PHENOMENOLOGY IN PARTICLE PHYSICS 1971

Proceedings of the Conference
Held at the California Institute of Technology
March 25 and 26, 1971

Edited by : *C.B. Chiu*
G.C. Fox
A.J.G. Hey

Sponsored by the Department of Physics, Mathematics and Astronomy, Caltech.

Published by the California Institute of Technology
Pasadena, California 91109

CONTENTS

PAGE

PREFACE v

MAP OF PHENOMENOLOGY WORLD vii

ABSTRACTS xi

1. WEAK INTERACTIONS

S.B. Treiman, Phenomenology of Weak Interactions.............................. 1

2. MULTIPARTICLE PROCESSES

U.E. Kruse, Some Recent Experimental Results for A_1, A_3, Q and L Mesons....... 27

W.R. Frazer, Phenomenology of Multiparticle Reactions.............................. 48

E.L. Berger, Phenomenological Applications of Dual Models.............................. 83

3. THE QUARK MODEL

R.P. Feynman, The Quark Model at Low Energies.............................. 224

4. THE A_2 MESON

K.W. Lai, Recent Results from Bubble Chamber Experiments on A_2.............................. 257

K.W.J. Barnham, Interfering Resonance Model Fit to $A_2^{+,-,0}$ Mass Spectrum....... 294

S.M. Flatté, The f^0 Mass Spectrum in 7 GeV/c π^+p Interactions.............................. 322

S. Ozaki, The Double Vee Magnetic Spectrometer: Experimental Setup and Current Results.............................. 326

M. Gettner, Measurements of the A_2^- and A_2^+ Mass Spectra.............................. 358

J.L. Rosner, Theoretical Remarks on the A_2 Meson.............................. 387

5. PHASE SHIFT ANALYSIS IN TWO-BODY REACTIONS

H. Steiner, Pion-Nucleon Scattering: Phase Shifts and Experiments.............................. 420

R.E. Cutkosky, Optimized Analytic Data Analysis and Application to K^+p Scattering.............................. 444

6. EXPERIMENTAL RESULTS IN TWO-BODY REACTIONS

B. Musgrave, A Review of Some Experimental Results on Hadron-Deuterium Scattering.............................. 467

D.W.G.S. Leith, Recent Results on $\pi^-p \to \rho^0n$ at Small Momentum Transfers....... 554

L. Dick, Some New Experimental Results with Polarized Targets--I.............................. 594

A. Yokosawa, Some New Experimental Results with Polarized Targets--II.............................. 612

7. PHENOMENOLOGY IN TWO-BODY REACTIONS

C. Schmid, Phenomenology at Intermediate Energies.............................. 629

C. Lovelace, Present and Future of Two-Body Phenomenology.............................. 668

G.C. Fox, On the Importance of Being an Amplitude.............................. 703

PREFACE

What is phenomenology? Reach not for your dictionary; make no vain efforts to pronounce it; we will come clean and explain all.

Science is noted for a competitive and helpful interaction between theorists and experimentalists. Unfortunately in almost all developing sciences, the moving hand of time drives a widening wedge between theory and experiment. Thus theorists are fully occupied in the mathematical and philosophical intricacies of their latest ideas. Again, experimentalists must concentrate on the design of their apparatus to insure they will get the best possible results current technology will allow. Phenomenology seeks to close the gap between those once close friends, theory and experiment, and so restore the interaction which is both vital to and characteristic of science. Although a classical concept, phenomenology is best known in its second-quantized form.

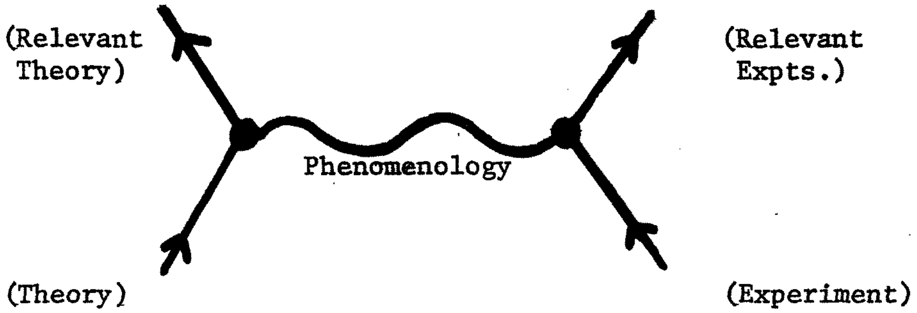

The basic tool of the phenomenologist is, first, the construction of simple models that embody important theoretical ideas, and then, the critical comparison of these models with all relevant experimental data. It follows that a phenomenologist must combine a broad understanding of theory with a complete knowledge of current and future feasible experiments in order to allow him to interact meaningfully with both major branches of a science. The impact of phenomenology is felt in both theory and experiment. Thus it can pinpoint unexpected experimental observations and so delineate areas where new theoretical ideas are needed. Further, it can suggest the most useful experiments to be done to test the latest theories. This is especially important in these barren days where funds are limited, experiments take many "physicist-years" to complete, and theories are multitudinous and complicated.

Phenomenology is applicable in many sciences but this conference was organized with the hope of emphasizing the wide scope and importance of phenomenology in particle physics. In fact, in the time available, not even all the important applications to particle physics could be covered. Some of these omissions were repaired in a workshop, held at Caltech just after the main conference reported here, and devoted to physics at intermediate energies ($\lesssim$ 5 GeV). This area is particularly suitable for phenomenology as the qualitative features have been well explored and further progress demands difficult experiments with high statistics. Phenomenology can indicate, for instance, which of the some hundred (quasi) two body reactions will be most fruitful to study. In the following we map some of the more active fields of phenomenology indicating where they have been covered in either the present volume, our companion workshop, or elsewhere. The contents of the current volume are summarized in more detail in the abstracts of the invited papers which have been collected together in pages xi to xvi.

We are indebted to many people for making this conference possible: Professor R.B. Leighton for his generous sponsorship; Nancy Hopkins and James Black of the Caltech Alumni Office for their efficient and cheerful organization; the session chairmen, M. Gell-Mann, W. Selove, J.D. Bjorken, M.J. Moravcsik, J.D. Jackson, T. Ferbel, R.L. Walker and S.C. Frautschi, for the smooth running of the conference; Susan Berger for her delightful cover; and our secretaries for their careful typing, with an especial thank you to Chris St.Clair who also drew the amusing illustrations. Alvin Tollestrup originally had the good idea of holding a phenomenology conference: We are grateful to him and our colleagues at Caltech for the encouragement which has made the organization and editing of this conference so enjoyable.

Editors:

C.B. Chiu

G.C. Fox

A.J.G. Hey

MAP OF PHENOMENOLOGY WORLD

In the following we indicate some of the main fields of phenomenology and some typical references: These are listed on Page ix.

I. Current Interactions

(a) Weak Interactions - Treiman[*]; Wolfenstein[1]; Lee and Wu[2].
(b) eN Scattering - Gilman[3]; Daresbury[4].
(c) νN Scattering - Treiman[*]; Llewellyn Smith[5].

II. Multiparticle Reactions

(a) General Properties - Frazer[*]; Berger[6].
(b) Inclusive Reactions - Frazer[*]; Quigg[1].
(c) Explicit Models (e.g., multiperipheral, B_5) - Berger[*,6].
See also III, IV(b) and V(b) (quasi two-body reactions).

III. Analysis and Interpretation of Production Experiments

(a) Extraction of Resonance Properties - Kruse[*]; A_2 Session[*]; Goldhaber[1].
(b) ππ and Kπ Phase Shifts - Argonne[7].
(c) Meson Spectroscopy - Feynman[*]; Rosner[1].
(a) to (c) are all covered by Reference 8.

IV. Analysis and Interpretation of Formation Experiments

(a) 2-body Phase-shifts - Steiner[*] (πN); Cutkosky[*] (KN); Moorhouse[1] (πN); Moravcsik[1] (KN, NN); Tripp[1] ($\bar{K}N$); Pfeil, Schwela[9] (γN).
(b) 3-body Phase-shifts - Cashmore[1].
(c) Baryon Spectroscopy - Feynman[*]; Plano[10]; Samios[10].
(d) Dispersion Relations - Ebel et al.[9]; Hohler, Strauss[11].

MAP OF PHENOMENOLOGY WORLD - (Page 2)

V. High and Intermediate Energy Two-Body Reactions

(a) Applications of Duality and Finite Energy Sum Rules

- (i) General Reviews - Schmid* (Intermediate Energies); Jackson[3].
- (ii) Dual Field Theory and Regge Cuts (Absorption) - Lovelace*.
- (iii) Veneziano Formulae - Berger*.
- (iv) SU_3 Constraints - Mandula et al.[1].
- (v) Relations between Absorption Model and Duality - Harari[3].

(b) Tests of High Energy Pole and Cut Models

- (i) Experimental Emphasis - Part 6*; Diebold[1].
- (ii) General Reviews - Jackson[13]; Fox (s-dependence[12], t-dependence*); Barger, Phillips[14].
- (iii) Empirical Rules for Cuts and Line Reversal Relations - Chiu[1].

(c) Further Topics

- (i) Diffraction Scattering - Morrison[10]; Gilman et al.[15]; Fox*.
- (ii) Photoproduction and Vector Dominance Model - Diebold[16]; Daresbury[4].
- (iii) Deuteron Corrections - Musgrave*.

REFERENCES FOR MAP

These are of course, only a representative collection: in particular, we refer, where possible, to reviews rather than the original phenomenology.

*This conference: see Table of Contents.

1. Proceedings of the *Workshop on Particle Physics at Intermediate Energies*, edited by R. D. Field, preprint UCRL - 20655 (1971)

2. T. D. Lee and C. S. Wu, Ann. Rev. Nuc. Sci. 15 and 16 (1965 and 1966).

3. Proceedings of the *International Conference on Duality and Symmetry in Hadron Physics* (Tel-Aviv 1971).

4. Proceedings of *4th International Symposium on Electron and Photon Interactions at High Energies*, (Daresbury Laboratory, Liverpool, 1969), edited by D. W. Braben and R. E. Rand.

5. C. H. Llewellyn Smith, to be published in Physics Reports.

6. E. L. Berger, invited talk at the Irvine Conference, 1969; preprint ANL/HEP 6927 (1970).

7. Proceedings of the *Conference on $\pi\pi$ and $K\pi$ Interactions*, edited by F. Loeffler and E. Malamud. (Argonne preprint, 1969).

8. *Experimental Meson Spectroscopy*, edited by C. Baltay and A. H. Rosenfeld. (Columbia Univ. Press, 1970).

9. *Low Energy Hadron Interactions*, Springer tracts in Modern Physics, Vol. 55 (1970).

10. *15th International Conference on High Energy Physics*, Kiev, (1970).

11. G. Höhler and R. Strauss, Karlsruhe preprint (1970).

12. *High Energy Collisions*, (Gordon and Breach, New York, 1970).

13. J. D. Jackson, Rev. Mod. Phys. 42, 12 (1970).

14. V. Barger and R. J. N. Phillips, *Phenomenology of Total Cross Sections and Forward Scattering at High Energies*, to be published in Nuclear Physics.

15. F. Gilman, J. Pumplin, A. Schwimmer and L. Stodolsky, Phys. Lett. 31B, 387 (1970).

16. R. E. Diebold, *Proceedings of 1969 Boulder Conference on High Energy Physics*, ed. K. Mahanthappa, W. Walker and W. Brittin, Colorado Assoc. Univ. Press, 1970.

ABSTRACTS

1. WEAK INTERACTIONS

S.B. TREIMAN, Phenomenology of Weak Interactions (Page 1)

The following recent developments of special interest in weak interactions are reviewed: status of the current-current picture and tests in diagonal processes, e.g., $\nu + e \rightarrow \nu + e$; speculations on the intermediate vector boson; new limits on neutral currents; a crisis developing for the process $K^o_L \rightarrow \mu^+\mu^-$; recent results on CP and T violation; theoretical anticipation for inelastic neutrino reactions.

2. MULTIPARTICLE PROCESSES

U.E. KRUSE, Some Recent Experimental Results for A_1, A_3, Q and L Mesons (Page 27)

After a brief description of the methods of analysis, some new results on the A_1, A_3, Q and L mesons are presented. A spin parity analysis of the 3π system in the A_1 region reveals 1^+ and 0^- components with both $\rho\pi$ and $\epsilon\pi$ decays. A preliminary analysis of the A_3 suggests spin 2^- and a $\rho\pi$ decay in addition to the dominant $f\pi$. The decay distribution of the A_1, A_3 and Q shows approximate t-channel helicity conservation in contrast to $\gamma p \rightarrow \rho^o p$ and πN elastic, which conserve helicity in the s-channel.

W.R. FRAZER, Phenomenology of Multiparticle Reactions (Page 48)

We discuss important qualitative features of multiparticle reactions. All models must explain the smallness of both the average transverse momentum and the multiplicity of produced particles. The longitudinal phase space plots, introduced by Van Hove, allow a convenient summary of low multiplicity events.

Single particle distributions are treated in detail—these test the theoretical ideas of scaling, limiting distribution, multiperipheralism and pionization. Most excitingly, the new diagrams, discovered by Mueller, suggest many new theoretical and phenomenological developments.

E.L. BERGER, Phenomenological Applications of Dual Models (Page 83)

Important applications of dual models to analysis of hadronic data are reviewed. A distinction is made between detailed quantitative fits, in which sums of Veneziano-type functions are employed, and more qualitative applications. Although quantitative fits have been generally unsuccessful, many valuable qualitative predictions can be abstracted from the models. Four-point (B_4) and five-point (B_5) models are treated thoroughly here; recent studies with higher order functions (B_6, B_8, $\ldots B_N$) are reviewed more briefly. A critical appraisal is given of evidence for and against predicted daughter states; in particular, the ρ' is examined in detail. Next, the important role played in dual models by dynamical zeroes is described and several applications are suggested. Analyses

(cont'd. on next page)

of Dalitz plots for the annihilation process $\bar{p}n \to 3\pi$ are discussed. There follows a section on B_5 phenomenology. Concerning quantitative applications, it is shown that new SLAC data on $K^0p \to K^+\pi^-p$ and $\bar{K}^0p \to K^-\pi^+p$ invalidate the simple B_5 approach of Chan, Raitio, Thomas and Törnqvist. New fits are proposed. Evidence against Rosner-Harari rules from some B_5 fits is disputed; discrepancies are shown to lie rather in improper unitarization of the model. Stressed is the importance of B_5 as a qualitative tool for understanding interference effects among competing channels in $2 \to 3$ particle reactions. It is demonstrated analytically that the model predicts asymptotic breaking of line-reversal symmetry in related production processes (e.g., $Kp \to K^*p$ and $\bar{K}p \to \bar{K}^*p$ or $\pi p \to KY^*$ and $\bar{K}p \to \pi Y^*$). The magnitude of symmetry breaking is directly proportional to the total width of the produced resonance. Examined closely is the possibility of using dual models to resolve the long-standing question of resonance or kinematical interpretation of A_1, Q, and other threshold enhancements. A simple counterexample is constructed to demonstrate the current dual models do not resolve this issue. The final section of the review concerns studies of inclusive reactions and of narrow resonances with large values of mass and spin. Throughout the paper, specific experimental and theoretical investigations are suggested in order to develop more understanding of the way duality and crossing-symmetry are manifest in hadronic data.

3. THE QUARK MODEL

R.P. FEYNMAN, The Quark Model at Low Energies (Page 224)

Matrix elements of vector and axial vector currents between one-hadron states are recalculated using a relativistic equation to represent the symmetric quark model of hadrons with harmonic interaction. Elements between states with large mass differences are too big compared to experiment, so a factor whose functional form involves one arbitrary constant is introduced to compensate for this. The vector elements are compared to experiments for photoelectric meson production, $K_{\ell 3}$ decay, and $\omega \to \pi\gamma$. Pseudo-scalar meson decay widths of hadrons are calculated supposing the amplitude is proportional (with one new scale constant) to the divergence of the axial current matrix elements. With only these two constants, the slope of the Regge trajectories, and the masses of the particles, more than 3/4 of the 75 calculated matrix elements agree with their experimental values within 40%.

4. THE A_2 MESON

K.W. LAI, Recent Results from Bubble Chamber Experiments on A_2 (Page 257)

Bubble chamber results on the A_2 meson in different charge states and for various decay modes are reviewed. Compared with the 7 GeV/c CERN π^- counter experiment, recent experiments, with both counter and bubble chamber techniques, have improved resolution but indicate "no-split" for the A_2. We present a compilation of angular distributions and spin-density matrix elements for $A_2^\pm$ production. Further it is shown that the decay branching ratios for A_2 and for K^{**} are in good agreement with SU_3 assuming a single resonance for A_2 and for K^{**}. Finally, we stress the advantages of having 4π geometry, as in bubble chamber data, for studying the A_2 mass spectrum and decay distributions.

K.W.J. BARNHAM, Interfering Resonance Model Fit to $A_2^{+,-,o}$ Mass Spectrum (Page 294)

This contribution is in the form of two papers: (A) New data; (B) Fit to all A_2 data.

(A) A study of the A_2^+ mass spectrum in π^+p interactions at 3.7 GeV/c is presented. For a cut of $-t' = 0.1 \rightarrow 2.0$ GeV^2 and on eliminating the Δ^{++} we find that the three pion mass spectrum in the A_2^+ region is fitted by the dipole formula with a confidence level of 53% and a single Breit-Wigner formula with a confidence level of 11%. Our result thus favors A_2 splitting although a single Breit-Wigner fit cannot be ruled out. We also report the A_2^+ decay branching fractions measured over all t' values. They are 0.78 ± 0.05 , 0.15 ± 0.04 , 0.06 ± 0.03 , and <0.02 for $\rho\pi$, $\eta\pi$, $K\bar{K}$, and $\eta'\pi$ respectively, in good agreement with other experiments.

(B) The $A_2^{+,-,o}$ three pion and missing mass spectra in the experiments with the best statistics to date, have been fitted with a two-interfering resonance model. Good fits are possible over a range of mass and width parameters for both the asymmetric case (wide and narrow resonances with nearly degenerate masses) and symmetric case (different mass values but approximately the same widths). Rather small changes in the relative amplitudes and phase of the two resonances are found to be necessary to change from the split A_2^- spectrum observed by the CERN Missing Mass Spectrometer and CERN Boson Spectrometer experiments to the unsplit A_2^+ observed by Alston-Garnjost et al.

S.M. FLATTÉ, The f^o Mass Spectrum in 7 GeV/c π^+p Interactions (Page 322)

We briefly report the f^o mass spectra and moments of the decay angular distribution in the reaction $\pi^+p \rightarrow \pi^+p\pi^+\pi^-$ at 7 GeV/c. No significant fine structure (e.g., splitting) is observed.

S. OZAKI, The Double Vee Magnetic Spectrometer: Experimental Setup and Current Results (Page 326)

The current status of the Double Vee Spectrometer experiment at the AGS is described. The experimental setup has both forward and recoil spectrometers. These are now both working, but the present data comes from runs using only the forward spectrometer. One of the two main reactions studied is:

$$\text{(a)}\quad \pi^- + p \rightarrow K^o + MM\ (\text{e.g., } \Lambda,\ \Sigma^o,\ Y^{*o})$$

$$\hookrightarrow \pi^+ + \pi^-$$

at 8 GeV/c. Preliminary results indicate that $d\sigma/dt$ for $\pi^-p \rightarrow K^o\Sigma^o$ is somewhat sharper than that for $\pi^-p \rightarrow K^o\Lambda$. The other reaction is:

$$\text{(b)}\quad \pi^-p \rightarrow A_2^- + p$$

$$\hookrightarrow K^- + K^o$$

$$\hookrightarrow \pi^+ + \pi^-$$

at 20.3 GeV/c. The data indicate "no-split" for the A_2 and the dominance of natural parity exchange in A_2 production. Similar A_2 results have also been obtained independently by the CERN-Munich group.

M. GETTNER, Measurements of the A_2^- and A_2^+ Mass Spectra (Page 358)

Observations of the mass distribution of the A_2 meson produced in the reaction $\pi p \rightarrow A_2 p$ are reported. The A_2's were observed using a missing mass technique. Measurements were made with 5 and 7 GeV π^- as well as 5 GeV π^+ beams. For each beam setting (5^-, 5^+, and 7^- GeV), more than 17,000 A_2's above background were observed with $0.20 \leq |t| \leq 0.29$ $(\text{GeV})^2$. The A_2 peaks are well described by a Breit-Wigner shape, whereas the dipole mass formula does not fit the data.

J.L. ROSNER, Theoretical Remarks on the A_2 Meson (Page 387)

The A_2 is in no way anomalous regarding its SU(3) properties or production mechanism. Evidence regarding substructure (or lack thereof) in the peak is discussed with particular regard to any further experiments that may be planned.

5. PHASE SHIFT ANALYSIS IN TWO-BODY REACTIONS

H. STEINER, Pion-Nucleon Scattering: Phase Shifts and Experiments (Page 420)

We give a brief survey of new low energy πN experiments and the status of current phase shift analyses. It is shown by Monte Carlo calculations, that A and R measurements will be very useful in limiting the number of acceptable phase shift solutions at a given energy.

R.E. CUTKOSKY, Optimized Analytic Data Analysis and Application to K^+p Scattering (Page 444)

A new approach to data analysis is described, which makes maximum use of general analyticity properties to extract interesting physics from experimental data. The analysis is applied to K^+p scattering, and preliminary results are discussed--in particular, the sensitivity of the results to the residues of the Λ and Σ poles.

6. EXPERIMENTAL RESULTS IN TWO-BODY REACTIONS

B. MUSGRAVE, A Review of Some Experimental Results on Hadron-Deuterium Scattering (Page 467)

The experimental techniques used in analyzing deuterium bubble chamber data are carefully reviewed. These are usually successful when tested via charge independence (symmetry) and hydrogen data. However, higher statistic data and a more uniform treatment of the corrections are needed for a really quantitative assessment of deuterium effects. Further, we give a brief survey of the important physics that can be studied in reactions on a neutron target.

D.W.G.S. LEITH, Recent Results on $\pi^- p \to \rho^0 n$ at Small Momentum Transfers (Page 554)

This contribution in in the form of 3 papers: (A) Data; (B) Tests of Vector Dominance Model; (C) Tests of (Strong) Absorption Model.

(A) The results of a wire spark chamber experiment studying the reaction $\pi^- p \to \pi^+ \pi^- n$ at 15 GeV/c are presented. The differential cross section, π-π mass distribution and density matrix elements have been determined from 10,000 $\pi\pi n$ events ($M_{\pi\pi} < 1.0$ GeV) produced with $-t < .30$ $(\mathrm{GeV/c})^2$. Both the density matrix elements and the differential cross section exhibit structure in the forward direction ($-t < m_\pi^2$).

(B) We present a comparison of new data on $\pi^- p \to \rho^0 n$ at 15 GeV/c with polarized and unpolarized single pion photoproduction data. Particular emphasis is placed upon the behavior of the differential cross sections and asymmetries in the forward direction ($-t < m_\pi^2$).

(C) The results of a wire spark chamber experiment studying the reaction $\pi^- p \to \pi^+ \pi^- n$ at 15 GeV/c are compared with the predictions of the absorptive one pion exchange model. The rich structure at small values of momentum transfer observed in the data is well described by the model.

L. DICK, Some New Experimental Results with Polarized Targets—I (Page 594)

We present the final results of an experiment performed at the CERN proton synchrotron by a CERN-Orsay-Pisa collaboration. The proton polarization in $\pi^- p$, $K^- p$, pp and $\bar{p}p$ elastic scattering has been measured at incident momenta of 6, 10, 14, and 17.5 GeV/c, and in the momentum transfer range $|t| = 0.1$ to 2.7 $(\mathrm{GeV/c})^2$.

A. YOKOSAWA, Some New Experimental Results with Polarized Targets—II (Page 612)

We report new polarization results for $\pi^\pm p$ and $K^+ p$ elastic scattering at large angles in the intermediate energy region, and also preliminary $\pi^- p$ charge exchange polarization measurements from CERN at 5 and 8 GeV/c.

7. PHENOMENOLOGY IN TWO-BODY REACTIONS

C. SCHMID, Phenomenology at Intermediate Energies (Page 629)

The following topics are discussed. Regge features are more easily and more clearly seen at intermediate energies (shrinkage, polarization structure in t). The direct (local) confrontation of Regge and phase shift amplitudes in $K^+ p$ scattering. The partial wave analysis of the imaginary part of the non-flip amplitude in $K^\pm p$ elastic scattering and the problem of the strength of the low partial waves. The new interference model as a tool above the phase shift region. Moravcsik's phase band method. Semi-local duality in $K^- p$ backward scattering and the qualitative difference between $K^+ p$ and $K^- p$ at intermediate angles.

C. Lovelace, Present and Future of Two-Body Phenomenology (Page 668)

We discuss the present state of strong interaction theory, especially Regge phenomenology, and likely directions for further progress. Elastic polarization experiments have strikingly confirmed exchange-degeneracy, and therefore pole-pole duality. Its corollaries have still not penetrated many theorists. Recent theoretical investigations have cast light on Regge cuts and the Pomeron. The NAL small-angle pp experiment will crucially test these new ideas.

G.C. Fox, On the Importance of Being an Amplitude (Page 703)

We review current experimental knowledge on the momentum transfer and spin dependence of the scattering amplitudes at high energy. We consider two-body, quasi two-body, and multiparticle reactions. (i) The small $-t$ data for natural parity exchange is shown to be inconsistent with all the current theories but consistent with several quite pleasing empirical rules. We document those $d\sigma/dt$, P, R and A measurements which can extend and clarify the present systematics. (ii) π exchange data at very small $-t$ is in amazing agreement with the poor man's absorption model which assumes smooth extrapolation from $t=m_\pi^2$ to $t=0$. At larger $-t \simeq .6\ (\mathrm{GeV}/c)^2$, $\rho_{00}\ d\sigma/dt$ for vector meson production shows similar systematics to the well-known natural parity exchange CEX reactions. (iii) We consider the behavior at large $-t \gtrsim 1\ (\mathrm{GeV}/c)^2$ of all two and quasi two-body data. In photoproduction, the data is well known to scale like $E_{\mathrm{lab}}^{-2}\ e^{3t}$. A similar t-dependence is observed for many hadronic reactions around 5 GeV/c. The energy dependence is less well studied: there is some suggestion that it is more like p_{lab}^{-3} for ρ and A_2 exchange. Explicit partial wave analysis of $\sqrt{d\sigma/dt}$ with various phase assumptions indicates that a large component of scattering is at small impact parameters. In photoproduction, this component takes a universal form which may reflect a new form of interaction present in all processes. (iv) We critically review quark model predictions for single and double resonance production. Although these are quite successful, the data seem to deviate from the quark relations, rather more than simple absorption models predict. This near equality between quark and absorption amplitudes implies one particularly amazing result. Thus absorption corrections to one pion exchange generates the Stodolsky-Sakurai distribution for the natural parity exchange component of Δ production. Further we show that many features of recent dual models based on the quark substructure are in qualitative agreement with experiment.

(Although it is not widely known, the beautiful princess' legendary sensitivity not only won her the hand of the handsome prince, but also landed her a job as part of the detection apparatus at one of our leading laboratories.)

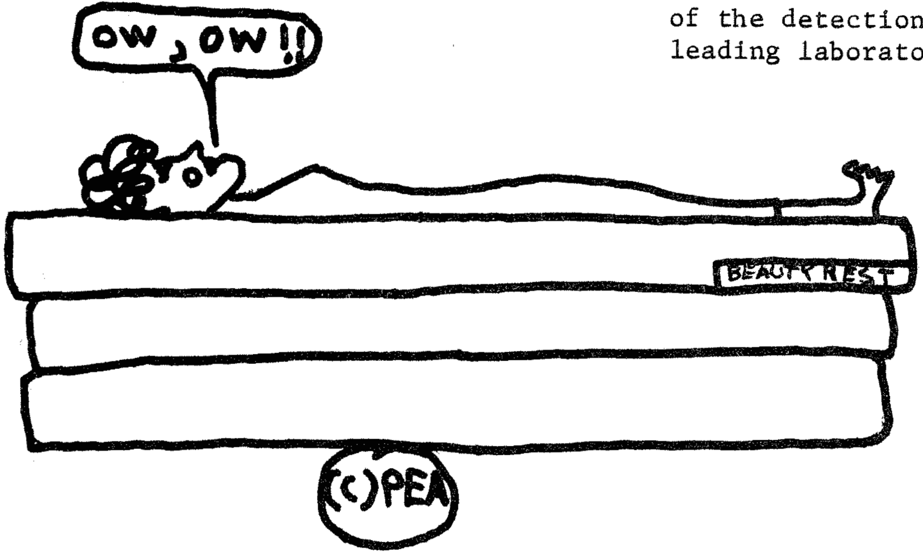

PHENOMENOLOGY OF WEAK INTERACTIONS*

S. B. Treiman

Joseph Henry Laboratories
Princeton University
Princeton, New Jersey 08540

---

* Research sponsored by the U.S. Atomic Energy Commission under Contract AT(30-1)-4159.

Most of our present ideas about the structure of weak interactions have been abstracted from the limited phenomenology of low energy decay processes. Each such process supplies at best a few pieces of information: the decay rate and perhaps several spectrum and polarization parameters. The wider prospects that would be afforded by study of weak interaction effects in collision reactions seems to be foreclosed for weak nonleptonic phenomena. But high energy neutrino physics, which has already yielded important results, is full of promise for the early future and has attracted a great deal of attention lately. Nevertheless, the low energy processes continue to produce new insights and occasional intimations that the standard phenomenology may be far from complete.

There is no need here for a systematic review of the whole of weak interaction physics. I will instead run through a subset of recent developments that seem to be of special interest. Let me begin by reminding you that on the present day picture one usually imagines that all classes of weak interactions -- nonleptonic, semileptonic, and pure leptonic -- arise from the effective self interaction of charged V, A currents composed of leptonic and hadronic parts. This picture rather directly summarizes what we read off from observations on muon decay and on various semileptonic processes; but owing to the complexities of hadron physics it goes beyond direct evidence so far as the nonleptonic interactions are concerned. Indeed, without the introduction of neutral currents or other speculative inputs, one has the familiar problem here of accounting for the empirical success of the $\Delta I = \frac{1}{2}$ rule. The subject has been endlessly discussed, without decisive outcome, and I shall not review it further. Equally speculative, still, is the question whether the weak interactions are mediated by heavy vector bosons.

For purely leptonic processes the current x current picture, at least on a straightforward and perhaps naive interpretation, provides a sharp prediction concerning $(\nu_e e)(\nu_e e)$ and $(\nu_\mu \mu)(\nu_\mu \mu)$ interactions: namely, that these have the same structure and strength as the $(\nu_e e)(\nu_\mu \mu)$ interaction responsible for muon decay. It has been therefore a matter of pressing interest for some time to test for the existence of these interactions, say through search for the elastic scattering process $\nu_e + e \rightarrow \nu_e + e$. The situation is made even more interesting by the speculations of Gell-Mann, Goldberger, Kroll, and Low,[1] who suggest that higher order weak interaction effects for such "diagonal" *processes can lead to an* *effective* *coupling strength which differs from that* describing muon decay. There have been several developments on these matters in the past year. An upper limit on $\nu_e - e$ scattering has been extracted by Steiner[2] from the data on electron production obtained in the 1963-64 CERN neutrino spark chamber experiment. Electron type neutrinos in the beam arise from K_{e3} decay and have a spectrum that peaks at ~ 1 Gev. Some 30 events compatible with the semileptonic process $\nu_e + n \rightarrow e^- + p$ were seen. At most one event was compatible with $\nu_e + e \rightarrow \nu_e + e$. This sets an upper limit $\sigma_{\nu e} \lesssim 40\, \sigma_{\text{theory}}$ ("theory" here refers to the standard expectation). More recently, Reines and Gurr[3] have reported negative results in a search for the reaction $\bar{\nu}_e + e \rightarrow \bar{\nu}_e + e$ induced by antineutrinos from the Savannah River reactor. They look in scintillator material for reactor-associated electron pulses corresponding to electrons in the energy range 3.8-5 Mev. The experimental upper limit is expressed by $\sigma_{\bar{\nu} e} < 4\, \sigma_{\text{theory}}$.

Another perennial concern of weak interaction physics has to do with the hypothetical intermediate vector bosons, W . When Yukawa introduced the pions as mediators of the nuclear force, he could infer from the known range of the force what the pion mass should roughly be. The mass M_W of the W particle is less well specified by its enthusiasts. Recall that if g is the dimensionless coupling constant that characterizes the interaction of the boson field with the lepton and hadron currents, then

$$\frac{g^2}{M_W^2} = \frac{1}{\sqrt{2}} G \,, \qquad G m_p^2 \approx 10^{-5}.$$

It has often seemed to people that a "natural" value for g might correspond to $g^2/4\pi \sim e^2/4\pi \sim \frac{1}{137}$. A more specific version of this association of weak and electromagnetic coupling constants has recently been suggested by Schechter and Uedu; and independently, T. D. Lee.[4] In Lee's notation, the idea is to define "charge" operators K_i according to

$$K_1 + i K_2 = \frac{1}{2} \int d^3x \; J_0^{weak}$$

$$K_1 - i K_2 = \frac{1}{2} \int d^3x \; J_0^{weak\,\dagger}$$

where J^{weak} here is the total lepton plus hadron current; and to define

$$i K_3 \equiv [K_1, K_2],$$

an equal-time commutator. With Q the usual electromagnetic charge operator, define also

$$Z = Q - K_3 \,.$$

In the usual quark model for the hadron part of the current one now finds the equal-time commutation relations

$$[K_i, K_j] = i \epsilon_{ijk} K_k \,,$$

$$[Z, K_i] = 0 \,.$$

With respect to K-spin one sees that the electromagnetic charge has a K=1 and a K=0 part, whereas the weak current is pure K=1. It is proposed now that $g J^{weak}$, $(e J^{em})_{K=1}$ and $g J^{weak\,\dagger}$ form a K=1 triplet. It then readily follows that

$$g = e/2\sqrt{2},$$

hence $M_W = 37.29$ Gev! If this is anything like right, the search for W particles is not going to be easy.

I mentioned earlier the speculative possibility that the weak nonleptonic interactions might involve the couplings of neutral hadron currents. The question also arises for purely leptonic interactions whether neutral lepton currents couple among themselves; or for semileptonic interactions, whether there are couplings of neutral lepton and neutral hadron currents. The latter might give rise to processes of the sort

$$\nu + \text{hadron} \rightarrow \nu + \text{hadron}$$

Upper limits derived from the CERN HLBC neutrino experiments have been reported during the past year for two such processes;[5] namely,

$$\frac{\sigma(\nu_\mu + p \rightarrow \nu + p)}{\sigma(\nu_\mu + n \rightarrow \mu^- + p)} = 0.12 \pm 0.06,$$

$$\frac{\sigma(\nu_\mu + p \rightarrow \nu + \pi^+ + n)}{\sigma(\nu_\mu + p \rightarrow \mu^- + p + \pi^+)} = 0.08 \pm 0.04 .$$

(I've taken the liberty to describe these as upper limits). Concerning neutral currents in purely leptonic processes, Albright[6] has noticed that the CERN neutrino data used to set a limit on elastic ν_e-e scattering also provides a limit on the reaction $\nu_\mu + e^- \rightarrow \nu_\mu + e^-$. He finds $\sigma(\nu_\mu e^- \rightarrow \nu_\mu e^-) < 0.40\ \sigma_{\text{theory}}$ ("theory" here refers to standard V-A coupling with standard strength). Another negative result, this one corresponding to the reaction $K^+ \rightarrow \pi^+ + \nu + \nu$, has been reported recently:[7] branching ratio $< 1.2 \times 10^{-6}$.

To be sure, any of these processes, if found, would not have to be interpreted as evidence of neutral current couplings. One could imagine that they arise instead from second order effects in conventional weak interactions, as illustrated in the diagram for the example of $K^+ \to \pi^+ + \nu + \bar{\nu}$:

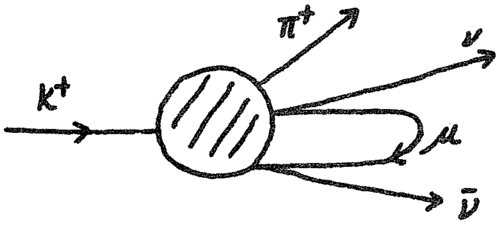

Formally one expects such second order effects to be "doubly" weak, but it's not clear what this means: naive perturbation calculations lead typically to divergent integrals. If evidence for processes of the type under discussion is some day found, one will begin to make distinctions among alternative interpretations on the basis of spectrum structure; e.g., according to whether the lepton pair seem to couple locally to the hadrons. But these points need hardly be pressed at the moment.

Of greater interest just now is the still unseen process

$$K_L^0 \to \mu^- + \mu^+ .$$

This is another example of a reaction that might arise from hypothetical neutral lepton couplings, or from higher order weak effects. But there is also another mechanism, one whose operation would seem to be indubitable: the sequence $K_L^0 \to$ two real or virtual photons $\to \mu^- + \mu^+$. On this latter mechanism, a rough estimate would suggest that[8]

$$\frac{\Gamma(K_L \to 2\mu)}{\Gamma(K_L \to 2\gamma)} \approx \alpha^2$$

hence

$$\text{branching ratio} = \frac{\Gamma(K_L \to 2\mu)}{\Gamma(K_L \to \text{all})} \approx 2 \times 10^{-8} .$$

In any case, if CP violating effects can be ignored, one gets a lower bound on the rate by taking the $K_L \to 2\mu$ amplitude to be purely absorptive. It can then be expressed, on the basis of unitarity considerations, as a sum of contributions coming from purely on-mass-shell intermediate states. To lowest relevant order in the fine structure constant only the 2γ, 3π, and $2\pi\gamma$ states need be considered. If the latter two channels are totally ignored (Pais calls this "naive unitarity") one then finds[9]

$$\text{b.r.} \gtrsim 6 \times 10^{-9} .$$

Let us now reinstate the $2\pi\gamma$ channel, continuing for a while longer to ignore the 3π state. Then one needs to know the amplitudes for $K_L \to 2\pi\gamma$ and $2\pi\gamma \to 2\mu$. The latter can be estimated with reliability in standard electrodynamics; the only unknown element is the electromagnetic form factor of the pion, which is however probably safely approximated in the ρ meson dominance model. As for $K_L \to 2\pi\gamma$, the process has not yet been seen and the bound ($\text{B.R.} < 4 \times 10^{-4}$) sets a limit on the modulus of the amplitude. Altogether, on the scale represented by "naive" unitarity, the net $2\pi\gamma$ contribution is unimportant. Finally, let us reinstate the 3π channel. It has two effects. Through the sequence $K_L \to 3\pi$, $3\pi \to 2\mu$ it makes a direct contribution to the absorptive $K_L \to 2\mu$ amplitude. The quantitative situation here is made uncertain because the process $3\pi \to 2\mu$ cannot be treated with theoretical reliability and is not yet accessible to experimental study. In addition the contribution of the 2γ state to the absorptive $K_L \to 2\mu$ amplitude is now made uncertain because the 3π state gives rise to an absorptive part for $K_L \to 2\gamma$, through the unitarity sequence $K_L \to 3\pi$, $3\pi \to 2\gamma$. And again the process $3\pi \to 2\gamma$ cannot be discussed with high reliability.

Despite all of these qualifications on the naive unitarity bound, estimates made by Martin, deRafael, and Smith suggest that it cannot easily be reduced by more than about 20%.[10] In advance of the experimental results that I will presently mention, most physicists would probably have regarded this bound as a safe betting proposition; and perhaps some of them still do. But the Berkeley group, Clark et. al.,[11] have earnestly looked for $K_L \to 2\mu$ events; and at least for the runs where K_L decay takes place in vacuum, they do not find any. The upper limit, at the 90% confidence level, is

$$\text{b.r.} \lesssim 1.8 \times 10^{-9}.$$

Insofar as this situation is sustained, there are the makings here of a first class crisis.

There is one more remark to be made. In the above discussion CP invariance has been assumed, so that it is decay into the ${}^1S_0$ state of two muons that is in question. Of course the K_L particle is in fact known to be very nearly pure with respect to CP. Let us ignore the small CP impurity and ignore also the 2π channels which this opens up for K_L decay. But let us allow for the possibility of substantial CP violation in the electromagnetic interactions of hadrons, so that we may comtemplate the CP violating decay of K_L into the ${}^3P_0$ state (spin-parity 0^+) of the muons. We similarly allow for CP violating $K_L \to 2\gamma$ and $2\pi\gamma$ decays. In this situation the absorptive amplitude for $K_L \to 2\mu({}^3P_0)$ decay can receive contributions only from the 2γ and $2\pi\gamma$ intermediate 0^+ states -- three pions cannot form a 0^+ state. For this same reason the amplitude for $K_L \to 2\gamma(0^+)$ has no absorptive part to leading electromagnetic order. Let us for a moment ignore the $2\pi\gamma$ contribution to the absorptive $K_L \to 2\mu({}^3P_0)$ amplitude. We then get a reliable lower (unitarity) bound on this absorptive amplitude in terms of the rate for $K_L \to 2\gamma(0^+)$. Or turning this around, we get an upper bound on the CP violating $K_L \to 2\gamma$ rate in terms of the $K_L \to 2\mu\,(^3P_0)$ rate. But the Berkeley results set an upper bound on the latter; and we hereby learn that[12]

$$\frac{\Gamma(K_L \to 2\gamma\,(0^+))}{\Gamma(K_L \to 2\gamma\,(\mathrm{all}))} \lesssim 0.37 .$$

On the basis of the kinds of considerations discussed earlier, it is found that the $2\pi\gamma$ contribution can be neglected with fair reliability and that the above result is secure to within about 20%, so long as the Berkeley results are sustained. These considerations of course do nothing to resolve the "crisis" for $K_L \to 2\mu\,(^1S_0)$ decay, but they have an interest of their own for the question of CP violation in electromagnetic interactions.

CP VIOLATION

Seven years after the initial discovery of CP breakdown it is still the case that the reasonably well established evidences of this breakdown are confined solely to the neutral K meson system, where one has detected the CP forbidden decays $K_L\to\pi^+\pi^-$ and $K_L\to 2\pi^0$ and has observed the CP forbidden asymmetry between $K_L\to\ell^-\pi^+\nu$ and $K_L\to\ell^+\pi^-\nu$ ($\ell = e$ and μ). This latter effect demonstrates directly that the K_L state is impure with respect to CP, whatever may be the fundamental origin of the impurity. One gloomy possibility, as you know, is that the origin lies in superweak, or other kinds of extravagant interactions which for all practical purposes can reveal themselves only through the generation of CP impurities in K_L and K_S. On this picture nothing of the symmetry violation would show up (at foreseeable levels of precision) outside the neutral kaon system; and even there, no additional on-mass-shell violations of the symmetry would be seen. In particular, for the $K_L\to 2\pi$ decays one would have $\eta_{00}=\eta_{+-}=\epsilon$, and $\arg\epsilon = \tan^{-1} 2\Delta m\,\tau_S = 43.2 \pm 0.4^\circ$.

Thanks to recent precision determinations of $\Delta m = m_L - m_S$ the phase of η_{+-} is now well determined on the basis of K_S-K_L interference effects in vacuum decay to $\pi^+\pi^-$: according to Aronson, et. al.[13] $\varphi_{+-} = 45.2 \pm 4.0^\circ$. The phase of η_{00} is less well determined. A recent report[14] gives $\varphi_{00} = 51 \pm 30^\circ$. The above results, especially that for φ_{+-}, are certainly compatible with the superweak class of theories. As for the moduli of the η parameters, the situation for $\pi^+\pi^-$ decay has been stable from the beginning: the present world average is $|\eta_{+-}| = 1.92 \pm 0.05 \times 10^{-3}$. For $|\eta_{00}|$ the situation is still problematic. In several experiments one finds results compatible with $|\eta_{00}| = |\eta_{+-}|$; in several others one finds that $|\eta_{00}|$ is noticeably bigger than $|\eta_{+-}|$. It's not for me to summarize these matters. Let me only mention two of the most recent published results. Chollet et. al.[14], in a CERN experiment, find $|\eta_{00}| = 3.3 \pm 0.6 \times 10^{-3}$. Barmin, et. al.[15], at DUBNA, find $|\eta_{00}| = 2.02 \pm 0.23 \times 10^{-3}$.

In contrast to the superweak alternative, it may be that CP violation resides in conventional nonleptonic and perhaps semileptonic interactions. The search for effects in weak processes outside the neutral K meson system has so far yielded only negative results. This is discouraging but not necessarily surprising if the scale is "milliweak", as would be suggested on this picture from the neutral K parameters. I will briefly mention here only a few recent results, which are beginning to approach the milliweak level of precision. Piroue and his collaborators[16] have collected data on 1.6×10^6 $K^+ \to \pi^+\pi^+\pi^-$ and an equal number of $K^- \to \pi^-\pi^-\pi^+$ decays. To the fraction of a percent accuracy which such large statistics implies, they find no significant differences between K^+ and K^- in any region of the Dalitz plot. As one measure of this they compare the usual odd pion slope parameters and find $\Delta a = (a^+ - a^-)/(a^+ + a^-) = -0.0070 \pm 0.0053$.

A new bound on time reversal violation in nuclear β decay has been obtained in the past year in an experiment of remarkable precision carried out by Calaprice et. al.[17]. They look for the T violating correlation $\vec{J}\cdot(\vec{p}_e \times \vec{p}_\nu)$ in β decay from polarized Ne^{19}: $Ne^{19} \to F^{19} + e^+ + \nu$. The coefficient of this correlation term measures the imaginary part of interference between the vector and axial matrix elements. They are relatively real in the absence of T violation -- apart from electromagnetic effects. The latter can be reliably computed and prove to be negligible at present levels of experimental accuracy. The experimental upper limit on phase difference between the vector and axial vector coefficients is found to be 0.3°. A similar high statistics study of muon polarization effects in $K_L \to \mu\nu\pi$ decay is currently being analyzed by Willis and collaborators, who have by now analyzed about a fourth of some 3 x 10^6 events. The components of muon polarization in the plane of decay provide information on the real part of the celebrated ξ parameter. The component normal to the plane measures Im ξ, which again ought to vanish in the absence of T violation. No indication of T violation has yet been detected here.

The most experimentally productive possibility for symmetry violation would be that C and T invariance are substantially violated in the (parity conserving) electromagnetic interactions of hadrons[18]. Two positive indications were reported some time ago. W. Lee and collaborators[19] looked for π^+, π^- asymmetries in the $\pi^+\pi^-\pi^0$ decay mode of η^0 mesons produced in the reaction $\pi^- p \to n \eta^0$. They reported a 1.5 ± 0.5% asymmetry for $A = [N(E^+ > E^-) - N(E^- < E^+)]/2N$. An interpretative difficulty here arises from possible interference produced by the small 3π continuum background under the η peak. The experiment has since been repeated at the PPA and the results are presently being analyzed. Some time ago also, Bartlett and Goulianos and their collaborators[20] studied the reaction $n + p \to d + \gamma$ at several energies and made a detailed balance comparison with the inverse reaction $\gamma + d \to n + p$ studied by others. They found a 2 1/2 standard deviation difference in the angular distributions for the events in the energy bin around the N + N*(1236) threshold. This experiment too has recently been repeated at the PPA and the results are now being analyzed.

In the meantime some new evidence has been reported for what could be a very substantial breakdown of detailed balance in electromagnetic processes. Berardo et. al.[21] have measured the differential cross section for $\pi^- p \to \gamma n$, at center-of-mass energies 1337 Mev and 1245 Mev. Information on the inverse reaction, obtained elsewhere, has to be extracted, unfortunately, from measurement of photo deuteron collisions. This involves problematic deuteron effects. Some confidence on the matter is claimed from the fact that detailed balance in fact works out well for the higher energy case (1337 Mev). On the other hand at 1245 Mev, near the N* region, the discrepancy between forward and inverse reactions seems to be substantial. For $\theta_{\gamma\pi} > 90^\circ$ the $\pi^- p \to n\gamma$ differential cross section is systematically smaller, by about 30%! It may take a while of course to digest and test the deuteron corrections.

SECOND CLASS CURRENTS

During the past year an interesting situation has developed with respect to mirror pairs of nuclear β decay, Wilkinson and Alburger[22] have surveyed available data and they report a systematic pattern of discrepancies, as big as 20% in a few cases, between the ft values of mirror pairs. At issue here are the G parity properties of the $\Delta S = 0$ hadron currents. Classification with respect to G parity was first suggested by Weinberg[23], who designated as "first class" the vector current with even G parity and axial current with odd G parity. The converse pieces he calls "second class". That the $\Delta S = 0$ currents have first class pieces we know from the occurence in nature of $\pi^{\pm}\to\pi^0 e^{\pm}\nu$ and $\pi\to\mu\nu$ decays. Here possible second class interactions cannot even contribute. But for semileptonic $\Delta S = 0$ processes connecting hadron states of indefinite G parity both classes of current can in general contribute. To test for the existence of second class interactions, let's see what things are implied by their absence. It will simplify the discussion if we ignore the possibility of T violation: insofar as we are concerned with observational effects which are even under time reversal there is no loss of generality in this. There are two different kinds of situations to be considered.

1. First consider a $\Delta S = 0$ semileptonic process between hadron states belonging to a common isotopic multiplet (e.g. $n\to p\bar{e}\nu$, $\nu_\mu + n\to p\mu^-$, etc.). For definiteness suppose that $\Delta Q = Q_f - Q_i = +1$. One encounters here the matrix element

$$\langle\alpha' | V_i + A_i | \alpha\rangle$$

where the labels α and α' specify spins and momenta. Suppose that the currents have definite isotopic spin I (in the examples cited only I = 1 can contribute; and more generally, on present phenomenology only I = 1 currents are envisaged). Then from the presumed first class G properties and from CPT invariance one can show that

$$\langle \alpha' | V_i + A_i | \alpha \rangle = (-1)^I \langle \alpha_T | V_i + A_i | \alpha'_T \rangle$$

where the subscript T means: reverse the sign of all spins and momenta. This result implies a restriction on the structure of the matrix element with respect to dependence on spins and momenta. For example, in neutron β decay the most general structures (independent of the above restriction) are

$$\langle p | V_\mu | n \rangle = \bar{u}(p) \left\{ g_V \gamma_\mu + \frac{G_V}{2m} \sigma_{\mu\nu} q_\nu + i \frac{h_V}{2m} q_\mu \right\} u(n),$$

$$\langle p | A_\mu | n \rangle = \bar{u}(p) \left\{ g_A \gamma_\mu \gamma_5 + i \frac{G_A}{2m} q_\mu \gamma_5 + \frac{h_A}{2m} \sigma_{\mu\nu} q_\nu \gamma_5 \right\} u(n),$$

where $q = p_n - p_p$ and where the form factors depend on q^2. The form factors must be relatively real if T invariance holds. Independent of this, one now observes that h_V and h_A can arise only from second class currents whereas the remaining form factors arise only from first class interactions. Second class effects are to be tested for by searching for the distinctive spectrum and spin effects induced by the form factors h_V and h_A. There are corresponding second class terms and effects for more general β decay processes connecting analog states. Unfortunately the second class coefficients multiply terms that are small for the small momentum transfers that occur in β decay, although the situation is by no means experimentally hopeless. For high energy neutrino processes like $\nu_\mu + n \rightarrow p + \mu^-$ this difficulty doesn't arise but there are other impediments: it is necessary to look at spin correlation effects in order to reliably observe contributions attributable to second class terms.

2. Next, consider a mirror pair of semileptonic processes: the $\Delta Q = +1$ process connecting hadron states α and β; and the $\Delta Q = -1$ processes connecting $\tilde{\alpha}$ and $\tilde{\beta}$, where $|\tilde{\alpha}\rangle = e^{i\pi I_2}|\alpha\rangle$, $|\tilde{\beta}\rangle = e^{i\pi I_2}|\beta\rangle$. In the former process one encounters the matrix element

$$\langle \beta | V_\mu + A_\mu | \alpha \rangle$$

in the latter,

$$\langle \tilde{\beta} | V_\mu^{+} + A_\mu^{+} | \tilde{\alpha} \rangle$$

From the presumed first class G parity properties of the currents, and from CPT and T invariance, one learns that

$$e^{i\pi I_2} (V_\mu + A_\mu) e^{-i\pi I_2} = V_\mu^{+} + A_\mu^{+}$$

hence

$$\langle \tilde{\beta} | V_\mu^{+} + A_\mu^{+} | \tilde{\alpha} \rangle = \langle \beta | V_\mu + A_\mu | \alpha \rangle .$$

In the context of β decay this implies, among other things, equality of decay rates for a mirror pair of processes. Of course the whole arguments presumes that electromagnetic violations of isospin independence can be safely ignored. In fact some of the electromagnetic effects are allowed for in the comparison not of rates but of ft values (this corrects for phase volume differences and for final state Coulomb interactions). But additional isospin impurity effects are more problematic and could conceivably account for the discrepancies noted by Wilkinson and Alburger. Because so much of our present thinking (CVC, the Cabibbo model, current algebra, etc.) excludes the possibility of second class currents, it is certainly a matter of high interest to pursue these hints of second class interactions.

INELASTIC NEUTRINO REACTIONS

I've deliberately left very little time for this subject, because the vast and growing literature, most of it theoretical, is anyhow too much to review. The topic that has most attracted attention concerns semileptonic processes in the situation where one sums over variables of the outgoing hadron system and indeed sums over all hadron channels as well as target spin. In this case the only variables retained are the incoming neutrino energy $\mathcal{E}$, the outgoing muon energy $\mathcal{E}'$, and the angle θ between the leptons (all, say, in the laboratory frame). Equivalently, let p be the 4 momentum of the target particle ($p^2 = -m^2$) and let q_ν and q_μ be neutrino and muon momenta, with $q = q_\nu - q_\mu$. Then the variables may be taken to be $\mathcal{E}$, q^2, and $\nu = -q \cdot p/m$.

In computing the cross section, for the sum over hadron channels, one encounters the object

$$W_{\nu\mu} = (2\pi)^3 \sum_X p_0 \langle p | j_\nu^+ | X \rangle \langle X | j_\mu | p \rangle \; \delta(p_X - p - q),$$

where j_μ is the weak current. The tensor $W_{\nu\mu}$ has the structure

$$W_{\nu\mu} = W_1 \left(\delta_{\nu\mu} - \frac{q_\nu q_\mu}{q^2}\right) + \frac{W_2}{m^2}\left(p_\nu - \frac{q \cdot p}{q^2} q_\nu\right)\left(p_\mu - \frac{q \cdot p}{q^2} q_\mu\right) + \frac{1}{2}\,\frac{W_3}{m^2} \epsilon_{\nu\mu\alpha\beta}\, q_\alpha p_\beta$$
$$+ \frac{W_4}{m^2} q_\nu q_\mu + \frac{W_5}{m^2}(p_\nu q_\mu + q_\nu p_\mu) + \frac{W_6}{m^2}(p_\nu q_\mu - q_\nu p_\mu),$$

where the W_i are real functions of ν and q^2. The structure function W_3 arises from vector-axial vector interference; the functions W_1 and W_2 are each $V\text{-}V$ and $A\text{-}A$; and if we accept the CVC hypothesis for the $\Delta S = 0$ currents and SU_3 generalization for the $\Delta S = 1$ currents, then W_4, W_5, and W_6 are pure $A\text{-}A$. Because the contraction of q_μ with the lepton current $\bar{u}_\mu \gamma_\mu (1+\gamma_5) v_\nu$ is proportional to the muon mass, W_4, W_5, and W_6 are expected to make only small contributions to the cross section. This is a pity, since they carry potentially interesting information. They have no counterpart in electro production and, for the reasons already noted, are expected to arise only from the axial current. They provide a measure, for one thing, of the non-vanishing of the divergence of the current. Moreover, the term with coefficient W_6 violates time reversal invariance and is therefore of interest on that count alone. This term gives rise to a non-vanishing component of muon polarization perpendicular to the plane defined by the leptons.

Having said all this, let me now ignore the lepton mass, hence ignore W_4, W_5, and W_6. Then for neutrino induced reactions the differential cross section is

$$\frac{\partial\sigma}{\partial q^2 \partial\nu} = \frac{G^2}{2\pi m}\,\frac{\varepsilon'}{\varepsilon}\left\{2W_1^{(\nu)}\sin^2\frac{\theta}{2} + W_2^{(\nu)}\cos^2\frac{\theta}{2} - \left(\frac{\varepsilon+\varepsilon'}{m}\right) W_3^{(\nu)}\sin^2\frac{\theta}{2}\right\}.$$

For antineutrino processes let $W_i^{(\nu)} \to W_i^{(\bar\nu)}$ and change the sign of the last term in the above equation. We have spoken here of the cross section when one sums over all outgoing hadron channels; but of course the structure is the same for each individual channel X if one integrates over all kinematic variables of the channel apart from invariant mass $M^{*2} = 2m\nu - q^2$. Let's also note the positivity conditions

$$\left(1+\frac{\nu^2}{q^2}\right) W_2 \geqslant W_1 \geqslant \frac{1}{2m}\sqrt{\nu^2+q^2}\,|W_3|\,.$$

So much for kinematics. Now for a few additional points of physical interest. For the question of second class currents, let us focus on $\Delta S = 0$ channels and compare the mirror processes

$$\nu + \alpha \to \mu^- + X\,,$$
$$\bar\nu + \tilde\alpha \to \mu^+ + \tilde X\,.$$

In the absence of second class currents one evidently has the relations

$$W_i^{(\nu)}(\alpha \to X) = W_i^{(\bar{\nu})}(\tilde{\alpha} \to \tilde{X}).$$

The simplest version arises when the hadron target is its own mirror, $\alpha = \tilde{\alpha}$ (e.g., deuterium, carbon, etc.). In this case one compares neutrino and antineutrino processes on the same target; and in fact, on summation over all $\Delta S = 0$ channels the prediction to be tested is

$$W_i^{(\nu)} = W_i^{(\bar{\nu})} \qquad (\Delta S = 0, \quad \alpha = \tilde{\alpha})$$

For the rest of the discussion let's accept that the currents are purely first class and let us turn to the fashionable matters of current algebra, Bjorken scaling, etc. The literature, as I've said, is vast. Among the various theoretical expectations, there is one which stands out for its special respectability. This is the Adler sum rule[23], which follows rather directly from the time-time commutators of Gell-Mann's current algebra, with a minimum of extra assumptions. For a target with isospin and hypercharge quantum numbers I_3 and Y it reads

$$\int_0^\infty \frac{d\nu}{m}\left[W_2^{(\bar{\nu})}(\nu,q^2) - W_2^{(\nu)}(\nu,q^2)\right] = 4I_3\cos^2\theta_c + (2I_3+3Y)\sin^2\theta_c ,$$

where θ_c is the Cabibbo angle. A remarkable feature is that the right hand side of the equation is independent of the variable q^2. It is an important, if difficult objective of neutrino physics to subject this relation to experimental test.

Next, let me remind you of Bjorken's scaling ideas[24]. For this purpose it is convenient to define

$$F_1 = W_1 ; \quad F_2 = \frac{\nu}{m} W_2 ; \quad F_3 = \frac{\nu}{m} W_3 ,$$

and to regard the F_i as functions of q^2 and

$$\omega = q^2/2m\nu .$$

Bjorken's conjecture[24] is that the $F_i \rightarrow F_i(\omega)$ have nontrivial limits as $q^2 \rightarrow \infty$, $\nu \rightarrow \infty$, ω fixed ($0 \lesssim \omega \lesssim 1$). The analogous conjecture for electroproduction seems, as you know, to be well supported by experiment, especially for F_2^{em}; and indeed the scaling limit sets in for surprisingly small q^2 (≈ 1 Gev$)^2$). For neutrino processes it is an immediate consequence of the scaling hypothesis that the total cross section σ grows linearly with neutrino energy ε as $\varepsilon \rightarrow \infty$:

$$\sigma^{(\nu)} \xrightarrow[\varepsilon \rightarrow \infty]{} \frac{G^2 m \varepsilon}{2\pi} \int_0^1 d\omega \left\{ F_2^{(\nu)}(\omega) + \frac{2}{3}\omega\, F_1^{(\nu)}(\omega) - \frac{2}{3}\omega\, F_3^{(\nu)}(\omega) \right\}$$

(of course a similar result holds for antineutrino processes, with $F_i^{(\nu)} \rightarrow F_i^{(\bar{\nu})}$ and with the last term given a sign change). Linear growth is strikingly supported by the CERN propane data, which give

$$\sigma\,(\text{nucleon}) \longrightarrow (0.52 \pm 0.13)\, \frac{G^2 m \varepsilon}{\pi}$$

Notice the inequalities

$$F_2(\omega) \geqslant 2\omega F_1(\omega) \geqslant \omega\, |F_3(\omega)| .$$

Within the scaling limit there are a great many further sum rules and predictions of other sorts, based on current algebra, parton models, field theoretic models, Reggeism, etc. Let me first mention here the Callan-Gross relation[25] which seems to arise in any picture where the currents are constructed out of elementary spin 1/2 fields (quarks?); namely

$$F_2(\omega) - 2\omega F_1(\omega) = 0 ,$$

a result whose analog in electroproduction seems to be very nearly supported by the SLAC data (σ_L/σ_T small, $\lesssim 0.2$). Moreover, from the space-space quark current algebra, Gross and Llewelyn Smith[26] obtained the sum rule

$$-\int_0^1 d\omega \left[F_3^{(\nu)}(\omega) + F_3^{(\bar{\nu})}(\omega) \right] = 4B + 2Y + \sin^2\theta_c \left[2I_3 - 3Y \right].$$

where B, Y, I_3 are the baryon, hypercharge, and isospin quantum numbers of the target hadron.

Then there are the more detailed predictions from parton models, e. g., relations connecting the neutrino and electroproduction structure functions[27]

$$12 \left(F_1^{\gamma p} - F_1^{\gamma n} \right) = F_3^{\nu p} - F_3^{\nu n}$$

and

$$F_1^{\gamma p} + F_1^{\gamma n} \geq \frac{5}{18} \left(F_1^{\nu p} + F_1^{\nu n} \right)$$

There's more, but, luckily, time doesn't permit...

REFERENCES

1. Gell-Mann, Goldberger, Kroll, and Low, Phys. Rev. 179, 1518 (1969).
2. H. J. Steiner, Phys. Rev. Letters 24, 746 (1970).
3. F. Reines and H. S. Gurr, Phys. Rev. Letters 24, 1448 (1970).
4. J. Schechter and Y. Ueda, Phys. Rev. D2, 736 (1970); T. D. Lee, to be published.
5. Cundy, Myatt, Nezrick, Pattison, Perkins, Ramm, Venus, and Wachsmuth, Phys. Letters 31B, 478 (1970).
6. C. Albright, Phys. Rev. 2D, 1330 (1970).
7. Klems, Hildebrand, and Steining, Phys. Rev. Letters 24, 1086 (1970).
8. M. A. Baqi Beg, Phys. Rev. 132, 426 (1963).
9. C. Quigg and J. D. Jackson, UCRL-18487 (unpublished); L. M. Seghal, Nuovo Cimento 45, 785 (1966) and Phys. Rev. 183, 1511 (1969).
10. Martin, deRafael, and Smith, Phys. Rev. D2, 179 (1970).
11. Clark, Elioff, Field, Frisch, Johnson, Kerth, and Wenzel, to be published.
12. These considerations were developed in collaboration with G. R. Farrar, to be published.
13. Aronson, Ehrlich, Hofer, Jensen, Swanson, Telegdi, Goldberg, Solomon, and Fryberger, Phys. Rev. Letters 25, 1057 (1970); and references therein.
14. Chollet, Gaillard, Jane, Ratcliffe, Repellin, Schubert, and Woff, Phys. Letters 31B, 658 (1970).
15. Barmin, Barylov, Borisov, Bysheva, Viselovsky, Golubchikov, Goldin, Davidenko, Dolgolenko, Demidov, Zombkovskaya, Kondratiev, Konoplev, Meshkovsky, Mirosidi, Tumanov, Chistyakova, Chuvilo, Shebanov, Bogdanovicz, Vinogradov, Ivanovskaya, Kanarek, Maximenko, Ogrzevalsi, Okhrimenko, and Strugalski, Phys. Letters 33B, 377 (1970).

16. Ford, Piroue, Remmel, Smith, and Sonder, Phys. Rev. Letters 25, 1370 (1970).

17. Calaprice, Cummins, and Girvin, unpublished.

18. Bernstein, Feinberg, and Lee, Phys. Rev. 139, 1650 (1965).

19. Gormley, Hyman, Lee, Nash, Peoples, Schultz, and Stein, Phys. Rev. Letters 21, 402 (1968).

20. Bartlett, Friedberg, Goulianos, Hammerman, and Hutchinson, Phys. Rev. Letters 23, 893 (1969).

21. Berardo, Haddock, Nefkens, Verhey, and Zeller, Phys. Rev. Letters 26, 201 (1971).

22. D. H. Wilkinson, Phys. Letters 31B, 447 (1970); D. H. Wilkinson and D. E. Alburger, Phys. Rev. Letters 24, 1170 (1970); D. H. Wilkinson and D. E. Alburger, Phys. Letters 32B, 190 (1970).

23. S. Weinberg, Phys. Rev. 112, 1375 (1958);

23'. S. Adler, Phys. Rev. 143, 1144 (1966).

24. J. D. Bjorken, Phys. Rev. 179, 1547 (1969).

25. C. G. Callan and D. J. Gross, Phys. Rev. Letters 22, 156 (1969).

26. D. J. Gross and C. H. Llewellyn-Smith, Nuclear Physics B14, 337 (1969).

27. See, for example, C. H. Llewellyn-Smith, Nuclear Physics B17, 277 (1970).

DISCUSSION

Yokosawa (Argonne): You mentioned neutrino experiments with polarized targets. How crucial are such experiments? We cannot do this next year, but if it is very crucial, maybe we can do something for you.

Treiman: We can take a vote! Such experiments are interesting on several scores. Of course, I've been burnt in suggesting experiments before, that cost people lots of trouble and at the end did not turn out. So I am reluctant to insist that you do it!

However, Bjorken has made some speculations on the spin-dependent effects which could be quite substantial. This represents another test, although I guess not of major importance, of the ideas of scaling and predictions of current algebra.

Time-reversal is a gamble. We are so desperate. If you find a violation, no excuse is needed for doing the experiment; if you don't, you'll hate me! I don't know what to say. The gloomy possibility may appear that we will never see it. Another possibility is that it is there, but down to the 10^{-3} level. We simply have to look all over the place. It will be a shame to pass up this possibility. We know such a thing was done in the analogous process of electroproduction, where a polarized target was used to do the so-called "Christ-Lee" experiment ($e + p \rightarrow e' +$ anything). Nothing was found to be sure. However, with neutrinos we can do the "Christ-Lee" experiment under circumstances where you can see the axial current contributing, because maybe the violation is in the axial current. There is, as I mentioned, the possibility of testing time-reversal without having a polarized target, if you are willing to look at the polarization of the muon. This is going to be very small and it seems better to do it with a polarized target.

Yovanovitch (Argonne): I would like to make two comments. One possible way to measure the polarization effects in weak interactions is not to build massive polarized targets, but to measure the recoil polarization, which sounds a bit cheaper at the moment. Also it probably will be done in ten years!

Secondly, for an inclusive experiment, one could measure the polarization of the muon.

Treiman: You understand that in the individual non-quasi-elastic process, the polarization does not bear on time-reversal; it is only in the quasi-elastic processes (2 → 2; e.g., $\nu + B \rightarrow \mu + B'$), or in experiments summing over all channels. The latter is because when you sum over all channels it corresponds to looking at the absorptive part of the forward scattering amplitude, and again time-reversal has something to say. Thus if you look at the polarization of the recoil nucleon, it is only for quasi-elastic processes that this bears on time-reversal; whereas if you polarize the parent, you can sum over all channels.

The trouble with the muon polarization is that the coefficient is down, certainly kinematically, and also for a variety of theoretical reasons -- but the latter should perhaps be discounted. It is true in the scaling limit, if you believe in the parton model, that the function W_6 is zero. But one should look in the non-scaling limit. The trouble here is closely related to the smallness of the muon mass.

Conforto (Rutherford): What is the situation with regard to second-class currents in muon capture where we have large momentum transfer?

Treiman: My colleague, Holstein, has looked into muon capture in hydrogen and helium. Unfortunately, what enters into the analysis is complicated for two reasons. First of all, for helium the two experiments give rather different answers, so there is an experimental problem. The other is that unfortunately, the induced pseudoscalar also enters in the analysis. This happens to enter in combinations with the second-class currents so that you cannot disentangle them. So, in order to interpret the result, you have to have some belief in what the induced pseudoscalar is. Now I'm one of the guilty parties; I have a belief! But it is not sure that you should believe this number, which comes from PCAC. That must be taken together with the fact that you don't know the axial-vector coupling because you are not at $q^2 = 0$. For the vector case, you can believe CVC; for the axial-vector you have no such guide. The q^2 is not so small, so just the thing which makes second-class currents important, makes g_A

uncertain. Holstein has looked at all these effects and concludes that, yes, you probably can say something if the experiment is good enough. However, it is marginal; you need some belief in g_A. Some day g_A will be measured as a function of q^2.

Conforto: What is your feeling? Is the limitation experimental or theoretical?

Treiman: They are about the same level.

Conforto: Then there is no point in doing the experiment!

Treiman: If you wait for the theorist to do the experiment, it will never be done.

Hey (Caltech): To disentangle the time-reversal violation in W_6 you need to know the electromagnetic corrections.

Treiman: That is a limitation on all remarks that I have made about time reversal.

Hey: De Rujula and de Rafael have a unitarity bound for the elastic case which is quite sizeable.

Treiman: It is a very crude bound. I think I would trust my instinct here. If you find something which is much bigger than α, then you should take it seriously. If it is of the order of α, you would always expect that. I don't have a technical comment on that. If you find a very small effect, you are right, you need to know the correction. That happened after all in the analogous electron "Christ-Lee" experiment. They found a very tiny effect which could quite well be second-order electromagnetic. So you are right, it is always a problem. The trouble is that we haven't even found a well-established small effect to quarrel over!

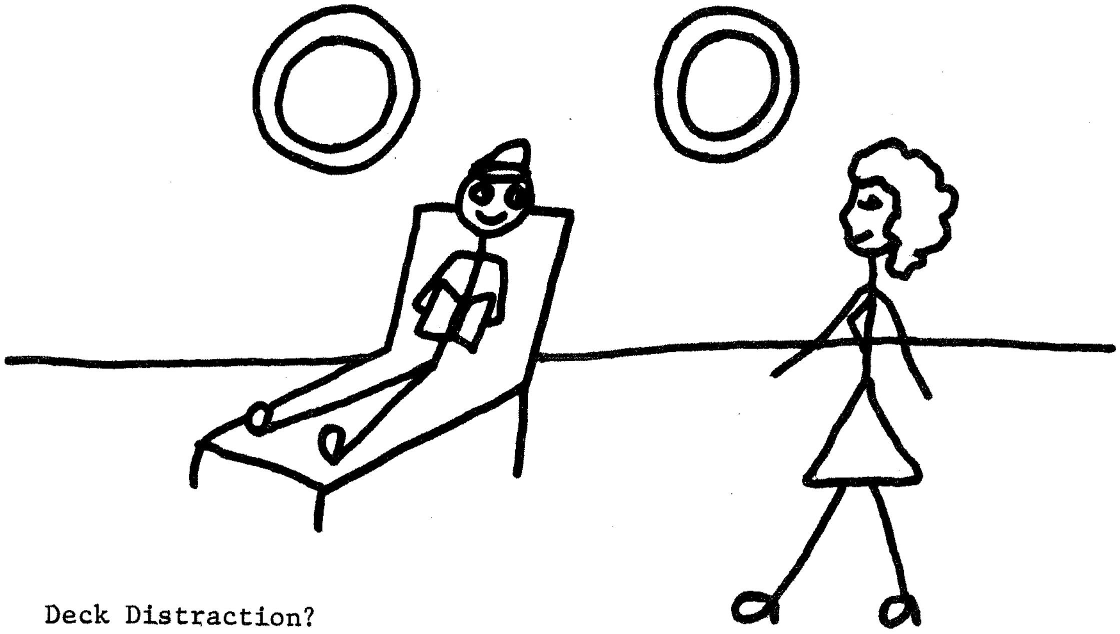

Deck Distraction?

SOME RECENT EXPERIMENTAL RESULTS FOR A_1, A_3, Q, and L MESONS[*]

U.E. Kruse

Department of Physics, University of Illinois at Urbana-Champaign
Urbana, Illinois 61801

---

[*] Work supported in part by the Atomic Energy Commission.

In the last year we have accumulated a great deal of information regarding boson enhancements which are seen primarily in diffractive production. If we take a brief look at production of 3π system by π mesons without change in charge we see the prominent A_1 and A_3 near 1060 and 1650 MeV. Similarly for the $K\pi\pi$ system produced by K mesons, we see a broad Q enhancement between 1200 and 1400 MeV and the L meson near 1750 MeV. I shall simply call these enhancements "mesons" for the sake of brevity and we shall examine some of the evidence to see if they are or are not "resonances".

There is general agreement that the A_1, A_3, Q, and L are strongly produced in π nucleon and K nucleon collisions in reactions with no change in charge, that the production is peripheral, and that the cross section falls off slowly with increasing beam momentum. There is also general agreement that the $\rho\pi$, $f\pi$, $K^*(890)\pi$, and $K^{**}(1420)\pi$ are strong decay modes for the A_1, A_3, Q, and L respectively. In each case the mass of the meson is roughly 200 MeV above threshold for these strong decays.

Other properties in production and decay are not so well established, and in this discussion I would like to select some of the topics of current interest. I will first briefly summarize the methods of analysis, then discuss some of the new results on the A_1 and A_3 then Q and L. I will leave to the end the discussion of polarization in production: that is, the question of s vs. t channel helicity conservation.

Some of the results such as those of the decay modes of the A_3 and L, and the possible structure in the Q are in a preliminary stage and there is disagreement between various experiments: more decisive determinations of these questions are needed. Nonetheless some of these preliminary results are very suggestive of resonance behavior and in the near future the experiments should clarify the nature of these mesons.

I. Methods of Analysis

The production of a system of three pseudoscalars is usually described by the mass of the system produced and the momentum transfer squared to the system. (In the present experiments there have been no measurements for the polarization of the target or outgoing proton.) There are then five further independent variables to describe the decay of the system into the three pseudoscalars. These are usually chosen to be the Dalitz plot variables S_1 and S_2 and three Euler angles. The variables S_1 and S_2 are the invariant masses squared of two of the pairs of pseudoscalars; the three Euler angles describe the orientation of the three particle system with respect to one of the standard coordinate systems.

Some of the data have been analyzed according to the distribution in the Dalitz plot. As an example, the Birmingham-Glasgow-Oxford collaboration(1) has explored this distribution for the $K\pi\pi$ system in the Q region and we will show some of their results for the Q decay modes. In other experiments, the data have been analyzed according to angular distributions. As an example the ABBCCHLV collaboration(2) has studied angular distributions for all events in the A_1 and Q mass bands to determine polarizations and examine the question of helicity conservation. Both of these types of analyses, Dalitz plot or angular distributions, will give the dominant features in the A_1 and Q region where presumably these mesons are strong and the background is relatively small. However, in the A_3 and L region the backgrounds are larger, particularly for low incident beam momenta. Hopefully we can obtain more information about the mesons as well as the background by examining all five variables at once by considering a whole set of partial waves for the 3 particle system. Our group at Illinois and in collaboration with other π^- experimental groups has examined the A_1 region with such an analysis[3),4)] and we have some preliminary data for the A_3 meson. In this partial wave analysis we make a maximum likelihood fit to the data using the theoretical probability as a function of the five variables for each event. In the theoretical probability distribution the production density matrix elements and the decay amplitudes are treated as variables. The maximum in the likelihood then gives us the best values for these variables. We can deduce the relative importance and polarization of various spin parity states from the density matrix elements and the magnitude and relative phase of the decay amplitudes for a particular spin parity state.

II. Some Results for the A_1 and A_3

The mass spectrum for the 3π system produced in $\pi^- p$ collisions is shown in figure 1. The data are taken from the high momentum contributions in a collaboration of $\pi^- p$ experiments$^{(4)}$. From the figure it is clear that even at these high momenta the A_2 still appears near the upper part of the A_1 and that there is considerable background under the A_3. When we look at the diagonal elements of the density matrix obtained in the partial wave analysis described above we obtain the relative contributions from the various spin parity states. In figure 2 the results of such an investigation are shown for the University of Illinois data at 5 and 7.5 GeV/c$^{(3)}$. Clearly the spin parity 1^+ dominates the A_1 region and the A_2 shows up in the 2^+ near 1.3 GeV as expected. A reasonable fraction of the events near 1.1 GeV is seen to have spin parity 0^-, and the peaking of the 0^- signal suggests that we also have an enhancement for this spin parity in the A_1 region. The decay modes of the 1^+ and 0^- have also been examined and are shown in figure 3. In both cases the S wave decay is strongest. For the 1^+ this is found to be the decay by S wave into $\rho\pi$ the P wave decay into $\epsilon\pi$ is also present. The ϵ is assumed to be a 0^+ resonance, in this analysis a mass of 765 MeV and width of 400 MeV gave a best fit. For the spin parity 0^- the strong S wave decay is into $\epsilon\pi$, P wave decay into $\rho\pi$ is also present.

The $\pi^- p$ collaboration has also examined the dependence on incident momentum of the production cross section in the A_1 region$^{(4)}$. In figure 4 the results are shown for events with spin parity 1^+ in the mass region from 1.0 to 1.2 GeV. There is a slow decrease with indident momentum, the cross section falls roughly as $P_{inc}^{-.4}$. A previous examination of this momentum dependence without the selection on 1^+ spin parity$^{(5)}$ indicates that the cross section continues to rise to lower momenta, thus the 5 GeV/c point should not be taken as the indication of a decrease for momenta below 6 GeV/c.

The A_1 is strongly produced only in diffractive reactions $\pi^\pm p \rightarrow p A_1^\pm$; the situation for production in other reactions is essentially unchanged from the summary presented by Garelick$^{(6)}$ who concluded there was evidence for production in other reactions and commented on the desirability of further work.

In the A_3 region, we are just above the threshold for $f\pi$ production, however well above the $\rho\pi$ threshold. A simple "Deck mechanism" explanation for the A_3 would predict only $f\pi$ decay. In earlier data at 6 GeV/c π^- the intensity distributions in the $\rho\pi$ and $f\pi$ bands of the Dalitz plot were examined as a function of 3π mass(7). There was no attempt to separate the various spin-parity contributions, and an enhancement was only seen in the $f\pi$ system, none in the $\rho\pi$. Preliminary results from a partial wave analysis of the A_3 region in the Illinois data at 5 and 7.5 GeV/c are shown in figure 5. In this analysis there is an enhancement for the spin parity 2^- the other spin parities 0^-, 1^+, 2^+ (not shown) and 3^+ show no significant structure in this region. In this analysis both $\rho\pi$ and $f\pi$ decay modes are seen for the spin parity 2^- as shown in figure 6. These results should be treated with caution, we have not performed all the checks that we would like to carry out. They are suggestive that the partial wave analysis may be able to pick out the contributions from a particular spin parity, and give us a better determination of the decay modes when large backgrounds are present. A confirmation of the $\rho\pi$ decay mode enhancement for the 2^- system in further analysis would argue for a "resonance" interpretation of the A_3.

III. Some Results For The Q and L Regions

A $K\pi\pi$ mass spectrum produced in K^+p collisions yielding $K^+\pi^+\pi^-p$ is shown in figure 7. The data are taken from the high momentum contributions of the International K^+ Collaboration. The Q enhancement between 1.2 and 1.4 is obvious. In this plot, however, the L meson near 1750 MeV is quite weak, many of the L events having been lost with the Δ^{++} cut. The purpose of this figure is twofold, to show the mass spectrum in the Q, and the large background in the L region.

The possible structure in the Q region has been discussed by Goldhaber(8) and most recently summarized by Firestone at the Philadelphia Conference(9). A broad peak, or perhaps a shallow valley between two peaks, can be most naturally associated with the existence of two strange meson states corresponding to the A_1 and B mesons. For the $K\pi\pi$ system, in the absence restrictions from G parity conservation, these can mix and produce complicated structures(8). Another possible explanation is the occurrence of Deck mechanism in both the $K^*\pi$ and $K\rho$ channels(10). Because of the lower $K^*\pi$ threshold the lower peak would then be expected to be mainly $K^*\pi$, the upper mainly $K\rho$.

The Birmingham-Glasgow-Oxford collaboration(1) has analyzed a large sample of K^+p interactions at 10 GeV/c using a Dalitz plot analysis. They have shown many fits to their data assuming both $K\rho$ and $K^*\pi$ decays and in one case they allowed for possible incoherence between these decays. The results for this fit, assuming spin 1^+ for the Q, are shown in figure 8. The upper plot shows the magnitude of the ratio of $K\rho$ decay amplitude to $K^*\pi$ amplitude, the lower shows the relative phase. These results are again very suggestive of structure in the Q region. As the authors point out, the variation of the relative phase shows a trend which we would expect if the lower Q is the analog of the A_1 with positive C conjugation and the upper Q the analog of the B with negative C conjugation. The variation of the magnitude of the $K\rho$ and $K^*\pi$ amplitudes is not consistent with a simple Deck picture. A detailed explanation of these data in terms of two partially interfering states has not been attempted.

With the Q, as with the A_1, the question of production in alternate channels continues to be of great interest. It is worthwhile to cite the two classic examples although they are not new. There is the C meson at 1242 MeV found in stopping $\bar{p}p$ reactions(11) and the K*(1300) seen in π^-p interactions at 6 GeV/c(12). The former would correspond to the lower part of the Q, the latter appears to be narrower than the overall Q but the statistics are limited for this reaction.

In the L region we can expect complications in the mass spectrum for the same reasons as in the Q region. If the L spin parity turns out to be 2^- we expect the analogs of the two possible 2^- non-strange states. At the moment there is no experimental evidence for a complication in the mass spectrum or in the decay modes. The question of the importance of various decay modes for the L has not yet been settled. The experiment in K^+p at 12 GeV/c has found a significant enhancement only in the $K^{**}(1420)\pi$ system(13). In contrast experiments in K^-p at 4.6(14) and 10 GeV/c(15) as well as K^+p at 10 GeV/c(16) find definite evidence that the L meson has decay modes other than $K^*(1420)\pi$. In all of these experiments there is a large background underneath the L meson; the determination of other decay modes will remain difficult without a better selection of the L events from the background.

IV. Results Of Polarization In Production

The ~~observ~~ation of s channel helicity conservation in the reaction $\gamma p \rightarrow \rho^o p$(17) led to the suggestion(18) that s channel helicity is also conserved in other diffractive processes such as A_1, A_3, Q, and L production.

The conservation of s-channel helicity predicts that for incident pseudoscalars the density matrix element $\rho^{s}_{oo} = 1$, that is $\rho_{oo} = 1$ when the angular distributions are examined in the s channel helicity frame with the z axis chosen to point opposite to the recoiling proton. In contrast, conservation of t-channel helicity predicts $\rho^{t}_{oo} = 1$, in this case the angular distributions are measured in the t channel helicity frame using the z axis along the incident pseudoscalar (the standard Gottfried-Jackson frame). The two reference frames are identical for $t = t_{min}$ but differ by a significant rotation about the normal to the production plane for larger t values.

Let us briefly summarize the current experimental situation. In the A_1 and Q regions the background is relatively small and the angular distributions in the mass bands have been investigated by two groups without selecting the 1^+ spin parity. The A_1 was studied at 8 GeV/c and 16 GeV/c, the Q^- at 10 GeV/c(2). A similar analysis was carried out for the Q^+ from the International K^+ collaboration(19). The A_1 and A_3 polarizations have also been studied using the partial wave analysis. The A_1^- has been examined by selecting the spin parity 1^+ component for π^- momenta between 5 and 25 GeV/c(4). A preliminary analysis has been carried out for the 2^- system in the A_3 region(20). For the A_3 the background is large and it was essential to use a method which selects the A_3 component.

We present some of the results in Table I showing the density matrix element ρ_{oo}. For simplicity we have grouped the data in rough t intervals. As can be seen in the table, there is general agreement that the experimental data do not fit s-channel helicity conservation, they are in better agreement with t channel helicity conservation. In the present data, there is no trend toward s channel helicity conservation with increasing beam momentum. We should stress that the data do not give complete agreement with t channel helicity conservation: in the π^-p collaboration data,(4) which is probably most independent of background difficulties, the real part of ρ_{10} is small, about -.1, but significantly different from zero.

V. Conclusions

The new experimental data therefore suggest the following conclusions:

1. In the A_1 there is evidence for enhancements in spin parities 1^+ and 0^- with each one having significant decay modes into $\rho\pi$ and $\epsilon\pi$.
2. In the A_3 the importance and exact nature of decay modes beyond $f\pi$ still needs further investigations; preliminary analysis of recent data favors spin parity 2^- for this enhancement and suggests the existence of a $\rho\pi$ decay mode.
3. In the Q, possible structure shows up in the mass spectrum and in the variations of the $K\rho$ and $K^*\pi$ decay amplitudes with Q mass.
4. In the L, the importance and exact nature of decay modes beyond $K^*(1420)\pi$ is still uncertain, though strong indications for other decay modes are seen in several experiments.
5. Helicity conservation has been investigated for the A_1, A_3 and Q. In each of them, s channel helicity conservation does not give a good fit; the data correspond more closely to t channel helicity conservation. However t channel helicity conservation does not give complete agreement, density matrix elements other than ρ_{oo}, although small, appear to be significantly non zero.

Acknowledgements

It is a pleasure to acknowledge the work and suggestions of many physicists who have contributed to the data discussed in this brief summary. I am particularly indebted to my colleagues at Illinois, G. Ascoli, L. Eisenstein, J. Hansen, and M. Ioffredo for many of the results presented for π^-p interactions as well as stimulating discussions.

REFERENCES

1. K. Barnham, et al, Nuclear Physics B25, 49(1970)
2. J. Beaupre, et al, Phys. Letters 34B, 160(1971)
3. D. V. Brockway, Ph.D. Thesis, Univ. of Illinois, (1970)
4. G. Ascoli, et al, Phys. Rev. Letters 26, 929(1971)
5. K. Paler, Nuclear Physics B18, 211(1970)
6. D. Garelick, Experimental Meson Spectroscopy, Edited by Baltay and Rosenfeld, Columbia Univ. Press, P205(1970)
7. D. Crennell, et al, Phys. Rev. Letters 24, 781(1970)
8. G. Goldhaber, Phys. Rev. Letters 19, 976(1967)
9. A. Firestone, Experimental Meson Spectroscopy, Edited by Baltay and Rosenfeld, Columbia Univ. Press, P229(1970)
10. D. R. O. Morrison, Kiev Conference Rapporteurs Talk, CERN, D.Ph.II, 70-64
11. A. Astier, et al, Nuclear Physics B10, 65(1969)
12. D. Crennell, et al, Phys. Rev. Letters 19, 44(1967)
13. A. Barbaro-Galtieri, et al, Phys. Rev. Letters 22, 1207(1969)
14. M. Aguilar-Benitez, et al, Phys. Rev. Letters 25, 54(1970)
15. J. Bartsch, et al, Phys. Letters 33B, 186(1970)
16. D. Colley, et al, Nuclear Physics B26, 71(1971)
17. J. Ballam, et al, Phys. Rev. Letters 24, 960(1970)
18. F. Gilman, et al, Phys. Letters 31B, 387(1970)
19. International K^+ Collaboration, CERN, D.Ph.II, 71-3
20. I am particularly indebted to L. Eisenstein and M. Ioffredo for these results.

Table I

Density Matrix Element ρ_{oo} for A_1, A_3, and Q

Particle	Momentum	ρ^t_{oo} t-channel helicity frame		ρ^s_{oo} s-channel helicity frame	
		$\|t-t_{min}\|$ 0-.1	.2 -.4	$\|t-t_{min}\|$ 0-.1	.2 -.4
A_1^-	5 - 7.5[a]	.94±.02	.87±.07	.89±.02	.41±.06
A_1^-	11 - 25[a]	.96±.05	.98±.20	.94±.05	.46±.03
A_3^-	5 - 7.5[b]	.95±.08	.84±.13	.58±.07	.13±.11
Q^-	10 [c]	.91±.05	.86±.09	.85±.05	.49±.1
Q^+	4.4 - 7.0[d]	.80±.06	.72±.09	.84±.06	.65±.09
Q^+	9.5 - 12.7[d]	.82±.04	.84±.09	.79±.04	.41±.10

[a] Reference 4

[b] Reference 20

[c] Reference 2

[d] Reference 19

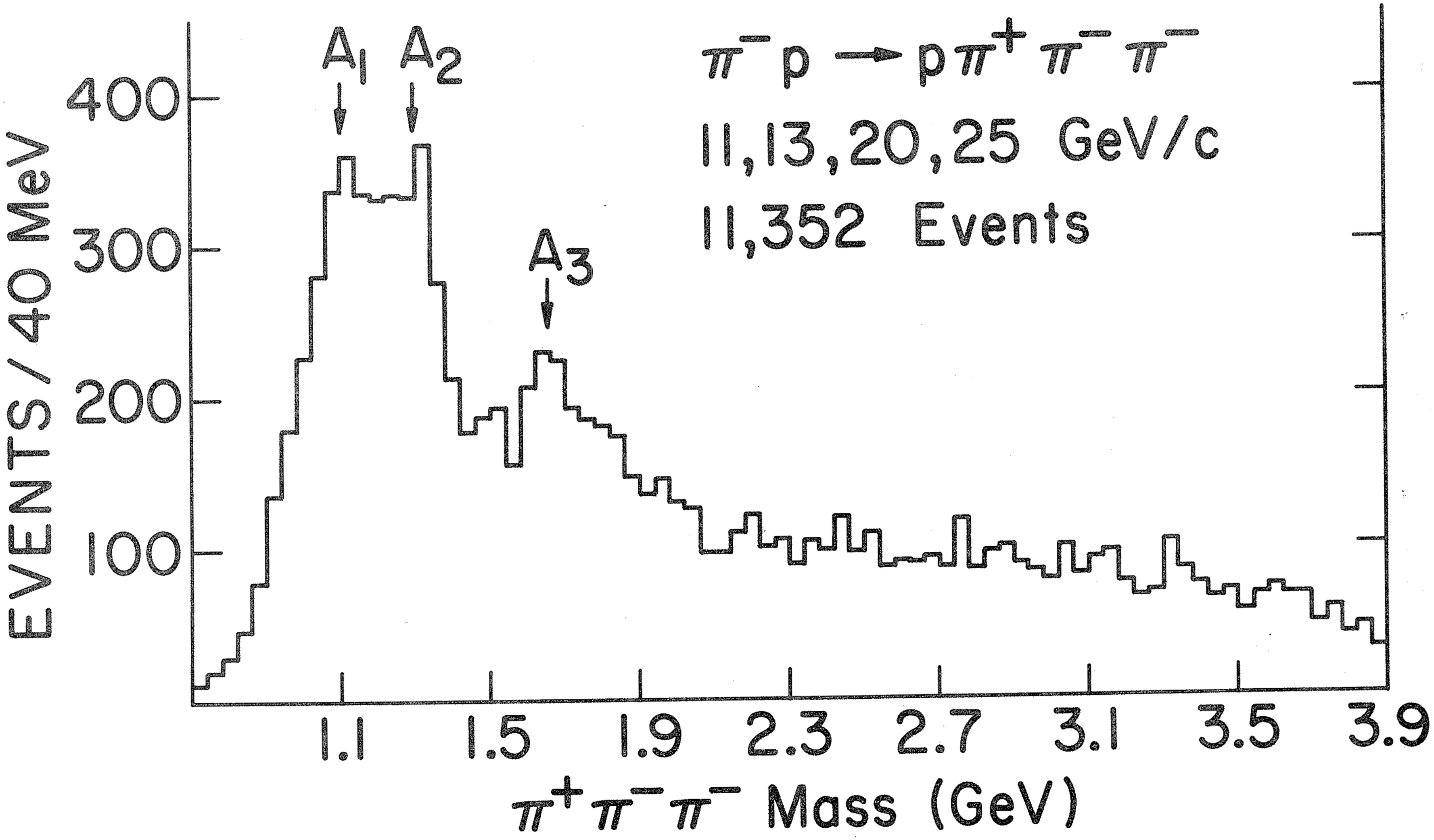

Figure 1. The $\pi^+\pi^-\pi^-$ Mass Spectrum for $\pi^- p \rightarrow p\pi^+\pi^-\pi^-$ at 11, 13, 20, and 25 GeV/c.

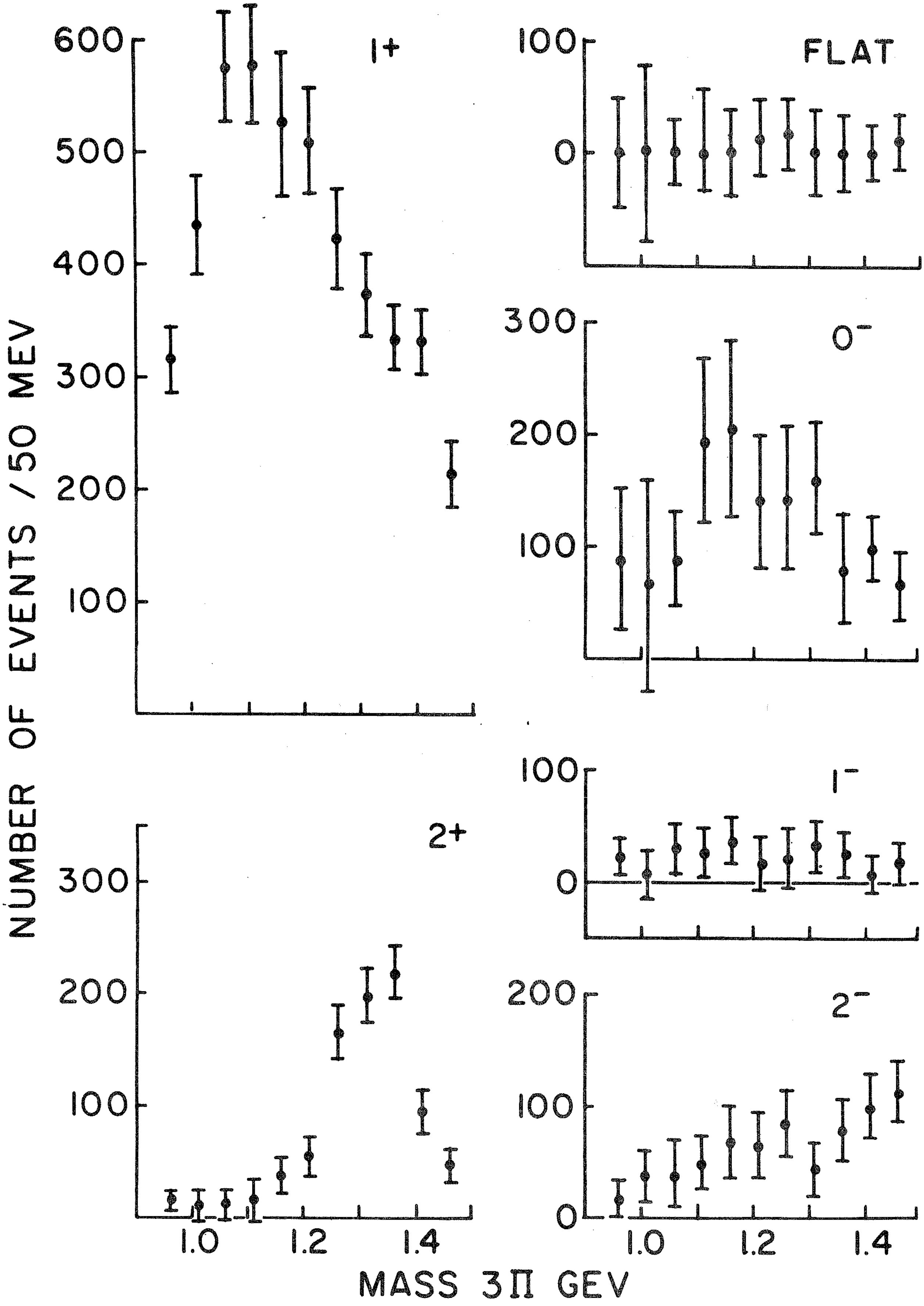

Figure 2. Number of events in the spin-parity states as a function of 3π mass for 5 and 7.5 GeV/c, A_1 region.

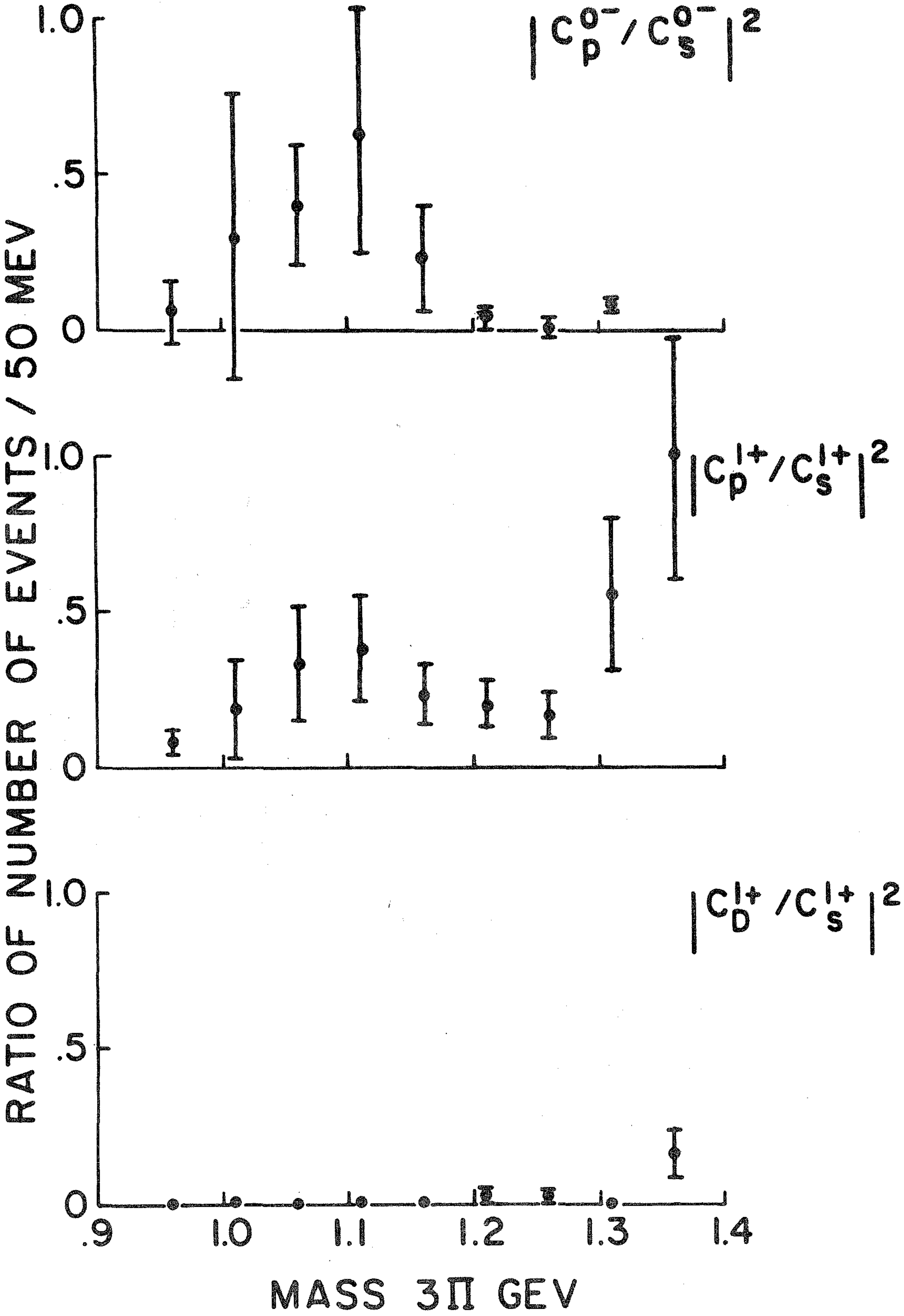

Figure 3. Ratio of magnitude squared of the decay amplitudes as a function of 3π mass for 5 and 7.5 GeV/c.

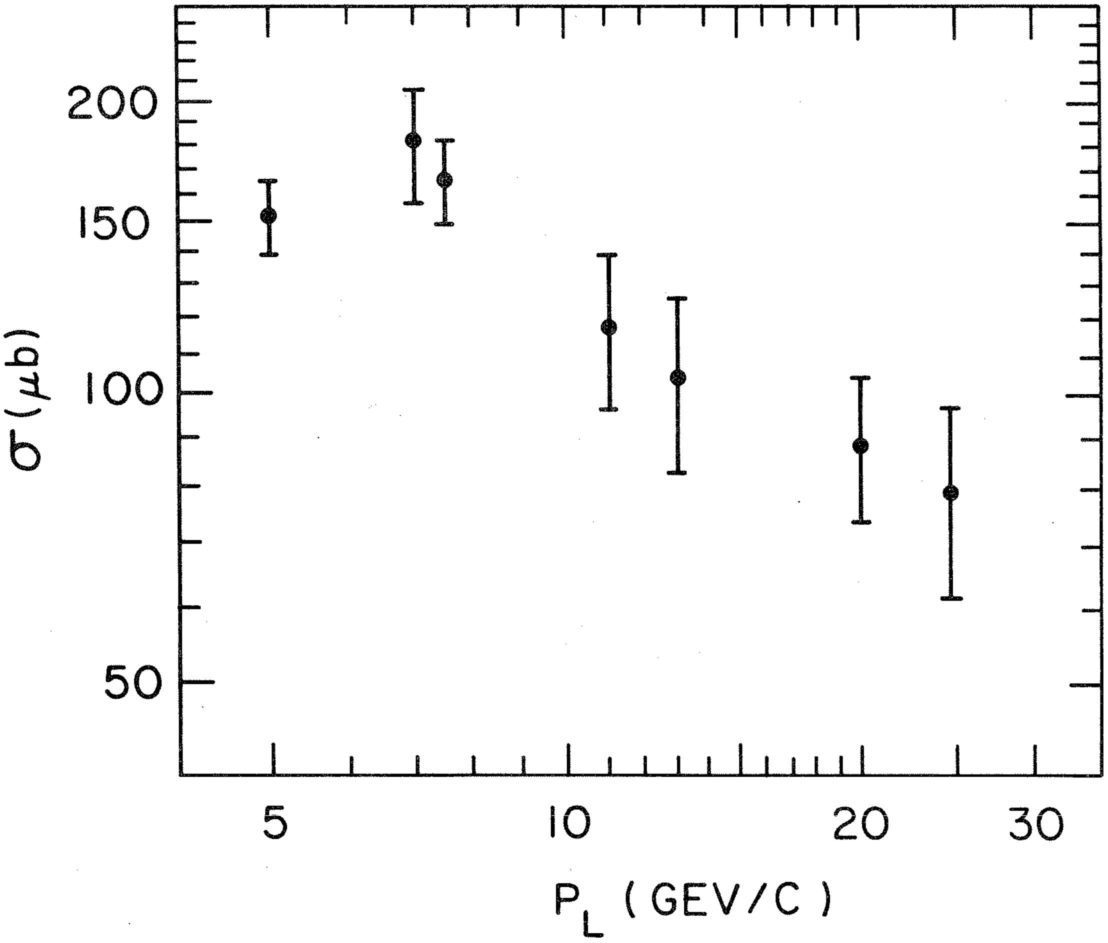

Figure 4. Cross section for $\pi^- p \rightarrow A_1^- p$ as a function of π^- momentum with A_1^- of spin parity 1^+ and mass between 1.0 and 1.2 GeV.

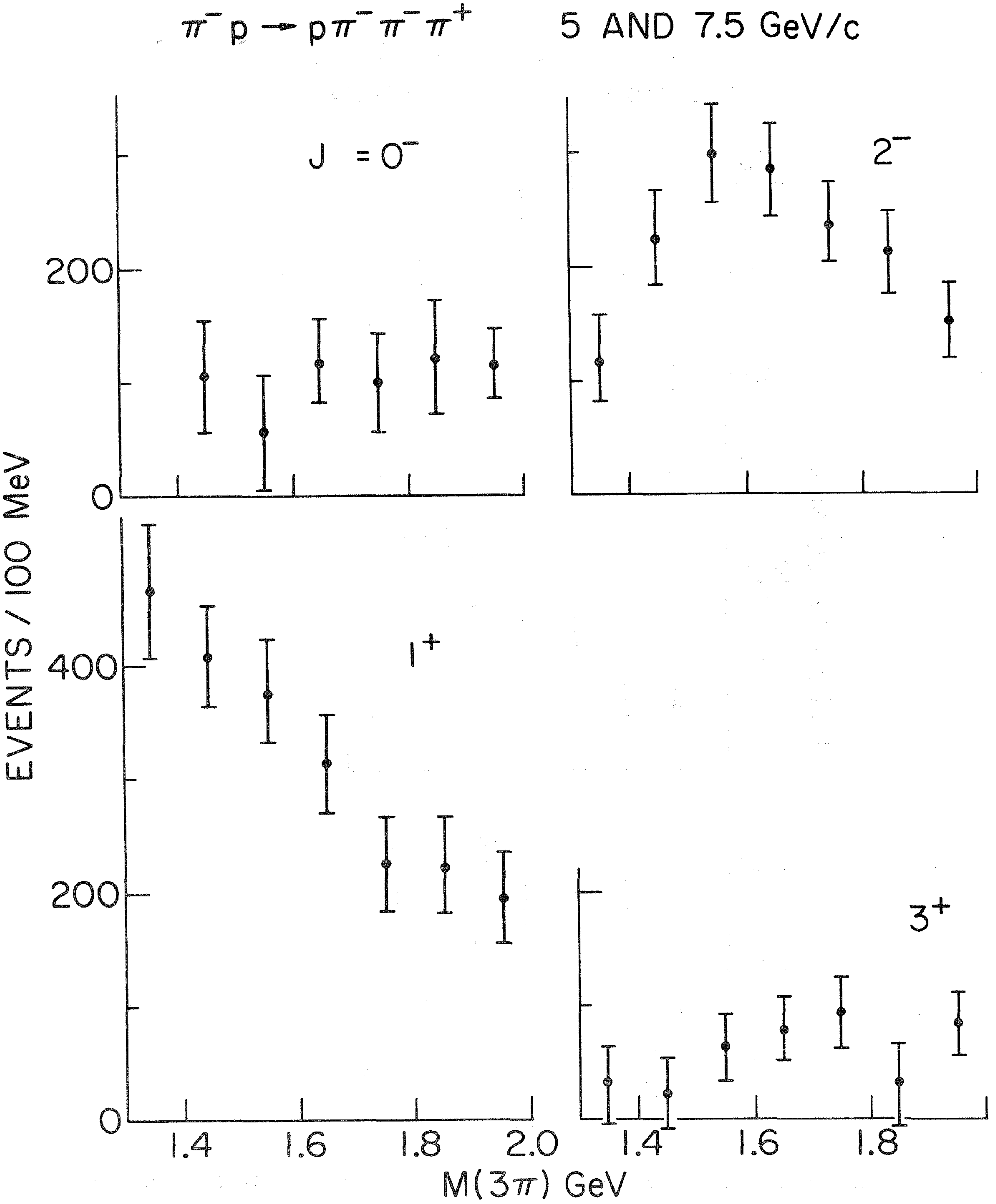

Figure 5. Number of events in the spin-parity states as a function of 3π mass for 5 and 7.5 GeV/c, A_3 region.

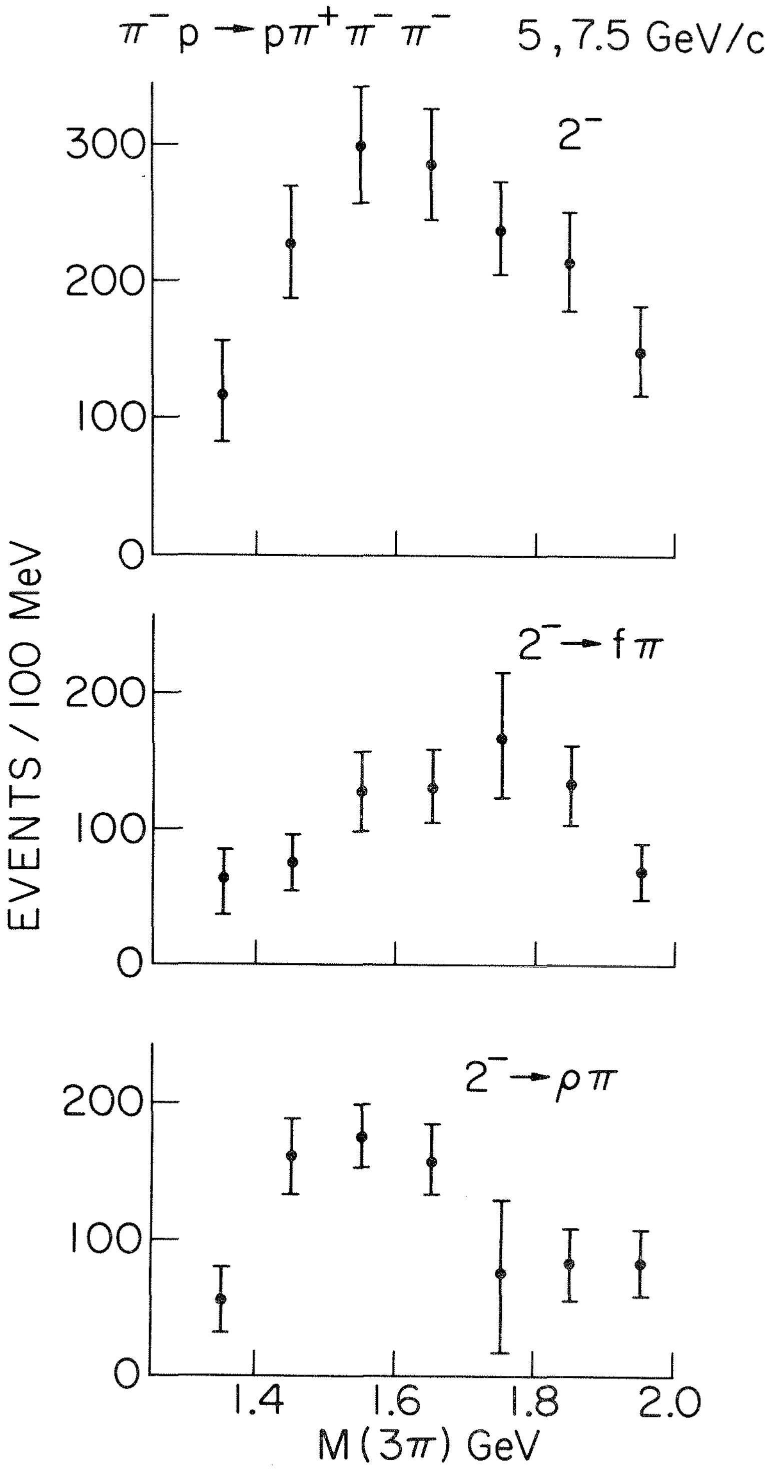

Figure 6. Number of events decay modes ρπ and fπ with spin parity 2^- as a function of 3π mass for 5 and 7.5 GeV/c.

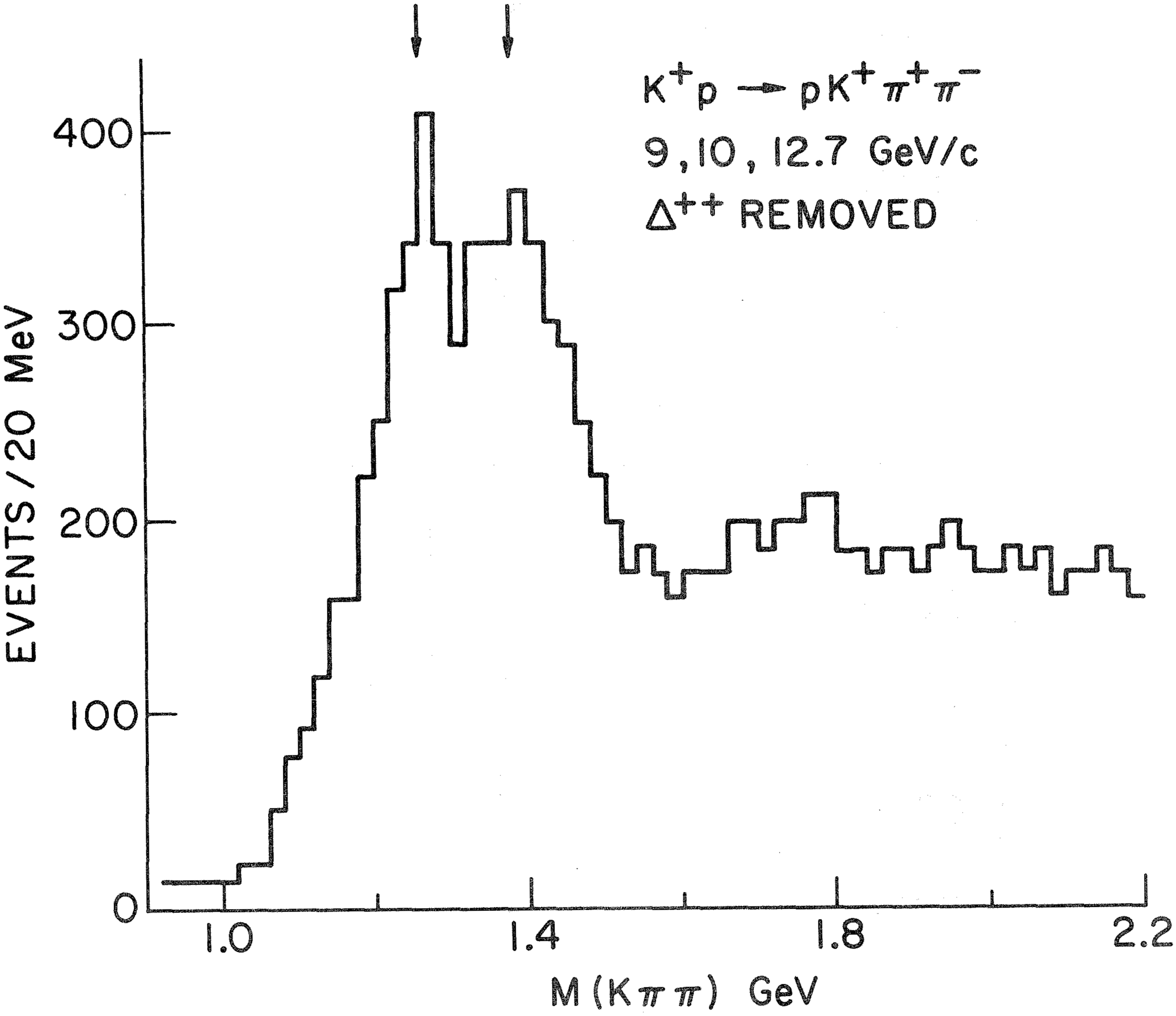

Figure 7. The $K^+\pi^-\pi^+$ Mass spectrum for $K^+p \rightarrow pK^+\pi^+\pi^-$ at 9, 10, 12.7 GeV/c with Δ^{++} removed.

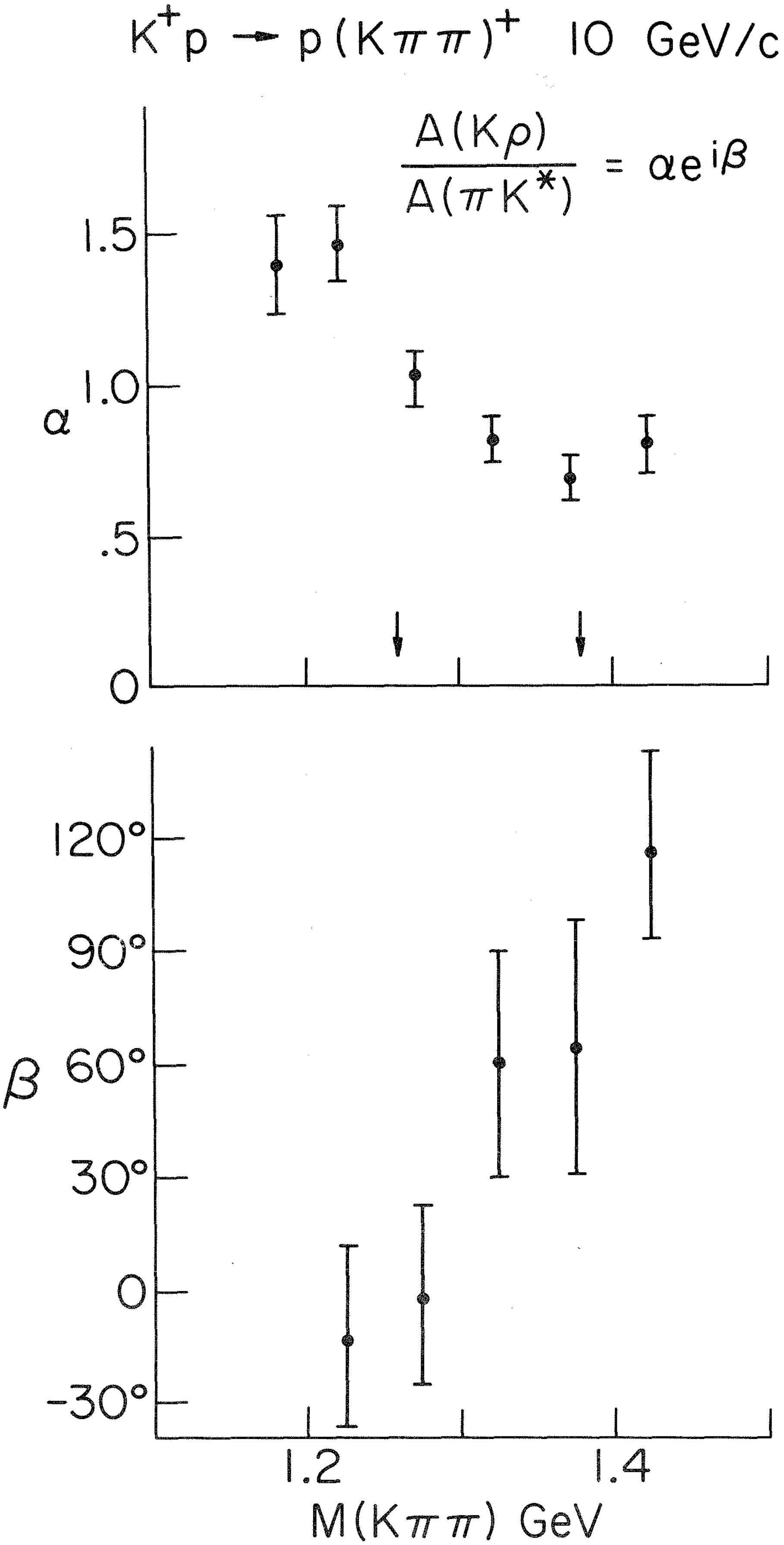

Figure 8. Variation of the relative magnitude and phase of K_ρ to $K^*\pi$ decay amplitudes for K^+p at 10 GeV/c.

DISCUSSION

Firestone (LRL): You remarked on a $p^{-0.4}$ fall-off in the A_1 cross section as a function of the incident momentum. Do you have similar information on the Q?

Kruse: We, ourselves, are not yet able to carry through a self-consistent analysis, as in the A_1 region, specifying spin-parity 1^+, and looking at a definite band in a consistent manner throughout the experiments. However, such a comparison has been done by the CERN group (Ref. 19). By choosing events carefully and so on, they find a fall-off of $p^{-0.6 \pm 0.15}$, unless my memory fails me.

At the moment, it is premature for us to do the same type of analysis for the A_3 and L.

Malamud (UCLA): How do you parameterize the mass dependence in your distribution?

Kruse: In what you saw here, we have simply divided the data into definite bins, in some cases 50 MeV wide, and in some cases 100 MeV wide where we did not have good statistics. We certainly didn't have mass dependences within that bin. In certain other studies, for instance in the A_2 study which we have published, we put in a definite Breit-Wigner dependence for the 2^+ amplitude to make certain tests.

Malamud: I meant two-body, not three-body.

Kruse: Of course, for the ρ and K^* we have also put in suitable Breit-Wigner amplitudes for the Dalitz plot densities. We recall that there is the product of a D-function with the Breit-Wigner amplitude for the particular resonance. For the ϵ, we used a mass of 760 with a width of 400 MeV as the parameters. All others, we take from the particle-data tables.

Lubatti (Washington): How do you determine the cross section for the A_1? What do you do about background?

Kruse: I will emphasize what the curve was. At each incident momentum, we do a spin parity analysis. We see 1^+ with the characteristic peaking around the A_1 region. We take a slice of the 1^+ piece from 1.0 to 1.2 GeV and call this the amount of "A_1". This is what is plotted as a function of the incident momentum.

Ferbel (Rochester): Do you have any estimate of the background included here?

Kruse: Our estimate on the A_1 is supposed to be background-free. We have just selected out the 1^+ contribution and called this the A_1.

Ferbel: What about the other partial waves, and what is their energy dependence?

Kruse: There are many other partial waves contributing besides the A_1 in this region. As shown in Fig. 2, the 0^- seems to be important. The energy dependence of the 0^- is relatively flat. The other waves behave in various ways with energy. For instance, the 2^+, which is the A_2 and will be discussed at length in Part 4, has somewhat steeper energy dependence than the 1^+ and 0^-.

Flatté (LRL): I would like to make a comment on the $\rho\pi$ band which you apparently see under the A_3. If you are going to produce $\rho\pi$ by diffraction, one expects the 1^+, 2^-, and 3^+ waves to come in. You see a very strong 1^+ in the A_1 region, then I would expect the next thing to see would be a 2^- $\rho\pi$ system at higher masses. So it seems very possible that you will see the 2^- wave rising and making a broad peak in the A_3 region. The establishment of a $\rho\pi$ decay for the A_3 is crucial for its resonance interpretation -- the standard $f^0\pi$ decay is confused by the Deck model enhancement. So it is important to see if the $\rho\pi$ mass distribution is just the broad kinematic effect discussed above, or rather a relatively narrow resonance like an A_3.

Kruse: Our data is very preliminary. At the moment the $\rho\pi$ 2^- mass distribution is similar to the overall 2^- mass distribution in our data. However, as we see from Fig. 6, both enhancements are rather broad. I really would like to dodge this question until we have looked at more data (cf. page 31).

Kim (Harvard): Do you also include the ϵ-π channel in the A_3 analysis?

Kruse: No, not as yet.

Kim: Also, how about the direct 3π decay mode?

Kruse: No again. What we have done in the A_3 region is to explore fits with the $f\pi$ and $\rho\pi$ decay modes and we have seen simply that these terms seem to account for most of what we need there. We have not done an exhaustive study as we have done for the A_1 region.

Kim: There must be background under $f^0\pi$ coming from the 3π mode.

Kruse: It is possible. As I said, in the A_1 region we have seen there is not much evidence of anything other than the $\rho\pi$. At present, we have not considered the possibilities you have mentioned for the A_3 region.

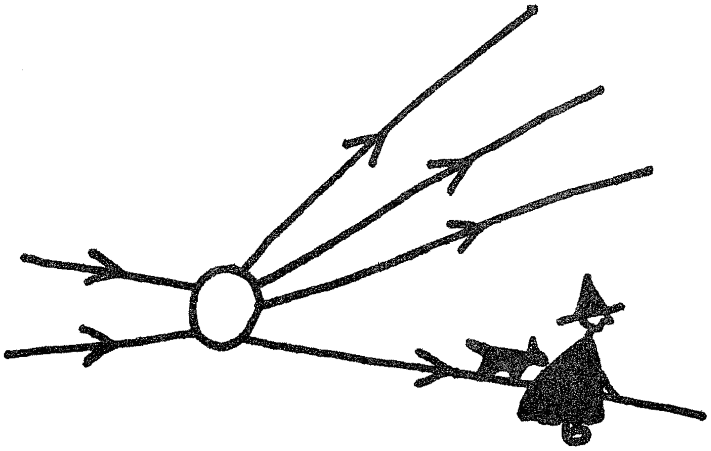

PHENOMENOLOGY OF MULTIPARTICLE REACTIONS

William R. Frazer

University of California at San Diego
La Jolla, California 92037

As I started to prepare this talk I realized that I didn't have a very clear understanding of that long, ugly word "phenomenology". My dictionary (American Heritage, 1969) didn't help much:

> phe-nom-e-nol-o-gy, n. 1. The study of all possible appearances in human experience, during which consideration of objective reality . . . is temporarily left out of account.

Certainly the study of all possible experiences is not what we mean by phenomenology. Nowhere in particle physics is this more evident than in the study of multiparticle reactions, where the large number of variables makes selectivity necessary.

One way in which physicists use the word phenomenology is to describe the stretching of elastic theories to cover as much data as possible; for example, the Regge pole theories of high-energy two-body reactions. No theory of multiparticle reactions is sufficiently well developed or sufficiently successful to inspire much of this sort of activity at this time, although some small areas have been successfully covered. The generalized Veneziano model B_5 fits, double Regge models, multiperipheral models, and the thermodynamical model are examples.

In general, however, phenomenology is at a much earlier stage in multiparticle reactions. It falls into two general categories:
(1) Suggestions for organization of data -- choice of variables, types of plots, etc., (for example, Van Hove's longitudinal phase space plots), and
(2) Attempts to abstract qualitative behavior from existing models, in hopes that the abstractions will prove to have greater validity than the models which inspire them (for example, scaling laws). I will concentrate on these two types of phenomenology, because I think they are the most appropriate guides we have at present for the selection among possible experiments. They impose the least bias and hopefully "maximize the possibility that the experimental data collected will remain useful despite continuing changes in theoretical fashions."[1]

I can start this talk at the beginning, avoiding assuming any previous knowledge of the field, because the beginning occurred so few years ago. I will start with two very general observations which are so influential in both phenomenology and the construction of models as to deserve priority of attention. They are

1) Smallness of transverse momenta: The number of particles produced falls off very rapidly with transverse momentum p_T (compatible with exponential or Gaussian). The average value, $\overline{p_T} \approx 0.4 - 0.5$ GeV/c, is approximately independent of the incident energy, and does not depend strongly on particle type or multiplicity of particles produced.

2) Low multiplicities: Recent cosmic ray measurements by the Michigan-Wisconsin group at Echo Lake find that the multiplicity of charged secondaries produced rises slowly compared to the total energy $W = s^{\frac{1}{2}}$ available in the center-of-mass system.[2] The data, shown in Fig. 1 are well fit by

$$\bar{n}_{ch} = A \ln Q + B \tag{1}$$

where $A = 1.41 \pm 0.20$, $B = 2.04 \pm 0.19$, and $Q = W - 2m_p$.

We shall return later to discussion of the importance of the logarithmic dependence of $\bar{n}$ on s as a way of distinguishing between various models. But at the moment the main point is that the available energy is not going primarily into particle creation (which would allow the multiplicity to rise as rapidly as $\bar{n} \propto \sqrt{s}$). This fact, together with the rule of smallness of transverse momenta, implies that most of the available energy goes into longitudinal momentum

$$\langle p_L \rangle \propto \frac{\sqrt{s}}{\ln s} \gg \langle p_T \rangle \tag{2}$$

Figure 2 sketches the elongation in p_L of a contour of constant cross section as s increases. Thus the longitudinal momenta are the only variables which are changing rapidly with energy, and great kinematical simplifications can be obtained by making use of this fact.

The simplifications obtained by focussing on the longitudinal momentum variables is shown in the longitudinal phase space (LPS) plots introduced by Van Hove.[3] To get some feeling for the nature of longitudinal phase space let us look first at the simplest case, a three-body final state. Since the three longitudinal momentum variables in the center-of-mass system, q_L^1, q_L^2, and q_L^3 are subject to the constraint that their sum is zero, a two-dimensional triangular plot is appropriate. The variables and kinematical boundaries are shown in Fig. 3. The experimental distribution for $\pi^+ p \to \pi^+ \pi^o p$ is shown in Fig. 4. Note the clustering of points near the boundary. The energy-conservation constraint would require all points to lie on the boundary if the transverse momenta were zero. Thus we see the rule of small transverse momenta appearing in this plot. Note also that practically all events lie in the left half plane, corresponding to the proton in the final state continuing in the same direction as the proton in the initial state. We lose very little information by looking only at the left half plane.

Continuing in the spirit of displaying only the dependence on longitudinal momenta, Van Hove reduces the two-dimensional plots of Fig. 3 and 4 to one dimension by projecting all events onto the boundary. In a similar manner four-body final states give rise to a two-dimensional LPS plot. The example of $\pi^- p \to 2\pi^- \pi^+ p$ at 11 and 16 GeV/c has been analyzed by Kittel, Ratti, and Van Hove[4]. For this reaction the only region of LPS plot with appreciable population is defined by $q_L^p < 0$, $q_L^f > 0$, where the superscripts p, +, f, and s refer to proton, π^+, and fast and slow π^-, respectively. The resulting distributions are shown in Fig. 5, where q_L^+ and q_L^s are used as independent variables.

Two facts emerge clearly from the elegant display in Fig. 5:

1) Only the regions favored by Pomeron exchange are heavily populated. Note the diagrams in Fig. 5 showing the Pomeron-exchange graphs and the regions in which they contribute.

2) In the heavily-populated regions the density of events does not vary significantly from 11 to 26 GeV/c, which confirms the assignment of these events to Pomeron exchange. The LPS plot has shown us in a very clear and detailed manner that single Pomeron exchange (diffraction dissociation) is the dominant mechanism in the reactions studied.

Since the complete display of dependence on all the longitudinal momenta is impractical for more than five particles in the final state, experimenters and theorists have turned to simpler distributions. The first to be investigated is the single-particle inclusive spectrum; that is,

$$p_a + p_b \to p + X \qquad (3)$$

where X stands for whatever else is produced, but not observed. (In case you have difficulty with the term "inclusive", just remember that it refers to experiments in which measurements of the other produced particles are excluded.) It is convenient to write the cross section in terms of a function $f(p_T, p_L, s)$ defined as follows:

$$E_p \frac{d^2\sigma}{dp_T{}^2\, dp_L} = f(p_T, p_L, s) \ . \qquad (4)$$

I hope that everyone will use this invariant form obtained by multiplying by the energy E_p . It multiplies out an uninteresting phase-space variation. As we shall see, the current situation in which some data is presented with the E_p factor and some without it makes comparisons difficult.

Organization of the data on single-particle spectra has been greatly facilitated by the scaling, or limiting distribution, hypothesis. This hypothesis has a long history, starting with the pioneering work of Amati, Fubini, and Stanghellini.[5] Wilson[6] recognized the generality of the scaling idea, and recent work has further underscored its generality and importance.[7-14]

In the center-of-mass system scaling takes the form proposed by Feynman,[7]

$$f(p_T, p_L, s) = f(p_T, x) \ , \text{ where } x = \frac{2p_L}{\sqrt{s}} \ , \qquad (5)$$

whereas in the lab or projectile frame it takes the form (easily shown to be equivalent) proposed by Benecke, Chou, Yang, and Yen,[8]

$$f(p_T, p_L, s) \rightarrow f(p_T, p_L) \quad \text{for} \quad p_L \ll \sqrt{s} \ . \qquad (6)$$

It is quite striking that scaling is implied by such diverse physical pictures as the diffractive and multiperipheral. If it is not verified everyone is on the wrong track!

The evidence I have been able to compile for this talk is shown in Figs. 6-11.[15-20] Figure 6 shows a compilation by VanderVelde.[15] The agreement with scaling is reasonably good, except for the 70 GeV/c data on aluminum at Serpukhov. Figures 7 and 8 show the data of Anthony et al.[16] (figure taken from Chen et al.).[17] The roughly flat curves at each value of x illustrate the lack of strong s-dependence, even at the low energies involved. Figures 9, 10, and 11 show some x-distributions for various reactions and energies.

It is possible to make some comparisons between the data of Ko and Lander[18] in Fig. 9, the data of the Notre Dame group[19] in Fig. 10, and the previously-reported work of the Wisconsin group at 25 GeV/c.[21] If all the distributions are fit by the form[22]

$$\frac{d\sigma}{dx} = c\, e^{-b|x|} , \qquad (7)$$

then one can infer the following values for the slope parameter b :

TABLE I

Reaction	P_{beam}	b, $x < 0$	b, $x > 0$
$K^+p \to \pi^- + X$	12 GeV/c	10.6 ± .7	7.0 ± 0.5
$\pi^+p \to \pi^- + X$	18.5 GeV/c	10.29 ± .07	7.62 ± 0.06
$\pi^-p \to \pi^- + X$	18.5 GeV/c	9.83 ± .08	6.10 ± 0.07
$\pi^-p \to \pi^- + X$	25 GeV/c	11.7 ± .7	6.6

The agreement is quite striking. Factorization leads us to expect this agreement for $x < 0$. In a fragmentation picture,

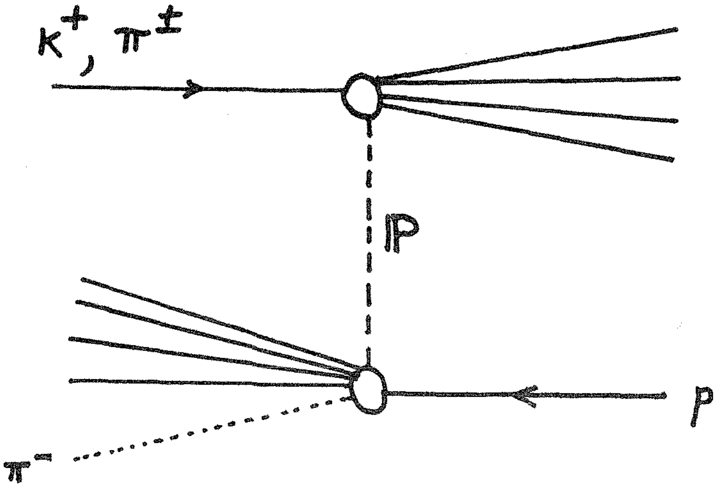

all four reactions are measuring the fragmentation $p \to \pi^- + X$, and should be independent, except for normalization, of the type of incident particle. The fact that there is also reasonable agreement among the b values for $x > 0$ is a statement about $K - \pi$ symmetry.

A factorization assumption (which can be understood most easily in terms of the Mueller diagrams I shall discuss later) allows comparison of magnitudes as well as slopes. This factorization assumption, together with scaling, predicts the equality at asymptotic energies of $\sigma_T^{-1}\ d\sigma/dp_L$ for small p_L in the lab system. Results from four different reactions at four different energies, all leading to $\pi^- + X$, have been compiled by Chen et al., a BNL, Rochester, Wisconsin collaboration.[23] Fig. 12, kindly supplied to me at this conference by Drs. L. L. Wang and T. Ferbel, shows the striking agreement among these reactions. The only one which differs strongly from the rest is $\pi^- p \to \pi^- + X$, the only reaction which is not "exotic" (more about this later).

To summarize the situation on scaling and factorization: the agreement is very encouraging, better than I would have expected at the energies surveyed. More data is rapidly becoming available, and we can expect considerable clarification in the next few months, with high-energy data eagerly awaited from NAL and the CERN-ISR.

What about the hypothesis often made by theorists that the distribution $f(p_T, x)$ factors in yet another sense, namely

$$f(p_T, x) \; = \; g(p_T)\cdot h(x)? \tag{8}$$

Figure 9, for example, shows that this is not strictly true. Perhaps it still has some utility for rough calculations.

The central region, $x \approx 0$, is very interesting. This is the region of multiperipheral events, often called the pionization region (I recommend dropping this term because it has come to mean different things to different authors). It is difficult to see this region in the x-plot, because so much is concentrated around $x = 0$. For this and other reasons it is advantageous to plot vs the rapidity variable y introduced by Wilson[6] and Feynman,[7] and discussed in detail by DeTar.[9]

To define the rapidity, consider the process

$$p_a + p_b \; \to \; p + X$$

where p_b is the beam four-momentum, p_a is the target four-momentum. Specialize to the lab frame, $p_a = 0$. Then the rapidity y is defined as

$$y = \sinh^{-1}\,(p_L/\mu) = \ell n\ \left(\frac{p_L + E_p}{\mu}\right) \tag{9}$$

where

$$\mu = (p_T{}^2 + m^2)^{\frac{1}{2}}$$

and m is the mass of the final state particle detected.

In terms of the rapidity y the four-momentum p in the laboratory system is given by

$$p = (\mu \cosh y \; , \; p_x \; , \; p_y \; , \; \mu \sinh y) \qquad (10)$$

where the z-direction has been chosen along the beam, so that

$$\vec{p_T} = (p_x, p_y) \qquad (11)$$

The rapidity y specifies the longitudinal Lorentz transformation that relates the lab frame to the frame in which particle p has zero longitudinal momentum.

The beam and target momenta are given by

$$\begin{aligned} p_b &= (m_b \cosh Y, 0, 0, m_b \sinh Y) \\ p_a &= (m_a, 0, 0, 0) \end{aligned} \qquad (12)$$

where $s = (p_a + p_b)^2$ is exponentially related to Y in the large s limit,

$$s \cong m_a m_b e^Y . \qquad (13)$$

All longitudinally moving frames are put on an equal footing by the use of the y variable, since such frames are all related by a simple shift of the scale. That is, a longitudinal Lorentz transformation characterized by $\gamma = \cosh u$ merely changes y to y', where $y' = y + u$, and $Y' = Y + u$.

In addition to this advantage of being essentially frame-independent, the y-variable has the advantage of expanding the central region so that it can be seen clearly. As DeTar has emphasized, a multiperipheral picture implies that the central region should be flat in y . Essentially y measures the distance from the end of the multiperipheral chain,

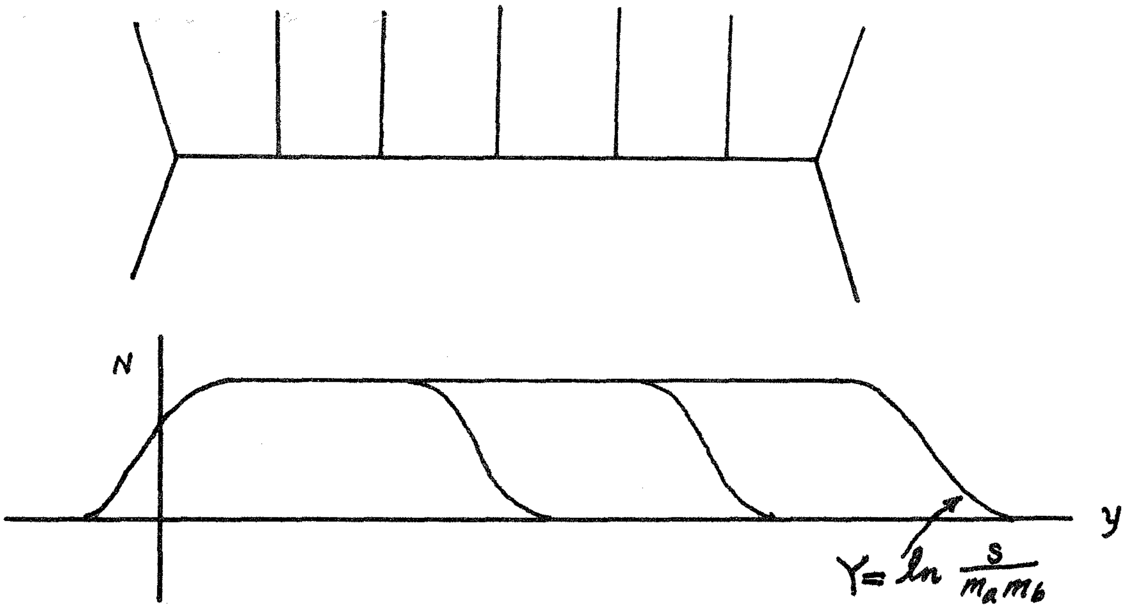

Now if it is farther from the ends than some correlation length L , then the amplitude should be independent of y . Distant parts of the multiperipheral chain are uncorrelated. Fig. 13, from the compilation of Chen et al, shows the situation at available energies.[23] The distribution is becoming more rounded with increasing energy, but it can hardly be called a plateau.

Higher energies are needed to test the plateau prediction than the limiting fragmentation or factorization predictions. The latter require the y-plot to be sufficiently long that the two ends are uncorrelated, or $Y > L$. The plateau requires that the central region is not correlated with either end, or $Y > 2L$. Since s is exponentially related to Y , this implies that the energy for the plateau goes like the square of the energy for the fragmentation limit.

DeTar has summarized the scaling and plateau predictions neatly in the following form:[9]

$$\frac{d^2\sigma}{dy\,dp_T^{\;2}} = f(p_T, y) = \begin{cases} A(p_T, y) & \text{for } y < L \\ f(p_T) & \text{for } L < y < Y - L \\ B(p_T, Y-y) & \text{for } y > Y - L \end{cases} \qquad (14)$$

Another way to test essentially the plateau prediction is to measure the average interval in y between two final-state particles. This has been done in the Echo Lake cosmic ray experiment at one of their lowest energies, 145 GeV/c. The variable they use is one long used by cosmic-ray physicists,

$\log_{10}\tan\theta$, which is not very different from y . Unfortunately, they cannot measure θ , but only its projection in a plane. The resulting intervals in this variable are shown in Fig. 14. Except for the end effect, the intervals are constant, as is expected from a multiperipheral model. Further studies of such two-particle correlations are eagerly awaited.

A plateau in y would give rise to logarithmically increasing multiplicities, since the contribution to the average multiplicity $\bar{n}$ from the plateau is given by

$$\bar{n} \approx \frac{1}{\sigma_T} \int^{Y} f(p_T)\, dy \sim cY = c \ln s + b \tag{15}$$

If we are actually seeing the beginning of a plateau at current accelerator energies, the central height should tell us the constant c in eq. (15). Bali et al., who first pointed this out, did indeed find consistency.[25]

The uncorrelated production of multiperipheral models predicts that the multiplicity distribution at a given energy should be some sort of Poisson distribution. The details depend on whether single particles are produced uncorrelated or pairs, or more complicated possibilities, but the distribution must be basically Poisson. Comparison of the Echo Lake data with various Poisson-type distributions is shown in Fig. 15, and is seen to be satisfactory.

Diffractive models predict that σ_n , the cross section for production of exactly n particles, remain constant with energy, whereas multiperipheral models predict a power-law decrease. The simple Chew-Pignotti model gives

$$\sigma_n \propto \frac{s^{2(\alpha_M(0)-1)} (g^2 \ln s)^n}{n!} \tag{16}$$

The data do not go to high enough energies to decide the issue, as can be seen in Fig. 16. This figure shows the n-charged-particle cross sections, which behave in the same way except for a different power in Eq. (16).

I conclude this talk with the most recent exciting development, Mueller's analysis.[10] Mueller has found a way to incorporate both diffractive and multiperipheral pictures in a new picture, which is already proving useful in suggesting further theoretical and phenomenological developments. First draw a diagram representing the inclusive cross sections we have been examining, $p_a + p_b \rightarrow p + X$:

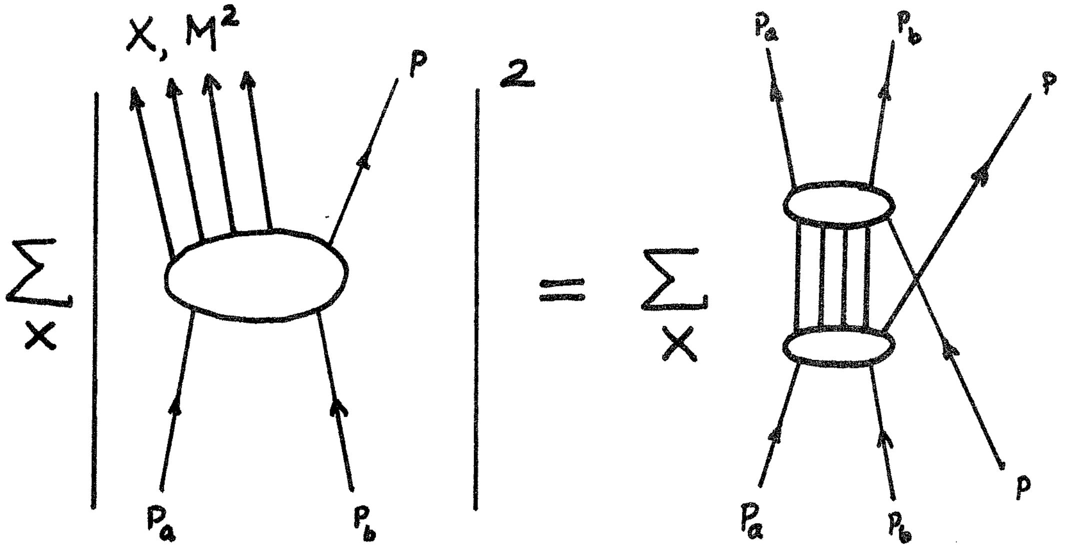
X, M²
p
2
Σ
X
=
Σ
X
Pa
Pb
Pa
Pb
p
Pa
Pb
p

Reversing the p-lines, Mueller writes this as the discontinuity of a three-body amplitude:

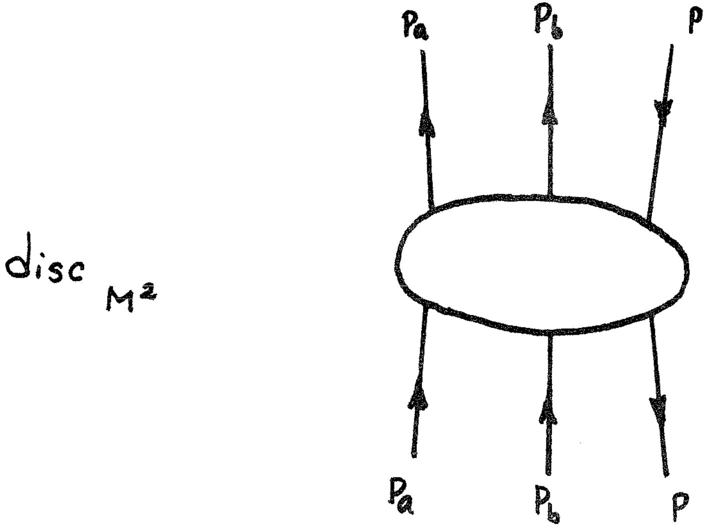
disc
M²
Pa
Pb
p
Pa
Pb
p

He expands the three-body amplitude in a Toller-type expansion, with three types of expansions appropriate to the two ends and center of the y plot. The dominant Pomeron-exchange terms can be represented diagramatically as follows:

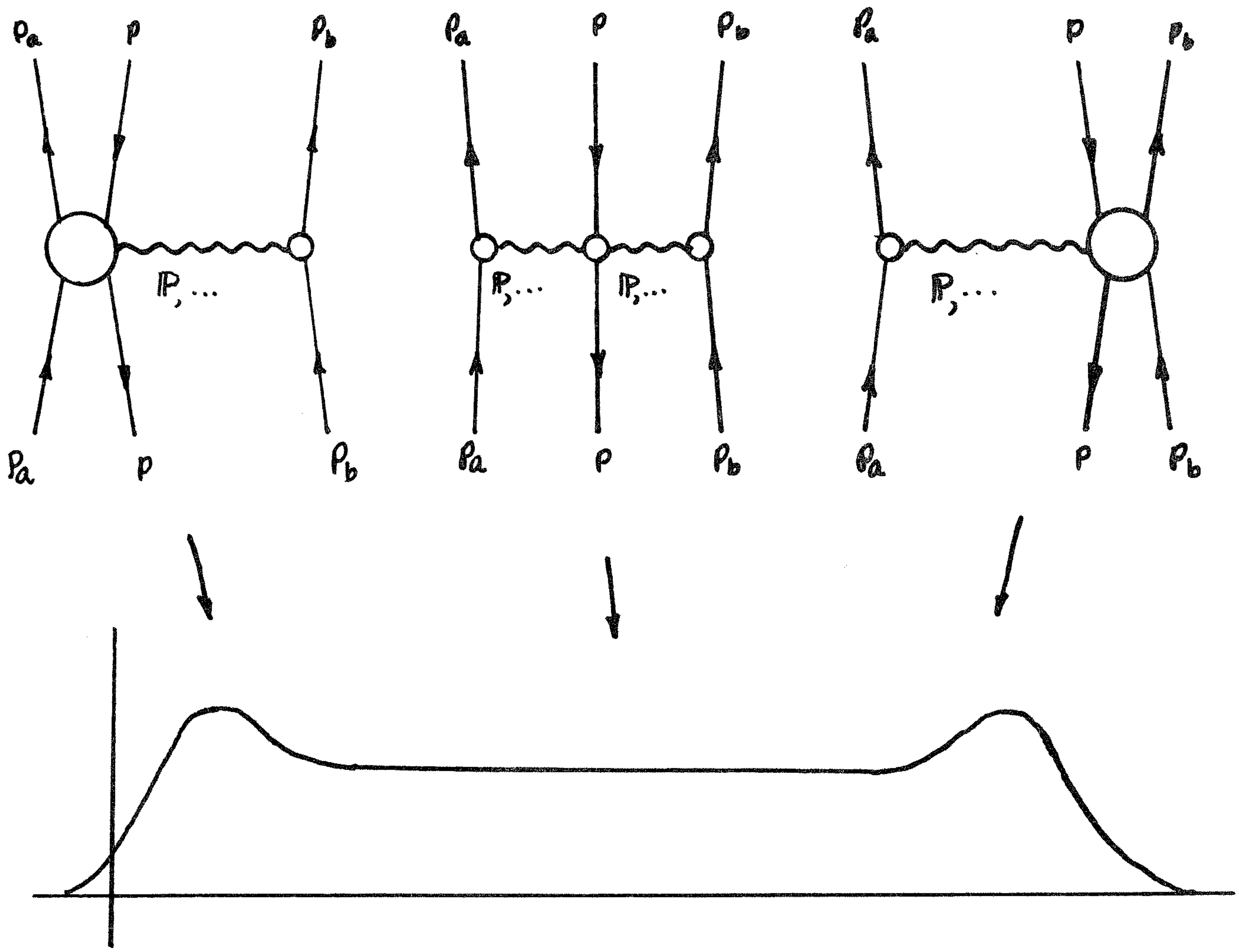

p_a
p
p_b
p_a
p
p_b
p_a
p
p_b
$\mathbb{P}, \ldots$
$\mathbb{P}, \ldots$
$\mathbb{P}, \ldots$
$\mathbb{P}, \ldots$
p_a
p
p_b
p_a
p
p_b
p_a
p
p_b

Theoretically, this is inspiring much activity. For example, the triple-Pomeron coupling has been identified as an object of great theoretical interest. It controls the strength of diffraction dissociation into high-mass states. Mueller diagrams are also leading to a complete Regge phenomenology of inclusive reactions, as pointed out by Chan, Hsue, Quigg, and J.-M. Wang.[26] They consider secondary trajectories, which tell about the rate of approach to limiting distributions. For example, in the target fragmentation region, diagrams of the types

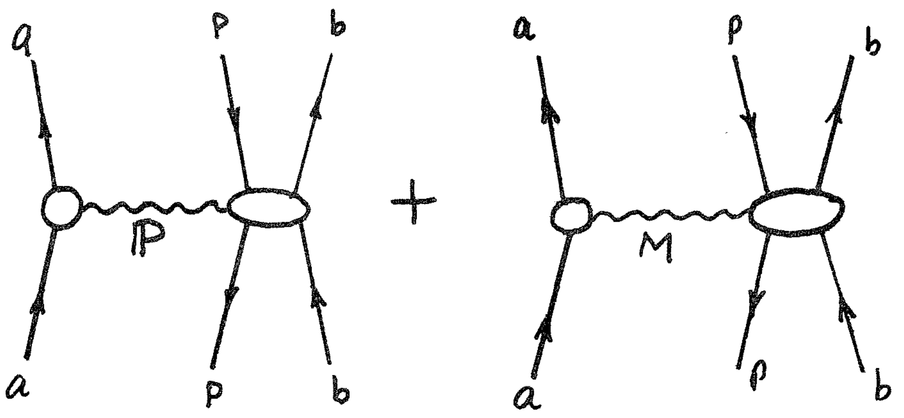

where M is some secondary trajectory, having intercept around $\alpha(0) \approx \frac{1}{2}$ give an amplitude of the form

$$f(p_T, p_L, s) \approx A(p_T, p_L) + B(p_T, p_L)\; s^{-\frac{1}{2}} \tag{17}$$

One can isolate secondary trajectories in the usual way. For example, the difference between π^+ and π^- on protons isolates the rho,

$$\begin{aligned} &\pi^+ + p \rightarrow c + X \\ &\pi^- + p \rightarrow c + X \\ &f^+(p_T, p_L, s) - f^-(p_T, p_L, s) = 2\, B_\rho(p_T, p_L)\; S^{\alpha_\rho(0) - 1} \end{aligned} \tag{18}$$

Another result is an extension of duality concepts to these reactions. For example, $K^+ + p \rightarrow \pi^\pm + X$ is related in Mueller's analysis to the three-body reaction $K^+ + p + \pi^\mp \rightarrow K^+ + p + \pi^\mp$. This reaction has exotic quantum numbers. Using the same reasoning as in two-body reactions, one can conclude that the contributions of the secondary meson trajectories vanishes, $B = 0$. Such reactions should then show limiting behavior at lower energies than non-exotic channels. Here are a few examples of exotic and non-exotic reactions.

Exotic	Non-exotic
$K^+ + p \to \pi^\pm + X$	$K^- + p \to \pi^\pm + X$
$\pi^+ + p \to \pi^- + X$	$\pi^\pm + p \to \pi^\pm + X$
$p + p \to \pi^\pm + X$	$p + p \to p + X$

Note that the three exotic reactions are just the ones which are clustering together in Fig. 12, whereas the non-exotic reaction is significantly different. The same behavior seems to be present in Table I. Perhaps my introductory remarks are already obsolete, and multiparticle phenomenology is becoming as well-developed as two-particle phenomenology at high energies.

FOOTNOTES

[1] Kenneth G. Wilson, Cornell University preliminary version of preprint.

[2] L. W. Jones, A. E. Bussian, G. D. DeMeester, B. W. Loo, D. E. Lyon, P. V. Ramana Murthy, R. F. Roth, J. G. Learned, F. E. Mills, D. D. Reeder, K. N. Erickson, and B. Cork, Phys. Rev. Letters 25, 1679 (1970).

[3] L. Van Hove, Nuclear Physics B9, 331 (1969).

[4] W. Kittel, S. Ratti, and L. Van Hove, paper submitted to Kiev Conference 1970.

[5] D. Amati, A. Stanghellini, and S. Fubini, Nuovo Cimento 25, 896 (1962).

[6] K. G. Wilson, Acta Physica Austriaca 17, 37 (1963).

[7] R. P. Feynman, Phys. Rev. Letters 23, 1415 (1969); in High Energy Collisions (Gordon and Breach, New York, 1969), p. 237.

[8] J. Benecke, T. T. Chou, C. N. Yang, and E. Yen, Phys. Rev. 188, 2159 (1969).

[9] C. E. DeTar, Phys. Rev. D3, 128 (1971).

[10] A. H. Mueller, Phys. Rev. D2, 2963 (1970).

[11] D. Silverman and C. -I. Tan, Phys. Rev. D3, 991 (1971).

[12] N. F. Bali, A. Pignotti, and D. Steele, Phys. Rev. D3, 1167 (1971).

[13] H. Cheng and T. T. Wu, Phys. Rev. Letters 23, 1311 (1969).

[14] S. Pinsky and W. Weisberger, private communication.

[15] J. C. Vander Velde, Physics Letters 32B, 501 (1970).

[16] R. W. Anthony, C. T. Coffin, E. S. Meanley, J. E. Rice, K. M. Terwilliger, and N. R. Stanton, Phys. Rev. Letters 26, 38 (1971).

[17] M. -S. Chen, L. -L. Wang, and T. F. Wong, Phys. Rev. Letters 26, 280 (1971).

[18] W. Ko and R. L. Lander, University of California, Davis, preprint.

[19] N. N. Biswas, N. M. Cason, V. P. Kenney, J. A. Poirer, J. T. Powers, C. A. Rey, O. R. Sander, W. D. Shephard, and D. W. Thomas, University of Notre Dame preprint.

[20] Aachen-Berlin-CERN-Imperial College-Vienna/Brussels-CERN collaboration. CERN-DPH2-Phys-70-52. V. Henri (private communication).

[21] J. W. Elbert, A. R. Erwin, and W. D. Walker, to be published.

[22] The factor E_p in Eq. (4) has not been included in all these data. This amounts to neglect of $4\mu^2/s$ compared to x, which leads to significant errors for small x. Now that more interest is being shown in scaling predictions, it is hoped that future data will be presented in a form more amenable to comparison.

[23] M. S. Chen, R. R. Kinsey, T. W. Morris, R. S. Panvini, L. L. Wang, T. F. Wong, S. L. Stone, T. Ferbel, P. Slattery, B. Werner, J. W. Elbert, and A. R. Erwin, private communication.

[24] D. E. Lyon, A. E. Bussian, G. D. DeMeester, L. W. Jones, B. W. Loo, P. V. Ramana Murthy, R. F. Roth, F. E. Mills, J. G. Learned, D. D. Reeder, K. N. Erickson, B. Cork, and C. Risk, Phys. Rev. Letters 26, 728 (1971).

[25] N. F. Bali, S. Brown, R. D. Peccei, and A. Pignotti, Phys. Rev. Letters 25, 557 (1970).

[26] Chan H. -M., C. S. Hsue, C. Quigg, and J.-M. Wang, Phys. Rev. Letters 26, 672 (1971).

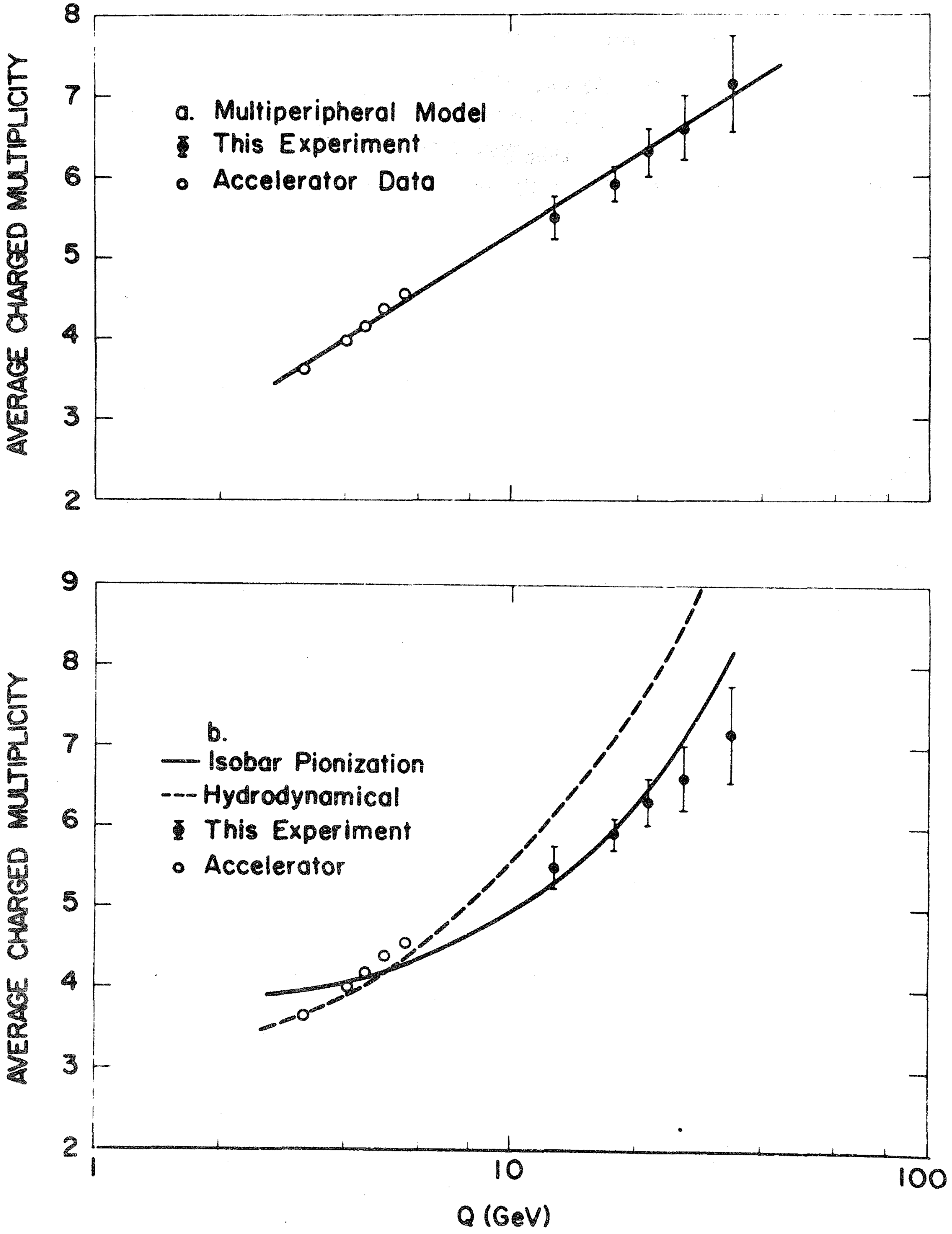

Fig. 1. Average multiplicity of charged secondaries as a function of center-of-mass energy in the Echo Lake cosmic ray experiment.[2]

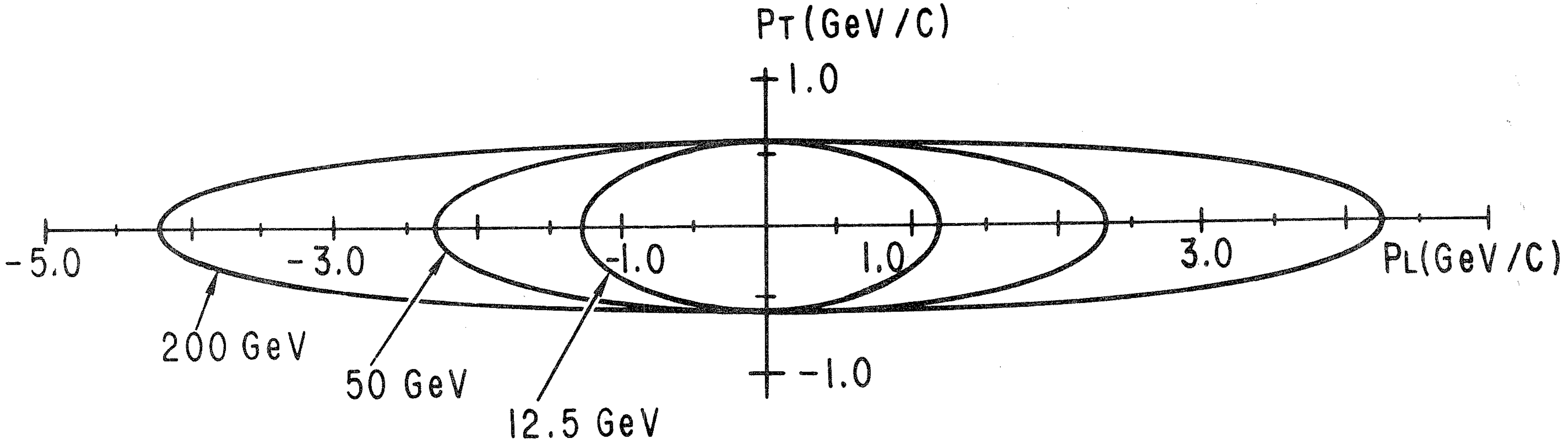

Fig. 2. Contours of constant cross section as a function of longitudinal and transverse momentum of secondary particle, for various beam momenta. The contour at 12.5 GeV/c is taken from Akerlof et al., Phys. Rev. D3, 645 (1971).

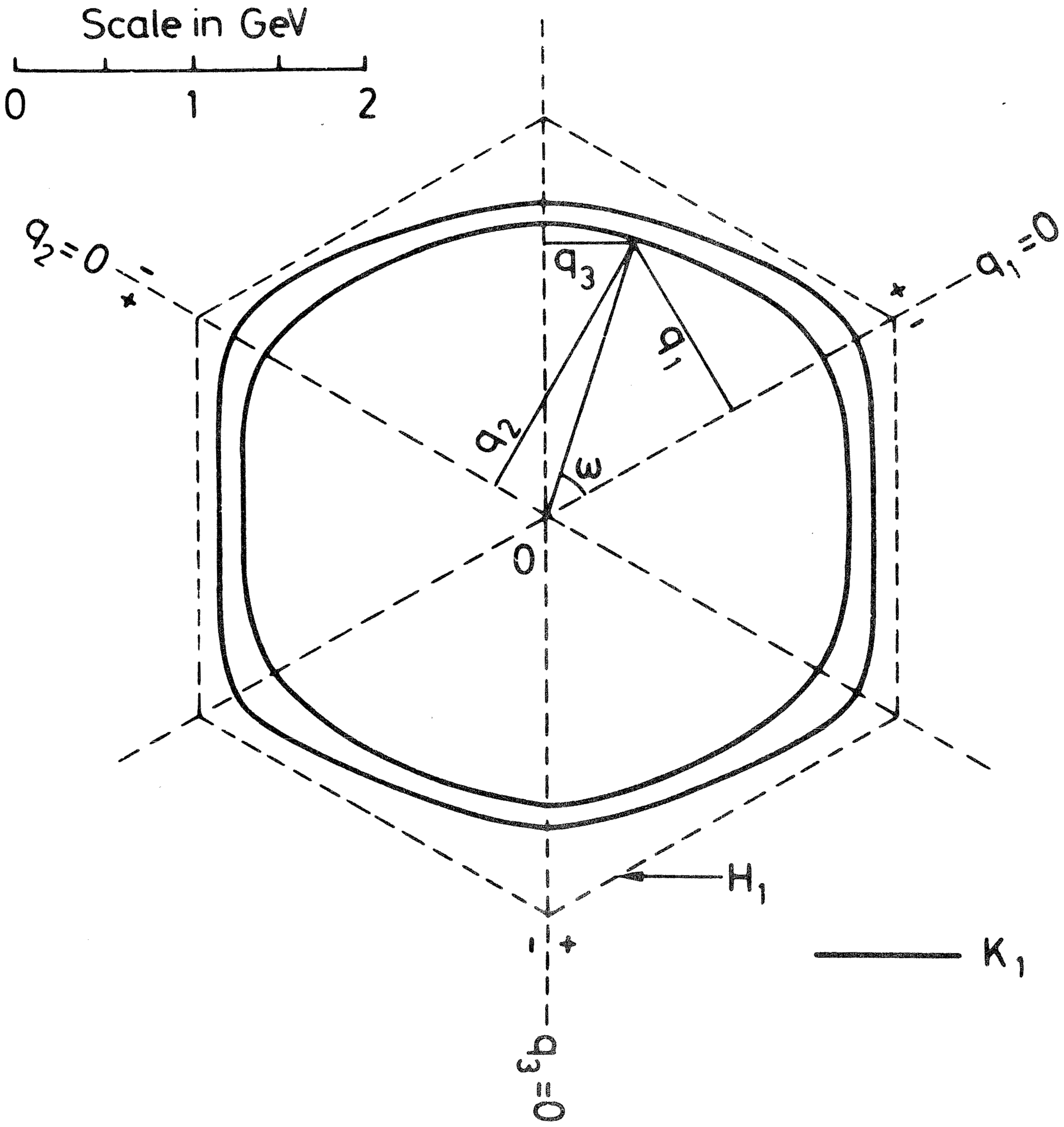
Scale in GeV
0
1
2
$q_2=0$
$q_1=0$
q_3
q_1
q_2
ω
0
H_1
K_1
$q_3=0$

ig. 3. Longitudinal phase space plot for ππN at c.m. energy W = 4 GeV. The inner full curve is for small typical transverse momenta, whereas the outer full curve is for zero transverse momenta. The dashed curve is the infinite-energy boundary.

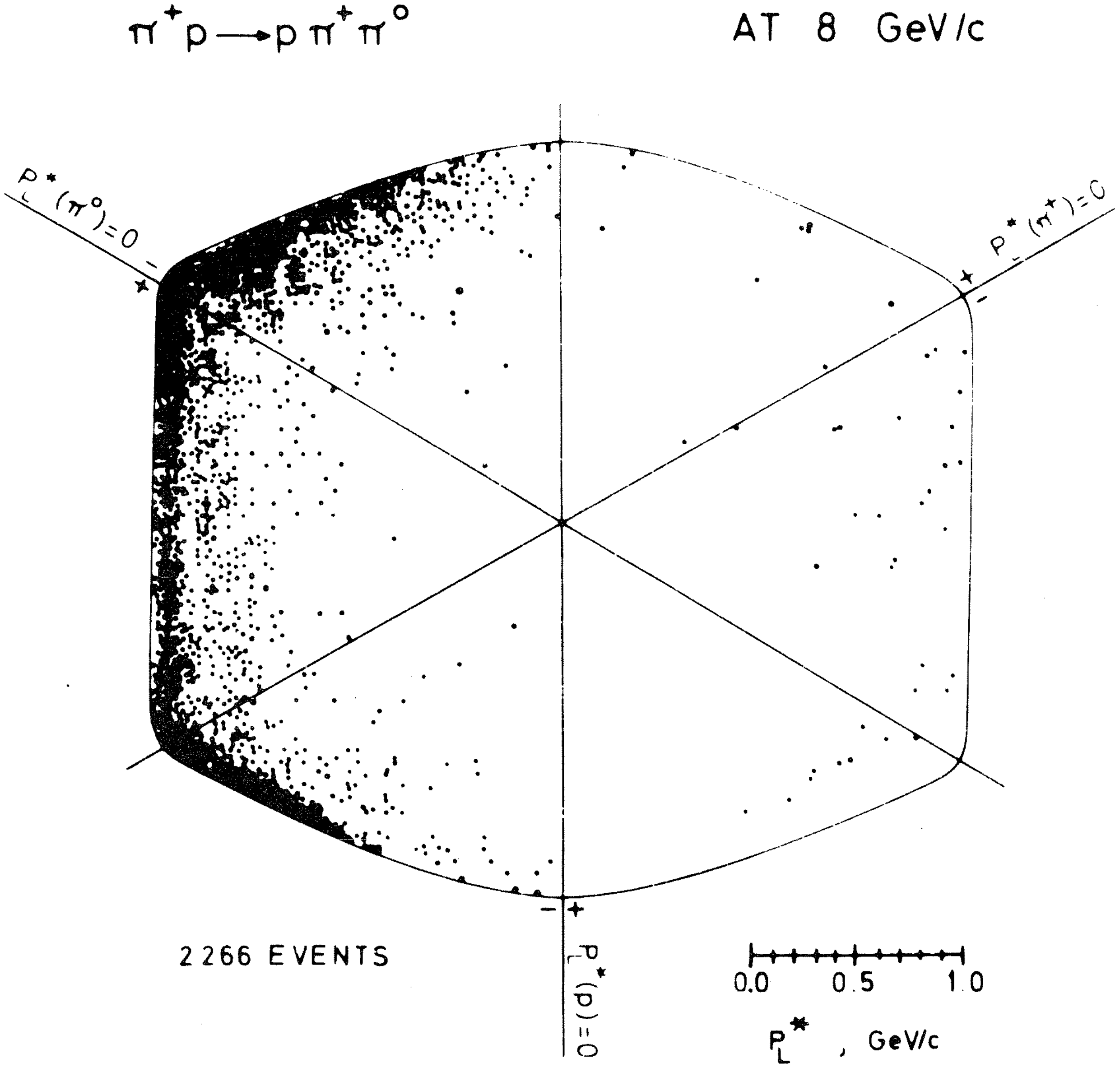

Fig.4. Experimental LPS plot for $\pi^+p \to \pi^+\pi^0p$ at 8 GeV/c, taken from Ref. 3.

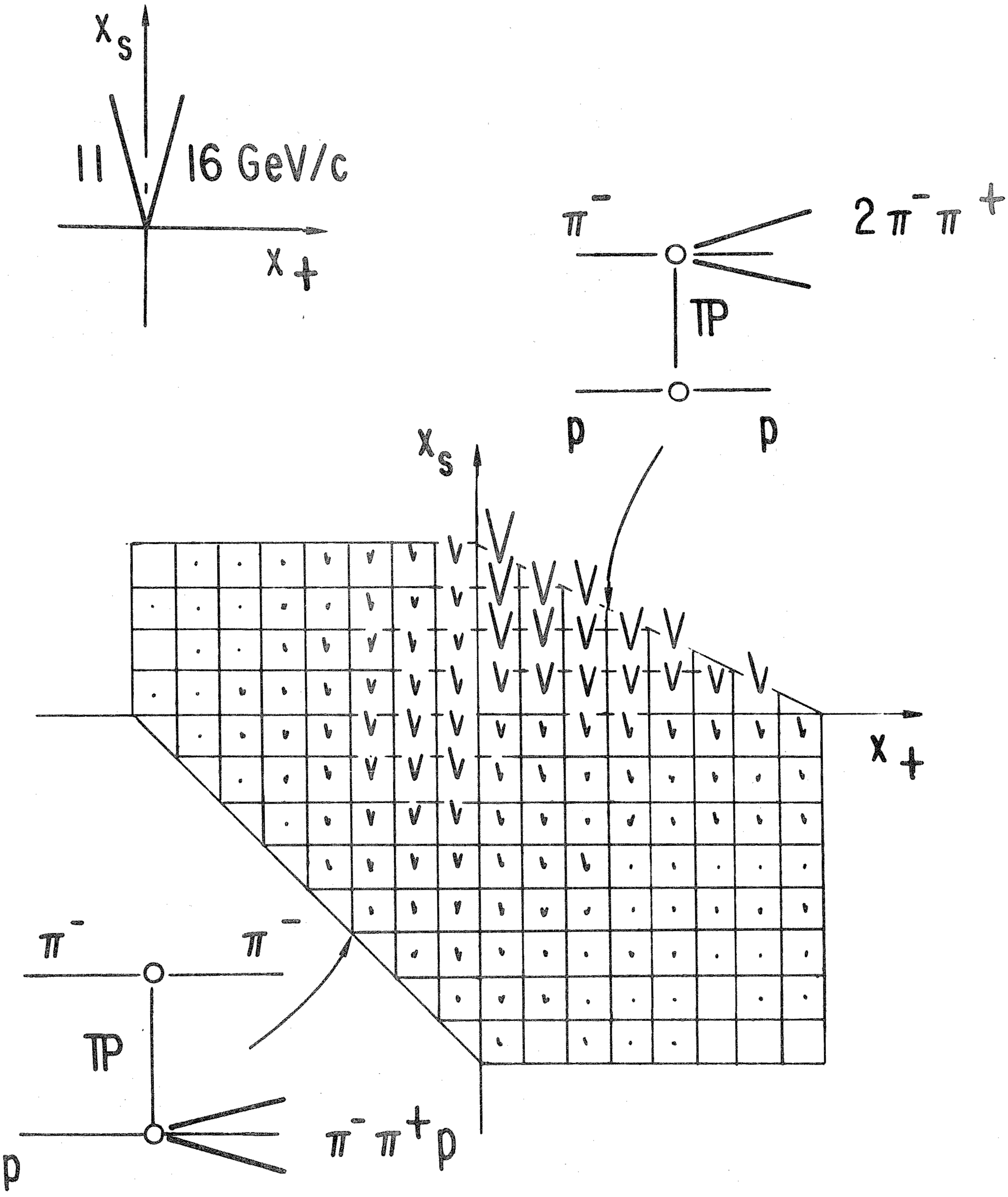

Fig.5. LPS distributions for $\pi^- p \to 2\pi^-\pi^+ p$ at 11 and 16 GeV/c. The oblique segments drawn upward from the bin centers measure the number of events in each bin at 11 GeV/c (left-hand segment) and 16 GeV/c (right-hand segment). The graphs show the possible Pomeron exchange processes.

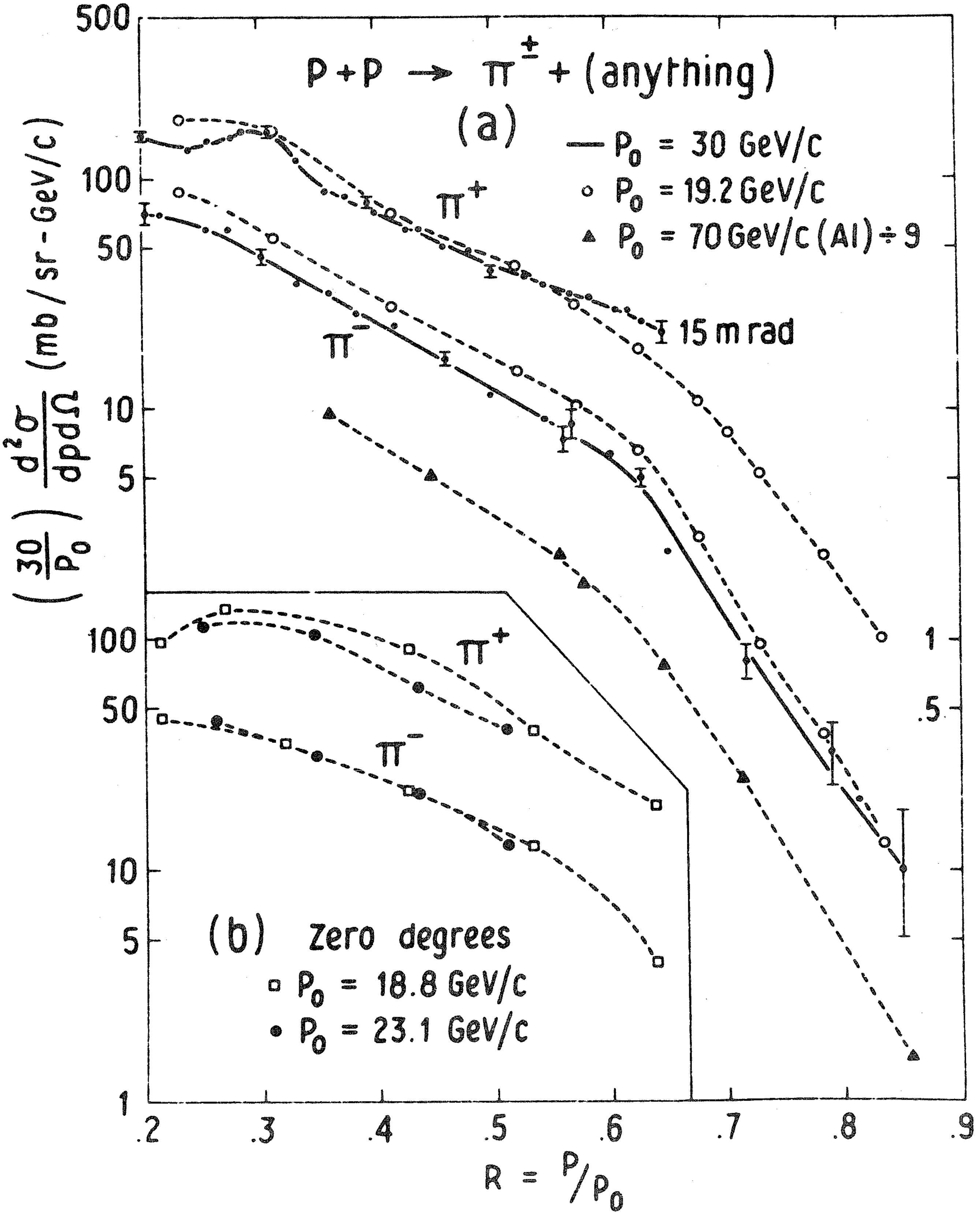

Fig.6. $\pi^{\pm}$ production compared at various energies, as a function of the scaling variable x (taken from Ref. 15).

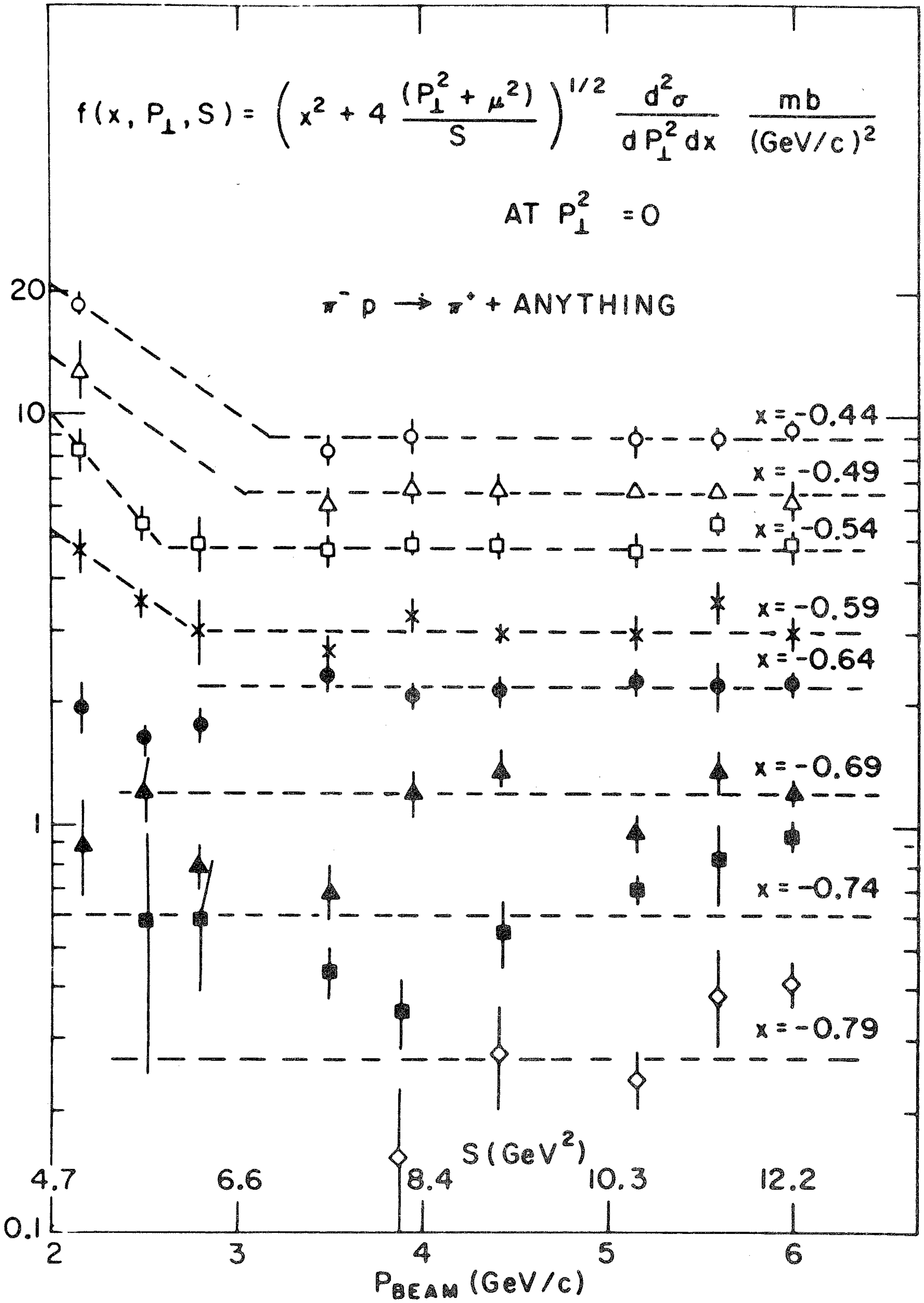

Fig.7. π^+ distribution as a function of incident energy at various x (from Ref. 16 and 17).

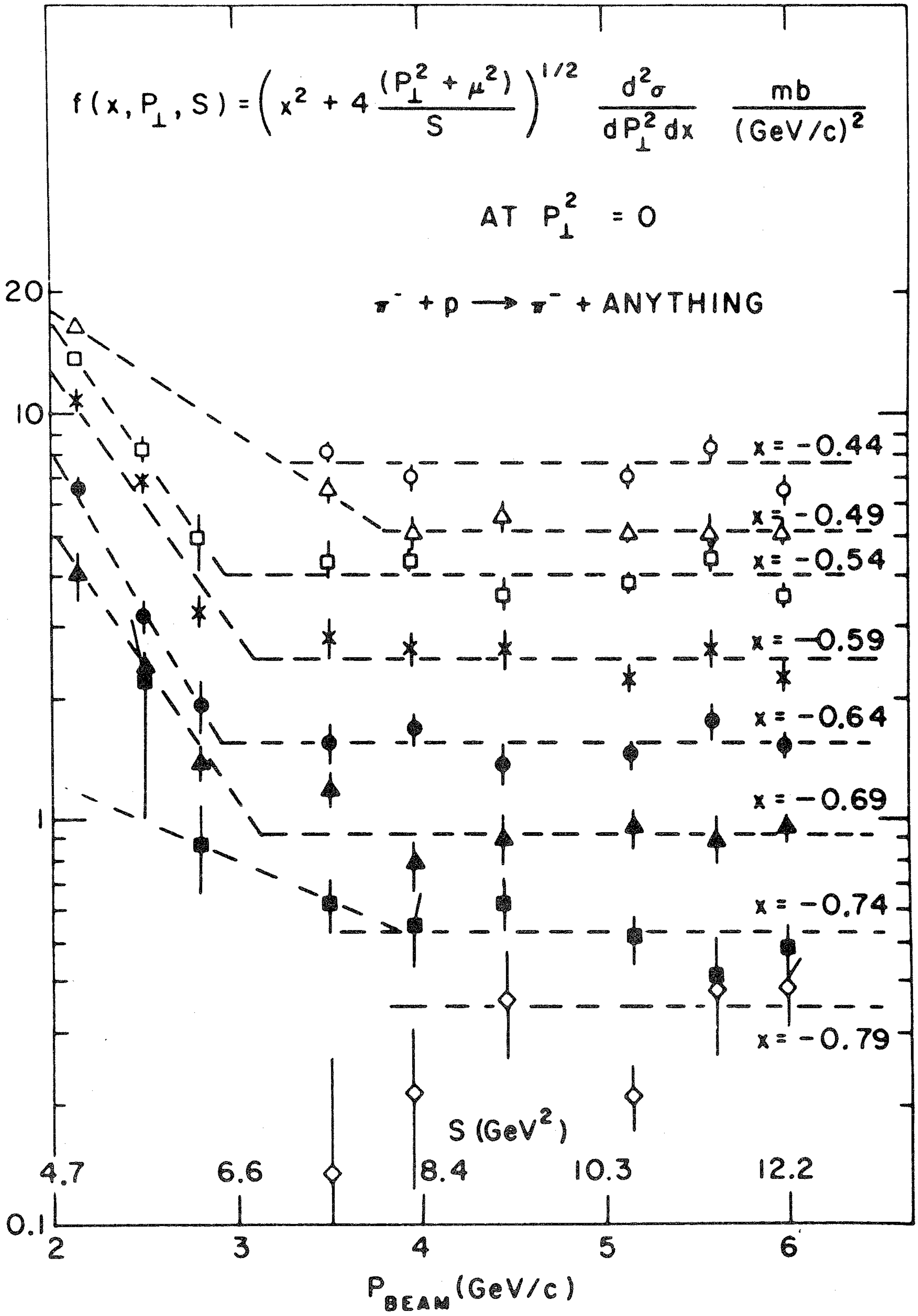

Fig.8. π^- distribution as a function of incident energy at various x (from Ref. 16 and 17).

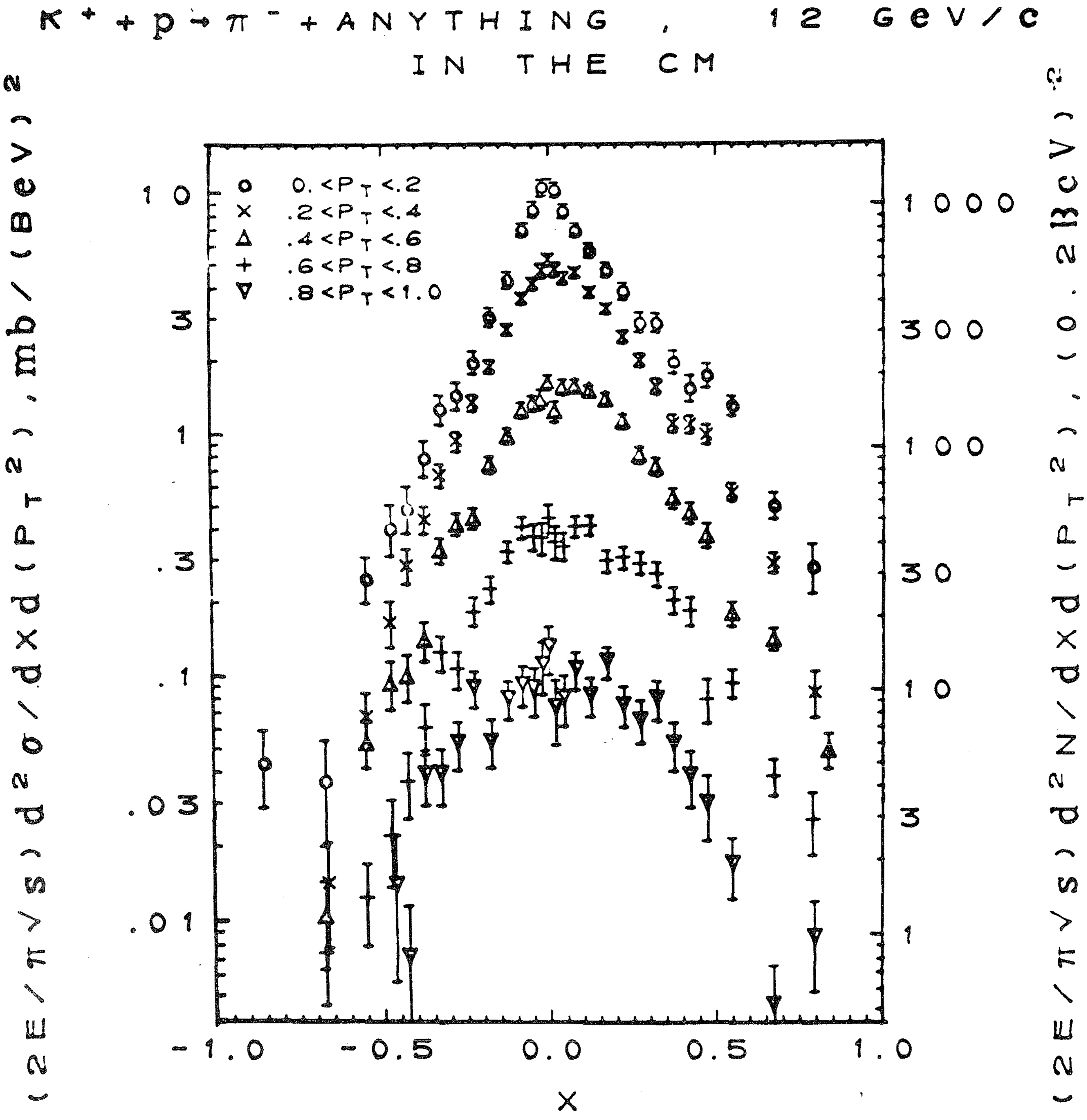

Fig.9. x-distribution for various p_T in $K^+p \rightarrow \pi^- +$ anything at 11.8 GeV/c, Ref. 18.

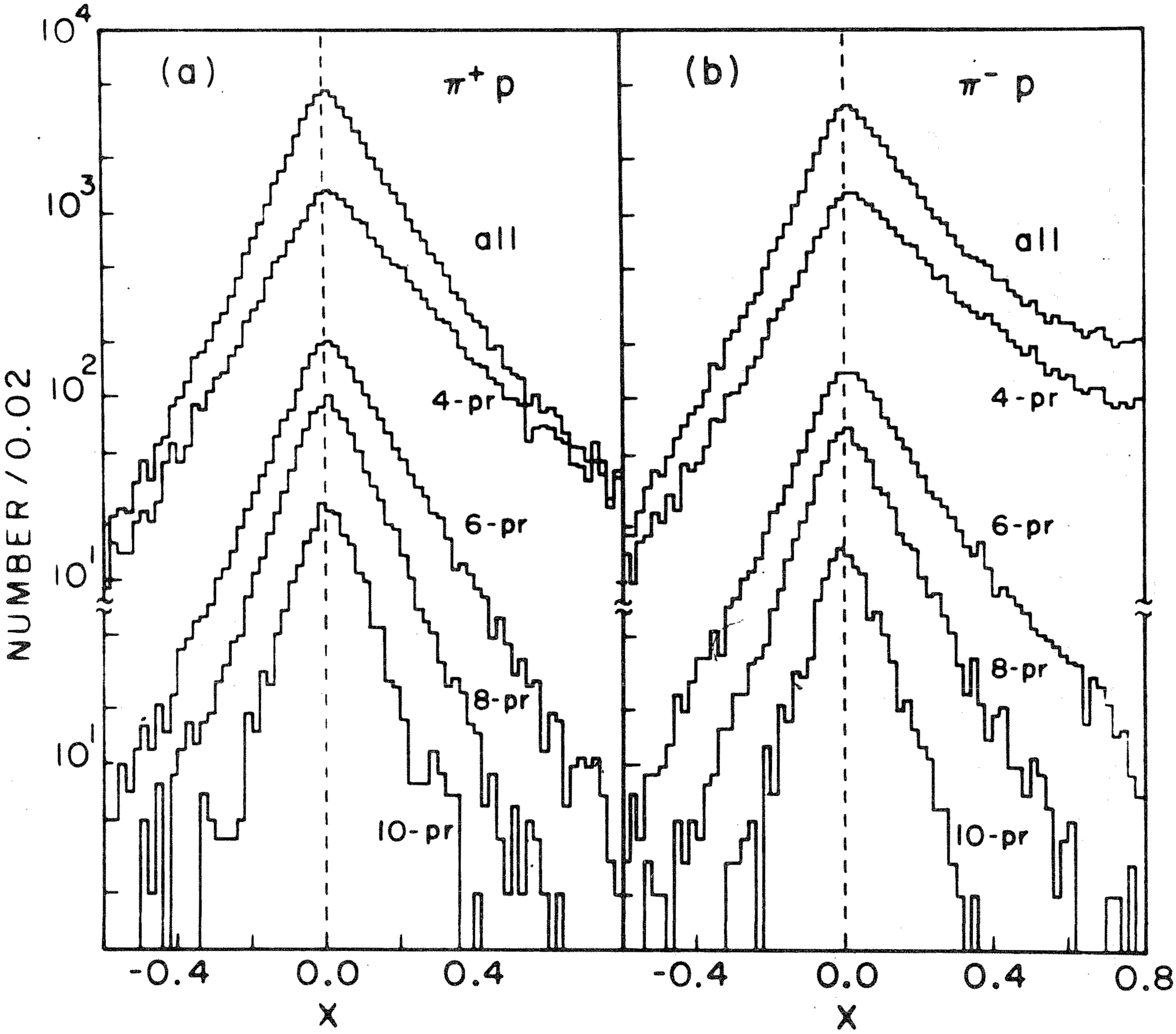

ig. 10. x-distribution for various charged multiplicities in $\pi^{\pm}p \rightarrow \pi^- + X$, at 18.5 GeV/c, Ref. 19.

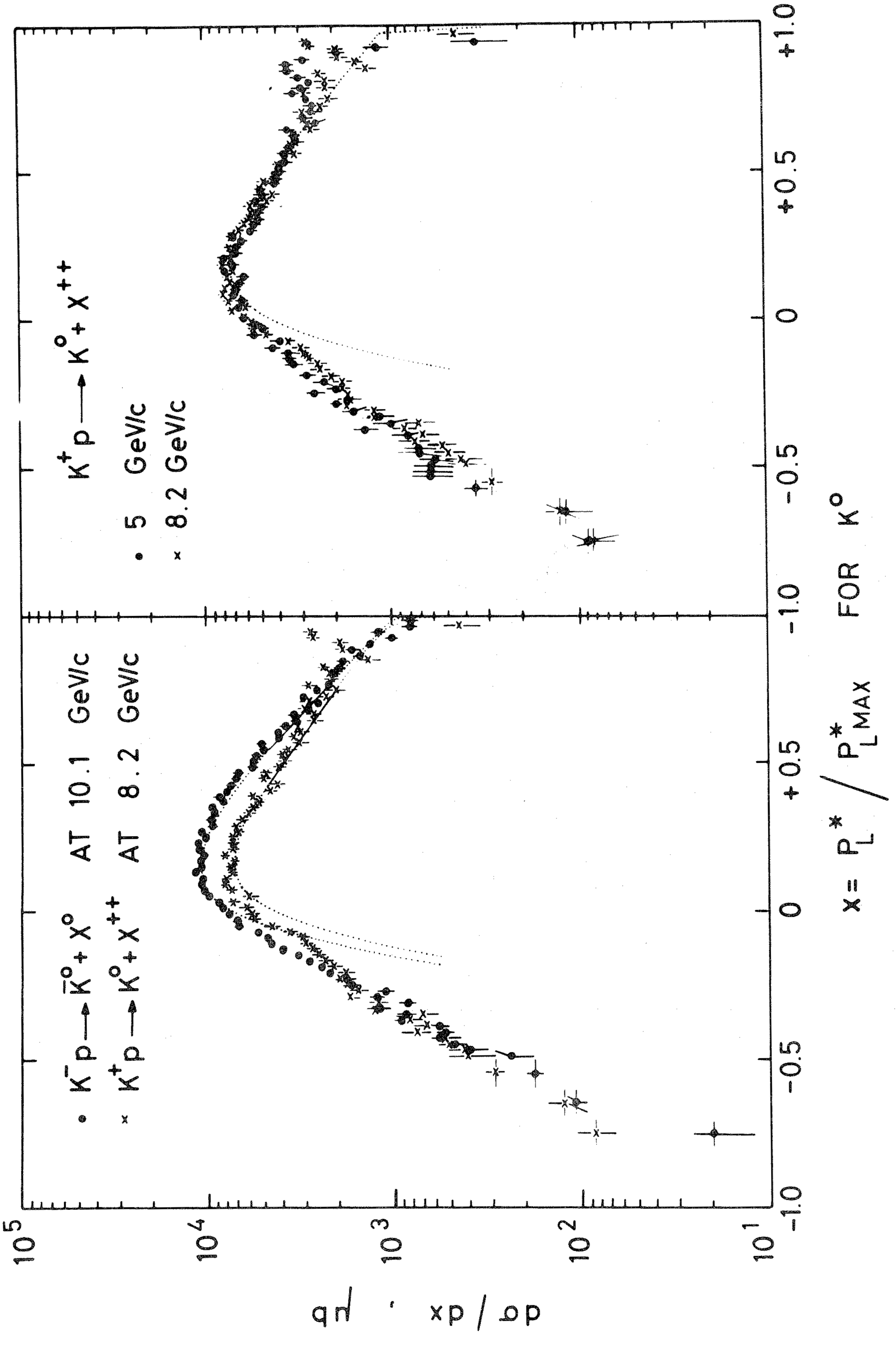

Fig. 11. x-distributions in K^o and $\bar{K}^o$ production, Ref. 20.

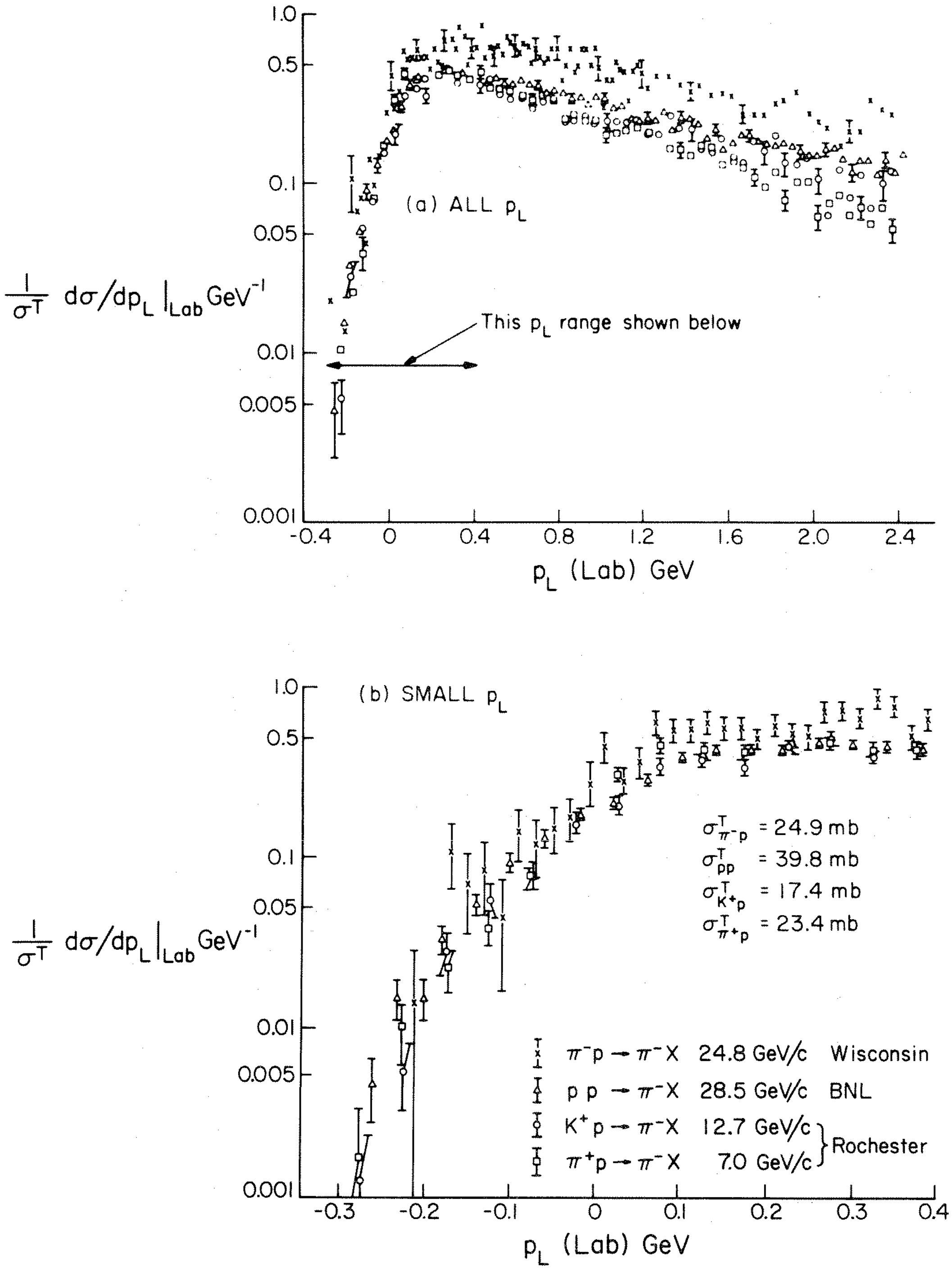

Fig. 12. Comparison of $d\sigma/dp_L$ in the lab system for various reactions, Ref. 23.

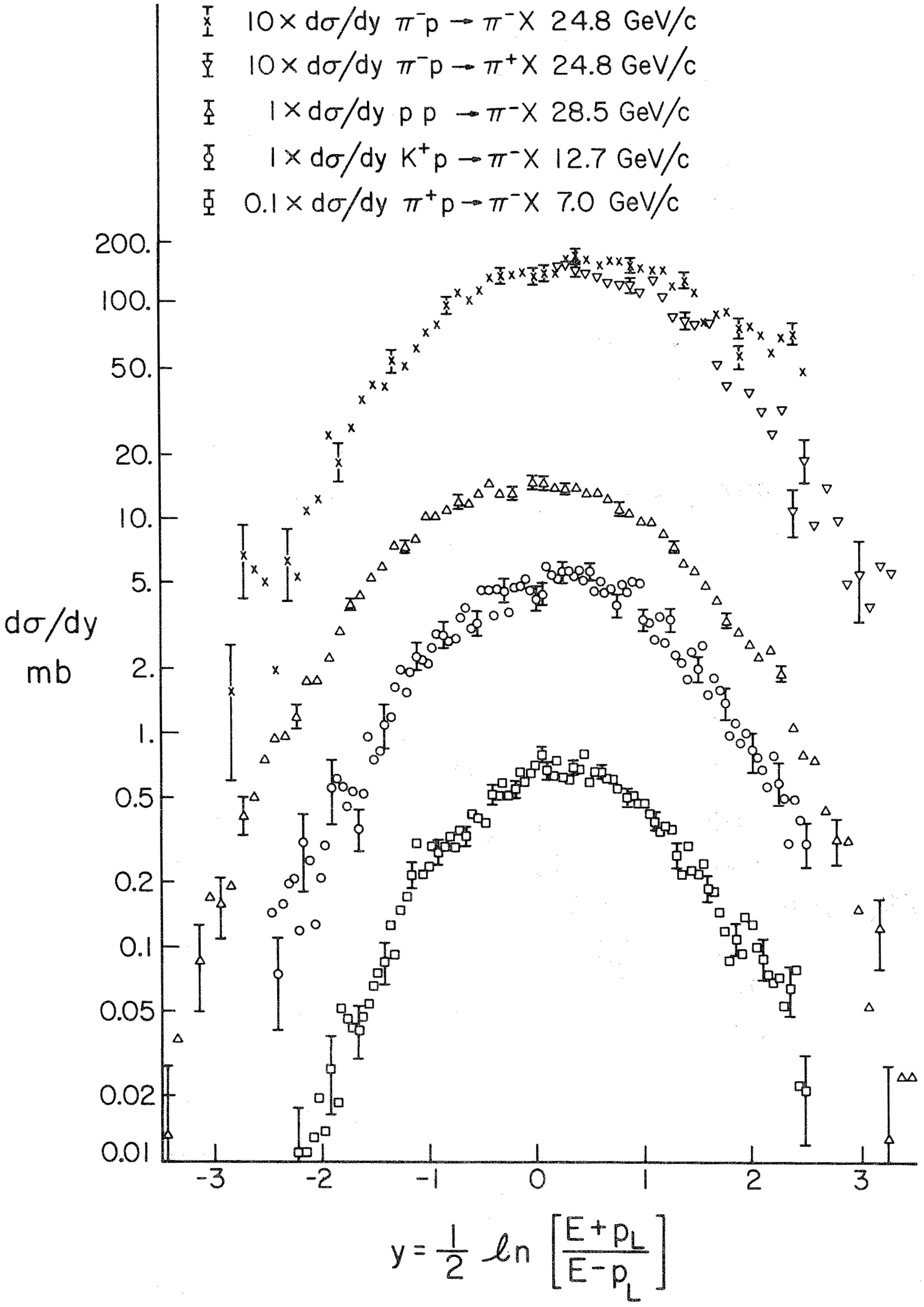

Fig. 13. Rapidity plots in several reactions, Ref. 23.

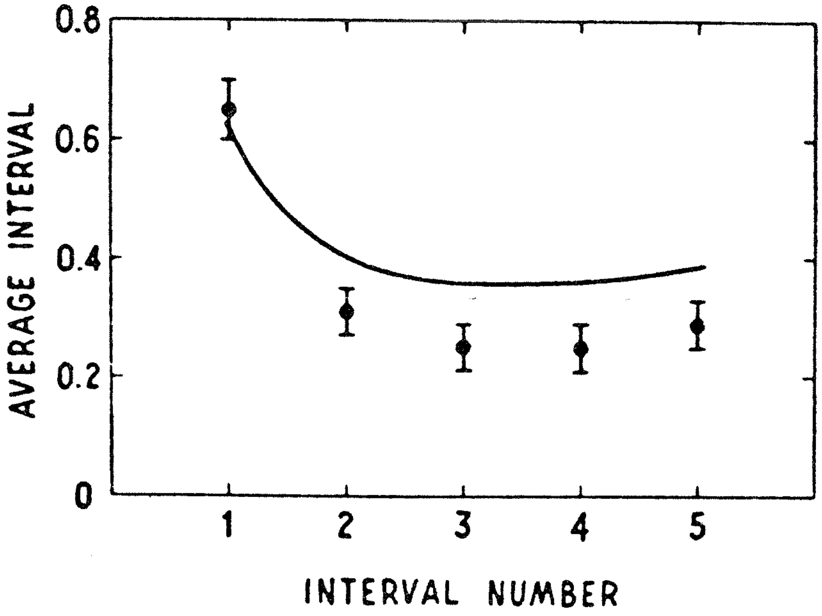

Fig. 14. Interval in log tan θ_p for six-prong events at 145 GeV/c, from Ref. 24. Solid curve is a multiperipheral model calculation.

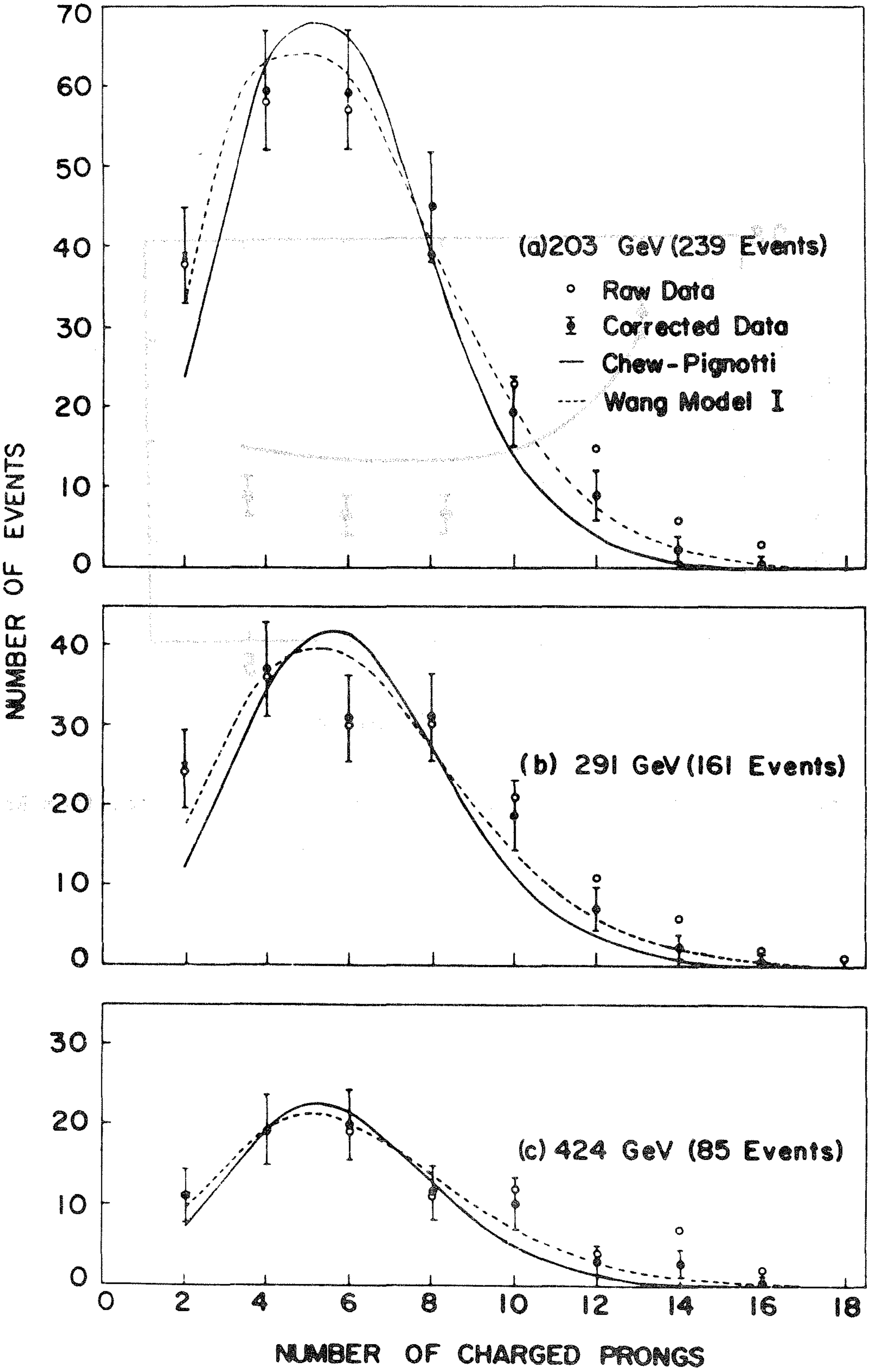

Fig.15. Multiplicity distributions in Echo Lake cosmic ray data, Ref. 2.

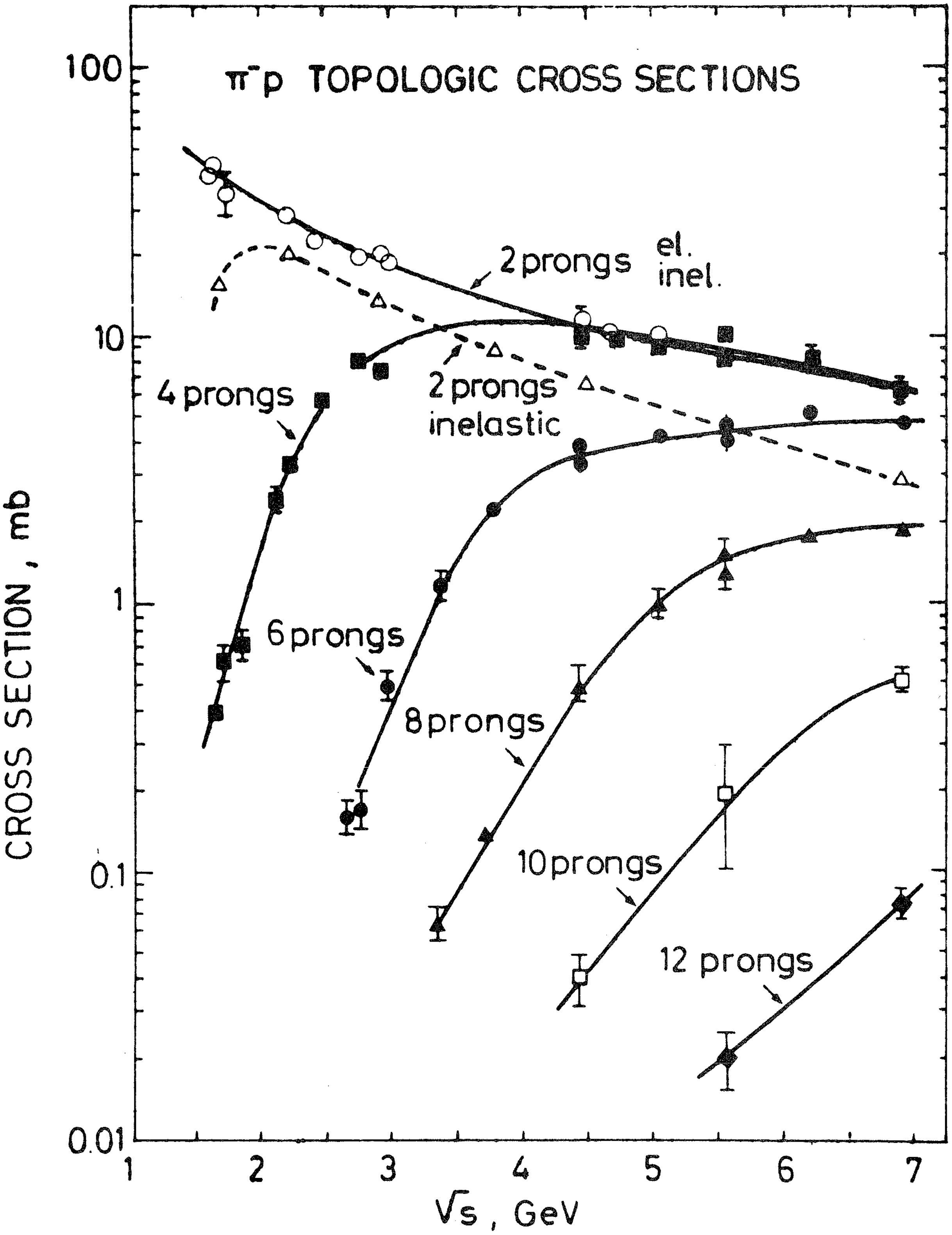

Fig. 16. Cross section versus c.m. energy for different numbers of charged particles produced (from W. D. Walker, in High Energy Collisions (Gordon and Breach, New York, 1969)).

DISCUSSION

Unidentified Voice: You noted some difference in π and proton induced reactions -- this suggests some dependence on the γ of the incident particle. Could you comment please.

Frazer: You are right. Recall that the length of the y (defined in Eq. (9)) plot is $Y \cong \ln(s/m_a m_b) \approx \ln(2\gamma_a)$ where a is the incident and b the target particle. As we discussed on page 56 it is conjectured that the high energy limit is reached when the particles are seperated by some distance (L or 2L, see again page 56) in the y plot -- if you have enough space in y, the particles are uncorrelated. Correspondingly, γ is important and at a given beam energy, this is higher for a π than a proton. It follows one is more likely to see any plateau in the y plot at lower energies for π's than protons. However, this is only a conjecture -- one could equally well say that the particles are uncorrelated if their relative s value is high enough -- this, of course, gives no particle dependence.

Gasiorowicz (Minnesota): It is commonly accepted, in the multiperipheral model, that multiple Pomeron exchange is very strongly suppressed. If you flip one of the lines in the Mueller diagram that is supposed to dominate the plateau region (see diagram 1 below), you get a double Pomeron exchange graph (see diagram 2 below). Is this a conflict?

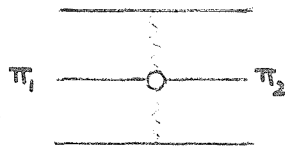

Diagram 1

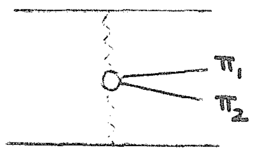

Diagram 2

Frazer: Yes, this is a question which I have been asking myself for some time. I didn't mention it because my student and I are trying to get the answer now. I don't want everybody to beat us to it. For example, consider one incoming pion (π_1) and one outgoing pion (π_2). You can flip one around and have two outgoing pions (π_1, π_2). If the second diagram exists, it would effect the logarithmic behavior on the multiplicity and this is very important. Again it, of course, requires that double Pomeron exchange producing a pair of pions should be found, whereas Lipes, Zweig, and Robertson (LZR) looked for it and did not find it (Phys. Rev. Letters 22, 433 (1969)). I don't know the answer, because there is an analytic continuation involved. Perhaps the continuation variable has an exponential fall off. Without having done the calculation, I would say if anybody wants to look at the double Pomeron exchange, they should look for it near the $\pi\pi$ threshold whereas LZR looked at higher $\pi\pi$ masses.

Yodh (Maryland): There is some question as to the interpretation of the $\ln s$ dependence on multiplicity. Thus in Figure 1, if you fit the points at low energy (where we think we've identified scaling), the $\ln s$ fit gets bad at high energy. Again, if you fit the high energy values, your χ^2 on the low energy points is poor.

Frazer: I agree.

Henri (CERN): Could you comment on the asymmetry for x > and < 0 shown, for instance, in our data of Figure 11.

Frazer: Yes, I would like to mention this asymmetry thing. The Wisconsin group (Elbert, Erwin, and Walker, preprint) found you could reduce the asymmetry to zero, by a suitable choice of reference frame. This turned out to be the quark-quark center of mass frame -- which naturally aroused some interest! Unfortunately you find the frame depends on the number of particles produced. Indeed, for eight final particles, the symmetry frame is more or less the usual center of mass. Such a behavior is easily understood within the multiperipheral model. For low multiplicity final states, "end effects" (e.g., resonance production) are important and lead to the observed asymmetry. For high multiplicities, the end effects are clearly less important and the particles are distributed symmetrically. This effect is not a very convincing argument for quarks.

Shephard (Notre Dame): Continuing on the same point, the reference frame in which the x distribution becomes symmetric has been determined by the Notre Dame group (Ref. 19) as a function of the number of outgoing charged particles (n) in the event. For each n, we characterize the frame in which there is no asymmetry by $R = |p(\text{target})/p(\text{incoming})|$. We find that R starts around 2-1/2 and decreases with increasing multiplicity; it seems to approach 1 (the c.m.s.) for large multiplicity. Thus it is difficult to interpret the values of $\langle R\rangle \approx 3/2$ obtained for averages over many multiplicities as evidence for the validity of a simple quark model of the interactions.

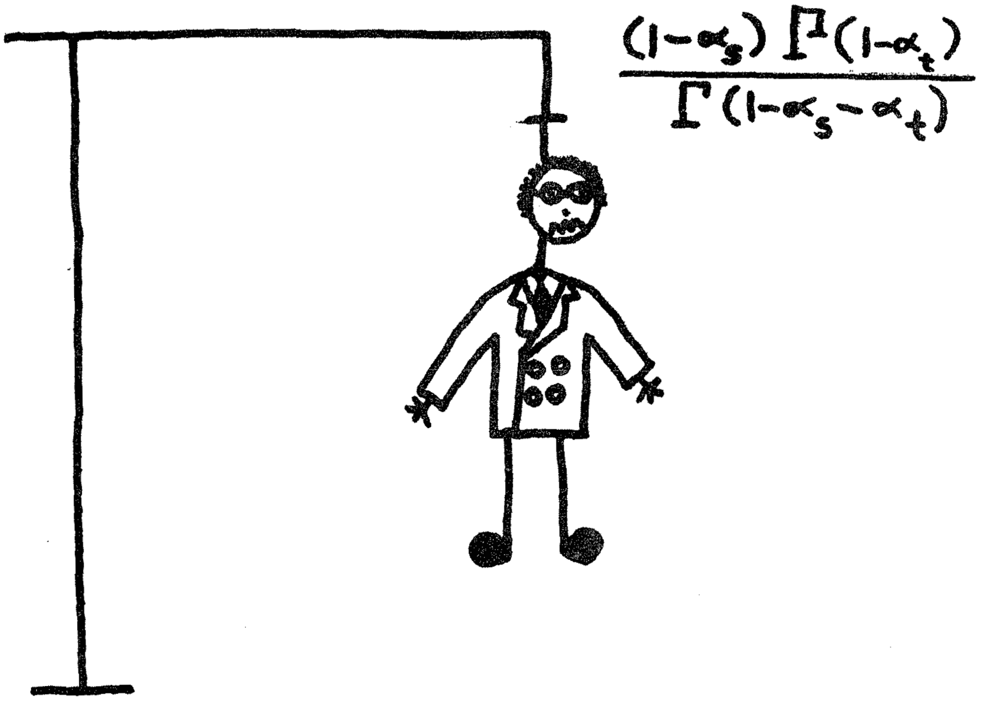
$\frac{(1-\alpha_s)\,\Gamma(1-\alpha_t)}{\Gamma(1-\alpha_s-\alpha_t)}$

PHENOMENOLOGICAL APPLICATIONS OF DUAL MODELS*

Edmond L. Berger

High Energy Physics Division,
Argonne National Laboratory
Argonne, Illinois 60439

---

*This work was performed under the auspices of the United States Atomic Energy Commission.

TABLE OF CONTENTS

1. Introduction. 87

2. Aspects of Four-Point Phenomenology. 90

2.1 Spectrum of Resonance States. 91

2.1.1 π-π Scattering. 91
2.1.1a The ϵ . 93
2.1.1b The ϵ' . 93
2.1.1c The ρ' . 93

2.1.2 Properties of the ρ' . 94

2.1.3 Experimental Search for the ρ' . 96
2.1.3a $\gamma p \rightarrow \pi\pi p$. 96
2.1.3b ρ' in $\pi\omega$ from $\bar{p}p \rightarrow \pi\pi\omega$. 101
2.1.3c ρ' in $\pi\omega$ from $\pi p \rightarrow \pi\omega p$. 102
2.1.3d ρ' in $\gamma p \rightarrow \pi\omega p$. 103

2.1.4 Search for ρ' in $\pi p \rightarrow \pi\pi N$. 104
2.1.4a Enhancement in Mass Plots. 105
2.1.4b Interference Effect in Angular Distributions 108

2.1.5 Conclusions. 110

2.2 Dynamical Zeroes, Dips in Differential Cross-Sections, and Relationships Among Coupling Constants. 111

2.2.1 Dynamical Veneziano Zeroes. 111

2.2.2 Evidence in Differential Cross-Sections. 113

2.2.3 The Goebel Construction. 115

2.2.4 Unitarity. 118

2.2.5 Coupling Constants and Residues. 120

2.3 Nucleon-Nucleon Annihilation into Mesons. 123

3. B_5 Phenomenology. 128

3.1 Work by the Chan Group. 129

3.1.1 Approximations and Choice of Functions. 129
3.1.2 Unitarity. 131
3.1.3 Fits to Data. 132
3.1.4 Conclusions from the Fits. 135

3.2 Relative Normalization. 136

3.2.1 K^* Subsamples. 136
3.2.2 Data from $K^o p$ and $\overline{K}^o p$ Reactions. 139

3.3 Line-Reversal Symmetry Breaking and Interference Effects Among Resonances in a Dalitz Plot. 141

3.3.1 $Kp \rightarrow K^* p$; A Specific Example. 141
3.3.2 The Sign of the Symmetry Breaking. 148
3.3.3 Other Predictions. 151
3.3.4 Experiments. 154

3.4 Allowed and Forbidden Quark-Duality Diagrams for the $\overline{K}N\Lambda\pi\pi$ System. 156

3.4.1 Quark-Duality Diagrams and Rosner-Harari Rules for B_5. 157
3.4.2 $\overline{K}N\Lambda\pi\pi$; The Approach of Törnqvist and Collaborators. 159
3.4.3 Criticism of the Anti-Rosner-Harari Conclusion. 160
3.4.4 A Virtue of the Rosner-Harari Alternative. 162

3.5 What Should be Done Next With B_5 ? 164

4. Dual Models for Diffraction Dissociation. 167

4.1 Brief History of A_1. 167

6

4.2 Opportunities with Dual Models. 168

4.3 A Counterexample. 169

4.4 Further Investigation. 172

4.4.1 Spin. 172
4.4.2 Pomeron. 173
4.4.3 Unitarity. 174
4.4.4 Helicity Conservation. 174

5. Miscellanea. 176

5.1 Inclusive Reactions. 176

5.1.1 Data. 176
5.1.2 Dual Models. 177
5.1.3 Questions. 178

5.2 Narrow Resonances with Large Mass and High-Spin. 181

6. Summary. 183
Acknowledgments. 184
References. 185
Figures. 194

1. Introduction.

The creation of Veneziano models has had more impact in high-energy physics than any other single development during the past three years. Based upon his experience with finite-energy-sum-rules, Veneziano (1968) proposed a simple, concise scattering amplitude for the reaction $\pi\pi \to \pi\omega$. His function is endowed with several desirable properties, including analyticity, crossing symmetry, duality, Regge-behavior at high energies, and explicit resonance structure at low energy. Generalizations of his amplitude now encompass most processes accessible to laboratory investigation. This explosion of activity has developed in two directions, which I term theoretical and practical (or phenomenological). In this article, I am concerned exclusively with practical uses of Veneziano models in the analysis of hadronic data. However, as an example of theoretical activity, let me mention continuing efforts to achieve a manifestly unitary framework in which to imbed the (non-unitary) Veneziano amplitude.

I sense that this is an opportune time for a critical appraisal of practical uses of Veneziano amplitudes. The initial surge of enthusiasm and activity has waned. After a series of important papers in which approximate solutions were proposed to overcome difficulties with spin and unitarity, the past year has witnessed few breakthroughs. In most of the recent papers, rather obvious modifications are made for slightly different experimental situations.

Concurrent with diminished activity, there has been growth of sentiment that dual models have outlived their usefulness. Further, it is said that rather little physical insight has resulted from the unusually large number of phenomenological papers. I cite this extreme view because I subscribe to it, to some degree. Upon greater reflection, however, I think the fault lies with the tendency of researchers to employ the model as if it were literally correct. This view characterizes almost all quantitative applications of the Veneziano model to 2 → 2 and 2 → 3 body processes. Indeed, theoretical amplitudes are expressed as specific linear combinations of Veneziano functions. Certain parameters are then varied in an attempt to achieve detailed fits to data (resonance widths, differential cross-sections, invariant-mass-spectra, and so forth). An example of this approach is the paper on πN and KN scattering which I wrote with Fox (E. Berger and G. Fox, 1969). Good fits can be achieved, but their physical significance is obscure.

Further progress in the practical application of dual models requires that the literal interpretation be deemphasized. This is one of the important conclusions to emerge from the present paper. As a substitute, I suggest identifying qualitative aspects of the model that may serve as useful guides to understanding. In spite of the fact that the model is not suitable for quantitative fits, we may inquire, nevertheless, whether important features of the model survive in Nature. Relevant questions in this qualitative approach include the following.

(a) What are the essential dynamical predictions of the model which may be confronted with data?

(b) Inasmuch as dual models provide an explicit analytic connection between high and low energies in 2 → 2 processes, between all regions of a Dalitz plot in 2 → 3 processes, and between all regions of phase-space in a 2 → n process, can we extract from the models practically useful information that helps us develop a broader perspective?

(c) Are relevant new ways suggested for looking at old data and for resolving longstanding ambiguities of interpretation?

(d) What new experimental investigations are suggested and why?

(e) Although not in themselves suitable as quantitative models, do dual models spawn theoretical investigations which lead to greater understanding?

These are questions I have in mind as I try to appraise applications made so far to analysis of hadronic data. In the pages that follow, I select for review those papers on dual model phenomenology which I think have made the greatest impact. Both four-point processes (2 → 2 scattering) and five-point reactions (2 → 3) are treated in some detail. Dual models for diffraction dissociation and for inclusive reactions are also discussed. Results are assessed for their physical content, and suggestions are made for futher exploration, both theoretical and experimental. In some cases, particularly in 2 → 3 scattering, I present previously unpublished calculations in order to demonstrate explicitly what new insight can be gained from the qualitative approach I advocate.

My overall conclusions are optimistic. In spite of obvious deficiencies, several of the fits I discuss illustrate the important roles played by duality and crossing symmetry, as manifest in the Veneziano model. Moreover, I think the potential of the model remains largely untapped. Because it embodies duality and crossing in an essential way, the model can be used to great advantage in developing qualitative understanding of the constraints which these principles impose on scattering amplitudes. Specific suggestions are given in the text.

The Table of Contents may be consulted for selection of topics. Most sections of this paper are fairly independent of each other. For instance, readers interested primarily in production processes may elect to omit Section 2. However, I assume readers have some basic familiarity with duality and the Veneziano amplitude. Here, I am fortunate in being able to refer to Jackson's review (1970), Jacob's paper at Schladming (Jacob, 1969), Jacob's review at the Lund conference (Jacob, 1970), Kugler's paper at Schladming (Kugler, 1970), the review by Sivers and Yellin (1971), and the papers by Schmid, Lovelace, and

Chan at the Discussion Meeting on Duality (Schmid, 1970; Lovelace, 1970; Chan, 1970). Mathematical questions associated with generalized Veneziano models and with the unitarization program are covered by Alessandrini, Amati, LeBellac, and Olive (1970).

2. Aspects of Four-Point Phenomenology.

There are two essential dynamical predictions of the Veneziano model. These are apparent upon cursory examination of the four-point Veneziano amplitude for any 2 → 2 scattering process. The model predicts a distinctive spectrum of resonance states as well as the existence of dynamical zeroes of the scattering amplitude. In this Section, I begin by examining evidence in Nature for predicted "towers" of resonances. Important in this context is some understanding of the changes which proper unitarization of the model is likely to make in the prediction of exact mass degeneracy of states in a given tower. Also crucial is the issue of total widths of resonances, inasmuch as in the Veneziano model, all resonances as well as "background" partial waves are approximated by zero-width poles, positioned on the real energy axis. These ambiguities are discussed. Subsequently, the existence and role of dynamical zeroes are explained. These have received little attention in the literature, but their consequences for phenomenology are intriguing and warrant further study. Finally, in subsection 2.3, I describe fits to data from the annihilation $\bar{p}n \rightarrow 3\pi$. In Veneziano model interpretations of these data, both resonance structure and dynamical zero structure of the model play a crucial role in generating the distinctive appearance of Dalitz plots.

2.1 Spectrum of Resonance States.

A most intriguing aspect of the Veneziano model is its prediction for the spectrum of states. Generally, the model predicts that whenever any trajectory* $\alpha(s)$ is equal to an integer value n, there will materialize a tower of $(n + 1)$ resonant states, degenerate in mass, whose spin values range from $J = \alpha = n$ down to $J = 0$.

2.1.1 π-π Scattering.

As an example, let us take the simplest B_4 amplitude describing $\pi^+\pi^-$ scattering (Shapiro, 1969; Lovelace, 1968). This is given by Eq. (1). Even within the narrow resonance framework, this amplitude is not, of course, the complete amplitude because diffractive effects (Pomeron exchange) are not present in the model; however, the Pomeron is said not to be dual to resonances (Freund, 1968; Harari, 1968). Therefore, the Pomeron part of the amplitude, whatever its structure, should not affect what I want to say here.

$$B_4(s,t) = -\frac{\Gamma(1-\alpha_\rho(s))\,\Gamma(1-\alpha_\rho(t))}{\Gamma(1-\alpha_\rho(s)-\alpha_\rho(t))} \quad . \tag{1}$$

The s and t channels are identified in Fig. 1a; α_ρ is the trajectory on which lie the familiar ρ and f mesons. For the completely uninitiated, I remark that $\Gamma(x)$ is Euler's Gamma function.

The spectrum of states predicted by this model is shown in Fig. 1b. Present, of course, are the resonances of the leading trajectory: the ρ, the f, the g, and other recurrences. These are well known, at least in principle, if not experimentally. Predicted to exist are daughter

---

[*] For baryon trajectories, substitute $\bar{\alpha} = \alpha - 1/2$ for α.

states: ϵ with $J^P = 0^+$, $I^G = 0^+$ and degenerate in mass with ρ; the ρ' ($J^P = 1^-$, $I^G = 1^+$) and ϵ', degenerate in mass with f^o, and so forth. The elastic couplings of all these states are also predicted; in particular

$$\frac{\Gamma^{el}_{\rho' \to \pi\pi}}{\Gamma^{el}_{\rho \to \pi\pi}} \simeq 1 \tag{2}$$

and

$$\frac{\Gamma^{el}_{\epsilon \to \pi\pi}}{\Gamma^{el}_{\rho \to \pi\pi}} \simeq 5 \; . \tag{3}$$

Now, the model is a zero total width model. Therefore, the predicted "resonances" really are poles positioned directly on the real energy axis. Resonances in Nature are seen as Breit-Wigner-like distributions in mass, not as Veneziano's zero-width, infinitely-high spikes. Clearly, some form of implicit, if not explicit, "unitarization" operation must be performed on the model before predictions can be confronted with data.* It is not altogether clear how this undefined unitarization will affect the predicted spectrum. Some Veneziano states may become ordinary experimental resonances. Other states in the model, for example low lying daughters, may become so spread out that they are merely background partial waves. Surely, the exact mass degeneracy in a given tower of states will also be broken. However, let us set aside such unsolved questions and begin instead to examine whether there is any evidence in Nature for Veneziano daughter states in $\pi^+\pi^-$ scattering.

---

* Someone offended by the fact that the Veneziano model is not unitarity should recall that it is endowed with analyticity, crossing-symmetry, and Regge-behavior. Were it to be unitarity also, it would satisfy all postulates of S-Matrix theory (Chew, 1966) and, therefore, be the ultimate theory.

2.1.1.a The ϵ.

It is universally agreed by people who extract $\pi\pi$ phase-shifts that there is indeed a substantial isospin zero, s-wave amplitude, which either resonates or comes very close to doing so in the neighborhood of 760 MeV. Primary evidence is, of course, the very asymmetric nature of the $\pi^+\pi^-$ angular distribution in the rho region. I need not dwell on this question.*

2.1.1.b The ϵ'.

Evidence here is less conclusive. However, various groups have reported evidence for an s-wave amplitude whose phase stays near 90° in the f^{o} region.** A recent paper is that of the ABC collaboration (J. V. Beaupre et al., 1971a). Again, an anomalous shape of the decay angular distribution of the f^{o} resonance gives us the clue.***

2.1.1.c The ρ'.

Although ϵ and ϵ' are observed (and seen easily, one might add), the ρ' has remained very elusive. Epitaphs for Veneziano have been written because ρ' is supposed not to exist. These dirges may well be as premature as those sung periodically for Regge theory as a whole. Let's look at the facts.

---

* For discussion, consult the Proceedings of the Conference on $\pi\pi$ and $K\pi$ Interactions, Argonne National Laboratory, May 1969.

** To demonstrate that this is a second s-wave resonance, it will be necessary to study carefully the behavior of the s-wave phase shift, as a function of π-π mass, from below the ϵ to well above the ϵ' position.

*** I do not take seriously the prediction (Shapiro, 1969) that ϵ' has negative elastic coupling. The kinematics are so sensitive that a reasonable shift in mass of ϵ' can make the prediction positive. Correct unitarization can easily supply the necessary shift in mass.

2.1.2 Properties of the ρ'.

Where would one expect to see this object? Obviously, because it is meant to be simply a heavy ρ, we may search for ρ' in all reactions in which ρ is produced. Moreover, ρ' will appear in a few additional channels. For example, it may show up as a p-wave resonance in the $\pi\omega$ system. Unfortunately, here it may be hard to disentangle* from B ($J^P = 1^+$, presumably an s-wave $\pi\omega$) which has nearly the same mass, 1250 MeV. The ρ' will also appear as an s-wave resonance in the πA_1 system. Here, it is subject to all the qualifications about whether the A_1 itself is a resonance. Nevertheless, four-pion mass distributions should be examined for evidence of a ρ', with and without a prior selection which forces $M(3\pi) \simeq M(``A_1")$.

The crucial question really is: What is the expected total width of ρ'? Should we be looking for a narrow object (say, $\Gamma_{tot} \simeq 100$ MeV), or something much more broad?

Theoretical guidance here is not entirely unambiguous. Let's try different approaches. First, let us abstract from the Veneziano model the simple assertions that (i) a ρ' exists, and (ii) that its elastic coupling to $\pi\pi$ is about 100 MeV. Then, let us assume that ρ' couples to all other channels allowed kinematically, with some universal, reduced coupling strength, derived from the value of $\Gamma_{\rho' \to \pi\pi}$. These other channels include $\bar{K}K$, $\pi\omega$, 4π, 6π, etc. Given these assumptions, and using trivial kinematic arguments (based on angular momentum barriers and distance from threshold), we can compute coupling strengths to each of the allowed channels. If we add up all these numbers, we get a total width. My answer is $\Gamma_{tot} \approx 300$ MeV, with partial width into $\pi\omega$ of 70 MeV.

---

* I'll comment more on this below, in Section 2.1.3.

A second way to obtain a total width for ρ' is to add up partial widths derived from explicit Veneziano-type models for all processes in which ρ' participates. For example, from an explicit B_4 model for $K\overline{K}$ scattering, we can obtain directly the partial width $\Gamma_{\rho' \to K\overline{K}}$, just as Eq. (1) gives us $(\Gamma_{\rho' \to \pi\pi}) \cong 100$ MeV. Although this method is possible in principle, there are practical difficulties. For example, there are non-trivial spin-complications in a proper treatment of, say, $\pi A_1 \to \pi A_1$, one of the channels which must be investigated (assume, for the moment, that A_1 is a resonance with $J^P = 1^+$). Moreover, what rule do we adopt concerning satellite* terms? By adding satellites, we can change the ρ' partial width by any amount we like. Nevertheless, if I specifically exclude unnecessary satellites, and do the best I can with spin, I again estimate a total ρ' width of 300 MeV.

It should be remarked, however, that this 300 MeV total width, derived from Veneziano formulas for various channels, is not divided up among channels in the same way that the previous number is. Indeed, the partial width for $\rho' \to \pi\omega$ is quite different. In the original B_4 amplitude for $\pi\pi \to \pi\omega$ (Veneziano, 1968), the ρ' is predicted to decouple dynamically from the $\pi\omega$ channel;** i.e. $(\Gamma_{\rho' \to \pi\omega}) = 0$. Previously, I estimated on kinematic grounds that $(\Gamma_{\rho' \to \pi\omega}) \cong 70$ MeV. Therefore, assuming ρ' is found in some channels, but not in $\pi\pi \to \pi\omega$, we would have an interesting check on whether satellite terms are necessary in meson-meson scattering.*

---

* By "satellite," I mean either terms which do not contribute to leading order asymptotically in one or more channels or those which do not contribute to the residue of the lowest-lying physical state on a given trajectory. I use the word "daughter" to denote any state in a given resonance tower whose spin J is less than that of the leading member. The term "exotic" denotes a meson state whose quantum numbers cannot be generated via the quark model as $(\overline{q}q)$; an exotic baryon is one for which (qqq) structure is not possible.

** Presence of satellite terms would change this conclusion.

In summary, then, current theoretical prejudices suggest that the ρ' is not a narrow resonance. Indeed, the total width may be as great as 300 MeV. This is a somewhat different view than was held in the earlier days of Veneziano phenomenology.

With respect to mass, ρ' should be located somewhere in the vicinity of f^o. However, again, unitarity will presumably break exact mass degeneracy; therefore, it is not unreasonable to suppose $M_{\rho'} \simeq M_f \pm 200$ MeV.

2.1.3 Experimental Search for the ρ'.

I will examine, in turn, various reactions in which we might expect to see a ρ'.

2.1.3.a $\gamma p \to \pi\pi p$.

In Table I, I give a list of some photoproduction experiments in which studies were made of pion pairs with high invariant-mass. Also cited is one experiment on massive $\mu^+\mu^-$ production in hadron collisions.

---

* Studies of $\pi N \to \pi N$ and $KN \to KN$ (Berger and Fox, 1969) show that satellites certainly are necessary in meson-baryon scattering.

TABLE I

Reaction	Authors	Results
1. $\gamma C \rightarrow \pi^+\pi^- C$ 10 GeV Bremsstrahlung beam	Cornell (McClellan et al., 1969)	$\sigma_\rho/\sigma_{\rho'} \simeq 10^2$
2. $\gamma C \rightarrow \pi^+\pi^- C$ 7.5 GeV Bremsstrahlung beam	DESY-MIT (Alvensleben et al., 1971)	$\sigma_\rho/\sigma_{\rho'} \simeq 10^2$
3. $\gamma B_e \rightarrow \pi\pi B_e$ 16 GeV Bremsstrahlung beam	SLAC (Bulos et al., 1971)	$\sigma_\rho/\sigma_{\rho'} \simeq 10^2$
4. $\gamma p \rightarrow \pi^+\pi^- p$ Monochromatic, linearly polarized γ in B.C.; $E_\gamma = 2.8$ and 4.7	SLAC-Berkeley-Tufts (Moffeit, 1970)	$\sigma_\rho/\sigma_{\rho'} > 40$
5. $pU \rightarrow \mu^+\mu^-$ + anything 29 GeV/c	Columbia-BNL (Christenson et al., 1970)	$d\sigma/dM_{\mu\mu} \propto M^{-5}$

There are differences in technique among the photoproduction experiments listed. Generally, the counter experiments (Table I, 1-3) have limited acceptance, and so are unable to view the entire range of angles in the $\pi^+\pi^-$ rest system. The bubble chamber experiment (Table I, 4) has 4π solid angle, and a monochromatic beam, but somewhat limited statistics. An example of counter spectra is given in Fig. 2. The spectrum decreases by ≥ 2 orders of magnitude from $M = m_\rho$ to $M \cong 1.3$ GeV, where ρ' is meant to be located. No statistically significant narrow enhancement is observed. However, a broad enhancement in the mass region $1.3 < m < 1.8$ GeV is present. Qualitatively similar results are reported by Bulos et al. (1971) and by McClellan et al. (1969). The broad enhancement may well be caused by background $\pi^+\pi^-$ pairs from $\gamma p \rightarrow \pi^+\pi^-\pi^o p$ and, therefore, have nothing to do with ρ'. Bubble chamber data, which should have no such contamination, are shown in Fig. 3. Here again, the signal in the region $M \simeq 1.3$ GeV is two orders of magnitude smaller than in the ρ region. Experimenters quote an upper limit of 0.5 μb for ρ' versus about 20 μb for ρ.

What does all this tell us about the ρ'? The important point, which is often missed, is that what is observed is the inseparable product of the production cross-section for the presumed vector particle and its branching fraction into 2 pions, $\Gamma_{\rho' \rightarrow \pi\pi}$. It is $\Gamma_{\rho' \rightarrow \pi\pi}$ which we discussed above in connection with the B_4 amplitude for $\pi\pi$ scattering.

In order to extract $\Gamma_{\rho' \rightarrow \pi\pi}$ from the γp data, we can try to write an explicit Veneziano amplitude for the five-point process $\gamma p \rightarrow \pi\pi p$. This amplitude should reflect correctly both the production and decay aspects of ρ' and, thus, allow identification of $\Gamma_{\rho' \rightarrow \pi\pi}$. One such attempt has been made (Satz and Schilling, 1970) but, unfortunately, this analysis contains several technical errors.* In principle, however, this is an excellent way to proceed. The analysis should be redone correctly.

---

* These errors include:
(i) The Pomeron is treated as a O^+ particle;
(ii) ρ production does not conserve helicity in the s-channel;
(iii) a kinematic factor $(t_{pp} - s_{\pi\pi})^{-1}$ is introduced which appears to suppress artificially ρ' relative to ρ;
(iv) no attempt is made to achieve an absolute prediction for normalization.

Lacking a complete amplitude, we may consider attributing the cross-section in the region around $m \simeq 1.3$ GeV to production of a vector meson which couples directly to the photon. We are directed to a diagram of the usual VDM type, shown in Fig. 4a.

The further assumptions of $\Gamma_{\rho'} = \Gamma_{\rho}$, and equal elastic cross-sections $\sigma_{\rho p} = \sigma_{\rho' p}$, lead us to deduce

$$\frac{g^2_{\rho'\gamma}}{g^2_{\rho\gamma}} \cdot \frac{\Gamma^2_{\rho' \to \pi\pi}}{\Gamma^2_{\rho \to \pi\pi}} \leq 10^{-2} \qquad (4)$$

Here, $g^2_{V\gamma}$ is the direct meson-photon coupling strength. This is not a very informative result, since we don't know whether to attribute the small product to $(\Gamma_{\rho' \to \pi\pi}/\Gamma_{\rho \to \pi\pi})^2 \ll 1$, in contradiction with Veneziano, or to $(g^2_{\rho'\gamma}/g^2_{\rho\gamma}) \ll 1$, meaning that the ρ' does not couple directly to photons.

On the other hand, a very instructive way in which to separate production and decay aspects is offered by the Drell diagram. This diagram is sketched in Fig. 4b. A beautiful feature of this diagram is that it provides an absolutely normalized cross-section (in terms of the values of electric charge and the πN elastic cross-section). Of course, it contains neither ρ nor ρ' resonances. However, by making a partial wave analysis of the Drell amplitude, I can determine the strength of the p-wave component near $m = 1.3$ GeV and near $m_\rho = 0.76$ GeV. Then, upon integrating the modulus squared of this p-wave component over the ρ and ρ' mass bands, I can get an estimate of the relative production strengths: $(g^2_{\gamma P \rho'}/g^2_{\gamma P \rho})$. Here, $g_{\gamma PV}$ denotes the three-particle coupling strength of incident γ, exchanged Pomeron P, and produced vector system V.

The estimate is expected to be good for two reasons. First, various people have used the diagram, along with final state interactions, to predict correctly the cross-section of $\gamma p \to \rho p$ (Kramer and Quinn, 1970). Second, I find that this diagram gives a good,* absolutely normalized representation of the cross-section $d^2\sigma/dM_{\pi\pi}dt_{pp}$ for $M_{\pi\pi} \geqslant 1$ GeV.

Defining effective coupling strengths, as indicated above, I obtain

$$\frac{g^2_{\gamma P\rho'}}{g^2_{\gamma P\rho}} \simeq 10^{-2} \quad . \tag{5}$$

Therefore, I conclude that

$$\frac{\Gamma_{\rho' \to \pi\pi}}{\Gamma_{\rho \to \pi\pi}} \sim 1 \quad ; \tag{6}$$

this result is fully consistent with the Veneziano model. The apparent suppression of ρ' and other higher vector mesons in $\gamma p \to \pi\pi p$ may be understood quite simply in terms of mass dependence inherent in the production mechanism.

In passing here, I think it is worth remarking that a Satz-Schilling type calculation, done correctly, would unify the VDM and Drell diagram approaches. Indeed, at high incident energy, the dual amplitude will take on the form shown in Fig. 5a, where the dashed line represents a Regge-exchange, presumably Pomeron. When factored at a pole in the $s_{\pi\pi}$ variable, the amplitude becomes a VDM type diagram shown in Fig. 5b. However, when factored at the t-channel π pole, the amplitude has the appearance of a Drell diagram, shown in Fig. 5c.

---

* Similar results are obtained by C. Schmid, K. Schilling, and P. Frampton, CERN (private communication from C. Schmid). I find that an extra, mild dependence on $t_{\gamma\pi}$ is necessary in the amplitude. The pure pion pole term $(t_{\gamma\pi} - m^2_\pi)^{-1}$ is not sufficiently peripheral. Reggeization of the pion supplies this extra t dependence, in the form of $s_{\pi\pi}^{\alpha_\pi(t_{\gamma\pi})} = \exp[(t_{\pi\gamma} - m^2_\pi) \log s_{\pi\pi}]$.

Although direct evidence for ρ' does not exist in data on $\gamma p \rightarrow \pi\pi p$, it is clear that experimental information is at least consistent with expectations of the Veneziano model. Let's now turn to other channels in which there might be a ρ' signal.

2.1.3.b ρ' in $\pi\omega$ from $\bar{p}p \rightarrow \pi\pi\omega$.

The most concrete suggestion of a $J^P = 1^- \pi\omega$ system comes from an analysis of ≈ 8000 examples of the annihilation at rest $\bar{p}p \rightarrow \pi\pi\omega$.* These data were examined by Diaz, Montanet and others at CERN (J. Diaz et al., 1970; S.U. Chung et al., 1970). Two analyses were performed. The first is a conventional decomposition of the final state amplitude into possible contributions from resonance and background partial waves; a fit is then made to the Dalitz plot to determine relative weights of various states. In the second analysis, explicit Veneziano B_4 functions are employed; this study is modeled on the Lovelace analysis of $\bar{p}n \rightarrow 3\pi$ (Lovelace, 1968).

In the conventional analysis, good fits require two resonances in the region of the B meson. Two such solutions are found. In the first, with χ^2 probability 33%, the resonances are B ($J^P = 1^+$) and $\rho'(?)$ ($J^P = 1^-$). In the second solution, with probability 45%, the resonances are B ($J^P = 1^+$) and $\epsilon'(?)$ with $J^P = 0^-$. The ρ' solution yields values for ρ' mass and width which are not at all unreasonable: $M_{\rho'} \simeq 1254$ MeV and $\Gamma_{\rho'} = 241$ MeV. The fit obtained to the $\pi\omega$ and $\pi\pi$ mass distributions is shown in Fig. 6.

---

* I am grateful to C. Lovelace and J. Diaz for bringing these results to my attention.

2.1.3.c ρ' in $\pi\omega$ from $\pi p \to \pi\omega p$.

Because of possible confusion with the B , a bump in the $\pi\omega$ spectrum cannot be taken as evidence for ρ', unless a careful partial wave analysis is performed. Conversely, bumps previously accepted uncritically as manifestations of B should be reexamined. In this connection, it is especially interesting to read those experimental papers on the B meson which are cited in the Particle Data Group Tables (1970).*

In experimental investigations of $\pi^{\pm}p \to \pi^{\pm}\omega p$, attempts to determine J^P of the "B" enhancement are rare. A notable exception is the study reported by Ascoli et al. (1968). These authors remark that their (subtracted) angular distributions are consistent with the assumption that their enhancement is in a state of pure J^P. They argue further that their data favor assignments $J^P = 1^+$ or $J^P = 2^+ 3^- 4^+ \dots$. The choice $J^P = 1^-$ is disfavored by about three standard deviations. It would be valuable if new detailed analyses were made, with a possible ρ' in mind. The question to be answered is this: To what extent do data allow or rule-out a $J^P = 1^-$ state, in addition to the (predominant) $J^P = 1^+$ system? One should bear in mind that the ρ' may have a full-width two or three times broader than the B .

Selections on momentum transfer may enhance ρ' relative to B. In $\pi p \to (\pi\omega)p$, B is presumably produced by ω and A_2 exchange, whereas, in ρ' production, π exchange may also contribute strongly. Because of the presence of the exchanged pion pole, events at small t should provide a relatively enriched sample of ρ'. This argument is somewhat weakened, however, because of the $\sqrt{-t}$ factor present in the π

---

* The reference to Bizarri et al. (1969) is superceded by the Diaz, Montanet et al. analysis mentioned just above in Section 2.1.3.b.

exchange amplitude associated with the nucleon vertex. On the other hand, no such $\sqrt{-t}$ factor is present at a $\bar{p}\Delta$ vertex. Therefore, small t events at high energy (10 GeV/c) from the reactions $\pi^+ p \to \pi^o \omega^o \Delta^{++}$ and $\pi^- n \to \pi^o \omega^o \Delta^-$ should provide a rich source of ρ'. Clearly, reactions of this type, in which there are two π^o's in the final state, are not easy to investigate. Bubble chambers with track-sensitive targets are presumably required.

2.1.3.d ρ' in $\gamma p \to \pi\omega p$.

Of special interest for observation of ρ' are experiments in which the $\pi\omega$ state is photoproduced diffractively. General theoretical arguments (Lorentz-invariance) allow diffractive photoproduction of both $1^+(B)$ and $1^-(\rho')$ states. However, the usual lore* about parity change in diffractive processes forbids diffractive photoproduction of B. The ρ' is favored strongly.

The channel $\gamma P \to \pi\omega p$ is also relatively more favorable to ρ' than is $\gamma p \to \pi\pi p$. In $\gamma p \to \pi\pi p$, as I pointed out above, the production cross-section for ρ' is expected theoretically to be suppressed by two orders of magnitude from that for ρ. Therefore, the ρ' signal is swamped by the much more obvious ρ. However, in $\gamma p \to \pi\omega p$, ρ is below $\pi\omega$ threshold. To estimate ρ' production in $\gamma p \to \pi\omega p$, we may construct a π exchange diagram (similar to the Drell diagram discussed earlier). Indications are that a healthy fraction of this amplitude is in the $J^P = 1^-$ state.

An experimental difficulty here again is that a neutral 4 pion ($\pi\omega$)

---

* Morrison's rule (D. Morrison, 1968) states that $\Delta P = (-1)^{\Delta J}$. This rule is consistent with available data on diffractive production of meson and baryon systems in meson-nucleon and nucleon-nucleon reactions. Strongest support for the rule comes from absence of a Pomeron contribution to $Kp \to K^* p$.

state with I = 1 decays into a system with two π^o's. Nevertheless, an enhancement in the $\pi\omega$ system near the B mass is observed in bubble chamber data, at low energy (J. Ballam et al., 1970). At higher energies, a bump near the B location is observed also in missing mass counter data (R. Anderson et al., 1970); this bump seems to be produced with energy-independent cross-section, suggesting a diffractive mechanism. If we hazard identification of the low-energy bubble chamber enhancement with the bump in the missing-mass spectrum, we can say that the $\pi\omega$ system is produced diffractively. Clearly, a partial wave analysis is important to determine the J^P of this bump. It is somewhat surprising, in view of our estimates above, that the $\pi\omega$ enhancement in bubble chamber data is only 100 MeV wide. This width is more suggestive of B; however, it is not unreasonable that the B, produced non-diffractively, should dominate at low-energy.

2.1.4 Search for ρ' in $\pi p \to \pi\pi N$.

Peripheral single-pion production reactions provide the traditional source of information on $\pi\pi$ scattering. These reactions include $\pi N \to \pi\pi N$ and $\pi N \to \pi\pi\Delta$. Discussion of techniques used to extract π-π amplitudes from these data may be found in review articles by Fox (1969), Kane (1970), and in various papers collected in the Proceedings of the Argonne Conference on $\pi\pi$ and $K\pi$ Interactions (1969).

Let us ask here whether the existence of ρ' (with $\Gamma^{el}_{\rho'} \simeq \Gamma^{el}_{\rho}$) is consistent with available information on (off-shell) $\pi\pi$ scattering. There are two aspects to this question. First, does any ρ' bump show up in plots of $\pi\pi$ invariant mass? Second, do we observe any hint of the existence of ρ' through interference with f^o? This second question speaks really to the most sensitive method for observing a broad p-wave resonance in $\pi^+\pi^-$ scattering. If ρ' and f are nearly degenerate, their interference will produce an asymmetric, forward peaked angular distribution in the $\pi^+\pi^-$ rest frame. The amount of asymmetry is a direct measure of the ratio $(\Gamma_{\rho'}^{el}/\Gamma_{\rho'}^{tot})^2$.

2.1.4.a Enhancement in Mass Plots.

Let's take up first the matter of a bump in $\pi\pi$ invariant mass plots. Because $f^o(I = 0,\ J^P = 2^+)$ is seen prominently in $\pi^+\pi^-$ spectra, it is advantageous to examine instead $I = 1$ distributions, such as $\pi^\pm\pi^o$. Data of Crennell et al. (1968) are shown in Fig. 7. Qualitatively similar results are reported by other groups (e.g., Wisconsin-Toronto, B. Oh et al., 1970). In the $\pi^-\pi^o$ mass distribution, Fig. 7e, we observe ρ and g production, but no hint of another peak in the mass region 1.2 to 1.4 GeV region, where ρ' should appear.

We can use the Crennell et al. data to obtain a rough upper limit on the ratio $(\Gamma_{\rho'}^{el}/\Gamma_{\rho'}^{tot})$. Let us assume that π exchange dominates $\pi^-p \rightarrow \pi^-\pi^o p$. An approximate form* for the absolute square of the invariant amplitude is therefore

$$|M|^2 = g^2 \frac{-t_{pp}}{(t_{pp} - M_\pi^2)^2} |A_{\pi\pi}|^2 \ ; \tag{7}$$

$$|A_{\pi\pi}|^2 = (8\pi)^2 s_{\pi\pi} (d\sigma_{\pi\pi}/d\Omega) \ . \tag{8}$$

Here, t_{pp} is the square of invariant momentum transfer from incident to final proton; $s_{\pi\pi} = M_{\pi\pi}^2$ is the square of the $\pi\pi$ invariant mass; $(g^2/4\pi) \simeq 14.5$. The doubly-differential cross-sectio-

---

* Because I am not proposing an explicit fit to data, effects of absorption are not crucial to the arguments developed here.

$$\frac{d^2\sigma}{dM_{\pi\pi}\, dt_{pp}} = G \int |M|^2 \, d\cos\theta_{\pi\pi}\, d\varphi_{\pi\pi} \; ; \tag{9}$$

where

$$G = \left(\frac{1}{2\pi}\right)^5 \left(\frac{\pi}{16 M_{\pi\pi}}\right) \frac{\lambda^{\frac{1}{2}}(s_{\pi\pi}, M_\pi^2, M_\pi^2)}{\lambda(s, M_\pi^2, M_p^2)} \tag{10}$$

and

$$\lambda(x, y, z) = x^2 + y^2 + z^2 - 2xy - 2xz - 2yz \; . \tag{11}$$

Angles $\theta_{\pi\pi}$ and $\varphi_{\pi\pi}$ are measured in the $\pi\pi$ rest frame. Entirely independently of $s_{\pi\pi}$ and t_{pp}, the ranges of integration for $\cos\theta_{\pi\pi}$ and $\varphi_{\pi\pi}$ are -1 to $+1$ and 0 to 2π, respectively.

If ρ' were purely elastic, as is ρ, then we could use the p-wave unitarity limit $(3/k_{\pi\pi}^2)$ to predict that the ratio of heights of the ρ' and ρ signals, in the $\pi^-\pi^0$ cross-section $\sigma_{\pi^-\pi^0}$, is given by $(k_\rho^2/k_{\rho'}^2) \cong 1/3$. Here $k_{\pi\pi}$ is the center of mass momentum in the π-π rest system. This result is sketched in Fig. 8. Any inelasticity reduces the ratio. Indeed,

$$\text{Experimental Ratio in } \sigma_{\pi^-\pi^0} \simeq \frac{1}{3}\left(\frac{\Gamma_{\rho'}^{el}}{\Gamma_{\rho'}^{tot}}\right)^2 \; . \tag{12}$$

Data shown in Fig. 7e do not give us $\sigma_{\pi^-\pi^0}$ directly. The data provide us with the left hand side of Eq. (9); we can extract $\sigma_{\pi^-\pi^0}$ by using Eqs. (7) through (11). To make this long story short, observe that kinematic quantity G (Eq. (10)) partially cancels the unitarity suppression of ρ' relative to ρ. Indeed, $G \propto k_{\pi\pi}$, where

$$k_{\pi\pi}^2 = \frac{\lambda(s_{\pi\pi}, M_\pi^2, M_\pi^2)}{4 s_{\pi\pi}} = \frac{(s_{\pi\pi} - 4M_\pi^2)}{4} \; . \tag{13}$$

As a result, in $d^2\sigma/dM_{\pi\pi}dt_{pp}$, suppression of ρ' is reduced from $\approx 1/3$ to $\approx \sqrt{1/3}$. However, there is a third factor which influences the final answer. Because amplitude $|M|^2$, Eq. (7), is damped strongly in its dependence on the variable t_{pp}, large values of $M_{\pi\pi}$ are suppressed in $d^2\sigma/dM_{\pi\pi}dt_{pp}$. This kinematic effect is well known. In other words, the cross-section in the ρ mass region is enhanced kinematically relative to that in the ρ' region.

The combined effect of p-wave unitarity, 3-body phase-space (G), and kinematic suppression of ρ' can only be determined numerically. I find that the 3-body phase-space and kinematic effects approximately cancel each other at 6 GeV/c. Therefore, after all effects are considered, we can indeed substitute data from Fig. 7e for the left hand side of Eq. (12).

Data indicate that there are about 180 events/40 MeV in the ρ region, and 30 events/40MeV in the ρ' region.* If I attribute 1/2 of the events in the ρ' region to (unseen) ρ' and the rest to background, I deduce

$$\left(\frac{\Gamma^{el}_{\rho'}}{\Gamma^{tot}_{\rho'}}\right) \simeq \left(3 \cdot \frac{15}{180}\right)^{1/2} = \frac{1}{2} \,. \qquad (14)$$

Note that this determination of the ratio $(\Gamma^{el}_{\rho'}/\Gamma^{tot}_{\rho'})$ is independent of assumptions about the precise value of $(\Gamma^{el}_{\rho'}/\Gamma^{el}_{\rho})$. In Fig. 8, I present the $\ell = 1$ portion of the $\pi\pi$ elastic cross-section. The shaded area represents the contribution of a ρ' resonance with $(\Gamma^{el}/\Gamma^{tot}) = 1/2$, the value deduced from the Crennell et al. data. Note that the combined effect of unitarity and inelasticity reduces the ρ' peak by a factor of $\frac{1}{3} \times \frac{1}{4} = \frac{1}{12}$ below the ρ peak.

---

[*] Very similar numbers may be obtained from the Wisconsin-Toronto data on $\pi^- p \to \pi^- \pi^0 p$ at 7 GeV/c (B. Oh et al., 1970).

I find that the Crennell et al. data do not militate against ρ'. This conclusion differs from that of previous authors (Shapiro, 1969; Jackson, 1970). However, in these earlier arguments, based on the same data, the assumption is made that ρ' is largely elastic. Recent developments (c.f. subsections 2.1.2, 5.2) suggest that this assumption is not justified. In the analysis just discussed, I use the Crennell et al. data to determine an upper limit on the elasticity of ρ', assuming that the resonance is present in the data.

2.1.4.b Interference Effect in Angular Distributions.

As remarked above, the most sensitive method for observing a p-wave resonance (ρ') nearly degenerate in mass with f^o is through interference of ρ' and f^o in the center-of-mass angular distribution for $\pi^+\pi^-$ scattering. It is instructive to compute this angular distribution based on the assumptions that (a) ρ' and f^o are perfectly degenerate in mass; (b) $(\Gamma^{el}_{\rho'}/\Gamma^{tot}_{\rho'}) \cong 1/2$, the value determined above; and (c) f^o is purely elastic.

Generally,

$$\frac{d\sigma}{d\Omega} = \left|\sum_{\ell} 2(2\ell+1)\left(\frac{1}{3} f_\ell^{(0)} + \frac{1}{2} f_\ell^{(1)} + \frac{1}{6} f_\ell^{(2)}\right) P_\ell(z)\right|^2 . \tag{15}$$

Here, the partial wave amplitude with isospin I is

$$f_\ell^{(I)} = \frac{e^{i\delta}\sin\delta}{k_{\pi\pi}} \rightarrow \frac{i}{k_{\pi\pi}} \left(\frac{\Gamma^{el}}{\Gamma^{tot}}\right) . \tag{16}$$

The last expression in Eq. (16) is the value at resonance. Given the assumptions above, we deduce that at resonance,

$$\frac{d\sigma}{d\Omega}(z = \pm 1) = \left| \frac{2}{3}(5) \pm 3\left(\frac{\Gamma^{el}}{\Gamma^{tot}}\right)\right|^2 . \tag{17}$$

Therefore, the ratio

$$\frac{d\sigma(z=+1)}{d\sigma(z=-1)} \cong 7 . \tag{18}$$

Experimentally (e.g., J. V. Beaupre et al., 1971a; B. Oh et al., 1970), this ratio is essentially 1. There can be no doubt, therefore, that ρ', with non-vanishing $\Gamma^{el}_{\rho' \to \pi\pi}$, cannot be degenerate in mass with f^o. However, these model calculations also show explicitly that if we shift the ρ' peak from the f^o peak by the amount $\Gamma^{tot}_{\rho'}$, then the interference effect in the f^o mass region essentially vanishes. A mass shift of the prescribed amount, either up or down from f^o, will accomplish the task. Mass shifts of this order of magnitude are certainly not unexpected as a result of unitarization of the original four-point dual amplitude.*

In summary, then, available information on $\pi\pi$ scattering (both mass plots and angular distributions) is perfectly consistent with the existence of ρ'. These data put certain fairly generous limits on its properties. Indeed, as we have discussed,

$$|\text{Mass}(\rho') - \text{Mass}(f^o)| \simeq \Gamma^{tot}_{\rho'} \; (> \Gamma^{tot}_{f}) \; . \tag{19}$$

$$(\Gamma_{\rho' \to \pi\pi} / \Gamma^{tot}_{\rho'}) \leq 1/2 \; . \tag{20}$$

If we take seriously the prediction of the simplest B_4 model for $\pi^+\pi^-$ scattering, then $\Gamma_{\rho' \to \pi\pi} = \Gamma_{\rho \to \pi\pi} = 120$ MeV (Shapiro, 1969). We can insert this value into Eqs. (19) and (20) to determine that

$$\Gamma^{tot}_{\rho'} \geq 240 \text{ MeV} \; ; \tag{21}$$

$$\text{and} \quad |\text{Mass}(\rho') - \text{Mass}(f^o)| \geq 240 \text{ MeV} \; . \tag{22}$$

Finally, it is amusing to note that some evidence exists in $\pi\pi$ scattering for a possible p-wave resonance in the mass region 1.08 to 1.22 GeV (B. Oh et al., 1970). The analysis is not conclusive, but if the resonant solution is accepted, $\Gamma^{tot} = 150 \, {}^{+100}_{-50}$ MeV.

---

* Note, also, that if this new estimate for ρ' mass is used in the analysis of subsection 2.1.4.a, the upper limit on ρ' elasticity increases.

2. 1. 5 Conclusions.

Towers of resonances and states on daughter trajectories are predicted in all processes, not simply in ππ channels.* I concentrated here on ππ reactions largely for historical reasons and because $\pi^+\pi^-$ scattering is the only process for which theorists have tried to argue that satellite B_4 terms are not present.** For this latter reason, we might feel comfortable in believing the (one-term) prediction*** $\Gamma^{el}_{\rho'} = \Gamma^{el}_{\rho}$.

I examined data on various channels in which ρ' might be expected. No conclusive evidence for or against ρ' was unearthed. Possible supporting evidence is found in the analyses of ππ scattering, by B. Oh et al. (1970), and of the πω system from $\bar{p}p \to \pi\pi\omega$, by Diaz et al. (1970).

The most concrete result of our study is a better definition of what one should be looking for in a search for ρ'.

(1) It seems clear that the total width is fairly large: 250 MeV.

(2) The resonance position is definitely shifted from f^o. A likely location is ~ 1.10 GeV. The value ~ 1.5 GeV is also suggested.

It is also clear that one must be careful to disentangle possible suppression of ρ' owing to production effects. This difficulty is serious in the reaction $\gamma p \to \pi\pi p$.

Reactions deserving much more careful experimental investigation are $\pi p \to \pi\pi N$ (or $\pi p \to \pi\pi\Delta$) and various processes in which the πω system is produced. In both ππ and πω , detailed phase shift analyses are required.

---

* For possible evidence of a $K^{*\prime}(J^P = 1^-)$ see A. Firestone et al., 1971.

** The argument has to do with positivity of residues of all states.

*** Satellite terms could quench ρ' and, as a result, $\Gamma^{el}_{\rho'} \ll \Gamma^{el}_{\rho}$.

Finally, let me try to put all this special pleading for ρ' into some semblance of perspective. I focused on ρ' because it is a daughter state which lies low enough in mass so that we should have a decent chance of observing it (i. e., seeing a bump in some mass plot and determining that the bump has $J^P = 1^-$). Surely, were the ρ' observed by now, everyone would regard its discovery as a great triumph for the Veneziano model. The ρ' has not been observed definitely. Some people hold this against the Veneziano model. However, the case is hardly closed.

Careful experimental investigation of all the channels I discussed here will be rewarding. I am the last person who would suggest another witch hunt for a spurious bump or split. What I do advocate with enthusiasm, however, is a concerted, systematic effort to accumulate enough events so that we can make a thorough spin-parity analysis (partial wave decomposition) from threshold to, say, 2 GeV in mass.

2. 2 Dynamical Zeroes, Dips in Differential Cross-Sections, and Relationships Among Coupling Constants.

The Veneziano model embodies not only a spectrum of resonant states, but predicts also the existence of dynamical zeroes with well defined spacing. These zeroes have interesting consequences for phenomenology. After a review of present understanding, I list possibilities in subsection 2. 2. 5 for new ways in which to exploit presence of the zeroes.

2. 2. 1 Dynamical Veneziano Zeroes.

In order to see whence these zeroes arise, let us examine the typical four-point function given in Eq. (23).

$$B_4(s,t) = -\frac{\Gamma(1-\alpha_1(s))\,\Gamma(1-\alpha_2(t))}{\Gamma(1-\alpha_1(s)-\alpha_2(t))} \quad . \tag{23}$$

Poles (resonances) of this function occur when the argument of one of the

Γ functions in the numerator becomes zero or a negative integer. Moreover, the function develops a dynamical zero whenever the argument of the Γ function in the denominator becomes zero or a negative integer. Therefore, except at isolated points of intersection between poles and zeroes, the function $B_4(s,t)$ is zero all along contours described by equations

$$\alpha_1(s) + \alpha_2(t) = N \geq 1 \quad . \tag{24}$$

In Eq. (24), N is a positive integer. We can use the kinematical relationship*

$$s + t + u = \Sigma \ , \tag{25}$$

plus the assumptions that trajectories are linear and have universal slope,** in order to recast Eq. (24) into a more useful form. Making these substitutions, we derive the equation

$$u = c_o - N/b \quad . \tag{26}$$

In Eq. (26), c_o is a constant.

Eq. (26) prescribes lines of constant u along which scattering amplitude $B_4(s,t)$ is zero. In Fig. 9, a sketch is given of a segment of the (s,t) plane. Shown are lines along which function $B_4(s,t)$ is zero and lines along which it is infinite (poles). Observe, especially, the behavior of the lines of zeroes in the scattering region. They occur at fixed u, with a spacing of about 1 $(\text{GeV})^2$. Moreover, if we move along a line t = constant, we will encounter, alternately, a resonance pole, followed by a dynamical zero, and so forth.

The zeroes represented by Eq. (26) are not be be confused with wrong-signature-nonsense-zeroes (WSNZ) or other such structure of high-energy amplitudes. In particular, a WSNZ at fixed u is associated with a u-channel exchange, whereas amplitude $B_4(s,t)$ contains no u-channel exchange trajectories. In the limit $s \to \infty$ at fixed u, $B_4(s,t)$ vanishes faster than any power.

---

* Σ denotes the sum of squares of external masses of particles participating in a scattering process for which Eq. (23) is a scattering amplitude.

** That is, $\alpha(s) = \alpha_o + bs$ where α_o and b are constants. Slope b is the same for all trajectories.

2.2.2 Evidence in Differential Cross-Sections.

Before inquiring into the physical significance of these Veneziano zeroes, let us first see whether there is any manifestation of their presence in Nature.

In order to expect to observe clear evidence for Veneziano zeroes in data, we must select processes which are simple from the standpoint of the model. For example $K^- p \to \overline{K}^o n$ is such a simple reaction, whereas $\pi^- p \to \pi^o n$ is not. In the latter case, there are resonances in all three channels (N^* in the s- and u-channels; $\rho, g, \ldots$ in the t-channel). Consequently, in addition to (s, t) terms of the type shown in Eq. (23), there should also be equally strong (u, t) and (s, u) terms. Zeroes would tend to be washed-out.

For $K^- p \to \overline{K}^o n$, the u-channel is exotic. Only (s, t) terms of the type shown in Eq. (23) are present, and zeroes should appear at fixed u. The s-channel trajectories include $(\Lambda_\alpha, \Lambda_\gamma)$ and $(\Sigma_\beta, \Sigma_\delta)$; the leading t-channel trajectories are (ρ, A_2). A sketch of the Mandelstam plane for the $\overline{K}N \to \overline{K}N$ complex is given in Fig. 10. For clarity, in the s-channel, only poles and zeroes associated with the Λ trajectory are given; poles and zeroes for Σ are displaced from those for Λ by the difference in intercepts, $\approx 0.3\ \text{GeV}^2$.

If only Λ trajectory poles are important in the direct channel, and if Veneziano zeroes are present in Nature, Fig. 10 indicates that we should observe dips in the differential cross-section for $K^- p \to \overline{K}^o n$ which occur at fixed values of $u \cong -0.6, -1.6, -2.6, \ldots\ (\text{GeV}/c)^2$. Data from

$K^- p \to \bar{K}^o n$ are shown in Fig. 11, for a sequence of values of laboratory momenta. As pointed out by Odorico (1971a), the figure shows clearly the presence of three dips occurring at remarkably constant values

$$u \simeq -0.1,\ -0.7,\ -1.7\ (\mathrm{GeV}/c)^2\ .$$

The exact positions of the observed dips do not coincide with naive theoretical expectations based on the value of the Λ intercept. However, it should be recalled that the Σ trajectory also contributes. The net contribution of Λ and Σ will certainly shift positions of predicted zeroes. Moreover, unitarity corrections (see subsection 2.2.4) are expected to shift dips somewhat from the values predicted by a simple non-unitary B_4 function. The remarkable fact is that fixed-u dips are observed at low-energy. Their spacing is approximately 1 $(\mathrm{GeV}/c)^2$. Because the u-channel is exotic, high-energy exchange models (and ordinary duality) make no statement about fixed u structure in $K^- p \to \bar{K}^o n$. Presence of these fixed-u dips is, therefore, a very intriguing qualitative confirmation of characteristic structure of the Veneziano model.

Odorico also examines the elastic process $K^- p \to K^- p$. Here, diffractive effects complicate the analyses. However, by studying invariant amplitude[*] $A(s,t)$, which should be free from diffraction, Odorico again observes structure at fixed u .

The processes $\bar{K}N \to \pi\Lambda$ and $\pi N \to K\Lambda$ present somewhat of a mystery. Resonances are present in all three channels. However, duality diagram arguments suggest that one should write only B_4 terms of the (s, u) and (t, u) variety.[**] Therefore, one may expect to see Veneziano dips at fixed t (from (s, u) terms) and at fixed s (from (t, u) terms), in addition to fixed u dips associated with WSNZ values of N exchanges. Instead, Odorico (1971b, c) presents evidence for a series of dips which occur at fixed values of (s-t) in $\overline{K}N \to \pi\Lambda$ and in[*] $\pi^- p \to K^o \Lambda$. His figures are reproduced here as Figs. 12 and 13. Dips at fixed (s-t) do not have any clear interpretation in terms of the Veneziano model. Odorico develops an alternative model which embodies such zeroes. However, his model has unfortunate side effects, such as resonances in some channels with exotic quantum numbers. Other possible explanations within the Veneziano framework should be studied before the Odorico alternative is accepted. Recall that, in spite of duality diagrams, $\overline{K}N \to \pi\Lambda$ and $\pi N \to K\Lambda$, are still reactions having resonances in all three channels. These reactions, therefore, do not provide as clear-cut a test as does $K^- p \to \overline{K}^o n$.

---

[*] Constructed from results of phase-shift analyses.

[**] The s-channel is the $\bar{K}N$ channel; the u-channel is the πN channel.

2.2.3 The Goebel Construction.[**]

Quite aside from whether one believes that data discussed in the last subsection confirm or defeat the Veneziano model, it is clear that the empirical approach taken by Odorico has uncovered some potentially significant regularities in data. It is interesting, now, to ask what theoretical features of the Veneziano model are connected with the lines of zeroes represented by Eqs. (24) and (26).

As we will see, dynamical zeroes are expected on the basis of rather general theoretical arguments. Indeed, contours in the (s, t, u) plane, along which the scattering amplitude is zero, have been discussed in various other contexts. In particular, I recall a series of illuminating papers on the subject by Eden and collaborators (Chiu, Eden, and Tan, 1968; Eden and Tan, 1968). The Veneziano model supplies a few crucial, additional ingredients; among these are the suggestions that the zeroes remain real, and that the contour, along which the function is zero, is a straight line.

---

[*] Recall that for $\pi p \to K\Lambda$, s is a momentum transfer.

[**] I learned first of the Veneziano formula from Charles Goebel during a brief visit to the University of Wisconsin in August, 1968. His explanation of the structure of the formula, in terms of lines of poles and of zeroes, is paraphrased here.

To see that dynamical zeroes must exist, let us examine a scattering amplitude $A(s,t)$ near the intersection point of an s-channel and a t-channel resonance. Although this intersection does not occur in the physical region for scattering, the assumption of analyticity allows us to write

$$A(s,t) \cong \frac{a}{s - M_1^2} + \frac{b}{t - M_2^2} \quad , \tag{27}$$

where a and b are the residues of the s and t channel poles, respectively, at the intersection point. This equation may be reexpressed as

$$A(s,t) = \frac{a(t - M_2^2) + b(s - M_1^2)}{(s - M_1^2)(t - M_2^2)} \quad . \tag{28}$$

The right hand side of Eq. (28) has the appearance of a double-pole, which is forbidden because it implies that the angular momentum of one or both of the resonances is infinite. Therefore, it is necessary that the numerator of Eq. (28) should vanish:

$$a(t - M_2^2) + b(s - M_1^2) = 0 \quad . \tag{29}$$

As a result, only a simple resonance pole remains at the intersection. Generally, a and b need not be constants. Nevertheless, Eq. (29) specifies a contour in the (s, t, u) (complex) plane along which $A(s,t)$ is zero.

Another general remark may be made. Let us rewrite Eq. (29) in the form

$$(a - b)(t - s) + (a + b)(t + s) = K \tag{30}$$

where K is a constant. Near the intersection, a and b are effectively constant; therefore, Eq. (30) defines the local orientation (tangent), in the Mandelstam plane, of the contour of zeroes associated with the two intersecting resonances. It is clear from Eq. (30) that this orientation is a direct measure of the ratio of resonance residues a/b .

The first special ingredient in our argument is local duality, which implies that a scattering amplitude may be written either in terms of s-channel resonance poles or in terms of t-channel resonance poles. According to this principle, the residues a and b are equal. Near the location of the resonance intersection, Eq. (30) reduces to

$$\begin{aligned} (t + s) &= \text{constant} , \\ \text{or} \qquad & \\ u &= \text{constant} . \end{aligned} \tag{31}$$

Finally, in the Veneziano formula, which imbodies strict local duality, Eq. (31) is asserted to hold not only near the intersection, but, indeed, globally. In addition, because the Veneziano amplitude is purely real, the line of zeroes remains in the real (s, t) plane.

It is interesting to consider other ways to satisfy Eq. (30), without requiring $a = b$. Other choices are certainly possible, but only $a = b$ seems simple and economical.

First, let us examine the upper right quadrant of Fig. 9. Because of its orientation $u =$ constant, the same contour of zeroes reduces not just one double-pole but, rather, as it propagates through the (s, t) plane, it satisfies the simple-pole-criterion at the intersection points of many different subsequent pairs of resonances. By contrast, if the contour of zeroes has arbitrary orientation at one intersection point, it would have to snake back and forth in the (s, t) plane in order to pass through the intersection point of a neighboring pair of resonance poles.

The choice[*] a = -b is as simple as the choice a = b, if our only criterion is reducing double-poles to single poles. This choice gives contours of zeroes running at right angles to those of the Veneziano formula. However, the angular momentum J of resonance poles must also be considered. The value of J is given directly by the number N of free zeroes which cross the pole in the (s, t) plane.[**] In Fig. 9, the first pole for $t > 0$ is crossed by one free zero and, therefore, has J = 1 ; the second pole has J = 2, and so forth. Were the lines of zeroes specified instead by the choice a = -b, then the first pole would have large J. With a = -b, the only way to avoid this conclusion is to introduce more poles. These must be placed in the u-channel, and we are led to a triple-product representation (Virasoro, 1969a; Odorico, 1970), having poles simultaneously in all three kinematic variables s, t, and u. Such representations run into difficulty when one of the three channels has exotic quantum numbers (e.g., $\pi^-\pi^-$; K^+n).

The Veneziano formula seems, therefore, to be the most economical and the simplest way to guarantee both simple resonance poles and desired angular momentum properties of these poles.

2.2.4 Unitarity.

It is useful to ask how unitarity will affect the Veneziano zeroes discussed above. Because no fully crossing-symmetric scheme exists for making the B_4 model unitarity, we certainly cannot answer the question completely. On the other hand, we can employ approximate unitarization methods in order to develop some intuition.

---

[*] This choice is advocated by Odorico (1971b, c) in order to interpret the dips at fixed values of (s - t) discussed in the previous subsection.

[**] "Free" zeroes are those not required to reduce double-poles.

Let us return to Eq. (1), which represents the $\pi^+\pi^-$ scattering amplitude. Lovelace has proposed unitarizing this amplitude by using a K-matrix method (Lovelace, 1969; Wagner, 1969). This technique may be strictly applied only below the first inelastic threshold. Nevertheless, it serves to dramatize possibilities.

Observe, first, that Veneziano zeroes of Eq. (1) occur when

$$\alpha_\rho(s) + \alpha_\rho(t) = 1, 2, 3, \ldots$$

Because $\alpha_\rho(s) \simeq 0.5 + 0.9\,t$, the first line of zeroes satisfies the equation*

$$-s = t \; . \tag{32}$$

In other words, the amplitude of Eq. (1) is zero at

$$\cos\theta \cong -1 \; , \tag{33}$$

for all values of $\pi^+\pi^-$ mass. Here, θ is the scattering angle in the π-π rest frame. The dashed curve in Fig. 14 shows the angular distribution, in the region $M^2_{\pi^+\pi^-} = M^2_\rho$, which is predicted by Eq. (1). Note the minimum at $\cos\theta = -1$. Also shown in Fig. 14 is the distribution obtained after Eq. (1) is unitarized by the K-matrix technique. Observe that the minimum of the angular distribution is moved from $\cos\theta = -1$ to $\cos\theta \simeq -0.2$. In momentum transfer units, this shift amounts to $\Delta u \simeq 0.2$ $(\mathrm{GeV}/c)^2$. Although the shape of the angular distribution changes significantly,* the shift Δu in the minimum position is not large compared to the $\simeq 1$ $(\mathrm{GeV}/c)^2$ spacing between locations of neighboring Veneziano zeroes. This is encouraging. Unfortunately, however, there is only a small range of values of $M^2_{\pi\pi}$ for which the K-matrix method is justified. Therefore, we are not in a position to estimate whether unitarization preserves the fixed-u character of Veneziano zeroes.

---

* I neglect the pion mass here. See also Fig. 9.

In examining data for evidence of Veneziano zeroes, one should bear in mind that unitarity may shift them somewhat from their predicted location. Moreover, their fixed-u (or fixed-t or fixed-s) character may be altered. It is, therefore, quite remarkable that fixed-u Veneziano zeroes are observed in $K^- p \to K^o n$ (c.f. subsection 2.2.2). From a theoretical standpoint, it would be useful to develop better estimates of the effects which unitarity is expected to have on Veneziano zeroes.

2.2.5 Coupling Constants and Residues.

In addition to the simple prediction of dips in differential cross-sections, the existence of dynamical zeroes has several interesting implications for phenomenology.

In subsection 2.2.3, we saw that the orientation, in the Mandelstam plane, of contours of dynamical zeroes of the scattering amplitude is determined by the ratio of coupling strengths (a/b) of resonances in crossed-channels. Lines of zeroes of amplitudes may be inferred from dips in differential cross-sections (c.f. subsection 2.2.2) or established by studying amplitudes reconstructed from phase shift analyses. The observation of a new relationship between zeroes (dips) and coupling constants opens an intriguing area for detailed theoretical exploration.

---

* Note that unitarization develops a backward peak in the angular distribution. Agreement of the solid curve in Fig. 14 with data is quite acceptable. The backward peak occurs in an exotic exchange channel. The K-matrix method shows that this exotic peripheral peak is caused by a "Regge-Regge cut" contribution.

It has been remarked (Berger and Fox, 1969; Odorico, 1969, 1971c) that the Veneziano hypothesis of equal residues (i. e., $a/b = 1$) is supported at the intersection point of N_α and Δ resonances in πN scattering. However, large deviations are observed at other intersections. It would be valuable to develop a systematic understanding of successes and failures of the predicted ratio $(a/b) = 1$. The investigation is likely to be most fruitful in $\bar{K}N$ channels because these processes are rather simple from the standpoint of dual models. Through an examination of ratios of the coupling strengths of resonances in crossed-channels* (and in the various spin-amplitudes) one would hope to gain a better understanding of how duality is manifest in low-energy data. Certainly, strictly local duality is not correct, but, at the present time, we have very little understanding of how this symmetry is broken (by unitarity?) or, indeed, whether it is even a (broken) symmetry of Nature.

The debate concerning the residue function of the Δ_δ trajectory illustrates a third type of question upon which useful light might be shed by the Odorico analysis. Fits to scattering data (Berger and Fox, 1969, 1971a) suggest strongly that the Δ_δ residue function does not have a factor $(\alpha_\Delta - \frac{1}{2})$. This conclusion is strengthened by the observation of negative sign for polarization at small u in recent high energy $\pi^+ p$ backward elastic scattering data (L. Dick, 1971). Exchange degeneracy of Δ_δ and

---

* For example, in $\bar{K}N \to \pi\Lambda$, we can study the *magnitude and sign, in* different spin amplitudes, of ratios of g^2_{N*}, g^2_{Y*}, and g^2_{K*}. Here, g^2_{N*}, g^2_{Y*}, and g^2_{K*} are coupling strength of nucleon-, hyperon-, and meson-resonances, respectively.

D_{15}, suggested by SU(3) arguments (Berger and Fox, 1969), implies that the residue function of Δ_δ should contain the factor $(\alpha_\Delta - \frac{1}{2})$, presumably in both spin amplitudes. Viewed in terms of intersecting poles and zeroes in the Mandelstam plane, Fig. 15, the zero at $\alpha_\Delta = \frac{1}{2}$ is generated by the line of zeroes necessary to cancel the double pole at the intersection of the N_α and ρ poles. This is a very different argument in support of the $(\alpha_\Delta - \frac{1}{2})$ factor. Moreover, it suggests that the factor need appear only in invariant amplitude B; it can be absent from A because the nucleon pole is also absent from A. A zero must still cross the ρ pole in amplitude A, Fig. 15a, in order that the ρ have correct angular momentum. However, this zero need not occur at $\alpha_\Delta = \frac{1}{2}$. The relationship of this argument to the SU(3) argument deserves clarification.

Existence of dynamical zeroes is relevant in a fourth context, also connected with residues and coupling strengths. It has been observed by various people* that the cross-section for $\pi^+ p$ scattering at low energy, as determined from the (3, 3) phase shift, is considerably smaller than predicted by a p-wave Breit-Wigner expression. It would appear that the Breit-Wigner expression should be damped strongly on the high-energy side. The presence of a dynamical Veneziano zero in the (3, 3) partial wave (at $\alpha_\Delta \simeq 2$ or $s \simeq 2\ \mathrm{GeV}^2$) can supply the needed suppression. The Veneziano formula suggests, therefore, a new parametrization of phase-shifts which takes into account presence of both resonances and dynamical zeroes.

---

* E. g., Berger and Fox, 1969, Footnote 32.

2. 3 Nucleon-Nucleon Annihilation into Mesons.

Of all processes, $\bar{p}n \to \pi^+\pi^-\pi^-$ has dramatized most vividly the remarkable structure of Veneziano functions. For annihilation at rest, Lovelace (1968) observed that the initial state has the quantum numbers of a pion. He then made the remarkable suggestion that one should use essentially the same four-point amplitude to describe both $\pi^+\pi^- \to \pi^+\pi^-$ and $\bar{p}n \to 3\pi$. The Lovelace ansatz gives a succinct interpretation to structure observed in the Dalitz plot for annihilation at rest. The pronounced minimum in the center of the plot (Anninos et al., 1968) is produced by the line of dynamical zeroes* at

$$\alpha(s) + \alpha(t) = 3 \quad .$$

This line of zeroes is generated by the Γ function in the denominator of Eq. (1).

The Lovelace fit has been reexamined by subsequent authors (Berger, 1969a; Altarelli and Rubinstein, 1969; Gopal et al., 1971). However, all of these authors agree with the basic hypothesis. Their contribution involves adding more Veneziano terms in an effort to reinterpret and improve the original fit. In the most recent of these analyses, by Gopal et al, a maximum likelihood fit is performed directly to the full two-dimensional surface of the experimental Dalitz plot.** Satellite terms are found to be essential. Nevertheless, an excellent fit is achieved with only four free parameters. By contrast, conventional phase-shift resonance models require fourteen parameters to do as well.

---

* C. f. subsection 2. 2.

** As an interesting byproduct of their work, Gopal et al. point out that the one-term Lovelace fit is better (smaller χ^2) than the five-term Altarelli-Rubinstein attempt. The Berger and Altarelli-Rubinstein fits do better at fitting the pronounced minimum in the center of the Dalitz plot. They also reproduce more adequately angular distributions in the ρ and f mass regions. These improvements are achieved essentially by multiplying the Lovelace amplitude by the factor $(3 - \alpha(t) - \alpha(s))$. Overall χ^2 is somewhat reduced, however, because this

In another recent paper, Pokorski and Thomas (1970) question the procedure of adding an imaginary part to the ρ trajectory. This ad-hoc unitarization procedure was suggested by Lovelace and is followed by all the other authors mentioned above. The difficulty with this Im α prescription is that all states in a given resonance tower acquire the same total width, even though partial widths of parents and daughters are very different. In order to investigate the problem, Pokorski and Thomas decompose Eq. (1) into a convergent sum of resonance terms. Then they "unitarize" each resonance term separately, assigning, for example, total widths of 410, 450, and 450 MeV to ϵ, ρ', and ϵ', respectively. The partial widths specified by Eq. (1) (and its off-shell continuation for $\bar{p}n$ kinematics) are retained. The final amplitude is obtained by summing the modified series. By using their different unitarization procedure, Pokorski and Thomas find some significant qualitative differences in overall fits.

Although no startling conclusions arise from the work of Pokorski and Thomas, I think their procedure is a useful phenomenological development. As we will see in subsection 3.4, the Im α prescription can lead to spurious conclusions. It is, therefore, valuable to develop and to use alternative methods for unitarizing the Veneziano amplitude, if for no other reason than to check sensitivity of results to the Im α prescription. The Pokorski-Thomas method allows also the possibility of manual

---

factor implies directly an unobserved strong depletion of events all along the line $M^2_{\pi^-\pi^-} = 4M^2_N + 3M^2_\pi - s - t \cong 4M^2_N + 3M^2_\pi - 2 + (3 - \alpha(t) - \alpha(s)) \simeq 1.6$ GeV^2, and not only in the middle of the plot.

intervention to break the exact mass degeneracy of states in a given tower.

The physical interpretation of Veneziano model fits to $\bar{p}n \to 3\pi$ is quite simple. At rest, the reaction is dominated by the five $\pi\pi$ resonances: ρ, ϵ, f, ρ', and ϵ'. Different fits differ only in the relative contributions from these five states. All fits agree that there is no role for any $I = 2$ $\pi\pi$ interaction.

Attempts have also been made to analyze data from $\bar{p}p$ annihilation at rest into three pions. Here, although the initial state is still in an s-wave, as for $\bar{p}n$, both singlet and triplet spin states are possible. Therefore, in an approach similar to that of Lovelace, one must consider contributions both from π, which couples to ${}^1S_0$, and from, say, ω which couples to the ${}^3S_1$ state of $\bar{p}p$. The number of four-point functions is increased correspondingly. Fits to data are adequate (Jengo and Remiddi, 1969) but much less compelling than those for $\bar{p}n \to 3\pi$.

Superficially, at any rate, one surprising aspect of all fits to $N\bar{N}$ annihilation at rest is that theoretical amplitudes contain no terms corresponding to baryon exchange. Because $\bar{p}n \to 3\pi$ is really a five-point process, we might expect some contribution from baryon graphs. In the Lovelace ansatz, such graphs are swept aside; a direct channel heavy π is asserted to dominate the reaction. To my knowledge, no adequate explanation has been offered for the minor role played by baryon exchange. The suppression does not seem to be purely kinematic. Indeed, as I remarked earlier (Berger, 1969a), if we define four momentum transfer $t_{N\pi} = (q_\pi - q_N)^2$, where q_N and q_π are four momenta of an initial nucleon and final pion, respectively, we find that the allowed kinematic range of $t_{N\pi}$ is given by

$$-M_N^2 + 2.5\, M_\pi^2 \leq t_{N\pi} \leq (M_N - M_\pi)^2 \cong 0.6\ \mathrm{GeV}^2 .$$

At the upper limit, $t_{N\pi}$ is not very far from the nucleon pole position ($0.88\ \mathrm{GeV}^2$). Large contributions to the amplitude from nucleon exchange should be expected. Incidentally, $t_{N\pi} \simeq 0.6\ \mathrm{GeV}^2$ is correlated kinematically with $M^2_{\pi^+\pi^-}$ being near its maximum allowed value. Therefore, the baryon exchange contribution should be largest in the two corners[*] of the Dalitz plot associated with large values of $M^2_{\pi^+\pi^-}$. Maxima of the density distribution are indeed observed near these corners. In the Lovelace analysis, these maxima are interpreted as part of the ρ resonance bands.

Data on the in-flight annihilation process $\bar{p}n \to 3\pi$ has been published (A. Bettini et al., 1971). An equal-density contour map of the experimental Dalitz plot is given in Fig. 16. Some features are similar to those observed for annihilation at rest. In particular, there is a pronounced minimum near the intersection of the lines $M^2_{\pi^+\pi^-_1} = 1\ \mathrm{GeV}^2 = M^2_{\pi^+\pi^-_2}$; moreover, there is again a significant enhancement in the plot near the intersection of the lines $M^2_{\pi^+\pi^-_1} = M^2_{\pi^+\pi^-_2} = 1.5\ \mathrm{GeV}^2$. These similarities may tempt one to try to extend the Lovelace method to the in-flight data. However, because $\bar{p}n$ is no longer at rest, one can no longer assert that a heavy pion adequately represents the initial state quantum numbers. Furthermore, there is no justification for assuming that the pion-trajectory dominates the direct channel.

It is clear from the data (Fig. 16), that some features agree with a Veneziano-like interpretation, whereas other features are mysterious. Absent from the plot are any hints of minima near the intersections[**]

---

[*] The third corner has $M^2_{\pi^-\pi^-}$ large. Because of the charges involved, exchange of Δ_δ would be required to populate this corner. This exchange is known to be suppressed. Therefore, we do not expect any maximum for large $M^2_{\pi^-\pi^-}$.

[**] To obtain the second intersection, interchange pion subscripts 1 and 2.

($M^2_{\pi^+\pi^-_1} = 2\ \mathrm{GeV}^2$, $M^2_{\pi^+\pi^-_2} = 1\ \mathrm{GeV}^2$). Such minima would be expected if a Lovelace-type amplitude were appropriate for annihilation in-flight. They would be generated by the line of zeroes $\alpha(s) + \alpha(t) = 4$. Their absence has prompted Odorico (1970) to develop an alternative model in which every other line of zeroes is reoriented. From a theoretical point of view, Odorico's model is unattractive because it implies the existence of exotic meson resonances with $I = 2$. From a practical standpoint, it is not at all clear that such a drastic assumption is required to fit the data. First, as discussed above, graphs with baryon exchange must be present to some degree. It seems entirely conceivable that such graphs could serve as "background," filling in some, but not all, minima predicted by graphs having only direct-channel meson poles.

The stark simplicity of the Lovelace interpretation of $\bar{p}n \rightarrow 3\pi$ at rest certainly encourages attempts to extend the analysis to annihilation in-flight. However, because of the additional phase-space involved, extra attention must be paid both to unitarity problems and to the role of baryon exchange.

3. B_5 Phenomenology.

Veneziano amplitudes were generalized to processes with five external particles by Bardacki and Ruegg (1969), and by Virasoro (1969). Five-point dual models offer the possibility of describing completely all facets of a production process, such as

$$K^- p \to \bar{K}^o \pi^- p \ .$$

The full amplitude is endowed with resonance poles in the entrance channel as well as resonance poles in all three of the final two particle sub-systems: $(\bar{K}^o p)$, $(\pi^- p)$, and $(\bar{K}^o \pi^-)$. In principle, the model allows a description of the entire Dalitz Plot, including all interference effects among competing resonances in the two particle sub-channels. Because both resonances and background are built into the model, along with their relative phase, difficult kinematical reflection problems are also solved (again, in principle). Moreover, the amplitude has correct Regge asymptotic behavior, allowing a description of quasi-two-body channels at high energy (e.g., $\bar{K}p \to \bar{K}^* p$ or $\bar{K}p \to \bar{K}\Delta$), along with specification of background under the resonances.

In sum, the five-point model is at one and the same time an isobar model, a model for background and for reflections, a model for "off-shell" effects, and a model for quasi-two-body scattering at high energy. There is one more crucial ingredient.

The important additional ingredient is crossing-symmetry. Legs of the B_5 formula can be permuted by crossing-symmetry so as to allow predictions for several observable reaction channels. For example, exactly the same amplitude which describes

$$K^- p \to \bar{K}^o \pi^- p \tag{34}$$

also applies to

$$K^+ p \to K^o \pi^+ p \quad , \tag{35}$$

$$\pi^- p \to K^o K^- p \quad , \tag{36}$$

$$K^o p \to K^+ \pi^- p \quad , \tag{37}$$

$$\overline{K}^o p \to K^- \pi^+ p \quad , \tag{38}$$

$$\overline{p}p \to K^- K^o \pi^+ \; , \tag{39}$$

and

$$\overline{p}p \to K^+ \overline{K}^o \pi^- \; . \tag{40}$$

3.1 Work by the Chan Group.

Chan, Ratio, Thomas, and Törnqvist (CRTT, 1970) exploited this crossing symmetry in attempting a simultaneous fit to available data on $K^- p \to \overline{K}^o \pi^- p$, $K^+ p \to K^o \pi^+ p$, and $\pi^- p \to K^o K^- p$. At the time of their analysis, $K^o p$ and $\overline{K}^o p$ data were not available. Recently, data on $K^o p \to K^+ \pi^- p$ and $\overline{K}^o p \to K^- \pi^+ p$ have been reported by a group from SLAC (A. Brody et al., 1970); these results provide an important check on the CRTT fit, as I will describe below. The CRTT approximations in treatment of spin and isospin preclude application of their model to the $\overline{p}p$ data.

The CRTT fit has become a model for many subsequent investigations, so its strengths and weaknesses deserve comment.

3.1.1 Approximations and Choice of Functions.

Complete treatment of spin and isospin for $Kp \to K\pi p$ requires at least thirty-six different B_5 functions.* However, even thirty-six is artificially low if experience with four-point models is any guide. For example, in a bare-bones B_4 representation of $Kp \rightarrow KN$ (Solution I of E. Berger and G. Fox, 1969), six B_4 functions are necessary, although only $2 \times 2 = 4$ are demanded on the basis of spin and isospin accounting.

---

* There are four spin amplitudes and three isospin states. For each of these twelve, there are three topologically different B_5 graphs which do not require exotic trajectories.

Because thirty-six B_5 functions are beyond reason, CRTT make certain controlled approximations in the treatment of spin and isospin. First, baryons are handled as if they were zero-spin mesons. Second, rather than attempting a general solution to the isospin problem, CRTT restrict themselves to specific charge states only. Third, although both $I = 0$ (ω, f) and $I = 1$ (ρ, A_2, π) exchanges can couple at the $\bar{p}p$ vertex, the authors use prior knowledge that ω exchange dominates K^* production in $Kp \rightarrow K^* p$ to limit themselves to exchange-degenerate (ω, f) exchange only. None of these approximations destroys crossing.

To make this long story short, when all is said and done, the CRTT amplitude has the form

$$A(s_1, s_2, s_3, s_4, s_5) = \beta K\left[B_5(a) + B_5(b) + B_5(c)\right] \quad . \tag{41}$$

Out of a possible thirty-six B_5 functions, only three are left.* These three graphs are shown in Fig.17. In Fig.17, arrows drawn on external lines are appropriate to $K^+ p \rightarrow K^o \pi^+ p$. The same set of graphs is repeated in Fig.18, but with arrows on external lines drawn for $K^- p \rightarrow \bar{K}^o \pi^- p$. For reasons described adequately in CRTT and discussed elsewhere (e. g. P. Hoyer et al., 1971), when there is a choice from among N_α, Δ_δ and other N^* trajectories, only N_α is retained. Moreover, in the $K^- p$

---

* This is not altogether true. As shown in Figs.17 and 18, one must still choose specific trajectories in various channels. If more than one choice is accepted, the number of functions increases accordingly.

channel only $(\Lambda_\alpha, \Lambda_\gamma)$ is retained; the $(\Sigma_\beta - \Sigma_\delta)$ pair is excluded. The choices of (ρ, A_2) in the $\overline{K}K$ channel and of (K^*, K^{**}) in the $K\pi$ channels are unique.

In Eq. (41), the full amplitude depends upon five channel invariants denoted s_i, $i = 1, 5$. There is an overall free normalization constant β; K is a well-defined kinematical factor which controls completely the angular distributions (θ and φ) in the region of the first resonance on each trajectory (i. e., A_2, K^*, Δ, Y_1^*, etc.). The relative weights and the relative signs of the three terms in Eq. (41) are determined entirely by the requirement of unique, correct signature in the N_α and Δ_δ channels.

It is interesting to examine the resonance structure of the three graphs shown in Fig. 18. Graph (a) has resonances in the $\overline{K}\pi$ and πp final channels, as well as in the entrance channel. Graph (b) has resonances only in the final $\overline{K}^o p$ channel; the other four kinematic variables in (b) are in the (space-like) momentum-transfer region. Graph (c) has resonances in the final πp and $\overline{K}^o p$ channels, as well as in the entrance channel. It is easy to visualize how changing the relative weights of these three graphs will change the predicted proportion of $\overline{K}^*$, Δ, and Y_1^* production in the total sample.

In Fig. 17, graph (a) provides K^* resonances in the final $K\pi$ mass variable; however, the other four kinematic variables in (a) are in the momentum transfer region. Similarly, (b) and (c) provide $\Delta(1238)$ and its recurrences; the other four variables in (b) and (c) are in the momentum transfer region.

3.1.2 Unitarity.

In addition to the approximations discussed already, detailed fits to data require one more approximation. Resonance poles must be moved off the real axis. This is done in an essentially parameter free way by adding an imaginary part to trajectory functions; the imaginary parts are adjusted beforehand to known resonance widths. Adding imaginary parts to trajectories is a completely ad hoc, approximate way to unitarize the amplitude. It has liabilities, the most severe of which is that all states in a given tower of resonances acquire the same total width. This can be embarrassing in situations (such as the ρ, ε tower) in which daughter states have much larger partial widths than the parents. As a practical consequence of this unitarization procedure, daughter states play an unnaturally large role in creating bumps in mass spectra and interference effects in angular distributions.*

The single most important roadblock to further progress in applying dual models to data is certainly development of a better way to cope with the unitarity-violating, zero-width aspect of the model. This is a problem on a fundamental level, whereas better handling of spin and isospin may be classed as engineering difficulties.

3.1.3 Fits to Data.

Having determined their amplitude, as described above, CRTT produce a reasonable fit to all available data on processes 34, 35 and 36 . The number of really free parameters is astonishingly small: There is only 1, the overall normalization constant. However, it must be recalled that judicious choices of trajectory functions were made, with an eye on the data.** It is also much to the credit of CRTT that they selected the set of reactions most suitable for application of the B_5 formalism.

---

* See also Section 3.4.

** A somewhat different parametrization for $K^- p \rightarrow \bar{K}^o \pi^- p$ is presented by the ABCLV collaboration (J. Bartsch et al., 1970a). This paper contains also a nice discussion of some of the ambiguities in the B_5 approach.

Curves obtained by CRTT have been published and reproduced in several conference proceedings. For this reason, I will not display them here. It is instructive, however, to examine a few of the distributions, on an expanded scale. In Figs. 19 through 23, data are shown from the reaction $K^- p \to \overline{K}^o \pi^- p$ at 5.5 GeV/c. The data were obtained by an Argonne-University of Chicago collaboration.* Geoffrey Fox and I computed the curves shown, using exactly the CRTT amplitudes and parameters. Curves are normalized to the data.

It is clear that the fits are not quantitative, although general features of experimental distributions are reproduced roughly. In Fig. 19 the ratio of K^* to K^{**} production is incorrect. In Fig. 20, the narrow spike in the theoretical curve at $M_{p\pi^-} \simeq 1.35$ GeV is produced by a spurious daughter state. The N_α trajectory controls the distribution in $M_{p\pi^-}$. The N_α signature factor removes the (parent) recurrence with $J^P = 3/2^\pm$, located at $M_{p\pi^-} = 1.35$ GeV, but does not annihilate the daughter state which has $J^P = 1/2^\pm$. It is this daughter which is manifest in the theory, but not in the data. On the other hand, data show some indication of Δ^o, at $M_{p\pi^-} \simeq 1.24$ GeV, but there is no Δ signal in the theory.

Distributions in momentum transfer variables are shown in Figs. 21 and 22. Theoretical distributions vanish at $t = t_{min}$ (and $u = u_{min}$), as a direct result of the CRTT choice of kinematic factor K. The theoretical distribution in t_{pp} is not sufficiently peripheral. Of course, neglected π exchange would tend to populate small values of t_{pp}. However, independent of π exchange, it seems to be a general feature of fits with dual amplitudes that t distributions are predicted to be too shallow.**

---

* B. Musgrave and H. Yuta, private communication.

** An additional t dependence of exp(t) seems called for.

A very similar effect is observed in the $t_{K\overline{K}}$ distribution, not shown here.

In Fig. 22, the dip observed in the theory at $u \simeq -0.2\ (\mathrm{GeV}/c)^2$ is an interesting effect. Although nearly coincident with the dip observed in π^+p backward elastic scattering, this dip has nothing to do with N_α exchange. Observe that Δ_δ controls the distribution in question. The dip is produced because two of the three graphs in Fig. 18 are proportional to the factor* $(\alpha_\Delta - \frac{1}{2})$. In order to compensate for their approximate handling of spin, CRTT choose the unorthodox value 0.63 for the α_Δ intercept.** Thus, a spurious dip is produced in $d\sigma/du$ at $u \simeq \frac{-0.13}{.9} \simeq -0.2\ (\mathrm{GeV}/c)^2$, whereas $(\alpha_\Delta - \frac{1}{2}) = 0$ normally corresponds to $u \simeq +0.4\ (\mathrm{GeV}/c)^2$.

In Fig. 23, angular distributions are presented. The angles θ_J and φ_{TY} are measured in the $\overline{K}\pi$ rest system. The absolute square $|K|^2$ of the CRTT kinematic K can be expressed as

$$|K|^2 \propto \sin^2\theta_J \sin^2\varphi_{TY} . \tag{42}$$

Therefore, independent of dynamics inherent in B_5,

$$\frac{d\sigma}{d\cos\theta_J} \propto \sin^2\theta_J , \tag{43}$$

and

$$\frac{d\sigma}{d\varphi} \propto (1 - \cos 2\varphi) . \tag{44}$$

---

[*] This factor in the Δ_δ residue function arises naturally in dual models. Consult E. Berger and G. Fox (1969 and 1971a) for discussion.

[**] This choice applies only when the πp variable is in the momentum-transfer region. The correct intercept (0.13) applies if $M_{p\pi} >$ threshold.

These equations explain the fact that theoretical distributions in Fig. 23 vanish at $\cos\theta_J = \pm 1$ and at $\varphi = 0$ and π.

Additional, dynamical dependence on θ and φ is provided by the B_5 amplitude, unless the B_5 functions are evaluated near the first resonance pole of a given trajectory, in which case the B_5 amplitude is essentially a constant. Consequently, angular distributions in the $K^*(890)$ region do not test B_5. The successful fits indicate that the choice of kinematic factor is sensible. On the other hand, angular distributions in the region $M(\bar{K}^o\pi^-) > 1.$ GeV do manifest structure of B_5. Figures show some disagreement between theory and experiment.

3.1.4 Conclusions from the Fits.

All of the discrepancies observed, in each distribution we have examined, can be excused directly in terms of approximations made. No one of these failures vitiates the basic model. However, this is hardly a conclusion from which to draw comfort. It implies that to achieve a quantitative fit to data, we must increase the number of B_5 functions and find a much better way to unitarize the model.

What has been learned from the CRTT fit and from others like it? One thing we have learned is that B_5 is by no means ridiculous. This is not an empty statement. After all, there are ridiculous models, such as unabsorbed OPE models for reactions like $\pi p \to \rho\Delta$ or baryon exchange models in which the baryon is treated as an elementary particle.

Admitting, therefore, that the model is not totally unreasonable and having made a partial list of successes and failures, we can ask: Has any important physical insight been gained into 2 → 3 body dynamics? I fear the answer is a qualified no. To too great a degree, the model has been viewed as an end in itself. Too much effort has been devoted to development of techniques (numerical methods, kinematic factors) and to the art of parameter variation, in order to achieve cosmetically attractive fits to data. Too little effort has gone into exploiting the fits for their possible physical content. If the B_5 model has really all the virtues I listed at the start of Section 3, surely even partially successful fits to data can be analyzed carefully to produce new insight into such intriguing questions as the connection between duality and interference effects among competing resonances on a Dalitz plot. In subsection 3.2, I develop a concrete example of this type of qualitative use of B_5.

3.2 Relative Normalization.

Perhaps the greatest success of the CRTT fit discussed in subsection 3.1 is nearly correct prediction of the relative normalization of cross-sections for $K^+p \to K^o\pi^+p$ and $K^-p \to \bar{K}^o\pi^-p$. This result is shown in Fig. 24 . Moreover, the fit fails by only a factor or two or so from reproducing the factor of 50 which separates experimental values of $\sigma(K^+p \to K^o\pi^+p)$ and $\sigma(\pi^-p \to K^-K^op)$.

These are non-trivial and intriguing predictions of the model. Expecially noteworthy is the fact that the reaction with exotic quantum numbers in the initial state (K^+p) is calculated to have a cross-section which is larger than that of the channel with non-exotic quantum numbers (K^-p).

3.2.1 K^* Subsamples.

Although not emphasized by CRTT, the same effect is present for the $K^*(890)$ subsamples, as shown in Table II. Observe that $\sigma(K^+p \to K^*p) > \sigma(K^-p \to \bar{K}^*p)$ at all energies.

TABLE II

Cross-sections presented in this table are obtained from the explicit B_5 parametrization of Chan, Ratio, Thomas, and Tornquist (1970). I calculate cross-section σ_a for "pure" K^* production by integrating the modulus squared of the graph in Fig. 17a, only. Cross-sections $\sigma_{tot}(K^*)$ and $\sigma_{tot}(\overline{K}^*)$ denote the total K^* cross-sections obtained from the modulus squared of the sum of the three graphs given in Figs. 17 and 18, respectively. The K^* is defined as all events in the interval $0.83 \leq$ Mass $(K\pi) \leq 0.95$ GeV. No "background" is subtracted. Overall normalization is arbitrary; only relative normalization is meaningful here.

p_{lab}(GeV/c)	σ_a	$\sigma_{tot}(K^*)$	$\sigma_{tot}(\overline{K}^*)$
5	3.69	4.70	2.56
10	1.20	1.50	.87
15	.66	.82	.48

It is difficult to confront results given in Table II directly with published cross-sections. In defining their K^* signals, experimenters make various cuts and are fond of substracting "background";* the methods used differ from group to group. Discrepancies in normalization for $K^- p \to \overline{K}^* p$ are especially notorious.** However, if I draw a reasonable

---

[*] Subtracting background and making cuts is not altogether appropriate; I discuss this again in Section 3.3.

[**] c.f., Fig. 56 from D. Johnson (1971).

curve which interpolates experimental results* at different energies, I obtain $\sigma(K^-p \to \overline{K}^*p) \cong .28 \pm .03$ mb and $\sigma(K^+p \to K^*p) \cong .38 \pm .03$ mb at 5.5 GeV/c. Given the ambiguities, the experimental ratio $\frac{\sigma(K^*)}{\sigma(\overline{K}^*)} \cong 1.3$ is not in gross disagreement with the CRTT ratio $\sigma(K^*)/\sigma(\overline{K}^*) \simeq 1.8$ at 5 GeV/c.

It is interesting to observe that the B_5 model, with perfectly exchange-degenerate input trajectories, predicts breaking of line-reversal-symmetry.** This effect is obvious from the numbers given in Table II: $\sigma(K^*) > \sigma(\overline{K}^*)$.

It is also intriguing that the quasi-two-body reaction with exotic quantum numbers in the s-channel (K^+p) is predicted to have a cross-section larger than that of its line-reversed partner. This result is in qualitative agreement with (as yet unexplained) systematics of broken-exchange-degeneracy. With few exceptions, data favor $\sigma_{\text{real}} > \sigma_{\text{rotating}}$, where σ_{real} and σ_{rotating} are differential cross-sections of a pair of processes related by line reversal (e.g., $K^-p \to \overline{K}^on$ and $K^+n \to K^op$). Here, σ_{real} $(\sigma_{\text{rotating}})$ corresponds to the process for which duality prescribes a real (rotating phase) production amplitude. The systematics appear to hold true for both two-body and quasi-two-body processes.

---

* For K^+p data, consult the Particle Data Group Compilation (L. R. Price et al., 1969).

** An analytic explanation of this effect is developed below. The usual concept of exchange degeneracy of Regge trajectories predicts that differential cross-sections should become equal asymptotically for a pair of processes related by line-reversal. Well-known examples of this prediction are $d\sigma/dt\ (K^-p \to \overline{K}^on) = d\sigma/dt\ (K^+n \to K^op)$, and $d\sigma/dt\ (\pi^+p \to K^+\Sigma^+) = d\sigma/dt\ (K^-p \to \pi^-\Sigma^+)$. Similar predictions are presumed to be true for reactions in which resonances are produced; e.g., $d\sigma/dt\ (K^+p \to K^*p) = d\sigma/dt\ (K^-p \to \overline{K}^*p)$.

3.2.2 Data from $K^o p$ and $\overline{K}^o p$ Reactions.

Recently, data (A. Brody et al., 1970) have become available on the reactions

$$K^o p \rightarrow K^+ \pi^- p$$

and

$$\overline{K}^o p \rightarrow K^- \pi^+ p \;.$$

These are related directly through crossing-symmetry to the three reactions treated by CRTT. Therefore, I can use the CRTT amplitudes to make absolute predictions for the $K^o p$ and $\overline{K}^o p$ reactions.

Experimental cross-sections are shown in Figs. 25 through 27 Available mass and momentum transfer distributions are not sufficiently comprehensive, so I restrict my remarks here to integrated cross-sections.

First, there are a few interesting qualitative remarks to be made. In Fig. 25, observe that the reaction with exotic quantum numbers in the direct channel ($K^o p$) has a smaller cross-section than its counterpart with non-exotic quantum numbers ($\overline{K}^o p$). The same effect is present also in Fig. 26 ; non-exotic $\sigma(\overline{K}^o p \rightarrow \overline{K}^* p) >$ exotic $\sigma(K^o p \rightarrow K^* p)$. However, as shown in Fig. 27 , the exotic cross-section $\sigma(K^+ p \rightarrow K^o \Delta^{++}) > \sigma(\overline{K}^o p \rightarrow K^- \Delta^{++})$; only this last result agrees with the systematics mentioned above. Quite apart from B_5, these SLAC data on K^* production complement previous results on $K^+ p \rightarrow K^* p$ and $K^- p \rightarrow K^* p$, and offer data-fitters a challenge.

From the B_5 point of view, the SLAC results are damaging for CRTT. In Table III, I give experimental cross-sections for $K^o p \rightarrow K^* p$ and $\overline{K}^o p \rightarrow \overline{K}^* p$, at 4.5 GeV/c, as well as theoretical values I computed from the CRTT amplitude.

TABLE III

Reaction	SLAC data (mb)	CRTT theory (mb)
$K^o p \rightarrow K^* p$ at 4.5 GeV/c	.26 ± .05	.36
$\overline{K}^o p \rightarrow \overline{K}^* p$ at 4.5 GeV/c	.32 ± .05	.25

The absolute value of theoretical cross-sections is of the right order of magnitude. However, observe that CRTT predict $\sigma(K^*)/\sigma(\overline{K}^*) \cong 1.5$, whereas, experimentally $\sigma(\overline{K}^*) > \sigma(K^*)$. The experimental relative normalization of K^o and $\overline{K}^o$ cross-sections should be essentially free from systematic error because both K^o and $\overline{K}^o$ initial particles are part of the same K_L beam. Although statistical errors are large on experimental values given in Table III, I take the results seriously because the same effect $(\sigma(\overline{K}^*) > \sigma(K^*))$ is present over a wide range of energies (Fig. 26). By contrast, CRTT predict $\sigma(K^*) > \sigma(\overline{K}^*)$ over the same range.

The obvious question is: Do the SLAC data, if correct, invalidate the CRTT approach or is it possible for CRTT to vary a few parameters and thus reproduce $K^o p$ and $\overline{K}^o p$ data, as well as $K^{\pm} p$ data? In subsection 3.3, I demonstrate analytically that the CRTT model must predict $\sigma_{real} > \sigma_{rotating}$. This result is completely insensitive to parameter variation. Therefore, the SLAC results $(\sigma(K^o p \rightarrow K^* p) < \sigma(\overline{K}^o p \rightarrow \overline{K}^* p))$ show conclusively that the simple CRTT model is wrong. However, neither

B_5 nor certainly, crossing symmetry are called into question. To accommodate both the SLAC data and the $K^{\pm}p$ results, it is necessary to include B_5 amplitudes in which $I = 1$ exchanges couple at the $\bar{p}p$ vertex. These may be (ρ, A_2) and/or π. Therefore, the minimum number of required B_5 functions is increased at least by the factor two. Moreover, because the spin coupling of either π or (ρ, A_2) to $\bar{p}p$ is different from that of (ω, f), a new treatment of spin (kinematic factor) is required.

3.3 Line-Reversal Symmetry Breaking and Interference Effects Among Resonances in a Dalitz Plot.

Other than indicating that normalization features of $K^{\pm}p$ data are described correctly, CRTT do not attempt to determine which aspect of the B_5 model gives this result. Therefore, a reader does not know whether the result is a fluke or a valid test of crossing symmetry in the model. Similarly, the importance of difficulties encountered with SLAC data is hard to assess. To remedy the situation, I will now show analytically how the result $\sigma(K^+p) > \sigma(K^-p)$ arises. My analysis leads to the remarkable conclusion that B_5 models predict asymptotic breaking of line-reversal symmetry in production reactions. This asymptotic inequality results from simple interference between resonances in different two-body channels in the final state.

3.3.1 $Kp \to K^*p$; A Specific Example.

Rather than handle the entire three-body final state, I consider only the morsels

$$K^-p \to \bar{K}^*p \qquad (45)$$

$$K^+p \to K^*p \ . \qquad (46)$$

I will show analytically that

$$\frac{\left[\frac{d\sigma}{dt}(K^+p \to K^* p) - \frac{d\sigma}{dt}(K^- p \to \overline{K}^* p)\right]}{\left[\frac{d\sigma}{dt}(K^+p \to K^* p) + \frac{d\sigma}{dt}(K^- p \to \overline{K}^* p)\right]} \propto \Gamma_{K^*} . \qquad (47)$$

The results here are more general than the CRTT approach and, perhaps, more general than B_5. The only essential ingredient here seems to be duality.

In order to indicate the generality of the argument, I must repeat some of the steps reviewed in subsection 2.1.1. First, as will become clear, baryon spin is an irrelevant complication. Therefore, I ignore spin completely. Second, because I am concerned with an asymptotic effect, satellite B_5 terms are not a problem. Out of a possible twelve non-equivalent topological permutations of the five external particles, only three do not involve exotic trajectories. These three graphs* are shown in Fig. 28. In Fig. 28, arrows drawn on external lines are appropriate to $K^+p \to K^o\pi^+p$. The same set of graphs is repeated in Fig. 29, but with arrows on external lines drawn for $K^-p \to \overline{K}^o\pi^-p$. Finally, we must specify trajectories which couple in each of the adjacent two particle channels of Fig. 28 and 29. In some channels, more than one choice is possible. Candidates are listed on the figures. Let us examine baryon channels first. Symbol Λ denotes the exchange degenerate $(\Lambda_\alpha, \Lambda_\gamma)$ pair; Σ denotes the pair $(\Sigma_\beta, \Sigma_\delta)$; and N stands for all $I = \frac{1}{2}$ nucleon trajectories $(N_\alpha, N_\gamma, N_\beta)$. As will be obvious shortly, because I take the asymptotic limit in all variables associated with baryon trajectories, I do not have to make definite choices from among possible baryon trajectories in any given channel. This simplifies the analysis considerably.* Specification of meson trajectories is straightforward. In $K\pi$ channels, choice of the exchange degenerate pair (K^*, K^{**}) is unique. Similarly, the isospin 1 exchange degenerate pair (ρ, A_2) is the only possibility in $\overline{K}K$ channels. Several trajectories may couple at the $\overline{p}p$ vertex. Obvious candidates are the $I = 0$ exchange-degenerate pair (ω, f) and the $I = 1$ exchange-degenerate pair (ρ, A_2). There is a strong π exchange amplitude, also. Because I am interested in an asymptotic effect, I retain only the highest lying trajectories (ω, f) and (ρ, A_2). For the moment, I ignore the fact that (ω, f) and (ρ, A_2) correspond to different isospin amplitudes, and I use a generic trajectory α_t to denote both sets. I return to this isospin question below.

---

* Throughout the following argument, these graphs may be thought of as quark-duality diagrams (Rosner, 1969; Harari, 1969). It should be clear that I do not invoke any detailed properties of B_5 functions in constructing my case.

For each graph shown in Fig. 28, there is an explicit B_5 function. The amplitude for $K^+p \to K^o\pi^+p$ is simply

$$A(K^+p \to K^o\pi^+p) = K[B_5(a) + c_1B_5(b) + c_2B_5(c)] . \tag{48}$$

Kinematic factor K is irrelevant in this analysis. I will discuss real constants c_i below.** The amplitude for $K^-p \to \overline{K}^o\pi^-p$ is identical to that given in Eq. (48); however, the B_5 functions are evaluated at different values of the five Mandlestam variables.

Given the preliminary comments above, I now proceed to the heart of the argument.

---

* In quantitative fits to data (e.g., CRTT), it is necessary to adopt specific parametrizations for trajectory functions and to give them added imaginary parts. We do not need to make such choices here.

** Recall that in CRTT, $c_i = +1$. I do not make this choice here.

I am interested in contributions from the three graphs of Fig. 28 in the limit that $s_{K^+p} \to \infty$, t_{pp} is fixed, and $s_{K^o\pi^+} \approx M^2_{K^*(890)}$. I first state the answers, then explain how they are derived, and finally discuss their significance.*

$$B_5(a) \to (s_{K^+p})^{\alpha_t} f_a(t_{pp})\, g_a(s_{K^o\pi^+}) \;; \tag{49-a}$$

$$B_5(b) \to e^{-i\pi\alpha_t}(s_{K^+p})^{\alpha_t} f_b(t_{pp})\, g_b(s_{K^o\pi^+}) \;; \tag{49-b}$$

and

$$B_5(c) \to 0 \quad . \tag{49-c}$$

In graph (c), there is no trajectory coupling to $\bar{p}p$. Near small t_{pp}, therefore, graph (c) gives an exponentially vanishing contribution as $s_{K^+p} \to \infty$. This statement explains Eq. (49-c).

An important point to observe about Eq. (49-a) is that graph (a) provides a real production amplitude. That is, the Regge phase is 1, not $(1 \pm e^{-i\pi\alpha})$, nor $e^{-i\pi\alpha}$. This result is prescribed by duality, because there are no resonances in the K^+p or K^*p channels. This result is quite familiar and need not be explained further. In Eq. (49-a), function $f_a(t) \propto \Gamma(1 - \alpha_t)$; B_5 also gives some additional weak dependence on t_{pp}, associated with the K^+ Reggeon $\to K^o\pi^+$ vertex. I ignore this extra mild dependence on t_{pp}. The most important quantity in Eq. (49-a) is function $g_a(s_{K^o\pi^+})$. In the strict zero-width B_5 limit,

$$g_a(s_{K^o\pi^+}) \;\propto\; \frac{-1}{1 - \alpha(s_{K^o\pi^+})} \tag{50}$$

where $\alpha(s)$ is real. I "unitarize" this expression by replacing it with the Breit-Wigner form

---

* In functions g_a and g_b of Eq. 49, I suppress dependence on decay angles (θ and φ) of the $K\pi$ system, as measured in the $K\pi$ rest frame.

$$g_a(s_{K^o\pi^+}) \propto \frac{-\Gamma M}{M^2 - s_{K^o\pi^+} - i\Gamma M} \quad . \tag{51}$$

Here, Γ and M are full width and mass, respectively, of the $K^*(890)$ resonance.

I now discuss Eq. (49-b). As in (49-a), $f_b(t) \propto \Gamma(1 - \alpha_t)$, except for additional mild (and ignored) t dependence associated with the K^+ Reggeon $\to \pi^+K^o$ vertex. The important point to notice about graph (b) is that it has no K^* resonance poles in the final $K^o\pi^+$ mass variable.* In Eq. (49-b), the real, positive function $g_b(s_{K^o\pi^+})$ is a smooth, featureless distribution. Graph (b) provides coherent background under the K^* pole of graph (a). Graph (b) does contribute to leading order asymptotically as $s_{K^+p} \to \infty$ with t_{pp} fixed.** In contrast to graph (a), however, (b) provides an amplitude with rotating phase, $e^{-i\pi\alpha_t}$. This result can be derived analytically using techniques developed in Bialas and Pokorski (1969). However, it is easy to obtain heuristically also. First, observe that if $s_{K^o\pi^+}$ and t_{pp} are bounded, then variables $t(K^+ \to \pi^+)$ and $t(K^+ \to K^o)$ are also constrained to be relatively small. As $s_{K^+p} \to \infty$, therefore, only the variables $t(p \to K^o)$ and $s_{p\pi^+}$ become large. Second, note that all variables in graph (b), except $s_{p\pi^+}$, are in the momentum transfer region and, therefore, are negative. The only way graph (b) can develop an imaginary part is through resonances (Δ_δ) which are present in the variable $s_{p\pi^+}$. Finally, in taking the limit $s_{K^+p} \to \infty$, we average over resonances present in $s_{\pi^+ p}$. The usual dual-Regge-average over resonances gives precisely a rotating phase: $e^{-i\pi\alpha} s^{\alpha}$.

---

* The (K^*, K^{**}) trajectory in (b) is exchanged (in the "u-channel"). In (a), (K^*, K^{**}) is in the direct ("s") channel.

** This is almost obvious from the fact that graph (b) has the leading t-channel trajectory coupling to the $\bar{p}p$ vertex. Explicit formulas for asymptotic limits of B_5 graphs are given by Bialas and Pokorski (1969).

The physical content of Eq. (49) may now be discussed. Upon substitution into Eq. (48), I derive

$$A(K^+ p \to K^* p) \;\propto\; s^{\alpha_t}\, \Gamma(1 - \alpha_t) \left[\frac{-\Gamma M}{M^2 - s_{K^0\pi^+} - i\Gamma M} + e^{-i\pi\alpha_t} g_b c_1 \right] \quad (52)$$

Observe that the K^* resonance term and the rotating phase background term interfere in both real and imaginary parts.* After I integrate over the K^* band, however, only the interference term involving imaginary parts is significant.** Therefore, for $K^+ p \to K^* p$, I obtain a major interference effect proportional to $(c_1 \Gamma_{K^*} g_b \sin \pi\alpha_t)$. The K^* signal is enhanced*** as a result of constructive interference of K^* with the entire spectrum of Δ resonances in the final state of $K^+ p \to K^0 \pi^+ p$. The B_5 model provides us with a dual, crossing-symmetric way to estimate effects of interference between competing two-particle sub-systems in the final-state. Interference occurs not only at the intersection point of two obvious resonance bands in a Dalitz plot, but also throughout the mass-spectrum. Duality specifies that, on the average, the phase in the $\pi^+ p$ sub-system is given by $e^{-i\pi\alpha_t}$, at large values of $\pi^+ p$ mass. This phase is not random. Therefore, there is coherent interference between the $K^*(890)$ amplitude, with definite Breit-Wigner phase, and the "background" term, with phase $e^{-i\pi\alpha_t}$ built up from N^* resonances. The interference effect is sizeable, as can be seen by a comparison of cross-sections given in columns 2 and 3 of Table II. Dual models suggest strongly, therefore, that there is no simple way to separate the $K^*(890)$ from its coherent background. A study of the entire Dalitz plot is required.

---

* Although I remarked above that spin is an irrelevant complication, the careful reader will note here that to obtain interference, it is essential that both the K^* resonance term and the rotating phase background term be in the same helicity amplitude. This is indeed the case. Although not shown here explicitly, Eq. (52) applies separately for each helicity amplitude. I thank Robert Diebold for remarking that this point deserved clarification.

** This is not completely true because graph (b) does not provide exactly a rotating phase factor, and because g_b is not a constant.

*** or diminished, depending on the sign of c_1.

A very similar analysis may be carried out for $K^- p \to \overline{K}^o \pi^- p$. Here both the $\overline{K}^*$ resonance graph (Fig. 29a) and the (Y^*) background graph (Fig. 29b) contribute a production amplitude with rotating Regge phase $e^{-i\pi\alpha_t}$. Therefore, the common phase may be factored out completely, and I derive

$$A(K^- p \to \overline{K}^* p) \propto e^{-i\pi\alpha_t} s^{\alpha_t} \Gamma(1 - \alpha_t) \times \left[\frac{-\Gamma M}{M^2 - s_{K^o\pi^+} - i\Gamma M} + g_b c_1\right] . \qquad (53)$$

Because interference now occurs primarily with the real part of the $\overline{K}^*$ Breit-Wigner term, its overall effect may integrate to a negligible contribution.* Note, however, that the position of the $\overline{K}^*$ peak will be shifted. Indeed, the explicit CRTT parametrization gives a downward shift of 5 MeV.

Combining K^* and $\overline{K}^*$ results, I predict that

---

* This is not completely true because graph (b) does not provide exactly a rotating phase factor, and because g_b is not a constant.

$$\frac{\left[\frac{d\sigma}{dt}(K^+p \to K^*p) - \frac{d\sigma}{dt}(K^-p \to \bar{K}^*p)\right]}{\left[\frac{d\sigma}{dt}(K^+p \to K^*p) + \frac{d\sigma}{dt}(K^-p \to \bar{K}^*p)\right]} \propto c_1 \Gamma_{K^*} \; . \tag{54}$$

Note, especially, that the difference[*] between Kp and $\bar{K}$p reactions remains finite at asymptotic energies, even though the trajectories exchanged, (ω, f_o) and/or (ρ, A_2), are perfectly exchange degenerate. This result may be contrasted with expectations for the difference between $K^-p \to \bar{K}^on$ and $K^+n \to K^op$ or between $K^-p \to \pi^-\Sigma^+$ and $\pi^+p \to K^+\Sigma^+$. For these stable-particle processes, the difference[*] between cross-sections for pairs related by line reversal must go to zero asymptotically.[**] Explicit values computed for K^* and $\bar{K}^*$ cross-sections are given in Table II, columns 3 and 4.

3.3.2 The Sign of the Symmetry Breaking.

The sign of real constant c_1 appearing in Eq.(54) is of considerable interest. As remarked above, with a few exceptions, data favor $\sigma_{\text{real}} > \sigma_{\text{rotating}}$. There are at least two ways to obtain the sign theoretically. Let us first examine the method followed by CRTT, and then I will present an alternate procedure.

Recall that CRTT determine $c_1 = +1$ by demanding that the N^*

---

[*] Actually, difference divided by the sum.

[**] In fact, the four-point model (B_4) predicts a difference in values of $d\sigma/dt$ which is proportional to $s^{2\alpha_t - 3}$, if t channel trajectories α_t are exchange degenerate. This difference arises because the asymptotic expansions of (s, t) and (u, t) terms differ in non-leading order as $s \to \infty$. In most other models also, if trajectories are exchange-degenerate, cross-sections differ only in non-leading order.

trajectory, in the $\pi^- p$ subchannel of $K^- p \rightarrow K^0 \pi^- p$, have precisely positive signature, appropriate to N_α. Therefore, according to Eq. (54), CRTT necessarily predict

$$\sigma(K^+ p \rightarrow K^* p) > \sigma(K^- p \rightarrow \bar{K}^* p) \ , \tag{55}$$

in agreement with data; but they also predict

$$\sigma(K^0 p \rightarrow K^* p) > \sigma(\bar{K}^0 p \rightarrow \bar{K}^* p) \ , \tag{56}$$

in disagreement with data. The CRTT model cannot accommodate both $K^\pm p$ data and the SLAC $K_L p$ data, as I have just shown analytically. Had CRTT chosen instead $c_1 = -1$, they would have obtained negative signature in the N^* channel, appropriate to the N_γ trajectory. Moreover, with $c_1 = -1$, although they might have obtained agreement with SLAC data, Eq. (54) shows that CRTT would necessarily fail to reproduce* the fact that $\sigma(K^+ p) > \sigma(K^- p)$. Incidently, with $c_1 = +1$, CRTT must obtain (correctly) the result

$$\sigma(K^+ p \rightarrow K^0 \Delta^{++}) > \sigma(\bar{K}^0 p \rightarrow K^- \Delta^{++}) \ . \tag{57}$$

Our analytic exercise indicates that if we want to achieve a B_5 fit to $K^\pm p$ data as well as to SLAC $K_L p$ data, then it is necessary to include at least six B_5 functions. Three of these will be exactly the functions used by CRTT. The other three will be similar, except for the fact that $c_1 = -1$. The relative contribution of these two sets of three functions must be determined by fitting. However, before attempting anything of that sort, we may ask whether there is more we can learn analytically about the second set of B_5 functions. This question leads me to the second method I mentioned for determining the sign of c_1.

---

* Although it is clear analytically, I do not claim to understand physically why there should be this mysterious connection between signature in the N^* channel and the sign of the difference between $\sigma(K^+ p \rightarrow K^* p)$ and $\sigma(K^- p \rightarrow \bar{K}^* p)$. However, it is an intriguing example of hidden treasure in B_5.

Let us examine the graphs shown in Fig. 30. These graphs are obtained by factoring the original B_5 amplitudes (Fig. 28) at the exchanged Regge pole; they represent scattering of Reggeon α_t with K^+ to produce $K^o\pi^+$. Reggeon α_t couples to the $\bar{p}p$ vertex and may have either isospin 0 or 1. If $I_t = 1$ (corresponding to $\alpha_t = \rho, A_2$) then, in order that there be no exotic isospin 3/2 poles in the $K\pi$ system, we must add four-point amplitudes corresponding to Fig. 30a and Fig. 30b with relative minus sign. Therefore, $I_t = 1$ requires $c_1 = -1$. However, if $I_t = 0$ (ω, f), symmetry requires $c_1 = +1$. Using this second method, we see quite clearly, therefore, that to predict the sign of the line-reversal violation, we must know whether (ρ, A_2) or (ω, f) exchange dominates K^* production. Empirically, (ω, f) dominance is well-established; therefore, I assert that $c_1 = +1$ in Eq. (54), in agreement with data.

Observe, however, that $I = 0$ (ω, f) exchange cannot be the whole story. Because $\sigma(\bar{K}^o p \to \bar{K}^* p) > \sigma(K^o p \to K^* p)$, SLAC data indicate a definite need for terms with $c_1 = -1$; i.e., some $I = 1$ exchange at the $\bar{p}p$ vertex. Either (ρ, A_2) or π may be contemplated. Density matrix elements of the K^* favor (ρ, A_2). On the other hand, if we take seriously the highest energy points in Fig. 26, we might be tempted to think that $\sigma(K^*) < \sigma(\bar{K}^*)$ is only a low energy effect. Thus, we might try a fit with only π exchange as the $I = 1$ candidate. Of course, π exchange implies large absorption corrections, which present additional intricacy. Sorting things out should be entertaining. In either case, whether π or (ρ, A_2) is chosen, a new method for handling spin will have to be devised. The CRTT kinematic factor is an appropriate representation of the spin coupling of (ω, f) to $\bar{p}p$, but it is not satisfactory for either π or (ρ, A_2).

3.3.3 Other Predictions.

The discussion above about the sign of c_1 points to an interesting correlation between isospin (and signature) of dominant exchanges and systematics of violation of line reversal symmetry. It shows also that to predict whether $\sigma_{\text{real}} > \sigma_{\text{rotating}}$, or vice-versa, we need more information than simple duality. Nevertheless, the procedure is quite straightforward, at least for production of meson resonances. For production of N^* or Y^* resonances, prediction of the sign of c_1 requires that some attention be paid to spin complications. For both meson and baryon resonance production, I prefer not to lengthen this paper by including details leading to specification of the sign of c_1. Therefore, I limit myself here to statements concerning absolute values of differences.

A few predictions follow.

$$\left|\frac{d\sigma}{dt}(K^+p \to K^*p) - \frac{d\sigma}{dt}(K^-p \to \bar{K}^*p)\right| \propto \Gamma_{K^*} \cdot \Sigma_{K^*} \tag{58}$$

$$\left|\frac{d\sigma}{dt}(\pi^+p \to K^+Y^{*+}) - \frac{d\sigma}{dt}(K^-p \to \pi^-Y^{*+})\right| \propto \Gamma_{Y^*} \cdot \Sigma_{Y^*} \tag{59}$$

$$\left|\frac{d\sigma}{dt}(K^+p \to K^o\Delta^{++}) - \frac{d\sigma}{dt}(\bar{K}^op \to K^-\Delta^{++})\right| \propto \Gamma_{\Delta} \cdot \Sigma_{\Delta} \ . \tag{60}$$

In these three equations and in all subsequent similar equations, symbol Σ_i appearing on the right hand side represents the sum of the two differential cross-sections whose difference is given on the left hand side. Equations similar to the three above are derived easily for other K^*, N^*, and Y^* resonances. I remark, however, that

$$\left|\frac{d\sigma}{dt}(K^-p \to \underset{\lfloor\!\to K^-\pi^+}{\bar{K}^*}n) - \frac{d\sigma}{dt}(K^+n \to \underset{\lfloor\!\to K^+\pi^-}{K^*}p)\right| \to \frac{1}{s}\ \Sigma_{K^*} \ . \tag{61}$$

This latter difference vanishes asymptotically because, for $K^+n \to K^+\pi^-p$ and its crossed process $K^-p \to K^-\pi^+n$, a background graph (b) does not exist.* Nevertheless, if we examine instead the neutral decay modes, we observe that

$$\left|\frac{d\sigma}{dt}(K^-p \to \underset{\llcorner\!\to \bar{K}^0\pi^0}{\bar{K}^{*}} n) - \frac{d\sigma}{dt}(K^+n \to \underset{\llcorner\!\to K^0\pi^0}{K^{*}} p)\right| \propto \Gamma_{K^*}\,\Sigma_{K^*} \ . \qquad (62)$$

In other words, for $K^+n \to K^0\pi^0p$ and its crossed-process $K^-p \to \bar{K}^0\pi^0n$, the background graph does exist. The astonishing contrast between Eqs. (61) and (62) would appear to violate fundamental notions about the definition of a resonance. However, bear in mind that when we write symbol K^*, we mean both the "proper" K^* resonance and the inseparable coherent background. Experimentally, it is not possible to subtract coherent background. The difference between Eqs. (61) and (62) is brought about by the fact that

$$2\,\frac{d\sigma}{dt}(K^+n \to \underset{\llcorner\!\to K^0\pi^0}{K^{*}} p) \neq \frac{d\sigma}{dt}(K^+n \to \underset{\llcorner\!\to K^+\pi^-}{K^{*}} p) \ . \qquad (63)$$

Equality in Eq. (63) is predicted if the K^* system has pure isospin 1/2; inequality results because of different background interference in the $K^0\pi^0$ and $K^+\pi^-$ charge states. The coherent background may have both $I = 3/2$ and $I = 1/2$ and will generally be a different mixture in the two reactions. We expect such "exotic" effects to show up more clearly as data become available for experiments with higher statistics.

As a final example of effects wrought by background interference,

---

* It would require an exotic $I = 3/2$ trajectory in the $K\pi$ channel. Note that no mass shift is predicted, either, for neutral $\bar{K}^*$ decaying into $K^-\pi^+$.

I consider reactions $\pi^+ p \to \pi^o \Delta^{++}$ and $\pi^+ p \to \pi^+ \Delta^+$. Both I = 1 and I = 2 amplitudes may be present in the t channel; I = 2 is exotic and is presumably suppressed. For I = 1, only, $\sigma(\Delta^{++})/\sigma(\Delta^+) \equiv 3/2$. I remark, however, that coherent background in the Δ^{++} and Δ^+ bands is likely to be very different. Even with only pure I = 1 exchange contributions, this inseparable interference effect will destroy the predicted ratio of cross-sections. If large violation of this isospin prediction is observed, naive analysis of data, without an understanding of coherent background interference effects, could lead one to postulate an excessively large isospin 2 amplitude (c. f., Boyarski, 1970).

Let us now discuss to what extent these predictions are independent of the B_5 model. It should be apparent that we have used very little of the explicit structure of B_5 amplitudes. First, we have used only single-Regge limits of B_5 functions. These asymptotic energy and phase predictions (either s^{α} or $e^{-i\pi\alpha} s^{\alpha}$) are certainly more general than B_5. Second, we have relied on the B_5 prescription for adding different resonances in a dual fashion. This is important, because it assures us that we are not double counting nor violating other dual restrictions when we combine $\overline{K}^*$, Y^*, and N^* effects in the final state of $\overline{K}p \to \overline{K}\pi p$. Presumably this duality manifest in B_5 is also more general than the model. The third important step in our argument involves not B_5 per se, but the way in which we unitarize the model. This step is the one which leads from Eq. (50) to Eq. (51). Observe that we have "unitarized" each graph in Fig. 28 (or Fig. 29) separately, rather than the amplitude as a whole. This is obviously a weak point in our analysis, but lacking a complete theory, we have little choice. On the positive side of the ledger, we have accommodated crossing symmetry, duality, Regge-behavior, and approximate unitarity. The interference effects we obtain are quite intriguing and warrant experimental investigation.

3.3.4 Experiments.

There has been considerable interest in confronting predictions of exchange-degeneracy with data. Failures of line-reversal symmetry are certainly observed at low-energy. However, for $p_{lab} \geq 10$ GeV/c, indications are that differential cross-sections become equal for pairs of stable-particle processes related by line reversal. Data on quasi-two-body processes are as yet inadequate for testing my assertion that line-reversal symmetry is not obeyed for these reactions. Nevertheless, there are at least qualitative indications of differences between purely stable particle reactions and resonance production processes. Indeed, at $p_{lab} \simeq 14$ GeV/c, whereas $\sigma(\pi^+ p \to K^+ \Sigma^+) \simeq \sigma(K^- p \to \pi^- \Sigma^+)$, $\sigma(K^- p \to \pi^- Y^{*+}) \simeq 1.6\, \sigma(\pi^+ p \to K^+ Y^{*+})$ (A. Bashian et al., 1970). Furthermore, over the present range of energies, $\sigma(K^+ p \to K^* \Delta^{++})$ and $\sigma(K^- n \to \overline{K}^* \Delta^-)$ differ considerably $(\frac{\sigma(K^+)}{\sigma(K^-)} \geq 1.5)$. Although errors are large, a plot of the two cross-sections gives no indication that they are approaching a common value.[*]

Some new experimental investigations of obvious value are listed below.

a. Most crucial is a systematic study of differential cross-sections for all processes related by line-reversal. Both two-body and quasi-two-body reactions should be examined. Absolute normalization and energy dependence of $d\sigma/dt$ should be measured carefully from 4 to 20 GeV/c for $0 < |t| < 1$ (GeV/c)^2, with care taken to eliminate systematic errors. For example, it is important to ascertain whether there is indeed a quantitative difference between Y^* production reactions and similar processes in which Σ^+ is produced. More precisely, it will be intriguing to see whether Eq. (59) is supported while, at the same time,

---

[*] I am grateful to Brian Musgrave for this remark.

$$\left|\frac{d\sigma}{dt}(\pi^+ p \to K^+\Sigma^+) - \frac{d\sigma}{dt}(K^- p \to \pi^-\Sigma^+)\right| \to \frac{1}{s}\,\Sigma_\Sigma \tag{64}$$

b. Our interference effect is predicted to be most pronounced in the resonance bands. Therefore, we expect, for example

$$\left|\frac{d\sigma}{dt}(K^+ p \to (K^o\pi^+)p) - \frac{d\sigma}{dt}(K^- p \to (\overline{K}^o\pi^-)p)\right| \tag{65}$$

$$\ll \left|\frac{d\sigma}{dt}(K^+ p \to K^* p) - \frac{d\sigma}{dt}(K^- p \to K^* p)\right| .$$

Here, $(K\pi)$ denotes an interval of $K\pi$ mass outside obvious resonance bands. At a given incident p_{lab}, it would be valuable to compare entire $(K\pi)$ and $(\overline{K}\pi)$ mass distributions directly with each other. This should be done without subtracting N^* or Y^* events from the sample. The only selection of relevance is a cut on the momentum transfer to the $(K\pi)$ system.

c. Although in b above, we indicate that coherent interference is stronger at the position of a resonance than it is away from resonance, we caution against the usual assertion which holds that once prominent resonances are subtracted from a sample, then other interference effects can be ignored. With considerable experimental support from 2 → 2 processes, duality suggests that resonances in a given channel build up a smooth high energy amplitude with definite Regge phase. This is presumably true in 2 → 3 processes also and is the basis for the interference effect we discuss in this section. In analyses of 2 → 3 reactions, these dual restrictions should be kept in mind; qualitative guidance from the B_5 model can lead to more meaningful categorization of events into various quasi-two-body subsamples.

3.4 Allowed and Forbidden Quark-Duality Diagrams for the $\bar{K}N\Lambda\pi\pi$ System.

Petersson and Törnqvist (1969) were the first people to employ B_5 amplitudes in the analysis of a production experiment. They studied

$$K^- p \to \Lambda \pi^+ \pi^- \quad . \tag{66}$$

In a subsequent paper, Törnqvist (1970) examined

$$\pi^+ p \to K^+ \pi^+ \Lambda \quad , \tag{67}$$

which is related to (66) by crossing symmetry. Finally, Hoyer, Petersson, and Törnqvist (1970) obtained a reasonable fit to data from a set of five different processes which are related to (66) by crossing and isospin.*

A remarkable conclusion emerges from these fits. The authors report that their results favor conclusively a set of B_5 functions which correspond to quark-duality diagrams forbidden by the Rosner-Harari rules (Rosner, 1969; Harari, 1969). Fits with allowed diagrams give a much poorer representation of data. If valid in a framework more general than B_5, this conclusion would have important significance. Therefore, it is appropriate here for us to examine somewhat carefully the analysis and basis for the conclusions.

I find that the conclusion is not substantiated, even within the B_5 framework. In the fits with diagrams allowed by Rosner-Harari rules, discrepancies may be attributed to improper unitarization of B_5 amplitudes. I will show this below, but first let me review briefly ideas behind the Rosner-Harari rules.

---

* Another B_5 fit to $K^- p \to \pi\pi\Lambda$ is given by Adjei et al., 1971. They use $U(6,6)$ to develop a different approximate treatment of baryon spin. The spin problem, without fits, is studied also by Hirshfeld and Schmidt, 1970.

3.4.1 Quark-Duality Diagrams and Rosner-Harari Rules for B_5.

In order to construct quark-duality diagrams for a given reaction, we begin by representing each external particle by its quark content. Mesons are $q\bar{q}$ pairs. Therefore, a meson can be represented by a pair of lines; thus,

meson ~

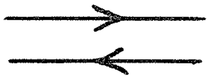

.

Direction of the arrow gives the "direction in which the quark travels." Baryons are (qqq) triplets; therefore,

baryon ~

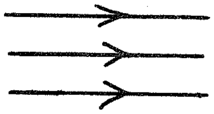

.

Quark-duality diagrams are then constructed by connecting together quark lines of various external particles. Of course, in making this connection, a λ quark from one particle is joined to a λ quark from another particle. The same is true for n and p quarks; one does not join, for example, a λ quark to a p quark. Moreover, no quark lines start and end at the same external particle.

In general, for a 2 → 2 process, one may draw up to three different quark-duality diagrams. These correspond to the (s, t), (s, u), and (t, u) terms in the language of Veneziano four-point phenomenology. For a 2 → 3 process, there can be as many as twelve different quark-duality diagrams. These are in one-to-one correspondence to each of the twelve topologically non-equivalent ways to order five external spokes (particles) emanating from a central hub (reaction vertex).

A quark-duality diagram is not drawn if the quantum numbers of two adjacent external particles add up to an exotic value (e.g., I = 3/2, 2, etc. for mesons). This is obvious because the exchange particle (attached to the exotic external pair in the diagram) would lie on an exotic trajectory, none of which is known to exist. Therefore, for the reaction $K^- p \rightarrow \pi^+ \pi^- \Lambda$, and all processes related to it by crossing symmetry, one may exclude a total of six graphs (potential duality diagrams) in which particles K^- and π^+ are adjacent.

For $\bar{K}p \rightarrow \Lambda\pi\pi$, the six remaining quark-duality diagrams are shown in Fig. 31. In a second variety of forbidden duality graphs, states internal to the diagram are exotic, even though all pairs of adjacent external particles have non-exotic quantum numbers. This possibility is illustrated by graph (a) and (b) of Fig. 31. A dotted line is also drawn on each of these graphs; it indicates a "cut" made across an internal state in the duality diagram. The internal state is composed of five quarks $(qqqq\bar{q})$ and is, thus, not an allowed state in the usual quark-model. Graphs (a) and (b) are forbidden by the rules drawn up by Rosner and Harari. The basic physical idea behind this exclusion is that all states which couple strongly in hadronic processes must have non-exotic representation in the quark model.

The Rosner-Harari rules make non-trivial predictions which can be examined experimentally. For example, the rules imply that the Regge-pole exchange amplitude for $K^- p \rightarrow \pi^- \Sigma^+$ is purely real at large s and small t. In the absence of cuts and so forth, this means that polarization should be zero. For further discussion of uses of duality diagrams in $2 \rightarrow 2$ scattering, consult Jackson (1970).

In $2 \rightarrow 3$ body processes, the Rosner-Harari rules can be invoked to reduce the number of possible B_5 graphs which should be considered. One may choose not to write B_5 graphs for those topological orderings of external particles which correspond to forbidden-duality diagrams. Applied to $\bar{K}p \rightarrow \pi\pi\Lambda$, this rule leaves us with four B_5 graphs, a reduction from the original six.

3.4.2 $\overline{K}N\Lambda\pi\pi$; The Approach of Törnqvist and Collaborators.

As remarked above, Törnqvist and collaborators try different B_5 fits to data on $K^-p \to \Lambda\pi\pi$ and processes related to it by crossing and isospin. I will not repeat details which can be found adequately in the original papers. It suffices to remark that they examine two different amplitudes:

$$A_{RH} \propto \left[\alpha_1 B_5(c) + \beta_1\left(B_5(d) + B_5(e)\right) + \gamma_1 B_5(f)\right] \tag{68}$$

$$A_{HPT} \propto \left[\alpha_2 B_5(a) + \beta_2 B_5(b) + \gamma_2 B_5(c)\right] \quad . \tag{69}$$

Symbol x in $B_5(x)$ labels the graphs of Fig. 31. In A_{RH}, only those four B_5 graphs are used which correspond to duality diagrams allowed by the Rosner-Harari rules. In amplitude A_{HPT}, forbidden graphs are used. Parametrizations of trajectories and values for the constants α_i, β_i, and γ_i are given and discussed in Hoyer, Petersson, and Törnqvist (1970).

Fits obtained with the two different amplitudes are compared with data in Fig. 32. Dashed curves were obtained from A_{RH} and solid lines computed from the forbidden amplitude A_{HPT}. Plots of $d\sigma/d\cos\theta$ for $\pi^+p \to K^+Y_1^*$ in Fig. 32a and b indicate that the smooth prediction of the A_{HPT} model agrees well with data. On the other hand, A_{RH} predicts an angular distribution with considerable structure not seen in the data. Törnqvist emphasizes that the success of A_{HPT} contrasted with the failure of A_{RH} to reproduce this angular distribution is the "most significant test of [the] anti-Harari-Rosner hypothesis."

3.4.3 Criticism of the Anti-Rosner-Harari Conclusion.

It is easy to understand analytically qualitative features present in theoretical curves of Fig. 32. First, curves are forced to vanish at $\cos\theta = \pm 1$ and at $t' = 0$ because of the choice of kinematic factor.* Second, for $\pi^+ p \to K^+ Y^{*+}$, A_{HPT} predicts no structure in $d\sigma/d\cos\theta$ because, in this model, there is no trajectory which couples in the direct $(\pi^+ p)$ channel. Structure in $d\sigma/d\cos\theta$ from A_{RH} is related to the fact that the Δ_δ trajectory couples strongly in allowed duality diagrams (d) and (e). Indeed, for $\pi^+ p \to K^+ Y^{*+}$, the B_5 amplitude collapses approximately to a sum of two B_4 terms $\left(\text{here, } B_4(x, y) = \frac{\Gamma(x)\Gamma(y)}{\Gamma(x+y)}\right)$

$$A_{RH} \propto B_4\left(\frac{3}{2} - \alpha_\Delta(s),\ 1 - \alpha_{K^*}(t)\right) + B_4\left(\frac{3}{2} - \alpha_\Delta(s),\ 1 - \alpha_\Lambda(u)\right) \quad . \tag{70}$$

Because background graphs** are present, Eq. (70) is not exactly correct; however, for present purposes, it is a reasonable approximation. The background terms are additive.

As expressed in Eq. (70), A_{RH} is a sum of two terms, the first of which has only a forward peak near $t = 0$ ($\cos\theta = +1$), and the second only a backward peak near $\cos\theta = -1$. It seems evident, therefore, that the resultant angular distribution will have a dip somewhere near $\cos\theta = 0$ (unless one of the two contributions is overwhelming). This latter conclusion depends crucially, however, on exactly what happens to the structure of the amplitude when it is "unitarized."

---

* The kinematic factor used by Törnqvist is identical to that used by CRTT; see subsection 3.2.

** I. e., graphs (c) and (f) which do not have a Y_1^{*+} pole.

It is not possible, of course, to develop an unambiguous procedure for unitarizing B_4 or B_5 amplitudes at ~ 2 - 3 GeV/c, where several inelastic channels are open. The trick used by Törnqvist and collaborators is to add an imaginary part to trajectories. This method, the same as that used by Lovelace (1968) and by CRTT (see subsection 3.2), preserves exactly the momentum transfer (or $\cos\theta$) dependence of the original B_4 or B_5 amplitude. More precisely, the first term of Eq. (70) vanishes[*] when $\frac{5}{2} - \alpha_\Delta(s) - \alpha_{K^*}(t) = 0, -1, \ldots, -N$. Consequently, there are functions $t = f_N(s)$ which specify values of t at which the first term is zero. These functions are essentially unchanged if an imaginary part is added to $\alpha_\Delta(s)$. The only difference is that zeroes become complex zeroes rather than remaining purely real.

We may entertain other methods of unitarization. A good example is provided by the Lovelace-Wagner K-matrix procedure discussed in subsection 2.2.4. Although the K-matrix procedure is not applicable for $\pi^+ p \to K^+ Y^*$ at 2 GeV/c, I think the $\pi^+\pi^-$ example developed in subsection 2.2.4, shows clearly that proper unitarization can change angular distributions drastically.[**] Therefore, I suggest that the failure of A_{RH} noted in Figs. 32a and b is a failure of the ad-hoc method of adding imaginary parts to trajectories. I do not believe any test has been made of the Rosner-Harari rules.

---

[*] These are the lines of zeroes discussed in subsection 2.2.

[**] Another, simpler way to change angular distributions is through addition of satellite terms. These change the parent to daughter ratio, and, therefore, allow one to adjust angular distributions almost at will. This technique is used by Y. Cho, Argonne National Laboratory, in a successful fit to $\bar{K}N \to \pi\pi\Sigma$. He uses only diagrams which obey the Rosner-Harari rules.

Other discrepancies between data and the Rosner-Harari alternative may be dismissed in a similar fashion. A short list follows.

a. Amplitude A_{RH} seems to predict that the total cross-section $\sigma(\pi^+ p \rightarrow K^+ Y^*)$ has a strong oscillating component as a function of energy, whereas A_{HPT} gives a smooth curve. The difficulty here is that when imaginary parts are added to trajectories, all states in a given resonance tower acquire the same total width. In reality, daughter states are much more broad and are displaced in mass from parents. These two effects (obtained by proper unitarization) smooth out oscillations.

b. As a byproduct of using only allowed duality diagrams, we are forced to install Y_1^* (1385) on an exchange degenerate trajectory. This implies a bump in $(\Lambda\pi^-)$ and $(\Lambda\pi^+)$ mass spectra at the position of Y_1^* (1765). The bump is not seen in data and not obtained in the A_{HPT} model (in which Y_1^* is not exchange-degenerate). Again, the fault lies in interpretation. The large bump generated by the A_{RH} model, with imaginary trajectories, is an incorrect superposition of parent and daughter signals. The daughters should be spread out and displaced.

c. Amplitude A_{RH} will have a substantial Δ_δ exchange term in (e.g.) $K^- p \rightarrow \pi^- Y_1^*$. A backward peak is not seen in data, Fig. 32 (d-f). However, it is well known that Δ_δ exchange is anomalously small in Nature (Berger and Fox, 1969). Although no satisfactory explanation for this problem exists, it is clearly not a fault of the Rosner-Harari rules.

3.4.4 A Virtue of the Rosner-Harari Alternative.

Having presented a set of apologies for the Rosner-Harari alternative, let me now demonstrate a distinct advantage one gains by using only these allowed diagrams.

Hoyer, Petersson, and Törnqvist remark that their (forbidden) model predicts

$$\sigma(K^- p \to \pi^- Y^{*+}) = \sigma(\pi^+ p \to K^+ Y^{*+}) \tag{71}$$

whereas, data indicate that

$$\sigma(K^- p \to \pi^- Y^{*+}) = 2\sigma(\pi^+ p \to K^+ Y^{*+}) \tag{72}$$

in the energy range 3 - 10 GeV/c. Moreover, if they normalize to $\sigma(K^- p \to \pi^- \pi^+ \Lambda)$, they predict too large a cross-section for the crossed reaction $\pi^- p \to \pi^- K^+ \Lambda$.

By contrast, I find that the allowed diagrams reproduce correctly the appropriate relative normalizations. If we use the analytic argument developed in subsection 3. 3, we can see easily why the present result follows. In amplitude A_{HPT}, favored by Törnqvist and collaborators, there is no background graph which can interfere with the Y_1^* graphs to produce a separation in cross-section between processes related by line-reversal. However, in A_{RH}, the necessary background is supplied by graph (c) of Fig. 31. As in subsection 3. 3, I predict $\sigma_{real} > \sigma_{rotating}$, in agreement with Eq. (72).

In summary, then, relative normalizations of reactions related by crossing are predicted correctly if we use amplitude A_{RH} (Eq. (68)), but not if A_{HPT} is used. In addition, as explained in the previous sub-sections, failure of A_{RH} to fit certain experimental distributions can be understood in terms of difficulties with unitarity, not with the Rosner-Harari rules. It would be valuable to document systematically any contradiction* of the Rosner-Harari rules. However, I do not believe existing analyses of $K^- p \to \Lambda\pi\pi$ and related processes indicate failure.

---

* For example, the rules forbid Ξ^* production in $\bar{K}p \to \Xi\pi K$. At 3. 3 GeV/c, the cross section for $\Xi^*(1530)$ production in this reaction is 12 ± 5 μb (Ross and Lyons, 1970).

3.5 What Should be Done Next With B_5 ?

My recommendations for future use of B_5 fall into two categories, corresponding to the literal and qualitative interpretation I mentioned in the introduction. I will treat each in turn.

I do not recommend that any new detailed fits be published until major technical advances are made in the treatment of spin and unitarity. As shown in this section, detailed fits with the five-point model have little proven quantitative relevance. Until major technical developments are made, the only option available is to increase the number of B_5 functions, in an effort to produce superficially better fits. This is a grim conclusion, because once the number of B_5 functions is increased, physical significance of fits becomes even more obscure. On the other hand, as I remarked earlier, the Veneziano model embodies more of the important principles of S-matrix theory than any previous model. I believe experimenters should understand these ideas and their simple realization in terms of the model. Fits to data may supply the necessary motivation for this learning process and be its inevitable by-product. Nevertheless, it should be clear from these statements that a critical attitude is indispensable. We may benefit from attempts to document systematically the successes and failures of the model in specific experimental situations, but we surely will not profit from a series of papers in which the only aim is to "dress-up" experimental distributions with meaningless theoretical curves.

I am considerably more positive with respect to qualitative uses of B_5. I am convinced that B_5 can bring a new dimension of understanding to bear on the analysis of Dalitz plots for $2 \rightarrow 3$ body processes. The model can also suggest significant improvements in present procedures for separating quasi-two-body reaction subsambles from a sample of

2 → 3 data. At the present time, duality constraints are essentially ignored by experimenters in their analyses of 2 → 3 body data. A few years ago, in 2 → 2 scattering, the lesson was learned that it is illegitimate to express a scattering amplitude as a sum of resonance terms and Regge-pole exchange terms. To do so is to count the same effect twice ("doubling-counting"; Dolen, Horn, Schmid, 1968). Analogous statements apply for 2 → 3 body reactions.

Terms which represent resonance (and background) contributions in different two-body channels of the 2 → 3 final state should not simply be added together to form an overall reaction amplitude. This popular type of analysis generally involves serious double counting. Although not suitable for detailed quantitative fits to the entire Dalitz-plot, dual models may be exploited at least for the restrictions they impose on scattering amplitudes in the vicinity of the intersection point of two prominent resonances on the plot. These restrictions will be qualitatively different in different reactions. For example, in $K^+p \rightarrow K^o\pi^+p$ (which has exotic quantum numbers in the initial state), terms corresponding to K^* and Δ resonances in the final state are additive in the overall amplitude (c.f., Fig. 28). Duality specifies only the relative phase of K^* and Δ poles. However, in $K^-p \rightarrow \bar{K}^o\pi^-p$, duality imposes a much stronger constraint; as illustrated in Fig. 29, the $\bar{K}^*$ and N^* resonance poles occur in the same B_5 function.

The discussion of subsection 3.3 provides a concrete example of a second type of qualitative use of B_5 in analyses of Dalitz plots. The idea that line-reversal symmetry is not valid for production processes, even asymptotically, is something which probably would not have occurred to anyone outside the framework of B_5. Other ramifications of this prediction deserve emphasis here. The effect results from inescapable coherent interference among states (not necessarily resonances!) in different two-body sub-channels of the final state. The interference effect appears to be a general manifestation of duality, more general than B_5. As well as its effect on relative normalizations, interference generates mass-shifts, skews mass-distributions, and alters significantly both production angular distributions and angular distributions in various two-particle rest frames. Therefore, these effects must be taken into consideration when studies are made of production mechanisms and of mass-splitting (e.g., $M(K^{*+}) - M(K^{*o})$). Furthermore, interference effects manifest in angular distributions are a serious complication in, for example attempts to extract $\pi\pi$ and $K\pi$ phase-shifts from $2 \rightarrow 3$ body data. The B_5 model does not yet supply a full quantitative alternative to present methods; however, it can now provide a good estimate of the magnitude of effects traditionally neglected.

With this new impetus from B_5, the development of better, practical methods for Dalitz plot analyses should blossom into a fertile field of endeavor.

4. Dual Models for Diffraction Dissociation.

Much speculation has centered about the interpretation of threshold enhancements which seem to be produced diffractively.* These enhancements** are known commonly as $A_1, A_3, Q, L, N^*(1400)$. No doubt others exist also. The question of interest is simply: Are they resonances or not? Dual models may shed new light on this issue.

4.1 Brief History of A_1.

Let us take A_1 as a particular example. This appears as an enhancement just above $\pi\rho$ threshold. For some time, it was thought that A_1 is a weak resonance supported by a large kinematic (Deck) background. This interpretation is difficult because both "resonance" and background appear to have spin-parity $J^P = 1^+$ (Kruse, 1971). On the other hand, the full width of the $\pi\rho$ mass distribution generated in simple Deck models is not as narrow as that of peaks observed experimentally; thus, it was also difficult to believe that the entire peak is kinematic background. This objection was removed by Berger (1968). In that and later papers, I showed that if the pion in the Deck diagram is Reggeized, then the predicted mass distribution is a reasonable representation of data, both in shape and absolute normalization. Chew and Pignotti (1968) subsequently invoked duality to assert that a kinematic enhancement, generated by particle exchange, is equivalent to a resonance. This statement would define the ambiguity out of existence, were it not for a few unusual ramifications. The first is that in my model, a Regge exchange amplitude is used at values of $\pi\rho$ subenergy near threshold. This lacks justification. The second is that the usual formulation of duality relates imaginary parts of Regge exchanges to resonances; pion exchange gives primarily a real exchange amplitude. Chew and Pignotti extend the application of duality in order to make statements about $|A|^2$ and not simply about Im A. Here, A denotes a scattering amplitude. Their extension has little support from studies of reasonably well understood 2 → 2 processes.* Therefore, debates over the resonance status of A_1 continue.

---

* See Berger (1969b) and papers cited therein. The same enhancements may be produced in non-diffractive processes, also. For example, backward production of A_1 in $\pi^- p \to pA_1^-$ is reported by Anderson et al. (1969). However, in this reaction and in every other situation in which they have been observed, the enhancements can be reproduced adequately as kinematical effects, rather than as resonances (Berger, 1969c).

** For an up-to-date review of the properties of A_1 and Q, consult U. Kruse (1971).

4.2 Opportunities with Dual Models.

Dual models present us with an opportunity to resolve the problem. Let us examine the diagram in Fig. 33. The dashed (P) line serves to indicate that the system (23) is produced diffractively. For the special case of A_1 production in reaction $\pi p \rightarrow \pi\rho p$, particles are identified in parentheses in Fig. 33; A_1 is a threshold enhancement in the (23) system.

Imagine that we construct a dual amplitude for reaction ab → 123. The amplitude should contain all known resonances present in the final state. For example, in the (23) channel, there may be an A_2 resonance as well as all recurrences of the pion (on the trajectory $\alpha_\pi(s_{23})$ which couples to $\pi\rho$). Furthermore, the amplitude will have a pion-exchange pole in the t_{b3} variable. It is this pion exchange term which supplies the usual Deck background. The advantage of the dual framework is that both Regge-exchange terms and direct channel resonances appear in the amplitude in an explicitly dual manner. In principle, therefore, we have an excellent framework in which to ask whether fits to experimental distributions require an A_1 resonance and/or an A_1 trajectory.

---

* Let A denote a Regge-pole exchange amplitude. The only processes for which $|A|^2$ remains a good approximation to data down near threshold are those for which the direct channel has no resonances (e.g. K^+p). This would suggest that A_1 is not a resonance!

Observe that the mere existence of dual models does not solve the problem of whether the A_1 is a resonance. Only data can decide, and so we must still fit data. Before fitting data, we are free to construct amplitudes which have explicit A_1 resonance poles as well as amplitudes which explicitly do not. However, we are not free to leave out pion exchange (pions are known to exist, and the coupling of $\rho \to \pi\pi$ is known to be large). The dual framework allows us to construct amplitudes which are meant to be a proper description of pion exchange, both in the high-energy (Regge) region and near threshold.

Unfortunately, these points are deemphasized in published papers on dual models for diffraction dissociation (Pokorski and Satz, 1970; J. Bartsch, 1970b). In these papers, it is assumed explicitly that threshold enhancements must be represented as resonance poles in dual models. To dispel this notion, I construct a simple counterexample. Subsequently, in subsection 4.4, suggestions are made for further investigations.

4.3 A Counterexample.

Although the Pomeron is not a simple exchange in dual models, it is convenient to make that assumption anyway. It is also made in papers cited above. Because I assume that incident energy is large, it is appropriate to think in terms of a Regge exchange approximation for the amplitude describing $ab \to 1(23)$. Therefore, interest centers on a parametrization of the diagram of Fig. 33. In this diagram, Pomeron exchange couples the upper $\bar{p}p$ vertex to the lower "dissociation" vertex.

Let us concentrate here on a description of the dissociation vertex. In my counterexample, I want no direct-channel poles near $\pi\rho$ threshold. Therefore, I exclude the A_1 trajectory explicitly. I must also eliminate the first recurrence pole of the pion trajectory. With $\alpha_\pi(s_{\pi\rho}) = b(s_{\pi\rho} - m_\pi^2)$, this first recurrence occurs at $\alpha_\pi(s_{\pi\rho}) = 1$ or $s_{\pi\rho}^2 \simeq 1$ (GeV)^2. The pion signature factor removes automatically the recurrence state on the leading trajectory ($J^P = 1^+$); however, to eliminate the daughter ($J^P = 0^-$), I add satellite terms. All this is done easily. The procedure is carried out, also, in a completely crossing-symmetric manner; whatever is done in the $\pi\rho$ direct (s_{23}) channel is done also in the exchange $\pi\rho$ exchange (t_{b3}) channel. In the second exchange (u) channel (variable t_{b2}) only the ρ-f trajectory appears. Finally, I ignore spin; this approximation is inconsequential for present purposes.

My amplitude has the form given in Eq. (73).

$$A_{\pi p\to\pi\rho p} = c\, s_{12}^{\alpha_P} \exp(\lambda t_{a1}) \Big[B_4\big(-\alpha_\pi(t_{b3}),\ 1 - \alpha_\rho(t_{b2})\big) + B_4\big(-\alpha_\pi(s_{23}),\ -\alpha_\pi(t_{b3})\big) + \ldots \Big] . \tag{73}$$

This amplitude has no resonances near the A_1 location. The three dots stand for uninspiring terms which are necessary to enforce crossing symmetry and to eliminate both parent and daughter states of the pion's first recurrence, as described above. The only term which is crucial in determining the $\pi\rho$ mass distribution near threshold is the first one shown explicitly in the square brackets of Eq. (73). The second term in the square brackets is displayed only because of the role it plays in generating the signature factor for the exchanged pion.

In the limit $s_{23} \to \infty$, with t_{b3} fixed, Eq. (73) becomes

$$A_{\pi p \to \pi \rho p} \longrightarrow c\, s_{12}^{\alpha_P} \exp(\lambda t_{a1}) \left[1 + e^{-i\pi\alpha_\pi(t_{b3})}\right] s_{23}^{\alpha_\pi(t_{b3})} \Gamma\left(-\alpha_\pi(t_{b3})\right) . \tag{74}$$

The amplitude has, therefore, correct (double) Regge behavior associated with a doubly-peripheral (π, P) exchange graph. It may also be normalized absolutely in terms of $g^2_{\rho\pi\pi}$ and $\sigma_{\pi p}$ (Berger, 1968, 1969b). Here, $g_{\rho\pi\pi}$ and $\sigma_{\pi p}$ are the coupling constant for $\rho \to \pi\pi$ and the πp total cross-section, respectively. In Eq. (73), the value $\lambda = 4$ is determined *a priori* from πN elastic scattering data.

The absolutely normalized cross-section $d\sigma/dM_{\pi\rho}$ ($M_{\pi\rho} = M_{23}$) computed from Eq. (73) is in good agreement with data,* as shown in Fig. 34. I use $\alpha_\pi(t) = 0.9\,(t - m_\pi^2)$, $\alpha_\rho(t) = 0.5 + 0.9t$ and $\alpha_P = 1$. Good agreement with data is obtained also for distributions (not shown here) in the variables s_{12}, t_{a1}, t_{b3}, and Treiman-Yang and Jackson angles (in both the $\pi\rho$ and πp rest frames). A partial wave analysis of the $M_{\pi\rho}$ enhancement yields predominantly $J^P = 1^+$, as observed experimentally (Kruse, 1971). It is obvious from this specific counterexample that *the A_1 bump can be explained perfectly well purely as π-exchange background, even within an explicitly dual framework.*

Should the above result be taken seriously? To a certain extent, the answer is yes. The calculation shows clearly that published papers on dual models for diffraction dissociation prove nothing about the A_1, Q, A_3, L, $N^*(1400)$ and other similar states. Anyone who prefers to doubt the resonance status of these enhancements can invoke my result to support his claim that the enhancements are not resonances, even when examined within a manifestly dual framework. On the other hand, technical facets of the calculation deserve improvement, as discussed in the next subsection.

---

* Data are taken from Brandenburg et al., 1971.

4.4 Further Investigation.

Approximations made in published papers and in subsection 4.3 fall into three categories: spin, unitarity, and the Pomeron. Significant improvement can be made in the way each of these is handled.

4.4.1 Spin.

In $\pi p \rightarrow \pi \rho p$, in which the incident pion dissociates into $\pi\rho$, neglect of proton spin is probably not a significant liability. A similar assumption is not valid, however, for baryon dissociation, such as $\pi N \rightarrow \pi(\pi N)$ and $NN \rightarrow N(\pi N)$. In these processes, proper treatment of baryon spin at the dissociation vertex would appear to be a crucial ingredient in answering questions about the resonance status of $N^*(1400)$. Even for $\pi p \rightarrow \pi \rho p$, however, improvements should be made in treating spin of the ρ and of the exchanged Pomeron. It is not difficult to write down dual amplitudes which represent properly the production of spin 1 particles (ρ). Moreover, rather than using a B_4 approximation for the lower vertex in Fig. 33, one may try B_5 amplitudes. In a B_5 approach, both $\rho(J^P = 1^-)$ and its s-wave daughter will be present. Inasmuch as A_1 has both $(\pi\rho)$ and $(\pi\varepsilon)$ components (Kruse, 1971), this is a more realistic representation of the experimental situation.

As to spin of the Pomeron, the problem can be approached on different levels. First, in spite of evidence to the contrary (Lovelace, 1971b), the common assumption can be made that P is a fixed singularity with $\alpha_P = 1$. If so, then P should at least be treated properly as a vector particle.* This would alleviate technical difficulties associated with achieving correct expressions for both single- and double-Regge limits of the overall amplitude for ab → 123; it would make more sense also for theoretical discussions of s- and t-channel helicity conservation. Second, entirely new approaches can be taken towards including the Pomeron, commensurate with its unique status in dual models.

4.4.2 Pomeron.

It is usually remarked that the Pomeron cannot be an ordinary Regge-trajectory in dual models. If it were dual to resonances, then exotic states would exist. Evidence for such states is lacking. Inasmuch as the Pomeron is a diffractive effect (associated with squares of invariant amplitudes, summed over all intermediate states), it is plausible that the Pomeron should be associated with dual loops, rather than with simple exchanges. In fact, Lovelace (1971a) has developed an explicit theory in which Pomerons are dual to Regge-Regge cuts. Several interesting statements emerge from his theory. The P and f are shown to have the same helicity coupling to the nucleon, in agreement with data. The Pomeron is predicted to have slope $\alpha'_P = \frac{1}{2}\alpha'$, where $\alpha' = 0.9\ \mathrm{GeV}^2$ is the slope of usual Regge trajectories. Lovelace also derives an explicit expression for the Pomeron propagator:

$$P(t) = e^{-i\pi\alpha^P/2}\,\Gamma(1-\alpha^P/2)/\Gamma(\alpha^P/2) \qquad (75)$$

with $\alpha^P = 1 + \alpha' t/2$. This propagator replaces the function $\Gamma(1-\alpha(t))$ appropriate for ordinary trajectories. Observe that the imaginary part of the Pomeron amplitude will be positive always, even though the trajectory moves. Finally, replacing the usual coupling constant, Lovelace derives a form factor to describe coupling of a Pomeron to two external hadrons; this is given by[*]

---

* It is not a 0^+ state, by any stretch of the imagination.

$$G(t) = B_4\left(\frac{1}{2};\ \frac{1}{4} - \frac{\alpha' t}{4}\right) \quad . \tag{76}$$

This new formalism for the Pomeron should be extended to diffraction dissociation. In analogy to Eq. (76), Lovelace will presumably specify a B_5 function[**] to describe the dissociation (lower) vertex in Fig. 33.

4. 4. 3 Unitarity.

Unitarity may well be more decisive than duality in an ultimate resolution of the resonance status of A_1 and other threshold enhancements. The general issue[***] here transcends the question of appropriateness of various approximate schemes for "unitarizing" Veneziano models. However, even within the dual framework, results should be examined for their sensitivity to these approximations. This is particularly true in models for diffraction dissociation of nucleons, inasmuch as the true daughter structure of the baryon spectrum is a far cry from that of naive models (Berger and Fox, 1969; Lovelace, 1971b).

4. 4. 4 Helicity Conservation.

It seems established that s-channel helicity is conserved in elastic scattering, whereas t-channel helicity is conserved in diffraction dissociation processes (Kruse, 1971; Beaupre et al., 1971b). This is superficially strange because the two processes have much in common otherwise. It would be interesting to see whether dual models can resolve this problem. It should be straightforward. A dual amplitude for the lower vertex of Fig. 33 can be factored at the pion pole in the s_{23} variable. In that event, the amplitude would represent πp elastic scattering. Suppose as input to our calculation, we impose the requirement that s-channel helicity be conserved in this πp elastic reaction. Can we then use the full dual model to derive t-channel helicity conservation for $\pi p \to A_1 p$?

---

[*] $B_4(x, y) = \Gamma(x)\Gamma(y)/\Gamma(x + y)$.

[**] B_6 if ρ is replaced by $(\pi\pi)$.

[***] In traditional N/D calculations, unitarity generates resonances if the exchange force is too strong. It would help in settling this question if the phase of A_1 relative to A_2 were to be determined experimentally.

A related question concerns the well-known crossover phenomenon.* It has been observed that the differential cross-sections for $\bar{K}^o p \to \bar{Q} p$ and $K^o p \to Q p$ crossover one another at $|t| \simeq 0.2$ $(GeV/c)^2$ (D. W. G. S. Leith, SLAC, private communication). Crossover is observed also in $\pi^\pm p$, in $K^\pm p$, and in $(pp, \bar{p}p)$ elastic scattering processes, where it is understood qualitatively, if not quantitatively, in terms of the contributions of ρ and ω exchanges. Evidently, at some level, we must also begin to include contributions of these secondary trajectories in our models for diffraction dissociation.

---

* Berger and Fox, 1969, Section II.

5. Miscellanea.

In previous sections, I have concentrated on practical uses of four- and five-point dual models. Some features of six-point and N-point models may also be useful in suggesting experiments and/or in the analysis of data. In this section, I review recent work in which B_6 is employed to derive predictions for particle spectra in inclusive reactions. Subsequently, I discuss a calculation of total widths of resonances from an N-point dual model (Chan and Tsou, 1971). These two examples by no means exhaust the possibilities for phenomenological use of B_N $(N \geq 6)$; however, they illustrate nicely how these higher order functions can be applied advantageously in developing qualitative understanding of fairly complex processes.

5. 1 Inclusive Reactions.

Inclusive reactions warrant a full review by themselves.* Here I can comment only briefly on recent efforts to understand inclusive spectra in terms of dual models. I begin by emphasizing one salient feature of data. I hope dual models will be used directly to provide understanding of this phenomenon.

5. 1. 1 Data.

Let us examine Fig. 35, in which data are presented from the inclusive reactions $pp \rightarrow \pi^{\pm}$ plus anything. Observe that data points for $p_T^2 \geqslant 1$ $(\mathrm{GeV}/c)^2$ fall on a curve of the approximate form $\exp(-3p_T^2)$. This result seems to be universal. More explicitly, in inclusive reactions of general type

---

* Consult E. L. Berger (1971).

$$a + b \rightarrow h + \text{anything} \quad , \tag{77}$$

the cross-section $d\sigma/dp_T^{\,2}$ for $p_T^{\,2} > 1\ (\mathrm{GeV}/c)^2$, is approximated well by the expression

$$\frac{d\sigma}{dp_T^{\,2}} \propto \exp(-3p_T^{\,2}) \quad . \tag{78}$$

This is true for all types of projectiles $(a = \pi, p, K, \gamma)$, of targets $(b = p, d, Be, C)$, and of produced hadrons* $(h = \pi^\pm, K^\pm, p, \overline{p})$. The result is true also over a very wide range of energies, from < 5 GeV/c to > 1100 GeV/c, as observed very recently in experiments at the CERN ISR facility.** The proportionality does fail for small $p_T^{\,2}$ (see Fig. 35) and also for values of longitudinal momentum p_L near kinematic limits. However, the fact that the rule is valid for a wide variety of particles and over a very wide kinematic range suggests that it reflects directly some universal, simple feature of hadron dynamics.

5.1.2 Dual Models.

DeTar, Kang, Tan, and Weis (1971) observe that dual models*** predict an exponential cutoff in $p_T^{\,2}$ which nearly reproduces the observed $\exp(-3p_T^{\,2})$ behavior. Following the suggestion of Mueller (1970), they relate the cross-section for

---

* To my knowledge, the only process which fails to follow this rule is the backward two-body process $\gamma p \rightarrow N\pi$; c. f. E. L. Berger and G. C. Fox, 1971b, Section 2. 4. 4.

** Argonne-Bologna-Michigan Collaboration, L. Ratner and A. D. Krisch, private communication.

*** Studies of dual models for inclusive reactions are reported also by Gordon and Veneziano (1971) and by Virasoro (1971).

$$a + b \rightarrow h + \text{anything}$$

to the imaginary part of the elastic amplitude for the 3 → 3 process

$$a + b + \bar{h} \rightarrow a + b + \bar{h} \ . \tag{79}$$

Here, $\bar{h}$ is the antiparticle of h. To describe process (79), they use six-point dual amplitudes (B_6). From B_6, they derive explicit forms for both energy and momentum transfer dependence of the inclusive reaction (77). In particular, at large p_T^2, they obtain

$$\frac{d\sigma}{dp_T^2} \propto \exp(-4bp_T^2) \ , \tag{80}$$

where the trajectory slope $b \simeq 0.9\ (\mathrm{GeV}/c)^2$. A curve from their paper is reproduced here as Fig. 36.

5.1.3 Questions.

Intriguing new investigations are suggested by the fact that dual models generate a distribution of the form $\exp(-4bp_T^2)$, in reasonable agreement with data. These prospects arise because dual models apply, in principle, in all regions[*] of phase space (resonance region, fragmentation region, central region, single-, double-, and triple-Regge regions, etc.). The models can be used, therefore, to relate phenomena characteristic of different regions.

The first important question seems to be: Why does the universal coefficient c in $\exp(-cp_T^2)$ have numerical value 3 and not some other random number (e.g. 1 or 8)? Indeed, to what other parameters of high energy distributions can c be related? Presumably, in a distribution which applies so universally, the value $c = 3$ cannot be simply accidental.

---

[*] See, e.g., DeTar et al. (1971) for definitions of various regions.

Second, can we understand in simple terms the fact that no shrinkage ($\log s$ dependence) is present in the distribution $\exp(-cp_T^2)$? As remarked above, c is approximately 3 from $p_{lab} \simeq 0$ to $p_{lab} \geq 1100$ GeV/c.

My third question is motivated by the shape of the distribution shown in Fig. 36. At large p_T^2, $f(p_T) \propto \exp(-4p_T^2)$, as we have discussed. However, for small p_T^2, $f(p_T) \propto \exp(-15p_T^2)$. The experimental distributions of Fig. 35 show similar behavior. Moreover, in Nature, for small p_T^2, the coefficient c' in the distribution $\exp(-c'p_T^2)$ is a strong function of the mass of particle h, whose inclusive spectrum is measured (Akerlof et al., 1971). For example, $c' \simeq 8$ for protons, but $c' \simeq 15$ for pions. An explanation for the steep forward peak and for the mass dependence of c' was given by Yen and Berger (1970). In the Yen-Berger interpretation, production and subsequent decay of low mass resonances play a crucial role in generating the steep forward peak. Indeed, the steep component is produced by secondary hadrons, the decay particles of resonances produced peripherally. Dual models, of course, have explicit resonance structure, as well as smooth large angle behavior. It is possible, therefore, that the steep forward peak present in Fig. 36 comes from low-mass resonances in the dual model. However, this is by no means clear from the work of DeTar et al.; it deserves clarification.

A fourth question concerns the shape of inclusive distributions as a function of logitudinal momentum p_L (or of $x = 2p_L^{c.m.}/\sqrt{s}$). This is being investigated by Arnold and Fenster at Argonne (private communication). After integrating B_6 over p_T^2, at fixed x, they obtain

$$x \frac{d\sigma}{dx} \simeq \exp(-dx^2) \tag{81}$$

with $d \simeq 6$ to 10. The gaussian cutoff in x is in good qualitative agreement with data* on $pp \to \pi^{\pm}$ plus anything (Akerlof et al., 1971), $\pi^{\pm}p \to \pi^{-}$ plus anything (Biswas et al., 1971), and $K^{+}p \to \pi^{-}$ plus anything (Ko and Lander, 1971). The theoretical doubly differential distribution $x d^2\sigma / dx\, dp_T{}^2$ also reproduces many qualitative features of the data, such as the tendency of the x variation to be less pronounced at large values of $p_T{}^2$. There are technical differences between the calculations of DeTar et al. and of Arnold and Fenster. For example, DeTar et al. use only one trajectory intercept in their B_6 model, whereas Arnold and Fenster consider two different intercepts. However, in both calculations, important qualitative results are insensitive to this ambiguity and also to the precise value chosen for intercepts. More theoretical effort is obviously necessary; however, the presence of a reasonably sharp cutoff in x^2 is an intriguing general prediction of the model. As with the value of the cutoff parameter in the $p_T{}^2$ distribution, it is important now to develop physical understanding of the fact that B_6 gives a gaussian cutoff in x of the correct magnitude.

Finally, within the framework of eight-point models B_8, we may investigate two-particle correlation functions. In terms of the notation of Benecke, Chou, Yang, and Yen (1969), interest centers on the function $\rho_2(p_c, p_d)$. This is measured in an inclusive process of the type

$$a + b \to c + d + \text{anything} \quad . \tag{82}$$

Specifically,

$$E_c E_d \frac{d^6\sigma}{d^3p_c\, d^3p_d} = \rho_2(p_c, p_d) \quad . \tag{83}$$

Here, (E_c, p_c) is the four-momentum of particle c.

---

[*] See also M. S. Chen et al. (1971).

Dual models could be useful in suggesting functional forms for $\rho_2(p_c, p_d)$ and in defining regions of phase-space of significant theoretical interest.

Experience with four-point and five-point functions teaches us that detailed models based upon B_6, B_8, . . . , B_N are unlikely to be useful for quantitative fits to data. Furthermore, some problems are accentuated at the level of B_N, with $N \geq 6$. Among these, I mention only difficulties with the Pomeron. A theory which is to predict "scaling," in the usual sense, must incorporate diffractive effects explicitly. In Regge exchange language, this means a trajectory with intercept $\alpha_v(0) = 1$. No self-consistent way has been devised yet to accomplish this in ordinary Veneziano models. Nevertheless, it remains very interesting, at least superficially, that B_6 provides exponential cutoffs in p_T^2 and in x^2 of approximately the right form. Proof of the relevance of B_6 awaits development of more physical insight into exactly why the model is successful.

5.2 Narrow Resonances with Large Mass and High-Spin.

As indicated earlier (c.f. subsection 2.1), resonance poles in dual models have zero total width. However, I remarked also that finite total widths Γ_{tot} may be calculated by the simple artifice of summing explicitly the partial widths for all decay modes. I showed how this is done for the ρ'. Chan and Tsou (1971) discuss the general case. After a formidable calculation, they predict the existence of heavy, narrow resonances. Moreover, they describe the dominant decay modes of these high-spin states and then suggest looking for them in certain production (not formation!) experiments. Their results, which are of obvious interest to meson spectroscopists, are summarized below.

First, as mass M is increased along a trajectory, the product $M\Gamma_{tot}$ decreases slightly with M. This result is shown in Fig. 37.

In order to obtain quantitative values, results may be normalized to the total width of the parent state at $\alpha = 1$. If $\Gamma_1 = 100$ MeV, as is appropriate for ρ, then Chan and Tsou predict that a meson resonance with $\alpha = 10$ ($J = 10$, $M^2 \simeq 10$ GeV^2) will have total width $\Gamma_{10} \simeq 24$ MeV.

Second, in a given tower of resonances (fixed J), the total width of the first daughter is a factor of five greater than that of her parent. Total widths continue to increase in this fashion as the "generation" index D grows. This result agrees with the observed ratio of ϵ and ρ total widths in $\pi\pi$ scattering. It suggests also that our earlier estimate of ρ' total width is, if anything, small (c.f. subsection 2.1).

Third, when decay occurs, states on the parent (leading) trajectory and on the first daughter trajectory ($D = 1$) move to a preferred final configuration consisting of a lower state on the parent trajectory plus one quantum (π).

Fourth, high-spin resonances decay preferentially by cascade into a number of basic mesons. A few units of spin are lost at each step; low final multiplicities are favored. A typical chain of decay for a parent with $\alpha = 6$ ($J = 6$, $M^2 \simeq 6$) is $(\alpha = 6) \to (\alpha = 3) \to (\alpha = 2) \to (\alpha = 1) \to (\alpha = 0)$.

Finally, because of their high spin, narrow resonances are not expected to be observed in formation experiments. Indeed, to form a narrow state on a parent trajectory, angular momentum $J = \alpha \propto s$ is required. However, in a formation process only states with $J \gtrsim a\sqrt{s}$ ($\ell \simeq ka$) are populated with appreciable probability (assume a classical interaction with effective radius a). Therefore, broad daughter states and not parents result from typical two-body scattering experiments. Nevertheless, once formed, broad states decay quickly, and, as remarked above, parent states are the preferred decay products of states on daughter trajectories. Therefore, Chan and Tsou suggest looking for narrow resonances in final states containing several (≥ 2) other particles.

There is no clear evidence in Nature for narrow resonances with high-mass. Although missing-mass spectrometer data suggest the existence of sharp resonance-like states, these data are compromised by the on-again off-again state of A_2 splitting. The trend of total widths for baryon resonances suggests that the Chan-Tsou prediction may not be correct, but duality for baryons is by no means on the same footing as duality for mesons (Lovelace, 1970). Therefore, this objection is possibly irrelevant. As things stand, it is safest to assume that the Chan-Tsou result is valid only for mesons. The prediction should obviously be borne in mind as data become available from careful new experiments in meson-spectroscopy.

6. Summary.

Specific conclusions were given at the end of each major subsection, so remarks here will be brief.

In this review, I have attempted to present a thorough, critical appraisal of practical uses made of dual models in the analysis of hadronic data. Wherever appropriate, I also extend the scope of published results in order to show more clearly their physical significance. This is particularly true in the section on B_5. In that section, I present several original calculations which illustrate the importance of B_5 as a qualitative tool for understanding complicated interference phenomena among competing two-body channels in a $2 \to 3$ particle reaction. Throughout the paper, suggestions are made for further theoretical and experimental investigations.

The most important conclusion to emerge from this study is that renewed efforts should be made to abstract from dual models statements about qualitative behavior of strong interaction processes. Although detailed quantitative fits with dual models are inappropriate, examples developed here show that abstractions from these models have much greater usefulness than the models themselves. Affirmative answers can be given to all of the questions posed in the Introduction. In the hands of conscientious, critical students, dual models should continue to provide valuable physical insight into the way in which duality, crossing-symmetry, and analyticity are manifest in hadronic data.

ACKNOWLEDGMENTS

I am indebted to Geoffrey Fox for many valuable discussions. I have benefited also from conversations with J. David Jackson, Claud Lovelace, Arthur Rosenfeld, Christoph Schmid, and Dennis Sivers. Mary Ann Rechtien deserves special praise for her cheerfulness and devotion to accuracy in typing this manuscript.

REFERENCES

1. S.A. Adjei, P.A. Collins, B.J. Hartley, R.W. Moore, and K.J.M. Moriarty, Phys. Rev. D3, 150 (1971).
2. C.W. Akerlof, D.G. Crabb, J.L. Day, N.P. Johnson, P. Kalbaci, A.D. Krisch, M.T. Lin, M.L. Marshak, J.K. Randolf, P. Schmueser, A.L. Read, K.W. Edwards, J.G. Asbury, G.J. Marmer, and L.G. Ratner, Phys. Rev. D3, 645 (1971).
3. V. Alessandrini, D. Amati, M. LeBellac, and D. Olive, "Dual Multiparticle Theory," CERN Lectures, CERN Report Ref. Th. 1160 (1970).
4. G. Altarelli and H.R. Rubinstein, Phys. Rev. 183, 1469 (1969).
5. H. Alvensleben, U.J. Becker, William K. Bertram, M. Chen, K.J. Cohen, R.T. Edwards, T.M. Knasel, R. Marshall, D.J. Quinn, M. Rohde, G.H. Sanders, H. Schubel, and Samuel C.C. Ting, Phys. Rev. Letters 26, 273 (1971).
6. E.W. Anderson, E.J. Bleser, H.R. Blieden, G.B. Collins, D. Garelick, J. Menes, F. Turkot, D. Birnbaum, R.M. Edelstein, N.C. Hien, T.J. McMahon, J. Mucci, and J. Russ, Phys. Rev. Letters 22, 1390 (1969).
7. R. Anderson, D. Gustavson, J. Johnson, D. Ritson, B.H. Wiik, W.G. Jones, D. Kreinick, F. Murphy, and R. Weinstein, Phys. Rev. D1, 27 (1970).
8. P. Anninos, L. Gray, P. Hagerty, T. Kalogeropoulos, S. Zenone, R. Bizzarri, G. Ciapetti, M. Gaspero, I. Laakso, S. Lichtman, and G. Moneti, Phys. Rev. Letters 20, 402 (1968).
9. G. Ascoli, H. Crawley, D. Mortara, and A. Shapiro, Phys. Rev. Letters 20, 1411 (1968).

10. J. Ballam, G.B. Chadwick, R. Gearhart, Z.G.T. Guiragossian, M. Menke, J.J. Murray, P. Seyboth, A. Shapira, C.K. Sinclair, I.O. Skillicorn, H. Spitzer, G. Wolf, R.H. Milburn, H.H. Bingham, W.B. Fretter, K.C. Moffeit, W.J. Podolsky, M.S. Rabin, A.H. Rosenfeld, and R. Windmolders, "Analysis of Δ, ρ, and A_2 Production in the Reaction $\gamma p \rightarrow N\, 3\pi$ and Evidence for Multineutral Decay Modes of Photo-Produced Mesons," SLAC Preprint, 1970; submitted to Kiev Conference.

11. K. Bardakci and H. Ruegg, Phys. Letters 28B, 342 (1969).

12. J. Bartsch, M. Deutschmann, R. Honecker, R. Schulte, R. Steinberg, H. Böttcher, U. Gensch, S. Nowak, H. Schiller, A. Angelopoulos, V.T. Cocconi, P.F. Dalpiaz, J.D. Hansen, W. Kittel, D.R.O. Morrison, K. Paler, H.J. Schreiber, H. Töfte, P.J. Dornan, S.J. Goldsack, M.J. Losty, M.E. Mermikides, A. Fröhlich, M. Markytan, G. Otter, P. Schmid, and H. Wahl, Nucl. Phys. B20, 63 (1970a).

13. J. Bartsch, R. Schulte, R. Steinberg, U. Gensch, S. Nowak, E. Ryseck, H. Schiller, V.T. Cocconi, P.F. Dalpiaz, J.D. Hansen, G. Kellner, W. Kittel, S. Matsumoto, D.R.O. Morrison, R. Stroynowski, J.B. Whittaker, M.J. Counihan, P.J. Dornan, S.J. Goldsack, G. Otter, B. Buschbeck, A. Fröhlich, P. Porth, P. Schmid, and H. Wahl, Nucl. Phys. B24, 221 (1970b).

14. A. Bashian, G. Finocchiaro, M.L. Good, P.D. Grannis, O. Guisan, J. Kirz, Y.Y. Lee, R. Pittman, G.C. Fischer, and D.D. Reeder, "Momentum Transfer Dependence of the Reaction $\pi^+ p \rightarrow K^+ Y^*(1385)$ from 3.5 to 14 GeV/c," Stony Brook Preprint (1970).

15. J.V. Beaupre, M. Deutschmann, H. Graessler, P. Schmitz, R. Speth, H. Böttcher, J. Kaltwasser, H. Kaufmann, S. Nowak,

A. Angelopoulos, K.W.J. Barnham, J.R. Campbell, V.T. Cocconi, P.F. Dalpiaz, J.D. Hansen, G. Kellner, W. Kittel, D.R.O. Morrison, Nucl. Phys. B28, 77 (1971a).

16. J.V. Beaupre, K. Boesebeck, M. Deutschmann, H. Grassler, R. Speth, J. Klugow, A. Meyer, E. Ryseck, M. Walter, K. Böckmann, W. Johnssen, M. Rost, K. Sternberger, T. Besliu, J.R. Campbell, V.T. Cocconi, P. F. Dalpiaz, W. Kittel, D.R.O. Morrison, H. Schiller, R. Stroynowski, J.B. Whittaker, D. Kisielewska, S. Brandt, T.P. Shah, M.J. Counihan, P.J. Dornan, S.J. Goldsack, M.J. Losty, D. Dallman, M. Markytan, G. Otter, P. Porth, P. Schmid, Phys. Letters 34B, 160 (1971b).

17. J. Benecke, T.T. Chou, C.N. Yang, and E. Yen, Phys. Rev. 188, 2159 (1969).

18. E.L. Berger, Phys. Rev. 166, 1525 (1968).

19. E.L. Berger, Proceedings of the Conference on $\pi\pi$ and $K\pi$ Interactions, Argonne, Illinois. F. Loeffler and E. Malamud, Eds. (1969a) p. 750.

20. E.L. Berger, Phys. Rev. 179, 1567 (1969b).

21. E.L. Berger, "Phenomenology of Multiparticle Production," Argonne Report ANL/HEP 6927, Proceedings of the Regge Pole Conference, Irvine, California (1969c).

22. E.L. Berger, "Inclusive Reactions," Invited Paper, Colloquium on Multiparticle Dynamics, Helsinki, May 1971.

23. E.L. Berger and G.C. Fox, Phys. Rev. 188, 2120 (1969).

24. E.L. Berger and G.C. Fox, Nucl. Phys. B26, 1 (1971a).

25. E.L. Berger and G.C. Fox, "Phenomenology of Backward Photoproduction," Argonne Report ANL/HEP 7103; to be published in Nucl. Phys. (1971b).

26. A. Bettini, M. Cresti, M. Mazzucato, L. Peruzzo, S. Sartori, G. Zumerle, M. Alston-Garnjost, R. Huesman, R. Ross, F. T. Solmitz, L. Bertanza, R. Carrara, R. Casali, P. Lariccia, R. Pazzi, G. Borreani, B. Quassiati, G. Rinaudo, M. Vigone, and A. Werbrouck, Il Nuovo Cimento 1A, 333 (1971).

27. A. Bialas and S. Pokorski, Nucl. Phys. B10, 399 (1969).

28. N. Biswas, N. Cason, V. Kenney, J. Powers, W. Shephard, and D. Thomas, Notre Dame Preprint; to be published in Phys. Rev. Letters (1971).

29. R. Bizzarri, M. Foster, Ph. Gavillet, G. Labrosse, L. Montanet, R. Salmeron, P. Villemoes, C. Ghesquiere, and E. Lillestol, Nucl. Phys. B14, 169 (1969).

30. A.M. Boyarski, R. Diebold, S. Ecklund, G. Fisher, Y. Murata, B. Richter, and M. Sands, Phys. Rev. Letters 25, 695 (1970).

31. G.W. Brandenburg, A.E. Brenner, M. Ioffredo, W. Johnson, J. Kim, M. Law, J. Mueller, B. Salzberg, J. Scharenguivel, L. Sisterson, and J. Szymanski, Nucl. Phys. B16, 287 (1970).

32. A.D. Brody, W.B. Johnson, B. Kehoe, D.W.G.S. Leith, J.S. Loos, G.J. Luste, K. Moriyasu, B.C. Shen, W.M. Smart, F.C. Winkelmann, and R.J. Yamartino, "K_L^o-p Interactions From 1-8 GeV/c," Stanford Preprint, SLAC-PUB-823, November 1970.

33. F. Bulos, W. Busza, R. Giese, E.E. Kluge, R.R. Larsen, D. Leith, B. Richter, S.H. Williams, B. Kehoe, M. Beniston, and A. Stetz, Phys. Rev. Letters 26, 149 (1971).

34. Chan Hong-Mo, Proc. Roy. Soc. Lond. A 318, 379 (1970).

35. Chan Hong-Mo, R.O. Ratio, G.H. Thomas, and N.A. Törnqvist, Nucl. Phys. B19, 173 (1970).

36. Chan Hong-Mo and Tsou Sheung Tsun, "The Decay Pattern of High Spin Resonances in the Generalized Veneziano Model," State

University of New York, Stony Brook, 1971.

37. M.S. Chen, R.R. Kinsey, T.W. Morris, R.S. Panvini, L.L. Wang, T.F. Wong, S.L. Stone, T. Ferbel, P. Slattery, B. Werner, J.W. Elbert, and A.R. Erwin, Rochester Preprint UR-875-340; to be published in Phys. Rev. Letters (1971).
38. G.F. Chew, The Analytic S Matrix (W.A. Benjamin, Inc., New York, 1966).
39. G.F. Chew and A. Pignotti, Phys. Rev. Letters 20, 1078 (1968).
40. C.B. Chiu, R.J. Eden, C-I.Tan, Phys. Rev. 170, 1490 (1968).
41. J.H. Christenson, G.S. Hicks, L.M. Lederman, P.J. Limon, B.G. Pope, and E. Zavattini, Phys. Rev. Letters 25, 1523 (1970).
42. S.U. Chung, L. Montanet, S. Rencroft, and P. Frenkiel, CERN Report D.Ph.II/Phys.70-18; submitted to Kiev Confernece, 1970.
43. D.J. Crennell, U. Karshon, K.W. Lai, J.M. Scarr, and I.O. Skillicorn, Phys. Letters 28B, 136 (1968).
44. G.V. Dass and C.D. Froggatt, Nucl. Phys. B19, 611 (1970).
45. C.E. DeTar, K. Kang, C-I. Tan, and J.H. Weis, "Duality and Single Particle Production," MIT Preprint, 1971.
46. J. Diaz, G. Labrosse, L. Montanet, P. Frenkiel, C. Ghesquiere, and E. Lillestol, CERN Report, D.Ph.II/Phys.70-16; submitted to Kiev Conference, 1970.
47. L. Dick, data presented at "Conference on the Phenomenology of Particle Physics," Caltech, 1971; see his talk in Part 6 of these proceedings.
48. R. Dolen, D. Horn, and C. Schmid, Phys. Rev. 166, 1768 (1968).
49. R.J. Eden and C-I. Tan, Phys. Rev. 170, 1516 (1968) and 172, 1583 (1968).
50. A. Firestone, G. Goldhaber, and D. Lissauer, UCRL-20261 (1971).

51. G. C. Fox in High Energy Collisions; Ed. by C. N. Yang, J. Cole, M. Good, R. Hwa, and J. Lee-Franzini (Gordon and Breach, Inc., N. Y., 1969).

52. P. Freund, Phys. Rev. Letters 20, 235 (1968).

53. G. P. Gopal, R. Migneron, A. Rothery, Phys. Rev. D, 1 April 1971.

54. D. Gordon and G. Veneziano, "Inclusive Reactions and Dual Models," Preprint, Institute for Advanced Studies, Princeton, 1971.

55. H. Harari, Phys. Rev. Letters 20, 1395 (1968).

56. H. Harari, Phys. Rev. Letters 22, 562 (1969).

57. A. Hirshfeld and M. Schmidt, "The Dual $\bar{K}N\bar{\Lambda}\pi\pi$ Amplitude with Spin," Heidelberg Preprint, fall, 1970.

58. P. Hoyer, B. Petersson, A. T. Lea, J. E. Paton, and G. H. Thomas, "Crossing Symmetric Description of the Complex $K^+K^-\pi^-p\bar{n}$," 1971; to be published in Nuclear Physics.

59. P. Hoyer, B. Petersson, and N. A. Törnqvist, Nucl. Phys. B22, 497 (1970).

60. J. D. Jackson, Rev. Mod. Phys. 42, 12 (1970).

61. M. Jacob, "Duality in Strong Interaction Physics," VIII Schladming Meeting, CERN Report Ref. Th. 1010 (1969).

62. M. Jacob, Proceedings of the Lund International Conference on Elementary Particles, G. von Dardel, Ed. (Berlingska Boktryckeriet, Lund, 1969).

63. R. Jengo and E. Remiddi, Lett. Nuovo Cimento 1, 637 (1969).

64. D. Johnson, "A Study of V^0 Final States in K^-d Interactions," Thesis, University of Kansas, 1971.

65. G. Kane in Experimental Meson Spectroscopy, '70 (Columbia Univ. Press, New York, 1970).

66. W. Ko and R. Lander, Phys. Rev. Letters 26, 1064 (1971).

67. G. Kramer and H. Quinn, "A Diffraction-Dissociation Model for High-Energy Rho-Photoproduction, DESY Report 70/23 (1970).

68. U. Kruse, "Current Experimental Status of A_1, A_3, Q and L Enhancements," Talk presented at Conference on the Phenomenology of Particle Physics, Caltech, 1971.

69. M. Kugler, "Duality," IX Schladming Meeting; Weizmann Institute Preprint (1970).

70. C. Lovelace, Phys. Letters 28B, 264 (1968).

71. C. Lovelace, Proceedings of the Conference on $\pi\pi$ and $K\pi$ Interactions, Argonne, Illinois, F. Loeffler and E. Malamud, Eds. (1969) p. 562.

72. C. Lovelace, Proc. Roy. Soc. Lond. A318, 321 (1970).

73. C. Lovelace, Phys. Letters 34B, 500 (1971a).

74. C. Lovelace, "Present and Future of Two-Particle Phenomenology," talk presented at Conference on the Phenomenology of Particle Physics, Caltech (1971b): see Part 7 of these proceedings.

75. G. McClellan, N. Mistry, P. Mostek, H. Ogren, A. Osborne, A. Silverman, J. Swartz, R. Talman, and G. Diambrini-Palazzi, Phys. Rev. Letters 23, 718 (1969).

76. K. C. Moffeit, "Bubble Chamber Study of Polarized $\gamma p \rightarrow \pi^+\pi^- p$ at 2.8 and 4.7 GeV," Ph.D. Thesis, University of California, Berkeley, UCRL-19890.

77. D. Morrison, Phys. Rev. 165, 1699 (1968).

78. A. H. Mueller, Phys. Rev. D2, 2963 (1970).

79. R. Odorico, Lett. al Nuovo Cimento 2, 655 (1969) and Erratum 3, 61 (1970).

80. R. Odorico, Phys. Letters 33B, 489 (1970).

81. R. Odorico, Phys. Letters 34B, 65 (1971a).
82. R. Odorico, "Experimental Evidence for Dual and Exchange-Degenerate Structure in $\bar{K}N \to \pi\Lambda$ and $\pi N \to K\Lambda$ at Intermediate Energies," CERN Report Ref. Th. 1277 (1971b).
83. R. Odorico, "Crucial Tests of the Veneziano Model from Dip Behavior at Low Energy," CERN Report Ref. Th. 1303 (1971c).
84. B. Oh, A. F. Garfinkel, R. Morse, W. D. Walker, J. D. Prentice, E. C. West, and T. S. Yoon, Phys. Rev. D1, 2494 (1970).
85. M. Roos, C. Bricman, A. Barbaro-Galtieri, L. R. Price, A. Rittenberg, A. H. Rosenfeld, N. Barash-Schmidt, P. Söding, Chih Yung Chien, C. G. Wohl, and T. Lasinski, Phys. Letters 33B, 1 (1970). PARTICLE DATA GROUP.
86. B. Petersson and N. A. Törnqvist, Nucl. Phys. B13, 629 (1969).
87. S. Pokorski and G. H. Thomas, "New Features in a Dual Description of $\bar{p}n \to \pi^+\pi^-\pi^-$ at Rest," Helsinki Preprint, October 1970.
88. S. Pokorski and H. Satz, Nucl. Phys. B19, 113 (1970).
89. L. R. Price, N. Barash-Schmidt, O. Benary, R. Bland, A. Rosenfeld, C. G. Wohl, "A Compilation of K^+N Reactions," UCRL-20000 K^+N (1969).
90. J. L. Rosner, Phys. Rev. Letters 22, 689 (1969).
91. R. Ross and L. Lyons, Oxford preprint, August 1970.
92. H. Satz and K. Schilling, Nuovo Cimento 67A, 511 (1970).
93. C. Schmid, Proc. Roy. Soc. Lond. A318, 257 (1970).
94. J. Shapiro, Phys. Rev. 179, 1345 (1969).
95. D. Sivers and J. Yellin, Rev. Mod. Phys., April (1971).
96. N. A. Törnqvist, Nucl. Phys. B18, 530 (1970).
97. G. Veneziano, Nuovo Cimento 57A, 190 (1968).
98. M. A. Virasoro, Phys. Rev. 177, 2309 (1969a).
99. M. A. Virasoro, Phys. Rev. Letters 22, 37 (1969b).

100. M. A. Virasoro, "A Simple Dual Model for Inclusive Reactions," Preprint, University of California, Berkeley, 1971.

101. F. Wagner, Nuovo Cimento 64A, 189 (1969).

102. E. Yen and E. L. Berger, Phys. Rev. Letters 24, 695 (1970).

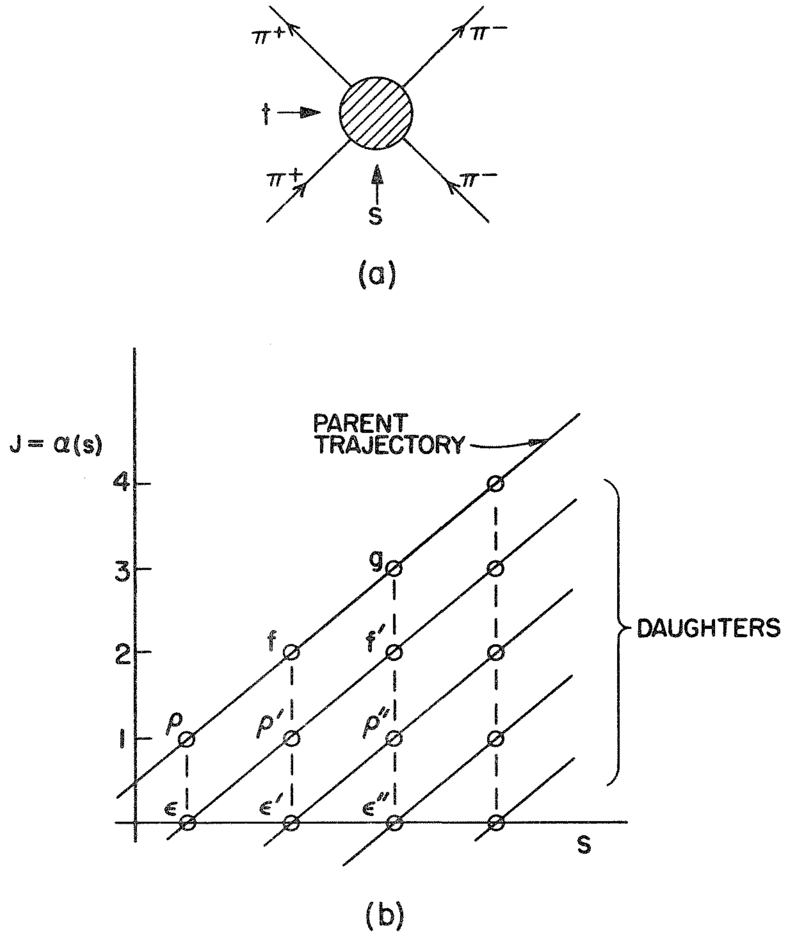

Fig. 1: (a) Diagram illustrating the kinematic variables s $(= M^2_{\pi\pi})$ and t for $\pi^+\pi^-$ elastic scattering. In (b), a sketch is given of the spectrum of resonance states in $\pi^+\pi^-$ scattering, as predicted by the Veneziano model (Eq. (1) of the text). Resonances are labeled by their common names (ρ, ε, etc.) and J designates their spin. The parent trajectory is given by $\alpha(s) = 0.48 + 0.85\ s$.

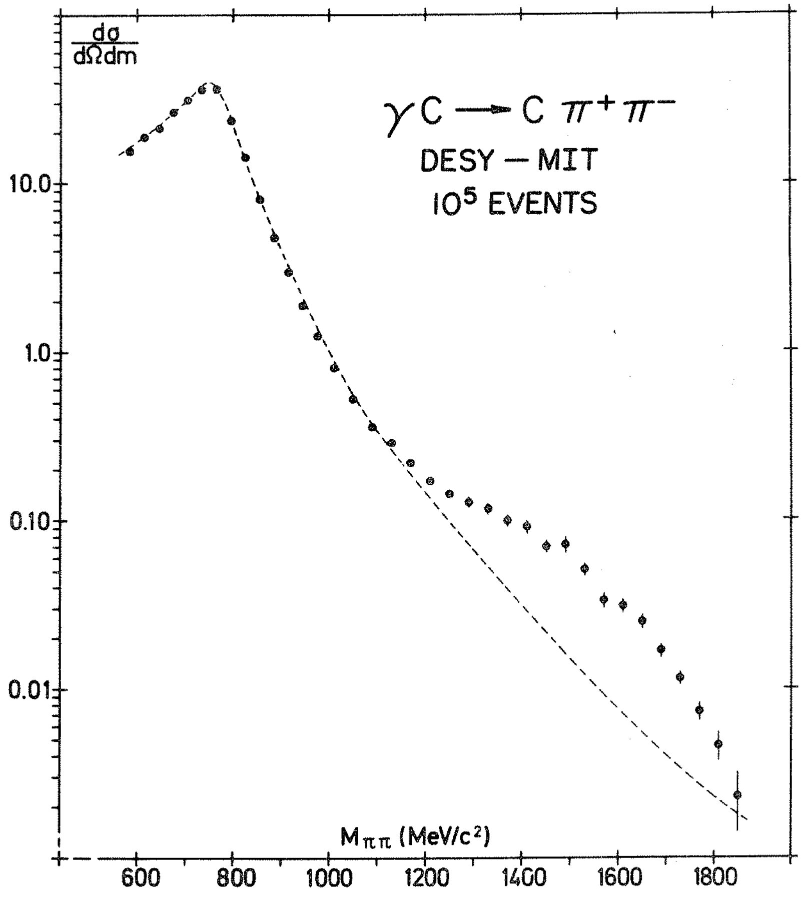

Fig. 2: Pion-pion mass spectrum measured in $\gamma C \Rightarrow C\pi^+\pi^-$ by Alvensleben et al. (1971). The dashed curve represents a fit made by Alvensleben et al. to events in the ρ region. Pion pairs are produced by a 7.5 GeV Bremsstrahlung beam and detected by a pair of magnetic spectrometers.

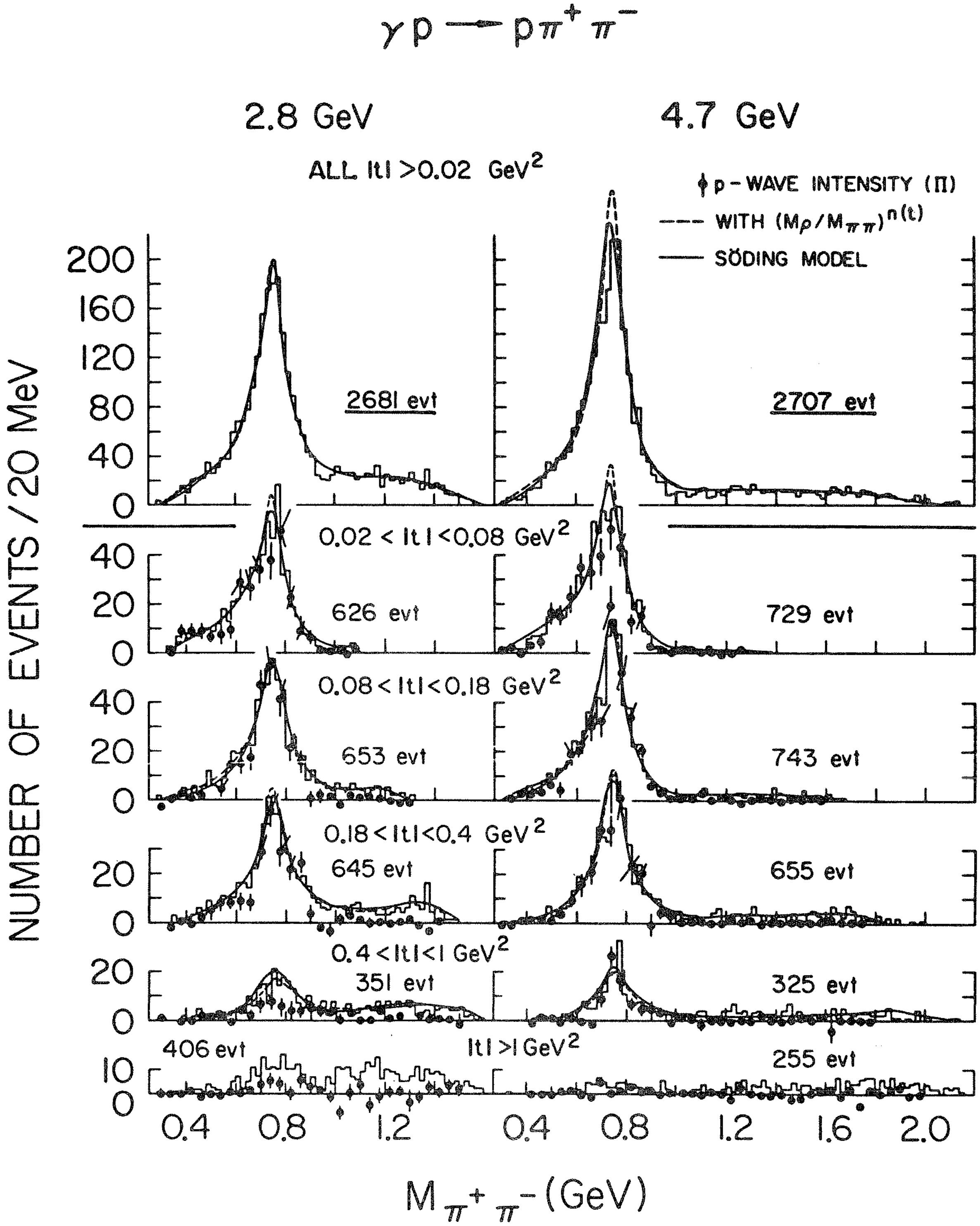

Figure 3: Di-pion mass distributions from $\gamma p \rightarrow \pi^+\pi^- p$ at 2.8 and 4.7 GeV (Moffeit, 1971). These are bubble chamber results obtained with a monochromatic, linearly polarized photon beam.

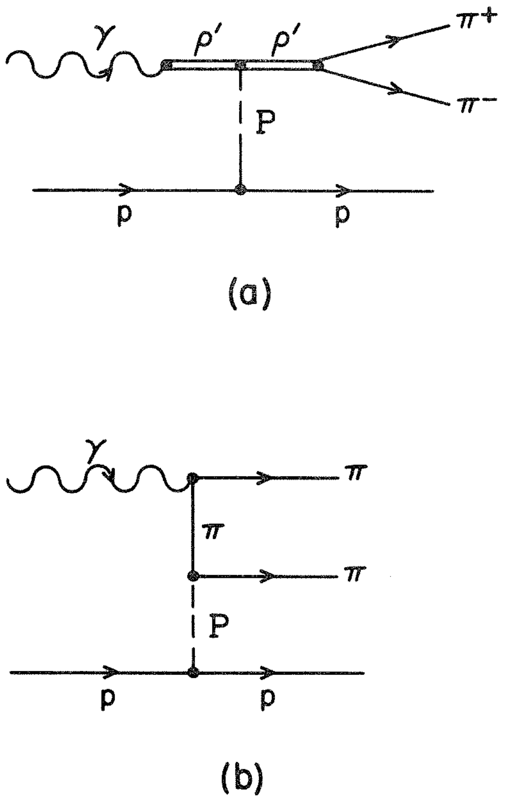

Fig. 4: (a) Vector-meson-dominance-model diagram for production of ρ'; symbol P denotes Pomeron exchange. (b) Drell diagram for diffraction-dissociation of γ into a pair of pions.

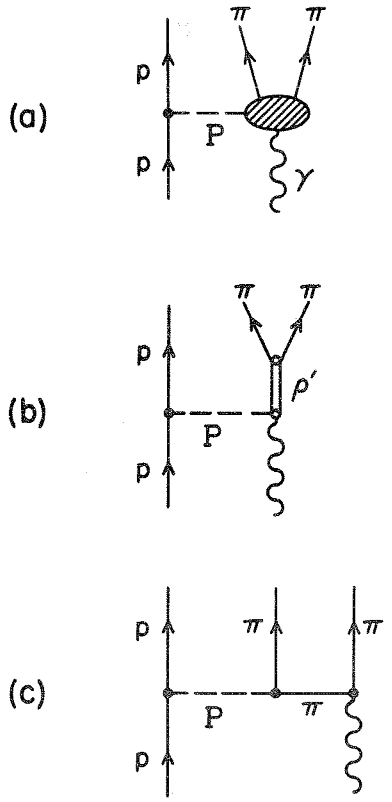

Fig. 5: Diagrams representing various approximate models for diffractive two pion photoproduction. In (a), the shaded oval denotes a four-point Veneziano model for process $\gamma P \to \pi\pi$. If this amplitude is expanded as a sum of terms, with each term representing a resonance pole in the $\pi\pi$ channel, individual terms in the sum have the appearance of (b). Alternatively, an expansion may be given in terms of exchange-channel poles, in which case (c) represents a typical term in the sum.

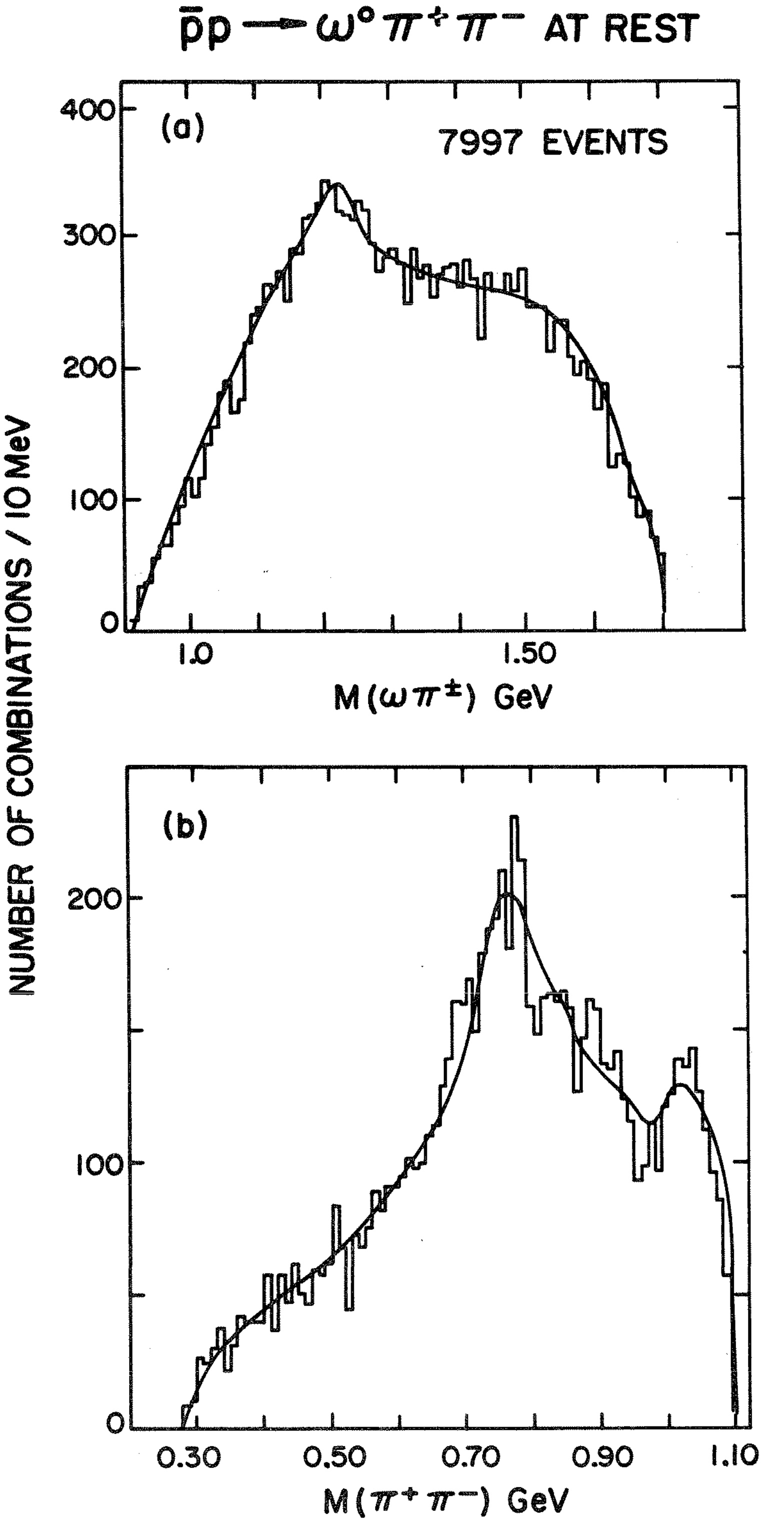

Figure 6: Distributions of the invariant mass of (a) $\omega\pi$ and (b) $\pi^+\pi^-$ from $\bar{p}p \Rightarrow \omega^o\pi^+\pi^-$, at rest (Diaz _et al_., 1970). Curves shown are results of a fit obtained by Diaz _et al_. to the entire Dalitz plot. Both ρ' and B mesons contribute to the peak near 1250 MeV in the $\pi\omega$ distribution.

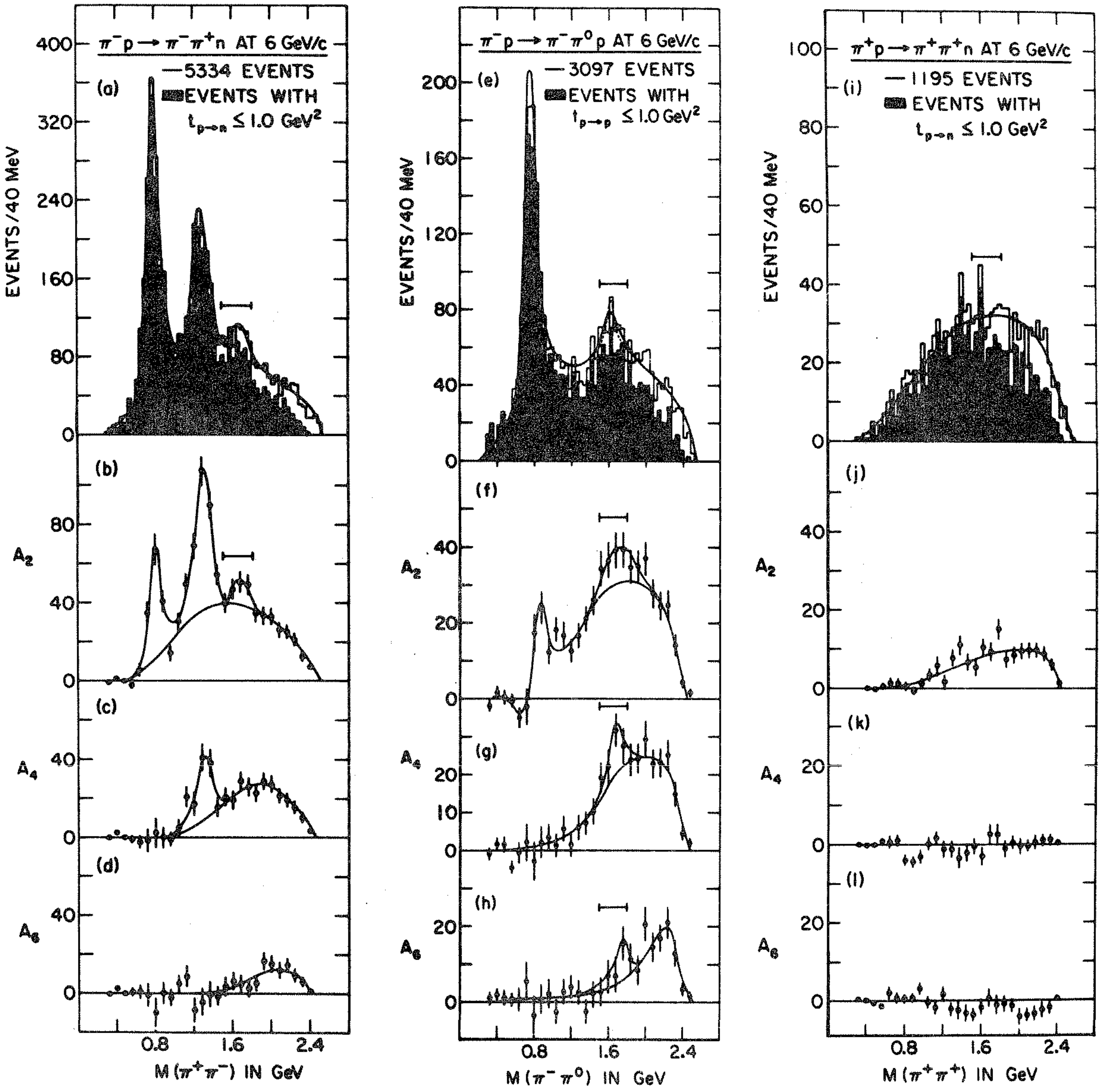

XBL 696-596

Figure 7: Pion-pion mass distributions and Legendre polynomial coefficients for $\pi N \to \pi\pi N$ at 6 GeV/c (from Crennell et al., 1968).

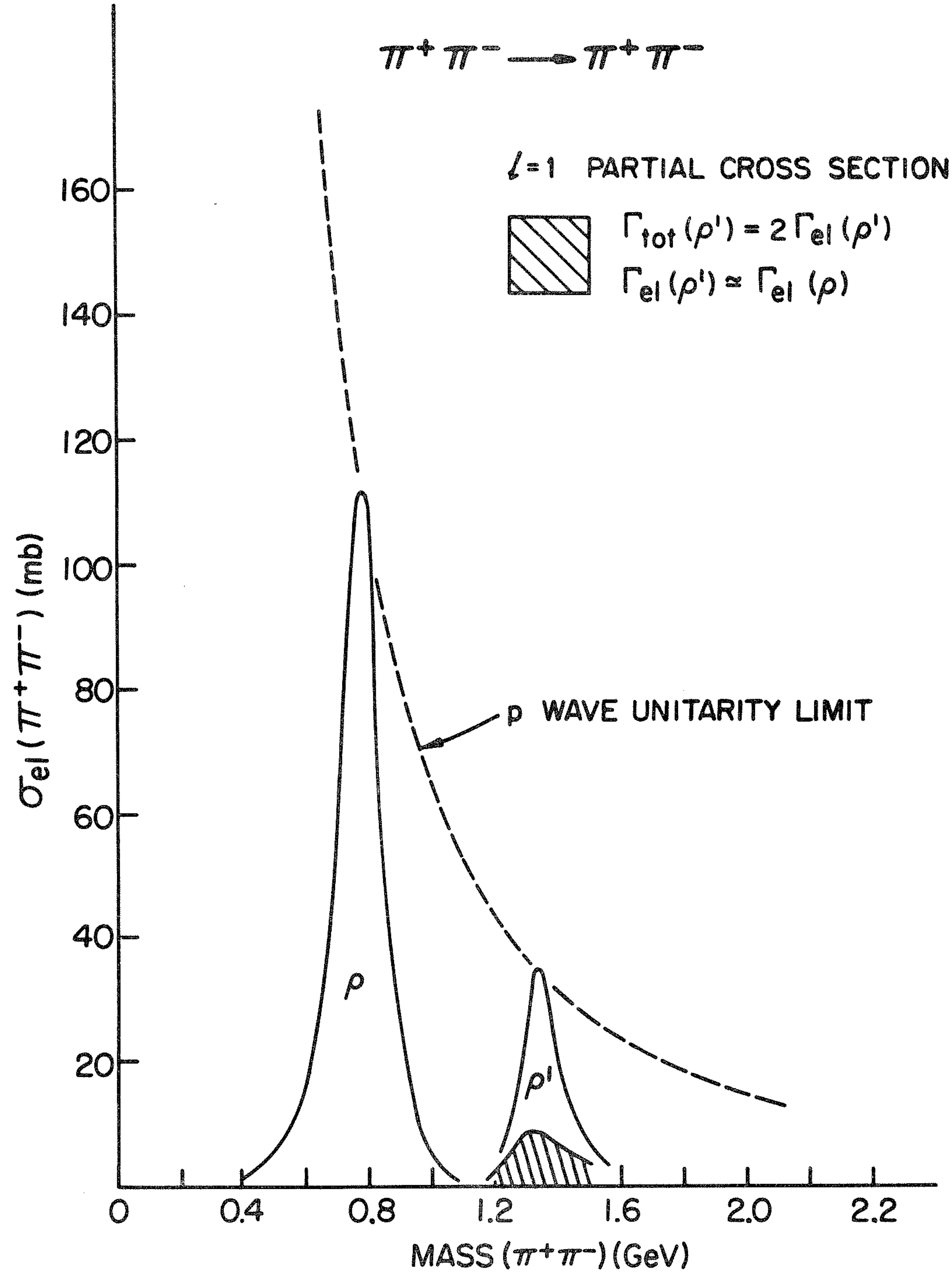

Figure 8: A sketch is given of the p-wave contribution to the $\pi^+\pi^-$ elastic cross section. Shown as a dashed curve is the p-wave unitarity limit, $4\pi(3/k^2)$, where k is the center of mass momentum in the $\pi\pi$ rest frame. The ρ is assumed to be perfectly elastic and is assigned a total width of 120 MeV. Two approximations are presented for ρ'. In the first, ρ' is perfectly elastic with Γ_{tot} = 120 MeV. In the second, shown cross-hatched, ρ' is assigned total width 240 MeV and partial width of 120 MeV for decay into $\pi^+\pi^-$. Masses of ρ and ρ' are computed from the trajectory $\alpha(s) = 0.48 + 0.85\,s$.

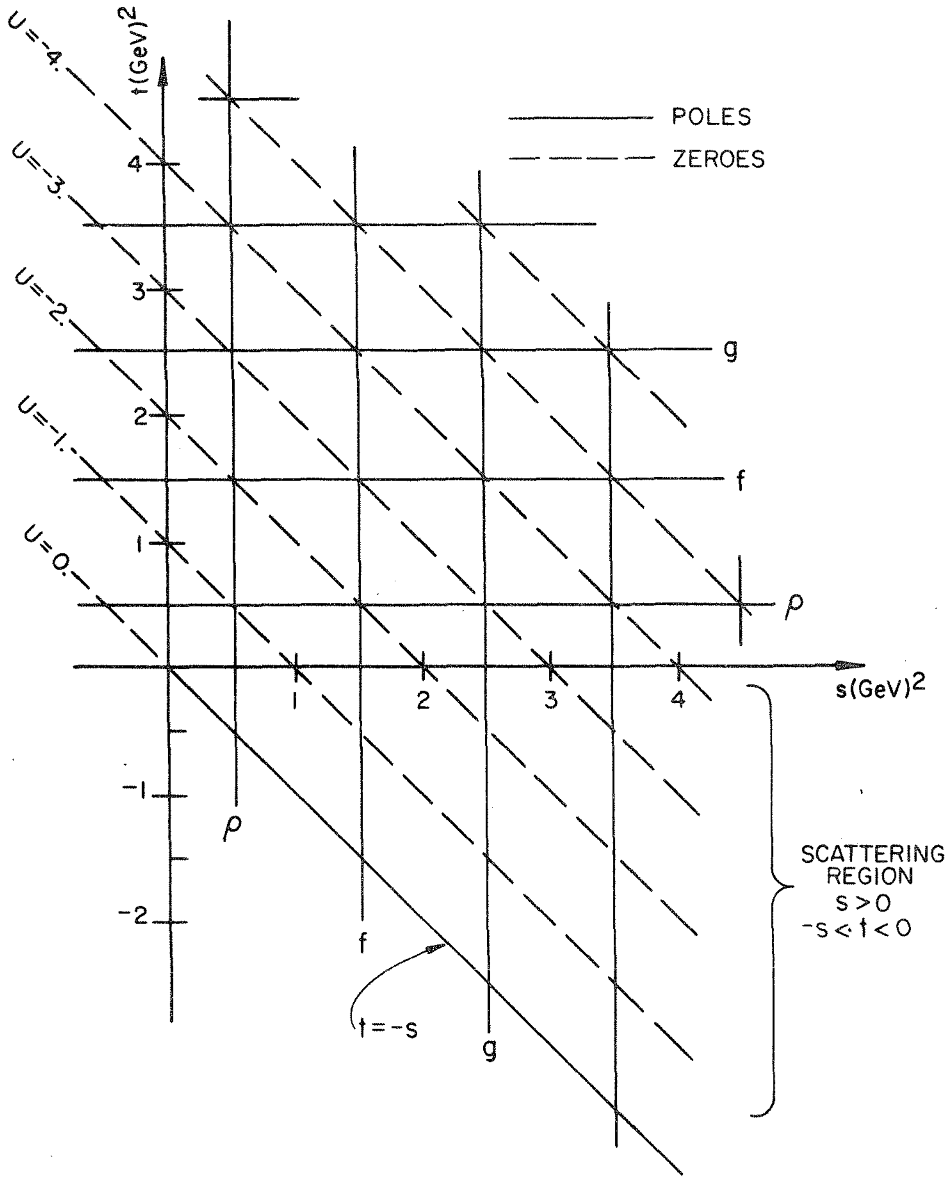

Figure 9: A segment of the (s,t) plane illustrating the dynamical structure of a simple four-point Veneziano amplitude. Shown are contours (straight lines) along which the function is zero and along which it is infinite (resonance poles). For convenience in illustration, Eq. (1) has been used, with $M_\pi = 0$ and $\alpha_\rho(s) = 0.5 + s$. Lines of zeroes appear at fixed values of $u = -s-t$, spaced by 1 $(\text{GeV}/c)^2$. In the unphysical region for ππ elastic scattering ($s > 0$, $t > 0$), resonance poles of the s and t channels intersect. At the intersection point, the resultant double pole is reduced to a single pole by the line of zeroes, which also crosses the intersection. In the physical scattering region ($s > 0$, $t < 0$), the intersection of a zero line and a pole results in an observable dip in the differential cross section.

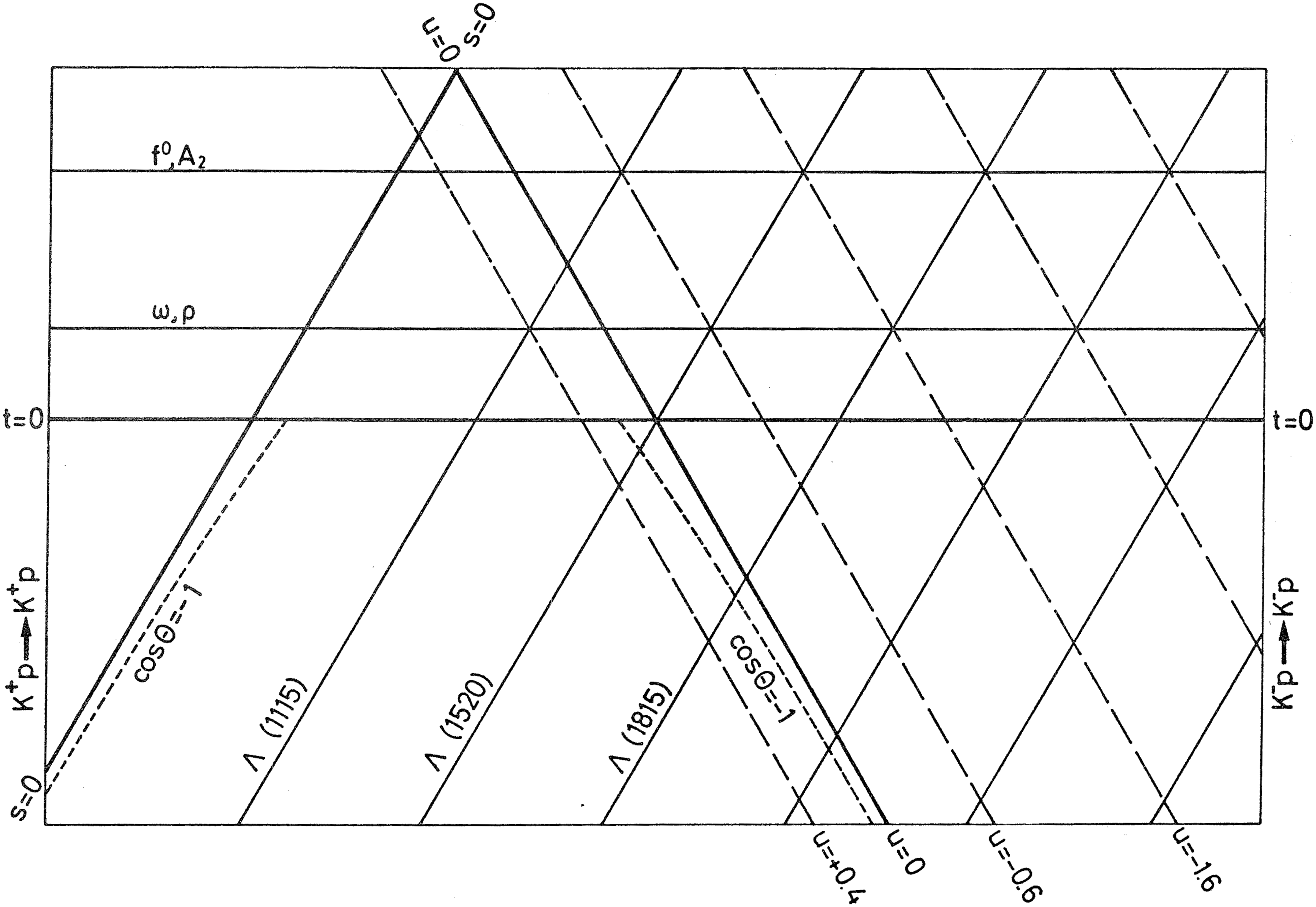
u=0
s=0
f^0, A_2
ω, ρ
t=0
t=0
$K^+p \rightarrow K^+p$
$K^-p \rightarrow K^-p$
$\cos\Theta = -1$
Λ (1115)
Λ (1520)
Λ (1815)
$\cos\Theta = -1$
s=0
u=+0.4
u=0
u=-0.6
u=-1.6

Figure 10: The (s,t,u) Mandelstam plane for $\bar{K}N \rightarrow \bar{K}N$ (from Odorico, 1971a). As in Fig. 9, solid lines represent resonance poles and dashed lines are dynamical zeroes. In the s-channel, poles represent states on the (Λ_α, Λ_γ) trajectory. In the t channel, meson resonances appear. There are no resonance poles in the exotic K^+p channel ($u > 0$).

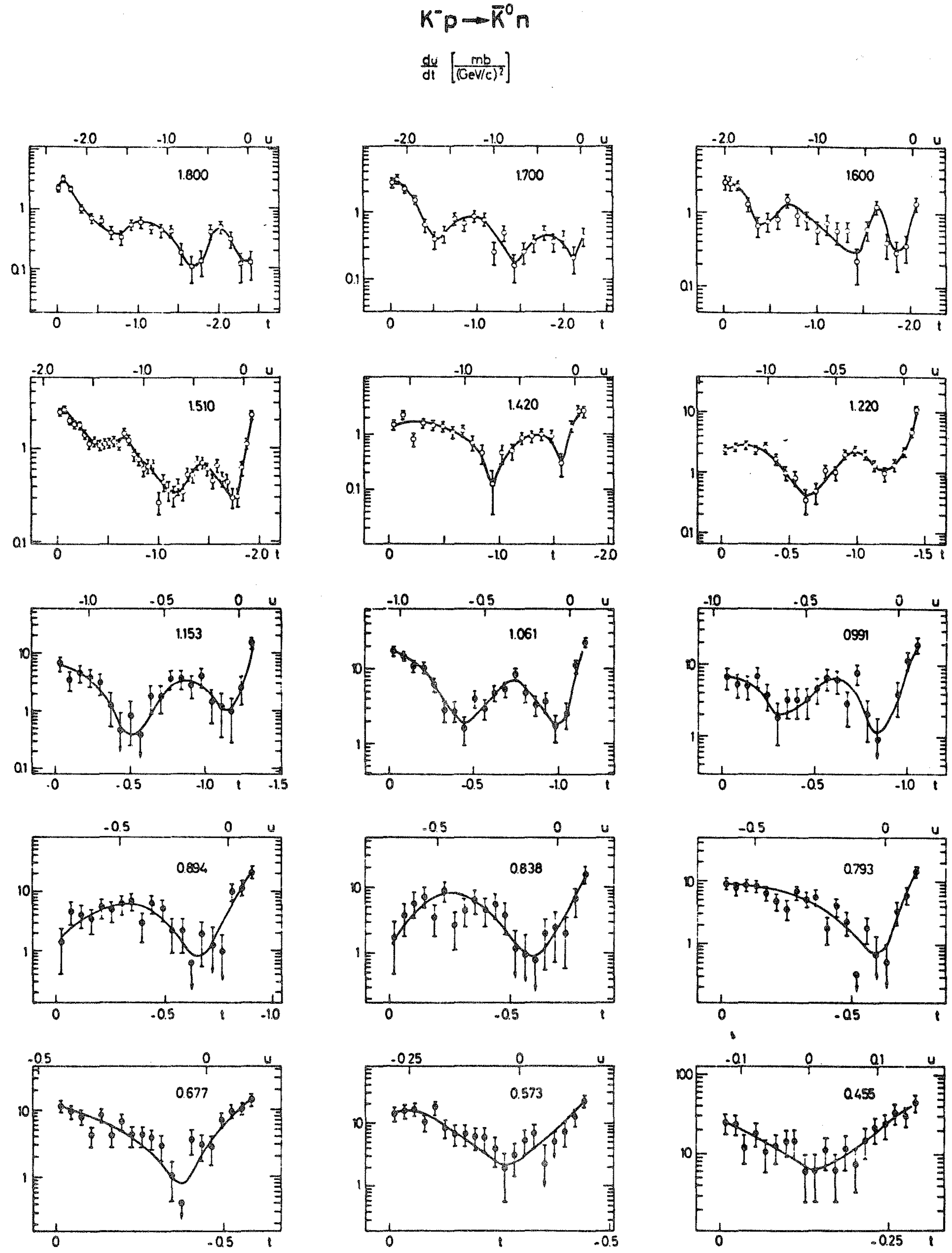

Figure 11: Compilation of low-energy $K^-p \Rightarrow \overline{K}^0n$ differential cross section data by Odorico (1971a). Solid lines are drawn to guide the eye. Indicated in each frame is the value of p_{lab} in GeV/c. The y-axis is labeled with the values of both u and t. Dips appear at constant $u \approx -0.1$, -0.7, and -1.7 $(GeV/c)^2$.

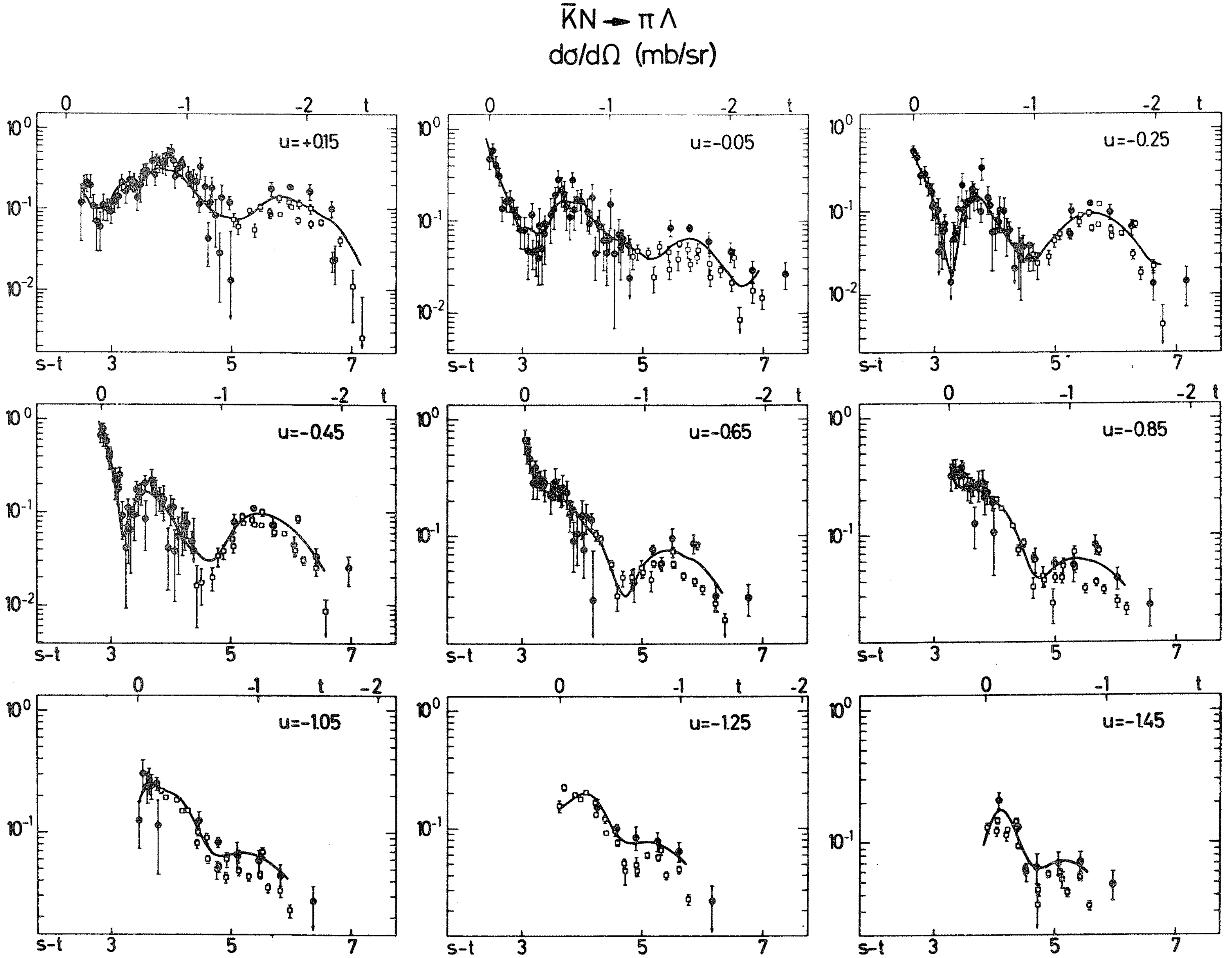

Figure 12: Compilation of $\overline{K}N \to \pi\Lambda$ differential cross section data from p_{lab} = 0.44 to 1.9 GeV/c (Odorico, 1971b,c). Data here are plotted versus t and versus (s - t), for several fixed values of u. (s is the $\overline{K}N$ c.m. energy squared; t is square of the invariant momentum transfer from $\overline{K}$ to π.) Observe the presence of dip structure at the values (s - t) = 3 and 5 GeV^2. Solid lines are drawn to guide the eye.

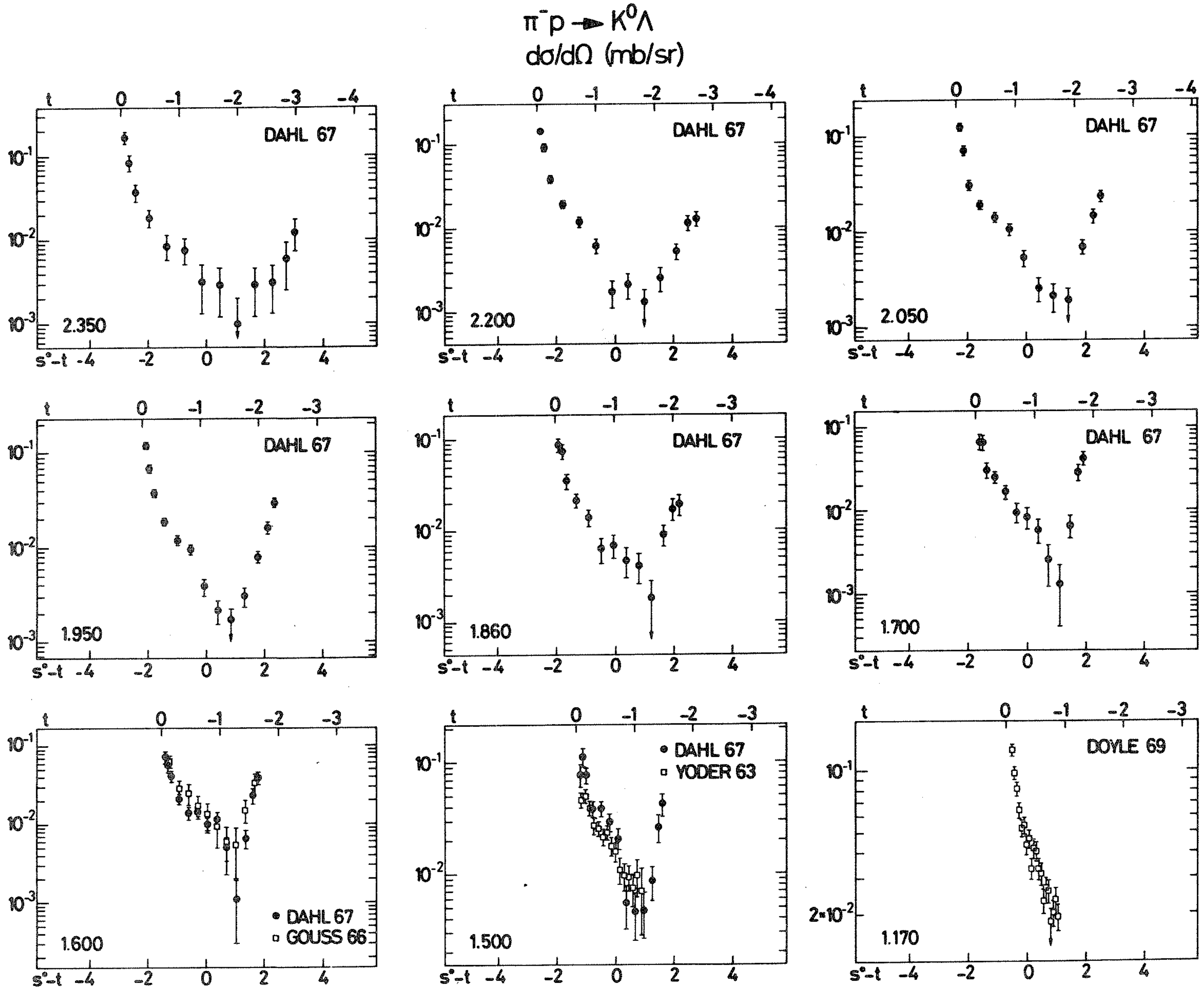

Figure 13: Compilation of low-energy differential cross section data from $\pi^- p \to K^0 \Lambda$ (Odorico, 1971b,c). Values of p_{lab} are indicated in each frame. Axis labels show values of t and of $(s^* - t)$. Here, s^* is the square of invariant momentum transfer from p to K^0. Observe the pronounced dip at $(s^* - t) = 1\ \mathrm{GeV}^2$.

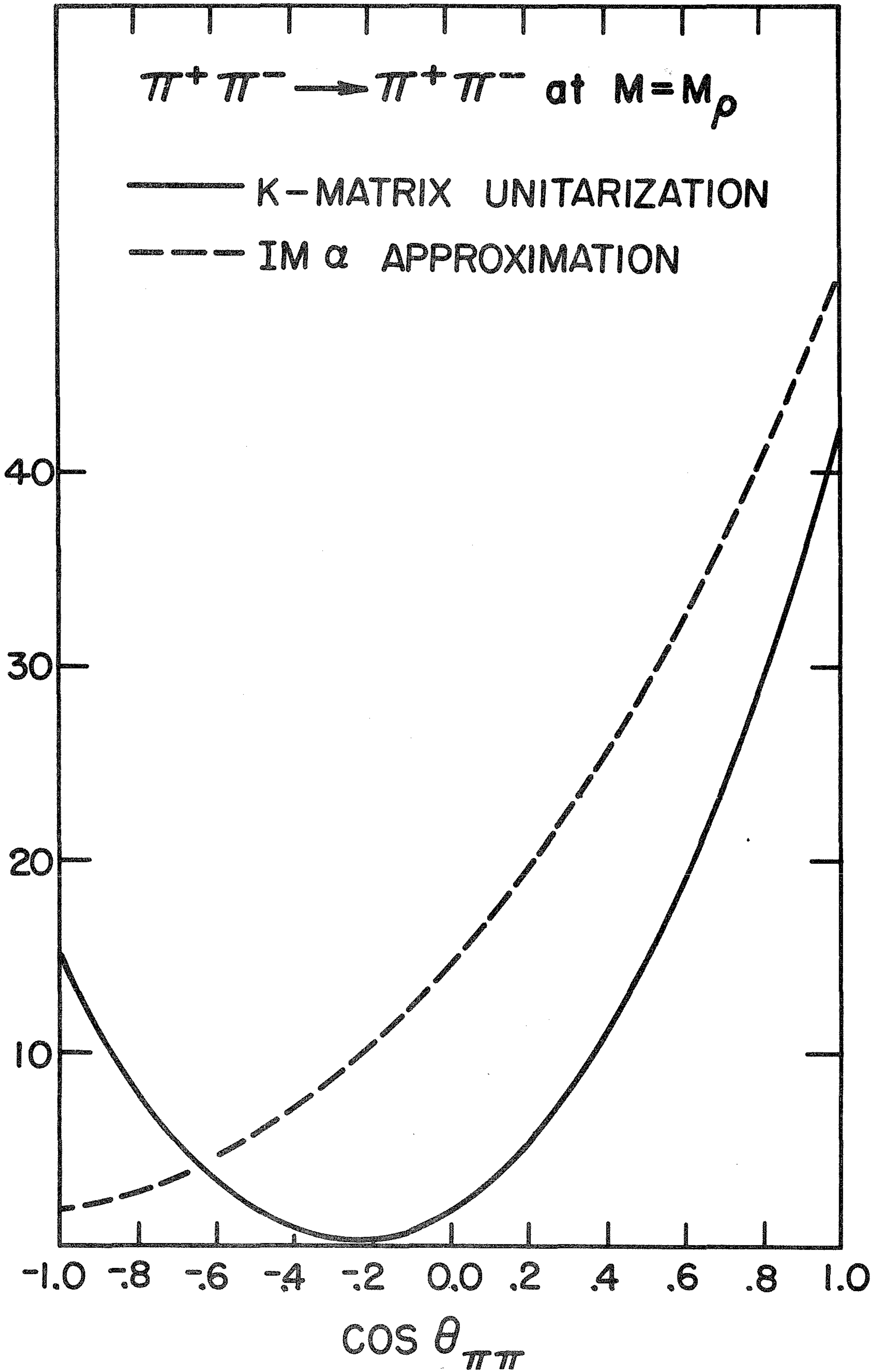

Figure 14: Differential cross sections (arbitrary units) for $\pi^+\pi^-$ elastic scattering at $\sqrt{s} = M = M_\rho$. Here, $\Theta_{\pi\pi}$ is the angle from π^+ to π^+ (as measured in the $\pi\pi$ rest frame). The dashed curve gives the prediction of a simple Veneziano model (Eqs. (1) of text). The solid curve shows the result obtained after Eq. (1) is unitarized by the Lovelace-Wagner K-matrix prescription.

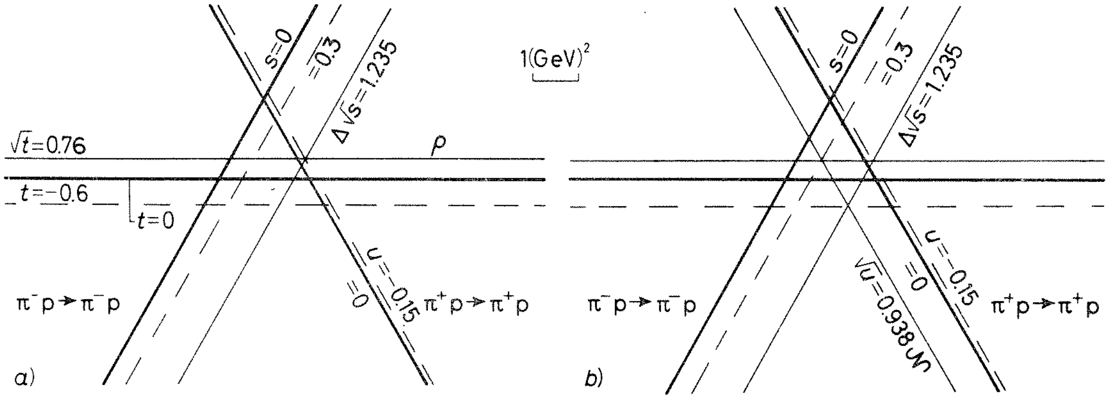

Figure 15: Mandelstam plane for πp elastic scattering. Shown as solid lines are poles representing the nucleon (N), Δ(1238), and ρ resonances. Dashed lines indicate dynamical Veneziano zeroes associated with the intersection points (ρ,N), (N,Δ), and (ρ,Δ). In (a), structure of invariant amplitude A is given; in (b), invariant amplitude B is represented. As usual (Berger and Fox, 1969), no N pole appears in A.

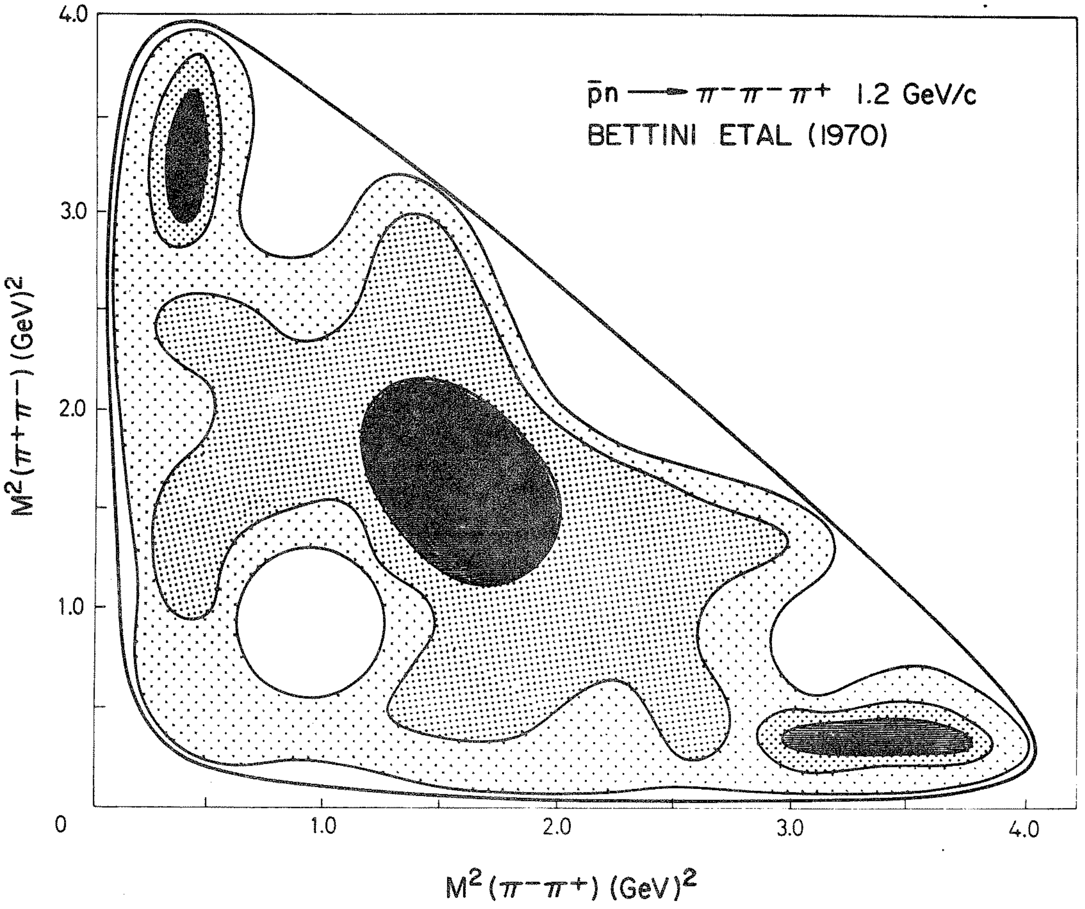

Figure 16: Equal density contour map of the experimental Dalitz plot for the annihilation $\bar{p}n \rightarrow \pi^+\pi^-\pi^-$ at 1.2 GeV/c (from Bettini et al., 1971).

$K^+p \longrightarrow K^\circ\pi^+p$

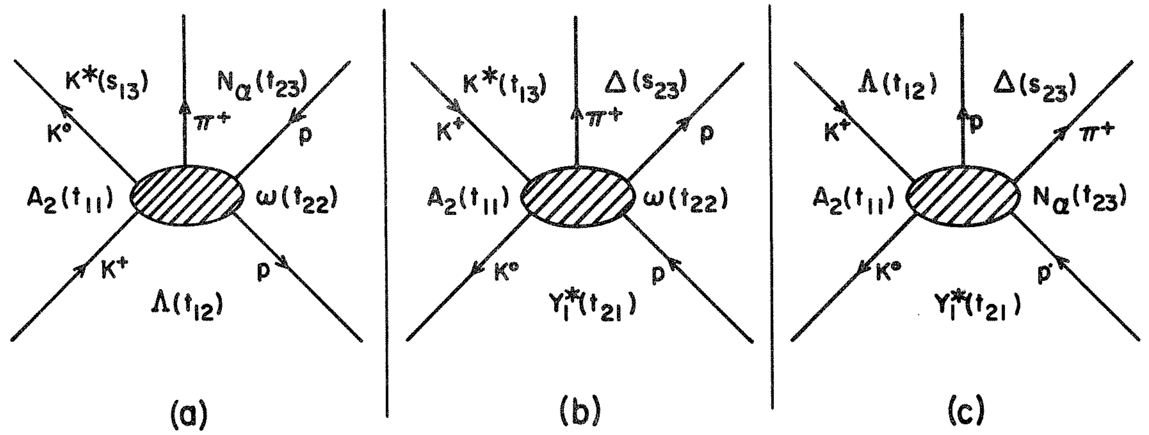
K*(s13)
Nα(t23)
K°
π+
p
A2(t11)
ω(t22)
K+
p
Λ(t12)
(a)
K*(t13)
Δ(s23)
K+
π+
p
A2(t11)
ω(t22)
K°
p
Y1*(t21)
(b)
Λ(t12)
Δ(s23)
K+
p
π+
A2(t11)
Nα(t23)
K°
p
Y1*(t21)
(c)

Figure 17: The three B_5 graphs used by Chan, Ratio, Thomas, and Tornqvist (1970). Arrows on external lines are drawn for the reaction $K^+p \to K^o\pi^+p$. Trajectories chosen by CRTT are indicated. Kinematic variables given in parenthesis (s_{ij}, t_{mn}) serve to indicate whether a trajectory is in the momentum transfer (t_{mn}) or resonance (s_{ij}) region.

$K^-p \longrightarrow \bar{K}^\circ\pi^-p$

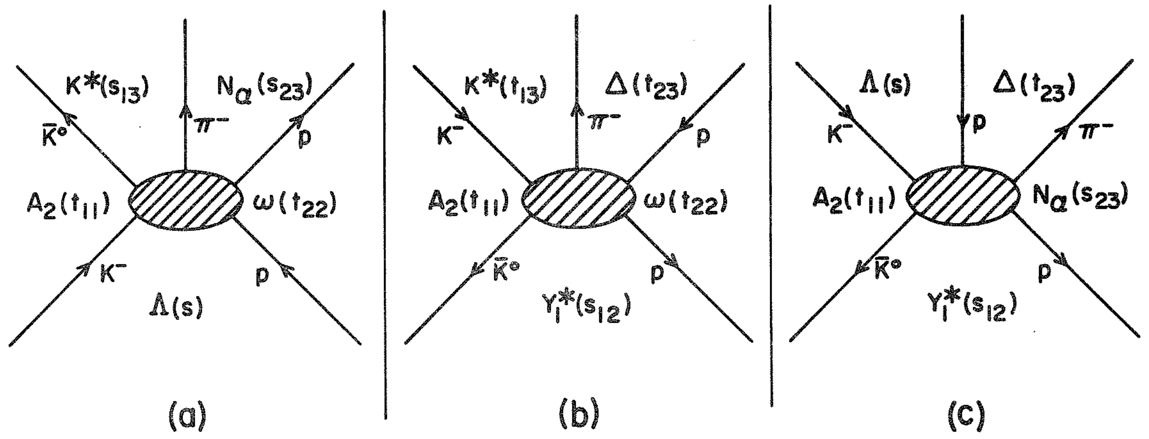
K*(s13)
Nα(s23)
K̄°
π−
p
A2(t11)
ω(t22)
K−
p
Λ(s)
(a)
K*(t13)
Δ(t23)
K−
π−
p
A2(t11)
ω(t22)
K̄°
p
Y1*(s12)
(b)
Λ(s)
Δ(t23)
K−
p
π−
A2(t11)
Nα(s23)
K̄°
p
Y1*(s12)
(c)

Figure 18: The graphs of Fig. 17 are repeated, except that arrows are drawn here for $K^-p \to \bar{K}^o\pi^-p$. Appropriate changes are made also in labeling of kinematic variables (s_{ij}, t_{mn}).

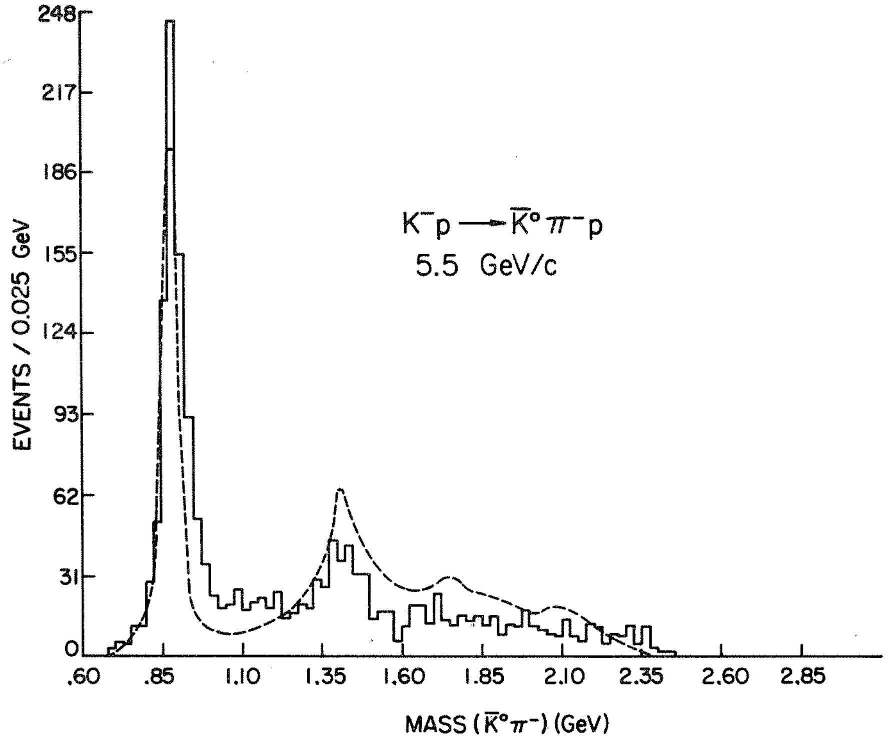

Figure 19: Histogram of cross section versus invariant mass of $(\bar{K}^o\pi^-)$ from $K^-p \to \bar{K}^o\pi^-p$ at 5.5 GeV/c. The dashed curve is the prediction of the CRTT model, normalized to data in this plot. Data were obtained by an Argonne-University of Chicago collaboration (B. Musgrave and H. Yuta, private communication); curves in this and in Figs. 20 to 23 were computed by Berger and Fox.

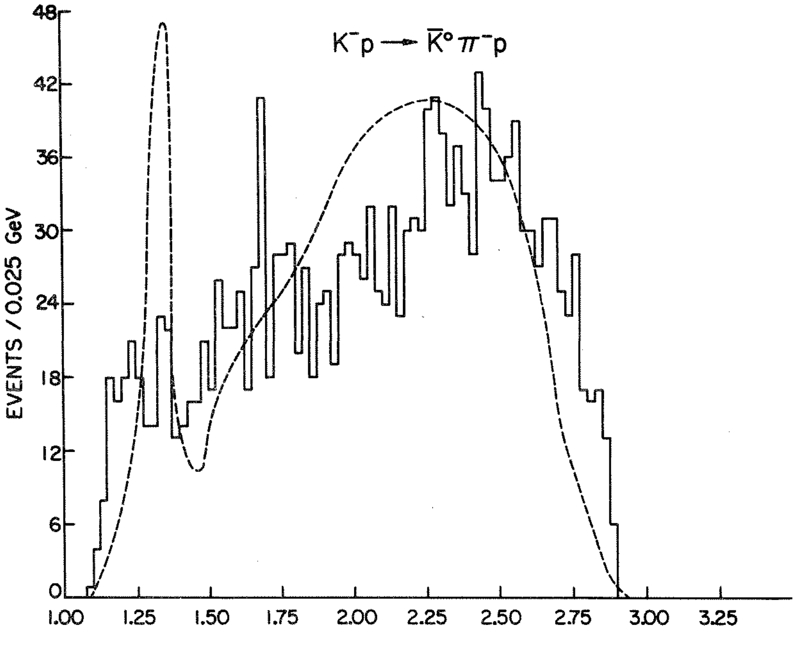

Figure 20: Histogram of cross section versus invariant mass of (π^-p) from $K^-p \to \bar{K}^o\pi^-p$, at 5.5 GeV/c, along with dashed line prediction of the CRTT model. See caption of Fig. 19 for further details.

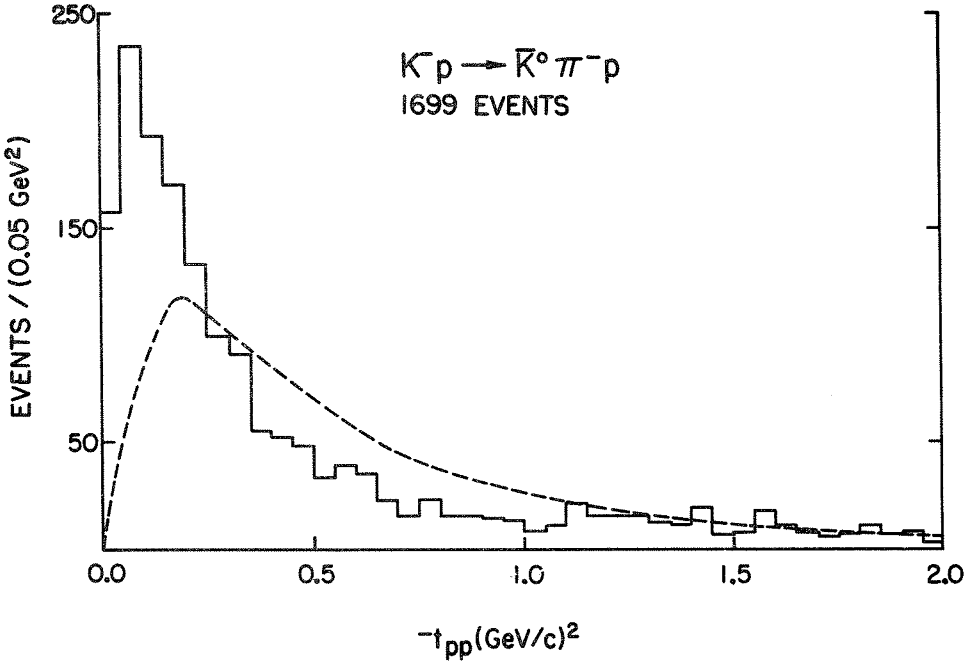

Figure 21: Histogram of differential cross section versus square of invariant momentum transfer from incident to final proton in the reaction $K^-p \rightarrow \bar{K}^0\pi^-p$. The dashed curve gives the prediction of the CRTT model. See text and caption of Fig. 19 for further details.

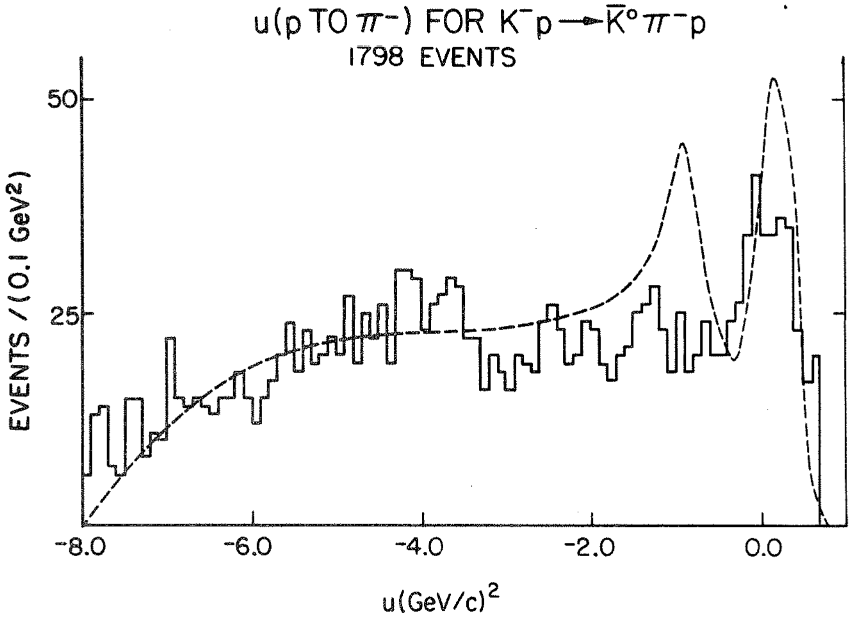

Figure 22: Histogram of differential cross section versus square of invariant momentum transfer from incident proton to final π^- in the reaction $K^-p \rightarrow \bar{K}^0\pi^-p$ at 5.5 GeV/c. The dashed curve gives the prediction of the CRTT model. See text and caption of Fig. 19 for further details.

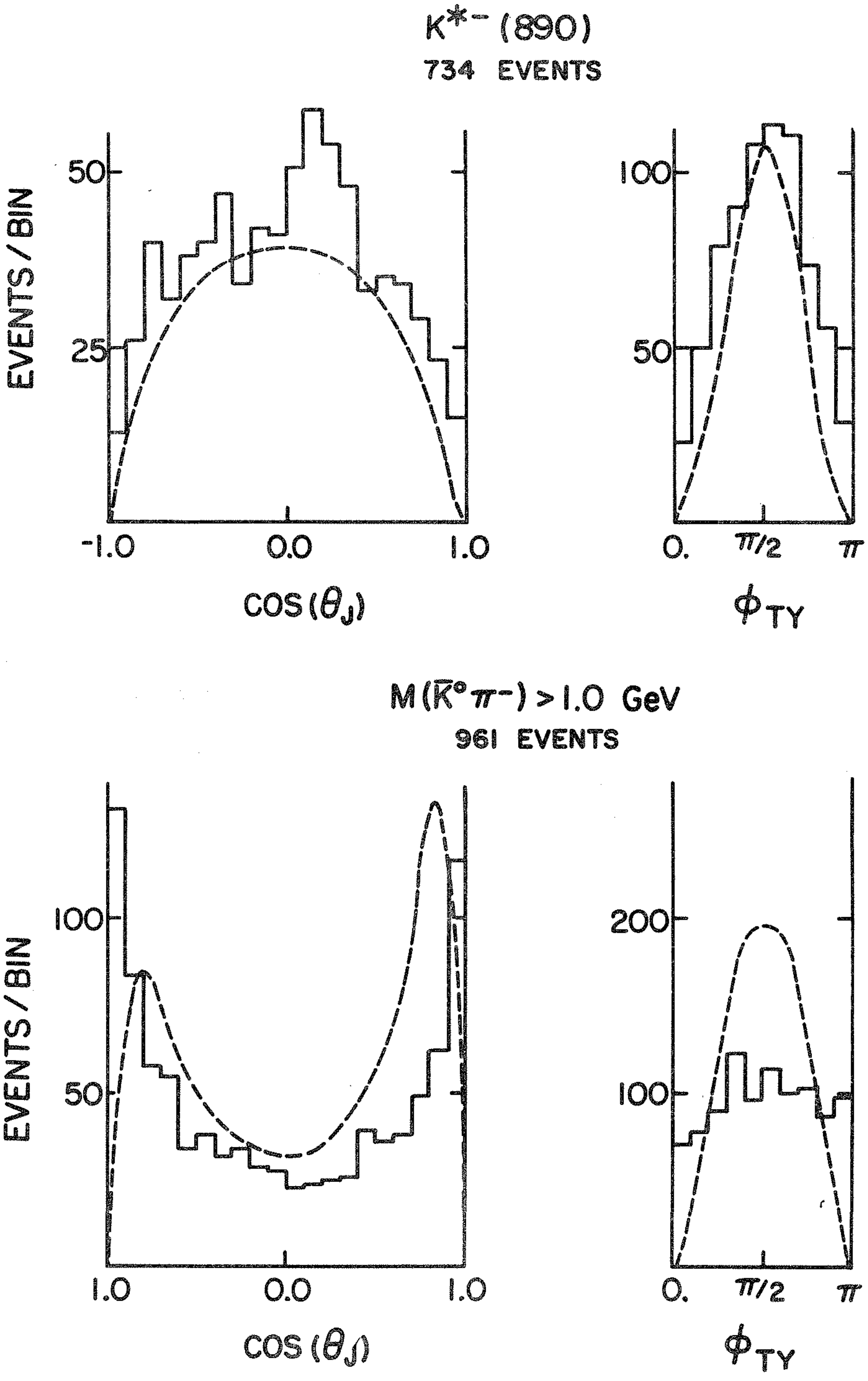

Figure 23: Angular distributions in the $K^*(890)$ mass region and for events with $\bar{K}^0\pi^-$ mass greater than 1 GeV. Here, Θ_J and ϕ_{TY} are the Jackson and Treiman-Yang angles, respectively, which define the direction of motion of $\bar{K}^0$ with respect to K^- in $\bar{K}^0\pi^-$ rest frame. Data are from $K^-p \rightarrow \bar{K}^0\pi^-p$ at 5.5 GeV/c and dashed curves are predictions of the CRTT B_5 model. See caption of Fig. 19 for further details.

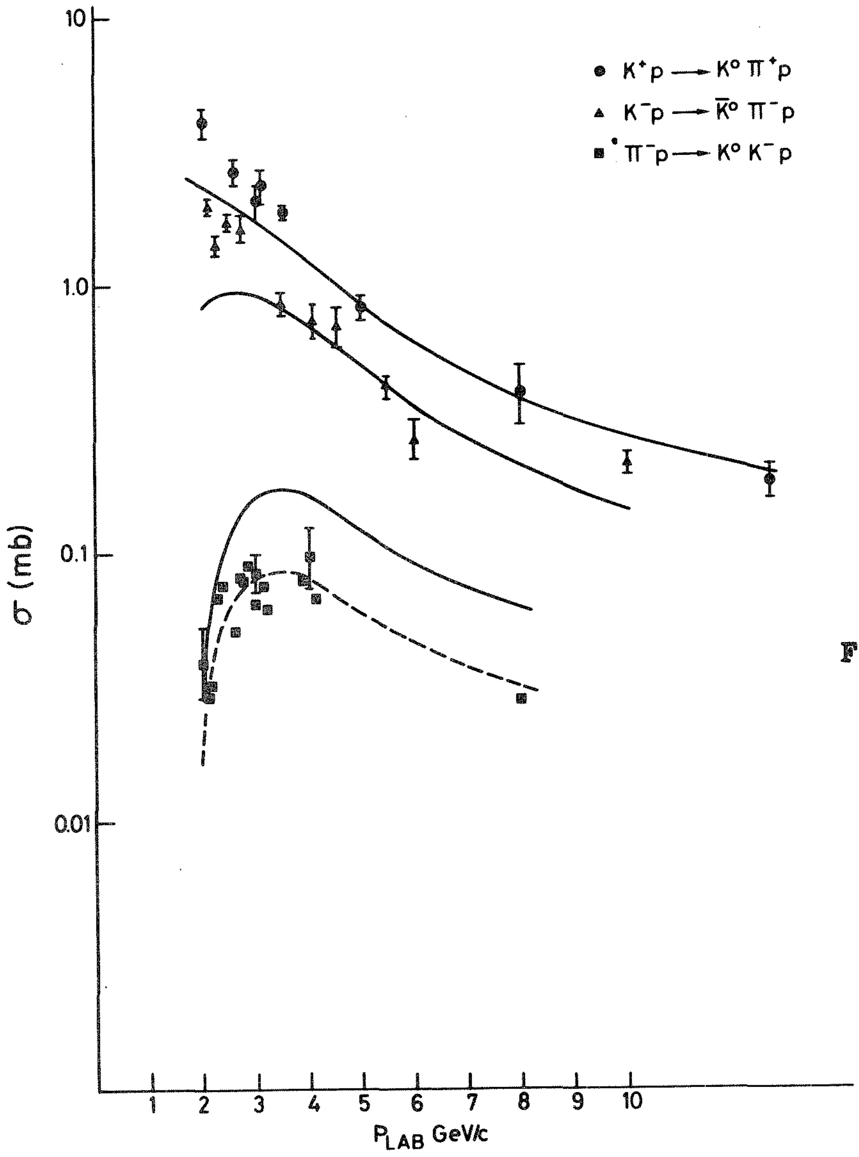

Fig. 24: Figure taken from the paper of Chan, Ratio, Thomas, and Tornqvist (1970). Their amplitude is normalized to the experimental total cross section for $K^+p \to K^o\pi^+p$ at 5 GeV/c. Solid lines give their predictions for cross section versus energy for three processes related by crossing symmetry: $K^+p \to K^o\pi^+p$, $K^-p \to \bar{K}^o\pi^-p$ and $\pi^-p \to K^oK^-p$. Their prediction agrees well with data for $K^-p \to \bar{K}^o\pi^-p$, but is too high by a factor of two for $\pi^-p \to K^oK^-p$. For this latter process, the dashed curve shows their prediction scaled by the factor 1/2. For experimental references, see CRTT (1970).

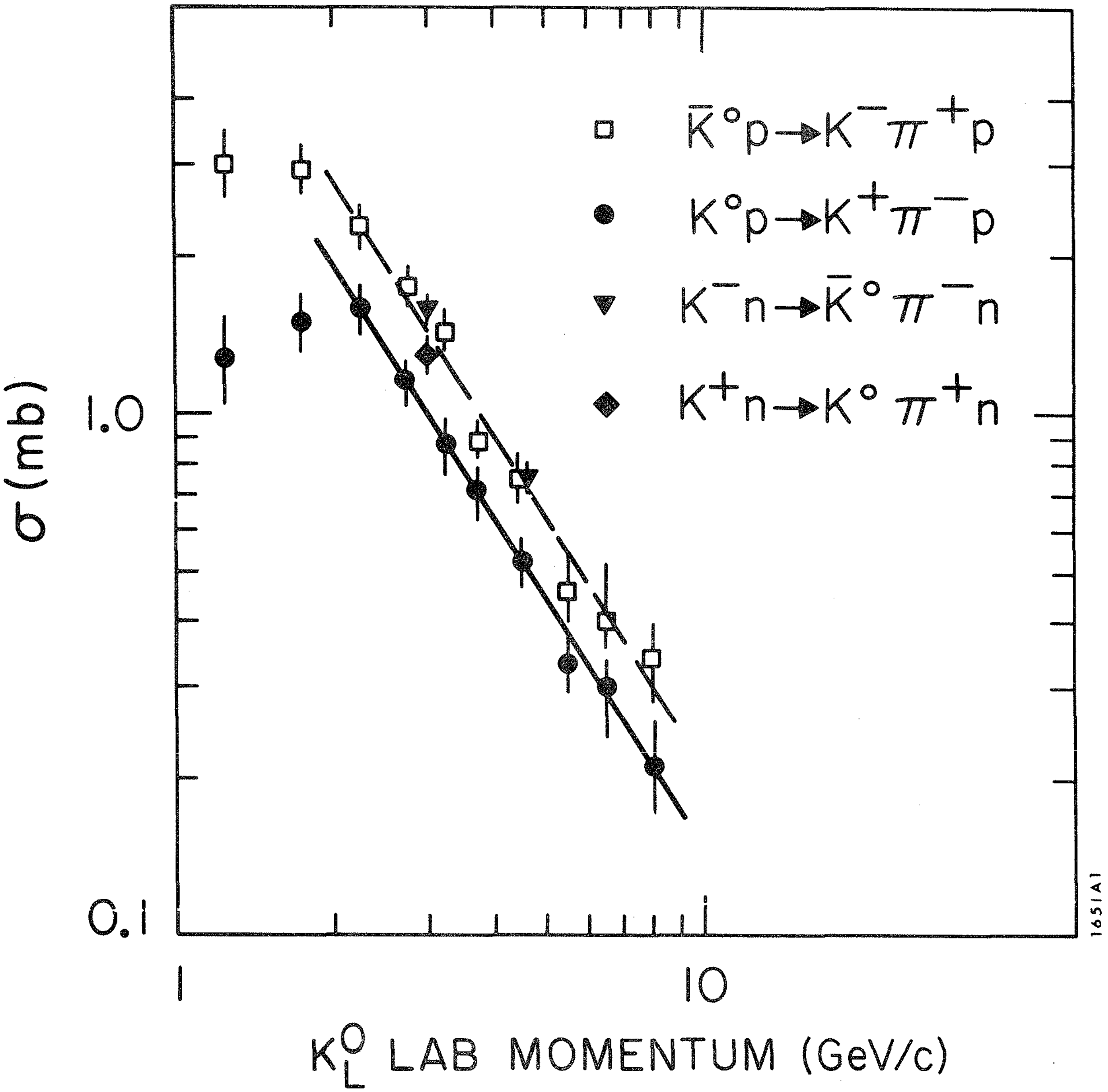

Figure 25: A figure from the paper of Brody et al. (1970) giving their measured values for total cross sections of $\bar{K}^0 p \to K^- \pi^+ p$ and $K^0 p \to K^+ \pi^- p$, as a function of lab momentum. For comparison, Brody et al. also list cross sections for the charge-symmetric processes $K^+ n \to K^0 \pi^+ n$ and $K^- n \to \bar{K}^0 \pi^- n$; see their paper for references. The solid and dashed lines are drawn to guide the eye; these lines have slope -1.6.

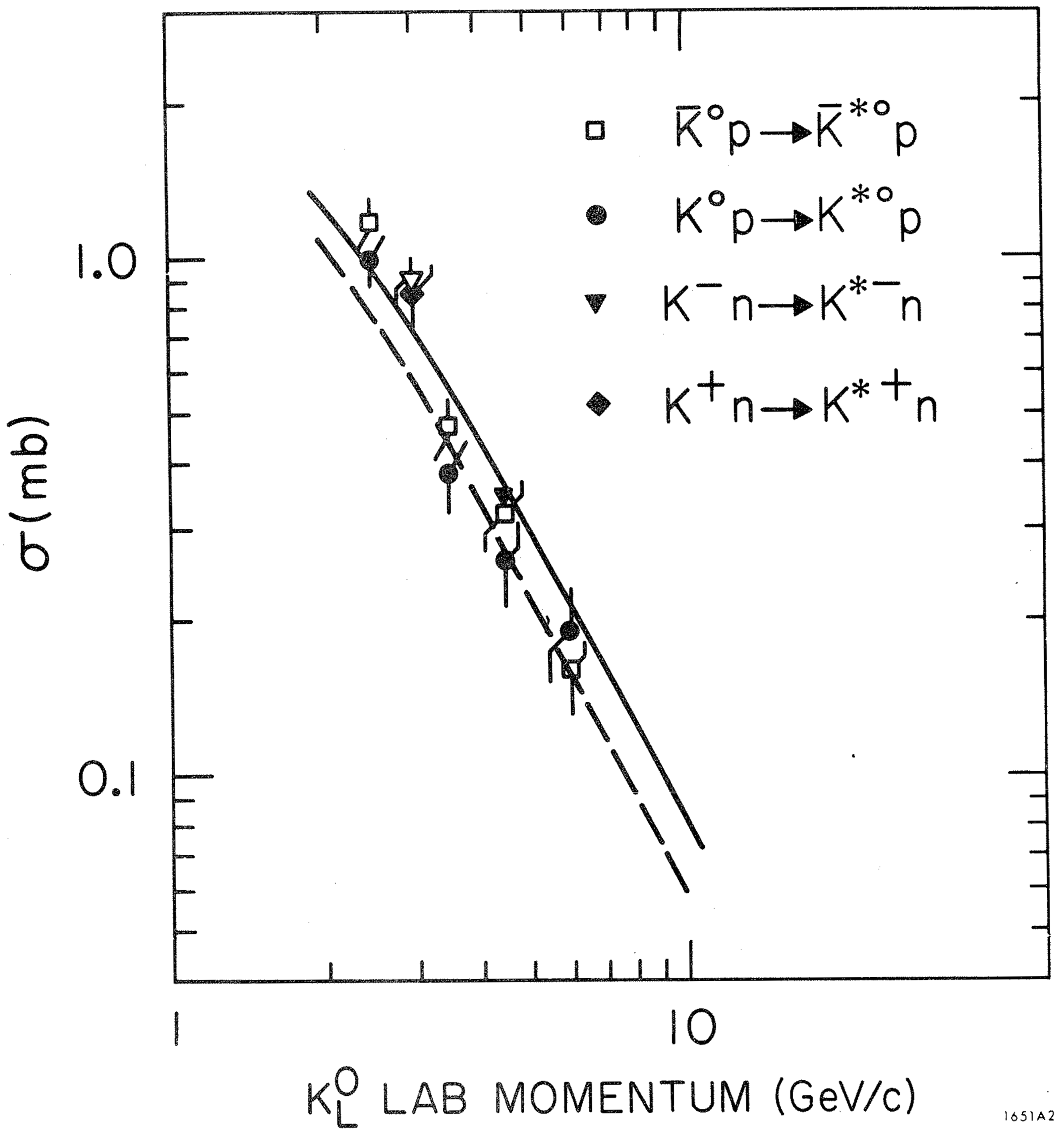

Figure 26: Total cross sections versus lab momentum for the K^*N subsamples in $K^0p \to K^+\pi^-p$ and $K^0p \to K^-\pi^+p$ (from Brody et al., 1970). Solid and dashed curves are predictions of a typical Regge pole model (Dass and Froggatt, 1970). If integrated from 2 to 7 GeV/c, the experimental ratio $\sigma(K^{*0}p)/\sigma(\bar{K}^{*0}p) = 0.88 \pm 0.10$, whereas the Dass-Froggatt model predicts 1.27.

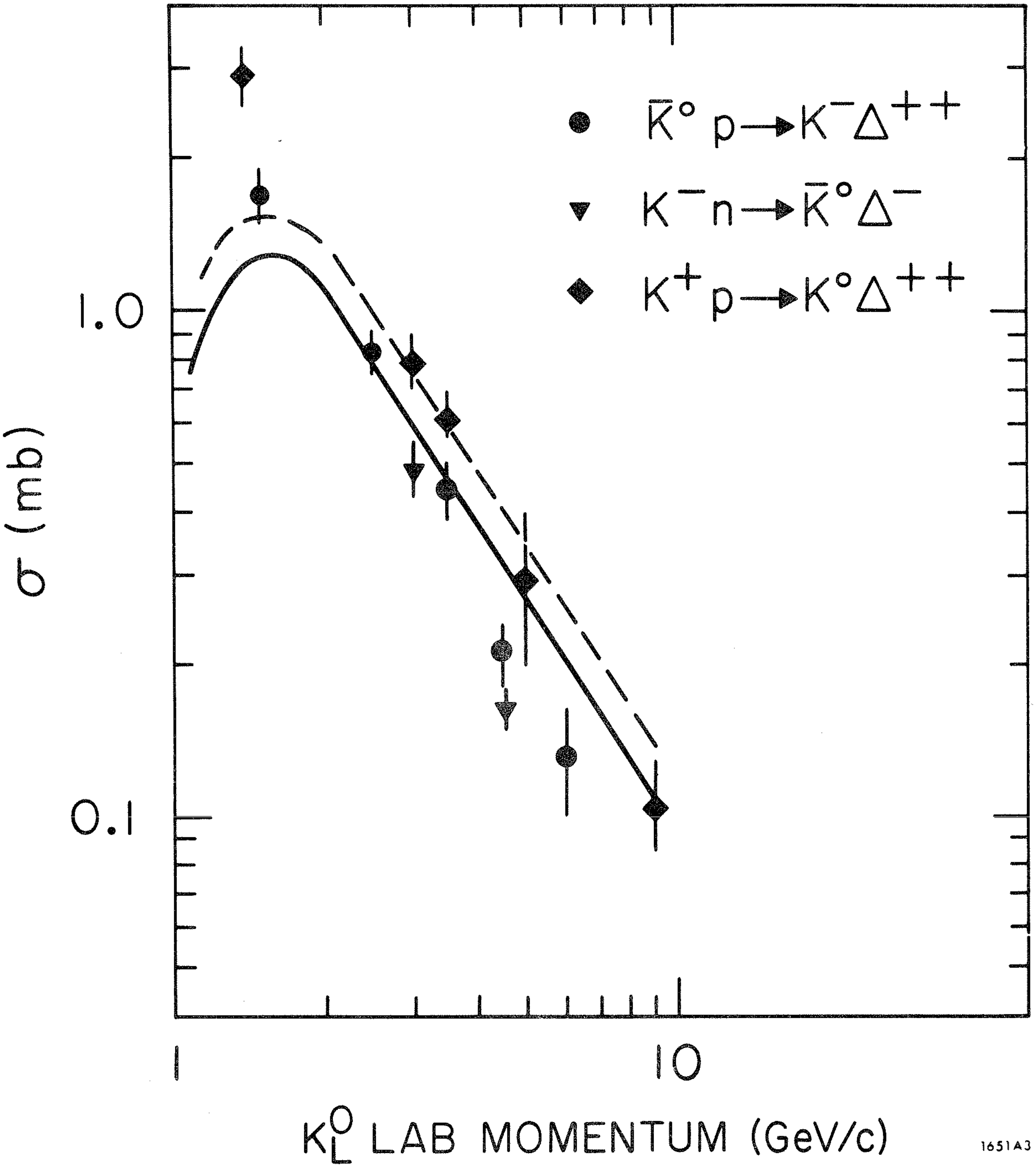

Figure 27: Another figure taken from Brody et al., 1970. Shown are total cross sections versus lab momentum for $\bar{K}^0 p \to K^- \Delta^{++}$ (Brody et al., 1970), $K^+ p \to K^0 \Delta^{++}$ (Price et al., 1969), and $K^- n \to \bar{K}^0 \Delta^-$. Solid and dashed curves are predictions of Dass and Froggatt (1970). Here, theory reproduces (qualitatively) the fact that $\sigma(K^+ p \to K^0 \Delta^{++}) > \sigma(\bar{K}^0 p \to K^- \Delta^{++})$.

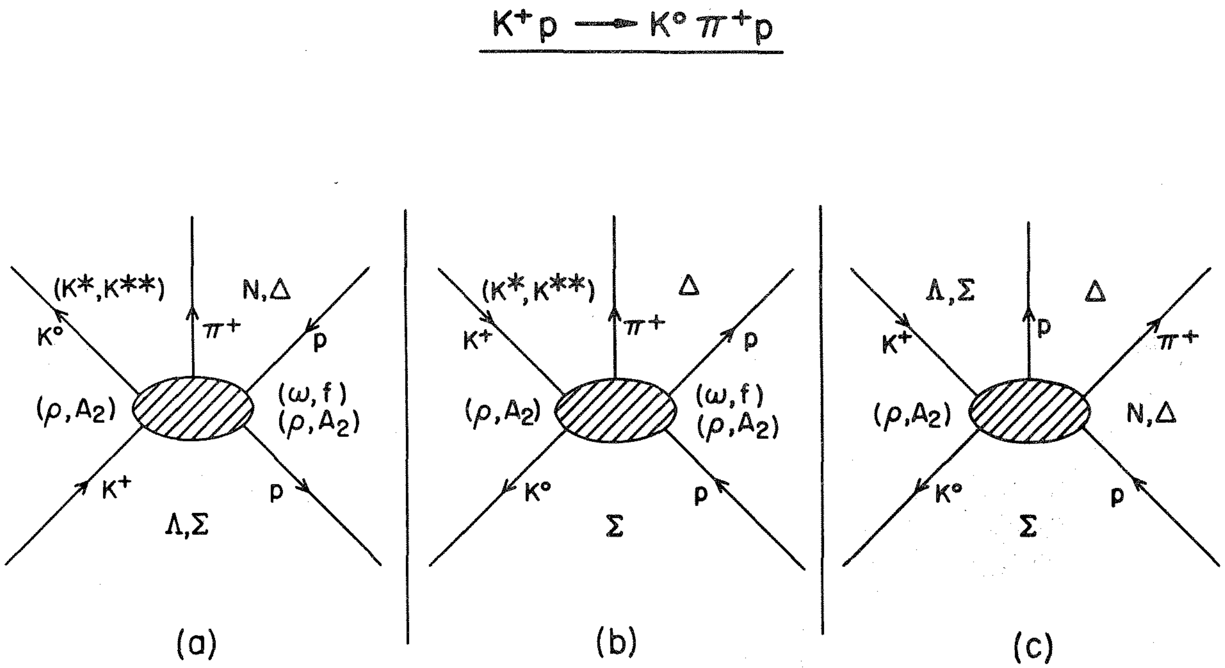
$K^+p \longrightarrow K^o \pi^+ p$
(K^*,K^{**})
N,Δ
K^o
π^+
p
(ρ,A_2)
(ω,f)
(ρ,A_2)
K^+
p
Λ,Σ
(a)
(K^*,K^{**})
Δ
K^+
π^+
p
(ρ,A_2)
(ω,f)
(ρ,A_2)
K^o
p
Σ
(b)
Λ,Σ
Δ
K^+
p
π^+
(ρ,A_2)
N,Δ
K^o
p
Σ
(c)

Figure 28: For $K^+p \to K^o\pi^+p$, these are the three B_5 graphs which correspond to the three allowed quark-duality diagrams. Possible choices of trajectories are listed for the various channels.

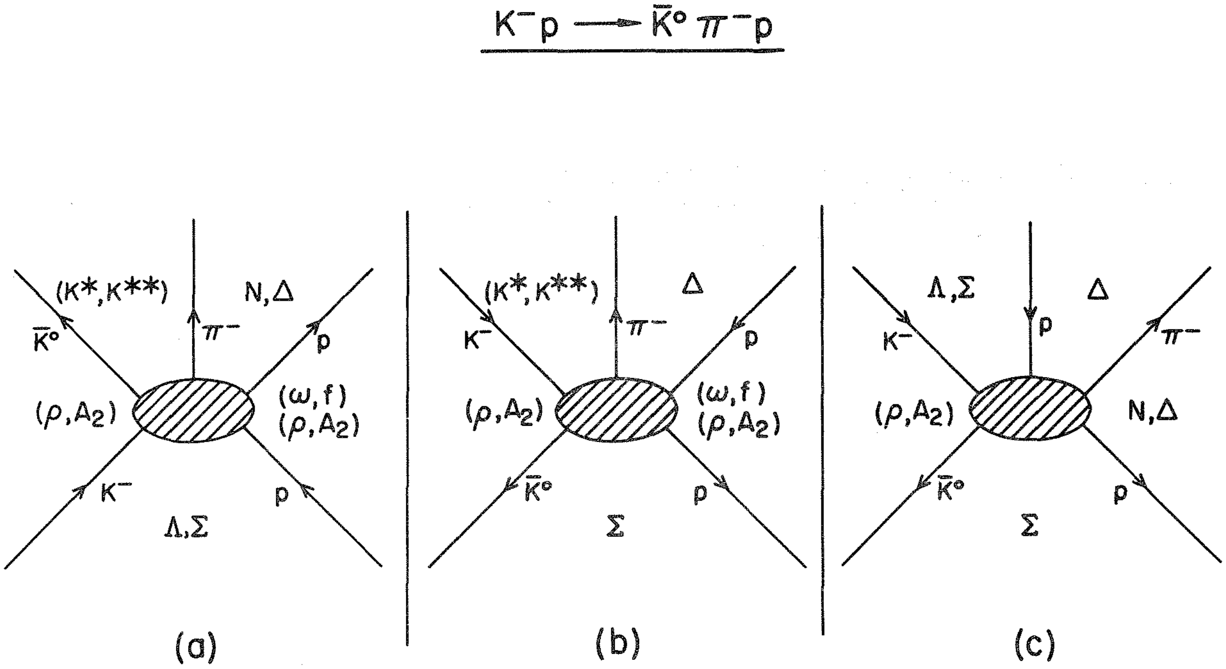
$K^-p \longrightarrow \bar{K}^o \pi^- p$
(K^*,K^{**})
N,Δ
$\bar{K}^o$
π^-
p
(ρ,A_2)
(ω,f)
(ρ,A_2)
K^-
p
Λ,Σ
(a)
(K^*,K^{**})
Δ
K^-
π^-
p
(ρ,A_2)
(ω,f)
(ρ,A_2)
$\bar{K}^o$
p
Σ
(b)
Λ,Σ
Δ
K^-
p
π^-
(ρ,A_2)
N,Δ
$\bar{K}^o$
p
Σ
(c)

Figure 29: The same set of graphs shown in Fig. 28, but with arrows on external lines drawn to correspond to $K^-p \to \bar{K}^o\pi^-p$.

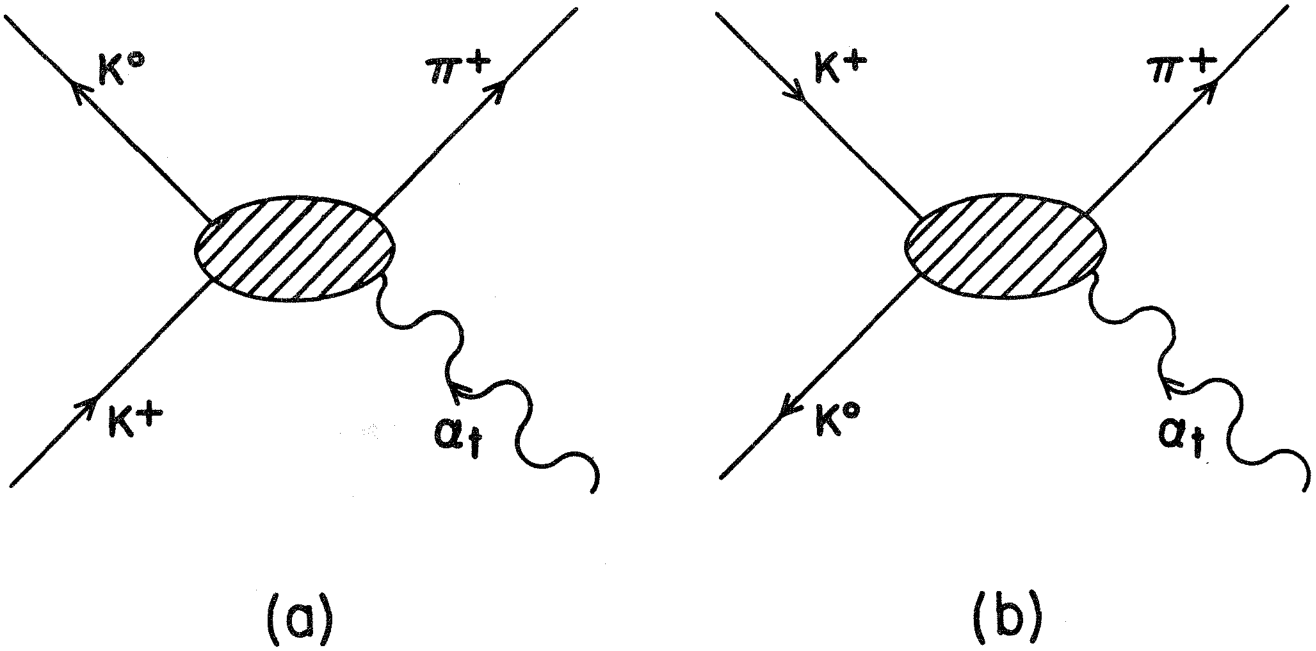

Figure 30: Four-point (2 → 2) processes obtained by factoring graphs (a) and (b) of Fig. 28 at the exchanged Regge pole α_t which couples to the $\bar{p}p$ vertex.

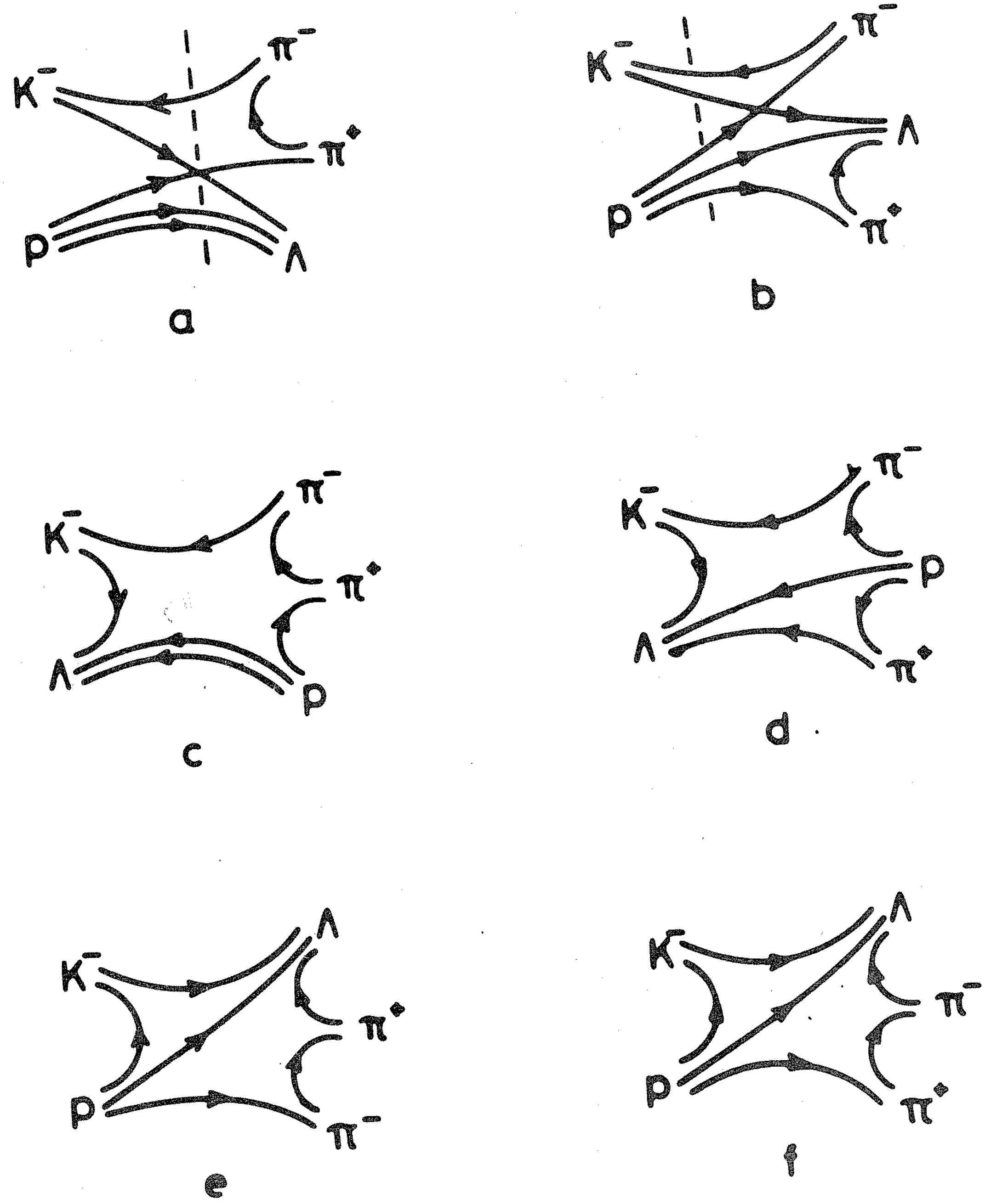
K⁻
π⁻
π⁺
p
Λ
a
K⁻
π⁻
Λ
p
π⁺
b
K⁻
π⁻
π⁺
Λ
p
c
K⁻
π⁻
p
Λ
π⁺
d
K⁻
Λ
π⁺
p
π⁻
e
K⁻
Λ
π⁻
p
π⁺
f

Figure 31: Quark-duality diagrams for the reaction $K^- p \rightarrow \pi^+ \pi^- \Lambda$.

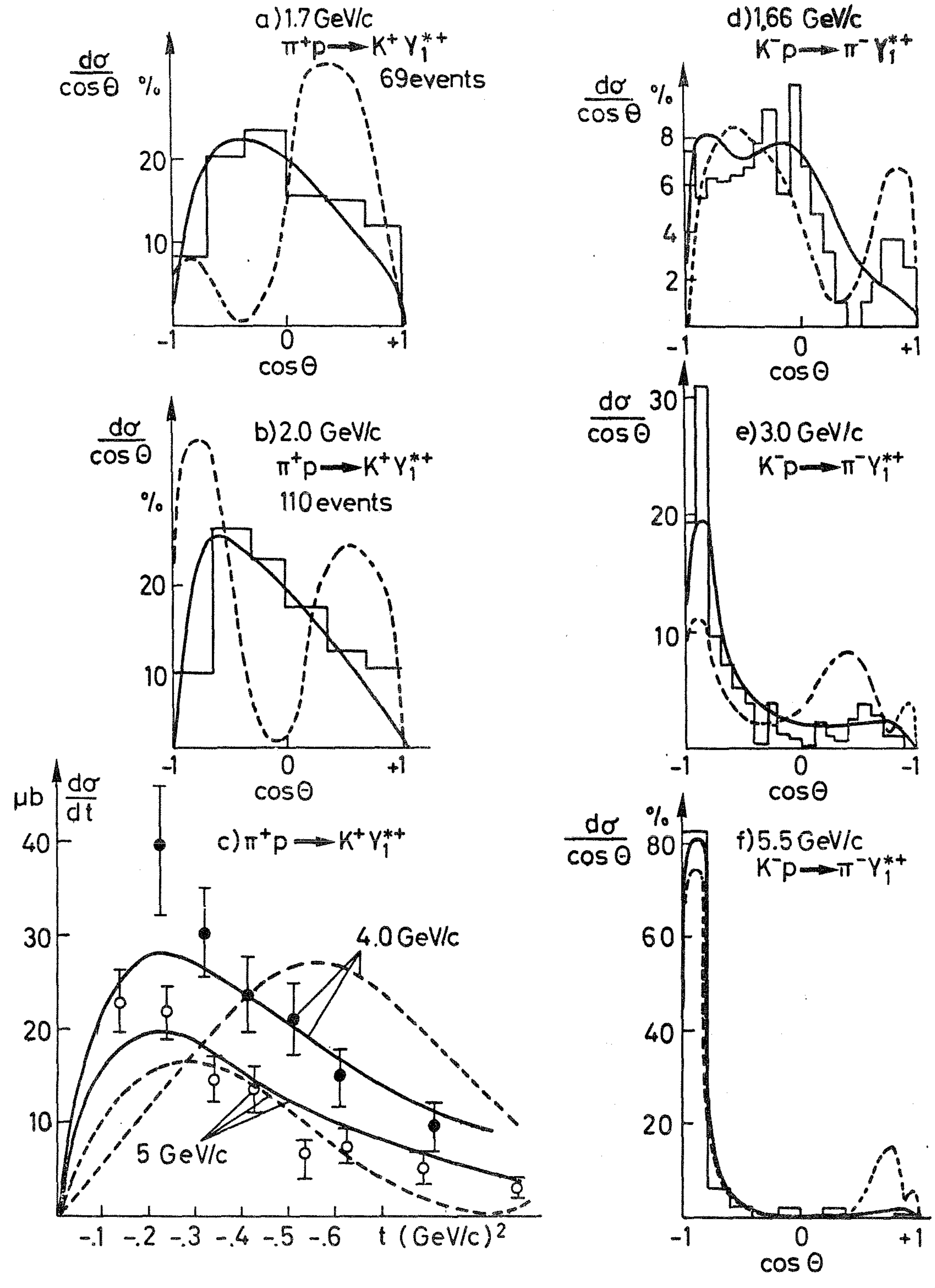

Figure 32: Distributions computed by Törnqvist (1970) for $\pi^+p \to K^+Y_1^{*+}$ and $K^-p \to \pi^-Y_1^{*+}$. Solid curves are obtained from a model in which B_5 functions correspond to quark-duality diagrams ((a) and (b) of Fig. 31) forbidden by the Rosner-Harari rules. Dashed curves are obtained from a second model in which only allowed diagrams are employed.

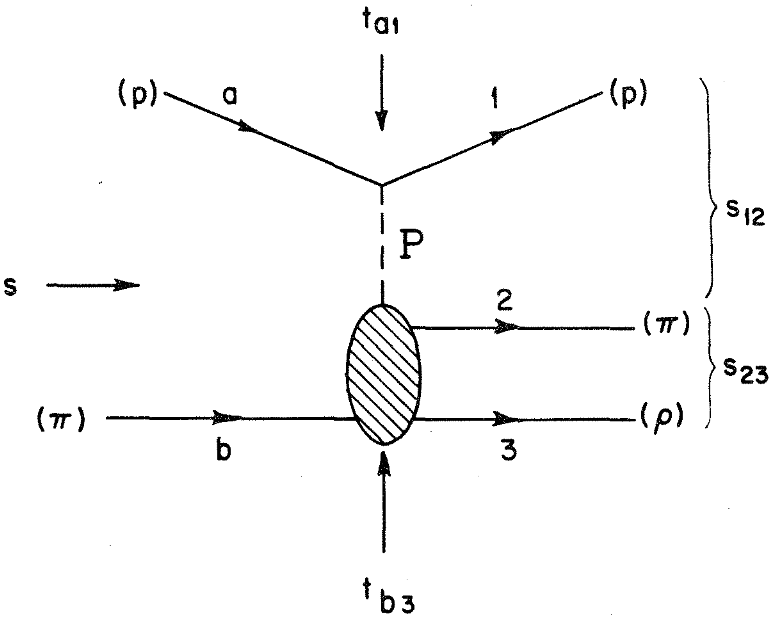

Figure 33: Diagram illustrating diffraction-dissociation of hadron b [π] into system (23) [ρπ]. Symbol P denotes Pomeron exchange.

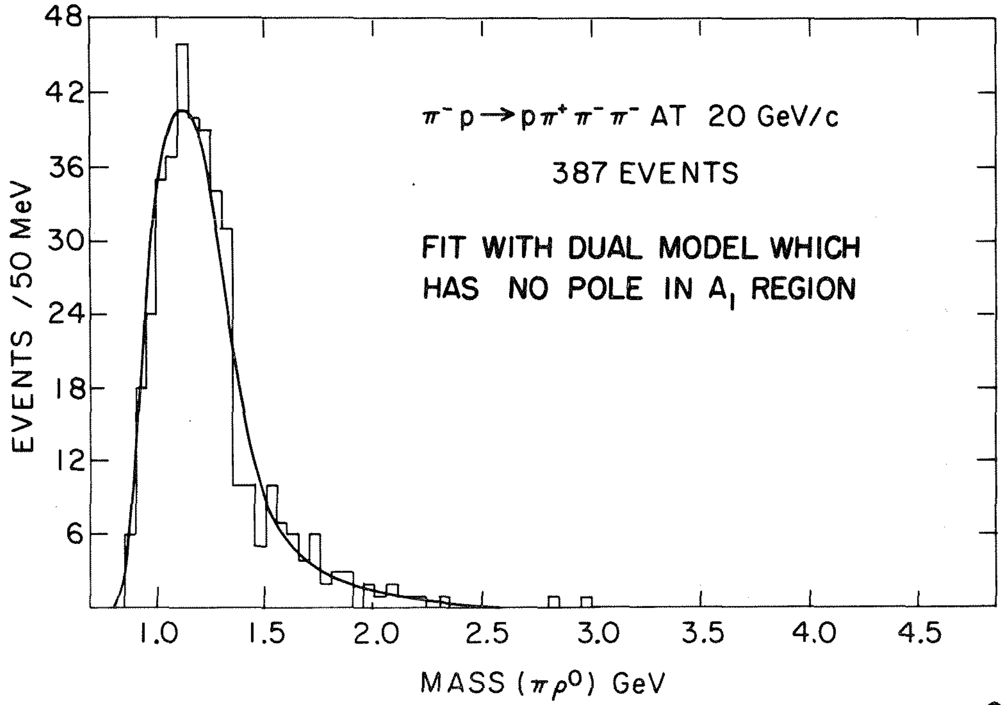

Figure 34: Histogram of the cross section vs. invariant mass of $\pi^-\rho^0$ from the reaction $\pi^- p \rightarrow \pi^- \rho^0 p$ at 20 GeV/c. The solid curve is obtained from a dual model which, as described in the text, has no resonance poles in the A_1 region (M ~ 1.1 GeV). Data are from Brandenburg et al. (1970). The following selections are made in both data and theory: Mass $(p\pi^-) \geq 2$ GeV and $|t_{\pi\rho}| \leq 1$ $(\mathrm{GeV}/c)^2$; these cuts do not alter quality of results.

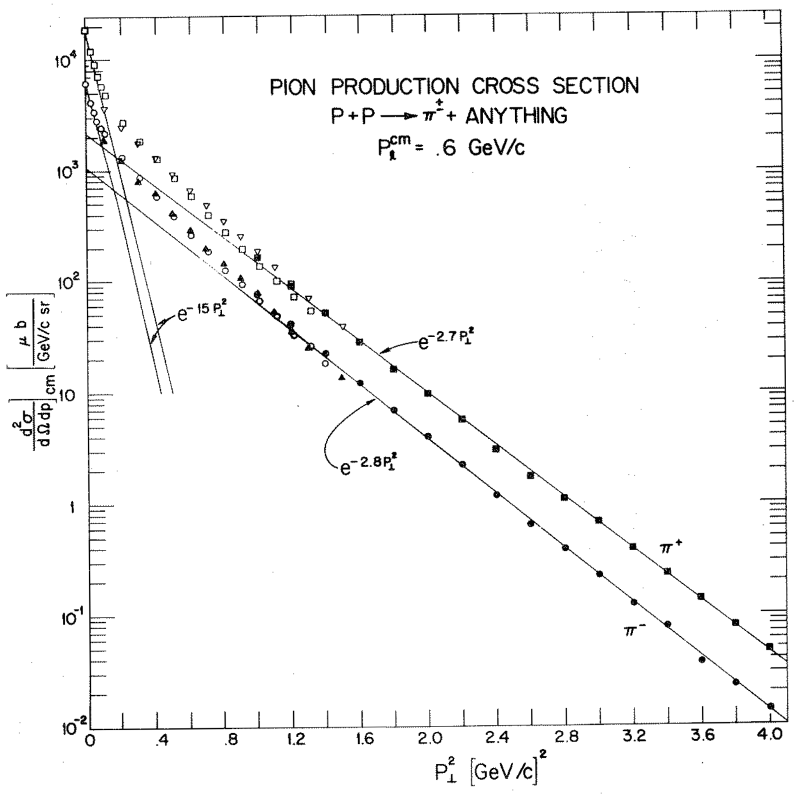

Fig. 35: Plot of $d^2\sigma/d\Omega\, dp$ versus p_T^2 for production of $\pi^\pm$ in the inclusive reactions $pp \rightarrow \pi^\pm$ plus anything (from Akerlof et al., 1971). Symbol p_T denotes the component of pion momentum transverse to the direction of the incident beam. Longitudinal momentum p_L of the pion in the c.m. frame is held fixed at 0.6 GeV/c. Curves are straight line fits to the data.

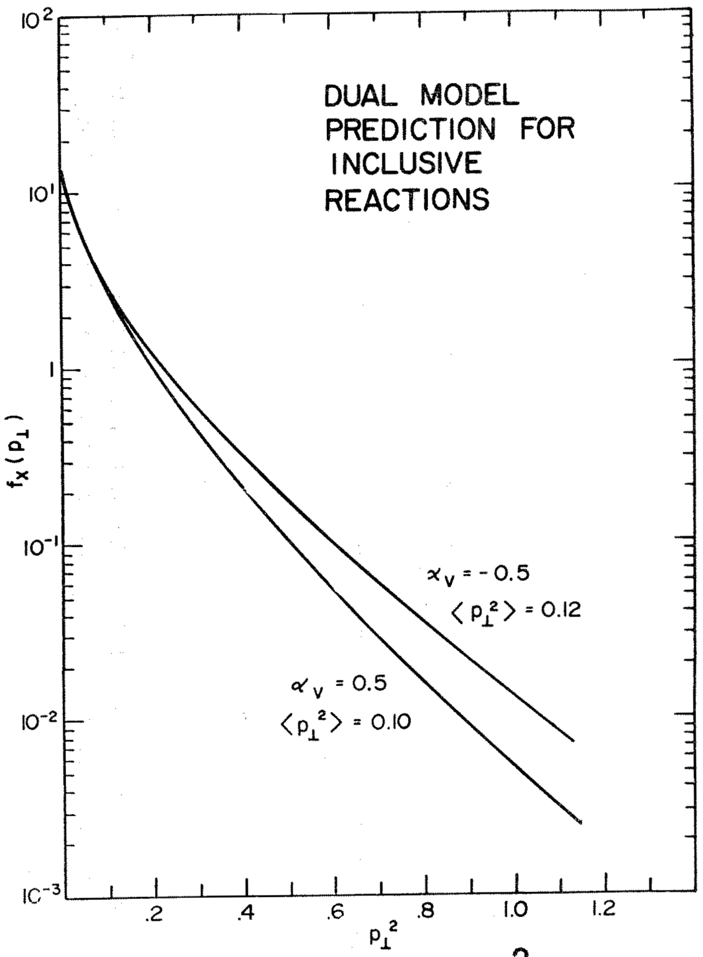

Fig. 36: A prediction for the p_T^2 dependence of $f_x(p_T)$ obtained from the six-point dual model (B_6) by deTar et al. (1971). Function $f_x(p_T)$ is related to the inclusive cross section $\sigma_{ab}^{\ x}$ for $ab \rightarrow x$ plus anything, as follows: $E_x(d\sigma_{ab}^{\ x}/d^3p_x) = \sigma_{ab}\, f_x(p_T)$. Here, σ_{ab} is the total cross section for ab scattering; (E_x, p_x) is the four-momentum of particle x.

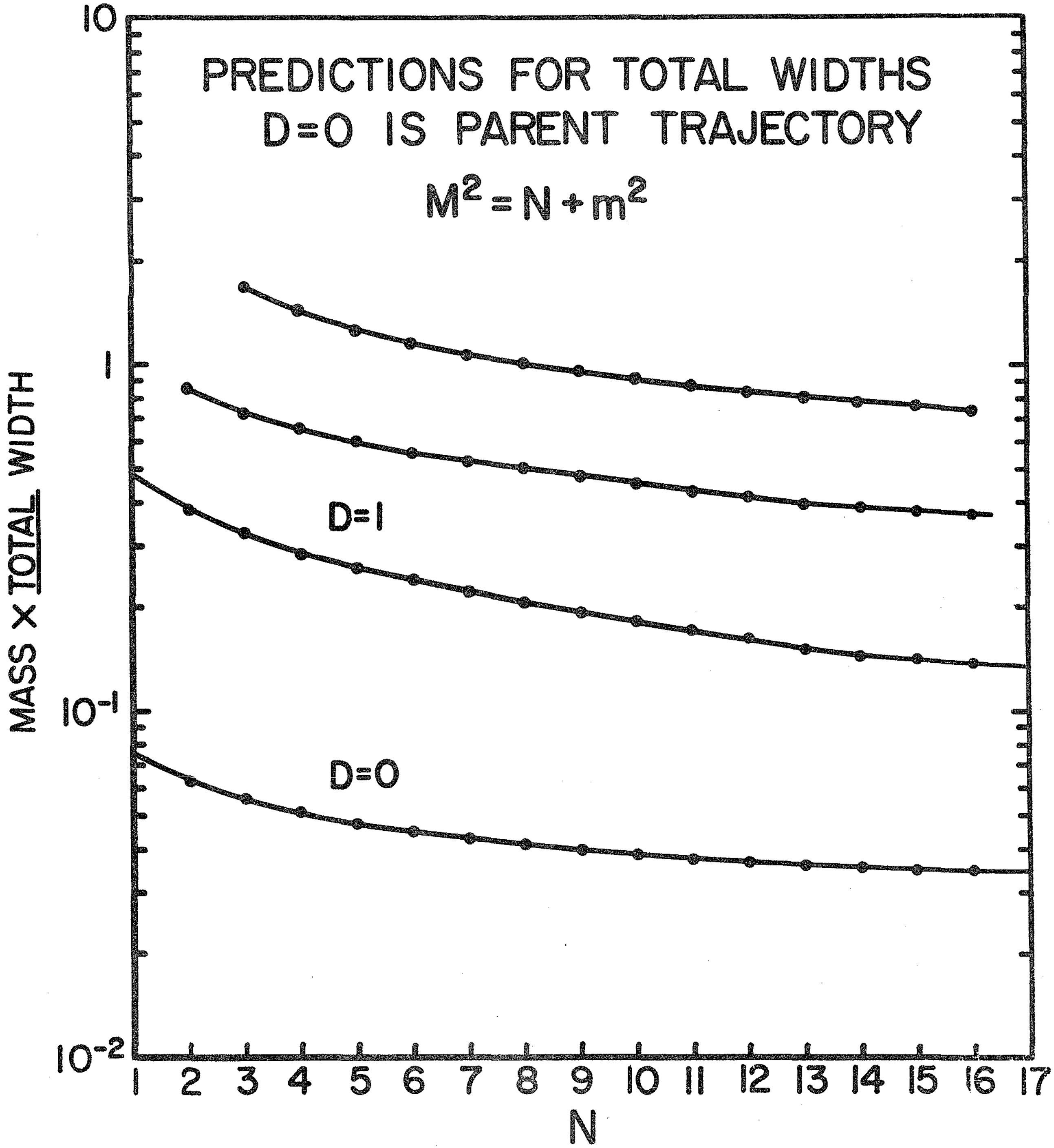

Figure 37: Predictions for the total widths of resonances obtained from an n-point dual model by Chan and Tsou. The resonance mass is denoted by M; m is a constant ($m \approx m_\pi$). Parameter D denotes the "generation index": D = 0 labels states on the parent trajectory, D = 1 labels states on the first daughter trajectory, and so forth.

DISCUSSION

Firestone (LRL): I have a comment on the evidence for the ρ' and the ϵ' under the f^0. One expects similar effects under the $K^*(1420)$. At Berkeley, in a 12 GeV $K^+n \rightarrow K^+\pi^-p$ experiment, we have discovered that in the neighborhood of the $K^*(1420)$ there is an additional resonance, whose spin-parity is most probably 0^+, but the 1^- hypothesis can't be excluded.

Berger: I'm sorry, I didn't have time to discuss this. I'll include it in my write-up (see footnote on page 110).

Schmid (CERN): This is about Chans' calculation (discussed on page 181) which predicts very narrow high spin mesons. For baryon resonances, experiments indicate that their widths are increasing as a function of energy. In dual models, there is no basic difference between mesons and baryons.

Berger: Yes there is. For baryons we have parity doubling.

Schmid: What has this to do with the sum over inelastic channels? . . . There is no evidence, except for one experiment, I guess, that the widths of mesons should behave differently. I have strong doubts about the relevance of Chans' calculation.

Lovelace (Rutgers): I think one must be careful here. There is the question of parents and daughters: the parents will eventually decouple from the elastic channel. Here, one knows certainly, that if the trajectory rises, whatever happens to the total width, the elastic width must go down exponentially. Therefore you are not going to see the high spin parents in formation experiments after all. So, at high energies, total cross sections don't tell you anything about the parent width: they tell you the width for some combination of daughters. The only way you can get at the very high spin parents is by doing production experiments. Thus the current experimental situation for mesons and baryons may be consistent with the narrow parent resonances suggested by the Chans. The πN, $\bar{K}N$ formation experiments just indicate that daughters are under their parents.

Schmid: I was talking about the comparison between the widths of the $3/2^+$, $5/2^-$, and $7/2^+$ resonances, observed in formation experiments. Given this increase of total width with J for baryons, and that the summation over inelastic channels is in principle similar for mesons and baryons, we deduce an increase of total width with J for mesons. (In disagreement with Chans' calculation.)

Lovelace: Yes. I think you will only get Chans' result asymptotically: you have to go much higher up than the $7/2^+$ to see the effect discussed by the Chans.

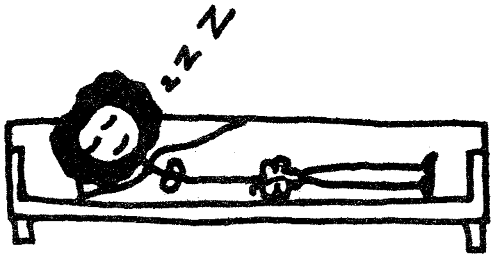

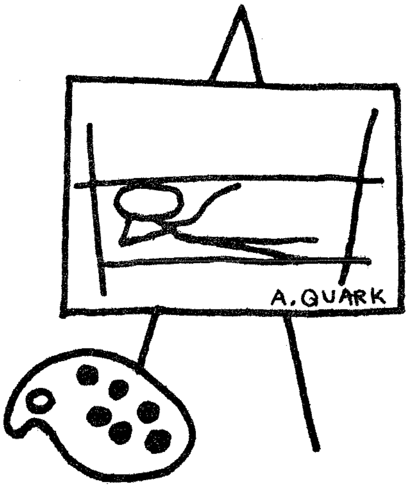

THE QUARK MODEL AT LOW ENERGIES

Richard P. Feynman
California Institute of Technology
Pasadena, California 91109

INTRODUCTION

The quark model has shown some promise of giving correct estimates for low energy matrix elements of currents between various resonant states.[1,2] We report here on how well it does, by remaking the calculations of the various workers in a uniform way. I am summarizing work done in collaboration with M. Kislinger and F. Ravndal, described in much greater mathematical detail in Ref. 3.

By the quark model, we mean the model that baryons consist of three quarks, and mesons of one quark and one antiquark. We suppose in the baryon, for example, that the three quarks are held together in a completely symmetrical, Bose state (in spite of the fact that quarks carry spin 1/2), by some kind of harmonic potential.

HADRON SPECTRUM

We shall first give a very brief review of how the actual baryon states and spectrum fits the pigeonholes of various multiplets expected from this quark model. The states in the harmonic oscillator quark model are characterized as follows. For the baryons of three quarks we have, besides the spin and unitary spin multiplets $\underset{\sim}{56}$, $\underset{\sim}{70}$, $\underset{\sim}{20}$, excitations of two independent three-dimensional modes of internal harmonic oscillation among the three particles. For the lower excitations a state can be uniquely described by giving the total N, the total number of excitations of all the modes, and the L or total orbital angular momentum. For higher states this is not unique (there may be several ways to make up the same total L from the two angular momenta of the two three-dimensional internal degrees of freedom). We shall write each SU_6 multiplet state as $[A, L^P]_N$ where A is 56, 70, or 20, L is the total orbital angular momentum, N the total quantum number, and the parity $P = (-1)^N$. If we further wish to specify an SU_3 multiplet within this, we adjoin ${}^d(\underset{\sim}{B})_J$ where B is the SU_3 multiplet which must be $\underset{\sim}{1}$, $\underset{\sim}{8}$, or $\underset{\sim}{10}$ (for singlet, octet, or decimets are all we can expect), d is the spin multiplicity (four for total of quark spins 3/2, two for total quark spin 1/2), and J is the total angular momentum of the state.

If we wish to speak of a particular particle within a multiplet, we finally add its name. Thus the neutron is N(938) ${}^2(\mathbf{8})_{1/2}\,[\mathbf{56},0^+]_0$. The $\mathbf{56}$ contains ${}^2(\mathbf{8})$ and ${}^4(\mathbf{10})$, the $\mathbf{70}$ is ${}^2(\mathbf{1})$; ${}^2(\mathbf{8})$; ${}^4(\mathbf{8})$; ${}^2(\mathbf{10})$; and the $\mathbf{20}$ is ${}^4(\mathbf{1})$; ${}^2(\mathbf{8})$. We have not yet identified any states belonging to the $\mathbf{20}$.

The multiplets we expect from the model and the observed mass squared of the highest hypercharge state of each multiplet (N for octets, Δ for decimets, Λ for singlets) are given in Table I. The other states of the multiplets are identified where known (as "accepted" in the tables of the Particle Data Group$^{4)}$) as in Table II.

The numbers after each state in Table I are the mass squared. In this variable we have noticed some regularities.$^{5)}$ First, of course, is the Regge relation, that adding $L = 2$ repeats the multiplet $2\Omega = 2.10\ (\mathrm{GeV})^2$ higher (e.g., compare $[\mathbf{56},0^+]_0$ and $[\mathbf{56},2^+]_2$ or $[\mathbf{70},1^-]_1$ and $[\mathbf{70},3^-]_3$). Masses seem to depend on L but there is little spin orbit coupling, each J has the same energy for given L. There is one enigmatic outstanding exception: $\Lambda(1405)$ ${}^2(\mathbf{1})_{1/2}$ and $\Lambda(1520)$ ${}^2(\mathbf{1})_{3/2}$. Inside the multiplets, the quark model expects Σ and Λ degenerate. If we calculate the average of Σ and Λ mass squared as the mass corresponding to strangeness $S = -1$ for an octet, we can see mass square rises by about 0.45 for each unit of $-S$ in octets, and by about 0.40 in decimets. (Here and in the following we measure mass squares in $(\mathrm{GeV})^2$.) Only the $\Sigma(1915)$ does not fit well into its octet, or even worse into the decimet at $J = 5/2^+$. There are strong differences in mass squared depending on the spin relation (quartet or doublet) of the quarks and the unitary spin relation ($\mathbf{1}$, $\mathbf{8}$, or $\mathbf{10}$). It does look like the energy can be nearly separated into a sum of terms, one for strangeness described above, one for SU_6 multiplet character:

$$\begin{array}{lll} \mathbf{56} & {}^2(\mathbf{8}) & 0.88 \\ & {}^4(\mathbf{10}) & 1.55 \\ \mathbf{70} & {}^2(\mathbf{1}) & 1.25\ \ (\text{or } 0.92) \\ & {}^2(\mathbf{8}) & 1.30 \\ & {}^4(\mathbf{8}) & 1.80 \\ & {}^2(\mathbf{10}) & 1.70 \end{array} \tag{1}$$

and one for orbital energy, 1.05 N. There is a possible additional correction for the $N = 2$ state depending on how the two orbits are compounded when they form a state of zero total angular momentum; -0.82 for the space-symmetric, -0.23 for the state of mixed spacial symmetry.

The lowest multiplets of each parity are seen to fit very well into their pigeonholes. The $N = 0$ fit was the origin of the quark model in the first place. For $N = 1$ all multiplets expected are found, except for a $3/2^-$ octet expected at about 1700. For higher N, e.g., $N = 2$, there are so many states available that little can be said. For calculating matrix elements, we identified the states as indicated.

We noticed empirically that the $\Sigma^2 - \Lambda^2$ mass square difference may alternate in sign with parity being about $0.16 \cdot$ parity -- again excepting the $\Sigma(1915)$, or supposing it to belong to the decimet. These rules give all the masses to within 1.5% except for the $\Lambda(1405)$ enigma and the $\Sigma(1915)$.

Our model will be an harmonic oscillator whose eigenvalues are m^2. This will describe the m^2 varying as $N\Omega$, but will leave out of account what spin orbit energy variation there really is, as well as the corrections for the $N = 2$ state. We shall simply suppose that, without disturbing the form of the Hamiltonian otherwise, a constant (around 0.4 $(\text{GeV})^2$) is added for each strange quark. Less satisfactory, the internal splits in the SU_6 multiplet are given no explanation, but are again represented by just adding the constants (1).

For mesons, the theoretical classification of the states of q and $\bar{q}$ is easier. There is just one SU_6 multiplet $\underset{\sim}{36}$ so we will not put that in our notation. It consists of a spin zero octet and singlet (or "nonet") and a spin one nonet. These we call singlet and triplet states, respectively. The internal angular momentum combines with this spin to make a total J. The experimental situation among the mesons is more confused than among the baryons and we have only chosen to try to identify the states of $N = 0$ and some for $N = 1$. (A more complete discussion is given by G. Zweig.$^{6)}$) We therefore need no elaborate notation, and use ${}^1S_0$, ${}^3S_1$ for the $N = 0$ singlet and triplet nonets; ${}^3P_2$, ${}^3P_1$, ${}^3P_0$ for the $N = 1$ states made from the triplet combined with $L = 1$ to make $J = 2, 1, 0$; and ${}^1P_1$ for the singlet combined with $L = 1$ to make $J = 1$. The S states have parity -, the P states parity +. We have identified the states as given in Table III.

Spin-orbit coupling is more obvious than in the baryons but we continue to ignore it in our "Hamiltonian for m^2". We suppose that in triplet nonets, states like ω, ϕ are mixed so ϕ and f' is made of pure strange quarks. We suppose there is no mixing in the states like η, η' for the singlet nonets. Again we suppose that on trajectories m^2 rises by 1.05 L (for example, $\rho_N(1670)$ 2.77 is probably 3^-, a repetition of ρ(765) 0.58 and possibly degenerate with the trajectory through the $^3P_2$, A_2 near $m^2 = 1.69$).

For s states, each strange quark supplies 0.24 $(\mathrm{GeV})^2$ to mass squared. The ϕ has two strange quarks, but η, η' are not diagonal in this quantity, the mean number is 4/3 for η and 2/3 for η'. Something must be assumed to push the SU_6 singlet (unitary singlet and spin singlet) η' up in energy.

BARYON DYNAMICS

We now turn to consider how matrix elements are to be calculated between states of the quark model. Our point of departure is the non-relativistic harmonic oscillator symmetric quark model of Greenberg.2) Usually this is interpreted by the non-relativistic Schrödinger equation for an oscillator, but mass differences between states are not small compared to the masses of the states themselves. This is especially true for meson states. This produces some ambiguity as to how mass factors are to enter matrix elements. It also leaves open the question of the mass of the quark itself. We avoid such ambiguities by using a relativistic equation. However, no relativistic quantum mechanical system is known that is not as complicated as field theory. We have kept the system relativistic, and as simple as the Schrödinger theory but at the expense of unitarity. We fix this lack crudely by modifying the matrix elements by a form factor. This form factor has an arbitrary adjustable constant which we chose to be the same for baryon and meson states, and whose numerical value was chosen to fit the experimental values best. It makes little effect when the mass of initial and final state are not too far apart, but decreases the matrix element when the masses differ more widely. It was designed to make the relativistic theory agree as closely as possible with calculated results made from the non-relativistic equation, for cases where the latter are not overly ambiguous.

In another paper we give the details of the calculations; here, a summary of the ideas must suffice. Our relativistic equation was motivated as follows. If the energies of excitation W of an harmonic oscillator of mass m_o, frequency ω_o, are small compared to m_o, they are calculated as eigenvalues of the operator

$$W = \frac{1}{2m_o} P^2 + \frac{m_o \omega_o^2}{2} X^2 \quad . \tag{2}$$

The masses squared of the states are $m^2 \approx m_o^2 + 2m_o W$ or

$$m^2 = P^2 + \Omega^2 X^2 + C$$

putting Ω for $m_o \omega_o$. Here C is a constant which determines where the series of m^2 values begins. The m^2 values rise linearly with the excitation quantum number N. The spacing in mass squared between levels is Ω. To fit the experimental masses, we choose our constant $\Omega = 1.05\ (\mathrm{GeV})^2$.

Instead of the simple oscillator of (2) we actually chose for baryons, consisting of three quarks, a, b, c, the operator (the propagator is K^{-1})

$$K = 3\, p_a^2 + 3\, p_b^2 + 3\, p_c^2 + \frac{\Omega^2}{36}\left[(u_a - u_b)^2 + (u_b - u_c)^2 + (u_c - u_a)^2\right] + C \tag{3}$$

where p_a, p_b, p_c are the four-vector momenta of the quarks and u_a, u_b, u_c are the corresponding four-vector positions. The total four-momentum operator

$$P = p_a + p_b + p_c \tag{4}$$

can be separated out so the reciprocal propagator becomes

$$K = P^2 - \mathcal{N} \tag{5}$$

where $\mathcal{N}$ involves only the internal relative variables. The eigenvalues of $\mathcal{N}$ are the mass squared values of the states. We suppose C has a contribution 0.45 for each strange quark in octets, etc., and varies within a multiplet as (1). In other words, we use the experimental values for the masses of each state, but the wave function (in four-dimensional variables) comes from the form of K (or rather, $\mathcal{N}$).

The four-dimensional nature of the oscillator is an embarrassment. Excitations in space-like directions act normally but excitation of the time-like direction gives states of negative norm. There is no need for them in Table I. We suppose that there is no excitation of the oscillators in the direction P_μ, of the overall four-momentum of the state.

The operator (3) does not seem to involve the spin, which is satisfactory as long as spin orbit forces can be neglected. When an external vector potential $A_\mu(x)$ acts, however, we interpret ${p_a}^2$ as $\not{p}_a \not{p}_a$ (here $\not{p}_a = p_{\mu a} \gamma_{\mu a}$ where $\gamma_{\mu a}$ acts on the spinor indices of particle a) or rather as $(\not{p}_a - e_a \not{A}(u_a))(\not{p}_a - e_a \not{A}(u_a))$ (where e_a is the charge on quark a). The first order perturbation in K due to A_μ is then written as $j_\mu A_\mu$ and the form of the operator j_μ for current read off. For axial currents in a given SU_3 direction, e_a is replaced by γ_{5a} times the matrix λ_a of the SU_3 system appropriate to the given direction. Again the axial vector current operator is determined. We calculate the first order matrix elements of these operators between the states defined by the wave functions from (3).

The equation (3), not containing the spin explicitly, has twice too many spinor solutions for each quark. We determine the spinor direction in each eigenstate of mass M, say by having the spinor appropriate to a quark (not an antiquark) in the rest system. Thus the triple spinor wave function U is taken to satisfy

$$P_\mu \gamma_{\mu a} U = M U \tag{6}$$

and similar equations for b, c.

For meson states, the appropriate operator is

$$K = 2 {p_a}^2 + 2 {p_b}^2 + \frac{\Omega^2}{16} \left[(u_a - u_b)^2 \right] \tag{7}$$

where a is the quark, b the antiquark. Everything is completely analogous to the hadron case.

ADJUSTABLE CONSTANTS

The restrictions on the states like (6), and the rule that states with oscillator excitation in the P_μ direction are omitted, destroys unitarity. For example, the restriction (6) has a peculiar effect. If an operator acts on one quark to change P from P_1 to P_2, the other quarks whose spins are not directly affected, nevertheless contribute a spin factor g, $g = (\bar{u}_2 u_1)$ because their four component spinors are projected into the new direction P_2. This factor is

$$g = \left(\frac{(m_1 + m_2)^2 - q^2}{4m_1 m_2}\right)^{1/2} \tag{8}$$

where $q = P_2 - P_1$ is the momentum transfer of the transition, and is greater than one. We have chosen to omit the factor g^3 from each matrix element between baryons (one g for each quark) and g^2 for elements between mesons.

The form factor we get from overlap of the four-dimensional Gaussian wave functions after a transfer of four momentum $q = (\nu, \vec{Q})$ is

$$G = \exp q^2/\Omega = \exp (\nu^2 - Q^2)/\Omega \tag{9}$$

whereas the non-relativistic wave functions give a form depending only on the space part of the momentum transfer Q, namely just $\exp(-Q^2/\Omega)$. Is the time part in (9) an artificiality of our four-dimensional wave functions? We have found empirically that an expression of the non-relativistic type depending more explicitly on Q fits better. Of course, Q^2 is not a relativistic invariant but $M_1{}^2 Q^2 = (P_1 \cdot P_2)^2 - P_1{}^2 P_2{}^2$ is, if M_1 is the mass of the state at rest in the system in which Q is measured. Therefore, for transitions between baryon states, we have artificially replaced a factor g^3 G (for meson states, g^2 G) by a new factor F of the form

$$F = \exp(-\alpha M_1{}^2 Q^2/(M_1{}^2 + M_2{}^2)) \tag{10}$$

where we have introduced an adjustable constant α that we chose to fit the data. For both meson and baryon cases we choose the same α, namely $\alpha = 1$. Only transitions where the mass change is large are much affected by this choice (10).

We calculate widths for decays of baryons into pseudoscalar mesons by the principle (PCAC) that the amplitude is proportional to the matrix element of the divergence of the axial current. This constant of proportionality is our second adjustable constant. We actually did all the calculations by choosing it so that the $NP\pi$ coupling would agree exactly with experiment. These are reported in Table II and Fig. 1. Results indicate that a decrease of 5% in this constant would make the average of all matrix elements fit a little better.

These are the only two adjustable constants. In calculating all matrix elements, momentum transfer values, and phase space factors, etc., we used the experimental masses from the particle tables (rather than theoretical masses from our equation, or mass fitting rules). The only additional constant we need is $\Omega = 1.05\ (\mathrm{GeV})^2$ which we chose from the slope of the Regge trajectories, and did not consider adjustable.

We need make no choice of quark mass. When comparing to the nonrelativistic theory, however, our theory corresponds most nearly to that theory with the quark mass equal to one-third the mass of the state for baryons (one-half for mesons).

MATRIX ELEMENTS OF VECTOR CURRENTS

We now compare the results of the quark model to experiment. First, there are the well-known results for the diagonal matrix elements of the vector current. The proton and neutron magnetic moments are +3.00 and -2.00 nuclear magnetons to compare to +2.79 and -1.91 experimentally. (We predict here not only the usual ratio $3 : -2$ but also the absolute values.) The Λ should be half the neutron or -1 of its magneton, or -0.84 nuclear magnetons (experiment is -0.74 ± 0.20).

For large q^2, however, our form factor is completely unsatisfactory. It falls too rapidly at large $-q^2$ (as a Gaussian instead of as an inverse power), and too slowly at small q^2 (as $1 + 0.64\, q^2$ instead of as $1 + 2.8\, q^2$). The latter effect is undoubtedly because we have not represented the ρ or ω pole in the photon coupling but to start to correct the theory in that direction requires an elaboration of our model that we do not know how to define generally as yet. The model is too simple.

The form factor for the $K_1\pi$ coupling in $K\pi e\nu$ or $K\pi\mu\nu$, usually written as

$$f_+(q^2)\,(K_\mu + \pi_\mu) + f_-(q^2)\,(K_\mu - \pi_\mu) \tag{11}$$

can be calculated from matrix elements of j_μ. We find

$$F\left[\left(1 + \frac{2q^2}{(m_K+m_\pi)^2 - q^2}\right)(K_\mu + \pi_\mu) - \frac{2\,(m_K{}^2 - m_\pi{}^2)}{(m_K+m_\pi)^2 - q^2}\,(K_\mu - \pi_\mu)\right] . \tag{12}$$

If $f(q^2)$ is written $f(0)(1+\lambda\, q^2/m_\pi{}^2)$ we find $f_-(0)/f_+(0) = -1.11$ (to compare to -0.94 ± 0.20 from polarization experiments$^{9)}$), $\lambda_+ = 0.11$ (experimentally $\lambda_+ \approx 0.04$) and $\lambda_- = 0.06$. Experimentally,$^{10)}$ $f_+(0) = 0.94 \pm 0.05$ (there is uncertainty from the Cabibbo angle) which agrees with 0.96 from the model. This latter value is very sensitive to our replacement of the factor g^2 G by F, otherwise $f_+(0)$ of the model would be 1.45. The formula (12) predicts a ratio for $\Gamma(K_{\mu 3})/\Gamma(K_{e3})$ of 0.65, whereas experiment$^{4)}$ gives 0.65 ± 0.02.

The non-diagonal photoelectric matrix elements ($q^2 = 0$) are given in Table IV. Aside from the $\omega \to \pi\gamma$ case, the form factor F makes no substantial contribution. It ranges from 0.96 for the $\Delta(1236)$ to 0.78 for the $F_{15}(1688)$. Thus the results are virtually unique, and as it turns out, are almost exactly the same as Walker's theoretical results, A^{NR}, obtained from the non-relativistic model.$^{7)}$ The experimental values are also from Walker, Ref. 7. One could say that our relativistic analysis only confirms the choices made in the non-relativistic model and has eliminated any effective free parameters (other than the observed masses and Ω, of course). The agreements shown here, in particular the small (or zero) values predicted here just when the experiment gives zero impressed Walker. The results are not at all sensitive to our choice of a harmonic potential, but the general way the spins and orbits line up are required for the cancellations and additions to get the general behavior correctly. In addition, the special values of F, D predicted by the model are needed for some of these numerical agreements. The model of three spin 1/2 quarks in a symmetrical overall state does seem to be strongly confirmed.

The worst photoelectric matrix element (the $F_{15}(1688)$, helicity $+3/2$ p) in Table IV is off by a factor of 2.3. We see no excuse for this as only one term contributes (the magnetic moment interaction does not contribute here). Most of our meson width calculations give amplitudes within a factor 1.4 where there is no cancellation of interfering terms. The $S_{11}(1535)$ helicity $+1/2$ p is off by 1.6 and is outside these limits also.

The signs of the quantities A given in the table involve a calculation of the sign of the pion coupling matrix element in addition to that of the photoelectric. These were calculated as described below using PCAC.

F. Ravndal$^{8)}$ has gone on to calculate electron $(e + N \rightarrow e + N^*)$ production rates and has concluded that the discrepancies between theory and experiment for the $F_{15}(1688)$ is at least as likely to be due to an error in interpreting the photoelectric experiments, as it is to be due to a failure of the quark model. The electron production probabilities are computed as a combination $\sigma_T + \epsilon\, \sigma_S$ of two cross sections σ_T, σ_S (corresponding to transverse and Coulomb virtual photons in an appropriate coordinate system). This ϵ depends on the conditions of the experiment (angles, energies, etc.) but is less than one.

To compute σ_T, σ_S by the quark model in the face of the fact that the elastic form factor is given so poorly in this model, Ravndal replaced F of (10) by an appropriate function of q^2 so the proton magnetic form factor would be correct (thus F for $q^2 = 0$ is unity and the photoelectric elements are not affected very much). Thus he effectively used the quark model to calculate the ratio of the electroproduction cross section at a given q^2 to the proton form factor at the same q^2. (He has also included a factor $(1 - q^2/4M^2)^{-N/2}$ for excitation to the N-th level of the harmonic oscillator so that this ratio would approach a constant for large q^2 as it seems to do. This somewhat alters the theoretical curves at higher q^2 but has no effects on the considerations we wish to make here.) Experimentally$^{12)}$ all the individual resonant peaks are not seen, only a bump at 1236 (which is an individual resonance $\Delta(1236)$), one near 1500 (which Ravndal calculates as $S_{11}(1535)$ plus $D_{13}(1520)$) and one near 1700 which is compared to the sum of five resonances. It is seen in Figs. 2, 3, 4 that the agreement, with no arbitrary constants is quite satisfactory. If the $F_{15}(1688)$ contributed $(2.3)^2$ or five times more strongly (as the photoelectric discrepancy suggests), no agreement would result. The entire 1700 electron production bump does extrapolate at $q^2 = 0$ to the photoelectric value, but only a minor part, theoretically, is due to the $F_{15}(1688)$. Walker, in private conversations, concedes that in the interests of simplicity he did not analyze his data including all the resonances near 1700, but left several out, so that possibly the experimental figure in Ref. 8 for the $F_{15}(1688)$ is wrong. He is planning calculations to see if this is true.

AXIAL CURRENT MATRIX ELEMENTS

As is well-known, the diagonal element of the axial current for the nucleon comes out $5/3 = 1.67$, while experiment is nearer 1.22, so the model is not doing well here. On the other hand, the predicted ratio of F, D is 2/3 while a recent evaluation[11)] gives $F = 0.49$, $D = 0.74$, which agrees perfectly (a check of the SU_6 aspect of the model).

We calculate the widths, Γ, of decay of resonances into pseudoscalar mesons using PCAC, from the non-diagonal matrix elements of the divergence of axial current.

The results of the calculations of pseudoscalar meson decay rates are given for hyperon decays in Table II. In this table, the first column gives the multiplet assignment and state, the second gives the mode of decay. We do not give the calculated matrix elements, but rather only the fully calculated width Γ_{calc} to be compared to experiment.[15)] Finally we give Γ_{exp} from the 1970 Particle Tables,[4)] and to make comparisons the last column gives $\ln(\Gamma_{calc}/\Gamma_{exp})$ for those cases where $\Gamma_{calc} \neq 0$. In cases where the theoretical result is zero because a numerical coefficient is zero for some special values of (F,D), we give the answer as $O(x)$ where x is the value one would get for Γ if the coefficient were unity (which was more typical), so working backward one can see how small the data indicates that the coefficient in fact is. We see none of these predicted zeros presents any real problem, experiment is small enough in all of them. The corresponding table for meson states is Table III.

In order to better discuss and understand the mass of figures in these tables, we have made a histogram of the results, Fig. 1, plotting the number of cases against the ℓn of the ratio of theoretical to experimental rates. The baryons are shaded squares, the mesons are open squares.

There is a peak near the center from -0.6 to +0.8 containing 3/4 the cases with the other 1/4 widely spread about, two cases at +4.4 and at -5.5 being completely off the scale of the drawing. The peak is not centered but the center lies near +0.1. We can move our axis there by renormalizing all our theoretical matrix elements up by choosing our coupling constant 5% lower meaning that the predicted nucleon coupling matrix is off to some extent, just like all the others. Doing this, we see that our bunch around the new center represents a spread of -0.7 to +0.7 in the logarithm, or 3/4 of the calculated partial widths are within a factor of two of the measured partial widths.

The next question we address ourselves to is to see whether we can learn anything about the character of the model's failings from the nature of the deviations. We list in Table V all the cases for which the ℓn is outside the limits -0.6 to +0.8. In making this comprehensive table, we have used all the data that is accepted to appear in the particle tables$^{4)}$ (but not in the data card listings, directly). Some of these data are of poor quality and we can not learn much from a deviation from theory if it is possibly experimental. Therefore, in Table V we have placed an approximate $\pm$ on the figure for ℓn which is a rough range of experimental widths. Cases in which this range could bring us into the region -0.6 to +0.8 do not represent anything of significance. These cases have been listed first and are all those before we get to $\Sigma(2030) \to \Sigma\pi$, which is marginal, as is $N(1535) \to N\pi$.

Cases labeled "β" in Table V are those for which the amplitude comes out as the interference of two terms of different Q dependences. The others are just a monomial in Q.

For the $\Lambda(1690) \to N\overline{K}$ we have no explanation and are unable to learn anything from it. No cancellation of interfering terms is involved and many similar disintegrations work quite adequately in other multiplets.

We have three apparently serious very large deviations. They are all states of spin 1/2 and involve cancellation of two terms. Such a situation is a sensitive test of the accuracy of calculations. Take the $\Lambda(1670) \to N\bar{K}$ at +4.4, for example. The theory is much too big. May that mean that experiment is, in a sense, too small? Theoretically, two terms are subtracting, they are three to one in ratio. Were they in reality closer together so in nature they nearly cancelled, then our theoretical result would be much too high. Again, in reverse, for $N(1780) \to N\pi$ at -5.5, the two terms theoretically cancel almost exactly. If in nature the balance were not so perfect, the rate could be much higher. It is also possible that we have misidentified this state. The Roper resonance N(1470) has a logarithmic error of 2.9, which may be due to the effect of cancellations also. However, we must remember that this orbital state requires a special mass squared correction of $-0.82\ (\mathrm{GeV})^2$ before it can be compared to the rest of the particles. Such a serious effect might well change the wave functions, and matrix elements in a serious way. We might well question whether the oscillator model is correctly describing these spin 1/2 states. In particular, the wave function of the states of zero total orbital angular momentum can not be trusted.

The $\Sigma(1915)\ {}^2(8)_{5/2}$ has all three of its modes in the list. The deviations are in opposite directions and experimental uncertainties do not seem to be large enough to account for anything like this.[14] It is this particle that does not fit well in our mass scheme.

In calculating some of the rates of Table III, where two pseudoscalar mesons are emitted, we are faced with a serious shortcoming of our theory. For instance, in the decay $K^*(892) \to K\pi$, the result is not symmetric in whether the π or the K is replaced (via PCAC) by the divergence of the axial current, the other meson being a state of two quarks. We therefore list both cases, $K^* \to K\pi$ and $K^* \to \pi K$, the last meson being the one replaced by the axial current. For the heavier mesons η and η', the situation is even worse. Using the K current always gives the higher value (by 0.7 in ℓn). When this theory is ultimately made more symmetrical, the πK rates will be reduced, and possibly the $\phi \to K\bar{K}$ rate will be reduced somewhat also. This makes it look like the somewhat high $\phi \to K\bar{K}$ rate is another sign of this need for another formulation. There is no numerical evidence that this difficulty extends to the baryons.

For the $A_1(1070)$ and $B(1235)$, some measurements of the ratio of the helicity +1 to helicity 0 amplitudes have been made. We get for these ratios

$$\frac{A_1(1)}{A_1(0)} = 0.76 \qquad\qquad \frac{B(0)}{B(1)} = 0.19 \qquad .$$

Two experiments for the A_1 [13)] give 0.5 or 0.9, respectively, while for the B(1235), measured values[13)] vary from 0.2 to 0.7.

DISCUSSION OF RESULTS

We emphasize that we do not have a theory in the ordinary sense but only a description useful to keep in mind as a way of remembering or organizing data when attempting to find a more satisfactory understanding of that data. In short, as is appropriate to this conference, we have a phenomenological system to describe experimental data on matrix elements of currents for low lying resonances.

From the phenomenological viewpoint, how good is our representation of data? If we call a reliable estimate of a matrix element one which is within a factor $\sqrt{2}$ (excepting those expected to be zero), we can say our system is generally as reliable as present-day data; except that partial widths of resonances of spin 1/2 are unreliable.

Finally we may ask if the deviations that do exist show any systematic trend so that we could improve our estimates in a frankly empirical way. The deviations of the spin 1/2 baryon widths seem capricious and not easily summarized in one rule. However, improvement results if all rates of meson decays (not baryon decays) calculated using PCAC for the K meson were reduced by a factor 2 or 2.5. In addition, the situation would be improved by supposing quarks to have their axial vector coupling renormalized by 0.70. This would change nothing except that the coupling constant of proportionality of PCAC determined experimentally from the Goldberger-Treiman relation could then be used instead of our adjustable value, and g_A of the nucleon would be reduced from 5/3 to 1.17, much closer to experiment.

TABLE I. Baryons.

J	1/2	3/2	5/2	7/2	9/2
$[\underset{\sim}{56}, 0^{+}]$	⑧ 0.88	⑩ 1.55			
$[\underset{\sim}{70}, 1^{-}]$	① 1.97	① 2.31			
	⑧ 2.36	⑧ 2.31			
	⑧ 2.89	⑧	⑧ 2.79		
	⑩ 2.72	⑩ 2.79			
$[\underset{\sim}{56}, 0^{+}]$	⑧ 2.16	⑩			
$[\underset{\sim}{56}, 2^{+}]$		⑧	⑧ 2.85		
	⑩ 3.65	⑩	⑩ 3.57	⑩ 3.80	
$[\underset{\sim}{70}, 0^{+}]$	①				
	⑧ 3.17	⑧			
	⑩				
$[\underset{\sim}{70}, 2^{+}]$		①	①		
		⑧ 3.46	⑧		
	⑧	⑧	⑧	⑧ 3.96	
		⑩	⑩		
$[\underset{\sim}{70}, 3^{-}]$			①	① 4.41	
			⑧	⑧	
		⑧	⑧	⑧ 4.80	⑧
			⑩	⑩	

TABLE II. Transition rates for decays into ground state baryons and pseudoscalar mesons.

State	Multiplet	Mode	Γ_{calc}(MeV)	Γ_{exp}(MeV)	$\ln(\Gamma_{calc}/\Gamma_{exp})$
$\Delta(1236)$	$^4\underset{\sim}{10}_{3/2}[\underset{\sim}{56},0^+]_0$	$N\pi$	94	120	-0.2
$\Sigma(1385)$	$^4\underset{\sim}{10}_{3/2}[\underset{\sim}{56},0^+]_0$	$\Lambda\pi$	35	32	+0.1
		$\Sigma\pi$	4	4	0
$\Xi(1530)$	$^4\underset{\sim}{10}_{3/2}[\underset{\sim}{56},0^+]_0$	$\Xi\pi$	12	7	+0.5
$\Lambda(1405)$	$^2\underset{\sim}{1}_{1/2}[\underset{\sim}{70},1^-]_1$	$\Sigma\pi$	56	40	+0.3
$\Lambda(1520)$	$^2\underset{\sim}{1}_{3/2}[\underset{\sim}{70},1^-]_1$	$N\bar{K}$	7	7	0
		$\Sigma\pi$	12	7	+0.5
$N(1535)$	$^2\underset{\sim}{8}_{1/2}[\underset{\sim}{70},1^-]_1$	$N\pi$	220	40	+1.7
		$N\eta$	71	77	-0.1
$\Lambda(1670)$	$^2\underset{\sim}{8}_{1/2}[\underset{\sim}{70},1^-]_1$	$\Sigma\pi$	22	11	+0.7
		$\Lambda\eta$	6	8	-0.3
		$N\bar{K}$	415	5	+4.4
$N(1520)$	$^2\underset{\sim}{8}_{3/2}[\underset{\sim}{70},1^-]_1$	$N\pi$	105	60	+0.6
		$N\eta$	0.2	~ 0.7	~ -1.3
$\Sigma(1670)$	$^2\underset{\sim}{8}_{3/2}[\underset{\sim}{70},1^-]_1$	$N\bar{K}$	3		
		$\Lambda\pi$	6		
		$\Sigma\pi$	49		
$\Lambda(1690)$	$^2\underset{\sim}{8}_{3/2}[\underset{\sim}{70},1^-]_1$	$N\bar{K}$	102	16	+1.9
		$\Sigma\pi$	11	21	-0.6

TABLE II (cont.)

State	Multiplet	Mode	Γ_{calc}(MeV)	Γ_{exp}(MeV)	$\ln(\Gamma_{calc}/\Gamma_{exp})$
$\Xi(1820)$	$^{2}\underset{\sim}{8}_{3/2}[\underset{\sim}{70},1^{-}]_{1}$	$\Lambda\bar{K}$	15		
		$\Xi\pi$	4		
		$\Sigma\bar{K}$	17		
		$\Xi^{*}\pi$	10		
$N(1700)$	$^{4}\underset{\sim}{8}_{1/2}[\underset{\sim}{70},1^{-}]_{1}$	$N\pi$	45	182	-1.4
		$N\eta$	112		
		ΛK	0 (74)	13	
$N(1670)$	$^{4}\underset{\sim}{8}_{5/2}[\underset{\sim}{70},1^{-}]_{1}$	$N\pi$	36	60	-0.5
		$N\eta$	7	< 1	
		ΛK	0 (0.2)	< 0.1	
$\Sigma(1765)$	$^{4}\underset{\sim}{8}_{5/2}[\underset{\sim}{70},1^{-}]_{1}$	$N\bar{K}$	66	53	+0.2
		$\Lambda\pi$	25	17	+0.4
		$\Sigma\pi$	10	~ 1	
		$\Sigma^{*}\pi$	6	15	-0.9
$\Lambda(1830)$	$^{4}\underset{\sim}{8}_{5/2}[\underset{\sim}{70},1^{-}]_{1}$	$N\bar{K}$	0 (48)	11	
		$\Sigma\pi$	73	33	+0.8
$\Xi(1930)$	$^{4}\underset{\sim}{8}_{5/2}[\underset{\sim}{70},1^{-}]_{1}$	$\Xi\pi$	83		
		$\Lambda\bar{K}$	24		
$\Delta(1650)$	$^{2}\underset{\sim}{10}_{1/2}[\underset{\sim}{70},1^{-}]_{1}$	$N\pi$	25	41	-0.5
$\Sigma(1750)$	$^{2}\underset{\sim}{10}_{1/2}[\underset{\sim}{70},1^{-}]_{1}$	$N\bar{K}$	14	~ 10	~ +0.3
		$\Lambda\pi$	9		
		$\Sigma\eta$	4		

TABLE II (cont.)

State	Multiplet	Mode	Γ_{calc}(MeV)	Γ_{exp}(MeV)	$\ln(\Gamma_{calc}/\Gamma_{exp})$
$\Delta(1670)$	${}^{2}\underset{\sim}{10}_{3/2}[\underset{\sim}{70},1^{-}]_{1}$	$N\pi$	30	31	0
$N(1470)$	${}^{2}\underset{\sim}{8}_{1/2}[\underset{\sim}{56},0^{+}]_{2}$	$N\pi$	8	150	-2.9
$N(1688)$	${}^{2}\underset{\sim}{8}_{5/2}[\underset{\sim}{56},2^{+}]_{2}$	$N\pi$	64	75	-0.1
		$\Lambda\bar{K}$	0.07	< 0.1	
		$N\eta$	0.27	< 0.6	
$\Sigma(1915)$	${}^{2}\underset{\sim}{8}_{5/2}[\underset{\sim}{56},2^{+}]_{2}$	$N\bar{K}$	3	8	-1.0
		$\Lambda\pi$	15	5	+1.1
		$\Sigma\pi$	24	3	+2.1
$\Lambda(1815)$	${}^{2}\underset{\sim}{8}_{5/2}[\underset{\sim}{56},2^{+}]_{2}$	$N\bar{K}$	35	53	-0.4
		$\Sigma\pi$	13	9	+0.4
		$\Sigma^{*}\pi$	16	14	+0.1
$\Xi(1930)$	${}^{2}\underset{\sim}{8}_{5/2}[\underset{\sim}{56},2^{+}]_{2}$	$\Xi\pi$	1		
		$\Lambda\bar{K}$	2		
		$\Sigma\bar{K}$	16		
$\Delta(1910)$	${}^{4}\underset{\sim}{10}_{1/2}[\underset{\sim}{56},2^{+}]_{2}$	$N\pi$	151	82	+0.6
$\Delta(1890)$	${}^{4}\underset{\sim}{10}_{5/2}[\underset{\sim}{56},2^{+}]_{2}$	$N\pi$	18	47	-1.0

TABLE II (cont.)

State	Multiplet	Mode	Γ_{calc}(MeV)	Γ_{exp}(MeV)	$\ln(\Gamma_{calc}/\Gamma_{exp})$
$\Delta(1950)$	$^4\underline{10}_{7/2}[\underline{56},2^+]_2$	$N\pi$	103	90	+0.1
		ΣK	7	5	+0.3
		$\Delta\pi$	43	~ 100	
		$\Sigma^* K$	0.1	3	
$\Sigma(2030)$	$^4\underline{10}_{7/2}[\underline{56},2^+]_2$	$N\bar{K}$	28	27	0
		$\Lambda\pi$	37	35	0
		$\Sigma\pi$	17	3	+1.7
		ΞK	1	< 2	
$N(1780)$	$^2\underline{8}_{1/2}[\underline{70},0^+]_2$	$N\pi$	0.5	120	−5.5
$N(1860)$	$^2\underline{8}_{3/2}[\underline{70},2^+]_2$	$N\pi$	75	90	−0.2
		ΛK	22	< 53	
		$N\eta$	19		
$N(1990)$	$^4\underline{8}_{7/2}[\underline{70},2^+]_2$	$N\pi$	15	26	−0.5
$\Delta(2420)$	$^4\underline{10}_{11/2}[\underline{56},4^+]_4$	$N\pi$	25	34	−0.3

TABLE III. Meson classification and decay rates.

State (mass)	Mass^2	Multiplet	Mode	Γ_{calc}(MeV)	Γ_{exp}(MeV)	$\ln(\Gamma_{calc}/\Gamma_{exp})$
$\eta'(958)$	0.92	$^1S_0$				
$\eta(549)$	0.30					
$K(494)$	0.24					
$\pi(140)$	0.02					
$\phi(1019)$	1.04	$^3S_1$	$K\bar{K}$	10	3.2	+1.1
			$\rho\pi$			
$\omega(784)$	0.61		$\pi\pi$	0		
$K^*(892)$	0.80		$K\pi$	66	51	+0.3
			πK	159	51	+1.1
$\rho(765)$	0.58		$\pi\pi$	157	125	+0.2
$K^*(1300)$	1.69	$^1P_1$				
$B(1235)$	1.53		$\omega\pi$	85	102	-0.2
$K^*(1240)$	1.54	$^3P_1$	$K^*\pi$	60	90	-0.4
$A_1(1070)$	1.14		$\rho\pi$	161	95	+0.5

TABLE III (cont.)

State (mass)	Mass^2	Multiplet	Mode	Γ_{calc}(MeV)	Γ_{exp}(MeV)	$\ln(\Gamma_{calc}/\Gamma_{exp})$
f'(1514)	2.29		$K\bar{K}$	103	52	+0.7
			$\bar{K}K^* + K\bar{K}^*$	15	7	+0.8
			$\pi\pi$	0	< 10	
f(1260)	1.59		$\pi\pi$	244	145	+0.5
			$K\bar{K}$	13	~ 5	+0.9
K^*(1420)	2.01		$K^*\pi$	22	35	-0.5
		$^3P_2$	ρK	8	8	0
			ωK	2	4	-0.7
			$K\pi$	87	48	+0.6
			πK	140	48	+1.1
			$K\eta$	5	~ 2	+0.9
			ηK	4	~ 2	+0.7
A_2(1300)	1.69		$\rho\pi$	66	64	+0.0
			$\eta\pi$	22	16	+0.3
			$\pi\eta$	45	16	+1.0
			$\bar{K}K$	17	10 ?	+0.5 ?

TABLE IV. Photoelectric matrix elements.

State	Multiplet	J_z	I_z	$\langle f \vert \mathcal{H}^V \vert i \rangle / F$	$A(\mathrm{GeV})^{-1/2}$	$A^{NR}(\mathrm{GeV})^{-1/2}$	$A^{exp}(\mathrm{GeV})^{-1/2}$
$P_{33}(1236)$	${}^4\underset{\sim}{10}_{3/2}[\underset{\sim}{56},0^+]_0$	+3/2	p	$-\sqrt{6}\,\rho$	−0.187	−0.178	−0.244
		+1/2	p	$-\sqrt{2}\,\rho$	−0.108	−0.103	−0.138
$D_{13}(1520)$	${}^2\underset{\sim}{8}_{3/2}[\underset{\sim}{70},1^-]_1$	+3/2	p	$+\sqrt{\Omega}$	+0.109	+0.112	+0.151
		+1/2	p	$-\sqrt{3}\,\lambda\rho + \sqrt{\frac{1}{3}}\sqrt{\Omega}$	−0.034	−0.029	−0.026
		+3/2	n	$-\sqrt{\Omega}$	−0.109	−0.112	−0.132
		+1/2	n	$+\sqrt{\frac{1}{3}}\,\lambda\rho - \sqrt{\frac{1}{3}}\sqrt{\Omega}$	−0.031	−0.030	
$S_{11}(1535)$	${}^2\underset{\sim}{8}_{1/2}[\underset{\sim}{70},1^-]_1$	+1/2	p	$+\sqrt{\frac{3}{2}}\,\lambda\rho + \sqrt{\frac{2}{3}}\sqrt{\Omega}$	+0.156	+0.160	+0.096
		+1/2	n	$-\sqrt{\frac{1}{6}}\,\lambda\rho - \sqrt{\frac{2}{3}}\sqrt{\Omega}$	−0.108	−0.109	−0.118
$D_{15}(1670)$	${}^4\underset{\sim}{8}_{5/2}[\underset{\sim}{70},1^-]_1$	+3/2	p	0	0	0	0.040 ?
		+1/2	p	0	0	0	~ 0
		+3/2	n	$-\sqrt{\frac{3}{5}}\,\lambda\rho$	−0.053	−0.053	
		+1/2	n	$-\sqrt{\frac{3}{10}}\,\lambda\rho$	−0.038	−0.038	
$S_{31}(1650)$	${}^2\underset{\sim}{10}_{1/2}[\underset{\sim}{70},1^-]_1$	+1/2	p	$-\sqrt{\frac{1}{6}}\,\lambda\rho + \sqrt{\frac{2}{3}}\sqrt{\Omega}$	+0.047	+0.047	

TABLE IV (cont.)

State	Multiplet	J_z	I_z	$\langle f \mid \mathcal{R}^V \mid i\rangle / F$	$A(\mathrm{GeV})^{-1/2}$	$A^{NR}(\mathrm{GeV})^{-1/2}$	$A^{exp}(\mathrm{GeV})^{-1/2}$
$D_{33}(1670)$	${}^2\underset{\sim}{10}_{3/2}[\underset{\sim}{70},1^-]_1$	+3/2	p	$+\sqrt{\Omega}$	+0.084	+0.091	
		+1/2	p	$+\sqrt{\frac{1}{3}}\,\lambda\rho + \sqrt{\frac{1}{3}}\,\sqrt{\Omega}$	+0.088	+0.092	
$P_{11}(1470)$	${}^2\underset{\sim}{8}_{1/2}[\underset{\sim}{56},0^+]_2$	+1/2	p	$(+\sqrt{\frac{3}{4}}\,\lambda\rho)\,\lambda$	+0.027	+0.032	
		+1/2	n	$(-\sqrt{\frac{1}{3}}\,\lambda\rho)\,\lambda$	-0.018	-0.020	
$F_{15}(1688)$	${}^2\underset{\sim}{8}_{5/2}[\underset{\sim}{56},2^+]_2$	+3/2	p	$(+\sqrt{\frac{4}{5}}\,\sqrt{\Omega})\,\lambda$	+0.059	+0.070	+0.139
		+1/2	p	$(-\sqrt{\frac{9}{10}}\,\lambda\rho + \sqrt{\frac{2}{5}}\,\sqrt{\Omega})\,\lambda$	-0.010	-0.015	~ 0
		+3/2	n	0	0	0	~ 0
		+1/2	n	$(+\sqrt{\frac{2}{5}}\,\lambda\rho)\,\lambda$	+0.035	+0.041	
$\omega(789)$	${}^3S_1$	0	π	$\sqrt{\frac{1}{2}}\,\rho$	0.172		0.13 ± 0.01
$\Lambda(1520)$	${}^2\underset{\sim}{1}_{3/2}[\underset{\sim}{70},1^-]$	+3/2	Λ	$+\frac{5}{6}\sqrt{\Omega}$	+0.107		0.095 ± 0.010
		+1/2	Λ	$-\frac{5}{6}\left[\sqrt{3}\,\lambda\rho - \sqrt{\frac{1}{3}}\,\sqrt{\Omega}\right]$	+0.012		

TABLE V. List of calculated transitions which seriously disagree with experiment.

State	J^P	Mode	$\ln (\Gamma_{calc}/\Gamma_{exp})$	β-Term
$K^*(1420)$	2^+	ωK	-0.7 ± 0.6	
$\Sigma(1765)$	$5/2^-$	$\Sigma^* K$	-0.9 ± 0.5	
$\Delta(1890)$	$5/2^+$	$N\pi$	-1.0 ± 0.5	
$N(1700)$	$1/2^-$	$N\pi$	-1.4 ± 0.7	β
$\Sigma(2030)$	$7/2^+$	$\Sigma\pi$	$+1.7 \pm 0.7$	
$N(1535)$	$1/2^-$	$N\pi$	$+1.7 \pm 0.6$	β
$\phi(1019)$	1^-	$K\bar{K}$	$+1.1 \pm 0.1$	
$\Lambda(1690)$	$3/2^-$	$N\bar{K}$	$+1.9 \pm 0.6$	
$\Sigma(1915)$	$5/2^+$	$N\bar{K}$	-1.0 ± 0.3	
		$\Lambda\pi$	$+1.1 \pm 0.6$	
		$\Sigma\pi$	$+2.1 \pm 1$	
$N(1470)$	$1/2^+$	$N\pi$	-2.9 ± 0.4	β
$\Lambda(1670)$	$1/2^-$	$N\bar{K}$	$+4.4 \pm 0.7$	β
$N(1780)$	$1/2^+$	$N\pi$	-5.5 ± 0.6	β

REFERENCES

1. M. Gell-Mann, Physics Letters 8, 214 (1964); G. Zweig, CERN Reports TH 401 and TH 412 (1964), unpublished; R. H. Dalitz, in 13th International Conference on High Energy Physics, Berkeley 1966 (University of California Press, 1967); D. L. Katyal and A. N. Mitra, Phys. Rev. D1, 338 (1970); D. K. Choudhury and A. N. Mitra, Phys. Rev. D1, 351 (1970).
2. O. W. Greenberg, Phys. Rev. Letters 13, 598 (1964); R. H. Dalitz, in Proceedings of the Conference on Particle Physics, University of Hawaii, 1967 (University of Hawaii Press, Honolulu, 1968); D. Faiman and A. W. Hendry, Phys. Rev. 173, 1720 (1968); D. Faiman and A. W. Hendry, Phys. Rev. 180, 1572 (1969); L. A. Copley, G. Karl, and E. Obryk, Physics Letters 29B, 117 (1969).
3. R. P. Feynman, M. Kislinger, and F. Ravndal, Phys. Rev. (to be published).
4. Review of Particle Properties, Particle Data Group, Physics Letters 33B, No. 1 (August 1970).
5. R. P. Feynman, S. Pakvasa, and S. F. Tuan, Phys. Rev. D2, 1267 (1970); C. A. Heusch and F. Ravndal, Phys. Rev. Letters 25, 253 (1970).
6. G. Zweig, in Meson Spectroscopy, ed. Baltay and Rosenfeld (W. A. Benjamin, Inc., New York, 1968), p. 485.
7. R. L. Walker, in Proceedings of the International Symposium on Electron and Photon Interactions at High Energies, Liverpool, 1969 (Daresbury Nuclear Physics Laboratory, Daresbury, Lancashire, England, 1970).
8. F. Ravndal, (private communication), Phys. Rev. (to be published).
9. M. K. Gaillard and L. M. Chounet, CERN Report 70-14 (May 1970); D. Haidt et al., (X_2 collaboration), Phys. Rev. (to be published). They find from three different measurements $\lambda_+ = 0.060 \pm 0.019$ and $\xi(0) = -1.0 \pm 0.5$.
10. This value of $f_+(0)$ is determined from the experimental rate of K_{e3} using for the Cabibbo angle $\theta_V = \theta_A = 0.235$ as given in Ref. 11.
11. H. Filthuth, in Proceedings of Topical Conference on Weak Interactions (CERN, Geneva, 1969).

12. A. B. Clegg, in Proceedings of the 4th International Symposium on Electron and Photon Interactions at High Energies, Liverpool, 1969 (Daresbury Nuclear Physics Laboratory, Daresbury, England, 1969).
13. A good review of the experimental situation can be found in E. W. Colglazier and J. L. Rosner, Caltech preprint CALT-68-278, to be published in Nuclear Physics. We thank Mr. Colglazier for many helpful discussions in this connection.
14. A. Barbaro-Galtieri has pointed out, at the meeting, that this pattern of deviations could result from just one experimental number being too high, the rate $\Gamma_{N\bar{K}}$ for $\Sigma(1915) \to N\bar{K}$, for the other two partial widths are determined from data giving their product with Γ_{KN}.
15. The relative signs of several resonant amplitudes have been determined for hyperons. They are reported by Levi Setti, Lund International Conference on Elementary Particles (1969), where he shows how closely they agree with SU_3 predictions using F/D ratios nearly the same as ours, except in the $^2[8]_{1/2^-}$ multiplet. With our F/D ratios we disagree with experiment in only one case, $\Sigma(1760)_{1/2^-} \to \Lambda\pi$ (for $\Sigma(1760)_{1/2^-} \to \Sigma\pi$, which is not yet measured, we predict the same sign as does Levi Setti). One of our signs is ambiguous for our theoretical matrix element for $\Lambda(1830)_{5/2^-} \to N\bar{K}$ is zero.

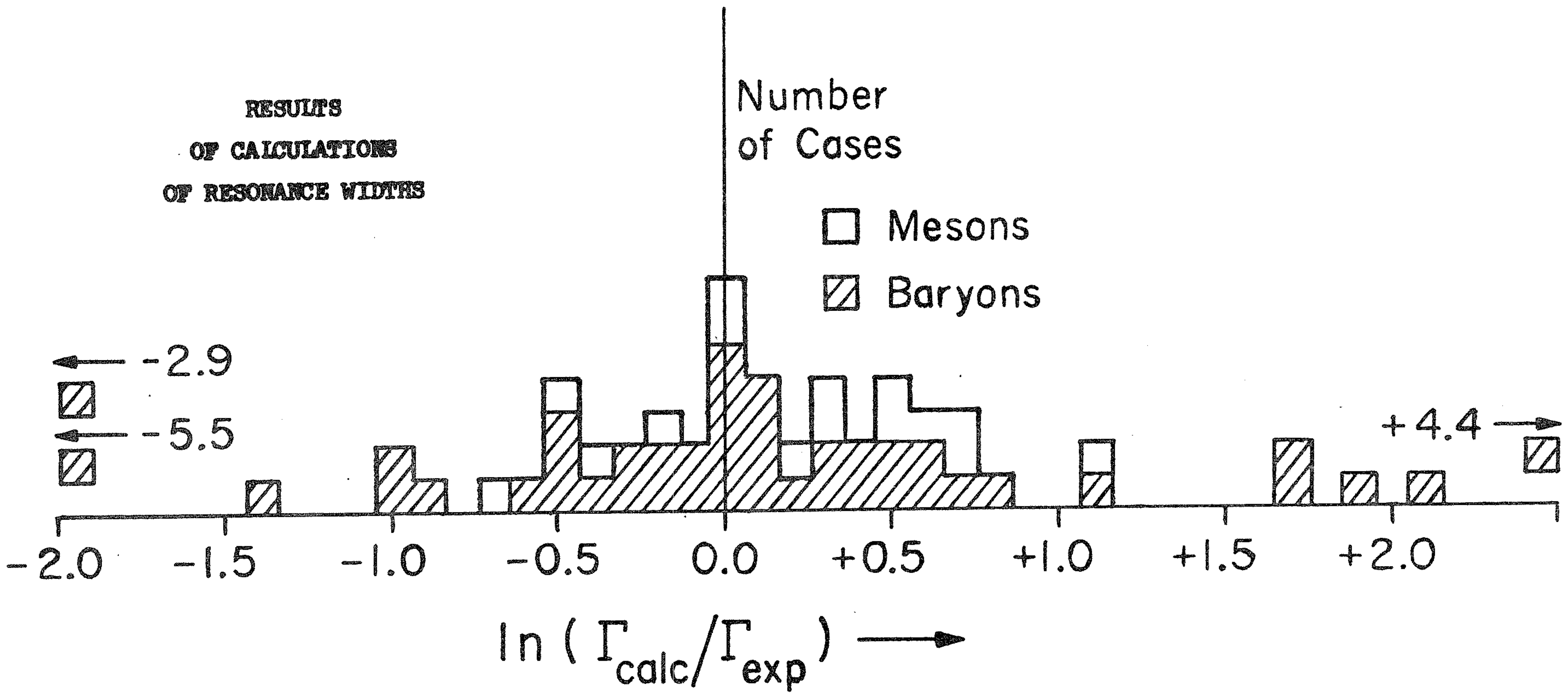

Fig. 1: Histogram of partial widths for pseudoscalar meson emission.

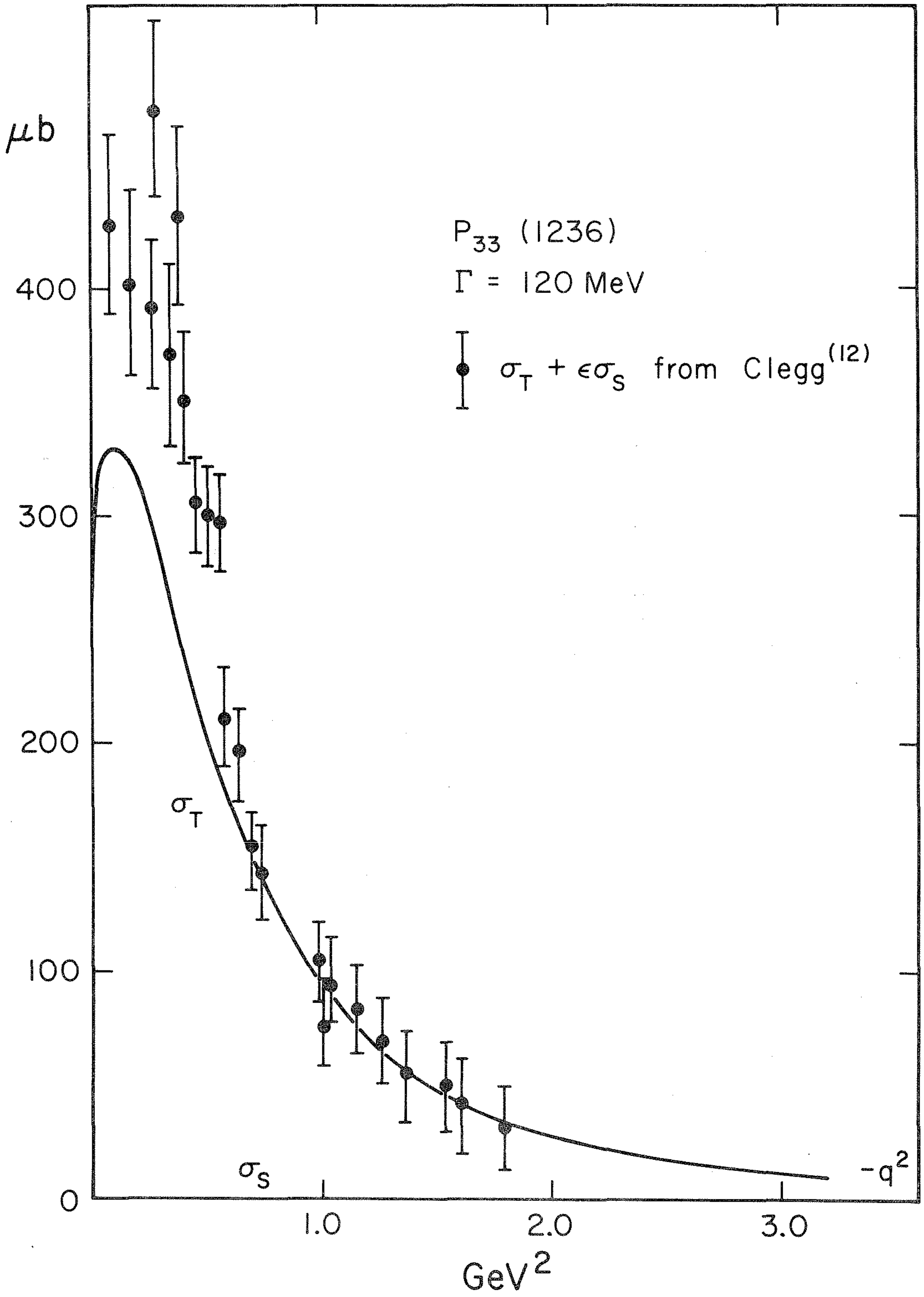

Fig. 2: Proton electroproduction cross section for the 1236 MeV resonance predicted by Ravndal 8) (solid line) compared to experimental results of Clegg. 12)

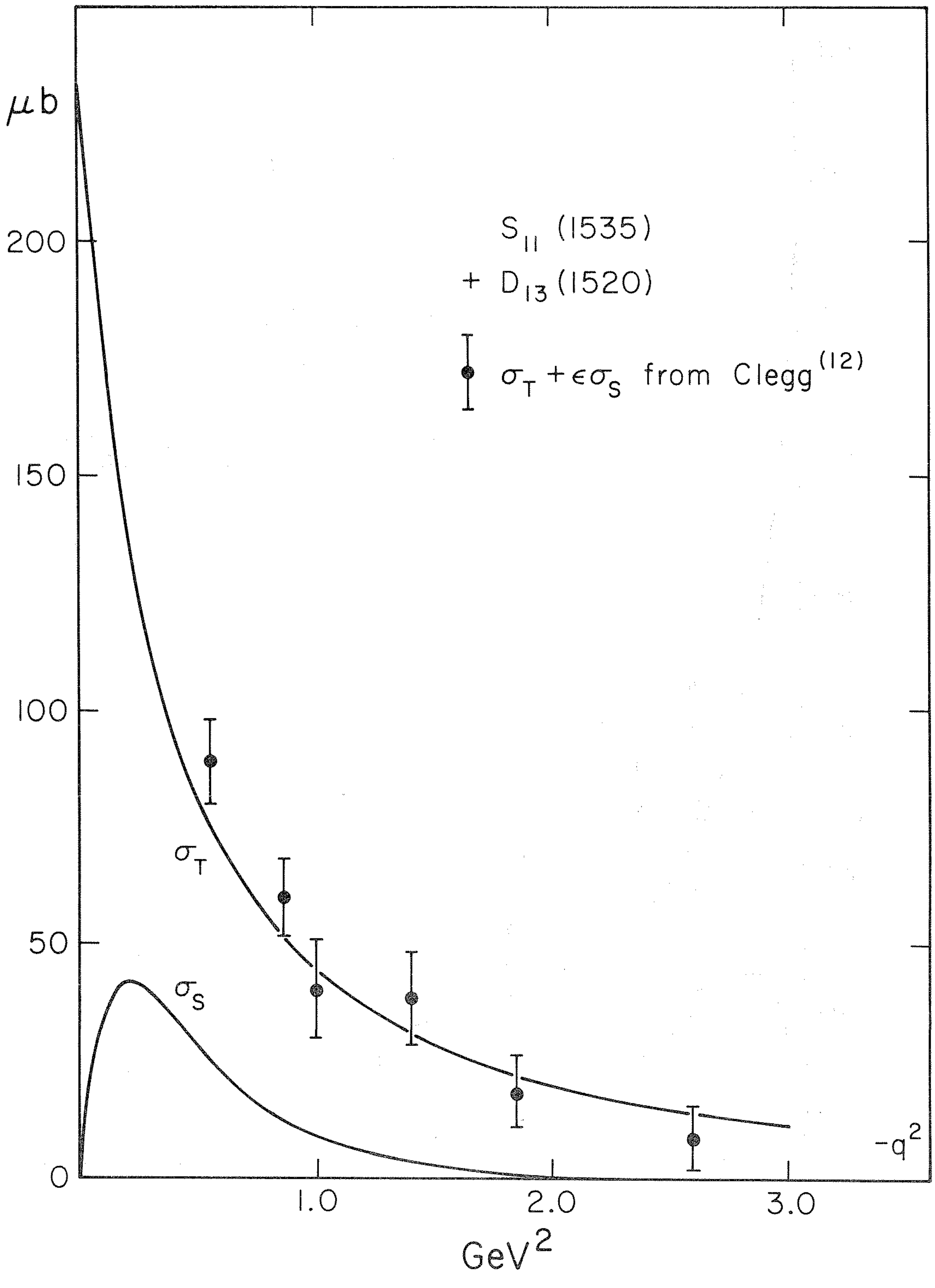

Fig. 3: Total transverse σ_T and scalar σ_S cross sections for resonances near the second peak at 1530 MeV.

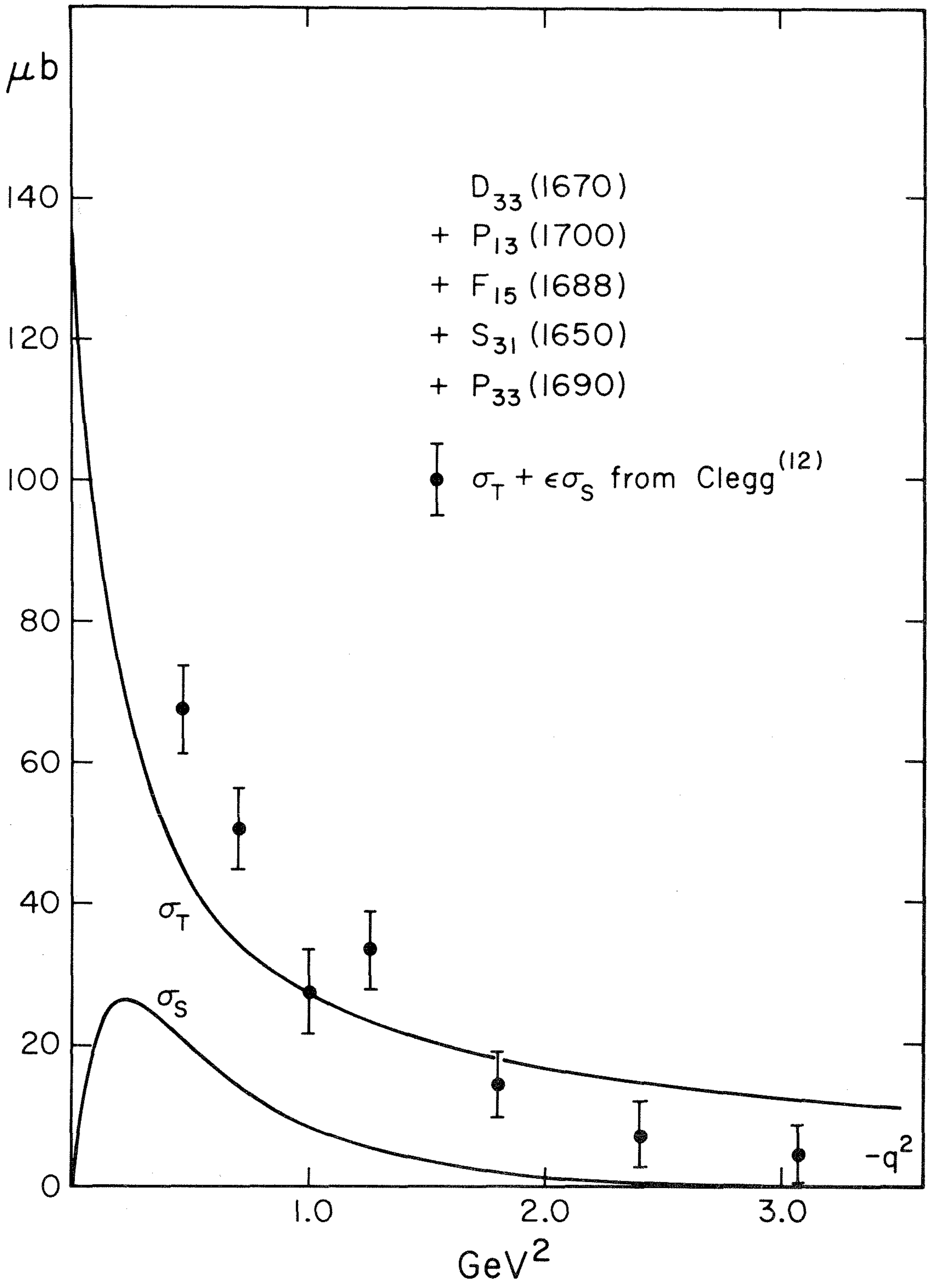

Fig. 4: Total transverse σ_T and scalar σ_S cross sections for resonances near the third peak at 1700 MeV.

DISCUSSION

Yovanovitch (Argonne): There were very few mesons on your chart (Fig. 1), and they seemed to have much less scatter than the baryons. Do you attach any significance to this?

Feynman: There are fewer meson matrix elements. It is true that we do not have mesons so far out, i.e., so bad, and this is interesting but I do not know what it means. I guess that the reason the meson results are good is that it happens for the meson calculations that we don't have one-half spin type terms which may or may not cancel; and it is these that are so delicate and difficult to handle.

Lovelace (Rutgers): Another possible reason for the better agreement of the theory for mesons is that mainly parents, and only very few daughters, have been observed. For instance, the three worst cases in Table V (all baryons) are daughters.

Gasiorowicz (Minnesota): Are there any systematics, say for the high angular momentum L isobars, whether they prefer to decay to the next lowest member, or anything of that sort?

Feynman: We calculated rates for high isobars going to intermediary isobars as well as to protons: all modes are included. There was no strong tendency: it did what the data did.

Schmid (CERN): It was surprising to find the ϕ meson on your list of bad results (Table V), since $\rho \to \pi\pi$ and $K^* \to K\pi$ are some of the successes of the nonet scheme. Isn't this just a question of ambiguity of the barrier factor? For $\phi \to K\overline{K}$ the barrier factor is huge compared with that for the ρ and K^* decays.

Feynman: Why should we be fooling around with barrier factors -- whatever they mean. The theory predicts the matrix element and all these dynamical features are automatically present. However, the $\phi \to K\overline{K}$ may be a symptom of a general disease that whenever we have meson systems decaying into K's, something is too high. (Note: see page 237.)

Rosner (Minnesota): The discrepancy associated with the $\Sigma(1910)\ 5/2^+$ state is a disease of any theory based on identification of this state as the Regge recurrence of the $\Sigma(1190)$. On the other hand, a decimet member (Σ, $5/2^+$) is also expected around (somewhat above) this mass. This would have a larger $\overline{K}N$ rate than that predicted for an octet member, and mixing could affect the result appreciably.

Feynman: We have also calculated the $\Sigma(1910)\ 5/2^+$ assuming a decimet assignment. As you suggest, it fits much better. If you take a less naive view of such things, then we took in our model, those particular states which are so terribly far off are exactly those for which configuration mixing would have a rather big effect on the matrix elements. It is not hard to find explanations for the deviations -- but perhaps that's rather a dangerous thing to do!

Ferbel (Rochester): Why do you use mass squared rather than mass? Mass squared may fit better in your model, but what about SU(3)? There, the mass seems to fit better. What sort of rationale can you use about which is best? Is there an answer to this?

Feynman: Yes. They cannot both be right. Consider, for example, the baryon octet and their recurrences. You cannot have the spacing of the masses equal in every one of these multiplets, and have all on straight lines in their mass squared. If the mass squares were nicely spaced in the multiplets by some regularities, then they can all be parallel on straight lines in a mass squared plot. There is no simple rule to argue whether it should be mass or mass squared; unless you have a theory of second-order corrections to the rule.

Ferbel: So the Ω^- will be an accident, for example?

Feynman: No. It is not so far off with equal spacing in mass squared: it is just much more perfect in mass. This "perfect agreement" may be an accident. We do have trajectories which seem to be pretty straight in mass squared, and we found that by using mass squares in our model, we got certain kinds of regularities and understandings. It's a little different from everyone else -- that is the way you write papers!

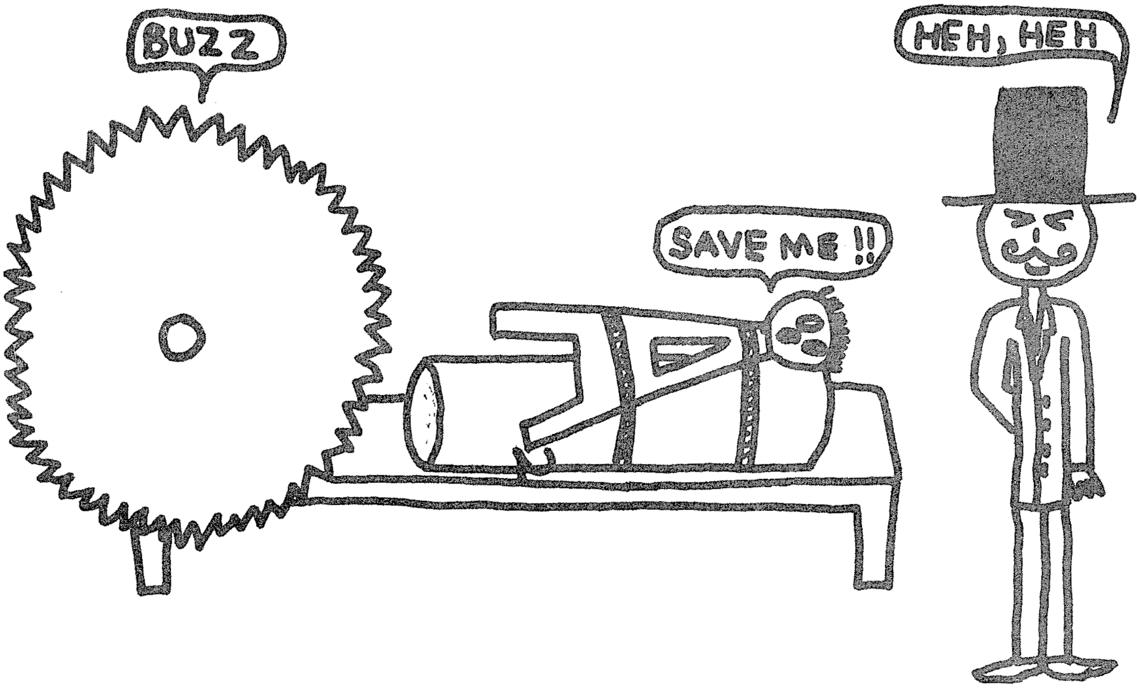

RECENT RESULTS FROM BUBBLE CHAMBER EXPERIMENTS ON A_2*

Kwan-Wu Lai

Physics Department
Brookhaven National Laboratory
Upton, New York

*Work supported by the U.S. Atomic Energy Commission.

In this talk I will discuss the experimental situation of A_2 meson from bubble chamber experiments and concentrate on recent results since the 1970 Philadelphia Conference on Meson Resonances. I will comment on:

A) Mass and fine structure of $A_2^{\pm}$

B) $\frac{d\sigma}{dt'}$ $(\pi^{\pm}p \rightarrow A_2^{\pm}p)$

C) Spin-Density matrix $\rho_{m,n}$ of A_2^{-}

D) Branching ratio of A_2^{+} and K^{**}

E) Experimental comments

Because of the status of A_2 is confused, I will try to examine the experimental results in each individual decay mode ($K\bar{K}$, $\eta\pi$ and $\rho\pi$) as well as the different charge states of A_2 (only new $A_2^{\pm}$ data available).

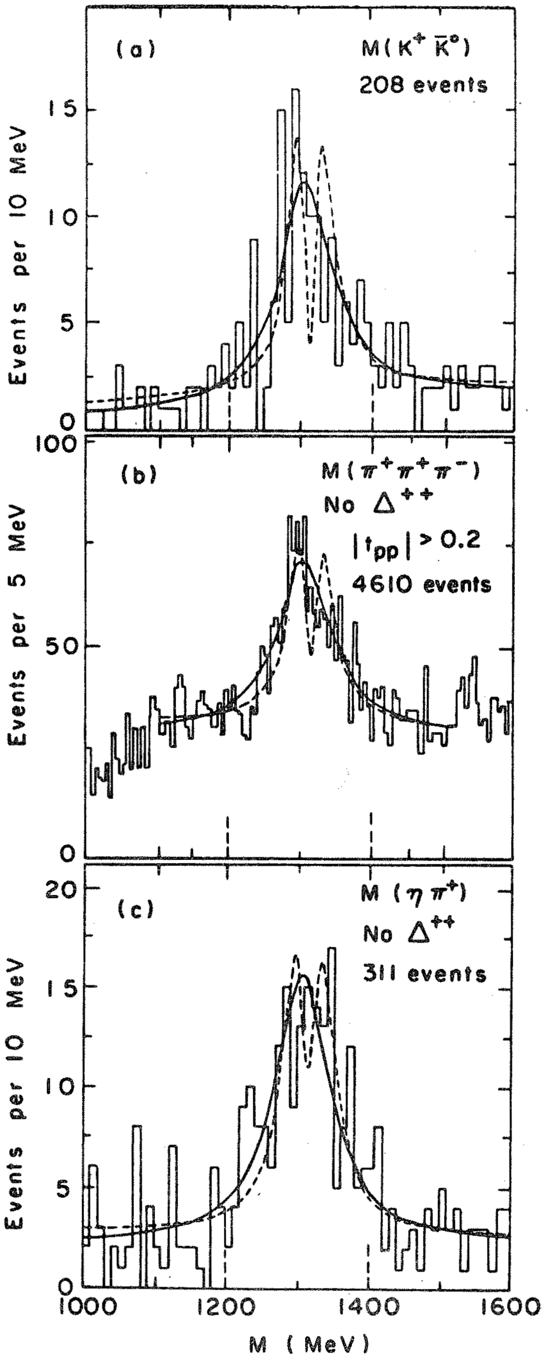

Fig. 1 Mass plots in the A_2 region. The curves are from the likelihood fit to the three decay modes simultaneously; BW (solid line) and DP (dashed line).

PART A - Mass and Fine Structure of A_2

$$
\underline{7\ \text{GeV/c}\ \pi^+ p \rightarrow A_2^+ p}
\\
\quad\quad\quad \hookrightarrow K_S^0 K^+
\\
\quad\quad\quad\quad \pi^+\pi^+\pi^-\ (\text{or}\ \rho^0\pi^+)
\\
\quad\quad\quad\quad \eta\ (550)\ \pi^+
$$

(LRL Group A, Physics Letters 33B, 607 (1970))

It is a high statistics bubble chamber experiment with good mass resolution. Single Breit-Wigner (BW) fit is favored over the "dipole" (DP) fit for all three decay modes. These results are in direct contradiction with the 7 GeV/c $\pi^- p \rightarrow A_2^- p$ results from CERN Boson Spectrometer experiment (Physics Letters 31B, 397 (1970)). The 7 GeV/c $\pi^- p \rightarrow p + X^-$ was a "Jacobian" type of counter experiment with limited $|t|$ range (0.2 to 0.29 GeV^2) but good statistics. The ma resolution, however, is not as good as that of the bubble chamber.

Bubble Chamber Experiment	"Jacobian" Counter Experiment
$\Gamma_{\text{res.}}(K_S^0 K^+) = 7.6$ MeV	$\Gamma_{\text{res.}}(K_S^0 K^-) = 20$ MeV
$\Gamma_{\text{res.}}(\pi^+\pi^+\pi^-) = 13.4$ MeV	$\Gamma_{\text{res.}}(X^-) = 16$ MeV
$\Gamma_{\text{res.}}(\eta\pi^+) = 18.4$ MeV	

There is no new information from bubble chamber results concerning the fine structure of $A_2 \rightarrow \rho\pi$ and $\eta\pi$, but there is a new result of $A_2^- \rightarrow K_S^0 K^-$ from BNL.

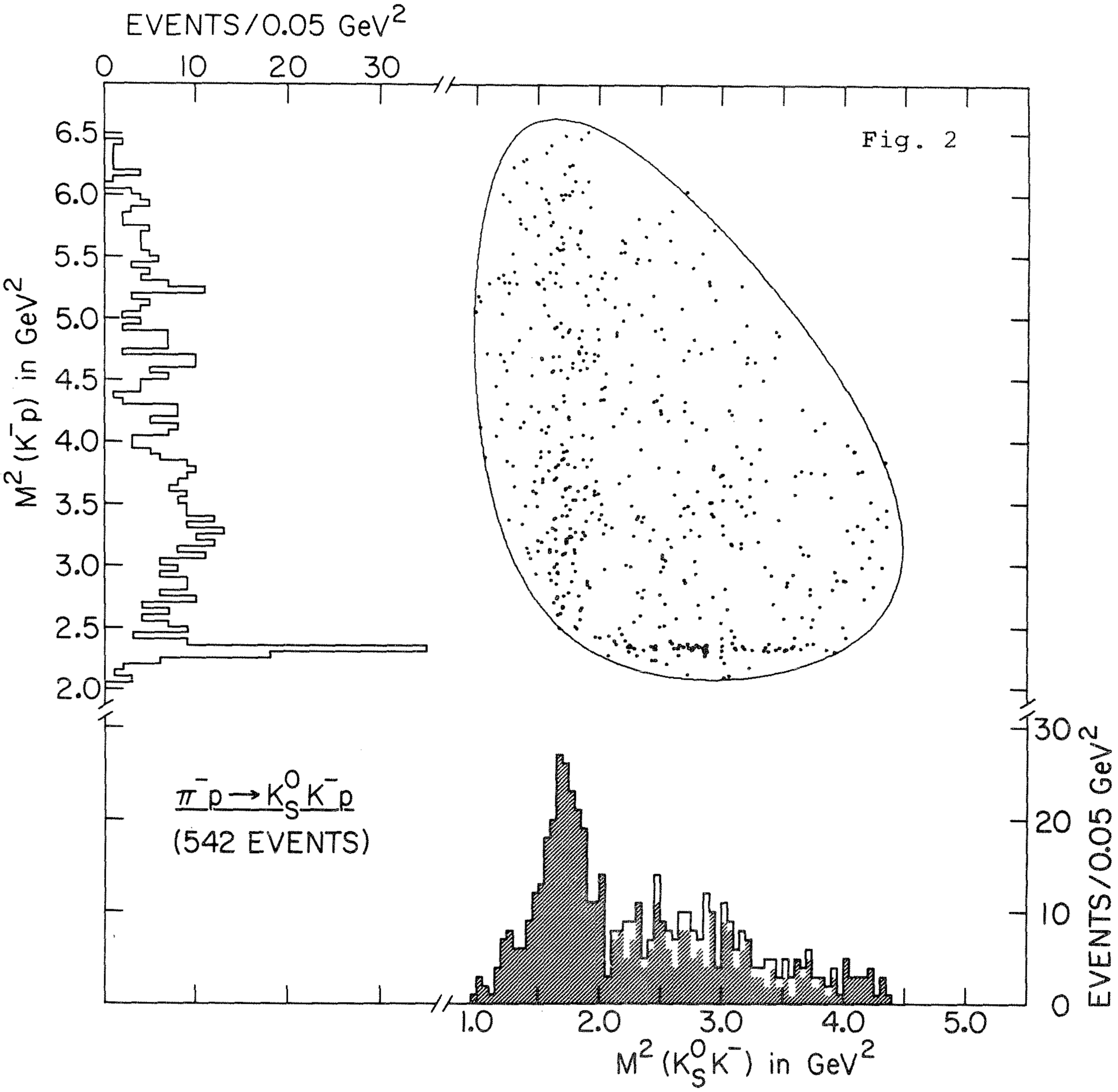

(BUBBLE CHAMBER)

4.5 GeV/c $\pi^- p \to A_2^- p$

$\hookrightarrow K^0_S K^-$

(New data from BNL: D.J. Crennell, H.A. Gordon, K.-W. Lai, and J.M. Scarr.) Strong $A_2^- \to K^0_S K^-$ and $\Lambda(1520) \to K^- p$ production in this final state. Kinematically, they do not overlap in the Dalitz plot. $\Gamma_{res}(K^0_S K^-) = 8 \pm 1$ MeV in A_2^- mass region. Events in the $\Lambda(1520)$ region provide independent check of systematics ($m = 1519.6 \pm 1.4$ and $\Gamma = 11^{+3}_{-2}$ MeV).

4.5 GeV/c $\pi^- p \rightarrow K_S^0 K^- p$

BNL (Bubble Chamber)

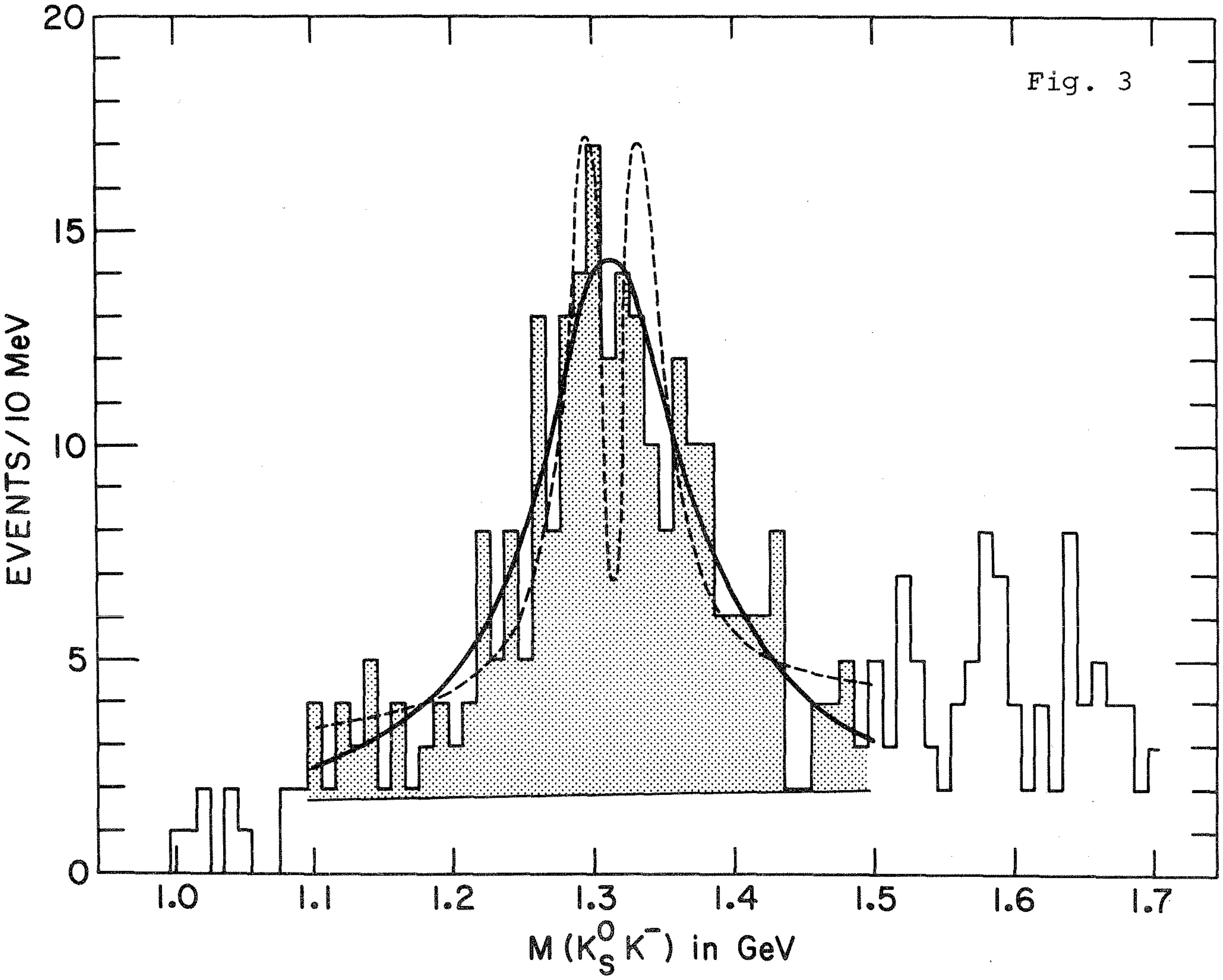

Fig. 3

A single Breit-Wigner resonance form plus a linear background was fitted to this mass spectrum by the maximum likelihood method; the result is shown by the solid curve where the resonance has mass 1313 ± 7 MeV and width 125^{+19}_{-16} MeV. A similar fit with a two parameter "dipole" plus a linear background yields two acceptable solutions with masses 1296 ± 2 and 1314^{+4}_{-3} MeV and widths 26 ± 4 and 30 ± 5 MeV, respectively. The latter fit is shown dashed in the figure. In an attempt to measure the acceptability of these fits we have calculated a χ^2 in the mass region from 1100 to 1500 MeV and obtain probabilities of 80% for the single Breit-Wigner resonance, 13% and 19% for the dipole fits. However, the χ^2 calculation depends greatly on the choice of bin size, so it is more reliable to examine the ratio of the likelihoods which show the Breit-Wigner fit is favored over either dipole fit by more than 240:1. Therefore, we conclude that, with the present statistics, we favor the single Breit-Wigner resonance interpretation even though we cannot rule out the "dipole" assumption on the χ^2-probability basis alone. However, we do not see the split in the $A_2^- \rightarrow K_S^o K^-$ reported by the 7 GeV/c $\pi^- p$ CERN experiment (with $0.2 < |t| < 0.29$ GeV^2) although we have a resolution less than half as broad. In fact, our data show remarkable similarity to the Berkeley 7 GeV/c $\pi^+ p$ data for $A_2^+ \rightarrow K_S^o K^+$.

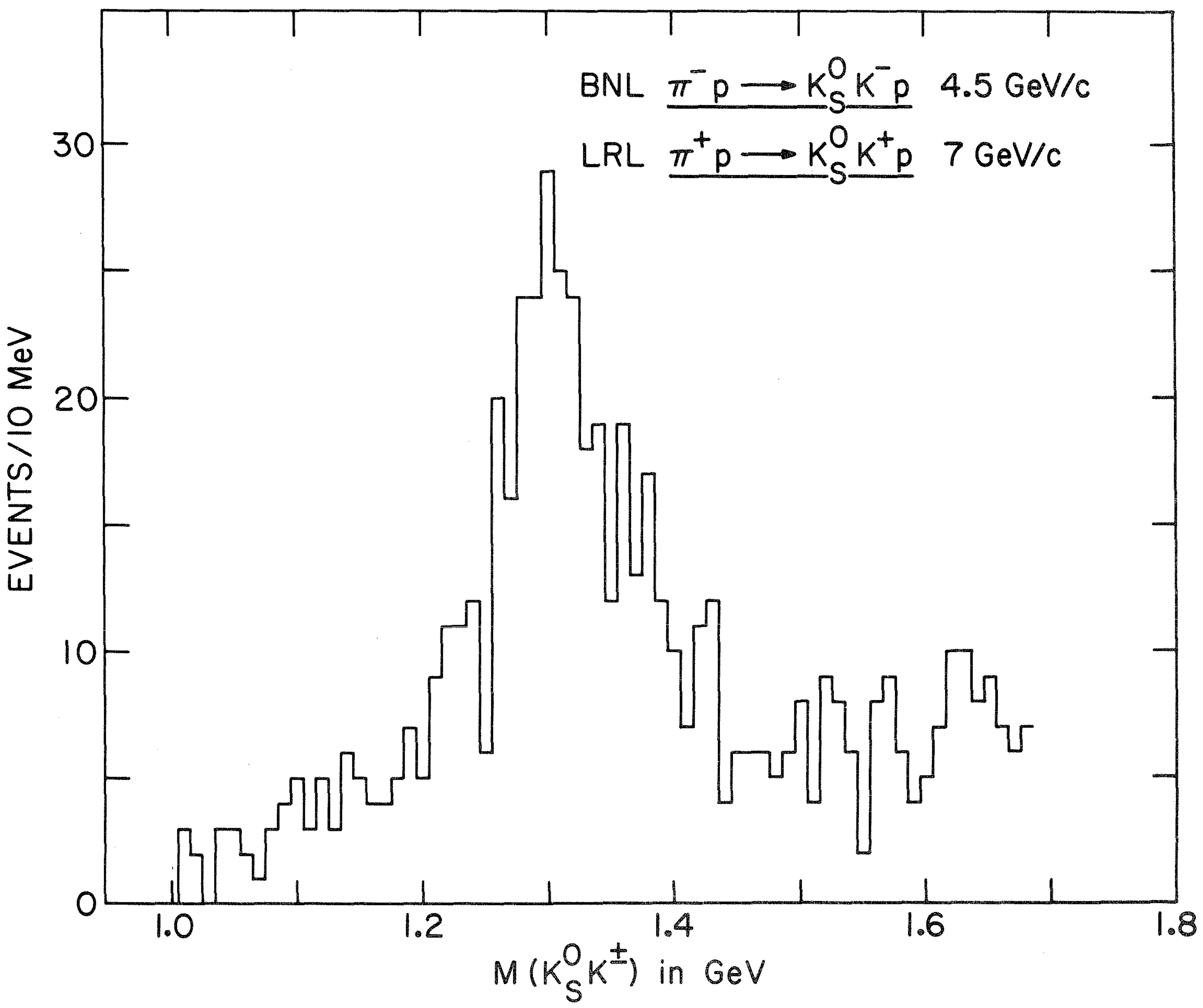
BNL $\pi^- p \rightarrow K^0_S K^- p$ 4.5 GeV/c
LRL $\pi^+ p \rightarrow K^0_S K^+ p$ 7 GeV/c
EVENTS/10 MeV
30
20
10
0
1.0
1.2
1.4
1.6
1.8
$M(K^0_S K^\pm)$ in GeV

Fig. 4

Combined $A_2^+ \rightarrow K_S^0 K^+$ and $A_2^- \rightarrow K_S^0 K^-$ from two bubble chamber experiments show: (a) no "split" in the mass spectrum with ~8 MeV mass resolution, and (b) no evidence for the 1425 MeV enhancement as reported by a BNL spectrometer experiment at 20.3 GeV/c (Phys. Rev. Letters 26, 413 (1971)).

$\pi^- p \rightarrow A_2^- p$, $A_2^- \rightarrow K_S^0 K^-$

4.5 GeV/c (BNL Bubble Chamber),
7 GeV/c (CERN Counter),
17.2 GeV/c (CERN and Munich Counter), and
20 GeV/c (BNL Counter).

$A_2^- \rightarrow K_s^0 K^-$

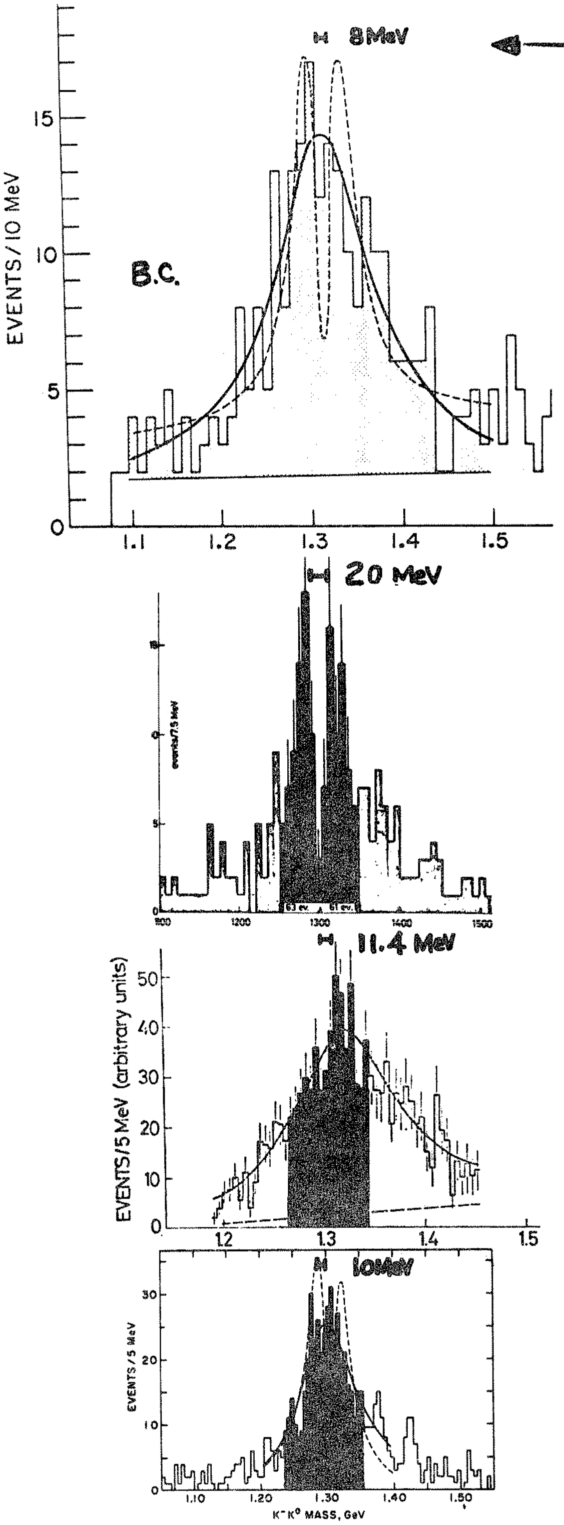

4.5 GeV/c

7 GeV/c

17.2 GeV/c

20.3 GeV/c

$A_2^+ \rightarrow K_s^0 K^+$

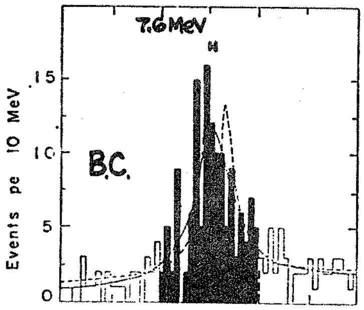

$\pi^+ p \rightarrow A_2^+$, $A_2^+ \rightarrow K_S^0 K^+$

7 GeV/c (LRL Bubble Chamber)

Fig. 5

Only the 7 GeV/c π^- experiment has less mass resolution than the others but shows the "split." In fact their "dipole" fit (60%) to the $A_2^- \rightarrow K_S^0K^-$ cannot rule out the assumption of a single Breit-Wigner fit (5%). With the exception of this 7 GeV/c π^- experiment, it is reasonable to conclude that the $A_2^- \rightarrow K_S^0K^-$ and $A_2^+ \rightarrow K_S^0K^+$ exhibit no obvious difference. In view of the recent 17.2 GeV/c π^-p CERN and 20.3 GeV/c π^-p BNL experiments of $A_2^- \rightarrow K_S^0K^-$ (no "split"), we further suggest that the structure (or non-structure) of $A_2^- \rightarrow K_S^0K^-$ has no energy dependence between 4.5 and ~ 20 GeV/c.

Summary on Mass and Fine Structure

- No new data on $\rho\pi$ and $\eta\pi$.
- "Old" results from LRL claimed no "split of $A_2^+ \to \rho^0\pi^+$ and $\eta^0\pi^+$ at 7 GeV/c.
- "New" data on $A_2^- \to K_S^0K^-$ from BNL -- no "split".
- No obvious difference between $A_2^+ \to K_S^0K^+$ at 7 GeV/c and $A_2^- \to K_S^0K^-$ at 4.5 GeV/c.
- No "split" reported from $A_2^- \to K_S^0K^-$ at 4.5 (Bubble Chamber) 17.2 (Counter), and 20.3 (Counter) GeV/c with good resolution 8-11.4 MeV whereas "split" reported at 7 GeV/c with poorer resolution (20 MeV).

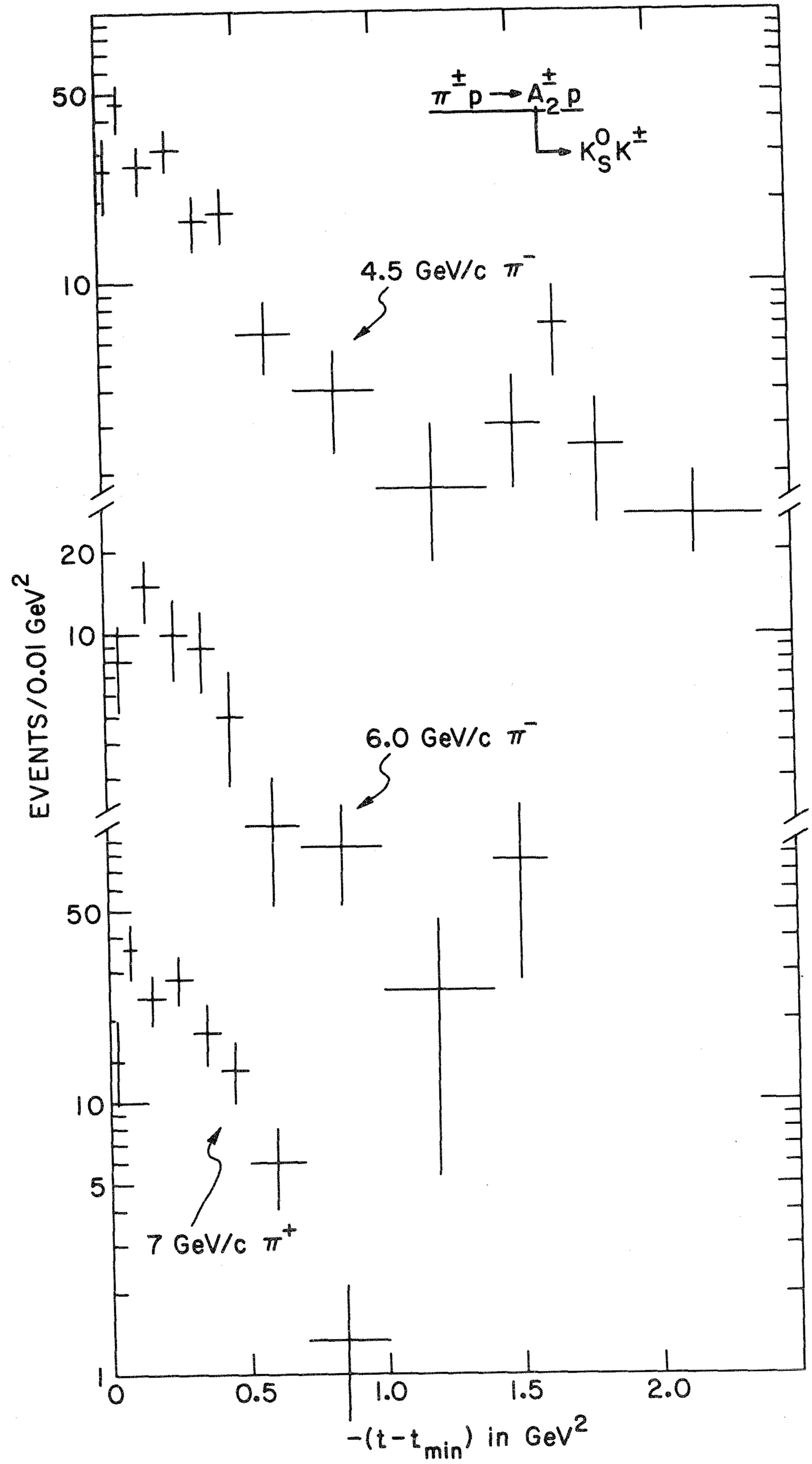

$\pi^{\pm}p \rightarrow A_2^{\pm}p$
$\rightarrow K_S^0 K^{\pm}$
4.5 GeV/c π^-
6.0 GeV/c π^-
7 GeV/c π^+
EVENTS/0.01 GeV^2
50
10
20
10
50
10
5
1
0
0.5
1.0
1.5
2.0
$-(t-t_{min})$ in GeV^2

Fig. 6

PART B $\frac{d\sigma}{dt'}(\pi^{\pm}p \rightarrow A_2^{\pm}p)$

$$\frac{d\sigma}{dt'}(\pi^{\pm}p \rightarrow \underbrace{A_2^{\pm}}_{\hookrightarrow K_S^0K^{\pm}}p)$$

4.5 and 6 GeV/c π^- BNL (unpublished data)
7 GeV/c π^+ LRL (Physics Letters 34B, 156 (1971)).

The production angular distribution of $A_2^{\pm}$ can best be studied in the $K_S^0K^{\pm}$ decay mode because of the small background (<20%) in the mass region (1.2-1.4 GeV). This figure displays the distributions as a function of $t' = t - t_{min}$ which can be fitted by the functional form $\sim e^{bt'}$ up to $|t'| \simeq 1$ GeV^2 with a value of $b = 3 \pm 0.5$ GeV^{-2} for the 4.5 and 6 GeV/c π^- data and somewhat steeper for the π^+ data. There is a dip in the forward direction ($t' = 0$ to -0.05 GeV^2) for both A_2^+ and A_2^-. In addition, there is a significant break in the distribution at $|t'| \sim 1.0$ GeV^2 in the 4.5 GeV/c data. Because of the limited t range studied so far by the counter experiments, the structure of the $A_2^- \rightarrow K_S^0K^-$ production at large $|t|$ region has not been revealed. We will return to this point after our examination of the decay correlations of the $A_2^- \rightarrow K_S^0K^-$.

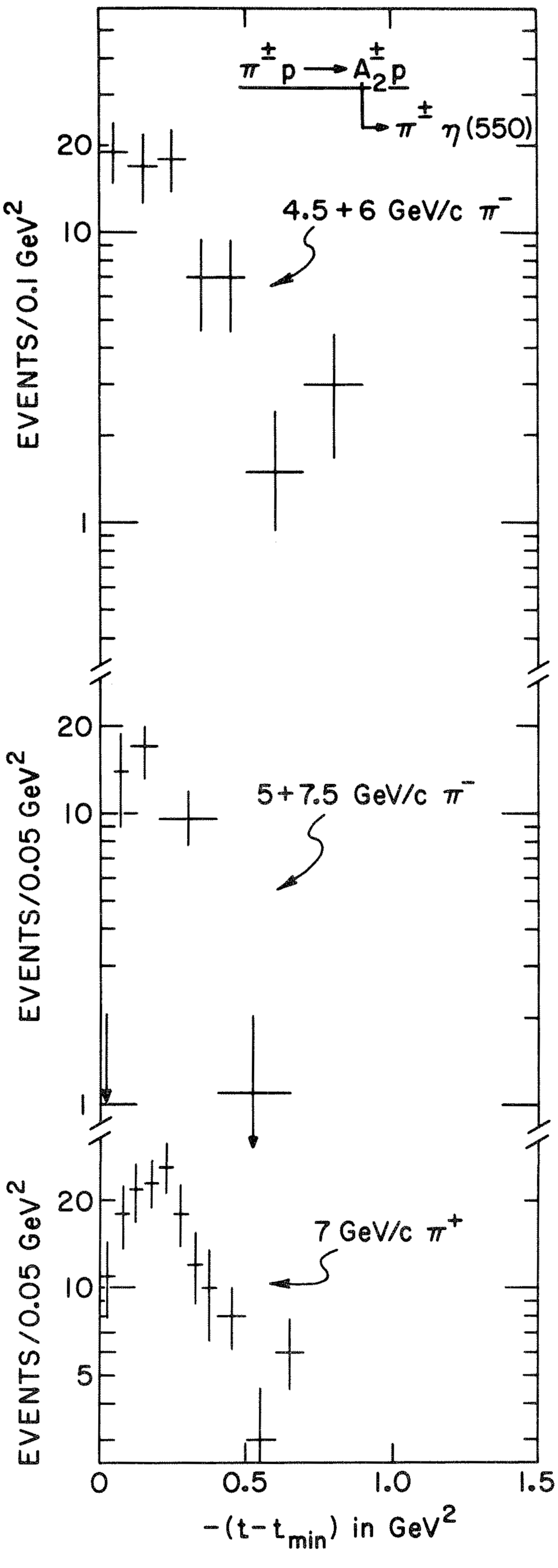
$\pi^\pm p \rightarrow A_2^\pm p$
$\hookrightarrow \pi^\pm \eta(550)$
4.5 + 6 GeV/c π^-
5 + 7.5 GeV/c π^-
7 GeV/c π^+
EVENTS/0.1 GeV^2
EVENTS/0.05 GeV^2
EVENTS/0.05 GeV^2
20
10
1
20
10
1
20
10
5
0
0.5
1.0
1.5
$-(t-t_{min})$ in GeV^2

Fig. 7

$$\frac{d\sigma}{dt'}(\pi^- p \to \underbrace{A_2^-}_{\hookrightarrow\ \pi^-\eta(550)} p)$$

4.5 and 6 GeV/c π^- BNL (unpublished results)
5 and 7.5 GeV/c π^- Illinois (M. Ioffredo, private communication)

Because of the small background in the $A_2^- \to \pi^-\eta(550)$ mass region (See Fig. 1), the $d\sigma/dt'$ can be obtained by a selection of $\pi^-\eta$ events in the A_2^- mass region (1.2 to 1.4 GeV). Limited statistics preclude a detailed study of the $A_2^- \to \pi^-\eta$ contribution in each t interval as performed for the $A_2^\pm \to \rho^o\pi^\pm$.

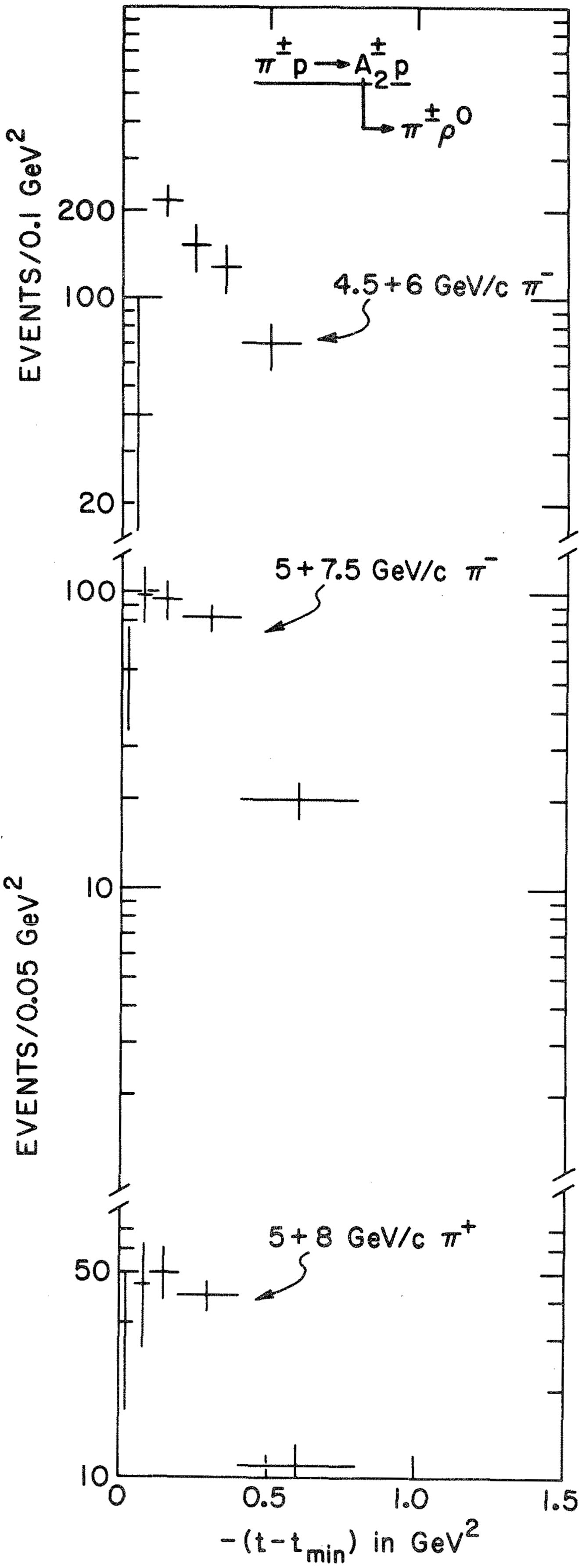
$\pi^{\pm} p \rightarrow A_2^{\pm} p$
$\hookrightarrow \pi^{\pm} \rho^0$
EVENTS/0.1 GeV^2
200
100
20
4.5+6 GeV/c π^-
5+7.5 GeV/c π^-
EVENTS/0.05 GeV^2
100
10
5+8 GeV/c π^+
50
10
0
0.5
1.0
1.5
$-(t-t_{min})$ in GeV^2

Fig. 8

$$\underline{\frac{d\sigma}{dt'}(\pi^{\pm}p \rightarrow A_2^{\pm}p)}$$
$$\hookrightarrow \rho^{0}\pi^{\pm}$$

4.5, 6 GeV/c π^- BNL (unpublished results)

$$\left.\begin{array}{l}\text{5, 7.5 GeV/c } \pi^- \text{ Illinois}\\ \text{5, "8" GeV/c } \pi^+ \text{ BDNPTRYABCCR}\end{array}\right\}\text{(Private communication, M. Ioffredo)}$$

Because of the large background in the $A_2^{\pm} \rightarrow \rho^0\pi^{\pm}$ mass region, the $d\sigma/dt'$ has to be obtained with special care. Two methods are generally used: (a) obtain $A_2^{\pm} \rightarrow \rho^0\pi^{\pm}$ contribution by fitting the mass spectrum for each interval of t' region (4.5 and 6 GeV/c data); (b) estimate the amount of $J^P = 2^+$ contribution from each interval of t region (5 and 7.5 GeV/c π^-, and 5 and 8 GeV/c π^+ data). Both cases are complicated by the large 1^+(s-wave) background of the A_1, in particular the low t' region. There is, however, a dip in the forward scattering ($t' = 0$ to ≈ 0.05 GeV^2) for both $A_2^+ \rightarrow \rho^0\pi^+$ and $A_2^- \rightarrow \rho^0\pi^-$. There is no obvious difference in $d\sigma/dt'$ between A_2^+ and A_2^-.

Summary of $\frac{d\sigma}{dt'}(\pi^{\pm} p \to A_2^{\pm} p)$

→ $\frac{d\sigma}{dt'}(A_2^{+}) \sim \frac{d\sigma}{dt'}(A_2^{-})$ for $K\bar{K}$, $\eta\pi$, and $\rho\pi$ decay modes.

→ Dip at $|t'| = 0$ to 0.05 GeV^2 for all modes.

→ A break at $|t'| = 1$ GeV^2 for $\frac{d\sigma}{dt'}(\pi^- p \to \underset{\hookrightarrow K_S^0 K^-}{A_2^-} p)$ at 4.5 GeV/c.

PART C Spin-Density Matrix Elements of A_2^-

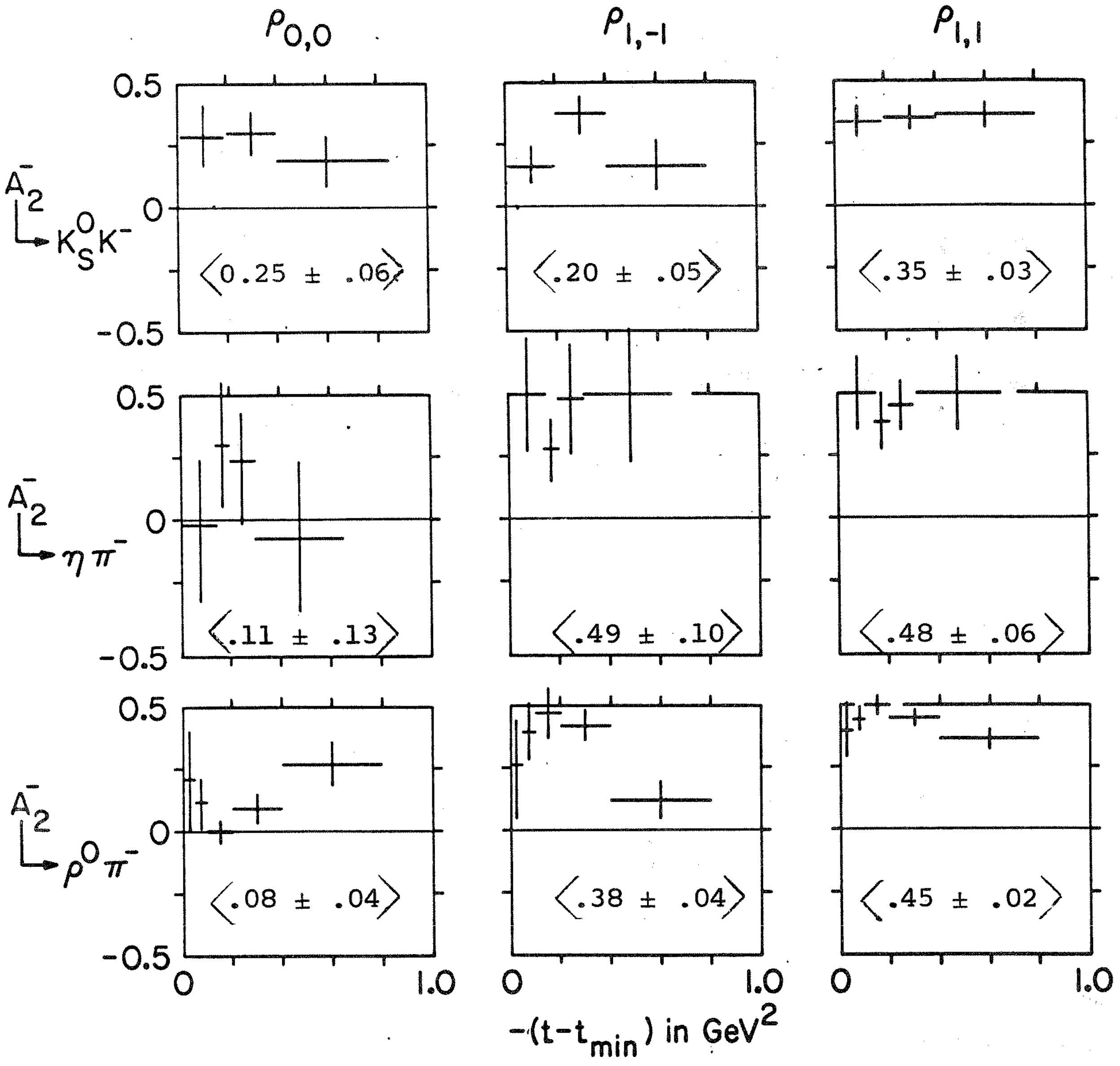

Fig. 9

$$\rho_{m,n}\ \text{vs. } t'\ \text{for } A_2^- \rightarrow \left\{ \begin{array}{l} K_S^0K^-\ \ 4.5\ \text{GeV/c}\ \pi^-\ \text{BNL unpublished data} \\ \left.\begin{array}{l}\eta\pi \\ \rho\pi\end{array}\right\}\ \begin{array}{l}\text{5 and 7.5 GeV/c } \pi^- \text{ Illinois data} \\ \text{(private communication, M. Ioffredo)}\end{array} \end{array}\right.$$

Maximum likelihood fit to the decay angles, assuming $J^P = 2^+$ for all three decay modes, gives spin-density matrix elements of $\rho_{0,0}$, $\rho_{1,-1}$, and $\rho_{1,1}$ with all the other elements consistent with zero. In this energy region, the values of $\rho_{1,1}$ and $\rho_{1,-1}$ reach to the maximum allowed value ($\rho_{1,1} = \rho_{1,-1} \simeq 0.5$ for a ρ exchange) for $|t'| \geq 0.4$ GeV^2. The value of $\rho_{0,0}$ seems to be non-zero for $|t'| \simeq 1.0$ GeV^2 for $A_2^- \rightarrow K_S^0K^-$ perhaps suggesting that trajectories other than ρ contribute to A_2^- production. There is no obvious s-dependence of $\rho_{m,n}$ for $A_2^- \rightarrow \rho^0\pi^-$ from $P_{\text{Lab.}} = \sim 5$ to 25 GeV/c. (Mike Ioffredo, private communication.)

Summary on Spin-Density Matrix of A_2^-

- $\rho_{1,1}$ and $\rho_{1,-1}$ large ~ 0.4 for all three decay modes
- $\rho_{0,0} \neq 0$ at moderate $|t'| = 0.4$ to 0.6 GeV^2 and $\frac{d\sigma}{dt'}(\pi^- p \to A_2^- p)$ at 4.5 GeV/c has a break at $|t'| \simeq 1$ GeV^2
  $\quad \hookrightarrow K_S^0 K^-$
  suggest trajectory other than ρ (such as B or f^0) being exchanged in t-channel.

PART D Branching Ratio of A_2 and K^{**}

$$A_2^+ \longrightarrow \frac{\eta(550)\pi}{\rho\pi} = 24.6 \pm 4.2\% \qquad \uparrow$$

$$\frac{K\bar{K}}{\rho\pi} = 9.7 \pm 1.8\% \qquad \uparrow$$

$$K^{**} \longrightarrow \frac{K^*\pi}{K\pi} = 44 \pm 9\% \qquad \downarrow$$

New A_2^+ and K^{**} Branching Rates

A_2^+ (7 GeV/c π^+ LRL data) branching rates are obtained for $|t| =$ 0.2 to 0.8 GeV^2 from the A_2^+ production from $\pi^+ p \rightarrow A_2^+ p$. The $\frac{(K\bar{K})^+}{(\rho\pi)^+}$ rate is about a factor two increased from some previous measurements. K^{**} (3.9 and 4.6 GeV/c K^- BNL data, Phys. Rev. Letters 25, 1362 (1970)) branching rates for $K\pi$ are increased and $K^*\pi$ are decreased substantially from previous measurements. Assuming A_2 and K^{**} are in the same $J^P = 2^+$ nonet, one can relate their $2^+ \rightarrow 1^-0^-$ and 0^-0^- transitions via SU_3 symmetry.

PARTIAL WIDTHS OF $J^P = 2^+$ NONET

$2^+ \to 1^-0^-$	$\lvert A\rvert^2$	Γ_{exp}	Γ_{SU_3}
$A_2 \to \rho\pi$	4	67 ± 8	71.2
$K^{**} \to K^*\pi$	3/2	26 ± 5.6	21.4
$K^{**} \to \rho K$	3/2	8.6 ± 3.5	5.9
$K^{**} \to \omega K$	$3/2\ \sin^2\theta_1$	2.9 ± 2.3	1.7
$f^* \to K^*K$	$6\ \cos^2\theta_2$	9 ± 9	10.5
$2^+ \to 0^-0^-$			
$A_2 \to K\overline{K}$	12	6.5 ± 1.3	7.4
$A_2 \to \eta\pi$	8	16.5 ± 3	14.4
$K^{**} \to K\pi$	18	58.5 ± 4.4	57.8
$K^{**} \to K\eta$	2	0 ± 1.0	1.9
$f^o \to \pi\pi$	$3(2\sin\theta_2 + \alpha\cos\theta_2)^2$	150 ± 25	140.2
$f^o \to K\overline{K}$	$4(\sin\theta_2 - \alpha\cos\theta_2)^2$	0 ± 3	5.3
$f^o \to \eta\eta$	$(2\sin\theta_2 - \alpha\cos\theta_2)^2$	0 ± 3	0.2
$f^* \to \pi\pi$	$3(2\cos\theta_2 - \alpha\sin\theta_2)^2$	0 ± 6	1.8
$f^* \to K\overline{K}$	$4(\cos\theta_2 + \alpha\sin\theta_2)^2$	62 ± 15	40.8
$f^* \to \eta\eta$	$(2\cos\theta_2 + \alpha\sin\theta_2)^2$	0 ± 16	12.3

$$\theta_1 = 39.6^o \quad (m^2)$$

$$\theta_2 = 31.7^o \quad (m^2)$$

SU_3 predictions are compared with recent measurements of A_2 and K^{**} branching rates assuming a single resonance in A_2 as well as K^{**}. Both $2^+ \to 1^-0^-$ and 0^-0^- experimental transition rates agree well with the predictions within the experimental errors. θ_1 (θ_2) is the mixing angle for vector (tensor) meson nonet using the mass-square mass formula.

Summary on Branching Ratios of A_2 and K^{**}

- Recent measurements suggest that $A_2^+ \rightarrow \frac{\eta\pi}{\rho\pi}$ and $\frac{K\bar{K}}{\rho\pi}$ increases and $K^{**} \rightarrow \frac{K^*\pi}{K\pi}$ decreases.

- Assuming a single resonance in A_2 and K^{**}, partial width predictions from SU_3 agree well with experimental measurements.

$A_2^- \rightarrow K_S^0 K^-$

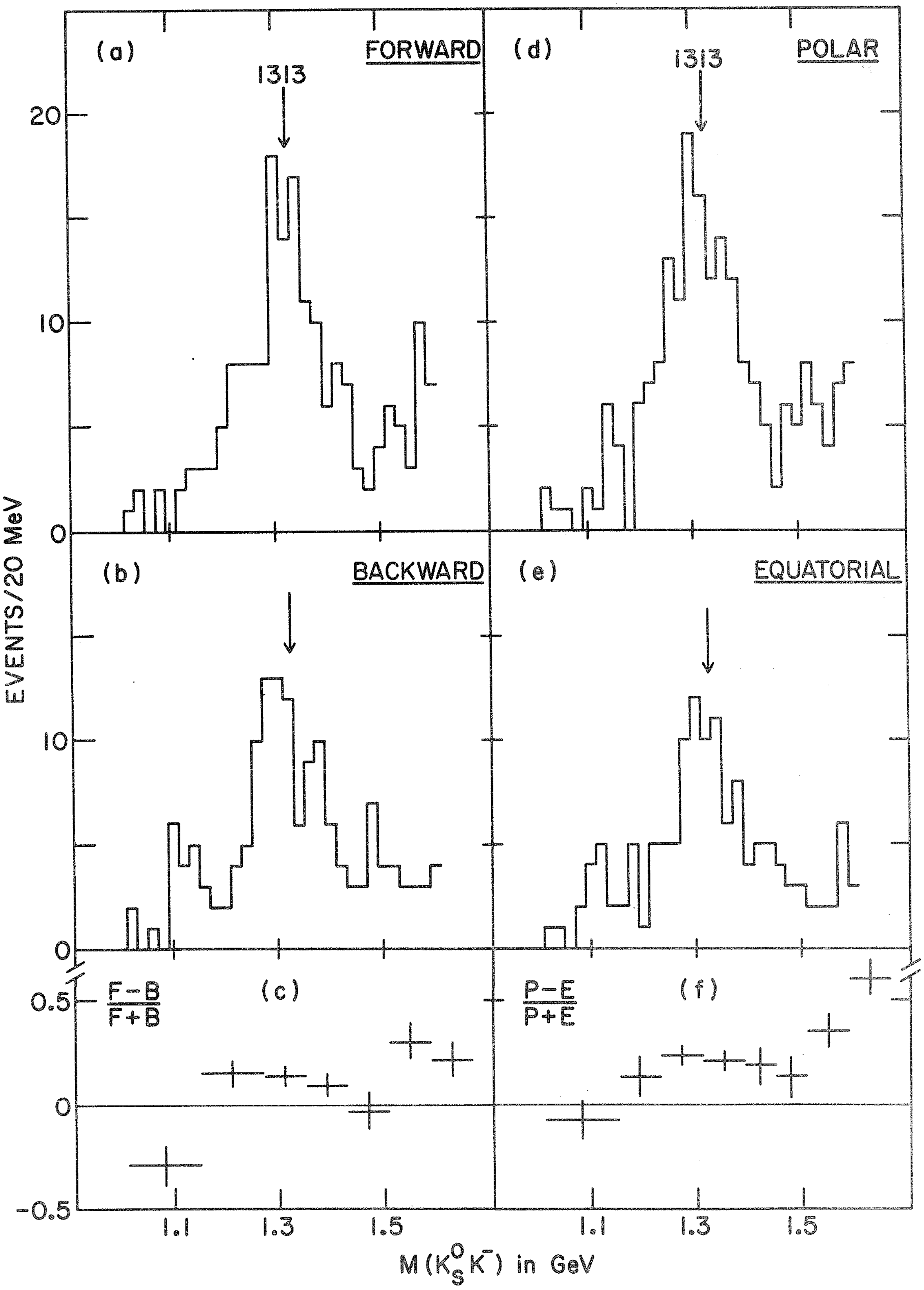

Fig. 10

PART E Experimental Comments for $A_2^- \to K_S^0K^-$

Since the 4.5 GeV/c π^- experiment has the largest sample of bubble chamber events in the $K_S^0K^-$ decay of the A_2^- from πN interactions, some experimental comments are necessary when one compares the 4π-solid angle $K_S^0K^-$ results (bubble chamber) with those of limited solid angle (counter). It is known that interference between states of different J^P may affect the $K_S^0K^-$ mass spectrum if one does not detect all of the solid angle of $K_S^0K^-$ decay. To illustrate this point, the Fig. 10 shows the $K_S^0K^-$ spectra in the A_2^- region subjected to the following cuts in the $K_S^0K^-$ rest frame: $\cos\theta>0$, $\cos\theta<0$ and $|\cos\theta| > 0.5$, $|\cos\theta| < 0.5$ corresponding to forward, backward and polar, equatorial regions as shown in (a), (b), (d), and (e) respectively where $\cos\theta$ is defined as $\pi_{in.} \cdot K_S^0$ in the $K_S^0K^-$ rest frame. These show that a possible mass shift of ~10 MeV, or a width difference of as much as ~20 MeV, or both can be achieved by these cuts. Furthermore, the forward-backward asymmetry $(\frac{F-B}{F+B})$ observed in (c) indicates interference between the A_2^- and the other amplitude(s) does indeed exist, whereas the asymmetry in $(\frac{P-E}{P+E})$, as shown in (f), is expected because of the nature of the A_2^- decay. Therefore, it is clear that different decay regions of $A_2^- \to K_S^0K^-$ from this experiment may exhibit different mass distributions of the A_2^-. This observation will make direct comparisons of $K_S^0K^-$ mass spectra between the "all" solid angle (such as bubble chamber) experiments and the "limited" solid angle (such as counter) experiments very difficult. This comment does not apply, of course, to missing mass experiments where no requirements were made of the decay products.

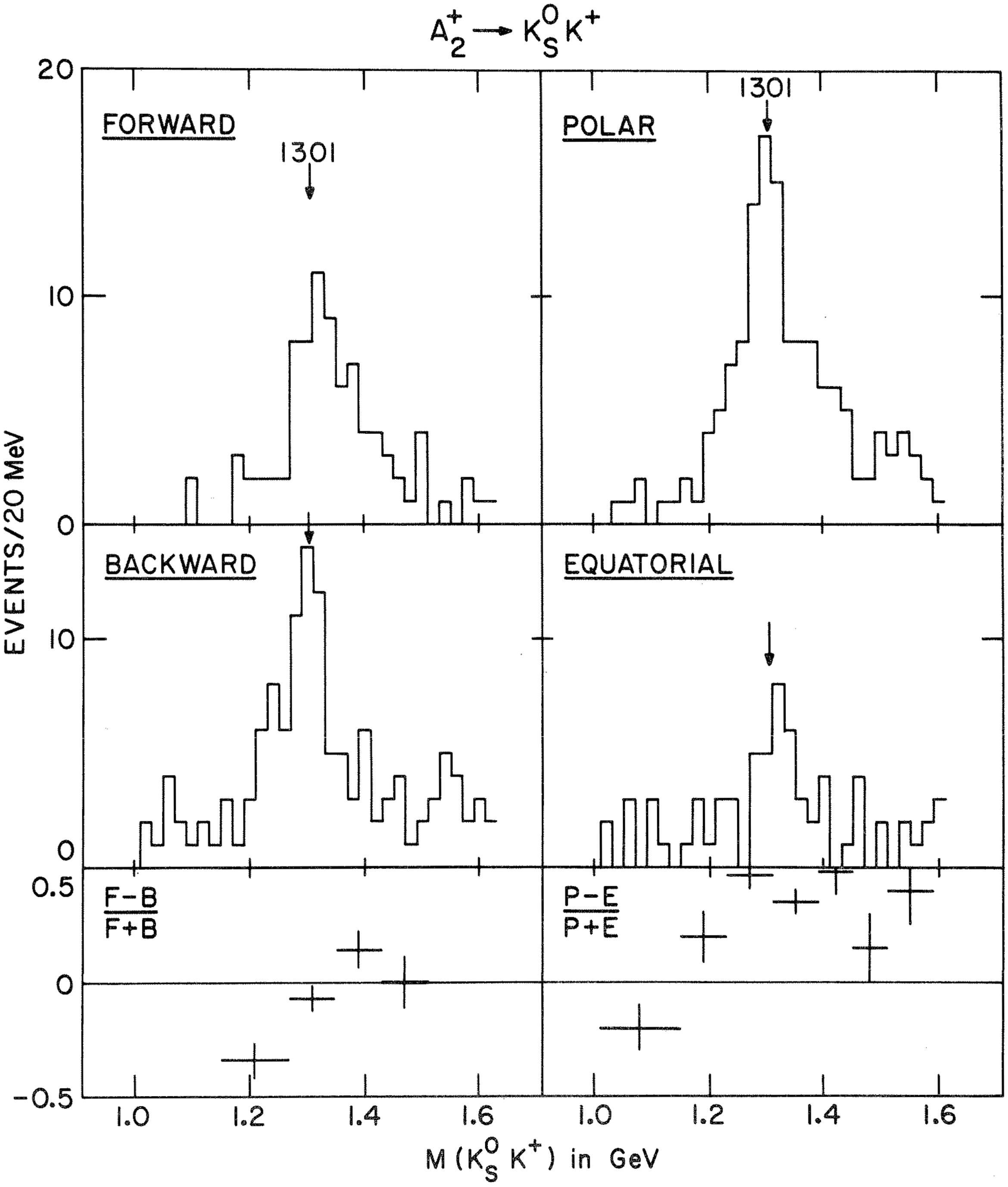
$A_2^+ \rightarrow K_S^0 K^+$
FORWARD
POLAR
BACKWARD
EQUATORIAL
1301
1301
$\frac{F-B}{F+B}$
$\frac{P-E}{P+E}$
EVENTS/20 MeV
20
10
0
10
0
0.5
0
-0.5
1.0
1.2
1.4
1.6
1.0
1.2
1.4
1.6
$M(K_S^0 K^+)$ in GeV

Fig. 11

Experimental Comments for $A_2^+ \rightarrow K_S^o K^+$

The same comments made for $A_2^- \rightarrow K_S^o K^-$ also apply here for $A_2^+ \rightarrow K_S^o K^+$ from the 7 GeV/c π^+ experiment. It is interesting to note that the $\frac{F-B}{F+B}$ seems to show opposite sign from that of $A_2^- \rightarrow K_S^o K^-$ (see Fig. 10).

Summary on Experimental Comments

- Small background amplitude does give substantial $\frac{F-B}{F+B}$ asymmetry in $A_2^{\pm} \rightarrow K_S^0K^{\pm}$ decays.
- Detailed comparisons of $K_S^0K^{\pm}$ mass spectrum between limited solid angle $K\bar{K}$ results with all solid angle $K\bar{K}$ results will be difficult since the interference may affect the $K_S^0K^{\pm}$ mass spectrum if one does not detect all of the solid angle of $K_S^0K^{\pm}$ decays.

Acknowledgment

I wish to thank Dr. Howard A. Gordon for careful reading of this manuscript and Dr. Michael Ioffredo, Dr. Monroe Rabin and Dr. Stanley Flatté for communicating their data for this talk.

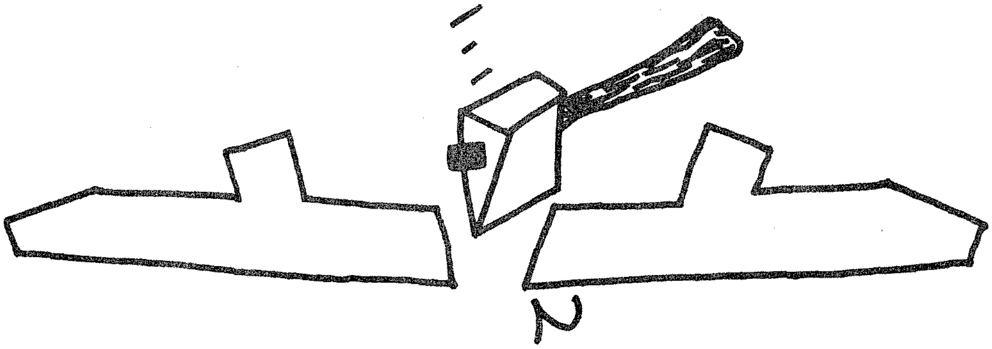

INTERFERING RESONANCE MODEL FIT TO $A_2^{+,-,0}$ MASS SPECTRUM*

K.W.J. Barnham

Lawrence Radiation Laboratory
University of California
Berkeley, California 94720

This talk is presented here in the form of two papers:

Paper A : "The A_2^+ Mass Spectrum in π^+p Interactions at 3.7 GeV/c". Page 295

Paper B : "Interfering Resonances and the A_2 Mass Spectrum". Page 307

---

*Work supported by the U.S. Atomic Energy Commission.

Paper A

THE A_2^+ MASS SPECTRUM IN π^+p INTERACTIONS AT 3.7 GeV/c*

K. W. J. Barnham, G. S. Abrams, W. R. Butler,† D. G. Coyne,‡
G. Goldhaber, B. H. Hall, J. MacNaughton, and G. H. Trilling

Department of Physics and Lawrence Radiation Laboratory
University of California, Berkeley, California 94720

The A_2 meson has been the subject of considerable experimental and theoretical investigation since the observation of the splitting of the A_2^- by the CERN Missing Mass Spectrometer and CERN Boson Spectrometer experiments.[1] Much less was known about the positive A_2 meson. The Bonn-Gurham-Nijmegen-Paris(E.P.)-Torino Collaboration reported[2] observing structure in the A_2^+ in 5 GeV/c π^+p interactions, but their statistics were rather limited. More recently Alston-Garnjost et al.[3] have reported on a high statistics π^+p bubble chamber experiment at 7 GeV/c, where they see no evidence for splitting. Furthermore a neutron missing mass spectrometer experiment[4] has recently

*Work supported by the U. S. Atomic Energy Commission.

†Present address: Department of Physics, David Lipscomb College, Nashville, Tennessee 37203.

‡Present address: Department of Physics, Princeton University, Princeton, New Jersey 08540.

studied the A_2^o in $\pi^- p$ interactions at 3.16 GeV/c incident momentum and observed splitting.

In this Letter we report some evidence favoring the splitting of the A_2^+ produced in $\pi^+ p$ interactions at 3.7 GeV/c with a sample of A_2^+ events intermediate in number between that of the 5 GeV/c and 7 GeV/c experiments. The data comes from a 180,000 picture exposure of the Lawrence Radiation Laboratory 72-inch hydrogen bubble chamber at the Bevatron. The experimental details have already been presented.[5,6] The exposure yielded the following numbers of events in the channels of interest to the A_2^+ study

$\pi^+ p \rightarrow p\pi^+\pi^+\pi^-$	16,445 events	(1)
$\pi^+ p \rightarrow p\pi^+\pi^+\pi^-\pi^o$	16,617 events	(2)
$\pi^+ p \rightarrow p\pi^+\pi^+\pi^- MM$	7,463 events	(3)
$\pi^+ p \rightarrow pK^+\bar{K}^o$	92 events	(4)

Reaction (3) consists of those events with two or more missing neutral particles for which the proton can be identified by ionization. In channel (4) we require the $K_1^o \rightarrow \pi^+\pi^-$ decay to be observed in the chamber. We have observed the A_2^+ decays to $\pi^+\pi^+\pi^-$, $\eta\pi^+$ and $K^+\bar{K}^o$ in channels (1), (2) and (4) respectively and searched for the $\eta'\pi^+$ decay mode in channel (3). However the statistics are limited for the $\eta\pi^+$, $K^+\bar{K}^o$ and $\eta'\pi^+$ decay modes with the result that we have information on decay branching ratios but can make no statement about structure in these cases.

Reaction (1) is dominated by the production of the $\Delta^{++}\rho^o$ quasi-two-body channel which has been discussed earlier.[6] To eliminate all contamination due to this and other Δ^{++} production channels, events with at least one $p\pi^+$ effective mass less than 1380 MeV were removed. The effect of making this selection can be seen in Fig. 1. The $\pi^+\pi^+\pi^-$ mass spectrum before making any cuts is shown in Fig. 1a. The A_2^+ stands on a very large background. The shaded histogram in Fig. 1a is the $\pi^+\pi^+\pi^-$ spectrum for the 12,117 events which have at least one $p\pi^+$ mass less than 1380 MeV, i.e., the events which are removed in order to study the A_2^+. It can be seen that there is no evidence for an A_2^+ signal in these events. There is however a shoulder at 1300 MeV. We cannot say whether the absence of an A_2^+ signal in the Δ^{++} region results from the dynamics of the $A_2^+ \rightarrow \rho^o\pi^+$ decay being such that there is little overlap with the Δ^{++} band on the $p\pi^+\rho^o$ Dalitz plot, or if some interference effect is occurring with the Δ^{++} amplitude. In Fig. 1b we show the $\pi^+\pi^+\pi^-$ mass spectrum when these Δ^{++} events have been removed. A clear A_2^+ signal is seen. Its mass however is shifted downwards somewhat from its value in the uncut spectrum in Fig. 1a primarily because of the shoulder at 1300 MeV in the Δ^{++} events. A fit of a single Breit-Wigner resonance, with a second-order polynomial in mass as background, made to the data in Fig. 1b (in 20-MeV bins in order to ignore possible structure), gives a resonance mass of 1307±4 MeV. A similar fit to the uncut spectrum in Fig. 1a gives a mass of 1324±6 MeV.

The number of A_2^+ events above the fitted background in Fig. 1b is 388±64. The error is the combination in quadrature of the statistical error on the total number of events in the fitted region (1100-1500 MeV) and the number of events under the background in this same region. It should be noted that on removing the Δ^{++} events we have a clear A_2^+ signal before applying any t cuts. We have been able to calculate A_2^+ branching ratios without making t selections. This is advantageous since, as has been pointed out,[7] if the A_2 consists of more than one resonance there could be a t dependence of the branching ratios. The branching fractions which we obtain for the $\rho\pi$, $\eta\pi$, $K\bar{K}$, and $\eta'\pi$ decay modes[8-13] are given in Table I. The results are in good agreement with the 5 GeV/c (Ref. 2) and 7 GeV/c (Ref. 7) π^+p values, and with the world averages.[14]

We have searched for evidence of structure by an examination of the 3π spectrum for various t' cuts. ($t' = |t - t_{min}|$ where $|t_{min}|$ is the minimum value of $|t|$ kinematically allowed for each event. At a 3π mass of 1300 MeV $|t_{min}| \approx 0.074$ GeV^2.) Figure 2 shows the 3π spectrum in 20-MeV bins for one such set of cuts. As has been observed in other experiments[2,3] the $t' < 0.1$ GeV^2 region (Fig. 2a) is dominated by the broad low mass A_1 enhancement with very little A_2 signal. The A_2 signal is clear in the t' interval 0.1-0.6 (Fig. 2b) and again for $t' > 1.0$ (Fig. 2d,e). There is no compelling evidence for A_2 production in the t' interval 0.6-1.0 (Fig. 2c).

Ideally one would like to study a very narrow t' range both for comparison with the missing mass experiments and for interfering resonance model considerations.[15] In such a model the two resonances can have different production mechanisms so that interference may only be observed over a limited region of t where coherence between the two amplitudes holds. As a compromise, in view of our limited statistics, we show in Fig. 3 the 3π mass distribution in 10-MeV bins for the t' interval 0.1-2.0 GeV^2. This t' interval gives a good A_2-to-background ratio and shows an indication of splitting.

Calibration studies of the mass errors obtained from the kinematic fitting program have been made in connection with the ω-ρ interference effect[5] and the determination of the width of the ω.[16] For the events in Fig. 3, $\Gamma_R/2 = 7$ MeV where Γ_R is the full width at half height of the resolution function. In order to ascertain the statistical significance of the dip centered at 1310 MeV in Fig. 3 we have followed the now "standard" procedure[1] of fitting the data to either a single Breit-Wigner resonance or a dipole shape[17] plus a linear background in each case. The theoretical curves were folded with the experimental resolution function and binned using the program EXTRACT,[18] to make the fit through a χ^2 minimization procedure. The parameters obtained from the fits are given in Table II. It can be seen that the dipole fit is favored over the single Breit-Wigner resonance, but with a confidence level[19] of 11% the Breit-Wigner cannot be completely ruled out. We also note that the interfering resonance model discussed in the following Letter[15] gives good fits to the mass spectrum.

The number of events in the dipole signal of Fig. 3 for the mass range 1200-1400 MeV is 297, and the background-to-signal ratio in this same region is 1.6/1. The values for the 5 GeV/c experiment are 108 and 1.3 respectively ($t' > 0.1$ GeV^2) and for the 7 GeV/c experiment 833 and 1.4 ($t > 0.2$ GeV^2).

The fitted dipole mass 1311.6±2.6 MeV is rather higher than the CERN value 1298±5 MeV but is more consistent with the value observed in the π^+p experiment[2] at 5 GeV/c 1306±4 MeV and the A_2^0 dipole mass[4] 1305.3±1.5 MeV. The errors we quote are those obtained from the fitting program and do not take into account systematic errors. We believe however that systematic mass errors in this channel are small. This is discussed in detail by Coyne et al.[16]

In conclusion we can state that we see some evidence for splitting in the A_2^+ mass spectrum for the t' range 0.1-2.0 GeV^2 when the Δ^{++} signal is removed. The dipole fit is favored over a single Breit-Wigner with confidence levels of 53% and 11% respectively. The single Breit-Wigner hypothesis cannot however be ruled out by our data.

Acknowledgments.—We gratefully acknowledge the help of the 72-inch bubble chamber crew under R. Watt and the Bevatron crew under W. Hartsough. We acknowledge the valuable support given by our scanning and programming staff, especially E. R. Burns and H. White and the FSD staff.

Table I. A_2^+ decay branching ratios.

Channel	Number of events observed	Number corrected for unseen decays[a]	Cross section μb	Branching fraction
$\rho\pi$	388±64	776±128	166±27	0.78±0.05
$\eta\pi$	34±8	149±34	32±7	0.15±0.04
$K\bar{K}$	17±8	55±25	13±6	0.06±0.03
$\eta'\pi$	2±2	6±6	< 4[b]	< 0.02[b]
A_2^+ total			212±29	

a. See Refs. 8-13.

b. This figure represents an upper limit at the two standard deviation level.

Table II. Fits to the three pion mass spectrum in 10 MeV bins for $t' = 0.1\text{-}2.0\ \text{GeV}^2$.

	Mass MeV	Γ MeV	χ^2/d.f. 1220-1380 MeV	C.L. 1220-1380 MeV
Dipole	1311.6±2.6	33.5±4.0	9.0/10	53%
Breit-Wigner	1304.0±4.5	111.4±18.0	15.7/10	11%

REFERENCES

1. G. Chikovani et al., Phys. Letters 25B, 44 (1967); H. Benz et al., Phys. Letters 28B, 233 (1968). For recent reviews of the experimental situation see A. Barbaro-Galtieri in Experimental Meson Spectroscopy, ed. C. Baltay and A. H. Rosenfeld (Columbia University Press, New York, 1970) and A. Astier, Proceedings of the XVth International Conference on High-Energy Physics, Kiev, USSR (1970), to be published.
2. K. Böckmann et al., Nuclear Physics B16, 221 (1970).
3. M. Alston-Garnjost et al., Phys. Letters 33B, 607 (1970).
4. M. Basile et al., Lettere al Nuovo Cimento 4, 838 (1970).
5. G. Goldhaber et al., Phys. Rev. Letters 23, 1351 (1969).
6. G. S. Abrams et al., Phys. Rev. Letters 25, 617 (1970).
7. M. Alston-Garnjost et al., Phys. Letters 34B, 156 (1971).
8. For $\pi\rho$ decay: As has been found in other experiments[2,3] the Dalitz plot in the A_2^+ region is consistent with the $\pi^+\pi^+\pi^-$ decay of the A_2^+ being entirely $\rho^o\pi^+$. We therefore multiply the observed number of events by two to allow for the unseen $A_2^+ \rightarrow \rho^+\pi^o \rightarrow \pi^+\pi^o\pi^o$ decays.
9. For $\eta\pi$ decay: To estimate the $\eta\pi^+$ branching ratio we have made the same Δ^{++} antiselection in reaction (2) as was used for reaction (1). We have selected the η events from the remaining events in reaction (2) by a 540-560 MeV cut on $\pi^+\pi^-\pi^o$ effective mass. We estimate that this cut includes as many non-η events as it cuts true η events from the tails of the distribution. A fit to the $\eta\pi^+$ mass spectrum with a phase space curve plus Breit-

Wigner gives an adequate fit and results in the number of events shown in Table I. We have corrected for the unseen η decays using the branching ratios in Ref. 14. For further details see Ref. 13.

10. For $K\bar{K}$ decay: We observe 17±8 events in the $K^+\bar{K}^0$ decay mode of the A_2^+ where the error includes uncertainty in estimating the background level. This when corrected for unseen $\bar{K}^0$ decays gives the total number of events shown in Table I. For further details see Ref. 11.
11. W. R. Butler (Ph.D. Thesis), UCRL-19845 (1970), unpublished.
12. For $\eta'\pi$ decay: We observe a strong η signal in the missing mass distribution for reaction (3) and a clear η' signal in the $\pi^+\pi^-\eta$ mass distribution for those events in this channel which fit the one constraint hypothesis $\pi^+p \rightarrow p\pi^+\pi^+\pi^-\eta$. We do not however see any compelling evidence for the $A_2^+ \rightarrow \eta'\pi^+$ decay, and can only set a rough limit at 2±2 events. The corrections for unseen decays allow for the presence of 75% of the $\pi^0\pi^0\eta$ decay of the η' where η decays to $\pi^+\pi^-\pi^0$, as this fraction of such decays has a $\pi^0\pi^0\pi^0$ mass within our η missing mass limits. For further details see Ref. 13.
13. G. S. Abrams et al., UCRL-20067, Contribution to the XVth International Conference on High-Energy Physics, Kiev, USSR, 1970.
14. Particle Data Group, Phys. Letters 33B, 1 (1970).
15. K. W. J. Barnham and G. Goldhaber, Phys. Rev. Letters (following Letter, UCRL-20293).
16. D. G. Coyne et al., UCRL-20088, submitted to Nuclear Physics B (1971).
17. $d\sigma/dm \sim (M - M_0)^2/[(M - M_0)^2 + (\Gamma/2)^2]^2$.
18. D. G. Coyne, EXTRACT, Lawrence Radiation Laboratory Trilling-Goldhaber Group Physics Note TG-175 (1969), unpublished.
19. The confidence levels in Table II were calculated using the same method

as was employed in Refs. 1 and 4. The fits were made over the entire region 1100-1500 MeV. The χ^2 was then calculated for the region 1220-1380 MeV and the total number of parameters (including one for normalization) subtracted from 16, the number of bins in this region, to obtain the number of degrees of freedom. The question of confidence levels is further discussed in Ref. 15.

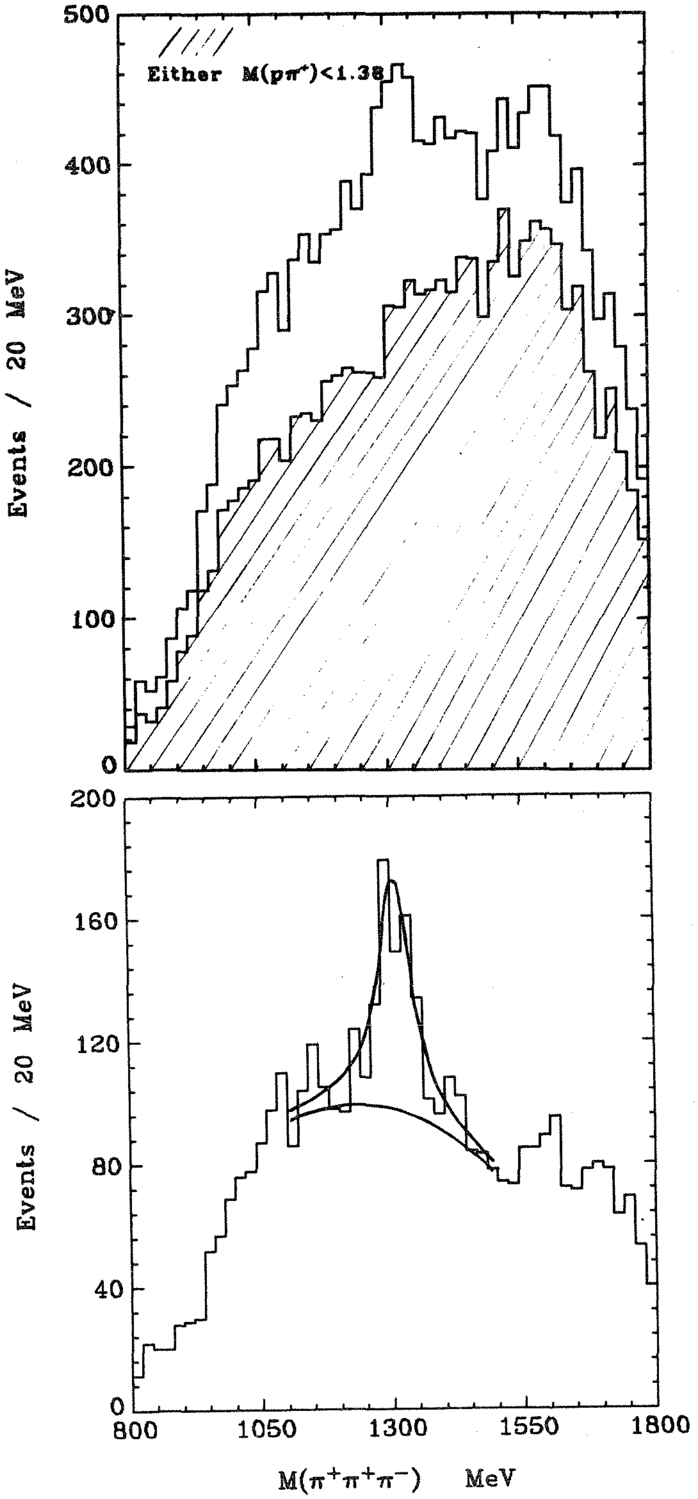

Figure 1: (a) Uncut $\pi^+\pi^+\pi^-$ mass spectrum for the events in reaction (1). The shaded histogram shows the $\pi^+\pi^+\pi^-$ mass spectrum for those events for which at least one π^+p combination has mass < 1380 MeV. (b) The $\pi^+\pi^+\pi^-$ mass spectrum for those events with both π^+p combinations having mass > 1380 MeV (Δ^{++} out). The curve is explained in the text.

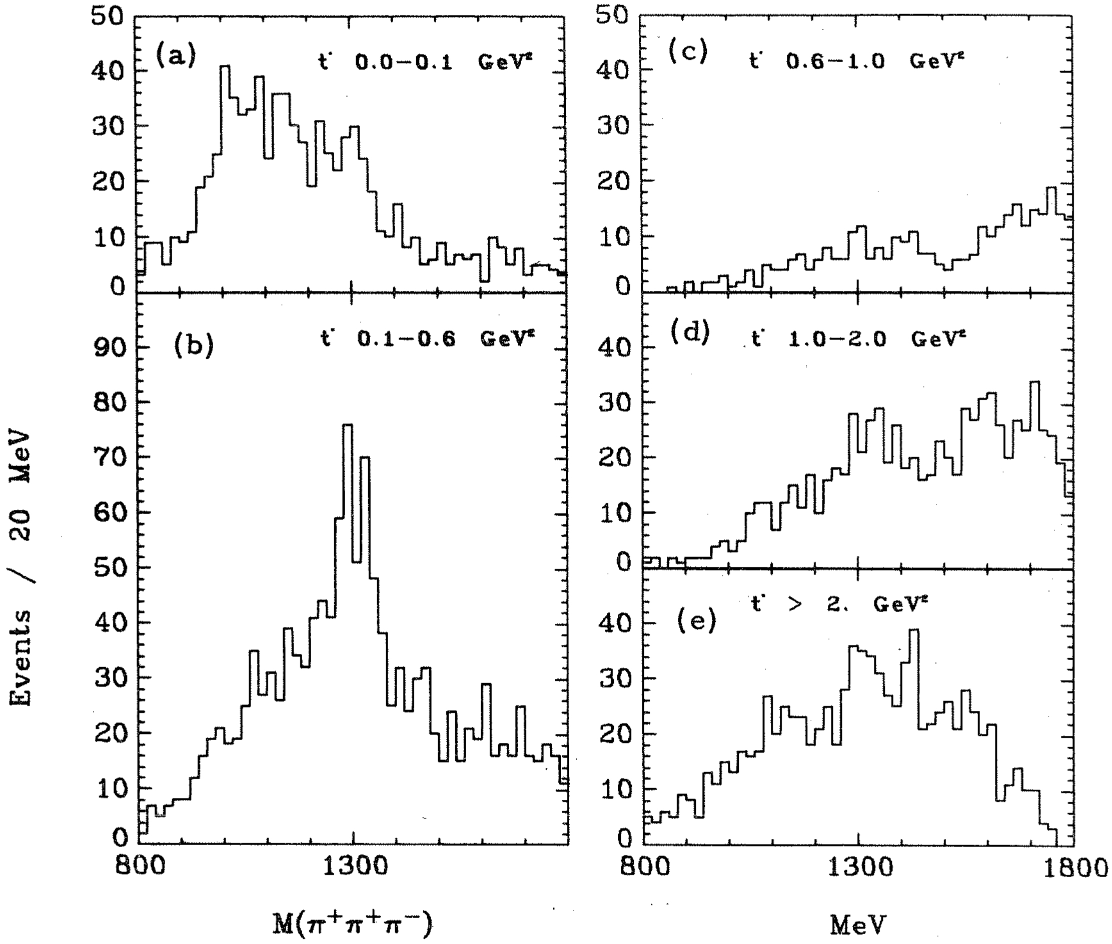

Figure 2: (a–e) The $\pi^+\pi^+\pi^-$ mass spectrum for the events with Δ^{++} out and the cuts on $t' = |t - t_{min}|$ indicated.

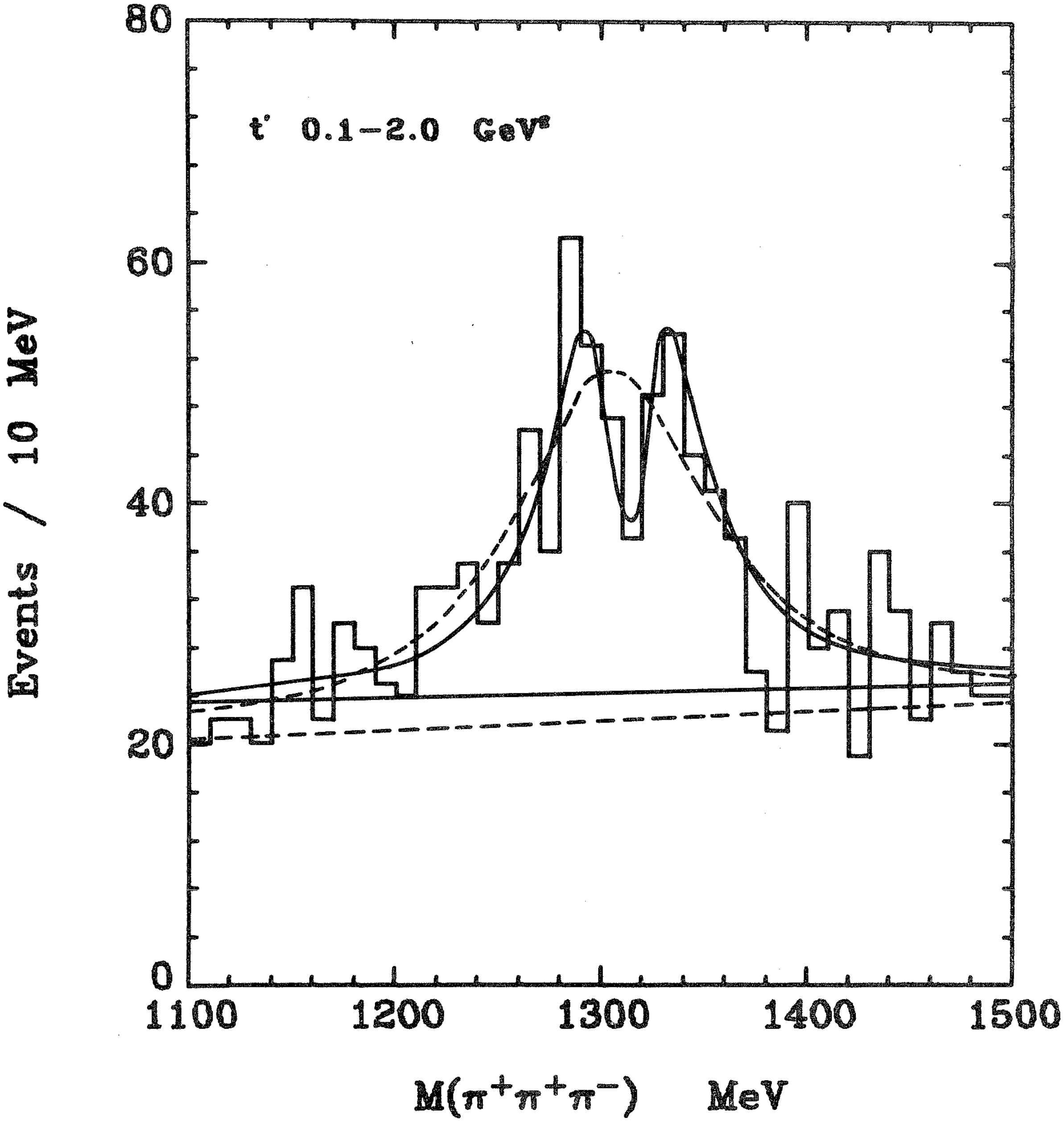

Figure 3: The $\pi^+\pi^+\pi^-$ mass spectrum in 10 MeV bins with Δ^{++} out and t' = 0.1 - 2.0 GeV^2. The parameters of the dipole fit (full curve) and Breit-Wigner fit (broken curve) are given in Table II. The curves connect the best fit points, the fits having been made by folding the theoretical distributions with the experimental resolution function and binning.

Paper B

INTERFERING RESONANCES AND THE A_2 MASS SPECTRUM*

K. W. J. Barnham and G. Goldhaber

Department of Physics and Lawrence Radiation Laboratory
University of California, Berkeley, California 94720

Alston-Garnjost et al.[1] have recently presented an unsplit A_2^+ spectrum in a high statistics π^+p bubble chamber experiment at 7 GeV/c. They find an acceptable fit to a single Breit-Wigner formula. On the other hand they obtain a poor fit with the "dipole" formula[2] which fits the split A_2^- originally observed by the CERN Missing Mass Spectrometer[3] experiment and confirmed by the CERN Boson Spectrometer experiment.[4,5]

In the present Letter we expand the point we made at the Kiev Conference[6] and show that if we abandon the simple dipole formula and consider two interfering resonances, a variation on the alternative solutions considered by

---

*Work supported by the U. S. Atomic Energy Commission.

the CBS group, the A_2^- and A_2^+ spectra can be reconciled. That is, both mass spectra can be fitted with the same mass and width parameters for the two interfering resonances with only small changes in other parameters discussed below. We also find that the model gives a good fit to the split A_2^0 observed by the Bologna-CERN neutron missing mass spectrometer,[7] and to the A_2^+ spectrum at 3.7 GeV/c reported in the preceding Letter.[8]

It is well known that the mass spectrum due to two interfering resonances with the same values of J^P and with arbitrary relative phase (φ) and amplitude (f) can take on a variety of shapes.[9] We have noted here however that under certain conditions the existence of a dip in the mass spectrum can be sensitively dependent on small variations in φ and f. We have not attempted to investigate the detailed dynamics of the interference.[10-12] Our aim has been for the simplest possible phenomenological parametrization and we find the data available at present requires nothing more complex.

For our analysis we have concentrated on the 3π or missing mass spectra with the highest statistics to date. We have not attempted to fit the $K\bar{K}$ and $\eta\pi$ decay channels both for reasons of statistics and because such an analysis could be complicated by the possible variations in shape with decay mode.[12] We have taken the sum of the negative missing mass spectra of the CERN MMS and CBS experiments (hereafter referred to as CBS or subscript C) from Fig. 5 of Ref. 4 plotted in 10-MeV bins, the A_2^+ spectrum of Alston-Garnjost et al.[1] also plotted in 10-MeV bins (referred to as LRL-A or subscript A), the A_2^0 mass spectrum[7] of the Bologna-CERN neutron missing mass spectrometer (referred to as BC) and the A_2^+ spectrum in the preceding Letter[8] (referred to as LRL-TG).

The parametrization we use is that of two resonance amplitudes B_λ with masses M_λ and widths Γ_λ

$$B_\lambda(M) = \frac{\sqrt{\Gamma_\lambda/2\pi}}{M_\lambda - M - i\Gamma_\lambda/2} \quad . \tag{1}$$

The amplitudes are assumed to be completely coherent and differ in relative phase by φ. The mass spectrum is then given by

$$\frac{dN}{dM} = \alpha|fB_1(M) + e^{i\varphi}B_2(M)|^2 \tag{2}$$

where α is a normalization constant and f a real number. We consider the two possibilities first tried by the CBS group. (a) The asymmetric case when the two resonances ($\lambda = 1, 2$) are wide (W) and narrow (N) resonances with widths Γ_W and Γ_N and approximately degenerate masses ($M_W \approx M_N$). This case is similar to the ω-ρ interference effect. (b) The symmetric case where the two resonances ($\lambda = 1, 2$) are lower mass M_L and higher mass M_H resonances with approximately equal widths ($\Gamma_L \approx \Gamma_H$).

The Breit-Wigner amplitudes have been normalized so that

$$\int_{-\infty}^{\infty} |B_\lambda(M)|^2 dM = 1 \quad . \tag{3}$$

If the total intensity of each resonance is I_1 and I_2 respectively then

$$f^2 = I_1/I_2 \quad . \tag{4}$$

A background contribution[13] consisting of a first-order polynomial in mass for all data except BC (for which a quadratic term was also needed) was added incoherently to the signal given by Eq. (1). The theoretical curves were folded with a resolution function[14] and binned, and fitted to the data using the χ^2 minimization program EXTRACT.[15]

We have introduced an additional parameter δ to allow for differences in absolute mass calibration between various experiments. This parameter was defined to be zero for the CBS data and positive when structure appears at a higher mass than the corresponding structure in the CBS data. Ideally the values of δ obtained should be comparable with the combined mass calibration errors of the two experiments being compared.

We reported at Kiev[6] that the CBS asymmetric case parameters (M_W = 1298 MeV, Γ_W = 90 MeV, M_N = 1297 MeV, Γ_N = 12 MeV, with $\delta_A = 0$) were a good fit to the 7 GeV/c A_2^+ mass spectrum, as reported by Barbaro-Galtieri[5] when a variation in φ was allowed. This has since been noted by Alston-Garnjost et al.[1] as well. As an example of the various shapes which result from the interference we show in Fig. 1 the mass spectrum obtained from the above parameters, with $f = 4.5$ (i.e., the narrow resonance has ~ 5% the intensity of the wide one), for various values of φ. The full line represents the theoretical curve, the broken line indicates what would be observed with an experimental resolution of $\Gamma_R/2 = 7$ MeV, where Γ_R is the FWHM of the resolution function.

Of the available data the largest variation in shape occurs between the CBS and LRL-A mass spectra. We have carried out a systematic search for parameters which would reconcile both these mass spectra. Our procedure was to determine M_1, M_2, Γ_1, and Γ_2 from the CBS data and then to fit the LRL-A data with these same parameters, allowing however for different phases φ_C and φ_A, amplitudes f_C and f_A and the possibility of a different absolute mass calibration δ_A. More specifically for the symmetric case we stepped in $\Delta M = M_H - M_L$, the spacing of the symmetric peaks, fixing $f_C = 1.0$ and varying M_L, Γ_L, Γ_H, and φ_C to fit the CBS data. For the search in the asymmetric case we stepped in Γ_W, fixing $\varphi_C = \pi$ (completely destructive interference at the peaks of the two approximately degenerate resonances) varying M_W, M_N, Γ_N, f_C and α_C to fit the CBS data. With each set of mass and width parameters obtained from the CBS data we attempted to fit the LRL-A data by varying $f_A \varphi_A \alpha_A$ and δ_A. The principal results are shown schematically in Figs. 2a and 2b.

It can be seen from Figs. 2a and 2b that the LRL-A data favors the asymmetric solution, the CBS data agrees well with either solution with a slight preference for the symmetric one. However both χ^2 curves[16] are sufficiently flat that satisfactory fits are possible over a wide range of mass and width parameters. It is also important to notice that for these satisfactory fits the difference in φ_C and φ_A is less than, and in some cases considerably less than, 0.6 radians. Also f_C and f_A do not have markedly different values.

The region of the asymmetric fits for which $\Gamma_W \lesssim 50$ MeV and the region of symmetric fits for $\Delta M \lesssim 10$ MeV, though good fits, are rather unsatisfactory when considered on the interfering resonance interpretation. In both cases two large Breit-Wigner amplitudes are interfering destructively, leaving only a relatively small total intensity. In such situations large changes in A_2 cross section occur for small changes in φ and f. There is currently no evidence for such large variations. Since few of the experiments we are comparing give cross sections we have not attempted any such constraints on our fits.

In view of the shallowness of the χ^2_C and χ^2_A curves in Figs. 2a and 2b we have not attempted an overall best fit to the presently available data. Furthermore the results presented in Figs. 2a and 2b do not completely exhaust the combinations of masses and widths which give acceptable fits to both sets of data but rather indicate the range of possibilities. In Tables I and II we give two representative fits, one each from the asymmetric and symmetric cases and show how well these two sets fit the other data. The corresponding curves are shown on Figs. 3a-d, for the asymmetric case. The curves for the symmetric fits are very similar.

It should be noted that for the asymmetric fits in Table I we have kept f constant at $f = f_C$ while in Fig. 2b f_A was allowed to vary. The fit to the LRL-A data turns out to be similar in Table I and Fig. 2b. The confidence levels[16] for all three experiments in Table I are very good. For comparison, we also show the confidence levels we obtain with the "most favored" hypothesis of the respective authors. For the LRL-TG and BC data the confidence levels are comparable to those obtained with a dipole fit. For the LRL-A data the confidence level is rather better than for a Breit-Wigner fit. A very important feature is the closeness of the values of φ to each other and to the CBS value of π.

For the symmetric fits in Table II we first tried keeping f fixed at $f = f_C = 1.0$ but found that the confidence level for the LRL-A data was unacceptable ($\ll 1\%$). In making the fits shown in Table II we therefore allowed f to vary. Good fits were obtained to the LRL-TG and BC data. The fit to the LRL-A spectrum has a confidence level comparable to that of a Breit-Wigner, which is acceptable, but not as good as in the asymmetric situation. As in the representative asymmetric fits the values of φ do not vary much from fit to fit.

Consideration must be given to whether the values of the mass shift δ we have obtained are reasonable. If, for example, we ascribe a systematic error on the absolute mass of 5 MeV to each experiment then we find the confidence level for the agreement of the three values of δ in Table I or II and the $\delta = 0$ for the CBS data is 15%. It should also be pointed out that δ can be traded off against φ. Namely, if δ_A is reduced φ_A moves further away from φ_C.

In conclusion we would like to state that we have found a range of mass and width parameters for interfering resonances over which satisfactory fits to both the CBS and LRL-A data are possible. In particular we would like to emphasize the small changes of φ and f necessary to reconcile these apparently conflicting mass spectra, provided not unreasonable shifts in absolute mass calibration are permitted. From the range of possible fits we have selected one set each of asymmetric and symmetric case mass and width parameters. The asymmetric case parameters fit the LRL-A, LRL-TG and BC data with the same f as for CBS and with only small changes in φ. For the LRL-A fits the confidence level is rather better than for a Breit-Wigner fit. For the LRL-TG and BC data the confidence levels are comparable with those for dipole fits. The representative symmetric mass and width parameters are not so satisfying as changes in f as well as φ are necessary to fit the LRL-A data and even then the confidence level is hardly increased over that for a Breit-Wigner.

Finally, it should be stressed that in our simplified treatment we have ignored variations in the degree of coherence between the two resonances and have considered data which involve wide t intervals over which both coherence and phase can change. To resolve the basic ambiguity between the symmetric and asymmetric situations, and before meaningful determinations of the best interfering resonance parameters are possible much more detailed experimental data will be needed.

While this work was in progress results of two new experiments on the $K\bar{K}$ decay mode at 17 GeV/c and 20 GeV/c have been reported.[17] Neither of these mass spectra show any evidence for splitting. Since these momenta are very much higher than those of the experiments we have been discussing, the lack of structure could be due to a number of different causes. For example, in the asymmetric case the relative intensity of the narrower resonance could be much reduced, or the degree of coherence between the wide and narrow resonances could be much smaller to the extent that we may be dealing effectively with the incoherent resonances. Preliminary studies suggest that either of these possibilities give reasonable fits; we have however not attempted an exhaustive search.

ACKNOWLEDGMENTS

We have benefitted by discussions with our colleagues Drs. G. S. Abrams, A. Barbaro-Galtieri, D. G. Coyne, G. Lynch, J. MacNaughton, M. Rabin, and G. H. Trilling.

POSTSCRIPT

Immediately after this work was presented at this Conference the results of the Northeastern University-Stony Brook missing mass spectrometer experiments at Brookhaven were announced. Under apparently identical conditions to the CERN MMS experiment and with superior statistics they see no evidence at all for structure. Clearly our model cannot account for differences in experiments performed under identical conditions. It appears to us that there are two possible situations which must hold for the A_2 problem.

(1) If the CERN MMS experiment and the NU-SUNY experiment indeed represent identical experiments, the interpretation of one of these experiments must be wrong. Extensive arguments have been presented at the 1971 Washington Meeting as to which of the experiments might be wrong, and we do not feel that this point is fully decided as yet.

(2) An alternative possibility is that the two experiments were not completely identical and hence do not necessarily contradict each other. One example which occurs to us would be the interference between two resonances with different spin parity. If this were the case, the NU-SUNY experiment, which has integrated over all decay angles, would not show an interference effect. On the other hand, the CERN MMS experiment by selecting on one or three decay particles of the A_2 possibly biased the A_2 decay distribution, and hence could in principle show interference effects between a broad $J^P = 2^+$ A_2 and a narrow resonance with a different spin parity value occurring at a low intensity level. It is interesting in this respect that we observe no evidence for structure in our A_2^+ mass spectrum at 3.7 GeV/c until the Δ^{++} events are removed. This cut is well known to bias the A_2^+ decay angular distribution. We do not however have sufficient statistics to investigate this point further.

Finally, we must note that the NU-SUNY experiment only contradicts the CERN MMS experiment. The CBS experiment was an independent one carried out under very different conditions, in that it was near threshold for A_2 production.

FOOTNOTES AND REFERENCES

1. M. Alston-Garnjost et al., Phys. Letters 33B, 607 (1970).
2. $dn/dm \sim (M - M_o)^2/[(M - M_o)^2 + \frac{1}{4}\Gamma^2]^2$.
3. G. Chikovani et al., Phys. Letters 25B, 44 (1967).
4. H. Benz et al., Phys. Letters 28B, 233 (1968).
5. For a review of the experimental evidence on the A_2 splitting see Ref. 6 and the talk by A. Barbaro-Galtieri in Experimental Meson Spectroscopy, ed. by C. Baltay and A. H. Rosenfeld (Columbia University Press, New York, 1970).
6. Reported in the review of meson resonances by A. Astier, Proceedings of the XVth International Conference on High-Energy Physics, Kiev, U.S.S.R. (1970), to be published.
7. M. Basile et al., Lettere al Nuovo Cimento 4, 838 (1970).
8. K. W. J. Barnham et al., Phys. Rev. Letters (preceding Letter, UCRL-20292).
9. G. Goldhaber, Phys. Rev. Letters 19, 976 (1967).
10. A possible approach to such an analysis has been outlined by D. G. Sutherland, Experimental Meson Spectroscopy, op. cit. See also Refs. 11 and 12.
11. C.-F. Chan, UCRL-20051, submitted to Phys. Rev. (1970).
12. C. Rebbi and R. Slansky, Phys. Rev. 185, 1838 (1969). We appreciate that the shapes we obtain from our model are similar to those which these authors obtain using the constraints of unitarity for a formation experiment.
13. The symmetric case fits to the CBS data were made with the background fixed at the level indicated in Fig. 4c of Ref. 4. In the asymmetric case we had to allow the background level to vary. We understand that the background levels we obtained are not unreasonable. We thank Drs. M. N. Kienzle-Focacci and P. Schübelin for private communications on this and other points.

14. For the CBS and BC data we assumed Gaussian resolution functions with $\Gamma_R/2 = 6$ MeV and 7.5 MeV respectively (Γ_R = FWHM of the resolution function) as quoted by the authors. For the LRL-A (G. R. Lynch, private communication) and the LRL-TG data we used the experimental resolution functions with $\Gamma_R/2 = 6.7$ MeV and 7 MeV respectively.

15. D. G. Coyne, EXTRACT, Lawrence Radiation Laboratory Trilling-Goldhaber Group Physics Note TG-175 (1969), unpublished.

16. We have estimated confidence levels with the method used on the CBS data and in Ref. 7 but not in Ref. 1. This consists in making a fit over the entire range of data available and then calculating the χ^2 for the mass region 1220-1380 MeV. The number of degrees of freedom is then taken to be the number of bins in this region minus the number of parameters used to fit over the entire spectrum. In Ref. 1 another method was used involving wider bins in the background region and they estimate the confidence level for a Breit-Wigner fit at 42%. Since what really matters are the relative confidence levels for various fits we compare the interference model fits with our results for the "favored" fits using the identical method for estimating confidence levels (see Tables I and II, Columns 6 and 8 respectively).

17. G. Grayer et al., Phys. Letters 34B, 333 (1971) and K. J. Foley et al., Phys. Rev. Letters 26, 413 (1971).

Table I. Fits with typical asymmetric parameters:
$M_W(C) = 1299.5$, $\Gamma_W(C) = 78.0$, $M_N(C) = 1298.1$, $\Gamma_N(C) = 9.6$ all in MeV,
$f_C = 2.85^a$ and $\varphi_C = \pi$ radians.

Data	f (fixed)	φ radians	δ^b MeV	χ^2/d.f.	C.L.	Favored fit χ^2/d.f.	Favored fit C.L.
LRL-A	2.85	2.67±0.12	16.5±1.9	10.8/12	55%	20.1/12	7% B.W.
LRL-TG	2.85	2.89±0.15	10.7±3.2	9.2/10	51%	9.0/10	53% dipole
BC	2.85	2.96±0.12	6.9±2.3	16.0/17	52%	10.4/17	89% dipole

a. The narrow resonance thus has 12% intensity of the wide one.

b. δ is the absolute mass shift; e.g., $M_W(A) = M_W(C) + \delta$, etc.

Table II. Fits with typical symmetric parameters:
$M_L(C) = 1291.2$, $\Gamma_L(C) = 26.4$, $M_H(C) = 1306.2$, $\Gamma_H(C) = 24.1$ all in MeV,
$f_C = 1.0$ and $\varphi_C = 4.21$ radians.

Data	f	φ radians	δ^a MeV	χ^2/d.f.	C.L.	Favored fit χ^2/d.f.	Favored fit C.L.
LRL-A	1.15±0.05	4.03±0.10	16.0±2.3	17.6/11	9%	20.1/12	7% B.W.
LRL-TG	1.11±0.03	4.21±0.16	11.7±2.1	9.8/9	37%	9.0/10	53% dipole
BC	1.06±0.01	4.02±0.09	6.6±2.0	9.8/16	88%	10.4/17	89% dipole

a. See footnote b in Table I.

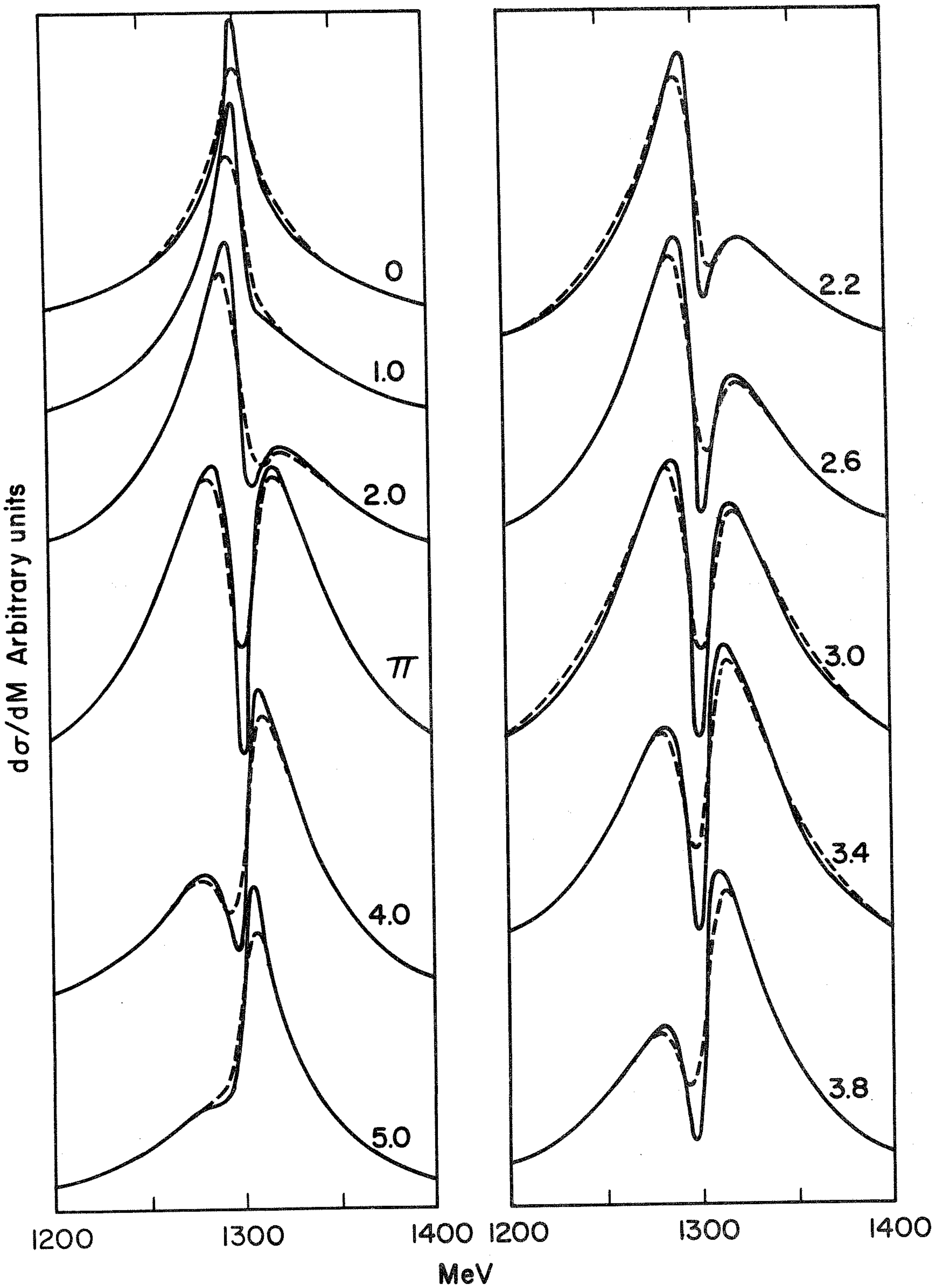

Figure 1: The shape of the mass spectrum for various values of ϕ (the relative phase in radians between the amplitudes of the two resonances) for the asymmetric case. The parameters used are $M_W = M_N = 1300$ MeV, $\Gamma_W = 90$ MeV, $\Gamma_N = 12$ MeV, and $f = 4.5$. The broken line assumes an experimental resolution with $\Gamma_R/2 = 7$ MeV.

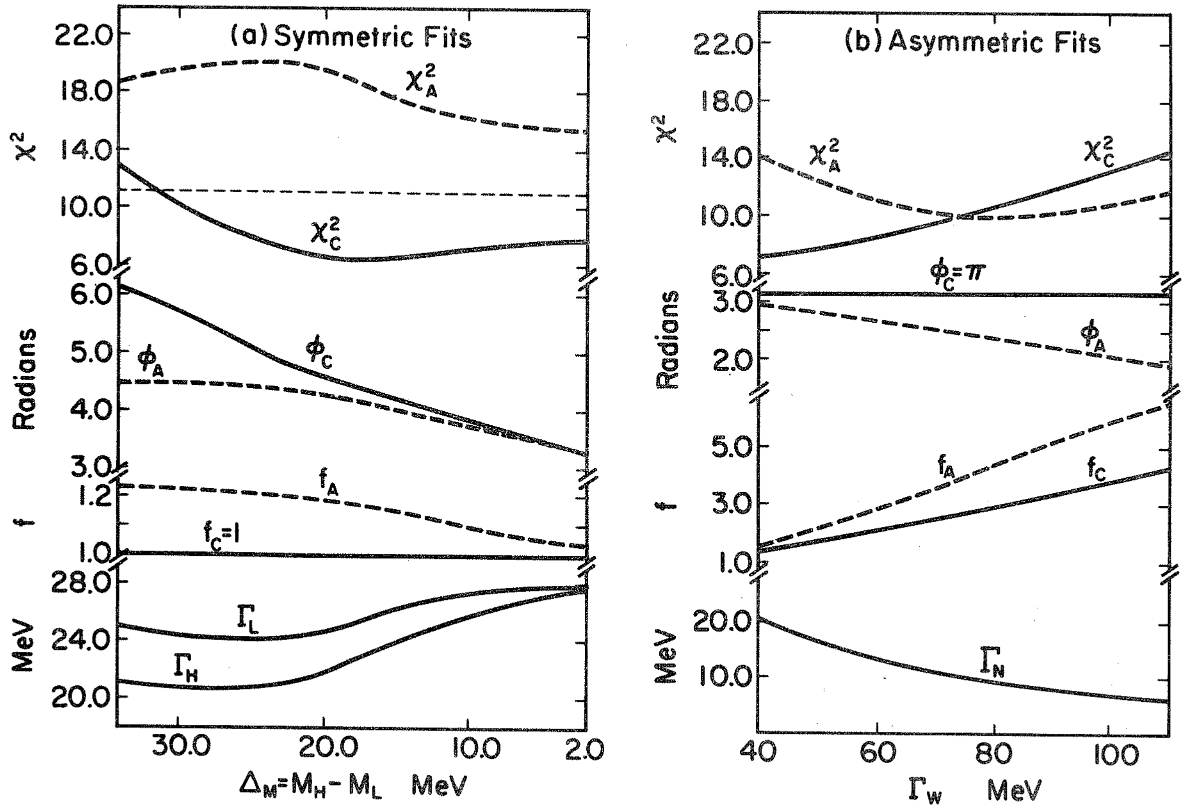

Figure 2: (a) Parameters Γ_L, Γ_H, ϕ obtained from a series of fits to CBS data stepping in $\Delta M = M_H - M_L$, the distance between the peak masses of the symmetric case resonances, with f_C fixed at 1.0. For all these fits $(M_L + M_H)/2 \approx 1299$ MeV. Also shown are the parameters f_A and ϕ_A which were varied along with δ_A and α_A in order to fit the LRL-A_2 data with each set of CBS mass and width parameters. The χ^2 for the fits (both 11 degrees freedom) are also shown. (b) Similar to (a) but for the asymmetric situation. In this case Γ_W was stepped and ϕ_C was fixed at π. For these fits M_W and M_H were within the range 1297 - 1301 MeV. χ_A^2 is for 11, χ_C^2 for 10 degrees of freedom.[13] In all the fits used to obtain both the figures δ_A had values similar to those given in Tables I and II.

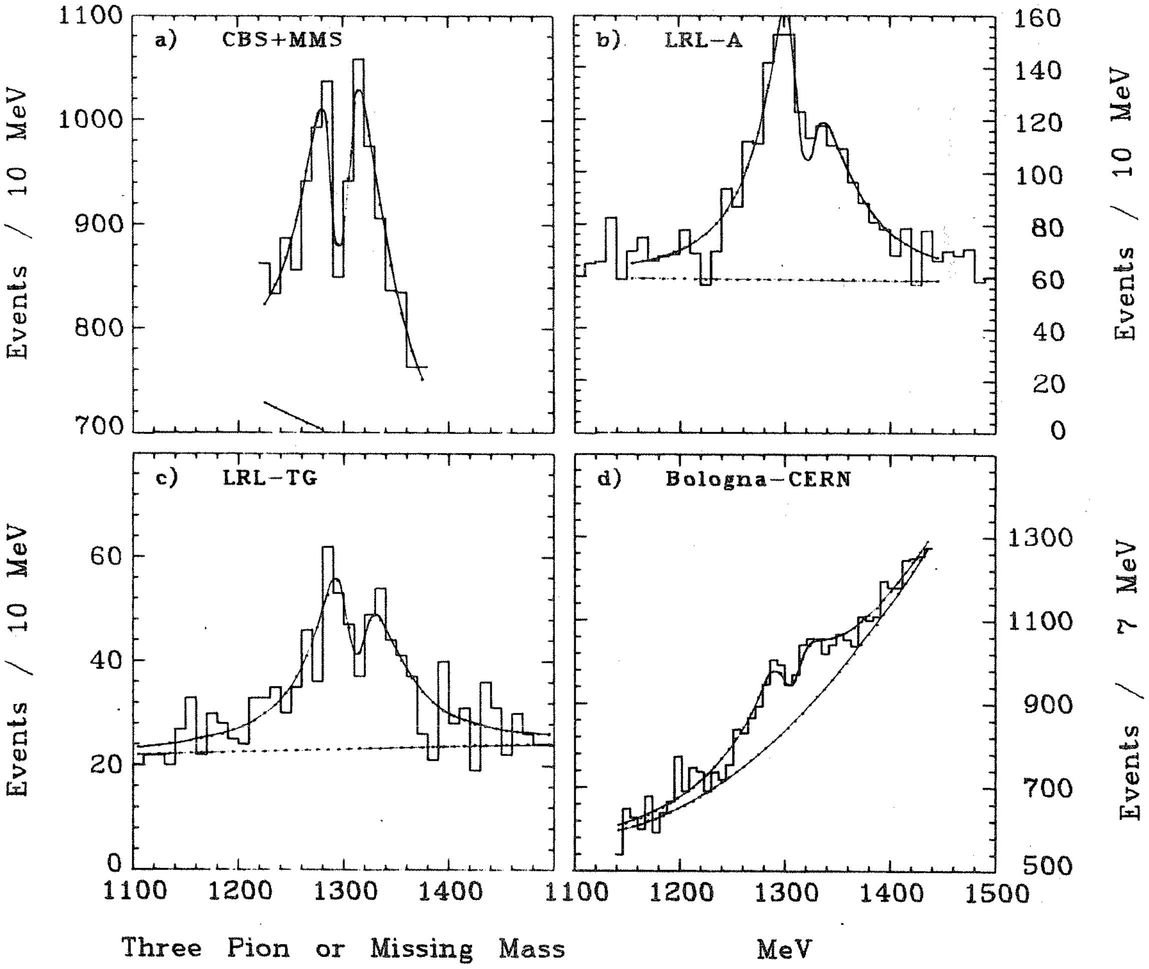

Figure 3: (a-d) Missing mass and three pion mass spectra in the A_2 region from Refs. 4, 1, 8, and 7. The curves correspond to the fits made with typical asymmetric parameters. Details of the fits are given in Table I. The background curves[13] are also shown (only partially in Fig. 3a). The ordinates on Fig. 3d are events/7 MeV.

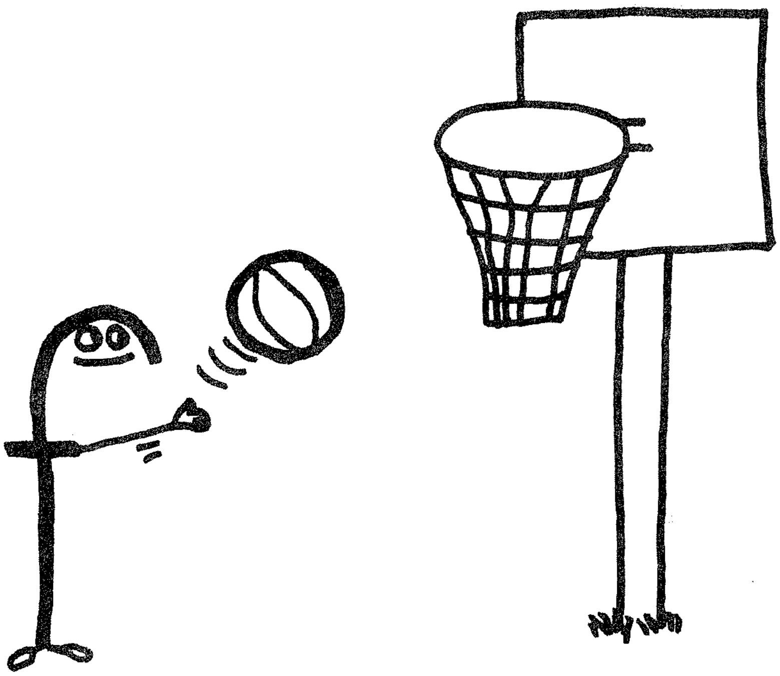

THE f^0 MASS SPECTRUM IN 7 GeV/c π^+p INTERACTIONS*

S.M. Flatté

Lawrence Radiation Laboratory
University of California
Berkeley, California 94720

---

*This work was performed under the auspices of the U.S. Atomic Energy Commission.

I want to talk very briefly about an experiment which has been carried out by people at LRL (Group A) on $\pi^+p \rightarrow \pi^+p\pi^+\pi^-$ at 7 GeV/c. We have 70,000 events of this reaction. Selection of the Δ^{++} reduces the number to 40,000 events. The experiment uses the same data as our analysis of the A_2 mass spectrum, so I don't have to discuss the resolution question here. Figure 1 shows the mass spectrum of $\pi^+\pi^-$ recoiling from a Δ^{++}. We want to look at the f^0. Why? Well, one must keep looking! Obviously, more searches for fine structure will always be in order. The spectrum here is in 50 MeV bins. We have about 5000 f^0 events. Figure 2a shows the spectrum in 5 MeV bins. Our resolution is 7.8 MeV half width at half maximum in the f^0 peak region. We see no narrow structure: A Breit-Wigner form fits quite well. The spectra for different t selections are shown in Fig. 2b-d. Again no structure. We have looked at all the moments up to $\ell = 4$ and $M = 4$. A few are shown in Fig. 3. The moments that we have examined do not show any significant narrow structure. (Note: These results have been published in Physics Letters 34B, 551 (1971).)

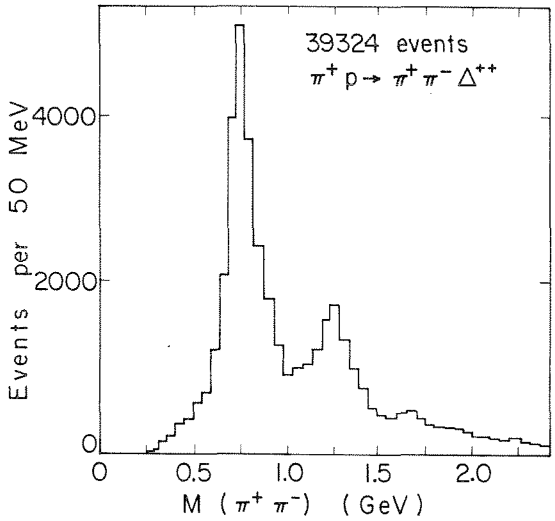

Fig. 1: Histogram of $\pi^+\pi^-$ mass in the reaction $\pi^+p \rightarrow \pi^+p\pi^+\pi^-$ for events in which the other π^+ and the proton form a Δ^{++} ($M(p\pi^+) < 1.4$ GeV).

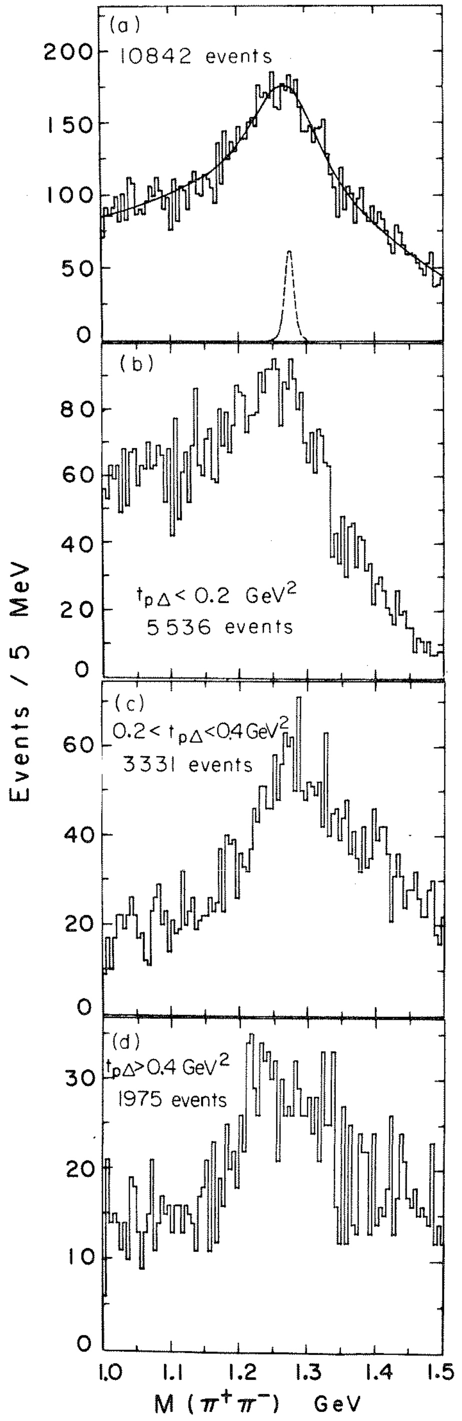

Fig. 2: Mass plots in the f^0 region. A Δ^{++} is always required. The solid curve is a fit with a Breit-Wigner s-wave resonance formula plus a linear background. The dashed curve is our resolution function normalized to 4% of the number of f^0 resonance events found in the fit.

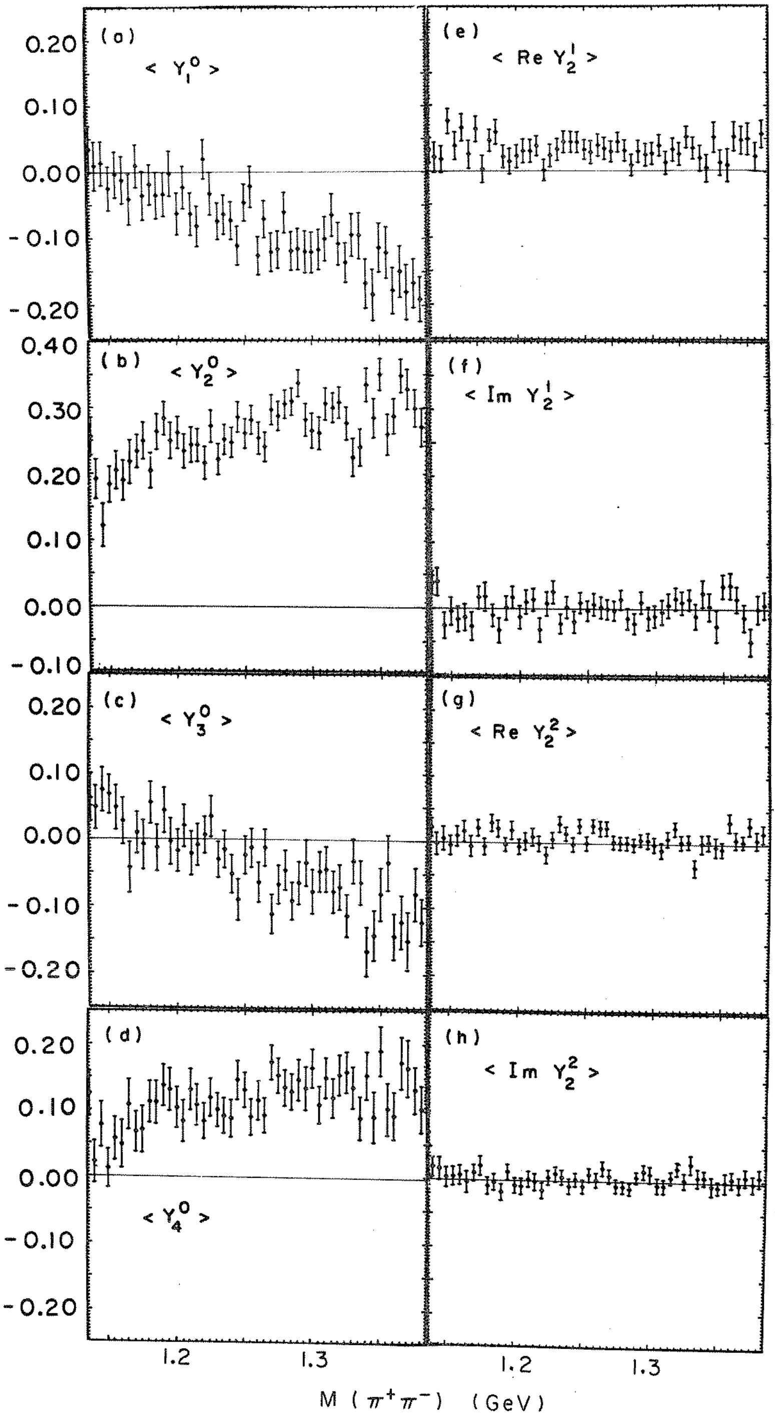

Figure 3: Some moments of the decay angle distribution in the f^0 region as a function of mass. A Δ^{++} is always required. The Z axis is the incoming π^+; the y axis is $p_{in} \times \Delta^{++}$. $\langle \mathrm{Im}\, Y_2^m \rangle$ are examples of parity-violating moments, and are thus expected to be equal to zero.

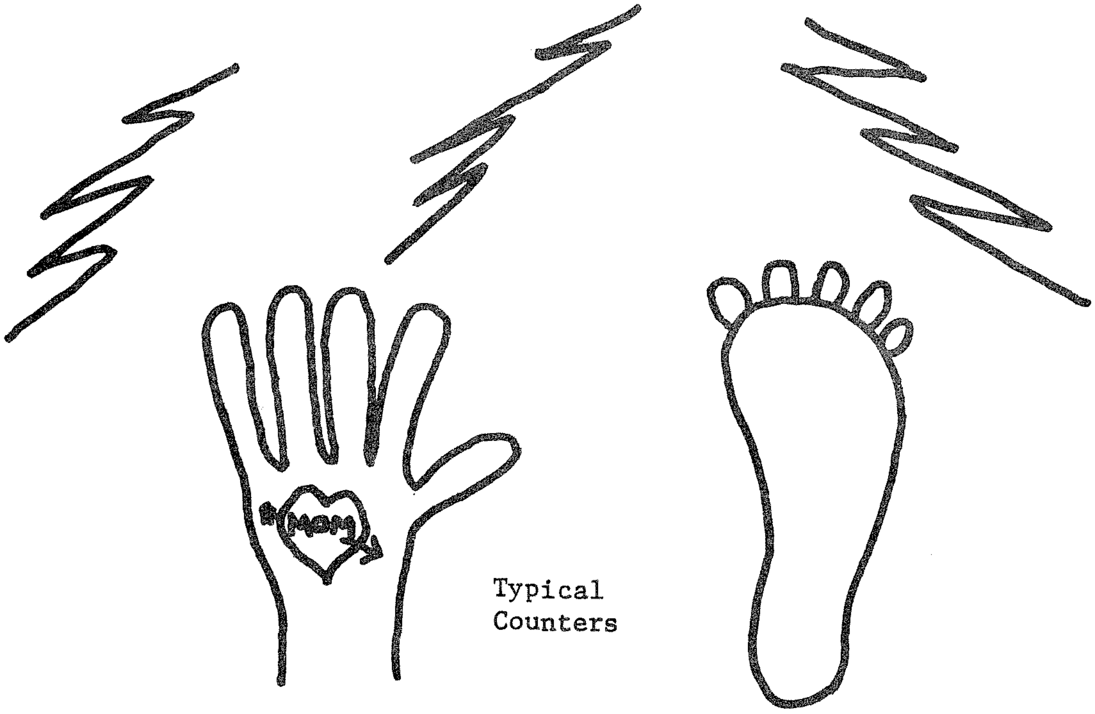

THE DOUBLE VEE MAGNETIC SPECTROMETER: EXPERIMENTAL SETUP AND CURRENT RESULTS*

S. Ozaki
Brookhaven National Laboratory
Upton, New York 11973

This afternoon I will talk about some of the experiments we have done at the Brookhaven AGS using the Double Vee Spectrometer. These experiments covered various reactions, and were, so to speak, survey experiments to see the performance of the spectrometer. Among the reactions we studied, I have chosen the following two for this talk on which we made a major effort:

$$\pi^- p \to K^0 + \Lambda,\ \Sigma^0,\ Y^{*0}$$
$$\qquad \lfloor\!\!\rightarrow \pi^+ + \pi^-$$

at 8.0 and

---

*This work was performed under the auspices of the U.S. Atomic Energy Commission.

$$\begin{array}{l} \pi^- + p \to A_2^- + p \\ \qquad\;\; \hookrightarrow K^- + K^0 \\ \qquad\qquad\quad\;\; \hookrightarrow \pi^+ + \pi^- \end{array}$$

at 20.3 GeV/c. In particular, a study of the second reaction is quite timely in view of the presently existing experimental controversy on the A_2 splitting.[1,2] From this experiment, we gave an answer to the question, "is the A_2 split?".[3] We completed this series of runs last January.

My colleagues who engaged in these experiments are Kenneth Foley, William Love, Edward Platner, Alfred Saulys, and Erich Willen from Brookhaven National Laboratory, and S. J. Lindenbaum from Brookhaven National Laboratory and the City College of the City University of New York. The experiment was done using the 0° secondary beam of the slow extracted proton beam at the AGS.

Figure 1 shows the experimental setup. The Double Vee Magnetic Spectrometer is preceded by an incident beam spectrometer, the downstream end of which (CT3 in the figure) is shown in the figure. This spectrometer consists of three 18D72 magnets and three sets of high resolution x-y scintillation counter hodoscopes. This measures the angle and the momentum of an individual incident particle to ~ .3 mrad base to base and ≤ .2% respectively up to 24 GeV/c. This spectrometer also includes three threshold Cerenkov counters, two which detect pions and one which detects pions and kaons. These are used in various combinations of "yesses" and "no's" to identify and tag whether the incoming particle for an event is a pion, kaon, or proton so that the reactions from these three incident particles, whenever feasible, can be studied simultaneously.

The target cell is four inches in diameter, 24 inches long, and can be filled either with liquid hydrogen or with liquid deuterium.

The forward leg of the Double Vee Spectrometer consists of 17 spark chambers upstream of the magnet in three modules. There are seven spark chamber gaps which measure the x coordinate, seven gaps which measure the y coordinate, and three gaps which measure 45° from them to resolve the ambiguity from multiple tracks. There are 14 spark chambers downstream of the magnet, six x, six y measuring chambers, and two 45° chambers. The magnet aperture is 48 inches wide by 18-1/2" high and has approximately 24 kg-meters of the field integral. With a detailed mapping of the field, we know the field integral along the particle path to better than .1%. The effective area of the chambers in the forward spectrometer ranges from 1 foot high by 3 feet wide for the first chamber to 4 feet high and 13 feet wide for the last chamber. The recoil spectrometer consists of ten spark chambers in front of a magnet which has an aperture 120 inches wide by 36 inches high by 36 inches deep with a 12.2 kgm field integral and five chambers behind it. The size of the first chamber is 5 feet high by 6 feet wide. The second is 6 feet high by 7 feet wide, and the last is 4 feet high by 13 feet wide. Both forward and recoil legs of the spectrometer are working, and we have some data. However, the data I will discuss here come from the forward spectrometer alone.

All of these chambers are wire spark chambers wound with 0.005 inch diameter aluminum wire, running parallel to form a transmission line, and with magnetostrictive readout. The special characteristics of these chambers are that they have a high spatial resolution, subtend a low mass to minimize the multiple scattering, and have a high multiple spark efficiency.

Two scintillation counter hodoscopes behind the forward spark chamber system provide a basic trigger. In addition to these, we used various configurations of trigger counter arrangements depending upon the process to be investigated. For example, to trigger on the production of K^o or Λ particles in the forward direction, we demanded that there be no count from a counter located immediately downstream of the target, a "yes" from a counter placed behind the first spark chamber module in the forward leg, and two or more coincidences registered in the last two hodoscopes. Typical trigger rate was 1 per 20,000. For triggering on $K\bar{K}$ decay of the A_2, the requirement was that the counter immediately downstream of the hydrogen target registered, via pulse height selection, no more than one charged particle, three counters in a 35 element scintillation counter hodoscope (H6) placed at 100 inches downstream from the target had the counts, and three coincidences were registered in the last two hodoscopes. A typical trigger rate in this case was 1 per 5×10^3. On-line monitoring of the experiment was done by the PDP-10 computer of the Brookhaven On-Line Data Facility. The analysis of the data was done by the CDC 6600 computer at Brookhaven. Figure 2 is a picture of the Double Vee Spectrometer as it is set up at the AGS experimental area. In the foreground the downstream end of the beam spectrometer can be seen.

The spatial resolution of these spark chambers, as measured by the scatter of the spark coordinates from a fit line segment, is 150-200 microns.

The angular resolution of the system , measured by comparison of two line segments, which are defined by the front and back section of the forward leg using a straight through beam, ranges from .25 mrad at 20 GeV/c to .35 mrad at 6 GeV/c. Below 6 GeV/c the multiple scattering starts to dominate and rapidly increases to .7 mrad at 2 GeV/c. These figures are consistent with the calculation based upon the multiple scattering and the spark chamber spatial resolution. This excellent angular resolution will play an important role in our A_2 experiment, since the accuracy in the opening angle measurement dominates the effective mass resolution of the $K\overline{K}$ system.

The combined resolution of the beam spectrometer and the forward spectrometer is .4-.45% between 4 and 15 GeV/c and increases up to .7% for 2 GeV/c and for 20 GeV/c. This increase is due to the increase in the multiple scattering of the beam momentum resolution which dominates at the low beam momentum and a decrease in the bending angle in the forward spectrometer magnet at higher momentum. This momentum resolution reflects to a major part on the missing recoil mass **resolution.**

In the $K^o\Lambda$ or $K^o\Sigma^o$ production experiment the data were analyzed with a requirement that K^o be a two-pronged vertex originating downstream of the "veto counter", but upstream of the first spark chamber module. The prongs, which were assumed to be pions and have opposite charges, go through a fiducial window at the magnet and reach the last hodoscope. It is also required that the effective mass of the π^+ and π^- from the vertex be in a region of 485-510 MeV. Figure 3 shows the distribution of this $\pi\pi$ effective mass at 8.0 GeV/c which shows clearly a K^o mass peak with very little background. The effective mass resolution here is 1.9 MeV (rms). The resolution increases to ~ 2.6 MeV at 15.7 GeV/c.

Figure 4 shows the missing mass distribution for $\pi^-+p \rightarrow K^o + MM$ at 8 GeV/c incident pion momentum. As can be seen clearly, Λ^o and Σ^o are separated. There is a first clear bump at about 1400 MeV which could be assigned to $\Sigma(1385)$ and $\Lambda(1405)$ unseparated, and the second bump at about 1500 MeV which could be assigned to $\Lambda(1520)$. The thing to note here is that between Σ^o and $\Sigma(1385)$ the missing mass spectrum falls down to 5% of the Σ^o peak, which suggests that the ΛY resonance at 1.32 GeV,[4] which was reported by a Dubna group at the Vienna Conference in 1968, is not seen in our data, or alternately, is at most a few percent of Σ^o production. Figures 5-6 show a missing mass square distribution in finer bins at 8.0 GeV/c. The line drawn on Figure 5 is the maximum likelihood fit to the Λ and Σ^o peak and the line on Figure 6 is the fit to an unresolved peak of $\Sigma(1385)$ and $\Lambda(1405)$, and to the resolved $\Lambda(1520)$ with a linear background. In both fits, the mass resolution in the missing mass square of .05 GeV^2, which corresponds to 25 MeV at 1 GeV mass, is used. From these fits, one can obtain the values of $d\sigma/dt$ versus t. As the analysis is still in the early stages for these processes, I cannot reach a definite conclusion on the t dependence, but the general feature of the data is that the ratio of $K^o\Sigma^o$ production to $K^o\Lambda$ production is about .7 and there is some indication that the slope is different for $K^o\Lambda$ and $K^o\Sigma^o$, the slope of $K^o\Sigma^o$ as expressed by the parameter b in[5] the form $d\sigma/dt \propto ae^{bt}$ being steeper by 1 to 2 $(\mathrm{GeV/c})^{-2}$. We have similar data at 10.7 GeV/c where $K^o\Lambda$ and $K^o\Sigma^o$ processes can still be resolved clearly. These data, together with that at 8 GeV/c, are presently being analyzed.

In our A_2^- experiment we studied the following process:

$$\pi^- + p \rightarrow A_2^- + p$$
$$A_2^- \rightarrow K^- + K^0$$
$$K^0 \rightarrow \pi^+ + \pi^-$$

and we determined the A_2^- mass from the direction and momentum of π^+, π^-, and K^- measured by the forward spectrometer. Therefore, this is not a missing mass experiment but a direct measurement of the effective mass. As we had no Cerenkov counter to identify K^-, we made an additional requirement that the mass of recoil particle be that of a proton in order to discriminate against K^* decaying into K^0 and π^-, thus determining that the forward going particle was indeed a candidate for the A_2^-. Though we have a reasonably large solid angle, our geometry still favors strongly the A_2^- decay with a forward K^0 over a forward K^-.

In detail, the analysis was carried out in the following way. The events of interest are to have the spark chamber tracks which show K^0 and an accompanying particle track with negative charge traced back to a point in a target and intersect the computed K^o trajectory. In this case, the K^o is required to be a two pronged vertex, originating downstream of the counter placed at the target exit, and upstream of the first chamber of the second spark chamber module. The prongs are assumed to be pions and the $\pi\pi$ effective mass is required to be within 485 MeV and 510 MeV. In fact, the $\pi\pi$ effective mass forms a clean peak at the K^o mass with a width of 3.0 MeV (rms) and with a negligible background. The effective mass of the forward going K^o and the negatively charged particle and the missing recoil mass were then calculated assuming that the charged particle was a K^- meson. The recoil mass distribution is shown in Figure 7. There is a clear peak corresponding to recoil protons from the reaction $\pi^- + p \rightarrow (K^- + K^o) + p$. In order to eliminate background from K^*'s, we cut the data requiring that the recoil mass be in the region 0.76 to 1.06 GeV. We estimate that the background with recoil particles other than protons is less than ~ 5%.

We estimate our mass resolution to be ≈ 4.7 MeV (one standard deviation) with 10% uncertainty, at a mass of 1.3 GeV at our incident momentum; the main contributions come from the measurement of the angles of the three particles and multiple scattering of the K^- in the hydrogen target. In this experiment, one of the important questions is whether our estimate of the mass resolution is correct or not. We have two good checks on our calculated resolution; namely, one is the K^o mass which we measured using this system and also during the course of this experiment. The other is that during actual data taking, we have triggered the system also on the incoming K^- beam particle which decays into three charged pions. From this data, we have reconstructed the K^- mass. Thus two good checks are the comparisons of the spread of the reconstructed effective mass with the predicted resolution and the reconstructed mass against the known mass for both K^o and K^-. From the known resolutions of the spectrometer, the mass resolution of the K^o is predicted to be $\approx$ 2.0 MeV (rms) at 8 GeV/c, and the experimental value is 1.9 MeV. The mass resolution of the K^- is predicted to be 4.2 MeV at 20.3 GeV/c and the experimental value is 3.9 MeV. Here, it should be noted that the K^o mass resolution depends mainly on angle measurements, whereas multiple scattering in the target makes a significant contribution to the K^- mass resolution. Our measured values for the K^o and

K^- masses are 497.9 MeV and 493.8 MeV respectively compared to the Table[6] values of 497.8 MeV and 493.8 MeV. Therefore, we estimate our mass scale to be accurate to $\approx$ 1 MeV in the region of the A_2 meson. Thus we feel that the resolution of the system is well understood and is certainly adequate to permit critical examination of the shape of the K^oK^- mass spectrum. In particular, the system is capable of resolving any dip of the type seen in data from the CERN missing mass spectrometers and other low energy measurements.

The K^oK^- mass spectrum in 5 MeV bins is shown in Figure 8. There are 730 events between 1.05 and 1.55 GeV. Our events cover the range of $|t-t_{min}|$ up to 0.7 with $\sim$ 60% of the events with $|t-t_{min}| < 0.2$ $(GeV/c)^2$. As you can see clearly, we do not see the expected dip. We have fitted the data with two separate functions, limiting the fits to the region 1.2 to 1.4 GeV which contains 564 events. A maximum likelihood fit was used. In order to present the data in such a way as to show the statistical significance more clearly, we have not corrected the data for the dependence of the acceptance of the apparatus on the K^oK^- effective mass; rather, we have corrected the shape of the function to be fitted. A Monte Carlo program was used to calculate our acceptance. There we assumed a decay correlation of $\cos^2\theta^* \sin^2\theta^* \sin^2\varphi^*$ in the Gottfried-Jackson frame[7] which is consistent with the decay distribution observed in this experiment. The mass dependence of the acceptance efficiency turned out to be only weakly dependent on the decay parameters used. The acceptance varies from 12.5% at the mass of 1.2 GeV to 6.5% at 1.4 GeV. As can be seen clearly, the background outside the A_2 peak is very small and is not strongly dependent on the K^oK^- mass. The first fit assumes a single Breit-Wigner form[8] which is added to a small flat background leaving the central mass and width of the BW and the height of the background as free parameters. This fit is shown as a solid line in Figure 8 and is clearly a good fit. The χ^2 of this fit is 35.1 for 37 degrees of freedom, a probability of ≈ 55%, with the parameters, $m_o = 1.313 \pm .004$ GeV, $\Gamma_o = .114 \pm .01$ GeV. Although it is not necessary to introduce any structure into the peak in order to fit the data, we have also tried the shape used for the CERN missing mass data; namely, the "double-pole" formula:

$$\left[\frac{\left(m - m_o\right)\ \Gamma}{\left(m - m_o\right)^2 + \left(\frac{\Gamma}{2}\right)^2}\right]^2$$

with m_o = 1.305 GeV, Γ = 29 MeV. A Gaussian resolution function with σ = 5 MeV had been folded into this formula and a small, flat background was added to this fit. The result is shown as a dashed line in Figure 8. The χ^2 of 149 for 39 degrees of freedom obtained for this fit is unacceptably bad. We also varied the peak position and width, but even for values much different from those found by the CERN MM group, we were unable to obtain a χ^2 of less than 100, still an unacceptably bad fit with a probability of $< 10^{-6}$. The data for $|t - t_{min}| > 0.2$ $(GeV/c)^2$ is shown in Figure 9. In this case the number of events in the A_2^- peak is reduced to 200 events in the region 1.2 to 1.4 GeV/c and the statistics are not really adequate to reach a definite conclusion. However, the fits made to this data using the parameters given for all t data still favor the single Breit-Wigner form with a χ^2 probability of $\approx$ 55% compared to $\approx$ 2.5% for the dipole fit.

Figures 10 and 11 show preliminary data on the $\cos\theta^*$ and φ^* decay distribution respectively of the A_2^- in the A_2^- rest frame. Here the usual coordinate system (Gottfried-Jackson system) is used; namely the π^- direction in the A_2 rest frame is taken as z-axis and the scattering plane is taken as the origin of the φ angle. The data are corrected for an acceptance of our spectrometer delivered using a Monte Carlo program which, as I said before, favors strongly for forward going K^o. The line drawn for the purpose of comparison in Figure 11 is A $\sin^2\theta^* \cos^2\theta^*$ and that for Figure 12 is B $\sin^2\varphi^*$, both indicating a good agreement to the data.

Figure 12 gives preliminary results on the t-distribution of A_2^-, and Figure 13 shows the same data with an expanded t scale at small $|t|$. The overall slope, as defined by b in e^{bt} dependence at $|t-t_{min}| > .1$, is about 4 $(GeV/c)^{-2}$, and the data shows a clear dip toward $|t-t_{min}| = 0$.

From these results, we conclude that the spin parity assignment for the A_2^- is 2^+, and the spin density element[9] ρ_{11} equals ρ_{1-1} and ρ_{oo} is small. The data is then consistent with the exchange of f^o and/or ρ in the production mechanism.

In a recent publication, report of another measurement of the K^oK^- effective mass in the A_2^- region was made by a CERN-MUNICH group.[10] Their experiment is quite similar to ours; namely, they also studied the K^oK^- decay of A_2^- produced in the π^-+p incident channel at 17.2 GeV/c and the effective mass of the A_2^- was made from π^+ and π^- for K^o decay and K^-. With approximately 1100 events in the mass region of 1.2-1.4 GeV and with stated mass resolution of 5.5-5.7 MeV, they concluded that a single Breit-Wigner form fit the data very well with $m_o = 1321 \pm 3$ MeV and $\Gamma_o = 123 \pm 7$ MeV giving a χ^2 probability of 32%. Although they do not give a result of the dipole fit to their data, they ruled out this possibility in their conclusion. In fact a visual inspection of their data for all $|t|$, $|t| < 0.2$ (GeV/c)^2 as well as 0.2 (GeV/c)$^2 < |t| < 0.7$ (GeV/c)^2 does not show any sign of a dip in the A_2^- mass spectrum. They also analyzed the A_2 decay distribution in the Gottfried-Jackson frame and found that their data show a characteristic structure of the angular distribution $\cos^2\theta^* \sin^2\theta^* \sin^2\varphi^*$.

REFERENCES

1. G. E. Chikovani, M. N. Focacci, W. Kienzle, C. Lechanoine, B. L. Leviat, B. Maglic, M. Martin, P. Schübelin, L. Dubal, M. Fischer, P. Grieder, H. A. Neal, and C. Nef, Phys. Letters 25B, 44 (1967); H. Benz, G. E. Chikovani, G. Damgaard, M. N. Focacci, W. Kienzle, C. Lechanoine, M. Martin, C. Nef, P. Schübelin, R. Band, B. Bosnjakovic, J. Cotteron, P. Cotteron, P. Klanner, and A. Weitsch, Phys. Letters 28B, 233 (1968); R. Baud, H. Benz, B. Bosnjakovic, D. R. Botterill, G. Damgaard, M. N. Focacci, W. Kienzle, R. Klanner, C. Lechanoine, M. Martin, C. Nef, P. Schübelin, A. Weitsch, H. Blumenfeld, H. Jostlein, and P. Lecomte, Phys. Letters 31B, 397 (1970).
2. M. Alston-Garnjost, A. Barbaro-Galtieri, W. F. Buhl, S. E. Derenzo, L. D. Epperson, S. M. Flatte, J. H. Friedman, G. R. Lynch, R. L. Ott, S. D. Protopopescu, M. S. Rabin, and F. T. Solmitz, Phys. Letters 33B, 607 (1970). See this paper for a full discussion of related work.
3. K. J. Foley, S. J. Lindenbaum, W. A. Love, S. Ozaki, E. D. Platner, A. C. Saulys, and E. H. Willen, Phys. Rev. Letters 26, 413 (1971).

4. Bogachev, N.P., Budagov, Yu. A., Vinogradov, V. B., Volodko, A. G., Dzhelepov, V.P., Ivanov, V. G., Kladnitsky, V. S., Klimenko, S. V., Lomakin, Yu. F., Merekov, Yu. P., Patocka, J., Flyugin, V.B., and Schyapnikov, P.V., "Resonance $Y_o^*(1327) \rightarrow \Lambda + \gamma$", (JINR Dubna), Paper 87, as reviewed by R. D. Tripp, 14th International Conference on High Energy Physics, Vienna, 1968.

5. Earlier preliminary results for this process were presented at the Kiev Conference, 1970: S. Ozaki, D. C. Cheng, K. J. Foley, S. J. Lindenbaum, W. A. Love, E. D. Platner, A. C. Saulys, and E. H. Willen, "K^o,Λ^o Production in the 8-16 GeV/c Incident Momentum Range", Presented at the XVth International Conference on High-Energy Physics, Kiev, August 26-September 4, 1970.

6. Particle Data Group, "Review of Particle Properties", UCRL 8030, Pt. 1, 1970.

7. K. Gottfried and J. D. Jackson, Nuovo Cimento 33, 3589 (1964).

8. The authors of Reference (7) have obtained a good fit to their K^oK^- mass spectrum from a similar experiment using the Breit-Wigner form:

$$\frac{m\, m_o\, \Gamma(m)}{\left(m^2 - m_o^2\right)^2 + m_o^2\, \Gamma^2(m)}$$

where

$$\Gamma(m) = \Gamma_o \left(\frac{q}{q_o}\right)^5 \left[\frac{9 + 3R^2 q_o^2 + R^4 q_o^4}{9 + 3R^2 q^2 + R^4 q^4}\right]$$

which is similar to ℓ=2 form of the angular momentum barrier calculated by Blatt and Weisskopf, Theoretical Nuclear Physics (published by John Wiley & Sons, 1952, p. 361). We have used the same functional form with $R^2 = 12\ (\mathrm{GeV}/c)^{-2}$.

9. R. H. Dalitz, Proc. of the International School of Physics, Enrico Fermi: Course XXXIII, Academic Press, p. 141, 1966.

10. G. Grayer, B. Hyams, C. Jones, P. Schlein, W. Blum, H. Dietl, W. Koch, H. Lippmann, E. Lorenz, G. Lütjens, W. Männer, J. Meissburger, U. Stierlin, and P. Weilhammer, Phys. Letters 34B, 333 (1971).

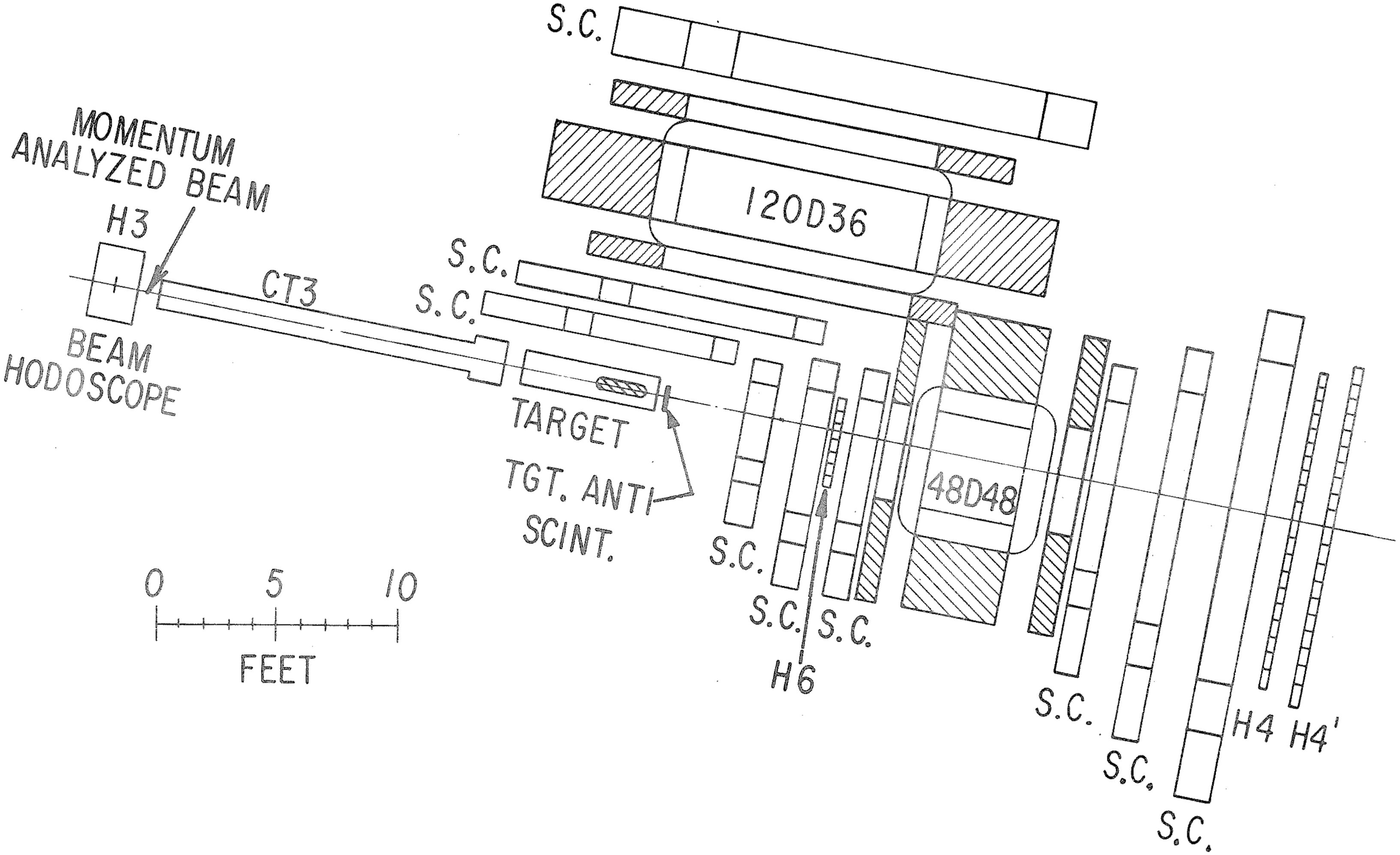
MOMENTUM ANALYZED BEAM
H3
BEAM HODOSCOPE
CT3
S.C.
S.C.
S.C.
120D36
TARGET
TGT. ANTI SCINT.
0
5
10
FEET
S.C.
S.C.
S.C.
H6
48D48
S.C.
S.C.
S.C.
H4
H4'

Figure 1: The Double Vee Magnetic Spectrometer as it was set up for the A_2^- experiment. For K^oY^o experiment, the hodoscope H6 was removed and instead a 3/16 inch thick trigger counter was placed behind the first spark chamber module in the forward leg.

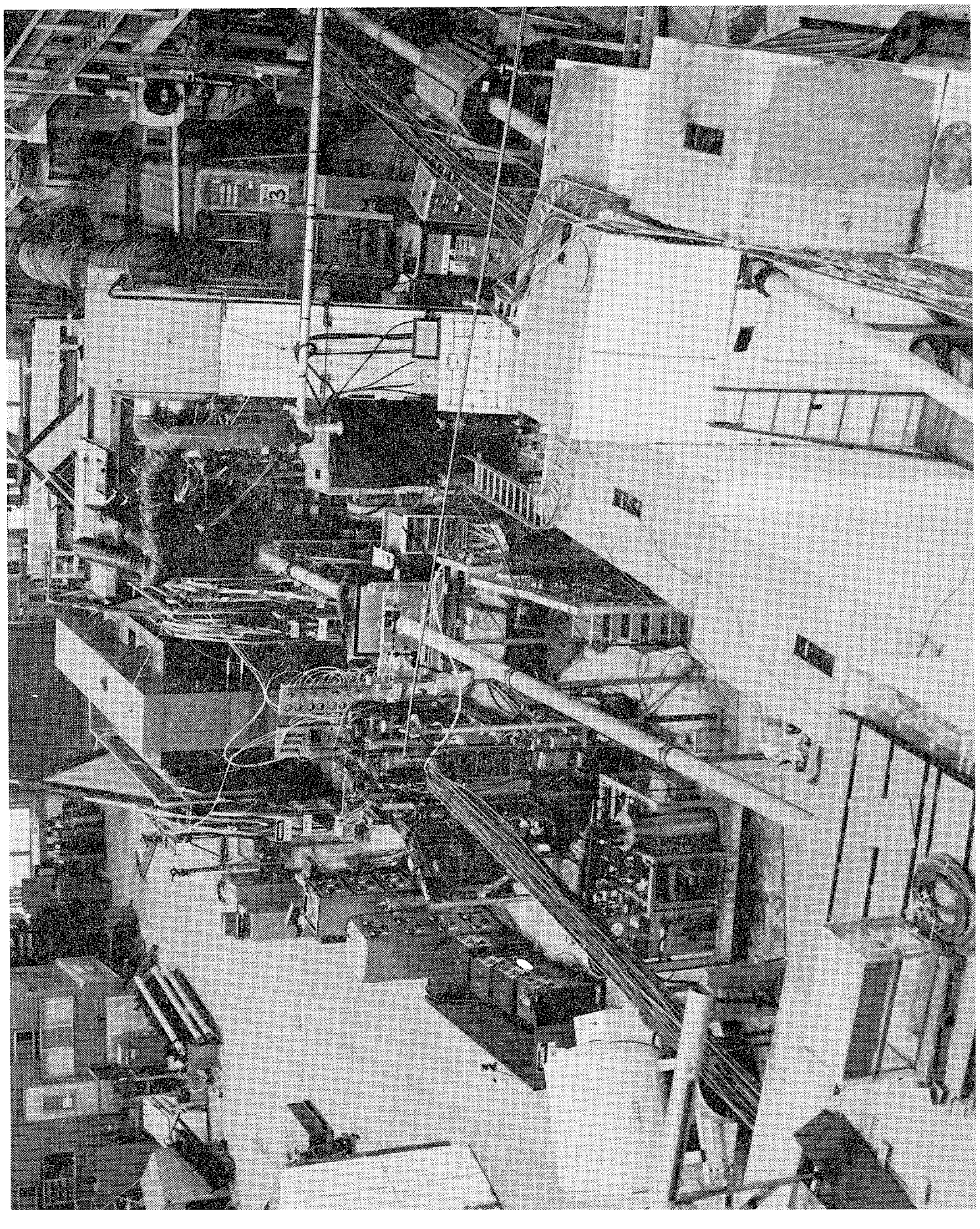

Figure 2: A picture of the Double Vee Magnetic Spectrometer setup on the AGS floor. In the foreground, an incoming beam pipe and the downstream end of the beam spectrometer can be seen. Target is located in a tent enclosure in the upper middle and from there the forward leg leads toward the top of the picture and recoil leg to the left.

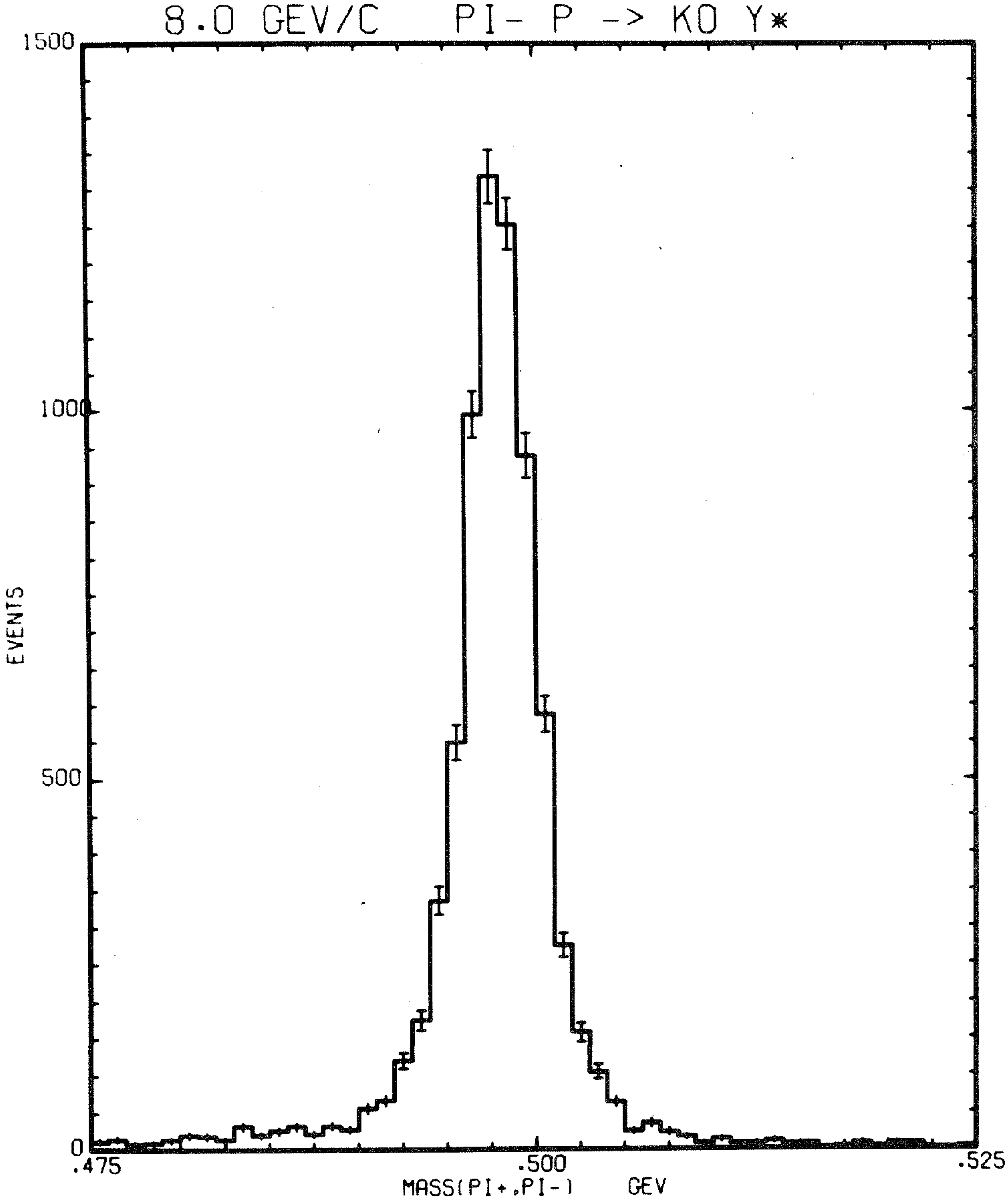

Figure 3: The $\pi^+\pi^-$ effective mass distribution obtained in the $\pi^- + p \rightarrow K^0 + Y^0$ experiment at 8.0 GeV/c. A standard deviation width of the peak is 1.9 MeV.

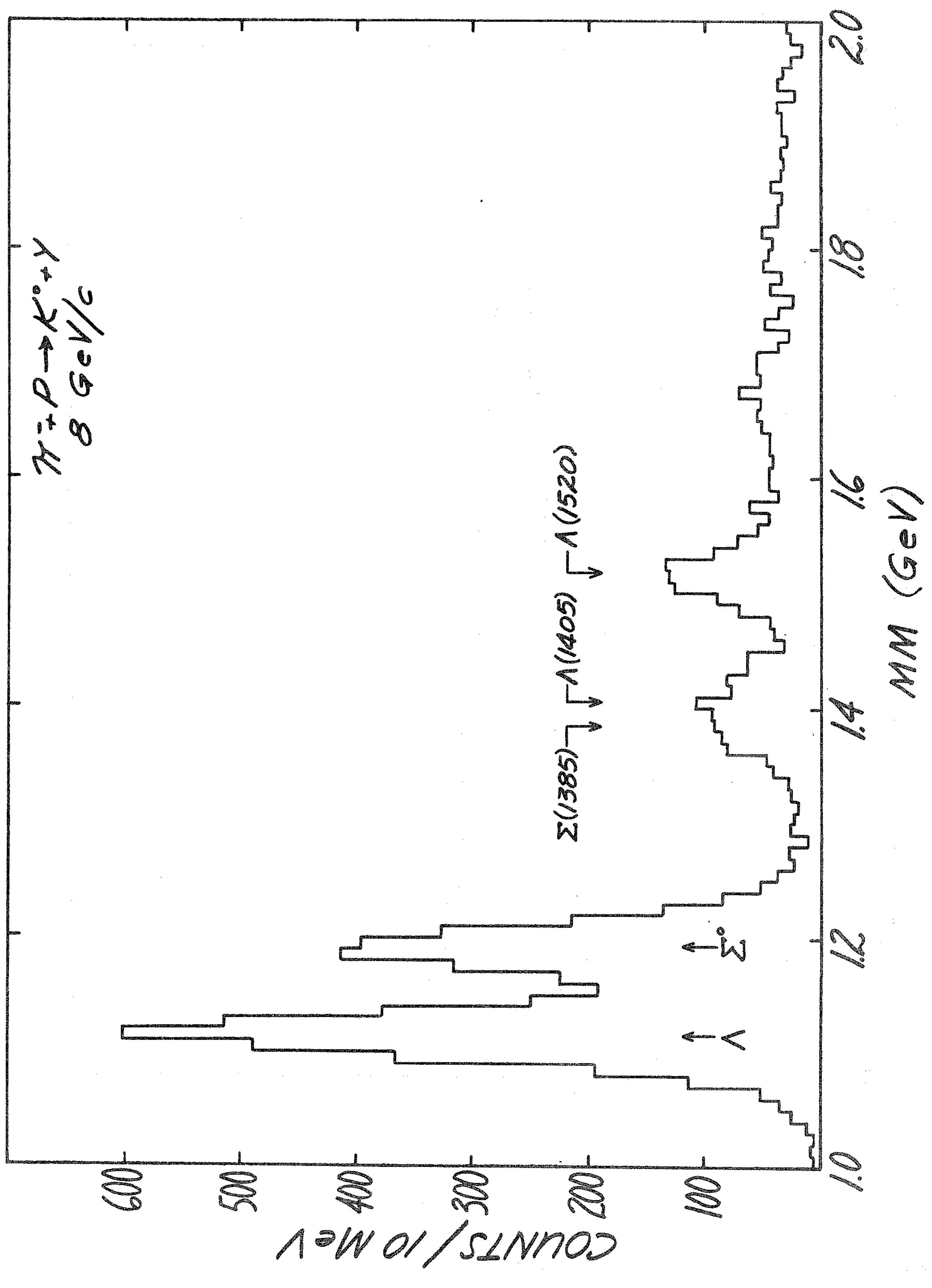

Figure 4: The missing recoil mass distribution for the process $\pi^- + p \to K^0 + (MM)$ at 8.0 GeV/c.

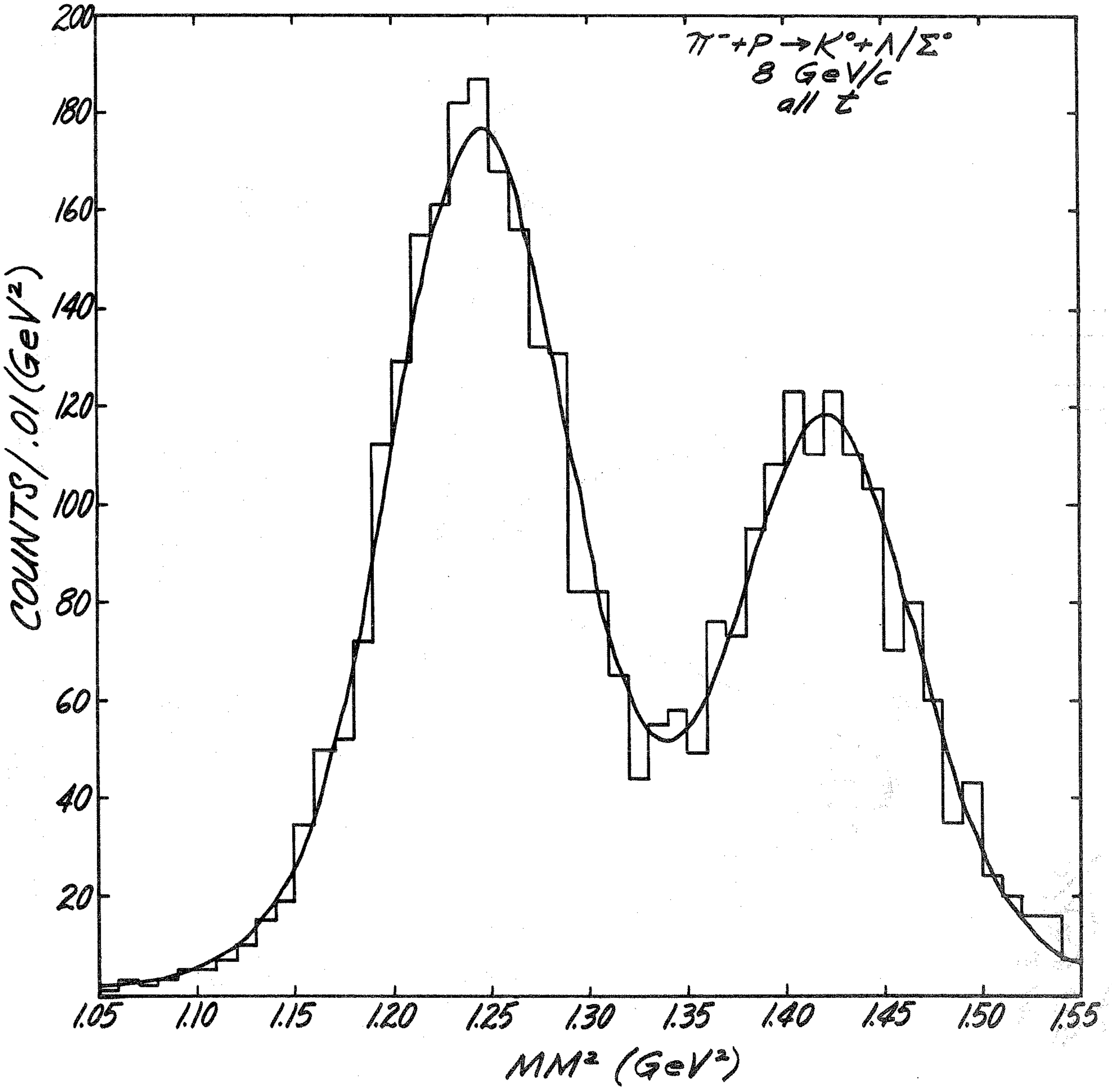

Figure 5: The missing recoil mass squared distribution in the mass region of Λ and Σ^0 for $\pi^- + p \to K^0 + (MM)$ process. The line is a maximum likelihood fit to the data with a Gaussian width of 0.05 GeV^2.

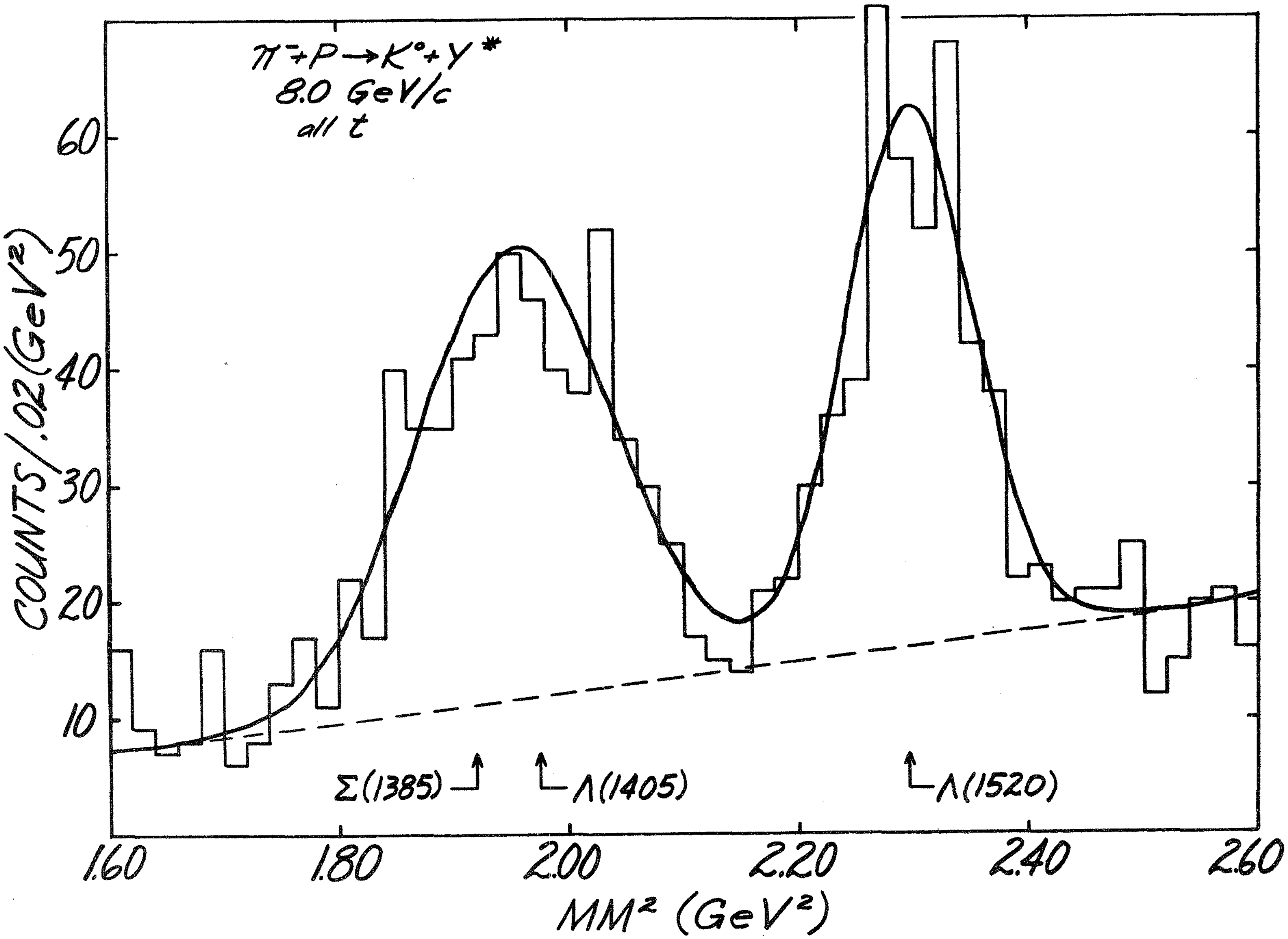

Figure 6: The missing recoil mass squared distribution in the mass region of $\Sigma(1385)$, $\Lambda(1405)$, and $\Lambda(1520)$. The solid line is the maximum likelihood fit to the data with a width which takes into account the resonance width and the resolution width.

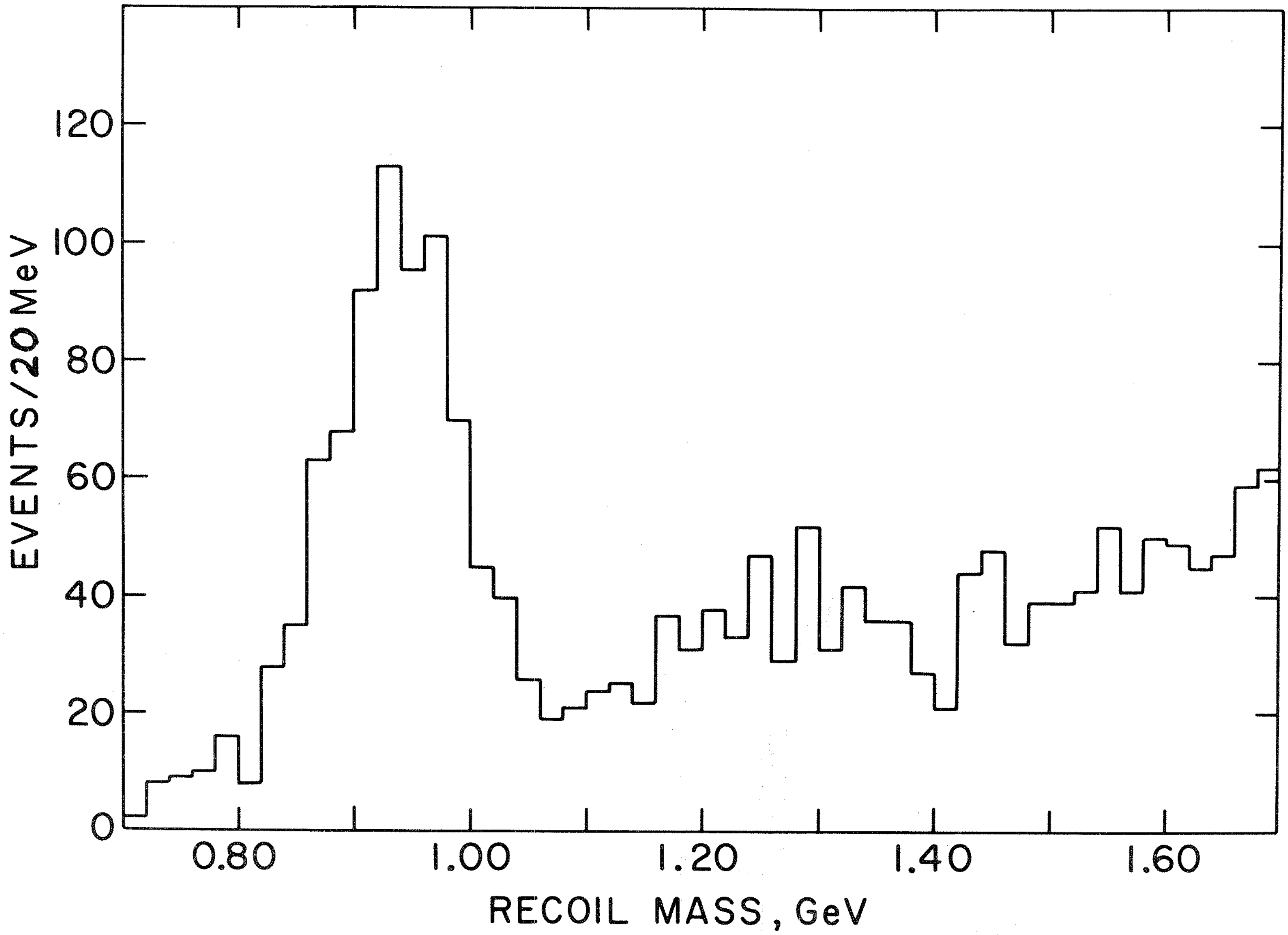

Figure 7: Missing recoil mass distribution for the $\pi^- + p \rightarrow A_2^- + (MM)$ process where K^0 from the A_2^- decay was identified and the accompanying negatively charged particle was assumed to be K^-. There is a clear peak at the proton mass. If the negative particle was misidentified π^-, the lightest recoil mass should have been that of Σ^+.

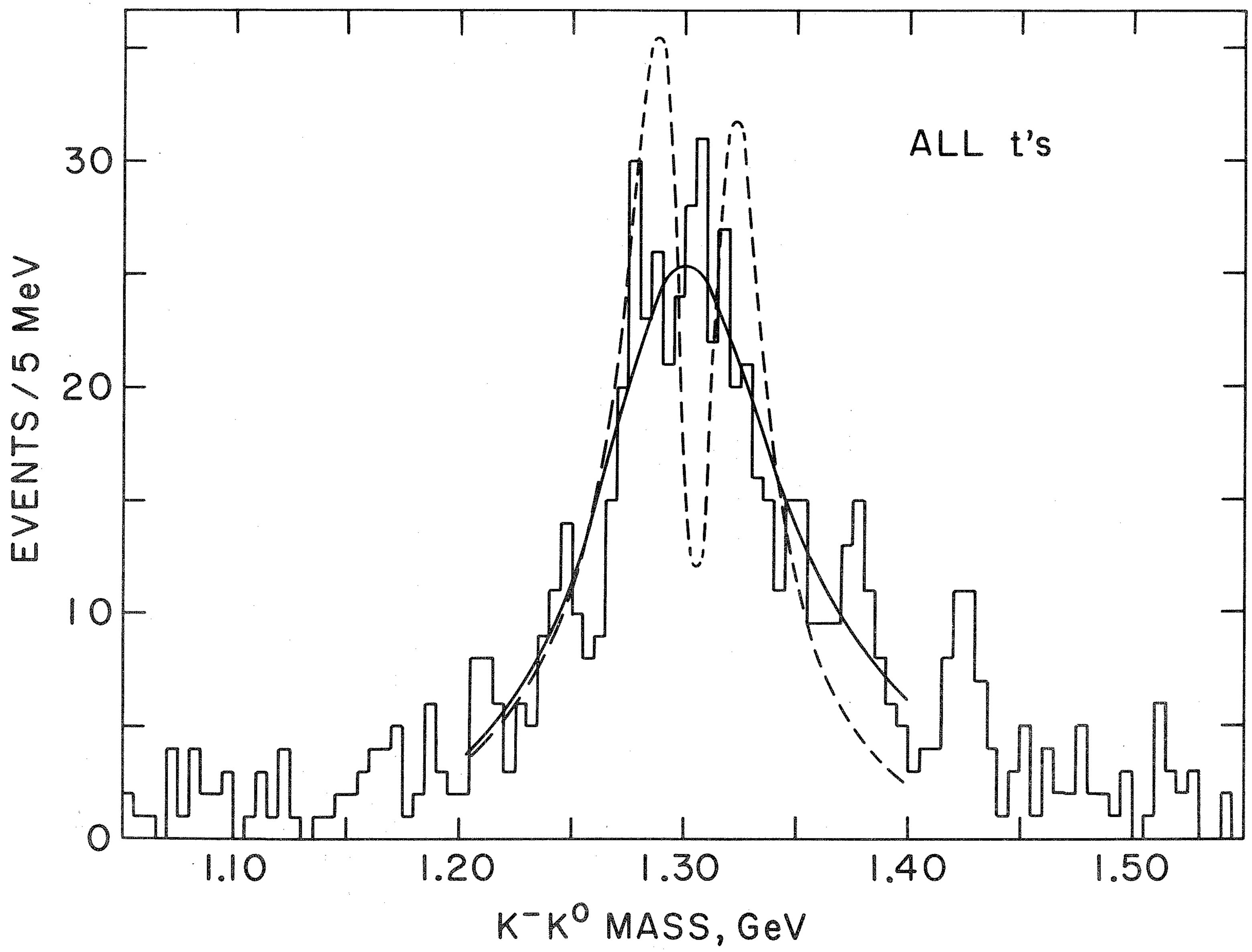

Figure 8: The K^-K^0 effective mass spectrum for K^-K^0 events with a recoil mass in the region 0.76 to 1.06 GeV. The data are not corrected for the spectrometer acceptance. The solid line is a fit of a single Breit-Wigner form and the dashed line is that for a dipole form.

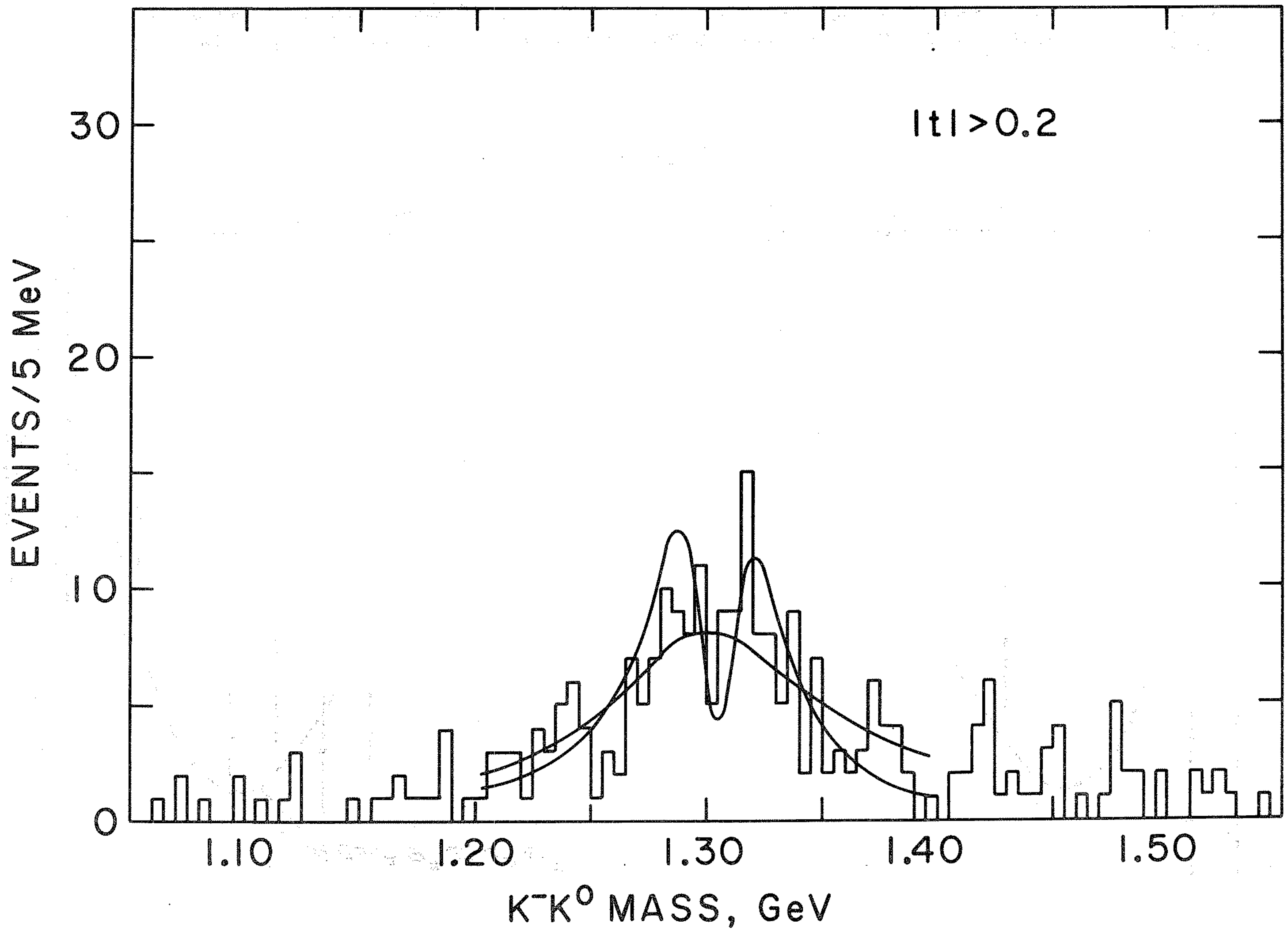

Figure 9: The K^-K^0 effective mass spectrum as in Figure 8, but with $|t - t_{min}| > 0.2\ (GeV/c)^2$. Two curves are those for a single Breit-Wigner form and a dipole form with a parameter used in Figure 8.

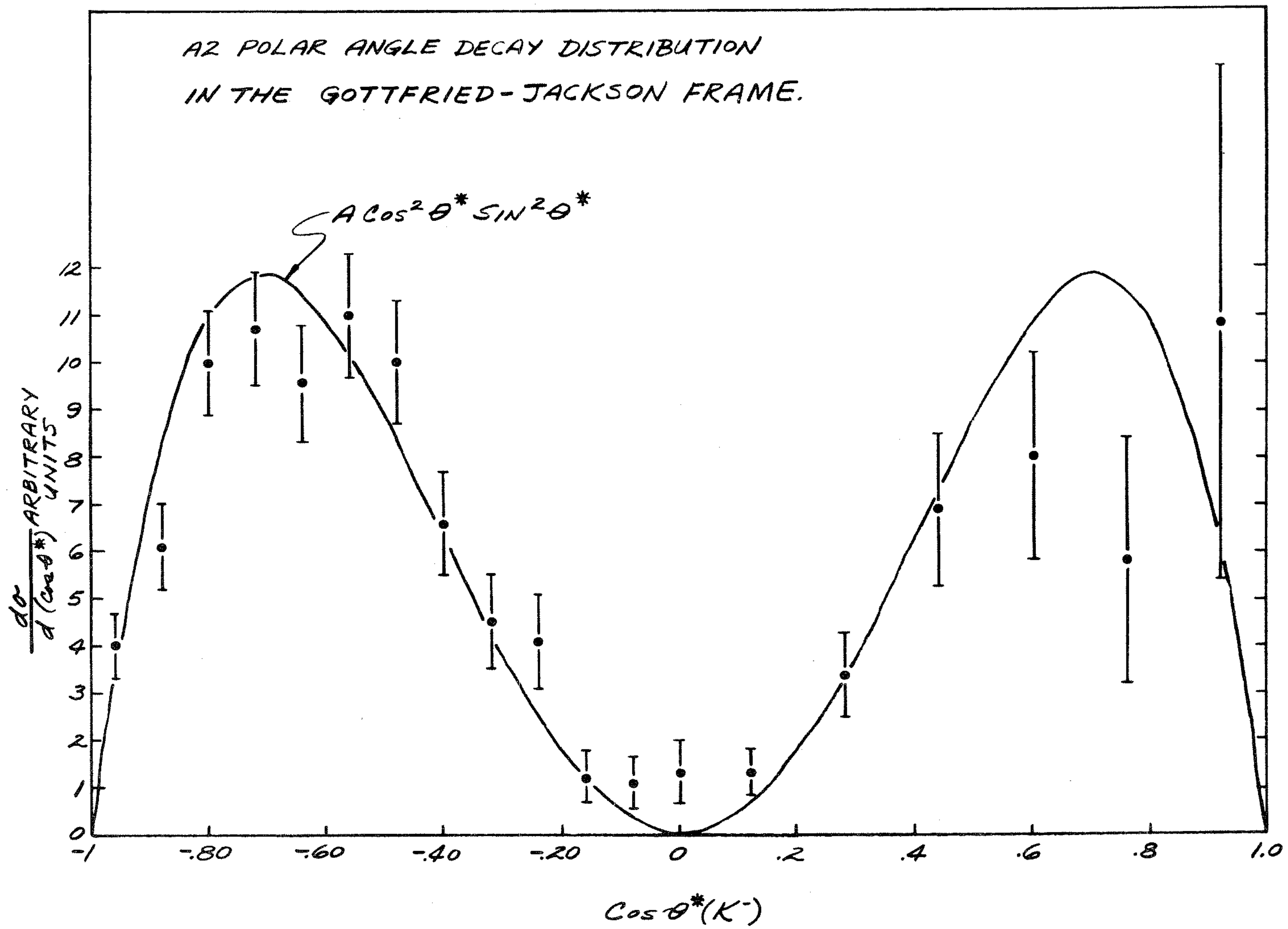

Figure 10: The preliminary result on the polar angle distribution of A_2^- decay into K^-K^0 in the Gottfried-Jackson frame. The data are corrected for the spectrometer acceptance. A curve for $A \cos^2\theta^* \sin^2\theta^*$ is also drawn in the figure for comparison.

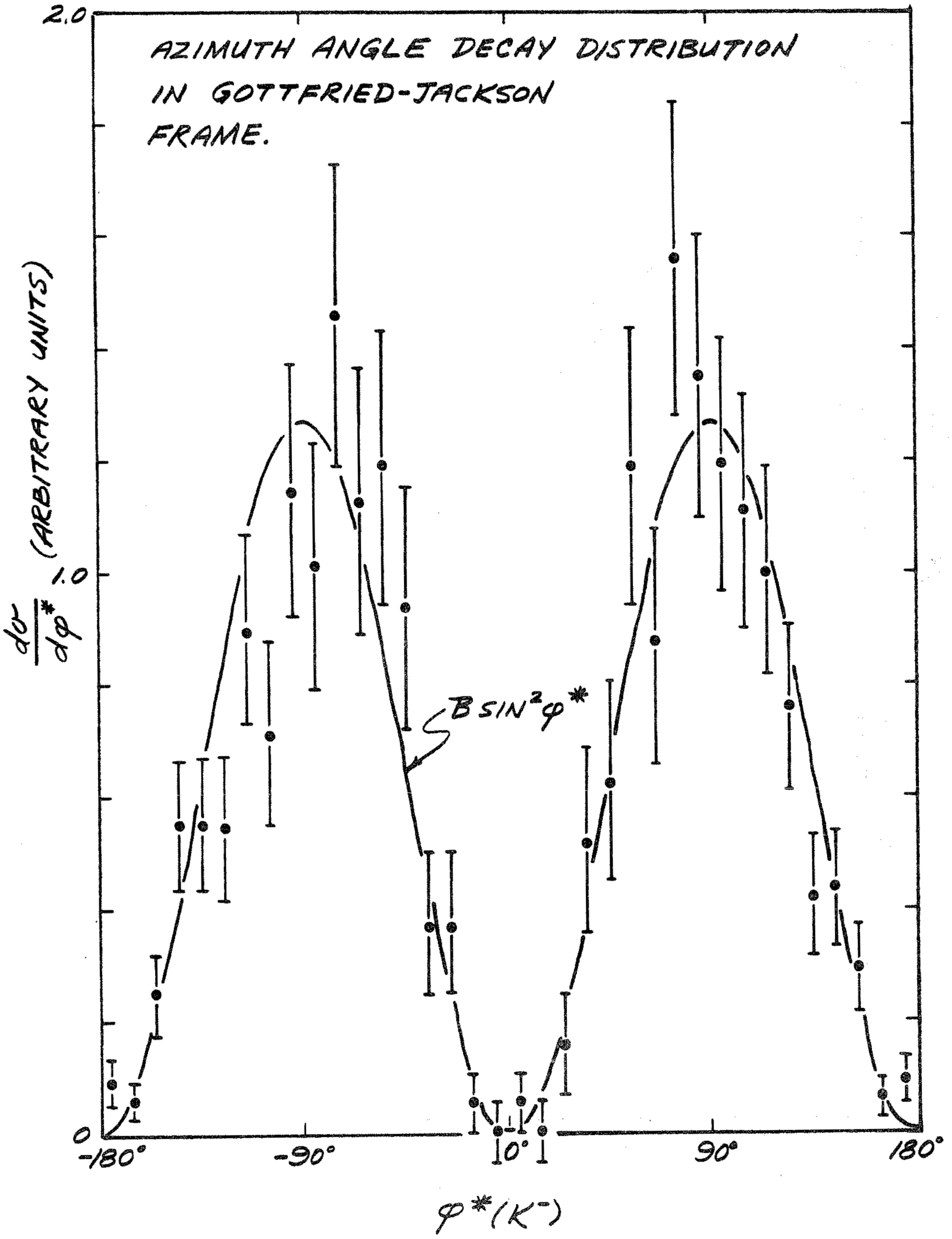

Figure 11: The preliminary result on the azimuth angle distribution of A_2^- decay into K^-K^0 in the Gottfried-Jackson frame. The data are corrected for the spectrometer acceptance. A curve for B $\sin^2\phi^*$ is also shown for comparison.

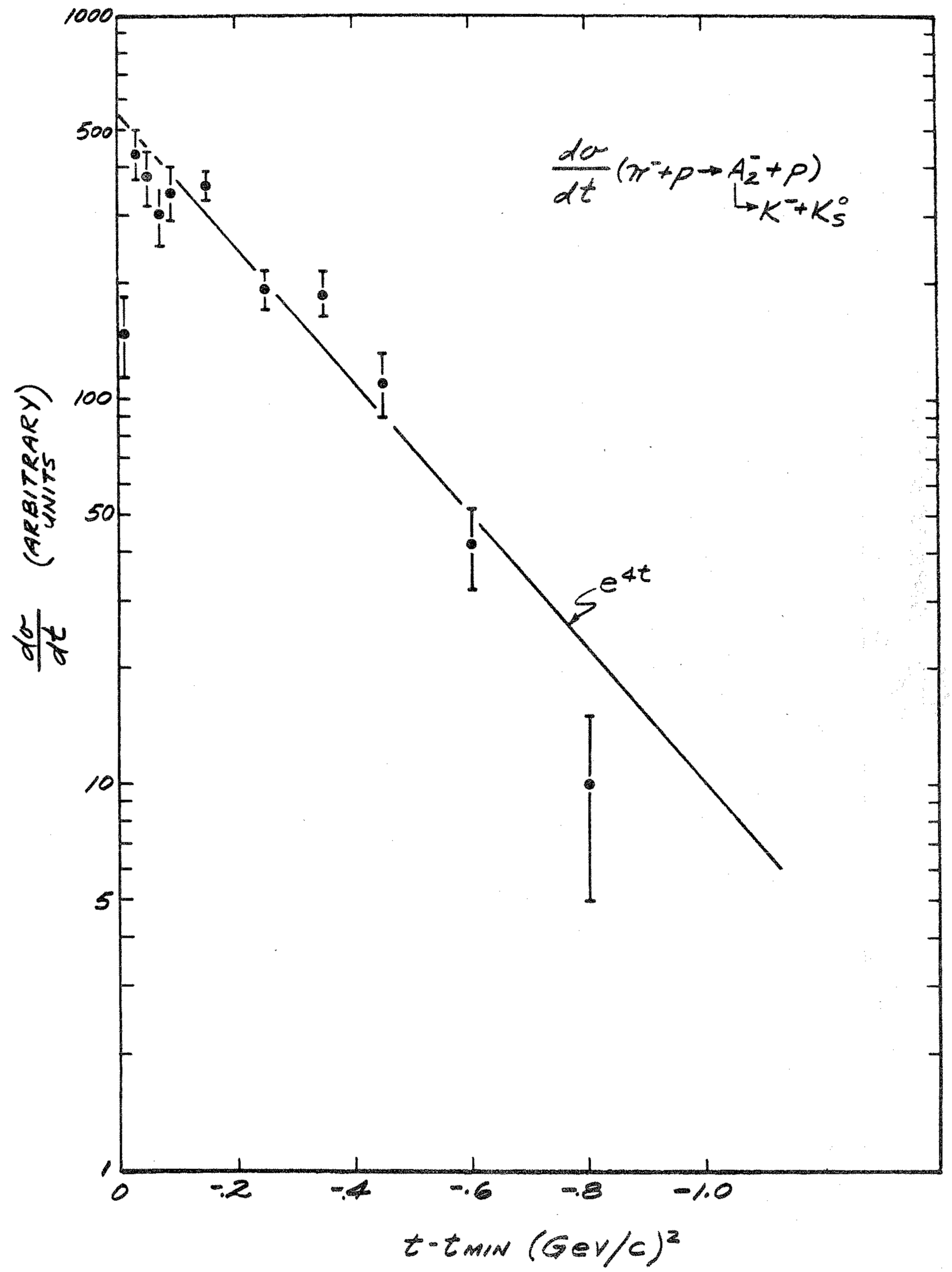

Figure 12: The preliminary result for the t distribution of $d\sigma/dt$ for $\pi^- + p \to A_2^- + p$

$\hookrightarrow K^0 + K^-$

in an arbitrary scale. The line drawn is e^{4t} for comparison with data.

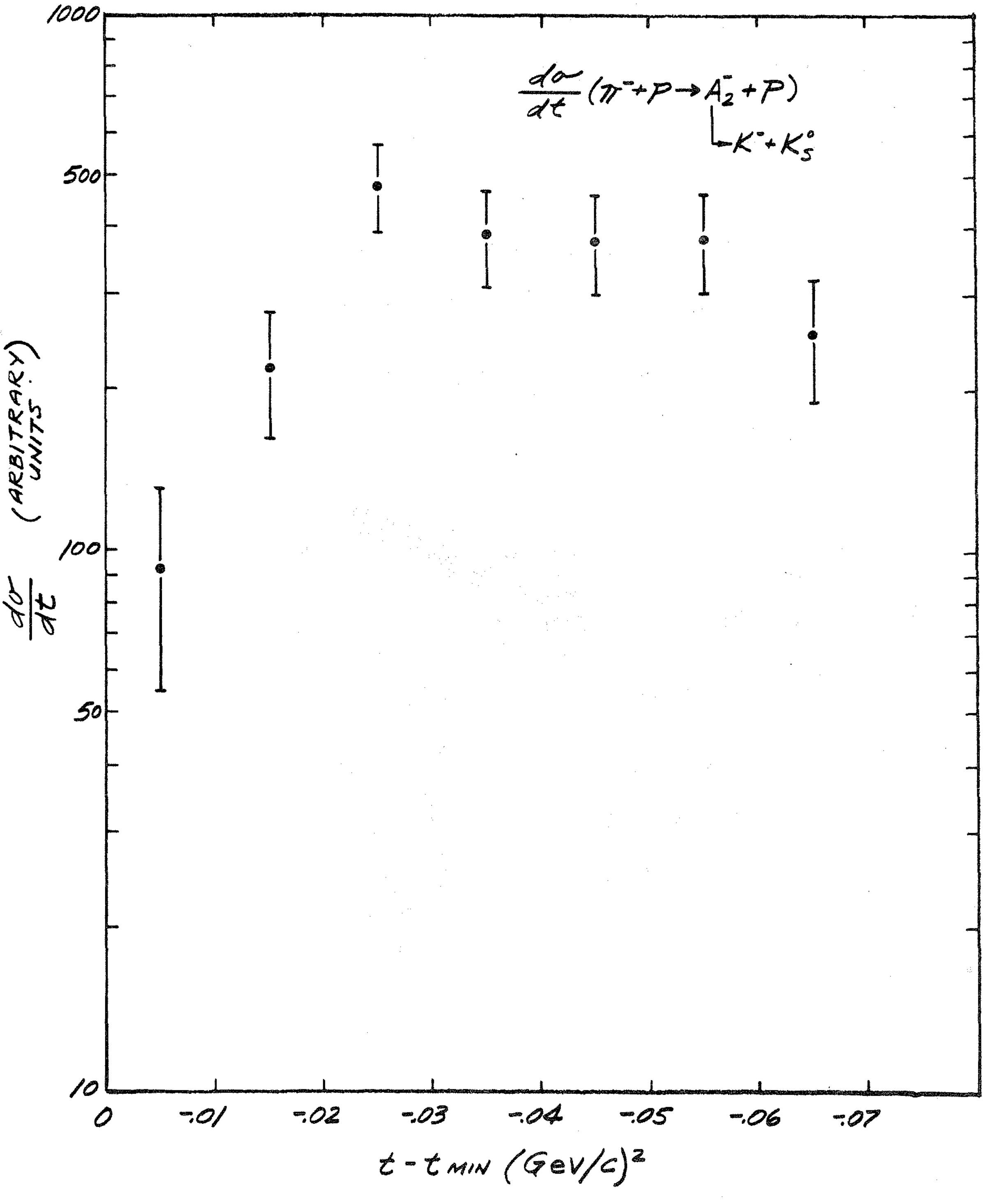

Figure 13: The same data as Figure 12 at smaller momentum transfer but expanded in the t scale. A clear forward dip of the cross section is seen.

MEASUREMENTS OF THE A_2^- AND A_2^+ MASS SPECTRA

D. Bowen, D. Earles, W. Faissler, D. Garelick, M. Gettner,
M.J. Glaubman, B. Gottschalk, G. Lutz, J. Moromisato[□],
E.I. Shibata, Y.W. Tang, and E. von Goeler
Northeastern University at Boston, Boston, Massachusetts 02115*

and

H. R. Blieden, G. Finocchiaro, J. Kirz,[†] and R. Thun
State University of New York at Stony Brook
Stony Brook, New York 11790[‡]

PRESENTED BY MARVIN GETTNER

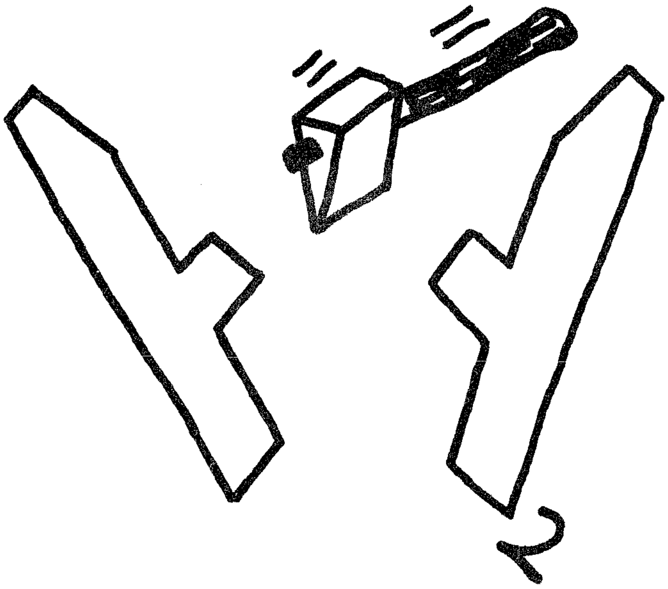

[□] On leave of absence from the University of San Marcos, Lima, Peru. Supported in part by a Ford Foundation Fellowship.

*Supported in part by the National Science Foundation under Grants GP 9217 and GP 25307.

[†] Alfred P. Sloan Foundation Fellow.

[‡] Supported in part by the U.S. Atomic Energy Commission.

I. Introduction

An experiment to investigate the A_2 mass distribution by the missing mass technique has been recently performed by a Northeastern University-Stony Brook collaboration at the Brookhaven AGS. Previously, the CERN missing mass group, hereafter referred to as the CMMS group, reported[1] that the A_2 meson's mass spectrum did not possess the usual Breit-Wigner distribution, but instead had a double peaked structure described by a "dipole" formula. Other experiments[2-7] have also examined the A_2 mass spectrum. In the experiment reported here data from the reaction $\pi + p \rightarrow A_2 + p$ were obtained in a similar manner and in the identical kinematic region as the original CMMS experiments. At an incident beam momentum of 5^- GeV/c about 28,000 A_2's above background were measured, 24,000 at 5^+ GeV/c*, and 17,000 at 7^- GeV/c. These data were in the four momentum transfer squared, t, range of - .20 to - .29 GeV^2 and the mass resolution was measured to be 16 ± 1 MeV (FWHM)[8] at 5 GeV/c and 21 ± 1 MeV at 7 GeV/c. The data show no fine structure in either the A_2^- or A_2^+ and their mass distributions are well described by the Breit-Wigner formula.

II. Apparatus

The experimental arrangement is shown in Fig. 1. The pion beam was derived from the slow external proton beam from the Brookhaven AGS. Three beam hodoscopes were used to determine the incident particle's direction, position at the hydrogen target, and to subdivide the momentum interval. The hydrogen target was 24" long with a 1" radius. Scintillation counters located around the target were used to record the approximate multiplicity of charged particles produced with each event. The beam was displaced towards the proton detector at the hydrogen target to minimize the coulomb scattering of recoil protons.

---

* The momentum and charge of the incident pion beam used in a particular measurement will be denoted simply as 5^+ GeV/c, 5^- GeV/c or 7^- GeV/c.

The recoil proton was detected in an easily rotatable telescope consisting of four spark chambers and five identical proton detectors which subdivided the vertical aperture. Each proton detector had an entrance aperture of 4" x 24" located about 5' from the target and they subtended a total solid angle of about 120 msr. Each consisted of a 1/2" scintillation counter to measure dE/dx and time of flight, followed by an 11¼" deep plastic scintillation counter to stop the proton and measure energy by pulse area,[9] and, finally, an anticoincidence counter to veto particles which did not stop. The proton kinetic energy acceptance ranged from .050 to .220 GeV and the lower limit could be adjusted by varying the discrimination level on the energy counter. The discrimination level on the dE/dx counters was set to twice the pulse from a relativistic pion. Using dE/dx, time of flight criterion, and checking for the consistency of a particle energy and energy loss, the detectors were able to identify protons with less than a 1% pion contamination. Although about 25% of the protons had nuclear interactions, 90% of these were excluded by the above requirements.

A second spectrometer, consisting of wire spark chambers and trigger counters located before and after a magnet was used to determine the production angles and momenta of particles produced in the forward direction. The magnet was placed about 19' from the target and had an aperture of 26" w x 5" h x 72" ℓ. This spectrometer, having a momentum resolution of 1% at 5 GeV/c, was used in this run to detect primarily elastically scattered π's.

The electronics defined three particles of interest, an incident beam particle, a proton recoil, and a "fast" particle detected through the forward magnetic spectrometer. A coincidence between the beam line scintillators, at least one count from each beam hodoscope, and a threshold Cerenkov counter set to count pions was required for a beam trigger. The proton logic demanded a coincidence between signals above the dE/dx and energy counters discrimination levels and no signal from the anti-counter. A "fast" particle was defined by coincidence between the four counters which defined the magnetic spectrometer aperture. The spark chamber pulses and data recording systems could be triggered by beam/proton, beam/fast, or beam/proton/fast coincidences. This could be done singly for each, or in proportions selected by the computer.

Data was recorded on magnetic tape with about a 3 ms dead time for beam-proton triggers. With a typical incident pion flux of about $.25 \times 10^6$ per pulse 30 to 50 events were recorded each pulse using a PDP9 computer as a data logger. The BNL OLDF's PDP10 reconstructed the data tapes typically within a few hours after they were taken. All the events for which a track was found in the proton spectrometer (about 40%) were recorded on "kinematic summary" tapes for off line analysis.

III. The Calibration, Stability, and Resolution of the Apparatus

A. Kinematics

The missing mass technique was used to study the reaction $\pi + p \rightarrow p + x$ where the mass, m, of x is determined from the knowledge of the incident beam momentum and the measurement of the proton energy and angle by the relationship:

$$m^2 = m_\pi^2 - 2[T\ (E_B + m_p) - P_B P \cos\theta] \qquad \text{(Eq. 1)}$$

where m_π, m_p, m are the pion, proton, and missing boson masses

E_B, P_B are the incident beam energy and momentum

T, P, θ are the recoil proton's kinetic energy, momentum and angle.

In Fig. 2 this relationship is shown for an incident momentum of 7 GeV/c for elastic scattering ($m = m_\pi = .14$ GeV) and for several values of m near the A_2 mass (m = 1.30 GeV). The proton spectrometer angle and energy acceptance used in the A_2 measurement is also shown. In this region ("Jacobian Peak") the missing mass is mainly determined by the proton angle, as can be seen from the figure. Also illustrated is the relationship between the elastic scattering and A_2 production kinematics. To detect protons from the elastic reaction in the same t range[10] as used in the A_2 reaction it was only necessary to rotate the proton spectrometer to a central angle about 20° larger than used for the A_2. Since all components of the proton spectrometer moved as a complete unit, most angular systematic errors would move with it. Thus the measurement of the proton angular distribution or equivalently the t-dependence, for elastic scattering is a good test for angle dependent systematic bias.

B. Calibration, Stability of the Mass Scale, and Beam Resolution

The mass scale is set by knowledge of the beam momentum, proton energy and scattering angle. The scattering angle was checked by measurements with the proton detector rotated into the beam and by surveying. To calibrate the mass scale and monitor its stability use was made of the elastic scattering reaction.

The beam momentum and resolution were determined from measurements of the elastically scattered pions detected with the magnetic spectrometer. These data which required a beam/fast coincidence were recorded along with the A_2 data and provided a continuous monitor of the beam momentum. They were analyzed by treating them as a missing mass experiment, but in this case the detected particle was the pion and the missing mass was that of the proton.

The beam momentum was initially set so that this mass distribution was centered at the proton mass. After this initial determination, no further adjustments were made and the missing mass for the A_2 data was calculated using these values of the beam momenta. All of the beam calibration data taken during the 7^- GeV/c A_2 run were added together and are shown in Fig. 3. Similar shapes were obtained during the 5^- and 5^+ GeV/c runs. The center of the distribution is at 948 ± 1 MeV indicating that the beam had drifted from its initial value during the data taking. It can be easily shown that the shift in apparent proton mass is directly proportional to the shift in beam momentum so that the average value of the beam for the data was 10 MeV/c higher than the initially assumed value. This would shift the mass scale at the A_2 by 1.1 MeV. These results are summarized in Table I for each value of the beam momentum used.

TABLE I

Beam Stability

Beam Momentum GeV/c	Observed Proton Mass (MeV)	Width of Proton Peak (MeV)	Beam Momentum Shift (MeV/c)	Mass Shift at A_2 (MeV)
5^-	943 ± 1	75	5	.7
5^+	930 ± 1	75	-8	-1.2
7^-	948 ± 1	82	10	1.1

The energy calibration of the proton detectors was done by requiring that the missing mass distribution determined by detecting only the protons from the elastic reaction be centered at the pion mass. Elastic scattering kinematics are more sensitive to the proton energy than are the kinematics in the A_2 region. (See Table III). Thus slight changes in the proton energy calibration could be easily detected. These calibration data which required a beam/proton trigger were obtained by moving the proton detector to a scattering angle about 20° larger than used for the A_2 runs, and were taken at frequent intervals throughout the experiment. In addition, during the recording of the 7^- GeV/c A_2 data protons from the elastic reaction were also detected and provided a simultaneous monitoring of the proton energy calibration.

Shown in Figure 4 is the sum of all the proton energy calibration data taken at 7^- GeV/c plotted as a function of mass squared. Similar shapes were obtained at 5^+ and 5^- GeV/c. The center is at .040 GeV^2 and indicates a calibration error of 3 MeV, at an average proton energy of 130 MeV. This calibration error shifts the mass scale at the A_2 mass by + .6 MeV and broadens the mass resolution by .3 MeV. The results for proton energy calibration data are shown in Table II.

TABLE II

Summary of Proton Energy Calibration Date

(For Proton Energy Between 105 and 155 MeV)

Beam Momentum (GeV/c)	Center of Distribution (GeV^2)	Width of Distribution (GeV^2)	Shift in Calibration (MeV)	Mass Scale Shift at A_2 (MeV)
5^-	.026 ± .001	.049	- 1.3	- .6
5^+	.029 ± .001	.051	- 1.8	- .9
7^-	.040 ± .001	.067	- 2.8	+ .6

The proton energy calibration has been checked by two other methods which are somewhat less precise, but are independent of any systematic error in the proton angle scale. During the calibration procedure, the pulse area for pions traversing the energy counter was recorded and the measured energy loss was within errors, equal to the predicted amount. In addition, the end point of the proton energy distribution (corrected for geometrical effects) was found to be in good agreement with the value predicted on the basis of the range-energy relationship.

Since the effects of the beam momentum and proton energy calibration drifts produced mass shifts at the A_2 significantly smaller than the mass resolution, all data have been summed with no adjustment of the mass scale.

The proton energy calibration measurements can be considered as a determination of the pion mass by the missing mass technique and thus can be used to study the mass resolution. The observed width of the pion mass squared has comparable contributions from the proton energy and angular resolutions, whereas for the A_2 mass region, the angular resolution dominates. Assuming that the observed pion width was due entirely to the angular resolution, upper limits to the A_2 mass resolution of 19 MeV for the 5 GeV/c data and 25 MeV for the 7 GeV/c data are obtained, including contribution from the beam momentum uncertainty.

C. Mass Resolution

The mass resolution is given by:

$$\Delta m^2 = \left[\left(\frac{\partial m^2}{\partial P_B}\,\Delta P_B\right)^2 + \left(\frac{\partial m^2}{\partial T}\,\Delta T\right)^2 + \left(\frac{\partial m^2}{\partial \theta}\,\Delta\theta\right)^2\right]^{\frac{1}{2}}$$

where $\frac{\partial m^2}{\partial P_B}$, $\frac{\partial m^2}{\partial T}$, $\frac{\partial m^2}{\partial \theta}$ are derivatives of Eq. 1 and ΔP_B, ΔT, $\Delta\theta$ are the beam momentum, proton energy, and proton angular resolutions. ΔP_B, ΔT, and $\Delta\theta$ are primarily properties of the apparatus. $\Delta\theta$ was mainly determined by the multiple scattering of the proton in the material preceeding the proton detectors and the thickness traversed is slightly dependent on the spectrometer angle. For convenience, these derivatives are listed in Table III for P_B = 5 and 7 GeV/c both for the elastic scattering and for the A_2 region.

TABLE III

Missing Mass Error Derivatives

(Proton Energy = 130 MeV, $|t|$ = .25 GeV^2)

Beam Momentum (GeV/c)	5		7	
M (GeV)	.14	1.3	.14	1.3
$\frac{\partial m^2}{\partial P_B}$ (GeV)	.047	.38	.033	.28
$\frac{\partial m^2}{\partial T}$ (GeV)	-5.58	+1.28	-7.45	.57
$\frac{\partial m^2}{\partial \theta}$ (GeV^2/rad)	-4.7	-3.8	-6.7	-6.0

The value of ΔP_B was determined from the width of the proton mass distribution, corrected for contributions from the intrinsic resolution of the magnetic spectrometer. For this determination, the width of the distribution obtained by combining all of the calibration data taken was used and thus the resolution obtained contains the effects of beam drifts.

To determine ΔT and $\Delta\theta$ elastic scattering events where the proton and scattered pion were detected in coincidence were analyzed. To illustrate the method used, the determination of $\Delta(\cos\theta)$ will be discussed, but the same technique was used to determine ΔT. For each elastic coincidence event, $\cos\theta$ could be obtained three ways: 1) the direct measurement, $\cos\theta_m$, 2) a value calculated from the beam momentum and the proton energy, $\cos\theta_1$, 3) calculated from the measured angle and momentum of the scattered pion, $\cos\theta_2$. Each of these has an uncertainty, which will be called α, β, and γ with $\alpha \equiv \Delta(\cos\theta)$ the quantity to be determined. Form the trio of differences:

$$A = \cos\theta_1 - \cos\theta_m$$

$$B = \cos\theta_2 - \cos\theta_m$$

$$C = \cos\theta_2 - \cos\theta_1$$

The distributions of the quantities A, B, and C have widths a, b, c; then, because α, β, and γ, are essentially independent, it follows that:

$$a^2 = \alpha^2 + \beta^2$$

$$b^2 = \alpha^2 + \gamma^2$$

$$c^2 = \beta^2 + \gamma^2$$

and

$$(\Delta(\cos\theta))^2 \equiv \alpha^2 = \frac{1}{2}(a^2 + b^2 - c^2).$$

In Fig. 5 a trio of histograms are shown. Elastic scattering data were analyzed at incident beam momenta of 5, 7, 11 GeV/c. The results obtained for $\Delta(\cos\theta)$ were all consistent and gave a value of $.0076 \pm .0004$.

The calculated expected value of $\Delta(\cos\theta)$ is .0075 with a contribution of .0069 from the multiple scattering[11] in the material in the proton's path (including the wires of the first spark chamber) and .003 from the uncertainty in the incident beam direction combined with the intrinsic angular resolution of the spark chambers. The latter contribution was measured by rotating the spark chambers into the beam.

The measured $\Delta(\cos\theta)$ of .0076 implies a $\Delta\theta$ of 8.0 mr. To determine $\Delta\theta$ for the A_2 measurements this value has to be increased to 8.6 ± .4 mr to account for the longer path length through the hydrogen target for protons produced at smaller angles in the inelastic process.

By a similar procedure to that used for $\Delta\theta$, ΔT of 5 ± 1 MeV was obtained for protons between 105 and 155 MeV. ΔT was determined for each of the five counters separately, as well as for the case where data from all of them were combined.

Table IV lists the measured values of ΔP_B, $\Delta\theta$, ΔT and shows their contribution to the A_2 mass resolution. As a consistency check the contributions to the width of pion peaks observed in the elastic scattering proton calibration data are also shown. They agree well with the values listed in Table II.

IV. Data Analysis

A total of 8.5 million triggers were recorded for incident beam momenta of 5^-, 5^+, 7^- GeV/c. For each beam momentum a single angle setting of the proton spectrometer was used in collecting the A_2 data. The data were obtained in five sets. The 5 GeV/c data were taken in a sequence of four runs of alternating beam polarity while the 7^- data were recorded in a single run. All of the events have been analyzed and data from different batches checked for consistency. About half the events survived geometric reconstruction.[12] In analyzing this data, further selections were made: 1) The production point of the event was restricted in order to exclude interactions from the target end windows and walls. 2) To exclude protons which had a nuclear interaction in the thick proton scintillator, a time-of-flight selection and energy and energy loss consistency were applied. 3) The position of the event in the entrance aperture of the proton counter was

TABLE IV

Measured Mass Resolutions

Proton Kinetic Energy 105 MeV to 155 MeV

$(.20 < |t| < .29)$

P_B (GeV/c)	5		7	
m (GeV)	1.3 (A_2)	.14(π)	1.3 (A_2)	.14(π)
$\Delta\theta$ (mr)	8.6 ± .4	8.0 ± .4	8.6 ± .4	8.0 ± .4
$\frac{\partial m}{\partial \theta} \cdot \Delta\theta$ (MeV)	13 ± .7		20 ± 1	
$\frac{\partial m^2}{\partial \theta} \Delta\theta$ (GeV^2)	.034		.052	
$\frac{\partial m^2}{\partial \theta} \cdot \Delta\theta$ (GeV^2)		.039		.055
ΔT (MeV)	5 ± 1	5 ± 1	5 ± 1	5 ± 1
$\frac{\partial m}{\partial T} \Delta T$ (MeV)	3.0 ± .5		1.0 ± .5	
$\frac{\partial m^2}{\partial T} \Delta T$ (GeV^2)	.008		.003	
$\frac{\partial m^2}{\partial T} \Delta T$ (GeV^2)		.028		.038
ΔP_B	54 ± 2	54 ± 2	61 ± 2	61 ± 2
$\frac{\partial m}{\partial P_B} \Delta P_B$ (MeV)	8.0 ± .4		6.4 ± .3	
$\frac{\partial m^2}{\partial P_B} \Delta P_B$ (GeV^2)	.021		.017	
$\frac{\partial m^2}{\partial P_B} \Delta P_B$ (GeV^2)		.003		.002
Δm (MeV)	16 ± 1		21 ± 1	
Δm^2 (GeV^2)	.041		.055	
Δm^2 (GeV^2)		.048		.067

restricted to a region slightly less than its physical size to insure that all the particle's energy would be deposited in the detector. 4) In order to have a direct comparison to the CMMS data[1], only those events in the $|t|$ range .20 to .29 were accepted. The fraction of events accepted by each of the selection criteria was determined for each of the data tapes (about 50,000 triggers per tape) and was found to remain constant. About 20% of the reconstructed events were accepted.[12]

The number of accepted events in the mass interval 1.25 to 1.35 GeV per incident pion was determined for each data tape. About 10% of the data tapes had a lower than average ratio and it was found that they had been recorded prior to the discovery of various equipment malfunctions. These were excluded from the analysis along with about an equal number for which the incident pion flux had not been recorded. For the remaining data the ratio was constant (within error) indicating that they were obtained under stable conditions.

In order to determine if the shape of the mass distributions remained constant, each block of data taken at a single value of the beam momentum was subdivided and values of χ^2 were obtained by comparing the mass distribution of each subset to that of the total sample. The χ^2's showed no systematic trend and their frequency distribution was as expected.

Mass distributions for each proton detector separately and for small intervals of the proton energy were obtained for each of the five sets of data. Corrections were made for the loss of events due to nuclear absorption in the proton detectors and for the geometrical detection efficiency. The correction factor has a broad maximum near 1.30 GeV and decreases by less than 15% in the interval 1.20 to 1.40 GeV.

The detection efficiencies were calculated assuming a production cross section of the form $d^2\sigma/dtdm = G(m)\, e^{(-B|t-t_m|)}$ where G(m) is the total cross section per unit mass for production of particles with an effective mass, m, and t_m is the minimum t possible for mass m. The value $B = 8\ (\text{GeV})^{-2}$, which approximates well the t dependence of all the data for $1.1 \leq m \leq 1.5$ GeV, was used in the calculations.

Fits to the final data showed that the A_2 mass, width, and the signal to noise ratio at a single value of the beam momentum, did not depend on the proton detector involved or on the proton energy (within errors).

To check the data selection criteria, the acceptance calculations, and to test for any angle dependent biases, the elastic scattering data where only a beam/proton coincidence was required were analyzed to obtain the t dependence and absolute cross section. The data is shown in Fig. 6 and in the $|t|$ range used in this experiment (.20 to .29 GeV^2). The agreement with data of Coffin et al., (Phys. Rev. 159, 1169 (1967)) is good.

V. Results

The A_2 mass distribution obtained at each value of beam momentum is shown in Figs. 7, 8, 9. The distributions contain at 5^-, 5^+, and 7^- about 28,000, 24,000, and 17,000 A_2 mesons above background. The statistical precision in the A_2 region is 2 - 3% per 5 MeV bin. Fits to the data have been made using a function consisting of a background term plus a resonance distribution which was folded with the experimental mass resolution. The data were fitted from 1.10 to 1.50 GeV in order to constrain the background to be smooth over the entire region. The form for the Breit-Wigner distribution was $B(M, M_o, \Gamma) = [(M - M_o)^2 + \frac{\Gamma^2}{4}]^{-1}$ and for the dipole was $D(M, M_o, \Gamma) \propto [BW(M_o, M, \Gamma)(M - M_o)]^2$.

The data were fitted with a Breit-Wigner, B, (or a dipole, D,) distribution plus a linear, L, or linear plus quadratic, Q, background. The number of degrees of freedom for the entire interval M = 1.1 - 1.5 GeV is 75 for the L fits and 74 for the Q fits. For each fit the χ^2 was determined from all points as well as for just the resonance region 1.22 to 1.38 GeV.

To investigate the consistency of the data with the dipole formula two different types of fits were used. In one, the dipole's width was fixed at 28 MeV, the value reported by the CMMS group[1] and the mass was allowed to vary to obtain the best fit. In the other, both the mass and width were allowed to vary. For this case, somewhat better fits were obtained. The results of these fits are shown in Table V and the χ^2 for various fits are shown in Fig. 10.

All the data agree well with a simple Breit-Wigner shape, regardless, of the form of the background assumed. In addition, at 5^-, 5^+ and 7^- GeV/c the A_2 mass and width are equal, within errors.

The apparent structure in the 5^- GeV/c data, Fig. 8, just below 1.3 GeV mass has been investigated by rebinning this data with the bin origins shifted by 2.5 MeV. Upon rebinning, the fluctuation is significantly reduced.

In Table V the $\Sigma \equiv (\chi^2_D - \chi^2_B)/(60)^{\frac{1}{2}}$ is the difference in χ^2 for the D and B fits for $1.22 \leq m \leq 1.38$ GeV divided by the approximate expected fluctuation in χ^2 for this mass interval. Σ is approximately equal to the number of standard deviations by which the data favors a Breit-Wigner fit over a dipole fit. This experiment yields a minimum Σ of 4 for the 7^- GeV/c data.

To investigate the significance of the disagreement between these results and the CMMS 6 and 7 GeV/c data[1], the 7^- GeV/c distribution (Fig. 9) was compared directly to that of CMMS. The data points in the region of the A_2 peak, $(1.29 \leq m \leq 1.31$ GeV$)$, differ by more than 7 standard deviations. Fig. 11 shows the data from the two experiments plotted together. Clearly the disagreement is only present at the peak of the A_2.

A special selection of 7^- GeV/c data was made in order to more closely approximate the conditions of the CMMS experiment. For this selection,

TABLE V

Results of the Fits. M_o, Γ, and R are the resonance mass, width, and signal to background ratio (at $M = M_o$) given by the fits. The uncertainties listed with M_o include the effects of possible systematic errors associated with determining this quantity. χ_T^2 and χ_R^2 are the total χ^2 for the regions M = 1.1 - 1.5 GeV and M = 1.22 - 1.38 GeV, respectively. For the definitions of Σ, D, B, L. and Q, see the text. $P(\chi^2_R)$ is the probability of observing a χ^2 larger than χ^2_R for 30 degrees of freedom.

Resonance and Background Distribution Used	Beam Momenta (GeV)	R	M_o (MeV)	Γ (MeV)	χ_T^2	χ_R^2	Σ	$P(\chi_R^2)$
B+L	5^-	0.79	1299 ± 6	105 ± 5	114	31		4×10^{-1}
D+L	5^-		1299 ± 6	26 ± 1	368	238	27	3×10^{-34}
D+L*	5^-		1298 ± 6	28*	374	252	29	6×10^{-37}
B+L	5^+	0.52	1300 ± 6	99 ± 5	94	27		6×10^{-1}
D+L	5^+		1300 ± 6	25 ± 1	271	79	20	4×10^{-23}
D+L*	5^+		1300 ± 6	28*	283	200	22	5×10^{-27}
B+L	7^-	0.89	1309 ± 4	103 ± 5	100	29		5×10^{-1}
D+L	7^-		1308 ± 4	27 ± 1	231	135	14	3×10^{-15}
D+L*	7^-		1308 ± 4	28*	231	138	14	9×10^{-16}
B+Q	5^-	0.82	1300 ± 6	118 ± 9	109	30		5×10^{-1}
D+Q	5^-		1298 ± 6	23 ± 1	243	114	11	1×10^{-11}
D+Q*	5^-		1298 ± 6	28*	281	166	18	9×10^{-21}
B+Q	5^+	0.61	1300 ± 6	113 ± 9	89	27		6×10^{-1}
D+Q	5^+		1301 ± 6	22 ± 1	195	94	9	2×10^{-8}
D+Q*	5^+		1299 ± 6	28*	234	146	15	3×10^{-17}
B+Q	7^-	0.81	1309 ± 4	96 ± 9	99	29		5×10^{-1}
D+Q	7^-		1309 ± 4	23 ± 1	138	58	4	2×10^{-3}
D+Q*	7^-		1308 ± 4	28*	159	87	7	2×10^{-7}

* For these fits the dipole width was fixed at $\Gamma = 28$ MeV.

data where one, two, or three charged particles were detected in a hodoscope which covered a large portion of forward direction (.30 sr.) were chosen. The result of fitting these data gave a Σ of about 12 in favor of the Breit-Wigner and does not differ significantly from the total 7^- GeV/c data.

To test the sensitivity of the results to the mass resolution, we have fitted the data with dipole distributions folded with resolutions larger than the measured value. To reduce Σ to three for the linear background fits, it would be necessary to increase the resolution at least a factor of two.

In summary, all results on the A_2 from this experiment are well described by a simple Breit-Wigner shape in disagreement with the findings of the CMMS group.

It is unlikely that the disagreement between the two experiments is either due to statistics or resolution.

FOOTNOTES AND REFERENCES

1. G. Chikhovani, M. N. Foccocci, W. Kienzle, C. Lechanoine, B. Levrat, B. C. Maglic, M. Martin, P. Shübelin, L. Dubal, M. Fischer, P. Grieder, C. Nef, Phys. Lett. 25B, 44 (1967).
2. For a summary of and for a list of references to the CMMS work and other A_2 experiments see P. Schübelin, Physics Today, Nov. 1970, 32. See also the reviews contained in Experimental Meson Spectroscopy, Baltay and Rosenfeld editors, Columbia Univ. Press, N.Y. (1970).
3. M. Aguilar-Benitez, et al., Phys. Lett. 29B, 62 (1969).
4. M. Basile, et al., Nuovo Cimento Letters 4, 838 (1970).
5. M. Alston-Garnjost, et al., Phys. Lett. 33B, 607 (1970).
6. G. Grayer, et al., Phys. Lett. 34B, 333 (1971).
7. K. J. Foley, et al., Phys. Rev. Lett. 26, 413 (1971).
8. All resolutions will be given as full width at half maximum (FWHM).
9. B. Gottschalk, Rev. Sci. Instr. 40, 22 (1969).
10. In this experiment, $t = -2m_p T$.
11. The multiple scattering was calculated using the theory of Nigam, Sundaresen, and Wu with the parameters given by R. Diebold (SLAC RD-11, 1967, unpublished). The material in the proton's path consisted of: hydrogen, 1.5×10^{-3} r.ℓ.; target container 1.39×10^{-3} r.ℓ; material between target and spark chamber wires, $.84 \times 10^{-3}$ r.ℓ. The resulting multiple scattering was increased by 10% to include the scattering in the spark chamber wires.
12. To check for possible bias in the software systems, the reconstruction and histogramming programs used were checked against other programs, independently written. Also they were tested with simulated events.

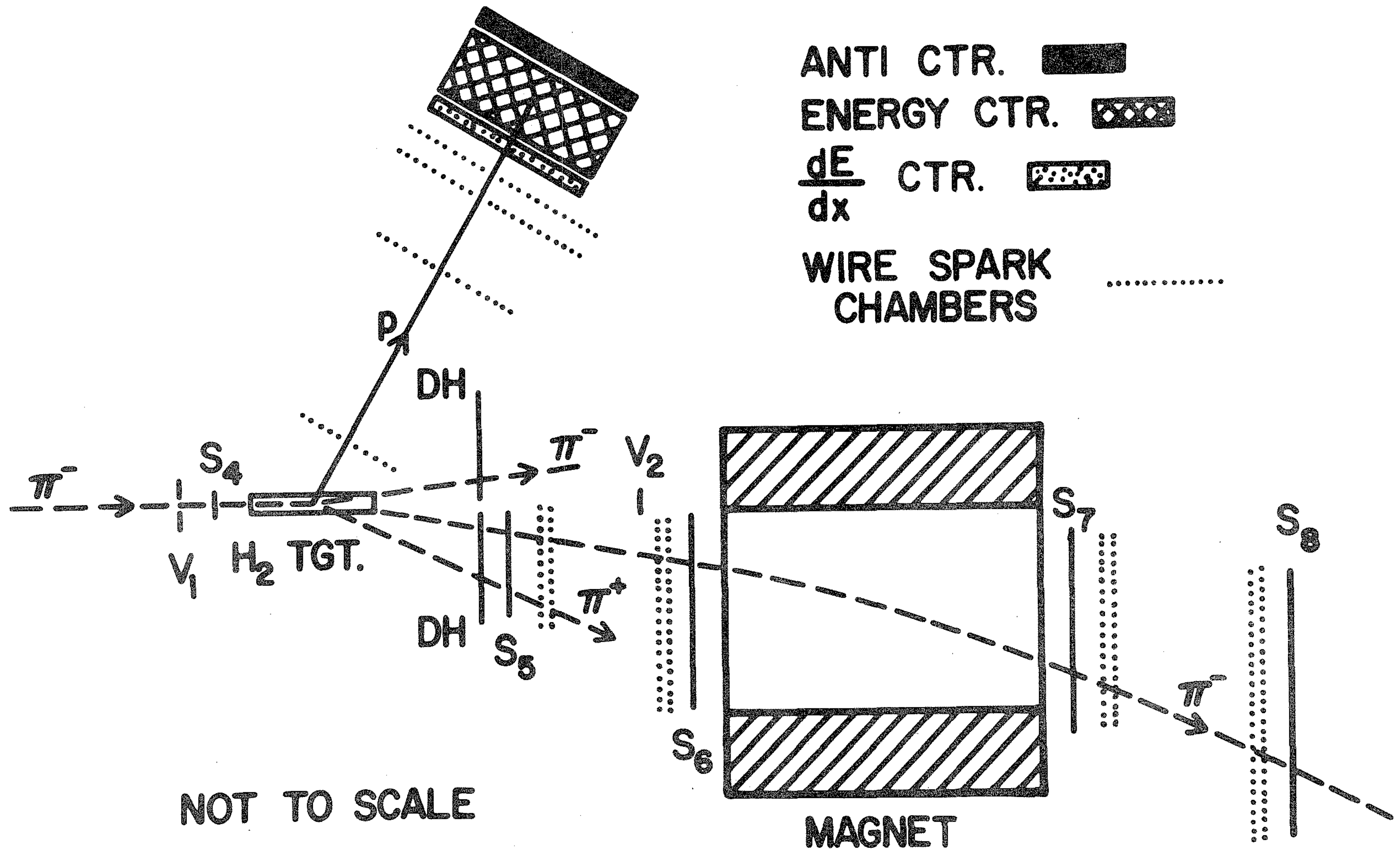
ANTI CTR. ■
ENERGY CTR. ▨
$\frac{dE}{dx}$ CTR. ▒
WIRE SPARK CHAMBERS ……………
π^-
V_1
S_4
H_2 TGT.
P
DH
DH
π^-
π^+
S_5
V_2
S_6
MAGNET
S_7
π^-
S_8
NOT TO SCALE

Figure 1: Experimental layout. The symbols S_1, S_2, . . . S_8 label aperture defining scintillation counters, V_1 and V_2 veto counters, and DH the decay hodoscope. The beam enters the apparatus from the left after traversing three beam hodoscopes and a threshold Cerenkov counter (not shown). For the charged boson missing mass data a beam/proton trigger was used.

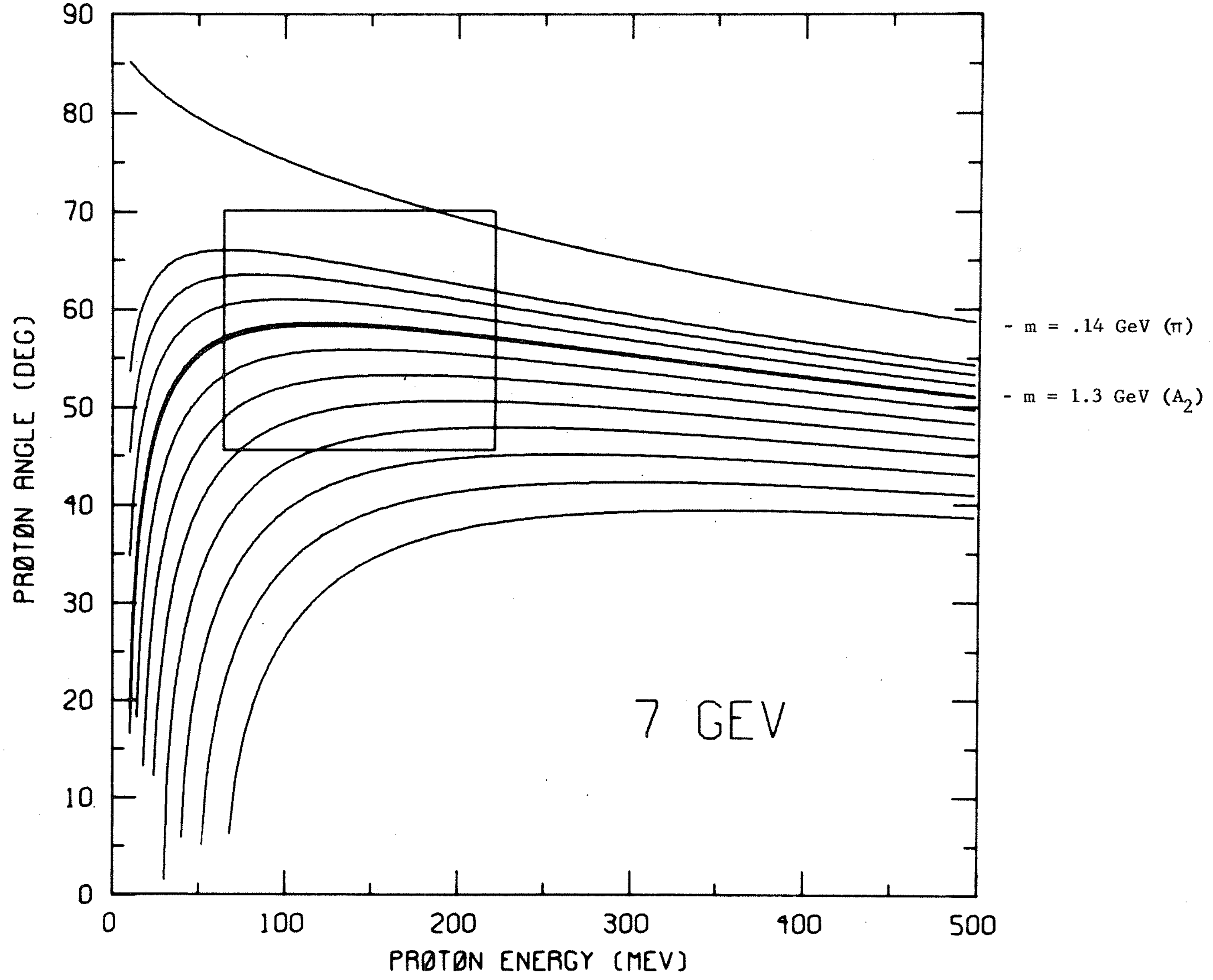

Figure 2: Missing mass kinematics at 7 GeV/c. The upper curve is for the elastic scattering reaction, the double curve is for a missing mass of 1.3 GeV. The other curves are for masses differing from 1.3 GeV in 100 MeV intervals. The approximate apparatus acceptance is shown by the rectangular box.

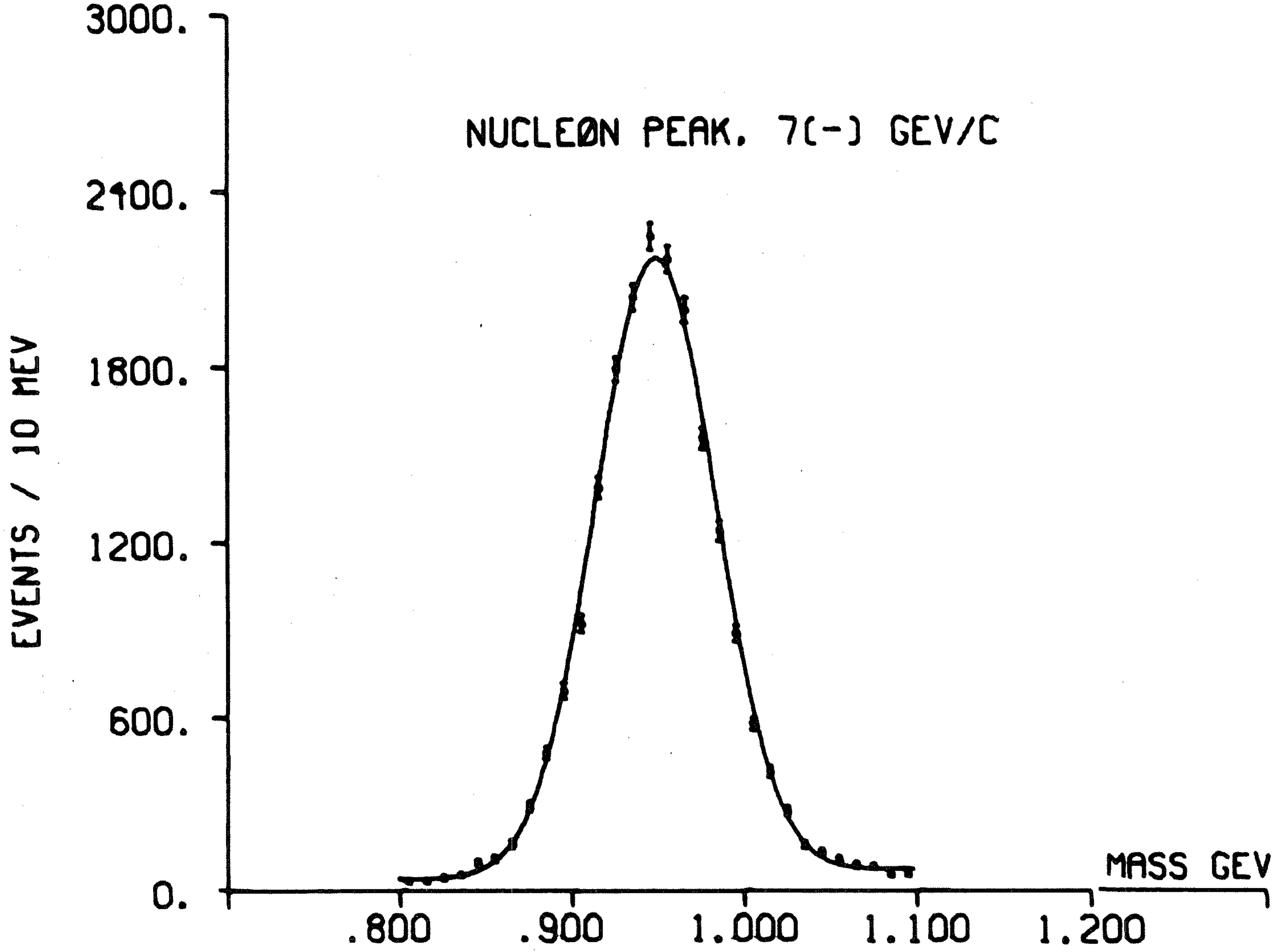

Figure 3: Beam momentum calibration data at 7^- GeV/c. The mass distribution was obtained from measurements of the scattered pion in the magnetic spectrometer and shows a peak from the reaction $\pi^- + p \rightarrow \pi^- + p$. These data required a beam/fast coincidence.

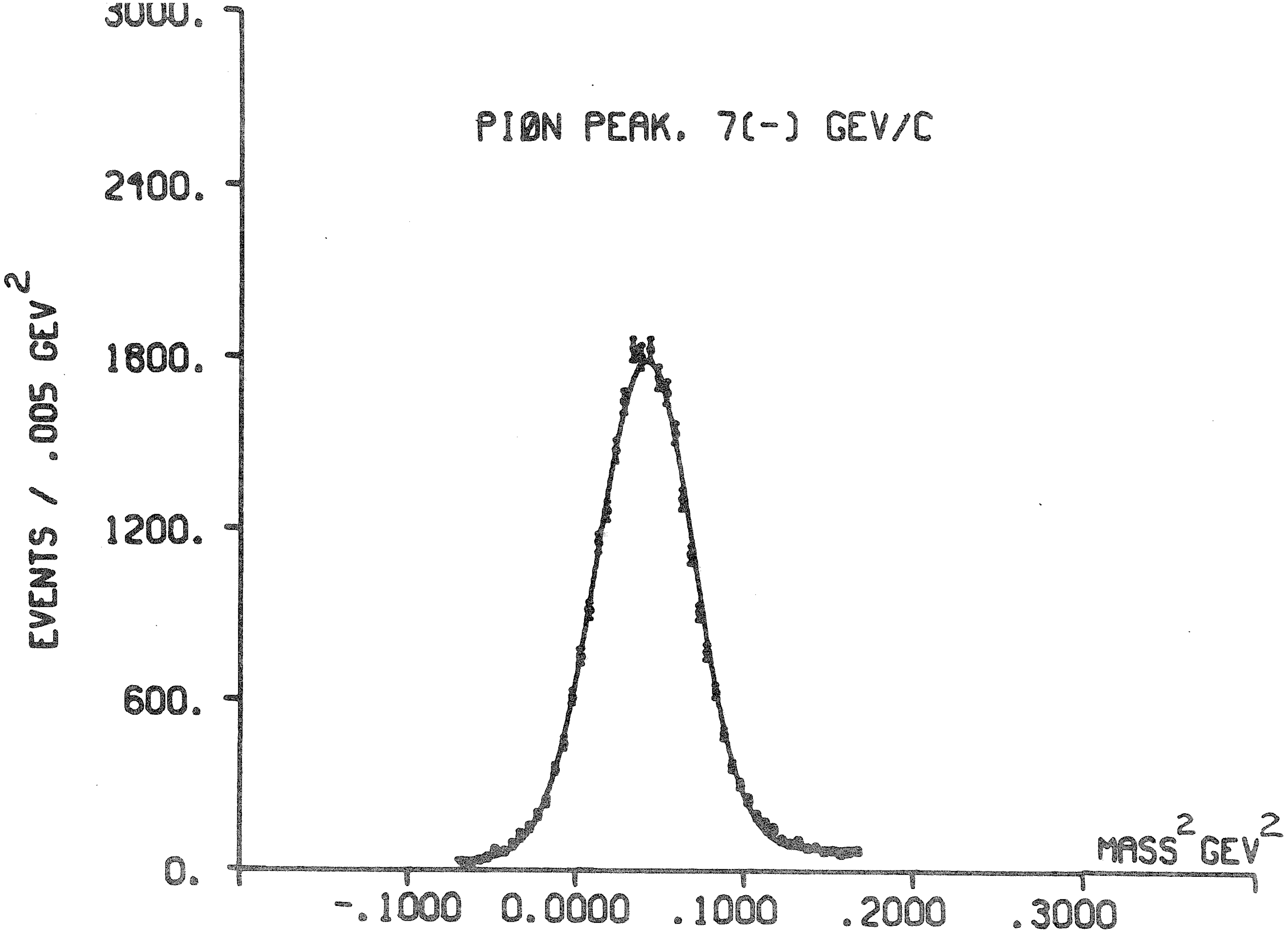

Figure 4: Proton energy calibration data taken at 7$^-$ GeV/c. The mass distribution was obtained from measurements of the recoil proton and shows a peak from the reaction $\pi^- + p \rightarrow \pi^- + p$. The data is plotted versus mass squared in order to avoid the artificial narrowing which would be present in a linear mass plot due to the effect of including data around zero mass. These data required a beam/proton trigger.

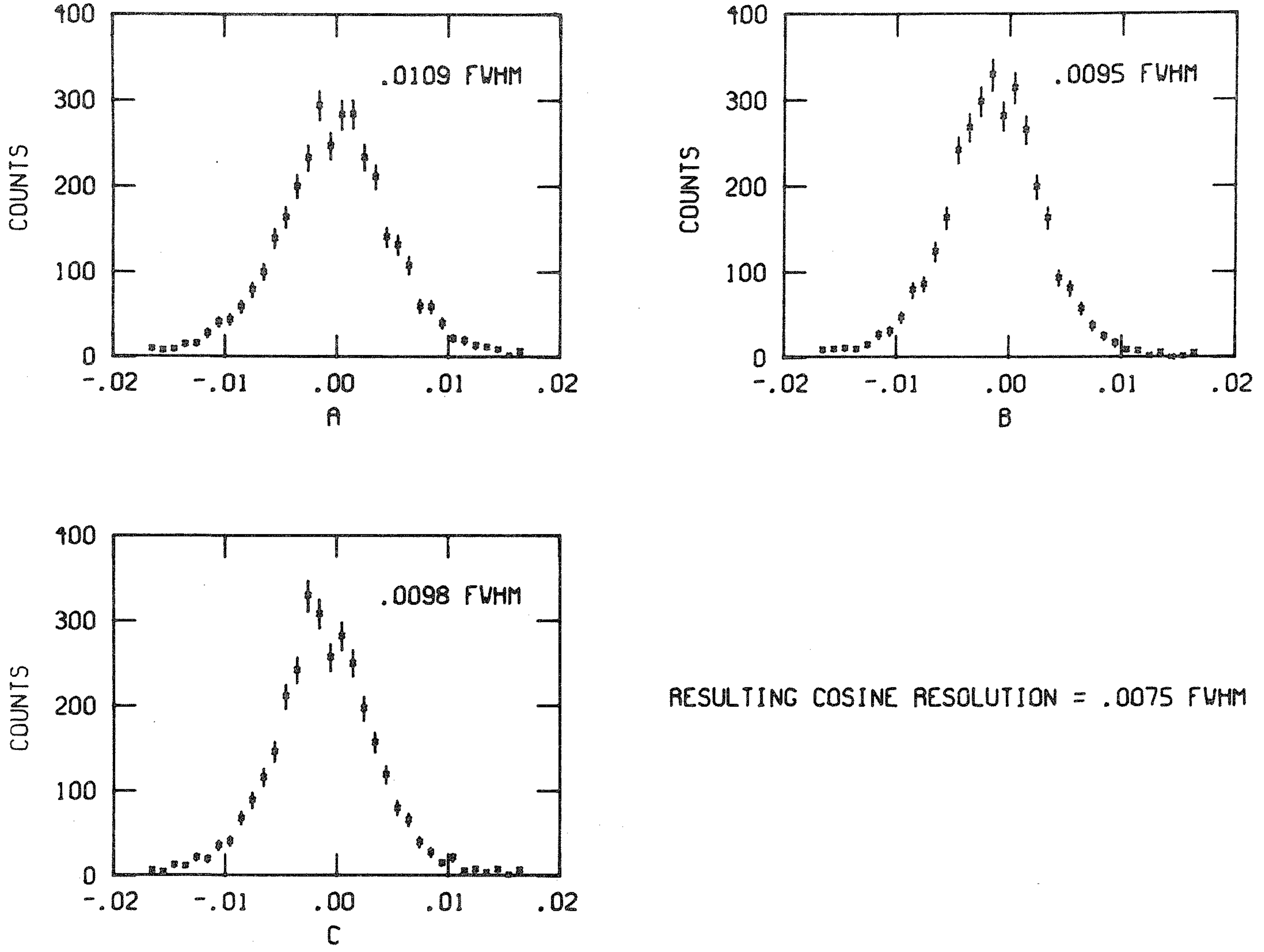

Figure 5: A trio of histograms for determining the angular resolution, Δ (cos Θ). Graph A shows the distribution for the quantity cos Θ_1 - cos Θ_m, B for cos Θ_2 - cos Θ_m, and C for cos Θ_2 - cos Θ_1. Cos Θ_1, cos Θ_2, and cos Θ_m are defined in the text. These data required a beam/proton/fast trigger.

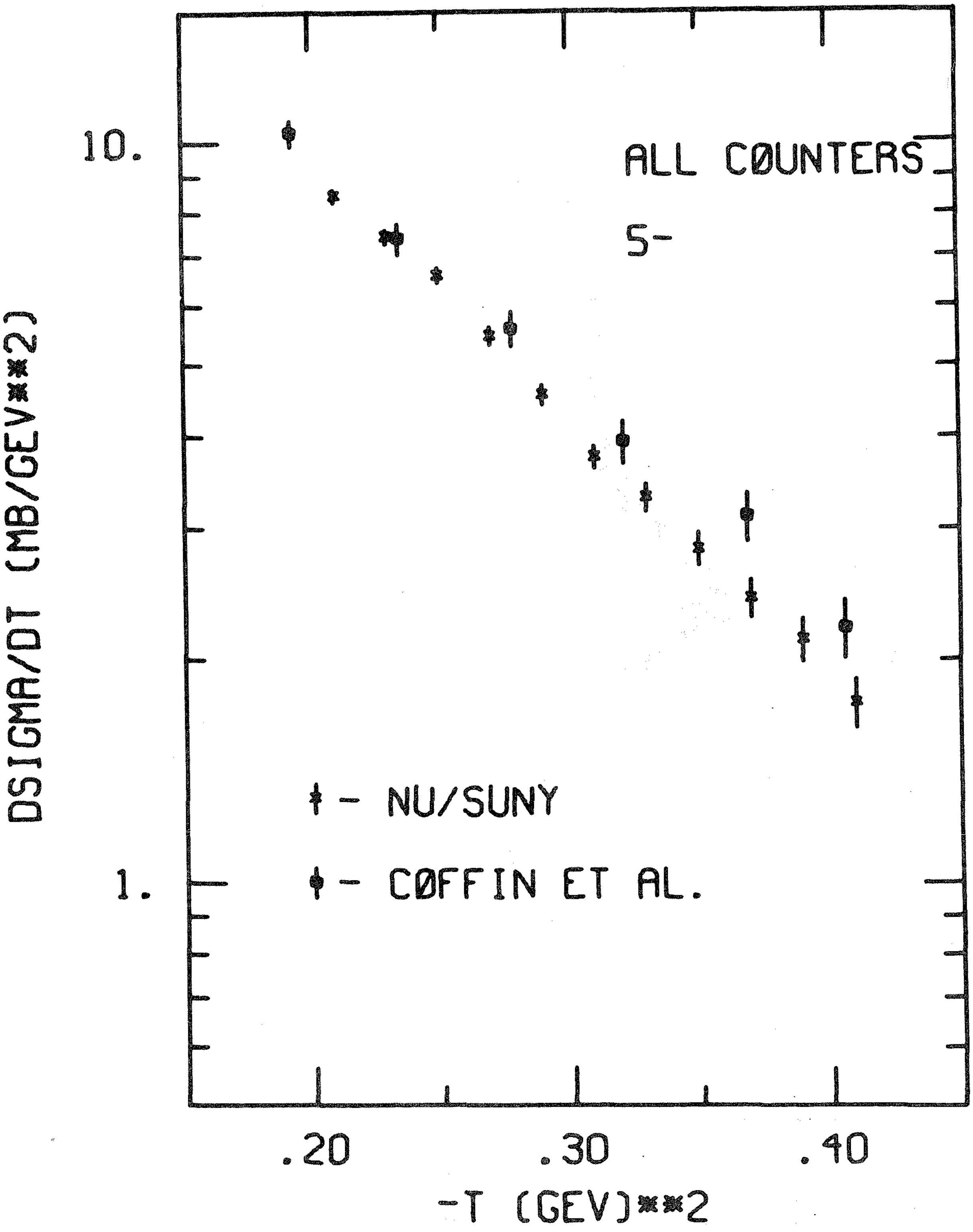

Figure 6: Elastic scattering cross section obtained from the calibration data compared with C. T. Coffin et al., Phys. Rev. 159, 1169 (1967). The NU/SUNY data for $|t| > 0.30$ has been corrected for decreases in detection efficiency of the ΔE counters for higher energy protons. This estimated correction factor varied between 1.1 and 1.3 in the $|t|$ range 0.3 to 0.4 GeV^2. The errors shown for these points include both statistics and an uncertainty arising from this correction.

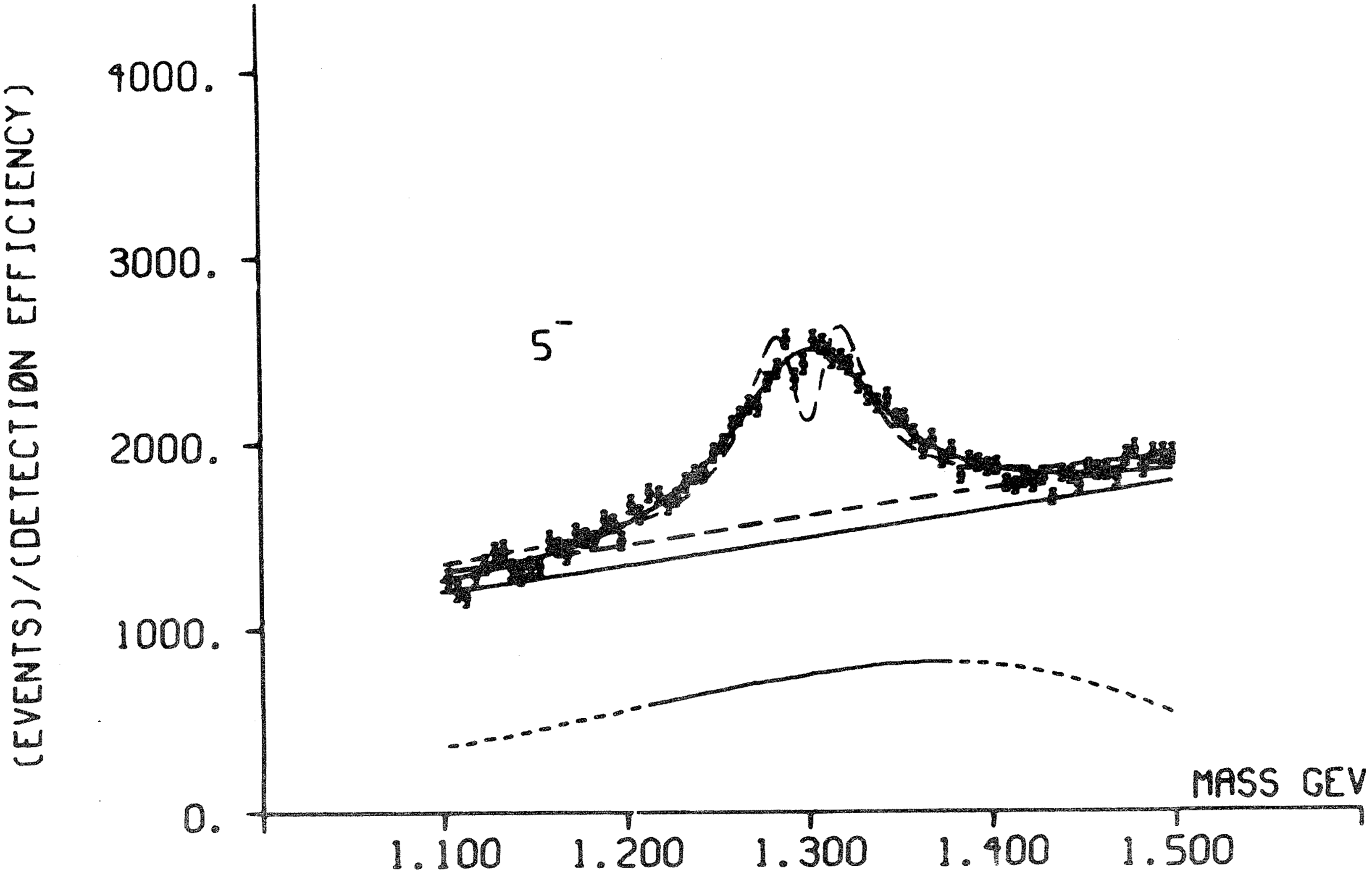

Figure 7: A_2 mass spectrum at 5^- GeV/c. The solid lines through the data are the Breit-Wigner fits, and the solid straight lines beneath the data are the associated fitted linear backgrounds. The dashed lines in the region of the data are the dipole fits (Γ dipole = 28 MeV, fixed) and their associated backgrounds. The calculated detection efficiencies vs. mass are shown (arbitrary units) as dashed lines (M = 1.10 - 1.22) and (M = 1.38 - 1.50 GeV) and as solid lines (M = 1.22 - 1.38 GeV). The detection efficiencies have been normalized so that at M = 1.300 GeV the ordinates indicate the actual number of events detected per 5 MeV bin.

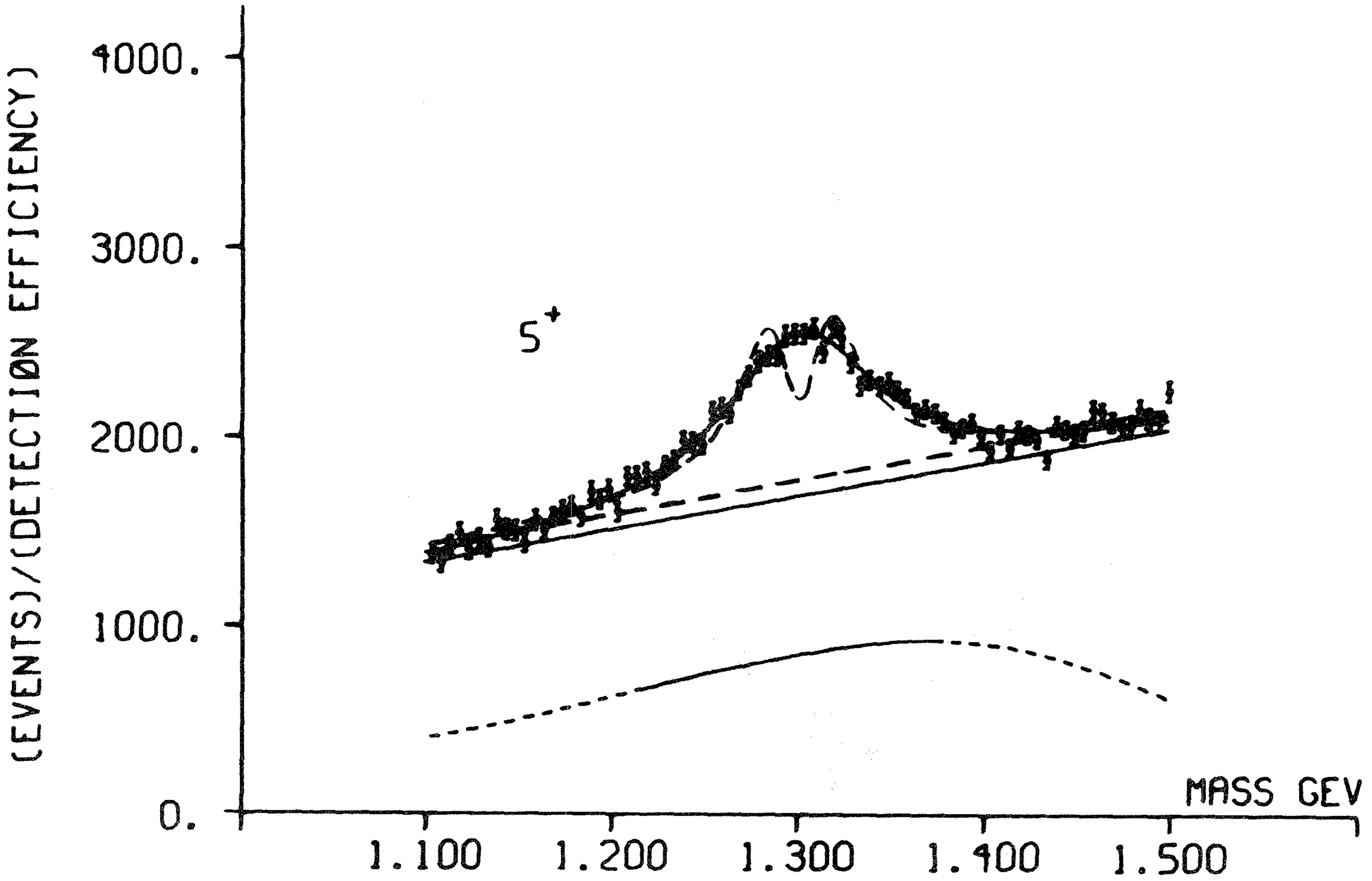

Figure 8: A_2 mass spectrum at 5^+ GeV/c. For further details, see the caption of Figure 7.

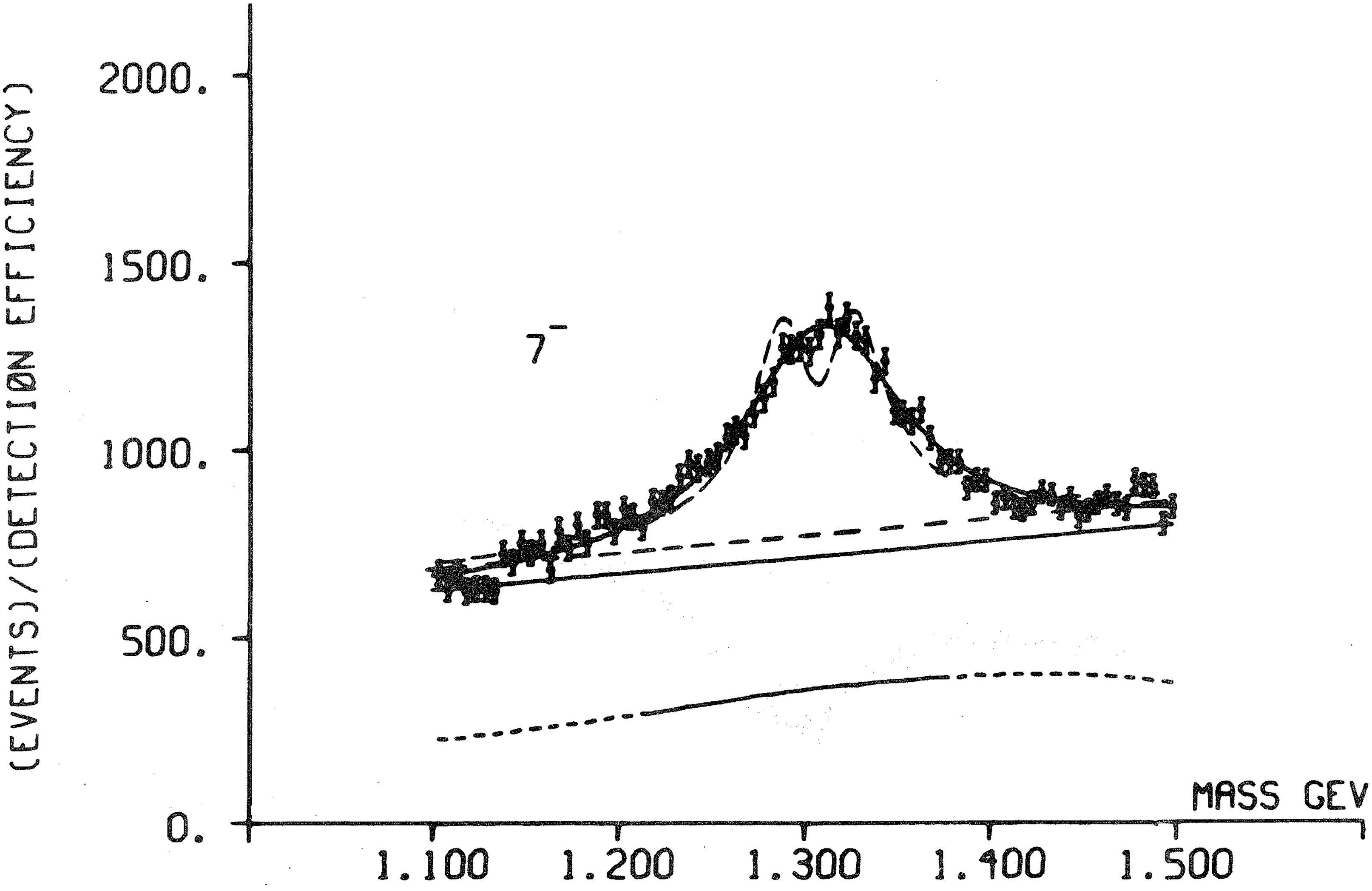

Figure 9: A_2 mass spectrum at 7^- GeV/c. For further details see the caption of Figure 7.

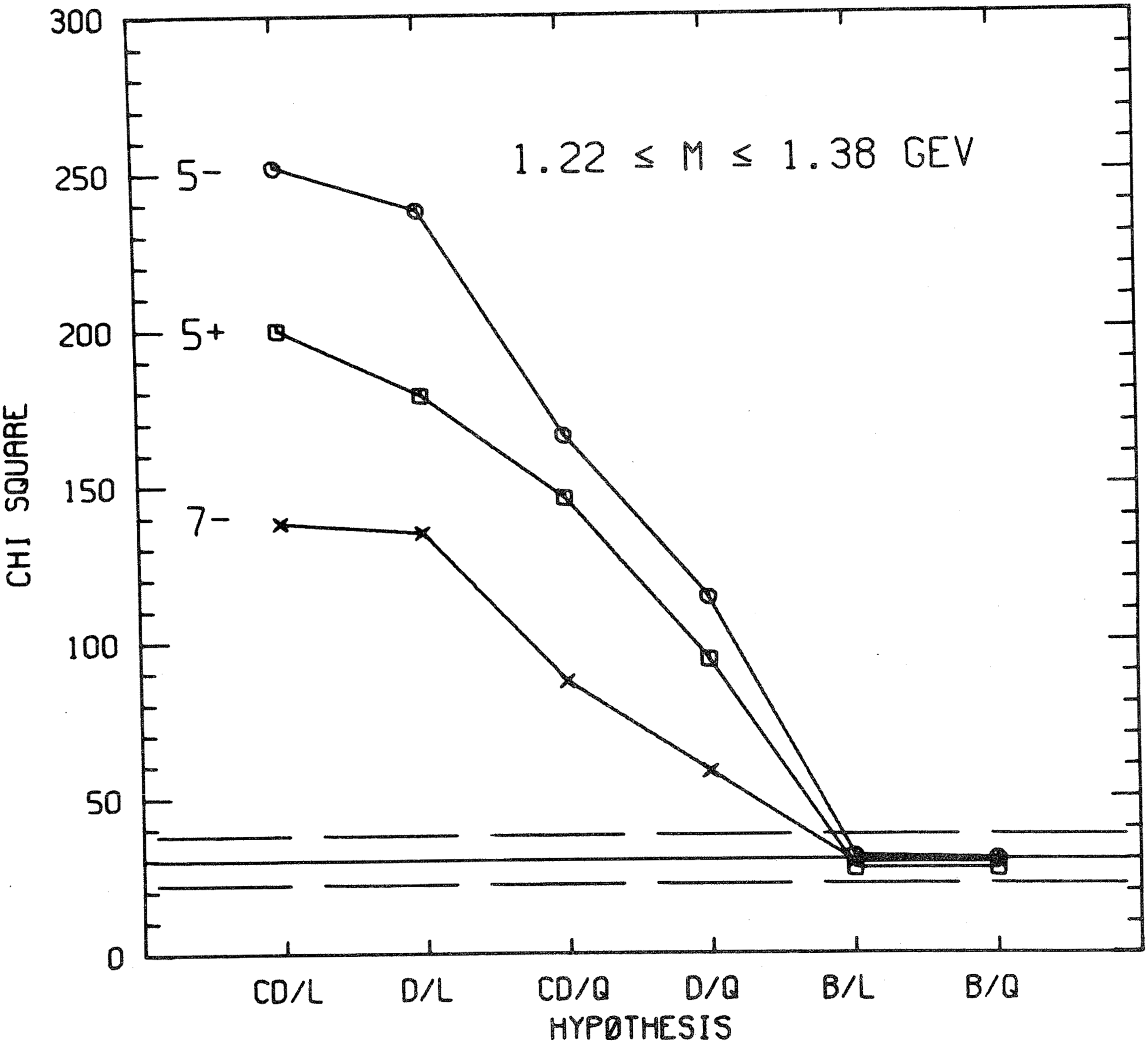

Figure 10: Summary of χ^2 for the mass region $1.22 \leq m \leq 1.38$ GeV for various hypotheses. The resonance distribution assumed in the fit is denoted by the first symbol, where CD is the dipole formula with a 28 MeV width, D the dipole with the width as a free parameter, and B the Breit-Wigner. The assumed form of the background is indicated by the symbol after the slash and L represents a linear background and Q a linear plus quadratic background. The solid line at $\chi^2 = 30$ is the most probable value of χ^2 and the dashed lines are one standard deviation above and below the most probable value.

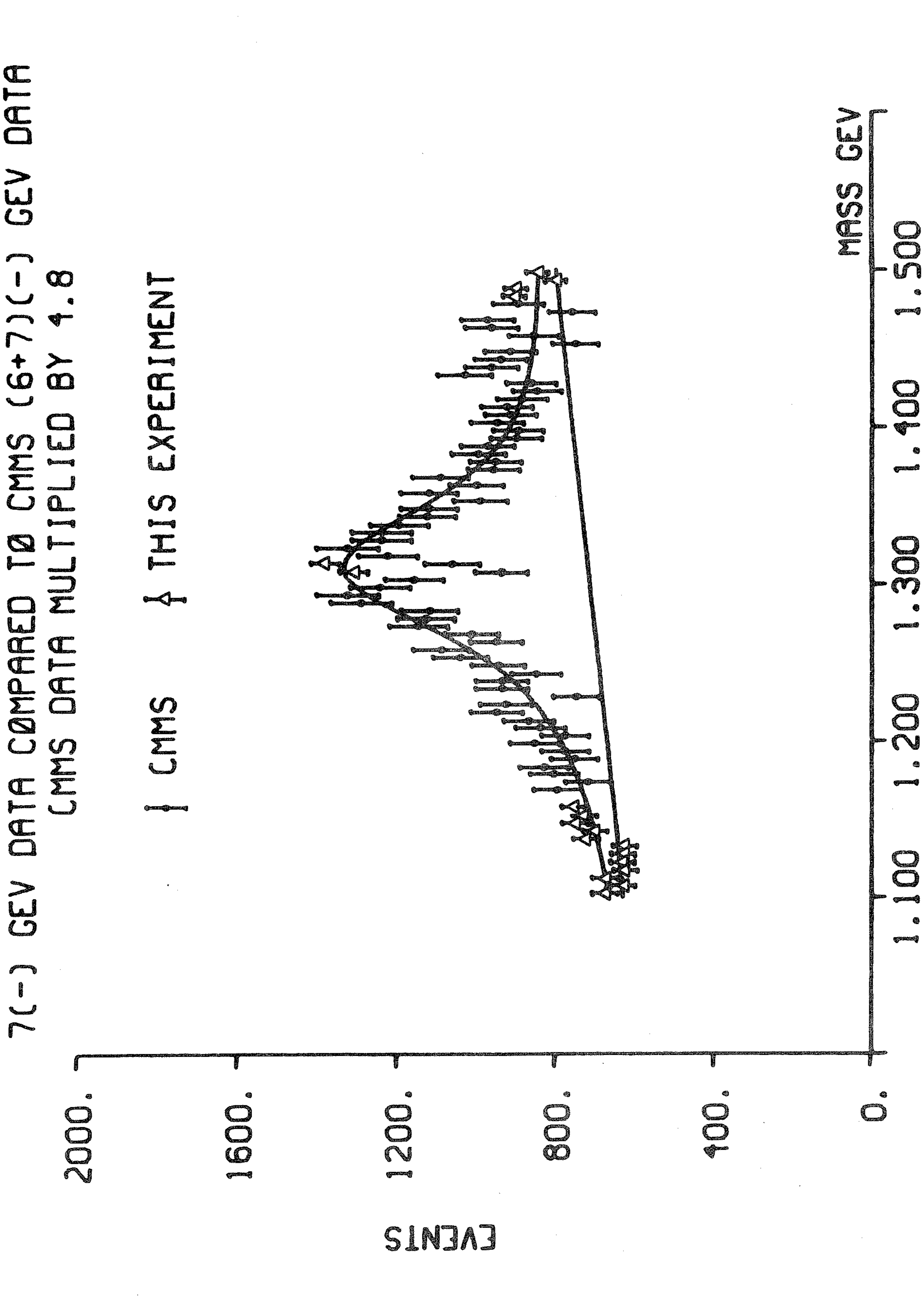

Figure 11: Comparison of the 7^- GeV/c data of this experiment to the CMMS data. The Breit-Wigner and linear background shown are those determined by the data of this experiment. For the sake of clarity only a few of our data points are included. The CMMS data has been shifted by +10 MeV for purposes of comparison.

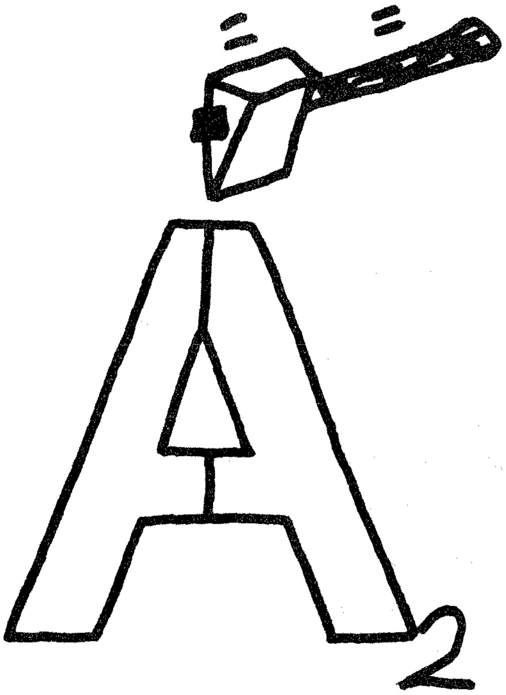

THEORETICAL REMARKS ON THE A_2 MESON[*]

Jonathan L. Rosner

School of Physics and Astronomy
University of Minnesota
Minneapolis, Minnesota 55455

---

[*] Work supported in part by the U.S. Atomic Energy Commission through Contract No. AT-(11-1)-1764.

Contents

I. Introduction. 389

II. Features of the unsplit A_2. 390

III. Production mechanism in $\pi N \to A_2 N'$. 391

- A. Isospin structure. 392
- B. Density matrices. 394
- C. Further experimental questions. 396

IV. A_2 Resonance shape. 398

- A. Two-peak hypothesis. 400
- B. Broad-narrow model. 401
- C. Effects of resolution. 404

V. Conclusions. 405

References. 407

I. Introduction.

The source of recent interest in the resonance shape of the A_2 meson was the report of a two-peak structure[1,2] observed in the missing-mass spectrum of X^-, $m(X^-) \simeq 1300$ MeV, in

$$\pi^- p \to A_2^- p \qquad (1)$$

for $p_{\pi^-} = 6$ and 7 GeV/c. Since 1967, when the effect was first considered to be statistically significant,[2] additional experiments under different conditions have given conflicting results.[3,4] The results of the first attempt to repeat the exact experiment of ref. 2 have been announced at this conference,[5] and they fail to confirm the effect.[5,6]

Given the parameters that one thinks are important in (1) - the beam momentum, and the angle, multiple scattering, and final momentum of the recoil proton, etc. - as quoted in refs. 1-2 ("CERN") and 5-6 ("Northeastern-Stony Brook" or "NE-SB"), the two sets of data contradict one another.[6] However, some models for the two-peak structure are more sensitive than others to variations in these parameters away from their quoted values. For this reason it may be useful to recall some theoretical aspects of the A_2 and its possible substructure despite the feeling on the part of many physicists that the splitting[2] may be irreproducible.

The role of the unsplit A_2 in our picture of the strongly interacting particles will be treated in section II, with particular regard to SU(3) properties. We shall discuss A_2 production mechanisms (sec. III) since one seems to have learned a great deal about them in recent high statistics experiments. Any discussion of possible splitting would require such information, as the effect is certainly dependent on s and probably on t if it is present at all.

Section IV deals with some experimental results on the splitting and their interpretation. We suggest that any further experiments to look for A_2 substructure reject the dipole[7] hypothesis in favor of the (much more demanding) possibility of the interference of a broad

($\Gamma \simeq$ 90 MeV) state with a narrow one ($\Gamma \simeq$ 5 MeV). Section V contains our conclusions.

II. Features of the unsplit A_2.

The existence of the A_2 was inferred[8] from arguments similar to considerations of exchange degeneracy.[9] (The K^{**} was also predicted in this manner). The broad "A" peak was clearly resolved into what we now call the A_1 and the A_2 fairly early.[10] Observation of K^-K^o, $K_S^oK_S^o$, and $(3\pi)^-$ modes near the same mass (1310 MeV) suggested the existence of a 2^+ resonance there, while the lower mass "A_1" effect has continued to elude unambiguous identification as a resonance.[11]

The A_2 appears to form a nonet with the other 2^+ resonances $f_o(1260)$, $K^{**}(1420)$, and f'(1515).[12] Recent experiments have been published on branching ratios of the (unsplit) A_2[13] and the K^{**}.[14] These new numbers have been used in a comparison of decay rates for $2^+ \to 1^-0^-$ and $2^+ \to 0^-0^-$ based on SU(3). From the observed partial widths, one derives reduced amplitudes[15,16] $\tilde{D}_i^{\,2}$ based on the expression

$$\tilde{D}_i^{\,2} = (M_i^{\,2}/p)(p_o/p)^4 \ \Gamma_i/C_i \tag{2}$$

where M_i is the mass of the decaying resonance, p is the 3-momentum of either decay product in the CM, p_o is an arbitrary constant taken to be 0.5 GeV/c for normalization, Γ_i is the partial width for the decay process i, and C_i is the square of an appropriately defined Clebsch-Gordan coefficient. The values of $\tilde{D}_i^{\,2}$ are shown in Fig. 1.[17] The two halves of this figure should lead to two independent consistent values of $\tilde{D}_i^{\,2}$ for couplings obeying SU(3), and to a single value of $\tilde{D}_i^{\,2}$ for various SU(6)-like models.[16,18,19]

One sees reasonable agreement with SU(3) and some possible deviation from SU(6) in the same direction as for the coupling ratio $(1^- \to 1^-0^-)/(1^- \to 0^-0^-)$.[20] As already noted,[21] to preserve SU(3) one would be reluctant to tamper with some of the partial widths in Fig. 1 too much without reestimating others as well. This would have been the case if (say) half of the A_2 peak had been ascribed to some other state not related to the f, K^{**}, and f'.

The A_2 is often described as a $^3P_2$ state of a quark (q) and an antiquark ($\bar{q}$).[22-26] If the $q\bar{q}$ spectrum is roughly that of a harmonic oscillator, $^3P_1$, ^3P_o, and $^1P_1$ $q\bar{q}$ states lie somewhere nearby in mass. One has reasonable candidates for all but a handful of these states.[24-26] Furthermore, there appear to be no additional P = + mesons[27] below 1.5 GeV, indicating little distortion of the harmonic oscillator sequence[23,24]

$$\begin{array}{lccccccccc} & n=0 & & n=1 & & n=2 & & n=3 & & \\ q\bar{q}: & L=0 & < & L=1 & < & L=2,0 & < & L=3,1 & < \cdots & (3) \\ & P=- & & P=+ & & P=- & & P=+ & & \end{array}$$

a fact of interest in connection with mechanisms for possible A_2 splitting.[26] In this respect, two states bear watching:

(a) The E(1420), if 0^-,[28] indicates some depression of the masses of the first radially excited states (n = 2, L = 0).

(b) The J^P assignment 1^+ has not been ruled out for the I = 1 $F_1(1540)$,[29] produced in $\bar{p}p$ annihilations. This state would have to come from the n = 3 group in eq. (3), if the A_1 and B were to fill the similar n = 1 slots as is usually assumed.[24-26]

Claims[4,30] for additional low-lying states with ordinary I, Y, and J^{PC} but which strain the scheme (3) would be every bit as important as the discovery of low-lying "exotic" mesons,[31] against which there is considerable evidence.[30] For the time being, the $q\bar{q}$; L picture seems as good as any other for classifying the broad, easily-observed low-lying mesons.

III. Production mechanism in $\pi N \rightarrow A_2 N'$.

The A_2 can be produced in the following pion-induced reactions with a recoil nucleon:

$$\pi^- p \rightarrow A_2^- p \tag{4a}$$

$$\pi^+ p \rightarrow A_2^+ p \tag{4b}$$

$$\left.\begin{array}{l} \pi^+ n \rightarrow A_2^o p \quad (4c) \\ \pi^- p \rightarrow A_2^o n \quad (4d) \end{array}\right\} \text{identical by isospin}$$

In the best-studied of these, process (4a), the mechanism suggested by all data above 5 GeV/c is f_o and ρ exchange, with f_o accounting for at least 75 per cent of the cross section at high energies, and with little coherence between the two. In addition there appears to be some evidence for B exchange at lower energies. Furthermore, present data do not rule out a small contribution from an I = 0 trajectory with intercept greater than 1/2. We now discuss the evidence.

A. Isospin structure of exchanges.

One may write, summing over t-values and helicity amplitudes i,

$$\sigma(A_2^{\pm}) = \sum_i |M_i^{(0)}|^2 + \sum_i |M_i^{(1)}|^2 + \pm 2 \sum_i \mathrm{Re}\,(M_i^{(0)*} M_i^{(1)}) \tag{5}$$

$$\sigma(A_2^o) = 2\sum_i |M_i^{(1)}|^2 \tag{6}$$

where the A_2 charge state refers to the appropriate reaction (4), and the superscript refers to the exchanged isospin. Then

$$\sigma_1 \equiv \sum |M_i^{(1)}|^2 = \sigma(A_2^o)/2 \tag{7}$$

$$\sigma_0 \equiv \sum |M_i^{(0)}|^2 = [\sigma(A_2^+) + \sigma(A_2^-) - \sigma(A_2^o)]/2 \tag{8}$$

Furthermore, one can define a coherence fraction f_c ($|f_c| \leq 1$) by

$$f_c \equiv \frac{\mathrm{Re}\sum_i M_i^{*(0)} M_i^{(1)}}{\sqrt{\sum_i |M_i^{(0)}|^2}\sqrt{\sum_i |M_i^{(1)}|^2}} = \frac{\sigma(A_2^+) - \sigma(A_2^-)}{4\sqrt{\sigma_0\sigma_1}} \qquad (9)$$

The value of f_c can be close to 0 for many reasons ($I_t = 0$ and $I_t = 1$ 90° out of phase for given i; $M_i^{(0)}$, $M_j^{(1)}$ nonzero only for $i \neq j$, etc.), so that deviations from 0 would be a stringent restriction on exchange models.

A comparison of σ_1 and σ_0 has been carried out at 5 and 7.5 GeV/c;[32] from this work it is also possible to estimate f_c. The results are shown in Table I. The cross sections represent only those for $A_2 \to 3\pi$, with the $A_2^{\pm}$ cross sections based on $A_2^{\pm} \to \pi^+\pi^{\pm}\pi^-$ and multiplied by 2 for the unseen $\pi^{\pm}\pi^0\pi^0$ modes.[33]

Table I. Comparison of A_2 production cross sections at 5 and 7.5 GeV/c. (From Ref. 32). Reactions (4a-c).

	$p_L = 5$	$p_L = 7.5$
$\sigma(A_2^+, \mu b)$	146±24	94±16
$\sigma(A_2^-)$	124±12	88±12
$\sigma(A_2^0)$	112±28	50±15
σ_1	56±14	25±8
σ_0	79±20	66±12
$R=\sigma_0/(\sigma_0+\sigma_1)$	.59±.11	.72±.10
$\sigma(A_2^+)-\sigma(A_2^-)$	22±29	6±20
f_c	.08±.13	.04±.14

Table I shows that:

(i) σ_0 is dominant already at 5 GeV/c and perhaps more so at 7.5.

(ii) σ_1 is non-negligible at both momenta.

(iii) No coherence between I_t=0 and I_t=1 amplitudes can be demonstrated.[32] This conclusion is strengthened by the study[32] of 2^+-1^+ interference, in which the I_t=0 amplitude for A_1 production and that for A_2 production display a large amount of coherence. No such coherence is seen between $I_t=0(A_1)$ and $I_t=1(A_2)$.

The $I_t=0$ amplitude probably becomes even more important relative to $I_t=1$ at higher energies. A comparison of reactions (4a) and (4c) at various energies[34] indicates that some portion of the $I_t=1$ amplitude is probably vanishing more rapidly than one would expect from pure ρ exchange. This comparison is shown in Fig. 2. Even if one were to fit both sets of data with an effective $1/p_L$ fall-off, however, one would expect $\sigma(A_2^0) \lesssim \sigma(A_2^-)/2$, and, assuming incoherence[32] to hold in general, one has $2\sigma_1 \lesssim (\sigma_1+\sigma_0)/2$ or

$$\sigma_1 \lesssim \sigma_0/3 \tag{10}$$

the result quoted earlier.

The best fit to reaction (4c) favors a fall-off more as p_L^{-2},[34] suggestive of a large contribution from a lower-lying trajectory such as B.[37] If this is the case, I=0 exchange becomes even more dominant in reaction (4a) at high energies.

The horizontal line in Fig. 2a shows that a leveling off of the cross section for (4a) cannot be excluded. Again, this would augment the dominance of $I_t=0$ at high energies.

B. Density matrices.

Above 5 GeV/c, reactions (4a) and (4b) seem to lead to A_2 with $J_z = \pm 1$ in its rest frame (z-axis: incident pion direction $\hat{q}$; y-axis: $\hat{p}'\times\hat{q}/|\hat{p}'\times\hat{q}|$ where $\hat{p}'$ is the direction of the recoil proton.[39] This is the "t-channel" or "Gottfried-Jackson" helicity system.) A compilation of density matrices for these reactions, averaged over t,[40] is shown in Table II and Fig. 3.

The figure shows a tendency toward $\rho_{11} \simeq \rho_{1-1} \simeq 1/2$ at high energy, a fact which favors *natural parity exchange*.[58,59]

At lower energies the indications of nonzero ρ_{00} would require the exchange of some unnatural parity trajectory. If this were to be the B(as expected; see Ref. 37) a large ρ_{00} should occur in the *charge-exchange reactions* (4c-d) at similar energies.

Table II. A_2 density matrices (Gottfried-Jackson system) in $\pi^{\pm}p \to A_2^{\pm}p$.

π^+	p_L	Ref.	Mode	ρ_{oo}	ρ_{11}	ρ_{22}	ρ_{1-1}
	3.7	42	$\eta\pi^+$	.15±.12	.42±.06	.00±.06	.20±.11
	5	43,41	$(3\pi)^+$	.03±.07	.45±.06	.03±.07	.16±.07
	5.4	44,41	$(3\pi)^+$	.09±.06	.46±.03	(set=0)	.37±.07
	"8"	45,41	$(3\pi)^+$	.04±.07	.42±.06	.06±.06	.42±.09
π^-							
	4.5	46	$K^-K_S^o$	.19±.05	.34±.03	.06±.04	.24±.04
	5	47,41	$(3\pi)^-$	.10±.05	.43±.04	.02±.05	.36±.05
	7	48,41	$(3\pi)^-$	.12±.11	.38±.08	.06±.10	.31±.10
	7	49,50	$K^-K_S^o$	$\leq$ .07	.45±.02	.05±.02	.37±.05
	7.5	47,41	$(3\pi)^-$	.06±.07	.44±.05	.03±.06	.33±.07
	5-16	53	$\eta\pi^-$	.11±.13	.48±.06	.03±.06	.49±.10
	11	54,41	$(3\pi)^-$	.08±.13	.40±.11	.06±.13	.34±.15
	13	55,41	$(3\pi)^-$	.05±.16	.44±.17	.04±.20	.35±.17
	"17"	56,41	$(3\pi)^-$	.09±.07	.43±.06	.03±.07	.38±.07
	17.2	35	$K^-K_S^o$	$\simeq$ 0	$\simeq$ .5	$\simeq$ 0	$\simeq$ .5
	20	55,41	$(3\pi)^-$	.04±.17	.41±.14	.06±.15	.35±.15
	25	34,57,41	$(3\pi)^-$	.07±.32	.39±.27	.08±.33	.36±.34

The suppression of ρ_{22} is a feature[59] which may be understood by a simple argument based on exchange degeneracy. Consider the process

$$\pi^+\pi^+ \rightarrow A_2^+\pi^+ \qquad (11)$$

which involves f_o and ρ exchange in the t channel. The s channel is exotic, so one expects the imaginary parts of the f_o and ρ exchange contributions to cancel. Consider the amplitude for (11) with A_2 t-channel helicity 2. It cannot have a ρ pole, so that the ρ residue must have a zero at $t = m_\rho^2$. By exchange degeneracy, then, so must the f_o residue. Since no such zero is required in $\pi^+\pi^+ \rightarrow \pi^+\pi^+$, factorization tells us this must be a property of the π-A_2-f_o coupling.

In processes (4a-b), one thus has a zero of ρ_{22}/ρ_{11} at $t = m_\rho^2$. Kinematics also gives a zero of order t of this quantity at t = 0. Assuming any sort of smooth behavior, one thus cannot expect ρ_{22}/ρ_{11} to be very large in the range of t ($t \gtrsim - 0.6(\text{GeV/c})^2$: see, e.g., Refs. 46, 47) for which A_2 production is appreciable.

The expectation of small ρ_{22} is confirmed in a simple model[60] for process (11) based on beta functions, in which,[61] as $s \rightarrow \infty$,

$$\frac{\rho_{22}}{\rho_{11}} \rightarrow \frac{-3t}{2}\left[\frac{1-2t}{3-4t}\right]^2 \qquad (12)$$

(units $2m_\rho^2 = 1$). This expression is quite small for the t range mention above, so that ρ_{22} would be essentially undetectable if a similar suppression held for processes (4a,b).

C. Further experimental questions.

The data discussed above, as stated at the outset, point to a picture of f_o-ρ exchange, with $\sigma_o \gtrsim 3\sigma_1$ at high energies and little coherence between I_t=0 and I_t=1 amplitudes. However, several interesting points could probably be cleared up with somewhat better data.

1. Magnitude of $\rho_{oo}\frac{d\sigma}{dt}$: is there evidence for B exchange? The

data of Refs. 46 and 47 show some evidence for a variation in ρ_{oo} with respect to t, but it is not even clear whether this quantity is larger for small $|t|$[46] or large $|t|$[47]! As suggested above, a study of reactions (4c,d) is probably the best way to see the effects of B exchange, but density-matrix analyses are technically more difficult: the $K\bar{K}$ mode comes from f_o as well as A_2^o, while $\eta\pi^o$ is hard to identify. One must then perform an analysis of the type in Ref. 47 (combined normal-to-production-plane[62] and Dalitz plot[63] analysis) on the $\pi^+\pi^-\pi^o$ mode. This presents no problem in principle; statistics would be the only limitation.

2. Possible π-B-A_2 coupling giving rise to $A_2^o \rightarrow \omega\pi^+\pi^-$. This decay would proceed via a virtual B and/or a virtual ρ. It should be present if the π-A_2-B coupling is of any importance.[64]

3. Energy dependence of σ_1 and σ_o. Does σ_1 continue to fall as p_L^{-2}? Does σ_o flatten out? (see Fig. 2). Both questions require high statistics at higher energies, and have interesting consequences. If σ_1/σ_o continues to fall, the ρ-f_o picture is called into question, with either (a) sizeable B contributions, or (b) an I = 0 exchange with $\alpha(0) > 1/2$. The latter might indicate a violation of the selection rule[65] for "diffraction dissociation":

$$P_f = P_i(-)^{J_f - J_i} \tag{13}$$

at a very small cross section level; the rule seems rather good in general.

4. Interference of f_o and A_2 in $K_S^oK_S^o$ and K^+K^- modes. This effect has received previous theoretical attention,[66] but a point of particular interest is the study of the mass spectrum arising from unnatural parity exchange in reactions like

$$\pi^- p \rightarrow (f_o, A_2^o)\, n \qquad \begin{cases} \rightarrow K^+K^- \\ \rightarrow K_S^oK_S^o \end{cases} \tag{14}$$

This requires good statistics, of course, but the measurement of a quantity such as

$$\rho_{oo}\ \frac{d^2\sigma}{dt\ \ dm(K\bar{K})} \tag{15}$$

allows one to separate out π and B exchange in f_o and A_2^o production, respectively. From experience with ρ-ω interference,[67] one thinks one knows the phases with which these amplitudes will occur,[38,68] whereas without projecting out unnatural parity exchange no such clean statement about phases seems possible.

5. Further studies of A_1-A_2 interference. The claim[32] for essentially complete coherence between $I_t=0(A_1)$ and $I_t=0(A_2)$ in $\pi^- p \to A_{1,2}^- p$ would be puzzling if only the Pomeranchuk trajectory contributed to A_1 production and only the f_o to A_2 production. The interference should be studied at higher energies to see if this complete coherence persists.

IV. A_2 resonance shape.

Table III summarizes some present and future data of high resolution and high statistics regarding this question. Only experiments with ≳ 150 events in the A_2 peak have been included; as shown by the χ^2 probabilities $P(\chi^2)$ for Breit-Wigner (BW) or dipole (DP), not all of these are terribly significant.

The salient point of this table is the contradiction between the two boxed results. The "best-resolution" sample[78] of ref. 2 (see the review by W. Kienzle, ref. 2, fig. 7) has two peaks separated by about 24 MeV and a deep dip near 1300 MeV in between these peaks. On the other hand, with at least 10 times as many events in the peak as this sample, the NE-SB experiment sees a distribution indistinguishable from a Breit-Wigner.

A model-independent comparison of the combined data of refs. 1-2 with those of refs. 5-6 indicates a significant discrepancy, quoted as at least 7 standard deviations,[6] which cannot be ascribed to the small

Table III. High (resolution/statistics) data regarding A_2 resonance shape in $\pi N \rightarrow A_2 N'$.

	p_L	Group	Ref.	Mode	Quoted Γ_R	Quoted p(BW)	Quoted p(DP)	Split ?
π^-:	(Low)*	RHEL	69	x^-	*	*	*	*
↓ A_2^-	2.6	CERN	70	x^-	10.4	*+	*+	Yes
	4.5	BNL	45	$K^- K_S^o$	8±1	80%	13%,19%‡	No
	5	NE-SB	5,6	x^-	16±1	B.W.favored by	≥11 s.d.	No
	6	UC-WIS	71	$\eta\pi^-, x^-$	15-20	*	*	*
	6,7	CERN	1,2	x^-	16±3(best)	0.1%	70%	Yes
	7	CERN	72	$K^- K_S^o$	≤20	5%	60%	Yes
	7	NE-SB	5,6	x^-	21±1	B.W.favored by	≥ 4 s.d.	No
	17.2	CERN-Munich	35	$K^- K_S^o$	13.5±1.4	32%**	.4%**	No
	20	BNL	73	$K^- K_S^o$	11	55%	2.5%	No
π^+:	3.7	LRL-G-T	74	$(3\pi)^+$	14	11%	53%	Yes
↓ A_2^+	5	NE-SB	5,6	x^+	16±1	B.W.favored by	≥ 9 s.d.	No
	7	LRL-A	75	$(3\pi)^+$	12.8	14%	0.3%	No
				$K^+ K_S^o$, π^+	7.2,16.4	13%	0.3%	No
π^-: ↓ A_2^o	3.2	CERN-Bologna	76	x^o	15	1%	65%	Yes
	4.5	Illinois	77	$(3\pi)^o$	7	*	*	*

*: unknown to author at present

+: fits to data of refs. 70 and 2 combined.

‡: two χ^2 minima.

**: sample fit.

differences in quoted mass resolution between the two experiments.

The other experiments in Table III which do not see the splitting are irrelevant if the NE-SB result is correct. Not one of them contradicts a report of splitting for comparable s, t, charge state, and decay mode. On the other hand, none of these other split-A_2 results is of comparable significance to that of ref. 2, which is really the keystone of the case for A_2 substructure.

Given the present contradiction between the two most significant sets of data[2,5,6], the question is how to avoid a third result which may be so indecisive as to call for a fourth experiment, etc.! The only suggestion I would dare to make if such experiments are still contemplated is that one proceed as if narrow structures were involved. Such structures are considerably more sensitive to resolution than the popular dipole[7] shape, as we shall show.

We shall not attempt a review of the many theoretical efforts[26,79-98] to explain A_2 substructure. We discuss only the "broad-narrow"[70] model. While the degeneracy of the A_2 (broad) and its possible narrow partner remains a puzzle in such a model, the "broad-narrow" hypothesis allows very easily both for differences among A_2 experiments under various conditions (e.g. s, charge; see Table III) and for differences among members of the 2^+ nonet (A. Barbaro-Galtieri, Ref. 3).

A. Two-peak hypothesis.

Spin-parity analyses in various decay modes of the A_2[3,35,43,47-49,51,75,99,100] agree that the only rapidly varying (resonant) amplitude in the $(3\pi)^\pm$ and $(K\bar{K})^\pm$ systems near m_{A_2} is that with $J^P=2^+$. In the $\eta\pi^-$ system, the 2^+ is certainly dominant[53] (for both high- and low-mass halves of the peak) but the possibility of interference with a very small, rapidly varying $J^{PC}=1^{-+}$ amplitude cannot be ruled out.[53,101] If there is any splitting, it must then occur in the 2^+ amplitude alone, to which we now restrict our discussion.

The dipole expression[7,80] used in the fits of Table III has the advantage that it allows a quick comparison of resonance shapes in various experiments. It is a "favored" shape theoretically only by virtue of economy of parameters, however. Once the shape depends on charge, s and possibly t, as suggested by the experiments in Table III prior to that of NE-SB,[5-6] this economy is lost, and comparisons based on the dipole shape alone[103] lose their theoretical significance.[104]

The dipole is a particular limit of the more general case of two 2^+ resonances which undergo mixing through real or virtual intermediate states.[79,80,88-94] These two resonances may have different production and decay properties, so that one would expect the shape to be invariant only under certain very special circumstances. In the next subsection we apply the formalism of production, mixing, and decay of two degenerate states to a simple model of the "broad-narrow" variety.

B. Broad-narrow model.

The "usual" A_2, with properties noted in Sections II and III, we denote by $A_2^{(1)}$ prior to mixing. Similarly, the unmixed "extra" state we denote by $A_2^{(2)}$.

Let us consider $A_2^{(1)}$ to have natural width Γ_1, and $A_2^{(2)}$ to be quite narrow;[79,86,96,105] we take $\Gamma_2 = 0$. One denotes production and decay processes by vectors

$$\vec{G}^{(r)} = \left[G_1^{(r)}, G_2^{(r)}\right] \quad \text{(production)} \tag{16}$$

$$\vec{F}^{(n)} = \left[F_1^{(n)}, F_2^{(n)}\right] \quad \text{(decay)} \tag{17}$$

where the components 1, 2, refer to $A_2^{(1,2)}$, and r, n label production and decay channels. The transition matrix is then given in the presence of mixing by

$$A^{nr} = -\vec{F}^{(n)} \cdot \overleftrightarrow{D} \cdot \vec{G}^{(r)} \tag{18}$$

where $\overleftrightarrow{D}$ is a 2 x 2 matrix propagator, with[38,79]

$$\vec{D}^{-1} = \begin{bmatrix} E - M_o + i\Gamma_1/2 & -V \\ -V & E-M_o \end{bmatrix} \tag{19}$$

The off-diagonal mixing term V is assumed real, as would be the case for mixing via virtual transitions.[90,107] We have taken the two states to have common mass M_o for simplicity. Performing the matrix inversion, one has

$$\vec{D} = (\mathrm{Det}\ D)^{-1} \begin{bmatrix} E-M_o & V \\ V & E-M_o+i\Gamma_1/2 \end{bmatrix} \tag{20}$$

$$\mathrm{Det}\ D = D_+D_- \tag{21}$$

$$D_\pm = E-M_o+i\Gamma_\pm/2 \tag{22}$$

where

$$V = \sqrt{\Gamma_+\Gamma_-}/2, \quad \Gamma_1 = \Gamma_+ + \Gamma_- \tag{23),(24}$$

determine $\Gamma_\pm$.

The poles of the S-matrix behave as shown in Fig. 4a, starting out for V = 0 at $\Gamma_+ = \Gamma_1$, $\Gamma_- = 0$; coalescing to the dipole shape[79] at $V = \Gamma_1/4$; and spreading apart in opposite real directions for larger V. One popular type of fit to split-A_2 spectra[70,74] is based on the pole positions illustrated in Fig. 4b. This is the class of models we shall be discussing here.

Assume that

$$\vec{F}^{(n)} = F_1^{(n)}\left[1,0\right]\ ;\ \vec{G}^{(r)} = G_1^{(r)}\left[1, \epsilon_r\right], \tag{25),(26}$$

corresponding to the following physical situation:

(a) $A_2^{(2)}$ has $\Gamma_2 = 0$ (no open decay channels), as mentioned above.

(b) $A_2^{(2)}$ is produced with amplitude ϵ_r relative to $A_2^{(1)}$ in channel r.

When ϵ_r is taken to be zero, one sees from Eqs. (18) and (20) that a symmetric two-peak structure results.[79] However, we retain ϵ_r in what follows.

The shape is then given by[108]

$$|A^{nr}|^2 = \left|\frac{F_1^{(n)}G_1^{(r)}}{D_+D_-}\right|^2 \left[(E-M_o+a_r)^2 + b_r^2\right] \qquad (27)$$

where

$$a_r = V\,\mathrm{Re}\,\epsilon_r; \quad b_r = V\mathrm{Im}\,\epsilon_r \qquad (28),(29)$$

One can parametrize even a single Breit-Wigner form using Eq. (27), since for

$$a_r = 0, \qquad b_r = \Gamma_-/2 \qquad (30)$$

the square-bracket term just cancels $|D_-|^2$. Hence Eq. (27) is an ideal form for quantitative comparison of resonance shapes independent of any theoretical ideas.[109] The two-state interpretation, however, is that ϵ_r is a relative production amplitude which may easily cause variations of any observed structure with respect to reaction, s, and t. The only relevant comparison in such a case, therefore, is that boxed in Table III.

Given a pair Γ_+, Γ_- claimed to be necessary to fit data with a symmetric shape (a_r=0) and a dip to 0 (b_r=0),[70,74] one may then attempt to obtain fits to A_2 shapes in other experiments.[110] If all these fits were to cluster around the values (30), one would not have seen the effect of the "second state" at all, and could just as well omit it altogether.

Needless to say, such fits are meaningless if one has no good idea of the true values of Γ_+ and Γ_-. One needs at least one experiment with resolution smaller than Γ_- in order to be sure that such parameters are being correctly determined, and even then one must rely on the happy accident a_r=b_r=0.

Eq. (27) is merely another form of the two-interfering-Breit-Wigner model of Ref. 74:

$$A^{nr} \sim \frac{f\sqrt{\Gamma_+}}{D_+} + \frac{e^{i\phi}\sqrt{\Gamma_-}}{D_-} \qquad (31)$$

The connection between (27) and (31) is:

$$z = f e^{-i\phi} \tag{32}$$

$$\epsilon_0 \equiv \sqrt{\Gamma_+/\Gamma_-} \tag{33}$$

$$\epsilon = i(z+\epsilon_0)/(1+z\epsilon_0) \quad , \tag{34}$$

i.e. a linear fractional transformation. It is amusing that, since ϵ and ϵ^* give the same resonance shape (see Eqs. (27)-(29)), so do $z(\epsilon)$ and $z_c \equiv z(\epsilon^*) \neq z(\epsilon)$.

The results of some fits to **Eqs.**(31) and (27) are shown in Fig. 5. Fits in Ref. 74 were constrained to have $|z| = \epsilon_0$. By comparing the closed circle with the open triangle (unconstrained fit to the same data, minus a low-statistics sample of $\eta\pi$ and $K\bar{K}$ [111]) in Fig. 5b one sees that such a constraint can be quite misleading. The best fit to the data of Ref. 75 on the basis of Eq. (27) is considerably closer to the case indistinguishable from the unsplit one ($z = \infty$, $\epsilon = i/\epsilon_0$) than the fit of Ref. 74.

Given parameters such as $\Gamma_+ = 90$, $\Gamma_- = 12$,[70] or $\Gamma_+ \cong 80$, $\Gamma_- \cong 10$,[74] the NE-SB data should lead to a fit to Eq. (27) with very small allowable deviation of a_r, b_r from the values in Eq. (30). One would then exhibit the contradiction between the CERN[2] and NE-SB[5,6] data by showing that on Fig. 5b, the derived values of ϵ were outside each other's error bars, despite the claimed identical nature of the experiments.[112]

In the next subsection we concentrate on the case for which the resonance shape would be symmetric (a_r=0) with a dip to 0 (b_r=0) in the limit of ideal resolution, and show that for $\Gamma_- \simeq 5$ MeV the resulting structure is rather sensitive to resolution.

C. Effects of resolution.[113]

We have folded a Gaussian resolution function $e^{-(x-y)^2/2\sigma^2}$ into resonance shapes corresponding to (i) dipole[7] (ii) broad-narrow with maximal destructive interference and symmetric shape (Eq. (27) with $a_r = b_r = 0$). The results are shown in Fig. 6. While the usual broad-narrow shape[70] with $\Gamma_- = 12$, $\Gamma_+ = 90$ is no more sensitive to resolution than the dipole form[2] (cf. Figs. 6a and 6b), more sensitivity sets in as Γ_- is reduced (Figs. 6c, 6d). For the cases of Figs. 6a, 6b to hold true in Nature, NE-SB would have to have made a gross underestimate of its resolution (the arrows indicate by how much; author's rough estimate). As Γ_- is reduced, one passes through a situation for which each group would have had to misjudge its resolution by some 40%. This appears to be around $\Gamma_- \simeq 5$ MeV. It is unlikely that CERN would have so overestimated its resolution as to have seen any substructure associated with Γ_- much less than this.

Other models can be invented to give considerable sensitivity to resolution. One of these is two line resonances separated by a given amount.[114] However, such a model is at odds with the discussion of sec. II unless all the 2^+ resonances were to have this pathological structure.

V. Conclusions.

In the past couple of years the A_2 has been behaving itself remarkably well: as if it were the "usual" $^3P_2$ state of a quark and an antiquark. This good behavior is reflected in well-observed SU(3) relations. We seem to have learned a good deal about A_2 production by pions, and it also shows no anomalies: f_o and ρ exchange describe it well. On the other hand, the question of possible substructure remains unsolved, with the original, most significant results in favor of a splitting[2] called into question.[5,6] Doubtless CERN[2] has seen some sort of anomalous effect; its interpretation in terms of a second A_2 state remains problematic.

If a third experiment is contemplated we urge some restraint in case narrow structures are involved. One must probably wait until experimental resolutions drop below 5 MeV(full width at half maximum) before re-opening the question. It may be a long time before our experimental techniques get that good.[115] Moreover, such an experiment should be capable of doing some other piece of physics should it again fail to see the splitting.

Should the A_2 substructure[2] turn out to have been merely an instrumental effect or a huge statistical fluctuation one would be left with the question of why the naive quark model predicts the meson spectrum below 1500 MeV so well.[22-26] In fact, however, not all of these predictions have been confirmed, and it might be useful to check them more systematically.[118]

ACKNOWLEDGEMENTS

The author thanks his colleagues at Minnesota for their unending patience and helpful suggestions since the time he was asked to prepare this report. Special thanks are due Wes Petersen for many fruitful discussions and help with computations.

The compilation of density matrix elements depended largely on the generosity of M. Ioffredo in sharing a large body of data[41] prior to publication. Thanks are also due to K. Barnham and M. Rabin for help in this respect and for discussions of two-peak fits to A_2 spectra.

Conversations with H. R. Blieden, T. Buhl, G. Conforto, G. Fox, M. Gettner, K. W. Lai, K. Lassila, B. Maglić, D. Mortara, C. Nef, R. Prepost, G. Ringland, A. Rosenfeld and P. Schübelin are also gratefully acknowledged.

NOTE ADDED IN PROOF:

After this manuscript was typed, we received a copy of "Comments on A_2 Production" by C. Michael and P. V. Ruuskanen, CERN preprint TH 1308, in which many of the results of Section III were obtained independently. (Note: This paper is now in Physics Letters 35B, 65 (1971).)

REFERENCES

[*] Work supported in part by the U.S. Atomic Energy Commission under Contract No. AT(11-1)-1764.

1. B. Levrat, *et al.*, Phys. Lett. 22, 714 (1966).
2. G. Chikovani, *et al.*, Phys. Lett. 25B, 44 (1967); W. Kienzle, in *Meson Spectroscopy* (1968 Phila. Meson Conference), eds. C. Baltay and A. Rosenfeld, New York, Benjamin, 1968, p. 265.
3. See, e.g., the talks by other participants in this conference, and the review in ref. 4; Other reviews: M. Martin, in *Experimental Meson Spectroscopy* (1970 Phila. Meson Conference), eds. C. Baltay and A. Rosenfeld, New York, Columbia University Press, 1970, p. 311; A. Barbaro-Galtieri, *Ibid*; p. 331.
4. A. Astier, in Proceedings of the XV International Conference on High Energy Physics, Kiev, 1970; Moscow, Atomizdat, to be published.
5. M. Gettner, this conference; B. Gottschalk, Bull. Am. Phys. Soc. 16, 610 (1971).
6. D. Bowen, *et al.*, subm. to Phys. Rev. Letters.
7. We mean by this a resonance shape of the form $(E-E_o)^2 \Gamma^2 / [(E-E_o)^2+\Gamma^2/4]^2$.
8. A. Pignotti, Phys. Rev. 134, B630 (1964).
9. R. Arnold, Phys. Rev. Lett. 14, 657 (1965).
10. Broad A: see, e.g., G. Goldhaber, *et.al.*, Phys. Rev. Lett. 12, 336 (1964); A_1 and A_2 resolved: S. U. Chung, *et al.*, Phys. Rev. Lett. 12, 621 (1964); Aachen-Berlin-Birmingham-Bonn-Hamburg-London (I.C.)-Munich collaboration, Phys. Lett. 10, 248 (1964).
11. See, e.g., U. E. Kruse, this conference.
12. S. Glashow and R. Socolow, Phys. Rev. Lett. 15, 324 (1965).
13. M. Alston-Garnjost, *et al.*, Phys. Lett. 34B, 156 (1971).
14. M. Aguilar-Benitez, *et al.*, Phys. Rev. Lett. 25, 1362 (1970).
15. The notation is that of ref. 16.
16. E. W. Colglazier and J. L. Rosner, Nucl. Phys. B27, 349 (1971).
17. The central values of the experimental numbers turned out to be identical to those chosen by K. W. Lai (this conference) in a similar fit, and are therefore not quoted. However: (a) his estimated

errors are larger (and, therefore, more to be trusted) than ours; (b) his fit takes account of mixing whereas ours assumes ideal nonet structure and quark model couplings, and (c) his fit uses an effective radius of interaction, whereas ours takes a D-wave matrix element behaving purely as $(p/p_o)^2$.

18. D. Horn, J. Coyne, S. Meshkov, and J. Carter, Phys. Rev. 147, 980 (1966). In this approach, when the 2^+ mesons are classified according to the 405 or 189 of SU(6), the C_i indicated in Fig. 1 hold only for A_2 and K^{**} decays.
19. The result of ref. 16 regarding fig. 1 is expected to hold even in the presence of a form of SU(6) breaking that decouples S-wave from D-wave decays of the $q\bar{q}$; L=1 mesons. Earlier results based on strict $SU(6)_W \times O(2)_{L_z}$ are quoted in ref. 16.
20. See, e.g., F. Gilman and H. Harari, Phys. Rev. 165, 1803 (1968).
21. N. Samios, Kiev Conf. op. cit.
22. M. Gell-Mann, Phys. Lett. 8, 214 (1964).
23. G. Zweig, CERN preprints TH-401 and TH-412 (unpublished).
24. G. Zweig, in Meson Spectroscopy, op. cit., p. 485.
25. R. H. Dalitz, in Meson Spectroscopy, op. cit., p. 497.
26. R. H. Dalitz, in Symmetries and Quark Models, ed. Ramesh Chand, New York, Gordon and Breach, 1970, p. 355.
27. These would have odd L in a $q\bar{q}$; L model.
28. P. Baillon, et. al., Nuovo Cimento 50A, 393 (1967).
29. M. Aguilar-Benitez, et.al., Phys. Lett. 29B, 379 (1969); Nucl. Phys. B14, 195 (1969).
30. J. Rosner, in Experimental Meson Spectroscopy, op. cit., p. 490.
31. "Exotic of type I": I,Y outside the octet; "exotic of type II": $J^{PC} = 0^{--}$ or 0^{+-}, 1^{-+}, 2^{+-}, ...
32. D. V. Brockway, et.al., Univ. of Illinois preprint COO-1195-202, presented at the Austin Meeting of the Division of Particles and Fields, November 1970; M. Ioffredo, private communication.
33. The usual assumption of $A_2 \to \rho\pi \to 3\pi$ is made here.
34. J. T. Carroll, et.al., Phys. Rev. Lett. 25, 1393 (1970).
35. G. Grayer, et.al., Phys. Lett. 34B, 333 (1971).
36. P. Schlein, private communication.

37. The B is thought to play a significant role in the reaction analogous to (4c) with A_2^o replaced by ω. (See, e.g., ref. 38; by analogy with their reasoning, one might expect B exchange to be as important in (4c) as is π exchange in $\pi^- p \to f_o n$!).

38. A. S. Goldhaber, G. C. Fox, and C. Quigg, Phys. Lett. 30B, 249 (1969).

39. K. Gottfried and J. D. Jackson, Nuovo Cimento 33, 309 (1964).

40. These averages reflect varying acceptances for different types of experiment, and should therefore be treated with some caution.

41. L. Eisenstein and M. Ioffredo, private communication; see also ref. 47.

42. K. W. J. Barnham, private communication (preliminary).

43. K. Böckmann, *et.al.*, Nucl. Phys. B16, 221 (1970).

44. I. J. Bloodworth, *et.al.*, Bull. Am. Phys. Soc. 16, 92 (1971).

45. Columbia-Rutgers-Rochester-Yale-ABC compilation. (For momenta and numbers of events see ref. 32).

46. K. W. Lai, this conference.

47. U. E. Kruse, in *Experimental Meson Spectroscopy*, *op.cit.*, p. 359; G. Ascoli, *et.al.*, Phys. Rev. Lett. 25, 962 (1970).

48. T. F. Johnston, *et.al.*, Nucl.Phys. B24, 253 (1970).

49. R. Baud, *et.al.*, Phys. Letters 31B, 397 (1970).

50. C. Nef, private communication. Very different results are obtained in this experiment for the 3π mode,[51] but the analysis in that case is apparently at fault (cf. ref. 52).

51. C. Nef, Thesis, University of Geneva, 1970 (unpublished).

52. H. Hogaasen, *et.al.*, Nuovo Cimento 42A, 323 (1966).

53. J. Lacy, thesis, University of Illinois, 1971 (unpublished), p. 47, based on data from refs. 47, 48, 54, and 16 GeV/c European collaboration (ABBCHW). Values in Fig. 3 adjusted for $\mathrm{Tr}\,\rho = 1$.

54. C. Caso, *et.al.*, Nuovo Cimento 67A, 613 (1970).

55. G. W. Brandenburg, *et.al.*, Nucl. Phys. B16, 287 (1970).

56. Average of 11, 13, 20, 25 GeV/c π^- data (refs. 54, 55, 57).

57. W. Robertson, private communication to L. Eisenstein and M. Ioffredo.

58. See, e.g., G. Ringland and R. Thews, Phys. Rev. 170, 1569 (1968).

59. One *cannot* conclude from this that only the ρ trajectory is exchanged, as we shall see. (cf. ref. 35).

60. C.Goebel, M. Blackmon, and K. C. Wali, Phys. Rev. 182, 1487 (1969).

61. W. Petersen and J. Rosner, unpublished.
62. S. M. Berman and M. Jacob, Phys. Rev. 139, B1023 (1965).
63. C. Zemach, Phys. Rev. 133, B1201 (1964).
64. The author thanks M. Ioffredo for this suggestion.
65. V. N. Gribov, Yad. Fiz. 5, 197 (1967) [Sov. J. Nucl. Phys. 5, 138 (1967)]; D. R. O. Morrison, Phys. Lett. 25B, 238 (1967). Here P_f, P_i and J_f, J_i are parities and spins of final and initial particles (assuming nucleon target, nucleon recoil.)
66. H. Lipkin, Phys. Rev. 176, 1709 (1968); K. Lassila, in "Physics with the Omega Spectrometer", informal conference at Cosener's House (RHEL), eds. R. J. N. Phillips and T. G. Walker, 1970, p. 113.
67. G. Goldhaber, in Experimental Meson Spectroscopy, op.cit., p. 59.
68. Given $\gamma_{\pi A_2 B}(t) = \gamma_{\pi f \pi}(t)$, a relation depending on arguments similar to those of ref. 38, one predicts f_o, A_2^o production amplitudes in (14) which are relatively imaginary, and the two different charge states of $K\bar{K}$ allow for a careful study of the interference effects.
69. D. Binnie, et.al., to be published (G. Fox, private communication; R. J. N. Phillips, private communication.)
70. H. Benz, et.al., Phys. Lett. 28B, 233 (1968).
71. G. Conforto, private communication: Argonne experiment E-259.
72. R. Baud, et.al., Phys. Lett. 31B, 397 (1970). See also M. Martin, ref. 3.
73. K. J. Foley, et.al., Phys. Rev. Lett. 26, 413 (1971).
74. G. Goldhaber, in Kiev Conf., op.cit; K. Barnham, this conference.
75. M. Alston-Garnjost, et.al., Phys. Lett. 33B, 607 (1970).
76. M. Basile et.al., Lett. Nuovo Cimento 4, 838 (1970).
77. D. W. Mortara, private communication: Argonne experiment E-237.
78. I thank Prof. B. Maglić for reminding me that these data involved a selection on downstream particles (1 or 3 charged) not used in the experiment of refs. 5,6.
79. K. Lassila and P. V. Ruuskanen, Phys. Rev. Lett. 17, 490 (1966); Ibid., 19, 762 (1967). The author also thanks K. Lassila for fruitful discussions of the mass-matrix method.
80. D. Sutherland and J. S. Bell, 1967 (unpublished), as quoted in ref. 2; J. S. Bell, CERN preprint TH-784, 1967 (unpublished).

81. J. V. Beaupre, et.al., Phys. Rev. Lett. 21, 1849 (1968).

82. T. P. Coleman, R. C. Stafford, and K. E. Lassila, Phys. Rev. D1, 2192 (1970).

83. H. Harari, in Proceedings of the XIV International Conference on High Energy Physics, Vienna, 1968, eds. J.Prentki and J. Steinberger, Geneva, CERN, 1968, p. 193 (various models for A_2 splitting cited).

84. A. S. Goldhaber, in Meson Spectroscopy, op.cit., p. 297.

85. D. Horn, Nuovo Cimento 62A, 581 (1969).

86. R. Arnold and J. Uretsky, Phys. Rev. Lett. 23, 444 (1969).

87. S. F. Tuan, Phys. Rev. Lett. 23, 1198 (1969).

88. C. Rebbi and R. Slansky, Phys. Rev. 185, 1838 (1969).

89. Y. Fujii and M. Kato, Phys. Rev. 188, 2319 (1969).

90. P. Coulter and G. Shaw, Phys. Rev. 188, 2443 (1969).

91. D. Sutherland, in Experimental Meson Spectroscopy, op.cit., p. 369.

92. L. Stodolsky, in Experimental Meson Spectroscopy, op.cit., p. 395.

93. S. Meshkov, in Experimental Meson Spectroscopy, op.cit., p. 535.

94. Y. Dothan and D. Horn, Phys. Rev. D1, 916 (1970).

95. L-H. Chan, R. Slansky and D. Sutherland, Phys. Rev. Letters 25, 482 (1970); L-H. Chan and R. Slansky, to be published.

96. J. Rosner, Phys. Lett. 33B, 493 (1970).

97. F. Gursey and M. Koca, Nuovo Cimento 1A, 429 (1971).

98. Chun-Fai Chan, Lawrence Radiation Laboratory report UCRL-20051 - Rev. , Phys. Rev. D3, to be published (1971).

99. D. Brockway, thesis, Univ. of Illinois (1970), unpublished.

100. R. Baud, et.al., Phys. Rev. Lett. 31B, 401 (1970).

101. A $J^{PC} = 1^{-+}$ $\eta\pi$ resonance seems unlikely in view of the considerations of ref. 102.

102. C. Levinson, H. Lipkin and S. Meshkov, Nuovo Cimento 32, 1376 (1964); H. Lipkin and S. Meshkov, Phys. Rev. Lett. 22, 212 (1969).

103. Particle Data Group, Rev. Mod. Phys. 43, XXX (1971).

104. Such comparisons are still valuable in demonstrating the remarkable propensity of a statistical fluctuation to look like an A_2 "splitting", however, and warn us against conclusions based on low-statistics experiments.

105. Such a circumstance would follow, for example, if the $A_2^{(2)}$ were a $qq\bar{q}\bar{q}$ object subject to the selection rules of ref. 106.

106. P. Freund, R. Waltz and J. Rosner, Nucl. Phys. B13, 237 (1969).

107. Eq. (19) may be verified by a simple summation procedure as well as using the more rigorous methods of various authors cited above. The author thanks D. Geffen for a discussion of this point.

108. We have checked that this form satisfies the unitarity constraints of ref. 88.

109. An analogous form may be used for the dipole shape, of course, by taking $\Gamma_+ = \Gamma_-$. If one took in addition $a_r = 0$, one would have the "duplicity" parametrization of ref. 103.

110. It may be necessary to add incoherent contributions by taking a sum of terms of the form (27). Shape is mode-independent in this model.

111. M. Rabin, private communication.

112. The error bars would reflect resolution as well as statistics.

113. This work was done in collaboration with W. Petersen.

114. The author thanks B. Maglić for this example.

115. The results of the experiment of ref. 77 bear watching; some crude calibration of resolution is presumably available in this case by looking at the ω and η' widths. However, we may be in for a considerably longer wait; note the time span between the first detailed measurements of optical spectra[116] and the first observation of hydrogen fine structure using new interferometric techniques.[117]

116. J. V. Fraunhofer, "Prismatic and Diffraction Spectra," (1817) ed. and trans. J. S. Ames, New York, Harper and Bros., 1898.

117. A. A. Michelson, Phil. Mag. 34, 280 (1892).

118. J. Rosner, in Proceedings of the Workshop on Physics at Intermediate Energies, Caltech, March 29-30, 1971, to appear as Lawrence Radiation Laboratory report; J. Rosner and E. W Colglazier, Phys. Rev. Lett. 26, 933 (1971).

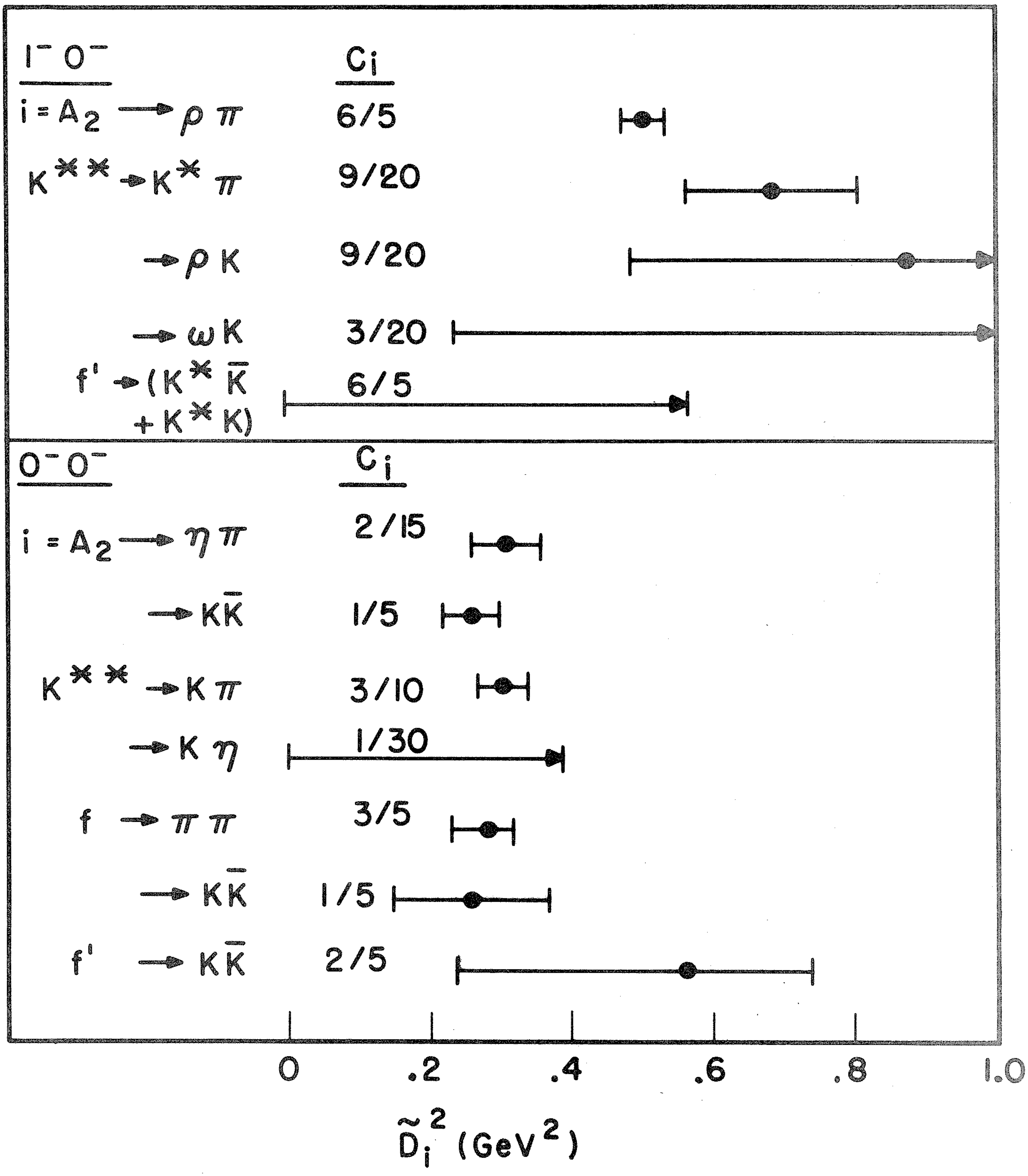

Figure 1: Comparison of $2^+ \to 1^- 0^-$ and $2^+ \to 0^- 0^-$ partial widths according to Eq. (2). The value of C_i is the square of a Clebsch-Gordan coefficient (see text); the reduced widths $\tilde{D}_i^2$ should be equal separately in the two sections of Fig. 1 if SU(3) holds, and in the whole figure if SU(6) holds.

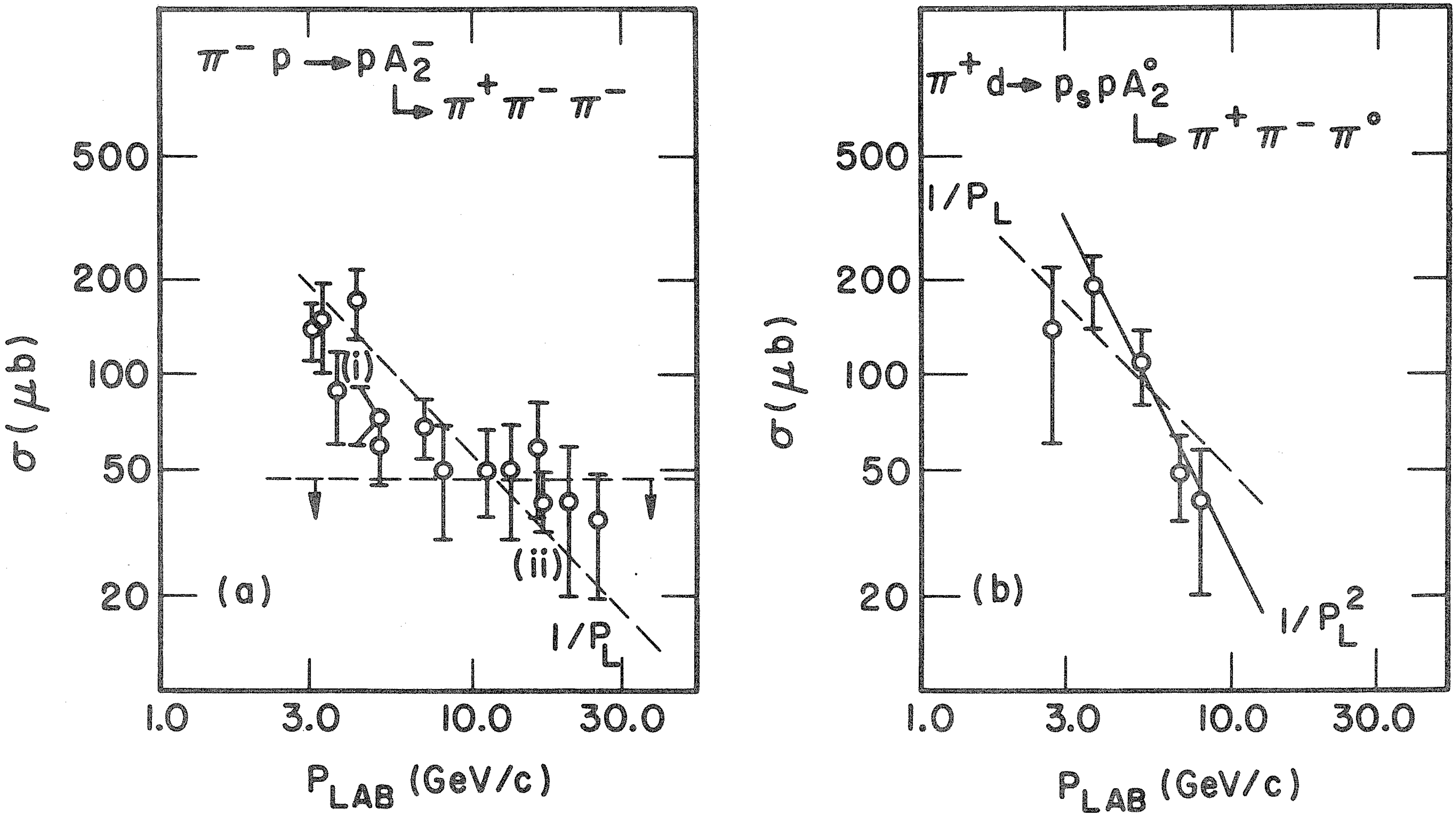

Figure 2: A_2 production cross sections from incident pions (from Ref. 34 except as noted). (a) $\pi^- p \to p A_2^- \to p\pi^+\pi^-\pi^-$. Point (i) represents a comparable value for $\pi^+ p \to A_2^+ p$ at 5 GeV/c (Table I). Point (ii) represents an estimate based on the $K^- K_S^\circ$ mode of the A_2^- produced in 17.2 GeV/c $\pi^- p \to A_2^- p$.[35,36] Diagonal dashed line:[34] fit to $\sigma(A_2^-) \sim p_L^{-1}$. Horizontal dashed line: present data are consistent with a constant limiting value of $\sigma\ (\pi^- p \to p\ A_2^- \to p\pi^+\pi^-\pi^-)$ as large as 50 μb. (b) $\pi^+ d \to p_S\ p\ A_2^\circ \to p_S\ p\pi^+\pi^-\pi^\circ$. Solid line:[35] fit to $\sigma(A_2^\circ) \sim p_L^{-2}$. Dashed line: $\sigma \sim p_L^{-1}$ also barely compatible with data.

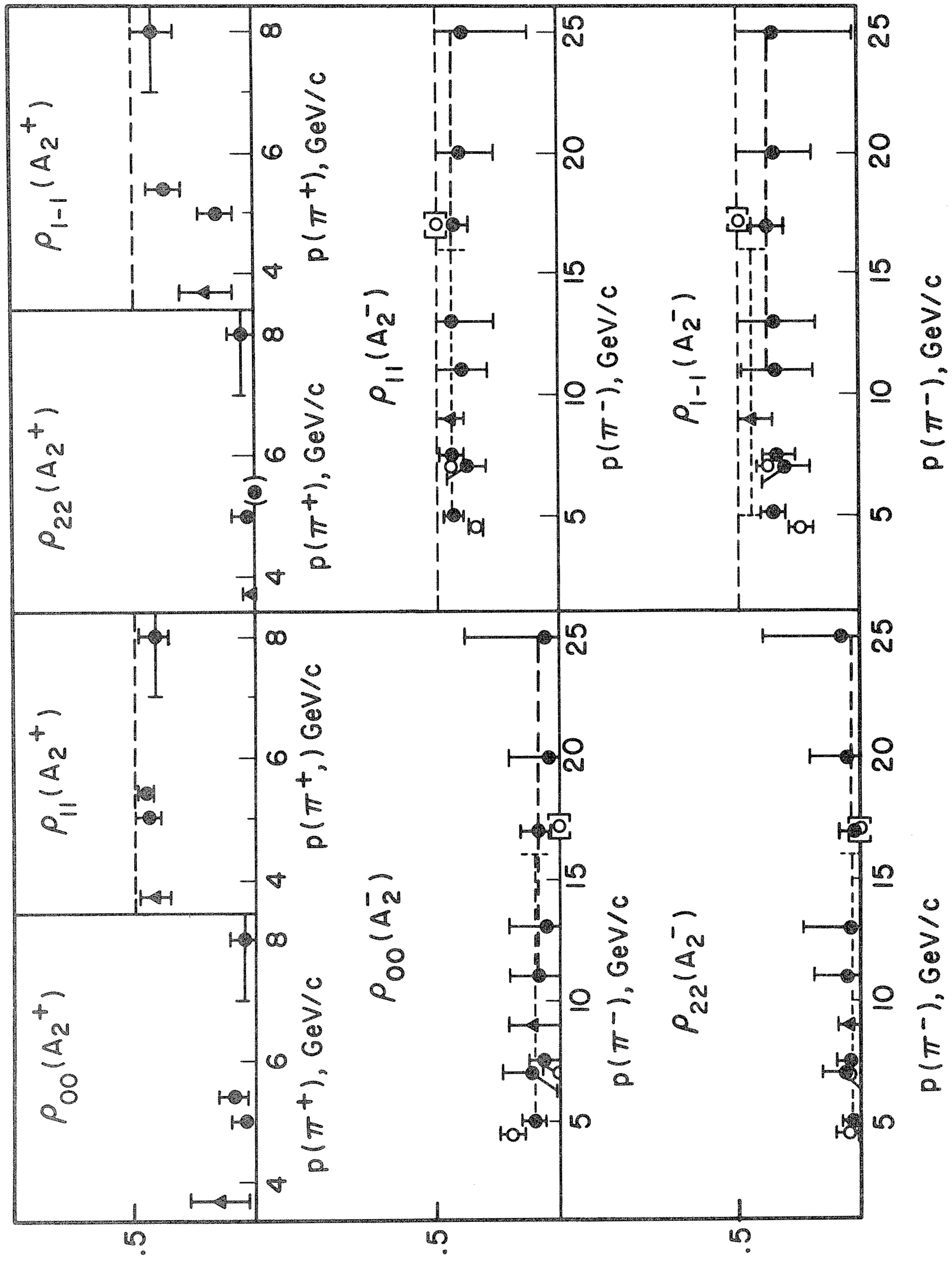

Figure 3: Compilation of density matrices for A_2 production in $\pi^{\pm}p \to A_2^{\pm}p$ as a function of P_L. (See Table II.) ●: 3π; O: $K\bar{K}$; ▲: ηπ.

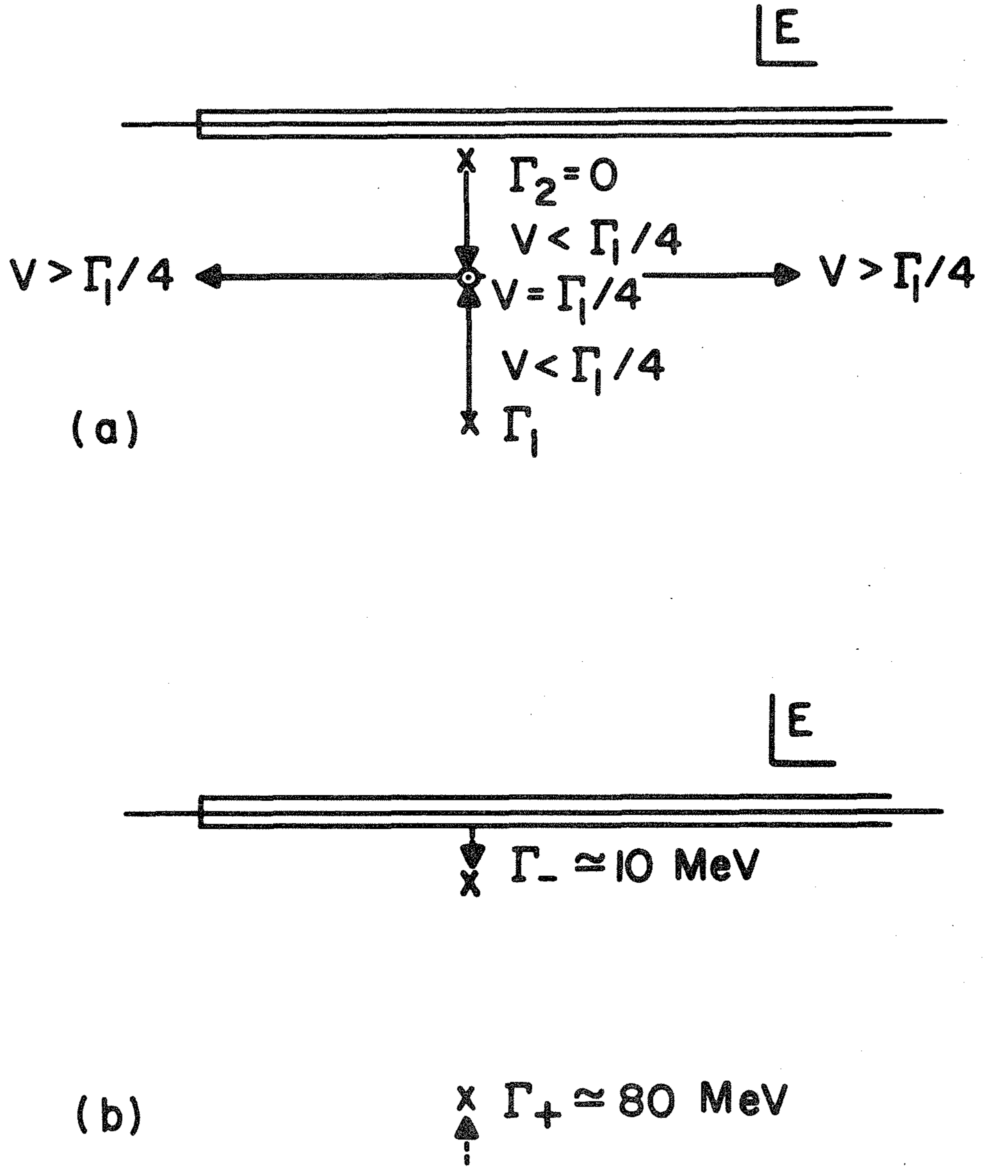
E
$\Gamma_2 = 0$
$V < \Gamma_1/4$
$V > \Gamma_1/4$
$V = \Gamma_1/4$
$V > \Gamma_1/4$
$V < \Gamma_1/4$
(a)
Γ_1
E
$\Gamma_- \simeq 10$ MeV
(b)
$\Gamma_+ \simeq 80$ MeV

Figure 4: (a) Behavior of poles in S-matrix as a function of V (see Eqs. (18) - (24)).
(b) Poles in "broad-narrow" solution.[70, 74]

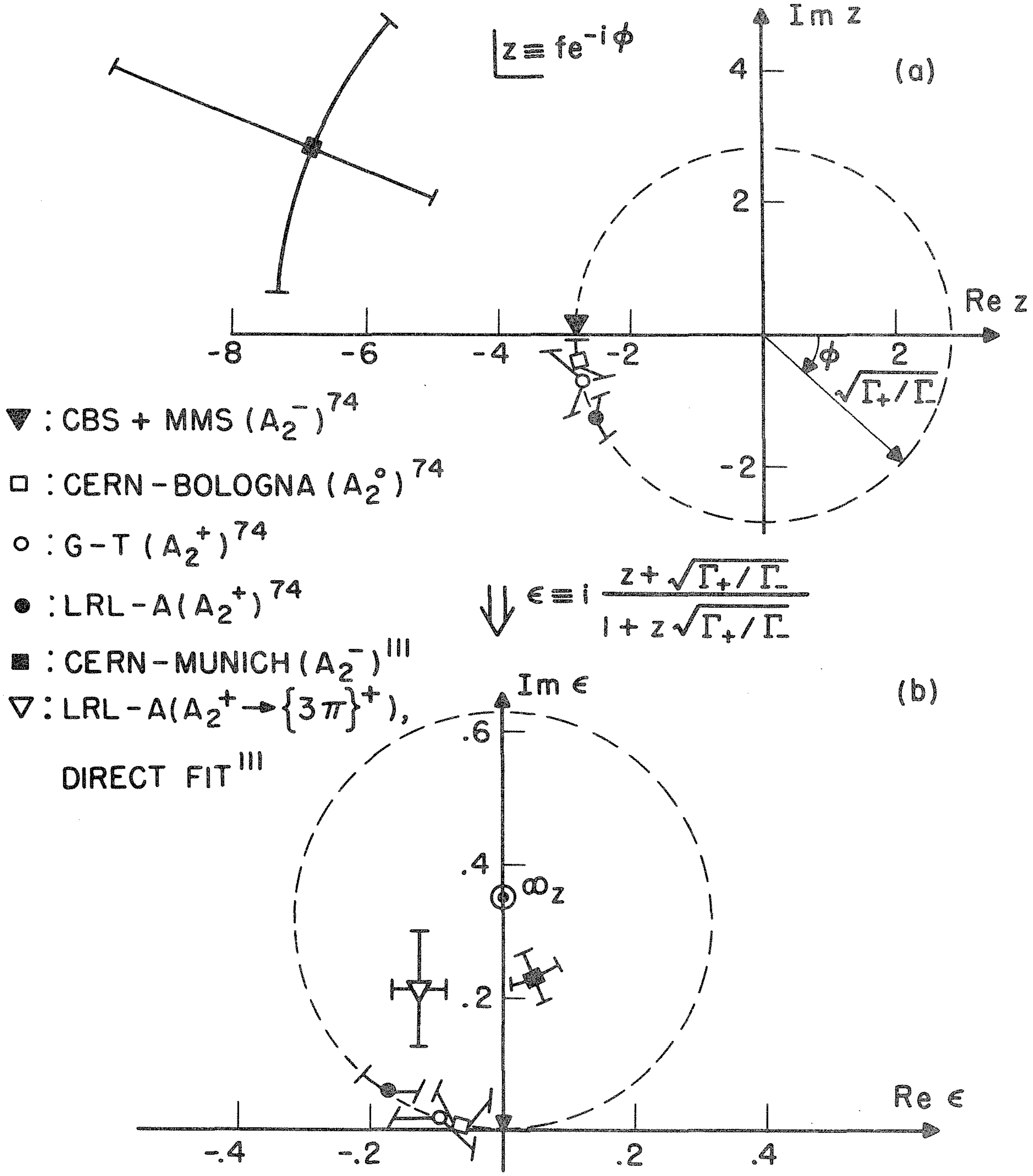

Figure 5: (a) Fits of A_2 spectra to expressions of the form (31).
(b) Fits to the expression (27), derived from those of (a) except in the case of the open triangle, where a direct fit was made. Parameters used: $\Gamma_+ = 78$ MeV, $\Gamma_- = 9.6$ MeV, M_0 variable (assuming calibration impossible[74]). The points $z = \infty$ (Fig. 5a) and $\epsilon = i\ \Gamma_-/\Gamma_+ \equiv \infty_z$ (Fig. 5b) correspond to a single B-W, width Γ_+.

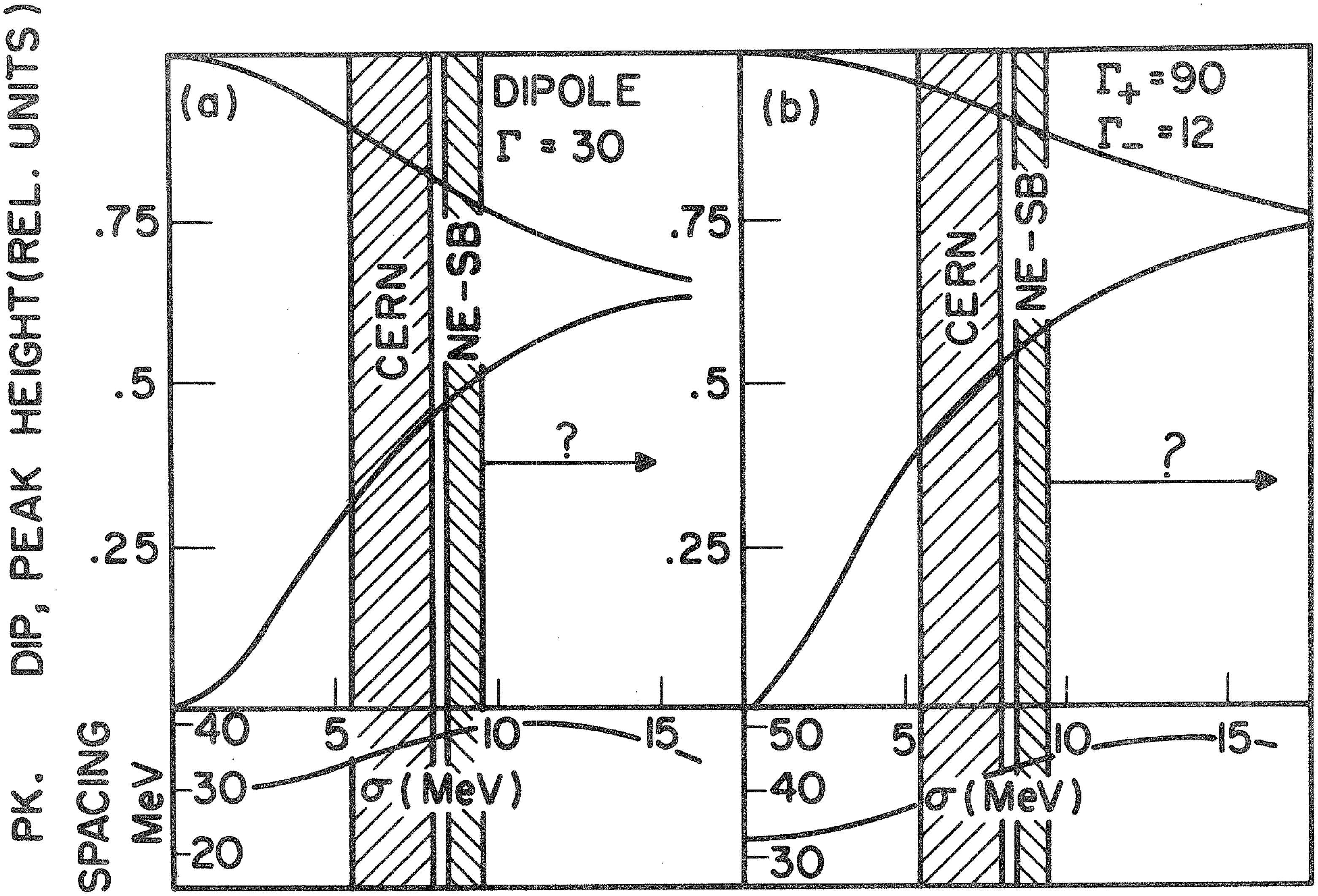

Figure 6: Relative double peak and dip height and peak spacings when folded with Gaussian resolution functions $e^{-(x-y)^2/2\sigma^2}$. (a) Dipole with $\Gamma = 30$ MeV.[2] (b) Broad-narrow form $(E-M_o)^2/|D_+D_-|^2$ (see Eq. (27)), $\Gamma_+ = 90$ MeV, $\Gamma_- = 12$ MeV. In all cases, shaded areas correspond to ranges of σ quoted in Refs. 2 (best resolution sample) and 5, 6 (7 GeV/c π^-). Arrows indicate shifts from quoted values of resolution needed to make results compatible with the given hypotheses.

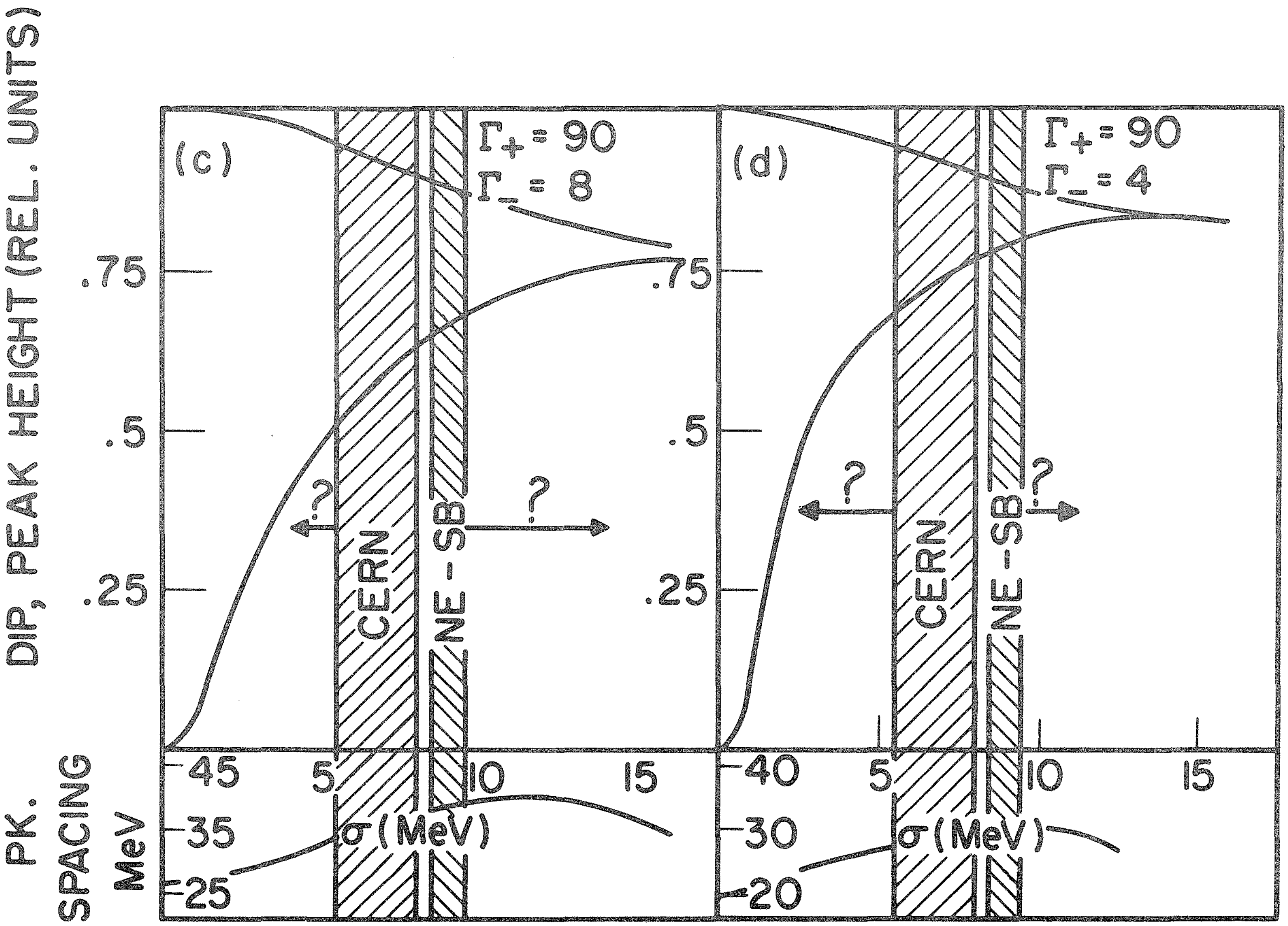

Figure 6 (continued): (c) and (d) same as (b) but $\Gamma_- = 8, 4$ MeV respectively. See the caption of Figs. 6a,b for details.

After a recent shipwreck, clutching his data in one hand and an inner tube in the other, Dr. Steiner floated aimlessly but bravely until he was cast ashore by a partial wave. In gratitude he named a method of analysis after this friendly force of Nature. He was also tempted to call it "Coconut Analysis" but decided against it because it sounded too much like a candy bar.

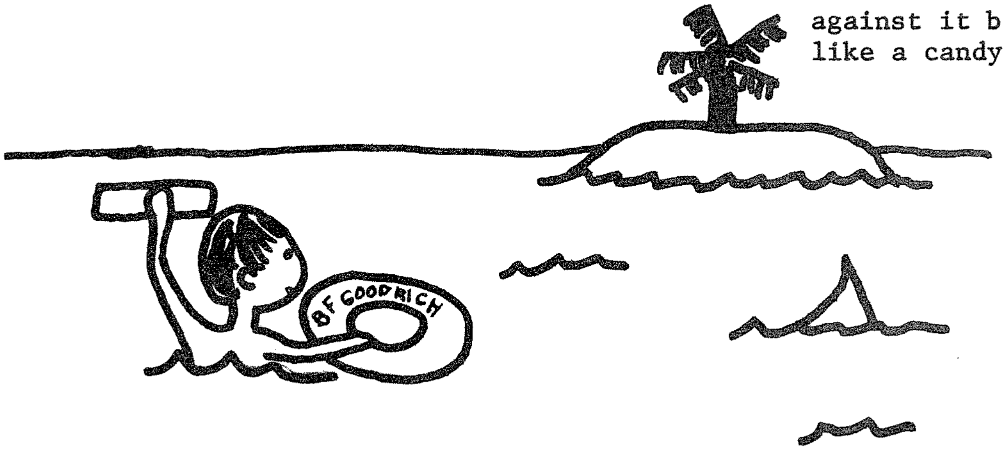

PION-NUCLEON SCATTERING: EXPERIMENTS AND PHASE SHIFTS

Herbert M. Steiner

Lawrence Radiation Laboratory
University of California
Berkeley, California 94720

I. Introduction

The major developments in low-energy pion-nucleon scattering during the last year or so have been (1) more extensive and accurate measurements of cross sections and polarization parameters, and (2) attempts to extend phase shift analyses to higher energies. In this brief status report it is not possible for me to discuss all of the new experimental work nor all of the phase shift analyses. Instead I have somewhat arbitrarily chosen some recent results which serve to illustrate what is happening in this area of research. A more complete summary of results reported prior to September 1970 is contained in Plano's rapporteur's talk at Kiev.[1]

II. Experiments

It is perhaps surprising that experimenters are still spending their time and the taxpayers' money making measurements of pion-nucleon scattering. After all, the pion-nucleon system -- because of its relative phenomenological simplicity and experimental accessibility -- has been studied much more extensively than any other two-body hadronic interaction. It is hardly necessary to point out that phase shift analyses are based on experimental data and that the "breakthroughs" in our understanding of the πN system -- such as, for example, the Saclay[2] and CERN[3] phase shift analyses -- were made possible by new and detailed measurements of cross sections and polarizations. Recent experiments have refined and extended these measurements even further, with the consequence that the existing phase shift solutions no longer give satisfactory fits to the data. To appreciate the significance of some of these measurements, let us look at a few examples.

(1) A Cavendish-Rutherford collaboration[4] has recently completed an extensive series of cross-section measurements at the CERN synchrocyclotron, including σ_T for both π^+p and π^-p scattering in the energy range $70 < T_\pi < 290$ MeV; i.e., around the first P_{33} or Δ resonance. The π^+p results are shown in Fig. 1. Note that the accuracy of the points is comparable to the thickness of the line passing through them. An interesting feature of the new data is an apparent shift of the peak of the cross section to a lower momentum. The authors quote the following experimental resonance parameters for the Δ^{++}: mass = 1231.0 ± 0.4 ± 1.4 MeV/c, elastic width = 111.1 ± 0.4 ± 1.8, total width = 111.1 ± 0.4 ± 1.8 MeV/c^2, where the first error is statistical and the second is an estimate of the error arising from uncertainties in the background. Because of the large χ^2 for this fit ($\chi^2 = 48$ for 11 degrees of freedom), the Particle Data Group[5] has tried some other fits--some having much more satisfactory χ^2's--for which $1231 < M < 1234$ MeV/c^2 and $110 < \Gamma < 120$ MeV/c^2, depending on the specific parametrization used. In any case the mass of the Δ^{++} seems to be at least 2 MeV/c^2 lower than had previously been thought. From an analysis of both the π^+p and π^-p cross sections, Carter et al.[4] determined the $\Delta^{++} - \Delta^o$ mass difference to be -2.9 ± 0.9 MeV/c^2, which is in good agreement with the predictions of Socolow[6] of 2.4 MeV/c^2 based on tadpole and baryon-octet self-energy diagrams. In another paper[7] the same group present $\pi^-p \to \pi^o n$ total charge-exchange cross sections for $90 < T_\pi < 290$ MeV/c. Again the results are of very high quality, having typical errors of 0.3 mb. Very accurate elastic differential cross sections were also obtained during the course of this experiment, and these are expected to be

published soon. The accuracy of these experiments is sufficiently good that more refined consideration of Coulomb effects must be taken into account in the analysis of the data.

(2) The polarized target group at the Rutherford Laboratory has recently completed a painstakingly thorough set of measurements at 68 different momenta of π^+p polarization in the momentum interval $0.68 < p_\pi < 2.5$ GeV/c(8). An example of the results obtained is shown in Fig. 2. For comparison the results of a 1965 LRL experiment at 1440 MeV/c are shown in Fig. 3. It is perhaps worth keeping in mind that practically all of the present-day phase shift analyses are based predominantly on pre-1966 data. It is also interesting to note that none of the existing phase shift solutions give satisfactory fits to these new data. (See Fig. 4.) We will see more of that later. The general qualitative trends of the data are usually reproduced reasonably well by the phase shift solutions, but the fits are completely unacceptable on a statistical basis.

(3) Recent polarization measurements at CERN[9] and Argonne[10] as well as differential cross-section measurements at CERN[9] are also generally not very well fit by existing phase shift solutions. As an example, some recent cross-section and polarization results are shown in Fig. 5 together with some of the phase shift fits.

(4) In the last year there have been several measurements of backward $\pi^\pm p$ differential cross sections at Saclay[11] and LRL.[12,13] The results are much more accurate and extensive (though in a very limited angular region) than previous measurements. Figure 6 shows the disagreement of some of the new Saclay results with earlier measurements at NIMROD. In Fig. 7 some of the new Saclay data are compared with the phase shift predictions. Some examples of the results obtained by the Iowa State-St. Louis University-McGill collaboration at the LRL Bevatron are shown in Figs. 8 and 9.

Several other very useful and accurate experiments have been reported during the last year, but the above serve as examples of the present state of the experimental information. A summary of existing measurements has been prepared by the polarized target group at the Rutherford Laboratory and is shown in Fig. 10. We note several things: (1) The new measurements extend to higher energies than previously. (2) Accuracy is much better. (3) Spacing of measurements in momentum is in many cases very close. (4) Existing phase shift solutions don't really fit the data well. The new data have been coming in so fast that the phase shifters have as yet not been able to keep up with them. (5) There are still potential unknown systematic errors. In some cases (e.g., total cross section) there exist several "high precision" experiments which give "accurate" but incompatible results. (6) The experimental effort has so far focused almost exclusively on the "easy" experiments (e.g., σ_T and $\frac{d\sigma}{d\Omega}$ for elastic and charge-exchange scattering, and P for elastic scattering).

A word about present developments and plans for the future. At first sight it might appear that the πN system below, say, 2 or 2.5 GeV/c^2 is now well understood in that most of the general features are common to the various phase shift solutions. There is, however, still an urgent need to improve the accuracy of these fits, to reduce the presently large number of acceptable solutions at a given energy, and to find better ways to make the energy continuation of the solutions. To this end the experimental efforts of several groups are being directed toward measurements of heretofore unmeasured quantities such as $P(\pi^- p \rightarrow \pi^0 n)$ (which is presently getting underway at LRL, RHEL, and ANL) and the so-called A and R parameters.

The A and R measurements involve the use of a polarized target and a subsequent analysis of the polarization of the recoil proton. Not only that, but all of the polarization vectors must lie in the plane of the scattering. (See Fig. 11.) Unlike the cross-section and polarization parameters which are proportional to $|G|^2 + |H|^2$ and Im GH^* (where G and H are the non-flip and the flip scattering amplitudes) A and R depend upon ReGH^* and $|G|^2 - |H|^2$. We have performed a rather simple exercise with the help of a computer which indicates the potential usefulness of some of these A and R measurements. We generated some typical $A(\pi^{\pm}p \rightarrow \pi^{\pm}p)$ and $R(\pi^{\pm}p \rightarrow \pi^{\pm}p)$ data from some of the existing phase shift solutions (see Fig. 12). To do this we distributed a representative number of data points statistically about the phase shift predicted curve. These fake computer-generated A and R data points were then put back into the computer as experimental data along with the real cross-section and polarization data. A new search was then started for sets of acceptable phase shifts which fit all of the input data. The matrix shown in Table I shows what happens to six different "good" solutions at 1080 MeV/c when they have to adjust themselves to fit all of the real data plus the six different sets of A and R results that are generated by each of these solutions. One sees that measurements of a total of 28 points for $A_{\pm}$ and $R_{\pm}$ with an accuracy of ± 0.1 serve to reject all but one or at most two of the original six solutions in each case. Thus it seems likely that A and R measurements of even modest accuracy are likely to be very useful in limiting the number of acceptable solutions at a given energy.

III. Phase Shifts

Although there are lots of groups, lots of methods, and lots of activity it should be made very clear that many of these analyses are not completely independent of each other. They often share common biases such as, for example, the smoothing techniques used in making the energy continuations which bias one against finding resonances, especially narrow ones. Sometimes the choice of "random" starting points used in initiating the minimization procedure to find the phase shifts is not at all random, but instead may be the best solution of a competitor. It may not only be a manifestation of the laws of nature that many different analyses are converging onto a common solution. The question of uniqueness of the existing solutions is not yet definitely settled, although I think most of the "experts" in the field feel that the general behavior of the dominant partial waves is unlikely to undergo major change.

I mentioned before that the phase shifters have not been keeping up with the new data. Instead, the most significant developments have been in extending the solutions to higher energies. For example the Saclay group[14] has recently reported phase shifts up to $p_\pi = 2.8$ GeV/c ($M = 2.5$ GeV). They cut off their partial-wave expansion at $\ell_{max} = 5$, which may be just a little low at the higher end of their range, especially since they claim to have found several new resonances such as $H_{1,9}(2200)$ and $H_{3,11}(2320)$ which are $\ell = 5$ states. These states, if they are confirmed by other analyses, could represent the Regge recurrences of the N(938) and the $\Delta(1234)$. The Saclay analysis fits 3150 data points with 44 parameters. Different variations of the "shortest path" method were used to make the energy continuation. Several other groups have extended their analyses to higher energies. In doing so, various model-dependent assumptions were involved. For example, Bransden and Ogden[15] at Durham have used a model in which the total scattering amplitude can be written as the sum of a Regge amplitude plus another term which can be parametrized as a function of s and t. They used this amplitude as the starting point for a phase shift search. In this way they obtained a solution for $1.95 < p_\pi < 3.5$ GeV/c. Nothing is yet known about the uniqueness of this solution. Bransden and Roychoudhury[16] have recently published a similar analysis in the energy range $1.5 < p_\pi < 2.5$ GeV/c. As one goes to higher and higher energies, especially when the available data are limited in scope, some model-dependent assumptions seem to be unavoidable. Assumptions are all right if they can be checked, but caution should be the watchword when one uses models which can't be tested. Quite a bit of effort has recently gone into making "suitable" models to fit the existing low-energy data. For example, there has been a revival of interest in trying to fit the data with a sum of Breit-Wigner resonances plus a background amplitude which is dominantly the imaginary part of an exponential diffraction-like term.[17]

As we go to higher and higher energies the complexity of standard phase shift method goes up rapidly as the number of parameters increases. To make such analyses tractable one needs ever-increasing computing power.

The present-day analyses have only been possible because of the availability of suitable computers. Clearly, other methods such as, for example, those suggested by Cutkosky,[18] in which the expansion of the scattering amplitude converges more rapidly than in the usual partial-wave decomposition, could significantly facilitate the computer searches.

Many questions remain to be answered. The behavior of the small partial-wave amplitudes is still not well established. The quality of the fits to even the old data is not satisfactory. The old question of how to extract resonance parameters from the phase shifts is still not settled. I think the theorists are falling somewhat behind the experimenters in the efforts they are devoting to this field of research. Hopefully, the availability of the new high-quality experimental data will revitalize not only the activities of the phase shifters but will stimulate the theorists to give renewed attention to the pion-nucleon system.

References

1. R. J. Plano, rapporteur's review talk, XV International Conference on High Energy Physics, Kiev, USSR, October 1970 (to be published).
2. P. Bareyre, C. Bricman, and G. Villet, Phys. Rev. 165, 1730 (1968).
3. A. Donnachie, R. G. Kirsopp, and C. Lovelace, Phys. Letters 26B, 161 (1968).
4. A. A. Carter, J. R. Williams, D. V. Bugg, P. J. Bussey, and D. R. Dance, Nucl. Phys. B26, 445 (1971).
5. Review of Particle Properties, to be published in Rev. Mod. Phys., April, 1971.
6. R. Socolow, Harvard University Thesis, 1964, unpublished.
7. D. V. Bugg, P. J. Bussey, D. R. Dance, A. R. Smith, A. A. Carter, and J. R. Williams, Nucl. Phys. B26, 588 (1971).
8. W. Holley, private communication.
9. M. G. Albrow, S. Anderson/Almehed, B. Bosnjakovec, C. Daum, F. C. Erne, J. P. Lagnaux, J. C. Sens, F. Udo, Nucl. Phys. B25, 9 (1971).
10. G. Burleson, D. Hill, S. Kato, P. F. M. Koehler, T. B. Novey, A. Yokosawa, D. Eartly, K. Pretzl, B. Barnett, A. Laasanen, and P. Steinberg, Phys. Rev. Letters 26, 338 (1971).
11. J. M. Abillon, A. Borg, M. Crozon, T. Leray, J. P. Mendiburu, and J. Tocqueville, Phys. Letters 32B, 712 (1970).
12. Iowa State-St. Louis University-McGill University Collaboration, L. Schroeder, private communication.
13. E. Jenkins, University of Arizona, private communication.
14. R. Ayed, P. Bareyre, and G. Villet, Phys. Letters, 31B, 598 (1970).
15. B. H. Bransden and P. J. Ogden, University of Durham, preprint, unpublished.
16. R. K. Roychoudhury and B. H. Bransden, Nucl. Phys. B27, 125 (1971).
17. R. G. Moorhouse, private communication.
18. R. Cutkosky, **this conference, page** 444.

19. O. Chamberlain, M. J. Hansroul, C. H. Johnson, P. D. Grannis, L. E. Holloway, L. Valetin, P. R. Robrish, and H. M. Steiner, Phys. Rev. Letters 17, 975 (1966).

20. P. J. Duke, D. P. Jones, M. A. R. Kemp, P. G. Murphy, J. D. Prentice, and J. J. Thresher, Phys. Rev. 149, 1077 (1966).

Table I. Effect of R and A Data on Phase Shift Analyses.

P_π = 1080 MeV/c. Initially 76 degrees of freedom.

With addition of new data, 100 degrees of freedom.

7 data points per experiment: $A^\pm$, $R^\pm$; $\cos\theta^* = .65, .55, .45, .35, .25, .15, .05$

$(\Delta A^\pm = \Delta R^\pm = \pm\ 0.1)$

Start Minimizing From Sol'n:

		B2/76	B8/78	C7/97	CH/83	QB/75	YB/90
"Fake"	B2	$\underline{106/0}$	156/14	176/13	149/14	560/11	310/15
$A^\pm$, $R^\pm$	B8	128/13	$\underline{104/0}$	169/3	120/7	$\underline{107/2}$	181/7
Data	C7	120/12	126/3	121/0	139/7	$\underline{103/5}$	149/6
From	CH	206/15	157/6	234/6	$\underline{106/1}$	144/7	121/2
Sol'n	QB	123/13	$\underline{109/1}$	156/2	129/7	$\underline{101/1}$	182/6
	YB	223/14	139/8	208/7	120/2	156/8	119/1

Numbers shown are the χ^2 of each fit together with a parameter which indicates how much the solution has shifted from the starting point. This parameter is small (i.e. 0 - 3) if the sol'n is essentially unchanged and large (i.e. > 10) if the solution differs appreciably from the initial one. The underlined numbers indicate "good" solution, i.e. solutions which fit all of the input data satisfactorily.

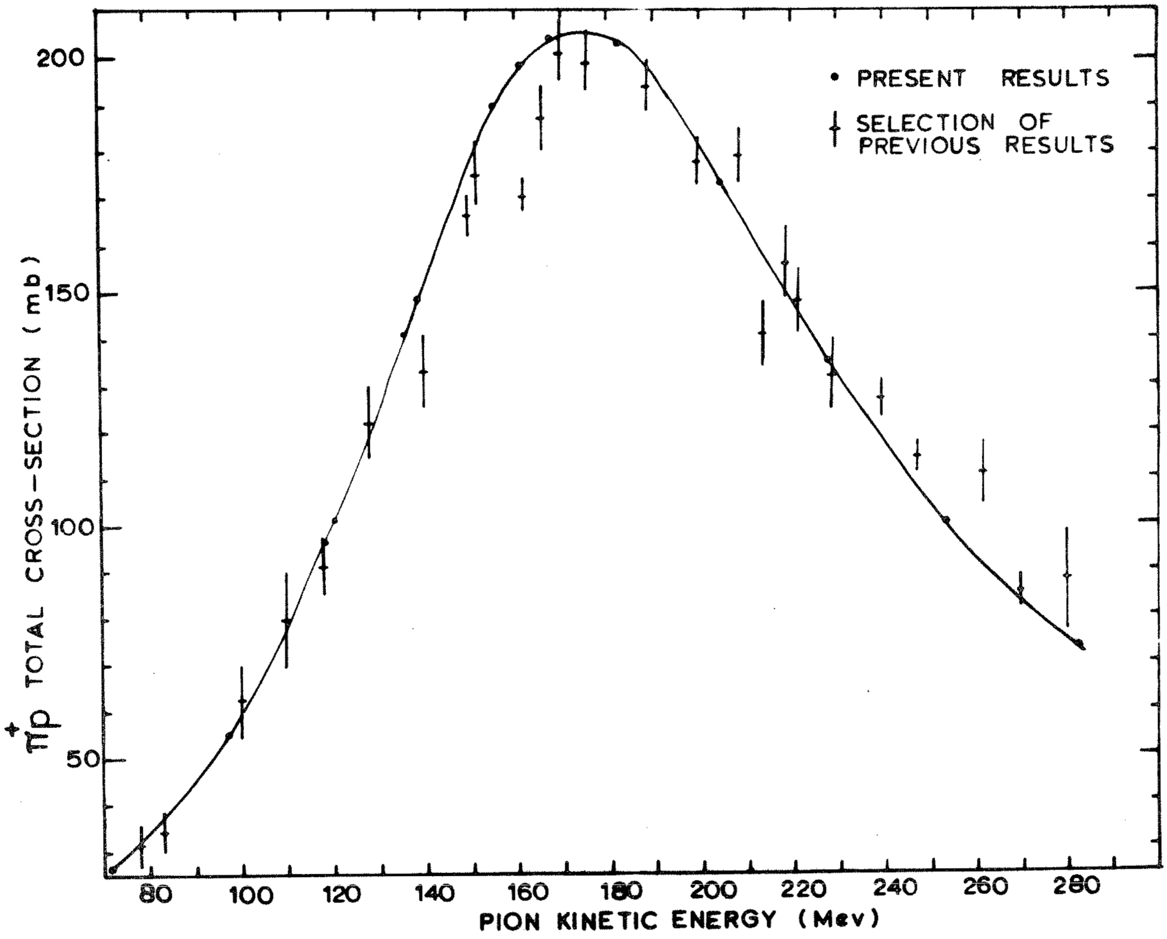

Fig. 1. π^+p total cross-section vs pion kinetic energy. The small points are the results of Carter et al.[4] whereas the points with error flags are a representative sampling of earlier measurements.

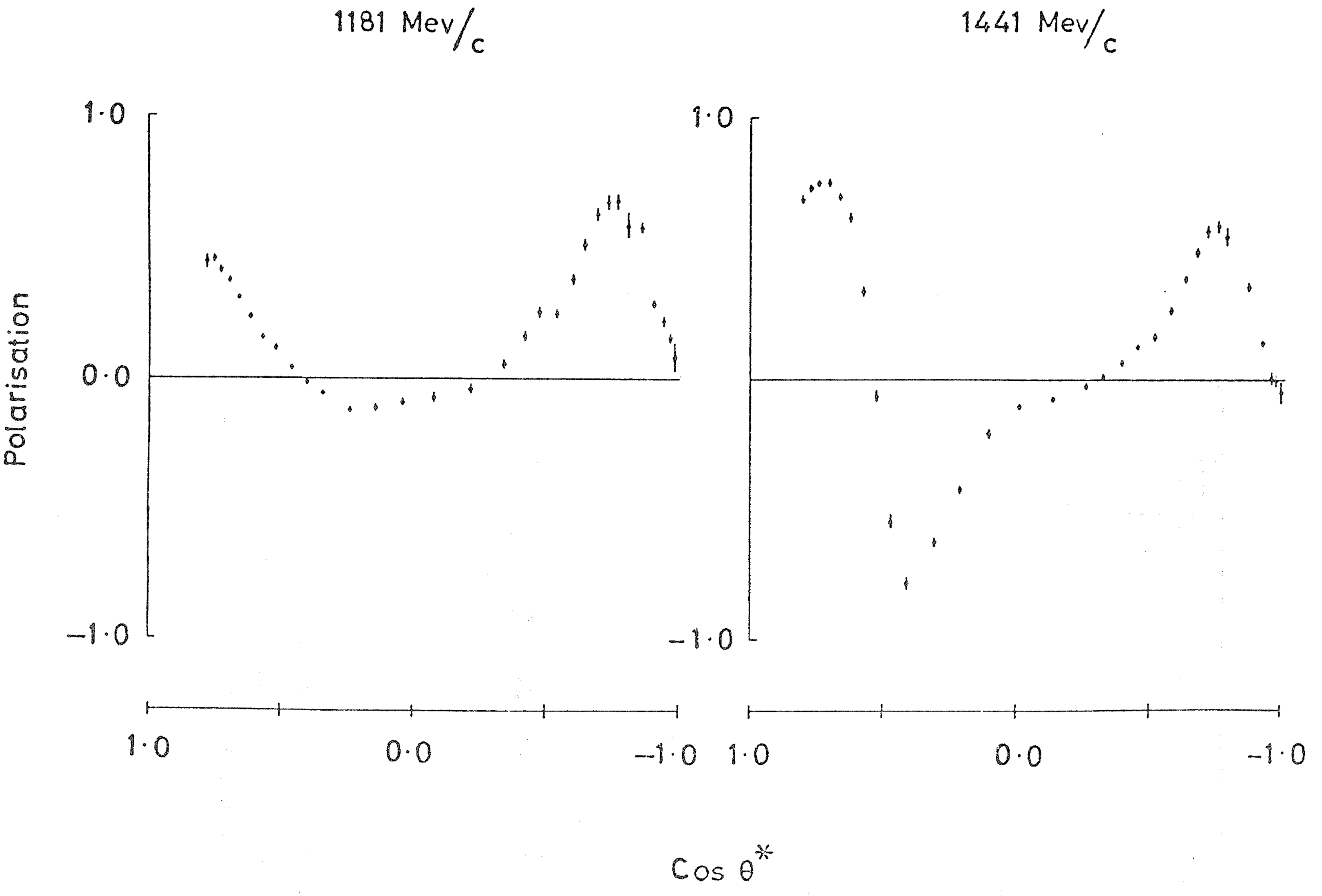

Fig. 2. Recent π^+p Polarization Results at 1181 and 1441 MeV/c as measured by the RHEL polarized target group.[8]

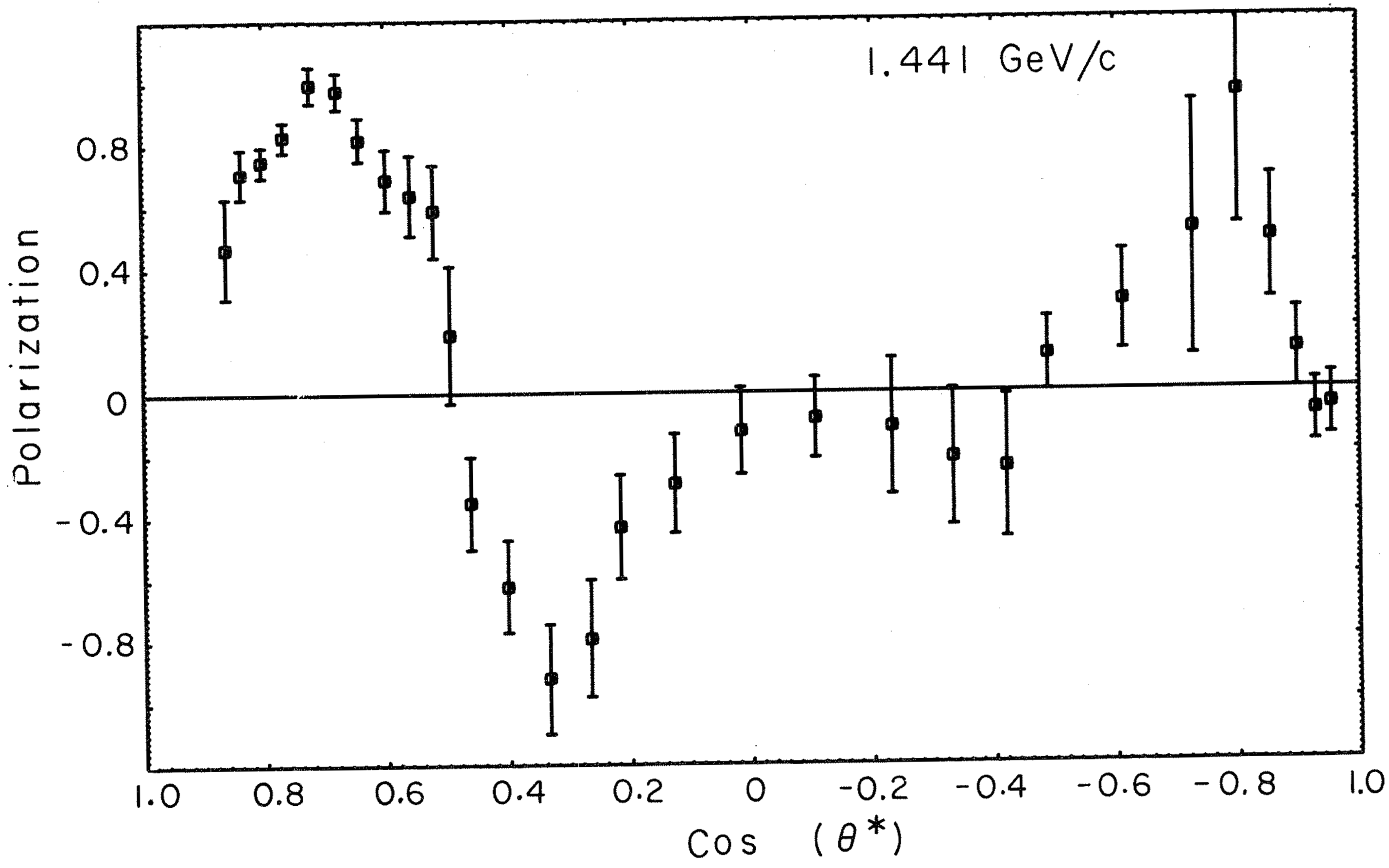

Fig. 3. Results of a 1965 LRL measurement of polarization in π^+p scattering at 1441 MeV/c.[19]

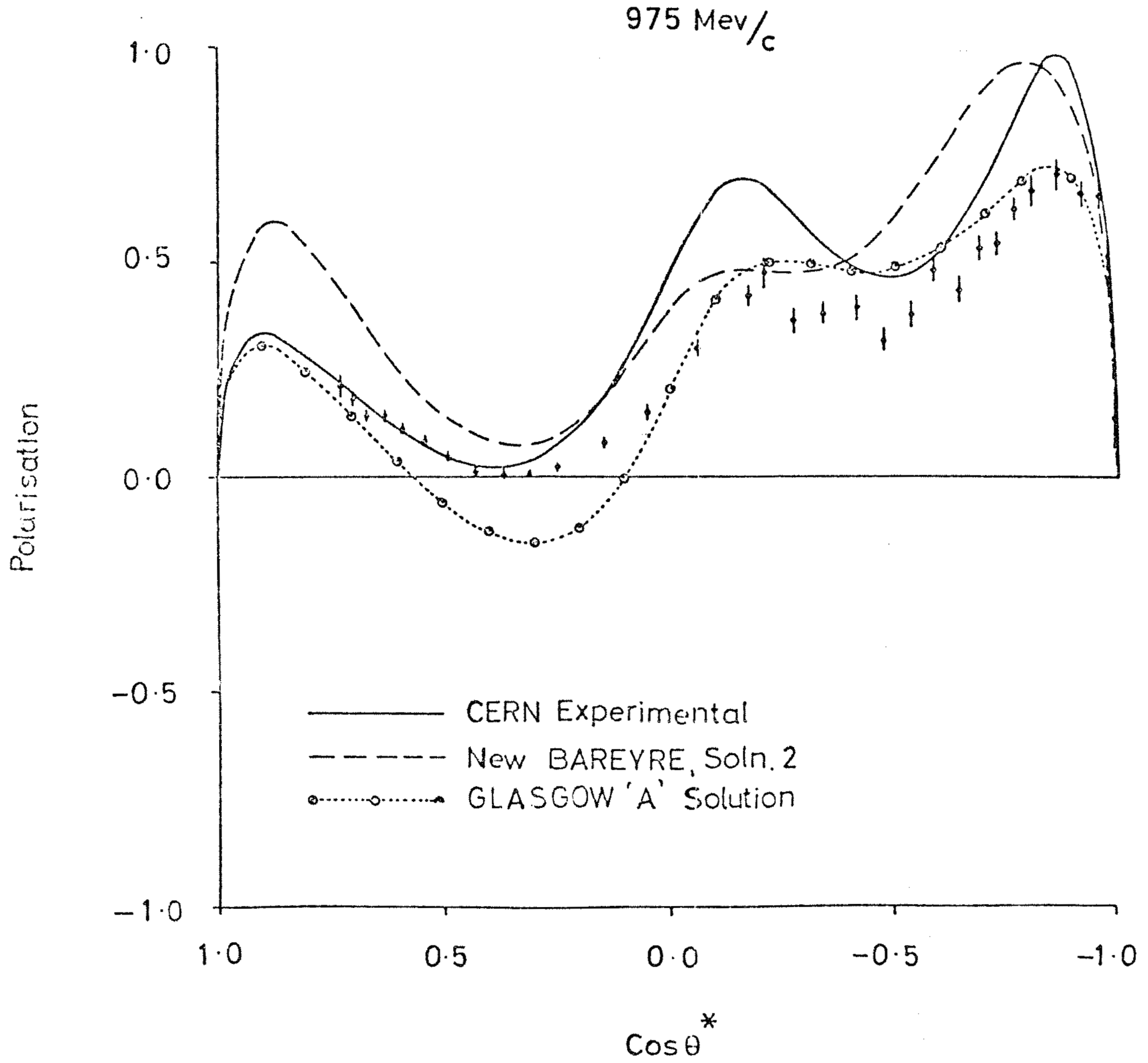

Fig. 4. Comparison of the new RHEL polarization data at 975 MeV/c[8] with various phase shift fits.

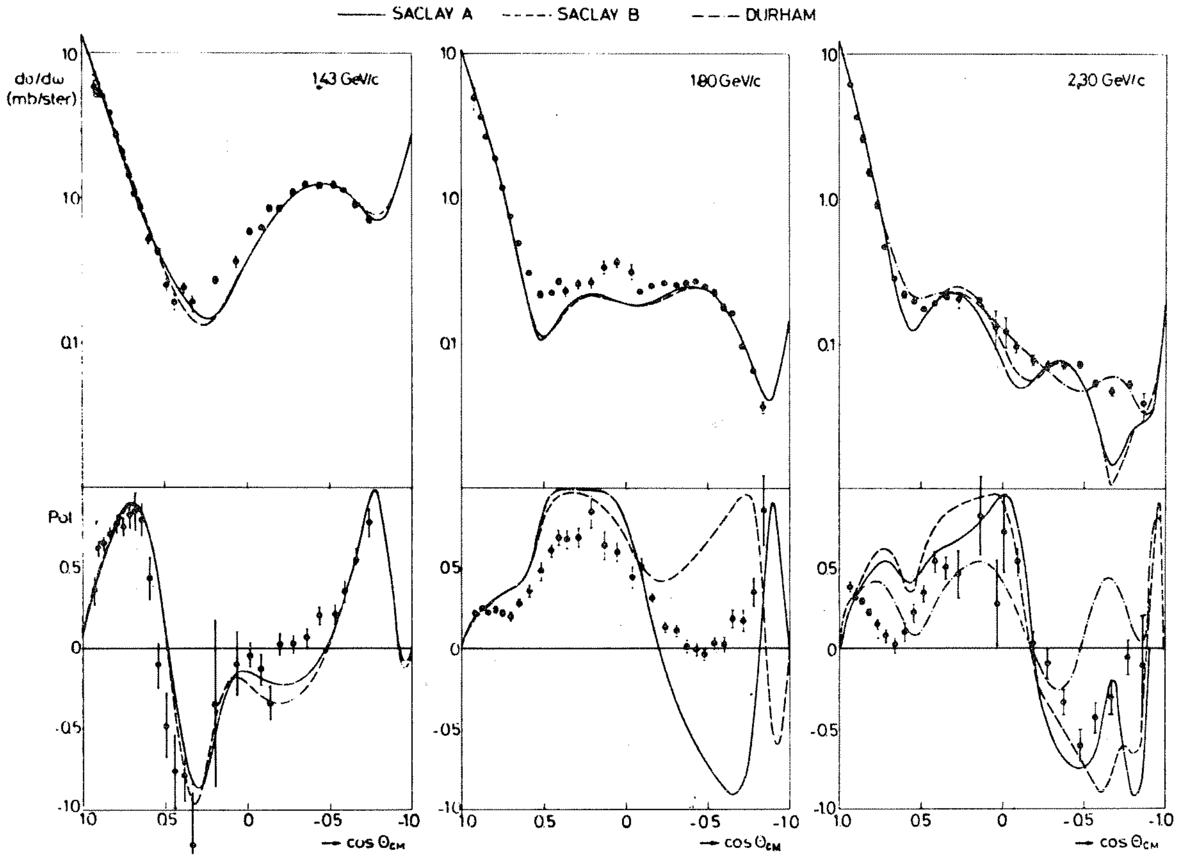

π⁺p ELASTIC SCATTERING
PHASE SHIFT PREDICTIONS (CERN - ALBROW, et al.)

Fig. 5. π^+p polarization and cross-section results obtained at CERN[9] compared with some existing phase shift predictions.

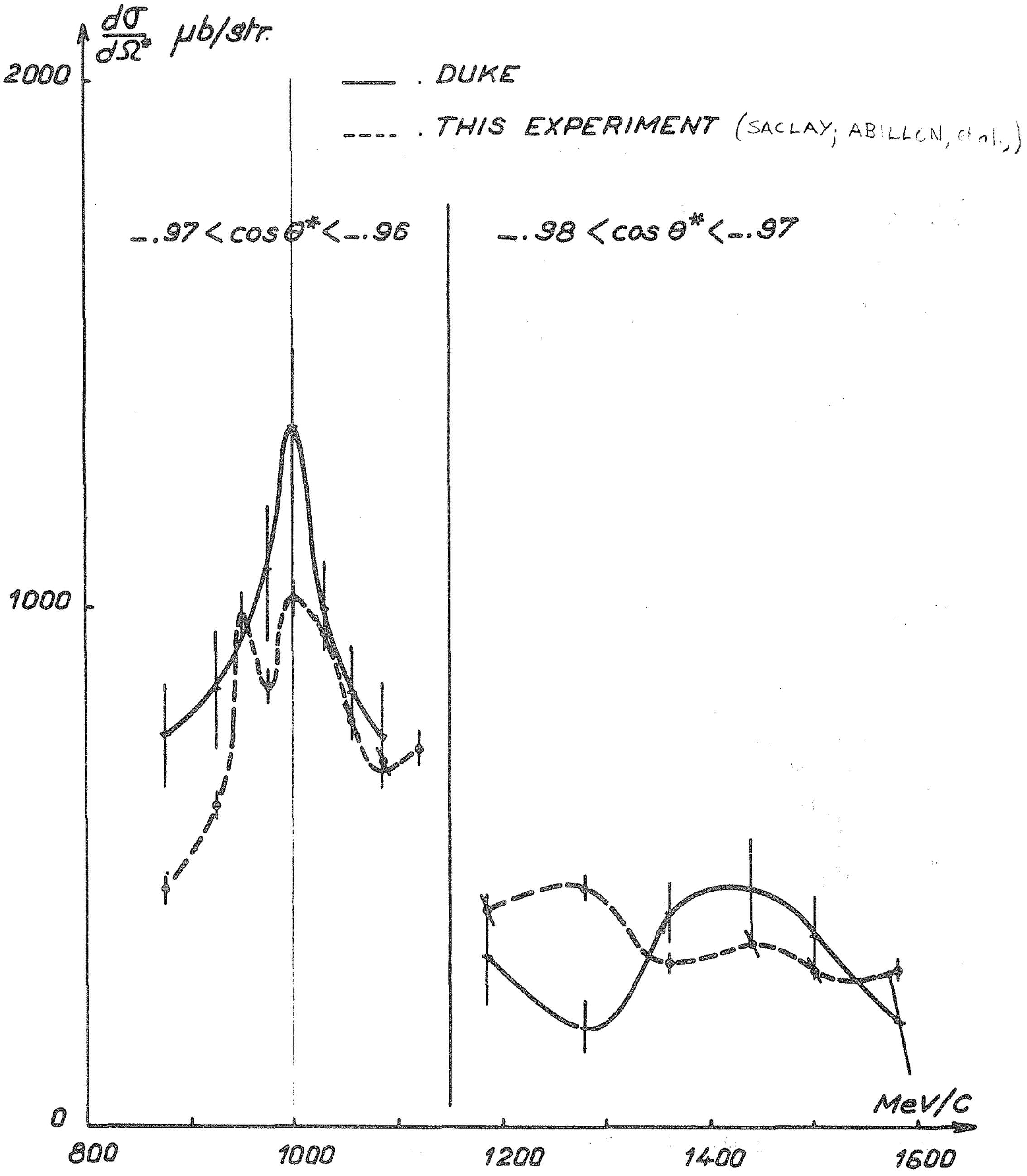

Fig. 6. Recent backward π^-p scattering results from Saclay[11] (dashed curve) and earlier measurements made at NIMROD by Duke et al. (solid curve).[20]

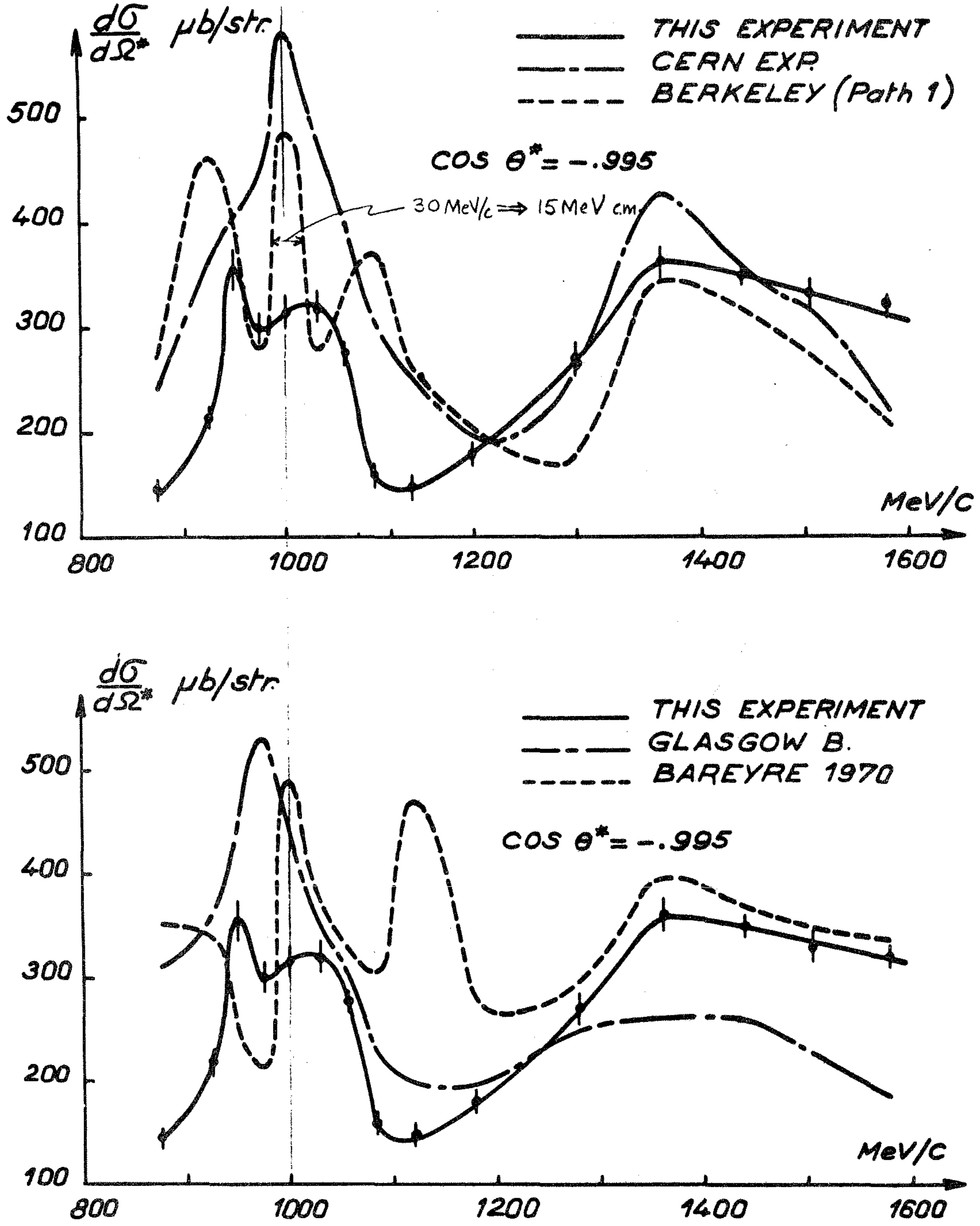

Fig. 7. Comparison of the Saclay backward π^-p scattering data[11] and various phase shift predictions.

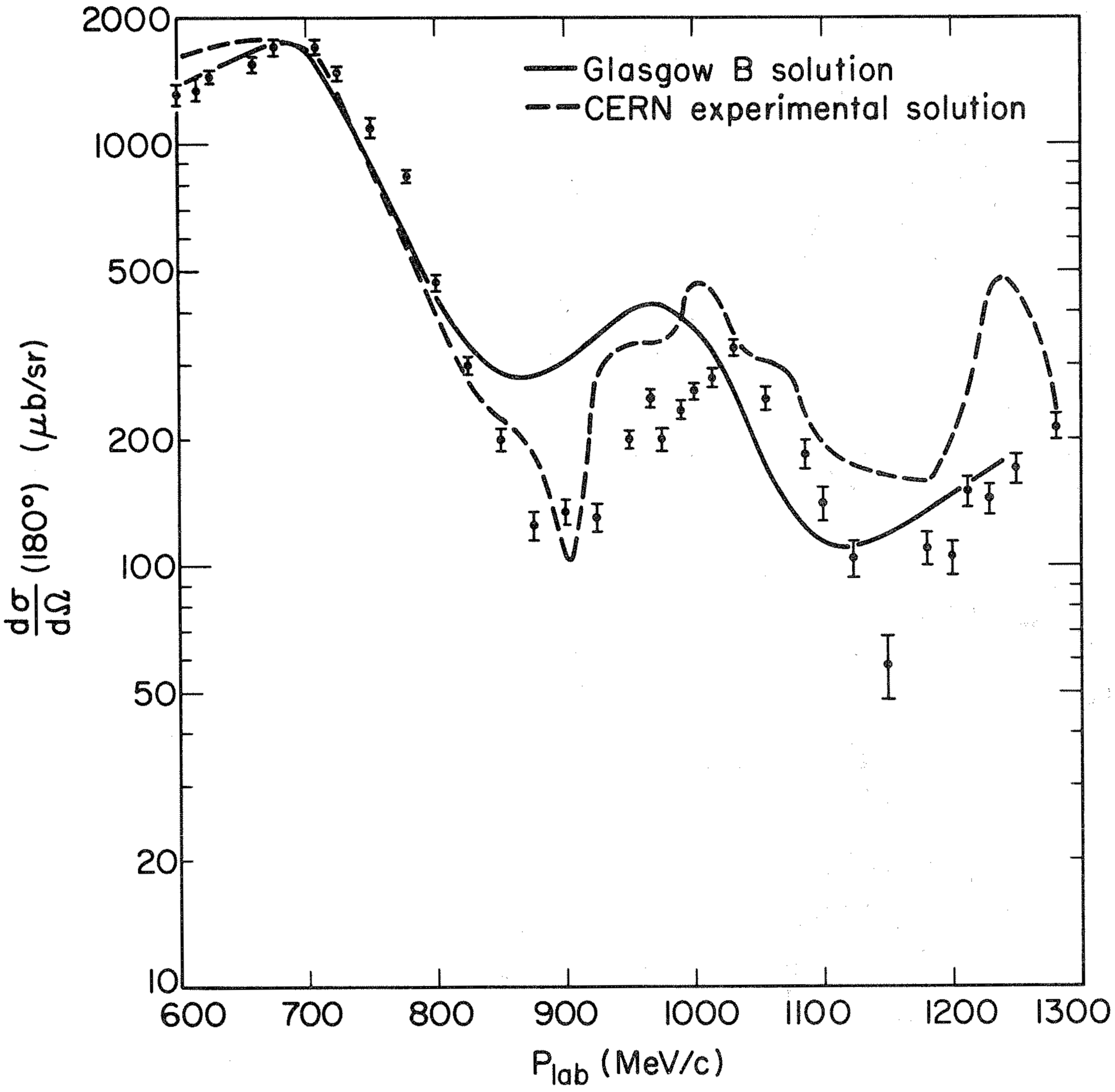

Fig. 8. Preliminary results on backward $\pi^- p \rightarrow \pi^- p$ scattering obtained by the Iowa State-St. Louis University-McGill University collaboration.[12]

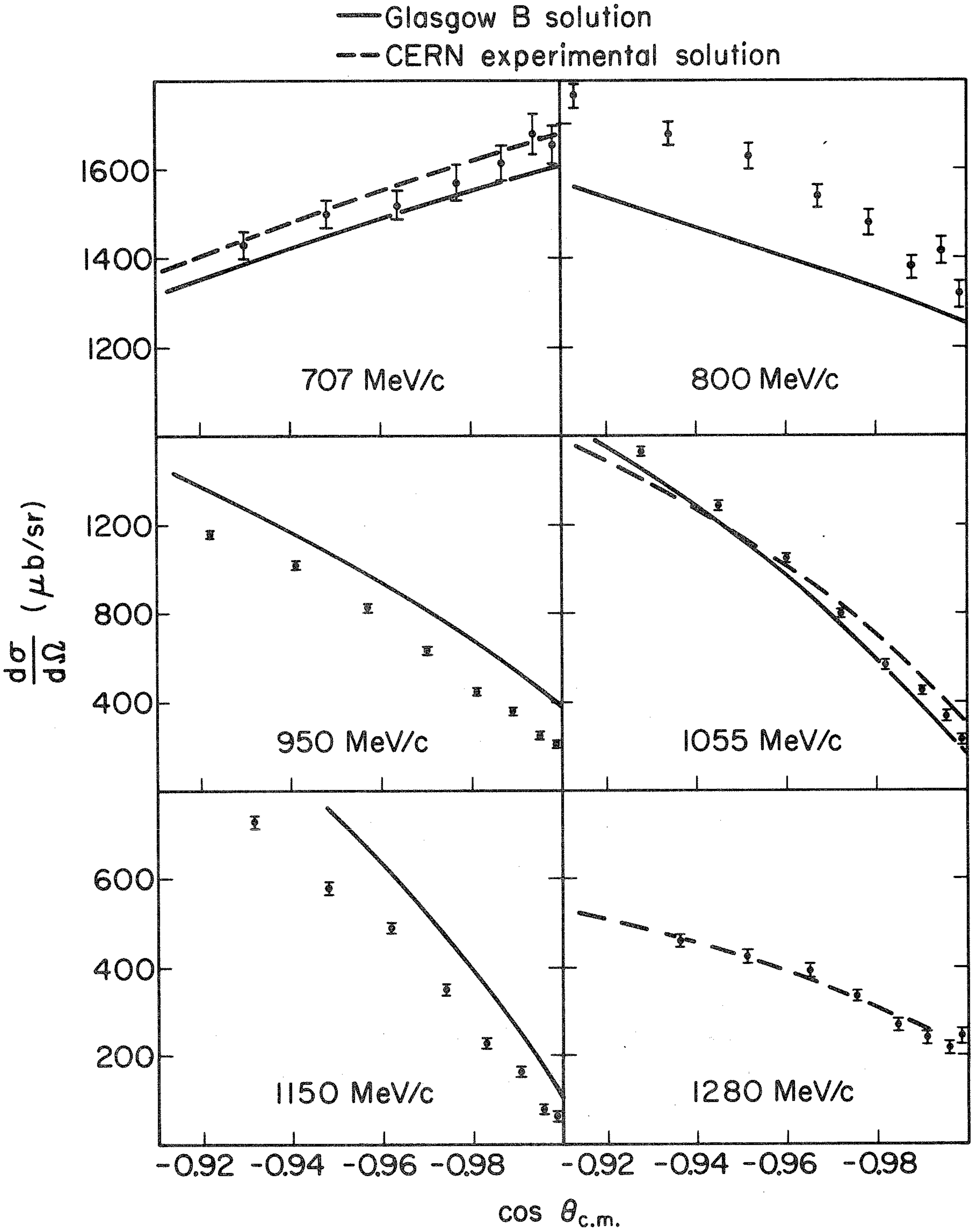

Fig. 9. Preliminary results of angular distributions near 180° for π^-p elastic scattering obtained by the Iowa State-St. Louis University-McGill University collaboration[12] and some phase shift predictions.

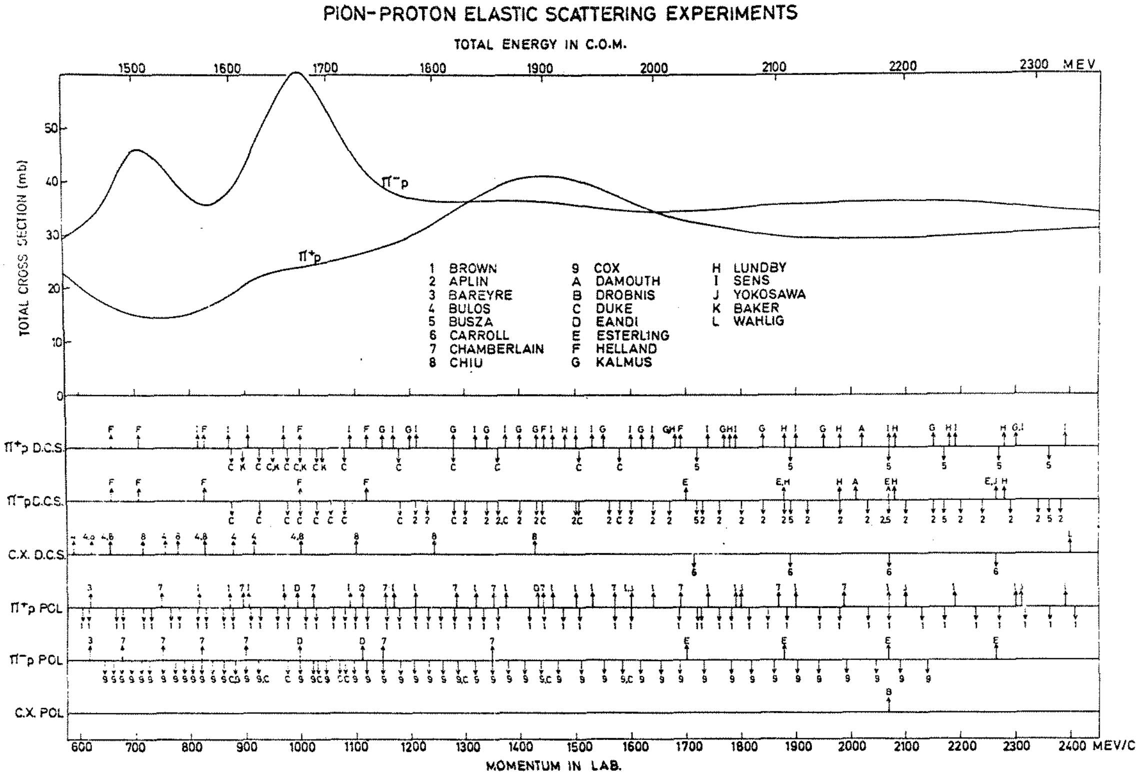

Fig. 10. Summary prepared by the RHEL polarized target group[8] of cross section and polarization measurements in pion nucleon scattering for $0.60 < p_\pi < 2.4$ GeV/c.

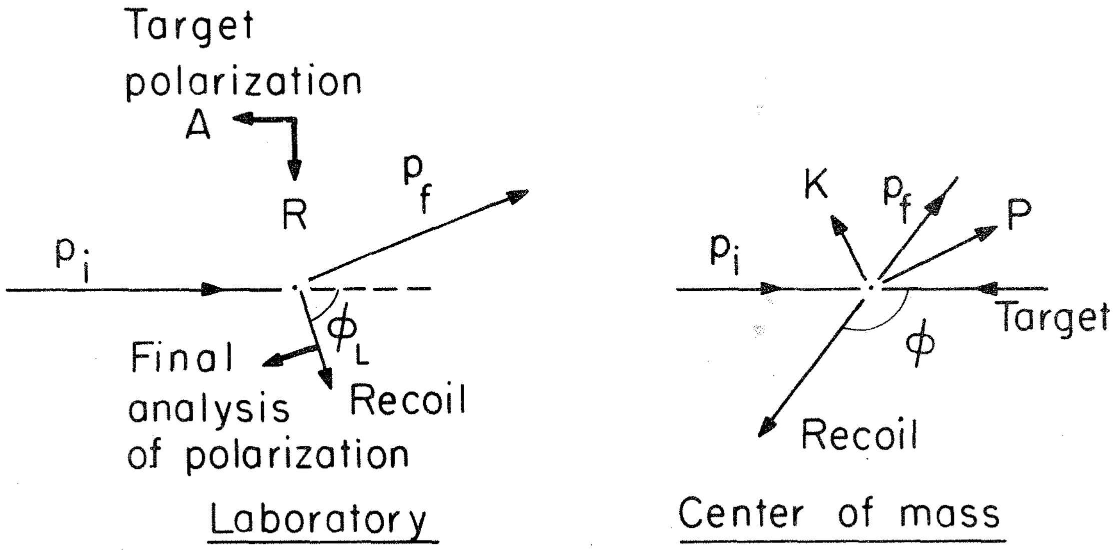
Target
polarization
A
R
p_f
p_i
ϕ_L
Final analysis of polarization
Recoil
Laboratory
K
p_f
P
p_i
Target
ϕ
Recoil
Center of mass

Fig. 11. Geometry for A and R measurements.

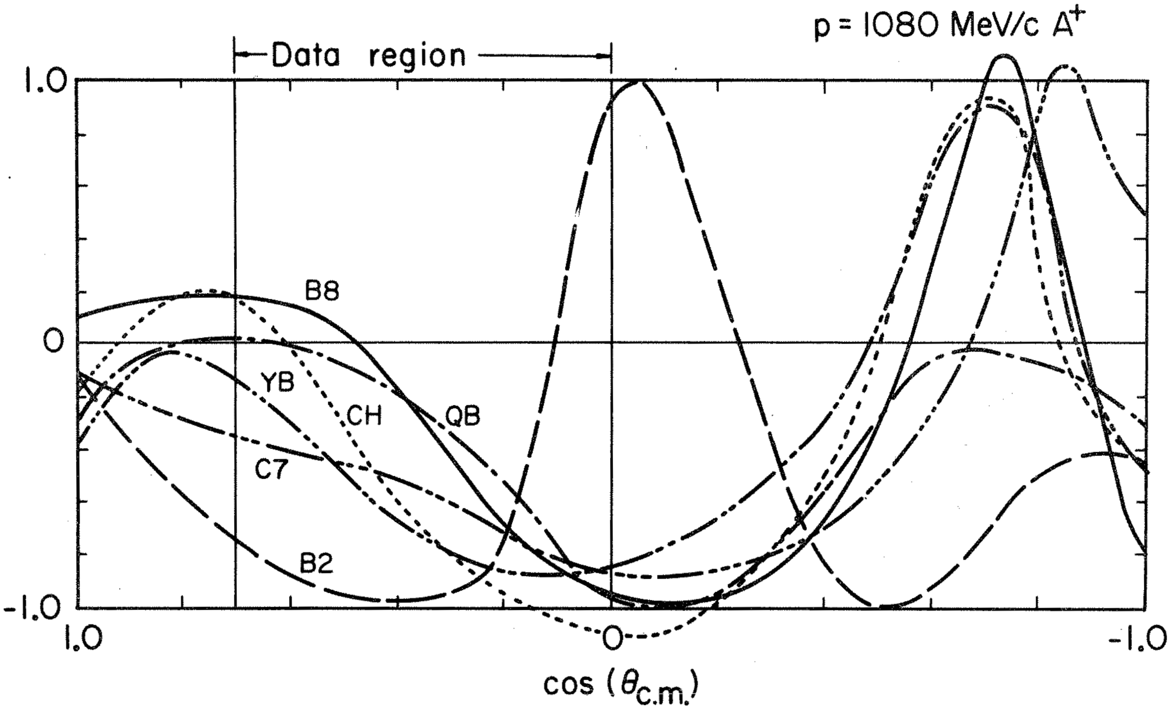

Fig. 12. Predictions of various phase shift solutions (labelled B8, YB, CH, QB, C7, and B2) for $A(\pi^+p \rightarrow \pi^+p)$ at p_π = 1080 MeV/c. From the experimental point of view most measurements would have to be made in the portion of the curves labelled "DATA REGION".

DISCUSSION

Yokosawa (Argonne): We compared the old CERN and Saclay phase shifts with our new backward πN polarization measurements. We concluded that the $\pi^+ p$ phase shifts could be believed up to 1.7 GeV/c and the $\pi^- p$ were pretty good to 2.1 GeV/c. This seems more optimistic than your analysis: is there really any point in complicated R and A measurements below these energies?

Steiner: I think there are two aspects which we have to keep separate. Firstly, we want to find out the general trend of the solution. I think that most people will agree that this has been established up to 1.7 GeV/c. However, there can be small variations. If you look at the energy continuations, they are still rather jagged. Secondly, the errors or the uncertainties of phase shifts will be reduced considerably, if you subject them to new experiments. Not just the same old ones. In this light, I think experiments for $I = 1/2$ states, for example the polarization in charge exchange scattering, will be very significant.

Barbaro-Galtieri (LRL): I have a comment on the $\Delta(1236)$. We have just put out a new up-to-date version of the tables. We have been trying to understand why there is this change in the mass and the width. And we came out with the conclusion that we do not know what the mass and the width are: it depends very much on the formula that you are using. For example, if you fit the δ_{33} phase shift with the conventional Breit-Wigner -- that is, with a conventional Blatt-Weisskopf barrier factor -- you find that the data cannot be fitted. The χ^2 is 48 on 11 data points (cf. page 422 of Steiner's talk).

Lovelace (Rutgers): There is a CDD zero just above the $\Delta(1236)$ (cf. his talk, page 673).

Barbaro-Galtieri (persistently): To fit the data, we have added another term to this barrier factor. The data is fitted very well then -- χ^2 is 11 when we expect 10. The mass is 1234 and the width is 120 MeV. We are back again to parameters similar to those we've been using for many years.

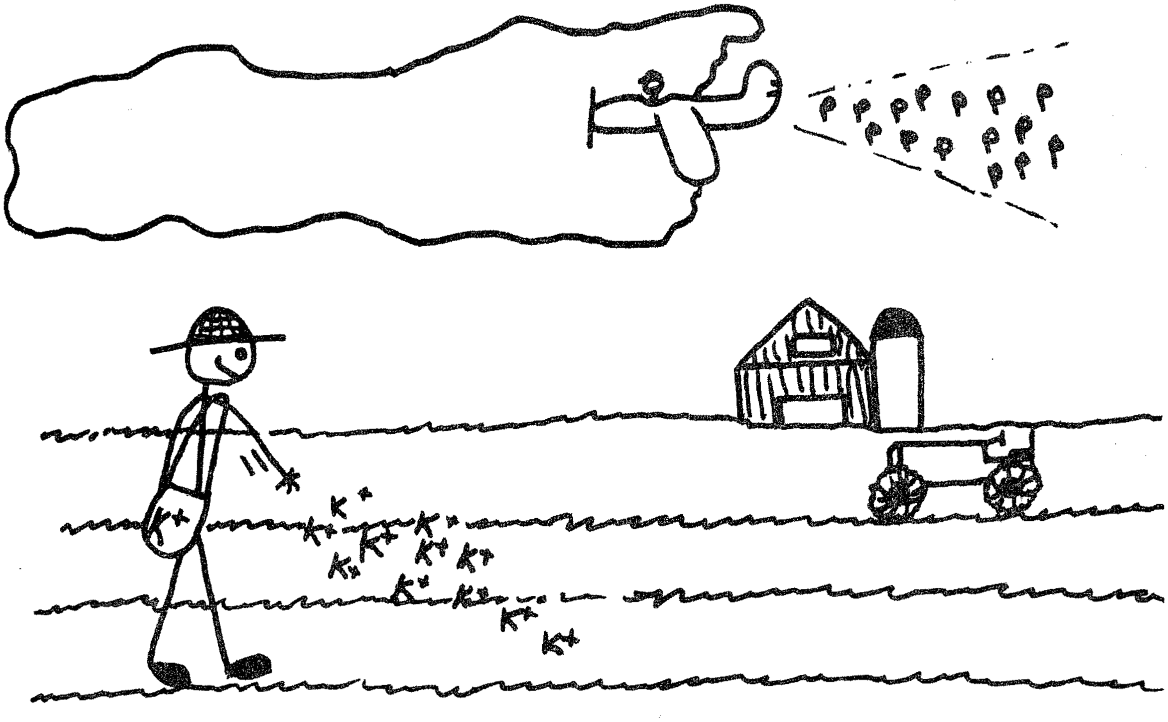

OPTIMIZED ANALYTIC DATA ANALYSIS AND APPLICATION TO K^+p SCATTERING*

R.E. Cutkosky

Physics Department, Carnegie-Mellon University
Pittsburgh, Pennsylvania

---

*Supported in part by the U.S. Atomic Energy Commission.

In this talk I wish, first, to advocate a new approach to data analysis, and, second, to report on some preliminary results obtained with the aid of my collaborators[1] in analyzing K^+-p data.

I. Optimized Analytic Data Analysis

The program being advocated here is one in which we try to get as much help as possible from general analyticity properties for the purpose of extracting interesting physics from experimental data. Some reasons for wanting to use more powerful mathematics in data analysis are:

1) We need to remove biases - a) overt bias, or model dependence; b) covert bias, or bias introduced by artifically restricting the number or kinds of parameters. The hidden bias is less easily recognized, and therefore more serious. We need to find general ways to aid in recognizing these problems, as well as ways to reduce model dependence.

2) We need to find more efficient parametrizations - a) to reduce computer searches to manageable proportions; b) to reduce hidden bias; c) to reduce noise effects (the fewer parameters you fit to lousy data, the fewer lousy results you will get); d) to reduce non-uniqueness (this is especially important in phase shift analysis).

3) We need to recognize the importance of, and to increase, stability - a) so that fits to data will converge stably when experimental information is increased; b) to provide stable extrapolations from data to physically interesting quantities.

What help can we get from mathematics in solving the above problems? They lie in the area known as "Analytic Approximation Theory". Many powerful theorems are known; see, for example, Walsh's book[2]. Building on these, one can prove some optimization theorems; the qualitative content of these theorems can be summarized as follows.

a) The "Convergence Principle": roughly speaking, the more analyticity is exploited (in particular, if one enlarges the domain in which an expansion converges), then the more rapidly an expansion will converge at a given point.[3,4]

b) The "Stability Principle": roughly speaking, the faster an expansion can be made to converge (by using more analyticity) the more stable the sum is against errors in the input information.[5,6]

Some specific techniques have been developed which use these ideas.

1) "Best" polynomial approximation - this involves mapping into the natural convergence domain of polynomial expansions.[3,4]

2) "Best" linear approximation - this involves looking for the best expansion functions (not necessarily polynomials), which turn out to be obtained from an eigenvalue problem.[5]

3) A "Convergence Test Function" Φ has been defined which can be added to χ^2 as $X^2 = \chi^2 + \Phi$. The use of Φ enables one to check that the convergence rate obeys theoretical expectations and at the same time to estimate the truncation error. By minimizing X^2 rather than χ^2, noise effects are discriminated against.[5]

II. Method of Analysis of K^+p Data

The method of the optimized polynomial expansion is being applied to the available data on K^+p elastic scattering.

The conventional partial wave expansion

$$f(x) = \sum a_\ell (2\ell + 1)\, P_\ell(x) \tag{1}$$

converges inside the Lehmann ellipse. In fitting to data, one cuts off the expansion at some value L. Now, for a large ℓ, the amplitudes decrease as

$$a_\ell \sim \exp(-\ell/\ell_0) \tag{2}$$

where

$$\ell_0 = \left[\ell n(a + (a^2 - 1)^{1/2})\right]^{-1} . \tag{3}$$

and where a is the semi-major axis of the ellipse. For large s, we have

$$\ell_o \sim s^{1/2}/4m_\pi \quad . \tag{4}$$

Note that the Λ and Σ poles lie far outside the Lehmann ellipse: the conventional expansion is completely insensitive to the coupling constants.

To increase a as much as possible, we map the cut x-plane into a unifocal ellipse in the z-plane, in such a way that the physical region $-1 \leq x \leq 1$ extends from $z = -1$ to $z = +1$. Then we write

$$f(x) = \sum_n b_n T_n(z(x)) + f_{Born}(x) \tag{5}$$

where $f_{Born}(x)$ is the pole contribution and the T_n are Chebysheff polynomials. We use the T_n because they are convenient for defining the convergence test function Φ. Since a is enlarged, the asymptotic convergence rate defined by $a_n \sim \exp(-n/n_o)$ is characterized by $n_o < \ell_o$, so we expect it is safe to cut off the sum (5) at a value $N < L$. In fact, for large s we have

$$n_o \sim \frac{2}{\pi^2} \ell n\ s \tag{6}$$

so the improvement in convergence rate becomes more and more dramatic as s increases.

The calculational procedure is as follows:[7]

We project out partial waves from (5):

$$\begin{aligned} a_\ell &= \sum_o^n \frac{1}{2}\int dx\ P_\ell(x)\ T_n(z)\ b_n + \frac{1}{2}\int dx\ P_\ell(x)\ f_{Born} \\ &= \sum_o^n C_{\ell n}\ b_n + a_\ell(\text{Born}) \quad . \end{aligned} \tag{7}$$

We solve (7) for b_n in terms of a_ℓ for $\ell \leq N$,

$$b_n = \sum_{0}^{n} C^{-1}_{n\ell} \quad (a_\ell - a_\ell(\text{Born})) \qquad (8)$$

and then insert this back into (7):

$$\underset{\ell > n}{a_\ell} = a_\ell(\text{Born}) + \sum_{n\ell'} C_{\ell n}\, C^{-1}_{n\ell'}\, (a_{\ell'} - a_{\ell'}(\text{Born})) \qquad (9)$$

(In meson-baryon scattering we must, of course, take spin into account and that makes the formulas more complicated). The a_ℓ for $\ell \leq n$ are used as the search parameters in the minimization procedure. It is more convenient to use these instead of the b_n because we are then able to enforce unitarity directly for $\ell \leq n$.

Thus we have a scheme to extrapolate from low partial waves to high partial waves. The formula (9) expresses the fact that analyticity requires the various partial waves to be strongly correlated with each other. One usually thinks of partial wave amplitudes as being independent of each other, in some statistical sense. However, if this were true, the cross section would exhibit Ericsson fluctuations. Since these fluctuations do not exist, the partial wave amplitudes must be correlated.

As is well known, the analyticity domain for Im f(x) is greater than for Re f(x); this is a consequence of unitarity. At energies where the inelasticity becomes appreciable, the nearest branch point is associated with two-pion exchange and with intermediate states such as K^+p. This branch point thus controls the rate of decrease of Im a_ℓ and leads to the high partial waves being quite inelastic. This is consistent with the fact that K^* production becomes highly peripheral quite soon after the threshold.

The Born term we have used for K^+p scattering incorporates a form factor suggested by the exchange-degenerate Regge-pole model. The Λ and Σ are treated as being degenerate at the Λ mass with an effective coupling constant equal to

$$g^2 = g_{KN\Lambda}{}^2 + g_{KN\Sigma}{}^2 \qquad (10)$$

There are several sources of information about g^2.

1) Forward $K^{\pm}p$ Dispersion Relations using a model-dependent extrapolation into the unphysical region. The Kim[8] extrapolation gives $g^2 = 13.5 \pm 2.5$. With other extrapolations the results have varied between 4 and 9 (with small quoted uncertainties). To allow for the model dependence of these results I take $g^2 = 9 \pm 7$ as the combined value.

2) Extrapolation of fixed (low) energy K^+p differential cross sections gave[9] $g^2 = 15 \pm 5$. (The error includes an estimate of truncation error).

3) From a Veneziano-Regge fit to high energy $K^{\pm}p$ data the value $g^2 = 9.5 \pm 3$ was obtained by Lovelace and Wagner.[10] This was raised to 10.5 ± 2.5 in their Veneziano-model phase shift analysis of K^+p data.[11]

4) Chao and Pietarinen[12] have applied the optimally convergent expansion method to the $K^{\pm}p$ dispersion relations. They take as the data region (on $-1 \le z \le 1$) the regions in which K^+p or K^-p forward real amplitudes are known, and map the unphysical region and the very low energy K^-p region where the total cross section is not reliable onto the ellipse. Estimating truncation error by use of Φ, they obtain $g^2 = 14 + 4/-3$.

III. Preliminary Results

We first undertook a detailed comparison of the optimally convergent method with the standard method, using the same number of parameters for each. The value $g^2 = 15$ was used, and a number of parameters chosen so that an adequate fit was obtained by the new method. Then we found that the minimum value of χ^2 was, on the average, about 20% higher when the conventional method was used. The relative improvement was greater for the data near 2 GeV/c than for the data in the 1 GeV/c region.

At our highest momentum (2.5 GeV/c) we only need 14 parameters, corresponding to the partial waves with $L \leq 3$. However, we found it necessary to include extrapolated partial waves with $L \leq 15$ in order to obtain a sufficiently accurate representation of the partial wave expansion. This is a very dramatic indication of the danger of truncating the conventional expansion.

Next we looked at the sensitivity to g^2 in the single energy fits. For this we included the convergence test function, which helped to stabilize the results. We combined the data below 2 GeV/c into groups of "High", "Middle", and "Low" energy, with about 500 data in each group. Each group, by itself, suggests a value $g^2 = 15 \pm 3$. Only a very minimal energy continuity was imposed; we just took the lowest value of X^2 obtained in a fixed number of randomly started searches, provided the energy dependence was not obviously ridiculous. These results are summarized in Fig. 1.

One of the problems which plagues phase shift analysis is that of multiple (ambiguous) fits. This problem is reduced with our new method, for two reasons: first, we can manage with fewer parameters. Second, we have found that we get a somewhat unexpected bonus from the fact that some of the fits obtained by the conventional method are artifacts of the sharp truncation; when we add on the extrapolated partial waves in these solutions, the fit gets worse instead of better.

In the single energy analyses below 1 GeV/c unique solutions were obtained. On passing over the "Brookhaven Bump" the uncertainty increases, but below 1.5 GeV/c there is still a unique group of solutions which can be joined onto the low energy region. Above 1.5 GeV/c the solutions spread out more. An "eyeball" continuity test shows that these results are roughly similar to the favored solution obtained by the conventional method and smoothed by the "shortest path" method.

We have drawn error ellipses at each momentum which are big enough to enclose the separate error ellipses obtained from all the reasonable solutions found at that momentum. These are shown in photographs of computer printout as Figures 2-5a, for the S_1, P_1, D_3, and P_3 amplitudes. At each momentum a cross is plotted with a separate number (or letter). The highest momentum plotted is 1.89 GeV/c in all cases, but we have also included results at 0.6 GeV/c from ref. 7 in the S and P waves, and in the S wave, two more points at lower momenta (also from ref. 7).

Also shown (Fig. 2-5b) is the preliminary result of an attempt to smooth the energy dependence using a new method. The method used is somewhat model dependent, that is, we fit using two-channel unitarity below the K-N*(1400) threshold, and take the second channel to be KΔ for the P_1, P_3 and D_3 partial waves, and to be K*p for the S_1 partial wave (the Δ and K* were also approximated as stable particles). In all the fits shown, it was assumed that no Z* resonance poles were present in any of the four sheets obtained by continuation through the two-channel cuts. The fit was made to the logarithm of Det D using the normed analytic approximation method.[5] It has been checked, by iteration, that these smoothed results are consistent with the actual data at the individual momenta. (Later fits, with a P_3 Z* pole assumed, look very much like Fig. 5b!).

In comparison with other phase shift analyses, it may be noticed that our smoothed results give a somewhat more elastic P_3 partial wave in the momentum region of the "Brookhaven Bump". We have looked into this, and discovered that a test of this point would be given by a measurement of the transverse polarization of recoil protons from a longitudinally polarized target. This polarization changes by amounts up to 0.5 in going between the two kinds of solution.

The most striking effect of our method is that we find significant contributions from the high partial waves: up to 40% of the inelastic cross section, and 25% of the total cross section, at the higher energies. This is consistent with the known fact that K^* production is highly peripheral.

REFERENCES

1. H. R. Hicks, R. L. Kelly, C. C. Shih (Carnegie-Mellon University); P. F. M. Koehler, T. B. Novey, A. Yokosawa (Argonne National Laboratory); G. Burleson (Northwestern University).
2. J. L. Walsh, "Interpolation and Approximation by Rational Functions in the Complex Domain", 2nd Ed., Vol. 20, American Mathematical Society, Providence, R. I., 1956.
3. R. E. Cutkosky and B. B. Deo, Phys. Rev. 174, 1859 (1968).
4. S. Ciulli, Nuovo Cimento 62A, 301 (1969).
5. R. E. Cutkosky, Annals of Phys., 54, 350 (1969).
6. R. E. Cutkosky and S. Ciulli, unpublished.
7. R. E. Cutkosky and B. B. Deo, Phys. Rev. D1, 2547 (1970).
8. J. L. Kim, Phys. Rev. Letters 19, 1079 (1967).
9. R. E. Cutkosky and B. B. Deo, Phys. Rev. Letters 20, 1272 (1968).
10. C. Lovelace and F. Wagner, Nucl. Phys. B28, 141 (1971).
11. It should be noted that Lovelace and Wagner use an expansion which is not stably convergent in the neighborhood of the poles.
12. Y. A. Chao and E. Pietarinen, Phys. Rev. Letters 26, 1060 (1971).

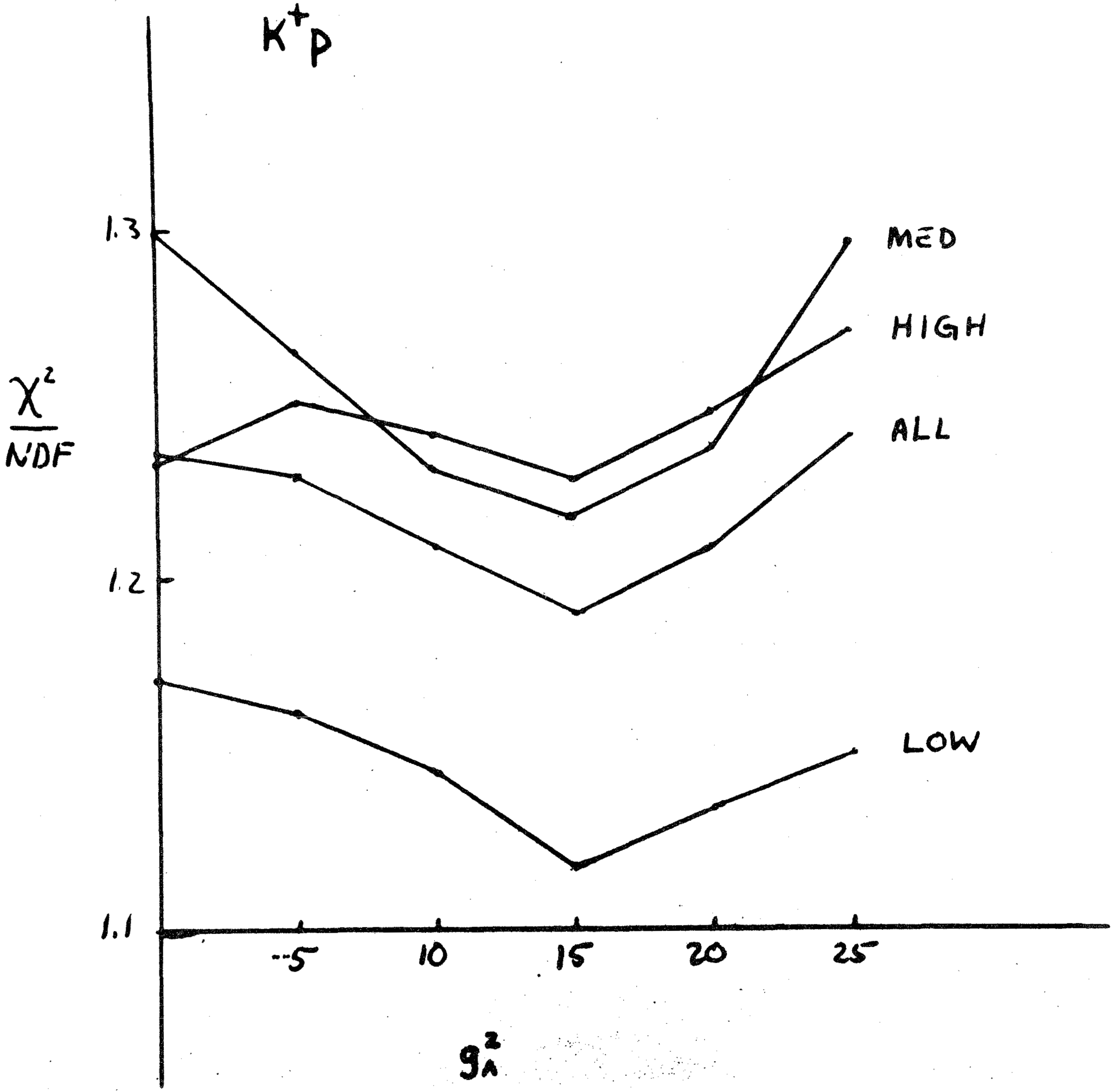

Figure 1: A summary of the sensitivity (measured by the value of χ^2/(degrees of freedom)) of the fits to the value of g_Λ^2 as described on page 450. LOW, MED, HIGH curves correspond to grouping of the data below 2 GeV/c into "low", "middle" and "high" energies. ALL denotes the total data.

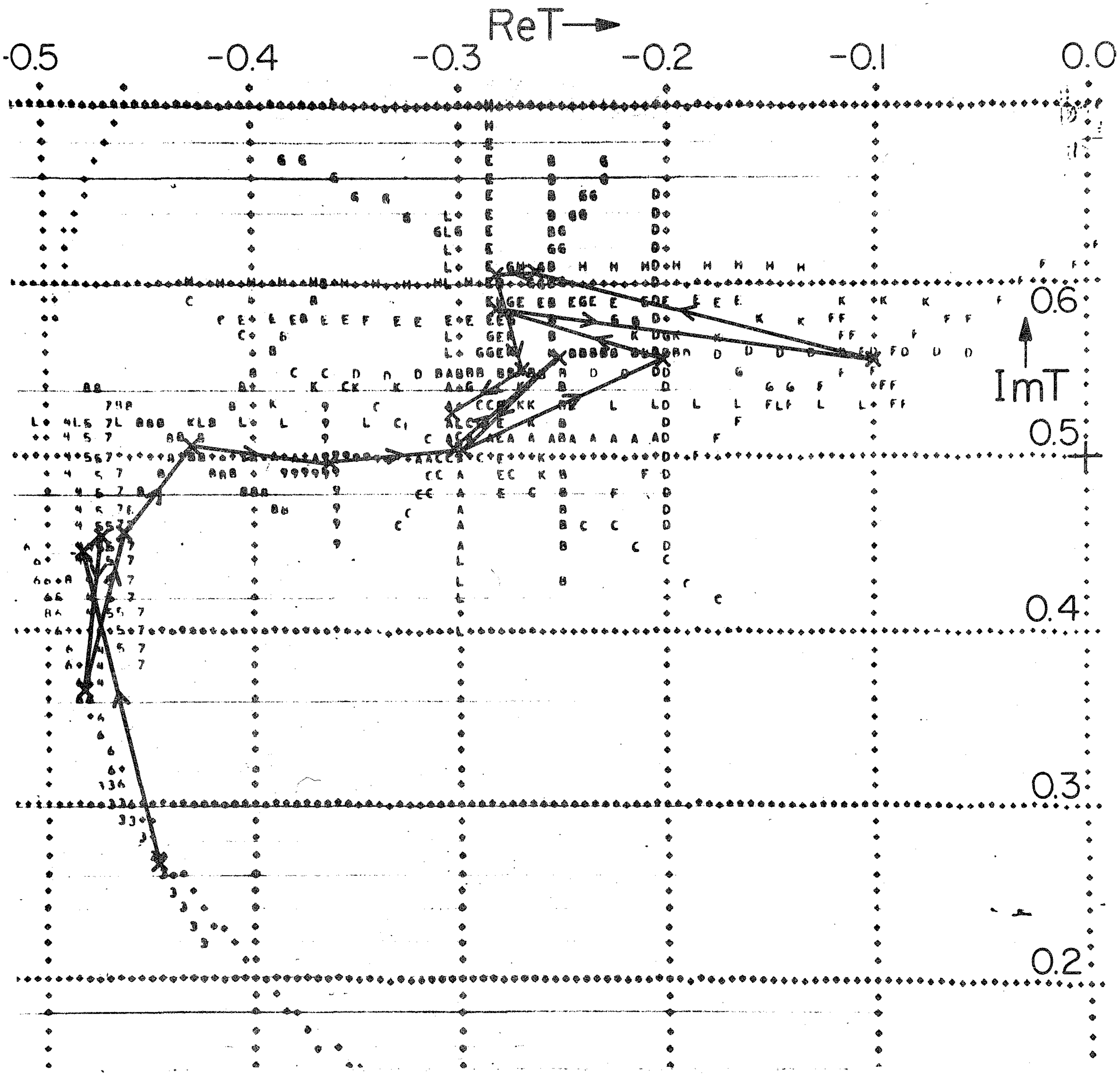

Figure 2(a): Argand plot for S_1 partial wave amplitude before smoothing described on page 451. x's mark centers of error ellipses at each energy and are joined by arrowed lines to guide the eye. The size of the errors is indicated by the computer crosses which also contain the code for the individual momenta. The momenta with their code in brackets are: .6 (3), .78 (4), .865 (5), .91 (6), .97 (7), 1.09 (8), 1.17 (9), 1.21 (A), 1.32 (B), 1.37 (C), 1.45 (D), 1.54 (E), 1.61 (F), 1.64 (G), 1.74 (H), 1.79 (L), 1.89 (K).

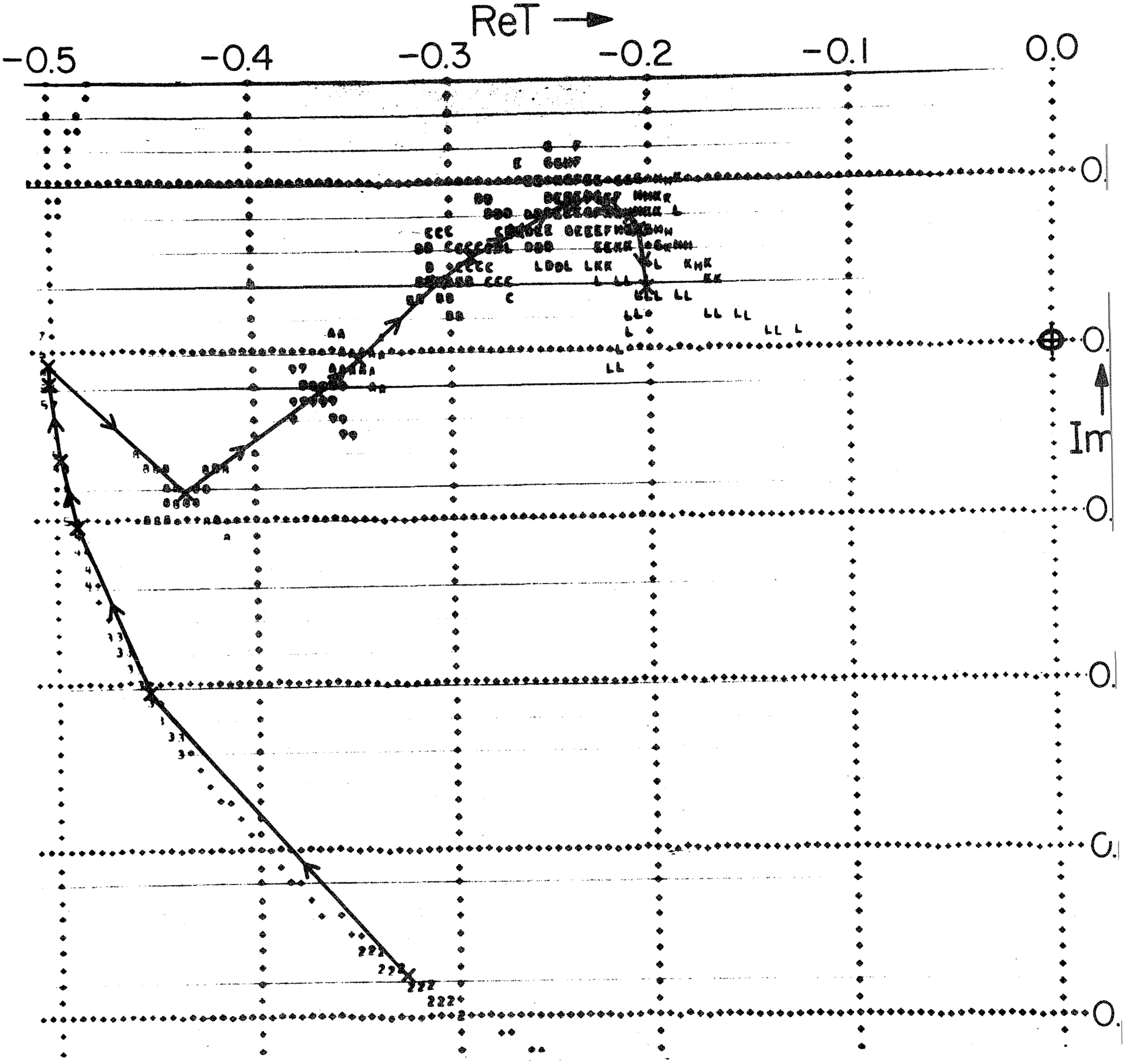

Figure 2(b): Argand plot for S_1 partial wave amplitude after smoothing described on page 451. The amplitude before smoothing is indicated in Fig. 2(a). The symbols have precisely the same meaning as in this latter figure. The code 2 denotes an unspecified momentum below .6 GeV/c. (Page 451).

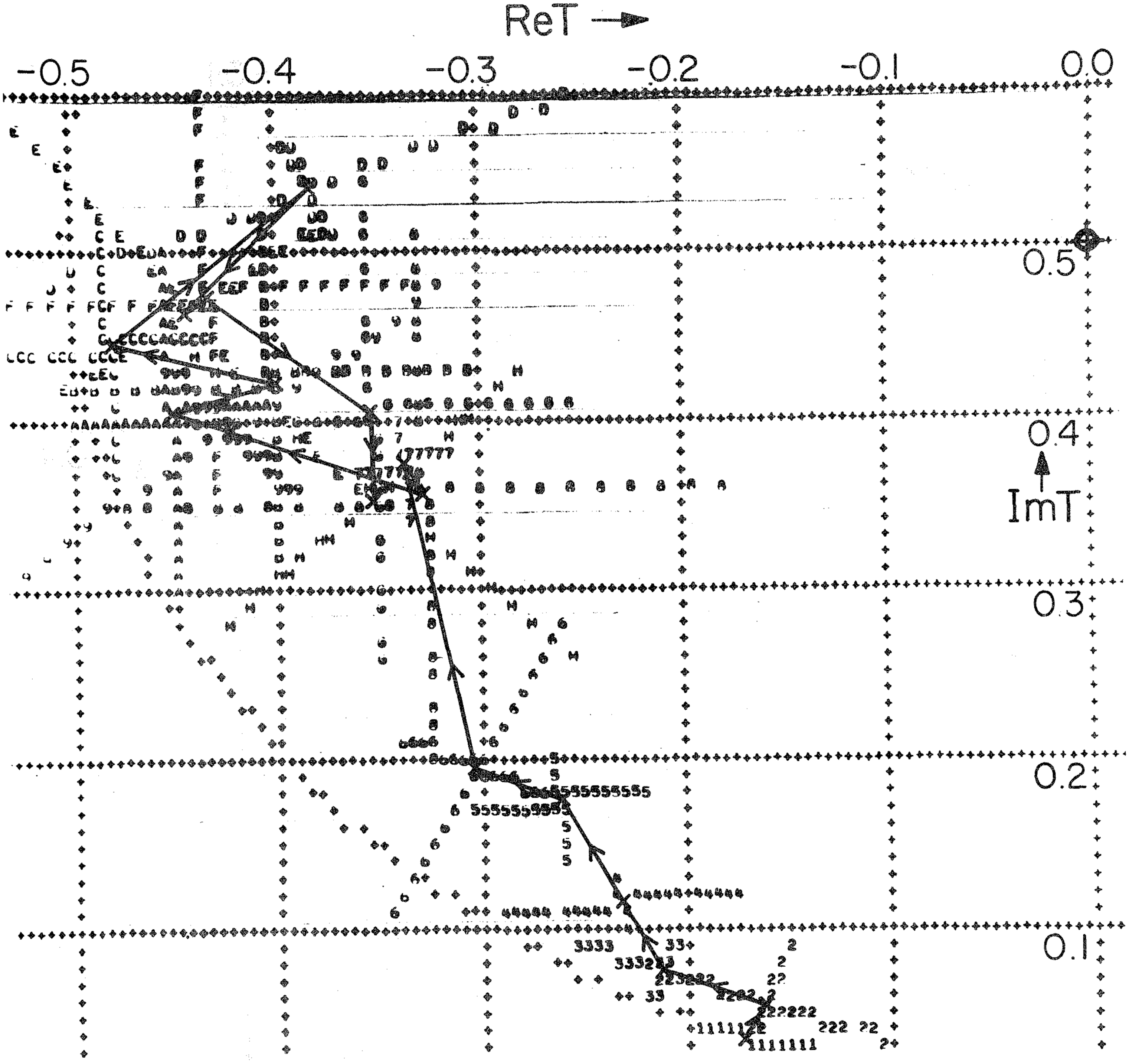

Figure 3(a): Argand plot for P_1 partial wave amplitude before smoothing described on page 451. x's mark centers of error ellipses at each energy and are joined by arrowed lines to guide the eye. The size of the errors is indicated by the computer crosses which also contain the code for the individual momenta. The momenta with their code in brackets are: .6 (1), .78 (2), .865 (3), .91 (4), .97 (5), 1.09 (6), 1.17 (7), 1.21 (8), 1.32 (9), 1.37 (A), 1.45 (B), 1.54 (C), 1.61 (D), 1.64 (E), 1.74 (F), 1.79 (G), 1.89 (H).

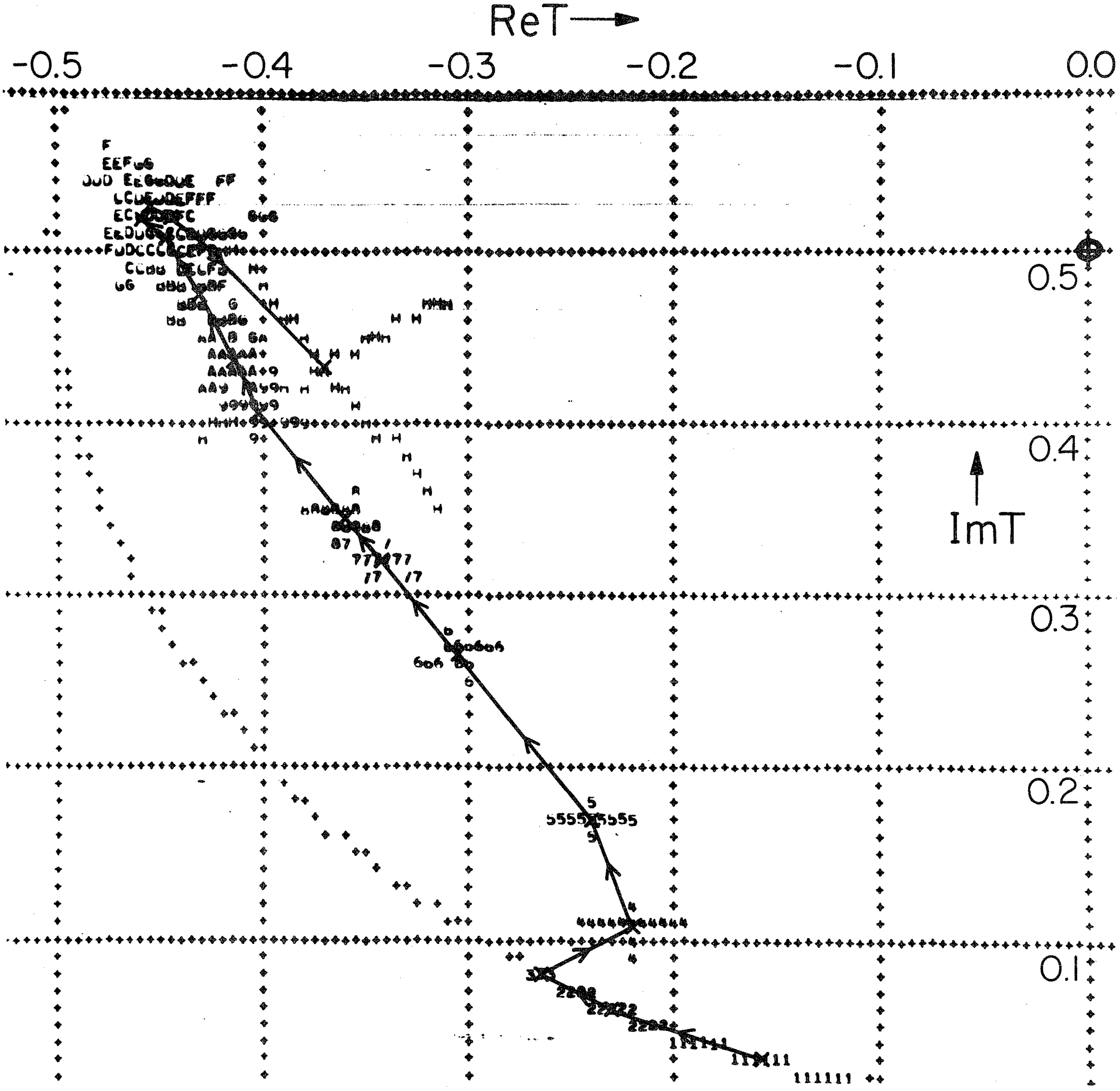

Figure 3(b): Argand plot for P_1 partial wave amplitude after smoothing described on page 451. The amplitude before smoothing is indicated in Fig. 3(a). The symbols have precisely the same meaning as in this latter figure.

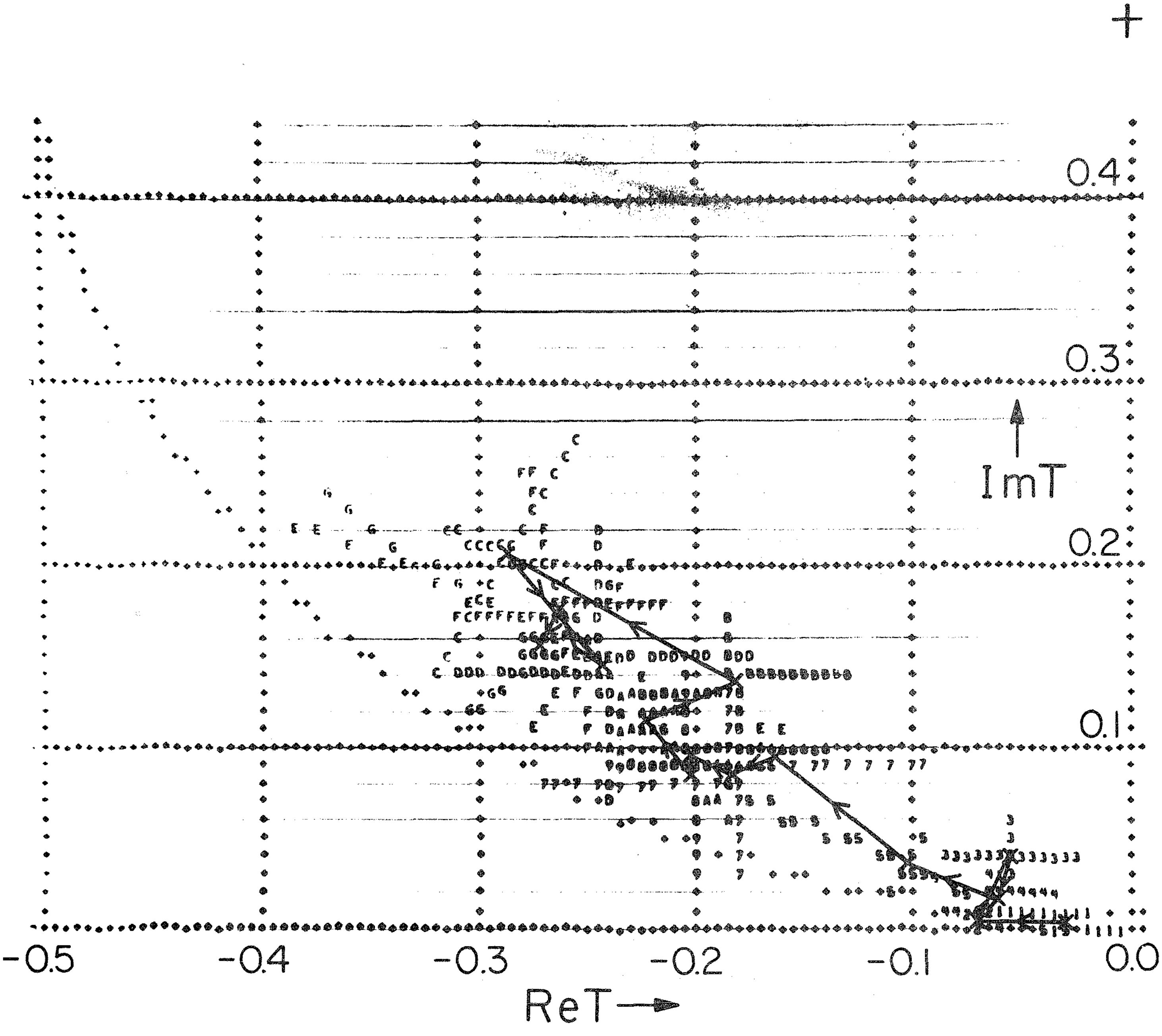

Figure 4(a): Argand plot for D_3 partial wave amplitude before smoothing described on page 451. x's mark centers of error ellipses at each energy and are joined by arrowed lines to guide the eye. The size of the errors is indicated by the computer crosses which also contain the code for the individual momenta. The momenta with their code in brackets are: .78 (1), .865 (2), .91 (3), .97 (4), 1.09 (5), 1.17 (6) 1.21 (7), 1.32 (8), 1.37 (9), 1.45 (A), 1.54 (B), 1.61 (C), 1.64 (D), 1.74 (E), 1.79 (F), 1.89 (G).

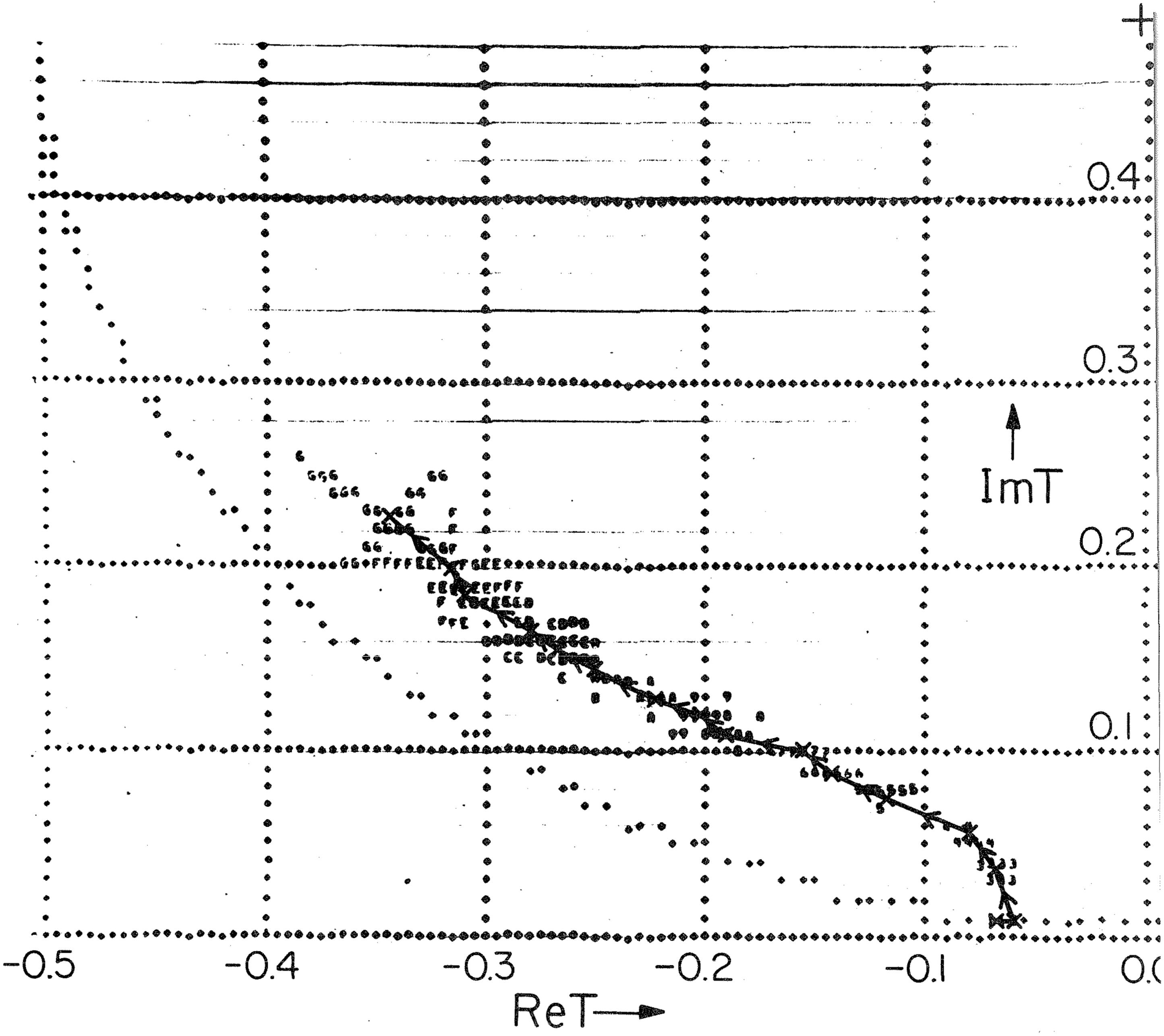

Figure 4(b): Argand plot for D_3 partial wave amplitude after smoothing described on page 451. The amplitude before smoothing is indicated in Fig. 4(a). The symbols have precisely the same meaning as in this latter figure.

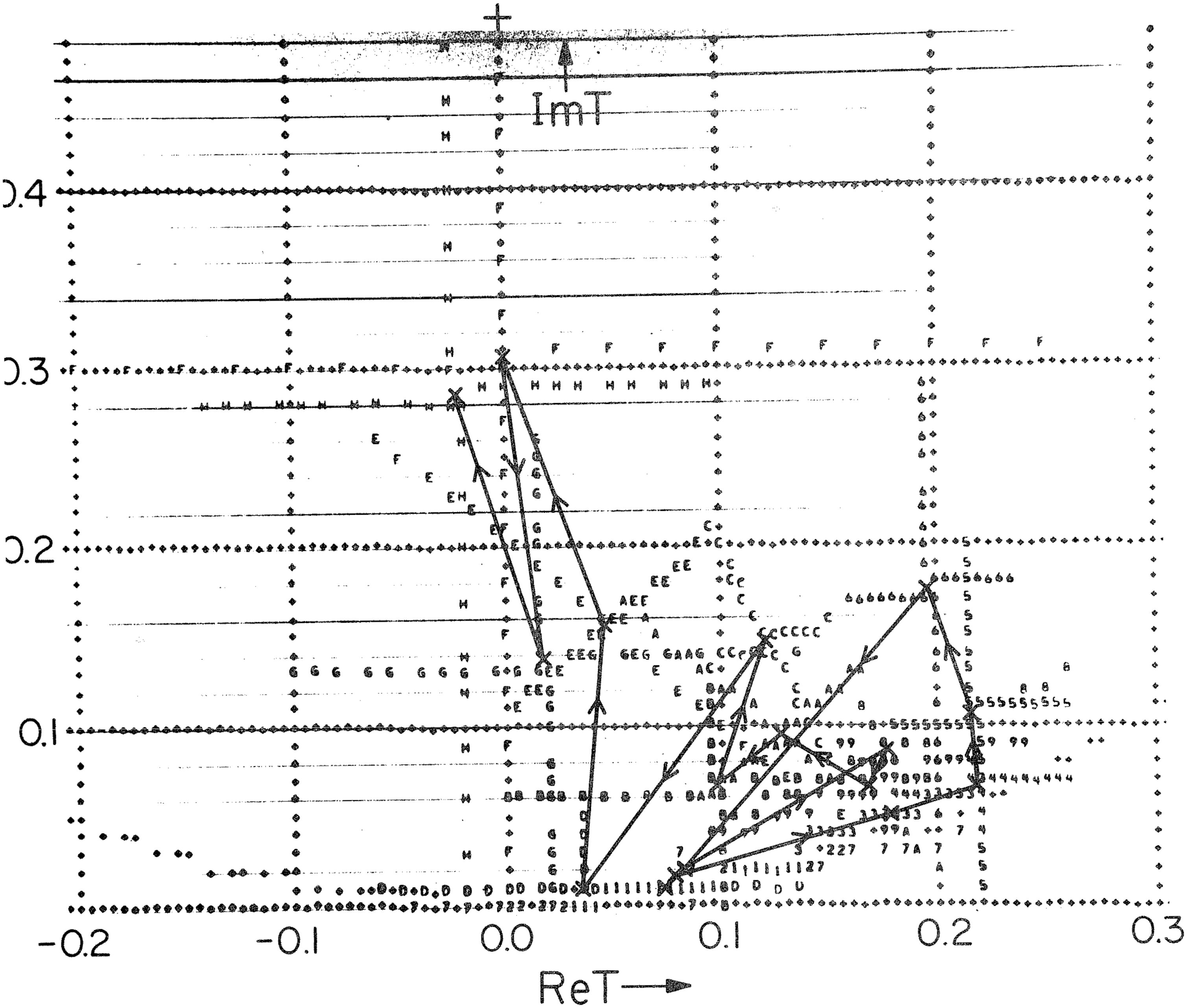

Figure 5(a): Argand plot for P_3 partial wave amplitude before smoothing described on page 451. x's mark centers of error ellipses at each energy and are joined by arrowed lines to guide the eye. The size of the errors is indicated by the computer crosses which also contain the code for the individual momenta. The momenta with their code in brackets are: .6 (1), .78 (2), .865 (3), .91 (4), .97 (5), 1.09 (6), 1.17 (7), 1.21 (8), 1.32 (9), 1.37 (A), 1.45 (B), 1.54 (C), 1.61 (D), 1.64 (E), 1.74 (F), 1.79 (G), 1.89 (H).

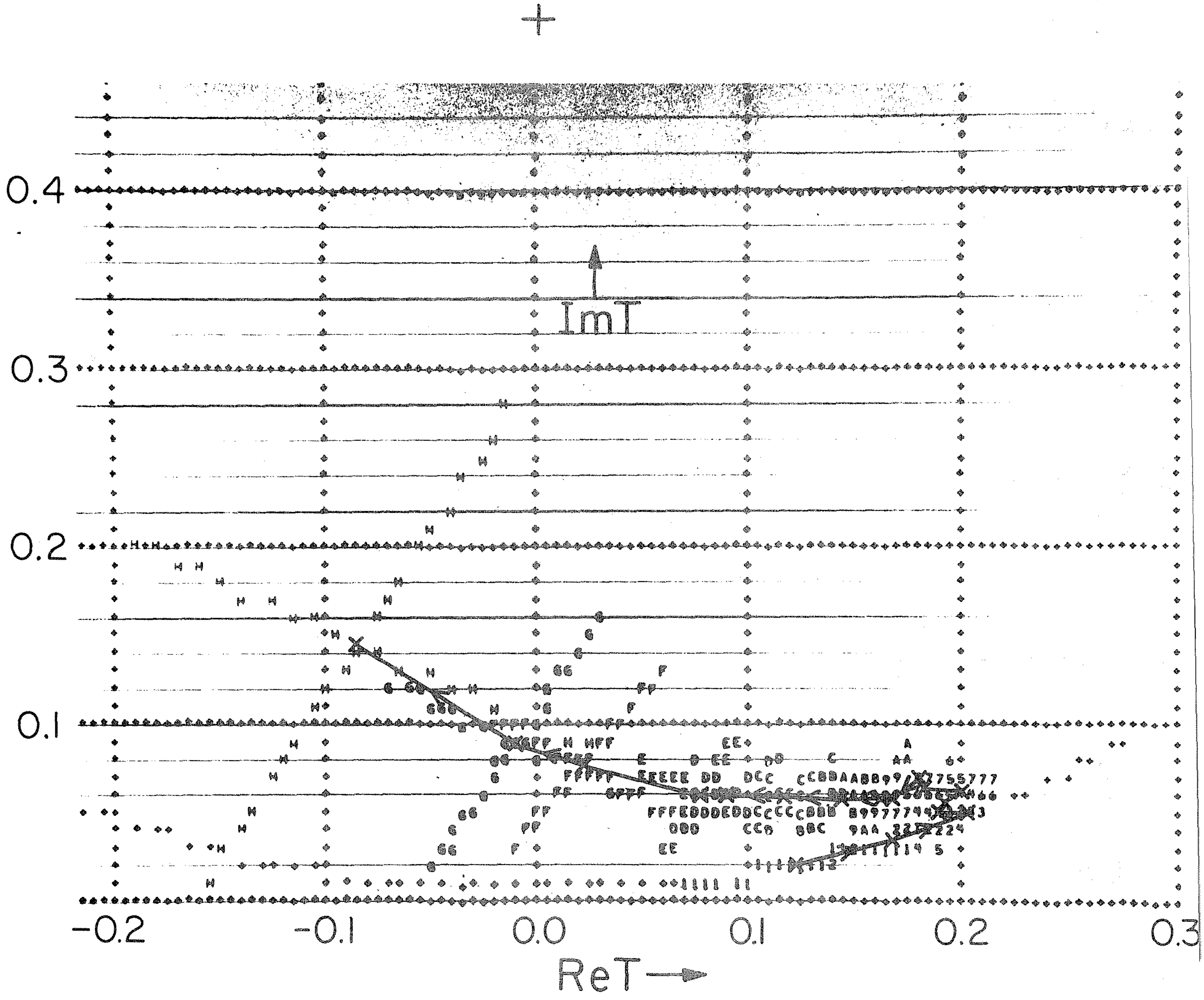

Figure 5(b): Argand plot for P_3 partial wave amplitude after smoothing described on page 451. The amplitude before smoothing is indicated in Fig. 5(a). The symbols have precisely the same meaning as in this latter figure. Fits with a Z^* pole give similar Argand plots (page 451).

DISCUSSION

Warnock (IIT): Since you have the high partial waves expressed in terms of the low partial waves, suppose that the low partial wave has a sharp resonance, what prevents this from occurring spuriously in the high partial waves?

Cutkosky: Well, this is something that has bothered me for a couple of years. I finally decided that it wouldn't be spurious. In fact, we know that there are good experimental and theoretical reasons indicating that there is a tendency for resonances to occur simultaneously--daughters and all that! An obvious theoretical example is the Veneziano model which uses analyticity much more strictly than we do here; as a consequence if you have a resonance in a high partial wave, this model gives similar resonances in all lower partial waves. Now we are using analyticity very loosely--one could say we were using a weak kind of duality. The result is that I think the (loose) correlation between resonances our model produces is not at all spurious--it is a very real part of physics.

Bjorken (SLAC): I wonder whether this procedure is stable with respect to perturbations of the analyticity. In other words, supposing there is a triple ice-cream-cone diagram, something which is very complicated and gives you a distant complex singularity in the cosine Θ plane, does that singularity remain distant, after your mapping?

Cutkosky: The answer is no--as far as I know. Actually, there is a certain amount of theoretical work that can be done here. First of all, to check the specific thing you have just mentioned. However, more generally, one can examine the sensitivity of the final answers to the input assumptions. This is something, in fact, not so much is known about in the mathematical literature, and there is little helpful work we can borrow for this. As an extreme example one can ask that maybe this whole analyticity picture is wrong. But how are we going to find this out except by using it in as stringent a way as possible? And presumably, if one has accurate enough data, you would eventually find out that there is something wrong by using the analyticity as much as possible. Certainly, as I discussed in the text, the model is sensitive to the residues and hence the existence of the Λ and Σ poles.

Yokosawa (Argonne): Could you comment on the errors in your calculated partial waves?

Cutkosky: There are two major sources on uncertainty in the calculations. The first comes from the model used in smoothing the energy independent phase shifts. We used the two-channel model below 2 GeV, with the unstable particle treated as a stable particle. There is some bias. We think that at the moment, one should add 10% of the amplitude to the error. Now we are in the process of trying another technique, which does not have the same assumption. It is more like the original Lovelace dispersion relations. The assumption going into this is quite different, and comparison of the two methods should give a good estimate of the error. Secondly, we have the intrinsic error in the analysis at each energy. This, in turn, has two parts to its uncertainty. The first part is just the usual error coming from the X^2 fit. (or more exactly X^2 when we include the convergence test function). The second part is the systematic error coming from neglecting higher terms in the partial wave series. To find a suitable cutoff in the series we look both for an acceptable X^2, and also at the convergence test function. One can, in fact, use the latter to estimate the error produced by the cutoff and fold this into the total error.

Moravcsik (Oregon): In your papers, you mention that the unitarity is not automatic in your theory. Thus, if the partial wave amplitude is outside the unitarity circle, you have to put it back in the circle by hand. Would you like to comment on this?

Cutkosky: Well, the general idea here is to call it the conformally mapped unitarized expansion--CMU for short! To be serious, this is something which worried Deo and I a great deal at the beginning. It turns out, expecially in the inelastic region, that there is no problem at all. Essentially, all the good solutions are with all the partial waves being unitary. This enables us to write fast computer programs to do the minimization. To be exact, there are some anomalous cases, where a few higher partial waves do not turn out to be unitary. In particular, in the region of the Cool bump, there is a tendency for the P_3 to have a high imaginary part, which is somehow correlated with non-unitary high partial waves. I don't know whether that is significant or not.

Rosner (Minnesota): What you are doing then, is to suppress the inelasticity in those partial waves which you know about, and this pops up in the other partial waves. Is this a fair statement? For instance, in the D_5 wave for the solution of S. Andersson et al. (Phys. Letters 30B, 56 (1969)), the amplitude goes inelastic fairly rapidly. This accounts for the Cool bump in this solution. What accounts for the Cool bump in your parameterization?

Cutkosky: It is a little obscure. It is sort of spread out between the various partial wave amplitudes; it is present in both high and low partial waves.

Initially we found solutions with a large D_5 inelasticity but, in fact, it turned out that this is something which is completely unconstrained by the data. The χ^2 did not change at all, while the inelasticity of D_5 varied over an enormous range. For this reason we put in the "soft" constraint that the D_5 have a similar imaginary part to the F_5 wave. When we put in this D_5 constraint, we found that it automatically constrains somewhat, all the higher partial waves with $J = \ell + \frac{1}{2}$. This is also reasonable, because these are precisely the ones with a large angular momentum barrier in the production channels. But to return to the question, the result is that the inelasticity is spread among the partial waves in a way I don't understand very well at present.

Yokosawa: I have a question to the chairman (Moravcsik) actually. You mentioned once that your phase band program and Cutkosky's method can be combined. I wonder if you can make a short comment on this.

Moravcsik: Maybe we can talk about this afterwards. Since we did not talk about my method at all, it is hard to answer the question about the combination of the two.

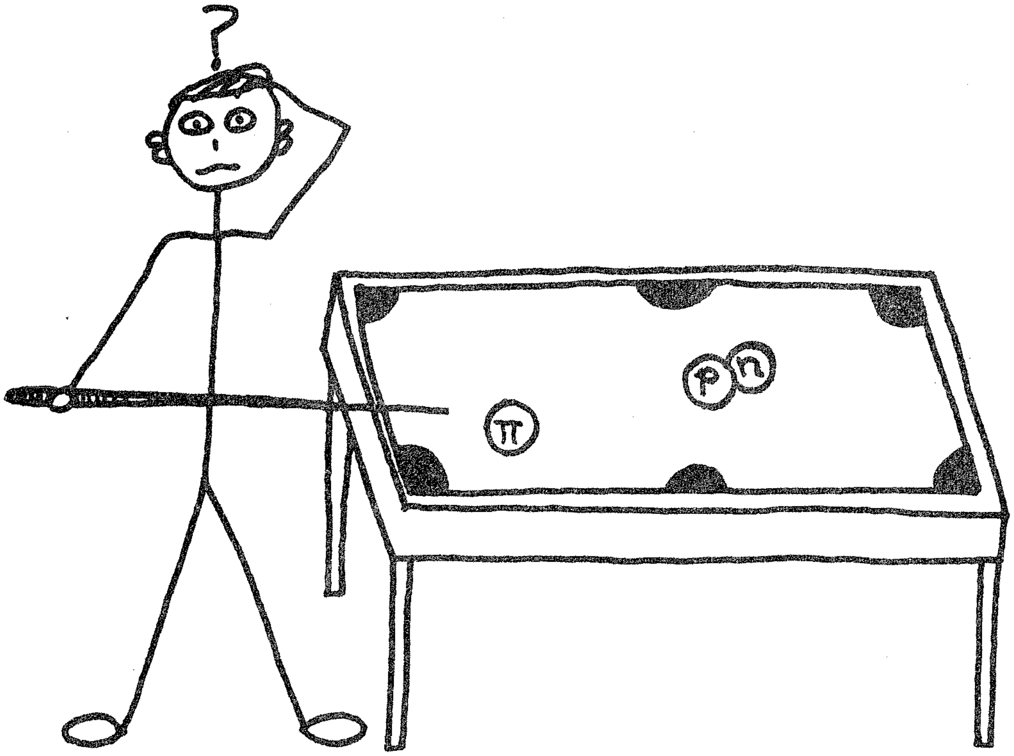

A REVIEW OF SOME EXPERIMENTAL RESULTS ON HADRON-DEUTERIUM SCATTERING

B. Musgrave*
Argonne National Laboratory
Argonne, Illinois 60439

I. Introduction

This talk considers some of the problems involved in obtaining cross sections, differential cross sections, and also decay angular distributions of resonances when the target is a neutron bound in deuterium. The various problems are illustrated mainly through π and K deuterium data for beam momenta above ∿ 2 GeV/c. Some of the π and K^--neutron results are related to hydrogen data through charge independence and charge symmetry.

---

*Work performed under the auspices of the U.S. Atomic Energy Commission.

II. The Impulse Model

Because the deuteron binding energy is small, it is generally asserted that the interaction of an incident hadron with a deuteron may be thought of in terms of its interaction with a free neutron or proton. This model(1) is usually thought to apply provided;

1) The radius of interaction of the incident particle is small compared to the nucleon - nucleon separation.

$$\lambda_{\text{inc}} < < r >_{\text{deuteron}}$$

2) The deuteron binding forces are negligible during the time of interaction and only serve to define the momentum of the target and hence of the bystander nucleon, since the two are equal and opposite in the impulse model.

These conditions are well satisfied for incident momenta above ~ 1 GeV/c, as is well known. A third assumption in the simple impulse model is(2):

3) Scattering of secondary particles on the spectator nucleon may be neglected.

The interaction then occurs on a moving target with a momentum distribution defined by the deuteron wave function. Generally the Hulthen wave function is assumed

$$\psi_d (r) = C \{ e^{-\alpha r} - e^{-\beta r} \} 1/r$$

$\alpha = \sqrt{2 \mu B} = 45.7$ MeV where μ = deuteron reduced mass and B = deuteron binding energy and with β usually within the range $\beta = 5.18\ \alpha$ to $\beta = 7\alpha$. The former value represents the best approximation of the Hulthen to the Gartenhaus numerical wave function as suggested by Moravcsik(3), and the latter value is due to Salpetre.(4) Moravcsik has also suggested more complicated analytic forms as better approximations to the Gartenhaus wave function. For the Hulthen wave function, the corresponding momentum distribution is

$$|\phi_d (p)|^2 p^2 dp = C' \left[\frac{1}{p^2 + \alpha^2} - \frac{1}{p^2 + \beta^2} \right] p^2 dp$$

This is illustrated in Fig. 1 for the reaction(5) $K^+d \rightarrow K^o p p$ at 600 MeV/c with the choice $\beta = 6\alpha$. Here, and generally for final states containing two nucleons, the spectator nucleon is defined to be the slower of the two. The Hulthen distribution is normalized to the data, and the agreement is good over the whole range of momentum. The Hulthen distribution peaks close to 50 MeV/c. To produce a visible track, i.e. ~ 1 mm in length, a minimum momentum of 80 MeV/c is required and 1/3 to 1/2 of the spectator nucleons satisfy this, depending on the chamber optics. When the spectator proton is not observed, the above reaction is sufficiently constrained that the fitted momentum distribution (shaded area in Fig. 1) agrees well with that obtained from the sample with observed spectator.

However, the reaction $K^+d \rightarrow K^o \pi^o p p$ is kinematically under constrained if the spectator nucleon is not seen. A kinematical fit is possible because the momentum of the unseen spectator nucleon is fairly well defined, being too small to produce a visible track, and its direction is randomly distributed with respect to the beam. The favoured choice of starting values for the kinematical fit is $p_x = p_y = p_z = 0$ with errors $\Delta p_x = \Delta p_y = 3/4\, \Delta p_z = 30$ MeV/c suggested by the momentum distribution discussed previously. In cases such as this the constraints are insufficient for the fitted spectator variables to conform with the impulse model. In particular the fitted momentum is essentially the same as the starting value and the angular distribution shows strong alignment with the beam direction, Fig. 2, reflecting the large momentum imbalance which usually exists in the beam direction.

In fact, due to the flux factor effect,(6) even in well constrained situations the angular distribution of the spectator nucleon with respect to the beam direction departs somewhat from isotropy. The observed counting rate is proportional to the cross section and the flux. The latter is proportional to the relative velocity of beam and target so that high momentum, forward spectators are favoured. This is demonstrated in Fig. 3 for the reaction $\pi^+ d \rightarrow \pi^+ \pi^- \pi^o$ p p at 1.5 GeV/c in which only even-pronged events were measured. The curves are from a Monte Carlo calculation including the flux factor(7) and assuming the Hulthen momentum distribution to apply. This experiment also illustrates one powerful advantage offered by deuterium, i.e. the study of neutral resonances, in this case a measurement of the natural width of ω^o. The width is found to be 9.3 ± 2.3 MeV using the experimental 3π effective mass resolution function in order to unfold the natural width. The stability of the width as a function of the error on the 3π effective mass is shown in Fig. 4.

In the reaction $\pi^+ d \rightarrow \pi^+ \pi^- \pi^o$ p p, the resolution in the 3π mass is less good for the sample of events where the spectator is unseen and the physics of this sample must be compared critically to that of the sample with seen spectator before combining both. In cases where the proton has insufficient energy to produce a visible track, its selection as the spectator is unambiguous and the spread in centre of mass energy is small, as shown in Fig. 5(b) for $K^- d \rightarrow K^- \pi^-$ p p at 5.5 GeV/c. Otherwise the spread is large, Fig. 5(a), and the effective range of beam momentum is in this case 4.8 to 6.2 GeV/c. The assumption is made, for momenta $\lesssim$ 2 GeV/c that the characteristics observed for any resonances produced correspond to those appropriate to a stationary target and the nominal beam momentum. At lower momenta, in the resonance formation region, the spread in CM energy due to target motion has been exploited to study baryon resonances in formation, covering a range of effective mass around the resonance mass.(6)

The previous good agreement shown between the Hulthen momentum distribution and experiment in Fig. 1 is not observed for higher beam momenta. Experiments generally observe a substantial excess (10 - 20%) of spectators with momenta greater than 300 MeV/c compared to the Hulthen prediction (~ 2%). This is seen in Fig. 6 for three different final states from a π^+d experiment at 1.1 - 2.4 GeV/c.(8) The excess of high momentum spectators over the Hulthen prediction is seen to be somewhat channel dependent. The strong η and ω^o production in the $\pi^+\pi^-\pi^o p\ (p_s)$ final state is found to be associated not only with events which could be claimed to satisfy the impulse model, but also with events having spectator momenta greater than a cut off around 300 MeV/c. The effect is also observed in final states containing a hyperon where no ambiguity exists in choosing the spectator nucleon, as shown for $K^- d \rightarrow \Lambda \pi^- p$ and $K^- d \rightarrow \Lambda p \pi^- + MM$ in Fig. 7.(9) The Hulthen wave function is not a good representation of the short range nucleon-nucleon interaction, i.e. the high momentum region of the momentum spectrum. Various other forms of the deuteron wave function have been tried and do not significantly improve the agreement. The SABRE Collaboration(10) have tried the various analytic forms suggested by Moravcsik and the Purdue Group(9) have used the McGee wave function which simulates some hard core behaviour and includes a small admixture of D-wave, enhancing high nucleon momenta somewhat relative to the lower momenta.(115)

Whilst most groups suggest the explanation for the high momentum excess lies in scattering of the outgoing particles on the spectator nucleon,(115) the effect is not handled consistently in the various experiments. In some cases only events with spectator momenta smaller than 250 to 300 MeV/c are used with a correction applied for those events excluded, assuming the Hulthen distribution to be true. In other experiments, the cross section determination includes all events regardless of disagreement between the observed and the Hulthen momentum distribution. This can result in systematic effects ~ 10 - 15%, i.e. of the same size as typical statistical errors in the cross section determination.(11)

III. Deuteron Corrections

Two further deuteron effects must be considered, where the first only arises for charge exchange reactions leading to two identical nucleons in the final state. The initial two nucleon state is S-state and the final two nucleons are not allowed to remain in this state unless spin-flip occurs in the interaction. The effect is only important for small momentum transfers to the struck nucleon and leads to a reduction in the differential cross section. In the impulse model approximation and using the closure approximation to evaluate terms involving the final two-nucleon wave function, the charge exchange differential cross section observed in deuterium is written(12)

$$\left(\frac{d\sigma}{dt}\right)^{d} = \left(\frac{d\sigma}{dt}\right)^{H}_{\text{flip}} \left[1 - 1/3\ S\ (q)\right] + \left(\frac{d\sigma}{dt}\right)^{H}_{\text{non-flip}} \left[1 - S\ (q)\right]$$

where $\left(\frac{d\sigma}{dt}\right)^{H}_{\text{flip}}$ and $\left(\frac{d\sigma}{dt}\right)^{H}_{\text{non-flip}}$ are the spin-flip and nonflip free nucleon differential cross sections and

$$S\ (q) = \int \left| \psi_d (r) \right|^2 e^{-i\ \vec{q}\ .\ \vec{r}}\ d^3\ \vec{r}$$

is the deuteron form factor(13) which defines the range of momentum transfer, t, over which the Pauli exclusion principle effect is important. The three momentum transfer to the deuteron is approximated by $q \sim \sqrt{-t}$ and S (0) = 1. Following Benson(14) we define the deuteron suppression ratio

$$R = \frac{(d\sigma\ /dt)^{d}}{(d\sigma\ /dt)^{H}}$$

and also the non-flip fraction of the free nucleon cross section

$$r = \frac{(d\sigma/dt)^{H}_{\text{non-flip}}}{(d\sigma/dt)^{H}} \quad \begin{cases} 0 & \text{pure flip} \\ 1 & \text{pure non-flip} \end{cases}$$

Then

$$R = 1 - S(t) \quad \left\{ \frac{1 + 2r}{3} \right\}$$

Benson has considered the magnitude of the correction for pure nonflip, ρ - exchange, A_2 exchange and finally pion exchange, as shown in Table 1. The nonflip fraction appropriate to ρ and A_2 exchange was obtained from the Regge pole analysis by Phillips and Rarita(15) of the reactions

$$\pi^- p \to \pi^o n \qquad (\rho)$$

$$\pi^- p \to \eta n \qquad (A_2)$$

The correction to the differential cross section is only significant for $|t| < 0.2\ (\text{GeV}/c)^{-2}$ and the reduction in the integrated cross section lies in the range 4 - 10% corresponding to the extremes of pure flip and pure nonflip processes. This is further illustrated in the table by the results of Cline et al(16) for the reaction $K^+d \to K^o\, p\, p$ at 5.5 GeV/c. The ratio of spin-flip to non-spin-flip free nucleon cross sections was estimated from $\pi^- p$ and $K^- p$ charge exchange. For reactions of the above type, the charge exchange cross section in deuterium vanishes in the forward direction because the free nucleon spin-flip amplitude vanishes there. This is not the case in photoproduction which is dominantly spin-flip and for which the exclusion principle effect has been demonstrated through the measured ratio $\dfrac{d\sigma/dt\,(\gamma d \to \pi^+ n n)}{d\sigma/dt\,(\gamma p \to \pi^+ n)}$ shown in Fig. 8. The ratio(17) agrees quite well with the value 2/3 in the forward direction.

Finally, a correction is made for the reduction in the number of target nuclei per unit volume resulting from shadowing by the spectator nucleon. It is usual to assume that the partial cross sections measured in bubble chamber experiments can be corrected according to the simple Glauber prescription applied to total cross section data, i.e.

$$\sigma_T(x\,d) = \sigma_T(x\,p) + \sigma_T(x\,n) - \delta$$

with $$\delta = [\,\sigma_T(x\,n)\,\sigma_T(x\,p)\,] \,/\, 4\pi\ \langle r^2\rangle$$

Typical values of this defect are;

2.5% of $\sigma_{tot}\,(\pi^+ d)$ at 2 GeV/c

5.0% of $\sigma_{tot}\,(K^- d)$ at 3 GeV/c

The difference between the above simple form and the more complicated form suggested by Wilkin(18) which satisfies charge independence, is small enough to be negligible even for the present very precise total cross section measurements.(19) Recent total cross section measurements by R. Cool et al(20) for $\pi^- d$, $\pi^+ p$ and $\pi^- p$ have been used to compute the $I = 1/2$ π N cross section in two independent ways;

1) Using $\sigma\,(\pi^+ p)$ and $\sigma\,(\pi^- p)$
2) Using $\sigma\,(\pi^- d)$ and $\sigma\,(\pi^- p)$ and unfolding $\sigma\,(\pi^- n)$

with the aid of an impulse model. A constant value of $\langle r^2\rangle = 31$ mb was assumed and the results were not sensitive to different forms of the deuteron wave function. The $I = 1/2$ cross section was then obtained from $\sigma\,(\pi^- n)$ and $\sigma\,(\pi^- p)$.

As shown in Fig. 9, the agreement between the two results is extremely good although this method of unfolding the π^- - neutron total cross section has been demonstrated to be unreliable for momenta below 1 GeV/c.(21)

Ebel and Pilkhun(22) have computed the Glauber correction and also Pauli principle corrections for the process $\pi^+ d \rightarrow \eta\, p\, p$ using Glauber multiple scattering theory. The shadow correction is consistent with that computed using the total cross section defect.

The question of correcting photoproduction processes for absorptive effects has been studied by Dar and Gal.(17, 23) for particular experiments of the single arm spectrometer type. They have contended that not only initial state shadowing but also final state shadowing should be considered. For processes of the kind

$$\begin{aligned} \gamma d &\rightarrow \pi^- p p \\ &\rightarrow \pi^+ n n \\ &\rightarrow \pi^- \Delta^{++} n \\ &\rightarrow \pi^+ \Delta^- p \\ &\rightarrow K^+ \Lambda^o n \end{aligned}$$

where a single particle is detected using a spectrometer, they have suggested a cross section correction

$$\frac{\sigma_T(\gamma N)}{4\pi <r^2>} + \frac{\sigma_T(M N)}{4\pi <r^2>}$$

where $\sigma_T(\gamma N)$ is replaced by the appropriate combination of vector meson-nucleon cross sections according to the Vector Dominance Model (VDM). This latter step substantially increases the magnitude of the correction. The results of this correction are shown in Fig. 8, where it is claimed that the deviation of the ratio $\frac{\sigma(\gamma d \rightarrow \pi^+ n n)}{\sigma(\gamma p \rightarrow \pi^+ n)}$ from unity at large t is satisfactorily accounted for. The exclusion principle effects at large t are negligible. Dar and Gal point out that a similar suppression of this ratio at large t is not seen in the SLAC data.(24) However, in view of the significant increase in the shadow correction following from use of vector meson-nucleon cross sections and also because of the possibility of significant systematic errors as suggested by the compilation of data on the π^+ ratio from D/H shown in Fig. 10, the need for the proposed correction cannot be considered established.

IV. Bound Proton Cross Sections

In two experiments, cross sections for reactions involving a bound proton (neutron spectator) have been compared to free proton data. At 3 GeV/c the SABRE Collaboration(10) have measured cross sections for states involving a hyperon with no ambiguity in selecting the spectator neutron. The substantial tail above 300 MeV/c in the neutron spectator momentum distribution is ignored in computing the cross sections shown in Table 2. There is no evidence of a systematic decrease in the deuterium results relative to hydrogen. However, the deuterium reactions are 1C processes and may include sufficient background to partially compensate the exclusion of high momentum spectator events, Fig. 11.

The cross section for the reaction $\pi^+ d \rightarrow \pi^+ \pi^- \pi^+ p\ (n_s)$ at 5.1 GeV/c(25) is substantially smaller than the free proton cross section, Table 3. It is not possible to account for the difference in terms of the high momentum spectator tail. The differential cross section for $\pi^+ p \rightarrow \rho^o \Delta^{++}$ shows excellent agreement with the free proton data, Table 4, with no evidence of bias. In each case the differential cross section is fitted using a sum of two exponentials.

V. π-N Charge Symmetric Cross Sections

The cross section for

$$\pi^- p \rightarrow \pi^- \pi^+ n$$
$$\pi^+ d \rightarrow \pi^- \pi^+ p\ (p_s)$$

are equal by charge symmetry. The data are compared in Fig. 12 and the π^+ data are systematically smaller than the π^- cross sections by 15-25%. Here the $\pi^- p$ reaction is less well constrained than the $\pi^+ d$ reaction and the cross section is quite likely to include more background. However, although the Glauber correction has been made, the π^+ data are not corrected for exclusion principle effects and the high momentum spectator tail is ignored in all except the 5.1 GeV/c case. Several of the π^+d experiments only use events where the proton spectator is observed and make the large correction for the remainder on the basis of the Hulthen momentum distribution. Neglect of the exclusion principle effect and the spectator momentum distribution tail might be expected to account for a large part of the observed discrepancy.

The ρ^o production cross sections for the above channels are actually in better agreement as shown in Fig. 13. In this case the exclusion principle correction has generally been made in the quoted cross section, otherwise a 4% (pure spin flip) correction has been applied. This much better agreement suggests that a large part of the discrepancy between the channel total cross sections should be attributed to background in the π^-p reaction. Benson$^{(14)}$ has given evidence that for processes known to have a strongly peripheral momentum transfer distribution, the fraction of events with spectator momentum exceeding 300 MeV/c is substantially reduced relative to that for less peripheral reactions. He conjectures that both the recoil and spectator momentum will be constrained as a result of the small four momentum transfers involved. The basis for this claim is summarized in Fig. 14 using the π^+d experiment at 3.65 GeV/c. The fraction of events with spectator momentum larger than 250 MeV/c is denoted by f and is studied, as a function of four momentum transfer. He also suggests this accounts for the good agreement shown in Fig. 1 where the four momentum transfer range available is again small.

The charge symmetric f^o cross sections provide a less stringent check of the deuterium data than is possible for the ρ, since the errors are much larger. The agreement in Fig. 15 is good apart, again, from the 4.5 GeV/c π^+d result. The cross section data for ρ and f production are collected in Tables 5 and 6.

A further check involves comparison of the differential cross section and density matrices for the charge symmetric ρ reactions. Such a comparison(26) has been made at 2.7 GeV/c and is shown in Fig. 16. At small momentum transfers a pure spin flip exclusion principle correction has been applied together with a scanning loss correction for the recoil proton. The agreement between differential cross sections and density matrices is good. The same observation is made at 7.0 GeV/c(27) in comparing density matrices for the two reactions. In this experiment both odd and even prong events were used. Table 7 shows a comparison of the $\pi^- p$ and $\pi^+ d$ results.

The experiments at 5.1(25) and 7.0(27) GeV/c provide extremely detailed information on ρ production. The differential cross section in both experiments is described by a sum of two exponentials with parameters shown in Table 8 and 9. This is similar to the structure observed in $\pi^+ p \rightarrow \rho^o \Delta^{++}$. At 7.0 GeV/c, combination of the $\pi^- p$ and $\pi^+ n$ data provides good statistics at large t, Fig. 17. The distribution in $(\rho_{00}^H - \rho_{11}^H)$ shows a dip at $|t| \sim 0.4\ (\mathrm{GeV/c})^2$ as is suggested by the strong absorption model of Ross et al.(28)

There is essentially no charge symmetric data to the reaction

$$\pi^+ d \rightarrow \pi^+ \pi^- \pi^o p\, p$$

which has been used to study η, ω, A_1^o, and A_2^o production.(29) Here, the odd prong events are pseudo - 1C and experiments are about equally divided over using these less well constrained events. The cross section data is shown in Fig. 18 and Table 10.

The cross section for $\pi^+ d \rightarrow \omega^o p\, p_s$ is shown in Fig. 19 and Table 10. The experiments have generally assumed spin-flip dominance in correcting for exclusion principle effects. At 7.0 GeV/c, the range $89.6 \pm 13.3 \leqslant \sigma\ (\omega\ p) \leqslant 96.2 \pm 14.2\ \mu b$ corresponding to the extremes of pure flip and pure non-flip dominance, with a measured cross section of $86.4 \pm 12.8\ \mu b$, is quoted. As has been pointed out on the basis of fewer data, $\sigma\ (\omega^o p)$ shows a momentum dependence of the form $\sigma\ (p) = A\,p^{-n}$ with $n = 2.1 \pm 0.1$. This reaction can be mediated by both ρ and B exchanges but this value of n is inconsistent with that expected for pure ρ - Regge exchange, i.e. $n = -(2\ \alpha_{eff}\ (0) - 2)$ so that $n \sim 0.7$. The observed value of n indicates $\alpha_{eff}\ (0) \sim 0.0$ such as might be expected for a π-B exchange degenerate Regge trajectory.

The cross section for this reaction is compared to that for the reaction $\pi^+ p \rightarrow \omega^o \Delta^{++}$, also expected to be mediated by ρ and B exchange, in Fig. 20. Both reactions show the same dependence on laboratory momentum and also quite good agreement in magnitude.

Recent experiments have attempted to isolate the natural and unnatural parity contributions to the exchange mechanism using (30)

a) ρ_{00}^{GJ} or $\rho_{00}^{GJ}\ d\sigma/dt$ which only contains contributions from B-like exchanges.

b) $\sigma^+ = \rho_{11} + \rho_{1-1}$ which isolates the ρ-like exchanges and is expected to be zero at $|t| \sim 0.6\ \text{GeV}^2$ corresponding to the ρ trajectory nonsense zero. The differential cross section may also show a dip at this $|t|$ value for the same reason.

The data are statistically not good enough to clearly demonstrate structure in any of these variables as shown in Figs. 21-26. for several of the experiments. The 4.19 and 5.1 GeV/c data show dips at $|t| \sim 0.2\ \text{GeV/c}^2$ in $d\sigma/dt$ and also ρ_{00}^{GJ} although the significance is 2-3 standard deviations. Recent experiments at 3.7(31) and 5.1 GeV/c(32) for $\pi^+ p \rightarrow \omega^o \Delta^{++}$ also show sharp dips, primarily in ρ_{00}^{GJ} at $|t| \sim 0.17\ (\text{GeV/c})^2$. It is difficult to relate such structure to the nonsense zero in the B-trajectory at $\alpha_B\ (t) = 0$. The dip is not described by a Regge model involving ρ and B exchange.(33) There is no conclusive evidence for structure in σ^+ from any of the $\pi^+ d$ experiments. The statistical significance of the $\pi^+ p \to \omega^o \Delta^{++}$ experiments at 3.7 and 5.1 GeV/c is better but does not clearly demonstrate the ρ nonsense zero $|t| \sim 0.6$ GeV/c^2.

The recent result for $\pi^+ d \to \omega^o p\, p$ at 7.0 GeV/c uses both odd and even prong events and the ω^o density matrices for the two samples agree everywhere within one standard deviation with the exception of ρ_{00} for $-t < 0.1$ $(\mathrm{GeV}/c)^2$.(113)

VI. $K^{\pm}$ - Deuterium Data and Tests of Exchange Degeneracy

In some cases it is possible to relate the $K^- n$ and $K^- p$ data through isotopic spin e.g.

$$\sigma\,(K^- p \to \Lambda + \text{meson}) = 1/2\ \sigma\,(K^- n \to \Lambda + \text{meson})$$

Also, a SLAC Group(37) has used charge symmetry to relate some $\bar{K}^o p$ and $K^- n$ reactions.

Although this survey is intended to cover the momentum region above 2 GeV/c, it is interesting to show the cross section measurements of the Birmingham Group for $K^- n \to \Lambda \pi^-$ which covers a CM energy range about the Σ (2030).(6) Here the internal motion of the target is utilized to cover this range of CM energy, but as this group first pointed out, it is necessary to include the flux factor in extracting the $K^- n$ cross section from the observed counting rate as a function of CM energy. They elect to use the high momentum proton spectator events in computing the cross section but not in making the phase shift analysis of the $\Lambda \pi^-$ system. The usual Glauber shadow correction is included. In Fig. 27 the cross section data is compared with measurements for $K^- p \to \Lambda^o \pi^o$ from two experiments in the same CM energy range. The agreement with the results of the Rutherford(34) experiment in the same chamber is generally quite good with a tendency to be systematically low by less than 10%. There is a large systematic difference between these results and those of Wohl et al.(35)

In both the above reactions, there exists the problem of minimizing the contamination from $K^-N \rightarrow \Sigma^o \pi$ which is expected to be easier starting from K^-d than from K^-p. This separation becomes more difficult at the higher beam momenta where the line reversed reactions

$$K^-p \rightarrow \Lambda \pi^o; \; K^-n \rightarrow \Lambda \pi^-$$

and

$$\pi^-p \rightarrow \Lambda K^o$$

have been used to check predictions based on the exchange degeneracy of the K^* and K^{**} Regge trajectories.(36) Briefly;

1) Strong EXD for K^* and K^{**} requires $d\sigma/dt$ to be identical for the line reversed pair with no Λ^o polarization in both cases.

2) Weak EXD requires the two reactions to have the same $d\sigma/dt$ with the Λ^o polarization showing mirror symmetry, as a function of t , between the two reactions.

In addition to the Σ^o contamination which is generally estimated to be less than 10% for the K^-n reaction but 10-20% for the K^-p case, there is a severe scanning loss problem which only exists for the deuterium reaction. The problem is associated with detecting the production vertex in the case of a fast forward π^- when the spectator proton is not seen and at 4.5(97) and 5.0 GeV/c(98) a correction factor 1.5 is applied to those events with $|t'| = |t - t_{min}| < 0.1 \; (\text{GeV}/c)^2$. This factor is suggested from comparison of the odd and even prong samples. In all cases the high momentum spectator events are not used and the usual Glauber correction is made. The cross section data is summarized in Table.11 and compared to K^-p data in Fig. 28. The errors are large and the agreement is good.

The differential cross section and Λ^o polarization data presently available are shown in Fig. 29-32. The errors on the polarization measurements of the two recent experiments at 5.0 and 5.5 GeV/c are large since they are based on 125 and 101 events respectively. For $|t| < 1.5$ GeV^2 the experiments up to 5.5 GeV/c indicate a large Λ^o polarization. This is also indicated by preliminary results(37) for $\bar{K}^o p \to \Lambda \pi^+$ with data from 1 - 8 GeV/c shown in Fig. 33. When the differential cross sections at 5.0 and 5.5 GeV/c are based only on events with visible spectator proton, the slope parameters in the two cases are 4.6 ± 1.2 and 5.7 ± 1.2 $(\text{GeV}/c)^{-2}$ over the range $0 < |t'| < 0.6$ (GeV/c). The observed number of events is too small in each case to reliably correct the differential cross section. Present data on the slope parameters for $\bar{K} N \to \Lambda \pi$ is summarized in Fig. 34. As suggested by the SLAC Group, the data indicate the differential cross section exhibits shrinkage and may be consistent with the line reversed reaction for laboratory momentum ~ 10 GeV/c.

The strong form of EXD in a pure pole model is well known to be inconsistent with the above data on Λ^o polarization. On the other hand,(38) the weak form of exchange degeneracy is able to describe the Λ^o polarization and differential cross section quite well for $K^- n \to \Lambda^o \pi^-$ but is not able to reproduce the Λ^o polarization in the line reversed reaction which also starts out positive at small $|t'|$ but then changes sign for $|t'| \sim 0.4$ GeV^2. A weak EXD pole plus cut model is able to describe the Λ^o polarization data in both reactions and requires the differential cross section for $\bar{K} N \to \Lambda \pi$ to shrink with increasing beam momentum and eventually agree with the line reversed reaction.(39)

There is less data available for the reaction $K^- d \to \Sigma^o \pi^- (p_s)$ but the differential cross section where measured shows a somewhat steeper slope than for $\Lambda \pi^-$, Table 12.

For completeness the cross sections for

$K^- d \rightarrow \Lambda \rho^- p_s$

$K^- p \rightarrow \Lambda \rho^o$

are compared in Fig. 35 and Table 13. Again, the Σ^o contamination is a severe problem but here the $K^- p$ reaction is the cleaner of the two. The production and decay properties of the ρ are very similar in the two reactions.

The hypothesis of EXD for (ρ, A_2) has been studied using the line reversed pair

$K^+ n \rightarrow K^o p$

$K^- p \rightarrow \bar{K}^o n$

The differential cross sections for these two reactions are well known to show marked disagreement at low momenta but good agreement above ~ 5 GeV/c,(40, 41) Fig. 36, 37. The exclusion principle correction has been made in the deuterium data assuming pure spin flip dominance except for the 5.5 GeV/c data(40) where the ratio of spin flip to non-flip cross section was estimated from $K^- P$ and $\pi^- P$ charge exchange data. The experiments differ in that some include the high momentum spectator events in computing a cross section, e.g. 5.5 and 12 GeV/c, whilst others do not. The total cross sections are shown in Fig. 38.

A similar test of (ρ, A_2) EXD(36) is possible using the line reversed pair

$K^+ p \rightarrow K^o \Delta^{++}$ (1236)

$K^- d \rightarrow \bar{K}^o \Delta^-$ (1236) p_s

but data only extend up to 5.5 GeV/c for the second reaction and the agreement in this case is markedly less good than seen previously. The K^- data areobtained from the channel $K^- d \rightarrow \bar{K}^o n \pi^- p_s$ and events satisfying this interpretation generally also satisfy the interpretation $K^- d \rightarrow \bar{K}^o \pi^- d$. Resolution of the ambiguity is straightforward,(42) particularly so when the deuteron produces a measurable track. Again, in defining the spectator the slowest nucleon is selected. The events excluded by this cut do not contain any Δ^- (1236) signal which would appear in the $n\pi^-$ effective mass.(43, 44) This reaction is pseudo - 1C if the spectator proton is not seen and then the fitted spectator characteristics do not agree with those expected assuming the impulse model. At 5.5 GeV/c there was, however, good agreement between the number of odd prong events observed and the number predicted by normalizing the Hulthen momentum distribution to the spectator momentum range 110 - 200 MeV/c for the even prong events.(43) Also, the density matrices for the K^* (890) (and Δ^-) resonances in the even and odd prong events showed agreement within the statistical errors. This is also shown in Table 14 for the same channel at 3 GeV/c.(60)

The channel cross sections are given in Table 15 and are compared to those for the charge symmetric reaction $\bar{K}^o p \rightarrow K^- \pi^+ p$ in Fig. 39. Note that here the SLAC Group have normalized the $\bar{K}^o$ p cross sections so as to agree with that for K^-d at 3 GeV/c and the agreement with the new K^-d results at 5.0 and 5.5 GeV/c is then good. In calculating the K^-d channel cross section, the high momentum spectator excess was ignored in all cases. In both the K^+p and K^-d channels the problem of extracting the Δ cross section is very similar and involves a fit to the Dalitz plot. The cross sections are compared in Fig. 40 and the agreement is poor in contrast to the situation for the charge exchange reactions previously considered. The preliminary SLAC data for $\bar{K}^o p \rightarrow K^- \Delta^{++}$ are compared to the K^-d cross sections in Fig. 41 and agree quite well at 5.0 and 5.5 GeV/c.

In comparing the differential cross section for the two reactions, the wide resonance introduces certain problems. No background correction is attempted and the mass range used to define the Δ varies somewhat between experiments. Use of t' rather than t makes little difference to the shape of the differential cross section and the data generally suggest the differential cross section flattens out at $|t'| \lesssim 0.2\ \text{GeV}^2$. Whilst the K^+P data are all described well by the form exp (bt') for $|t'| \gtrsim 0.15$, the K^-d data suggest some structure for $|t'| \sim 0.5\ \text{GeV}^2$. However, both K^+ and K^- data show roughly the same shape,(36) as indicated by the results in Table 16.

In computing the cross section for $K^-d \rightarrow \bar{K}^o \pi^- np_s$ the loss into the coherent channel $K^-d \rightarrow \bar{K}^o \pi^- d$ has been neglected. According to the simple impulse model and using the closure approximation, we can write(42)

$$\left(\frac{d\sigma}{dt}\right)_{\text{coherent}} = \left[\frac{d\sigma p}{dt} + \frac{d\sigma n}{dt} + 2\,\text{Re}\, f_p^* f_n\right] S^2\,(q/2)$$

so that some part of this cross section must be included in estimating the free neutron cross section. Any significant loss of Δ^- events to this channel would show up as the d^* (2200) enhancement in $d\pi^-$ mass where $M(d^*) \sim M(\Delta) + M(N)$. At 5.5 GeV/c it is estimated that the loss to the cross section for $K^-n \rightarrow \bar{K}^o\Delta^-$ which results from both the coherent process and the selection of the slowest nucleon as the spectator, is less than 5%.(43)

Attempts to fit the reactions

$$\pi^+ p \rightarrow \pi^o \Delta^{++}$$
$$\rightarrow \eta\, \Delta^{++}$$
$$K^+ p \rightarrow K^o \Delta^{++}$$

over a wide range of beam momentum using a Regge model involving ρ and A_2 Regge exchanges have been quite successful.(46) The reaction $K^- n \rightarrow \bar{K}^o \Delta^-$ is not easily included in this group, as discussed previously. It may be possible to describe all four reactions by including absorption in addition to ρ and A_2 exchanges.(47)

$K^- d \rightarrow \bar{K}^o n \pi^- p_s$ also contains strong $\bar{K}^*$ (890) production and it is interesting to compare

$$K^- d \rightarrow K^* (890)\ n\ (p_s)$$
$$K^- P \rightarrow \bar{K}^* (890)\ p.$$

which should have the same cross section provided interference between ω and π exchange can be ignored. Such interference, possible because of absorption effects, will be small, opposite in sign between the two reactions and only observable at very small momentum transfers. Attempts to observe this effect(48) have been unsuccessful and interpretation would anyway be complicated by factors such as loss to the coherent process $K^- d \rightarrow \bar{K}^* d$ and the problem of interference between the neutron and proton amplitudes. The cross sections for both reactions are shown in Table 17, Fig. 42, and the agreement is apparently good except for the $K^- p$ results at 4.6 and 5.0 GeV/c.

VII. K^* Production by Charge Exchange

The deuterium target is essential to study K^* production by charge exchange, e.g.

$$K^- p \rightarrow \bar{K}^{*o} (890)\ n$$
$$K^+ d \rightarrow K^{*o} (890)\ p\ p_s$$

These reactions are known to be described fairly well at any given evergy by OPE with absorption.(49, 50) Extensive data exist on the first of these and agreement is good on the shape of $d\sigma/dt$ (slope ~ 5 GeV^2 for $|t| < 0.5$ GeV^2) and on density matrices. There are normalization disagreements. Much less data exists on the second reaction.(50, 51, 52) Fig. 43 shows the available differential cross sections, corrected for the exclusion principle effect by us. The CERN-Brussels experiment at 3 GeV/c indicates a slope of ~ 9 GeV^{-2} for $d\sigma/dt$ (not influenced much by our correction). The other distributions show slightly smaller slopes but all are substantially steeper than for the K^-p reaction. A similar, preliminary observation is made by a UCLA Group who study both reactions at 2 GeV/c.(53) OPE with absorption is then not able to explain both reactions.

This difference in slope between the K^+ and K^- data is shown to be due to the dominance of $\rho_{11}\, d\sigma/dt$ at large t. The slopes of $\rho^{GJ}_{00}\, d\sigma/dt$ and $\rho^{H}_{00}\, d\sigma/dt$ are much larger than for $d\sigma/dt$ in the case of K^-P and in fact they approach those for the K^+n reaction.

One model to explain this has been proposed by Fox(54) who uses VDM and SU (3) to relate

$$\rho^{H}_{11}\ \frac{d\sigma}{dt}\,(K^- p \to \bar{K}^* (890) n) \to \frac{d\sigma}{dt}\,(\gamma\, p \to \pi^+ n)$$

$$\rho^{H}_{11}\ \frac{d\sigma}{dt}\,(K^+ n \to K^* (890)\, p\,) \to \frac{d\sigma}{dt}\,(\gamma\, n \to \pi^- p)$$

In single π photo-production, the π^-/π^+ ratio from deuterium, Fig. 54,is explained by invoking ρ and π exchange with absorption. The difference in slope is due to interference of the ρ with the pion-cut, of opposite sign in the two cases. The same thing is supposed to happen in the $K^\pm$ reactions and the connection to photoproduction establishes the interference as constructive for K^-p and destructive for K^+n.

The model assumes π and ρ, A_2 Regge exchanges with strong absorption (SCRAM). The parameters are determined by fitting to all available data on both reactions with results shown for the 5.5 GeV/c K^-p(114) and 3 GeV/c K^+n data. First $d\sigma/dt$ for

$K^-P \to \bar{K}^*$ (890) n, Fig. 44. Then ρ_{00}^{GJ} $d\sigma/dt$ and ρ_{00}^{H} $d\sigma/dt$ for $K^-P \to \bar{K}^*$ (890) n at 5.5 GeV/c, Fig. 45. The second is steeper than the first since the absorption allows the ρ to contribute in the Jackson but not in the helicity frame. The ρ_{00}^{GJ} $d\sigma/dt$ and ρ_{00}^{H} $d\sigma/dt$ for $K^+n \to K^*(890)p$ at 3 GeV/c are also shown, Fig. 46. Density matrices are shown in Fig. 47-49. Further data are needed for the K^+d reaction to make the comparison with well known normalization and over a wide range of momenta.

A similar comparison may be made for the reactions

$$K^+p \to K^*(890)\,\Delta^{++}(1236)$$
$$K^-d \to \bar{K}^*(890)\,\Delta^-(1236)\,p_s$$

where the latter is obtained from the channel

$$K^-d \to K^-\pi^+\pi^-n\,(p_s)$$

As discussed in Section VI, this process must be separated from the coherent reaction,in this case $K^-d \to K^-\pi^+\pi^-d$. Up to 5.5 GeV/c, this latter is less than 10% of the breakup cross section, Fig. 50. As the momentum increases and diffractive processes dominate, these cross sections approach one another. Again, some part of the coherent process should be apportioned to the breakup cross section to obtain the "free" neutron cross section.(42)

The problems involved in isolating a sample of breakup events representing neutron target events are several.(55, 56, 116) Separation of the breakup events from the coherent events is fairly straightforward but severe ambiguity is observed between interpretation of events as $K^-d \to K^-\pi^-\pi^+np$ and $K^-d \to \pi^-\pi^-\pi^+\Lambda p$. In all three experiments presently available, it is concluded that these ambiguous events should have the former rather than the latter interpretation. The dominant features of each experiment are then strong $\bar{K}^*$ (890) and Δ^- (1236) formation, with substantial double resonance production, $K^-d \to \bar{K}^*(890)\,\Delta^-(1236)\,p_s$. The cross section data are contained in Table 18. The result at 7.3 GeV/c(57) is based only on the events having an unseen spectator proton and is seen to be substantially higher than the trend indicated by the other results.

Although the choice of spectator nucleon is perhaps less ambiguous for this sample of events, the chance of including substantial background is much higher than when the spectator nucleon produces a measurable track. As is usual with such double resonance reactions, all events in the overlap region of the two resonance bands are used to study the reaction $K^-d \rightarrow \bar{K}^{*}\Delta p_s$. At 5.5 GeV/c, the bias in this differential cross section due to loss into the coherent channel $K^-d \rightarrow \bar{K}^*(890)d^*(2200)$ is shown in Fig. 52(b) to be a small effect, confined to small momentum transfer(55). The differential cross section in all three K^-d experiments is very similar in shape with a slope $\sim 5(\text{GeV}/c)^{-2}$. This is shown in Fig. 51(c) at 3 GeV/c, 52(b) at 5.5 GeV/c, 53 (c) at 7.3 GeV/c. However, the slopes typical of the K^+P reaction are significantly higher. A recent compilation(58) suggests the slope increases with beam momentum from 7.5 $(\text{GeV}/c)^{-2}$ at 3 GeV/c to 10.5 $(\text{GeV}/c)^{-2}$ at 5.0 GeV/c. This difference in slopes is similar to the $KN \rightarrow K^*N$ reaction discussed earlier. Indeed, the same VDM + absorption model(54) relates to K^+/K^- ratio to photoproduction: this time to $\gamma N \rightarrow \pi\Delta$. Fig. 54 shows the ratio $R = d\sigma/dt(\gamma d \rightarrow \pi^-\Delta^{++}n)/d\sigma/dt(\gamma d \rightarrow \pi^+\Delta^-p)$ and in agreement with the model(54) this is similar to the single pion photoproduction π^-/π^+ ratio previously referred to.

Conclusions

At the existing statistical level of bubble chamber results, there appear to be no serious problems in extracting "free" neutron data from deuterium experiments. Where checks can be applied, they are generally satisfied. Further studies of deuterium effects with high statistics experiments will be interesting and are needed to make more quantitative assessments of deuterium effects.

Several groups generously supplied unpublished data for use in this talk. In particular I am grateful to Dr. J. Mathews, Dr. W. Fickinger, Dr. K. Anderson, and Dr. Y. Chien.

References

1) G. Chew and H. Lewis, Phys. Rev. 84, 779 (1951).

2) Reference 1 contains a discussion of the transparency condition.

3) M. J. Moravcsik, Nucl. Phys. B7, 113 (1958).

4) R. L. Gluckstern and H. A. Bethe, Phys. Rev. 81, 761 (1951).

5) Private communication from Dr. Y. Cho, Argonne National Lab.

6) G. F. Cox et al., Nucl. Phys. B19, 61 (1970).

7) P. Katz, Ph D Thesis, University of Minnesota 1970, Unpublished. The flux factor was from R. G. Newton, "Scattering Theory of Waves and Particles". (McGraw-Hill 1966) Chapter 8.

8) J. S. Danburg, Ph D Thesis (1969), Unpublished UCRL-19275.

9) J. Tebes et al., Nucl. Phys. B20, 565 (1970).

10) D. Merrill et al., Nucl. Phys. B18, 403 (1970).

11) In Reference 8, the cross section for

$$\begin{aligned} \pi^+ d &\rightarrow \pi^+\pi^- p\,p \\ &\rightarrow \pi^+\pi^-\pi^o\, p\,p \\ &\rightarrow p\,p + MM \end{aligned}$$

was normalized to that for

$$\begin{aligned} \pi^- p &\rightarrow \pi^+\pi^- n \\ &\rightarrow \pi^+\pi^- + MM \end{aligned}$$

This, aside from channel to channel variations in the high momentum spectator proton excess, cirumvents this problem in determining cross sections.

12) B. M. Schwartzschild, Ph D Thesis (1967), Unpublished UCRL-17572.

13) Reference 1 gives for the deuteron form factor using the Hulthen wave function

$$S(q) = \left[\frac{1}{2\alpha} + \frac{1}{2\beta} - \frac{2}{\alpha+\beta}\right]^{-1} \frac{1}{q}\left[\tan^{-1}\left(\frac{q}{2\alpha}\right) + \tan^{-1}\left(\frac{q}{2\beta}\right) - 2\tan^{-1}\left(\frac{q}{\alpha+\beta}\right)\right]$$

Generally, one takes the relation $q^2 = -t$ as defining the transferred three momentum. This is true in the beam - deuteron CM frame but the q should really be defined in the laboratory where $q^2 = -t + t^2/4M_d^2 \sim -t$ for small angle scattering.

14) G. C. Benson, Ph D Thesis (1968), University of Michigan, Unpublished.

15) R.J.N. Phillips and W. Rarita, Phys. Rev. 139, 1336 (1965).

16) D. Cline et al., Nucl. Phys. B22, 247 (1970).

17) A. Dar and A. Gal, Phys. Rev. Letters 21, 444 (1968).

18) C. Wilkin, Phys. Rev. Letters 17, 561 (1966).

19) G. Lynch in "Hyperon Resonances - 70", Edited by E. C. Fowler. Published by Moore Publishing Company.

20) R. Cool et al., Phys. Rev. D1, 1887 (1970).

21) A. A. Carter et al., Phys. Rev. 168, 1457 (1968).

22) G. Ebel and H. Pilkhun, Nucl. Phys. B7, 147 (1968).

23) Dar and Gal, Phys. Rev. 1D, 2714 (1970).

24) A. Boyarski et al., Phys. Rev. Letters 21, 1767 (1968).

25) N. Armenise et al., Nuovo Cimento 65, 637 (1970).

26) R. J. Miller et al., Phys. Rev. 178, 2061 (1969).

27) Private communication from J. Mathew, University of Toronto.

28) M. Ross et al., Nucl. Phys. B23, 269 (1970).

29) A.M. Cnops et al., Phys. Letters 29B, 45 (1969).

30) H. Hogaasen and H. Lubatti, Phys. Letters 26B, 166 (1968).

31) G. S. Abrams et al., Phys. Rev. Letters 25, 617 (1970).

32) C. L. Pols et al., Nucl. Phys. B25, 109 (1971).

33) G. S. Abrams and U. Maor, Phys. Rev. Letters 25, 621 (1970).

34) A. Berthon et al., Submitted to the LUND International Conference on Elementary Particles 1969.

35) C. G. Wohl et al., Phys. Rev. Letters 17, 107 (1966).

36) K. W. Lai and J. Louie, Nucl. Phys. B19, 205 (1970).

37) A. D. Brody et al., SLAC-PUB-823 (1970).

38) J. D. Jackson and R. Field, Symposium on Polarization, Argonne National Laboratory (1970).

39) A. C. Irving et al., TH. 1304 - CERN (1971).

40) D. Cline et al., Phys. Rev. Letters 23, 958 (1970).

41) A. Firestone et al., Phys. Rev. Letters 25, 958 (1970).

42) P. Fleury, Methods in Subnuclear Physics (Gordon and Breach, Science Publishers, Inc., New York 1967) 2, p560.

43) D. Johnson, Ph D Thesis, University of Kansas (1971), Unpublished.

44) D. D. Carmony et al., Phys. Rev. 1D, 30 (1970).

45) G. Bakker et al., Nucl. Phys. B16, 53 (1970).

46) R. D. Mathews, Nucl. Phys. B11, 339 (1969); M. Krammer and U. Maor, Nucl. Phys. B13, 651 (1969) and Nuovo Cimento 52A, 308 (1967); F. Gilman, Phys. Letters 29B, 673 (1969).

47) Private communication from G. C. Fox.

48) R. L. Eisner et al., Phys. Letters 28B, 356 (1968).

49) F. Schweingruber et al., Phys. Rev. 166, 1317 (1968).

50) G. Bassompierre et al., Nucl. Phys. B16, 125 (1970).

51) S. Goldhaber et al., Phys. Rev. Letters 15, 737 (1965).

52) The 12 GeV/c K^+d result is private communication from A. Firestone.

53) D. Davies et al., Paper submitted to the KIEV Conference on High Energy Physics (1970).

54) G. C. Fox et al., Paper submitted to KIEV Conference on High Energy Physics (1970), To be published.

55) B. Werner et al., Nucl. Phys. B23, 37 (1970).

56) B. Haber et al., Nucl. Phys. B17, 289 (1970).

57) Private communication from K. Anderson, University of Colorado.

58) G.S. Abrams et al., Phys. Rev. 1D, 2433 (1970).
59) A. Boyarski et al., Phys. Rev. Letters 25, 695 (1970).
60) S.A. de Witt, Ph D Thesis (1968), University of Amsterdam,

π N Data

61) J. Alitti et al., Nuovo Cimento 29, 515 (1963).
62) T.C. Bacon et al., Phys. Rev. 157, 1263 (1967).
63) E. West et al., Phys. Rev. 149, 1089 (1966).
64) V. Hagopian and Y. Pan, Phys. Rev. 152, 1183 (1966).
65) B.G. Reynolds et al., Phys. Rev. 184, 1424 (1969).
66) D.H. Miller et al., Phys. Rev. 153, 1423 (1967).
67) J. Baton et al., Nuovo Cimento 35, 713 (1965).
68) Y.Y. Lee et al., Phys. Rev. 159, 1156 (1967).
69) A-B-B-H-L-M Collab., Nuovo Cimento 31, 729 (1964).
70) I. Derado et al., Phys. Rev. Letters 14, 872 (1965).
71) R.L. Eisner et al., Phys. Rev. 164, 1699 (1967).
72) D.J. Crennell et al., Phys. Letters 28B, 136 (1968).
73) Private communication from J.A.J. Mathews, University of Toronto.
74) J.A. Poirer et al., Phys. Rev. 163, 1462 (1967).
75) O-M-B Collaboration, Nuovo Cimento 53A, 798 (1967).
76) P. Fleury et al., Proc. of the 1962 International Conf. on High Energy Physics at CERN, p597.
77) C. Caso et al., Nuovo Cimento 62A, 755 (1969).
78) B.D. Hyams et al., Nucl. Phys. B7, 1 (1968).
79) O-M-B Collaboration, Nuovo Cimento 53A, 798 (1967).
80) J. Ballam et al., Phys. Letters 31B, 489 (1970).
81) T.C. Bacon et al., Phys. Rev. 157, 1263 (1967).
82) R.J. Miller et al., Phys. Rev. 178, 2061 (1969).
83) L.W. Lovell, Ph D Thesis (1969) Unpublished, University of Michigan; G.C. Benson, Ph D Thesis (1968) Unpublished, University of Michigan; G.C. Benson et al., Phys. Rev. Letters 22

1074 (1969); F. Henyey et al., Phys. Rev. Letters 21, 1782 (1968).

84) G.S. Abrams et al., Phys. Rev. Letters 23, 673 (1969) and private communication from Dr. B. Eisenstein, University of Illinois.

85) A. Forino et al., Phys. Letters 19, 68 (1965).

86) The cross sections for the 5.1 GeV/c $\pi^+ d$ experiment are normalized by equating $\sigma\ (\pi^+ d \rightarrow \eta\, p\, p_s)$ and $\sigma\ (\pi^- p \rightarrow \eta\, n)$ at this momentum, N. Armenise et al., Phys. Letters 26B, 336 (1968). The latest cross section data for this experiment are in N.Armenise et al., Nuovo Cimento 65A, 637 (1970); N. Armenise et al., Nuovo cimento 54, 999 (1968).

87) M.S. Farber et al., Notre Dame University Preprint (1970). The normalization in this experiment is made by equating $\sigma\ (\pi^+ d \rightarrow \pi^+ \pi^-\, p\, p_s)$ and $\sigma\ (\pi^- p \rightarrow \pi^- \pi^+ n)$ at the same momentum. An internal normalization is also quoted.

88) Private communication from J.A.J. Mathews for the Toronto-Wisconsin Collaboration.

89) Private communication from Dr. G. Condo, University of Tennessee.

$\bar{K}$ N Data

90) C.G. Wohl et al., Phys. Rev. Letters 17, 107 (1966).

91) L.T. Smith et al., Athens Conference, Ohio (1965).

92) G. London et al., Phys. Rev. 143, 1034 (1966).

93) J. Badier et al., CEA (Saclay Report) 68-7.

94) N. Hague et al., Phys. Rev. 152, 1148 (1966).

95) D.C. Colley et al., Nuovo Cimento 53A, 522 (1968).

96) R. Barloutaud et al., Nucl. Phys. B9, 493 (1969).

97) W.L. Yen et al., Phys. Rev. 188, 2011 (1969).

98) Private communication from Dr. W. Fickinger, Case-Western Reserve University.

99) D. Johnson, Ph D Thesis (1971) Unpublished, University of Kansas.

100) Private communication from Dr. Chien, Johns Hopkins University.

101) D.O. Huwe, Phys. Rev. 181, 1824 (1969).

102) K. Jaeger, Ph D Thesis, Syracuse University (1970) Unpublished.

103) J. Mott et al., Phys. Rev. 177, 1966 (1968).

104) M. Aderholz et al., Nucl. Phys. B5, 606 (1968).

105) M. Dickenson et al., Phys. Letters 23, 505 (1966).

106) J.H. Friedman et al., Phys. Rev. Letters 16, 485 (1966).

107) B-G-L-O-R Collaboration RPP/H/29 Rutherford Laboratory Preprint (1967).

108) F. Schweingruber et al., Phys. Rev. 166, 1317 (1968).

109) M. Aderholz et al., Nucl. Phys. B5, 567 (1968).

K N Data

110) A Compilation of K^+N Reactions, UCRL-20000 K^+N (1969).

111) V.G. Lind et al., Nucl. Phys. B14, 1 (1969).

112) K.W.J. Barnham et al., Nucl. Phys. B28, 171 (1971).

113) Private communication from R. Holloway, University of Illinois (Seminar at ANL, April 1971) of preliminary results for $\pi^- p \to \omega^o n$ at 3.65, 4.5 and 5.5 GeV/c indicate for ρ^{GJ}_{00} a stronger dependence on momentum transfer than that observed in bubble chamber experiments on $\pi^+ d \to \omega^o\ p\ p_s$. This is an optical spark chamber experiment which provides about 500 events at each momentum at present. A broad dip is seen in ρ^{GJ}_{00} extending from $|t| \sim 0.1$ to $\sim 0.5\ \text{GeV}^2$. As discussed in Section V, the bubble chamber results are not

statistically good enough to clearly establish structure in ρ_{00}^{GJ} versus t. The experiments at 4.19 and 7.0 GeV/c could be consistent with the $\pi^- p$ data, the errors are large. A further complication pointed out in reference 84 is that background corrections can be important in determining the t-dependence. The differential cross section for $\pi^- p \to \omega^o n$ at 5.5 GeV/c clearly demonstrates a dip in the forward direction ($|t| < 0.15$ GeV^2). Such a dip is also clearly indicated by the $\pi^+ d$ bubble chamber experiments at 5.1, 7.0, and 9.0 GeV/c but less clearly or not at all by the experiments at 2.7, 3.65, and 4.19 GeV/c.

114) New data. R. Engelmann et al., ANL - University of Chicago, To be published.

115) A comparison of the Hulthen prediction with that from the repulsive core deuteron wave function is given by D. C. Brunt et al., Phys. Rev. 187, 1856 (1969). The authors also use a statistical model calculation, assuming the impulse approximation, to show that for $p\,d \to n\,p\,p\,\pi^+\pi^-$ at 2.11 GeV/c the choice of the slowest nucleon as the spectator misidentifies less than 0.6% of the spectator nucleons with momentum > 150 MeV/c. They also point out that misidentification of slower spectators is even less likely.

116) J. Rhode et al., University of Indiana Preprint.

Table 1a

Values Used to Predict the Effect of Pauli Exclusion on the Deuterium Cross Section. R Is the Reduction and r Is the Fraction of the Cross Section Which Is Spin Nonflip

$-t$	$S(t)$	η^o	π^o	$r = 1$			$r = 0$
$(GeV/c)^2$	(β =5.18α)	$r_{A_{2ex}}$	$r_{\rho\, ex}$	R_{nf}	$R_{A_{2ex}}$	$R_{\rho\, ex}$	$R_{\pi\, ex}$
0	1	1	1	0	0	0	0.667
.01	.608	.80	.71	.392	.472	.509	.797
.02	.434	.67	.55	.566	.661	.696	.855
.03	.333	.60	.41	.667	.756	.795	.889
.04	.267	.54	.32	.733	.815	.854	.911
.05	.220	.50	.26	.780	.854	.889	.927
.06	.185	.44	.21	.815	.883	.912	.938
.07	.159	.40	.16	.841	.905	.930	.947
.08	.138	.36	.13	.862	.921	.942	.954
.09	.117	.34	.10	.883	.934	.953	.961
.10	.104	.31	.08	.896	.943	.959	.965
.15	.062	.25	.01	.938	.969	.979	.979
.20	.041	.20	.00	.959	.980	.986	.986
.25	.030	.18	.01	.970	.986	.990	.990
.30	.022	.16	.06	.978	.991	.992	.993

Table 1b

Momentum Transfer Distribution for $K^+d \rightarrow K^o pp$ in $\mu b/(GeV/c)^2$. Integrated Cross Section = 174.8 ± 20.0 μb

$-t$ $(GeV/c)^2$		$d\sigma/dt\ (K^+d \rightarrow K^o pp)$ (uncorrected)	$d\sigma/dt\ (K^+n \rightarrow K^o p)$
0.0	0.05	328.9 ± 82	539.2 ± 135
0.05	0.10	740.4 ± 148	807.4 ± 161
0.10	0.15	527.7 ± 106	538.5 ± 108
0.15	0.25	243.7 ± 37	243.7 ± 37
0.25	0.35	132.5 ± 25	132.5 ± 25
0.35	0.45	140.1 ± 29	140.1 ± 29
0.45	0.65	55.4 ± 14	55.4 ± 14
0.65	0.85	38.9 ± 17.5	38.9 ± 17.5
0.85	1.05	40.1 ± 13.6	40.1 ± 13.6
1.05	1.25	10.1 ± 7.	10.1 ± 7.

Table 2

Comparison of Hydrogen Cross Sections for Free and for Bound Protons at 3 GeV/c SABRE Collaboration (Ref. 10)

K^-d^* σ (μb)	K^-P σ (μb)
$\sigma\ (n_s\ \Lambda\pi^+\pi^-) = 490 \pm 56$	$\sigma\ (\Lambda\pi^+\pi^-) = 505 \pm 40$
$\sigma\ (n_s\ \Lambda\pi^+\pi^+\pi^-\pi^-) = 116 \pm 25$	$\sigma\ (\Lambda\pi^+\pi^+\pi^-\pi^-) = 157 \pm 12$
$\sigma\ (n_s\ \Sigma^-\pi^+\pi^+\pi^-) = 180 \pm 20$	$\sigma\ (\Sigma^-\pi^+\pi^+\pi^-) = 169 \pm 10$
$\sigma\ (n_s\ \Sigma^+\pi^+\pi^-\pi^-) = 281 \pm 32\ \mu b$	$\sigma\ (\Sigma^+\pi^+\pi^-\pi^-) = 221 \pm 16$

*Includes 5% Glauber shadow correction. Restricted to $n_s \leq 300$ MeV/c and $0.66 \leq (MM)^2 \leq 1.18\ (GeV/c)^2$.

Table 3

$\pi^+ p \rightarrow \pi^+ \pi^- \pi^+ p \rightarrow \rho^o \Delta^{++}$*

	Momentum	$\sigma(\pi^+\pi^-\pi^+p)$ (mb)	$\sigma(\rho^o\Delta^{++})$ (mb)
$\pi^+ p$	4 GeV/c	3.09 ± 0.09	0.9 ± 0.1
$\pi^+ p$	5 GeV/c	2.76 ± 0.04	0.87 ± 0.08
$\pi^+ d$	5.1 GeV/c	1.96 ± 0.2	0.632 ± 0.06
$\pi^+ p$	8.0 GeV/c	2.05 ± 0.06	0.31 ± 0.24

Table 4

Reaction $\pi^+ p \rightarrow \rho^o \Delta^{++}$**

Fitted to $dN/dt \sim Ae^{-at} + Be^{-bt}$

Reaction	Momentum (GeV/c)	Variable Range $(GeV/c)^2$	a $(GeV/c)^{-2}$	b $(GeV/c)^{-2}$
$\pi^+ p \rightarrow \rho^o \Delta^{++}$	5.0	$-t'$ 0.0 - 1.4	16.7 ± 0.9	2.71 ± 0.2
$\pi^+ d \rightarrow \rho^o \Delta^{++}(n_s)$	5.1	$-t'$ 0.0 - 0.7	20.1 ± 1.2	3.4 ± 0.4
$\pi^+ p \rightarrow \rho^o \Delta^{++}$	8.0	$-t'$ 0.0 - 2.0	19.1 ± 2.0	3.2 ± 0.7
$\pi^+ p \rightarrow \rho^o \Delta^{++}$	13.0	$-t'$ 0.0 - 0.7	20	3.8

* The $\pi^+ p$ data is given in Ref. 32.

**The $\pi^+ d$ data is from Ref. 25.

Table 5

Cross Section $\pi^- p \rightarrow \pi^- \pi^+ n$, $\rho^o n$, $f^o n$, $g^o n$

Reference	Momentum GeV/c	$\sigma (\pi^+ \pi^- n)$ mb	$\sigma (\rho^o n)$ mb	$\sigma (f^o n)$ mb	$\sigma (g^o n)$ mb
61	1.59	6.45 ± 0.17			
62	1.71	7.4 ± 0.5			
63	2.1	5.67 ± 0.1	~ 3.5		
64	2.14	5.4 ± 0.3			
65	2.26	5.67 ± 0.17	2.89 ± 0.11		
66	2.7	3.9 ± 0.2	2.3 ± 0.2	0.15 ± 0.10	
67	2.75	3.9 ± 0.1	1.1	< 0.1	
68	3.63	4.33 ±			
69	4.0	3.16 ± 0.13	0.75 ± 0.13	0.42 ± 0.06	
70	4.0	3.16 ± 0.13	1.1		
71	4.16	2.85 ± 0.07	1.15 ± 0.047	0.53 ± 0.056	
72	6.0	1.16 ± 0.18			
73	6.93		0.390 ± 0.050	0.220 ± 0.060	0.049 ± 0.015
74	8.0	0.96 ± 0.05	0.234 ± 0.021	0.165 ± 0.018	0.054 ± 0.013
75	8.0		0.39 ± 0.07	0.14 ± 0.05	0.08 ± 0.04
76	10.0	0.85 ± 0.12	< 0.09		
77	11.0	0.70 ± 0.10	0.11 ± 0.014	0.075 ± 0.014	0.055 ± 0.014
78	11.2		0.128 ± 0.016		
79	16.0		0.182 ± 0.047	0.081 ± 0.022	< 0.015
80	16.0	0.40 ± 0.08	0.052 ± 0.013	0.038 ± 0.009	

Table 6

Cross Section $\pi^+ d \rightarrow \pi^+\pi^- pp_s$, $\rho^o pp_s$, $f^o pp_s$, $g^o pp_s$

Reference	Momentum	$\sigma(\pi^+\pi^- p)$ mb	$\sigma(\rho^o p)$ mb	$\sigma(f^o p)$ mb	$\sigma(gp)$ mb
81	1.68	6.6 ± 0.3			
82	2.7	3.42 ± 0.3	2.2 ± 0.25	0.51 ± 0.2$^+$	
83	3.65	2.58 ± 0.21	1.6 ± 0.15	0.63 ± 0.105	
84	4.19	2.40 ± 0.12	1.27 ± 0.07	0.66 ± 0.04	
85	4.5	1.56 ± 0.04	0.544 ± 0.030	0.285 ± 0.021	
				(0.149 ± 0.015)	
86	5.1	1.39 ± 0.17	0.65 ± 0.083	0.46 ± 0.061	0.083 ± 0.019
				(0.210 ± 0.03)	
87	5.4	1.3 ± 0.4	0.433 ± 0.133	0.262 ± 0.081	0.035 ± 0.014
			0.533 ± 0.1*	0.322 ± 0.064*	0.043 ± 0.014*
88	6.95		0.37 ± 0.07	0.26 ± 0.05	0.049 ± 0.008

$^+$Corrected for decay $f^o \rightarrow \pi^o\pi^o$; ( ) is for $f^o \rightarrow \pi^o\pi^o$.

*With the normalization $\sigma(\pi^+ n \rightarrow \pi^+\pi^- p) = \sigma(\pi^- p \rightarrow \pi^+\pi^- n)$.

Table 7

Comparison of ρ, f, and g Production in
$\pi^+ n \rightarrow \pi^+ \pi^- p$ and $\pi^- p \rightarrow \pi^+ \pi^- n$
at 7.0 GeV/c [Toronto-Wisconsin Collaboration] Ref. 88

Resonance	Variable	$\pi^+ n$	$\pi^- n$
ρ^o	Mass (MeV)	781 ± 3	783 ± 3
	Width (MeV)	162 ± 8	142 ± 10
	Cross Section (μb)	370 ± 70	390 ± 50
f^o	Mass (MeV)	1266 ± 4	1278 ± 5
	Width (MeV)	189 ± 12	155 ± 14
	Cross Section (μb)	260 ± 50	220 ± 60
g^o	Mass (MeV)	1670 ± 10	1660 ± 10
	Width (MeV)	141 ± 10	127 ± 10
	Cross Section (μb)	49 ± 8	49 ± 15

Table 8

Reaction $\pi N \rightarrow f^o N$

Fitted to $dN/dt \sim Ae^{at} + Be^{bt}$

Reaction	Momentum	Variable Range	a	b
$\pi^+ n \rightarrow f^o p$	5. 1	t' 0. 0 - 0. 7	11. 7 ± 1. 4	2. 7 ± 1. 0
$\pi^+ n \rightarrow f^o p$ $\pi^- p \rightarrow f^o n$	7. 0	t' 0. 0 - 1. 4	12. 51 ± 0. 52	2. 65 ± 0. 28

Table 9

Reaction $\pi N \rightarrow \rho^o N$

Fitted to $dN/dt \sim Ae^{at} + Be^{bt}$

Reaction	Momentum GeV/c	Range $(GeV/c)^2$	a $(GeV/c)^{-2}$	b $(GeV/c)^{-2}$
$\pi^+ n \rightarrow \rho^o p$	5. 1	t' 0. 0 → 0. 7	14. 0 ± 1. 2	2. 7 ± 1. 0
$\pi^+ n \rightarrow \rho^o p$ $\pi^- p \rightarrow \rho^o n$	7. 0	t' 0. 0 → 1. 4	13. 98 ± 0. 53	2. 84 ± 0. 26

Table 10

Cross Section $\pi^+ d \to \pi^+\pi^-\pi^0 pp_s$, $\omega^0 pp_s$, ηpp_s

Reference	Momentum	$\sigma(\pi^+\pi^-\pi^0 p)$	$\sigma(\omega p)$	$\sigma(\eta p)$
62	1.68	5.0 ± 0.3	1.8 ± 0.2	0.15 ± 0.04
82	2.7	4.22 ± 0.37	$0.8 \pm 0.03^+$	$0.21 \pm 0.04^+$
83	3.65	3.44 ± 0.31	0.46 ± 0.05 $(0.50 \pm 0.06)^+$	
84	4.19	2.19 ± 0.11	$0.345 \pm 0.05^+$	
85	4.5	1.62 ± 0.24		
86	5.1	2.12 ± 0.60	0.195 ± 0.040	
87	5.4	1.162 ± 0.195 $1.43 \pm 0.24^*$	$0.121 \pm 0.028^+$ $0.149 \pm 0.035^{*+}$	$0.117 \pm 0.042^*$
88	7.0		$0.086 \pm 0.0128^+$	
89	8.0		$0.085 \pm 0.015^+$	

$^+$Corrected for unseen decays.

*Normalized by equating $\sigma(\pi^+ n \to \pi^+\pi^- p)$ to $\sigma(\pi^- p = \pi^+\pi^- n)$.

Table 11

Cross Sections for $K^-p \rightarrow \Lambda\pi^o$; $K^-n \rightarrow \Lambda\pi^-$

P_{K^-} (GeV/c)	σ_T (μb)	Reference
	$K^-p \rightarrow \Lambda\pi^o$	
1.22	1580 ± 70	90
1.42	1370 ± 60	90
1.51	1370 ± 60	90
1.60	1100 ± 70	90
1.70	940 ± 50	90
1.72	930 ± 80	90
1.80	640 ± 50	91
1.95	530 ± 50	91
2.24	315 ± 47	92
3.0	138 ± 15	93
3.5	115 ± 40	94
6.0	24 ± 6	95
	$K^-n \rightarrow \Lambda\pi^-$	
3.0	310 ± 40	96
4.5	83 ± 11	97
5.0	59 ± 10	98
5.5	53 ± 13	99
13.0	14 ± 6	100

Table 12

$K^-n \rightarrow \Sigma^o\pi^-$

P_{K^-}	σ_T (μb)	Slope (GeV/c)$^{-2}$	Reference
3.0	170 ± 30	5.4 ± 0.4	96
4.5	32 ± 10	5.0 ± 2.5	97
5.0	17 ± 4		98

Table 13

Cross Sections for $K^- p \rightarrow \Lambda\rho^o$; $K^- n \rightarrow \Lambda\rho^-$

P_{K^-} (GeV/c)	σ_T (μb)	Reference
$K^- p \rightarrow \Lambda\rho^o$		
1.15 - 1.30	0 ± 70	101
1.30 - 1.45	290 ± 90	101
1.45 - 1.60	460 ± 90	101
1.60 - 1.75	140 ± 90	101
1.8	390 ± 60	91
1.95	330 ± 40	91
2.24	83 ± 14	92
3.0	110 ± 26	93
3.82	108 ± 19	102
4.1	66 ± 23	103
4.6	58 ± 8	102
5.0	41 ± 10	102
5.5	22 ± 4	103
6.0	9 ± 3	95
10.1	3 ± 2	104
$K^- n \rightarrow \Lambda\rho^-$		
4.5	70 ± 13	97
5.0	44 ± 9	98
5.5	41 ± 8	99

Table 14

3 GeV/c $\left\{\begin{array}{l} K^- d \rightarrow \bar{K}^o \pi^- n p_s \\ K^- d \rightarrow K^o \Delta^-(1236) p_s \\ K^- d \rightarrow K^{*-}(890) n p_s \end{array}\right.$

$K^*(890)$

	Seen Sp.	Unseen Sp.	All
ρ_{00}	0.21 (5)	0.16 (3)	0.18 (3)
ρ_{1-1}	0.25 (5)	0.34 (3)	0.31 (2)
$\mathrm{Re}\,\rho_{10}$	-0.08 (3)	-0.07 (3)	-0.07 (2)

$\Delta^-(1236)$

	Seen Sp.	Unseen Sp.	All
ρ_{33}	0.29 (4)	0.33 (4)	0.31 (3)
$\mathrm{Re}\,\rho_{3-1}$	0.26 (5)	0.22 (4)	0.24 (3)
$\mathrm{Re}\,\rho_{31}$	-0.09 (5)	-0.09 (4)	-0.09 (3)

$\left\{\begin{array}{l} K^- d \rightarrow K^- \pi^+ \pi^- n p_s \\ \quad\quad \rightarrow K^*(890)\, \Delta^-(1236) p_s \end{array}\right.$

$K^*(890)$

	Seen Sp.	Unseen Sp.	All
ρ_{00}	0.52 (4)	0.50 (3)	0.51 (3)
ρ_{1-1}	-0.05 (4)	0.01 (3)	-0.01 (2)
$\mathrm{Re}\,\rho_{10}$	-0.03 (3)	0.03 (2)	0.00 (2)

$\Delta^-(1236)$

	Seen Sp.	Unseen Sp.	All
ρ_{33}	0.07 (3)	0.11 (3)	0.09 (2)
$\mathrm{Re}\,\rho_{3-1}$	-0.02 (3)	0.06 (3)	0.03 (2)
$\mathrm{Re}\,\rho_{31}$	-0.07 (3)	-0.02 (3)	-0.04 (2)

The errors in parentheses are in the least significant figure.

Table 15

Cross Sections $K^- n \to \bar{K}^0 n \pi^-$

Reference	Momentum GeV/c	σ (mb)
45	3.0	1.60 ± 0.11
44	4.5	0.758 ± 0.021
98	5.0	0.568 ± 0.063
99	5.5	0.441 ± 0.050

Table 16

$K^+ p \to K^0 \Delta^{++}$

Reference	Momentum GeV/c	Momentum Transfer Range $(GeV/c)^2$	Slope $(GeV/c)^{-2}$
110	3.0	$\lvert t \rvert$; 0.05 - 1.0	3.26 ± 0.6
110	3.5	$\lvert t \rvert$; 0.05 - 1.0	3.5 ± 0.5
110	5.0	$\lvert t \rvert$; 0.05 - 1.0	4.1 ± 0.7
111	9.0	$\lvert t \rvert$; 0.0 - 0.9	4.18 ± 0.49
112	10.0	$\lvert t \rvert$; 0.05 - 0.7	5.2 ± 0.4
110	13.0	$\lvert t' \rvert$; 0.0 - 0.7	5 ± 1

$K^- n \to \bar{K}^0 \Delta^-$

Reference	Momentum GeV/c	Momentum Transfer Range $(GeV/c)^2$	Slope $(GeV/c)^{-2}$
45	3.0	$\lvert t \rvert$; 0.1 - 0.5	3.3 ± 0.7
44	4.5	$\lvert t \rvert$; 0.05 - 0.7	4.0 ± 0.7
98	5.0	$\lvert t' \rvert$; 0.15 - 0.6	4.1 ± 0.7
99	5.5	$\lvert t' \rvert$; 0.15 - 0.6	3.9 ± 0.6

Table 17

Cross Sections for $K^-p \to pK^{*-}(890)$; $K^-n \to K^{*-}(890)n$

$K^-p \to K^{*-}(890)p$		
P_{K^-} (GeV/c)	σ_T (μb)	Reference
1.8	1890 ± 135	91
1.95	1875 ± 150	91
2.0	1300 ± 80	105
2.1	2010 ± 120	106
2.24	1375 ± 175	92
2.45	1650 ± 120	106
2.64	1245 ± 75	106
3.0	839 ± 45	93
3.5	760 ± 60	107
3.82	623 ± 137	102
4.1	500 ± 60	108
4.6	529 ± 65	102
5.0	511 ± 85	102
5.5	279 ± 26	108
6.0	165 ± 38	95
10.1	92 ± 9	109
$K^-n \to K^*(890)^-n$		
3.0	885 ± 90	45
4.5	354 ± 18	44
5.0	264 ± 45	98
5.5	170 ± 30	99

Table 18

$K^-d \rightarrow K^-\pi^-\pi^+ n\, p_s$; $K^*(890)\, \Delta^-(1236)\, p_s$

Reference	Momentum GeV/c	$\sigma\ (K^-\pi^-\pi^+ n\, p_s)$ mb	$\sigma\ (K^*(890)\Delta^-(1236)\, p_s)$ mb
116	2.24	1.94 ± 0.5	~ 0.12
56	3.0	1.74 ± 0.13	0.93 ± 0.07
55	5.5	1.30 ± 0.20	0.28 ± 0.05
57	7.3	2.17 ± 0.29	0.24 ± 0.03
100	13.0	0.70 ± 0.07	~ 0.06 ± 0.025

Y. Cho et al (CMU-BNL)
600 Mev/c K+d

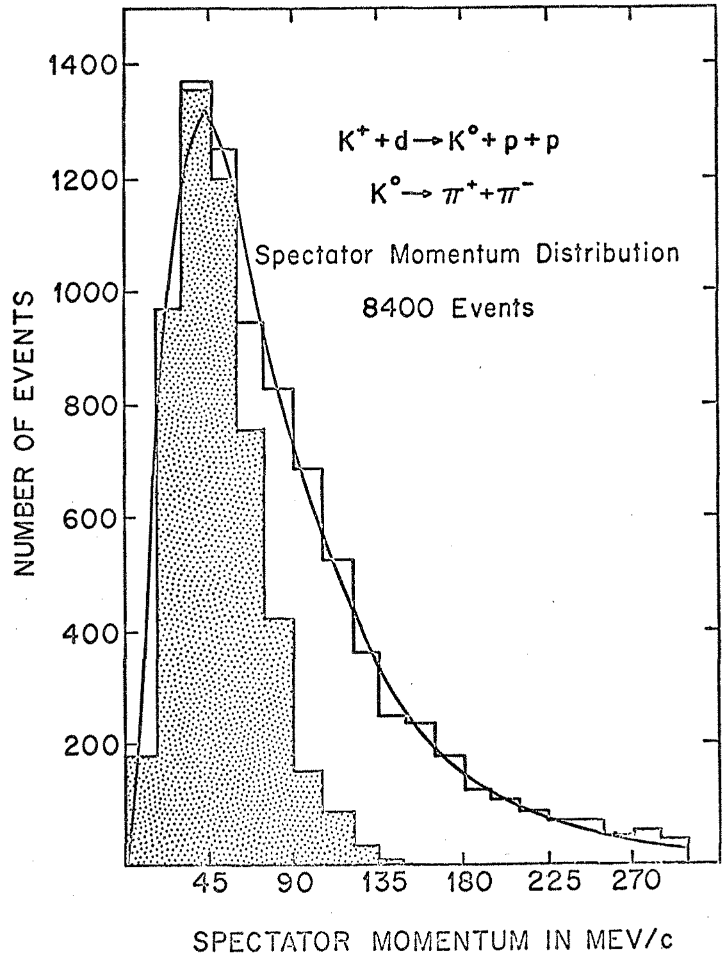

Figure 1: Spectator laboratory momentum distribution for both visible and unseen spectator tracks.

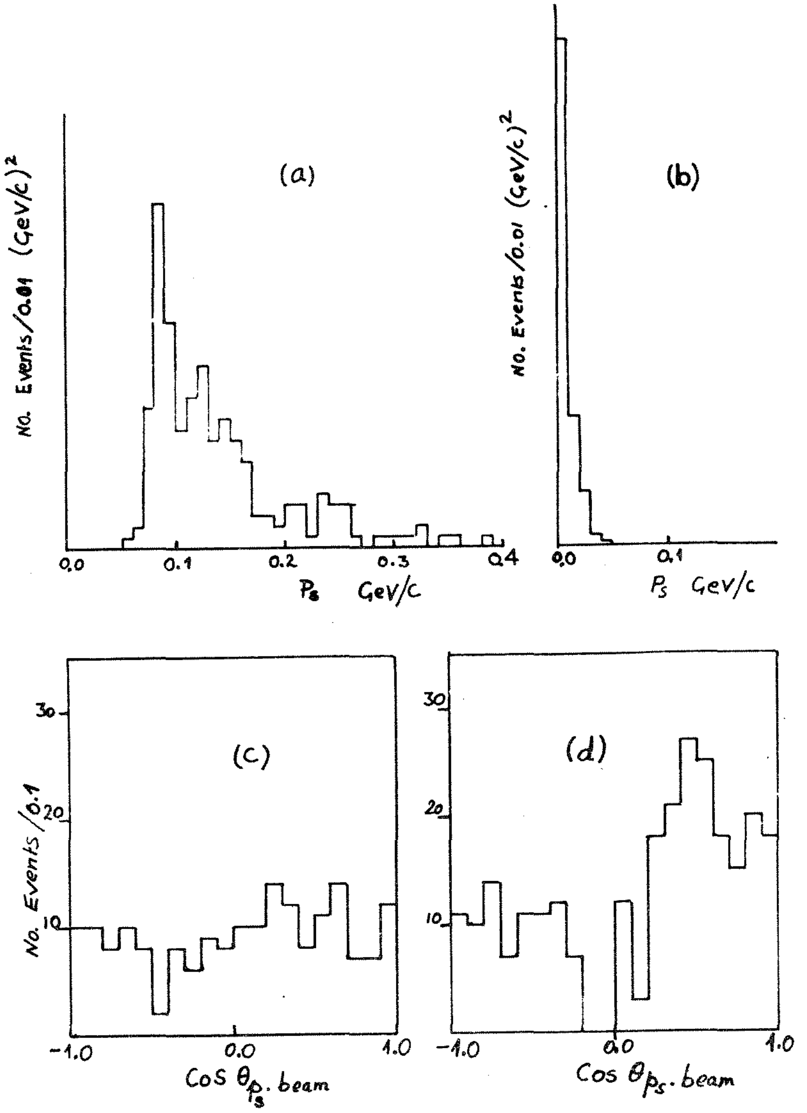

Figure 2: Spectator momentum and angular distribution for (a), (c) visible spectator tracks and (b), (d) unseen tracks, in the reaction $K^+d \rightarrow K^0\pi^0pp$ at 600 MeV/c (Ref. 5).

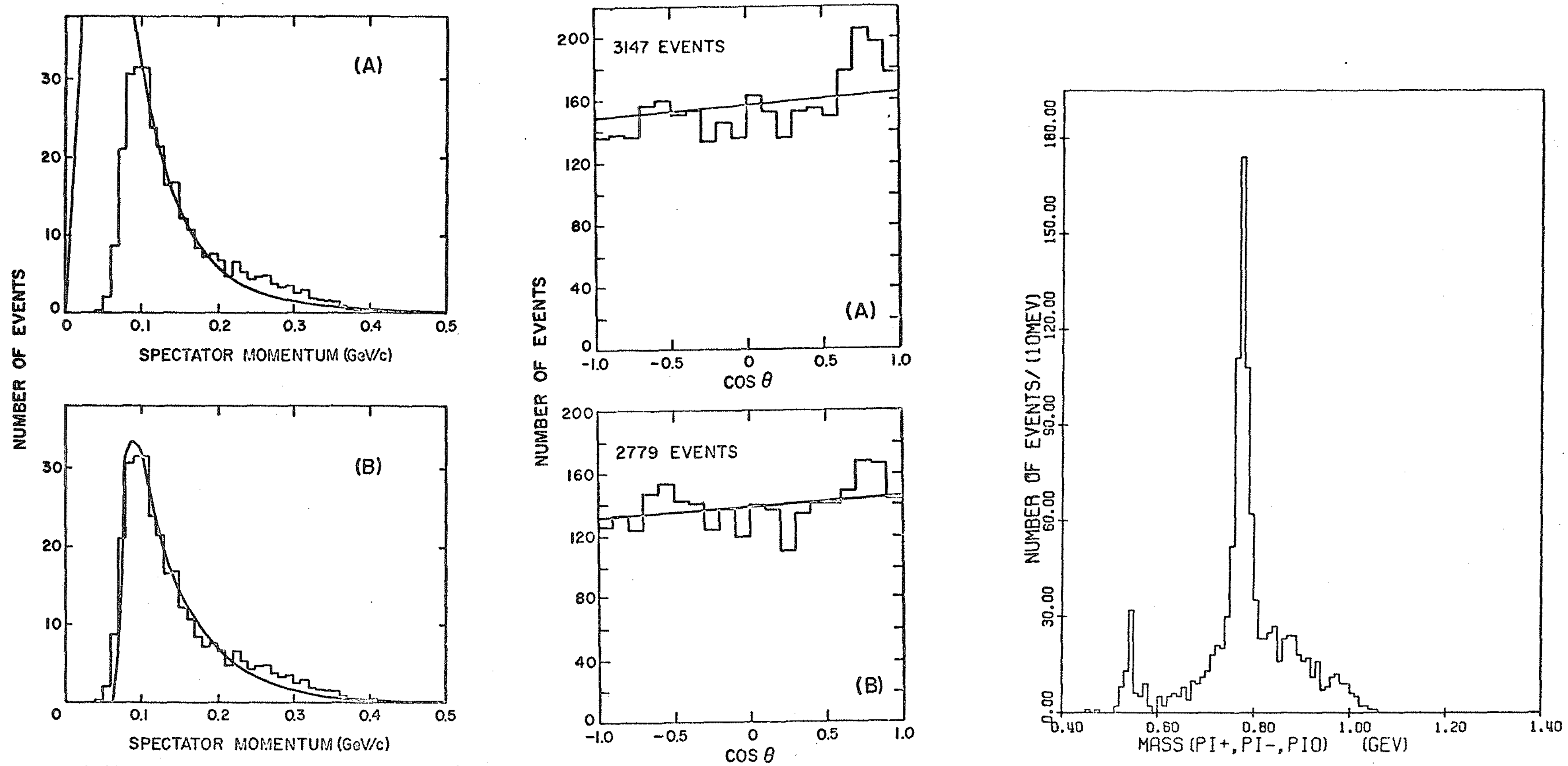

a) Momentum of spectator proton compared to Hulthèn wave function normalized to $110 < p < 180$ MeV/c.

b) Momentum of spectator proton compared to the Hulthèn wave function with the requirement that $p_{proj.} > 70$ MeV/c.

a) Distribution in cos (angle between spectator proton and beam) for all 4c and 1c events. The smooth curve is the Monte Carlo calculation.

b) Same comparison as above for events with $p_{spec} \leq 250$ MeV/c.

Mass $(\pi^+\pi^-\pi^o)$ for events fitting $\pi^+ n \rightarrow p\pi^+\pi^-\pi^o$.

Figure 3: Some distributions from 1.5 GeV/c π^+d experiment by an ANL Group, Reference 7.

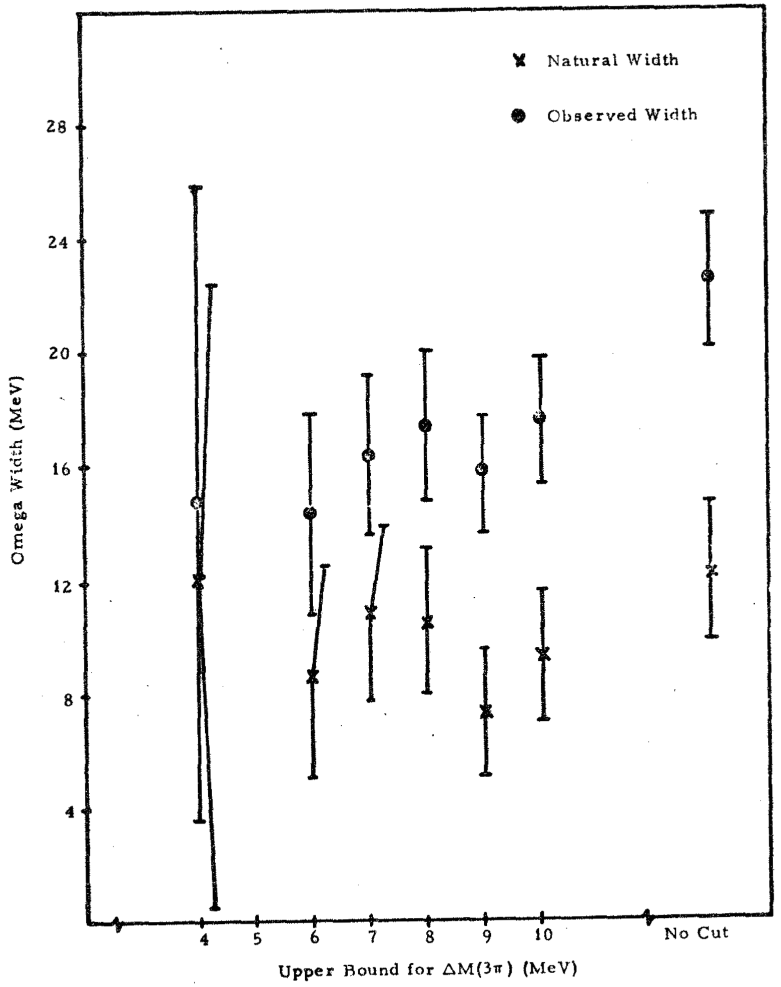

Figure 4: The ω^o width as a function of the error on the 3π mass from $\pi^+d \rightarrow \omega^o pp$ at 1.5 GeV/c.

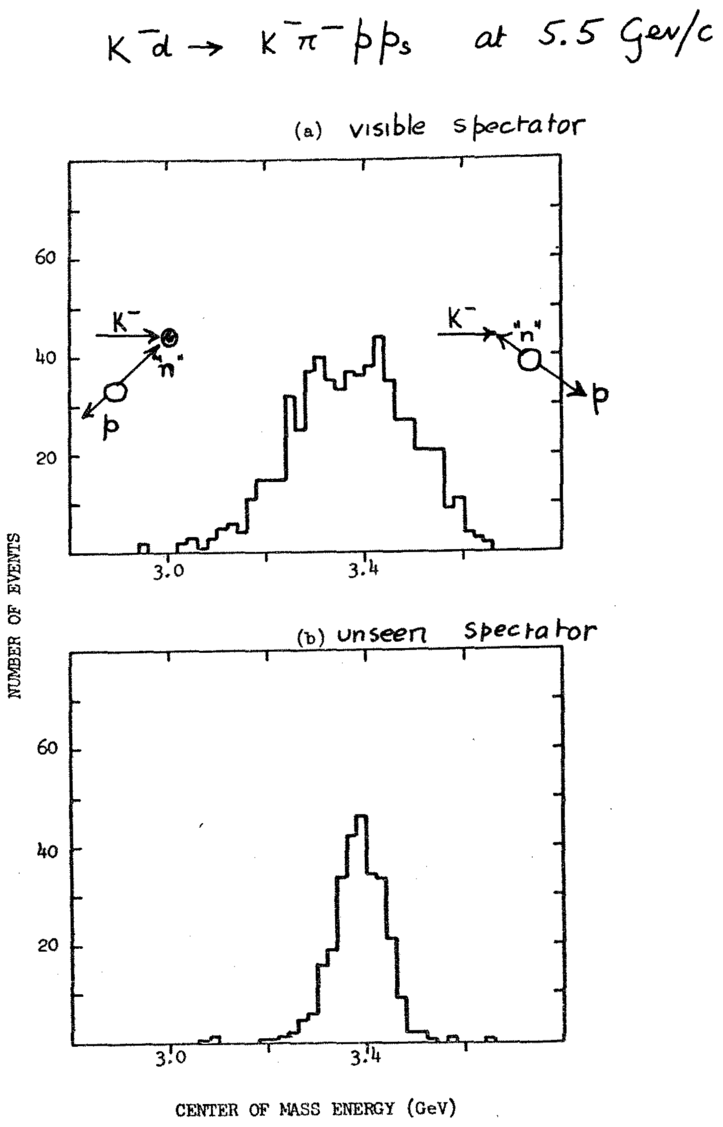

Figure 5: Centre of mass energy for the reaction $K^-n \rightarrow K^-\pi^-p$ for beam momentum 5.5 GeV/c when (a) the spectator proton track is seen and (b) when it is unseen.

(a, b) Spectator momentum distribution for a) "good" 4-pronged events from the final state $p\ p\ \pi^+\ \pi^-$ and (b)

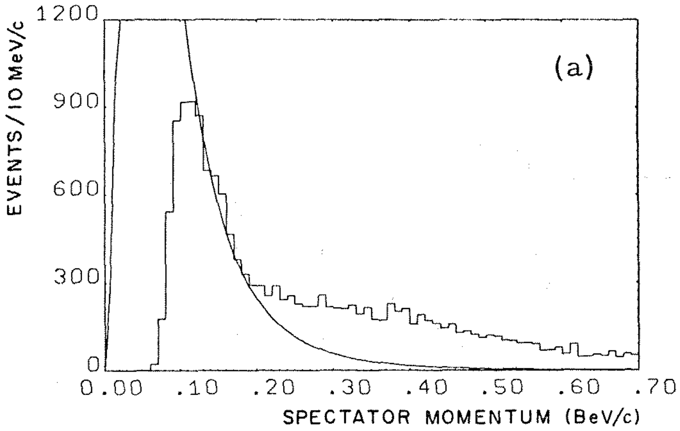

"good" events from the final state (n) $p\pi^+\pi^+\pi^-$. The curves are the Hulthén distribution, normalized to have the same area as the histogram in the interval (110 MeV/c < p < 160 MeV/c) for a) and (0 < p < 160 MeV/c) for b).

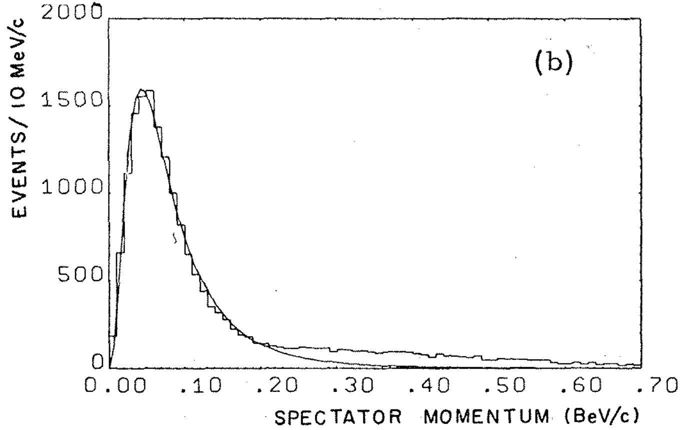

(c) Laboratory momentum of lower-momentum proton in the final state $p\ p\ \pi^+\ \pi^-\ \pi^0$ for 4-pronged events; the curve is the Hulthén distribution normalized to have the same area as the histogram in the interval (110 MeV/c < p < 160 MeV/c).

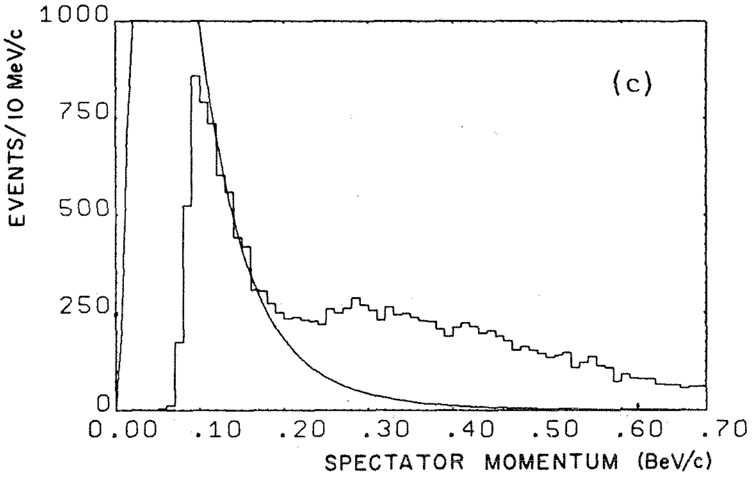

Figure 6: Laboratory spectator momentum distribution for three reactions from π^+d interactions in the momentum range 1.1 - 2.4 GeV/c.

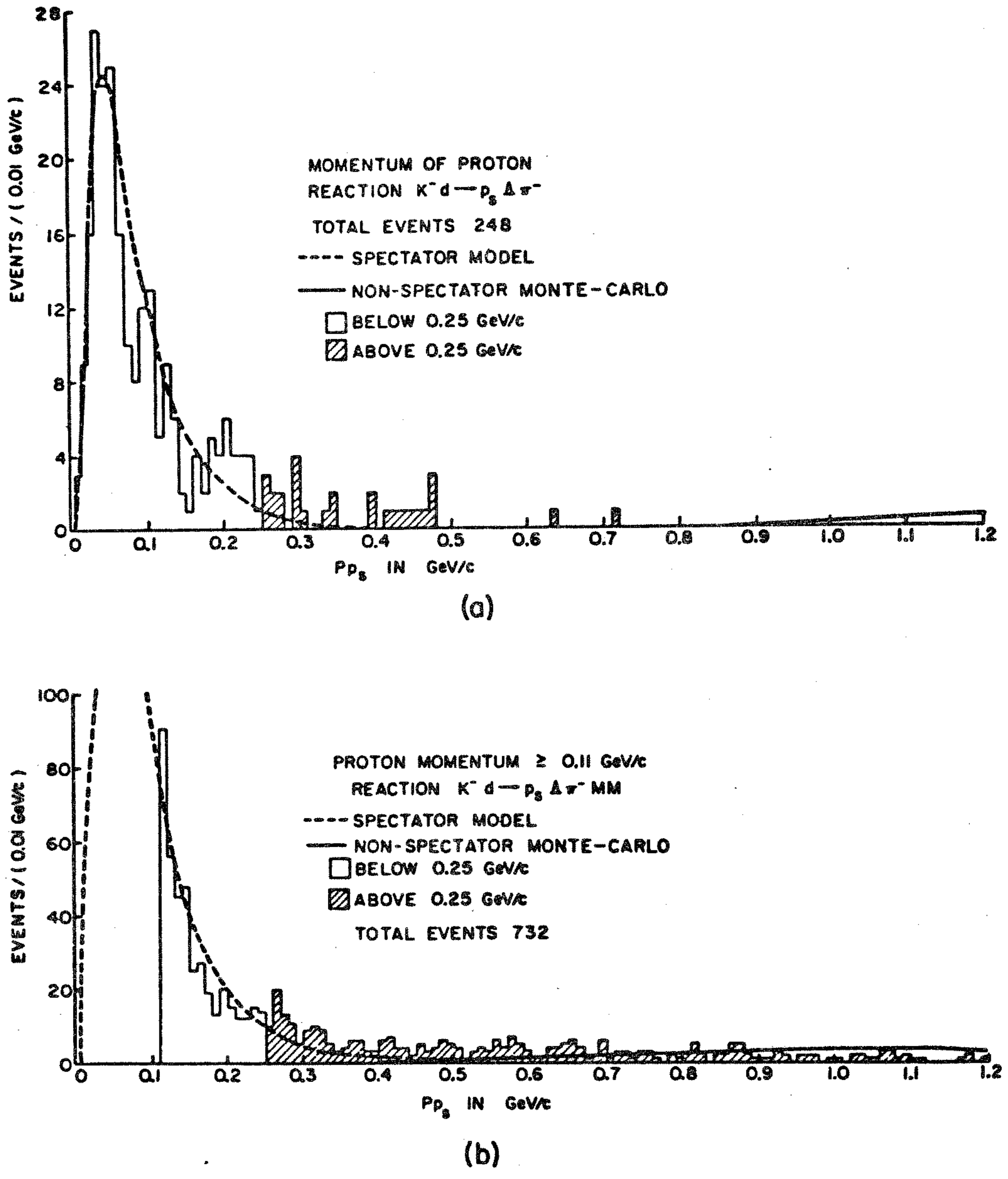

Momentum distribution of proton for final states (a) $p\Lambda\pi^-$, (b) $p\Lambda\pi^-$mm. The dotted line shows the Hulthén distribution with $\beta = 7\alpha$ normalized to events with proton momentum in the range (0.11 - 0.25 GeV/c). The solid line is a non-spectator Monte-Carlo calculation of the expected distribution of protons assuming K^- interacted with deuterium normalized to events in the range 0.25 - 1.2 GeV/c.

Figure 7: **Laboratory spectator momentum distribution for states containing a Λ^0 from K^-d interactions at 4.5 GeV/c.**

More specifically, the authors have tested the relations

$$\frac{d\sigma/dt(\gamma d\rightarrow K^+\Sigma^0 n)+d\sigma/dt(\gamma d\rightarrow K^+\Sigma^- p)}{d\sigma/dt(\gamma p\rightarrow K^+\Sigma^0)}=3, \quad (1a)$$

$$\frac{d\sigma/dt(\gamma d\rightarrow \pi^+ N^{*0} n)+d\sigma/dt(\gamma d\rightarrow \pi^+ N^{*-} p)}{d\sigma/dt(\gamma p\rightarrow \pi^+ N^{*0})}=4, \quad (1b)$$

$$\frac{d\sigma/dt(\gamma d\rightarrow \pi^- N^{*++} n)+d\sigma/dt(\gamma d\rightarrow \pi^- N^{*+} p)}{d\sigma/dt(\gamma p\rightarrow \pi^- N^{*++})}=\tfrac{4}{3}, \quad (1c)$$

where $-t$ is the square of the four-momentum transferred from the incident photon to the produced meson.

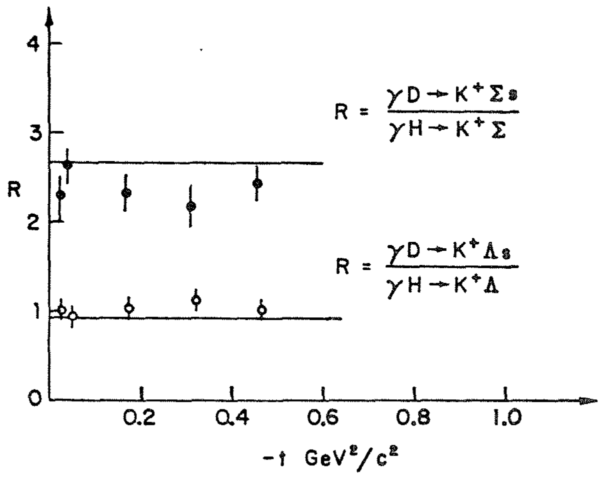

(a) Comparison between experimental results (Ref. 1) and theoretical predictions, as described in the text, for the ratios

$[d\sigma/dt(\gamma d\rightarrow K^+\Sigma s)]/[d\sigma/dt(\gamma p\rightarrow K^+\Sigma)]$

and

$[d\sigma/dt(\gamma d\rightarrow K^+\Lambda n)]/[d\sigma/dt(\gamma p\rightarrow K^+\Lambda)]$.

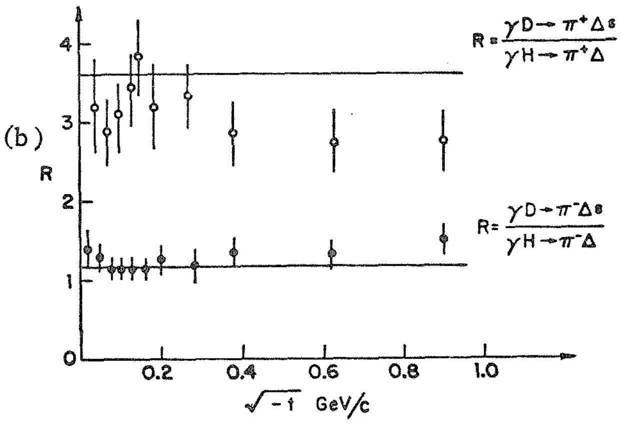

(c) Comparison between experimental results (Ref. 5) and theoretical predictions, as decribed in the text, for the ratio

$$\frac{d\sigma/dt(\gamma d\rightarrow\pi^+ nn)}{d\sigma/dt(\gamma p\rightarrow\pi^+ n)}$$

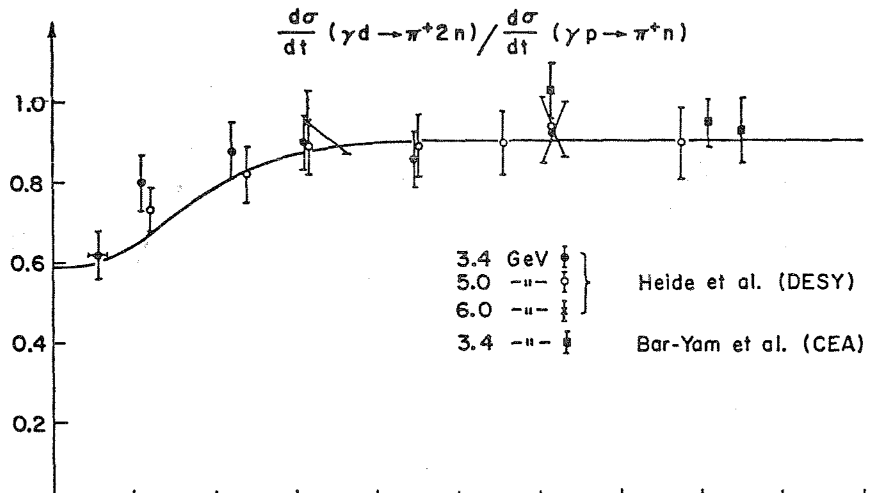

Figure 8: (a) and (b) show hydrogen-deuterium ratios which differ significantly from their expected values (1 a,b,c above). The solid curves on (a) (b) represent the values (1 a,b,c) reduced by the deuterium shadow effects calculated by Ref. 23. Deviations of the data from these curves indicate exotic t-channel exchange. Figure 8(c) indicates that the theory of Ref. 23 correctly reproduces the data in a case where there can be no exotic exchange. (See, however, the data of Fig. 10(a) -- the SLAC data lies higher than the DESY data near t = 0.)

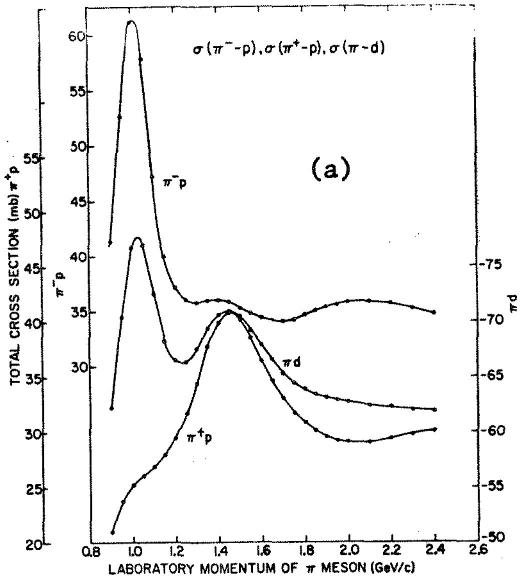

(a) $\pi^- - p$, $\pi^+ - d$, and $\pi^- - d$ total cross sections. For all points shown, statistical errors are smaller than the size of the data points.

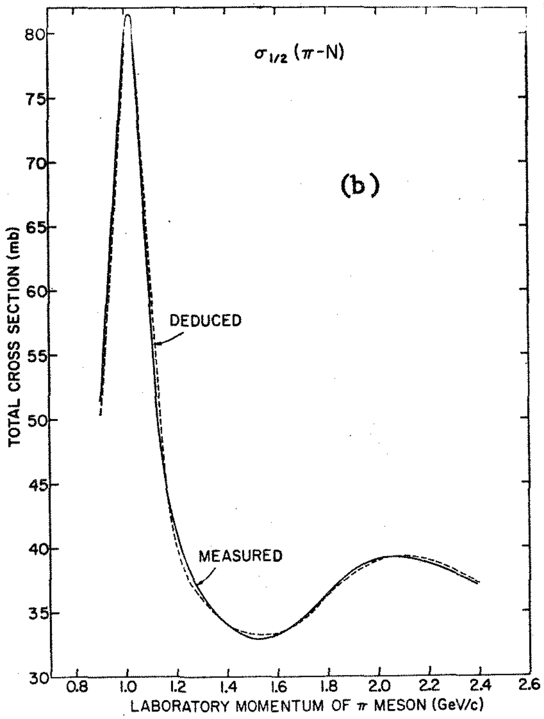

(b) $I = \frac{1}{2}$ pion-nucleon total cross section. Solid line was computed algebraically from $\pi^- - p$ and $\pi^+ - p$ data; dashed line was computed using $\pi^- - p$ and $\pi^- - d$ data, taking into account the effects of screening and Fermi motion in the deuteron.

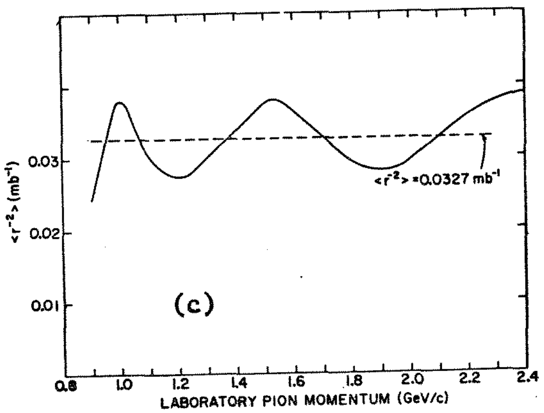

(c) $\langle r^{-2} \rangle$, the average value of the inverse of the square of the neutron-proton separation in the deuteron, computed from t e pion data.

Figure 9: (a), (b) Total cross section data; (c) the nucleon-nucleon separation deduced using $\sigma_{tot}(\pi^- d)$ expressed in terms of $\sigma_{tot}(\pi^+ p)$ and $\sigma_{tot}(\pi^- p)$.

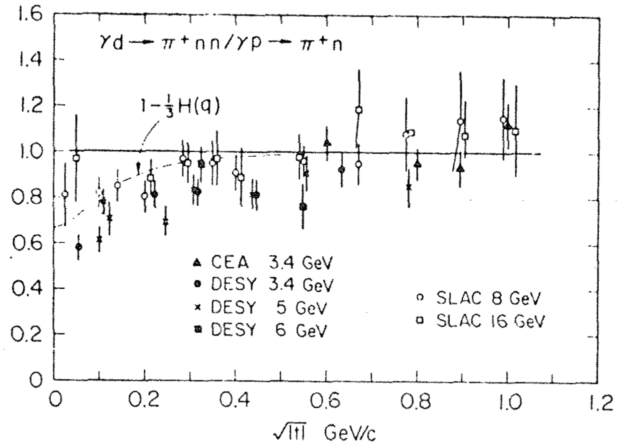

(a) The ratio of π^+ production from deuterium and hydrogen. Lower energy data from Cambridge Electron Accelerator and DESY (Ref. 5) are also shown. The curve $1-\frac{1}{3}H(q)$ represents the exclusion-principle effects expected for the spin-flip amplitudes. The data are plotted versus $\sqrt{|t|}$ to display the points at small t better.

(a) A. Boyarski et al.
Phys. Rev. Letters
21, 1767 (1968)

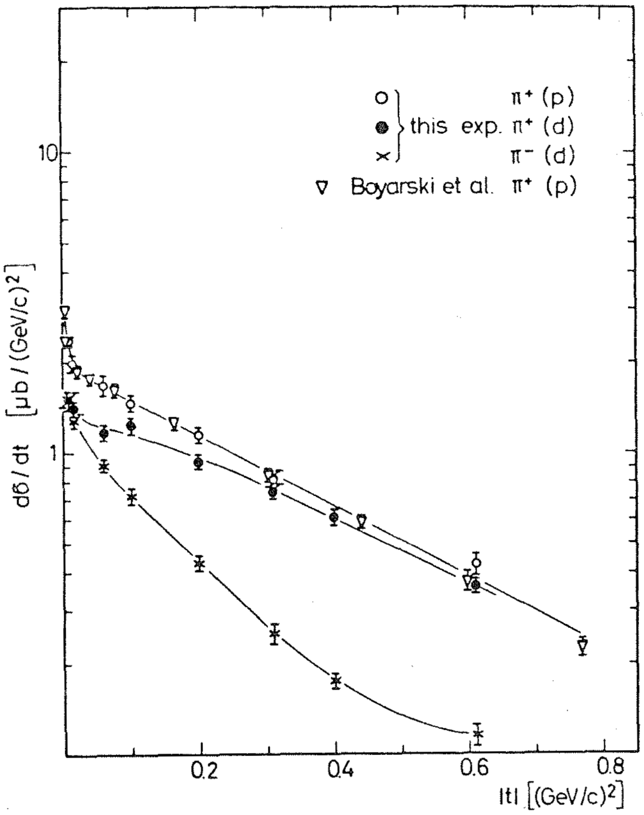

(b) Differential cross sections for the reactions $\gamma p \to \pi^+ n$, $\gamma d \to \pi^+ nn$, and $\gamma d \to \pi^- pp$ at $E_\gamma = 5$ GeV as functions of momentum transfer $|t|$. The curves are drawn to guide the reader.

(b) P. Heide et al.
Phys. Rev. Letters
21, 248 (1968)

Figure 10: Single pion photoproduction data (a) compilation of the hydrogen-deuterium π^+ ratio (b) comparison of π^+ and π^- photoproduction from hydrogen and deuterium.

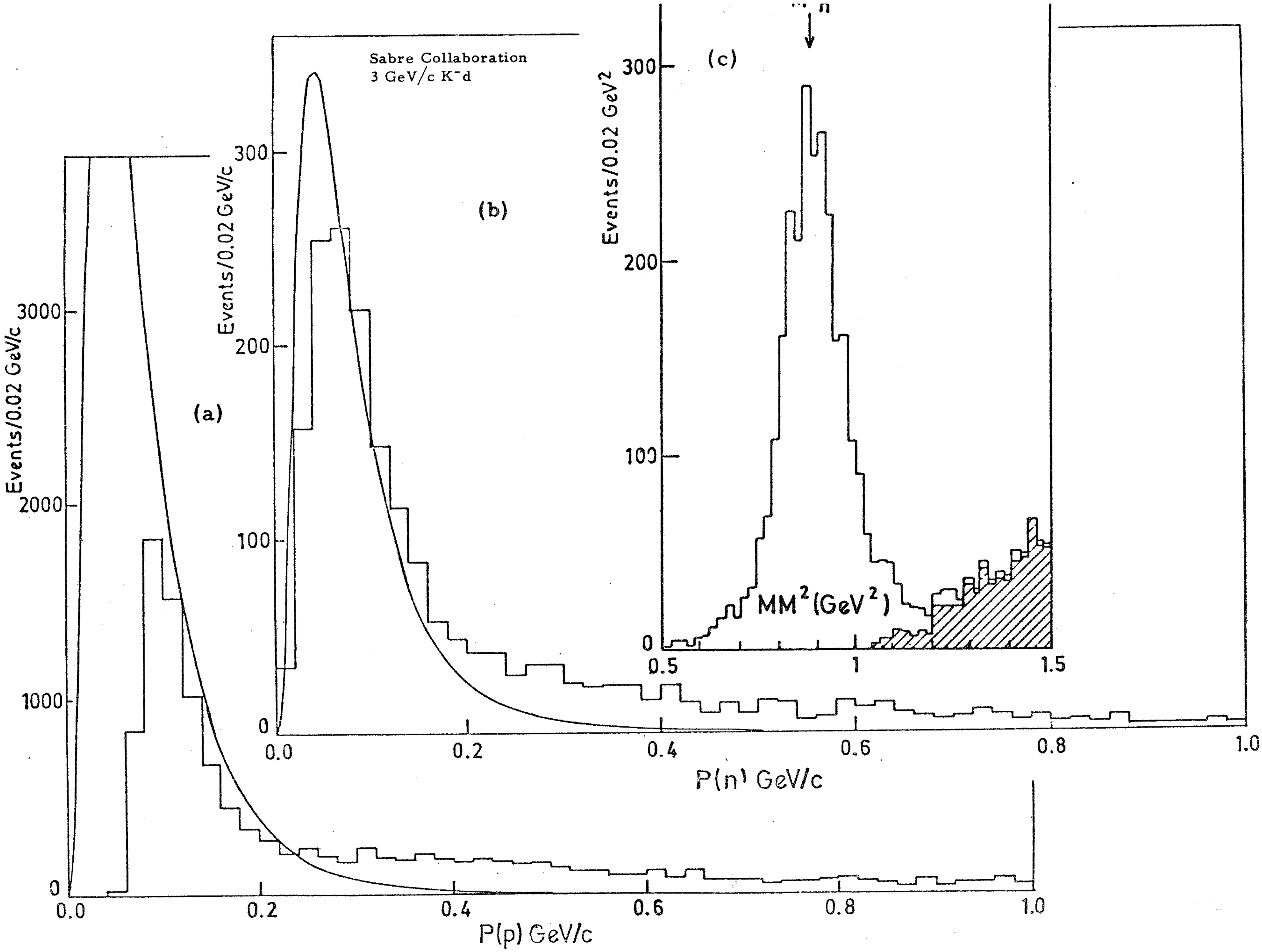

Figure 11: (a), (b) spectator momentum distributions for (a) seen proton and (b) neutron for events with a Λ or Σ in the final state. (c) neutron missing mass peak for $K^-d \rightarrow p_s n \bar{K}^0 \pi^- + m\pi^0$ (K^-d at 3 GeV/c, Ref. 10). In (a), (b) the theoretical curve is the Hulthén distribution normalized to events below 300 MeV/c.

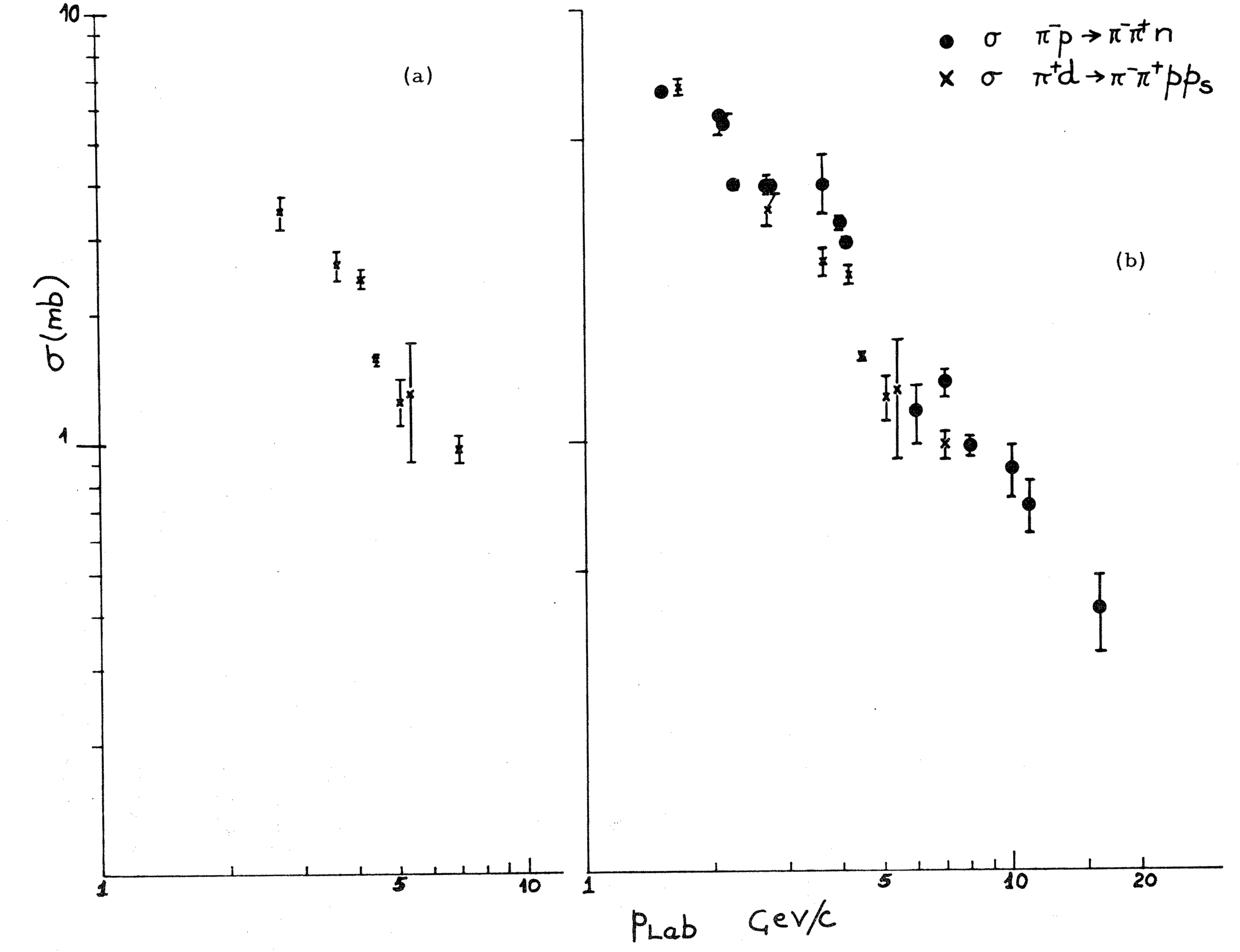

Figure 12: (a) Cross sections for $\pi^+d \rightarrow \pi^+\pi^- pp_s$ (b) Comparison of channel cross-sections for $\pi^+d \rightarrow \pi^+\pi^- pp_s$

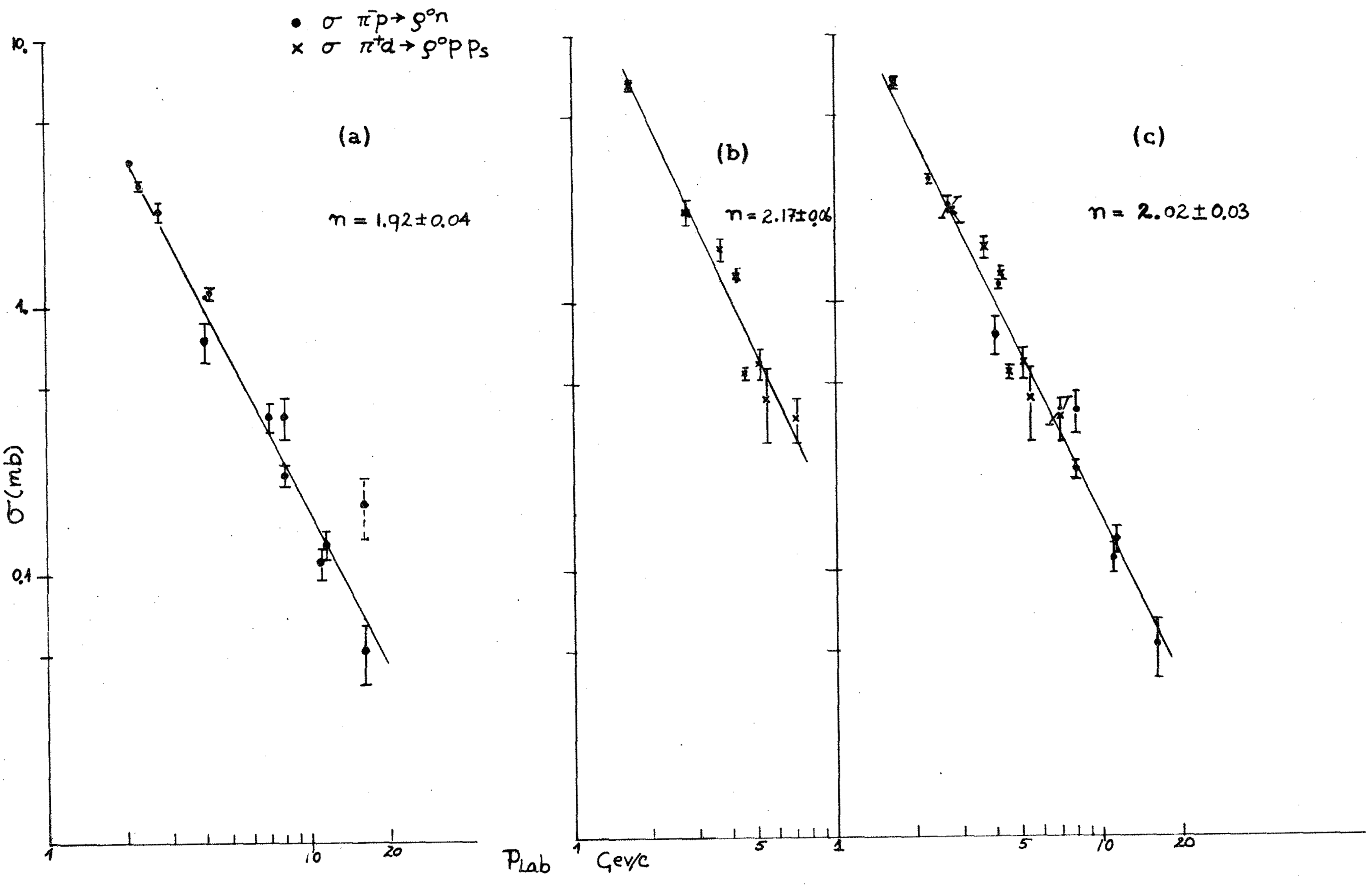

Figure 13: Channel cross sections for $\pi^+ d \to \rho^o p p_s$ and $\pi^- p \to \rho^o n$. (a) Shows $\pi^- p \to \rho^o n$; (b) $\pi^+ n \to \rho^o p$ and (c) both of them. The marked values of n are found from fitting the data in each graph to the form $A p_{lab}^{-n}$.

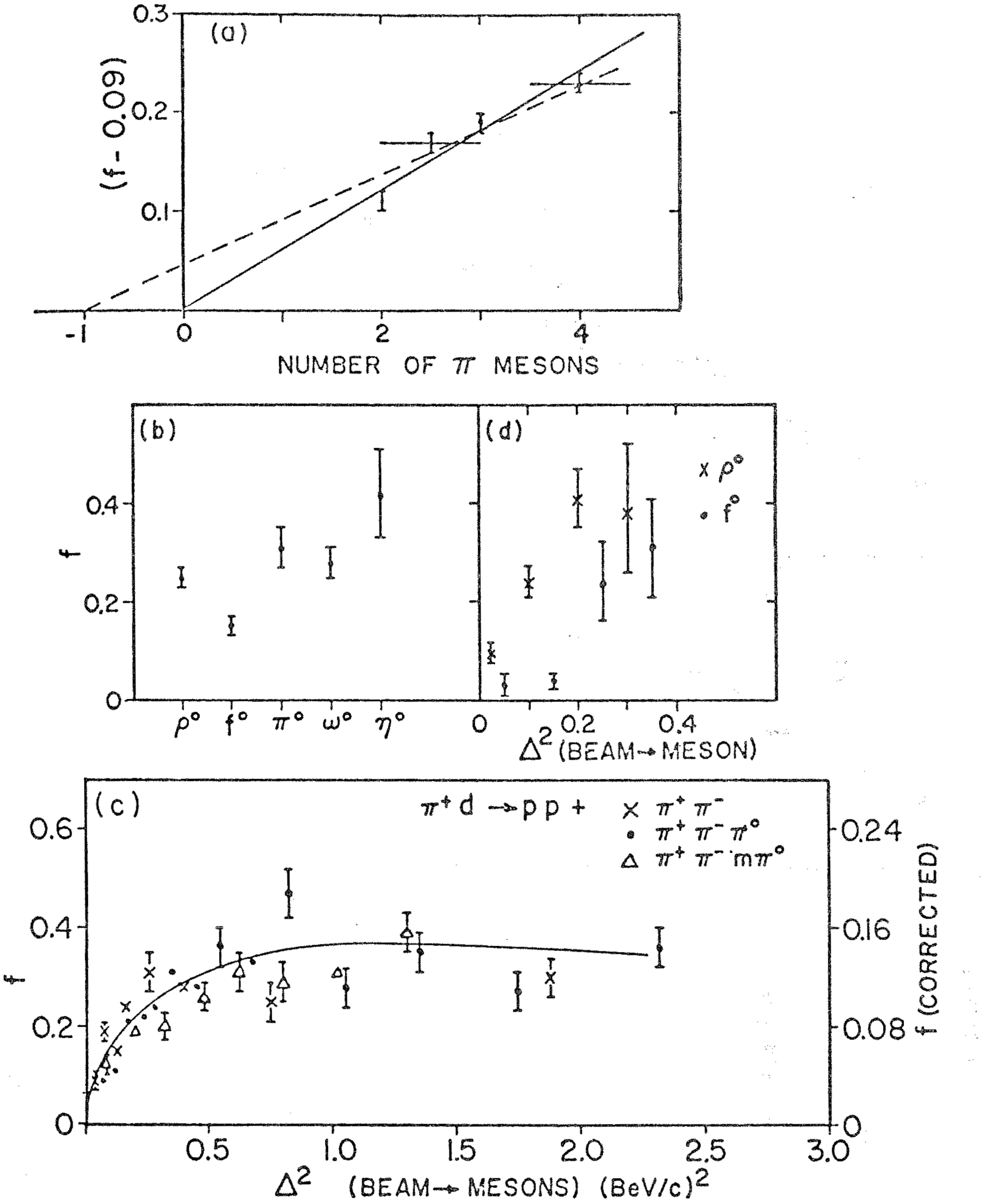

(a) The fraction of events with a spectator proton of momentum greater than 250 MeV/c, f, less the Hulthén prediction for $\pi^+\pi^-$, $m\pi^0$, $\pi^+\pi^-\pi^0$, and $\pi^+\pi^- m\pi^0$ final states. (b) f for production of ρ^0, f^0, π^0, ω^0, and η^0 particles only. (c) f as a function of Δ^2 (beam → mesons). (d) f as a function of Δ^2 (beam → meson) for ρ^0 and f^0 production only. The smooth curve and lines are drawn arbitrarily.

Figure 14: Study of high momentum tail of spectator momentum distribution for the reactions $\pi^+ d \rightarrow \pi^0 pp$, $m\pi^0 pp$, $\pi^+\pi^- pp$, $\pi^+\pi^-\pi^0 pp$ and $\pi^+\pi^- m\pi^0 pp$ at 3.65 GeV/c.

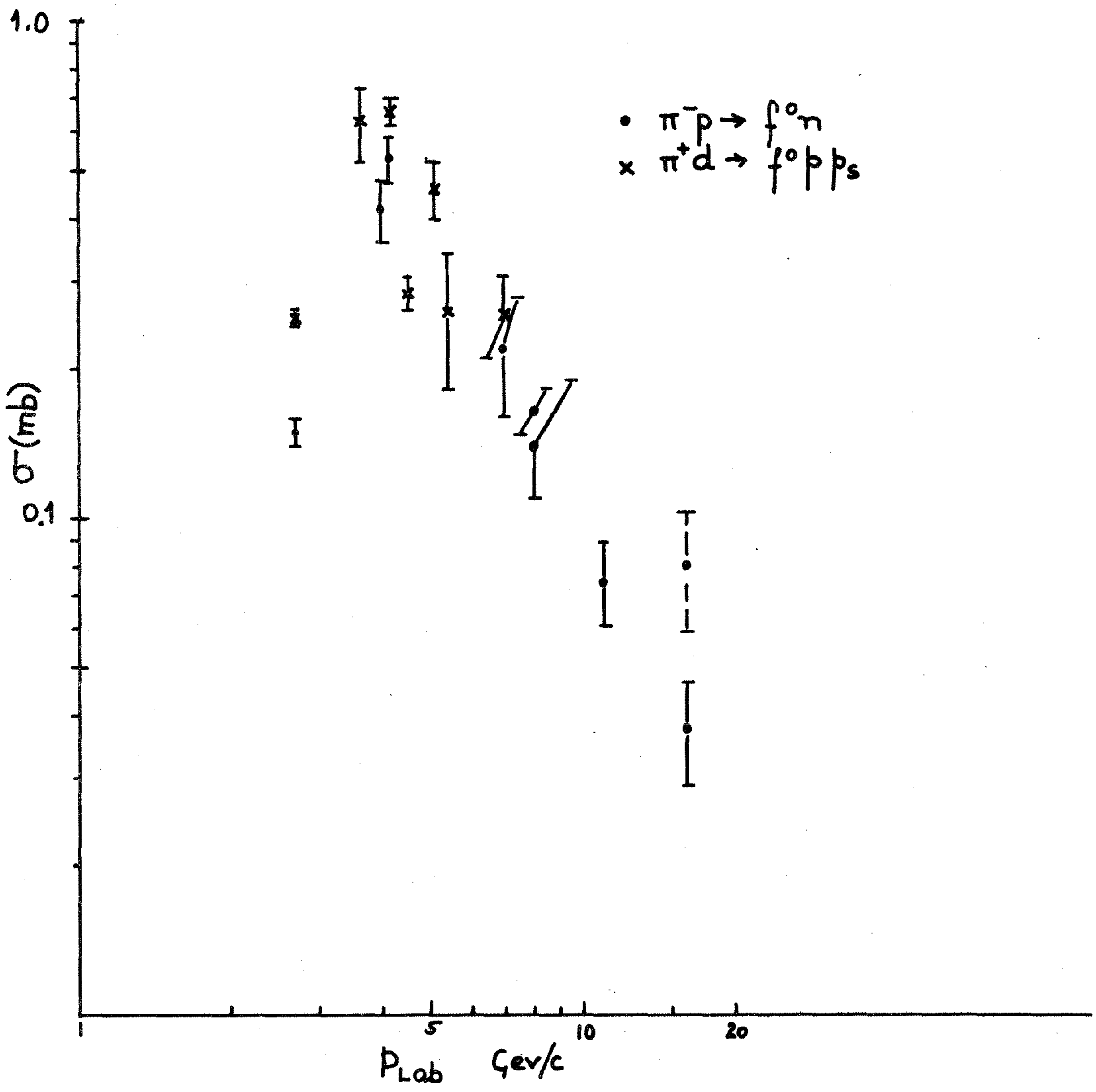

Figure 15: Channel cross sections for $\pi^+ n \to p f^0$ and $\pi^- p \to f^0 n$.

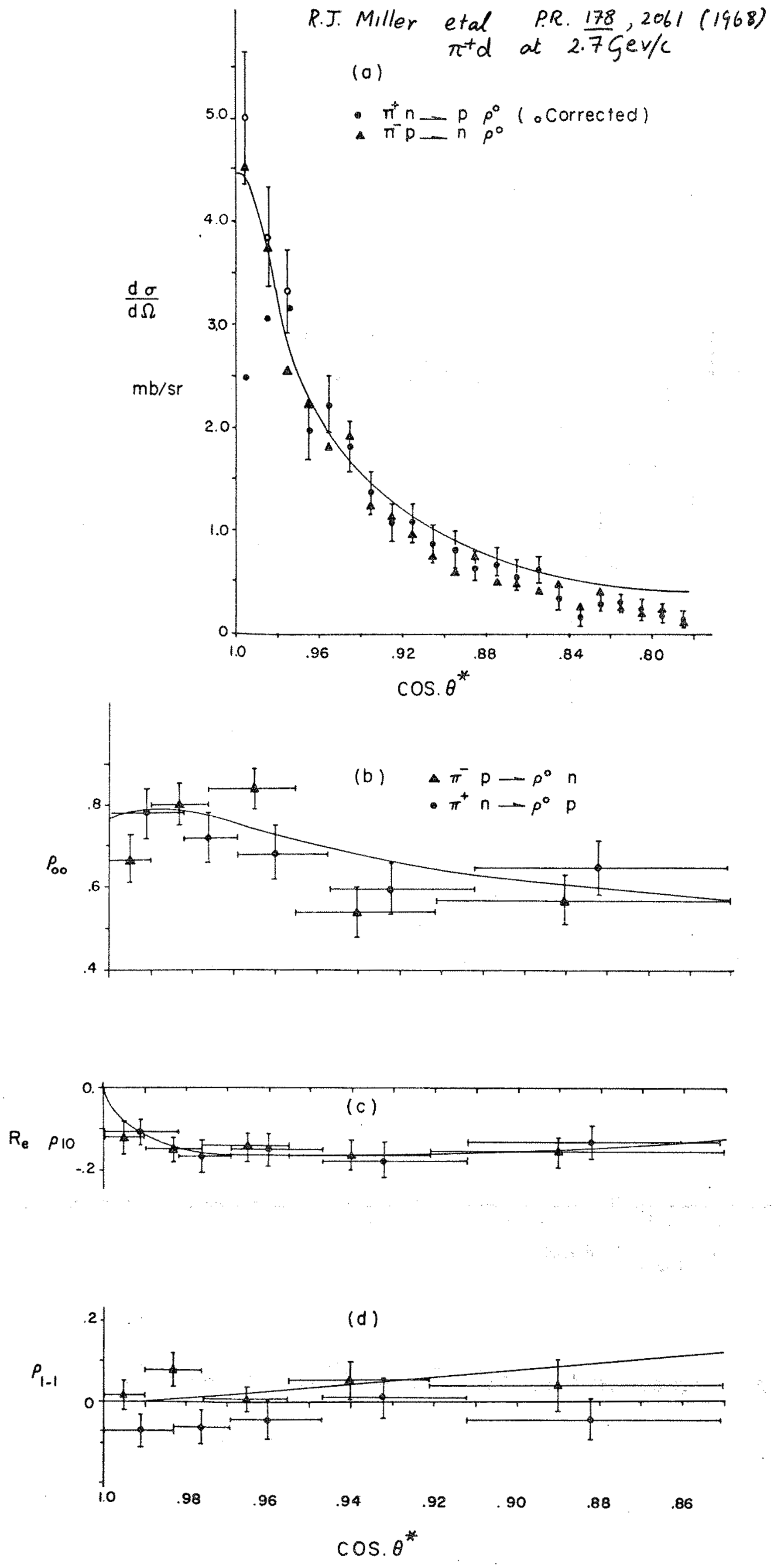
R.J. Miller etal P.R. 178, 2061 (1968)
π^+d at 2.7 Gev/c

Fig. 16: Comparison of production angular distribution and decay density matrices for $\pi^+n \rightarrow \rho^0 p$ and $\pi^-p \rightarrow \rho^0 n$.

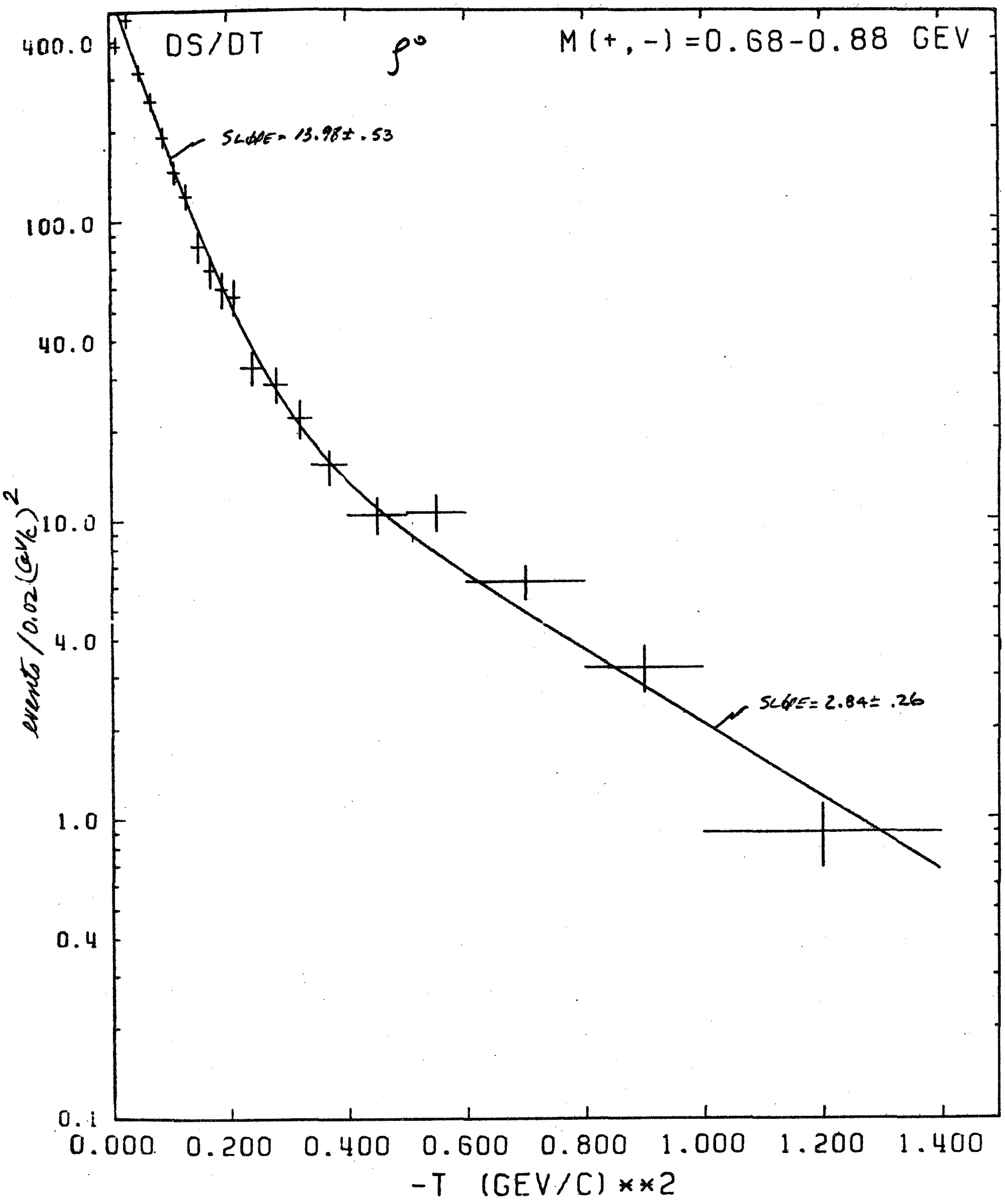

Figure 17: Four momentum transfer distribution for ρ^0 production in $\pi^- p \rightarrow \rho^0 n$ and $\pi^+ n \rightarrow \rho^0 p$ (both reactions combined) at 6.95 GeV/c.

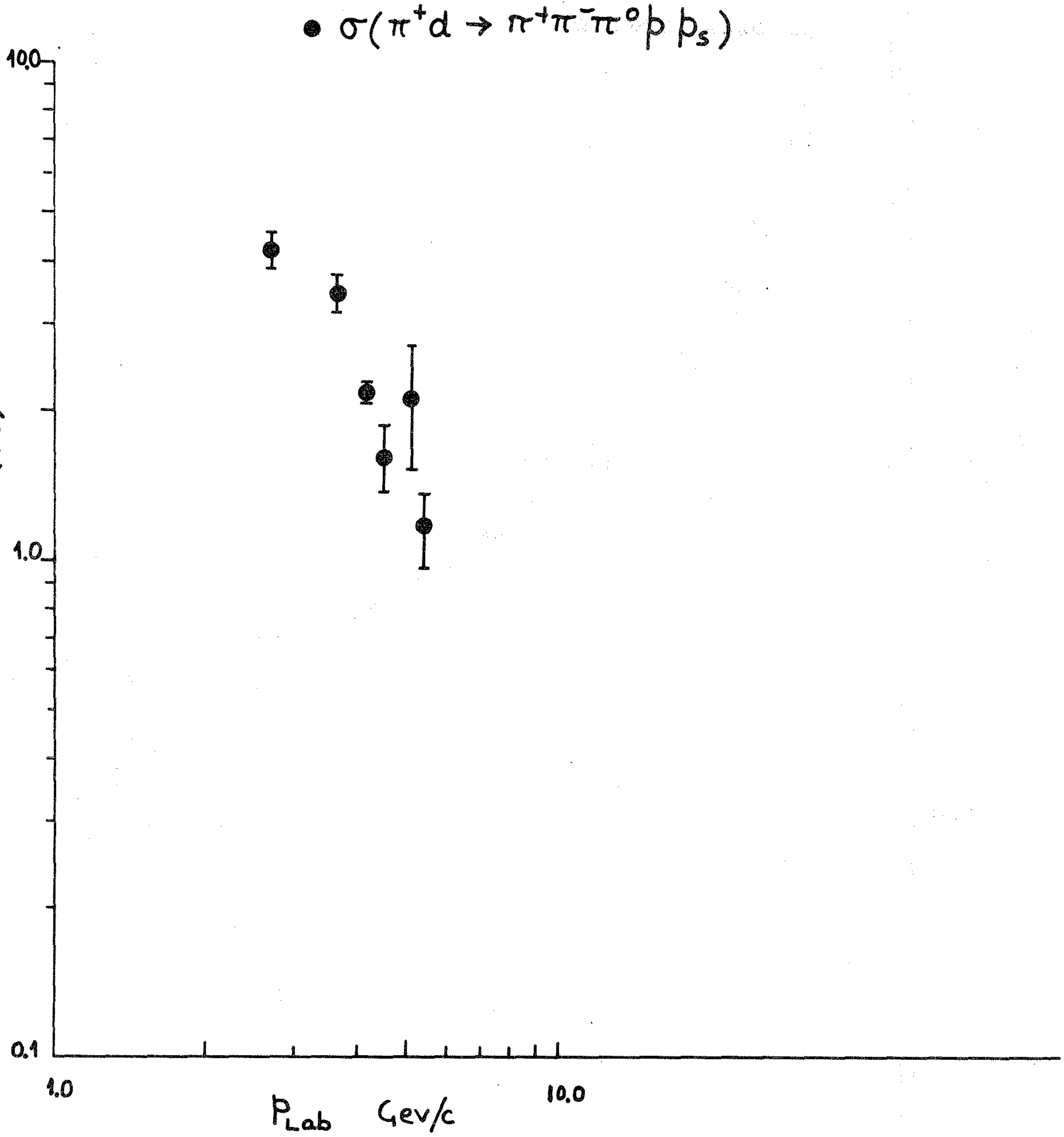

Figure 18: Channel cross section for $\pi^+ d \rightarrow \pi^+\pi^-\pi^0 p\ p_s$.

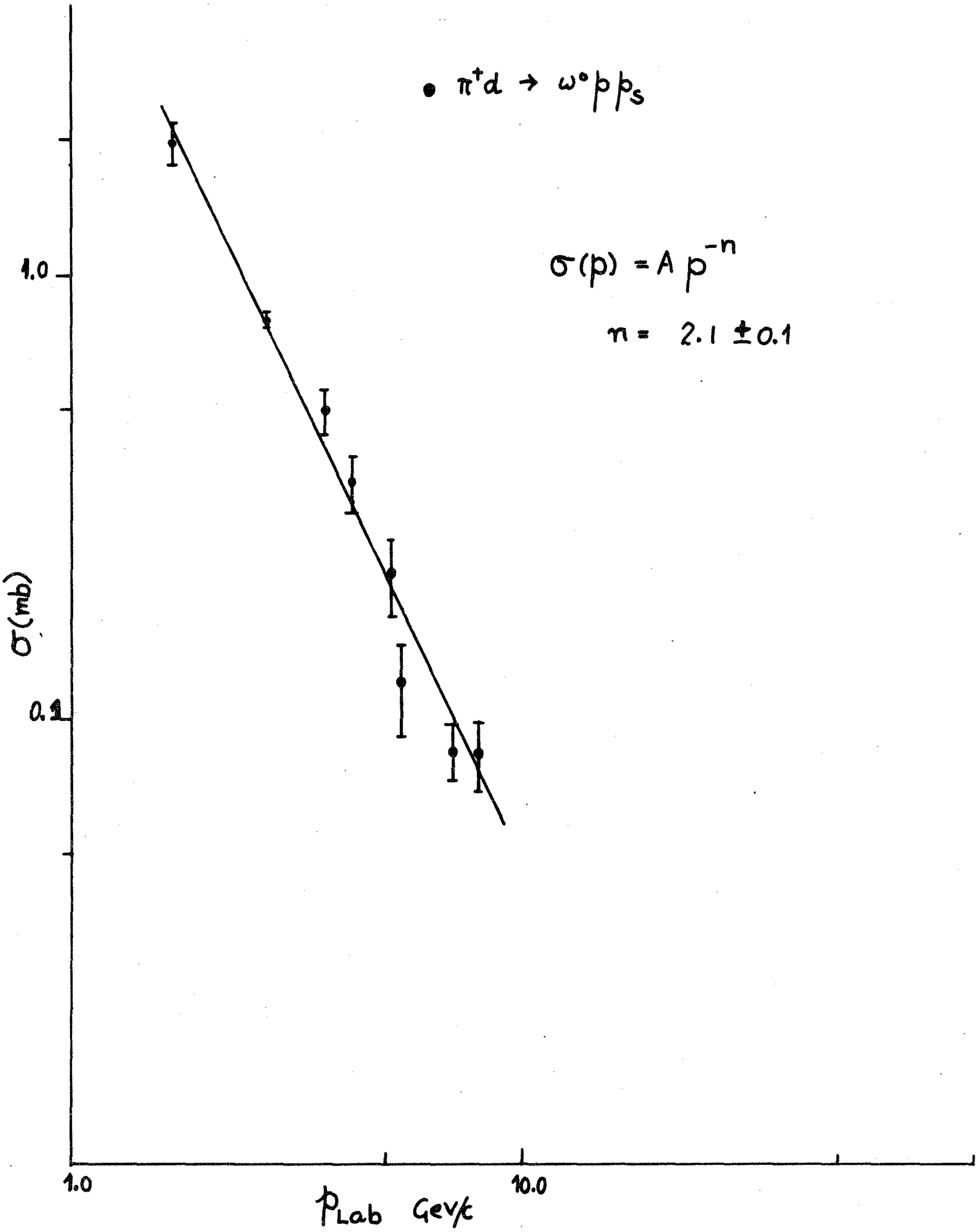

Figure 19: Channel cross section for $\pi^+d \rightarrow \omega^o p\, p_s$.

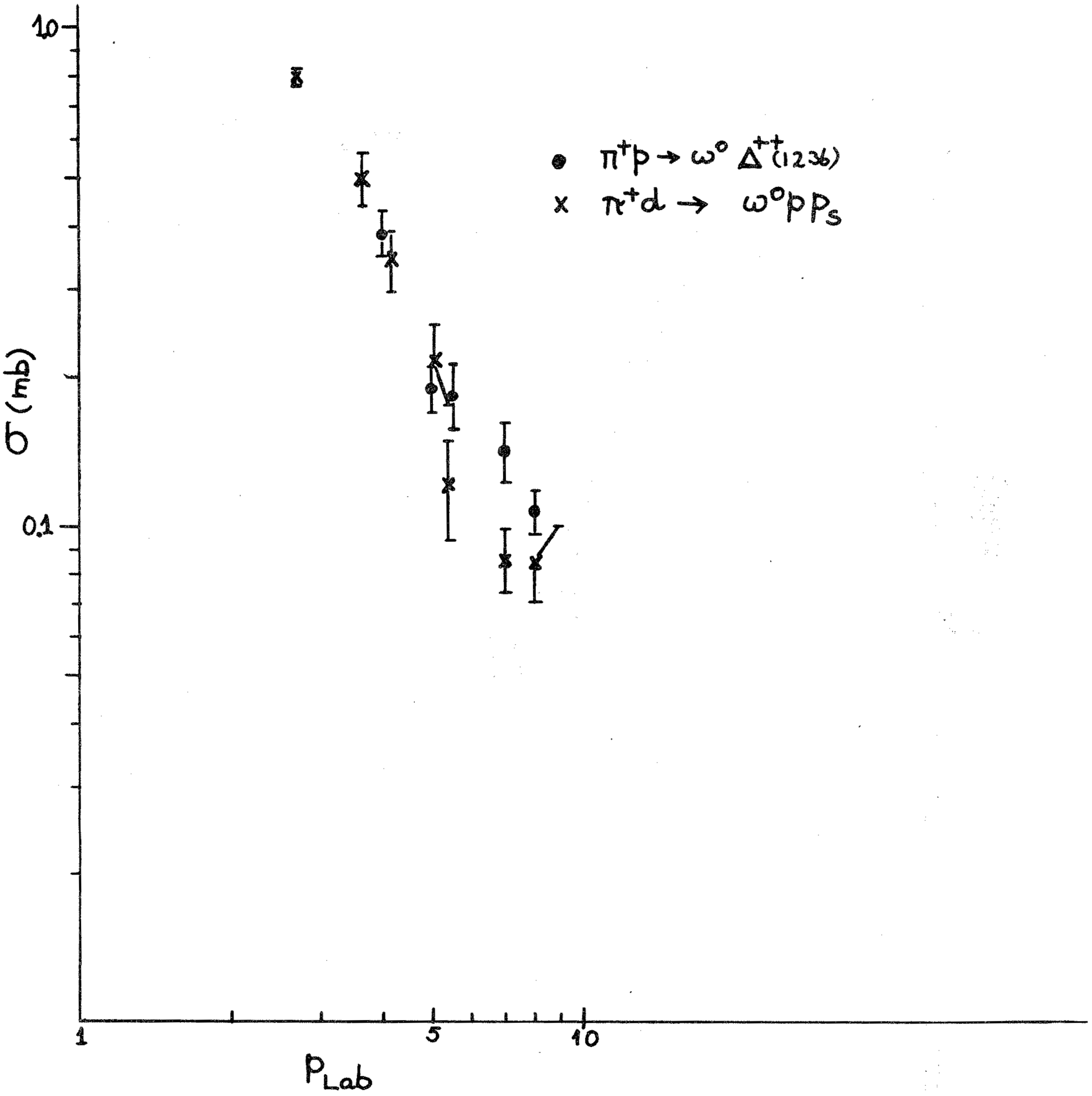

Figure 20: Comparison of channel cross sections for $\pi^+n \rightarrow \omega^0 p$ and $\pi^+p \rightarrow \omega^0\Delta^{++}$.

R. J. Miller et al.
P.R. 178, 2061 (1968)

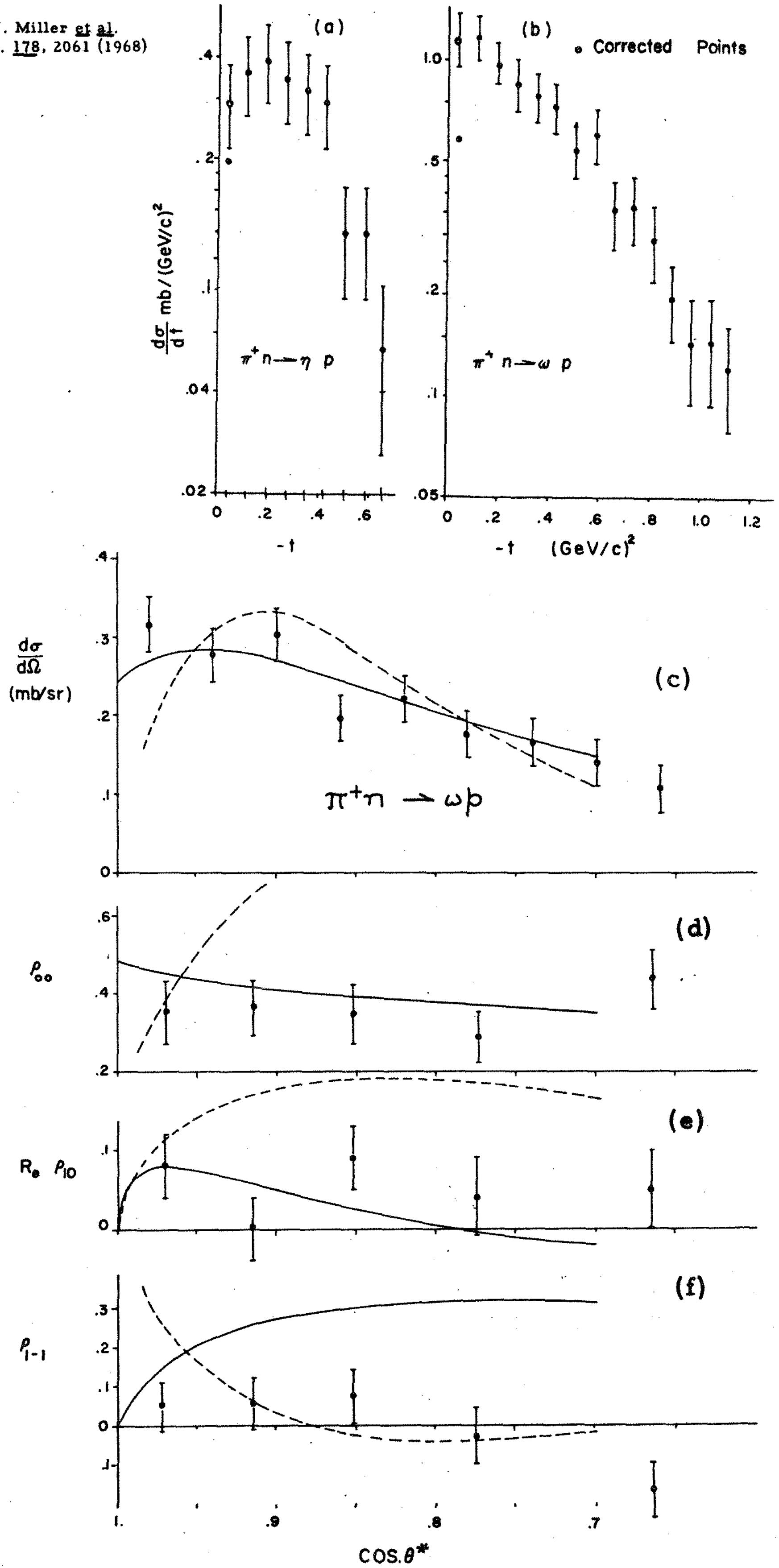

Figure 21: Four momentum transfer distribution and density matrices for $\pi^+ n \rightarrow \omega^0 p$ at 2.7 GeV/c, (b), (c) differential cross-section and (d), (e), (f) density matrix elements.

G. C. Benson et al.
Phys. Rev. Letters 22, 1074 (1969)
$\pi^+ d \rightarrow \pi^+\pi^-\pi^0 p p_s$
3.65 GeV/c

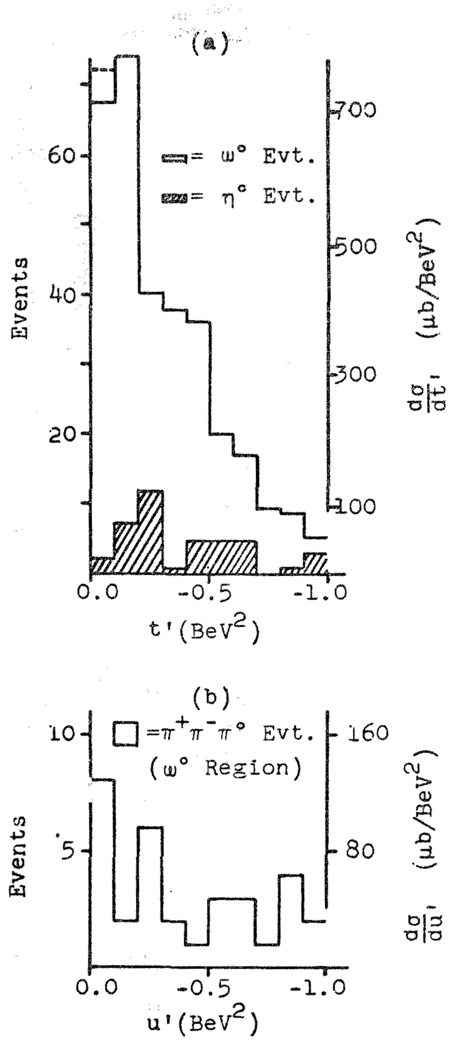

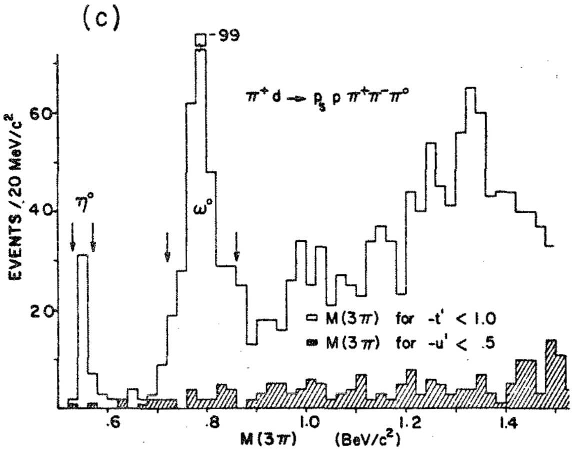

(c) Unshaded: invariant mass of $\pi^+\pi^-\pi^0$ for events with $-t' < 1.0$ BeV^2. Shaded: invariant mass of $\pi^+\pi^-\pi^0$ for events with $-u' < 0.5$ BeV^2. The regions of ω^0 and η^0 selection for Figs. (a) and (b) are indicated by the arrows. The definitions of t' and u' can be found in the ref.

(a) Unshaded: differential cross section for $\pi^+ d \rightarrow p_s p + (\omega^0 \rightarrow \pi^+\pi^-\pi^0)$. The dotted line in the first bin shows correction to approximate the production on a free neutron. Shaded: differential cross section for $\pi^+ d \rightarrow p_s p + (\eta^0 \rightarrow \pi^+\pi^-\pi^0$ or $\pi^+\pi^-\gamma)$. (b) Differential cross section for $\pi^+\pi^-\pi^0$ production near the backward direction and in the ω^0 mass region. See Fig. (c) (shaded). All cross sections have been corrected for undetected events with invisible spectator protons.

Figure 22: Forward (a) and backward (b) momentum transfer distributions for $\pi^+ n \rightarrow \omega^0 p$ at 3.65 GeV/c. (c) shows the corresponding $\pi^+\pi^-\pi^0$ mass distributions.

G. S. Abrams et al.
Phys. Rev. Letters 23, 673 (1969)
$\pi^+ d \rightarrow \pi^+\pi^-\pi^0 p p_s$
at 4.19 GeV/c

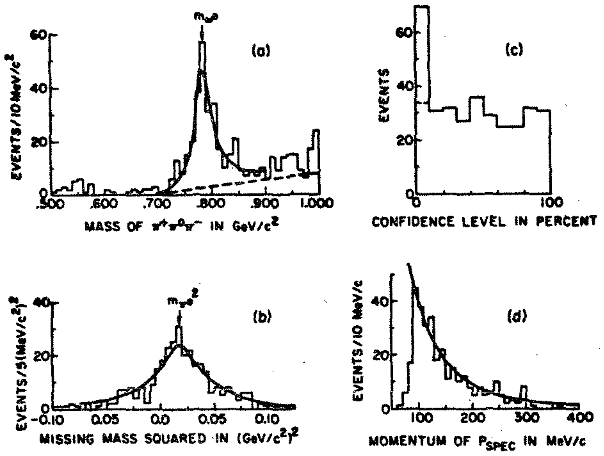

(a) Invariant-mass distribution of $\pi^+\pi^-\pi^0$ in the region of the ω^0. The curve indicates the best least-squares fit to find the mass and width of the ω^0. The dashed line shows a linear estimate of the background. (b) Missing-mass—squared distribution of π^0. Curve represents resolution function normalized to the number of events. (c) Confidence-level distribution. Dashed line indicates the number of events in the first bin which have confidence level >2%. (d) Spectator-momentum distribution. Curve represents Hulthén wave function normalized to the number of events between 120 and 200 MeV/c.

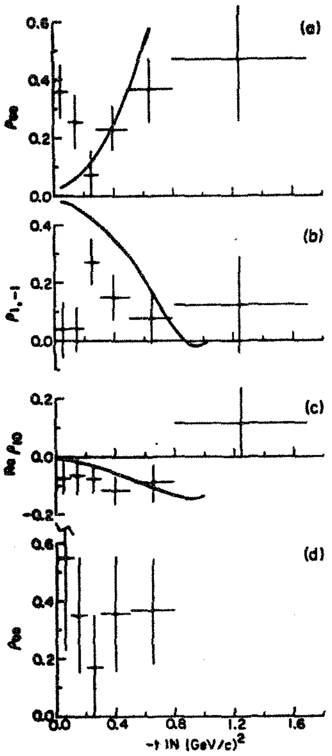

Density matrix elements (a) ρ_{00}, (b) $\rho_{1,-1}$, (c) Re ρ_{10}, and (d) ρ_{00} after background subtraction described in the ref. The solid curves are the prediction of the Regge model.

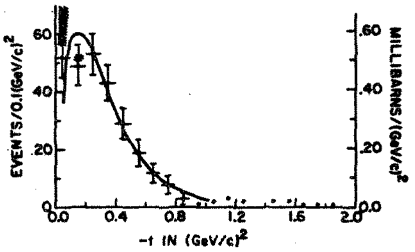

Differential cross section for $\pi^+ n \rightarrow \omega^0 p$. The curve represents the predictions of the Regge model and parameters in Ref. 11. The Pauli correction is indicated by the cross hatching in the first two bins. The limits correspond to the values 0.1 and 10.0 for the ratio of spin-flip to spin-nonflip amplitudes.

Figure 23: Four momentum transfer distribution, density matrix elements and mass distributions for $\pi^+ n \rightarrow \omega^0 p$ at 4.19 GeV/c.

π^+d 5.1 GeV/c

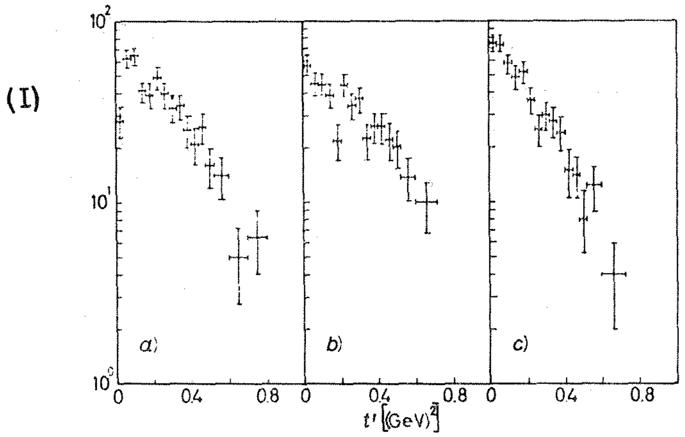

– dN/dt' distributions from the reactions: *a*) $\pi^+n \to p\omega$; *b*) $\pi^+n \to pA_2^0$; *c*) $\pi^+p \to pA_2^+$

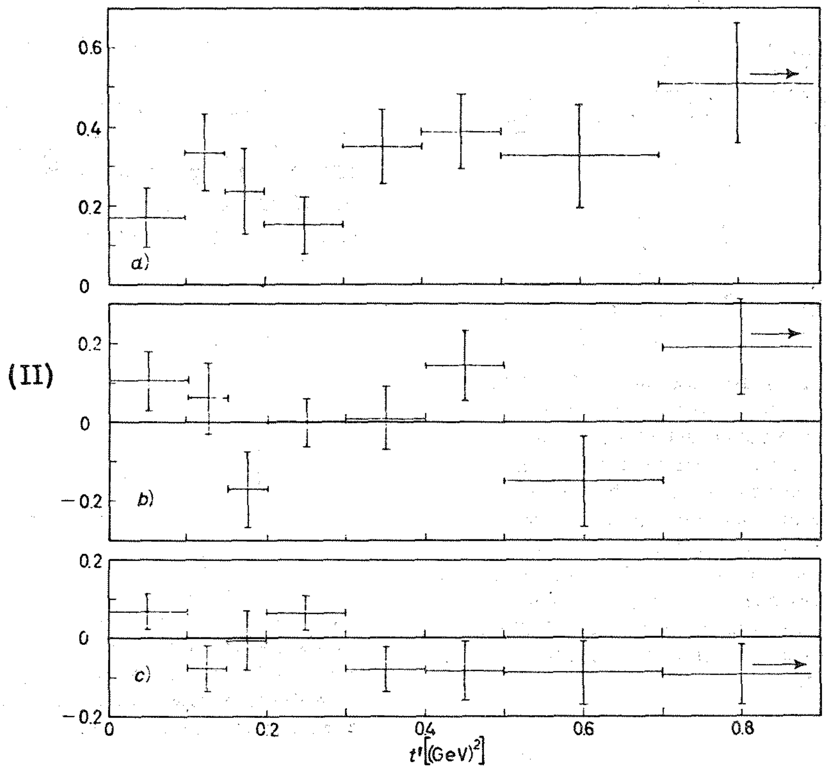

– ϱ_{ik} *vs.* t' for the reaction $\pi^+n \to p\omega$, *a*) $\varrho_{0,0}$; *b*) $\varrho_{1,-1}$; *c*) Re $\varrho_{1,0}$.

Figure 24: (I) (a) dσ/dt and (II) density matrix elements (a) ρ_{00}; (b) $\rho_{1,-1}$; (c) ρ_{10} for $\pi^+n \to \omega^0p$ at 5.1 GeV/c.

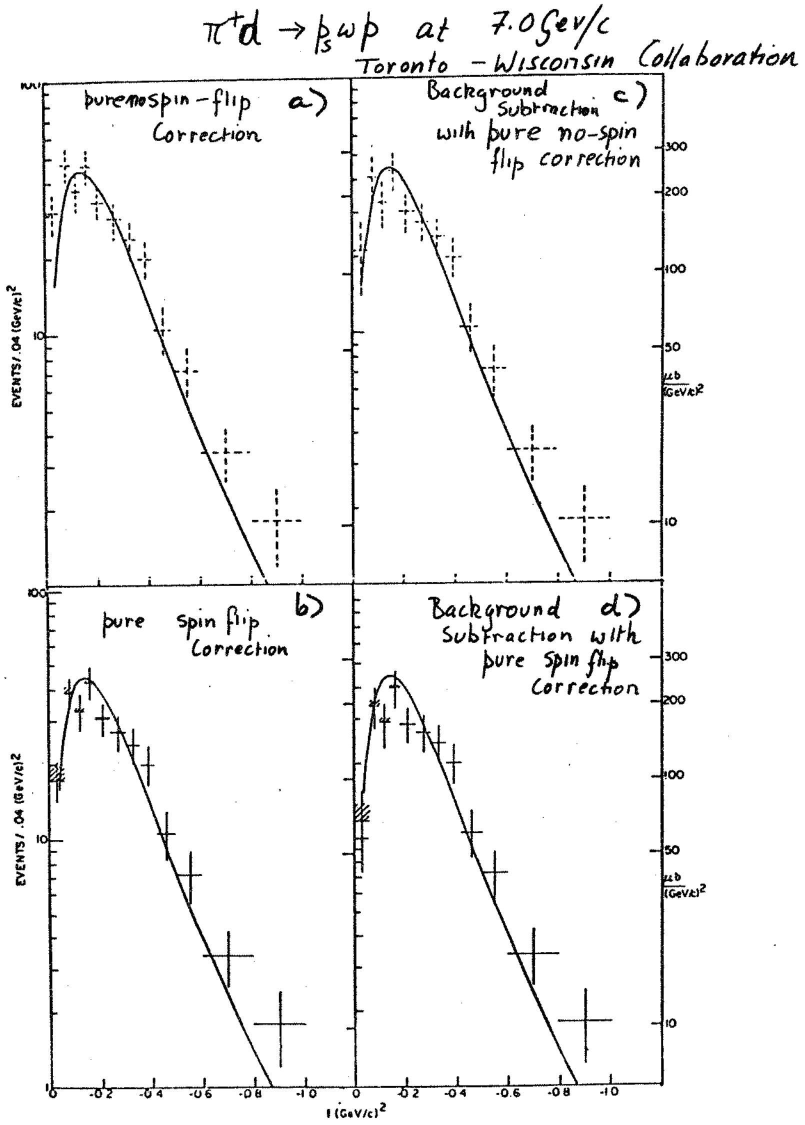

Fig. 25: Four momentum transfer distribution for $\pi^+n \to \omega^0 p$ at 7.0 GeV/c. In (b) and (d) the shaded region indicates the magnitude of the pure spin flip correction. The fitted curves come from a ρ, ρ' and B exchange Regge pole model.

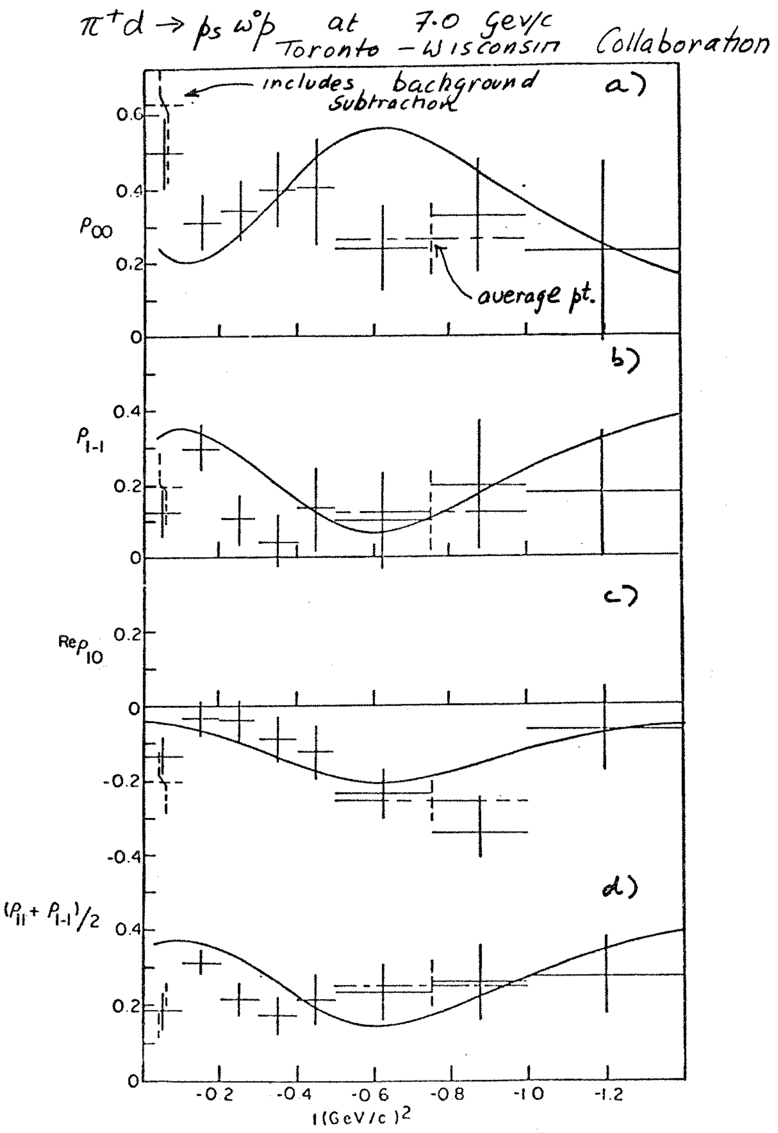

Fig. 26: The density matrices for ω^0 at 7.0 GeV/c. The fitted curves come from a ρ, ρ' and B exchange Regge pole model.

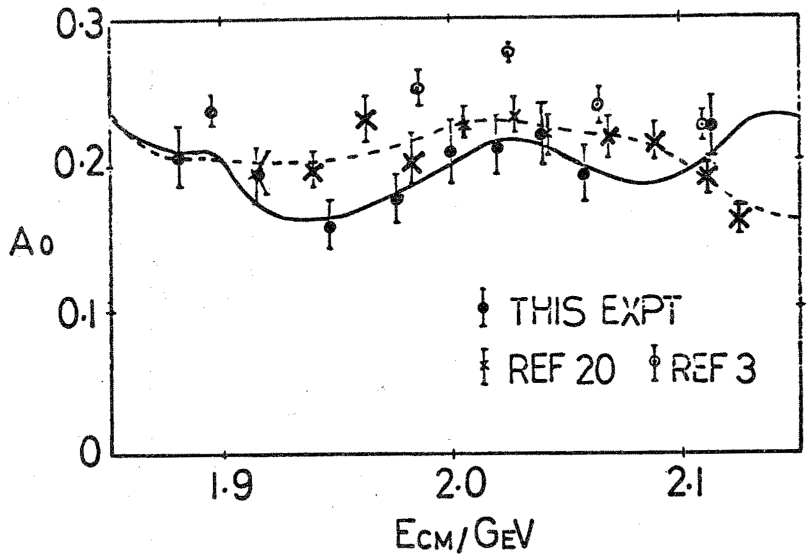

Fig. 27: Half of the total cross section for $K^-n \to \Lambda\pi^-$ (dot); total cross section for $K^-p \to \Lambda\pi^0$, (cross) Rutherford Lab-Saclay, and LRL (circle).

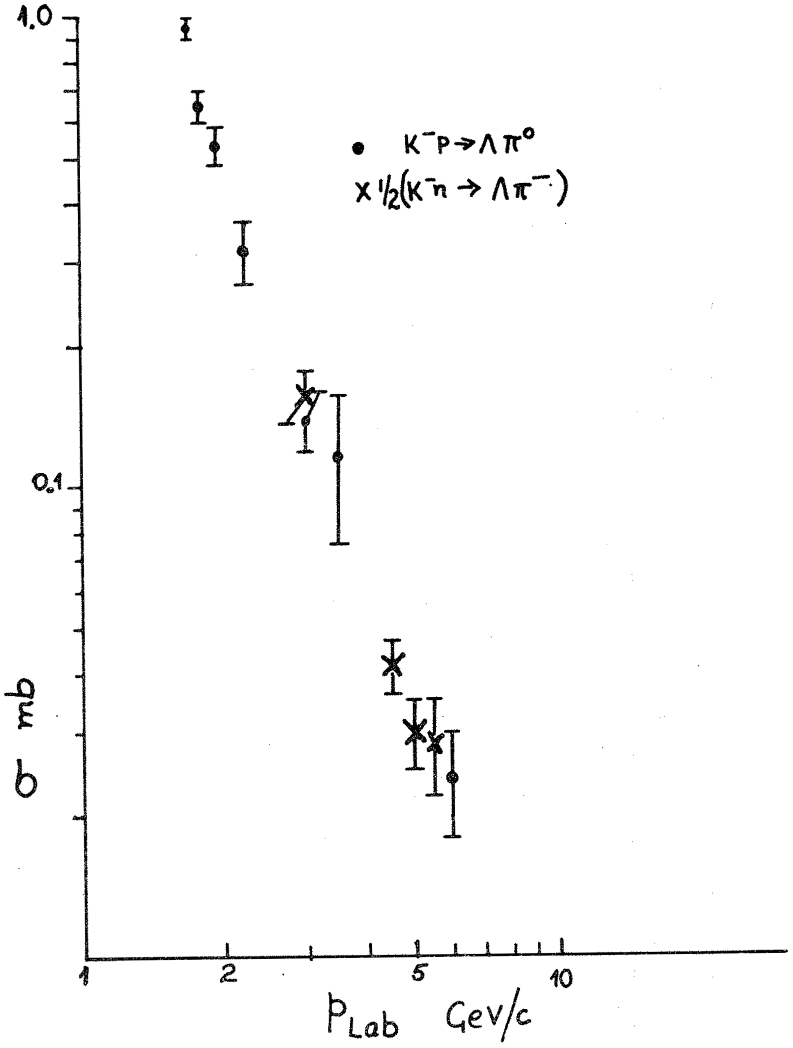

Fig. 28: Comparison of channel cross sections for $K^-n \to \Lambda\pi^-$ and $K^-p \to \Lambda\pi^0$.

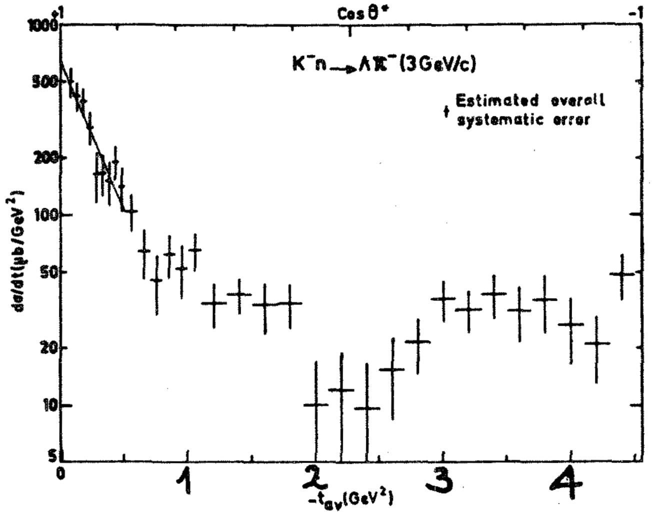

Distribution of $d\sigma/dt$ for events of reaction (1), after application of corrections for unseen events. The fitted curve represents $d\sigma/dt = Ae^{at}$ where $a = 3.6\,\mathrm{GeV}^{-2}$ and $A = 674\ \mu\mathrm{b/GeV}^2$. The distribution shown corresponds to $N(1) = N_S - N_G = 1100$ events.

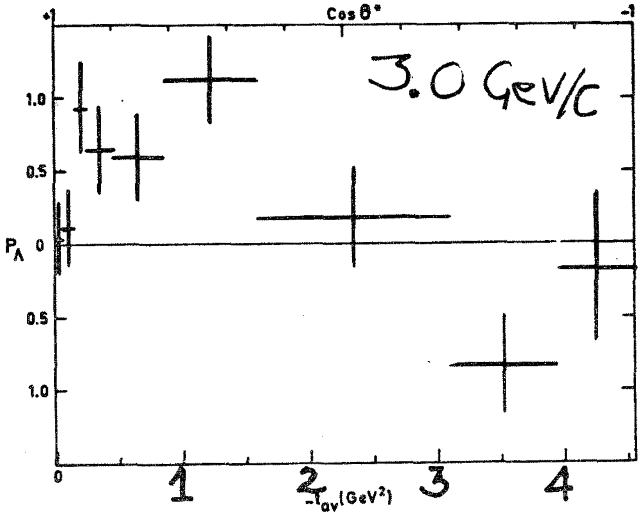

Distribution of Λ polarization $P_\Lambda(t)$, for events of reaction (1). Each point plotted corresponds to approximately 120 events.

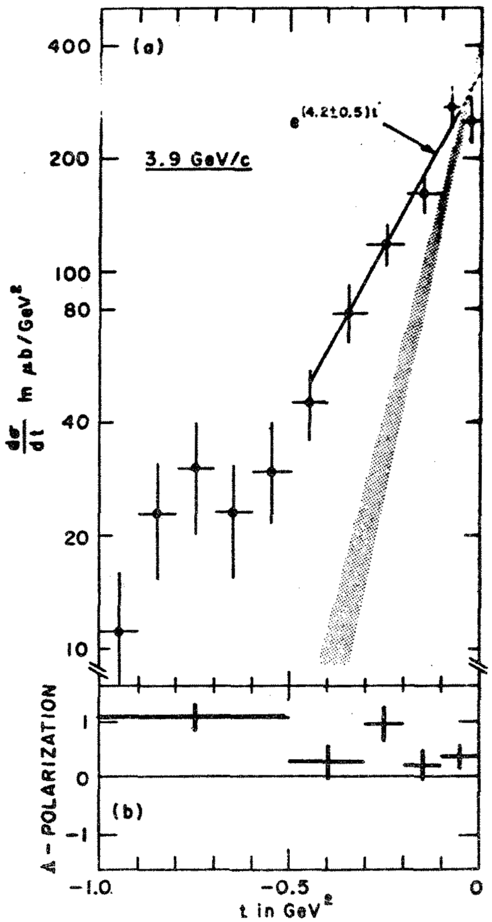

(a) Differential cross section in the forward region. Solid line is an exponential fit to the data from $0.05 < |t| < 0.45\ \mathrm{GeV}^2$. The shaded area, presented for the purpose of comparison, shows the slope and its error for the differential cross section of the line-reversed reaction, $\pi^- p \to \Lambda K^0$, at ~4 GeV/c (Ref. 8). See text for details. (b) Λ polarization in the forward region.

Figure 29: The four momentum transfer distribution and Λ^0 polarization for $K^- n \to \Lambda\pi^-$ at 3.0 and 3.9 GeV/c.

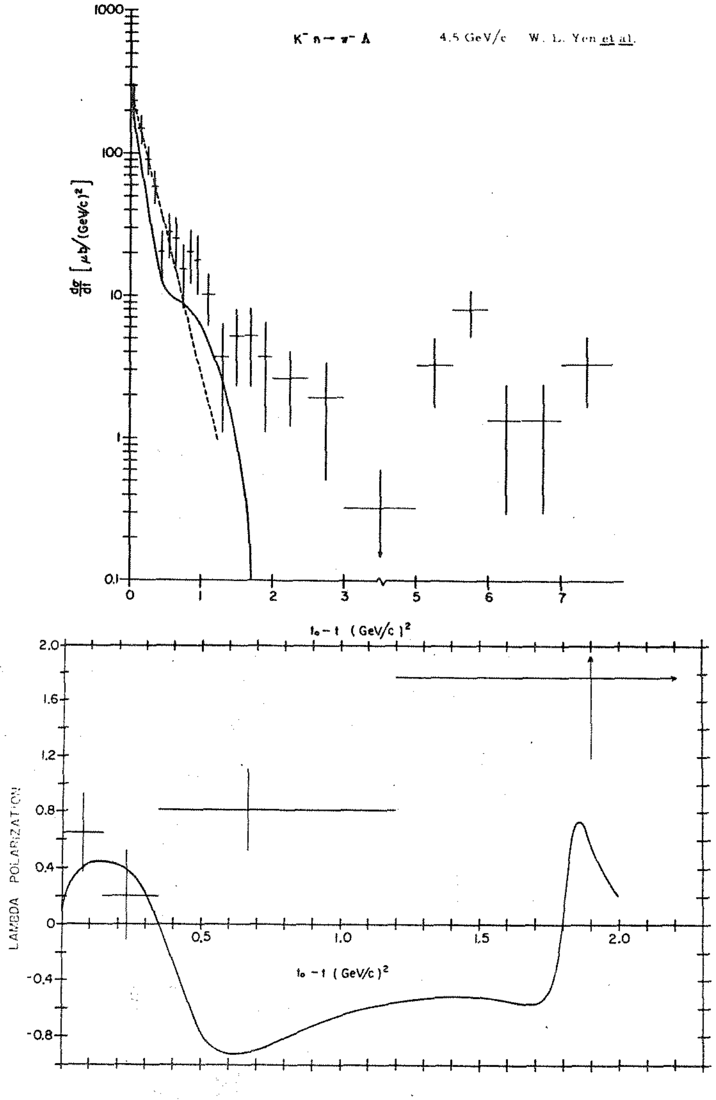

Figure 30: The four momentum transfer distribution and Λ^0 polarization for $K^- n \to \Lambda\pi^-$ at 4.5 GeV/c.

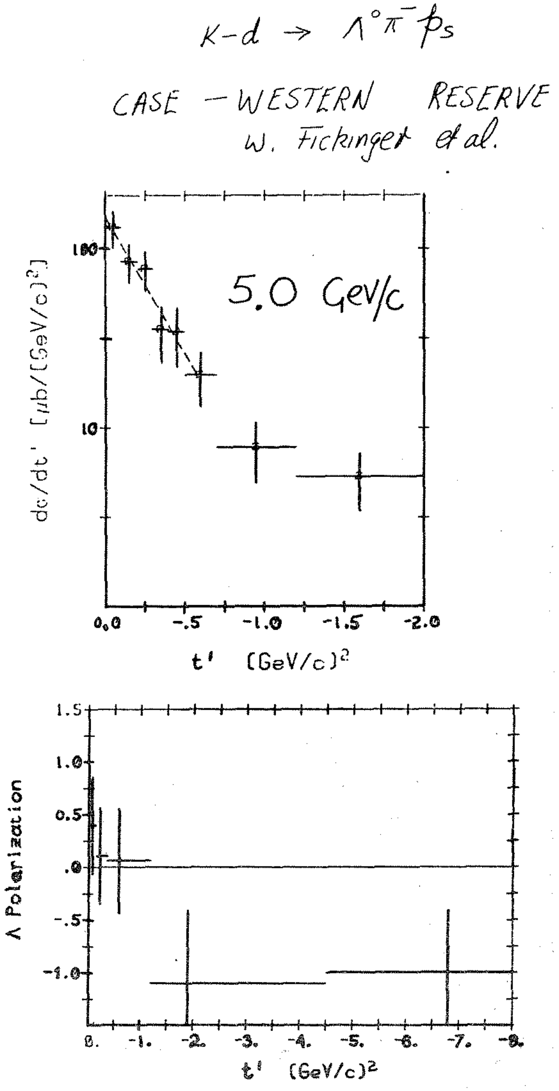
$K\text{-}d \to \Lambda^0 \pi^- p_s$

CASE – WESTERN RESERVE
W. Fickinger et al.

Figure 31: The four momentum transfer distribution and Λ^0 polarization for $K^- n \to \Lambda\pi^-$ at 5.0 GeV/c.

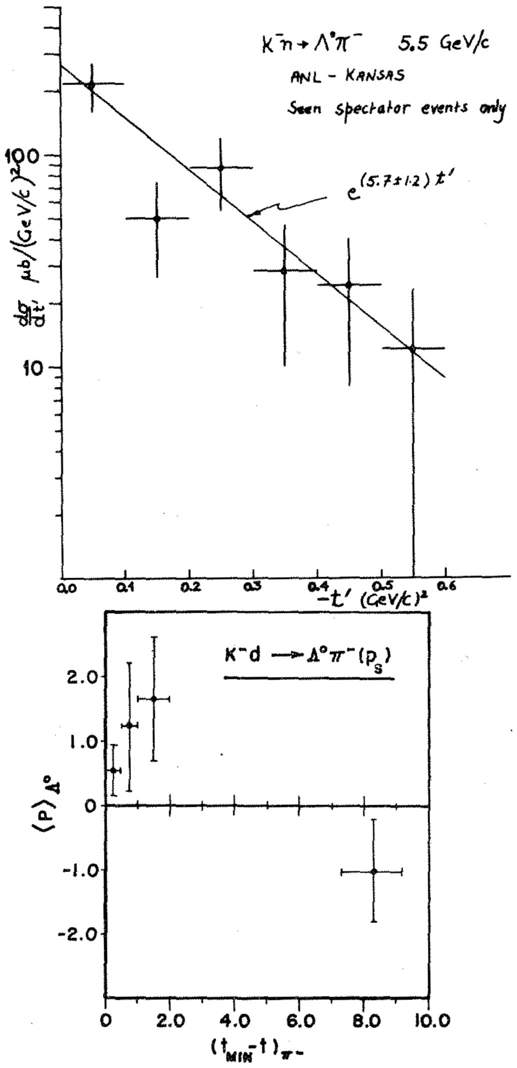

Fig. 32: The four momentum transfer distribution and Λ^0 polarization for $K^-d \to \Lambda\pi^- p_s$ at 5.5 GeV/c. The differential cross section is based only on events where the spectator track is visible but the polarization is based on all events.

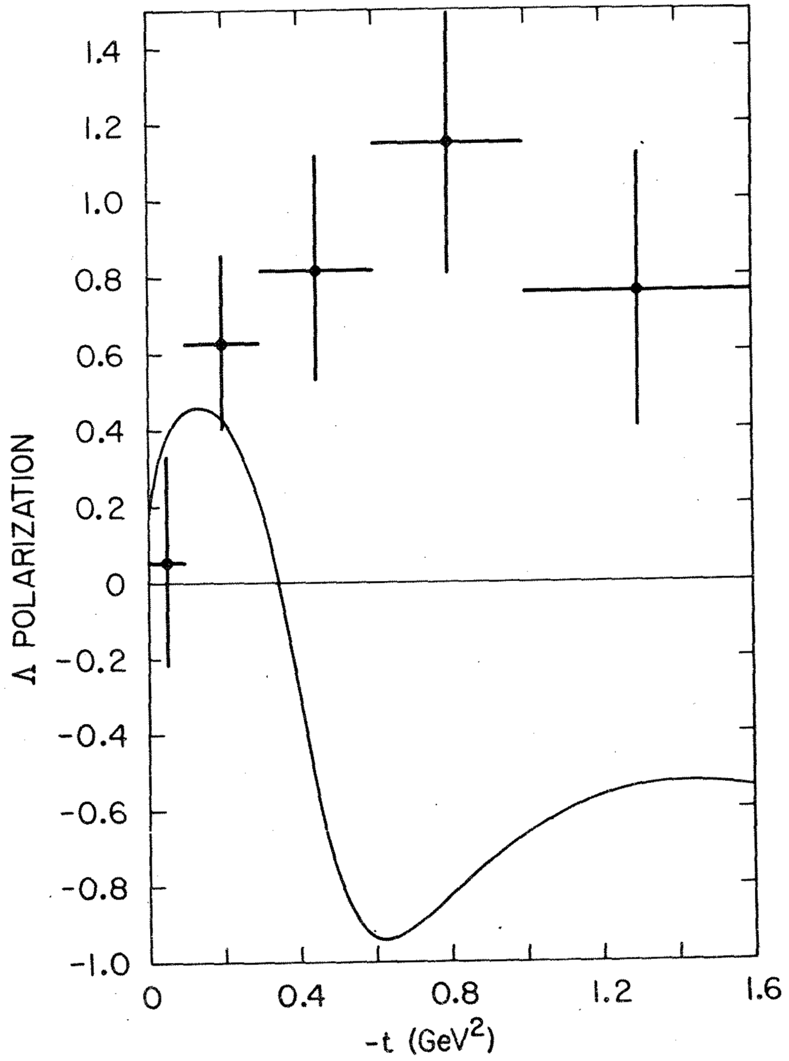

Fig. 33: The Λ^0 polarization for $\bar{K}^0 p \to \Lambda\pi^+$ over the lab. momentum range 1 - 8 GeV/c.

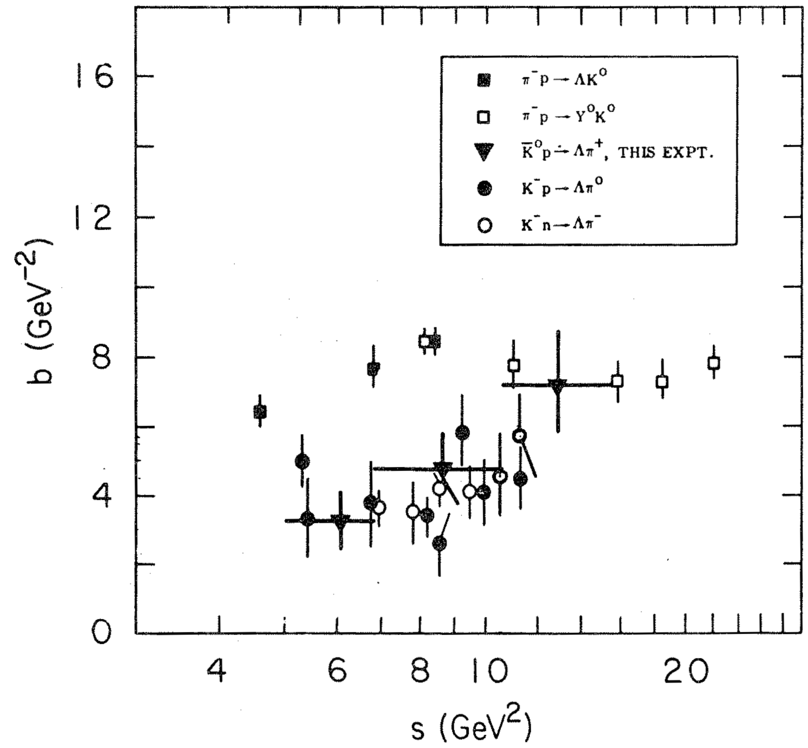

Fig. 34: Comparison of the slope parameter b for the $\overline{KN} \Rightarrow \Lambda\pi$ and $\pi^-_t p \Rightarrow \Lambda K^0$ reactions where $d\sigma/dt = Ae^{bt}$.

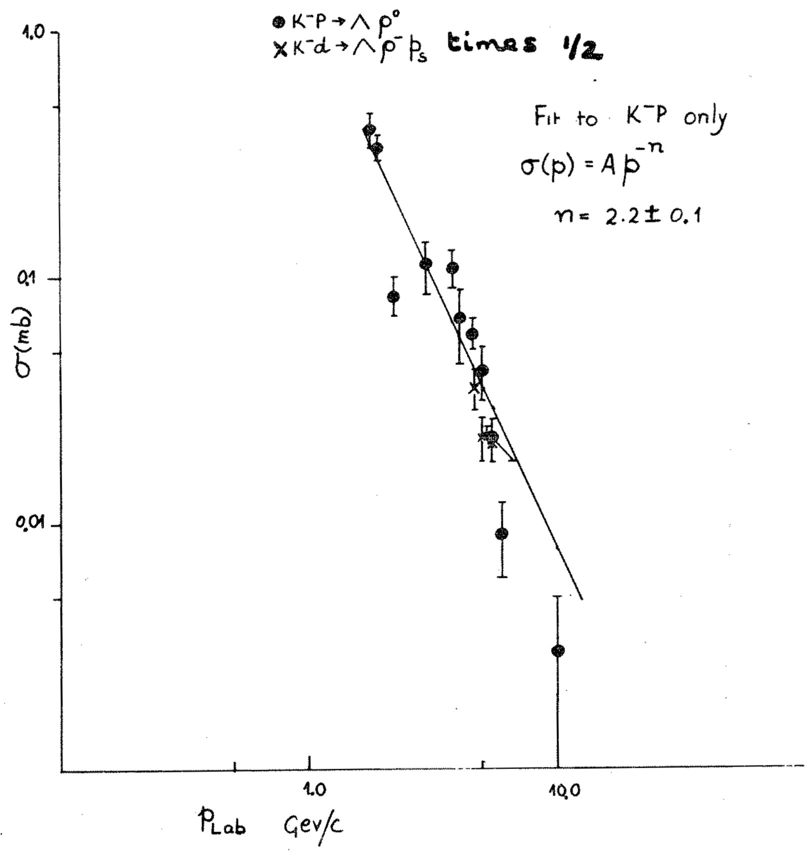

Fig. 35: Comparison of channel cross sections for $K^- n \Rightarrow \Lambda\rho^-$ and $K^- p \Rightarrow \Lambda\rho^0$.

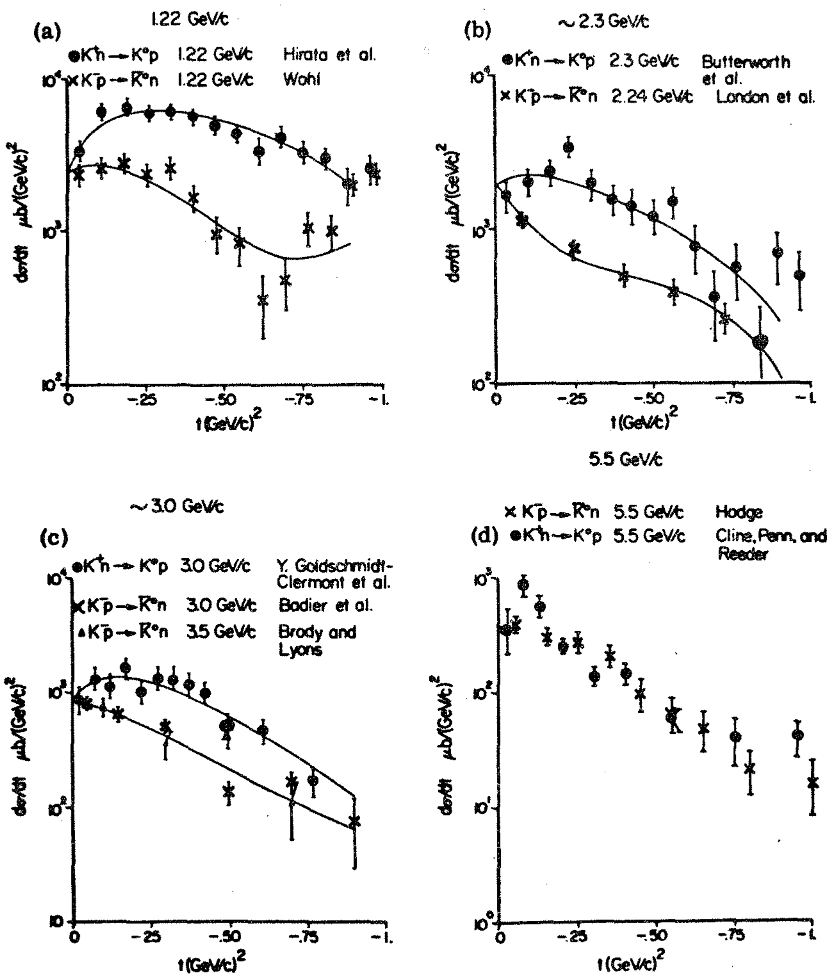

Fits to $K^{\pm}N$ charge-exchange data with parametrization of Ref. 9 and data from Refs. 7 and 8.

Figure 36: Comparison of differential cross sections for the charge exchange reactions $K^-p \to \bar{K}^0 n$ and $K^+n \to K^0 p$. See Fig. 37 for a similar comparison of data at 12 GeV/c.

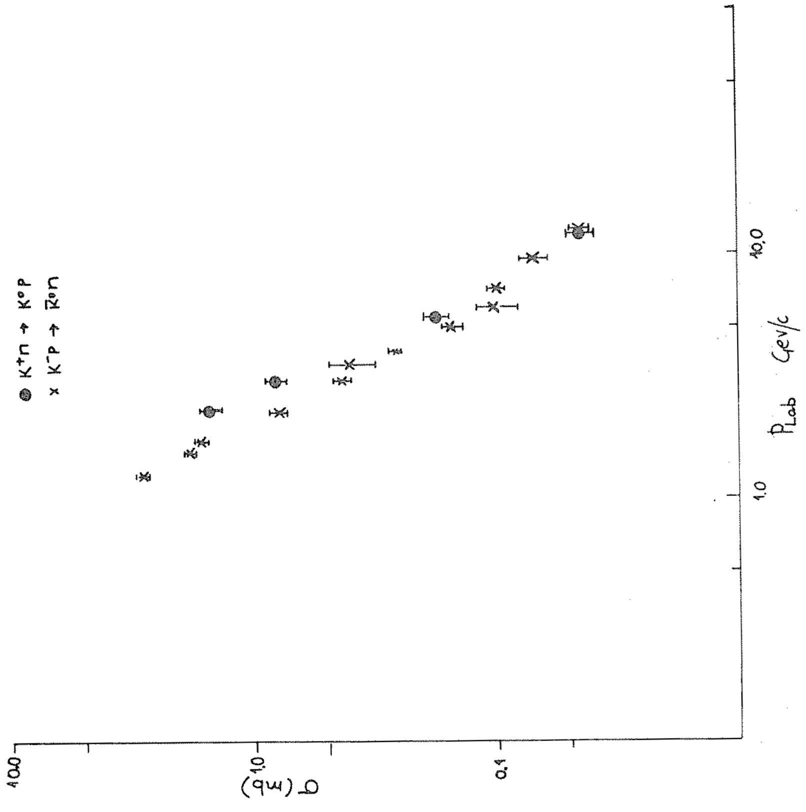

Fig. 38: Comparison of channel cross sections for $K^-p \rightarrow \bar{K}^0n$ and $K^+n \rightarrow K^0p$.

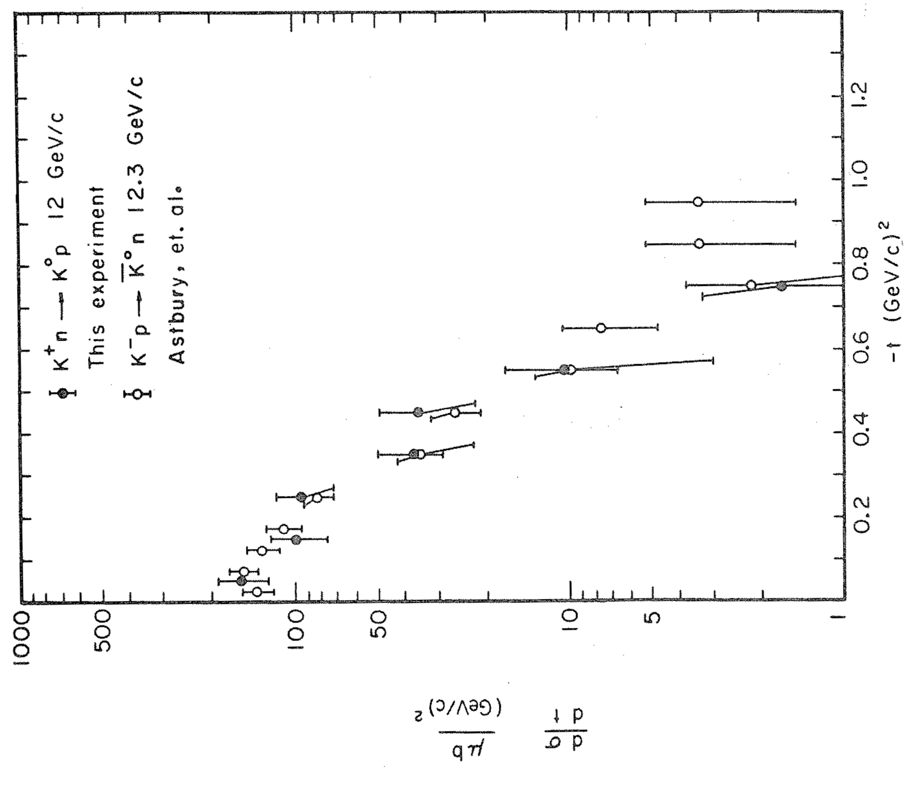

Fig. 37: Comparison of differential cross sections for $K^-p \rightarrow \bar{K}^0n$ and $K^+n \rightarrow K^0p$ at 12 GeV/c.

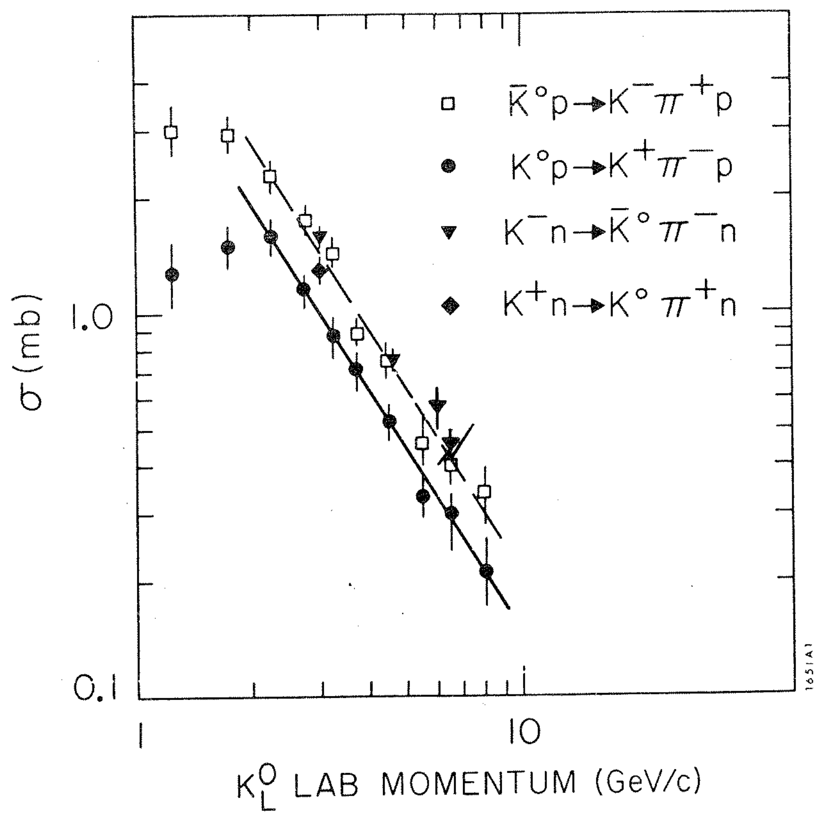

Fig. 39: Comparison of channel cross sections for $\bar{K}^0 p \to K^- \pi^+ p$ and $K^- n \to \bar{K}^0 \pi^- n$, also for $K^0 p \to K^+ \pi^- p$ and $K^+ n \to K^0 \pi^+ n$.

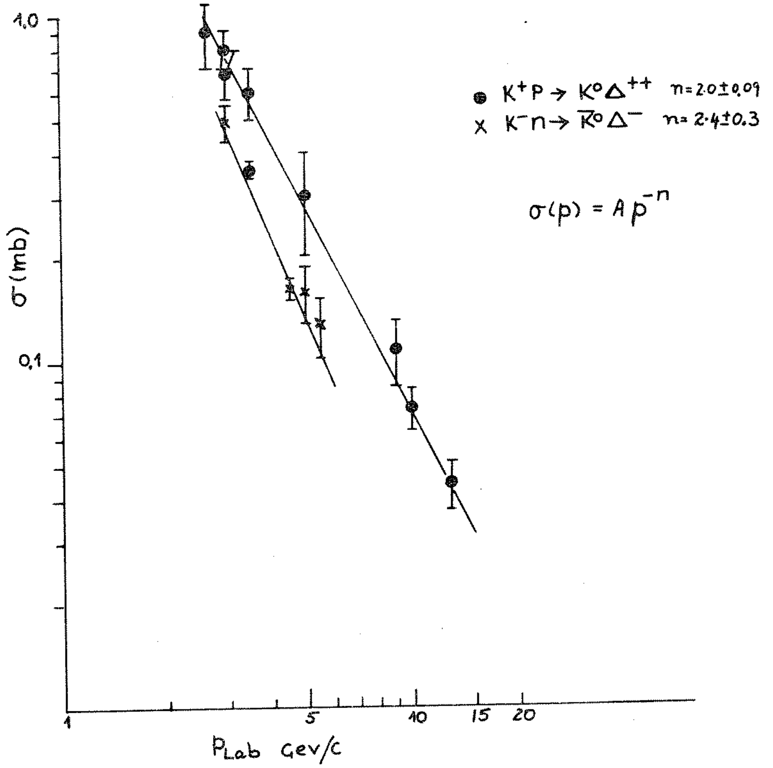

Fig. 40: Comparison of channel cross sections for $K^+ p \to K^0 \Delta^{++}$ and $K^- n \to \bar{K}^0 \Delta^-$.

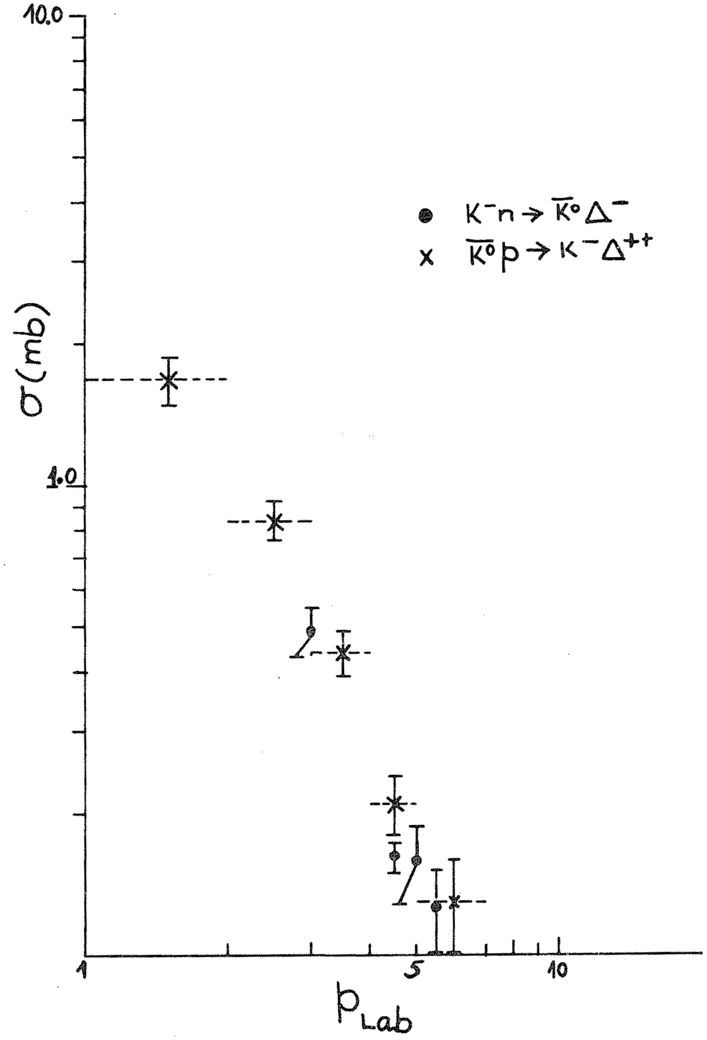

Fig. 41: Comparison of channel cross sections for $K^-n \to \overline{K}^0\Delta^-$ and $\overline{K}^0p \to K^-\Delta^{++}$.

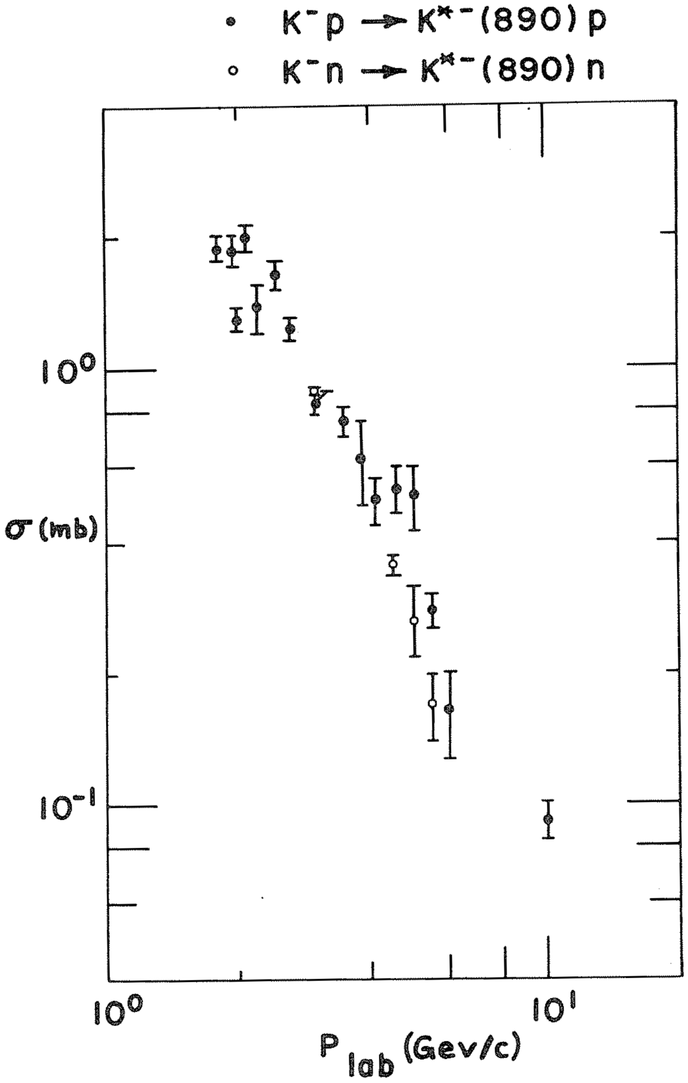

Fig. 42: Comparison of channel cross sections for $K^-p \to \overline{K}^{*}(890)p$ and $K^-n \to \overline{K}^{*}(890)n$.

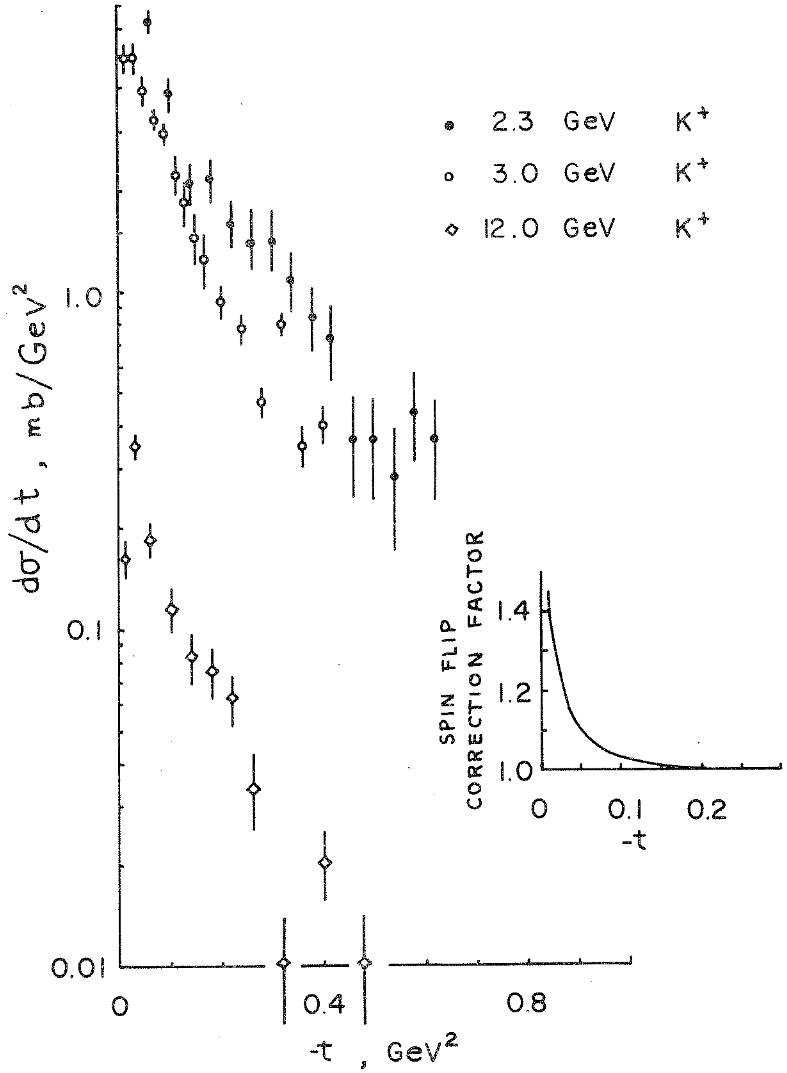

Fig. 43: The four momentum transfer distribution for $K^+n \rightarrow K^*(890)p$. The exclusion principle correction has been made in each case.

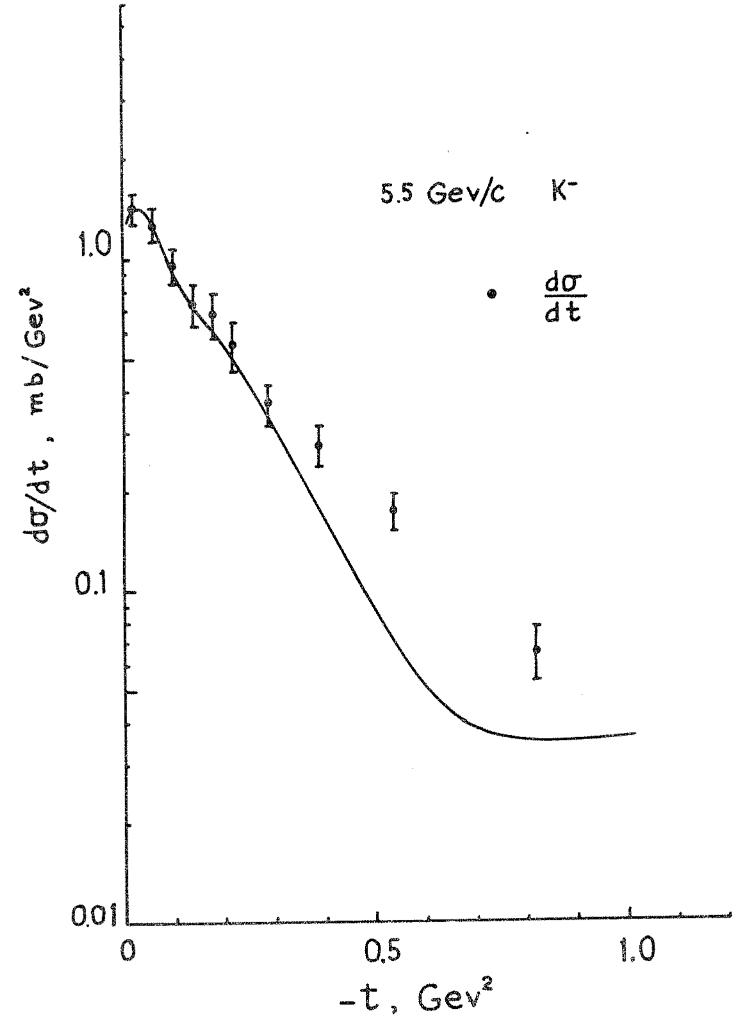

Figure 44: The differential cross section for $K^-p \rightarrow \bar{K}^*(890)n$ at 5.5 GeV/c. The fitted curve is from the SCRAM model of ref. 54.

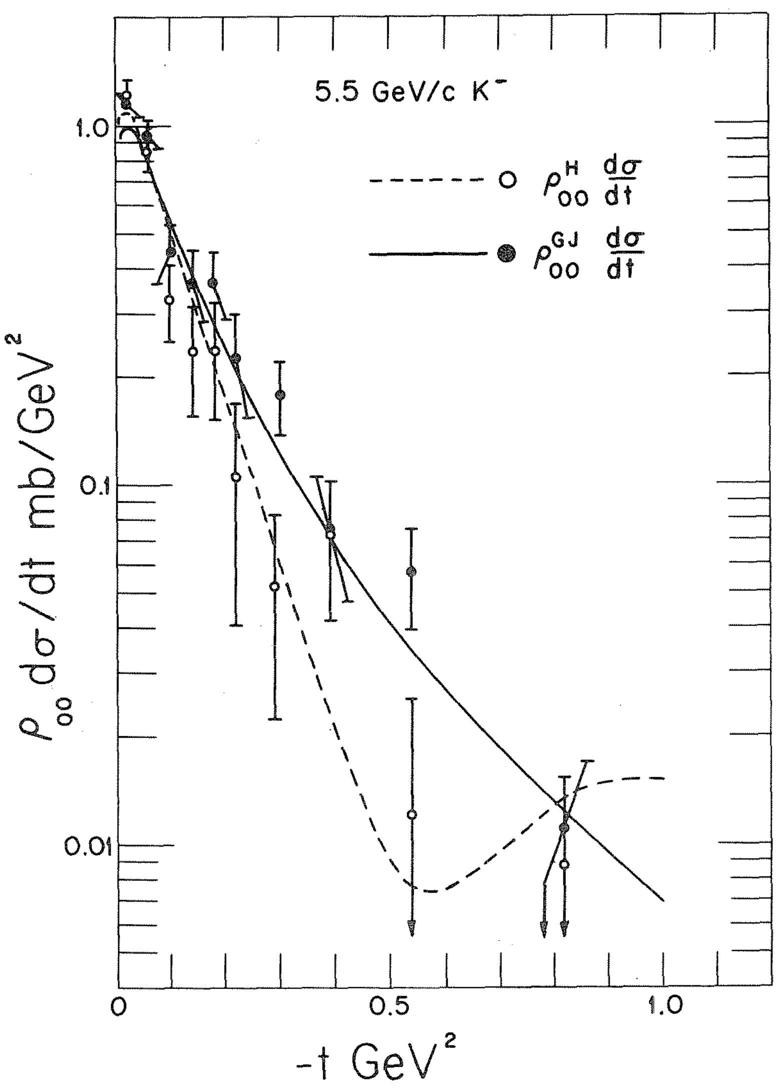

Figure 45: ρ^{H}_{00} dσ/dt and ρ^{GJ}_{00} dσ/dt for $K^{-}p \rightarrow \bar{K}^{*}(890)n$ at 5.5 GeV/c. The fitted curves are from the SCRAM model of ref. 54.

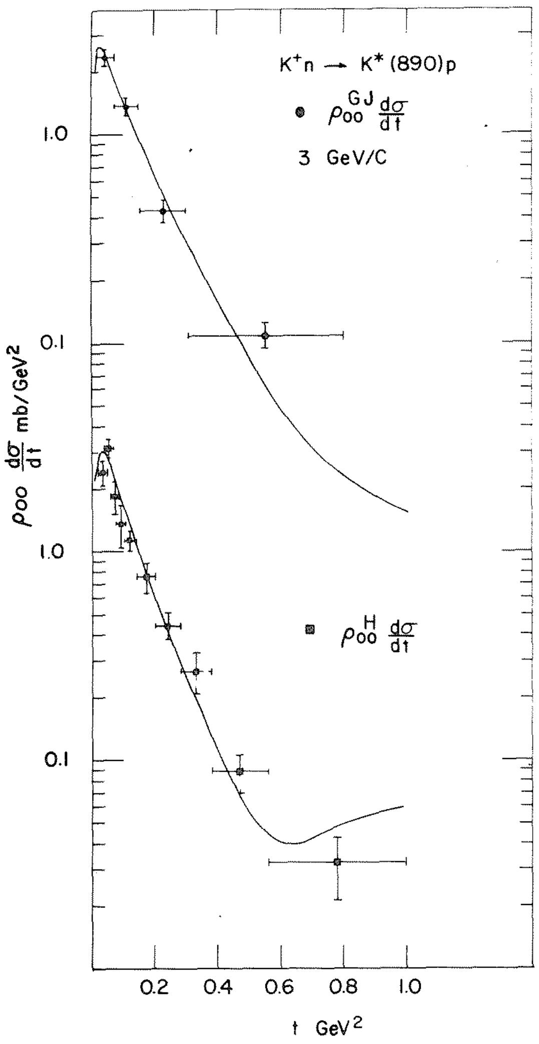

Figure 46: ρ^{H}_{00} dσ/dt and ρ^{GJ}_{00} dσ/dt for $K^{+}n \rightarrow K^{*}(890)p$ at 3.0 GeV/c. The fitted curves are from the SCRAM model of ref. 54.

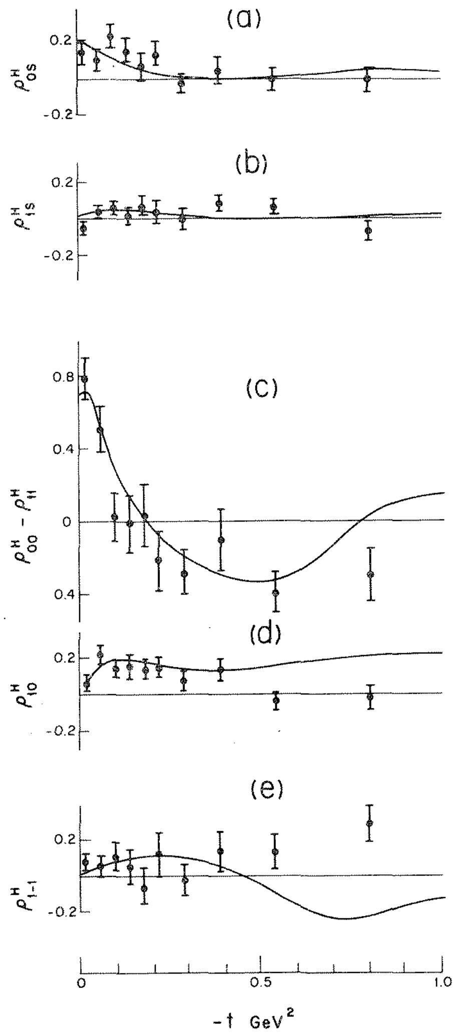

Figure 47: s-channel density matrices for $\bar{K}^*(890)$ in $K^-p \to \bar{K}^*(890)n$ at 5.5 GeV/c. The fitted curves are from the SCRAM model of ref. 54.

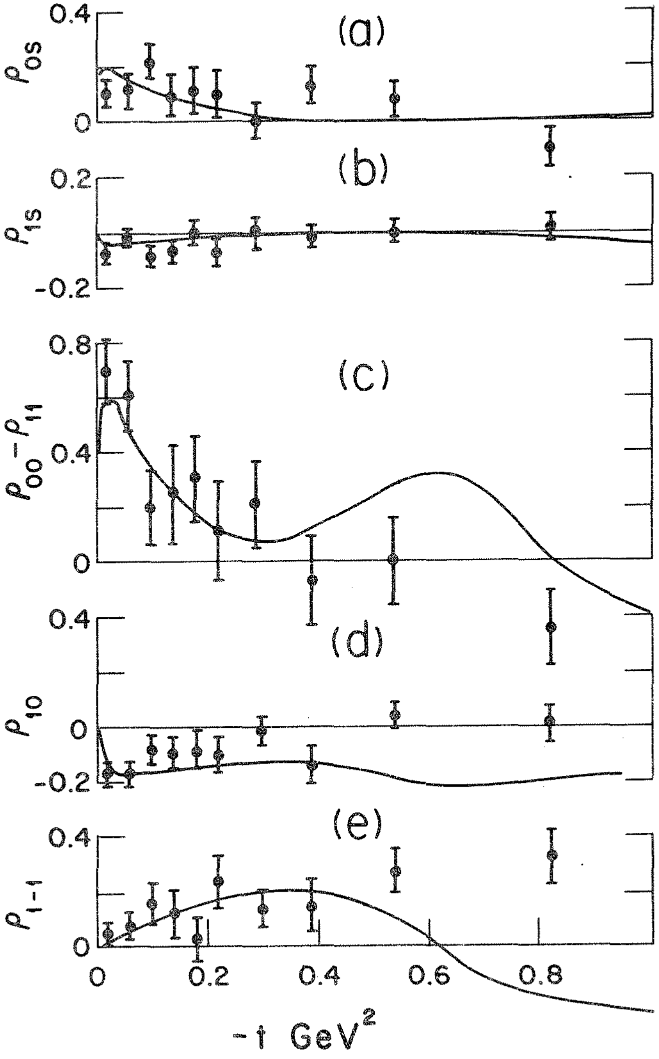

Figure 48: t-channel density matrices for $\bar{K}^*(890)$ in $K^-p \to \bar{K}^*(890)n$ at 5.5 GeV/c. The fitted curves are from the SCRAM model of ref. 54.

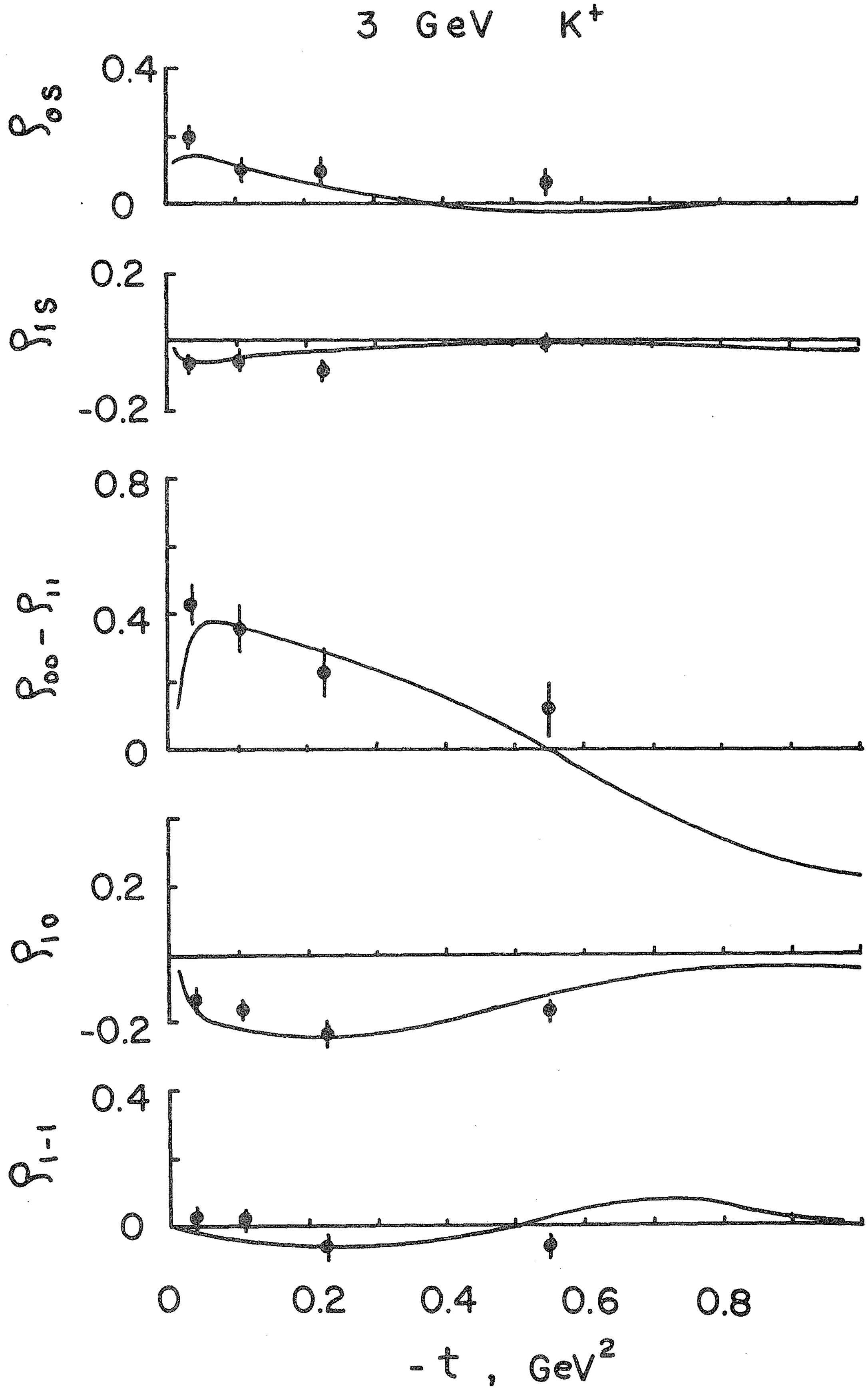

Figure 49: t-channel density matrices for $K^*(890)$ in $K^+n \rightarrow K^*(890)p$ at 3 GeV/c. The fitted curves are from the SCRAM model of ref. 54.

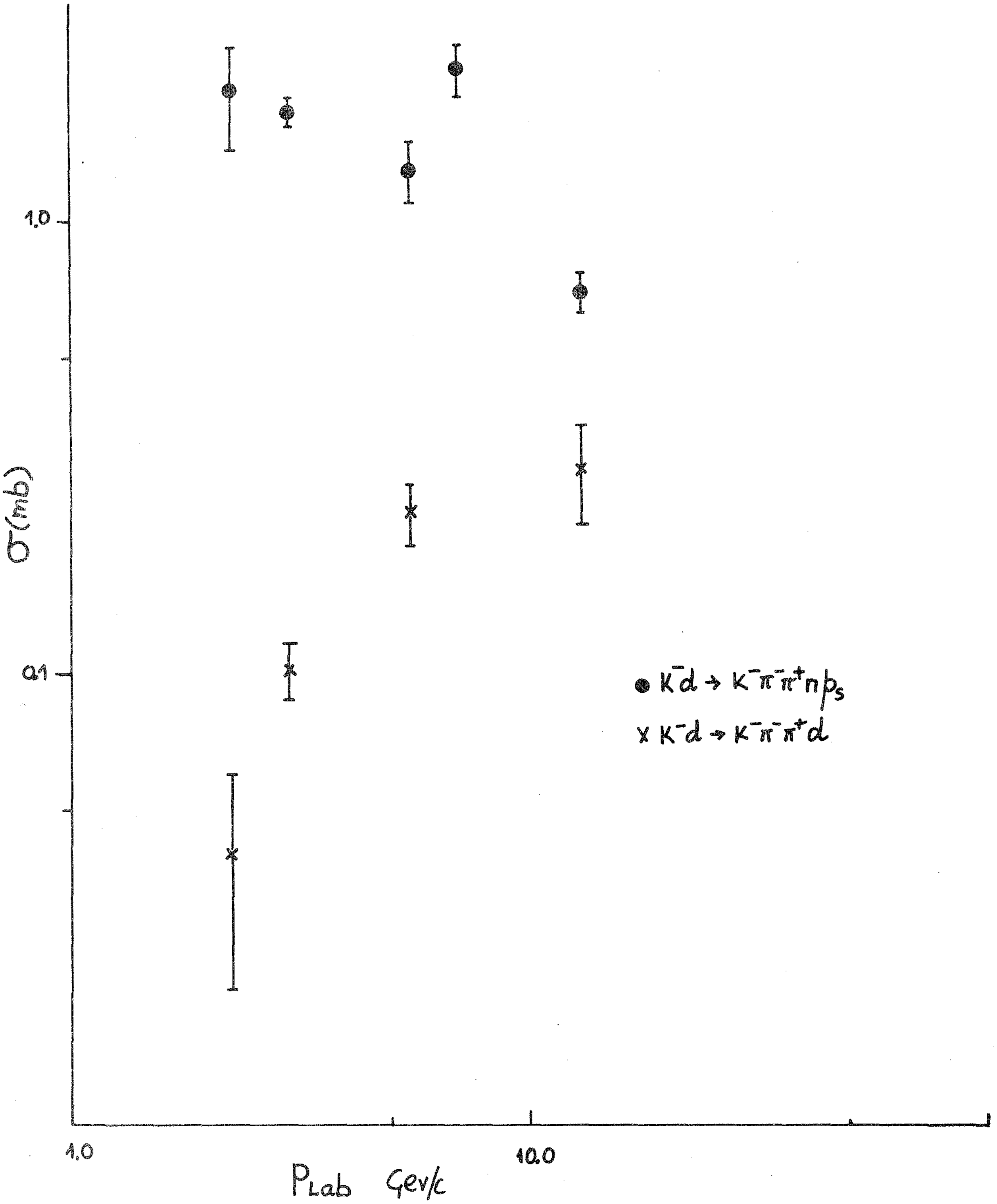

Figure 50: Comparison of channel cross sections for $K^-d \rightarrow K^-\pi^-\pi^+np_s$ and $K^-d \rightarrow K^-\pi^+\pi^-d$.

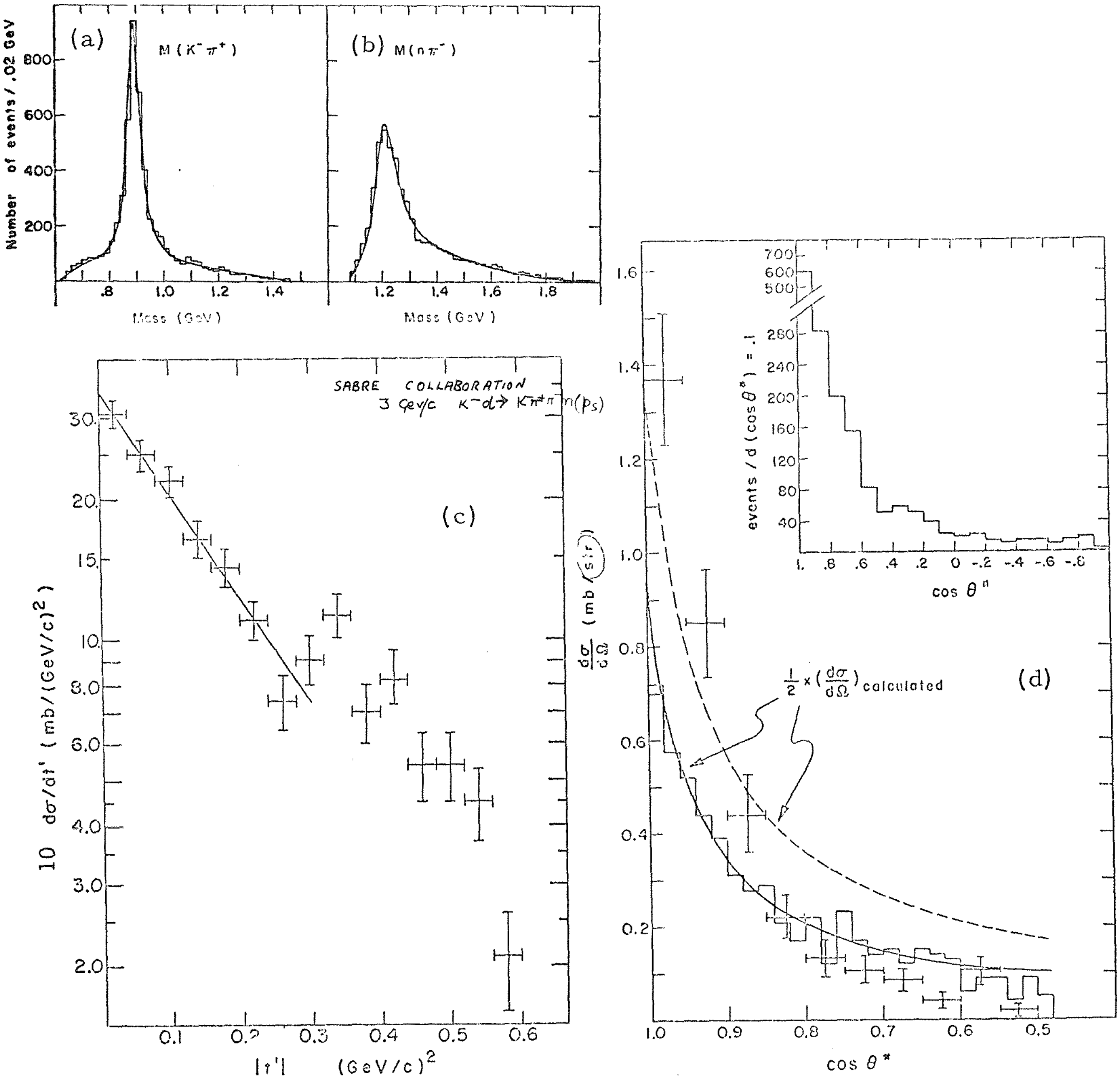

Figure 51: $K^-d \rightarrow K^-\pi^+\pi^-np$ at 3 GeV/c: (a) and (b), invariant mass distributions for $K^-\pi^+$ and $n\pi^-$ respectively; (c) $d\sigma/dt'$ for $K^-n \rightarrow \bar{K}^*\Delta^-(1236)$, and (d) comparison of differential cross sections for $K^-n \rightarrow \bar{K}^*\Delta^-(1236)$ (histogram) and $K^+p \rightarrow K^*\Delta^{++}(1236)$ (crosses). See Ref. 56 for further details and a discussion of the absorption model curves in (d). The scale on (c) in Ref. 56 was wrong by a factor of 10: the ordinate has been relabelled to account for this.

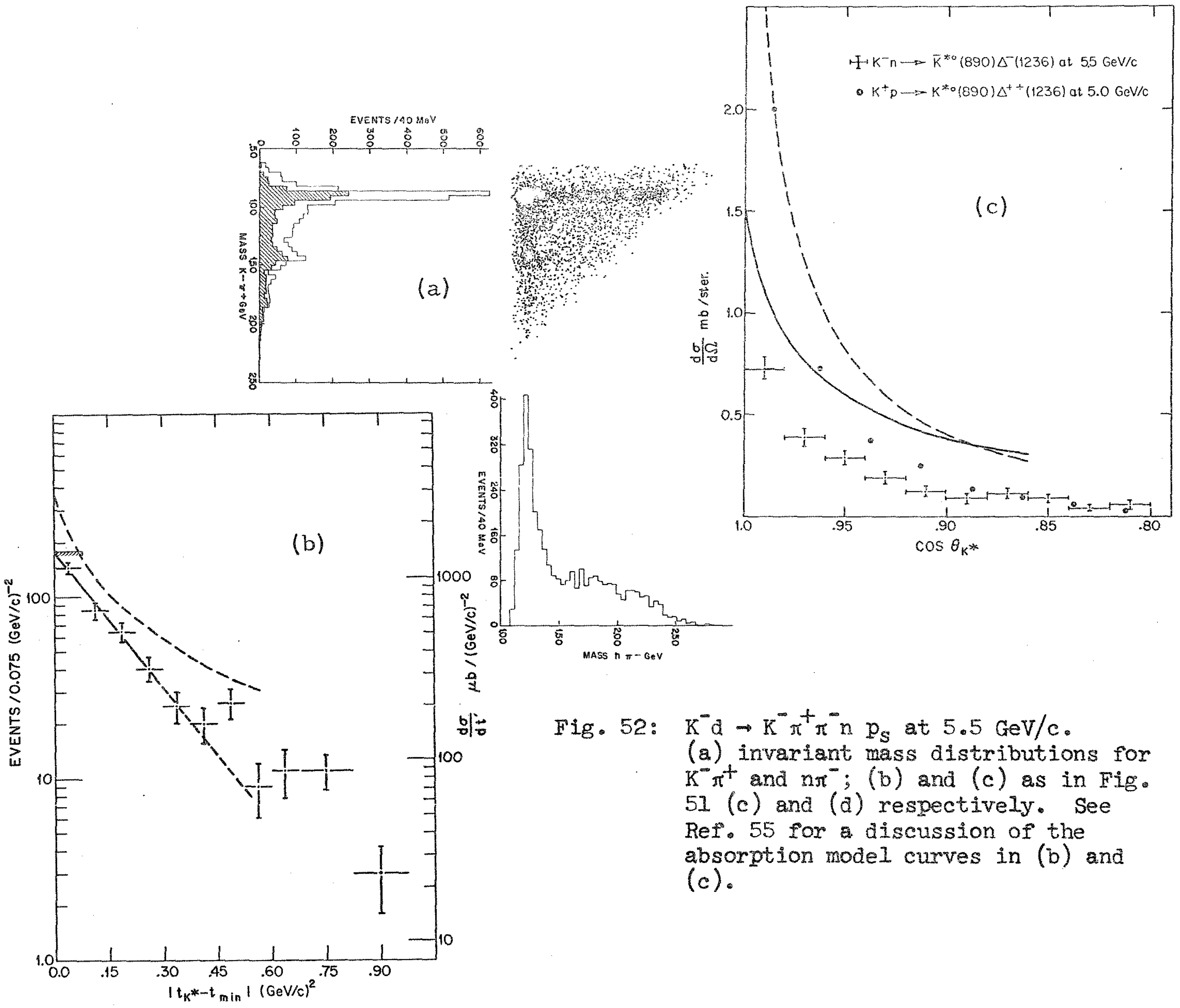

Fig. 52: $K^-d \rightarrow K^-\pi^+\pi^- n\, p_s$ at 5.5 GeV/c. (a) invariant mass distributions for $K^-\pi^+$ and $n\pi^-$; (b) and (c) as in Fig. 51 (c) and (d) respectively. See Ref. 55 for a discussion of the absorption model curves in (b) and (c).

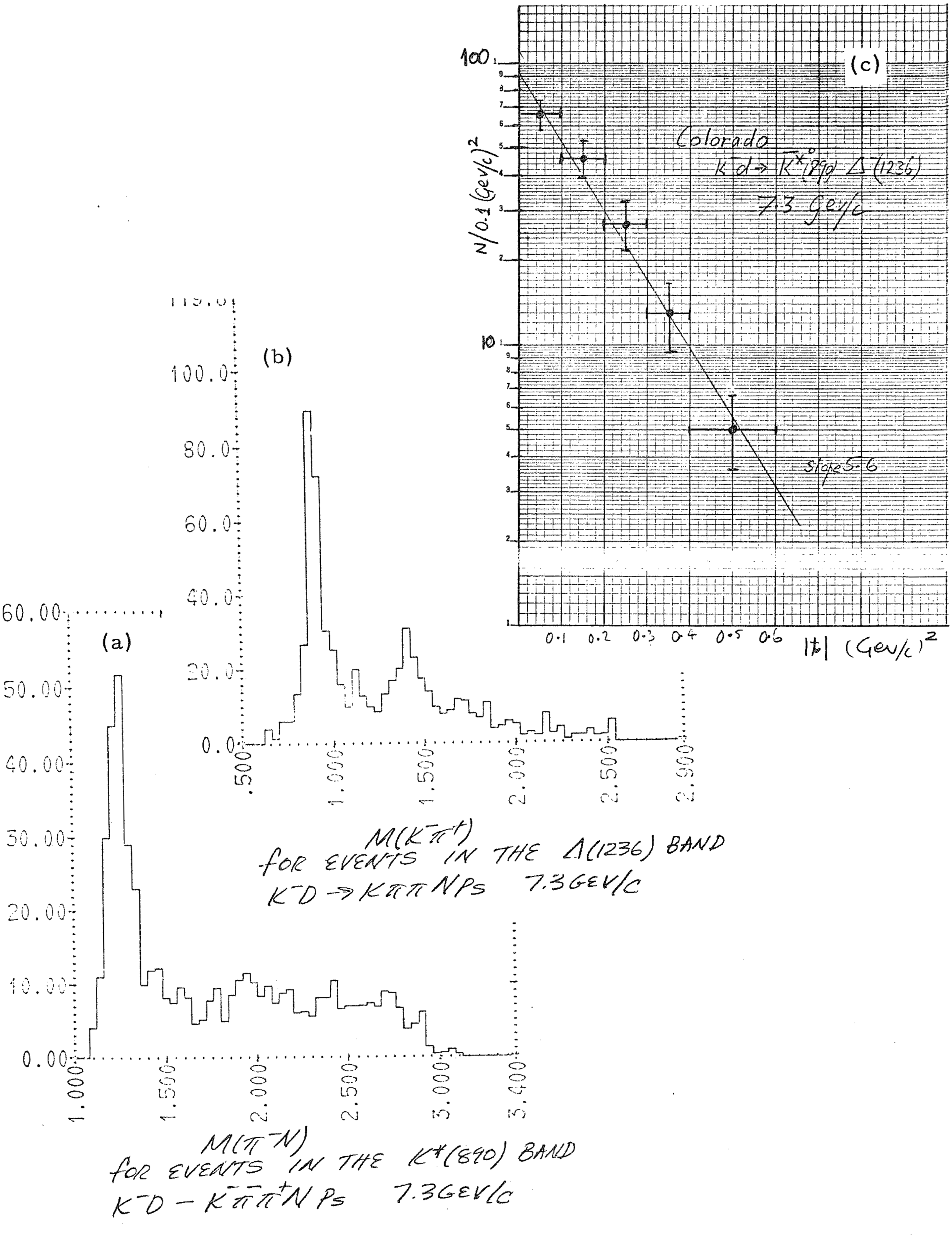

Figure 53: $K^-d \rightarrow K^-\pi^+\pi^- n\ p_s$ at 7.3 GeV/c. (a) and (b), invariant mass distributions for $n\pi^-$ and $K^-\pi^+$ respectively. (c) differential cross-section for $K^-d \rightarrow \bar{K}^*(890)\ \Delta^-(1236)\ p_s$.

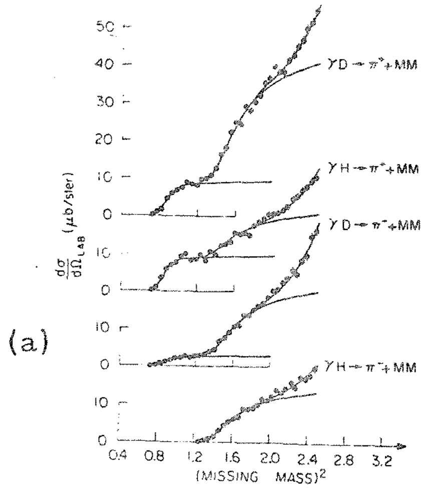

Fits to the π^+ and π^- data from hydrogen and deuterium for $d\sigma/d\Omega_{lab}$ vs MM^2 at 1.4°. The curves show the single nucleon, the Δ, and the ρ processes folded with a $0.03X_0$ bremsstrahlung spectrum including a Fermi smearing for the deuterium case as given by the Hulthén momentum distribution.

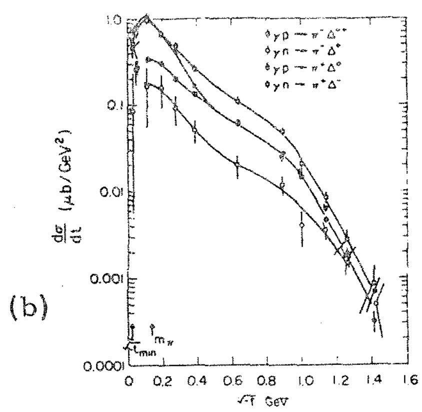

Measured cross sections for $\pi^\pm\Delta$ photoproduction versus momentum transfer $(-t)^{1/2}$. The γn cross sections result from deuterium minus hydrogen subtractions. Fits made to missing-mass spectra included the single-nucleon process, the Δ, background from $\gamma N \rightarrow \rho N$, and a correction for phase space $\gamma N \rightarrow \pi\pi N$. A Jackson-type Breit-Wigner form was used to calculate the shape of the Δ contribution. Smooth curves are drawn to guide the eye.

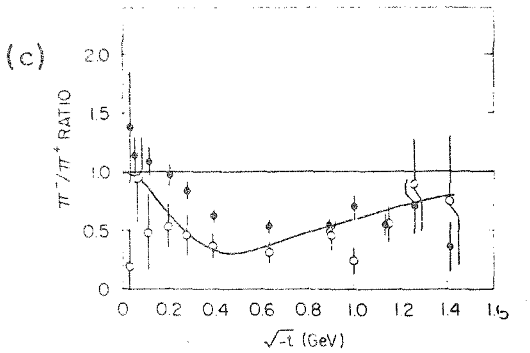

The ratios $(\gamma p \rightarrow \pi^-\Delta^{++})/(\gamma n \rightarrow \pi^+\Delta^-)$ (closed circles with error bars) and $(\gamma n \rightarrow \pi^-\Delta^+)/(\gamma p \rightarrow \pi^+\Delta^0)$ versus $(-t)^{1/2}$ (open circles with error bars). These ratios, where different from 1, indicate an interference between isoscalar (ω-like photon) and isovector (ρ^0-like photon) amplitudes. For comparison the curve shows the ratio $(\gamma n \rightarrow \pi^- p)/(\gamma p \rightarrow \pi^+ n)$, Ref. 6.

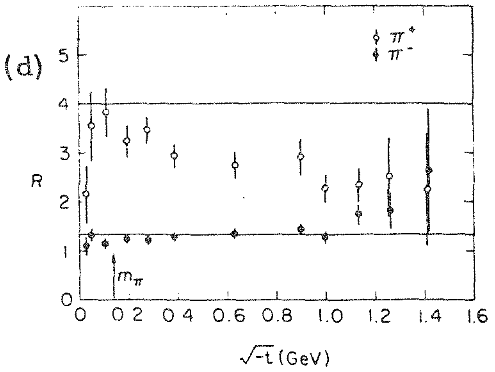

The deuterium-to-hydrogen ratios versus $(-t)^{1/2}$. Neglecting absorption effects in deuterium, which were found to be negligible in our $\gamma d \rightarrow \pi^+ nn$ data, dominance of isospin-1 exchange implies $R = 4$ for π^+ and $R = \frac{4}{3}$ for π^-. The π^+ data indicate that isospin-1 exchange alone does not fit the data for $|t| \sim 0.15$ GeV^2.

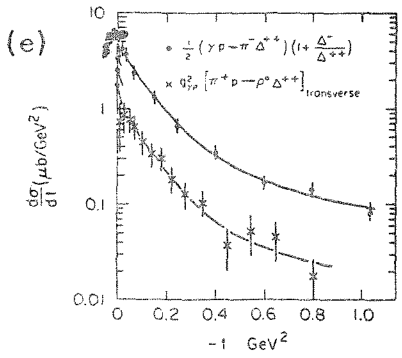

Test of the vector-dominance model. The average of Δ^{++} and Δ^- is compared with that predicted from the $\pi^+ p \rightarrow \rho^0\Delta^{++}$ data at 8 GeV by vector dominance. There is disagreement by about a factor of 5. Smooth curves are drawn to guide the eye.

Figure 54: Δ(1236) photoproduction data from hydrogen and deuterium at 16 GeV/c. The ratio $(\gamma p \rightarrow \pi^-\Delta^{++})/(\gamma n \rightarrow \pi^+\Delta^-)$ shown in (c) as ɸ is predicted to be similar to the solid line in (c). This latter is a smooth curve representing the ratio $(\gamma n \rightarrow \pi^- p)/(\gamma p \rightarrow \pi^+ n)$. The model which relates these two photoproduction both to each other and the K^*N and $K^*\Delta$ strong interaction data is discussed in Section VII of the text.

DISCUSSION

Deuteron Corrections

Dean (Iowa): One can evaluate, à la Glauber, the multiple scattering contributions to, say, $\pi d \to \pi\pi d$, where the two pions are not resonating, and compare with $\pi d \to \rho d$ assuming the rho doesn't decay inside the deuteron. The two are qualitatively quite different; the latter involves high-energy ρN scattering, whereas the former includes the pion-nucleon amplitude at substantially lower energy, and may therefore be much larger. Thus the differences you note between resonant and non-resonant final states are not surprising. (Cf. page 477).

Physics of $\pi^- p \to \rho^o n$, $\pi^+ n \to \omega^o p$ and $KN \to K^* N$.

Ferbel (Rochester): You mentioned (page 479) the $1/p^2_{lab}$ scaling law observed in many resonance production reactions, (e.g., $\pi N \to \omega N$, $\pi N \to \rho N$, $KN \to K^* N$). This was also commented on by Fox in his talk at this conference. For instance, in $KN \to K^* N$, you see from the decay of the K^*, it is mainly vector exchange, yet it exhibits this same $1/p^2_{lab}$ behavior characteristic of elementary π exchange.

Fox (Caltech): As mentioned by Musgrave (page 487), vector dominance relates K^*, ρ and ω production to photoproduction. The latter also shows a $1/p^2_{lab}$ behavior. Thus the strong and photoproduction data show the same mystery. At low $-t \lesssim 0.75$ $(GeV/c)^2$, it can be "understood" as a complicated effect from the mixture of π, B, ρ and A_2 pole and cut exchange with their sundry energy dependencies. However, the universal $e^{3t}\, p^{-2}_{lab}$ structure of photoproduction for $-t \gtrsim 1$ $(GeV/c)^2$ has no such simple (or complicated) "explanation". Unfortunately there is little information on the hadronic vector meson production reactions in this t range. It is a crucial experiment. It is also important to see if $\rho_{oo} d\sigma/dt$ (π, B exchange only) behaves like p^{-3}_{lab} (as in a pole theory) or p^{-2}_{lab} at lower $-t \approx 0.6$ $(GeV/c)^2$.

Jackson (LRL): I would like to make a comment on the $\pi^+ n \to \omega^o p$ data. At the low momentum, say, up to 3 GeV/c, there is a strong signal over the whole angular region. In addition to the peripheral peak, there is large backward production. We all know ω is strongly coupled to the nucleon, so the u-channel nucleon exchange is important. I would say that the cross section at the low s is probably artificially enhanced by this, and that if you plot only the peripheral part which you would associate with t-channel exchange, it might have a flatter slope in energy.

SPECIAL EVENT:
SMALL MOMENTUM TRANSFERS
HEP
RELAYS

RECENT RESULTS ON $\pi^- p \to \rho^0 n$ AT SMALL MOMENTUM TRANSFERS

D.W.G.S. Leith
Stanford Linear Accelerator Center
Stanford University, Stanford, California 94305

This paper is divided into three parts:

Paper A : Presentation of Data : "A Study of the Reaction $\pi^- p \to \rho^0 n$ at 15 GeV/c." Page 555

Paper B : Tests of Vector Dominance Model : "A Comparison of $\pi^- p \to \rho^0 n$ with Single Pion Photoproduction at 15 GeV/c." Page 574

Paper C : Tests of (Strong) Absorption Model : "Comparison of Absorptive One Pion Exchange Model with Measurements of $\pi^- p \to \pi^+ \pi^- n$." Page 584

Paper A

A STUDY OF THE REACTION $\pi^- p \to \rho^o n$ AT 15 GeV/c [*]

F. Bulos, R. K. Carnegie, G. E. Fischer, E. E. Kluge,
D.W.G.S. Leith, H. L. Lynch, B. Ratcliff, B. Richter,
H. H. Williams, and S. H. Williams

Stanford Linear Accelerator Center
Stanford University, Stanford, California 94305

and

M. Beniston

IBM, Palo Alto, California 94304

ABSTRACT

The results of a wire spark chamber experiment studying the reaction $\pi^- p \to \pi^+ \pi^- n$ at 15 GeV/c are presented. The differential cross section, π-π mass distribution and density matrix elements have been determined from 10,000 $\pi\pi n$ events ($M_{\pi\pi} < 1.0$ GeV) produced with $-t < 0.30$ $(\text{GeV}/c)^2$. Both the density matrix elements and the differential cross section exhibit structure in the forward direction ($-t < m_\pi^{\ 2}$).

(SLAC-PUB-884: A shorter version of this paper was submitted to Phys. Rev. Letters.)

---

[*] Work supported by the U. S. Atomic Energy Commission.

We report the results of a wire spark chamber experiment performed at SLAC to study the reaction $\pi^- p \rightarrow \pi^+ \pi^- n$ at an incident beam momentum of 15 GeV/c.[1] This reaction has been previously studied at lower energies,[2] but prior to this experiment no accurate determination of the density matrix elements or the differential cross section, $d\sigma/dt$, has been available at high energies ($t \equiv$ momentum transfer squared to the nucleon). In addition, knowledge of these quantities for very small momentum transfers has been lacking at all energies. Absorption models[3] and also the vector dominance model (VDM) predict that the $\pi^- p \rightarrow \rho^0 n$ differential cross section for transversely polarized rho mesons should have a sharp rise in the forward direction, ($-t < m_\pi^2$), as does the reaction $\gamma N \rightarrow \pi^{\pm} N$. For a detailed comparison of the data with VDM, see Ref. 4.

The experimental apparatus, which is described in more detail elsewhere,[5] is shown in Fig. 1. The momentum of the incident π^- was determined to an accuracy of $\pm .3\%$ and the horizontal and vertical projected π^- angles at the target were determined to an accuracy of $\pm .5$ mr by counter hodoscopes placed in the beam line. The spectrometer, which measured the momenta and angles of the outgoing pions, consisted of seven 2-gap spark chambers, an analyzing magnet ($100 \times 38 \times 120$ cm aperture), and trigger hodoscopes. Three chambers were placed upstream of the magnet and four downstream. The inside faces of the magnet gap were lined with scintillation counters to veto events in which a particle intersected the pole faces. The trigger logic required an incident beam particle, two or more charged particles downstream of the magnet, and no signal from the magnet veto counters. In addition, scintillator-Pb sandwich counters surrounded the 1 m long LH_2 target to detect particles which escaped the spectrometer. A gas Čerenkov counter placed downstream of the spectrometer distinguished π's from heavier particles. The information from both the Čerenkov counter and target counters was used only in the off-line analysis.

Because the main pion beam passed through the spectrometer system, and because of the high instantaneous fluxes ($8\,\pi^-/1.6\,\mu$sec burst), a small region of the chambers was desensitized by the installation of a polyurethane plug. As a result, very asymmetric ρ decays could not be observed. This limitation of the plug was matched by the low momentum cutoff of the magnet which also prohibited observation of very asymmetric decays. For $|\cos\theta| < .8$ (where θ is the polar angle of the π^- in the helicity frame), the average acceptance was 25%, and varied slowly as a function of $M_{\pi\pi}$ and t for ρ-n events. The π-π mass resolution was less than ±10 MeV at the mass of the rho; the missing mass resolution was ±80 MeV, and the t resolution was calculated to be $\pm 0.016\ \sqrt{-t}\ (\mathrm{GeV/c})^2$.

The density matrix elements of the di-pion system were determined as a function of t by fitting the observed decay angular distribution to the form $\omega(\theta,\phi) = W(\theta,\phi)\ E(\theta,\phi)$ where

$$W(\theta,\phi) = \frac{1}{4\pi}\Big[1 + (\rho_{00}-\rho_{11})(3\cos^2\theta - 1) + 2\sqrt{3}\,\mathrm{Re}(\rho_{0S})\cos\theta - 3\sqrt{2}\,\mathrm{Re}(\rho_{10})\sin 2\theta\cos\phi - 2\sqrt{6}\,\mathrm{Re}(\rho_{1S})\sin\theta\cos\phi - 3\rho_{1-1}\sin^2\theta\cos 2\phi\Big] \qquad (1)$$

is the angular distribution for S and P waves, $E(\theta,\phi)$ is the detection efficiency of the spectrometer, and θ,ϕ are the polar and azimuthal decay angles of the π^- in the ρ rest frame. The normalization of the density matrix elements was $\rho_{00}+2\rho_{11}+\rho_{00}^{S}=1$. The analysis was performed on the events in the mass interval $.665 < M_{\pi\pi} < .865$ GeV. A Monte Carlo program was used to calculate $E(\theta,\phi)$ to correct for geometrical losses. By refitting the data with more restrictive geometrical cutoffs than those imposed by the apparatus, it was ascertained that the ρ_{ij} obtained were not affected by the geometry of the apparatus. The density matrix elements were obtained in the helicity (ρ_{ij}^{H}) and Jackson (ρ_{ij}^{J}) frames and their consistency checked by rotating from one frame to the other. By varying the missing mass cutoff and using the information from the target counters, it was determined that 12 ± 2% of the event sample was $\pi^+\pi^- N^*$ events and that this contribution did not affect the values of ρ_{ij}.[6]

Recently Biswas et al.[7] have suggested that higher partial waves than $\ell=1$ may contribute in the ρ region of $\pi\pi$ mass. They find that their 4 GeV data are inconsistent with the relation $\langle \cos 2\phi \rangle = -\frac{3}{4}\rho_{1-1} \sin^2\theta$ which is valid if only S and P waves are present, and they also find ρ_{1-1} to be mass dependent. Our data show no evidence of these discrepancies: $\langle \cos 2\phi \rangle$ is consistent with $-\frac{3}{4}\rho_{1-1} \sin^2\theta$ ($\chi^2 = 16.5$ for 18 degrees of freedom) and there is no evidence for a mass dependence of ρ_{1-1} ($\chi^2 = 10.6$ for 10 degrees of freedom).[8] In addition, there are no systematic deviations of the fit from the data in any particular region of $\cos\theta, \phi$. Hence, we conclude that partial waves with $\ell \geq 2$ are not required to describe the decay angular distribution.

The density matrix elements are shown in Figs. 2a-e and 3a-e, and are listed in Tables 1 and 2. The error bars shown are statistical only; systematic errors, which could result if there were small unknown biases in the apparatus or event reconstruction, are estimated to be less than the statistical errors. The fact that Re ρ_{0S} and Re ρ_{1S} do not vanish is conclusive evidence that the dipion system may not be described by a pure P wave.

Many of the density matrix elements exhibit structure for momentum transfers less than m_π^2; in particular there is a striking dip in $\rho_{00}-\rho_{11}$ (helicity and Jackson frames) and in Re ρ_{10}^J for $-t < m_\pi^2/2$, a region which has not been studied in previous experiments.[9] The narrow dip in $\rho_{00}-\rho_{11}$ is predicted by one-pion-exchange absorption models (OPEA).[3] OPEA also predicts that $\rho_{1-1}^J \approx 0$ for $-t < m_\pi^2$, as is observed in the data.

It is not possible to determine separately ρ_{11} or ρ^S_{00} from the angular distribution alone; however, the Schwartz inequalities on the helicity amplitudes and the requirement that the diagonal elements of the density matrix be positive-definite enable one to establish limits on ρ^S_{00} and ρ_{11}. The limits on ρ_{11} calculated in this manner are shown in Figs. 2f and 3f.

Independent information on ρ^S_{00} (and hence ρ_{11}) may be obtained from the existing $\pi^- p \to \pi^o \pi^o n$ data.[10] The curves in Figs. 2f and 3f show the values of ρ_{11} calculated assuming $d\sigma/dt\,(\text{S-wave}) \propto |t|\,e^{7t}/(t-m_\pi^2)^2$, which is a good representation of the t-dependence of the $\pi^o\pi^o$ data; the normalization was obtained by scaling the $\pi^o\pi^o$ cross section to 15 GeV.[11] The values of ρ_{11} obtained in this manner are consistent with the limits described above. We have also calculated ρ_{11} taking the amount of S-wave from our fits to the π-π mass spectrum (see discussion below) and assuming the same t-dependence as above. The results obtained agree within errors.

A peak in the calculated value of ρ_{11} is observed in the forward direction. The structure does not strongly depend on the details of the S-wave t-dependence; for example, if the S-wave is assumed to decrease by only 25% from $t=-m_\pi^2$ to $t=t_{min}$, rather than vanishing as predicted by OPEA, the peak in ρ_{11} is decreased by only 20%.

The total differential cross section $d\sigma/dt\,(\pi^- p \to \pi^+\pi^- n)$ and the transversely polarized cross section in the helicity frame, $2\rho^H_{11}\frac{d\sigma}{dt}(\pi^- p \to \pi^+\pi^- n)$, are shown in Fig. 4 for the mass interval $.665 < M_{\pi\pi} < .865$ GeV. The transverse and longitudinal cross sections for the Jackson frame are shown in Fig. 5. The cross sections are listed in Table 3. The error in the overall normalization is ± 5% and results from uncertainties in the counter and spark chamber efficiencies, thick target corrections, and track reconstruction efficiency. As a check on our absolute normalization, we have measured the elastic cross section, $\frac{d\sigma}{dt}(\pi^- p \to \pi^- p)$, with the same apparatus. Our measurements agree well with those of Foley et al.[12] as shown in Fig. 6.

The sharp rise in the helicity transverse cross section and the dip in the total cross section are predicted by OPEA models and verify that the reaction is dominated by pion exchange for small momentum transfers. The transverse cross section in the Jackson frame is expected to be flat (i.e., no peak or dip); this is consistent with the data. The total rho cross section, which is also shown in Fig. 4, has been obtained from the $\pi^+\pi^-$ cross section by subtracting the amount of S-wave and correcting for the fraction of the rho mass spectrum outside our mass interval. The normalization error is ±25%, the dominant contribution coming from the uncertainty in the rho line shape.

The π-π mass distribution shown in Fig. 7 is described from .4 - .9 GeV using only a P-wave resonance and an S-wave background. The P-wave is parameterized by a Breit-Wigner form which was used by Pišut and Roos[13] to fit both ρ^- and ρ^0 mass distributions at lower energies:

$$\frac{d\sigma}{dm} \propto \frac{1}{q} \frac{m^2 m_0^2 \Gamma_\ell^2(m)}{\left(m_0^2 - m^2\right)^2 + m_0^2 \Gamma_\ell^2(m)} \int_{t_{min}(m)}^{T} e^{At}\, dt$$

where $\Gamma_\ell(m) = \Gamma_0 \left(\frac{q}{q_0}\right)^{2\ell+1} \frac{m_0}{m} \frac{1+R^2q_0^2}{1+R^2q^2}$; ℓ = angular momentum of resonance,

$$q = \left(\frac{m^2}{4} - m_\pi^2\right)^{1/2}$$

$$q_0 = \left(\frac{m_0^2}{4} - m_\pi^2\right)^{1/2}$$

m_0, Γ_0 = the mass and width,

A is the slope of $d\sigma/dt(\pi^- p \to \rho^0 n)$,

$t_{min}(m)$ is the kinematical lower limit of t,

T is the upper limit of $|t|$ for the event sample, and

R is a parameter which corresponds to the range of the interaction.

The S-wave contribution is also parameterized by the above form with a mass of .7 GeV and a width of .4 GeV; this is consistent with the $\pi^o\pi^o$ mass distribution.[10] The fit yields a rho mass and width of $M_\rho = .771 \pm .004$ GeV, $\Gamma_\rho = .160 \pm .014$ GeV, and $R^2 = 4.8 \pm 3.2$ $(\mathrm{GeV}/c)^{-2}$. The amount of S-wave required is 11 ± 2% which agrees well with the 12% predicted by scaling the $\pi^o\pi^o n$ data.[11] Other acceptable fits to the mass spectrum may also be obtained by changing R or by choosing different Breit-Wigner functions, such as the standard P-wave form discussed by Jackson.[14] Although these forms are indistinguishable within the interval .4 - .9 GeV, the high mass behavior results in normalizations differing by ±20%. Since this region is complicated by the presence of other resonances, it is difficult to distinguish between the forms by extending the fits to higher masses.

We summarize our results as follows: The dipion density matrix elements have been determined as a function of t for $.665 < M_{\pi\pi} < .865$ GeV and exhibit pronounced structure at small momentum transfers. We note that the angular distribution is well described by S and P waves alone. The differential cross sections for $\pi^- p \to \rho^o n$ and $\pi^- p \to \pi^+\pi^- n$ for the above mass interval have also been determined. The total and longitudinal cross sections show a dip at small t, whereas the transverse cross section in the helicity frame has a strong forward peak.

FOOTNOTES AND REFERENCES

1. These results supersede the preliminary data presented at the XVth International Conference on High Energy Physics, Kiev (1970).
2. B. D. Hyams *et al.*, Nucl. Phys. B7, 1 (1968); P. B. Johnson *et al.*, Phys. Rev. 176, 1651 (1968); J. P. Baton and G. Laurens, Phys. Rev. 176, 1574 (1968). Additional references may be found in these papers.
3. K. Gottfried and J. D. Jackson, Nuovo Cimento 34, 735 (1964); F. Henyey, G. L. Kane, Jon Pumplin, and M. H. Ross, Phys. Rev. 182, 1579 (1969).
4. F. Bulos *et al.*, following article (B), submitted to Phys. Rev. Letters. This article contains a list of references on VDM.
5. G. T. Armstrong *et al.*, "Wire chamber spectrometer at SLAC," Report No. SLAC-PUB-801 (1970).
6. This event sample was selected by making both missing mass and target-counter cuts. The missing mass cut was .8 - 1.06 GeV; the cut on the targer-counter information was such that ≈30% of the $\pi^+\pi^- N^*$ events were removed while the $\pi^+\pi^- n$ events were unaffected.
7. N. N. Biswas *et al.*, Phys. Rev. D1, 2705 (1970).
8. These checks were made on the data sample $-.1 < t < 0$ $(\mathrm{GeV}/c)^2$ and $.665 < M_{\pi\pi} < .865$ GeV.
9. The region $-t < m_\pi^2/2$ is inaccessible to low energy experiments because of kinematical limits on t. For example, t_{min} (4 GeV) $\approx m_\pi^2/3$ whereas t_{min} (15 GeV) $\approx m_\pi^2/50$.
10. P. Sonderegger and P. Bonamy, Lund International Conference on Elementary Particles (Abstract 372) (1969); E. I. Shibata, D. H. Frisch, and M. A. Wahlig, Phys. Rev. 25, 1227 (1970).

11. The $\pi^0\pi^0 n$ data were scaled according to p^{-2} where p is the incident beam energy. Sonderegger and Bonamy (Ref. 10) have shown that this scaling works well over a range of 3 to 18 GeV/c. It has been assumed that the $\pi^0\pi^0$ cross section is I=0.

12. K. J. Foley et al., Phys. Rev. 181, 1775 (1969).

13. J. Pišut and M. Roos, Nucl. Phys. B6, 325 (1968).

14. J. D. Jackson, Nuovo Cimento 34, 1644 (1964).

TABLE 1

Density Matrix Elements Evaluated in the Helicity Frame for $\pi^- p \to \pi^+ \pi^- n$, $.665 < M_{\pi\pi} < .865$ GeV

-t $(\mathrm{GeV/c})^2$	$\rho^H_{00}-\rho^H_{11}$	Re ρ^H_{10}	ρ^H_{1-1}	Re ρ^H_{0S}	Re ρ^H_{1S}	ρ^H_{11} *
t_{min} - .0025	.248 ± .127	-.067 ± .040	-.025 ± .033	.296 ± .048	-.038 ± .021	.228 ± .042
.0025 - .0050	.595 ± .080	-.053 ± .031	.023 ± .020	.180 ± .045	-.048 ± .012	.097 ± .027
.0050 - .0075	.699 ± .061	-.034 ± .030	.015 ± .020	.202 ± .042	-.022 ± .011	.054 ± .020
.0075 - .0100	.734 ± .054	-.079 ± .028	.014 ± .016	.257 ± .037	-.029 ± .010	.038 ± .018
.0100 - .0125	.778 ± .045	-.068 ± .035	.015 ± .016	.268 ± .038	-.010 ± .009	.024 ± .015
.0125 - .0200	.722 ± .033	-.020 ± .010	.044 ± .010	.280 ± .020	.005 ± .006	.038 ± .011
.0200 - .0275	.760 ± .028	.028 ± .013	.038 ± .010	.280 ± .020	.017 ± .005	.031 ± .009
.0275 - .0350	.734 ± .036	.037 ± .015	.039 ± .011	.283 ± .023	.012 ± .007	.034 ± .012
.035 - .045	.705 ± .035	.078 ± .016	.040 ± .012	.247 ± .023	.022 ± .007	.040 ± .012
.045 - .060	.644 ± .034	.098 ± .014	.035 ± .012	.274 ± .021	.037 ± .007	.057 ± .011
.060 - .080	.656 ± .033	.145 ± .013	.023 ± .011	.240 ± .020	.045 ± .006	.061 ± .011
.080 - .100	.580 ± .047	.174 ± .017	.017 ± .018	.219 ± .026	.057 ± .009	.079 ± .016
.100 - .150	.454 ± .039	.186 ± .012	.019 ± .016	.225 ± .020	.077 ± .008	.123 ± .013
.150 - .200	.250 ± .073	.203 ± .020	.024 ± .027	.194 ± .012	.077 ± .012	.197 ± .024
.200 - .300	-.086 ± .099	.211 ± .022	.041 ± .034	.077 ± .033	.053 ± .016	.306 ± .033

---

*Note: The values of ρ^H_{11} are not directly measured and depend on certain assumptions concerning the S-wave. See discussion in text.

TABLE 2

Density Matrix Elements Evaluated in the Jackson Frame for $\pi^- p \rightarrow \pi^+ \pi^- n$, $.665 < M_{\pi\pi} < .865$ GeV

$-t\ (\mathrm{GeV}/c)^2$	$\rho^J_{00}-\rho^J_{11}$	Re ρ^J_{10}	ρ^J_{1-1}	Re ρ^J_{0S}	Re ρ^J_{1S}	ρ^J_{11} *
t_{min} - .0025	.206 ± .128	-.076 ± .040	-.033 ± .034	.306 ± .047	-.055 ± .021	.243 ± .043
.0025 - .005	.482 ± .090	-.117 ± .031	.002 ± .022	.173 ± .046	-.074 ± .015	.136 ± .030
.005 - .0075	.586 ± .068	-.141 ± .029	-.007 ± .021	.203 ± .042	-.057 ± .013	.092 ± .023
.0075 - .010	.579 ± .055	-.187 ± .027	-.030 ± .019	.254 ± .035	-.072 ± .010	.090 ± .018
.010 - .0125	.584 ± .063	-.216 ± .030	-.049 ± .021	.258 ± .038	-.069 ± .009	.089 ± .021
.0125 - .020	.557 ± .037	-.181 ± .009	-.007 ± .012	.267 ± .020	-.063 ± .008	.094 ± .012
.020 - .0275	.590 ± .033	-.185 ± .011	-.012 ± .011	.260 ± .020	-.062 ± .008	.088 ± .011
.0275 - .035	.541 ± .043	-.200 ± .005	-.021 ± .013	.274 ± .021	-.085 ± .008	.098 ± .014
.035 - .045	.559 ± .038	-.195 ± .012	-.005 ± .013	.235 ± .021	-.071 ± .009	.089 ± .013
.045 - .060	.479 ± .040	-.183 ± .011	-.005 ± .015	.257 ± .020	-.079 ± .009	.113 ± .013
.060 - .080	.525 ± .036	-.205 ± .011	-.011 ± .014	.229 ± .019	-.076 ± .008	.104 ± .012
.080 - .100	.492 ± .038	-.213 ± .015	-.004 ± .017	.216 ± .024	-.071 ± .009	.108 ± .013
.100 - .150	.374 ± .039	-.189 ± .009	.027 ± .019	.225 ± .020	-.072 ± .009	.150 ± .013
.150 - .200	.252 ± .062	-.172 ± .023	.064 ± .037	.182 ± .026	-.083 ± .015	.196 ± .021
.200 - .300	.185 ± .071	-.134 ± .023	.168 ± .042	.106 ± .029	-.036 ± .019	.216 ± .024

---

*Note: The values ρ^J_{11} are not directly measured and are dependent on certain assumptions concerning the S-wave. See discussion in text.

TABLE 3

Differential Cross Sections for $\pi^- p \to \pi^+ \pi^- n$

-t $(\mathrm{GeV/c})^2$	$\frac{d\sigma}{dt}(\pi\pi)$ $\mu b/(\mathrm{GeV/c})^2$	$\rho_{11}^H \frac{d\sigma}{dt}(\pi\pi)$ * $\mu b/(\mathrm{GeV/c})^2$	$\rho_{11}^J \frac{d\sigma}{dt}(\pi\pi)$ * $\mu b/(\mathrm{GeV/c})^2$	$\frac{d\sigma}{dt}(\rho)$ * $\mu b/(\mathrm{GeV/c})^2$
t_{min} - .0025	221 ± 29	50.5 ± 11.4	53.6 ± 11.7	368 ± 51
.0025 - .005	307 ± 36	29.9 ± 8.9	41.6 ± 10.4	487 ± 65
.005 - .0075	332 ± 36	17.9 ± 7.0	30.6 ± 8.2	511 ± 65
.0075 - .010	344 ± 36	13.0 ± 6.3	30.8 ± 7.0	521 ± 64
.010 - .0125	377 ± 38	9.2 ± 5.8	33.7 ± 8.6	574 ± 68
.0125 - .020	355 ± 17	13.6 ± 4.0	33.2 ± 4.7	531 ± 30
.020 - .0275	375 ± 23	11.7 ± 3.5	33.1 ± 4.6	572 ± 41
.0275 - .035	301 ± 21	10.1 ± 3.7	29.4 ± 4.8	448 ± 38
.035 - .045	250 ± 17	10.0 ± 3.0	22.3 ± 3.5	368 ± 30
.045 - .060	195 ± 12	11.2 ± 2.3	21.9 ± 3.0	284 ± 22
.060 - .080	168 ± 10	10.2 ± 1.9	17.5 ± 2.3	252 ± 18
.080 - .100	111 ± 8.5	8.7 ± 1.8	12.0 ± 1.7	162 ± 15
.100 - .150	74.1 ± 3.9	9.1 ± 1.1	11.1 ± 1.1	109 ± 7.0
.150 - .200	44.7 ± 3.5	8.8 ± 1.3	8.8 ± 1.2	67.0 ± 6.3
.200 - .300	20.5 ± 1.7	6.3 ± 0.8	4.4 ± 0.6	30.5 ± 3.0

$$\frac{d\sigma}{dt}(\pi\pi) \equiv \frac{d\sigma}{dt}(\pi^- p \to \pi^+ \pi^- n), \quad .665 < M_{\pi\pi} < .865 \text{ GeV}$$

$$\frac{d\sigma}{dt}(\rho) \equiv \frac{d\sigma}{dt}(\pi^- p \to \rho^o n)$$

---

*Note: The values of $\rho_{11}^H \frac{d\sigma}{dt}$, $\rho_{11}^J \frac{d\sigma}{dt}$, and $\frac{d\sigma}{dt}(\rho)$ are not directly measured and depend on certain assumptions concerning the S-wave. See discussion in text.

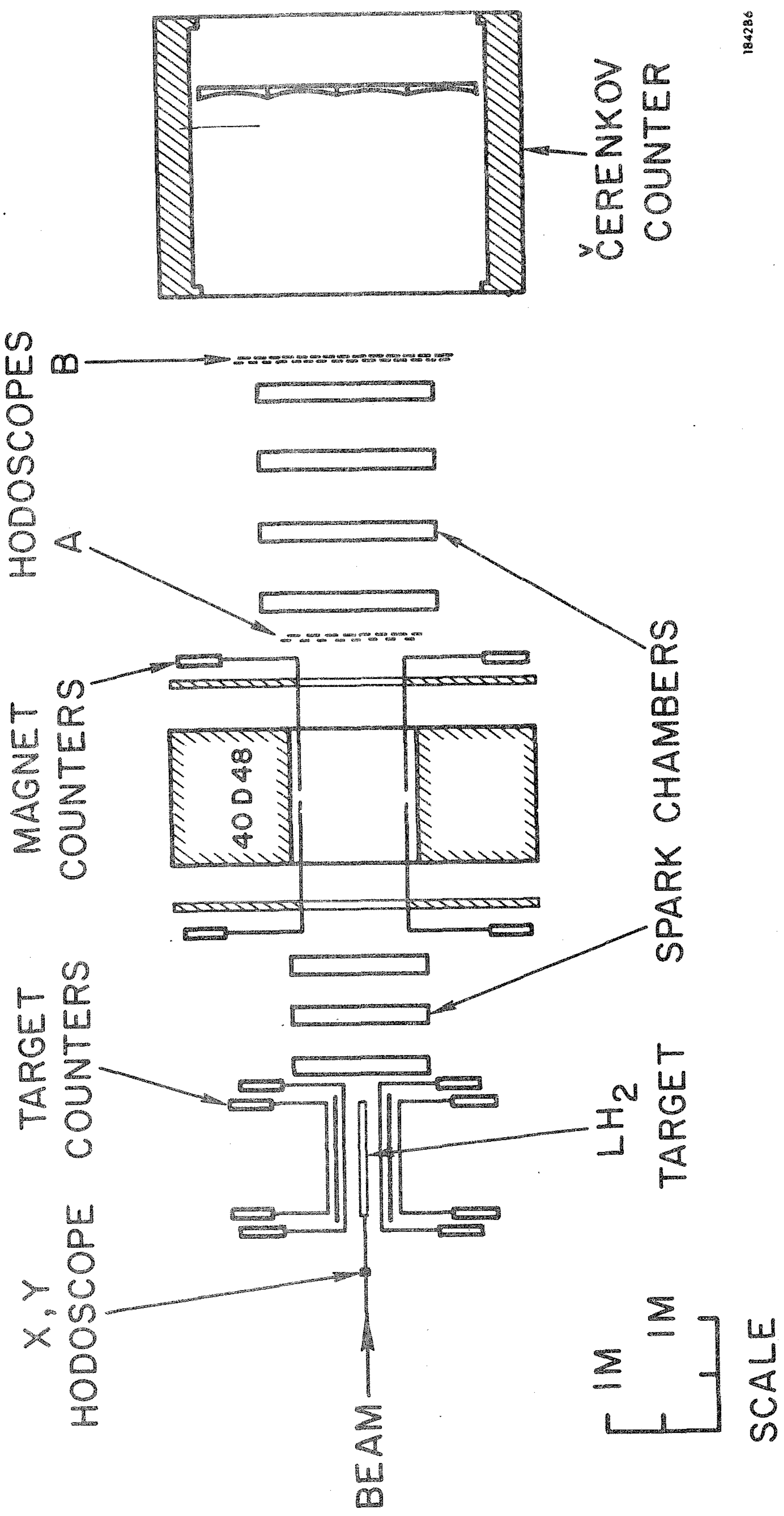
HODOSCOPES
A
B
ČERENKOV
COUNTER
MAGNET
COUNTERS
40 D 48
SPARK CHAMBERS
TARGET
COUNTERS
LH_2
TARGET
X,Y
HODOSCOPE
BEAM
IM
IM
SCALE
184286

Figure 1: A plan view of the experimental apparatus.

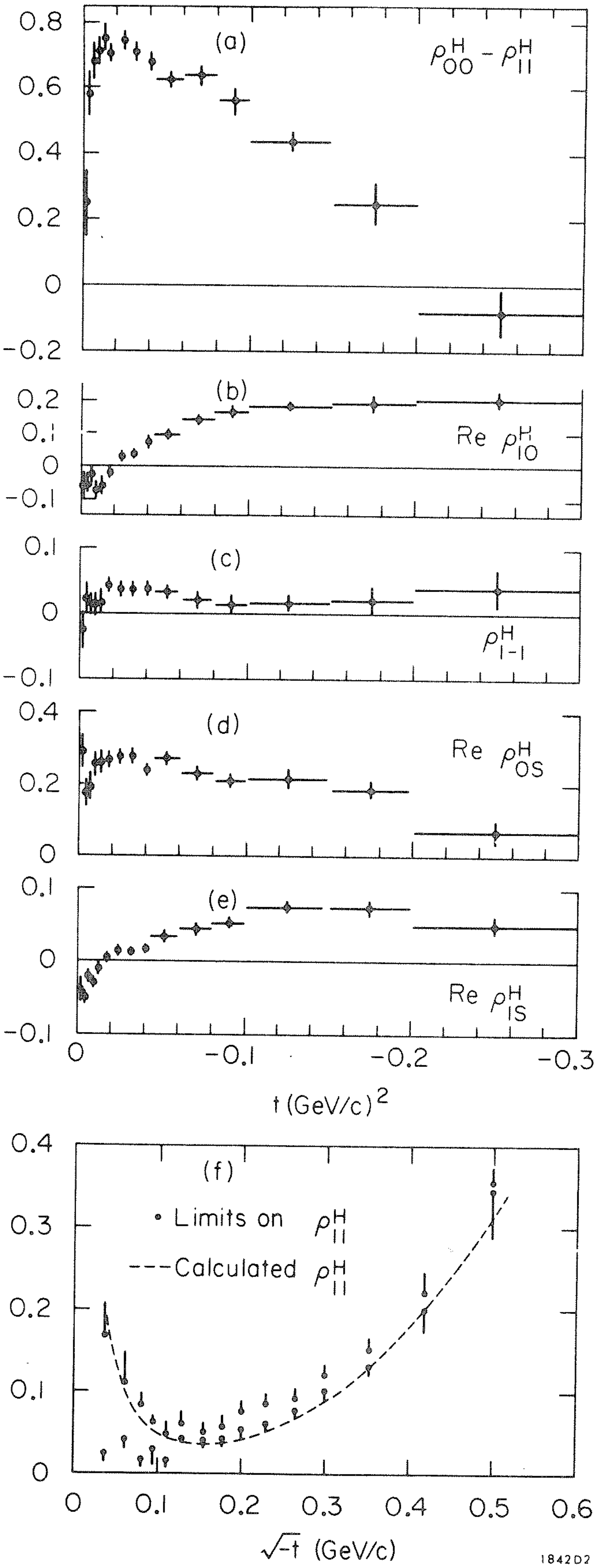

Figure 2: (a-e) The density matrix elements in the helicity frame for $0.665 < M_{\pi\pi} < 0.865$ GeV. The error bars indicate the statistical errors. (f) The upper and lower limits on ρ_{11} which are determined from the Schwartz inequalities on the helicity amplitudes and the requirement that the diagonal density matrix elements be positive definite. The errors on the limits result from the propagation of the errors on the density matrix elements. The curve is the calculated value of ρ_{11}^H obtained when the amount of S-wave is estimated from the $\pi^- p \Rightarrow \pi^0 \pi^0 n$ data.

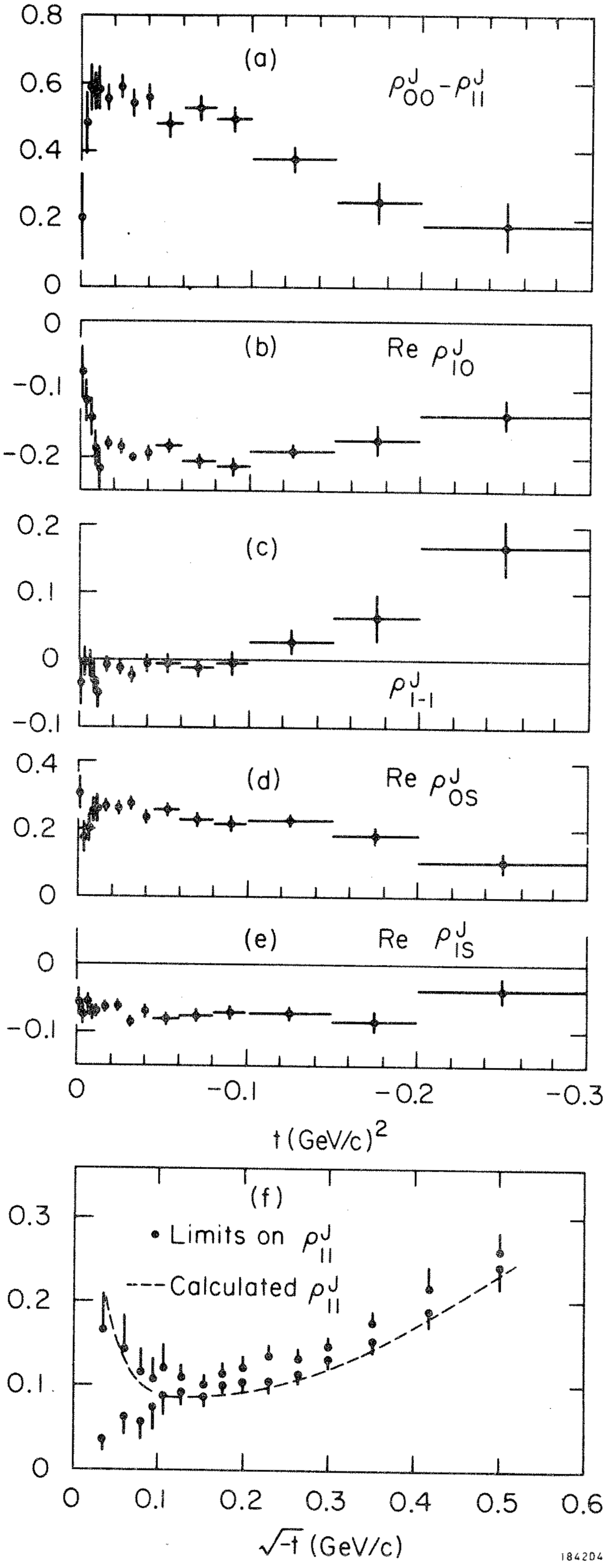

Figure 3: The density matrix elements evaluated in the Gottfried-Jackson frame. See the discussion in the caption of Fig. 2.

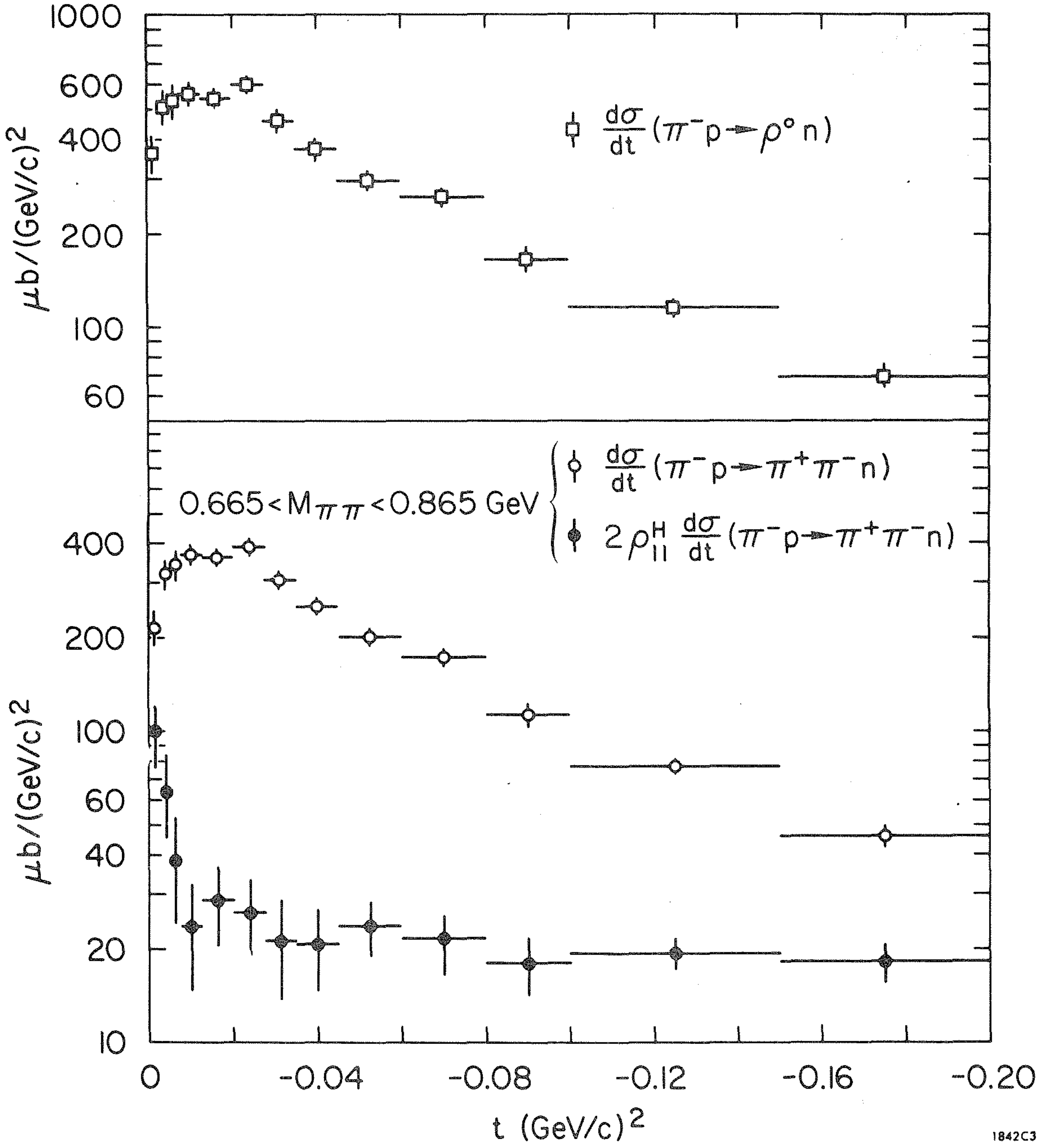

Figure 4: The total and transverse differential cross sections (helicity frame) as a function of momentum transfer for $\pi^- p \to \pi^+\pi^- n$, $0.665 < M_{\pi\pi} < 0.865$ GeV and the total cross section for $\pi^- p \to \rho^0 n$. The error bars indicate the statistical errors.

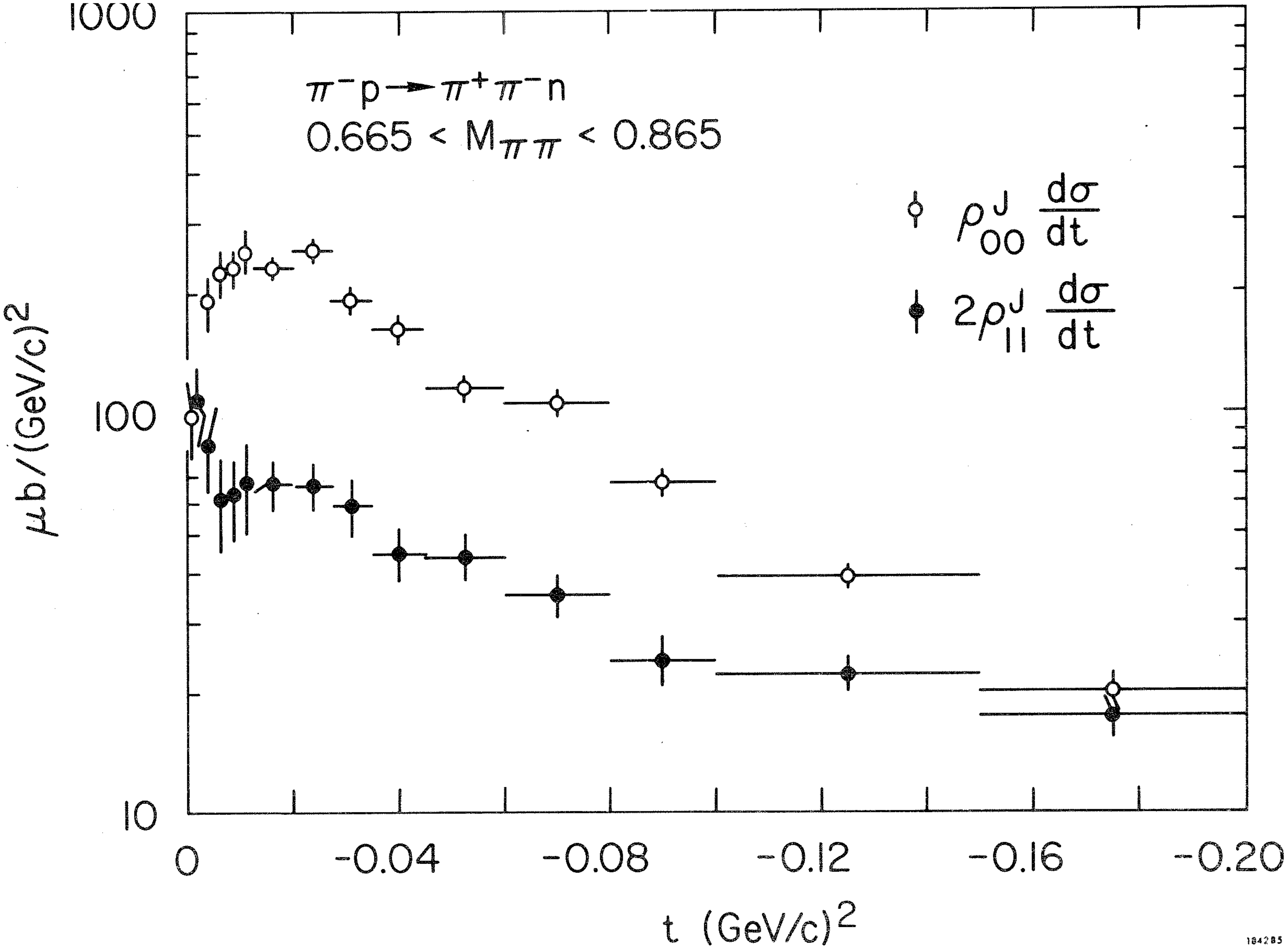

Figure 5: The longitudinal and transverse differential cross sections in the Jackson frame for $\pi^- p \rightarrow \pi^+ \pi^- n$, $0.665 < M_{\pi\pi} < 0.865$ GeV.

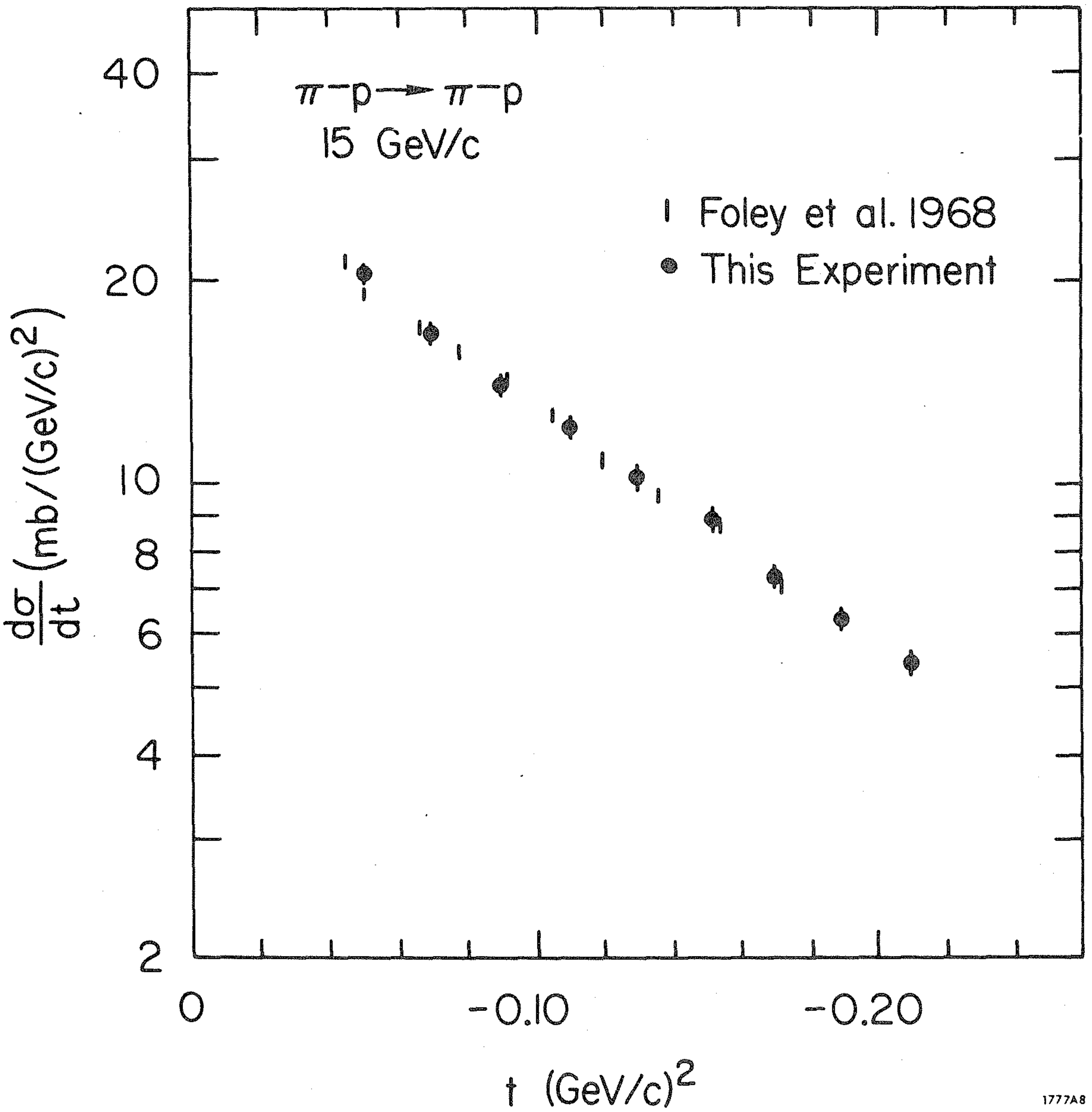

Figure 6: A comparison of $d\sigma/dt$ ($\pi^- p \to \pi^- p$) as measured in this experiment with the measurements of Foley et al.[12]

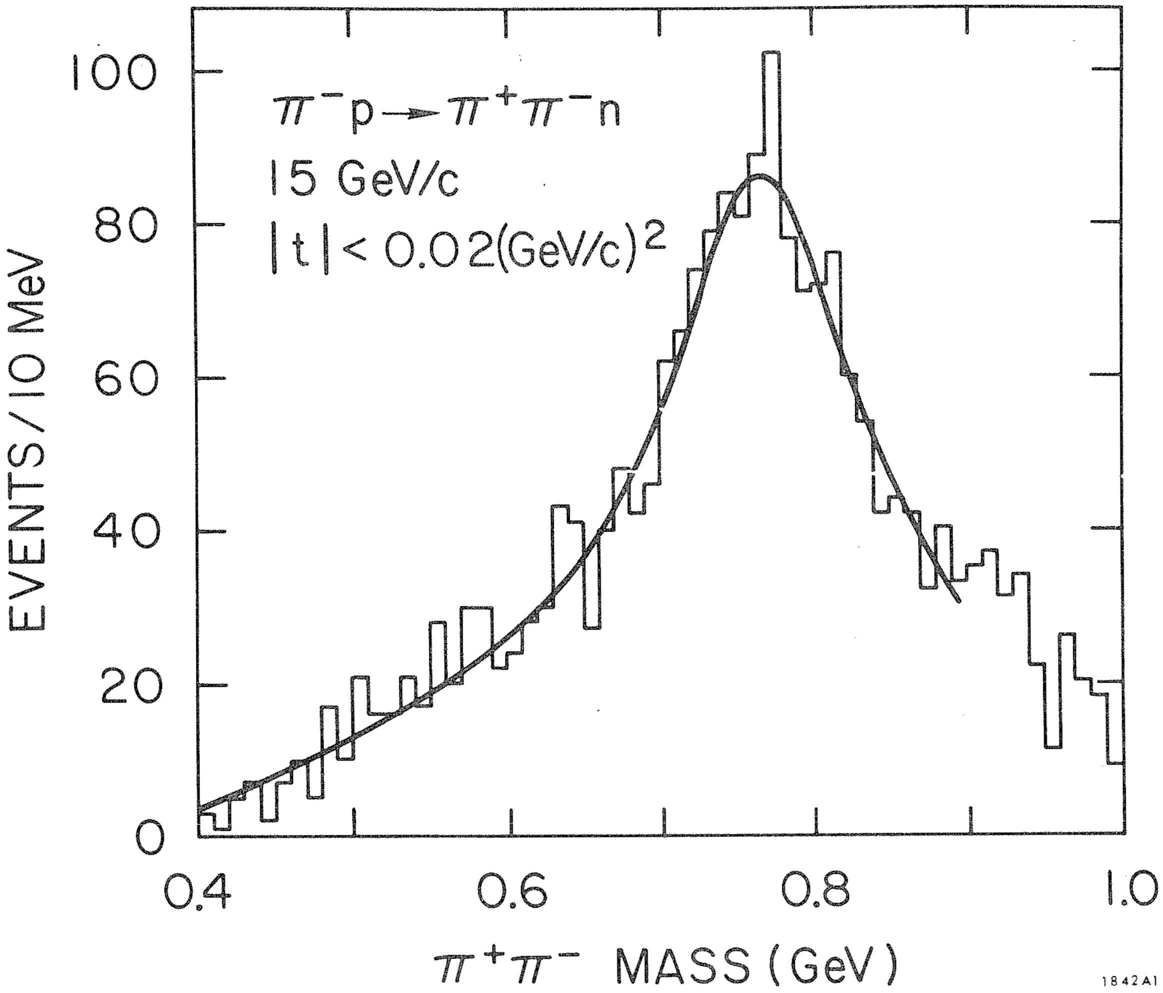

Figure 7: The observed $\pi^+\pi^-$ mass spectrum for $|t| < 0.02$ (GeV/c)^2. The curve represents the fit described in the text, after it has been folded with the acceptance.

Paper B

A COMPARISON OF $\pi^- p \rightarrow \rho^o n$ WITH SINGLE PION PHOTOPRODUCTION AT 15 GeV/c [*]

F. Bulos, R. K. Carnegie, G. E. Fischer, E. E. Kluge,
D.W.G.S. Leith, H. L. Lynch, B. Ratcliff, B. Richter,
H. H. Williams, and S. H. Williams

Stanford Linear Accelerator Center
Stanford University, Stanford, California 94305

ABSTRACT

We present a comparison of new data on $\pi^- p \rightarrow \rho^o n$ at 15 GeV/c with polarized and unpolarized single pion photoproduction data. Particular emphasis is placed upon the behavior of the differential cross sections and asymmetries in the forward direction, $(-t < m_\pi^2)$.

---

[*] Work supported by the U. S. Atomic Energy Commission.

Studies of single pion photoproduction at SLAC[1] and DESY[2] have shown a sharp increase in the differential cross section, $d\sigma/dt$, for momentum transfers to the nucleon $-t < m_\pi^2$, over a large energy range. In addition, experiments with linearly polarized photons have shown that the asymmetry parameter, which is zero in the forward direction, rises rapidly to unity[3] at $-t \approx m_\pi^2$. Single pion photoproduction is related to the reaction

$$\pi^- p \to \rho^0 n \qquad (1)$$

through the vector dominance model (VDM).[4] Since the small t behavior of the photoproduction processes is so striking, it is important to look for similar structure in the forward direction in reaction (1). Furthermore, this reaction is interesting from the point of view of exchange models which also make predictions concerning forward structure in $\pi^- p \to \rho^0 n$. The strong cut absorption model[5] shows a sharp peak in the transverse cross section for momentum transfers less than m_π^2. In contrast, the one pion exchange model requires that the cross section should vanish in the forward direction, whereas Avni and Harari[6] have predicted no pronounced structure in the transverse cross section. Although previous comparisons of $\pi^- p \to \rho^0 n$ with single pion photoproduction have been published,[7] the new data presented in the previous letter[8] allow this comparison to be made in the small t region ($-t < m_\pi^2$) for the first time.

In the preceding letter we presented the differential cross sections and density matrix elements for the reaction $\pi^- p \to \pi^+ \pi^- n$ at an incident beam momentum of 15 GeV/c. The density matrix elements for the ρ^0 in the helicity frame are shown in Fig. 1. They have been obtained from the dipion density matrix elements described in Ref. 8 by imposing the normalization condition $2\rho_{11} + \rho_{00} = 1$. The S-wave cross section was assumed to be of the form

$$\frac{d\sigma}{dt}(\text{S-wave}) = B \, \frac{|t|}{(t - m_\pi^2)^2} \, e^{7t}$$

as obtained from the data of Sonderegger and Bonamy[9] for the reaction $\pi^- p \to \pi^0 \pi^0 n$ and extrapolated to 15 GeV/c. The behavior of the ρ^0 density matrix elements for small t does not depend strongly on the assumed t dependence of the S-wave background.[8]

The VDM directly relates the reaction $\gamma N \to \pi N$, to the reaction, $\pi^- p \to V^0 n$, where N is the nucleon and V^0 is a mixture of ρ^0, ω, and ϕ. Since the coupling of the ϕ to nonstrange mesons is small, we can neglect its contribution in the direct term and in ω-ϕ interference. The VDM then predicts[4]

$$\frac{1}{2}\left[\frac{d\sigma}{dt}(\gamma p \to \pi^+ n) + \frac{d\sigma}{dt}(\gamma n \to \pi^- p)\right] = \frac{\pi\alpha}{\gamma_\rho^2}\left[\rho_{11}\right]_\rho \frac{d\sigma}{dt}(\pi^- p \to \rho^0 n) + \frac{\pi\alpha}{\gamma_\omega^2}\left[\rho_{11}\right]_\omega \frac{d\sigma}{dt}(\pi^- p \to \omega n) \tag{2}$$

where $[\rho_{11}]_\rho \left([\rho_{11}]_\omega\right)$ is the density matrix element which projects out the transversely polarized ρ^0 (ω) mesons. We take the sum of the photoproduction cross sections to cancel ρ-ω and ρ-ϕ interference effects. The photon-vector-meson coupling constants have been measured[10] to be in the ratio $(1/\gamma_\rho^2):(1/\gamma_\omega^2) = (7.51 \pm 1.52):1$ and $(d\sigma/dt)\ (\pi^- p \to \rho^0 n):(d\sigma/dt)(\pi^- p \to \omega n)$ is approximately 10:1 in the forward direction at 8 GeV.[11] Assuming that this ratio does not change greatly at 15 GeV/c, the second term in Eq. (2) contributes only a few percent compared with the ρ^0 term and can be ignored. Equation (2) then becomes

$$\frac{(1+R)}{2}\frac{d\sigma}{dt}(\gamma p \to \pi^+ n) = \frac{\pi\alpha}{\gamma_\rho^2}\rho_{11}^H \frac{d\sigma}{dt}(\pi^- p \to \rho^0 n) , \tag{3}$$

where

$$R = \frac{d\sigma}{dt}(\gamma n \to \pi^- p) \Big/ \frac{d\sigma}{dt}(\gamma p \to \pi^+ n)$$

is taken from the π^-/π^+ ratio on deuterium.[1] For the comparisons in this paper, we take $\gamma_\rho^2/4\pi = 0.50$.[10]

It is also possible to extract the components of linear polarization for the ρ^0 which may be compared with the photoproduction data obtained with linearly polarized photons. The VDM predicts[4]

$$\frac{1}{2}\left[\frac{d\sigma_\perp}{dt}(\gamma n \to \pi^- p) + \frac{d\sigma_\perp}{dt}(\gamma p \to \pi^+ n)\right] = \frac{\pi\alpha}{\gamma_\rho^2}\left(\rho^H_{11} + \rho^H_{1-1}\right)\frac{d\sigma}{dt}(\pi^- p \to \rho^o n) \tag{4}$$

$$\frac{1}{2}\left[\frac{d\sigma_\parallel}{dt}(\gamma n \to \pi^- p) + \frac{d\sigma_\parallel}{dt}(\gamma p \to \pi^+ n)\right] = \frac{\pi\alpha}{\gamma_\rho^2}\left(\rho^H_{11} - \rho^H_{1-1}\right)\frac{d\sigma}{dt}(\pi^- p \to \rho^o n) \tag{5}$$

where $\sigma_\perp (\sigma_\parallel)$ denotes the cross section $d\sigma/dt$ for pions produced in a plane perpendicular (parallel) to the electric vector of the photon, and where we have neglected the small contribution of the other vector mesons as before. Equations (4) and (5) correspond to processes with natural and unnatural parity exchanged in the t-channel.[12] Equation (4) is invariant under rotations about the normal to the production plane, and is thus independent of certain frame ambiguities of the VDM which arise since the helicity of a massive particle is not Lorentz invariant.[13] Several theoretical arguments have been made,[14] however, which suggest that at high energies the helicity frame is the correct choice.

A consequence of Eqs. (4) and (5) is

$$\frac{\rho_{1-1}}{\rho_{11}} = \frac{A^+ + RA^-}{1+R} , \tag{6}$$

a comparison which is independent of the normalization of the two sets of data, and the value of the rho-photon coupling constant. The asymmetry parameters are defined by

$$A^\pm = \frac{\sigma_\perp^\pm - \sigma_\parallel^\pm}{\sigma_\perp^\pm + \sigma_\parallel^\pm}$$

where, for example, $\sigma_\perp^+$ is the cross section $d\sigma_\perp/dt$ for π^+ photoproduction.

In Figs. 2a,b,c and d the photoproduction data are compared to our results for reaction (1) using Eqs. (3), (4), (5), and (6) respectively. Since polarized photoproduction cross sections are not yet available at high energy, the photoproduction data shown in Figs. 2b-d were obtained by combining the asymmetry parameters $A^{\pm}$ measured at lower energies[3, 15] with the unpolarized cross sections and π^-/π^+ ratios at 16 GeV/c.[1]

The overall behavior in t of the data in Fig. 2a, b, c, d shows qualitative agreement, and indeed, the forward, t=0, cross sections are in good agreement. The transverse rho cross section (Fig. 2a) agrees rather well for larger t, but falls more sharply than the unpolarized photoproduction cross section for $-t < m_\pi^2$. Except for the forward point in Fig. 2b, the rho data fall a factor of two below the photoproduction data, but display similar shape. It is interesting to note in Fig. 2c the dramatic rise of the cross sections for $-t < m_\pi^2$, and the remarkable agreement between the rho production and photoproduction data. The asymmetry comparison, shown in Fig. 2d, shows good agreement for momentum transfers less than $2m_\pi^2$, but the asymmetry in the rho data falls more rapidly for larger t.

Cho and Sakurai[16] have extended the vector dominance model to predict the dominant longitudinal amplitude for reaction (1) in addition to the usual predictions of the transverse amplitudes. In Fig. 3 we show both the transverse and total rho cross sections. The dotted line is the input to the calculation of Cho and Sakurai based on the single pion photoproduction cross sections, while the solid line is their prediction for the total rho cross section. The agreement in the total cross section is good for $-t < 0.1\ (\mathrm{GeV}/c)^2$.

In drawing quantitative conclusions from Figs. 2 and 3, it should be noted that the errors shown are statistical only and do not include the contribution from the uncertainty in the S-wave normalization.[17]

In conclusion, our rho production results show structure similar to the single pion photoproduction data. The magnitudes of the forward cross section are the same and the existence of a sharp forward peak and the rapid change in the asymmetry are features present in both reactions. In detail, the unnatural parity exchange cross section agrees very well, as does the asymmetry for $-t < 2m_\pi^2$. However, elsewhere either in the sharpness of the structure or the absolute cross section, there are pronounced differences which may not be resolved by changes of scale (e.g., change in value of $\gamma_\rho^2/4\pi$). These differences indicate some inadequacy in the VDM description of the details for the rho production process.

REFERENCES

1. A. M. Boyarski et al., Phys. Rev. Letters 20, 300 (1968); A. M. Boyarski et al., Phys. Rev. Letters 21, 1767 (1968); and private communication.
2. P. Heide et al., Phys. Rev. Letters 21, 248 (1968).
3. H. Burfeindt et al., Phys. Letters 33B, 509 (1970); C. Geweniger et al., Phys. Letters 29B, 41 (1969); H. Burfeindt et al., 1969 International Symposium on Electron and Photon Interactions at High Energies, Daresbury, England (Abstract 86).
4. J. J. Sakurai, Ann. Phys. (N.Y.) 11, 1 (1960) and Proc. of Int. School of Physics (Academic Press, New York, 1963), p. 41; D. S. Beder, Phys. Rev. 149, 1203 (1966); H. Joos, Acta Physica Austriaca, Suppl. IV (1967); C. Iso and H. Yoshii, Ann. Phys. (N.Y.) 47, 424 (1968); M. Krammer and D. Schildknecht, Nucl. Phys. B7, 583 (1968).
5. F. Henyey et al., Phys. Rev. 182, 1579 (1969).
6. Y. Avni and H. Harari, Phys. Rev. Letters 23, 262 (1969).
7. R. Diebold and J. A. Poirier, Phys. Rev. Letters 20, 1532 (1968); I. Derado and Z.G.T. Guiragossian, Phys. Rev. Letters 21, 1556 (1968); R. Diebold and J. A. Poirier Phys. Rev. Letters 22, 255 (1969) and 22, 906 (1969).

8. F. Bulos et al., preceding article (A).

9. P. Sonderegger and P. Bonamy, Lund International Conference on Elementary Particles (Abstract 372) June 25 - July 1, 1969.
10. J. E. Augustin et al., Phys. Letters 28B, 503 (1969).
11. J. F. Allard et al., Nuovo Cimento 50A, 106 (1967).
12. P. Stichel, Zeitschrift f. Phys. 180, 170 (1964); G. Cohen-Tannoudji and Ph. Salin, Nuovo Cimento 55A, 412 (1968); J. P. Ader et al., Nuovo Cimento 56A, 952 (1968).
13. A. Bialas and K. Zalewski, Phys. Letters 28B, 436 (1969).
14. H. Fraas and D. Schildknecht, DESY Preprint 68/4 (1968); C. F. Cho and J. J. Sakurai, Phys. Letters 30B, 119 (1969); M. LeBellac and G. Plaut, Nuovo Cimento 64A, 95 (1969).
15. Recent measurements of A^+ at 12 GeV/c are consistent with the values at 3.4 GeV/c; S. Ecklund, private communication. A^- has not been measured at small values of momentum transfer ($-t < m_\pi^2$), so we assume that $A^- = A^+$.
16. C. F. Cho and J. J. Sakurai, Phys. Rev. D2, 517 (1970), and private communication.
17. For example, a 30% decrease in the S-wave cross section would result in a 30% increase in the transverse rho cross section for the interval $0.1 < \sqrt{-t} < 0.2$, the most sensitive region. For the limits on ρ_{11}, see Ref. 8.

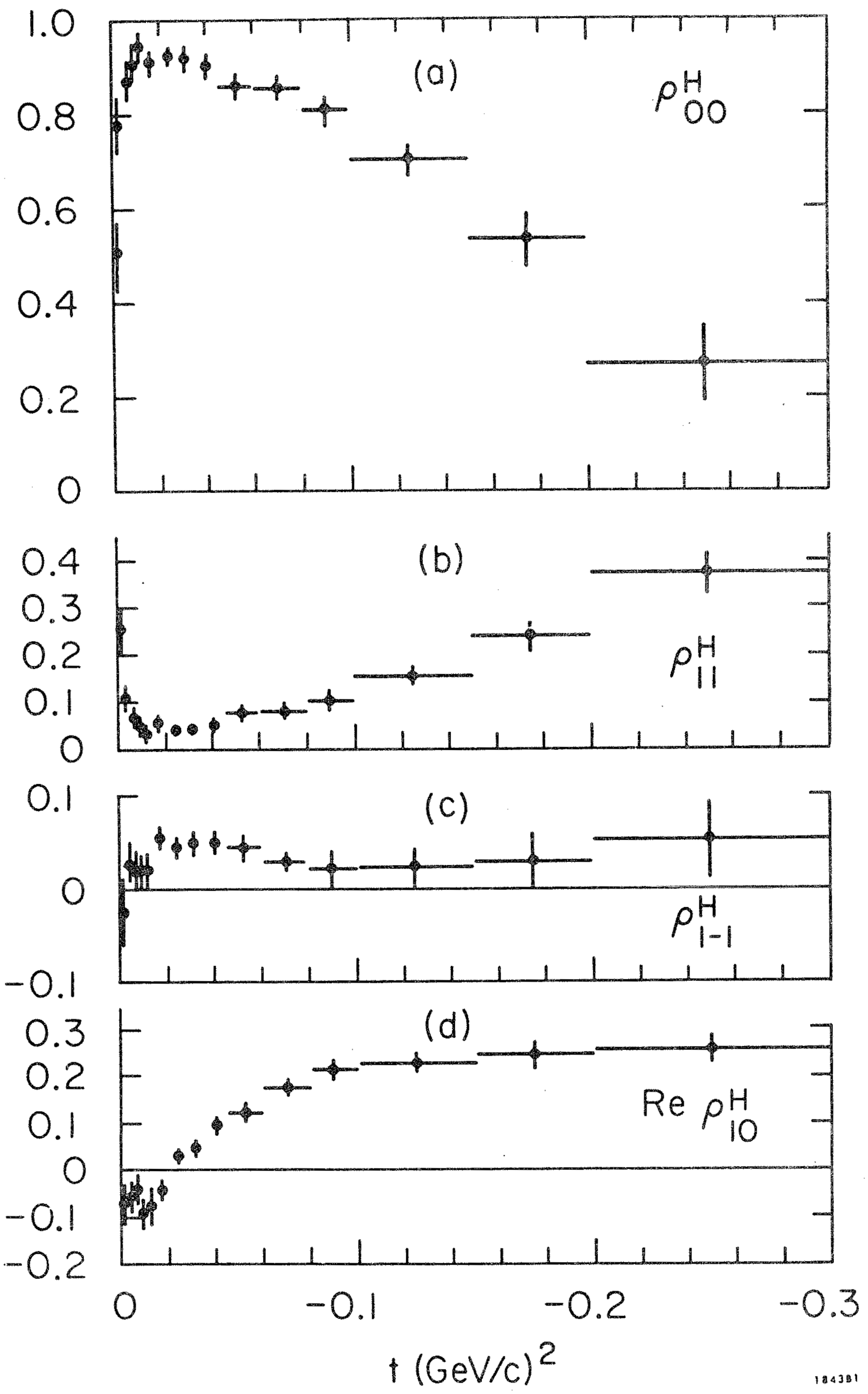

Figure 1: The spin density matrix elements in the helicity frame for the ρ^0 with the normalization $2\rho_{11} + \rho_{00} = 1$. The data are obtained from Ref. 8.

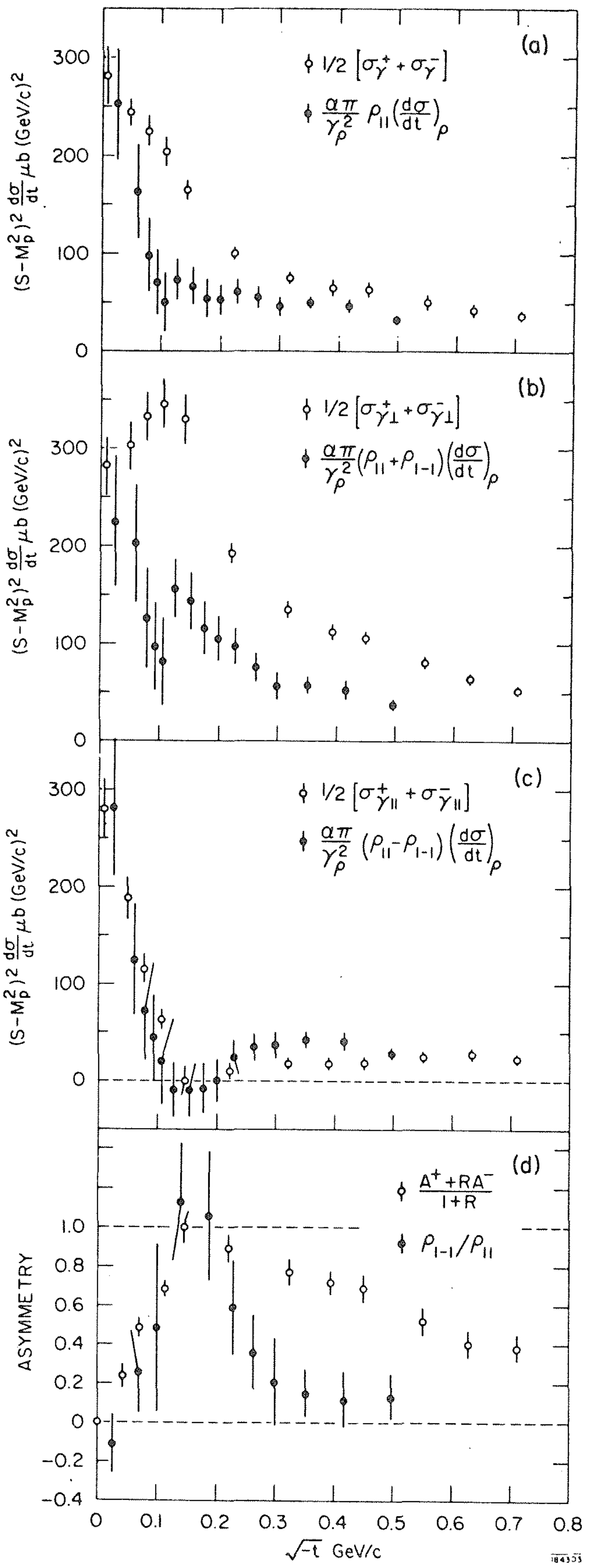

Figure 2: Differential cross sections and asymmetries for single pion photoproduction and rho production in $\pi^- p \to \rho^0 n$, $(d\sigma/dt)_\rho$:

(a) the unpolarized cross section (see Eq. (3) of text);
(b) The natural parity cross section (see Eq. (4) of text);
(c) the unnatural parity cross section (see Eq. (5) of text);
(d) the asymmetry (see Eq. (6) of text).

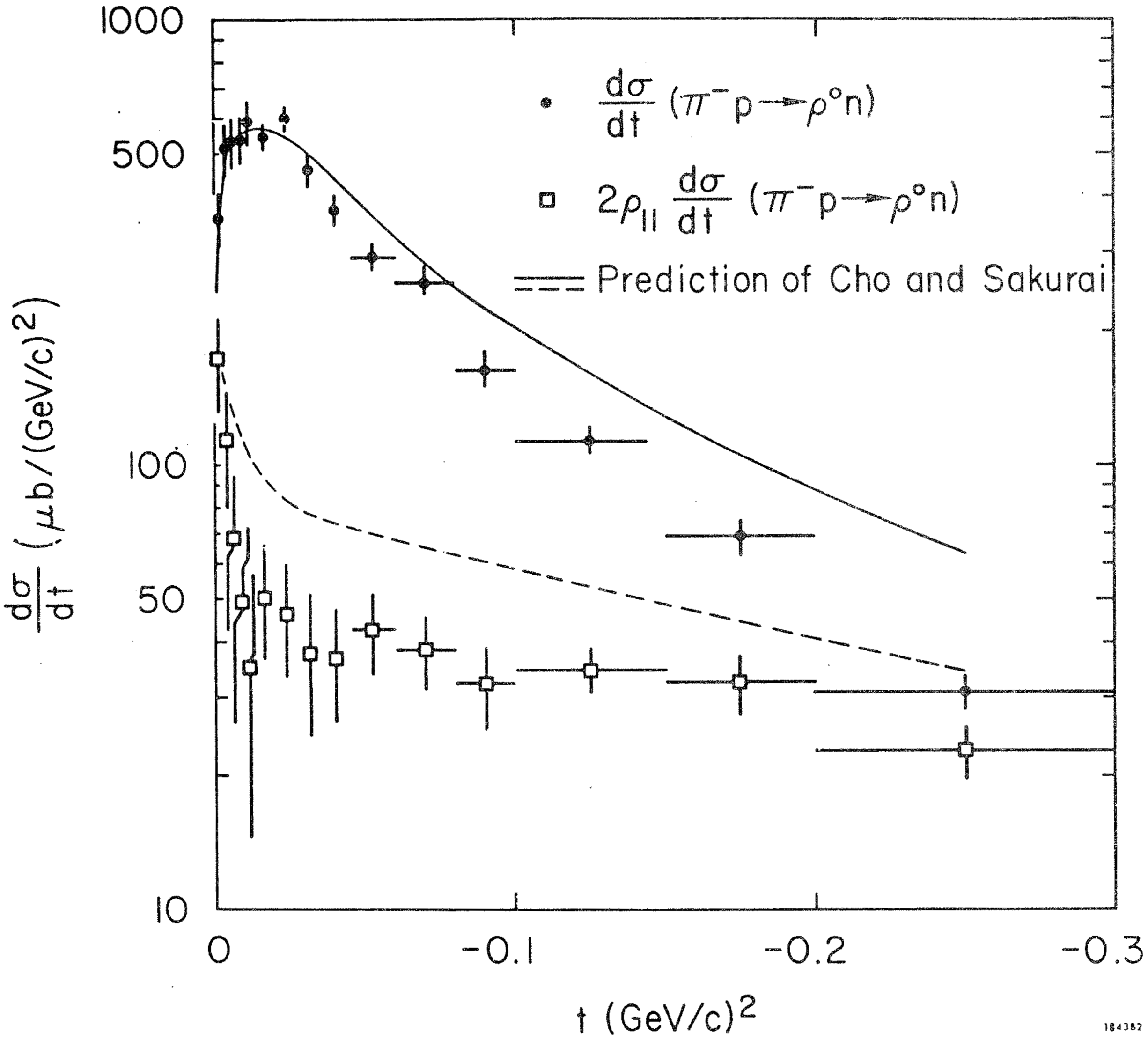

Figure 3: Differential cross sections $d\sigma/dt$ and $2\rho_{11}(d\sigma/dt)$ for $\pi^- p \rightarrow \rho^0 n$ at 15 GeV. The solid line represents the prediction of Cho and Sakurai,[16] and the dotted line represents the input to their calculation.

Paper C

COMPARISON OF ABSORPTIVE ONE PION EXCHANGE MODEL WITH MEASUREMENTS OF $\pi^- p \rightarrow \pi^+\pi^- n$ [*]

P. Baillon, F. Bulos, R. K. Carnegie, G. E. Fischer,
E. E. Kluge, D.W.G.S. Leith, H. L. Lynch,
B. Ratcliff, B. Richter, H. H. Williams, and S. Williams

Stanford Linear Accelerator Center
Stanford University, Stanford, California 94305

ABSTRACT

The results of a wire spark chamber experiment studying the reaction $\pi^- p \rightarrow \pi^+\pi^- n$ at 15 GeV/c are compared with the predictions of the absorptive one pion exchange model. The rich structure at small values of momentum transfer observed in the data is well described by the model.

---

[*] Work supported by the U. S. Atomic Energy Commission.

The absorptive one pion exchange model[1,2] (OPEA) makes some particular predictions for the small momentum transfer behavior of the reaction $\pi^- p \to \pi^+ \pi^- n$, quite different from that of the elementary one pion exchange model[3,4] (OPE) or form factor modified[5,6,7] OPE models. Specifically, a sharp rise is predicted in the forward differential cross-section for transversely polarized rho mesons; this is also expected in the vector dominance model[8] (VDM). Furthermore, it has been pointed out[2], that the behavior of $\pi^- p \to \pi^+ \pi^- n$ should be dominated at small momentum transfers by the propagator of the exchanged particle and by the minimal t-dependence required by angular momentum conservation. Any other t dependence is expected to be smooth and slowly varying. It is then possible to make very definitive predictions about the structure of the dipion matrix elements and the differential cross-section for $-t < m_\pi^2$. In the special parameterization of P.K. Williams[9] the prediction of the model for the small t behavior of the density matrix elements enable us to make a detailed comparison with our measurements of the reaction $\pi^- p \to \pi^+ \pi^- n$.

A detailed study of the reaction $\pi N \to \pi\pi N$ at small t is of further interest, because this process can in principle yield information on the elastic $\pi\pi$ cross section by extrapolating to the pion pole. However, the Chew-Low[4] method does not give a recipe for the extrapolation, and consequently a model is needed either to select a suitable variable, expected to be a smooth function of t, or even to prescribe a certain t dependence.

Lately the absorption model, as suggested by Kane and Ross[10], has been used by Chan et al.[11] to obtain the extrapolated $\pi\pi$ cross-section. Since the model makes some striking predictions for the momentum transfer region $-m_\pi^2 \leq -t \leq m_\pi^2$, it is important to test the model in the physical region.

We have studied the reaction $\pi^- p \rightarrow \pi^+\pi^- n$ at 15 GeV using a wire spark chamber spectrometer at SLAC. In a recent publication[12] we have presented the results of our experiment on the $\pi^+\pi^-$ differential cross-section and density matrix elements. In this report we are comparing the data with the predictions of the absorption model.

A pronounced structure of the density matrix elements in the helicity (H) or Gottfried-Jackson (GJ) reference frame[13] for small values of -t is expected in the absorption model. Below we list a number of predictions for the small t region given by M. Ross et al.[17]. Prior to this experiment they have not been verified.

(1) ρ_{11}^{GJ} and $\rho_{11}^{H} d\sigma/dt$ will have sharp forward peaks

(2) ρ_{00}^{GJ} and $d\sigma/dt$ will have forward turnovers

(3) $\rho_{11}^{GJ} d\sigma/dt$ will have no structure

(4) $\rho_{1-1}^{H}/\rho_{11}^{H}$ behaves like $-t/m_\pi^2$

(5) $\rho_{1-1}^{GJ} \approx 0$

In Figs. 1 and 2a we present our measurements of the above quantities in the momentum transfer interval $0 \leq -t \leq .15$ GeV^2 for the dipion mass region $.665 \leq m_{\pi\pi} \leq .865$ GeV. In the presence of S-wave, it is not possible to determine directly the longitudinal (i.e. ρ_{00}) and transverse (i.e. $2\rho_{11}$) fraction of the ρ meson and hence the density matrix elements shown have been obtained by using additional information on the S-wave background, as discussed previously[12]. Our matrix elements are normalized such that $\rho_{00} + 2\rho_{11} + \rho_{00}^S = 1$, where ρ_{00}^S is the relative amount of S-wave.

Our results confirm all 5 qualitative predictions listed above; we proceed to make a more quantitative comparison between our data and the absorption model. We use the parameterization of P.K. Williams[9], who predicts the magnitude and momentum transfer dependence of the pure rho density matrix elements. However, the measureable dipion matrix elements depend on the interference with the S-wave; the amount of S-wave and its relative phase are free parameters. In the context of this model the helicity amplitudes are assumed to possess a common t dependence characterized by a form factor in addition to their individual dependence of $(-t)^{n/2}$ required by angular momentum conservation, where n is the net helicity change.[17] The form factor is supposed to represent the collimating effect of absorption and in the case under discussion is chosen to be of the form[9] $\exp(A(t-m_\pi^2))$. By retaining only the nucleon helicity flip contribution and evaluating the amplitudes at the pion pole, the subsequent relations can be obtained:[9]

$$d^2\sigma/dtdm_{\pi\pi}^2 = \frac{\gamma(m_{\pi\pi})}{s^2(t-m_\pi^2)^2} \; \xi(t) \; \exp(2A(t-m_\pi^2))$$

$$\text{with} \quad \xi(t) = 1 + (\tfrac{1}{2}x + \epsilon)\delta + \delta^2$$

$$\rho_{00}-\rho_{11} = \tfrac{1}{2}(x\delta - \delta^2 - 1)/\xi(t)$$

$$\rho_{1-1} = \delta/\xi(t)$$

$$\text{Re}\;\rho_{10} = \tfrac{1}{2}(\tfrac{1}{2}x\delta)^{1/2}\;(\delta-1)/\xi(t)$$

$$\text{Re}\;\rho_{0S} = \cos(\phi)\delta\;\;(\tfrac{1}{2}x\;\epsilon)^{1/2}/\xi(t)$$

$$\text{Re}\;\rho_{1S} = \cos(\phi)\tfrac{1}{2}(\delta-1)(\delta\epsilon)^{1/2}/\xi(t)$$

$$\text{where} \quad \delta = -t/m_\pi^2 \; .$$

The parameter x is related to the ratio of longitudinal to transverse rhos and assumes in P.K. Williams' model the value $x = (m_{\pi\pi}/m_\pi)^2$. The square of the total CMS energy for $\pi N \to \pi\pi N$ is denoted by s.

The parameters to be fitted are $\cos\phi$, ϵ, A, and γ, where γ is the average value of $\gamma(m)$ in our mass interval. Note that $\rho_{00}-\rho_{11}$, ρ_{1-1} and Re ρ_{10} depend only on one free parameter, ϵ. In addition, this dependence is quite weak, since ϵ, a parameter describing the amount of S-wave background, is small compared to x. The interference terms of S and P wave, Re ρ_{0S} and Re ρ_{1S}, are scaled by $\cos\phi$, an S-P mixing parameter. The magnitude of $d\sigma/dt$ is given by γ, whereas its slope is determined by the parameter A.

The resulting best fit is shown in Fig. 2 together with our measurement of $d\sigma/dt$ and the density matrix elements in the helicity system.

Since our sample of events from the reaction $\pi^- p \to \pi^+\pi^- n$ contains a $(12 \pm 2)\%$ contamination from $\pi^- p \to \pi^+\pi^-\Delta^0$, as discussed in Ref. 12, the actual fit shown in Fig. 2 was obtained allowing for a fixed non spin flip contribution of this size. The parameters for the non flip amplitudes were obtained from a study of our $\pi^+\pi^-\Delta^0$ events.

We are able to obtain a satisfactory fit to the data with a χ^2 of 65 for 73 degrees of freedom in which the rich structure observed in the data is well described by the model. Specifically the change of sign of Re ρ_{10} and Re ρ_{1S} at $-t = m_\pi^2$ in the data is a simple consequence of the assumed t-dependence and the requirement of parity conservation for the amplitudes at the pion pole[9]. Similar structure for Re ρ_{10} is expected in the model of Cho and Sakurai[14], who use the vector dominance model to derive the prediction.

The fit was performed in a restricted momentum transfer region only, $0 \leq -t \leq .15$ GeV^2, since the model is not expected to describe the data adequately for larger values of -t. We obtain the following results for the free parameters: $\phi = 0 \pm 0.2$, $\epsilon = 1.8 \pm 0.1$, $\gamma = 145 \pm 7$ and $A = 5.0 \pm 0.3$. We also tried a fit by varying x, which describes the ratio of longitudinal to transverse rhos. The resulting x is, within its error, compatible with the value given in the model[9], $x = (m_{\pi\pi}/m_\pi)^2$, where $m_{\pi\pi}$ was chosen to be the weighted average dipion mass in our interval.

As was pointed out above, the density matrix elements ρ_{00} and ρ_{11} cannot be measured directly, but have to be determined by making assumptions on the S-wave background. This model fit gives a determination of $d\sigma/dt$ for the S-wave, which is in good agreement with the one used in Ref. 12.

Having determined the free parameters of P.K. Williams' model, we can calculate the on shell $\pi\pi$ cross-section $\sigma_{\pi\pi}$ as an additional check on the results.

$$\sigma_{\pi\pi} = \frac{\pi(4M^2 \; P_L^2/s^2)}{(G^2/4\pi)m_\pi^2 \; P_1 \; m_{\pi\pi}} \; \gamma \; (1/2 \; x + \epsilon - 2)$$

where P_L is the laboratory momentum of the incident pion, $G^2/4\pi = 14.6$ is the π-N coupling constant, P_1 is the momentum of the outgoing pion in the $\pi\pi$ CMS and M is the proton mass. We obtain an average cross-section for the mass interval $.665 \leq m_{\pi\pi} \leq .865$ GeV of $\sigma_{\pi\pi} = (85 \pm 15)$mb. By taking the observed form[12] of the $\pi\pi$ mass distribution into account we derive a $\pi\pi$ cross-section $\sigma_{\pi\pi} = (118 \pm 20)$mb at $m_{\pi\pi} = .765$ GeV.

It is important to note, that our data strongly indicate a nonzero forward cross-section for $\pi^- p \to \pi^+\pi^- n$. In contrast to our results it has been often assumed in Chew-Low extrapolations that the differential cross-section vanishes at $t = 0$. Our results therefore justify the proposed[9,10,15,16] use of nonevasive extrapolation methods to obtain the $\pi\pi$ cross-section.

To conclude, we have shown that the qualitative predictions of the absorptive one pion exchange model for the region of very small momentum transfer, $-t \leq m_\pi^2$, are in very good agreement with our experimental data. Furthermore, the special form of the model by P.K. Williams provides a good quantitative description of the density matrix elements and the differential cross-section out to larger values of t ($-t \lesssim 10 \; m_\pi^2$). The rich structure observed in the data can be explained in the absorption model by the minimum t dependence of $(-t)^{n/2}$ required by angular momentum conservation.

References

1. K. Gottfried and J. D. Jackson, Nuovo Cimento 34, 735 (1964).
2. F. Henyey et al., Phys. Rev. 182, 1579 (1969).
3. C. Goebel, Phys. Rev. Letters 1, 337 (1958).
4. G. F. Chew and F. E. Low, Phys. Rev. 113, 1640 (1959).
5. H. P. Dürr and H. Pilkuhn, Nuovo Cimento 40, 899 (1965).
6. J. Benecke and H. P. Dürr, Nuovo Cimento 56, 269 (1968).
7. G. Wolf, Phys. Rev. 182, 1538 (1969)
8. J. J. Sakurai, Ann. Phys. (N.Y.) 11, 1 (1960) and Proc. of Int. School of Physics (Academic Press, New York, 1963), p 41; D. S. Beder, Phys. Rev. 149, 1203 (1966).
9. P. K. Williams, Phys. Rev. D1, 1312 (1970).
10. G. L. Kane and M. Ross, Phys. Rev. 177, 2353 (1969).
11. L. Chan et al., Phys. Rev. D2, 583 (1970).
12. F. Bulos et al., **first article (A).**
13. K. Gottfried and J. D. Jackson, Nuovo Cimento 33, 309 (1964).
14. C. F. Cho and J. J. Sakurai, Phys. Rev. D2, 517 (1970).
15. C. D. Froggatt and D. Morgan, Phys. Rev. 187, 2044 (1969).
16. J. D. Kimel, Phys. Rev. D2, 862 (1970).
17. M. Ross et al., Nucl. Physics B23, 269 (1970).

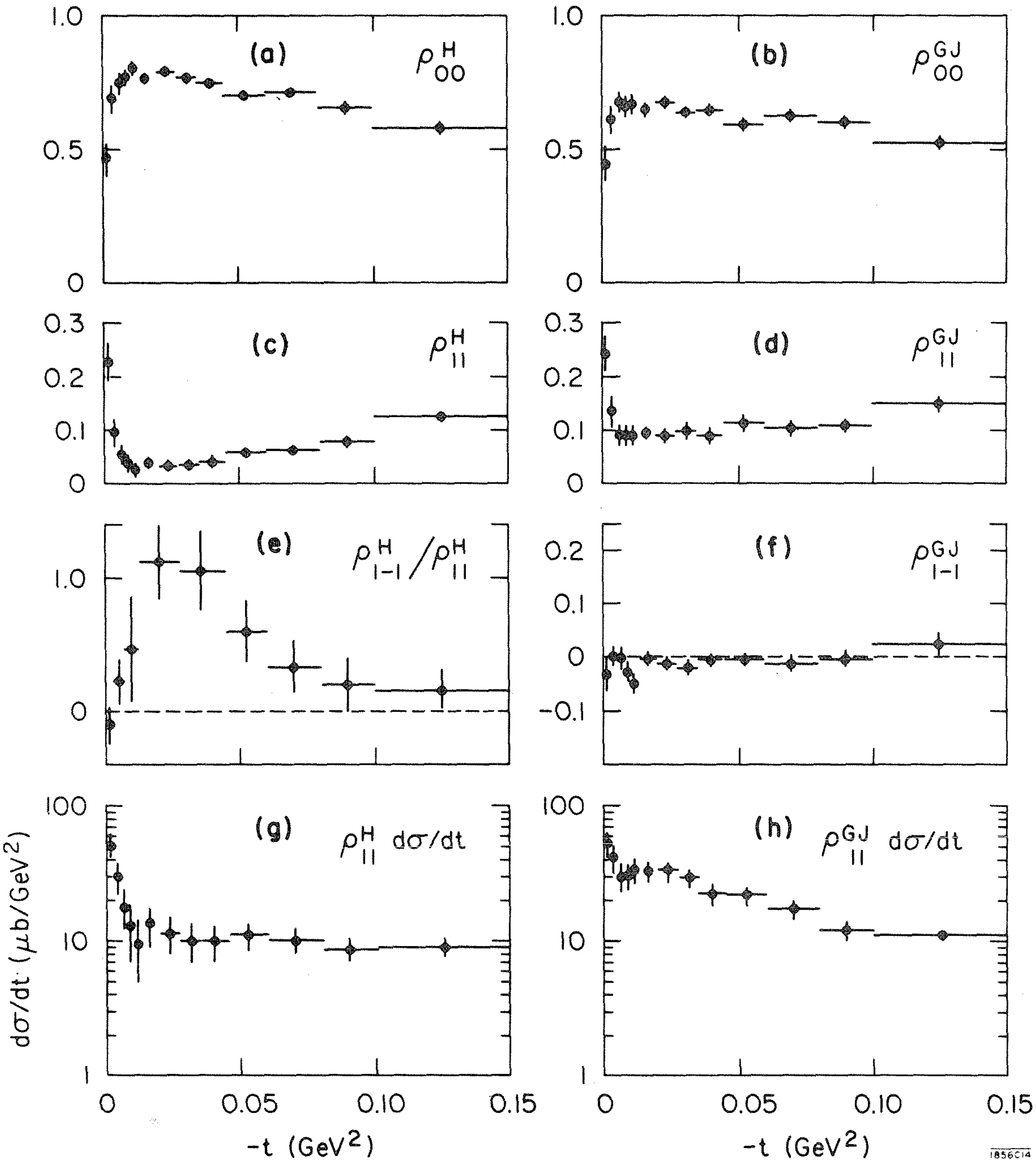

Figure 1: Density matrix elements expected to exhibit particular behavior for $-t < m_\pi^2$ in the helicity (H) and Gottfried-Jackson (GJ) frames as a function of momentum transfer for $\pi^- p \rightarrow \pi^+\pi^- n$ in the dipion mass interval $0.665 \leq m_{\pi\pi} \leq 0.865$ GeV. (a) ρ^H_{00}, (b) ρ^{GJ}_{00}, (c) ρ^H_{11}, (d) ρ^{GJ}_{11}, (e) ρ^H_{1-1}/ρ^H_{11}, (f) ρ^{GJ}_{1-1}, (g) ρ^H_{11} dσ/dt, (h) ρ^{GJ}_{11} dσ/dt.

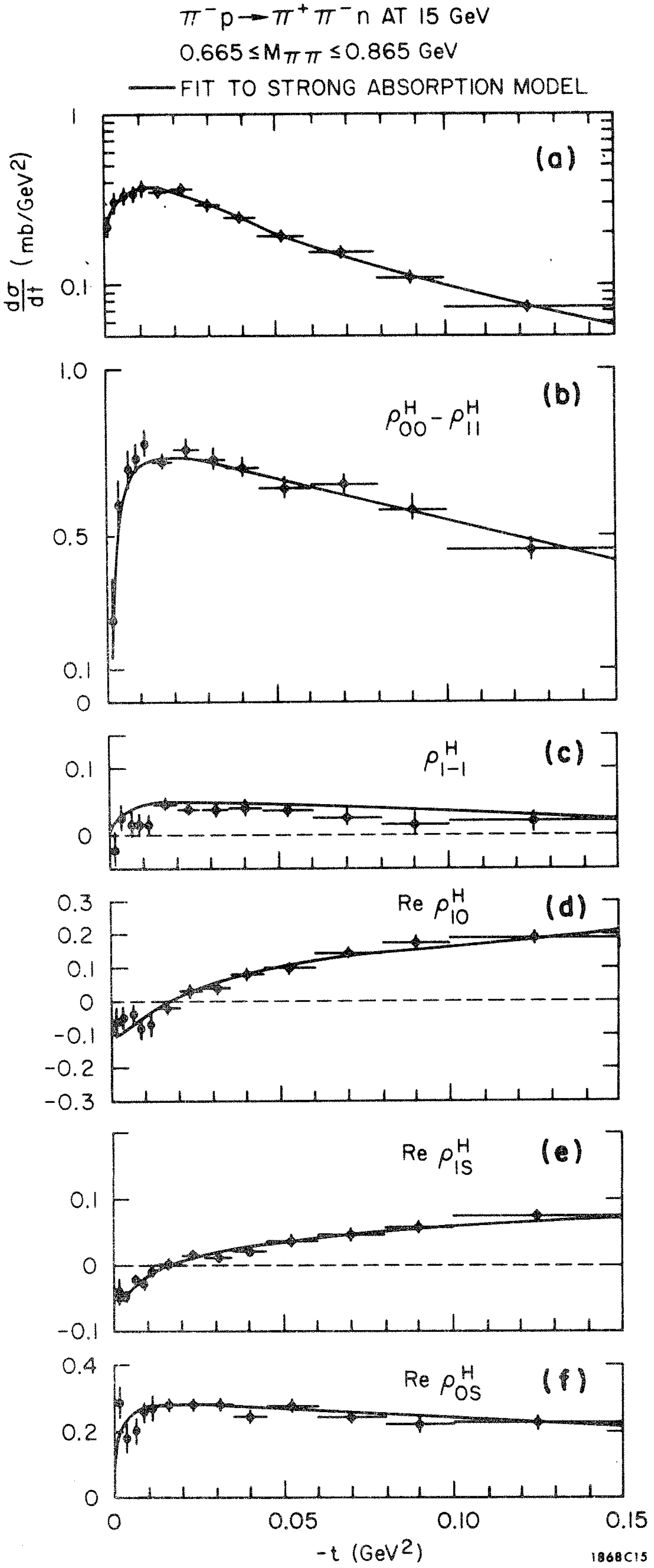

Figure 2: The differential cross section, $d\sigma/dt$, and density matrix elements in the helicity frame for $\pi^- p \to \pi^+\pi^- n$ with $0.665 \le m_{\pi\pi} \le 0.865$ GeV as a function of t. The solid line represents a fit to the absorption model in the parameterization of P. K. Williams with additional terms allowing for a small non-spin-flip background.

(a) $d\sigma/dt$,
(b) $\rho^H_{00} - \rho^H_{11}$,
(c) ρ^H_{1-1},
(d) Re ρ^H_{10},
(e) Re ρ^H_{1S},
(f) Re ρ^H_{0S}.

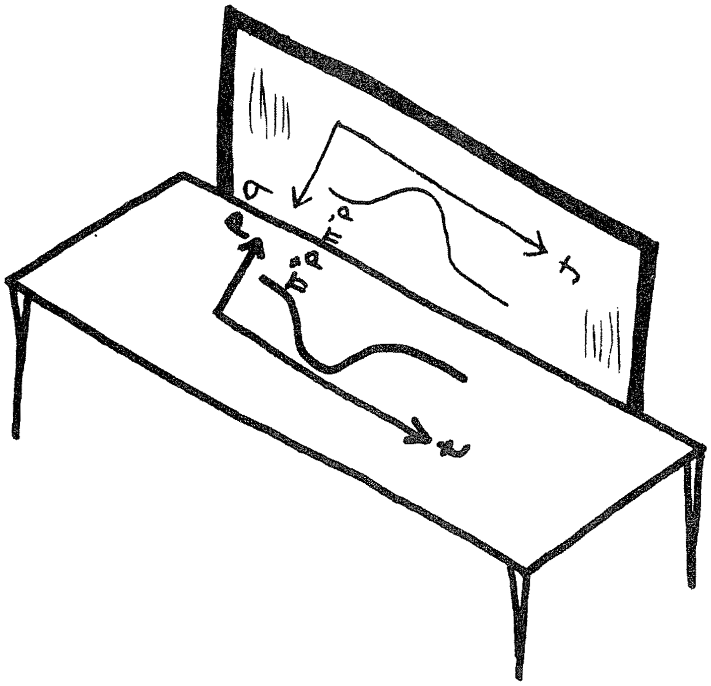

Mirror, mirror on the wall,
which is the loveliest theory
of them all?

SOME NEW EXPERIMENTAL RESULTS WITH POLARIZED TARGETS--I*

L. Dick

CERN, Geneva, Switzerland

---

* Report on Experiments by the CERN-ORSAY-PISA Collaboration.

We present here the final results of an experiment performed at CERN proton synchrotron by a CERN-ORSAY-PISA Collaboration. We have measured the recoil proton polarization in $\pi^{\pm}$, $K^{\pm}$, p and $\bar{p}$ elastic scattering by using a polarized target. Incident momenta were 6, 10, 14 and 17.5 GeV/c and the absolute value of the momentum transfer ranged from $|t| = 0.1$ to $|t| = 2.7$ $(\text{GeV/c})^2$. Preliminary results have already been published for 6, 10 and 14 GeV/c $^{1)}$.

The experimental set-up is rather standard, with the following important features:

a) We used an unseparated high intensity beam containing between 4×10^6 and 20×10^6 particles per PS burst.

b) The polarized target was made of butanol doped with porphyrexide. The first part of the experiment was performed with an average proton polarization of 35% at a target temperature of 1° K whereas the other part used a He^3 refrigerator giving a temperature of 0.5° K and a polarization of 65%.

c) Particle coordinates were recorded by means of a large set of 600 scintillation counter hodoscopes.

d) The data acquisition system was linked to an IBM 360/44 computer performing on-line geometrical and kinematical reconstruction of each event. We have recorded data at a rate up to 500 events in a burst.

e) 6 threshold Čerenkov counters identified the incident and scattered particles. The average contamination of rare events ($K^{\pm}$, $\bar{p}$ scatterings) never exceeds 5%.

Elastically scattered events were separated from the background by plots of coplanarity, angular correlation and interaction point in the target along the beam line. By comparing the tails of such distributions outside the elastic peak for positive and negative target polarization a normalization factor between the two sets of runs was obtained.

The background which still remains under the elastic peak has been evaluated in two different ways: the first used a polynomial fit adjusted to the tails of the spectra and extrapolated under the elastic peak. The second way was to measure this background using a dummy target having the same composition as the true target, except for the absence of hydrogen.

Our final results are presented in the figures. The π^+p and π^-p (fig. 1, 2, 3) elastic scattering data are nearly mirror-symetric up to 2 $(GeV/c)^2$ and display a minimum around $|t| = 0.6$ $(GeV/c)^2$ which has been seen in previous experiments 2). This minimum is commonly interpreted as being due to a vanishing ρ-meson Regge exchange amplitude at $|t| = 0.6$ $(GeV/c)^2$. The behaviour of P_o $(\pi^{\pm}p)$ in the range $0.6 \leq |t| \leq 1.8$ $(GeV/c)^2$ is believed to be dominated by a ρ-P' interference. The polarization seems to be slowly varying function of the incident momentum, and only very elaborate Regge models are able to reproduce the detailed trend of these data 3).

K^+p and K^-p polarization (fig. 4, 5, 6) are both seen to be positive up to $|t| = 0.9$ $(GeV/c)^2$. The K^+p data do not show any structure whereas the corresponding K^-p results show a change of sign around $|t| = 1.0$ $(GeV/c)^2$. There is a minimum in the differential cross section at the same t-value. This behaviour may be explained by assuming the exchange of the (ρ, A_2) and (P', ω) trajectories respectively, which lead to an approximate relation between the polarization parameters $P^+(P^-)$ respectively for $K^+(K^-)$ proton scattering.

$$P^- \cong P^+ \cos \pi\alpha$$

We are able to draw the following conclusions:

a) $P^- \leqslant P^+$ for $|t| < 1.0\ (\mathrm{GeV/c})^2$

and for $|t| = 0$ $P^- = 0$ and grows as $|t|^{3/2}$.

b) Around $|t| = 0.6\ (\mathrm{GeV/c})^2$ corresponding to $\alpha(t) = 0$ the polarization P^+ and P^- are equal $P^+ = P^-$.

c) P^- and P^+ have opposite signs for $|t|$ values bigger than $1.0\ (\mathrm{GeV/c})^2$.

Experimental results confirm these predictions:

P^- rises slowly from $t = 0$ but has the same order of magnitude as P^+ for $|t| = 0.6\ (\mathrm{GeV/c})^2$. The strong evidence for a change of sign for P^- confirm the opposite sign for P^+ and P^- at $|t| > 1\ (\mathrm{GeV/c})^2$.

The measurements of P_o in pp elastic scattering have a very good accuracy (fig. 7, 8, 9, 10). No significant structure appears for low values of the momentum transfer. But its amplitude seems to be strongly energy dependent, dropping from 14% at 6 GeV/c to some 5% at 17.5 GeV/c incident momentum.

For higher momentum transfers the polarization has a shallow minimum around $|t| = 0.8\ (\mathrm{GeV/c})^2$. At 10 GeV/c incident momentum, in the range of momentum transfer $1 < |t| < 2\ (\mathrm{GeV/c})^2$, the polarization exhibits a strong structure with a maximum at $|t| = 1.5\ (\mathrm{GeV/c})^2$.

This peak in polarization corresponds with the region where the pp differential cross section has a discontinuity in slope.

Associating this observed change of slope with a smeared out diffraction minimum implies that at this momentum transfer either the real part is significant or the flip contribution does not vanish or both are relevant. The strong polarization which we observed points to the latter possibility.

The $\bar{p}p$ results are given as an indication of the shape, although statistical errors are large (fig. 11). Nevertheless, for $|t|<0.4$ $(GeV/c)^2$ the polarization is very small and compatible with 0.

As a final remark, for small t, we observe a polarization close to 0 for K^-p and $\bar{p}p$ scattering and a positive value comparable in order of magnitude for K^+p and pp scattering.

REFERENCES

1) M. Borghini, L. Dick, L. di Lella, A. Navarro, J.C. Olivier, K. Reibel, G. Coignet, D. Cronenberger, G. Grégoire, K. Kuroda, A. Michalowicz, M. Poulet, D. Sillou, G. Bellettini, P.L. Braccini, T. del Prete, L. Foà, G. Sanguinetti, M. Valdata, Phys. Letters 31B (1970) 405, and Proc. of the XVth International Conference on High Energy Physics, Kiev, 26 August - 4 September 1970.

2) M. Borghini, G. Coignet, L. Dick, K. Kuroda, L. di Lella, P.C. Macq, A. Michalowicz and J.C. Olivier, Phys. Letters 24B (1967) 77 ; R. J. Esterling, N.E. Booth, G. Conforto, J. Parey, J. Scheid, D. Sherden and A. Yokosawa, Phys. Rev. Letters 21 (1968) 1410.

3) See for example: V. Barger, R.J.N. Phillips, Phys. Letters 29B (1969) 1924.

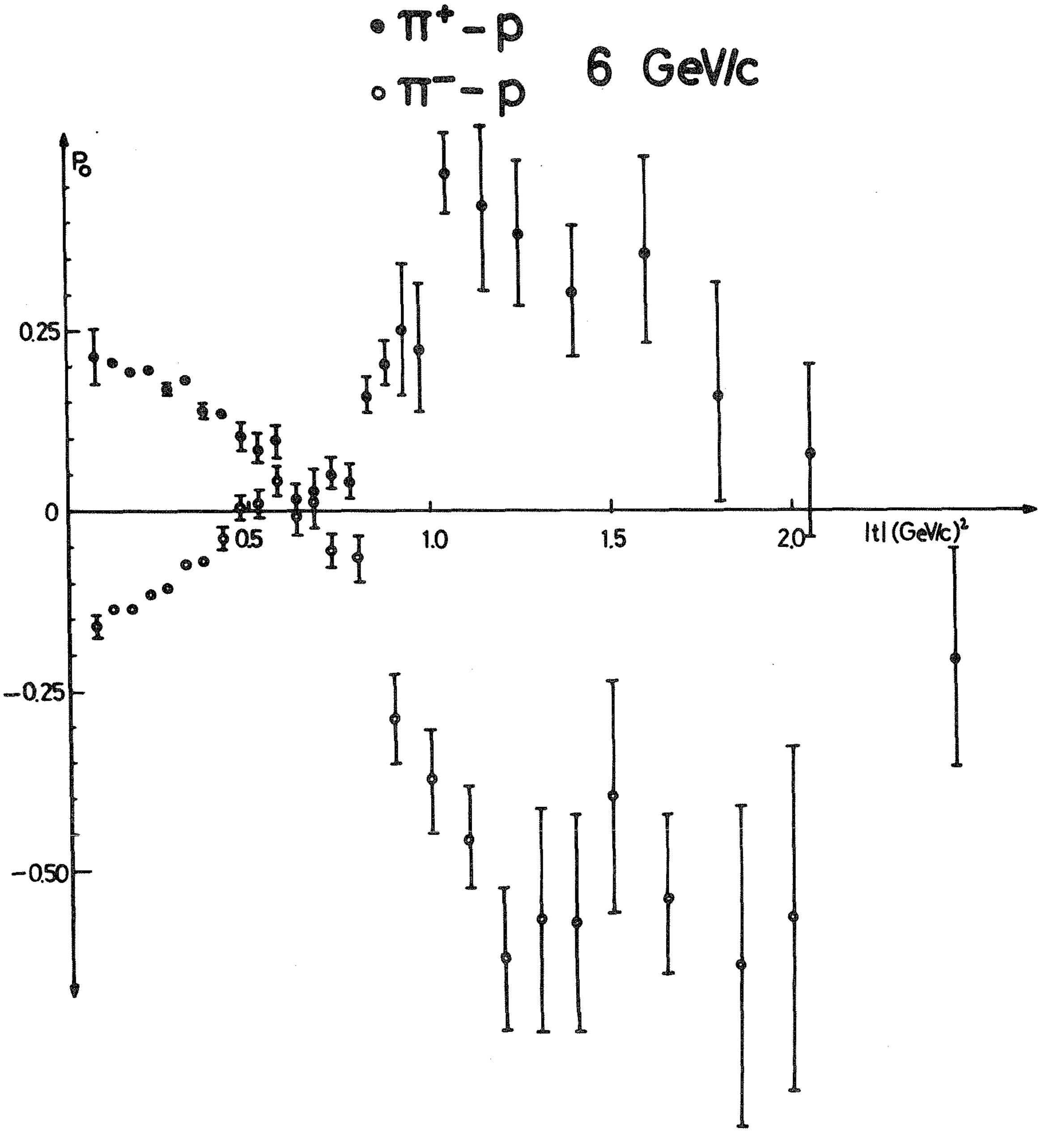

Figure 1: Polarization P_0 for $\pi^{\pm}p$ scattering at 6 GeV/c incident momentum.

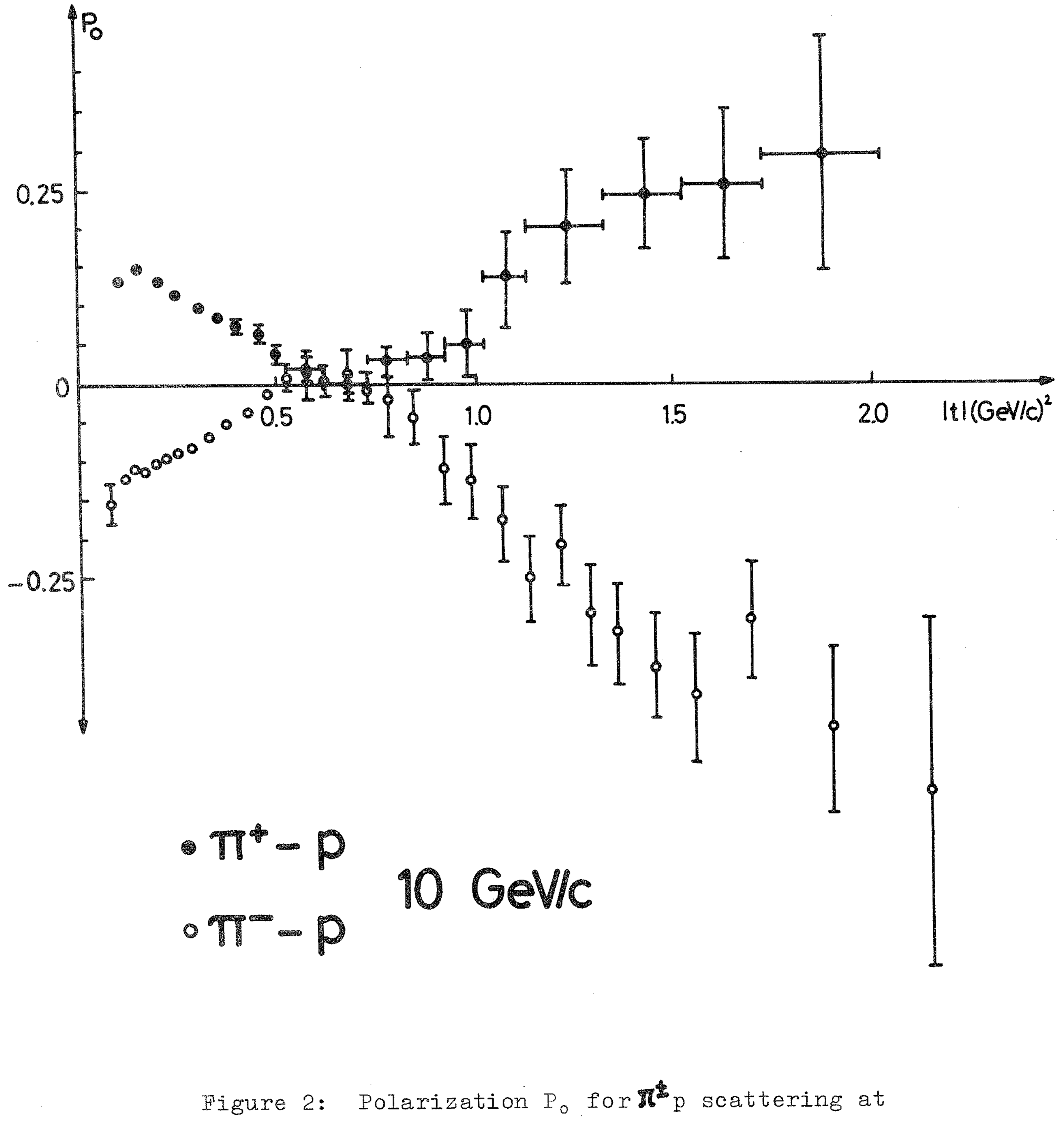

Figure 2: Polarization P_0 for $\pi^{\pm}p$ scattering at 10 GeV/c incident momentum.

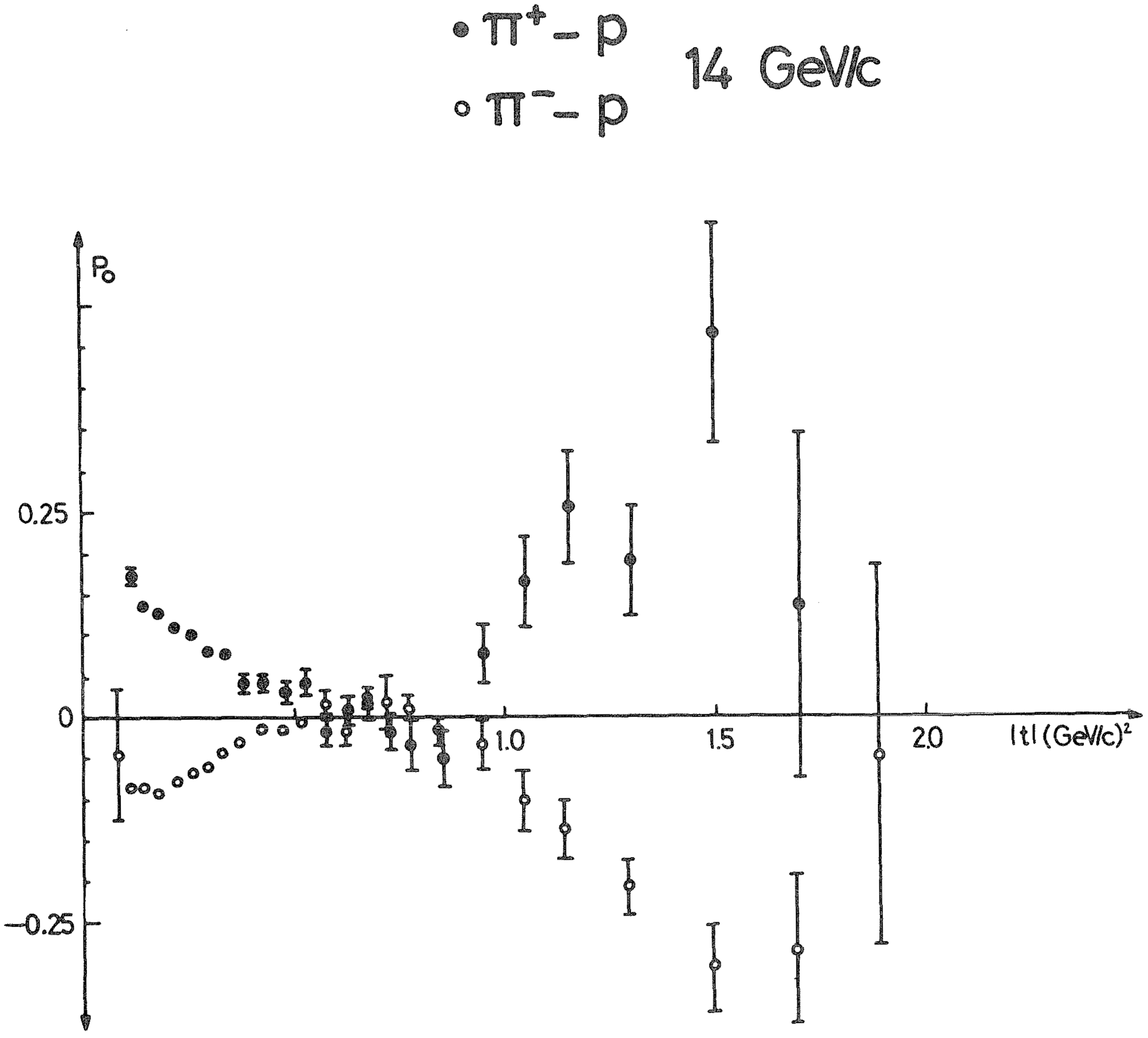

Figure 3: Polarization P_0 for $\pi^{\pm}p$ scattering at 14 GeV/c incident momentum.

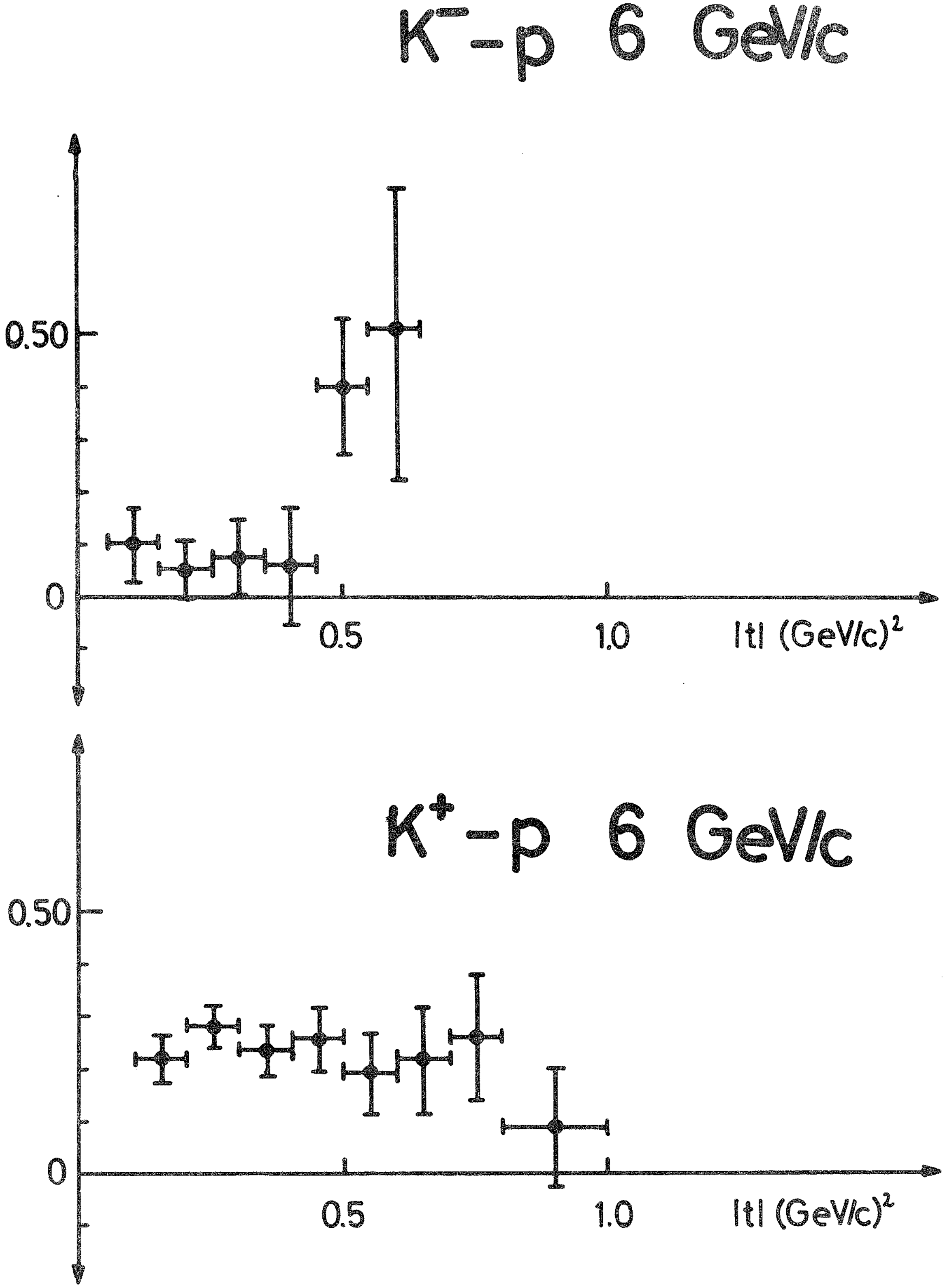

Figure 4: Polarization P_o for $K^{\pm}$ p scattering at 6 GeV/c incident momentum,

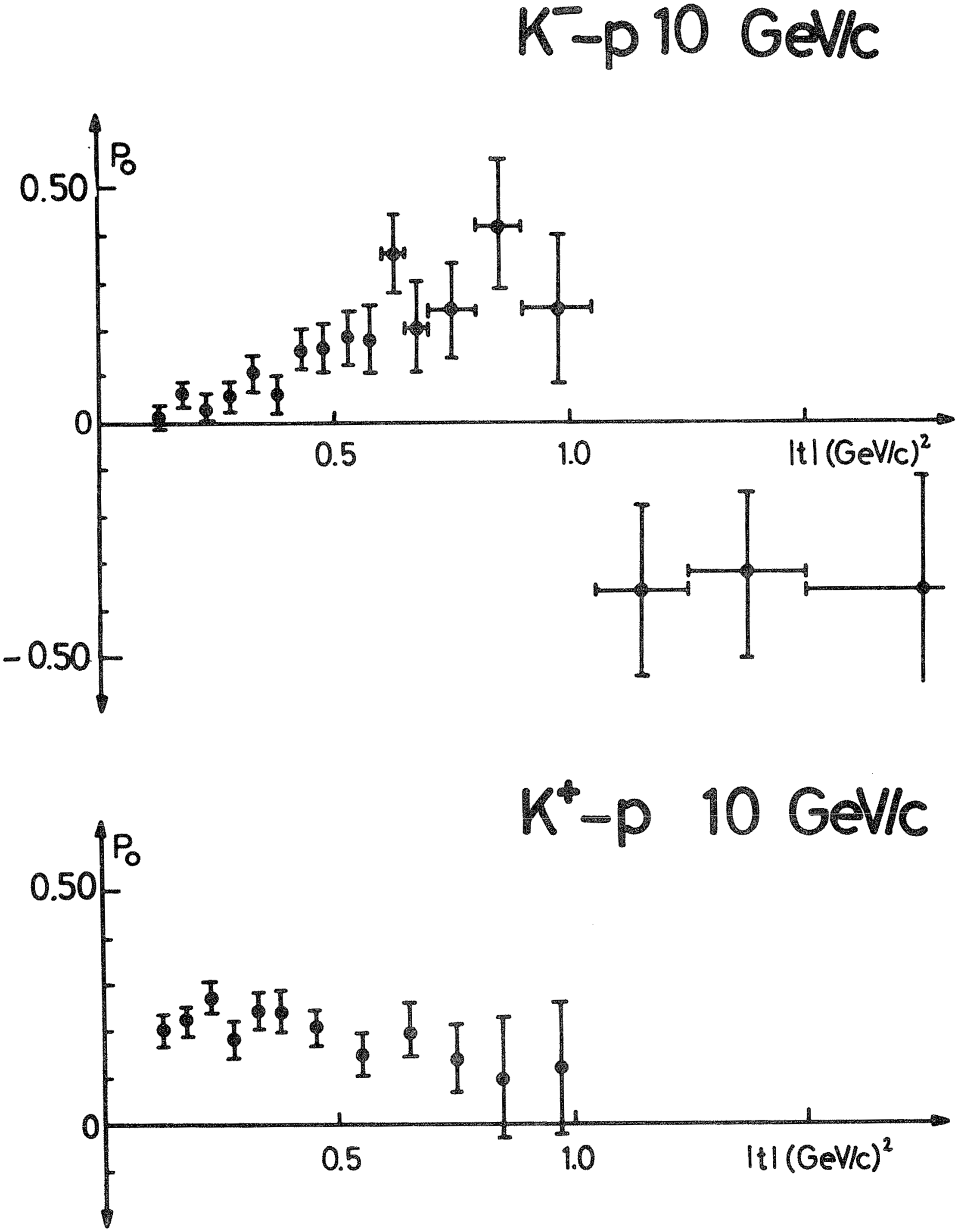

Figure 5: Polarization P_0 for $K^{\pm}p$ scattering at 10 GeV/c incident momentum.

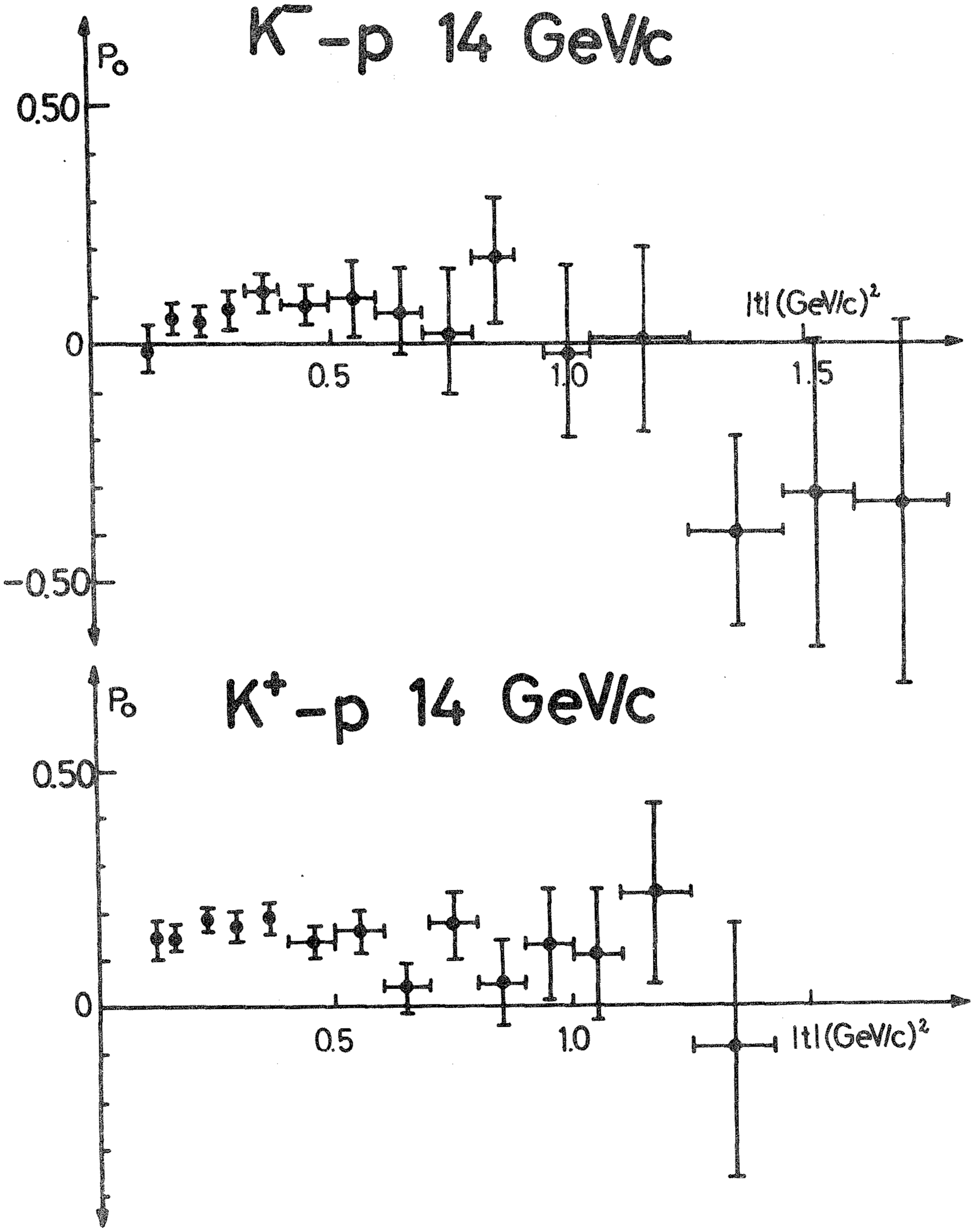

Figure 6: Polarization P_0 for $K^{\pm}$ p scattering at 14 GeV/c incident momentum.

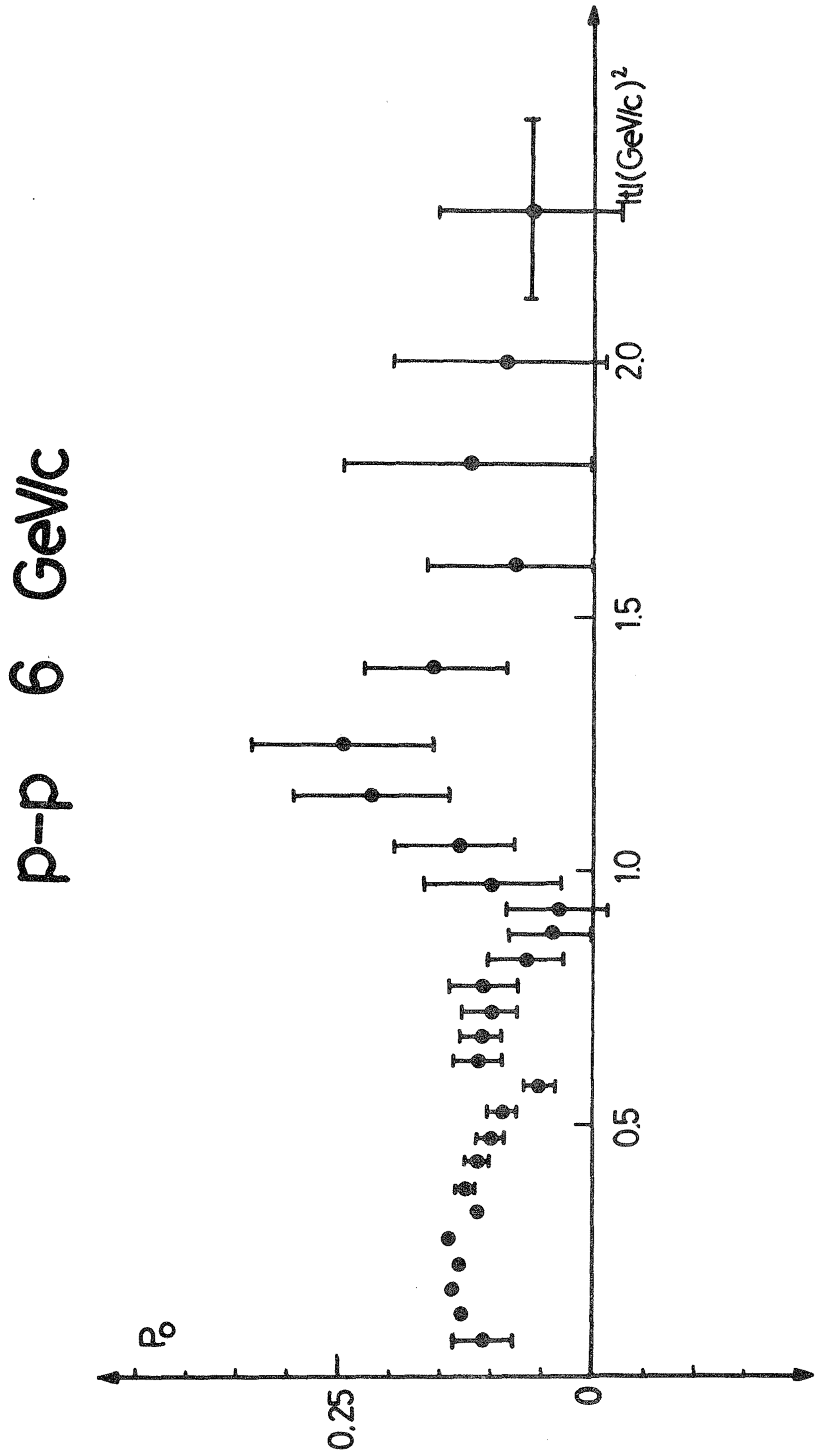

Figure 7: Polarization P_o for pp scattering at 6 GeV/c incident momentum.

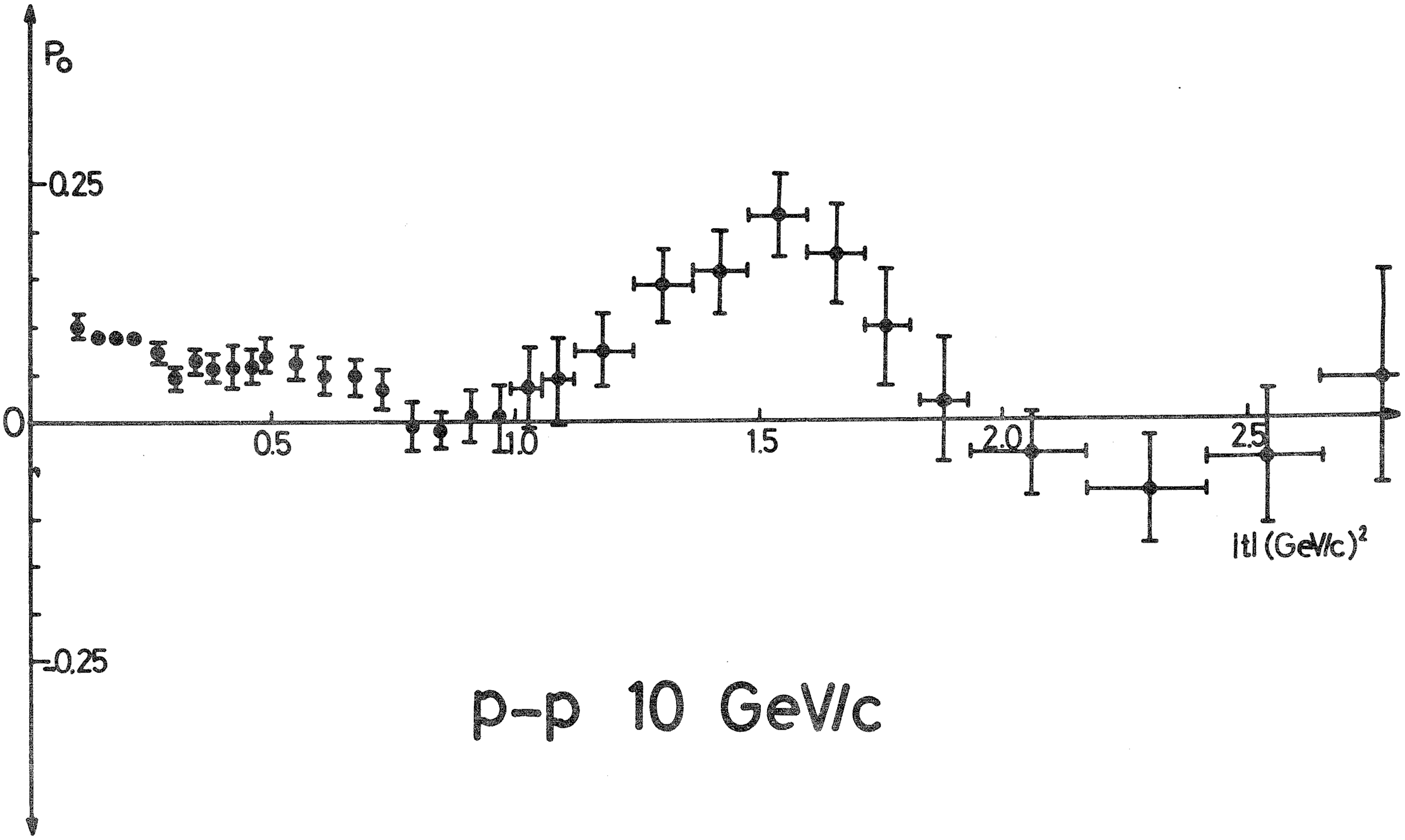

Figure 8: Polarization P_o for pp scattering at 10 GeV/c incident momentum.

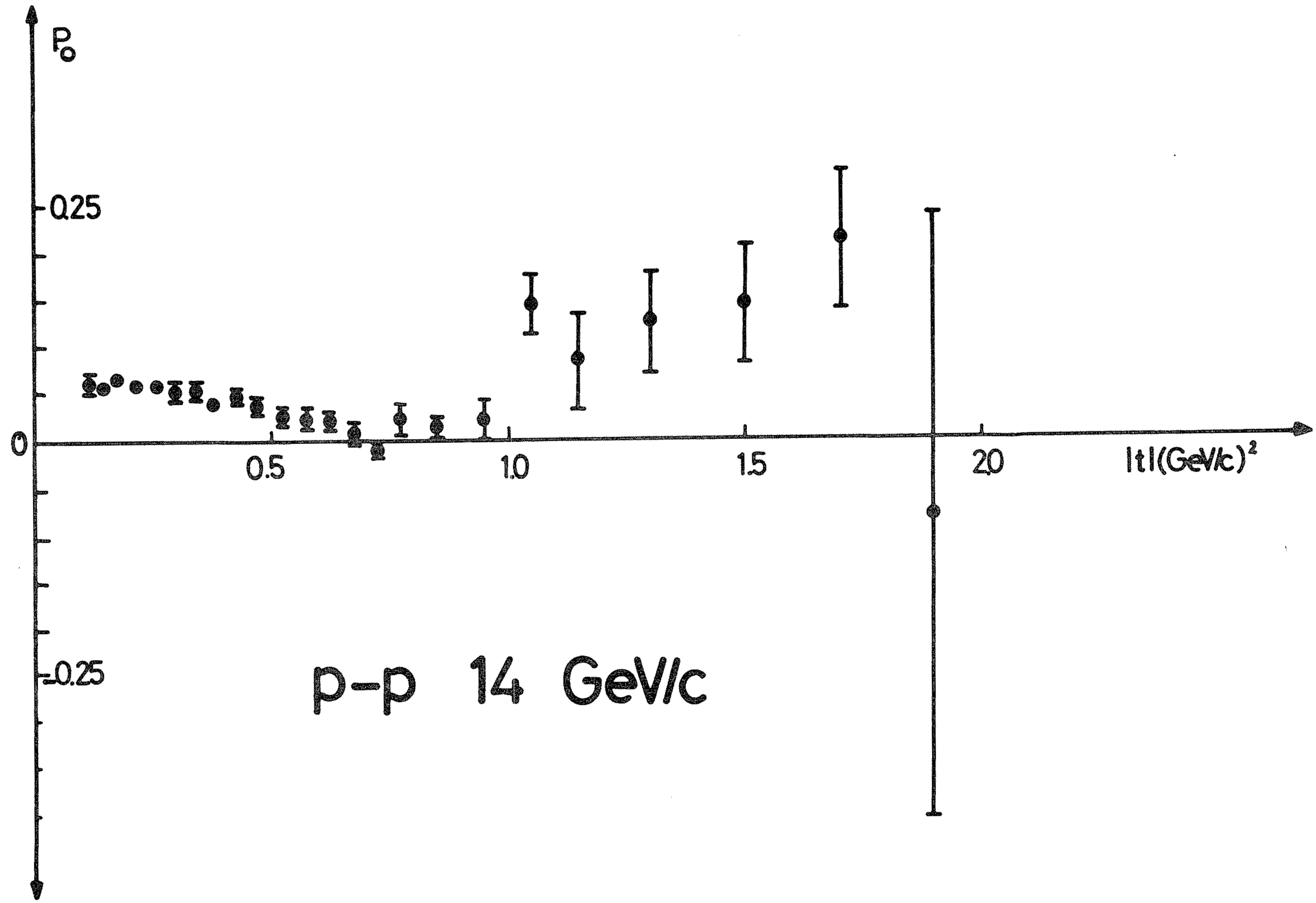

Figure 9: Polarization P_o for pp scattering at 14 GeV/c incident momentum.

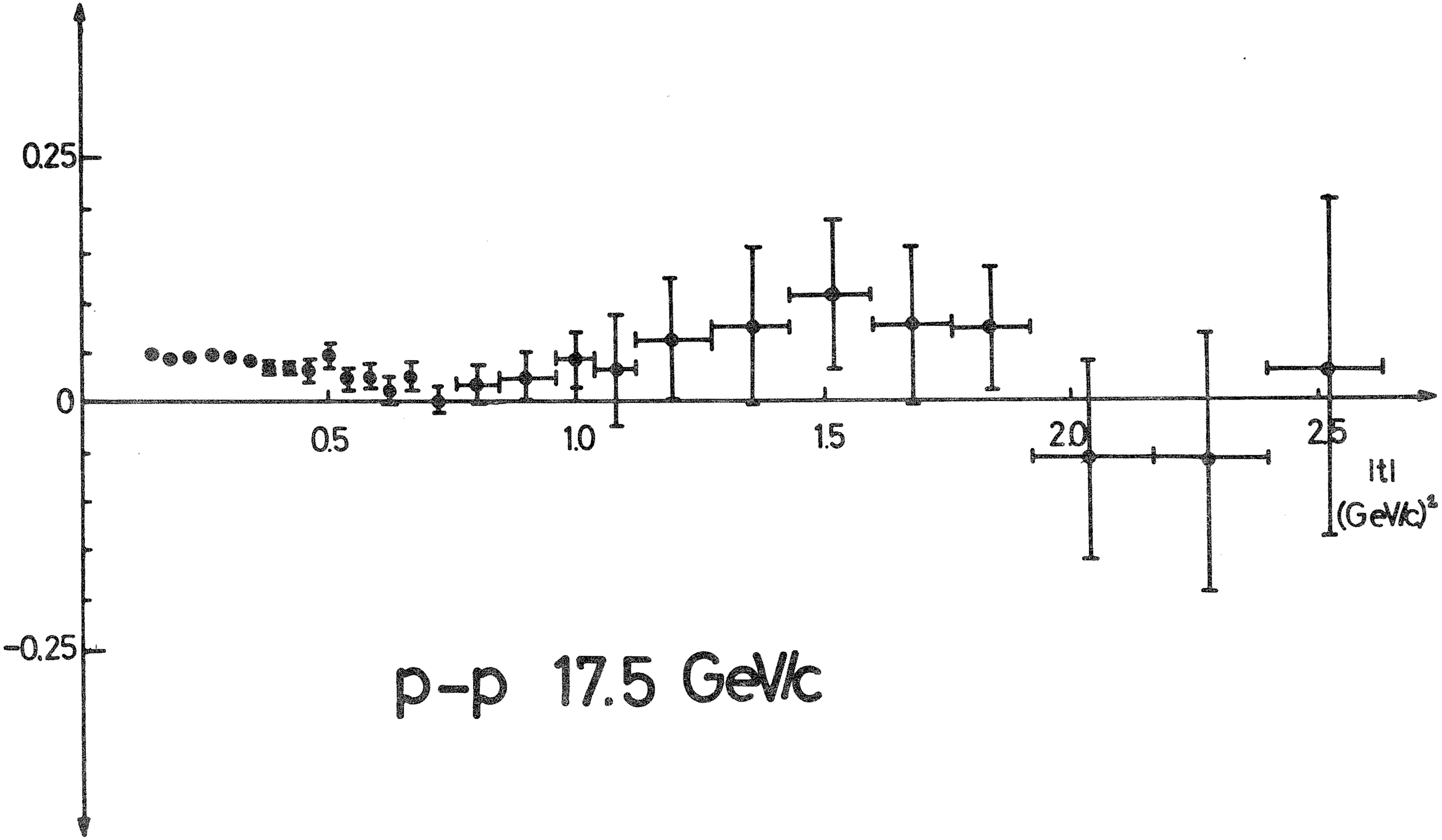

Figure 10: Polarization P_0 for pp scattering at 17.5 GeV/c incident momentum,

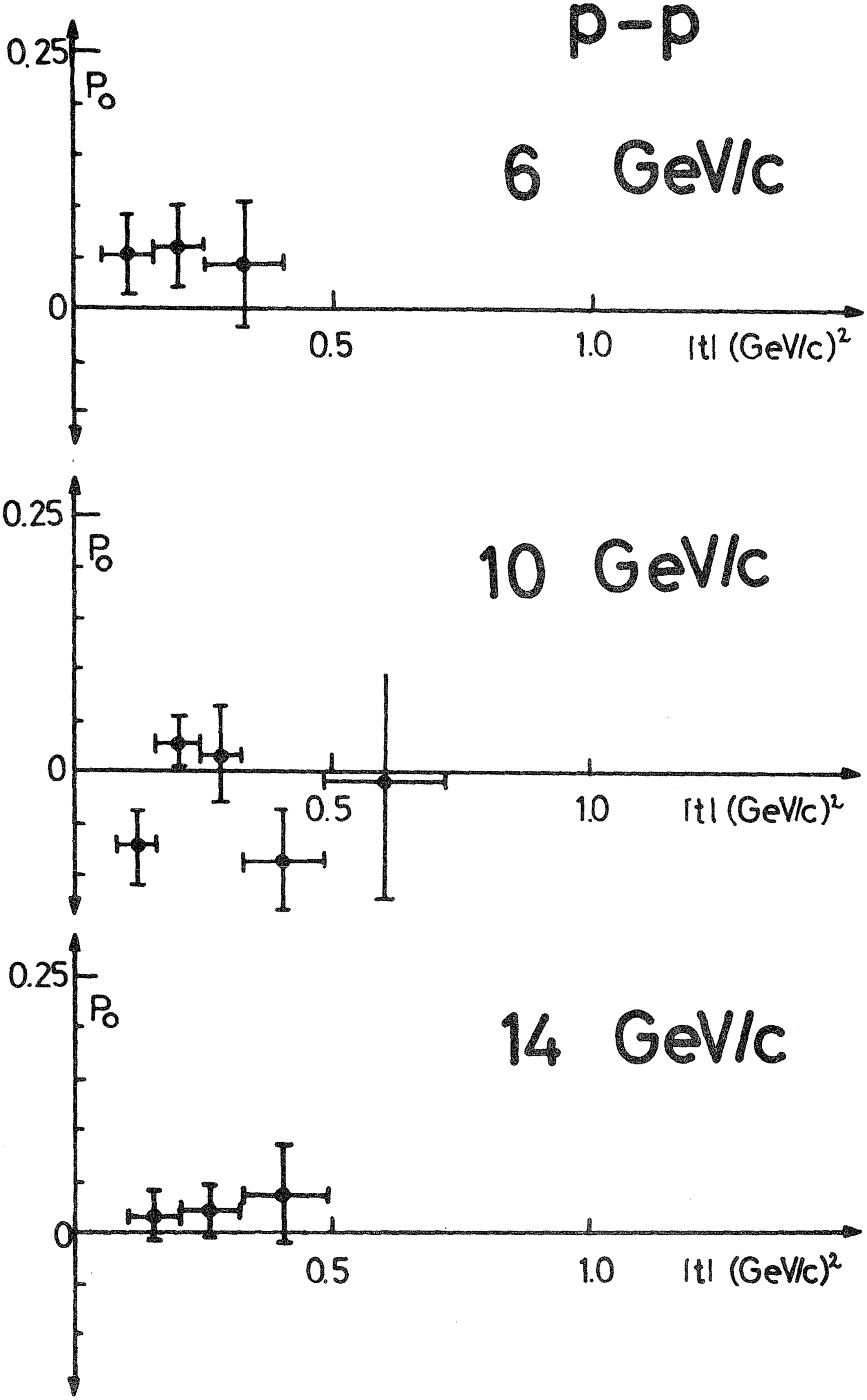

Figure 11: Polarization P_0 for $\bar{p}p$ scattering at 6, 10, 14 GeV/c incident momentum.

DISCUSSION

Gell-Mann (Chairman): Thank you very much. The next conference will be for the computers connected directly to one another and not bothering to send their human representative. Just so we won't think that these remarkable curves from this remarkable new kind of experimental work will have to send all theorists back to their drawing board, Professor Lovelace would like to make a remark or two about these remarkable clusterings of zero values at the particular values of t.

Lovelace (Rutgers) commented on the startling agreement of the elastic polarization data with the predictions of the exchange degenerate Regge phase. See page 596 of Dick's talk. Further comments can be found on pages 632, 682, and 713 of these proceedings. But...

Gell-Mann: That's very nice, thank you. Some day of course, we will have to explain why the cuts and other terms accompanying the poles participate in this thing, or maybe as we go up higher and higher in energy, the picture will become less and less simple. That picture will be very unfortunate.

Polarized targets are the greatest invention since

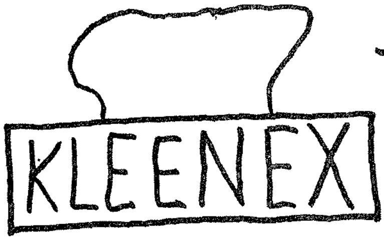

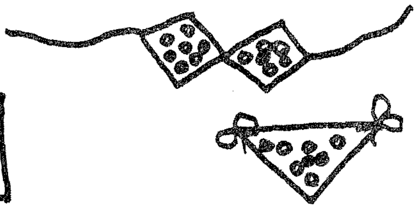

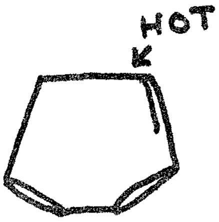

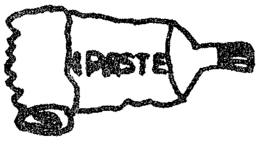

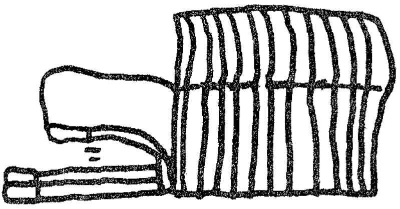

SOME NEW EXPERIMENTAL RESULTS WITH POLARIZED TARGETS*--II

A. Yokosawa

Argonne National Laboratory
Argonne, Illinois 60439

---

* Work performed under the auspices of the U.S. Atomic Energy Commission.

I would like to report the new results on: (1) $\pi^{\pm}p$ and $K^{+}p$ measurements at large angles, and (2) preliminary $\pi^{-}p$ charge exchange polarization results from CERN. (These results have been presented during the Moriond Conference, March 13-20, 1971, Meribel, France.)

(1) Polarization Measurements at Large Angles

$\pi^{+}p$ Elastic Scattering

It is known that the $\pi^{+}p$ elastic scattering reactions at high energy show peaking of the cross sections at $\cos\theta_{cm} = -1.0$ and a dip in $d\sigma/du$ which appears at $u \approx -0.15$. Results of recent polarization measurements in the backward region from 1.60 to 3.75 GeV/c [1,2] incident π^{+} momenta are shown in Fig. 1. The 3.25 and 3.75 GeV/c [1] data together with preliminary 6.00 GeV/c results presented by the previous speaker (L. Dick) as shown in Fig. 2, indicate that polarization is negative in the range of $0 > u > -0.1$ and then positive for $-0.1 > u > -0.2$. However, values of polarization are small, suggesting that the phases of flip and non-flip amplitudes are similar, or that the real or imaginary amplitude is dominant in the region of $0 > u > -0.2$. For the region of $|u| > 0.2$, the polarization becomes large and negative. There is very little energy dependence in polarization from 2.50 to 2.93 GeV/c, in spite of possible influence of the direct channel $\Delta_{\delta}(2420)$. However, a drastic variation from 1.60 to 2.50 GeV/c suggests an interference of u-channel effects with either t-channel or direct channel effects or possibly both.

A comprehensive study of all existing baryon exchange models, with or without Regge cuts, has been recently made by Berger and Fox.[3] The qualitative features of available cross section data at high energies were represented adequately by all models. Figure 1 shows their predicted polarization (solid) at 2.93 GeV/c based upon exchange of N_{α}, N_{γ}, and Δ_{δ} Regge trajectories (pure pole model); these parameters were obtained by fitting to existing $\pi^{+}p$, $\pi^{-}p$, and $\pi^{-}p$ charge exchange data in the backward region at higher energies. The obvious discrepancy between the model and the experimental data was investigated by including the effect of cuts. Two predictions[3] based upon "weak" cuts and "strong" cuts are also shown in Fig. 1 at 2.75 GeV/c. These Regge cuts models seem to explain qualitatively the experimental data from 2.50 to 2.93 GeV/c, but they do not agree very well with data at 3.25, 3.75, and 6.00 GeV/c, as shown in Fig. 2. High energy data for the large $|u|$ region are in fairly good agreement with a pole plus fixed cut model,[3)] based upon prescriptions by Bardacki-Halpern and Carlitz-Kislinger. (See Fig. 2.)

So far, we have discussed the effect of u-channel and direct channel; however, we also expect to see t-channel effects, even in the very backward region, especially at the lower energy. A comparison[2)] of the data below 2.30 GeV/c with predictions of the t-channel Regge pole model of Barger and Phillips,[4)] which was fitted to the high energy data, is shown by the dotted curves in Fig. 3. The agreement at 2.11 and 2.31 GeV/c is reasonably good over the entire angular region.

Figure 3 also shows predictions of the CERN and Berkeley phase shift analyses.[5)] Above 1.80 GeV/c, the overall agreement is poor, particularly in the backward region. The angular range of the data available at the time of the above analysis is shown by an arrow.

$\pi^- p$ Elastic Scattering

Preliminary results of large angle $\pi^- p$ polarization measurements at 1.88, 2.28,[6)] and 2.74 GeV/c [7)] are shown in Figs. 4, 5, and 6, respectively.

The data at 2.28 and 2.74 GeV/c cover the region of dips in the differential $\pi^- p$ cross section at $t \approx -0.6$ and -2.8 $(\text{GeV}/c)^2$. Both sets of data reveal a remarkable structure in the vicinity of $|t| = 2.8$ as shown in Figs. 5 and 6. The predictions of Ref. 4 are in excellent agreement with the data. An earlier phase shift analysis[8)] at 2.28 GeV/c also predicts this new structure very well. An arrow in Fig. 5 indicates the $|t|$ region of the data available at the time of the phase shift analysis.

Comparison of $\pi^+ p$ and $\pi^- p$ Scattering

Earlier measurements up to $|t| = 2.0$ at 5.15 GeV/c [9)] have shown remarkable behavior of $P^{\pi^+ p}(t) \approx -P^{\pi^- p}(t)$ in the entire $|t|$ range. What will happen beyond $|t| = 2.0$? The data at 2.30 GeV/c seem to indicate the same behavior as mentioned above up to $|t| = 3.0$. In Fig. 7, both the 5.15 and 2.31 GeV/c data are plotted for the range of $0 < |t| < 2.0$ and $2.0 < |t| < 3.0$, respectively. In addition to Ref. 4, which predicted this interesting behavior, a similar conclusion has been made by a model[10)] which is different from the Regge pole approach. It is interesting to observe the behavior beyond $|t| = 2.0$ at high energies.

K^+p Elastic Scattering

The differential cross sections exhibit a backward peak, which is explained by Reggeized baryon exchange. The two trajectories involved here are expected to be exchange degenerate, and thus the polarization is predicted to be zero. Recent polarization measurements from 1.60 to 2.31 GeV/c [11)] are shown in Fig. 8. We observe practically no energy dependence in the backward region, in contrast to the drastic changes in the case of πp scattering. In addition, polarization values are consistent with zero for $|u| < 0.5$ $(\text{GeV/c})^2$. The t dependence is also shown in Fig. 8 and unlike the πp case, no obvious structure is observed over the entire angular range.[12)]

(2) π^-p Charge Exchange at CERN

I was asked by authors of "Polarization in Charge Exchange Reactions"[13)] to present their new results at this conference. Although the details will be available in the Moriond Proceedings, a brief summary will be given here.

Previous polarization data[14)] measured up to $|t| = 0.3$ $(\text{GeV/c})^2$ indicate non-zero positive values in this range of momenta transfer. The results have been interpreted variously by over 100 theoretical papers. The predicted polarizations in the range $|t| > 0.3$ differ from model to model; however, I will present them in two groups: (1) a pole model[4)] based on the finite energy sum rules, and (2) absorption models including "weak"[15)] and "strong"[16)] cuts. The first one predicts a large positive value[17)] for the range $|t| > 0.3$ and the latter a large negative value as shown in Fig. 9.

A new experimental technique has been used in this experiment: They used only a shower spark chamber and instead of employing neutron counters, they computed the hydrogen effect by measuring the effects of CH_2 and C separately and taking the difference CH_2-C. The validity of this method has been tested previously.[18)]

Their preliminary data[19)] are shown in Fig. 10 and the comparison with other results[14)] is given in Fig. 11. The cut models, mentioned above, are clearly inadequate to explain the data, but the pole model is remarkably consistent with the data.

REFERENCES

1. D. Sherden et al., Phys. Rev. Letters 25, 898 (1970).
2. G. Burleson et al., Phys. Rev. Letters 26, 338 (1971).
3. E. L. Berger and G. Fox, Nucl. Phys. B26, 1 (1971).
4. V. Barger and R.J.N. Phillips, Phys. Rev. 187, 2210 (1969).
5. Particle Data Group, "πN Partial-Wave Amplitudes, a Compilation", UCRL-20030 (1970).
6. ANL-Northwestern-NAL Collaboration, preliminary data.
7. Preliminary CERN data, private communication from J. C. Sens.
8. A. Yokosawa et al., Phys. Rev. Letters 16, 714 (1966); R. Hill et al., Phys. Rev. D1, 729 (1970).
9. R. Esterling et al., Phys. Rev. Letters 21, 1410 (1968).
10. G. Berlad, A. Dar, and G. Eilam, preprint, Haifa, Israel (1970).
11. ANL-Maryland-Northwestern-NAL Collaboration, to be published.
12. We note that K^+p polarization measurements at the intermediate region have been carried out at ANL, BNL, and CERN by several groups.
13. O. Guisan, P. Sonderegger et al., presented during the Moriond Conference, France (March 1971).
14. P. Bonamy et al., Nucl. Phys. B16, 335 (1970); D. D. Drobnis et al., Phys. Rev. Letters 20, 274 (1968).
15. R. C. Arnold and M. L. Blackmon, Phys. Rev. 176, 2082 (1968).
16. F. Henyey, G. L. Kane, J. Pumplin, and M. H. Ross, Phys. Rev. 182, 1579 (1969).
17. Similar predictions were also made by R. E. Kreps and J. W. Moffat (see Phys. Rev. 175, 1942 (1968)) who used a dipole ρ meson model, and by F. Schrempp (Nucl. Phys. B6, 487 (1968)).
18. O. Guisan et al., submitted to Nucl. Phys.
19. The statistics will be improved in the near future by a factor of 1.3 at 5.0 GeV/c and almost 4.0 at 8 GeV/c (see Ref. 13).

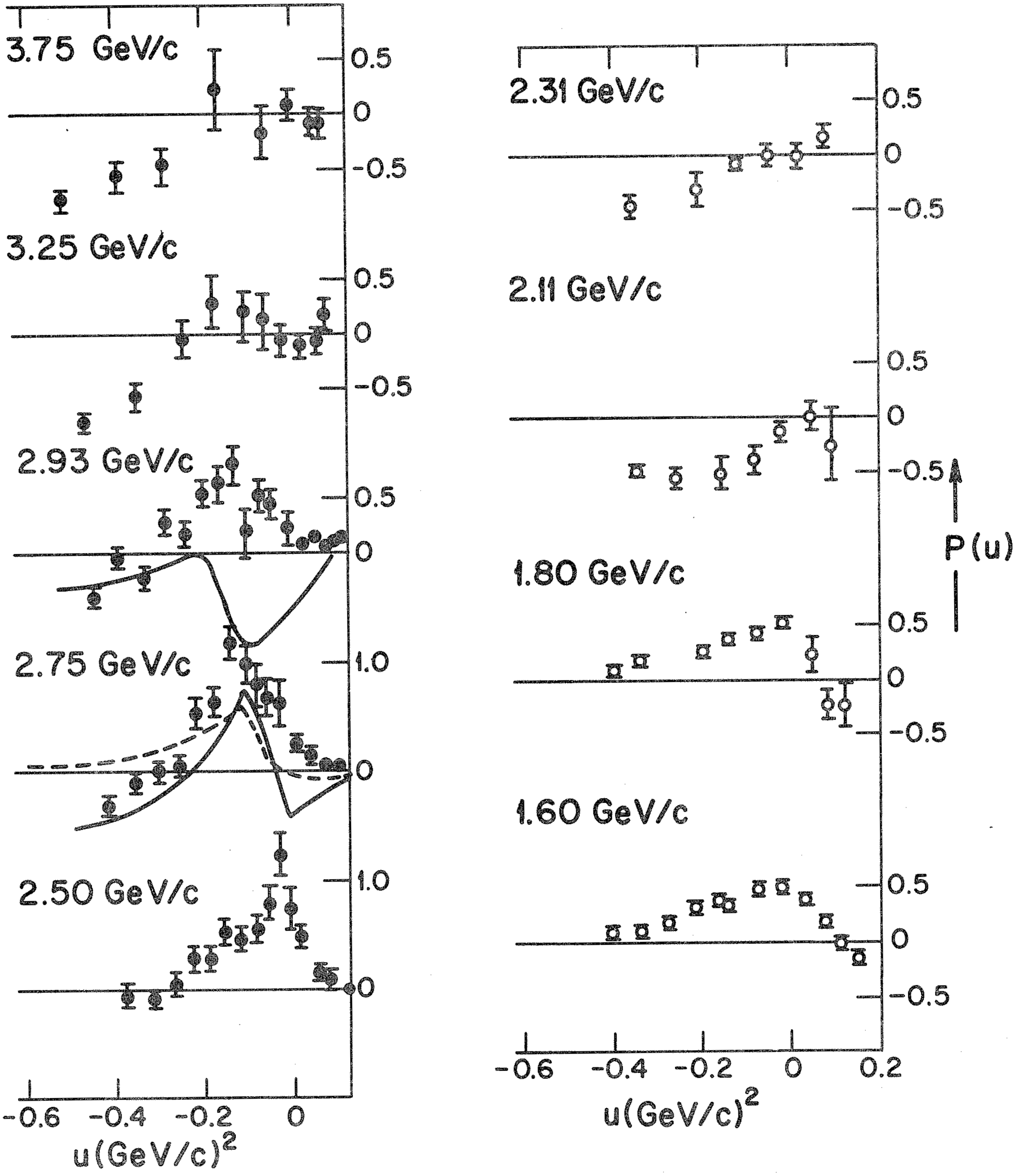

Figure 1: π^+p polarization as a function of u . The solid curve represents the pure pole model at 2.93 GeV/c as described in the text, and the solid and dashed curves represent the "weak" and "strong" cuts models at 2.75 GeV/c, respectively.

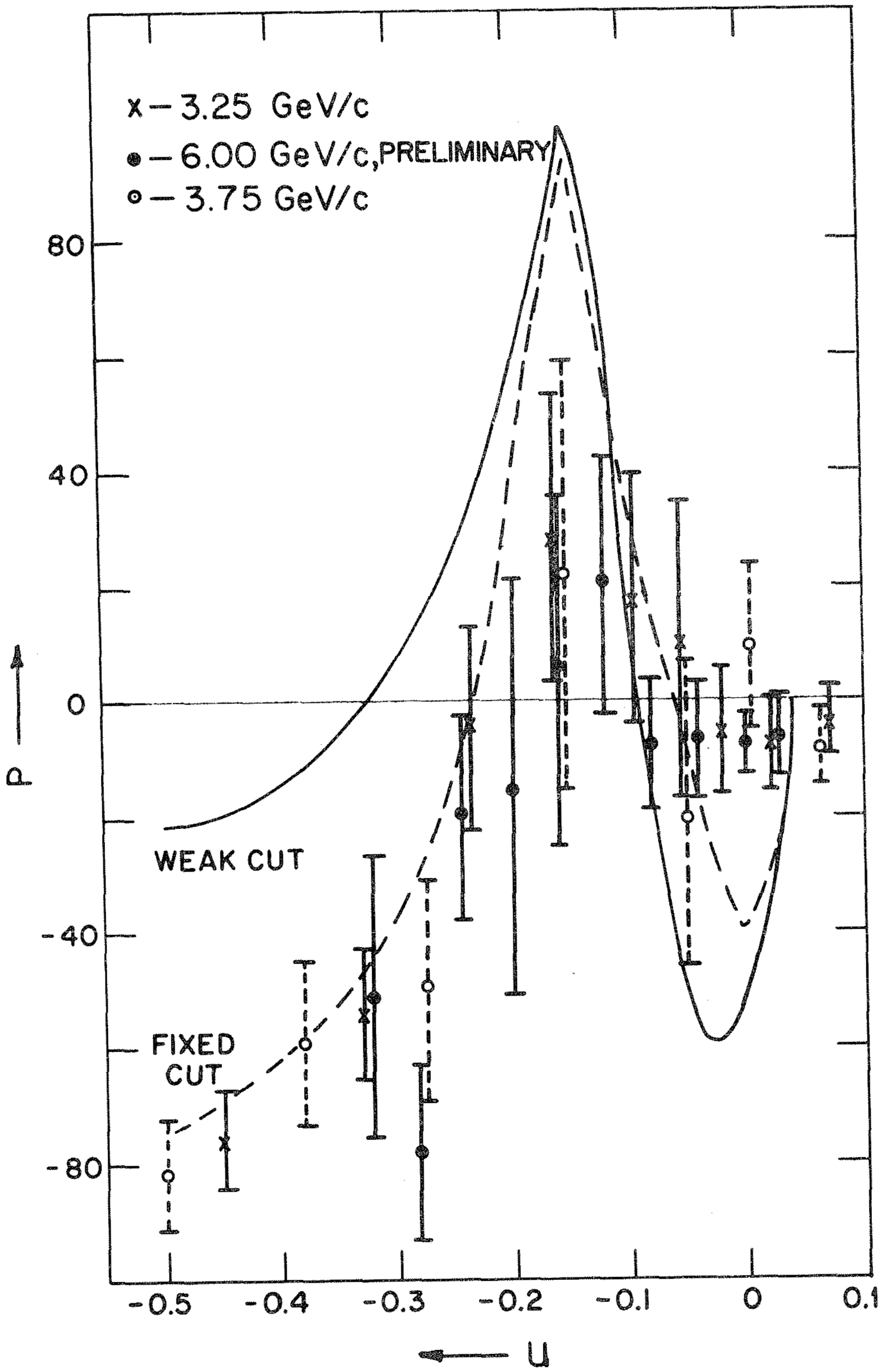

Figure 2: π^+p polarization as a function of u at 3.25, 3.75, and 6.00 GeV/c. The 6.00 GeV/c data are preliminary data from CERN. The solid and dashed curves represent the "weak" and "fixed" cut (see text) calculated at 5.2 GeV/c.

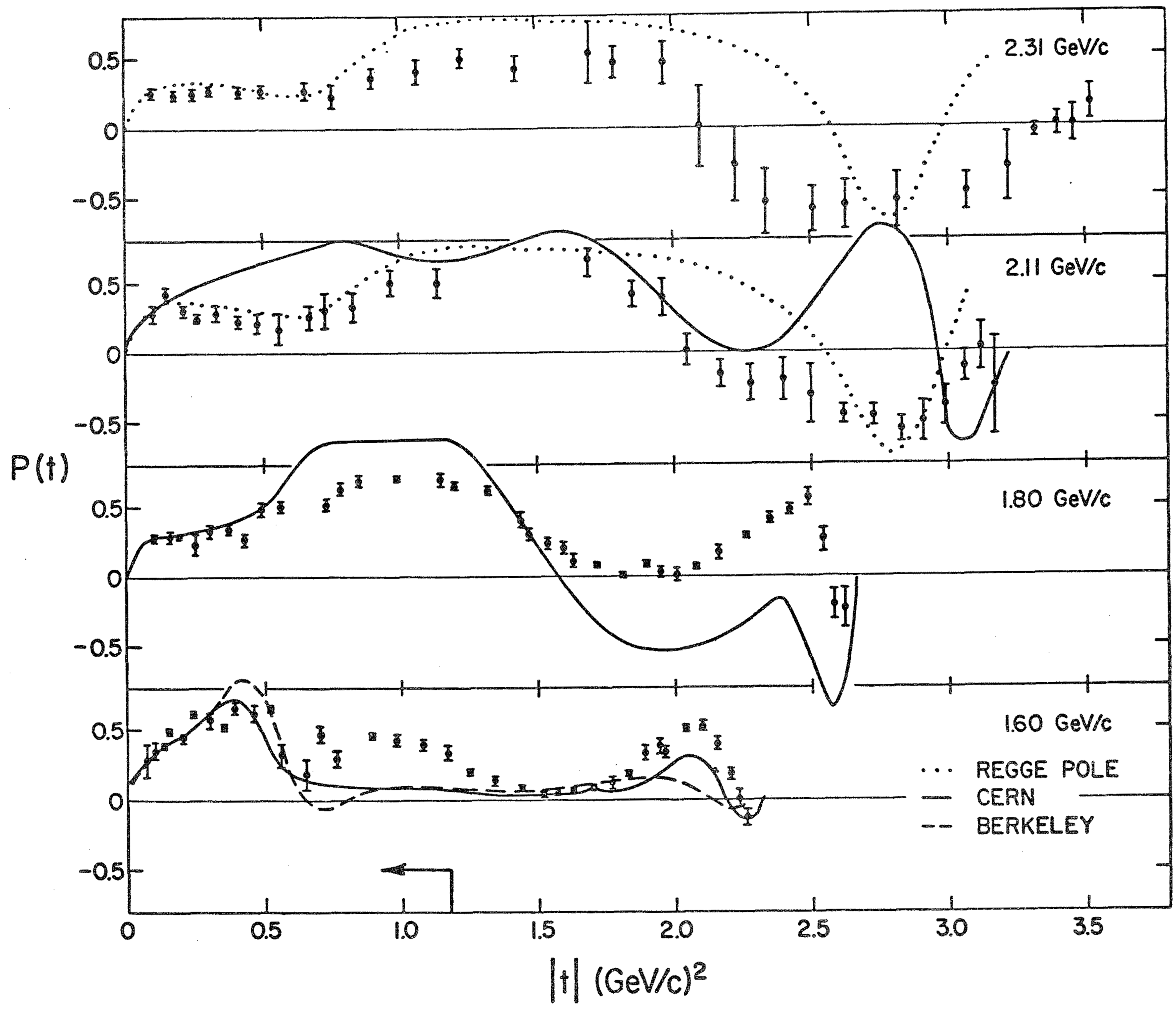

Figure 3: π^+p polarization as a function of $|t|$. The dotted curve represents the Regge pole model as described in the text and the solid and dashed curves represent the CERN and Berkeley phase shift analyses, respectively.

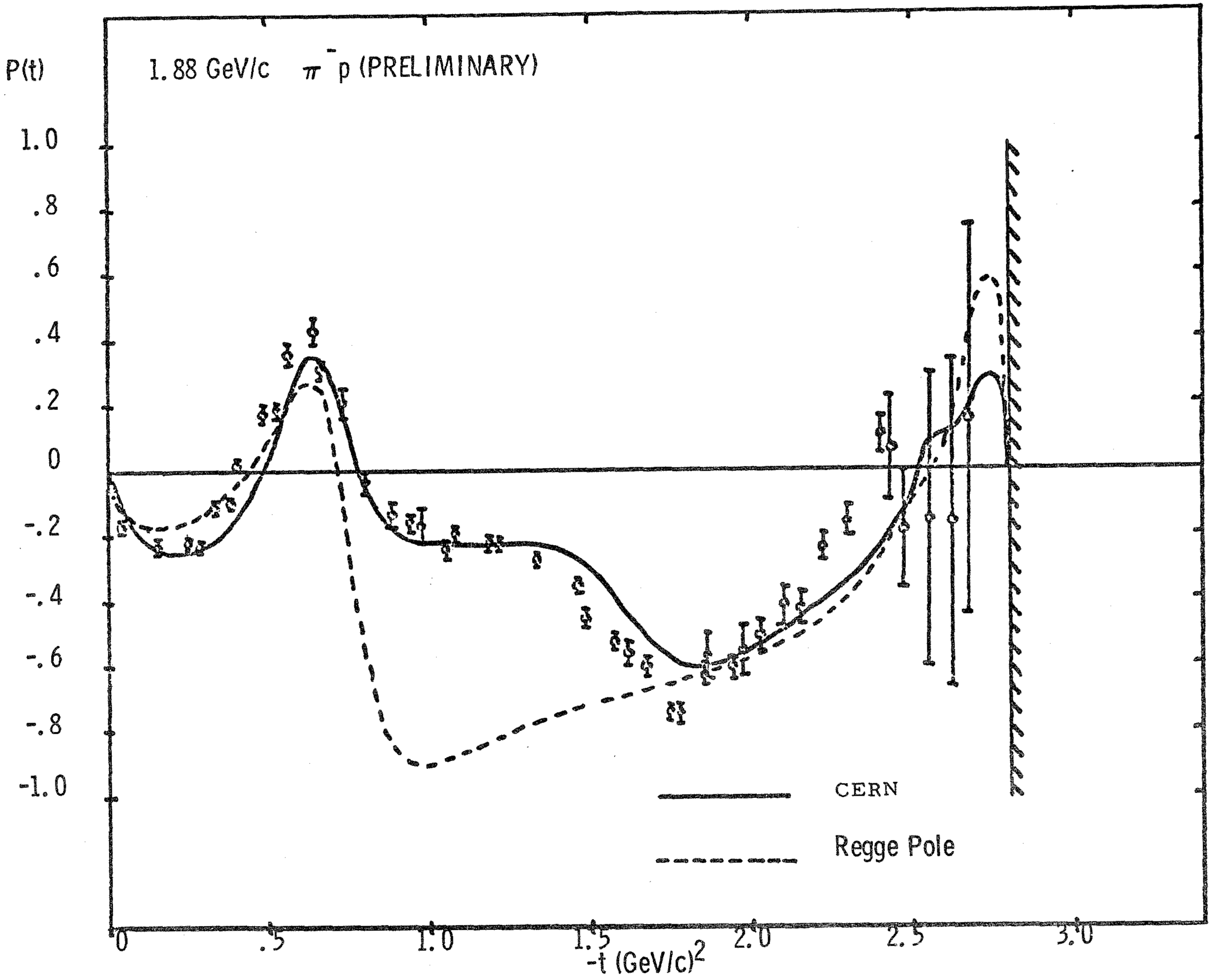

Figure 4: π^-p polarization at 1.88 GeV/c. The solid curve represents the CERN phase shift analysis,[7] while the dashed curve represents the Regge pole model as described in the text.

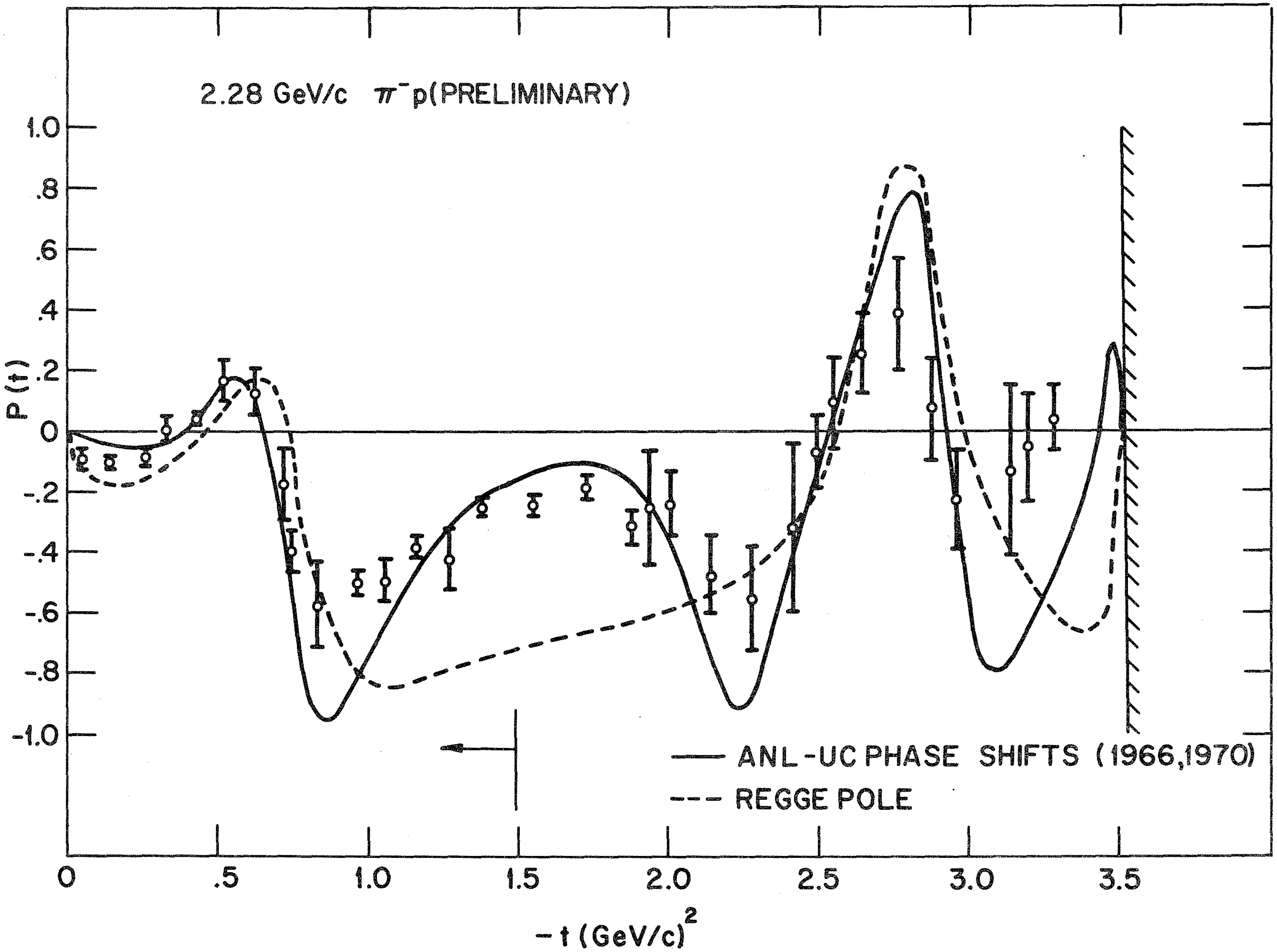

Figure 5: $\pi^- p$ polarization at 2.28 GeV/c. The solid curve represents the ANL-UC phase shift analysis and the dashed curve represents the Regge pole model as described in the text.

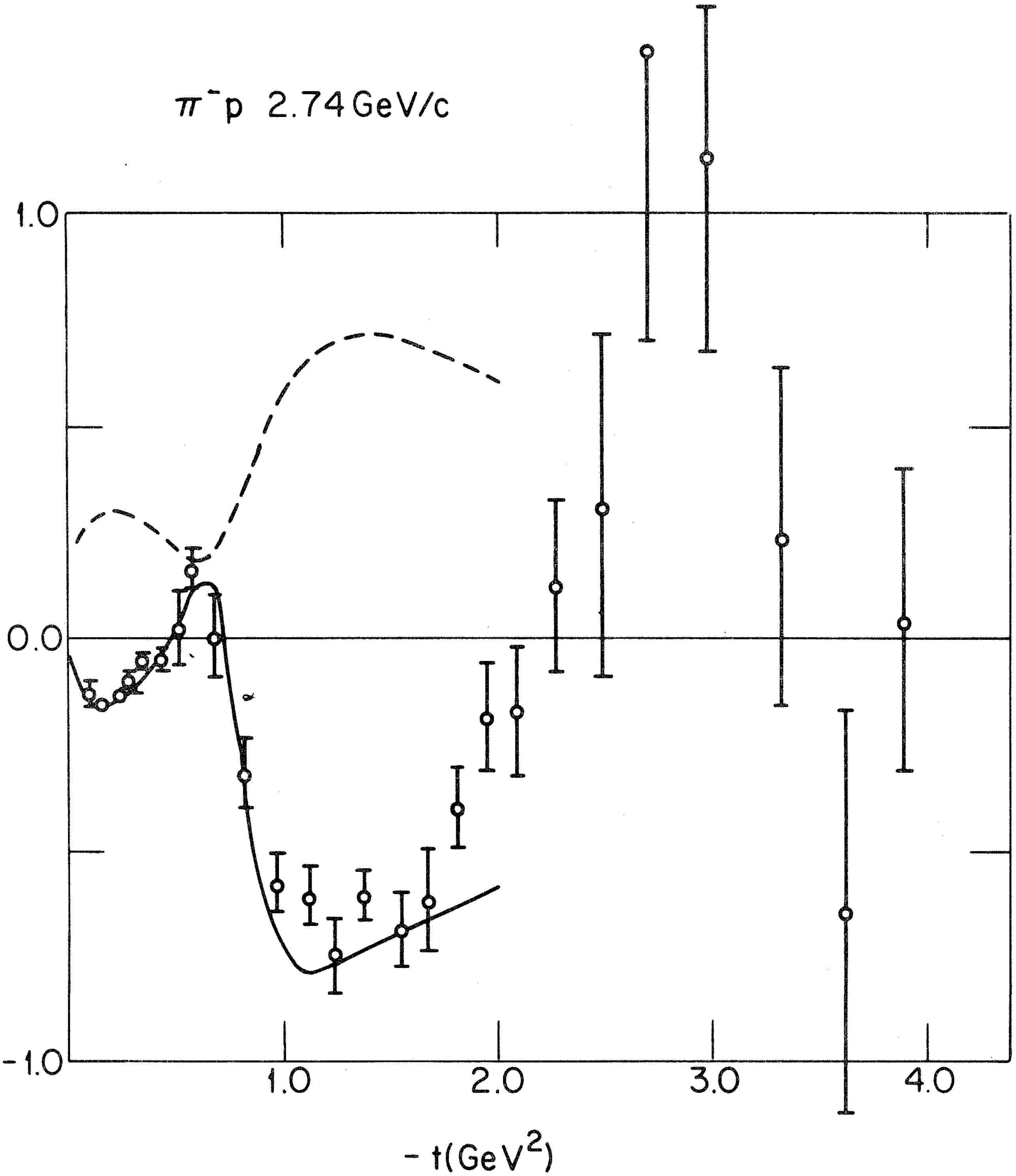

Figure 6: π^-p polarization at 2.74 GeV/c.

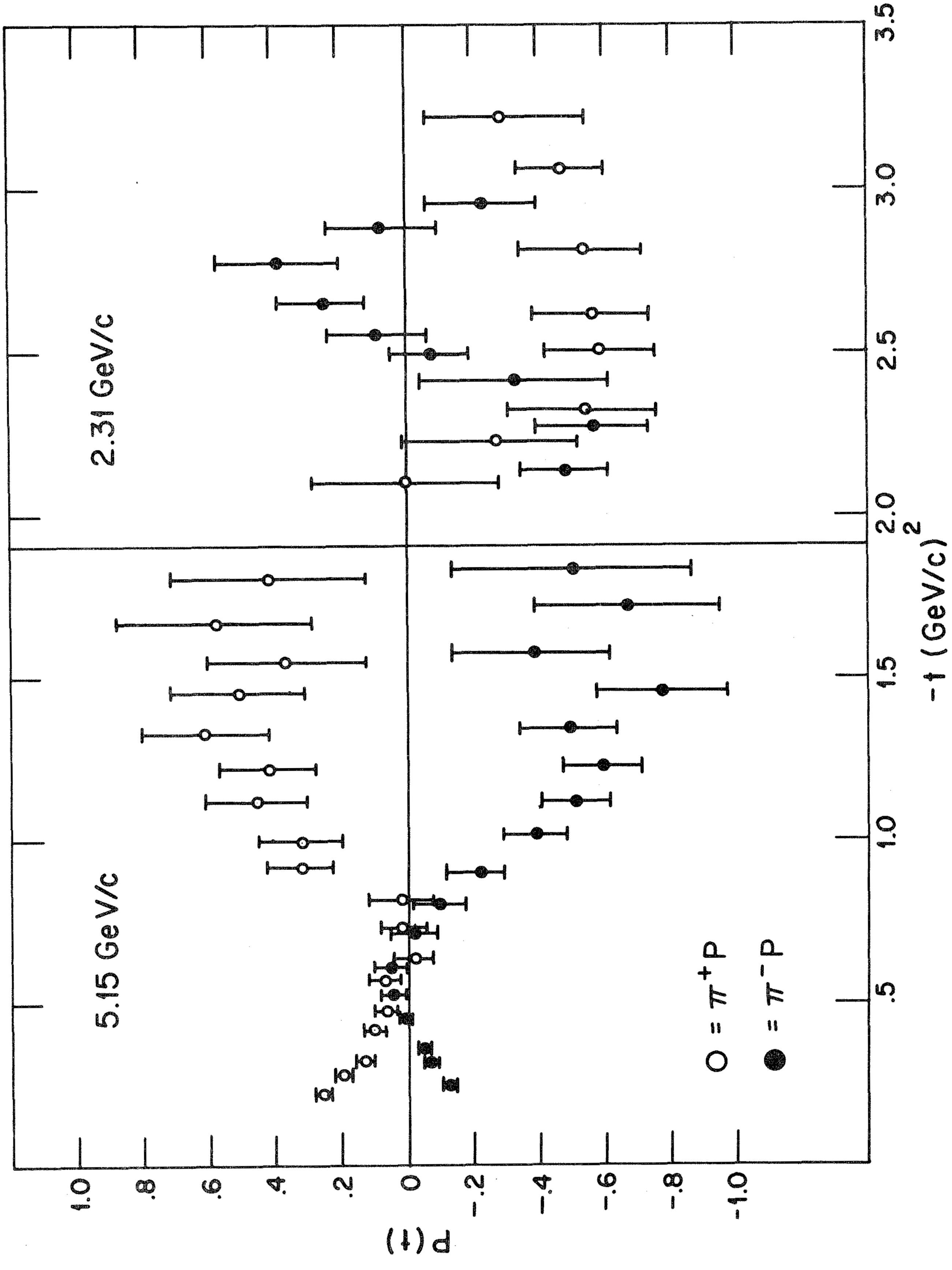

Figure 7: Comparison of π^+p and π^-p polarization.

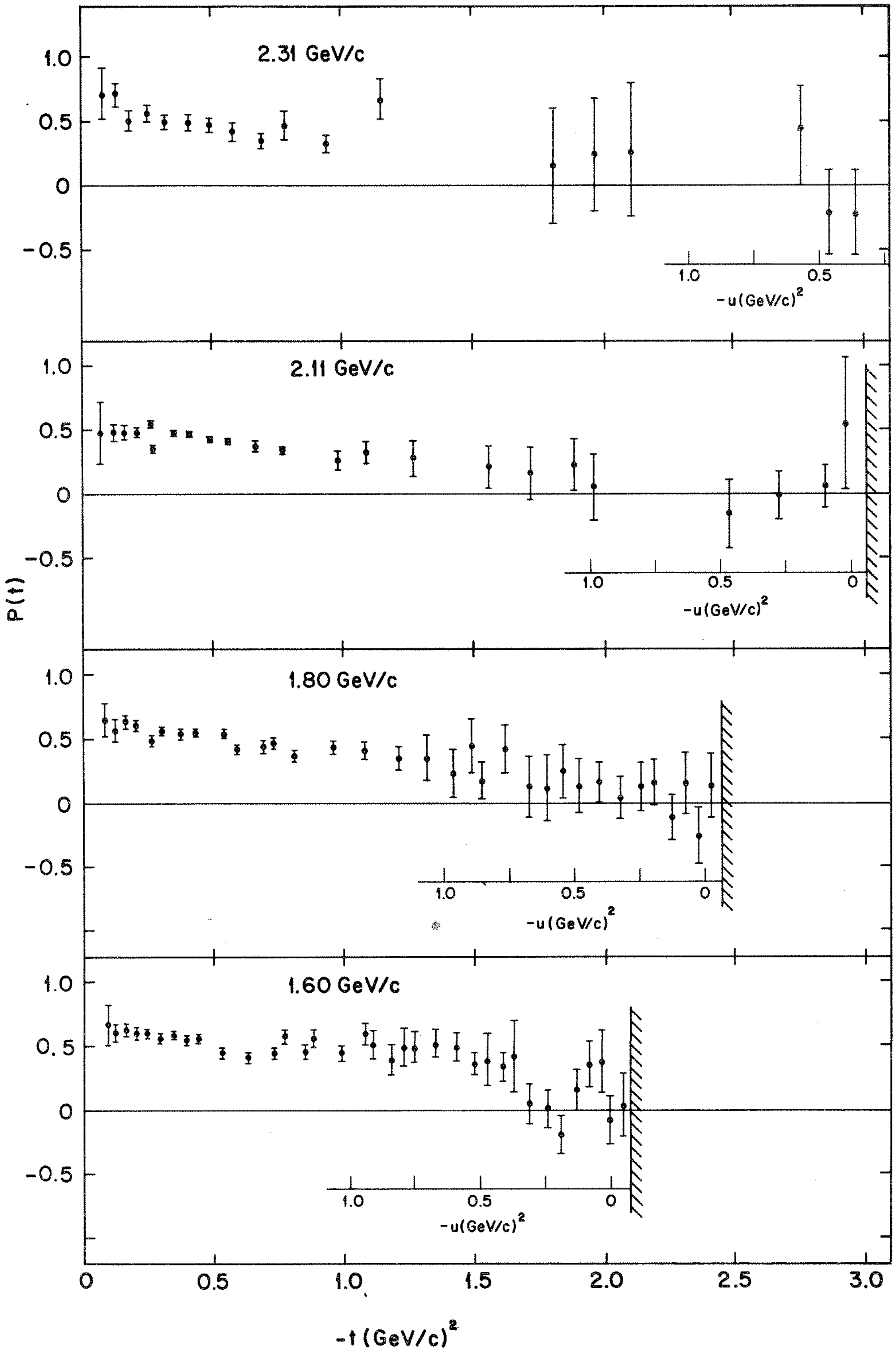

Figure 8: K$^+$p polarization, from 1.60 to 2.31 GeV/c.

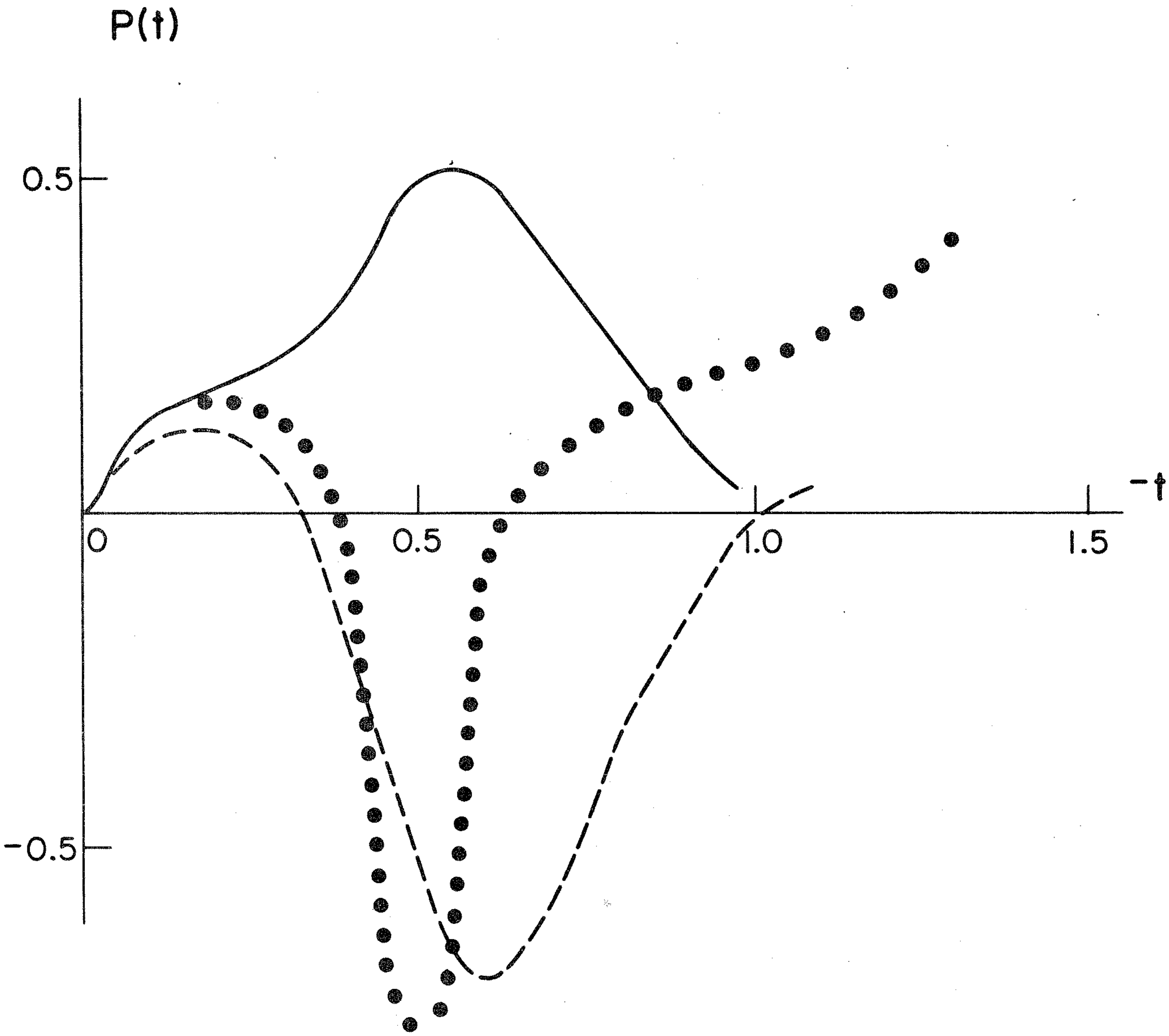

Figure 9: Theoretical predictions; the solid curve represents the pure pole model, and the dotted and dashed curves represent the "weak" and "strong" cuts models, respectively.

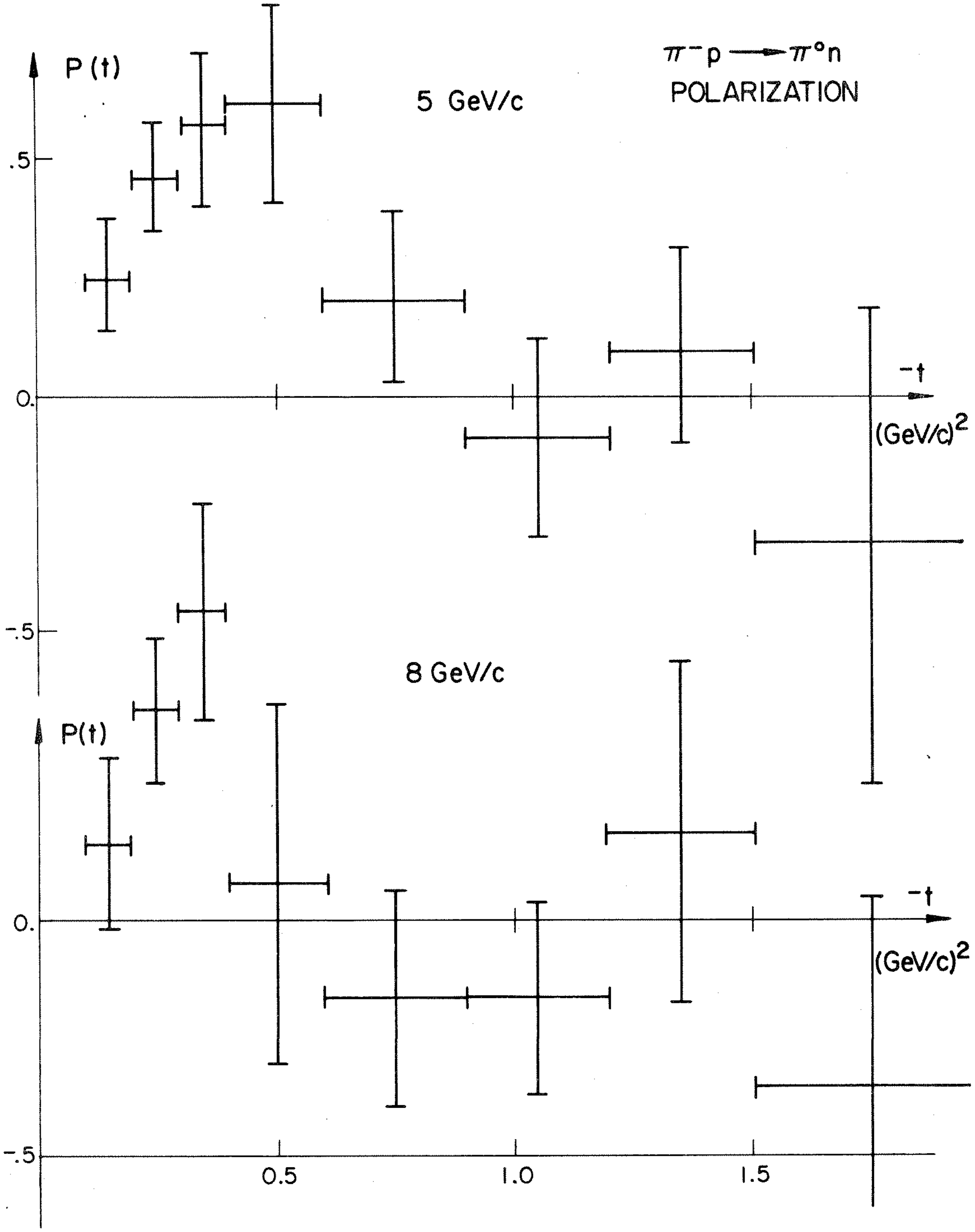

Figure 10: π^-p charge exchange polarization data.[13)]

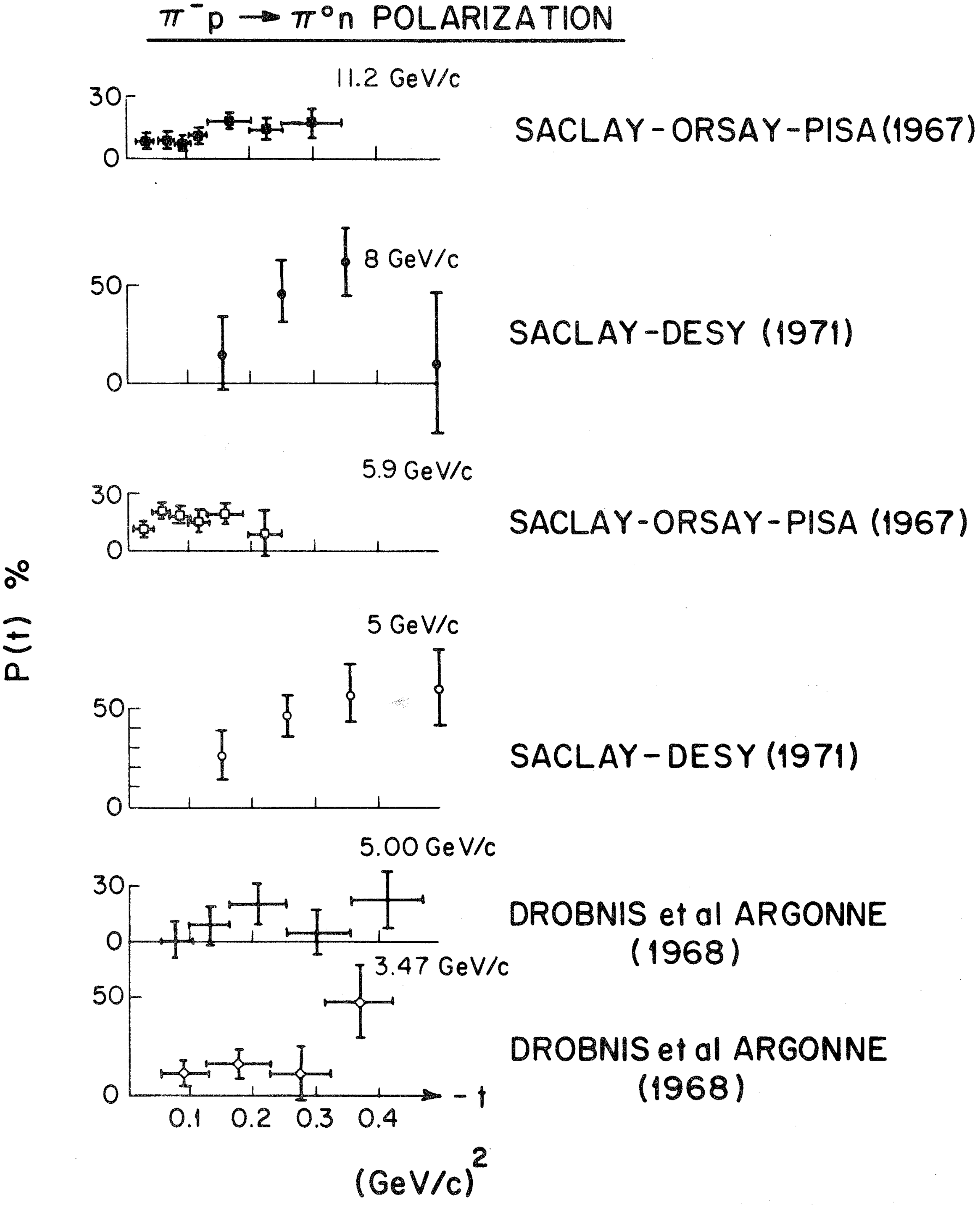

Figure 11: Comparison of new data[13) with other data.

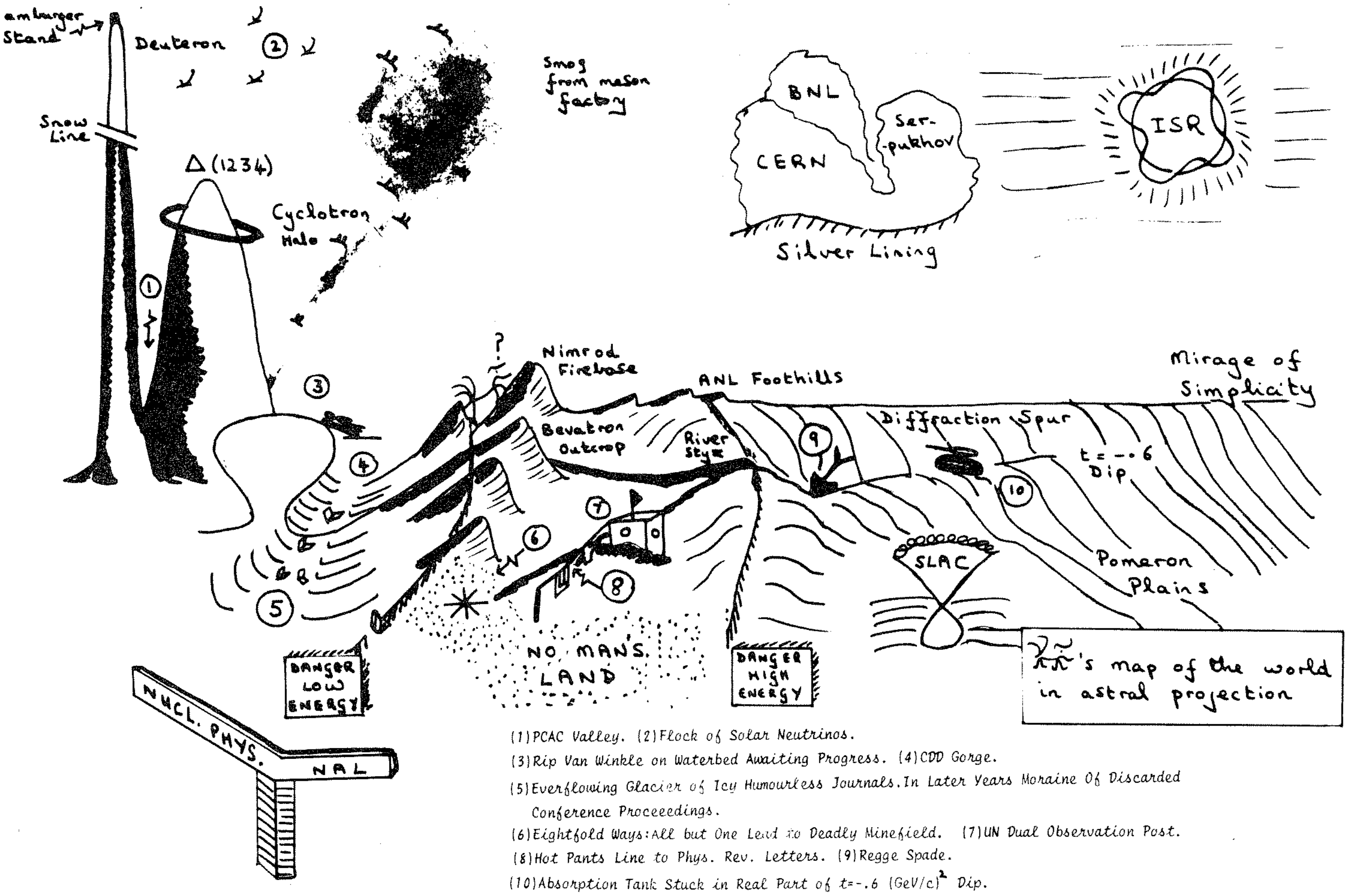
amburger Stand
Deuteron
②
Snow Line
Δ(1234)
Smog from meson factory
BNL
CERN
Ser-pukhov
ISR
Silver Lining
Cyclotron Halo
①
③
④
⑤
?
Nimrod Firebase
Bevatron Outcrop
ANL Foothills
River Styx
⑥
⑦
⑧
⑨
Diffraction Spur
t = -.6 Dip
⑩
Mirage of Simplicity
SLAC
Pomeron Plains
NO MANS LAND
DANGER LOW ENERGY
DANGER HIGH ENERGY
NUCL. PHYS.
NAL
$\overset{\tilde{\gamma}}{\pi\tilde{\pi}}$'s map of the world in astral projection

(1)PCAC Valley. (2)Flock of Solar Neutrinos.

(3)Rip Van Winkle on Waterbed Awaiting Progress. (4)CDD Gorge.

(5)Everflowing Glacier of Icy Humourless Journals.In Later Years Moraine Of Discarded Conference Proceeedings.

(6)Eightfold Ways:All but One Lead to Deadly Minefield. (7)UN Dual Observation Post.

(8)Hot Pants Line to Phys. Rev. Letters. (9)Regge Spade.

(10)Absorption Tank Stuck in Real Part of $t=-.6$ $(GeV/c)^2$ Dip.

PHENOMENOLOGY AT INTERMEDIATE ENERGIES

Christoph Schmid
CERN, Geneva, Switzerland

1. - THE SIGNIFICANCE OF INTERMEDIATE ENERGY EXPERIMENTS FOR REGGEOLOGY

1.1. - Where does Regge start ?

It is surprising that simple Regge type features persist down to low energies in many reactions. As an operational definition for the beginning of the Regge region we require that the fluctuations in s at fixed t are quite small, say $\delta A/A \lesssim 15\%$.

A - In near forward elastic scattering, Regge features persist down to $p_{lab} \approx 1.5$ GeV/c. This came as a surprise to the CERN-Holland group 1). They set out to discover Y^* resonances in $K^-p - K^-p$ in the region $p_L = 1.5 - 2.5$ GeV/c by measuring the polarization. Instead they found surprising Regge type regularities : they observed a dip at $t \approx -0.8$ GeV^2, whose position is pretty much independent of p_{lab} ; similarly the position of the first zero in the polarization is at $t \approx -0.8$ GeV^2 for all energies in the interval.

The new Argonne data 2) on the full angular distribution for the π^+p polarization at $p_L = 1.8 - 2.3$ GeV show, for $|t| \lesssim 1.5$ GeV^2, a great similarity to the polarization at higher momenta, Fig. 1. In fact the FESR Regge fit of Barger and Phillips 3) gives a good description for $|t| \leq 2.0$ GeV^2 and $p_L \geq 2.1$ GeV/c.

B - In inelastic reactions, we have to distinguish between amplitudes where the low energy resonances add and those where the resonances cancel. The former type of amplitude is big and shows small fluctuations, the latter type is small and shows big fluctuations. An example for the former type is the spin-flip amplitude of π^-p CEX, for the latter type the non-flip π^-p CEX. Where we can isolate the latter type, as in $\sigma_{tot}(\pi^-p) - \sigma_{tot}(\pi^+p)$, we observe strong fluctuations up to $p_L = 2.5$ GeV/c. Where the former type dominates, as in $d\sigma/dt$ (π^-p CEX) for $t \neq 0$, no s dependent (resonance type) structure is seen above $p_L \gtrsim 2.0$ GeV (with the present accuracy).

C - In πN backward scattering, one observes dramatic dips in $\sigma(180^\circ)$ at $p_L \approx 2.1$ GeV/c for π^+p, π^-p and π^-p CEX. The $\Delta(11/2^+, 2420)$ at $p_L = 2.6$ still appears as a marked peak and the π^+p polarization at 2.75 GeV/c 2) looks qualitatively very different from the new results at 6 GeV 4). Therefore Regge type experiments in the backward peak should not be done below $p_L = 4.0$ or 3.5 GeV/c. An exception is the exotic channel $K^+p \rightarrow K^+p$. According to exchange degeneracy the backward peak should be purely real, and the polarization should vanish. Within statistical errors this is the case down to momenta as low as $p_L = 1.80$ GeV/c, see Fig. 2 5).

1.2. - Regge shrinkage

Regge shrinkage is dramatic at large t, (say, $|t| \sim 1\text{-}3$ GeV^2), see the π^+p data 6) in Fig. 3, and the effective trajectory in Fig. 4.

- The conclusion for the experimentalist : Regge features are more dramatic at large t, and in the past the gross structure in t over a large t interval has been more illuminating than fine details near $t = 0$.
- The conclusion for the theorist : the present cut models (weak or strong) fail badly beyond $|t| \sim 0.5$ GeV^2, they do not reproduce the strong shrinkage exhibited by the data, Fig. 4. One of the important tasks is to find a reasonable cut model for beyond $|t| \sim 0.5$ GeV^2.

Regge shrinkage is also observed for π^+p backward scattering in the intermediate energy region, $3.25 \leq p_L \leq 5.25$ GeV/c, see Fig. 5 from Ref. 7).

Plots of $\alpha_{\text{effective}}$ can be misleading, if the cross-section is a sum of several terms (particularly if there is destructive interference). It is cleaner to isolate a single term, e.g., $[d\sigma/dt(K^-p) - d\sigma/dt(K^+p)]$ in a pole model is the interference term between the

Pomeron and the vector mesons (ω, ρ). Therefore it should follow a simple power law $s^{\alpha_P + \alpha_M - 2}$. In Fig. 6, Ref. 8), we see that the data follow such as a simple power law from $p_L = 15$ GeV/c all the way down to $p_L = 1.5$ GeV/c. Note particularly $|t| = 0.5 - 0.8\ \mathrm{GeV}^2$, where the statistics for the difference are good. The fitted exponent $n = \alpha_P + \alpha_M$ is shown on Fig. 7. We see that the shrinkage is even somewhat stronger than $\alpha'_P = 0.3$ and $\alpha'_M = 0.9\ \mathrm{GeV}^{-2}$.

1.3. - Structure in t

Regge experiments at large t, $|t| \approx 1.0 - 3.0\ \mathrm{GeV}^2$, are also important, because they teach us something about the qualitative behaviour of the amplitudes near the points $\alpha = 0, -1, -2$.

The qualitative features of the elastic $K^{\pm}p$ and $\pi^{\pm}p$ polarizations are simply explained by exchange degeneracy. The polarization arises from a Pomeron-meson interference.

Assuming the Pomeron to be purely imaginary, non-flip and without structure in t, the polarization becomes proportional to $\mathrm{Re}\, B_{\mathrm{meson}}$. Exchange degeneracy implies that the phase of the combined meson poles is $-e^{-i\pi\alpha}$ for K^-p, -1 for K^+p and $+1-e^{-i\pi\alpha}$ for the ρ term. Therefore the polarization is

$$\begin{array}{llll} \mathrm{Pol.} \sim -\mathrm{Re}\, B_{\mathrm{meson}} & \sim +1 & \text{for} & K^+p \\ & \sim +\cos\pi\alpha & \text{"} & K^-p \\ & \sim +1-\cos\pi\alpha & \text{"} & P\sigma(\pi^+p) - P\sigma(\pi^-p) \end{array}$$

This correctly gives the structure shown in Fig. 8, Refs. 9), 10) : the rise $\sim t^{\frac{3}{2}}$ of K^-p near $t = 0$, the comparable magnitude and positive relative sign of $K^{\pm}p$ near $\alpha = 0$, the zero of K^-p near $\alpha = -\frac{1}{2}$, the comparable magnitude and opposite sign for $K^{\pm}p$ near $\alpha = -1$, the zero of K^-p near $\alpha = -1.5$. In $\pi^{\pm}p$ it gives the well-known double zero of the difference of the polarization at $\alpha = 0$. Note that the low energy experiments ($K^{\pm}p$ at 2.7 GeV, $\pi^{\pm}p$ at 5 GeV) were more useful to Regge phenomenology than the experiments at higher momenta (available at that time), because the former covered a larger t interval with better statistics.

1.4. - Why experiments at intermediate energy ?

Because of interesting structure in t and because of dramatic Regge shrinkage at large t, experiments in the range $|t| \sim 1 - 3$ GeV^2 are important. But statistics becomes a problem at large t, therefore the experimentalist is forced to do Regge experiments at intermediate energies. Luckily, Regge features persist down to low energies (see 1.1). For elastic scattering and $|t| \lesssim 2.0$ GeV^2 one can do Regge experiments at a momentum as low as $p_L = 2.5$ or even 2.0 GeV/c.

It is a widely held misconception that Reggeology is "purest" and "simplest" at very small t and at the highest available energies. The last few years have taught us the opposite ; we must not close our eyes at the dramatic schrinkage at large t and at the beautifully simple large t structure of the polarization.

One might wonder whether Regge phenomenology will look very different at 70 - 500 GeV from 2 - 5 GeV. This is quite possible ; the relative importance of cuts may be very different. If at some future time there would be two simplified formulations, one useful and simple for 2 - 20 GeV, the other one for 20 - 200 GeV, then it would be the former which would be relevant for duality. The interlocking via FESR of the resonance region with the Regge region refers more to the intermediate energy Regge description than to the very high energy models.

2. - THE CONFRONTATION OF THE REGGE DESCRIPTION WITH THE PHASE SHIFT DESCRIPTION IN K^+p SCATTERING

K^+p scattering is a good place to compare directly (locally) the Regge and the phase shift descriptions. At fixed t, the data $(d\sigma/dt, P)$ for K^+p appear Regge behaved down to $p_L \approx 1.4$ GeV. On the other hand, phase shifts exist up to $p_L = 2.5$ GeV.

At each energy and momentum transfer, the present experiments give us only two quantities $d\sigma/dt$ and P. How is it possible to determine all four quantities, Re and Im of non-flip and flip ?

The crucial hypothesis for a phase shift analysis is that all partial waves above ℓ_{max} are either zero or fixed as a theoretical input (from partial wave dispersion relations or from Veneziano). If σ_{tot} and all moments A_n (of $d\sigma/d\Omega$) and B_n (of $P\, d\sigma/d\Omega$) up to $n = 2\ell_{max}$ are experimentally well determined, one has the same number of unknowns and of equations, namely $2\,(2\ell_{max}+1)$. In principle this allows us to arrive at the knowledge of four quantities at each energy and momentum transfer. Unfortunately, almost all equations are quadratic, and one is faced with an enormous ambiguity problem ; there are of the order of $2^{2L_{max}+1}$ solutions $^{11)}$.

In a Regge model the phase of an amplitude can be obtained from the s dependence of the absolute magnitude of this amplitude. This allows us to arrive at the knowledge of three quantities at each energy and momentum transfer. The fourth quantity can never be determined in a Regge framework, because (for t not near zero) one can always rotate a Regge solution in the $a-b$ plane (spin non-flip/spin flip plane) without changing cross-sections or polarizations [for details, see Ref. 12)].

In a confrontation between phase shifts and Regge, one must compare this third quantity, which can be defined as the "effective phase" :

$$\tan \varphi \equiv \left[\frac{(\mathrm{Im}\, a)^2 + (\mathrm{Im}\, b)^2}{(\mathrm{Re}\, a)^2 + (\mathrm{Re}\, b)^2} \right]^{1/2}$$

where a and b are t channel helicity amplitudes with kinematical factors absorbed such that $d\sigma/dt = |a|^2 + |b|^2$ and $P d\sigma/dt = -2\, \mathrm{Im}(ab^*)$. It is useful to define the third quantity also in another way, which is equivalent, if $d\sigma/dt$ and P are measured (and fitted) at one given (s, t) with infinite accuracy. One considers the a - b plane (non-flip - flip plane) and draws the vectors $\vec{\mathrm{Re}} = (\mathrm{Re}\, a, \mathrm{Re}\, b)$ and $\vec{\mathrm{Im}} = (\mathrm{Im}\, a, \mathrm{Im}\, b)$. The angle between the two vectors, $\vartheta(\vec{\mathrm{Re}}, \vec{\mathrm{Im}})$, is this second possibility to define the third quantity.

In Fig. 9, such a comparison is made for K^+p scattering at $p_L = 1.45$ GeV/c. The solid lines show the predictions of various phase shift solutions 13),14) for two possible (equivalent) definitions of the third quantity. We see that the various phase shift solutions strongly disagree among each other, although they look quite similar on the Argand plots. For example, at $t = -1$ GeV^2, the solutions have φ values from 20° (predominantly real) to 60° (predominantly imaginary). Some solutions tend to $\varphi \approx 90°$ (purely imaginary) towards the backward direction, in contradiction with the exchange degeneracy prediction that K^+p backward scattering should be purely real (and therefore $P = 0$, see Fig. 2).

The dots show the predictions of the effective pole model of Daum et al. 12). An effective pole model was chosen because the presently available cut models fail badly if one goes out to $|t| = 1.5$ GeV^2, e.g., they cannot reproduce the dramatic shrinkage shown by the data, Fig. 7, while our effective three-pole model gives quantitative fits. We see on Fig. 9 that the Regge predictions strongly discriminate against the solutions ANL II, III, IV. They disfavour the solutions ANL I, CERN α , γ, while the agreement is moderate with CERN β .

We conclude that in principle the Regge approach allows us to discriminate among phase shift solutions. What is now needed are Regge models which are quantitatively reliable out to 1.5 GeV^2.

3. - THE GEOMETRICAL PICTURE

A useful "language" for the Reggeologist is to plot his amplitudes not versus t (at fixed p_{lab}) but versus ℓ or equivalently versus this impact parameter $b \equiv \ell/k$. In general a partial wave analysis at high energy requires reliable Regge amplitudes out to fairly large t as an input. In special cases, however, there are shortcuts, if one is willing to make certain approximations. Davier and Harari 15) use, for $K^\pm p$ elastic scattering at 5 GeV, the following approximations :

(i) neglect R^2 terms compared to P^2, but keep the interference terms $P \cdot R$, where P = Pomeron, R = ordinary Regge pole ;

(ii) assume the Pomeron to be purely imaginary for $t \neq 0$;

(iii) assume that R is purely real in K^+p since there are no resonances.

With these assumptions, one obtains :

$$d\sigma/dt\ (K^+p) \approx |P|^2$$

$$d\sigma/dt\ (K^-p) \approx |P|^2 + 2|P|\ \mathrm{Im}\, R_{\Delta\lambda=0}$$

In the differential cross-section, interference with P is only possible for that part of the R amplitude which has the same phase and spin structure as P (s channel helicity non-flip, $\Delta\lambda = 0$). Solving for Im $R_{\Delta\lambda=0}$, we obtain

$$\mathrm{Im}\, R_{\Delta\lambda=0} = \frac{\frac{d\sigma}{dt}(K^-p) - \frac{d\sigma}{dt}(K^+p)}{2\sqrt{\frac{d\sigma}{dt}(K^+p)}}$$

Im $R_{\Delta\lambda=0}$ is shown in Fig. 10. We see the well-known cross-over zeros at $|t| = 0.2$ and 1.3 GeV^2. They are shifted (by cuts) compared to the positions in an exchange degenerate pole model, $\alpha(t) = 0, -1$.

The position of the first zero is simply connected (via FESR) to the first zero of the intermediate energy resonances. Helicity non-flip corresponds to an angular dependence $P_\ell(\cos\vartheta)$ while helicity flip corresponds to $P'_\ell(\cos\vartheta)$. Therefore the first zero in the non-flip amplitude must be closer to $t = 0$ than the first zero in the flip amplitude. This means that the exchange degeneracy of the t channel Regge amplitudes must be broken (by cuts), because of the spin structure of the direct channel resonances.

The curve drawn through the points in Fig. 10 is motivated by the picture of one dominant (band of) partial wave(s) containing the zeros of $P_\ell(\cos\vartheta)$ or of its asymptotic form $J_0(c\sqrt{-t})$. Since a fundamental feature of the difference plotted in Fig. 10 is the strong Regge shrinking shown in Figs. 6, 7, J_0 must be multiplied by a shrinkage factor $\exp[B(s)t]$. In partial wave language this means that one needs an expanding band (Δb) of impact parameters participating, i.e., we must have a collective effect of many partial waves.

Figure 11 shows the partial wave analysis of Im $R_{\Delta\lambda=0}$ *). We see indeed a peaking for an impact parameter of about one fermi ; this means that the imaginary part of the ordinary Regge amplitude is a

---

*) It makes no sense to partial wave analyze differential cross-sections. What one analyzes here is the imaginary part of an amplitude (approximately). The result can be trusted for low and intermediate ℓ, but not for high ℓ.

peripheral effect. We also see that a broad band of partial waves is needed, $\delta\ell \approx 6$. At $p_{lab} = 5$ GeV the parent trajectory $(Y_0^* : \frac{1}{2}^+, \frac{3}{2}^-, \frac{5}{2}^+ \ldots)$ is at $\ell = 10$, while the dominant partial wave, $\ell = kb \sim \sqrt{s}$, is at $\ell \approx 7$.

The unabsorbed Veneziano amplitude and the empirical amplitude in Fig. 11 have the common feature of a collective effect of many partial waves, from $\ell = \ell_{parent} \sim s$ down to $\ell = 0$. In both cases the partial waves which are dominant for $-1 < \cos\vartheta < +1$, are near $\ell = \ell_{dominant} \sim \sqrt{s}$. The difference lies in a strong suppression of the very low partial waves in the empirical amplitude ($\ell \lesssim 3$ at 5 GeV) compared to the unabsorbed Veneziano amplitude.

Veneziano models for KN, $\bar{K}N$ with weak or no absorption have the following feature : if fitted to $\sigma_{tot}(K^\pm p, K^\pm n)$, and with the flip - non-flip ratio from $d\sigma/dt$ (CEX) and from the assumption that ω-f decouple from s channel flip, one predicts the strength of the Y^* parent resonances too small by about a factor 2. This statement can be turned around : if the parent resonance strength is the input, then the forward amplitudes which are the sum of parents and all daughters, $\sum_\ell (2\ell + 1)\, a_\ell$, come out too large by about a factor 2. In other words the daughters must be absorbed more strongly. What is needed is a new absorption model which uses non-sense wrong signature zeros in the input (e.g., a Veneziano input) like the Argonne model, but which has stronger absorption in the very low partial waves than the Argonne model.

If one has a broad band of partial waves centered at ℓ_{dom}, the first (and in our case also the second) zero of the angular distribution will be given by the zero(s) of P_ℓ with $\ell = \ell_{dom}$. Further out in t there will be strong cancellations within the band of important waves in order to give the Regge shrinkage ; therefore the zeros are not expected to be given by the wave with $\ell = \ell_{dom}$. Experimentally the second and third cross-over zeros (at $|t| = 1.3$ and about 2.2 GeV^2) are approximately given by the exchange degeneracy positions, $\alpha = -1, -2$.

For pp and $p\bar{p}$ elastic scattering the second and third cross-overs disappear, $d\sigma/dt(p\bar{p})$ stays smaller than $d\sigma/dt(pp)$ after the first cross-over. In this case both the exchange degeneracy picture and the ℓ_{dom} picture (J_0 picture) need important corrections.

Why is the scattering (at 5 GeV) strongest near an impact parameter of 1 fermi (see Fig. 11) ? The effective impact parameter is directly connected to the first zero of the angular distribution. This first zero occurs at a t value, which is independent of s, and which is the same for the Regge amplitude at 5 GeV and for the intermediate energy resonances. Therefore the dominant impact parameter is independent of s, and the value of 1 fermi is the value given by the intermediate energy resonances, $Y^*(\frac{5}{2}^\pm \frac{7}{2}^\pm \frac{9}{2}^\pm)$.

In Fig. 12, we see that the Pomeron is mostly in low partial waves.

Only the imaginary part of the (non-Pomeron) Regge amplitude is peripheral. The real part is central in K^+n CEX, but peripheral in K^-p CEX. This comes from the Regge signature factors which give :

$$K^-p \text{ CEX} : -e^{-i\pi\alpha}$$

$$K^+n \text{ CEX} : -1$$

The slope of the forward peak is directly related to the average radius of interaction :

$$F(t) = C\, e^{\frac{1}{2}Bt}$$

$$\frac{1}{2}B = \left.\frac{dF/dt}{F}\right|_{t=0} = \frac{\sum_\ell (2\ell+1)\, a_\ell \frac{\ell(\ell+1)}{4q^2}}{\sum_\ell (2\ell+1)\, a_\ell} = \left\langle \frac{b^2}{4} \right\rangle$$

Predazzi 16) has plotted this experimental slope B of the forward peak for $\pi^+ p - \pi^+ p$, as a function of energy, see Fig. 13. As we come to the $\Delta(\frac{7}{2}^+, 1920)$, the average radius of interaction shows a sharp increase. This is still another indication that intermediate energy resonances are peripheral effects.

There is a funny change of roles. A few years back, in the interference model, people thought that resonances correspond to central collisions and Regge exchanges correspond to peripheral collisions. Now we have seen that resonances are quite peripheral effects ($b \sim 1$ fermi) and that the unabsorbed Regge amplitude is not peripheral enough.

4. - THE NEW INTERFERENCE MODEL

Above the present phase shift region, $p_L \gtrsim 2.5$ GeV/c in πN, one still sees resonance structure, particularly in the backward direction. What model could be used to fit this region ? The Veneziano model is not flexible enough (in practice) to give quantitative fits, quite apart from the difficulties with treating fermions correctly. Therefore one considers a model with resonances plus "something else".

Duality assumes resonance saturation for the imaginary part, therefore the imaginary part is represented either by resonances or by Regge exchanges. In addition we have the Pomeron. While the usual duality framework is explicit about the imaginary part, it says little about the real part, which must be computed from dispersion relations. In this sense the K^+n charge exchange (CEX) amplitude, which is purely real, is built by the long range tails of the Y^* resonances in the crossed channel.

Before discussing the real part in more detail, let us look at the Indiana model 17). They fit the π^+p backward peak as a sum of resonances only. The inconsistency of this ansatz is evident when applied to K^+p backward scattering. Since there are no (strong) K^+p resonances the Indiana approach would imply that there is no (strong) backward peak in K^+p, while duality merely says that the imaginary part of the K^+p backward peak should be zero. Experimentally K^+p has a strong backward peak (Λ, Σ exchange), but the polarization is 0 ± 20% for $p_L = 1.6 - 2.3$ GeV/c (see Fig. 2), in agreement with the duality prediction.

A step forward in the treatment of the real part is the new interference model by Coulter, Ma and Shaw 18). It is useful to consider separately the u channel and s channel resonances in the FESR :

$$\int_{-N}^{+N} \frac{\mathrm{Im}\, F_{\text{res.}}\, ds'}{s'-s} \approx \sum u \text{ reson.} + \sum s \text{ reson.} \qquad (4.1)$$

Similarly it is useful to split up the full Regge term not into even signature and odd signature parts, but rather into parts which have only either a s channel ($\cos\vartheta_t > +1$) or a u channel ($\cos\vartheta_t < -1$) cut :

$$\left[\mp 1 - e^{-i\pi\alpha(t)}\right] s^{\alpha(t)} = \mp s^{\alpha(t)} - (-s)^{\alpha(t)} \qquad (4.2)$$

(For definiteness we assume that we are in the s channel, s positive.) Duality (i.e., resonance saturation and Regge pole dominance) implies that we can either use both types of resonances or both types of Regge terms (in the absence of the Pomeron). But we note that there is a one-to-one correspondence between the splitting up into two terms in (4.1) and (4.2), e.g., the first terms in both expressions have no s channel discontinuities. The new interference model uses, when working in the s channel, the second term of (4.1) and the first term of (4.2), i.e., they take the s channel resonances and add that part of the t channel Regge pole which has the discontinuity in the u channel *). In the Veneziano model, the decomposition looks as follows :

$$\text{in the } s \text{ channel}: \quad \underbrace{V_{st} + V_{su}}_{\substack{\downarrow \\ s \text{ resonances}}} \quad + \quad \underset{\substack{\downarrow \\ \text{purely real} \\ \text{Regge term}}}{V_{ut}}$$

where V_{ut} has singularities in u and t only.

For the real part and the problem of tails this is quite a step forward, the tails of the u channel resonances are now neatly parametrized by the V_{ut} Regge term. We are still faced with the problem of the tails of low energy s channel resonances.

Yokosawa tries to circumvent this by using resonances only in the imaginary part and taking for the real part the full Regge real part. This is not good, because any s dependent structure in the imaginary part is reflected (via analyticity) in an equally important structure in the real part.

The problem of high energy tails of low energy resonances is intimately tied to the problem of daughter partial waves at intermediate energies. The necessity for daughters is obvious, because $|f(0^\circ)| \gg |f(180^\circ)|$. The backward amplitude is small because many (large) partial waves cancel against each other. There have been many fits which used (at any given energy) only a few parent partial waves (in the imaginary part). They could obtain fits to some small u

---

*) Practically this means dropping the term $e^{-i\pi\alpha}$ in the Regge signature factor.

interval, say $0 \leq |u| \leq 1$ GeV^2. These models would not be able to build up the large (non-Pomeron contribution to the imaginary part of the) forward peak.

The test question to ask for any calculation with the new interference model is the following : does it have enough daughter resonances to build up $\sigma_{tot} - \sigma_{tot}$ (Pom) ? Figure 14 [Ref. 19] shows that after subtracting all the established and half-established Y^* resonances from $\sigma_{tot}(K^-p)$, one is still 7 mb above $\sigma_{tot}(K^-p$, Pom) for $p_L = 1.5 - 3.0$ GeV/c. Since σ_{tot}(resonances) $\approx$ $\approx$ 5 mb at 2 GeV, the resonance amplitude must be more than doubled. If one sticks to the model, one needs a lot of new resonances for which there is not yet direct evidence. If one parametrizes the 7 mb difference as background, this background would correspond to the daughter partial waves of the ordinary Regge exchange, while the higher partial waves of Regge would correspond to the explicit resonances. Such an approach would be similar to the phase band method (discussed in Section 5), with the difference that here the background is parametrized in (s,t) with a simple s dependence, while there the parametrization is in ℓ (in the impact parameters) with little emphasis on the s dependence.

The best place to try out the new interference model is in those cases where at least one of the three ingredients (s resonances, u-t Regge term, Pomeron) is absent : (i) $\bar{K}N$ elastic scattering : Pomeron + resonances 20) ; (ii) $K^-p - \bar{K}^0n$: only resonances 19) ; (iii) $\pi^-p - \pi^0n$: resonances + u-t Regge term.

A consistent fit in the new interference model needs a lot of parameters, and in order to tie them down one must fit the full angular range of $d\sigma/d\Omega$ and P over a large energy interval. So we are almost back to an energy dependent phase shift analysis, with the exception that the background parametrization is more economical and physically more meaningful.

5. - THE PHASE BAND METHOD

Moravcsik has proposed another tool for analyzing data above the phase shift region 21). He parametrizes the low partial waves, $0 \leq \ell \leq \ell'$, in a collective way (phase band), practically by cubic functions for $\delta(\ell)$ and $\eta(\ell)$. The high partial waves, $\ell' < \ell \leq \ell_{max}$, are parametrized individually as in the usual phase shift analysis, therefore they are allowed to contain resonances. The method has been applied by Bridges, Moravcsik and Yokosawa 22) to π^+p scattering at $p_L = 2.5$ and 2.75 GeV with $\ell' = 4$ and $\ell_{max} = 6$. It is now important to notice that there is not one phase band, but rather there are eight phase bands : we need a separate parametrization for $j = \ell + \frac{1}{2}$ and $j = \ell - \frac{1}{2}$, for even ℓ and odd ℓ, for Re and Im or equivalently for δ and η. If we have a cubic fit in each phase band we need $8 \times 3 = 24$ parameters, while the conventional analysis uses only $2(2\ell' + 1) = 18$ parameters. This means that one must go to much higher energies in order to make this method economical. Bridges et al. 22) halve their number of free parameters by not distinguishing even ℓ from odd ℓ.

One might ask whether it might be all right not to distinguish between even and odd ℓ nor between $j > \ell + \frac{1}{2}$ and $j = \ell - \frac{1}{2}$, or to put the real parts to zero, for low partial waves. All this corresponds to the assumptions : (i) that the low partial waves are dominated by Pomeron exchange, which is verified by Fig. 12, and (ii) that the non-Pomeron part in the low partial waves $\ell \leq \ell'$ is negligible compared to the non-Pomeron part in the high partial waves $\ell > \ell'$, which is certainly not true according to Fig. 11.

Also we know independently of the figure that it is impossible to build an ordinary Regge exchange (with shrinkage) out of only two partial waves at 2.5 GeV, one needs a collective effect of many. We conclude that we really need eight phase bands.

In $K^-p - K^-p$ there is no backward peak at intermediate energies, therefore it is reasonable to drop the distinction between even ℓ and odd ℓ in the phase band. (Even in the peripheral waves there is, in an average sense, no distinction between even and odd partial waves, since the peripheral resonances are exchange degenerate.) This reduces the phase band parameters by a factor of two and makes this reaction a preferred place to apply the method.

6. - K^-p BACKWARD SCATTERING

At high energy, $\bar{K}N - \bar{K}N$ backward scattering is an exotic reaction : the exchanged Regge pole would have to be a Z^* resonance which cannot be built from three quarks.

The new data of the CERN-Orsay-Paris-Stockholm collaboration 23) show that at $p_L = 5$ GeV the 180° cross-section for K^-p is very much suppressed compared to K^+p : $\sigma_{K^-p}(180^\circ) : \sigma_{K^+p}(180^\circ) \approx 1 : 100$, see Fig. 15. From $p_L = 1$ to $p_L = 5$ GeV, one has a steep falling off in $\sigma_{K^-p}(u = 0)$. The point at 5 GeV may or may not indicate the beginning of a different power law (Regge cut ?). This suspicion is strengthened by the observation that the K^-p angular distribution has a backward peak of the same relative height and width as the K^+p backward peak, see Fig. 16. In our context here it is important that this effect is very small in absolute terms.

If the high energy reaction is exotic, the low-energy resonances Y^* should average to zero at fixed u according to FESR duality. Let us consider $K^-p - \bar{K}^0n$ backward scattering. For $p_L < 1.7$ GeV one observes a strong backward peak. We shall now show that this strong backward peak is consistent with duality. We must consider the amplitudes rather than the differential cross-section.

In Fig. 17 [from Ref. 24], we show the imaginary and real parts of the backward amplitude ; they perform a damped oscillation around zero. We have a semi-local cancellation involving resonances spaced by $\delta(m^2) = 1\ \mathrm{GeV}^2$, as opposed to a local parent-daughter cancellation. Note that, e.g., near $p_L = 1$ GeV the $\Sigma(\frac{5}{2}^-)$ and $\Lambda(\frac{5}{2}^+)$ contribute with the same sign and that daughter contributions are rather unimportant in this case (the dashed curve for resonances qualitatively agrees with the full phase shift amplitudes).

The exotic behaviour in the Veneziano model, e.g., for $\pi^+\pi^- - \pi^+\pi^-$ backward scattering, is produced by an increasing overlap of subsequent resonance towers (semi-local cancellation) and not by a local parent-daughter cancellation. In fact the magnitude of the combined parent-daughter contribution is symmetric with respect to the point $t + \frac{1}{2} = u$, which is approximately the point $\vartheta = 90^\circ$. For instance, at $u = -0.5\ \mathrm{GeV}^2$ the combined parent-daughter contribution is as large as the secondary forward peak at $t = -1.0\ \mathrm{GeV}^2$. The crucial difference between $t = -1.0\ \mathrm{GeV}^2$ (non-exotic) and $u = -0.5\ \mathrm{GeV}^2$ (exotic) as s becomes large, is the alternating sign of subsequent resonance towers in the exotic case. It is only through an increasing overlap (increasing $m\Gamma$) that the exotic behaviour for u fixed $(u \neq 0)$ and $s \to \infty$ is produced. Therefore the rate of decrease of the backward K^-p cross-section $(d\sigma/du \sim p_L^{-9})$ is intimately tied to the increase of resonance widths.

Let us now consider large angle scattering (between the forward and the backward peaks), Fig. 16, and see how duality gives us some understanding of the qualitative features. The angular distributions look very different for K^+p and K^-p at large angles, $+0.3 \geq \cos\vartheta \geq -0.7$, at 5 GeV : K^+p is quite flat in this angular range, while K^-p falls far below in a skew V shaped manner. At 90° we have $d\sigma/dt(K^-p) : d\sigma/dt(K^+p) \approx 1{:}40$, see Fig. 16. Let us study the one-term Veneziano model in the analogous case of $\pi^\pm\pi^+$ elastic scattering :

$$V = -\frac{\Gamma(1-\alpha_s)\,\Gamma(1-\alpha_t)}{\Gamma(1-\alpha_s-\alpha_t)}$$

The s channel is $\pi^+\pi^- - \pi^+\pi^-$ (non-exotic, like K^-p), the u channel is $\pi^+\pi^+$ (exotic, like K^+p). For $s \to \infty$ and $t + \frac{1}{2} = u$ ($\vartheta_s \approx 90^\circ$) we obtain

$$|V| \to e^{-s\log 2}\,\sqrt{2\pi}\;e^{-\frac{\pi}{2}\,\mathrm{Im}\,\alpha(s)}$$

and for $u \to \infty$ and $t + \frac{1}{2} = s$ ($\vartheta_u \approx 90^\circ$) :

$$|V| \to e^{-u\log 2}\,\sqrt{2\pi}\;\sqrt{u}$$

The crucial difference between the exotic channel, $\pi^+\pi^+$, and the non-exotic channel, $\pi^+\pi^-$, is the factor $\exp\left[-\frac{\pi}{2}\,\mathrm{Im}\,\alpha(s)\right]$ which comes from the alternating sign of successive resonance towers in $\pi^+\pi^-$ for fixed angle. As $\mathrm{Im}\,\alpha(s) \to \infty$ these towers overlap increasingly and cancel each other more and more. In $\pi^+\pi^+$ no cancellations can occur. This explains qualitatively why K^-p falls far below K^+p at large angles.

REFERENCES

1) C. Daum, F.C. Erné, J.P. Lagnaux, J.C. Sens, M. Steuer and F. Udo - Nuclear Phys. B6, 273 (1968) ;

S. Andersson, C. Daum, F.C. Erné, J.P. Lagnaux, J.C. Sens, C. Schmid and F. Udo - 1969 Stony Brook Conference, "Hign Energy Collisions", Gordon and Breach (1969).

2) G. Burleson, D. Hill, S. Kato, P.F.M. Koehler, T.B. Novey, A. Yokosawa, D. Eartly, K. Pretzl, B. Barnett, A. Laasanen and P. Steinberg - Phys.Rev.Letters 26, 338 (1971).

3) V. Barger and R.J.N. Phillips - Phys.Rev. 187, 2210 (1969).

4) H. Aoi, N.E. Booth, C. Caverzasio, L. Dick, A. Gonidec, Z. Janout, K. Kuroda, A. Michalowicz, M. Poulet, D. Sillou, C.M. Spencer and W.S.C. Williams - Phys. Letters 35B, 90 (1971).

5) B.A. Barnett, A.T. Laasanen, P.H. Steinberg, D. Hill, S. Kato, P.F.M. Koehler, T.B. Novey, A. Yokosawa, G. Burleson, D. Eartly and K. Pretzl - Phys.Letters 34B, 655 (1971).

6) B.B. Brabson, R.R. Crittenden, R.M. Heinz, R.C. Kammerud, H.A. Neal, H.W. Paik and R.A. Sidwell - Phys.Rev.Letters 25, 553 (1970).

7) R.A. Sidwell, R.R. Crittenden, K.F. Galloway, R.M. Heinz and H.A. Neal - Phys.Rev. D3, 1523 (1971).

8) C. Daum, C. Michael and C. Schmid - unpublished.

9) Ref. 1), for K^+p polarization see also Ref. 13).

10) C. Schmid - 1969 Erice Lectures, Academic Press (1970) ;

P. Sonderegger - 1969 Moriond Lecture, Orsay Report, unpublished.

11) A. Gersten - Nuclear Phys. B12, 537 (1969).

12) C. Daum, C. Michael and C. Schmid - Phys.Letters 31B, 222 (1970), and preprint in preparation.

13) M.G. Albrow, S. Andersson/Almehed, B. Bosnjakovic, C. Daum, F.C. Erné, Y. Kimura, J.P. Lagnaux, J.C. Sens, F. Udo and F. Wagner - CERN Preprint((Dec. 1970), to be published in Nuclear Phys.

14) S. Kato, P. Koehler, T. Novey, A. Yokosawa and G. Burleson - Phys.Rev.Letters 24, 615 (1970).

15) M. Davier and H. Harari - SLAC Preprint (1971).

16) Y. Hama and E. Predazzi - Sao Paolo Preprint

T. Lasinski, R. Levi Setti and E. Predazzi - Phys.Rev. 179, 1426 (1969).

17) R.R. Crittenden, R.M. Heinz, D.B. Lichtenberg and E. Predazzi - Phys.Rev. D1, 169 (1970) ;

P.G. Tomlinson, R.A. Sidwell, D.B. Lichtenberg, R.M. Heinz, R.R. Crittenden and E. Predazzi - Nuclear Phys. B25, 443 (1971).

18) P.W. Coulter, E.S. Ma and G.L. Shaw - Phys.Rev.Letters 23, 106 (1969).

19) C. Bricman, M. Ferro-Luzzi, J.M. Perreau, G. Bizard, Y. Declais, J. Duchon, J. Seguinot and G. Valladas - Phys.Letters 31B, 152 (1970).

20) T.A. Lasinski - Nuclear Phys. B29, 125 (1971).

21) M.J. Moravcsik - Phys.Rev. 177, 2587 (1969).

22) D. Bridges, M.J. Moravcsik and A. Yokosawa - Phys.Rev.Letters 25, 770 (1970) ; Erratum Phys.Rev.Letters 26, 155 (1971).

23) C. Baglin et al. (CERN-Orsay-Paris-Stockholm Collaboration) - to be published.

24) C. Bricman, E. Pagiola and C. Schmid - CERN Preprint D.Ph.II/Phys. 71-15 (1971).

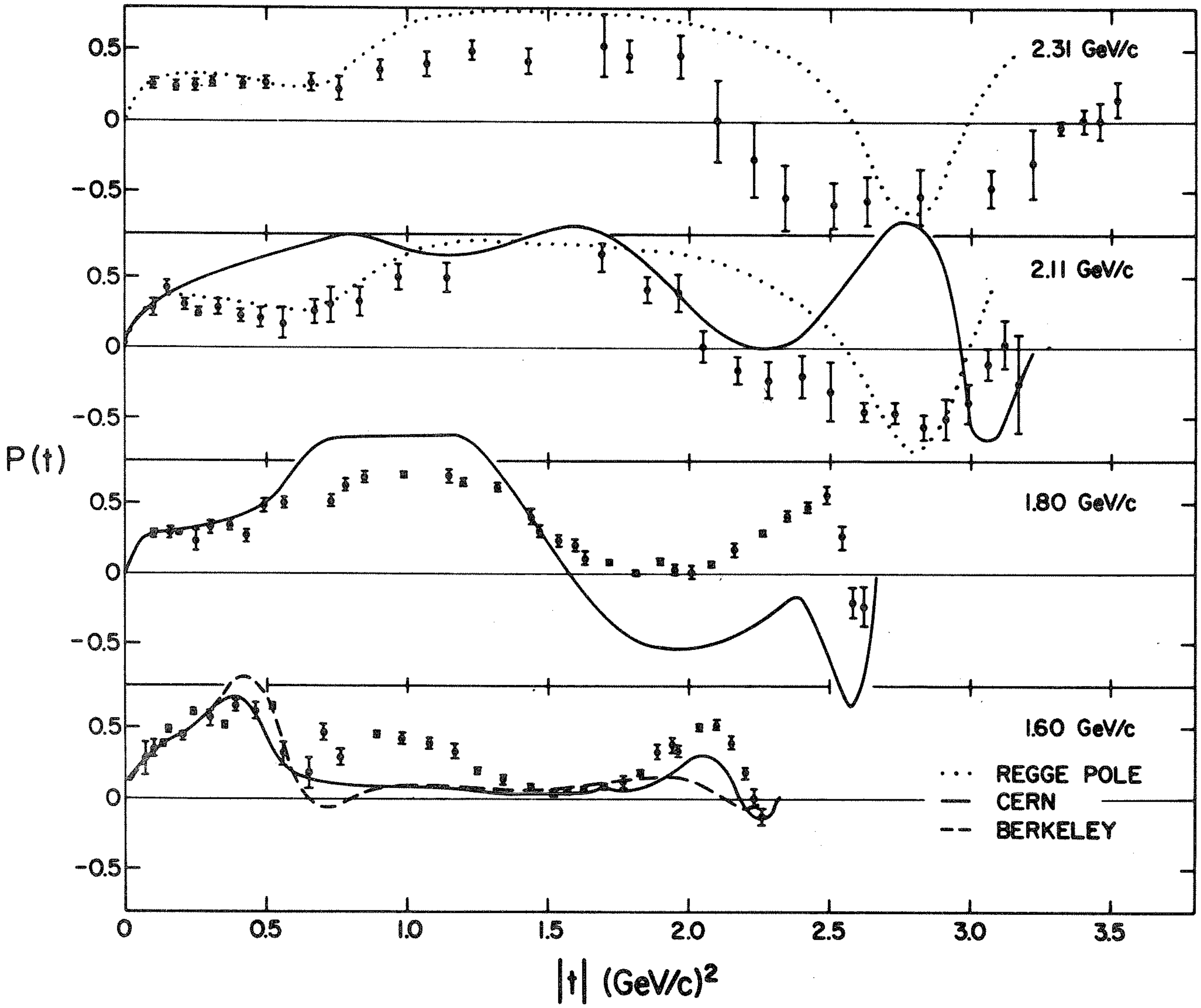

Figure 1 π^+p polarizations, Ref. 2). The Regge pole prediction is from Ref. 3).

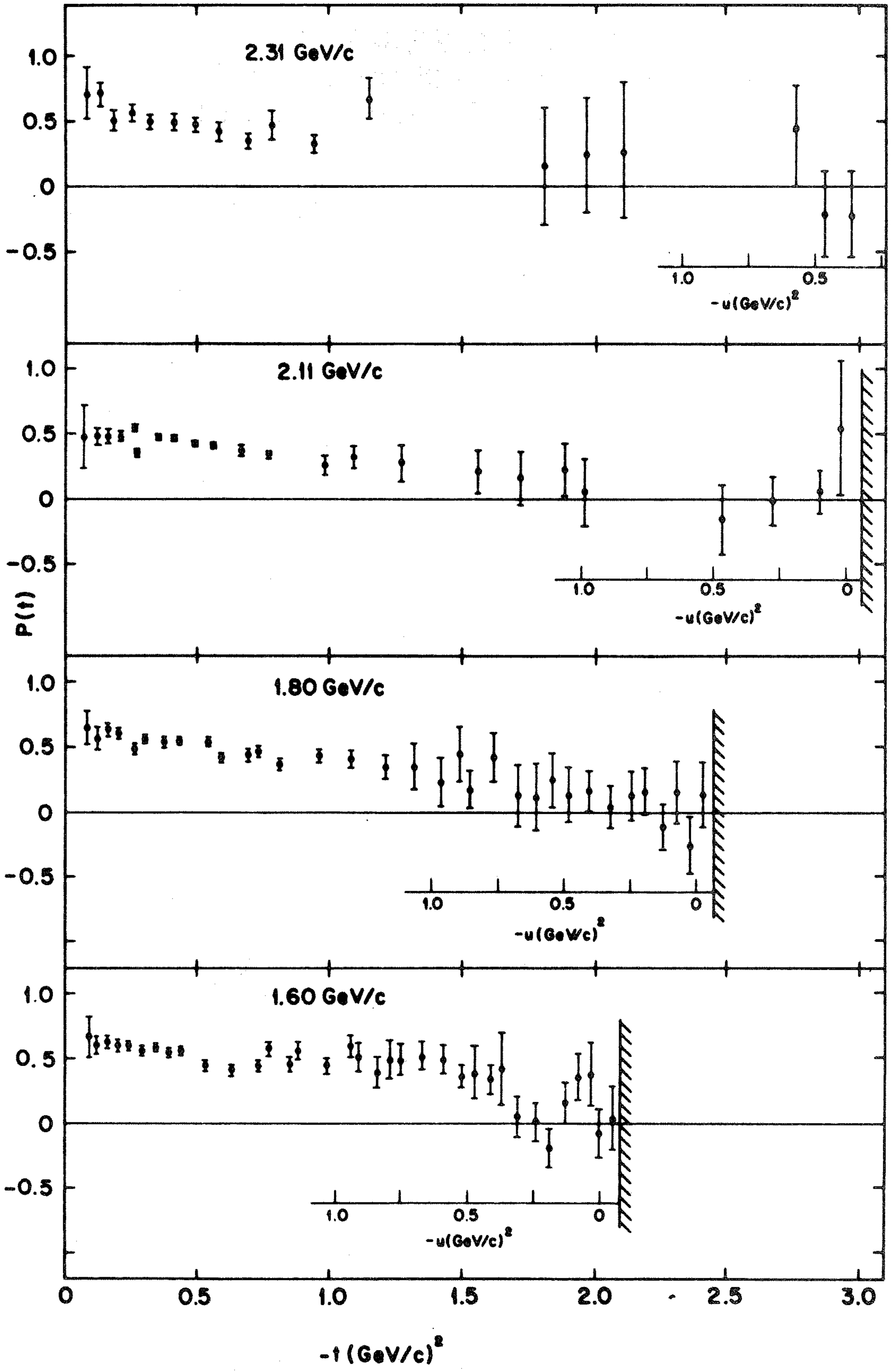

Figure 2 K^+p polarizations, Ref. 5).

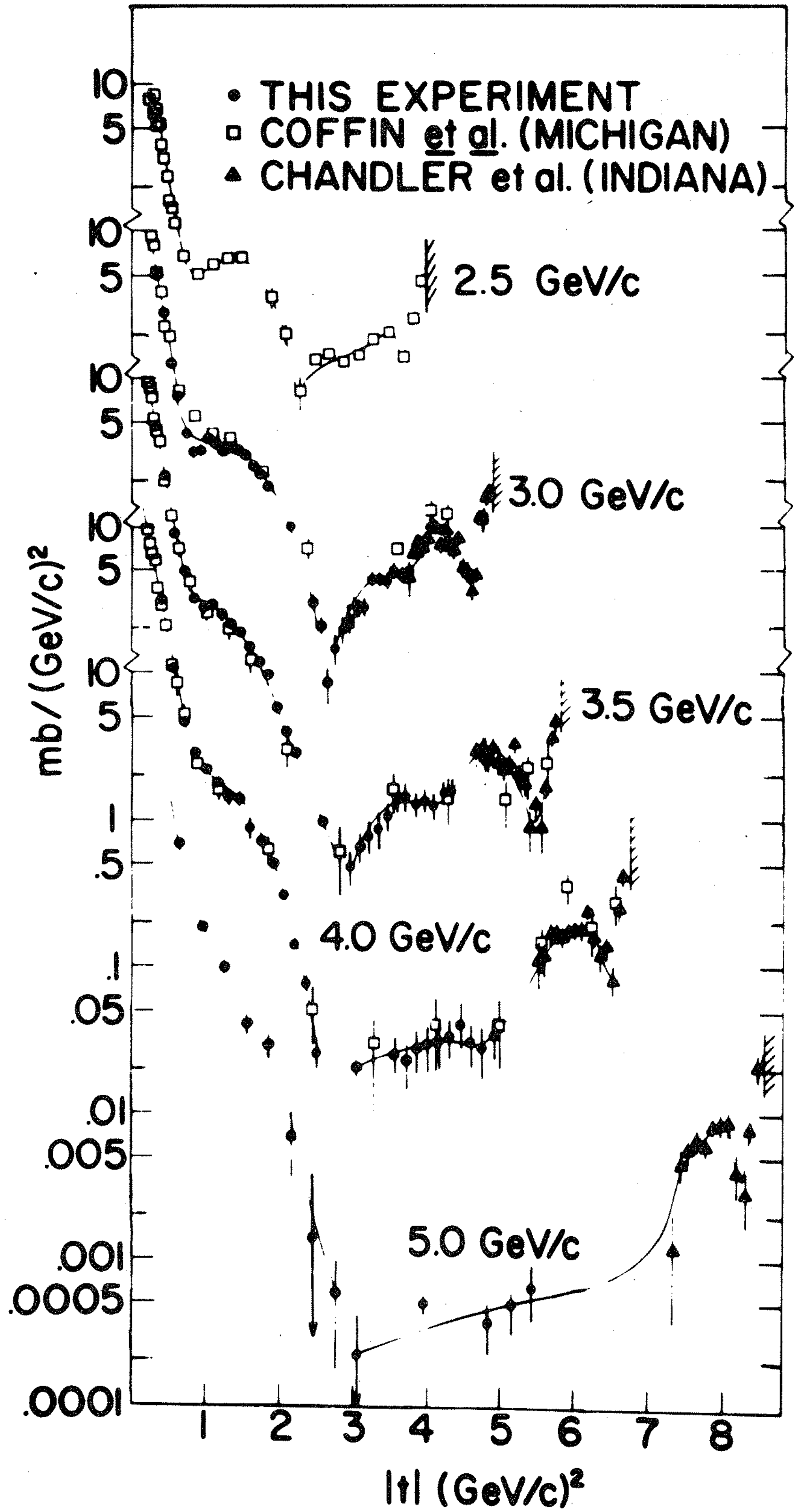

Figure 3 π^+p differential cross-sections, Ref. 6). $\theta_{cm} > 180^\circ$ is marked by a hatched area.

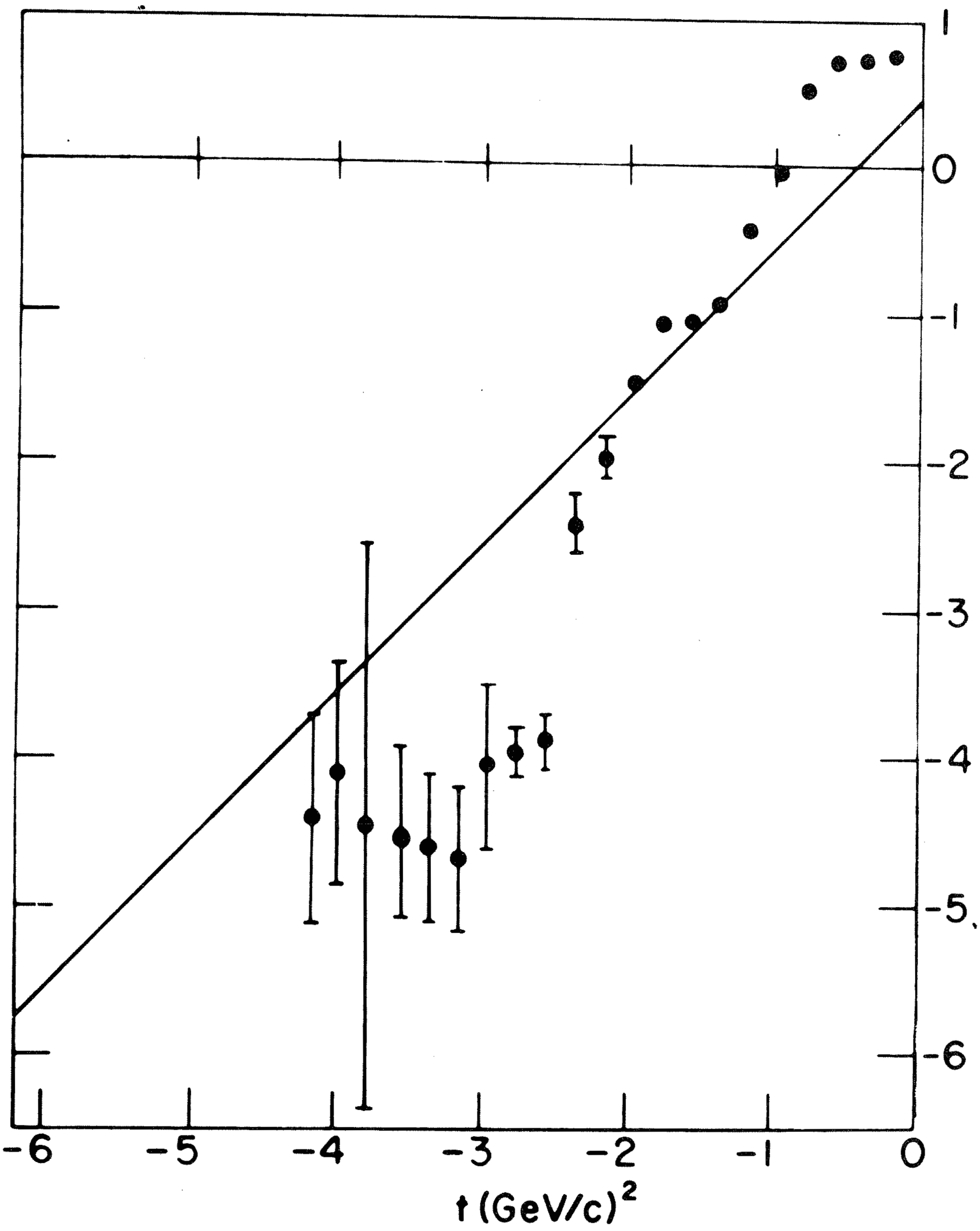

Figure 4 $\alpha_{\text{eff}}(t)$ for π^+p above p_L = 2.5 GeV/c from Ref. 6). The solid line represents a trajectory of slope 1 GeV^{-2} with the ρ intercept.

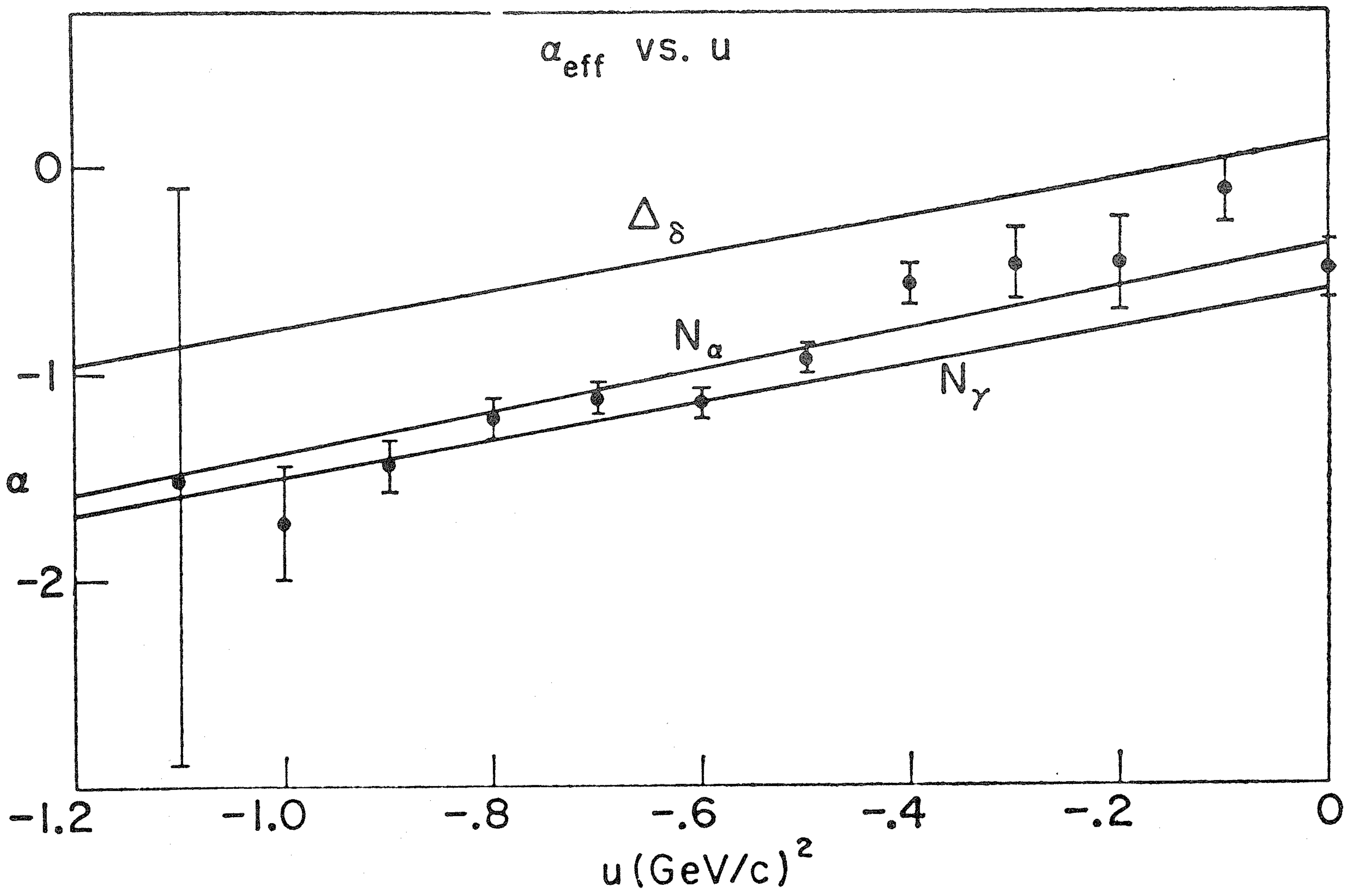

Figure 5 Effective trajectory for π^+p backward elastic scattering with $3.25 \leq p_L \leq 5.25$ GeV/c, from Ref. 7).

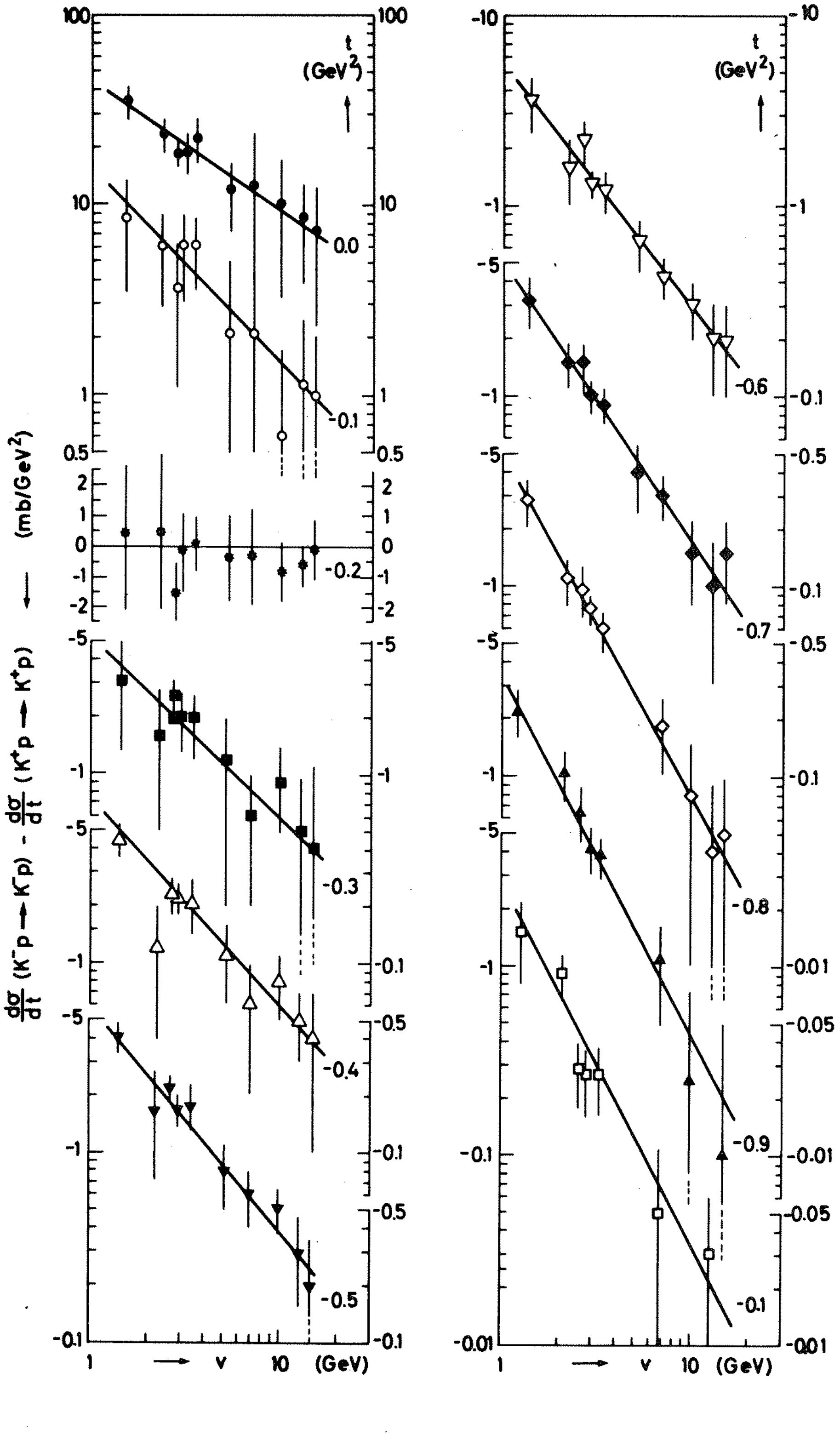

Figure 6 The difference of K^-p and K^+p differential cross-sections plotted against $\nu = \omega_L + t/4M$ for fixed t values between 0 and $-1\ GeV^2$, from Ref. 8).

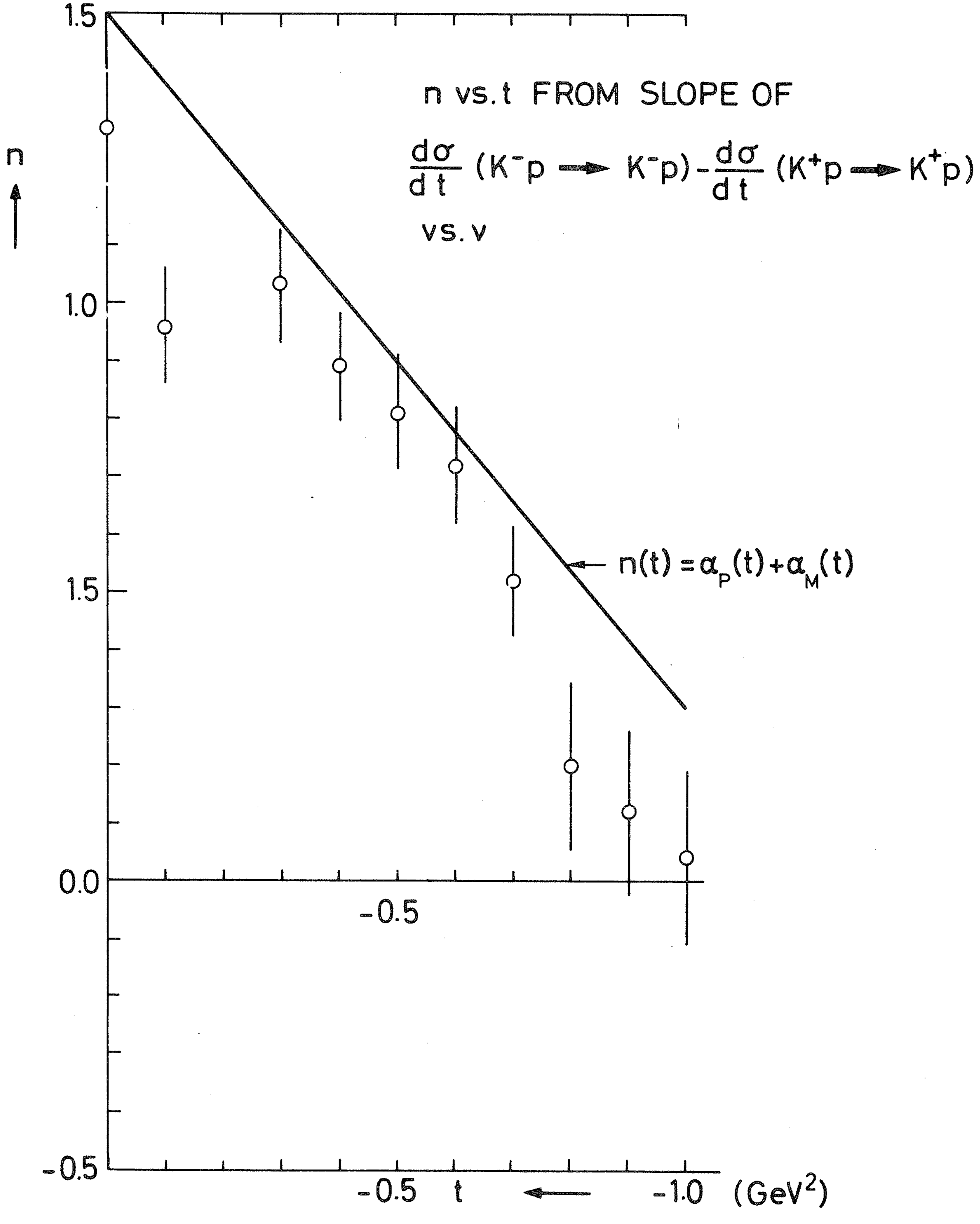

Figure 7 The Regge exponent $n(t) = \alpha_P(t) + \alpha_M(t)$ from the fits in Fig. 6. The solid line corresponds to $\alpha_P = 1 + 0.3\ t$ and $\alpha_M = 0.5 + 0.9\ t$; Ref. 8).

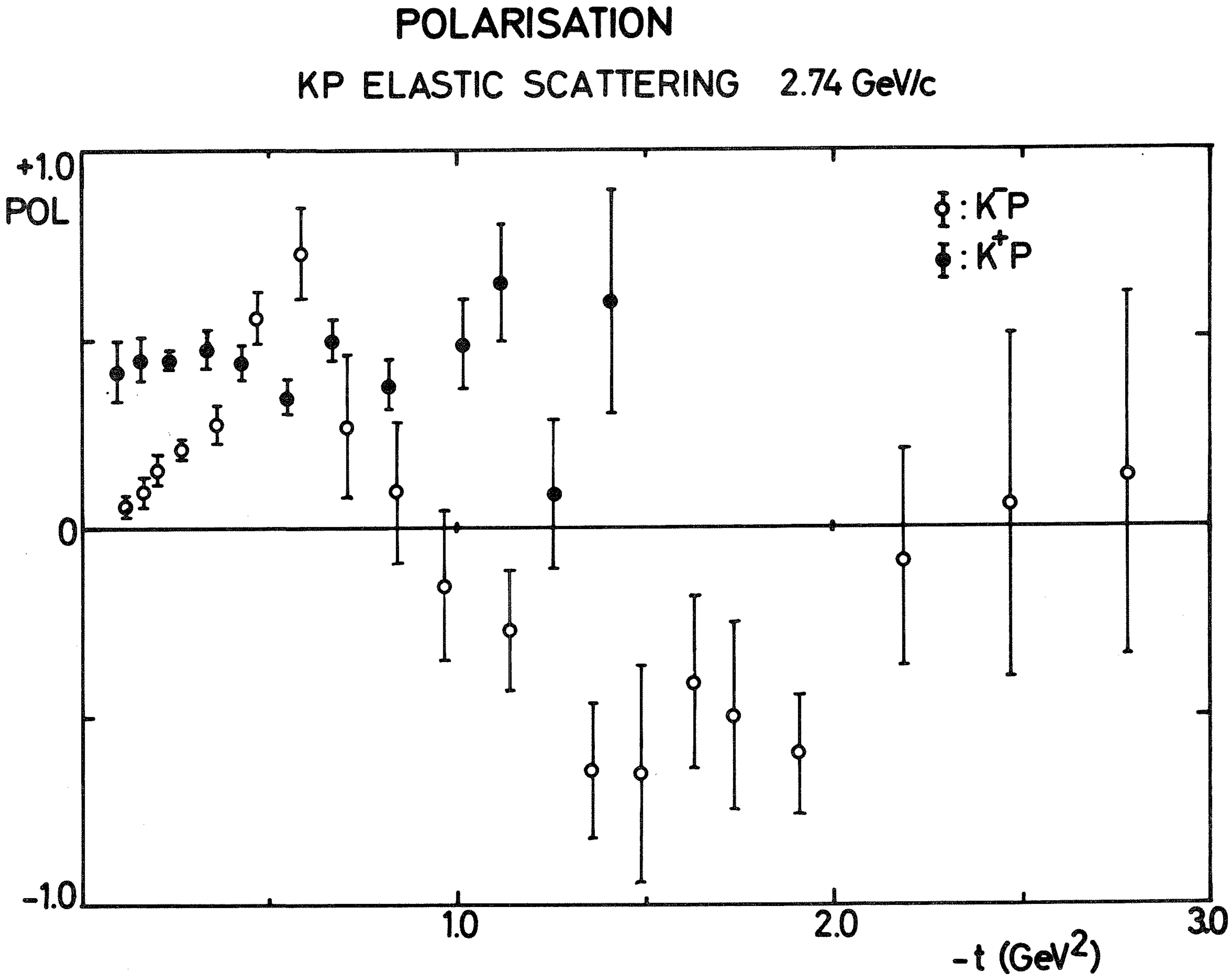

Figure 8 Polarizations for $K^{\pm}p$ elastic scattering at $p_L = 2.74$ GeV/c, Ref. 9).

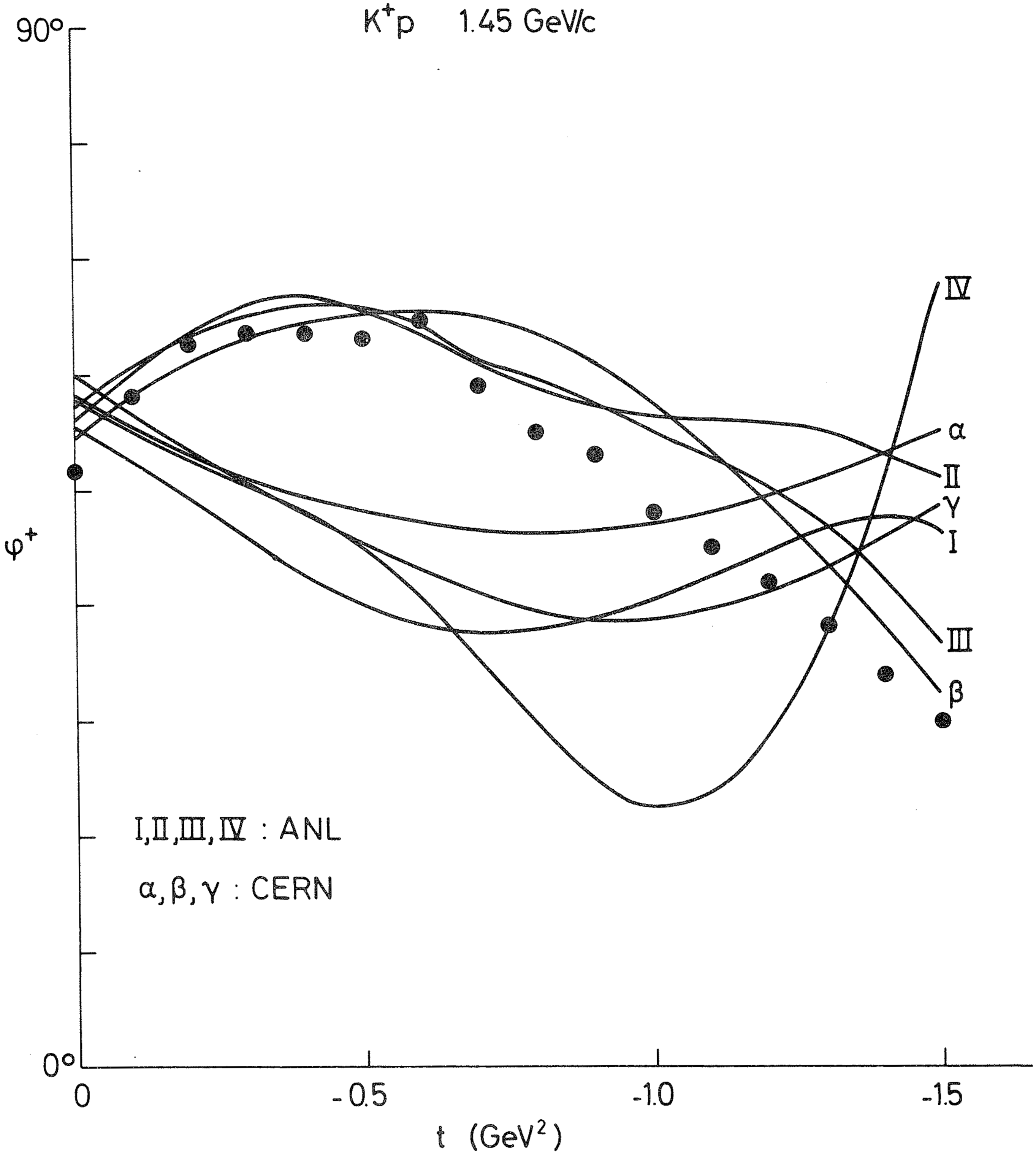

Figure 9(a) Comparison of phase shift and Regge predictions for K^+p elastic scattering at p_L = 1.45 GeV/c against t for the effective phase ϕ defined in the text. Solid lines are phase shift solutions α, β, γ of CERN, Ref. 13), and I - IV of Argonne, Ref. 14). The dots are the fixed t Regge predictions, Ref. 12).

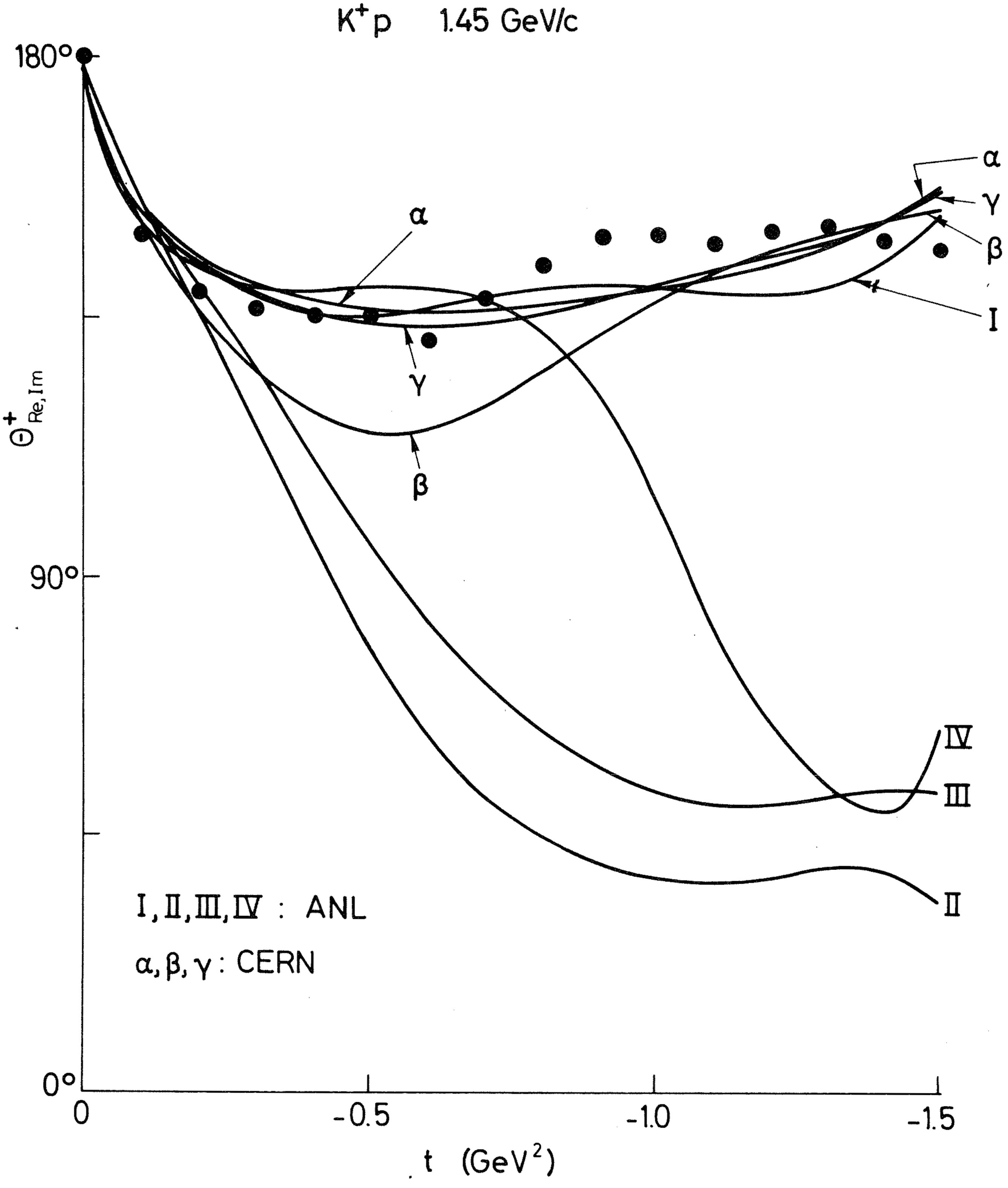

Figure 9(b) Comparison of phase shift and Regge predictions for $K^{+}p$ elastic scattering at p_L = 1.45 GeV/c against t for the angle $\theta(\vec{Re}, \vec{Im})$ in the nonflip/flip plane. For further details see caption of Fig. 9(a).

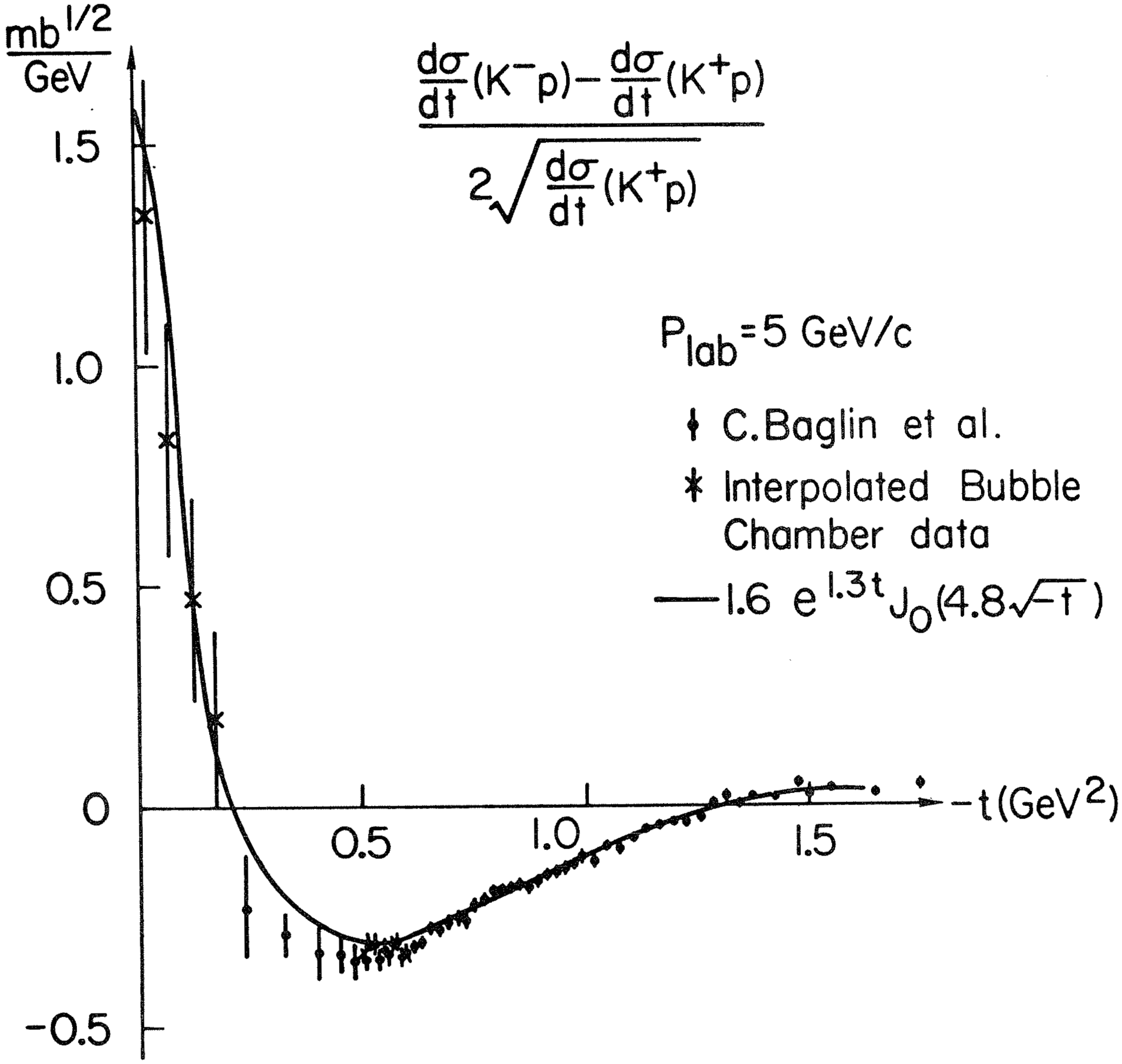

Figure 10 The experimental results for $\frac{1}{2}[d\sigma/dt(K^-p) - d\sigma/dt(K^+p)]\cdot$ $\cdot\ [d\sigma/dt(K^+p)]^{-\frac{1}{2}} \approx \mathrm{Im}\, R_{\Delta\lambda=0}$ as a function of t at $p_{lab} = 5$ GeV, Ref. 15).

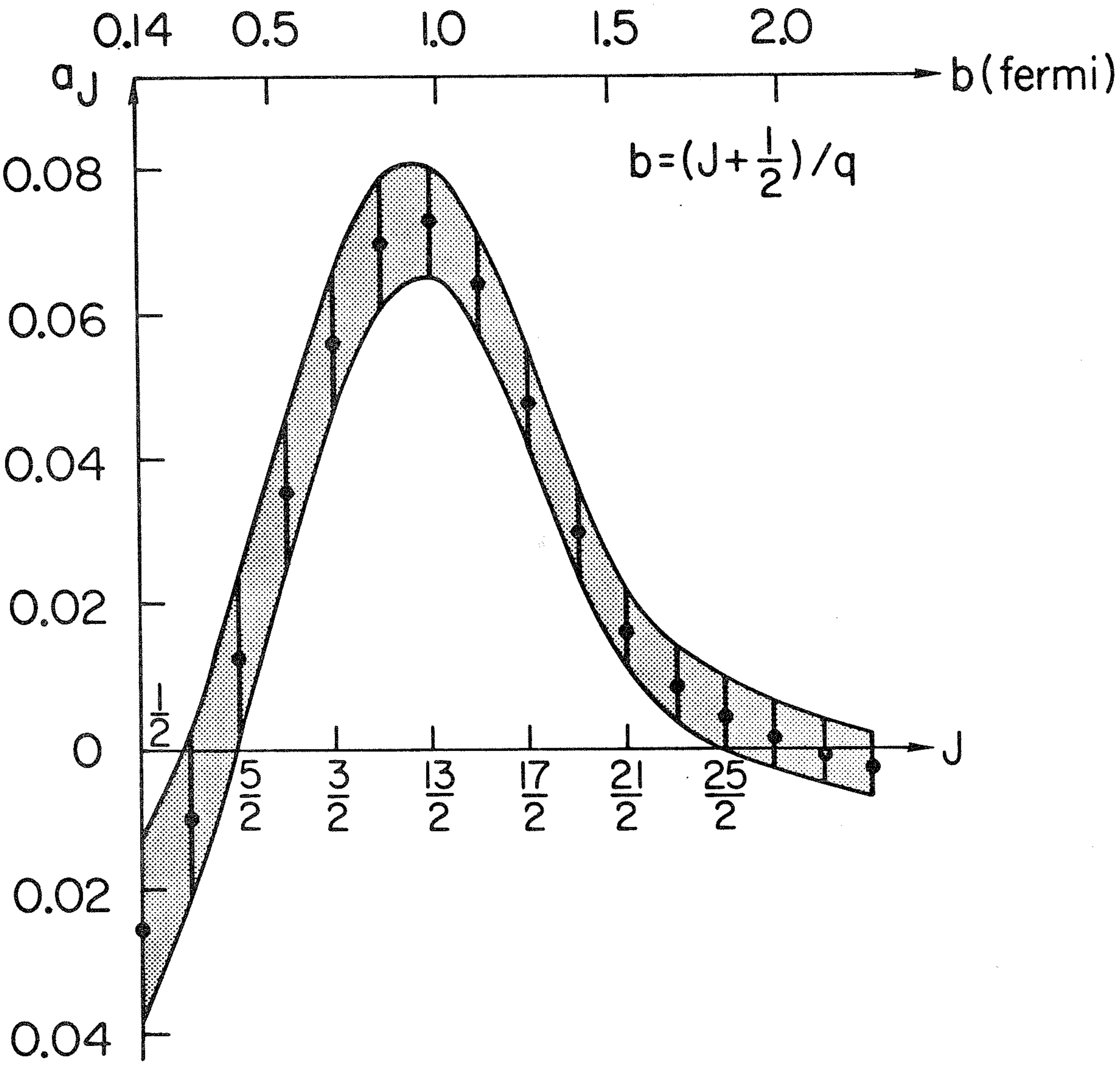

Figure 11 Legendre coefficients for the amplitude $\mathrm{Im}\,R_{\Delta\lambda=0}$ of Fig. 10. The dashed area between the two curves represents the uncertainty introduced by both statistical and systematic errors, Ref. 15).

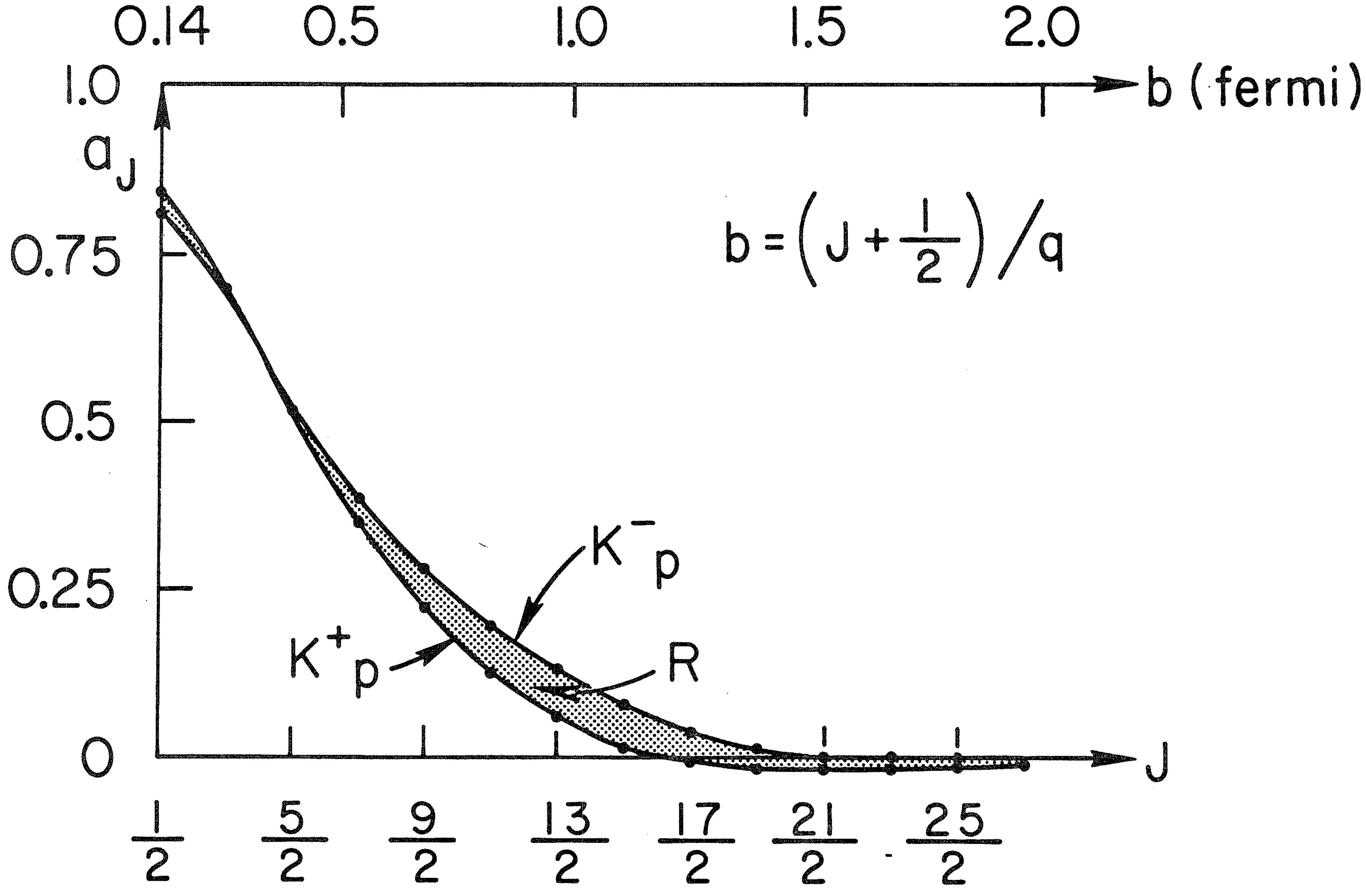

Figure 12 Legendre coefficients for $\sqrt{d\sigma/dt}(K^+p) \approx P$ and for $\sqrt{d\sigma/dt}(K^-p) \approx P + \text{Im}\, R_{\Delta\lambda=0}$, where Pomeron $\approx iP$.

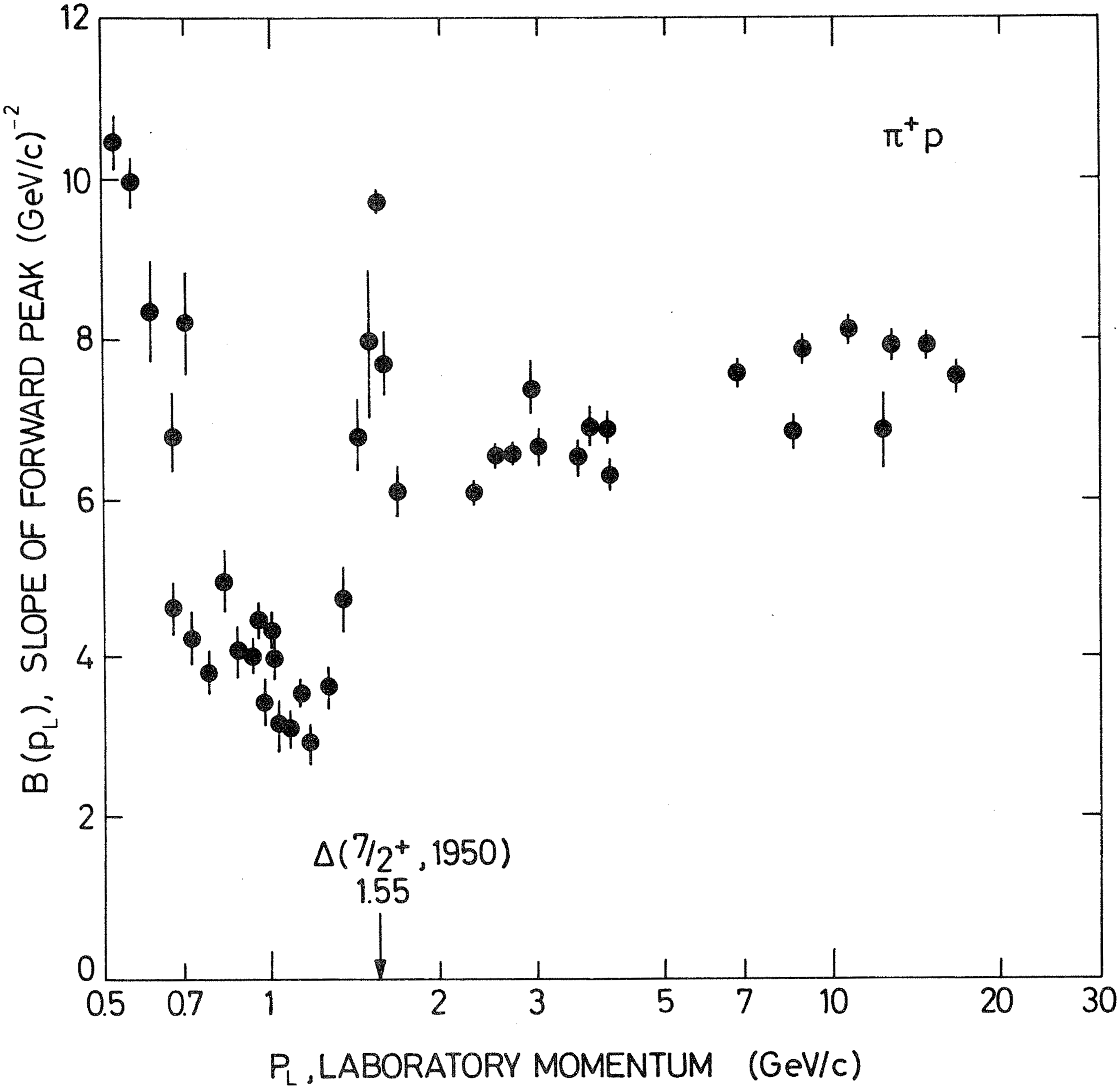

Figure 13 The slope B of the forward peak for π^+p elastic scattering as a function of p_{lab}.

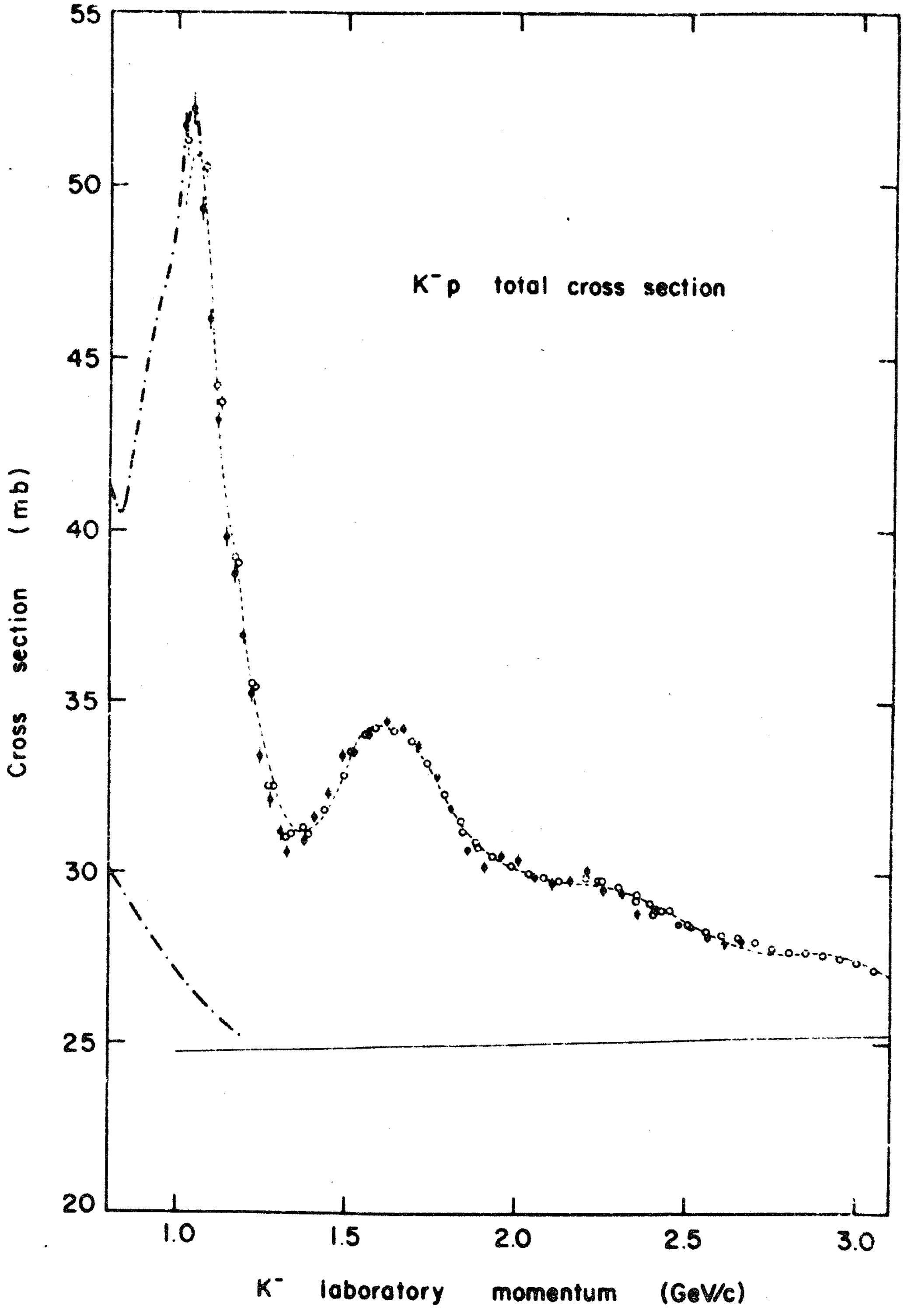

Figure 14 K^-p total cross-section as a function of the K^- lab. momentum. The dashed curve is the fit by resonances plus background, the solid curve is the background contribution, Ref. 19).

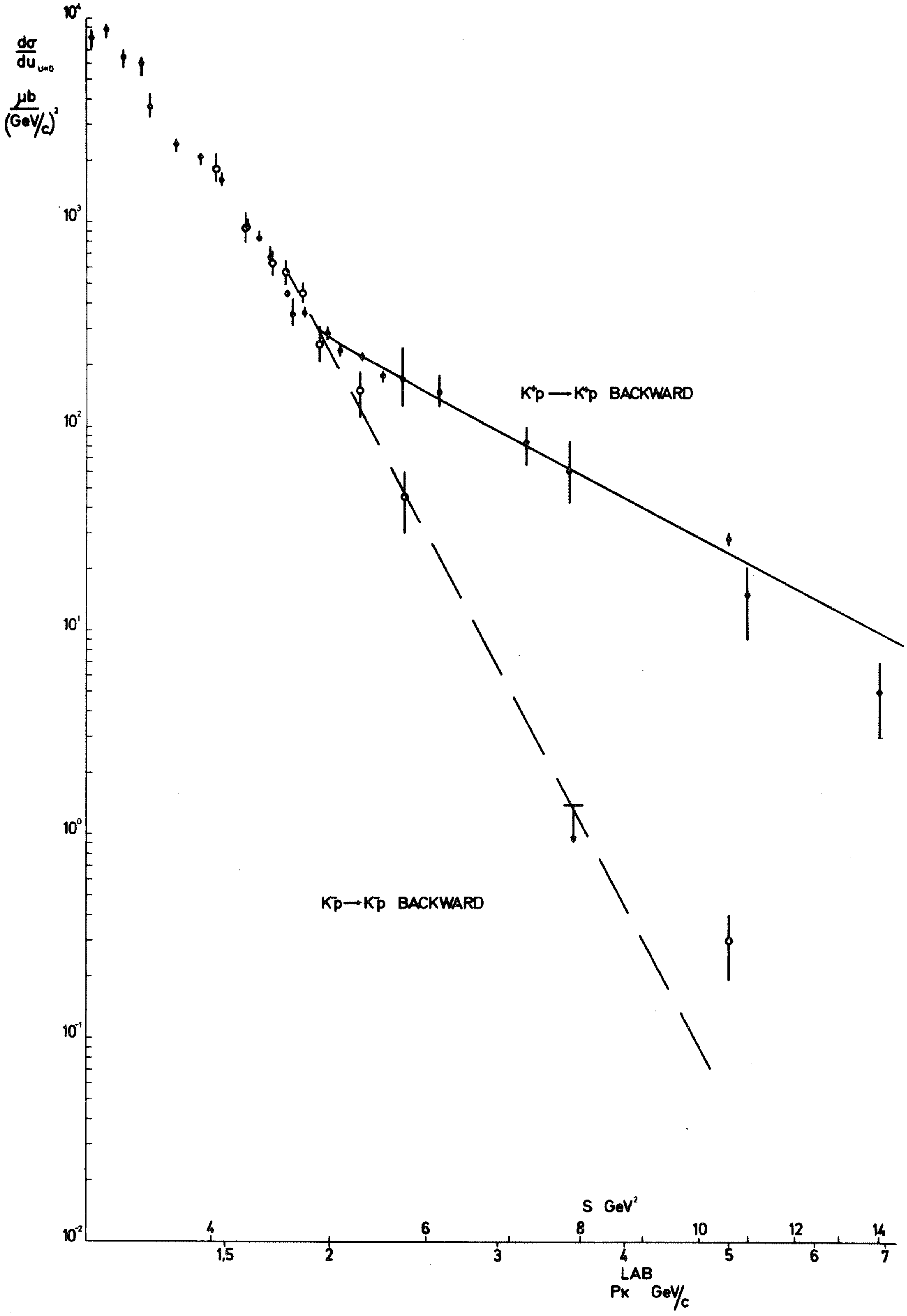

Figure 15 K^+p and K^-p differential cross-sections at $u = 0$ versus p_L. The new 5 GeV points are from Ref. 23).

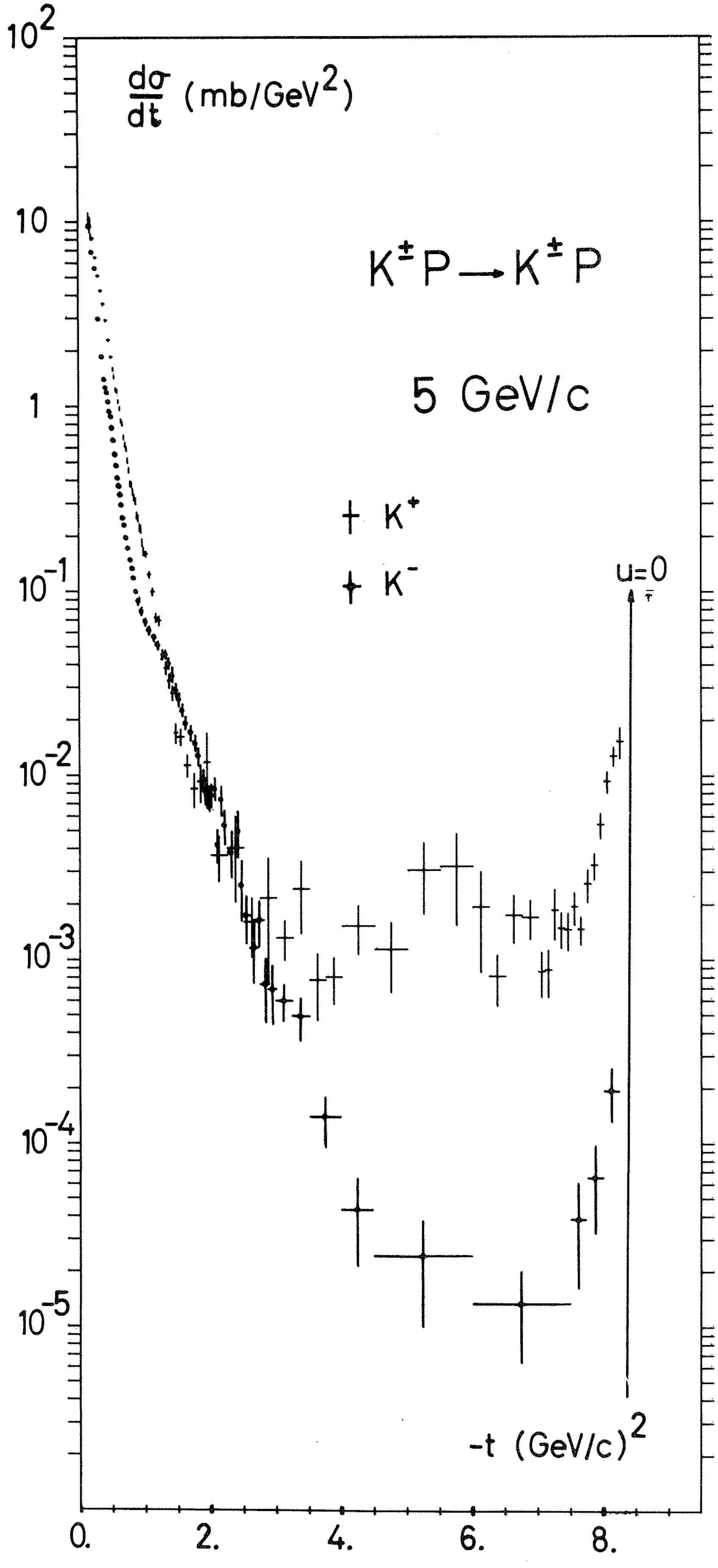

Figure 16 K^+p and K^-p angular distributions at 5 GeV, Ref. 23).

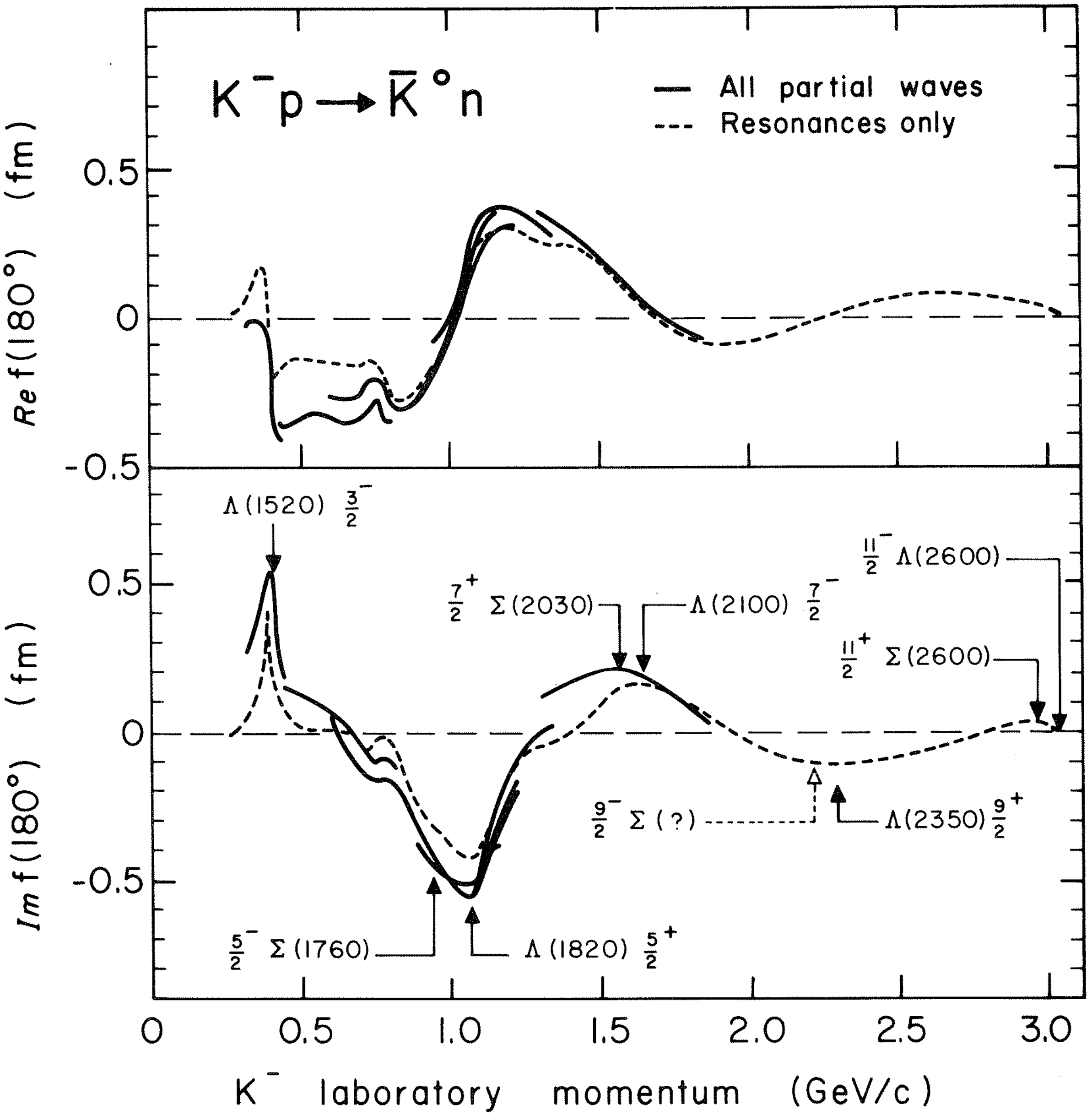

Figure 17 The imaginary and real parts for K^-p - $\bar{K}^0n$ backward scattering. The full lines are computed from various partial wave analyses, the dotted lines correspond to resonances only, Ref. 24).

"The other speakers are showing you the trees....What pattern is emerging...?"

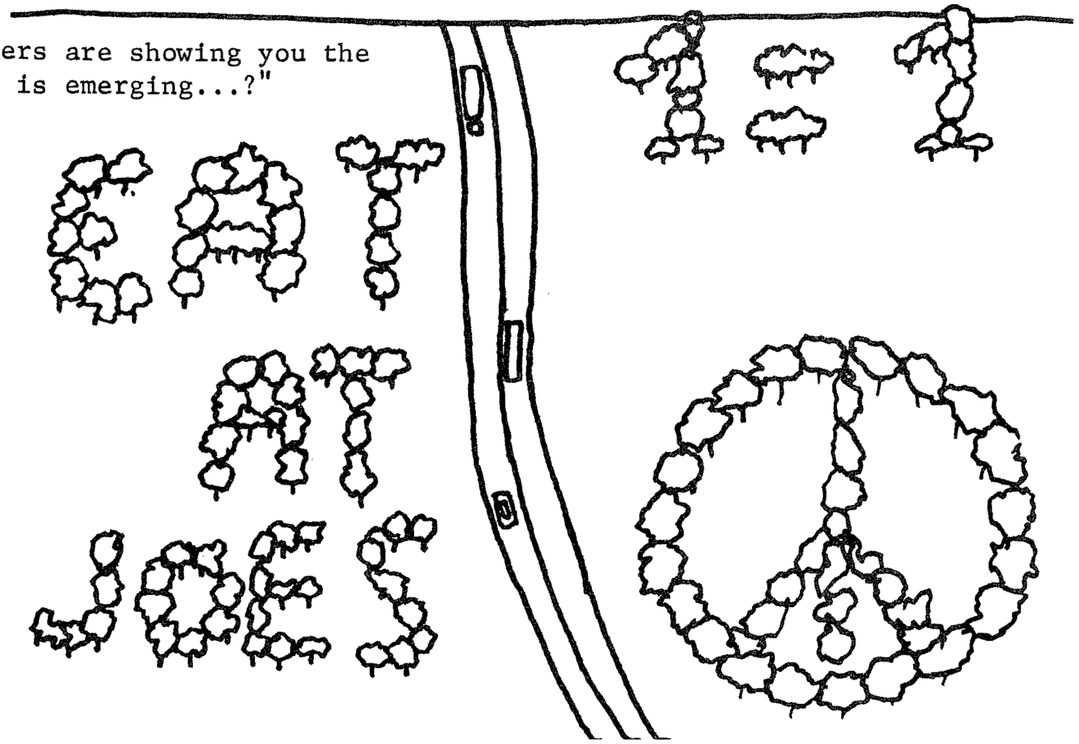

PRESENT AND FUTURE OF TWO-PARTICLE PHENOMENOLOGY

C. Lovelace*

Department of Physics
Rutgers - The State University
New Brunswick, New Jersey 08903

---

[*] Also at CERN, Geneva.

1. Introduction

The other speakers are showing you the trees. This talk will be about the wood. What pattern is emerging from strong interaction phenomenology? Where are the major gaps? How should we set about filling them?

2. Resonances on the average

As phase-shift analysis proceeds to higher energies, how many more resonances will be discovered? There is an old and simple argument[1] which partly answers this question. (It is evidently unknown to both authors of a recent "review" of dual models.) Take a phenomenological Regge fit[2], and analyse it into s-channel partial waves. As observed by Schmid[3], you will see circles just like resonances. According to duality they are resonances. Phenomenological Regge amplitudes contain factors e^{ict}, where c only varies logarithmically in s. Therefore these circles will lie on roughly linearly rising trajectories in s, accompanied by parallel daughters[1]. This means that s-channel daughter trajectories must rise linearly (up to log s factors) for as long as t-channel Regge fits remain valid. Even assuming this to be 25 GeV/c, would already imply that baryon trajectories rise to $J > 40$, and that more than 40 descendants with the quantum numbers of the nucleon exist!

There are only two ways to escape this conclusion: (1) You may disbelieve all Regge fits, (2) You may deny that Schmid circles are true resonances. Discussion of (1) would be superfluous at a phenomenology conference. Besides the original arguments[4] against (2), there is an inductive one. Unless Schmid circles are true resonances, there is no reason to exclude them in exotic channels. Therefore the well known consequences[5] about exotic amplitudes being pure real, thus implying exchange degeneracy (EXD) and wrong signature nonsense zeros (WSNZ)[6], would not follow. Similarly if Regge poles in one channel were dual to

Regge cuts in another channel[7], these consequences would not follow, since Regge cuts in exotic channels are certainly required by unitarity. Therefore any experimental evidence for EXD and WSNZ, is also experimental evidence that Schmid circles are real resonances and that poles are dual to poles.

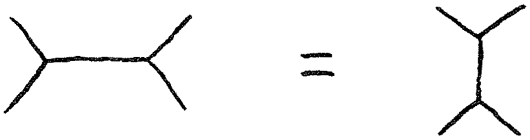

If Schmid circles are nondegenerate resonances, then they must by definition have factorizing residues. Comparing different channels, shows that this holds for parents but not daughters. Much effort to construct dual models with consistent factorization properties, has always given degeneracy increasing at least exponentially with mass[8]. I am afraid this is probably true in the real world.

Three particles with the quantum numbers of the nucleon are now listed in the Tables. As we have seen, indirect evidence suggests that there are some 40 more at higher masses. It is therefore a sad comment on specialization in physics that recent rapporteurs on current algebra have completely ignored dual models in favor of fallacious[9] saturation schemes, based on the absurd assumption that only one meson of each quantum number exists. This is particularly silly when there is direct experimental evidence that the photon current is not saturated by the known vector mesons[9,10] and that amplitudes with external leptons satisfy duality[11].

I now come to another string of obvious statements, whose corollary is evidently beyond the deductive power of many theorists. Pion beams are more intense than K beams. Nucleon targets are easier to make than meson targets. Total cross-sections get measured before angular distributions. High spin resonances are narrower because of the centrifugal barrier. They stick up higher because of the $(J + \frac{1}{2})$ factor. These elementary facts mean that the hadron spectrum is inevitably disentangled in fixed chronological order: nucleons → hyperons → mesons; parents → daughters → granddaughters → ... Nevertheless theorists who learned in graduate school that only parent trajectories existed, still occasionally say so on conference platforms.

Meson resonances are so hard to detect that theorists have often inferred them years earlier from indirect arguments. Thus the π and ω were predicted from nuclear forces[12,13], the ρ from electromagnetic form factors[14], the f from the earliest Regge fit[15], a broad ε from πN backward dispersion relations[16]. Each of these predictions was greeted with skepticism, and each was eventually proved right, though masses were usually underestimated.

The latest ridiculed prediction is the ρ', required at 1300 MeV by the $\pi\pi$ Veneziano formula[17], and at some mass below 2 GeV by electromagnetic form factors[9,18]. The ρ' partial widths should be 105 MeV into $\pi\pi$[19], 36 MeV in $K\bar{K}$[19], between 70 and 200 MeV into πA_1[20], probably as much again into $\pi\omega$, etc. A total ρ' width of 400 MeV is by no means unreasonable. I don't know who gave experimentalists the false idea that a narrow ρ' was wanted.

Though no experiment has firmly claimed a ρ', at least four[21] have an unexplained broad enhancement at 1500 MeV, with the right quantum numbers. Certainly nothing excludes a ρ' of the expected total width and inelasticity, at this mass.

Resonances 400 MeV broad can only be established by phase shift analysis. I recall that two CERN groups performed experiments designed solely to detect a claimed narrow ε, after a CERN theorist had told them the ε ought to be broad. Eventually $\pi\pi$ phase shift analysis was done[22], and the ε was found. After the present conference, even the dumbest experimentalist must realize that detailed phase shift analysis is more cost-effective than searching over and over again for narrow bumps or splits in mass spectra. There has been some $K\pi$ phase shift analysis[23], and, given enough data, it looks practicable for $\pi\pi \to K\bar{K}$, $\pi\pi \to \pi\eta$, and $\pi\pi \to \pi\omega$. All these processes have dubious resonances waiting to be disentangled.

3. Resonances viewed locally

The local systematics of daughter resonances is clearly wrong in the Veneziano formula. Even in the meson case, the masses of $\kappa(1100)$, $\delta(965)$, and probably $\rho'(1500)$, were all underestimated by 200 MeV[19], while for baryon daughters there is virtually no resemblance to experiment[24]. However, it must be emphasized that exact daughter degeneracy is a disease of dual Born terms, not of dual field theories[25]. Furthermore, one dual field theory is now known to be renormalizable[26].

What does work locally for baryons is SU(6) with ℓ-excitation[27] The success of a nonrelativistic model up to 2 GeV is obviously puzzling. Not only are the parity doublets expected relativistically absent, but the simplest fixed cut mechanism[28] for cancelling them is disfavored by backward Regge fits[29]. More πN phase shift analyses from 1.5 to 2.5 GeV/c are badly needed, both to give information on daughters, and to constrain backward Regge fits by FESR. I am not convinced that any of the recent πN analyses[30,31] have really improved on our 1967 work.[32] They are certainly no better at predicting π^+p polarizations[33].

As I described at Irvine[34], single energy phase shift analysis proceeds in three stages: random searching, energy linkage and smoothing. When smoothing is performed, it is very important that the results be fed back into the experimental fits and iterated. This was done in the 1967 CERN analysis[32], but apparently not yet in the 1970 Saclay work[35]. The different partial waves are highly correlated. Therefore, if your individual waves contain structures which are neither physically significant (new resonances), nor statistically insignificant (smooth within diagonal errors), you have thrown away experimental information on the other waves. The smoothness of the whole answer tests the credibility of all its parts.

In $\bar{K}N$ scattering, there is not enough data for single-energy analysis. However energy-dependent $\bar{K}N$ fits typically assume

Breit-Wigner resonance formulae plus linear background. This is plainly inadequate to fit the accurately known πN phase shifts. It is very important, both for $\overline{K}N$ phase shift analysis and for numerology, to devise resonance formulae which fit πN quantitatively.* Clearly they will have to allow for several resonances in the same partial wave, separated by CDD zeros. I can think of three approaches:

(1) Fits with parametrized partial wave dispersion relations, as in the 1967 CERN analysis[32,34]. They could be improved by using Veneziano formulae for the left hand cut, and other distant effects[36]. The advantages are: (a) ghosts are impossible, (b) no restrictions on CDD zeros, (c) no need to decide in advance whether a particular wave resonates. The disadvantage is that 15-25 parameters are needed per wave, and even then narrow resonances are not well fit.

(2) Veneziano formulae used as coupled channel K-matrices[19,37]. The advantage is that they contain CDD zeros, and hence give reasonable shapes and backgrounds. The disadvantages are that CDD zeros stay where they are put, and liability to ghosts[38].

(3) Optimized dispersion relation or K-matrix fits, as discussed by Dr. Cutkosky[39].

Devising better resonance formulae sounds unglamorous, but I think it could be lucrative.

As we have seen, t-channel Regge fits imply that huge numbers of yet unobserved daughters must exist in the s-channel. In the past, phase-shift analysts were so scared of announcing new resonances that they built heavy antiresonance biasses into their programs, e.g. shortest path[40]. I think this no longer makes much sense, except in exotic channels. If phenomenologists are going to be biassed, they should try to please theorists rather than to save paper for Rosenfeld. Regge fits should therefore be used as trial solutions in phase shift analysis, at energies where exhaustive searching would be uneconomical. Linkage programs should try to minimize deviation from Regge, rather than deviations from a straight line.

---

*Nuclear physicists live down a square well, and therefore know their barrier penetration factors. We do not.

Looking in the other direction, the most reliable way to evaluate sum rules is certainly to use phase shifts. Where no phase shift analysis is available, the next best is to construct a Veneziano model which fits both channels . This should at least give some statistical average of the daughters correctly. To use a few high spin resonances, that happen to be already listed in the Tables, is worst of all. I am mystified how physicists can assume that anything not directly observed by March 1971 is unlikely to exist. It is amusing to recall that attempts to eliminate the "atomic hypothesis" from physics continued till the end of the nineteenth century.

Another sensible use of Veneziano fits is to calculate the effect of distant singularities in partial wave dispersion relations[36] This avoids the gross pathologies resulting from uncorrected Born terms, or from employing asymptotic Regge formulae at low energies.

In KN elastic scattering, at least eight B_4 terms are needed to get reasonable spin structure of the leading Y* trajectories, thougl fortunately there are only 3 independent coupling constants[24,36]. Existing B_5 fits have been very slapdash about putting in spin[41], pion exchange and diffraction dissociation. It seemed from Dr. Berger's talk that the result is a sort of up-to-date phase space. The conclusion I would draw is perhaps not the one he intended. The existence of B_5 is already a miracle. It would be utterly unreasonable to think we can construct a more sophisticated theory of many-body processes, and still have it amenable to calculation. Therefore, if B_5 fits cannot be made any better, all detailed many-particle phenomenology is futile, and we should only perform quasi-two-body and inclusive experiments. The fate of B_5 is thus closely linked to the fate of bubble chambers.

4. Regge cuts.

All reputable phenomenologists now agree that Regge cuts are significant, and that the sign of the first cut is opposite to the pole. The evidence for this negative sign is enormous. It comes from (a) the effect on the pion pole in np charge exchange[42] and in photoproduction[43], (b) the existence of "crossovers"[44], (c) the flattening of Serpukhov total cross-sections[45], (d) the structure in wide-angle pp scattering[46], (e) innumerable successful fits with the reggeized absorption model[47,36,48], (f) Feynman graphs when correctly handled[49], (g) Glauber theory[50], (h) dual loops[51]. The positive sign came from a wrong argument about box graphs, and from the original form of the multiperipheral bootstrap[52] (which in my opinion there was never any experimental evidence for anyway). One still occasionally sees papers which want positive or zero Regge cuts. They can be thrown away safely.

To disentangle Regge poles from data, we need to understand Regge cuts. This understanding can only come from models. There are three relevant models: (1) Glauber theory[50], (2) summing high energy limits of Feynman graphs[49,53,54], (3) dual loops[51]. All three agree that a q-number eikonal formula should be valid, at fixed t, to leading order in s

$$(1)\quad F(\underset{\sim}{\Delta}, s) = -2is \int d^2 b \, . \, e^{-i(\underset{\sim}{\Delta}\,\underset{\sim}{b})} \times$$

$$\times \left\{ \exp\left[2i\eta(\underset{\sim}{b}, s)\right] - 1 \right\} + O(s^{-1}),$$

where $\underset{\sim}{\Delta}^2 = -t$, and η is an operator in the space of internal quantum numbers. In Glauber theory, η is related to the optical potential by

$$(2)\quad \eta(\underset{\sim}{b}, s) = (16\pi^2 s)^{-1} \int d^2 k \, . \, e^{i(\underset{\sim}{k}\,\underset{\sim}{b})} \, V(-\underset{\sim}{k}^2, s).$$

The Regge absorption model[55] puts

$$(3)\quad V(t, s) = P(t, s) + R(t, s),$$

where P and R are the elastic Regge amplitudes for exchange of a pomeron or reggeon. η is then a c-number except for spin. When the exponential in (1) is expanded, the multiple scattering terms contain Regge cuts.

The result from dual loops[51] is so pretty that I can't resist quoting it. Just add to the impact parameter $\underset{\sim}{b}$ in (2), a Nambu-Susskind internal field[56]

$$\underset{\sim}{b}(e^{i\vartheta}, e^{i\vartheta'}) = \underset{\sim}{b} + \sum_{n=1}^{\infty} n^{-\frac{1}{2}} . i\left[(\underset{\sim}{a}_n - \underset{\sim}{a}_n^{+})\cos(n\vartheta) + (\underset{\sim}{c}_n - c_n^{+})\cos(n\vartheta')\right] \tag{4}$$

Here $\underset{\sim}{a}_n$ and $\underset{\sim}{c}_n$ are harmonic oscillators which describe the excited states of the two scattered particles[8,56]. θ and θ' are circular "space" variables in a two-dimensional internal "space-time"[56]. A reggeon can be emitted only at $\theta = 0$ or π, a pomeron anywhere with probability

$$\rho(\vartheta, \underset{\sim}{k}) = |2\sin\vartheta|^{\alpha_P(-\underset{\sim}{k}^2) - \alpha_f(-\underset{\sim}{k}^2) - 1} . \tag{5}$$

(To form a Regge cut, they must be emitted at the same "time"[51].) The eikonal for a pomeron is then

$$\eta_P(\underset{\sim}{b}, s) = (16\pi^2 s)^{-1} \int d^2k \, P(-\underset{\sim}{k}^2, s) \times (2\pi)^{-2} \int_0^{2\pi} d\vartheta . \rho(\vartheta, \underset{\sim}{k}) \int_0^{2\pi} d\vartheta' . \rho(\vartheta', \underset{\sim}{k}) \times \exp\left[i\left(\underset{\sim}{b}(e^{i\vartheta}, e^{i\vartheta'})\underset{\sim}{k}\right)\right], \tag{6}$$

and for a reggeon

$$\eta_R^{\pm}(\underset{\sim}{b}, s) = (16\pi^2 s)^{-1} \int d^2k \; \times \tag{7}$$

$$\times \; D(-\underset{\sim}{k}^2, s) . \exp\left[i\left(\underset{\sim}{b}(\pm 1, \pm 1)\underset{\sim}{k}\right)\right] .$$

They are q-numbers because of the harmonic oscillators. (1) needs slight modification because more than two reggeons cannot form a cut: Elastic scattering of ground state particles is

$$F(\underset{\sim}{\Delta}, s) = -2is \int d^2b . \, e^{-i(\underset{\sim}{\Delta}\underset{\sim}{b})} \; \times \tag{8}$$

$$\times \langle 0 | \left\{ \exp\left[2i\eta_P(\underset{\sim}{b}, s)\right] . \left[1 + 2i\eta_R^{+}(\underset{\sim}{b}, s) - \right.\right.$$

$$\left.\left. - \, 2\eta_R^{+}(\underset{\sim}{b}, s)\,\eta_R^{-}(\underset{\sim}{b}, s)\right] - 1 \right\} | 0 \rangle ,$$

where $|0\rangle$ is the harmonic oscillator vacuum. Taking other matrix elements gives us the scattering amplitudes for excited states*.

If we expand in powers of $\eta_P(\underset{\sim}{b}, s)$, we can evaluate the harmonic oscillator matrix elements. Transforming to the momentum representation, then leads to Gribov's reggeon calculus[53]. The term with M pomerons and N reggeons exchanged gives the Regge cut

$$F_{M,N} = (M!\,N!)^{-1} . \left[\frac{i}{8\pi^2 |s|}\right]^{M+N-1} \; \times \tag{9}$$

$$\times \int d^2k_1 \ldots d^2k_{M+N} \, . \, \delta^{(2)}\left(\underset{\sim}{\Delta} - \sum_{j=1}^{M+N} \underset{\sim}{k}_j\right) \times$$

$$\times \left[G_{M,N}(\underset{\sim}{k}_1, \ldots, \underset{\sim}{k}_{M+N})\right]^2 . \prod_{j=1}^{M} P(-\underset{\sim}{k}_j^2, s) . \prod_{j=M+1}^{M+N} R(-\underset{\sim}{k}_j^2, s) ,$$

---

*This last statement is a slight oversimplification.

or graphically

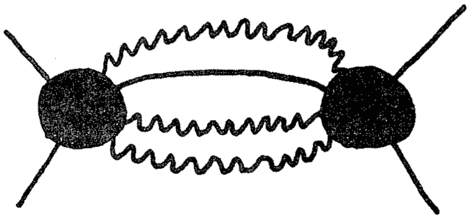

Here the black blobs are "Gribov vertices". They are fixed pole residues of the big vertices, independent of s, and come from the third double spectral function[53]. In the dual loop model, the Gribov vertices result from evaluating the harmonic oscillator matrix elements in (8), and are just the partition functions of two-dimensional Coulomb gases confined to the unit circle, with the exchanged momenta $\underset{\sim}{k}_j$ as charges[51]. Dual loops thus justify both q-number Glauber theory[50] and Gribov's reggeon calculus[53], explain the relation between them, and fill in, for one model, all the unknown quantities. This obviously ought to influence future phenomenology.

The tip of the Regge cut corresponds to the leading power of log s. Evaluating the integrals in (9) asymptotically, shows that the exchanged momenta $\underset{\sim}{k}_j$ are then distributed in fixed ratios, determined by the slopes of the trajectories. In particular at $t = 0$ and the tip of the cut, all $\underset{\sim}{k}_j = 0$. Eqs. (4), (5), (7) then show that the harmonic oscillators decouple, so the eikonal becomes a c-number and we are back with the weak absorption model (3). The dual loop cuts thus converge to the weak absorption model at $t = 0$, $s \to \infty$. For more general dual models, there may be additional scalar oscillators which need not decouple, but still only a small fraction of the excited states will contribute to the absorption asymptotically.

Phenomenologists need formulae valid in as many models as possible. Unfortunately the people[54] who calculate high energy Feynman graphs are very lazy, and have not even checked the Gribov formula (9), let alone calculated the vertices. In the dual loop model, the Gribov vertices are partition functions and therefore have linked cluster expansions, which describe the deviations from weak absorption at finite s and t. For the pomeron-pomeron (PP) and pomeron-reggeon (PR) cuts (but not for RR), the first cluster integral (average potential) vanishes, and convergence to weak absorption is rapid. If similar expansions are valid in other models, the elementary cluster integrals would make very suitable phenomenological parameters.

The Michigan group have suggested[48] that the PR cut be multiplied by a factor $\lambda \sim 2$ because elastic unitarity in (1) needs to be supplemented by diffraction dissociation. There are four things wrong with this argument: (1) Identifiable diffraction dissociation is small experimentally: 5% of the total cross-section as against 15% for elastic scattering.[57] (2) If diffraction dissociation dominated the inelastic scattering asymptotically, this would constitute the two-fireball model, which is disproved by inclusive experiments[58*], (3) Despite its vast quantity of resonances, the dual loop model[51] makes all cuts converge to the weak absorption model as $s \to \infty$ and $t \to 0$, (4) Glauber theory with a disintegrating deuteron[59] likewise gives λ near 1.

There is certainly no evidence in any model that deviations from weak absorption will jack the whole cut up by a constant λ-factor, independent of s and t.

Experimentally the ordinary absorption model works reasonably well for the cuts generated by a pomeron plus a vector or tensor meson[47,24,36,60,61]. It somewhat underestimates them in the noflip amplitude, as is shown by the K^-p - K^+p crossover[36]. It seems to overestimate them in the flip amplitude, since the EXD polarization predictions (see below) are less distorted by the cut than expected. Measurement of backward K^+p and π^-p polarization would give very direct information on the size of the pomeron-baryon cuts. Forward np charge exchange[42] suggests that the absorption model may underestimate the pomeron-pion cut by as much as a factor 2. However, Jackson and Quigg found that the corresponding statement in photoproduction was very model-dependent[43].

---

*I am grateful to Dr. A. Mueller for this remark.

Regge-regge cuts (not involving a pomeron) dominate K^-p backward scattering[62], which has just been measured[63], as well as[64] forward $K^-p \rightarrow K^+\Xi^-$. I expect them to become of phenomenological interest quite soon. Dual loops predict large deviations from the absorption model (except at u = 0 or t = 0) for RR cuts[51].

The tip of the cut (9) is at

$$\ell = M(\alpha_P^0 - 1) + N(\alpha_R^0 - 1) + 1 + \alpha' t/(2M+N), \tag{10}$$

which is flatter in t, the larger M and N. Therefore cuts will inevitably dominate poles at large t. Fortunately they are only ∿30% as big at t = 0. Crossovers at t ∿ -0.25 show where cuts become larger than poles in the noflip amplitude. They are expected to be less important for flip. By correcting for cuts, we can certainly view the poles near t = 0[61], and possibly even out to t = -1, without getting hopelessly model dependent.

Now Regge poles are clearly the fundamental objects, just as in Glauber theory neutron scattering is more interesting than the deuteron wave function. They generate the Regge cuts by a mechanism which is ingenious, but in principle understood. In wide-angle scattering, numerous cuts interfere[46] to produce a small cross-section, only remotely connected to the input pole. Wide-angle scattering is therefore unlikely to teach us anything fundamental. It is just high energy nuclear physics.

5. Dip mechanisms

Because of this uncertainty in disentangling the poles, there were till recently two possible views on them.

Argonne phenomenology[47,55] says that Regge poles are exchange degenerate because of no-exotic constraints and that dips therefore came from wrong-signature nonsense zeros (WSNZ). The cuts convert zeros into dips. If the elastic eikonal formula (1) - (3) is used, the cuts are generated with no extra parameters. Argonne-type fits are actually more economical than pure Regge poles, since they allow one to fit experiment with simpler pole formulae. In modern Argonne fits[24] the trajectories are fixed from the particle masses, and the residues constrained by duality. In one ultramodern one[36], almost all KN and $\bar{K}N$ data above 3 GeV/c (forward and backward) was explained with only 4 parameters, and the result also joined on smoothly to K^+p phase shifts at 2 GeV/c.

Michigan phenomenology[48] said that dips were due to pole-cut interference. This requires that the cuts be jacked up by a λ-factor $\sim$2-3, which they varied independently for the different exchanges. Also the Michigan group avoided elastic channels, and disliked working below 8 GeV/c, thus eliminating duality information in practice. Therefore, Michigan fits were much less economical even than conventional Regge fits, let alone Argonne ones. This made them rather slippery to test. However, though Argonne and Michigan give similar cross-sections and polarizations, the amplitudes are completely different[65]. A firm test can therefore only be performed where the amplitudes are known. Most Regge phenomenologists would agree that this is so in πN scattering for $t > -1$. To determine amplitudes there, we have d.c.s. and polarizations in three channels (π^+p, π^-p and π^0n), as well as R and A measurements for π^-p, and most important the FESR constraints from the elastic phase shifts. These actually predicted[66] R and A correctly before they were measured[67].

The $\pi^{\pm}p$ polarizations[68,69] are mirror symmetric, proving that they are entirely due to interference between I = 0 and I = 1 exchange. Michigan says that I = 1 should have a single zero at $t = -0.6$. EXD predicts a double zero. The data[68,69] has a double zero (Fig. 1). The solid line is Argonne, the dotted line is the best[71] that can be done for Michigan by varying the pomeron. Trying to put the extra zero into the pomeron would conflict with FESR[71], and also with the absence of any zero at $t = -0.6$ in K^+p and pp polarization[68]. New π^-p polarization data at 14 GeV/c[68], shows the same double zero, with no change except overall reduction Therefore claiming this as a low energy effect would be very implausible.

EXD predicts[47,5,70] that the exotic channels K^+p and pp should have smooth positive polarization, K^-p should have single zeros where $\alpha_\rho = \pm\frac{1}{2}$, and $\pi^{\pm}p$ a double zero at $\alpha_\rho = 0$. All these predictions agree with experiment[68]. The mirror symmetry in Fig. 1 implies that the pomeron and f must have the same helicity coupling to the nucleon. FESR with CERN 1967 phase shifts[32] show this to be helicity noflip in the s-channel[66] (P and f decouple from the πN A amplitude). The π^-p spin rotation parameters[67] confirm this. SACLAY 1970 phase shifts[30] give the same result[71], except for a sudden change near the forward direction, where there is no polarization data to constrain the phase shifts. In my opinion this is an argument against SACLAY 1970 rather than against s-channel helicity conservation.

Absence of KN exotic resonances requires that f and ω be exchange degenerate and therefore have the same helicity coupling to the nucleon. So $f \not\twoheadrightarrow A$ predicts $\omega \not\twoheadrightarrow A$, which agrees with nucleon electromagnetic form factors[47]. Similarly ρ and A_2 must have the same helicity coupling. This explains why $\pi^-p \to \pi^0 n$, $\pi^-p \to \eta n$, $K^-p \to \bar{K}^0 n$ all have the forward flattening characteristic of spin-flip, while only $\pi^-p \to \pi^0 n$ has a dip at $t = -0.6$. Detailed Argonne fits have been very successful in these[47,36] and similar[72] processes.

Duality also predicts that backward K^+p should be pure real. Therefore, there should be no dip, unlike backward π^+p, and no polarization. New K^+p data at 5 GeV/c indeed show no backward dip[63]. The backward polarization has unfortunately only been measured up to 2 GeV/c[74] (where it vanishes).

All these facts are inexplicable to Michigan, despite their statement[48] that "whenever a distinction can be made, the strong cut model is favored over the conventional models (even including cuts determined by conventional absorption models)".

When EXD is combined with exact SU(3), many more predictions follow. They are summarized by duality diagrams[75]. Experimentally these SU(3) + EXD predictions are much worse than those which follow directly from no exotics. A spectacular example is N_α-N_γ EXD, which would reduce the backward π^+p dip to a shoulder. Likewise $K\Lambda$ backward polarization shows that the Σ_α F/D ratio deviates considerably from the EXD prediction[75]. More seriously, the WSNZ at $\alpha_\Delta = \frac{1}{2}$ is not confirmed by backward πN charge-exchange[29]. Despite repeated dogmatic assertions by Mandula et al[77], Regge fits make it perfectly clear that EXD is more exact for vector and tensor meson than for baryon exchange.

There are two places where existing Argonne phenomenology is at a serious disadvantage relative to Michigan: (1) np charge-exchange[42] probably requires the pion-pomeron cut to be much bigger than the weak absorption model. (2) Some dips required by WSNZ are totally absent in photo production[48]. (2) may have a trivial explanation in terms of fixed poles (see below).

There is a simple way you can predict which of these two existing Regge phenomenologies will work better: The fewer the number of Regge exchanges, and therefore the less the number of parameters, the more superior is Argonne to Michigan. The whole history of physics tells us that a theory with few parameters which works only in simple situations, is more likely to be basically correct than a theory with many parameters which works only in complicated situations.

6. The pomeron

If the pomeron were dual to resonances, then exotics would have to exist in K^+p. This is disfavored by phase shift analysis[36]. If the pomeron were EXD, then either a strong photon would exist, or the WSNZ[6] would make total cross-sections vanish. (This shows in particular that the pomeron cannot be the trajectory in the Veneziano model, as some people have been claiming.)

Regge cuts, as described by the eikonal formulae (1) - (3), will be very important for the pomeron. Let us define the bare pomeron to be what goes in (P), and the clothed pomeron to be the experimental quantity F which comes out. We have no model-independent way to disentangle the bare pomeron from its shielding cuts, nor even the experimental checks provided by crossovers and WSNZ in the reggeon case. Nevertheless, different theoretical calculations[78,51] indicate that the "bare pomeron" is a meaningful and indeed fundamental concept.

If the bare pomeron intercept α_P^0 is above one, the eikonal formula (1) will automatically pull the clothed pomeron down, till it satisfies the unitarity bound[78]. However, models[78,79] indicate that two things will then happen: (1) the total cross-section will increase logarithmically, (2) the d.c.s. will have a $\sqrt{-t}$ branch point at $t = 0$. There is no sign of either experimentally. Therefore, α_P^0 is probably close to one. If $\alpha_P^0 = 1$ exactly, this would be a remarkable fact, not attributable to any trivial unitarity bound. It might indicate some underlying scale invariance of the strong interactions.

There are three pieces of experimental evidence that the pomeron shrinks:

(1) Small angle pp scattering, as measured at Serpukhov[80]. To second order, the eikonal formula (1) - (3) gives[61] for the slope of the diffraction peak at $t = 0$

$$b(s) = 2\alpha'_P \ln(s/s_0) + \sigma_\infty/32\pi. \tag{11}$$

Thus the second order cut correction to α'_P vanish at $t = 0$, and the Serpukhov experiment measures the slope of the bare pomeron, to good approximation. It gives $\alpha'_P = 0.40 \pm 0.09$ GeV^{-2}.

(2) According to duality, the ordinary Regge poles are pure real in K^+p and pp. Also the pomeron-reggeon cut is pure real[81]. If the pomeron were a fixed pole, it would be pure imaginary. Therefore, there would be no interference, and pp and K^+p should rapidly approach a fixed DCS. In contrast, they show the biggest shrinkage of any elastic process[82] (Fig. 2). Pomeron exchange seems to dominate the K^+p imaginary part as low as 1.5 GeV/c[83]*. Therefore α'_P can be deduced from K^+p and pp scattering at comparatively low energies (below 20 GeV/c), and again[82] gives $\alpha'_P \simeq 0.5$ (Fig. 2).

(3) According to the quark model, $\gamma p \to \phi p$ should be pure pomeron exchange. Barger and Phillips[84] again deduced $\alpha'_P = 0.5$ from fits to this process at 2 - 10 GeV/c. However, polarization has recently been observed[85], so this pure pomeron assumption is questionable.

People who still use naive fixed-pole optical models do so for non-experimental reasons. There is only one indirect upper bound on α'_P. This comes from wide angle K^-p scattering at $t \simeq -1$, where the DCS dip and polarization zero predicted at $\alpha_\rho = -\frac{1}{2}$ by EXD[86], would be shifted unless the background were positive imaginary. However, the background at $t = -1$ is certainly dominated by cuts and not by the bare pomeron. Nevertheless, eikonal models have trouble with K^-p if $\alpha_P(-1) < \frac{1}{2}$.

As I pointed out at the beginning, EXD and WSNZ test the statement that poles are dual to poles 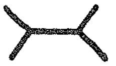 = 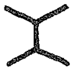. Regge cuts test the statement that poles can be fed into unitarity equations. Combining the two, we necessarily have duality relations for Regge cuts. These can be derived from duality diagrams with closed loops[87]. Fig. 3a shows a very important diagram. In one channel it has a Regge-Regge (RR) cut (2 ribbons). In the other channel it has a closed pipe: the "pipe hypothesis" says that this is a bare pomeron. It was suggested by a model calculation[88,51]. There are a whole series of nice consequences:

---

*This also proves that the pomeron does not generate itself by a multiperipheral bootstrap[52,79], since inelastic K^+p scattering at ~1.5 GeV/c is not even dominated by $I = 0$ exchange.

(1) Since the boundaries of the duality diagram are quark lines, the pomeron contains no quarks, and therefore no isospin, etc.

(2) The pomeron form factor is f-dominated, in the same sense that e.m. form factors are ρ-dominated.[89] This is proved in Fig. 3b. Therefore the P and f must have the same helicity coupling to the nucleon. This explains the mirror symmetry of the $\pi^{\pm}p$ polarizations (Fig. 1).

(3) In the $K^{+}p$ s-channel, the RR pipe is the two-particle unitarity correction (imaginary part and rescattering). Therefore the pomeron is dual to low energy nonresonant background, in accord with the Harari-Freund.

(4) As everyone who has played with dual models will know, trajectories which are dual to each other must have the same slope. The RR cut has slope $\frac{1}{2}\alpha'_R$ (see eq. (10) for $M = 0$, $N = 2$). Therefore the bare pomeron, which is dual to it, again has slope[88]

$$\alpha'_P = \tfrac{1}{2}\alpha'_R = 0.45 \text{ GeV}^{-2}$$

compared to the experimental[80] 0.40 ± 0.09 GeV^{-2}.

(5) Any satisfactory pomeron residue must be nonzero at $\alpha_P = 1$ (no WSNZ). Model calculation[51] indeed verifies this. At $\alpha_P = -1$, etc. the pomeron has multiplicative fixed poles, the reggeon additive ones.

(6) The iterated PP cuts, which clothe the pomeron, correspond to duality diagrams with several pipes exchanged.

Another consequence of this diagram (Fig. 3a) was noticed by Finkelstein[90]. Exchange of an RR cut cannot contribute to forward KN or $\bar{K}N$ elastic scattering. This is easily seen, because

4 quarks have to be exchanged permanently, and there is nowhere for the λ-quarks to go. Therefore RR cuts cannot explain the difference between $K^+n \to K^0p$ and $\bar{K}^-p \to \bar{K}^0n$ below 5 GeV/c.

7. Photoproduction

The salient experimental feature[91] of photoproduction ($\gamma N \to \pi N$) is that $\alpha_{eff}(t)$ is constant at 0, and $\alpha_{eff}(u)$ is constant at $-\frac{1}{2}$. This is in drastic contrast to strong processes. The natural explanation for it is not Michigan phenomenology, but fixed poles. Fixed poles should certainly occur in Compton scattering[92], but there is no proof either way for photoproduction. If πN elastic scattering satisfied Levinson's theorem, e.g.

$$\delta_{P_{33}}(\infty) = 0, \qquad \delta_{P_{11}}(\infty) = -\pi, \tag{12}$$

then there would be no fixed poles in photoproduction[93]. However (12) is clearly false experimentally[32].

The CDD zeros, which break Levinson's theorem, generate arbitrary parameters[94] in the Omnés equation for photoproduction. That for P_{33} is actually important in low energy fits[95]. If πN scattering has 40 resonances in each partial wave, then existing theories of photoproduction will have 40 free parameters. Clearly something must determine them. Finding it should be the goal of photoproduction phenomenology. It will almost certainly be related to the fixed pole mechanism.

Previous dual models for photoproduction had great difficulty reconciling poles in the off-shell masses with consistent factorization in other channels[96]. It was recently pointed out[51,97] that the amplitudes with external pomerons factored from the pipe diagram of Fig. 3 have no such difficulty, and therefore provide a natural model for currents, very much in the spirit of Wu-Yang. Such models certainly have fixed poles even for one current. In fact the fixed poles support the Regge cuts I discussed earlier. This suggestion would therefore relate fixed pole residues in photoproduction to the Gribov vertex of the pomeron-reggeon cut (which generates the corrections to the weak absorption model).

8. Exotic mesons and nuclear forces

There has been much discussion of the duality diagram[75]

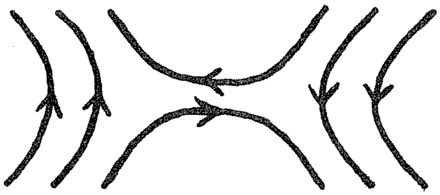

In my opinion, it means exactly what it says: (1) Exotic mesons exist[98]. (2) They couple only to $N\bar{N}$. (3) Ordinary mesons in the $N\bar{N} \rightarrow N\bar{N}$ t-channel are dual to exotic mesons in the $N\bar{N} \rightarrow N\bar{N}$ u-channel, and vice-versa. This implies that one-boson-exchange models of NN scattering do not involve double counting, unlike K^+p[99]. No exotics are expected in NN → NN. Probably[100,101] dual models for NN will be just sums of (t,u) Veneziano terms, except that one trajectory in each term will be a Rosner exotic. Now (t,u) Veneziano models are very successful in K^+p[36], where they explain the strong repulsive S wave force. Anybody constructing such an NN model, and unitarizing it, will find a great deal of phase shifts and Regge data to fit. Factorization uniquely determines the vector and tensor meson Regge limits, since they are well established in πN, KN[24], $\pi\pi$ and $K\bar{K}$[19].

Nuclear physicists are still wailing that they don't understand the repulsive core quantitatively, and astrophysicists that they can't tell the stability limit of neutron stars. A correct* Veneziano model for NN would clearly be an advance on boundary condition nonrelativistic potentials, and would probably predict the mass of Rosner's exotic mesons[98], as well as closing this ancient story of nuclear forces.

---

*Despite several previous attempts at NN Veneziano formulae, I only know of one[101] which even uses the right duality diagram, and this merely considers the Regge limit (without absorption).

9. Conclusions*

Recently a few far-sighted people have been constructing dual field theories, whose Born term satisfies 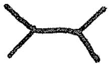 = 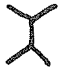, and therefore contains an exponentially infinite particle spectrum. One ϕ^3-like model is actually complete and renormalized. A few other people have been building more realistic Born terms.

Figure 4 shows the whole deductive scheme, describing the present state of strong interaction dynamics. The arrows are not proofs in the sense of Wightman, but are nevertheless very plausible. The ticks indicate statements which have been checked experimentally. My conclusion is: If any simple theory of strong interactions exists, then it must be a dual field theory.

Small angle pp scattering, as measured at NAL and ISR, will soon give a crucial test of this deduction. Three situations can be envisaged:

(1) It continues to shrink with $\alpha_P' = 0.45$ GeV^{-2}. This Regge effect is in conflict with naive intuition (like the bending of light in a gravitational field). Only the "pipe hypothesis", which is essential to any dual field theory, predicts a definite nonzero number.

(2) It stops shrinking. This would be very difficult to reconcile with the shrinkage of pp and K^+p at observed energies (Fig. 2), without effectively discarding duality.

(3) The s-channel trajectories at last turn over. According to duality, the whole t-channel Regge description will then collapse, and we will find ourselves in a new land of giant resonances.

---

*It is difficult to present the complete case without being unkind to some people. However, I only get really angry with the authors of incorrect papers, when they write "reviews" in which opposing work is not answered but systematically ignored.

References

1. C. Chiu and A. Kotanski, Nucl. Phys. B7, 615 (1968).
2. V. Barger and R. Phillips, Phys. Rev. 187, 2210 (1969).
3. C. Schmid, Phys. Rev. Lett. 20, 689 (1968).
4. C. Schmid, Nuovo Cim. 61A, 288 (1969).
5. C. Chiu and J. Finkelstein, Phys. Lett. 27B, 510 (1968); C. Schmid, Lett. Nuovo Cim. 1, 165 (1969).
6. J. Finkelstein, Phys. Rev. Lett. 22, 362 (1969).
7. G. Cohen-Tannoudji et al., Phys. Rev. Lett. 26, 112 (1971).
8. S. Fubini, D. Gordon and G. Veneziano, Phys. Lett. 29B, 679 (1969).
9. It is popularly asserted [T. Massam and A. Zichichi, Nuovo Cim. 43, 1137 (1966); N. M. Kroll, T. D. Lee and B. Zumino, Phys. Rev. 157, 1376 (1967); etc.] that an off-shell $\rho N\bar{N}$ vertex would reconcile the observed $<t^{-2}$ asymptotics of nucleon form factors with single ρ saturation. This argument is false from neglect of unitarity. Any reader of Muskhelishvili's book or of Ref. 94, ought to be able to construct a counter theorem, relating asymptotic behavior of e.m. form factors to the number of CDD zeroes. The precise fallacy in MZ-KLZ is easily traced from comparison with "deuteron-dominance". A correctly unitary theory of off-shell effects was given long ago [C. Lovelace, Phys. Rev. 135, B1225 (1964)], and is well confirmed by nd scattering experiments [A. C. Phillips, Phys. Rev. 142, 984 (1966)]. If the off-shell ρ vertex were really so important, then by unitarity the ρ propagator could not be approximated by a pole for all t. In the absence of a second vector meson, the net effect has to cancel in the asymptotic e.m. form factor for reasons related to Levinson's theorem.
10. R. Diebold and J. Poirier, Phys. Rev. Lett. 22, 255 (1969); L. Gutay et al., Phys. Rev. Lett. 22, 424 (1969); C. F. Cho and J. Sakurai, Phys. Lett. 31B, 22 (1970); D. Schildknecht, DESY 70/31; M. Nauenberg, Phys. Lett. 32B, 383 (1970);

G. Greenhut and R. Weinstein, Phys. Lett. 33B, 363 (1970);
R. Manweiler and W. Schmidt, Phys. Lett. 34B, 366 (1970);
A. M. Boyarski et al., Phys. Rev. Lett 25, 695 (1970);
Z. Bar-Yam et al., Phys. Rev. Lett. 25, 1053 (1970).

11. E. Bloom and F. Gilman, Phys. Rev. Lett. 25, 1140 (1970).
12. H. Yukawa, Proc. Phys. Math. Soc. Japan 17, 48 (1935).
13. Y. Nambu, Phys. Rev. 106, 1366 (1957).
14. W. Frazer and J. Fulco, Phys. Rev. Lett. 2, 365 (1959).
15. C. Lovelace, Proc. Aix Conf. I, 125 (1961);
    Nuovo Cim. 25, 730 (1962).
16. C. Lovelace, R. Heinz and A. Donnachie, Phys. Lett. 22, 332 (1966).
17. J. Shapiro, Phys. Rev. 179, 1345 (1969);
    C. Lovelace, Phys. Lett. 28B, 265 (1968).
18. G. Höhler, R. Strauss and G. Wunder, Vienna Conf. (1968).
19. C. Lovelace, Proc. Argonne Conf. on ππ and Kπ (1969), p. 562.
20. J. Rosner and H. Suura, Phys. Rev. 187, 1905 (1969).
21. M. Davier et al., SLAC-PUB-666 (1969);
    H. Alvensleben et al., Phys. Rev. Lett. 26, 273 (1971);
    F. Bulos et al., Phys. Rev. Lett. 26, 149 (1971);
    J. Diaz et al., CERN Internal Report (1970).
22. E. Malamud and P. Schlein, Phys. Rev. Lett. 19, 1056 (1967);
    Many authors in Proc. Argonne Conf. on ππ and Kπ (1969).
23. T. Trippe et al., Phys. Lett. 28B, 203 (1968);
    Proc. Argonne Conf. on ππ and Kπ (1969);
    H. Yuta et al., ANL (1971).
24. C. Lovelace, Nucl. Phys. B12, 253 (1969).
25. T. Eguchi, Tokyo UT-86 (1971).
26. J. Scherk, Orsay LPTHE 71/7.
27. R. Dalitz in "Pion-nucleon scattering", ed. Shaw and Wong
    (Wiley, N.Y. 1969);
    O. Greenberg, Proc. Lund Conf. (1969), p. 387.
28. R. Carlitz and M. Kisslinger, Phys. Rev. Lett. 24, 186 (1970).
29. E. Berger and G. Fox, Nucl. Phys. B26, 1 (1971).
30. R. Ayed et al., Phys. Lett. 31B, 598 (1970).

31. R. K. Roychoudhury et al., Nucl. Phys. B16, 461 (1970).

32. C. Lovelace, Proc. Heidelberg Conf. (1967), p. 79;
A. Donnachie, R. Kirsopp and C. Lovelace, Phys. Lett. 26B, 161 (1968).

33. M. G. Albrow et al., Nucl. Phys. B25, 9 (1971);
G. Burleson et al., Phys. Rev. Lett. 26, 338 (1971);
R. M. Brown et al., Kiev Conf. (1970).

34. C. Lovelace, in "Pion-Nucleon Scattering", ed. Shaw and Wong (Wiley, N.Y. 1969).

35. R. Plano, Proc. Kiev Conf. (1970).

36. C. Lovelace and F. Wagner, CERN Th.1251 (1970), to be published in Nucl. Phys. B.

37. F. Wagner, Nuovo Cim. 64A, 189 (1969);
G. Bassompierre et al., Nucl. Phys. B16, 125 (1970).

38. E. Tryon, Columbia NYO-1932(2)-177 (1971).

39. R. Cutkosky, this conference.

40. C. Johnson and H. Steiner in "Pion Nucleon Scattering" ed. Shaw and Wong (Wiley, N.Y. 1969);
F. Wagner and C. Lovelace, Nucl. Phys. B25, 411 (1971).

41. B. Petersson and G. Thomas, Nucl. Phys. B20, 451 (1970).

42. M. LeBellac, Phys. Lett. 25B, 524 (1967);
R. Phillips and G. Ringland "Regge Phenomenology", RHEL (1971) §V̄A.

43. J. D. Jackson and C. Quigg, Phys. Lett. 29B, 236 (1969);
Nucl. Phys. B22, 301 (1970).

44. J. Finkelstein and M. Jacob, Nuovo Cim. 56A, 681 (1968).

45. V. Barger and R. Phillips, Phys. Rev. Lett. 24, 291 (1970).

46. A. Anselm and I. Dyatlov, Yad. Fiz. 6, 591 (1968);
S. Frautschi and B. Margolis, Nuovo Cim. 56A, 1155 (1968).

47. R. Arnold and M. Blackmon, Phys. Rev. 176, 2028 (1968);
M. Blackmon and G. Goldstein, Phys. Rev. 179, 1480 (1969);
M. Blackmon et al., Phys. Rev. 183, 1452 (1969);
Nucl. Phys. B12, 495 (1969).

48. M. Ross, F. Henyey and G. Kane, Nucl. Phys. B23, 269 (1970).

49. S. Mandelstam, Nuovo Cim. 30, 1127, 1148 (1963).

50. R. Glauber, Boulder Lectures I, 362 (1958).

51. C. Lovelace, Phys. Lett. 34B, 500 (1971).

52. G. Chew, F. Low and M. Goldberger, Phys. Rev. Lett. 22, 208 (1969).

53. V. Gribov, JETP 53, 654 (1967);
G. Winbow, Phys. Rev. 177, 2533 (1969).

54. H. Cheng and T. T. Wu, DESY 70/67.

55. R. Arnold, Phys. Rev. 153, 1523 (1967);
C. Chiu and J. Finkelstein, Nuovo Cim. 57, 649 (1968);
G. Cohen-Tannoudji et al., Nuovo Cim. 48, 1075 (1967).

56. Y. Nambu, Chicago EFI 69-64;
L. Susskind, Nuovo Cim. 59A, 457 (1970);
S. Fubini and G. Veneziano, Nuovo Cim. 57A, 29 (1970).

57. H. Satz, Priv. Comm. I think this number originated from D. Morrison, but cannot trace the reference within the editorial deadline. All the 64 inelastic channels analysed by J. D. Hansen et al. [Nucl. Phys. B25, 605 (1971)] have $\alpha_{eff} < \frac{1}{2}$.

58. C. DeTar, UCRL-19882 (1970);
C. Akerlof et al., Phys. Rev. D3, 645 (1971).

59. D. Harrington, Phys. Rev. D1, 2615 (1970).

60. C. Meyers et al., Nucl. Phys. B23, 99 (1970);
A. Irving et al., CERN.TH.1304 (1971).

61. S. Frautschi, C. Hamer and F. Ravndal, Phys. Rev. D2, 2681, 2687 (1970).

62. C. Michael, Phys. Lett. 29B, 230 (1969).

63. A. Carroll et al., CERN (1971).

64. C. Quigg, unpublished.

65. E. Berger and G. Fox, Phys. Rev. Lett. 25, 1783 (1970).

66. V. Barger and R. Phillips, Phys. Lett. 26B, 730 (1968).

67. B. Amblard et al., Lund Conf. (1969).

68. L. Dick, this conference.

69. M. Borghini et al., Phys. Lett. 31B, 405 (1970).

70. E. Berger, ANL/HEP 7034 (1970), p. 100.

71. G. Ringland and R. Phillips, RHEL preprint RPP/C/8 (1971).

72. C. Chiu, Cal.Tech. CALT-68-281 (1970).

73. C. Schmid, Lett. Nuovo Cim. 1, 165 (1969);
V. Barger, Phys. Rev. 179, 1371 (1969).

74. B. Barnett et al., ANL (1971).

75. M. Imachi et al., Progr. Theor. Phys. 40, 353 (1968);
H. Harari, Phys. Rev. Lett. 22, 562 (1969);
J. Rosner, Phys. Rev. Lett. 22, 689 (1969).

76. C. Schmid and J. Storrow, CERN TH.1216 (1970).

77. J. Mandula et al., Phys. Rev. Lett. 22, 1147 (1969);
23, 266 (1969); Ann. Rev. Nucl. Sci. 20, 289 (1970).

78. S. J. Chang and T. M. Yan, Urbana, Ill. (TH)-71-4.

79. J. Finkelstein and F. Zachariasen, CERN.TH.1297 (1971).

80. G. Beznogikh et al., Phys. Lett. 30B, 274 (1969).

81. V. Barger and R. Phillips, Phys. Lett. 29B, 676 (1969).

82. V. Barger and D. Cline, Nucl. Phys. B23, 227 (1970).

83. C. Meyers and Ph. Salin, Nucl. Phys. B27, 33 (1971);
M. Bander and T. Stone, Irvine preprint (1971).

84. V. Barger and D. Cline, Phys. Rev. Lett. 24, 1313 (1970).

85. G. McClellan et al., Cornell CLNS-140,141 (1971).

86. C. Lovelace, Proc. Lund Conf. (1969), p. 266.

87. K. Kikkawa, S. A. Klein, B. Sakita and M. Virasoro,
Phys. Rev. 184, 1701 (1969); D1, 3258 (1970).

88. G. Frye and L. Susskind, Phys. Lett. 31B, 589 (1970);
D. Gross et al., Phys. Lett. 31B, 592 (1970).

89. Because of the strong form factors, t-channel unitarity corrections could make the P trajectory very nonlinear (cf. footnote 9). This would explain the absence of narrow particles, and is not disfavored by Regge fits (cf. Ref. 36).

90. J. Finkelstein, CERN. TH.1306 (1971).

91. K. Lübelsmeyer, Proc. Daresbury Conf. (1969);
E. Berger and G. Fox, ANL/HEP 7103 (1971).

92. J. Bronzan et al., Phys. Rev. 157, 1448 (1967).
93. R. Dashen and S. Frautschi, Phys. Rev. 143, 1171 (1968);
R. Dashen and S. Y. Lee, Phys. Rev. Lett. 22, 366 (1969).
94. C. Lovelace, Commun. Math. Phys. 4, 261 (1967).
95. H. Rollnik, Proc. Heidelberg Conf. (1967), p. 400.
96. B. Hasslacher and D. Sinclair, Stony Brook preprint (1970).
97. I. Drummond, CERN.TH.1301 (1971).
98. J. Rosner, Phys. Rev. Lett. 21, 950 (1968).
99. K. Kinoshita and K. Shiga, Kyushu-71-HE-1.
100. S. Ellis et al., Nucl. Phys. B24, 1 (1971).
101. G. Joshi and A. Pagnamenta, Part. Fi. 1, 220 (1970).

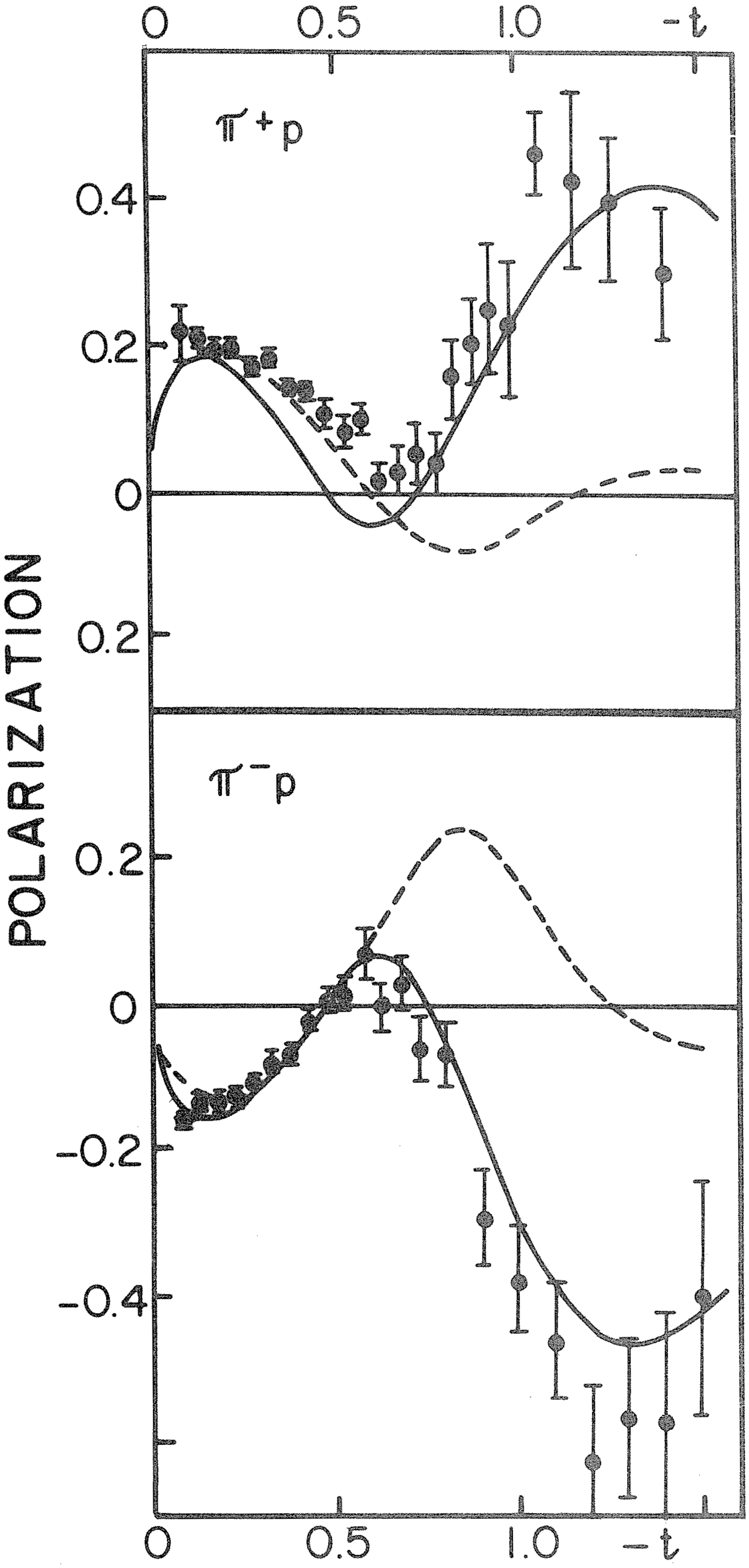

Fig. 1 $\pi^{\pm}p$ polarization at 6 GeV/c[69]. New data[68] at 10 and 14 GeV/c is very similar. The solid line is Argonne, the dotted Michigan[71].

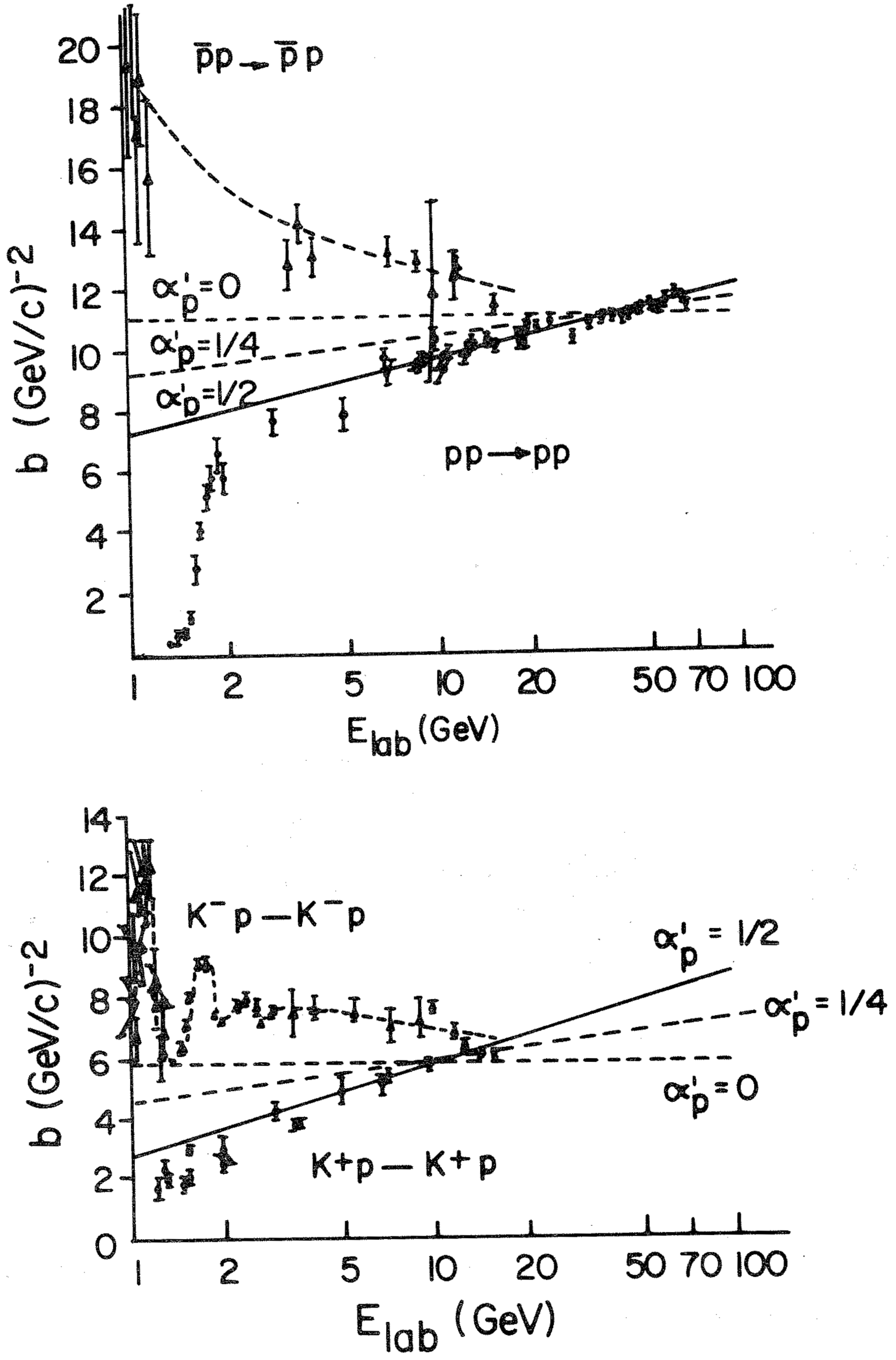

Fig. 2 Slope of the diffraction peak as a function of energy for various processes[82].

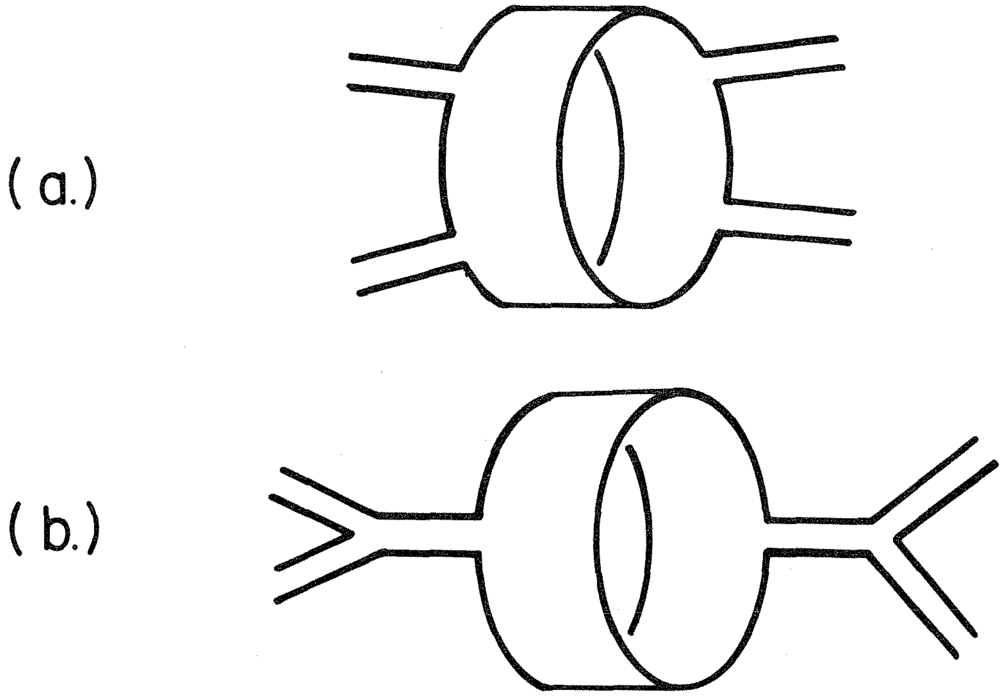

Fig. 3 (a) The duality diagram for a RR cut (vertical) dual to a bare pomeron (horizontal).

(b) The pomeron form factors have poles from the f and its daughters.

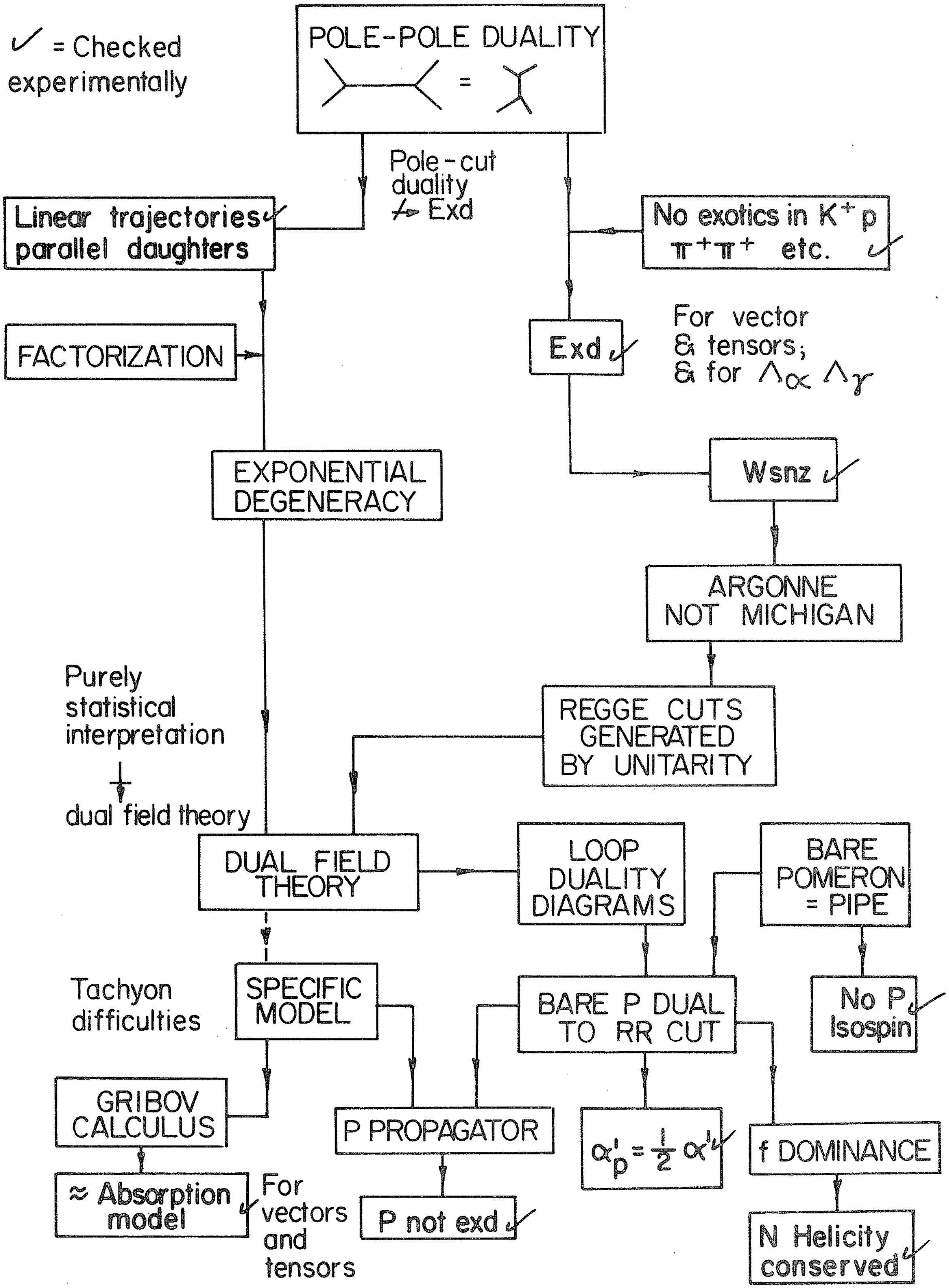
✓ = Checked experimentally
POLE-POLE DUALITY
Pole-cut duality ↛ Exd
Linear trajectories parallel daughters ✓
No exotics in K^+p $\pi^+\pi^+$ etc. ✓
FACTORIZATION
Exd ✓
For vector & tensors; & for Λ_α Λ_γ
EXPONENTIAL DEGENERACY
Wsnz ✓
ARGONNE NOT MICHIGAN
REGGE CUTS GENERATED BY UNITARITY
Purely statistical interpretation ↓ dual field theory
DUAL FIELD THEORY
LOOP DUALITY DIAGRAMS
BARE POMERON = PIPE
Tachyon difficulties
SPECIFIC MODEL
BARE P DUAL TO RR CUT
No P, Isospin ✓
GRIBOV CALCULUS
P PROPAGATOR
$\alpha'_p = \frac{1}{2}\alpha'$ ✓
f DOMINANCE
≈ Absorption model ✓
For vectors and tensors
P not exd ✓
N Helicity conserved ✓

Fig. 4 Deductions from strong interaction phenomenology. Ticks show experimentally checked results.

DISCUSSION

Yokosawa (Argonne): I have a general question on Regge cuts. We experimenters began to hear about this Regge cut several years ago, year after year, stronger and stronger. We began to catch up. And we started to believe it. And also there are many predictions from cuts in various channels. Finally we understood that there are very important channels, that they can make very strong predictions, such as in πN charge exchange or backward scattering. People who worked on the weak cut model and the Michigan model said that the predictions here are very firm and no more parameters to be determined. If they don't agree with experiment, the models are through . . . Now, the experiment at 5 GeV, which is high enough in energy, disagrees completely with the cut prediction (see Yokosawa's talk, page 615). My question is, from the experimentalist point of view, are theorists really going in the right direction with Regge cuts?

Lovelace: Of course! There wouldn't be fun being an experimentalist if you cannot prove theorists wrong, especially the ones of your own laboratory. However, the charge exchange polarization, if I am not mistaken, depends on the interference between the first order cut and the second order cut,* so it is much a less basic test than things like the forward peak in the np charge exchange, which is the direct test of the first order cut.

Henyey (Michigan): I won't go into all the successes of the Michigan model. Instead I would like to use duality as the test of the various models. According to my understanding, if you take the isospin one channel of $\pi\pi$ scattering, and ask where the zero is in ordinary dual model with the nonsense-wrong signature zero, you find that the zero comes out about -0.6 $(\mathrm{GeV}/c)^2$, slightly moved in because of the weak cut. The Michigan model predicts a dip at -0.2. At the mass of the ρ, in the $I = 1$ channel, the ρ is the only thing that is resonating. The zero occurs at -0.26.

---

*Editor's footnote: This does not seem to be borne out by a detailed investigation. Negative polarization at $t \approx -0.6$ $(\mathrm{GeV}/c)^2$ seems an unambiguous prediction of absorption cut models, and is not sensitive to (small) second order corrections. See Section 2.1B (715) (Table 1A) of Fox's talk at this conference.

Lovelace: Well, the first statement is that the Michigan model does not actually predict a zero at any particular place. You are supposed to fit the data by adjusting the cut strength: the zero can be anywhere. The second statement is that there are two separate pieces of the Michigan model which have to be tested separately. First is the dip mechanism: is the dip due to the pole WSNZ or is it due to the pole-cut interference effect. The latter gives a very bad prediction for the $\pi^{\pm}p$ elastic polarization (Figure 1, Lovelace's paper). The second thing is whether the cut is stronger than that predicted by the eikonal form. The case you are describing, tests the second, not the first. In fact, I think there is evidence that the eikonal formula underestimates the cuts in zero helicity flip. This is the case in your $\pi\pi$ case, np charge exchange and the crossover phenomena.

Henyey: By how much do you need to increase the absorption in this non-flip amplitude?

Lovelace: I don't think that it is the question of a multiplicative factor here. It is a failure of the Gribov vertex to factorize. There is no evidence from any model that one can describe the correction to the eikonal model just simply by jacking up the normalization (cf. page 679 of Lovelace's talk).

Kelly (Carnegie-Mellon): I just want to comment on how much you can adjust the parameters in the Michigan model in order to get agreement with data. An important constraint which has been ignored in many discussions of this, is that, in the Michigan model, if you take the amplitude and extract the residue at a particle pole, it gives a reasonable coupling constant. We looked at many previous fits and we have noticed some bad disagreements.

Lovelace: Do you fit the K^-p charge exchange or $\pi^-p \rightarrow \eta n$? For these cases there is the forward turnover, but no dip at -0.6 $(\mathrm{GeV}/c)^2$.

Kelly: I don't know the latest status of this.

Flatté (LRL): I would like to understand little more basically what you think the Pomeron is. From what you say, I don't see any difference between the Pomeron and any other particle.

Lovelace: Certainly, there is difference. The difference is firstly it has slope half, and secondly it has a multiplicative fixed pole and the over-compensation mechanism. This is predicted by dual loops. While everything else has exchange degeneracy, nonsense-wrong signature zeros and additive fixed poles, the Pomeron does not have an EXD partner or nonsense-wrong signature zeros: further it has a multiplicative fixed pole. The Pomeron is dual to a Regge-Regge cut. Other poles are dual to each other.

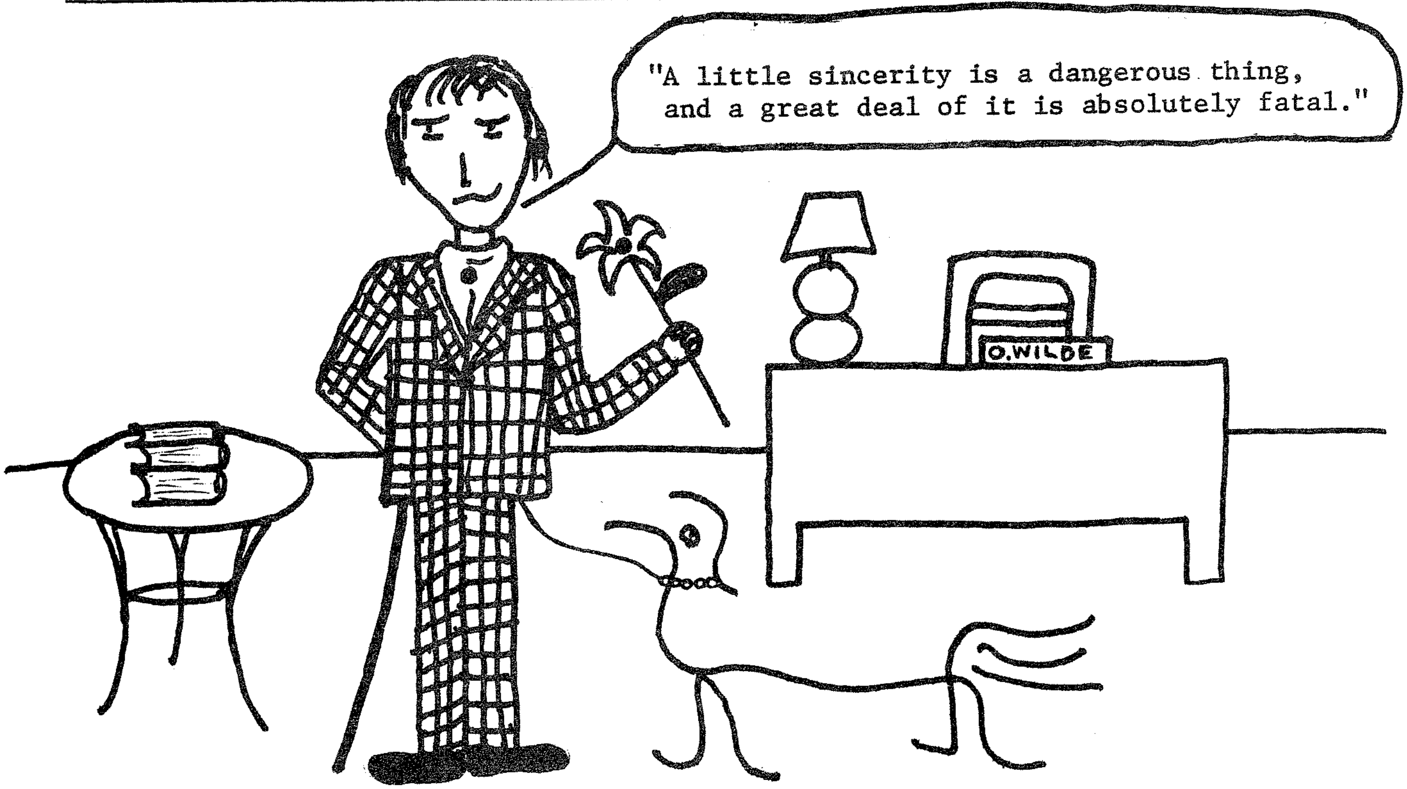
"A little sincerity is a dangerous thing,
and a great deal of it is absolutely fatal."
O.WILDE

ON THE IMPORTANCE OF BEING AN AMPLITUDE*

Geoffrey C. Fox
California Institute of Technology
Pasadena, California

---

*Work supported by the U.S. Atomic Energy Commission under Contract No. (11-1)-68.

TABLE OF CONTENTS

		PAGE
1.	Introduction	705
2.	Small Momentum Transfer ($-t \lesssim 1$ (GeV/c)^2)	709
	2.1. Natural Parity Exchange: zero structure of amplitudes	709
	2.2. Unnatural Parity Exchange: zero structure of amplitudes (ρ_{00} $d\sigma/dt$)	720
	2.3. Backward scattering	724
	2.4. π exchange (Poor Man's Absorption, conspiracy)	726
	2.5. EXD and SU_3	731
	2.6. Diffraction scattering	732
3.	Large Momentum Transfer ($-t \gtrsim 1$ (GeV/c)^2)	734
	3.1. Experimental t distributions	734
	3.2. Interpretation in the b-plane	738
4.	Quark Model	743
	4.1. The Model	743
	4.2. Stodolsky-Sakurai Distribution	743
	4.3. Additivity Frame: Perversity Amplitudes	744
	4.4. Dynamics of the Black Box	745
	4.5. Double Resonance Production	749
	4.6. Absorption Model	750
	4.7. Summary	753
5.	Multiparticle Reactions	756
References and Footnotes		758
Table 1A:	Forward Polarizations	715
Table 1B:	Backward Polarizations	725
Table 2:	ρ_{00} $d\sigma/dt$ Predictions	722
Table 3:	Large $-t$ Slopes	740
Table 4:	Polarized Target Observables	757

1. INTRODUCTION

I would like to review theoretical and experimental understanding of the scattering amplitudes at high energy. Most experiments measure for the process $1+2 \to 3+4$,

$$d\sigma/dt = K(s) \sum_{i=1}^{m} \left|H_{\lambda_1\lambda_2 \to \lambda_3\lambda_4}(s,t)\right|^2 \qquad (1)$$

with $K(s)$ a known kinematic factor.1) This is a sum over m independent complex amplitudes, labelled by the helicities of particles; m varies from 2 in, say, πN scattering to 24 in $\gamma N \to \omega\Delta$. One can analyze data in two distinct ways:

(i) Fixed t (momentum transfer), variable s (energy):

This tests the infamous $s^{2\alpha-2}$ prediction of Regge theory for $d\sigma/dt$ and its modification in absorption models. I reviewed the situation in such tests some time ago2) and there has unfortunately been little new data since then.

(ii) Fixed s and variable t:

We will concentrate on this study of the t-dependence of the amplitudes H in the current article. We note first that (i) and (ii) approximately separate because it is true in most models -- at least for a given exchange -- that

$$H_{\lambda_1\lambda_2 \to \lambda_3\lambda_4}(s,t) \sim g_{\lambda_1\lambda_2 \to \lambda_3\lambda_4}(t) \;\; f(s,t) \qquad (2)$$

where $f(s,t)$ is, for example, $s^{\alpha(t)}$ in Regge theory, and generally depends only weakly on the helicities λ. The ansatz (2) has not been stringently tested but is in reasonable accord with experiment. We discuss the spin structure of amplitudes, i.e., which spin amplitudes H contribute to a given reaction and what are the ratios of these for different helicities. Further, we consider the t-dependence for each given amplitude.

The studies (ii) are, in one way, easier than (i) because the conditions are satisfied in a single experiment. However, there is a crucial difficulty that t-dependence not only depends greatly on the labels λ_i but also differs for the real and the imaginary part of H. The extraction of the t-dependence of a given amplitude from $d\sigma/dt$ data is usually indirect;

it can come from explicit model fits, symmetry constraints on amplitude ratios or interference effects. (E.g., the cross-over in $\pi^\pm p$ is sensitive to the imaginary part of the ρ nonflip amplitude.) Most directly, further experimental observables give us more information about amplitudes and their t-dependence. For instance, in meson-baryon scattering we have

$$P\, d\sigma/dt \;=\; 2K(s)\ \mathrm{Im}\left[H_{+\to+}\ H^{*}_{-\to+}\right] \tag{3}$$

where P is polarization. Again, in vector meson production -- say $\pi N \to \rho N$ --

$$\rho_{00}\ d\sigma/dt \;=\; K(s)\left\{\left|H_{0+\to0+}\right|^2+\left|H_{0+\to0-}\right|^2\right\} \tag{4}$$

selects two out of the six independent helicity amplitudes. The decay density matrix elements for resonance production and their information on the basic amplitude structure, represents the main reason for studying such reactions. For simple $d\sigma/dt$ studies, they, of course, suffer from a lack of statistics and background subtraction problems, compared with stable particle data.

In spite of the paucity of polarization data and the corresponding indirectness of the inferences, there has been striking progress recently in unravelling the t-dependence -- in particular, the zero structure -- of amplitudes. The data has given us only a few pieces of the cosmic jigsaw but even these are sufficient to rule out all explicit theories so far proposed. Thus both Regge pole and Regge pole plus absorption cut models4,5) give distinctive predictions for the zeros of amplitudes.3) Although each model has some interesting successes, neither is universally correct. Indeed, it appears that the correct picture of scattering must involve an intriguing mixture of geometric (absorption) and analyticity (Regge) constraints. One can try to suggest the structure of this correct theory by empirical rules4,6) that summarize the current data. Our present knowledge is sufficiently incomplete that there are, of course, many possible rules. Only experiment can delineate the precise regions of validity of the simple theories and so clarify and extend the present rules. Such studies must emphasize amplitude determination -- for instance, in the well-measured $\pi^- p \to \pi^0 n$ reaction, the spin flip amplitude agrees well with Regge theory but in the same reaction (the imaginary part of) the nonflip amplitude can only be understood in an absorption model. This ambivalence is general: correspondingly, simple dσ/dt studies are usually difficult to interpret in any one model. This unambiguous failure of all explicit models renders it essential to design experiments that can be interpreted independently of detailed model fits. In particular, the usefulness of experiments that measure all the observables of a given reaction (e.g., dσ/dt, P, R, and A for meson-baryon scattering) cannot be overemphasized:3) they determine the amplitude structure -- up to an overall phase -- without any model-dependent assumptions. In the following sections we will try to indicate precisely which experiments will best illuminate the barren patches of our giant jigsaw. I will often use explicit model fits as a guide in suggesting interesting experiments. Although the theories are not quantitatively correct, they are a valuable guide to the expected size of interesting effects. At the very least, this indicates the statistical accuracy necessary in any given experiment.

In Section 2 we discuss the amplitude structure at small momentum transfer ($-t \lesssim 1$ $(\mathrm{GeV/c})^2$) for natural and unnatural parity exchange. We first consider the zero structure of the amplitudes and then the inhabited amplitude systematics (i.e., F/D ratios, conspiracy, etc.). In the natural parity exchange segment, we consider dσ/dt, FESR, CMSR, elastic, and inelastic polarizations plus R and A measurements. Particularly interesting is the real part of the nonflip amplitude -- several indirect inferences from current data suggest it has a t-dependence quite different from the predictions of any model. Further, we apply the lessons from this well-studied segment to π exchange processes. This emphasizes the surprising nature of the well-known systematics of the latter reactions. The natural parity exchange data appears to discredit the usual and superficially successful SCRAM calculations7) for π exchange. On the other hand, recent data lends support to an alternative PMA (poor man's absorption) model8) which emphasizes smoothness in the amplitude extrapolation from $t = 0$ to $t = m_\pi^2$. At larger $-t \approx 0.6$ $(\mathrm{GeV/c})^2$, we study $\rho_{00}\, d\sigma/dt$ for vector meson production. The current data agree, within limited statistics, with the empirical rules deduced from natural parity exchange. Higher statistics data, particularly on $\pi^- p \to \rho^0 n$, will provide decisive new information.

In Section 3 we examine the systematics of large momentum transfer data of all possible inelastic two- and quasi-two-body data.9) This is a summary of unpublished work by Charles Chiu and myself. We compare photoproduction and strong interaction data and show that a naive interpretation of the present data in a geometric picture suggests that a large component of scattering is at small impact parameter. Photoproduction exhibits a universal e^{3t} dependence at and above 5 GeV/c.10) Hadronic data has only been well measured around 5 GeV/c but here it too, often shows an e^{3t} behavior. Urgent experimental work is necessary to clarify the universality of the e^{3t} momentum transfer dependence and its energy dependence in hadronic data. Further explicit partial wave analysis of $\sqrt{d\sigma/dt}$ with various phase assumptions allows us to interpret large -t $d\sigma/dt$ data in the impact parameter (b) plane. There are striking differences for both the signs and sizes of the small b component, between real and imaginary parts and between strong interaction and photoproduction data. This behavior if confirmed and shown (experimentally) to be universal, would be in intriguing challenge for theory.

In Section 4 we review the current status of the quark model relations for resonance production reactions.11) We compare the data, the quark model and simple absorption models of, for instance, one pion exchange in $\pi N \to \rho\Delta$. At present all three -- data, quarks, and absorption -- are indistinguishable. We suggest experiments that will remedy this distressing situation. Further, we show that many features of recent dual models,12,13) based on the quark substructure, are in qualitative agreement with experiment.

In Section 5 we lament the essentially non-existent knowledge of amplitudes in multiparticle reactions.

2. SMALL MOMENTUM TRANSFER ($-t \lesssim 1$ (GeV/c)^2)

2.1. Natural Parity Exchange: Zero Structure of Amplitudes

In this section we review knowledge of natural parity exchange for those amplitudes unencumbered by π exchange. Section 2.4 treats the natural parity component of complicated reactions, e.g., $\pi N \Rightarrow \omega\Delta$ and photoproduction. Again, I will only consider exchange processes here as diffraction scattering is postponed to Section 2.6. First we give a short theoretical motivation (Section 2.1A), then a summary of the experimental evidence (Section 2.1B), and finally present some conclusions (Section 2.1C).

2.1A. Theoretical Motivation

Let us first state some qualitative conclusions on which the various phenomenological analyses$^{3-7,14)}$ seem to agree. We extend and make these more accurate in Section 2.1C.

→ (C1) Imaginary parts of amplitudes have "absorption zeros".

→ (C2F) The real parts of spin flip amplitudes approximately agree with Regge theory. In particular, they do not have the absorption zeros.

→ (C2N) The real part of the nonflip amplitude is badly determined. There is some evidence that it, again, does not have the absorption zeros.

Even these systematics are sufficient to rule out all theories so far proposed. Let us recall the three canonical theories and their rather dubious acronyms.

→ (T1) Regge pole theory with exchange degeneracy (EXD) and hence wrong signature nonsense zeros (WSNZ) = GORE.

→ (T2) Regge poles as in (T1) $\oplus$ weak absorption = Argonne model = WIZKID.

→ (T3) Regge poles without WSNZ $\oplus$ strong absorption = Michigan model = SCRAM.

Then (T1) and (T2) disagree with (C1) for the nonflip amplitude, but agree with (C1) for the flip; they approximately agree with (C2F). (T3) agrees with (C1) but disagrees with (C2F).

Figures 1 - 6 present typical curves for the amplitudes in our three theories. These come from explicit fits$^{15)}$ to the data and are calculated at 5 GeV/c and absolutely normalized -- not as in Eq. (1) -- but so that

$$d\sigma/dt \;=\; \left\{|N|^2 + |F|^2\right\} \mathrm{mb}/(\mathrm{GeV}/c)^2 \qquad (1a)$$

where we have introduced the shorthand $N = H_{+\Rightarrow+}$ and $F = H_{-\Rightarrow+}$ for the s-channel helicity amplitudes. We also give in Figs. 1-6 the Fourier-Bessel transforms of these amplitudes defined by

$$f_{N,F}(s,b) \;=\; 1/(32\pi\sqrt{sK(s)}\;\; q\, b^n) \int_0^\infty N,F(s,t)\; J_n(b\sqrt{-t})\; d(-t) \qquad (5)$$

where $n = |\lambda_1 - \lambda_2 - \lambda_3 + \lambda_4|$ is the total s-channel helicity flip and $f(b)$ is normalized so that the S-matrix $S(b) = 1 + 2i\, f(b)\, b^n$ where we have removed the kinematic zero b^n. The impact parameter b is in units of $(\mathrm{GeV}/c)^{-1}$ so that $b = 5\ (\mathrm{GeV}/c)^{-1} \approx$ the magic value 1 fermi. The absorption prescriptions[2,5,7] (T2) and (T3) are, in their simplest form, given by:

$$f_{\mathrm{TOTAL}}(b) \;=\; f_{\mathrm{REGGE}}(b)\left\{1 - C\exp(-b^2/2a)\right\} \qquad (6)$$

with $a \approx 8\ (\mathrm{GeV}/c)^{-2}$, the slope of elastic scattering and $C \approx 0.5$ to 0.75 in (T2) and approximately twice this in (T3).

We have taken the four distinctive types of process, characterizing them by the Regge pole signature factors. The latter determine the zero structure of amplitudes in the simple theory (T1).

→ (R1) $\pi^- p \Rightarrow \pi^0 n$: (Figs. 1 and 5.) ρ-ω exchange:
These have signature factor $1 - e^{-i\pi\alpha}$ (7/1)
in Regge theory. Similar reactions are $\pi^+ p \Rightarrow \pi^0 \Delta^{++}$ and $K^0_L p \Rightarrow K^0_S p$.
(These examples have, of course, different ratios N/F.)

→ (R2) $\pi^- p \Rightarrow \eta n$: (Figs. 2 and 6.) A_2 exchange:
Signature factor is in Regge theory $1 + e^{-i\pi\alpha}$ (7/2)
and similar is $\pi^+ p \Rightarrow \eta^0 \Delta^{++}$.

→ (R3) $K^- p \Rightarrow \bar{K}^0 n$: (Fig. 3.) ρ, A_2; $K^* - K^{**}$ exchange:
Signature factor is in Regge theory $e^{-i\pi\alpha}$ (moving phase) . (7/3)
Similar are $K^- n \Rightarrow \bar{K}^0 \Delta^-$, $\pi^- p \Rightarrow K^0 \Lambda$, $\pi^+ p \Rightarrow K^+ \Sigma^+$.

→ (R4) $K^+ n \Rightarrow K^0 p$: (Fig. 4.) ρ, A_2; $K^* - K^{**}$ exchange:
Signature factor is in Regge theory 1 (real) . (7/4)
Similar are $K^+ p \Rightarrow K^0 \Delta^{++}$, $K^- n \Rightarrow \Lambda\pi^-$, and $K^- p \Rightarrow \pi^- \Sigma^+$.

We do not give SCRAM curves for (R3) and (R4) as the lack of pole EXD in this theory allows flexibility in the relative components of, say, the ρ and A_2 exchange. The SU_3 constraints for the amplitudes

$$\begin{aligned}\sqrt{2}\,(K^-p \Rightarrow \bar{K}^0 n) &= -(\pi^-p \Rightarrow \pi^0 n) + \sqrt{3}\,(\pi^-p \Rightarrow \eta^0 n)\\ \sqrt{2}\,(K^+n \Rightarrow K^0 p) &= (\pi^-p \Rightarrow \pi^0 n) + \sqrt{3}\,(\pi^-p \Rightarrow \eta^0 n)\end{aligned} \tag{8}$$

allow approximate predictions for (R3) and (R4) in SCRAM.

2.1B. Experimental Evidence

(i) Zero Structure of Im N:

The imaginary part of the nonflip amplitude N has the notorious crossover zero at $t \approx -0.2\ (\mathrm{GeV}/c)^2$. Evidence comes from (a) finite energy sum rules (FESR),16,17) and (b) $\pi^\pm p$, $K^\pm p$, pp, and $\overline{pp}$ differential cross sections.7,18) Harari and Davier18) have used recent new $K^\pm p$ elastic scattering data in an interesting way. Assuming the scattering is dominated by $I = 0$ exchange, and that the Pomeron part of this only contributes to Im N, one can write

$$2\ \mathrm{Im}\ N\ (\omega) \approx \frac{d\sigma/dt\ (K^-p) - d\sigma/dt\ (K^+p)}{2\left[d\sigma/dt\ (K^+p)\right]^{1/2}} \tag{9}$$

and their "experimental" result for $2\ \mathrm{Im}\ N\ (\omega)$ is shown in Fig. 7(a). Further, they partial wave analyzed $2\ \mathrm{Im}\ N\ (\omega)$ -- using the equivalent of Eq. (5) -- to find the value of $2\ \mathrm{Im}\ f_N(\omega)$ shown in Fig. 7(b).

It is clear from comparing Figs. 1(a) and 5(a) with Fig. 7(a) that theories (T1) and (T2) cannot reproduce the data at all. This is well-known. The strong cut (T3) is able to generate the correct position for the first zero in $\mathrm{Im}\ N(\omega)$ with $C \approx 1.33$. However in this case, Im N is too large for $t \approx -1\ (\mathrm{GeV}/c)^2$. In particular, the second zero of Fig. 7(a) is not reproduced. In the Fourier-Bessel transforms, this difference shows up in the large negative value of $\mathrm{Im}\ f_N(\omega)$ at $b \approx 0$ for (T3). The small central ($b \approx 0$) component in Fig. 7(b) follows from the second zero in $\mathrm{Im}\ N(\omega)$ of Fig. 7(a). (Remember, $J_0(b\sqrt{-t})$, $b = 5\ (\mathrm{GeV}/c)^{-1}$, has zeros at $-t = 0.23$ and $1.2\ (\mathrm{GeV}/c)^2$.) As we shall discover again in Section 3, this is a crucial point, i.e., is there a second crossover in $\mathrm{Im}\ N(\omega)$?, or, ≈ equivalently, is there a central component in Im $f_N(\omega)$? Unfortunately, the data is not as convincing as Fig. 7(a) suggests. Thus the assumptions used in generating it become very dubious for $-t \approx 1\ (\mathrm{GeV}/c)^2$. In particular there could well be a sizeable real part/spin flip component of diffraction scattering in this region. For example, if the Pomeron has slope 1/2 as a naive interpretation of the Serpukhov pp data suggests, then diffraction has equal real and imaginary parts in this region. Other data also indicate that this question is not settled yet. Figures 8(a) and 8(c) show pp ($\bar{p}p$) scattering at 3 and 16 GeV/c. pp and $\bar{p}p$ graze at $t \approx -1\ (\mathrm{GeV}/c)^2$ at 16 GeV/c but there is no clear-cut second crossover at either energy.

The sensitivity of $f_N(b)$ to assumptions on the large $-t$ behavior of Im N is illustrated in Fig. 9. This shows the partial wave projection of

$$(\text{———})\quad N(t) = \mathcal{A}(t) \quad \text{all } t \tag{10a}$$

with $\mathcal{A}(t) = 4.6\, J_o(5.84\sqrt{-t})\, e^{0.7t}$. Also shown is

$$\begin{aligned}(\cdots\cdots)\quad N(t) &= \mathcal{A}(t) \qquad -t \lesssim 1.3\ (\mathrm{GeV}/c)^2\\ &= \mathcal{A}(-1.3)\exp\left(1.5\,(t+1.3)\right) \qquad -t > 1.3\end{aligned} \tag{10b}$$

$$\begin{aligned}(\text{-----})\quad N(t) &= \mathcal{A}(t) \qquad -t \lesssim 0.6\ (\mathrm{GeV}/c)^2\\ &= \mathcal{A}(-0.6)\exp\left(1.5\,(t+0.6)\right) \qquad -t > 0.6\end{aligned} \tag{10c}$$

All three forms are identical for $-t \lesssim 0.6\ (\mathrm{GeV}/c)^2$ where they give a good representation to 2 Im $N(\omega)$ determined, just as in Eq. (9), from pp ($\bar{p}p$) scattering at 5 GeV/c. However, Fig. 9 strikingly shows that the three forms have quite different small b components. Until one can extract Im $N(\omega)$ reliably at large $-t$, no conclusion can be drawn at present about the amount of scattering at small impact parameter b.

Figures 8(a), (b), (c) also show up another interesting point. The first crossover in pp seems to move to lower $-t$ as energy increases. This behavior is expected in cut models (T2), (T3) and is also exhibited in K^-p scattering. This is the best established violation of the factorization rule of Eq. (2).

(ii) Zero Structure of Im F

It seems universally agreed that there is a single zero in Im F around $t \approx -0.6\ (\mathrm{GeV}/c)^2$. This is determined from (a) FESR's, and (b) dips in the single flip dominated, ρ exchange $\pi^- p \to \pi^0 n$, $\pi^+ p \to \pi^0 \Delta^{++}$; ω exchange $\gamma p \to \pi^0 p$, $\pi^{\pm} p \to \rho^{\pm} p$. Figures 1(b) and 5(b) indicate that this behavior is predicted in all three theories.

Most direct experimental evidence for Im N and Im F tests the zero structure of the odd signature ρ and ω exchange. However, EXD (supported by FESR's) suggests a similar behavior for the even signature P' and A_2 exchange. It is important to check this directly -- obvious experiments are the measurements of polarization in $K^+ n \to K^0 p$ and backward $K^+ p \to p K^+$.

(iii) Zero Structure of Real Parts

We now consider Re N and Re F; the evidence for the t-dependence of these is less familiar. It comes from:

(E1) Coulomb interference for elastic reactions.

(E2) t-dependence of real reactions -- type (R4).

(E3) Continuous moment sum rules (CMSR).

(E4) Elastic polarizations.

(E5) Polarizations in exchange reactions.

(E6) Particularly potent reactions: πN elastic, $K^0_L p \to K^0_S p$.

(E1) requires no comment except to say that the derived values of Re N (t = 0) agree quite well with those expected from the Regge signature factor. The essential feature of (E2) is that exchange processes in the exotic Kp, pp channels show no dip structure at all -- this directly suggests that the corresponding real amplitudes have no zeros in the momentum transfer region so far studied. In particular, there is excellent and well-documented agreement of the reactions $K^+ n \to K^0 p$ and $K^+ p \to K^0 \Delta^{++}$ with EXD Regge theory.[4,19] This supports (C2F), Re F ≈ Regge pole prediction. The only nonflip "real" reactions, unencumbered by π exchange, are backward $K^+ p \to p K^+$ which again shows no structure and $K^- n \to \pi^- \Lambda$, $K^- p \to \pi^- \Sigma^+$. The latter two reactions do not correspond to exotic channels but are predicted by duality diagrams to be purely real. Presumably this is approximately true[20] and it is interesting to note that the "real" $K^- n \to \pi^- \Lambda$, $K^- p \to \pi^- \Sigma^+$ are significantly flatter than their line reversed compatriots, $\pi^- p \to K^0\Lambda$ and $\pi^+ p \to K^+\Sigma^+$.55) These last two reactions are dominantly imaginary, and so the line reversal breaking suggests that Re N is less peripheral than Im N -- in particular, it may not have the magic zero around $t = -0.2$ $(\mathrm{GeV}/c)^2$.

Turning to (E3), we note that it is possible to write CMSR's that are directly sensitive to the real parts of the high energy amplitudes (in the pole approximation). Figure 10 shows some curves -- unfortunately without any estimate of errors or sensitivity to the sundry phase shift analyses -- from a recent paper by Phillips and Ringland.14) It is notable that the FESR's show the absorption zeros while the CMSR's show (a) approximate agreement with GORE for Re F(ρ), (b) neither absorption zeros nor agreement with GORE for Re N(ρ). This result for Re N is quite surprising (to me); the success of CMSR for Re F perhaps lends credibility to the Re N curve.

(E4) Elastic polarizations: These are the cleanest tests for Re $F(\rho, A_2)$. Using the same assumptions that led to Eq. (9), one finds that

$$\mathbb{P}\mathrm{ol}\ (\mathrm{elastic})\ \alpha\ \mathrm{Im}\ N(\mathrm{Pom}) \times \mathrm{Re}\ F(\rho, A_2) \quad . \qquad (11)$$

The old data at 6 GeV/c is summarized in Fig. 11. The t-dependence for all elastic reactions for $-t \lesssim 1$ $(\mathrm{GeV}/c)^2$ agrees amazingly with featureless Im N(Pom) and GORE for Re F. In particular, a single "absorption" zero in Re F at $t \approx -0.6$ $(\mathrm{GeV}/c)^2$ is ruled out by the data: to be precise it has been proposed22) that such a zero is possible if Im N(Pom) also has a zero at the same t value. Such a scheme does not appear compatible with all the information summarized here and in Section 2.6. In fact, it is rather alarming that the agreement with Eq. (11) extends to arbitrarily large -t -- as with Eq. (9) the assumptions leading to (11) are surely wrong above $-t \approx 1$ $(\mathrm{GeV}/c)^2$. Data presented by Dick at this Conference (page 607) shows structure in pp polarizations at $t \approx -1$ $(\mathrm{GeV}/c)^2$ -- which is inexplicable in this simple model; however, the same data perversely indicate the expected zero in $K^- p$ polarizations at this t value. It is clearly important to clarify the validity of Eqs. (9) and (11) at large -t.

(E5) Exchange polarizations: In general, polarizations are not interpretable without a specific model ($\mathbb{P}$ol and $d\sigma/dt$ not being a complete set of observables). However if we *assume* a simple t-structure for Im N and Im F, (zeros at -0.2 and -0.6 $(\text{GeV}/c)^2$ respectively), one can use the data to give important constraints on the real parts. Thus from Eq. (3),

$$\text{Pol} \propto \text{Re}\ F \times \text{Im}\ N - \text{Im}\ F \times \text{Re}\ N \qquad (12)$$

and so at $t = -0.2\ (\text{GeV}/c)^2$, where Im N is said to vanish, we find Pol α - Im F x Re N: this relates the sign of Pol to the *sign* of Re N as the *sign* of Im F certainly agrees with Regge theory. Actually putting in the magnitude of Im F from Regge theory would also allow a deduction of Re N in *sign* and *size*. However, here let us just discuss the sign predictions. For convenience, define $\hat{N}(t) = \text{Re}\ N(t)\ \epsilon_N$, $\hat{F}(t) = \text{Re}\ F(t)\ \epsilon_F$, where ϵ_N and $\epsilon_F = \pm 1$ are chosen so that in GORE, $\hat{N}$ and $\hat{F}$ are $\gtrsim 0$ -- or more precisely have the signs at $t = 0$ of the Regge signature factors (7/1-4). The table below summarizes the predicted polarization signs[23] in terms of $\hat{N}$, $\hat{F}$, and the experimental results when known.

TABLE 1A

		Sign		
Reaction	$t(\text{GeV}/c)^2$	Theory	Experiment	Ref.
(a) $\pi^- p \to \pi^0 n$	-0.2	$\hat{N}$	> 0	24
(b)	-0.6	$\hat{F}$	> 0	
	-1.2	$-\hat{N}$	(?)	
(c) $\pi^- p \to \eta n$	-0.2	$-\hat{N}$	> 0 (?)	25
	-0.6	$-\hat{F}$	(?)	
	-1.2	$\hat{N}$	(?)	
(d) $\pi^+ p \to K^+ \Sigma^+$	-0.2	$\hat{N}$	≈ 0	26
(e)	-0.6	$\hat{F}$	> 0	
(f)	-1.2	$-\hat{N}$	> 0	
(g) $\pi^- p \to K^0 \Lambda$	-0.2	$-\hat{N}$	> 0	27
(h)	-0.6	$-\hat{F}$	< 0	
	-1.2	$\hat{N}$	(?)	
$K^- p \to \bar{K}^0 n$	-0.2	$-\hat{N}$	(?)	
	-0.6	$-\hat{F}$	(?)	
	-1.2	$\hat{N}$	(?)	

Here we have omitted type (R4) reactions as their imaginary part is zero to first approximation. From the above table we can now read off the signs of $\hat{N}$ and $\hat{F}$ at the particular t values: a negative value indicates a sign change compared with $t = 0$. For instance, (a) shows that $\hat{N}(\rho)$ is positive at $t \approx -0.2$ $(\mathrm{GeV}/c)^2$ and so Re $N(\rho)$ has no zeros between $t = 0$ and -0.2 $(\mathrm{GeV}/c)^2$, i.e., it is less peripheral than Im $N(\rho)$ and vanishes -- if at all -- at larger $-t$. This agrees with our previous evidence on Re N but disagrees with the theories (T2) and (T3) -- Figures 1(a) and 5(a) show they predict Re $N(\rho)$ vanishing before Im $N(\rho)$. We should note here that most published (including all (T2) fits) cut predictions for such inelastic polarizations seem irrelevant: thus these models do not get the correct crossover zero position in Im N. This zero is clearly vital in determining the systematics of the inelastic polarizations.

Returning to our goldmine, row (b) shows that $\hat{F}(\rho)$ is positive at $t \approx -0.6$ $(\mathrm{GeV}/c)^2$. This suggests that Re $F(\rho)$ behaves like

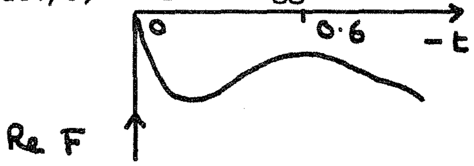

$(\epsilon_F = -1)$,

which disagrees with GORE and the absorption models. In the latter, the much-lauded destructive cut makes Re $F > 0$ at -0.6 $(\mathrm{GeV}/c)^2$. (See Figs. 1(b), 5(b).) A negative Re F at $t \approx -0.6$ does however agree with CMSR (Fig. 10). (e) and (h) show in reactions (R3) that again Re F agrees with GORE at -0.6 $(\mathrm{GeV}/c)^2$. Re N in (R3) seems curious: the data ((d) and (g)) suggest in $\pi^+p \to K^+\Sigma^+$:

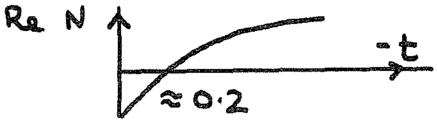

not

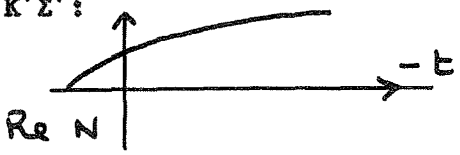

as in GORE; in $\pi^-p \to K^0\Lambda$ the zero in Re N seems to be at larger $-t$. Such behavior is consistent with cut models although the Σ, Λ difference is surprising.

(c) is particularly exciting: the data seems to have the opposite sign to expectations -- further polarization measurements in $\pi^-p \to \eta^0 n$ will be interesting.

The $t \approx -1.2$ results are perhaps dubious as the zero in Im N there is not well established. However, (d) and (f) suggest a zero in Re N between -0.2 and -1.2 $(\mathrm{GeV}/c)^2$. This is expected in (T1) from the signature zero at $\alpha_{K*} = -1/2$. $(t \approx -1\ (\mathrm{GeV}/c)^2)$

(E6) Potent reactions: In the $\pi N \to \pi N$ system, there are four independent amplitudes (including both isospin states) and so seven independent observables. These could be $d\sigma/dt$ and polarization for the three reactions $\pi^- p \to \pi^- p$, $\pi^+ p \to \pi^+ p$, and $\pi^- p \to \pi^0 n$ plus, say, R for $\pi^- p \to \pi^- p$. Measurements of all these quantities exist around 5 GeV/c! It would be interesting to find all the amplitudes in a model-independent way.

More modestly, let us look at $K_L^0 p \to K_S^0 p$ which allows ρ and ω exchange with

$$d\sigma/dt = \mathrm{Re}\ N^2 + \mathrm{Im}\ N^2 + |F(\rho)|^2 \tag{13}$$

The last two terms in this can easily be estimated: the second from Eq. (9), the last from SU_3 and $\pi^- p \to \pi^0 n$ (the nonflip part of $\pi^- p \to \pi^0 n$ can be lumped into the first two terms). Figure 12 shows these two contributions to $K_L^0 p \to K_S^0 p$, their sum, and the total (experimental) $d\sigma/dt$ at $p_{\mathrm{lab}} \sim 3$ and 5 GeV/c. $|\mathrm{Re}\ N|^2$ is found by subtracting the last two curves. Let us not dwell on the uncertainties in this analysis (e.g., SU_3 breaking, non-monoenergetic K_L^0 data) but emphasize that the figure shows this data is quite consistent with a Re N which has no zeros in $0 \leq -t \leq 1\ (\mathrm{GeV}/c)^2$. However, such a Re N is not a smooth exponential but rather has a break for $-t \approx 0.3\ (\mathrm{GeV}/c)^2$.

Higher statistic experiments on both $\pi N \to \pi N$ and $K_L^0 p \to K_S^0 p$ would clearly be desirable. In the former case, collection of the desired seven independent observables at the same energy clearly requires some coordination of the experimental effort.

(iv) R and A Measurements

In the previous pages we have had to resort to indirect methods to find the various amplitudes. There is a class of feasible experiments which will render such subterfuge unnecessary and provide immediate decisive tests of your favorite model. These are measurements of R and A, which are the components of final nucleon polarization observed in scattering off a polarized target. At high energy they take the form:

$$\begin{aligned} R &= 2\,\mathrm{Re}(N^{*}F)/(|N|^{2}+|F|^{2}) \quad , \\ A &= (|N|^{2}-|F|^{2})/(|N|^{2}+|F|^{2}) \quad . \end{aligned} \tag{14}$$

Figure 13 shows the predicted$^{3)}$ R and A for $K^{-}p \to \pi^{-}\Sigma^{+}$ in the GORE and SCRAM models. It is clear that there is a great difference in the theoretical curves and that the SCRAM predictions reflect the distinctive structure at $t \approx -0.2$ and -0.6 (GeV/c)^{2} in this model. Model independently, such data will render it rather easy to extract the mysterious Re N which proved so difficult to disentangle from the current data. Again, the perceptive reader will have noted that most of the previous tests did not determine if the magic zeros were in the s- or the t-channel amplitudes. This ambiguity stems from the rotation invariance of ℙol and dσ/dt. R and A are not so invariant and their measurement will be able to determine the preferred frame.$^{28)}$

These experiments on $\pi N \to K(\Sigma,\Lambda)$, $\bar{K}N \to \pi(\Sigma,\Lambda)$ with a polarized target are feasible (because the hyperons analyze their own polarization). The measurements will be important at all energies; at low energies for phase shift analysis, and at high energy, of course, they test your favorite dynamical model. At intermediate energies they will be invaluable for understanding the origin of the line reversal violation between, say, $\bar{K}N \to \pi\Sigma$ and $\pi N \to K\Sigma$ (cf. discussion in Section 2.1B (E2)). Further, it would be useful -- when designing an experiment -- to be able to observe the corresponding Y^{*} reactions (e.g., $\pi N \to KY^{*}$). The latter provide the cleanest way to examine $n = 2$ amplitudes and also determine the conjectured "quark additivity frame". This is discussed again in Section 4.6 and Fig. 45.

2.1C. Conclusions

We have surveyed many relatively model independent analyses of the current data. This has isolated many reactions of particular interest. These included: polarization in $K^{+}n \to K^{o}p$, $K^{+}p \to pK^{+}$, and $\pi^{-}p \to \eta^{o}n$; dσ/dt and polarization in $K^{o}_{L}p \to K^{o}_{S}p$;$^{29)}$ complete set of observables in elastic scattering (isospin made this easier than in the general reaction); R and A in, for example, $\pi N \to K\Sigma$ and $\pi N \to KY^{*}$.

We can now sharpen our conclusions (C1 - C3) of Section 2.1A.

→ (C1) Im N and Im F have the first absorption zero. In the impact parameter (b) plane this corresponds to a large component of scattering around $b \approx 1$ fermi. However, the discussion in Section 2.1B(i) plus Figs. 1 - 7 and 9 show there are still two possibilities.

→ (C1a) Absorption picture breaks down at larger -t. Im N,F have a large central component (Figs. 9(c), 5(c),(d), 6(c),(d), ----- line).

→ (C1b) Im N,F have second absorption zero and very small scattering at small b. (Figs. 7, 9(a).)

There is strong evidence for (C1a) -- especially for Im F -- from the large -t data examined in Section 3. In particular the dip at $t \approx -1.4 \ (\mathrm{GeV/c})^2$ in $\pi^- p \to \eta^0 n$ and $\pi^+ p \to \eta^0 \Delta^{++}$ directly contradicts the absorption picture which predicts a dip at $t \approx -2 \ (\mathrm{GeV/c})^2$ ($J_1(5\sqrt{-t})$ has its second zero there). Further evidence for (C1a) comes from the large -t behavior of π^0 photoproduction. Indirect evidence to the contrary on Im N, i.e. for (C1b), comes from the elastic polarization data which suggests that the assumptions leading to Fig. 7 are valid up to $t \approx -1 \ (\mathrm{GeV/c})^2$.

→ (C2F) Re F agrees amazingly with Regge pole theory. This corresponds (Figs. 1(d) - 4(d)) to large scattering at small impact parameter.[3,6] The unambiguous identification of a large real part at small impact parameters emphasizes the importance of distinguishing (C1a), and (c1b); if (C1b) is true, there is little imaginary part at small b -- physically, such absorption seems unexplicable if it is not present in the real part. In (C1a) we have only one difference between real and imaginary parts; the latter are large for $b \approx 5 \ (\mathrm{GeV/c})^{-1}$ -- no particular difference is claimed for small b.

→ (C2N) There are several pieces of evidence (each rather dubious) that Re $N(\rho,\omega)$ does not vanish for small t.[30] This difference from Im N is inexplicable in cut models (cf. Figs. 1(a), 5(a)) and Regge models (where the Im N zero is obtained from an explicit residue zero).

Experimentally, (C1,2) imply that the major unknowns are Im N,F and Re F at largish -t and Re N at all t values.

Theoretically, the situation is unsatisfactory. The quantitative demise of our much loved theories (T1) - (T3) has led to a splintering of current interpretations into empirical rules which cover only a small fraction of the data. Their extension to the general reaction is ambiguous and so explicit calculations of any given process are very hard. Charles Chiu4) has proposed:

⟶ (I1) Poles have WSNZ. The absorption constant C is different in the various spin amplitudes (e.g., $C_{n=0} \approx 1.3$, $C_{n=1} \approx 0$, $C_{n=2} \approx ?$). This agrees with current data except (C2N) if the lack of zero in Re $N(\rho)$ is confirmed. Harari6) has pointed out the possibility (C1b) and emphasized:

⟶ (I2) The agreement of Re F with GORE is correlated with the coincidence of the $\alpha = 0$ WSNZ with the absorption zero in Im F 31) ($t \approx -0.6\ (\mathrm{GeV}/c)^2$). This is very attractive except that it is now impossible to predict real parts of amplitudes when -- as is usual -- this happy circumstance does not occur. However, it may mean that determination of such unhappy real parts will give important clues as to the underlying dynamics. Unhappy amplitudes include the mysterious Re N and those controlling the τP^- exchange $\rho_{00}\ d\sigma/dt$. So now let us turn to the latter misery.

2.2. Unnatural Parity Exchange: Zero Structure of Amplitudes ($\rho_{00}\ d\sigma/dt$)

In this section we discuss the current experimental situation for the zero systematics for unnatural parity exchange. It will become obvious that both the theoretical and experimental situations are unclear. To isolate unnatural parity exchange, one can look at reactions of the type

$$\pi N \Rightarrow (\pi\pi)_{\text{s-wave}} N: \quad d\sigma/dt \tag{15a}$$

$$\pi N \Rightarrow \rho N \quad : \quad \rho_{00}\ d\sigma/dt \tag{15b}$$

$$\pi N \Rightarrow (\pi\pi)_{\text{s-wave}} \Delta: \quad d\sigma/dt \tag{15c}$$

$$\pi N \Rightarrow \rho\Delta \quad : \quad \rho_{00}\ d\sigma/dt \tag{15d}$$

(and their SU_3 friends) .

The reactions involving Δ's are complicated: $\rho_{00}\ d\sigma/dt$ being a mixture of $n = 0, 1$, and 2 in the s-channel. We do not expect any particular dip structure, unless one of these n values dominates. There is a report of a dip at $t \approx -0.75\ (\mathrm{GeV}/c)^2$ in $\pi^+ p \Rightarrow \rho^0 \Delta^{++}$ at

3.7 GeV/c;$^{32)}$ it would be exciting to see this re-examined with higher statistics and consideration of the double correlations to find the Δ^{++} spin structure. Here, in view of the limited statistics of the current experiment and the complication of the theory, I will ignore Δ production. Again, there is no relevant $(\pi\pi)_{s\text{-wave}}$ data of which I am aware. So I will discuss the reaction $\pi N \rightarrow \rho N$ and its SU_3 analogues. Here π exchange in $\rho_{00}\, d\sigma/dt$ corresponds to pure $n = 1$ and hence is particularly clean theoretically. Again, it is exactly analogous to the πN CEX family discussed in Section 2.1 which were also dominantly $n = 1$. We can calculate ρ_{00} in any frame and so test the t-dependence of the amplitudes in different frames. For completeness we remember that:

> s-channel amplitudes correspond to helicity frame density matrix elements -- y axis along the normal ($\underline{1} \times \underline{3}$) to the scattering plane and z axis along the $-\underline{4}$ direction in 3's rest frame. t-channel amplitudes correspond to the Gottfried-Jackson frame which is as above but with z axis in the $\underline{1}$ direction. (16)

First consider $\rho_{00}\, d\sigma/dt$ in the s-channel for the four reactions:

Reaction	Exchange	
$1/2\ (\pi^- p \rightarrow \rho^0 n)$ or $\pi^\pm p \rightarrow \rho^\pm p$	$\lvert\pi\rvert^2$	(17a)
$1/2\ (\pi^+ n \rightarrow \omega^0 p)$	$\lvert B\rvert^2$	(17b)
$K^- p \rightarrow \bar{K}^{0*} n$	$\lvert\pi + B\rvert^2$	(17c)
$K^+ n \rightarrow K^{0*} p$	$\lvert\pi - B\rvert^2$	(17d)

where we have normalized so that SU_3 gives

$$2\left[(17a) + (17b)\right] = (17c) + (17d)$$

or

$$(17c) = (17d) = (17a) + (17b) \qquad (18)$$

if there is no line reversal differences between (17c) and (17d). Now consider four theories:

(i) Pure absorption (T3):$^{7)}$ There is a dip in all four reactions at $t \approx -0.6\ (\text{GeV}/c)^2$.

(ii) Regge theory (T1) in SU_6 Limit: The π one unit in below the ρ and will have a WSNZ at $t \approx -0.6$ $(GeV/c)^2$ where $\alpha_\pi = -1$. $\rho_{00}\, d\sigma/dt$ for (17a) will vanish there. The B is one unit below the A_2 and will be non-vanishing at $t \approx -0.6$ $(GeV/c)^2$. (17b) should look like $\pi^- p \rightarrow \eta^o n$ and be very smooth near $t \approx -0.6$ $(GeV/c)^2$.

(iii) Regge theory (T1): realistic trajectories: As (ii) except (17a) should vanish $t \approx -1.1$ $(GeV/c)^2$ $\left[\alpha_\pi = -1 \approx 0.9\ (t - m_\pi^{\ 2})\right]$. At $t \approx -0.6$ $(GeV/c)^2$, $(17a)/(17b) = \cot^2 \pi\alpha_\pi/2$ from EXD. This is then the model of Chiu[4)] with no cut corrections in spinflip amplitudes. (Section 2.1C (I1).)

(iv) Hybrid model of Harari (Ref. 6 and Section 2.1C (I2)): Absorption zeros at $-0.6 (GeV/c)^2$ in imaginary parts. The real parts are unhappy and hence unknown because the absorption dip (-0.6) no longer coincides with the WSNZ ($\alpha_\pi = -1$). Note that in the SU_6 limit (ii) the amplitudes are happy and the real parts of GORE are expected to be reliable. In the realistic limit perhaps -- mirabile dictu and Sic Transit analyticity -- the real parts are still given by EXD Regge pole theory. Then $(17a)/(17b) = \cot^4 \pi\alpha_\pi/2$ at $t \approx -0.6$ $(GeV/c)^2$.

The expectation for the relative values of $\rho_{00}\, d\sigma/dt$ near $t \approx -0.6$ $(GeV/c)^2$ is summarized in the table below: here the results for (17c,d) are found from (18).

TABLE 2

	$1/2(\pi^+ n \rightarrow \omega^o p)$	$1/2(\pi^- p \rightarrow \rho^o n)$	$K^- p \rightarrow \bar{K}^{*o} n = K^+ n \rightarrow K^{*o} p$
Pure absorption	0	0	0
SU_6	1	0	1
Regge	1	1	2
Regge real: Zero Im	1	1	2

The experimental data for ρ_{00} in the helicity frame is shown in Figs. 14 through 17. I have multiplied the data by e^{-4t} $(p_{lab}/5)^2$ to clarify the presentation. The statistics for the higher energy data for $\pi^+ n \rightarrow \omega^o p$ shown in Fig. 14 could be usefully improved. However, it seems reasonable to deduce that $\pi^+ n \rightarrow \omega^o p$ does not dip near $t \approx -0.6$ $(GeV/c)^2$

and is quite smooth near there. This then agrees with theories (ii) to (iv) and rules out the pure absorption model -- theory (i). (This will be our last definite conclusion!) For reference on this and the following ρ and ω figures, we mark the magic line 0.15 which gives a reasonable representation for $1/2\ e^{-4t}\ (p_{lab}/5)^2\ \rho_{00}\ d\sigma/dt$ in $\pi^+ n \rightarrow \omega^0 p$ at the higher energies. In the K^* figures -- motivated by the last two theories -- we mark double this.

$\overset{(-)}{K}N \rightarrow \overset{(-)}{K}{}^{*}N$ is shown on the next figure (No. 15). It is very striking that the forward peak due to π exchange is followed by a sharp break which has a similar magnitude and t-dependence to sad old $\pi N \rightarrow \omega N$ -- which has struggled along with this staid t-dependence right from the forward direction. The $\overset{(-)}{K}{}^{*}$ data seems again to prefer no dip around -0.6 but it is a brave man who comments on the normalization (given the standard background and resonance definition ambiguities). If anything, theories (iii) and (iv) with $\overset{(-)}{K}{}^{*} = 2(\omega)$ are favored but decisive tests await new data. The behavior after the break in $\pi N \rightarrow \rho N$, shown in Figs. 16 and 17, is again strikingly similar to the ω data. However, the data is inconclusive as to the presence or absence of a dip near $t \approx -0.6\ (\mathrm{GeV}/c)^2$. Thus it is clearly not present below 3 GeV/c (where background problems are severe), but the beautiful data at 6.95 GeV/c just runs out of statistics at the vital point.

In the above we have considered -- influenced by the absorption picture -- ρ_{00} in the s-channel frame. It is also interesting to look in the t-channel and Figs. 18 through 21 give the analogous curves to those just discussed. Similar comments are in order, although in the ρ and K^* cases, the s-channel $\rho_{00}\ d\sigma/dt$ is significantly sharper than its t-channel analogue.

To summarize, we have shown that the present data (a) have ruled out the pure absorption model$^{7)}$ -- just as the natural parity exchange data did in Section 2.1; (b) is consistent with the theories (ii) to (iv) above, but theories (iii) and (iv) with no dip in $\pi^- p \rightarrow \rho^0 n$ are favored by low energy data; (c) shows no striking differences in the dip structure in the s- and t-channels.

It clearly does not require a great increase in statistics to sharpen these conclusions. These reactions provide very clean tests of theories for the dip structure in a situation (i.e., unhappy amplitudes) which is very different from the well-established natural parity case. The measurements are thus very important.

Finally, we should mention that we have tacitly assumed there is no A_1 (which inhabits $n = 0$ amplitudes) exchange. This can be checked at once by a polarized target experiment. Any non-zero polarization at high energies indicates the presence of the A_1.

2.3. Backward Scattering

(i) There is essentially no understanding of the amplitude structure for backward scattering. As will become apparent, even the relative signs of the amplitudes at $u = 0$ are unknown; it follows that the most important experiments are R and A measurements in backward $\bar{K}N \to \Lambda\pi$ and $\bar{K}N \to \Sigma\pi$. These will provide the vital quantitative clues (i.e., $|N|^2$, $|F|^2$, and sign (N/F)[33]) necessary for understanding all other backward reactions.

(ii) Dips in $K^-n \to \Lambda\pi^-$, $\pi^+p \to p\pi^+$, and $\pi^-p \to n\pi^0$ at $u \approx -0.15$ $(\mathrm{GeV}/c)^2$, [34,35] suggest a single zero in Im N (N_α exchange there). This is in agreement with both Regge pole theory (WSNZ, $\alpha_{N_\alpha} = -1/2$) and the absorption picture (standard $n = 0$ dip). Correspondingly, in the language of Section 2.1C, the Re N amplitude is happy, (i.e., Regge theory is right), but Re F is unhappy. Thus, amusingly enough, the situation is completely reversed from the forward direction! Hence the models of Chiu (I1) and Harari (I2 of Section 2.1C) give opposite predictions for the amplitudes in which cuts are large. We need more Pol (R and A) data before tests can be made.

(iii) As in Section 2.1, we can relate backward polarizations to the sign of the real parts at $u = -0.2$ and -0.6 $(\mathrm{GeV}/c)^2$. This is summarized in the table below -- where the polarizations correspond to the usual forward convention (i.e., in $M_1B_1 \to B_2M_2$ the normal is $M_1 \times M_2$).

TABLE 1B

Reaction	$u(\mathrm{GeV}/c)^2$	Sign		Ref.
		Theory	Experiment	
$\pi^+ p \rightarrow p\pi^+$	-0.2	$\hat{N}$	≈ 0	36
	-0.6	$\hat{F}$	< 0	
$\pi^- p \rightarrow p\pi^-$	-0.2	$\hat{N}$	(?)	
	-0.6	$\hat{F}$	(?)	
$K^- n \rightarrow \Lambda\pi^-$	-0.2	$\hat{N}$	< 0	35
	-0.6	$\hat{F}$	< 0	

In forward scattering, the polarizations -- especially at -0.6 -- agreed well with the Regge predictions $\hat{N}, \hat{F} > 0$. The table indicates this is not true for backward scattering. However, it must be emphasized that in preparing the table, I assumed the sign of N/F at $u = 0$. This came -- as is true in all backward fits -- from finding this sign at the particle pole position ($u = m_N^2, m_\Delta^2$) and assuming it did not change in extrapolating to $u = 0$. There is no other check of this assumption and it seems quite likely that it is wrong. Thus the same assumption plus EXD leads to the wrong relative sign for nonflip $I_u = 1/2$ and $I_u = 3/2$ amplitudes at $u = 0$. (Experimentally determined from the ratio $\pi^+ p \rightarrow p\pi^+ / \pi^- p \rightarrow n\pi^0$ — see Ref. 34.) Other checks of the assumption could come from (a) FESR's,[38)] (b) signs of low energy amplitudes from phase shift analyses. It would be nice to improve both (a) and (b) -- as may now be possible in view of the new low energy backward scattering data. At high energy the assumption can only be checked through the R and A measurements we mentioned earlier.

(iv) Finally, we mention that there are a large number of essentially single exchange backward scattering processes. Measurement of Δ_δ exchange, $\pi^- p \rightarrow p\pi^-$, $\gamma p \rightarrow \Delta^{++}\pi^-$, and $K^- p \rightarrow \Sigma^+\pi^-$; or $N_\alpha - N_\gamma$ exchange, $\bar{K}n \rightarrow \Lambda\pi^-$, $\pi^+ d \rightarrow pp$, and $\gamma d \rightarrow np$ will be valuable.[34,39)] In this respect, backward scattering is simpler than forward scattering but the low cross sections have prevented exploitation of this good fortune.

2.4. π Exchange

The experimental systematics are easily stated if we divide reactions into three classes distinguished by the t-dependence of the usual Feynman diagram Born terms.

(I) Crippled π: Born Term $= g_I t/(t - m_\pi^2)$ (19/I)

Examples are $p\bar{p} \to n\bar{n}$, $np \to pn$, $\gamma p \to \pi^+ n$, $\gamma n \to p\pi^-$, $2\rho_{11}^H\, d\sigma/dt$ ($\pi^- p \to \rho^0 n$, $K^- p \to \bar{K}^{*0} n$, $\pi^- p \to f^0 n$, etc.).

(II) Half Asleep π: Born Term $= g_{II} \sqrt{-t}/(t - m_\pi^2)$ (19/II)

Examples are $\rho_{00}^H\, d\sigma/dt$ ($\pi^- p \to \rho^0 n$, etc.), $pp \to n\Delta^{++}$, $\gamma p \to \pi^- \Delta^{++}$, $\gamma p \to \omega p$.

(III) Fully Fledged π: Born Term $= g_{III}/(t - m_\pi^2)$ (19/III)

Examples are $p\bar{p} \to \Delta\bar{\Delta}$, $\pi^+ p \to \rho^0 \Delta^{++}$, $\pi^+ p \to f^0 \Delta^{++}$, etc.

Now divide any amplitude into three pieces:

$$A(t) = A_\pi^{LOW}(t) + A_\pi^{HIGH}(t) + A_{other}(t) \quad . \tag{20}$$

A_π^{LOW}, A_π^{HIGH} are the contributions to π exchange coming from low $b \leq b_0$ and high $b \geq b_0$ partial waves. Here b_0 may be conveniently chosen as:

$$b_0 = \frac{1}{m_\pi} \approx 7\ (\mathrm{GeV}/c)^{-1} \quad . \tag{21}$$

$A_{other}(t)$ is the contribution of everything else except π exchange. A_{other} is dominated by waves for $b < b_0$ whereas A_π^{HIGH} is 60% for (19/III) and 80% for (19/II) of the total Born term at $t = 0$.

⟶ (π1) All theories agree that $A_\pi^{HIGH}(t)$ exists, and is essentially unaffected by absorption and other dynamical myths -- it is given uniquely by the residue of the nearly π pole. The total amplitude $A(t)$ is determined by the relative sizes of the sacrosanct piece $A_\pi^{HIGH}(t)$, $A_\pi^{LOW}(t)$, and $A_{other}(t)$.

⟶ (π2) $A_\pi^{HIGH}(t)$ is enormous for the fully fledged π -- at least in the examples quoted below (19/III). This is graphically illustrated in Fig. 22 which compares $\pi^+ p \to \rho^0 \Delta^{++}$ and $\pi^+ p \to \omega^0 \Delta^{++}$. The latter is essentially an upper bound on $A_{other}(t)$ for ρ^0 production. Thus, from

EXD, the A_2 exchange in $\rho^o\Delta^{++}$ = the ρ exchange in $\omega^o\Delta^{++}$ at $t = 0$ and the latter will be less than the total $d\sigma/dt$ for $\omega^o\Delta^{++}$ which has as well substantial B exchange.

→ (π3) $A_\pi^{HIGH}(t)$ also dominates over $A_{other}(t)$ for $-t \approx m_\pi^2$ in the half asleep class (II). However this time, comparison of $\pi^- p \to \rho^o n$ and $\pi^+ n \to \omega^o p$ shown in Figs. 14, 16, 18, 20 indicates that whereas $|A_\pi^{HIGH}(t \approx 0)|^2/|A_{other}(t \approx 0)|^2 \approx 200$ for class III (Fig. 22), the ratio is only around 10 for class II at $t \approx -m_\pi^2$. An immediate corollary is: class III reactions are much better for studying π-π scattering than class II.[40)]

Figures 23 and 24 show the amplitudes and their Fourier-Bessel transforms -- defined and normalized as in Eq. (1a) and (3) -- for $K^- p \to \bar{K}^{*o} n$ at 5 GeV/c.[41)] Only two of the amplitudes are presented. The nonflip amplitude $N \propto H_{0,-1/2 \to 1,1/2}$ is shown in Figs. 23(a),(b),(d) and 24, with the spinflip amplitude $F \propto H_{0,-1/2 \to 0,1/2}$ in Figs. 23(c) and (e). F is half asleep π; the latter two figures indicate that (a) $f_F(b)$ for unabsorbed π is not especially large at small b and (b) modification with strong cuts, which mutilates F_π^{LOW} -- leaving F_π^{HIGH} unchanged, changes F very little at small t. The same is true for fully fledged π (not shown) and it follows that the small t behavior of classes (II) and (III) is unambiguous and all theories will give similar predictions. At larger $-t \gg m_\pi^2$ the behavior is sensitive to the details of A_π^{LOW}, e.g., the relative size of $f_F(b)$ for $b = 0$ and $b = 5\ (\text{GeV/c})^{-1}$. It is controlled by the same dynamics as the better studied natural parity exchange discussed in Section 2.1. These were discussed for the half asleep case in Section 2.2.

It follows that the only special features of the π exchange occur in the crippled class (I) and we now turn to this. Clearly $A_\pi^{HIGH}(t)$ has an identical t-dependence for classes (I) and (III). They only differ in their overall normalization which is determined by the relative size of g_I and g_{III} in (19/I) and (19/III), i.e., by the size of the π pole coupling constants. In the quoted examples, the amplitude $A_\pi^{HIGH}(t)$ is a full order of magnitude smaller for class (I) compared with class (III). It follows that class (I) cross sections near $t = 0$ are much more sensitive to the details of the low partial waves: $A_\pi^{LOW}(t)$ and $A_{other}(t)$. Write for $-t$ of $O(m_\pi^2)$,

$$N = \frac{g_I\, t}{(t - m_\pi^2)} + C_1 \quad . \tag{22}$$

Then in the Born term: $C_1 = 0$ and the cross section vanishes at $t = 0$ in complete disagreement with experiment. In the Poor Man's Absorption Model (PMA) we put $C_1 = -g_I + C_2$ giving

$$N = \frac{g_I\, m_\pi^2}{(t - m_\pi^2)} + C_2 \tag{22a}$$

and assume C_2 small. In the t-plane this corresponds to the (reasonable) assumption of a smooth extrapolation of the π pole from $t = m_\pi^2$ to $t \approx 0$. In the b plane, Fig. 23(d), it corresponds to the nondescript behavior

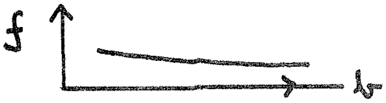

not the change of sign

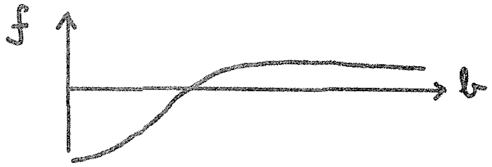

of the Born term. The PMA model gives absolute predictions for all crippled π cross sections at $t = 0$.

In units of $mb/(GeV/c)^2$, some examples are:

$$\begin{aligned} &\gamma p \to n\pi^+,\ \gamma n \to p\pi^-: && d\sigma/dt = 3.01 \times 10^{-3}\,(p_{lab}/5)^{-2} \\ &np \to pn,\ \bar{p}p \to \bar{n}n: && d\sigma/dt = 5.8\,(p_{lab}/5)^{-2} \\ &\pi^- p \to \rho^o n: && 2\rho_{11}^H\, d\sigma/dt = 1.48\,(p_{lab}/5)^{-2} \quad . \end{aligned} \tag{23}$$

This is compared with experiment in Fig. 25 in which various crippled π cross sections are plotted in a normalization such that PMA would predict 1 at $t = 0$. This simple model is in amazing agreement with experiment.

The absorption model[2,7] gives similar predictions for C_1 but:

(i) One needs a strong cut (SCRAM) corresponding to $C \approx 1.3$ in Eq. (6). This leads in Fig. 23(d) to the implausible snake-like

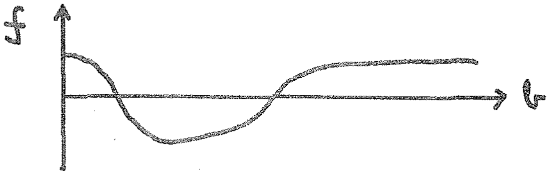

for the partial wave amplitude $f(b)$.

(ii) Philosophically the PMA prediction at $t = 0$ seems prettier as it depends only on a simple extrapolation in t through m_π^2. The SCRAM value at $t = 0$ is a complicated combination of two parameters: the strength C of the absorption and the t-dependence of the input π (Regge) pole.

(iii) This is reinforced by the observation that —— and ---- in Fig. 23(d) indicate that the values of the low partial waves of π exchange are not anomalously large (at 5 GeV/c). (Compare Figs. 1 - 6, 9, 23, and 24.) Real parts of amplitudes were not absorbed for natural parity exchange. (Section 2.1 for the spin flip amplitude at least.) Hence the explanation of crippled π exchange in terms of the absorption model lacks conviction. Why should we use it for the π when it fails for the ρ and A_2?

Interpreting the PMA model in the j plane leads to a complicated structure. Considering just nonflip and single flip vertices, the PMA model may be decomposed into precisely three "trajectories". These consist of two $\tau P-$ exchanges -- one $M = 0$ and one $M = 1$, plus one $\tau P + M = 1$ trajectory. (M is the Toller quantum number.[42]) Section 4.6(ii) discusses this further.

We finish with some disconnected remarks on PMA and its relation to other models of π exchange.

(a) PMA is consistent with VDM. Indeed, the success of the Cho-Sakurai[43] model may be interpreted not as a success for VDM but rather as a success of PMA. In the more general Jackson-Quigg pseudomodel,[44] PMA follows from the dominance of the π FESR by the nucleon Born term.

(b) PMA is consistent with the coherent droplet model[45] -- it corresponds to a particular form near $t = 0$ of the droplet.

(c) In $\pi^- p \rightarrow \rho^0 n$, PMA specifies the amplitude structure near $t = 0$ and hence all the density matrix elements of the ρ. The excellent agreement of this with experiment is in fact documented in Leith's talk at this conference (pages 585 to 593). Indeed, the absorption model of Williams,[46] used by Leith, is precisely the PMA model specialized to $\pi^- p \rightarrow \rho^0 n$. PMA also predicts the small t density matrix elements for all $\pi\pi$ masses. For instance, for $\pi^- p \rightarrow (\pi\pi)n$,

$$2\rho_{11}^H/\rho_{00}^H \approx 2(m_\pi^2/-t)\ (m_\pi/m_{\pi\pi})^2\ \epsilon_L \qquad (24)$$

where $\epsilon_L = 0, 1,$ and 3 for S, P, and D $\pi\pi$ waves respectively.[47] Note that the "absorption" corrections decrease with increasing mass $(1/m_{\pi\pi}^2)$ but increase with increasing angular momentum L. These predictions are, I believe, unchecked at present. The PMA model should be invaluable for extracting $K\pi$, $\pi\pi$ phase shifts from such data.[48]

(d) In $\gamma p \to \pi^- \Delta^{++}$, PMA coincides with the gauge invariant Born term (just as it did for $\gamma p \to \pi^+ n$). Analogously to Eq. (24) we write[49]

$$(\gamma p \to \pi^-\Delta^{++}) \text{ crippled } \pi \text{ part}/(\gamma p \to \pi^-\Delta^{++}) \text{ half asleep part}$$
$$\approx 2\left[m_\pi^2/-t\right]\left[m_\Delta m_\pi/(m_\Delta^2 - m_N^2)\right]^2 \qquad (25)$$

which predicts the (non-zero) cross section at $t = 0$ in agreement with experiment. (Ref. 10, Fig. 30.)

(e) The behavior of the curves in Fig. 25 away from $t = 0$ are of some dynamical interest. (i) $np \to pn$ has a sharper t-dependence than $\bar{p}p \to \bar{n}n$, $\gamma n \to p\pi^-$ is sharper than $\gamma p \to n\pi^+$. This is "explained" by the interference of ρ exchange, which (approximately) vanishes at $t = 0$ (cf. Fig. 24(a)), with the PMA π exchange. The data imply a relative sign of π and ρ exchange in agreement with the quark model -- Section 4.6(ii). (ii) The very sharp $\pi^- p \to \rho^0 n$ forward peak is incomprehensible. I would have expected it to lie somewhere between $np \to pn$ and $\bar{p}p \to \bar{n}n$. The current data (Leith, this conference, pages 555 to 573) has quite large errors -- it is important to confirm this surprising feature. (iii) Photoproduction after the natural PMA normalization at $t = 0$ is notably bigger at large $-t$ than the strong interaction data shown. (Compare $\gamma p \to n\pi^+$ with $\bar{p}p \to \bar{n}n$; $\gamma n \to p\pi^-$ with $np \to pn$.) This may reflect some basic dynamical difference between photoproduction and strong interactions (e.g., fixed poles in the former) -- see Section 3.

(f) The argument in (e) (i) is the only unambiguous separation of ρ (A_2) exchange from the natural parity component of π exchange generated by PMA. In principle they can be separated by their energy dependence $(\alpha_\rho(0) - \alpha_\pi(0) \approx 0.5)$ but present data are over too small an energy range for this to work. Indirect arguments (e.g., use SU_3/EXD on ω exchange in $\gamma p \to \pi^0 p$, $\pi^\pm p \to \rho^\pm p$) and explicit fits suggest ρ, A_2 exchange will be sizeable for $-t \approx 0.5$ $(\text{GeV}/c)^2$. This is only accurate to a factor of two;

correspondingly it is not obvious whether the much debated (lack of) dip at $t \approx -0.6\ (\mathrm{GeV}/c)^2$ in $\pi^+p \to \omega^0\Delta^{++}$, $\pi^-p \to \omega n$, and $\gamma p \to \eta n$ [4-7] is due to PMA $\pi(B)$ corrections or lack of WSNZ in ρ exchange.

In conclusion, the simple PMA model gives an excellent description of π exchange for small $-t$. It is important to check it in other reactions, e.g., angular decay of $\pi^-p \to f^0n$ and $np \to pn$ at NAL energies. In the latter case, ρ and A_2 contributions to $A_{\text{other}}(t \approx 0)$ may swallow up dull old PMA.

2.5. Symmetry and Exchange Degeneracy for Regge Residues

(i) Coupling Structure for $B\bar{B} \to (V,T)$ (e.g., $N\bar{N} \to \rho$, $N\bar{\Sigma} \to K^*$)

Current knowledge on SU_3 and the F/D values for the $B\bar{B} \to (V,T)$ couplings has been well summarized by Michael[50] and Michael and Odorico.[51] Highlights include decoupling of the ω and P' from the $N\bar{N}$ s-channel helicity flip amplitude and the prediction of equal and opposite polarizations in Λ and Σ production.[3,52] (Cf. Table 1A for $\pi^-p \to K^0\Lambda$ and $\pi^+p \to K^+\Sigma^+$.) Experimentally, the analysis is only clean in the forward direction, where there is but one spin amplitude and total cross section and $d\sigma/dt$ data. The new SLAC $K_L^0p \to K_S^0p$ data gives $F/D|_{\rho,\omega\ \text{non-flip}} = -6.8^{+1.3}_{-2.0}$, in agreement with the σ_{tot} determination.[53] At non-zero t, the presence of both flip and non-flip amplitudes with different F/D values renders the analysis complicated. In particular, we have yet to determine if the F/D values are constant with t and, if so, what channel this holds in (e.g., constant F/D values for t-channel amplitudes imply t-variation in the s-channel F/D's). Experimentally the best determination of F/D will come from the R and A measurements in $\pi p \to K(\Sigma,\Lambda)$ and $\bar{K}p \to \pi(\Sigma,\Lambda)$. Current $d\sigma/dt$ measurements give ambiguous and model dependent values for F/D. However, R and A will give at once $|N|^2$ and $|F|^2$, and an immediate value for F/D by comparing Λ and Σ production.

Theoretically, we note that the quark model predicts $F/D|_{\text{nonflip}} = \infty$ and $F/D|_{\text{flip}} = 2/3$ which is in reasonable accord with the data -- assuming the quark model is predicting t-channel amplitudes. Actually there is no other test that the quark relations should be applied to in the t-channel and indeed in Section 4 we find theories with a different "quark additivity frame" which varies with both s and t. Current data is not good enough to test this although it can rule out dramatic changes in frame -- for instance, the quark relations are certainly not true in the s-channel.

(ii) Exchange Degeneracy (EXD)

The predictions of SU_3 and EXD are summarized by duality diagrams (DUDES).$^{54)}$ Over and above the usual constraints from exotic channels, DUDES embody the so-called strong EXD condition $F/D|_V = F/D|_T$. Although there are well-known difficulties with EXD/DUDES$^{55)}$ (e.g., line reversal breaking in $d\sigma/dt$, non-zero polarization in $np \Rightarrow pn$,$^{56)}$ and $K^-n \Rightarrow \pi^-\Lambda$), there is no evidence for violent disagreement with these rules.$^{20)}$ In particular, the signs at $t = 0$ of all couplings seem to be right. Recent successes for EXD include small polarization in backward $K^+p \Rightarrow pK^+$ $^{57)}$ and equality of $d\sigma/dt$ for $K^-p \Rightarrow \bar{K}^0n$ and $K^+n \Rightarrow K^0p$ at 12 GeV/c.$^{58)}$ EXD is not only successful in $PB \Rightarrow PB$ collisions but also in both vector meson production $PB \Rightarrow VB$ and photoproduction. In the latter, of course, Regge pole theory is a disaster but the signs and rough magnitudes of the amplitudes at $t \approx 0$ can be determined from FESR's$^{44,59a)}$ and high energy data. These values are approximately consistent with EXD/DUDES -- just as are the vector dominance related reactions $PB \Rightarrow VB$. The most striking test of EXD signs in the latter case comes from ρ-ω interference which verifies the EXD sign between the much-maligned π and B trajectories.$^{59b)}$

We conclude that EXD and duality diagrams (and hence factorization except for the well-defined PMA violations) are in qualitative agreement with experiment wherever they have been well studied.

2.6. Diffraction Scattering

Although the amplitude structure of diffraction scattering is a rich field of study, I will only treat it very briefly. The quantum selection rules$^{60)}$ for the spin, parity, and SU_6 structure of diffractively produced states have been summarized by Zachariasen.$^{61)}$ Further, one can report that:

(i) Factorization has not been stringently tested but is consistent$^{62)}$ with current data on $pp \Rightarrow pN^*$ and $\pi p \Rightarrow \pi N^*$. Single particle distributions give similar qualitative agreement with factorization.$^{63)}$ The recently proposed tests$^{64)}$ for the M value of the Pomeron in two particle distributions may be more stringent.

(ii) Helicity conservation[65)] has been observed in the s-channel for meson-baryon scattering ($\pi N \to \pi N$, $\overset{(-)}{K}N \to \overset{(-)}{K}N$) and ρ photoproduction[66)] but in the t-channel for the diffractive production of "kinematic enhancements" ($\pi N \to A_1 N$, $\overset{(-)}{K}N \to \overset{(-)}{Q}N$).[67)] Further progress awaits either a theoretical consensus (there are plenty of models which I will not even begin to list) or an experimental investigation of the systematics. What happens in $\gamma N \to \gamma N$ (polarized γ), $NN \to NN$ (R and A type measurements), $NN \to NN^*_{1400}$ and in the production of nucleon recurrences (N^*_{1520}, N^*_{1688})?

(iii) Detailed investigation of the t-dependence and Re/Im ratio for diffraction scattering is possible in πN elastic scattering.[17)] Information comes from finite energy sum rules and high energy data. There is really no evidence for any real part or any s-channel helicity flip component for diffraction scattering.[68)] This is particularly surprising at $p_{lab} = 5$ GeV/c where one would expect sizeable real parts from P' exchange at $t \sim -0.6 \to -1\ (\mathrm{GeV}/c)^2$ whereas experimentally it is the total $P + P'$ $I = 0$ exchange that has small Re/Im. Similar conspiracy between the P and P' is exhibited by the fact that both conserve s-channel helicity.

3. LARGE MOMENTUM TRANSFER ($-t \gtrsim 1$ (GeV/c)^2)

3.1. Experimental t-Distributions

Here I would like to summarize an empirical investigation of large $-t$ exchange data[9,69)] carried out in collaboration with Charles Chiu. In the forward direction there is a great variety of sizes and shapes for $d\sigma/dt$, e.g., π exchange peaks, spinflip $t = 0$ dips, absorption -0.2, -0.6 dips, etc. The different t dependencies for $-t \lesssim 1$ in photoproduction[10)] are schematically represented in Fig. 27. Strong interactions are similar: one particularly dramatic contrast is shown in Fig. 22. However, around t of -1 (GeV/c)^2 many of these differences have died away and cross sections have settled down to a monotonous equality. This is illustrated in Fig. 26 which compiles (all) $d\sigma/dt$ at $t = -1$ (GeV/c)^2 and $p_{lab} = 5$ GeV/c.[70,71)] We can draw the following conclusions:

→ (L1) The size of the $d\sigma/dt$ at $t \approx -1$ (GeV/c)^2 is still correlated with t-channel quantum numbers. It shows the natural ordering: Pomeron > meson S=0 > meson S=1 > baryon S=0 > baryon S=1 exchange. In more detail, we find $\tau P+ > \tau P-$ meson exchange, proton induced > similar meson induced reactions.[72)] In Fig. 26, the photoproduction data has been scaled by the natural[39,41)] coefficient 550, (for $\gamma_\rho^2/4\pi = 0.5$) so that VDM predicts, for instance, (scaled) $\gamma p \to \pi^+ n = 2\rho^H_{11}\, d\sigma/dt\ (\pi^- p \to \rho^0 n)$. It is noteworthy that -- in disagreement with exact VDM -- photoproduction is larger than strong interaction data. This was also indicated in Fig. 25.

After considering the size (L1), we turn to t-dependence or slope (L2) for $-t \gtrsim 1$ (GeV/c)^2 and to the s-dependence (L3) of both size and t slope. Both these appear to be well established and universal in photoproduction.

→ (L2, L3-PHOTO) Photoproduction scales with energy like p_{lab}^{-2} and has the (energy-independent) t-dependence e^{3t}. This has been established for large $-t \gtrsim 1.5$(GeV/c)^2 in $\gamma p \to \pi^+ n$, $\gamma p \to \pi^- \Delta^{++}$, and $\gamma p \to \pi^0 p$, and Fig. 27 hints at this behavior for other photoproduction processes. It would be interesting to extend the measurements of $\gamma n \to \pi^- p$, $\gamma p \to K^+(\Sigma^0, \Lambda)$, and $\gamma p \to \eta^0 p$ to larger $-t$ to check that e^{3t} is truly universal. The evidence for the energy dependence is summarized in, for instance, Refs. 2 and 10, the slopes are listed in Table 3A at the end of this section and show that indeed $d\sigma/dt$ is $\propto e^{3t}$ for $p_{lab} \gtrsim 5$ GeV/c. We thus deduce the scaling law

$$\boxed{p_{lab} \gtrsim 5\ \text{GeV/c: Forward}\ \ d\sigma/dt \ = \ \epsilon\, e^{3(t+1)}\, (p_{lab}/5)^{-2}} \tag{26}$$

where, from Fig. 26:

Forward Photoproduction:

$$S = 0 \ \ \text{exchange:} \ \ \epsilon \approx 1/5\ \mu b/(\text{GeV/c})^2 \tag{27a}$$

$$S = 1 \ \ \text{exchange:} \ \ \epsilon \approx 1/20\ \mu b/(\text{GeV/c})^2 \tag{27b}$$

(26) suggests that scattering amplitudes may be written as the sum of two components.

$$A(s,t) \ = \ A_R(s,t) + A_{FP}(s,t) \qquad . \tag{28}$$

A_R controls small t photoproduction and clearly exhibits both the s and t dependence of the Regge pole exchange expected in the various reactions. Thus in Fig. 27, all the small -t behaviors are precisely what you expect from the dominant exchange. Explicitly:

$\gamma p \rightarrow \pi^- \Delta^{++}$: forward peak due to $\sqrt{-t}/(t - m_\pi^2)$ π-pole (half asleep π), cf. Eq. (25).

$\gamma n \rightarrow \pi^- n$, $\gamma p \rightarrow \pi^+ n$: forward peak due to $1/(t - m_\pi^2)$ π-pole (crippled π). π^-/π^+ ratio < 1 due to ρ exchange (vanishing at $t = 0$).

$\gamma p \rightarrow \pi^o p$: dip at $t = 0$ and -0.5 (GeV/c)^2 due to spin flip ω exchange (related by SU_3 to ρ exchange above).

$\gamma p \rightarrow K^+(\Sigma^o, \Lambda^o)$: forward dip due to single and double flip $K^* - K^{**}$ exchange. K exchange small as $1/(m_K^2 - t) \ll 1/(m_\pi^2 - t)$ for $t \sim 0$. Some difference in Λ and Σ^o near $t = 0$ (e.g., $0 \approx \alpha_{eff}(0)|_\Lambda < \alpha_{eff}(0)|_\Sigma \approx 0.3$) may be due to larger K exchange in the former. ($g^2_{\bar{N}K\Lambda} \gg g^2_{\bar{N}K\Sigma}$.)

The relevance of Regge poles ($A_R(s,t)$ in Eq. (28)) dies away at larger -t and both the s and t dependence of Eq. (26) are inexplicable in simple models. Thus Eq. (28) postulates a new component of scattering ($A_{FP}(s,t)$) which dominates large -t scattering leading to the universal form (26). In the j-plane A_{FP} corresponds to a Fixed Pole at $j = 0$.

Now VDM suggests that the universal form (26), and hence the decomposition (28), should hold for strong interaction vector meson production. Indeed, it may be valid for all forward hadronic reactions if, as expected, a common dynamics mediates all strong processes.

$\longrightarrow$ (L1) The experimental data on sizes at $t \approx -1\ (\mathrm{GeV}/c)^2$ has already been illustrated in Fig. 26; this allows one to read off the expected value of ϵ in the conjectured scaling law (26).

$\longrightarrow$ (L2) The evidence for t slopes is summarized in Tables 3B and 3C at the end of this section. There is very little data above 5 GeV/c. In detail:

$\longrightarrow$ (L2A) The tables and Fig. 28, for $\gamma p \to \pi^0 p$ and $\pi^- p \to \pi^0 n$, indicate that there is a rapid change in large -t slope from 2 to 5 GeV/c in both photoproduction and strong interactions.

$\longrightarrow$ (L2B) Around 5 GeV/c much hadronic data exhibits the e^{3t} behavior of photoproduction; there is no evidence for or against the hypothesis -- Eq. (26) -- that the t slope remains fixed in strong interactions above 5 GeV/c. This is an obvious area for experimental investigation. Projected cross sections may be estimated from Eq. (26) and Fig. 26. Arbitrary samples of the present data are shown in Figs. 29 through 31. ($\pi^+ p \to K^+ \Sigma^+$, $\pi^- p \to \omega^0 n$, $\gamma p \to \pi^- \Delta^{++}$, $K^- p \to \bar{K}^{*0} n$, $\pi^- p \to \rho^0 n$, $pp \to n\Delta^{++}$, $K^- p \to \bar{K}^0 n$, $\pi^+ p \to \eta^0 \Delta^{++}$, $\pi^- p \to \eta n$.) We can draw the following conclusions:

$\longrightarrow$ (I4) The ratio A_{FP}/A_R in the wondrous Regge octet ($\pi N \to \pi(N,\Delta)$, $\overset{(-)}{K}N \to \overset{(-)}{K}(N,\Delta)$ CEX, $\pi N \to \eta(N,\Delta)$) is smaller than in photoproduction. Evidence comes from several sources.

(i) $\pi^- p \to \pi^0 n$ and $\gamma p \to \pi^0 p$ are superficially similar with dips at $t = 0$ and $-0.5\ (\mathrm{GeV}/c)^2$ and $d\sigma/dt \propto e^{3t}$ above $-t = 1\ (\mathrm{GeV}/c)^2$. However, (Fig. 28), the coefficient of the e^{3t} term (relative, say, to the maximum value of $d\sigma/dt$) is smaller in $\pi^- p \to \pi^0 n$ at 5 GeV/c. Further, the value at $t = -1\ (\mathrm{GeV}/c)^2$ falls faster with energy than Eq. (26) suggests. Comparison of 18.2 with 4.83 or 4.83 with 3.67 GeV/c suggests at least a ${p_{\mathrm{lab}}}^{-3}$ energy dependence.

(ii) Again, $\alpha_{\mathrm{eff}}(t)$ is much flatter[2)] in $\gamma p \to \pi^0 p$ than $\pi^- p \to \pi^0 n$.

(iii) A dip has been observed in $\pi^+ p \to \eta^0 \Delta^{++}$ [73)] and $\pi^- p \to \eta^0 n$ [74)] at $t \approx -1.4\ (\mathrm{GeV}/c)^2$. This amazing data is shown in Fig. 31, where we also mark the Regge expectation[75)] for $\pi^- p \to \eta^0 n$ in Fig. 31(c). This is clear evidence for the importance of Regge pole effects (A_2 WSNZ at $\alpha = -1$) for $-t \gtrsim 1\ (\mathrm{GeV}/c)^2$. The dip in the t distribution goes hand in hand with a very fast fall with energy. (${p_{\mathrm{lab}}}^{-3}$ to ${p_{\mathrm{lab}}}^{-4}$.) Indeed, Fig. 31(c) shows that $p_{\text{lab}}^2\, d\sigma/dt$ at 4.83 GeV lies significantly below the same quantity at 3.67 GeV/c. A similar effect is shown in the $\pi^- p \to \pi^0 n$ data of Fig. 28(b). Chiu,$^{4)}$ guided by the quark model, has noted the approximate equalities $\pi^+ p \to \pi^0 \Delta^{++} = C(\pi^- p \to \pi^0 n)$, $\pi^+ p \to \eta^0 \Delta^{++} = C(\pi^- p \to \eta n)$, $K^+ p \to K^0 \Delta^{++} = C(K^+ n \to K^0 p)$, with $C \approx 1.5$. The solid curve in Fig. 31(a) shows that this result is good up to $t \approx -3\ (\text{GeV}/c)^2$!

→ (L5) In spite of the above evidence for important Regge pole effects at large $-t$, Fig. 30 shows that for π exchange reactions there is little qualitative difference between photoproduction (a Regge disaster area) and strong interactions. We superimpose $\gamma p \to \pi^- \Delta^{++}$ on data for $K^- p \to \bar{K}^{*0} n$, $\pi^- p \to \rho^0 n$, and $pp \to n\Delta^{++}$. The similarity is striking. Note from Fig. 29(b) that resonance production data show the same shrinkage from 2 to 5 GeV/c as other strong interaction and photoproduction processes. The rather flat $K^- p \to \bar{K}^{*0} n$ t-distribution at 3.9 GeV/c is probably not an asymptotic effect.

→ (L6) Backward scattering has been reviewed in Ref. 39. In the decomposition (28), fermion exchange shifts the fixed pole in A_{FP} to $J = -1/2$. Correspondingly, in the conjectured scaling law (26) the energy dependence becomes p_{lab}^{-3}. Experimentally photoproduction exhibits this energy scaling but falls off very slowly with u (like e^u -- see Fig. 32(a) and Table 3D). Hadronic data, however, appear to fall like e^{3u} as in the forward direction (Fig. 32(b) and Table 3E).$^{76)}$ This difference -- and disagreement with VDM -- is not understood.

In summary, photoproduction has suggested a new type of interaction A_{FP} (Eq. (28)) which dominates large $-t$ scattering. Strong interaction data show that the ratio A_{FP}/A_R varies from process to process. It appears that the ratio is large in, for instance, photoproduction and $\pi^- p \to \rho^0 n$ but small in $\pi^- p \to \eta^0 n$. But even the latter can have a non-zero A_{FP} component hidden at the current low energies by an A_R which is large but falling fast with energy. Only more experiments for a wider range of reactions and energies can confirm or deny the existence of an A_{FP} component in all scattering amplitudes.

3.2. Interpretation in the b-Plane

The analysis of Section 2.1 indicated the relevance of the Fourier-Bessel transform in summarizing the dip structure of small $-t$ data. It is tempting to do the same for large momentum transfer data. So, rather than use an explicit model (remember they are all wrong anyway), we risk eternal damnation and naively insert for the amplitude in Eq. (5) the $\sqrt{d\sigma/dt}$.

Operationally we have:

(i) Assumed a given spin amplitude dominates.

(ii) Given $\sqrt{d\sigma/dt}$ a smooth sign change if $d\sigma/dt$ has a dip.

(iii) Partial wave analyzed both $\sqrt{d\sigma/dt}$ and $\sqrt{d\sigma/dt}$ with the Regge pole phase. The latter gives a more meaningful distribution into real and imaginary parts: however, it is not very relevant if the data do not exhibit the Regge energy dependence, i.e., it is probably irrelevant for photoproduction.

(iv) Assumed $d\sigma/dt$ has a smooth exponential tail for $-t >$ measured values. We used $\exp(3t)$ if no other information was available.

The partial wave analyses are shown in Figs. 31(d), 33, 34 and 35 for $\pi^- p \to \eta^0 n$, $\pi^- p \to \pi^0 n$, $K^- p \to \bar{K}^0 n$, $K^+ n \to K^0 p$, $\pi^+ p \to K^+ \Sigma^+$, $p\bar{p} \to n\bar{n}$, $np \to pn$, $\gamma p \to \pi^+ n$, $\gamma n \to \pi^- p$, $\gamma p \to \pi^0 p$, and backward $\pi^+ p \to p\pi^+$, $\gamma p \to n\pi^+$, $\gamma p \to p\pi^0$ (cf. also Figs. 7 and 9). Note the result:

$$d\sigma/dt = A\, e^{at} \left(\sqrt{-t}\right)^{2n}$$

implies:

$$f_n(b) = \frac{0.45\, e^{a/2}}{a^{n+1}} \quad e^{-b^2/2a} \sqrt{d\sigma/dt}\Big|_{t=-1\ (\mathrm{GeV}/c)^2} \tag{29}$$

assuming the cross section is dominated by a spin flip n amplitude.

⟶ (L7) The universal e^{3t} behavior in (26) translates into $e^{-b^2/6}$ partial wave amplitude: b is typically $2.5\ (\mathrm{GeV}/c)^{-1}$, half the value 5 which led in Section 2.1 to low $-t$ dips. The relative size of $b \approx 5$ with respect to $b \approx 0$ directly reflects the relative size of small and large $-t$ respectively. We conclude from the figures:

→ (L8) Real parts are always dominated by small b, imaginary parts are large for $b \sim 5\ (\mathrm{GeV}/c)^{-1}$; they are typically smaller than real parts for $b \approx 0$. This agrees with the small $-t$ data surveyed in Section 2.1.

→ (L9) Harari has speculated that there is little or no scattering at small b (Section 2.1C). Present data for strong interactions is inconclusive: our partial wave analyses give a small b component that varies all the way from zero to a value similar in absolute magnitude to that at $b \approx 5\ (\mathrm{GeV}/c)^{-1}$. However, $\gamma p \to \pi^o p$ suggests a large small b component for an imaginary part. This follows because it is crossing odd,$^{77)}$ and the only such function which leads to $d\sigma/dt \propto p_{\mathrm{lab}}^{-2}$ (amplitude constant with energy) is the well-loved number i: it is purely imaginary! So it is reasonable to attribute $\sqrt{d\sigma/dt}$ to the imaginary part of the spinflip amplitude. This leads to the large small b component shown by the solid line in Fig. 33(a).

→ (L10) More generally, the $\sqrt{d\sigma/dt}$ curves without Regge phase are perhaps most relevant for photoproduction where the Regge energy dependence is such a disaster. It is amusing to note that real parts of the b plane amplitudes have the same sign at large and small b; the imaginary parts have a sign change and the opposite sign between $b = 0$ and $b = 5\ (\mathrm{GeV}/c)^{-1}$ (compare Figs. 33(a), 35(a)). The latter is in perfect agreement with SCRAM (cf. Figs. 5, 6) with its overabsorption at small b; SCRAM has perhaps the right magnitude but the wrong sign at small b for the real parts. This particular empirical feature of photoproduction disagrees with all current models.

→ (L4 again) The b plots confirm that A_{FP}/A_R is smaller in strong interactions than photoproductions. (Compare in Fig. 33 the dip reactions $\pi^+ p \to p\pi^+$, $\gamma p \to p\pi^o$, $\pi^- p \to \pi^o n$, cf. Figs. 7, 9.)

To conclude, we have surveyed the present data on large $-t$ behavior. Photoproduction has indicated a universal structure which can be immediately interpreted as a universal amplitude in the b plane with well-defined s and b dependence. ($f(b) \propto 1/p_{\mathrm{lab}}\, e^{-b^2/6}$.) Such a behavior is of fundamental importance in any geometric picture of high energy scattering. Some differences have been observed between real and imaginary parts and between strong and photoproduction processes. Further progress requires a systematic study of many reactions, determination of amplitudes (as opposed to "$\sqrt{d\sigma/dt}$"!), and energy dependence. (Regge s dependence → Regge phase?)

TABLE 3

Large -t Slopes

				$e^{(c\pm\Delta c)t}$ fit	
Reaction	p_{lab} GeV/c	-t range $(GeV/c)^2$		c	Δc
A. Forward Photoproduction					
$\gamma p \rightarrow \pi^+ n$	5	0.5	1.15	2.19	0.21
	8	0.5	2.13	3.06	0.06
	11	0.5	2.06	3.26	0.08
	16	0.5	3	3.49	0.06
$\gamma p \rightarrow \pi^- \Delta^{++}$	16	0.5	2	3.46	0.15
$\gamma p \rightarrow \pi^o p$	2.5	1	3.12	0.26	0.07
	3	1	2.81	1.87	0.16
	3.5	1	2.84	2.0	0.34
	4	1	3.41	2.86	0.27
	5	1	2.82	2.97	0.26
	6	1	3	2.39	0.05
	12	1	3	2.92	0.08
	18	1	3	2.86	0.17
B. Forward Strong Interactions					
$\pi^- p \rightarrow \pi^o n$	1.71	1.2	2.45	0.82	0.38
	2.26	1.2	2.36	2.35	0.67
	2.8	1.2	2.24	1.65	0.54
	3.67	1.2	2.5	2.71	0.15
	4.83	1.2	2.4	2.81	0.25
	5.9	1.2	2.5	3.6	0.54
	10	1.2	2.32	2.48	1.28
	13.3	1.2	2.5	3.68	1.36
$K^- p \rightarrow \overline{K}^o n$	3.95	0.5	3	1.33	0.14
	7.1	0.5	1.5	2.48	0.46

TABLE 3 (cont.)

				$e^{(c \pm \Delta c)t}$ fit	
Reaction	p_{lab} GeV/c	$-t$ range $(GeV/c)^2$		c	Δc
$\pi^+ p \to K^+ \Sigma^+$	4	1.3	2.2	2.12	0.27
	5.05	1.25	2.95	2.12	0.08
$K^- p \to \pi^- \Sigma^+$	3	1.25	2.87	-0.6	0.21
$K^- n \to \pi^- \Sigma^0$	3	1.25	2.9	0.05	0.28
$p\bar{p} \to n\bar{n}$	5	0.5	1.3	4.98	0.66
	6	0.5	1.3	4.41	0.62
	7	0.5	1.3	3.02	0.74
	9	0.5	1.3	2.56	0.59
C. Resonance Production					
$\pi^- p \to \rho^0 n$	2.77	0.5	1.9	1.75	0.07
	6.95	0.5	1.4	3.82	0.4
$\pi^- p \to \rho^- p$	2.77	1	2	2.32	0.18
$\pi^+ p \to \rho^+ p$	3.7	0.5	1.4	0.68	0.25
	5	0.5	1.6	1.78	0.64
	8	0.5	2	1.93	0.38
$K^- p \to K^{*-} p$	3.9	0.8	1.6	1.1	0.3
$K^- n \to K^{*-} n$	3.9	0.8	2	2	0.3
$K^- p \to \bar{K}^{*0} n$	2	0.5	2	1.08	0.05
	3.9	0.5	2	2.25	0.19
	5.5	0.8	3	2.85	0.6
	10.1	0.5	2	2.55	0.95
$\pi^- p \to \omega^0 n$	1.5	0.5	1.2	2.64	0.22
	2.7	0.5	1.14	3.07	0.56
	3.65	0.25	2.1	2.97	0.28
	5.1	0.25	0.8	4.32	0.64
	6.95	0.25	1	4.83	0.5
$pp \to n\Delta^{++}$	6.6	1	3	1.42	0.25

TABLE 3 (cont.)

Reaction	p_{lab} GeV/c	-t range $(GeV/c)^2$		$e^{(c \pm \Delta c)t}$ fit c	Δc
D. Backward Photoproduction					
$\gamma p \rightarrow n\pi^+$	5	0.2	1.69	1.18	0.06
	9.55	0.2	1.72	1.16	0.09
$\gamma p \rightarrow p\pi^0$	8	0.5	1.01	0.82	0.42
	12	0.5	1.21	1.58	0.48
	18	0.5	1.23	1.36	0.66
E. Backward Strong Interactions					
$\pi^+ p \rightarrow p\pi^+$	2.85	0.55	1.7	1.02	0.35
	3.55	0.55	2.25	1.06	0.25
	9.85	0.55	2.03	2.37	0.32
	13.73	0.55	2.48	2.6	0.42
$\pi^- p \rightarrow n\pi^0$	4	0.7	1.7	1.45	0.3
	5.9	0.7	2.04	3.09	0.25
	10.1	0.7	2.04	3.48	0.45
$pp \rightarrow d\pi^+$	4.76	0.1	0.98	1.26	0.98
	21.1	0.1	1.12	3.47	0.26
$pp \rightarrow d\rho^+$	21.1	0.1	1.15	3.47	0.22

4. QUARK MODEL

4.1 The Model

Bialas and Zalewski$^{11)}$ have given a beautiful summary of the quark model predictions for high energy scattering processes. The derivation, predictions and relation of the model to other scattering theories is relatively unfamiliar. As it agrees quite well with experiment, the quark spin structure may be an important symmetry and so I will go into some detail here. Our conclusions are summarized in Section 4.7.

The SU_3 predictions of the quark model are well known and successful: they have been considered in a more general context in Section 2.5. They are represented,$^{78)}$ as usual, by the duality diagrams$^{54)}$ typified by Fig. 36(a). Here the dotted lines represent δ-functions in the SU_3 indices of the quark wave functions of the external particles. More generally we can calculate the predictions for spin structure in terms of the diagram of Fig. 36(b) where we replace the explicit vertical lines of 36(a) by an unknown black box for quark (anti-)quark scattering. This time we use the full SU_6 wave functions and so express all helicity amplitudes for the hadronic process in terms of the eight independent black box amplitudes.

4.2 Stodolsky-Sakurai Distribution (SSD)

(i) Considering, for example, $\pi^+ p \to \pi^0 \Delta^{++}$, the quark diagram of Fig. 36(b) predicts

$$H_{0\;1/2 \to 0\;3/2} = -\sqrt{3}\;\; H_{0\;1/2 \to 0\;-1/2}$$

α 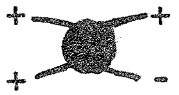

$+$ 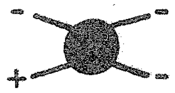

(30a)

where 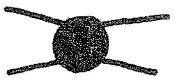 is a black box amplitude with the given helicities, and

$$H_{0\;1/2 \to 0\;1/2} = H_{0\;1/2 \to 0\;-3/2} = 0 \tag{30b}$$

and all the $\pi N \to \pi\Delta$ helicity amplitudes are given in terms of one complex number--the sum of two black box amplitudes. The relations (30a) and (30b) imply the well-known Stodolsky-Sakurai distribution (SSD) for the decay of Δ, i.e.,

$$\rho_{33} = 3/8 \ : \ \rho_{3-1} = \sqrt{3}/8 \ : \ \rho_{31} = 0 \qquad (31)$$

Some typical experimental evidence for the validity of this is given in Fig. 37, where the theoretical curves should be ignored at present. The data clearly agrees rather well with (31).

(ii) Theorem

More generally it is easy to show that the quark model implies the SSD for the Δ (and its SU_3 companions) whenever it is produced by natural parity exchange. (32)

We will return to a rather surprising implication of this in Section 4.6.

4.3. The Additivity Frame: Perversity Amplitudes

So far we have been rather gay about the correct relativistic definition of spin states to be used in conjunction with Fig. 36(b). In particular, the relations (30a), (30b) can only be true in one frame--they are not rotation invariant. This frame, which is termed the quark additivity frame, is in simple models the t-channel[79]: for instance, the quark relation $H_{0\ 1/2 \rightarrow 0\ -3/2} = 0$ of (30b), at the ρ-pole $t = m^2_\rho$, must be true in the t-channel (and this only) where it follows because the ρ particle has spin 1, and so no helicity flip two coupling. However, although the amplitude relations (30a), (30b) are frame dependent, the resultant density matrix element predictions (31) are in fact rotation invariant. This follows generally for all quark relations involving unpolarized targets: this can easily be seen in terms of perversity (commonly denoted by the lugubrious, if more descriptive, epithet transversity) amplitudes. These correspond to matrix elements between spin states with:

z axis along the normal ($\underline{1}$ x $\underline{3}$) to the scattering plane and the -y axis along the $\underline{1}$ (t-channel) or $-\underline{4}$ (s-channel) direction in the rest frame of 3. (33)

Thus they are related to the corresponding longitudinal frames defined in (16) by a rotation through $-\pi/2$ about the x direction.

A δ-function in a particular longitudinal frame for our basic quark line ⇒-⇒- of Fig. 36(b) becomes a diagonal matrix $\begin{bmatrix} e^{i\theta_1} & \cdot \\ \cdot & e^{i\theta_2} \end{bmatrix}$ in any perversity frame. The additivity frame is distinguished by the fact that $\Theta_1 = \Theta_2$ in its related perversity frame. However, all relations for unpolarized targets are clearly insensitive to Θ_1, Θ_2 and so rotation invariant.

The quark relations are thus most naturally expressed in terms of perversity amplitudes and this is done by Bialas and Zalewski. For example, the SSD, (31) in a longitudinal frame, becomes

$$\begin{aligned} &\rho_{\widetilde{33}} = 0 \\ &\mathrm{Re}\ \rho_{\widetilde{3-1}} = 0 \qquad \mathrm{Im}\ \rho_{\widetilde{3-1}} = 0 \end{aligned} \tag{34}$$

in a perversity frame $(\rho_{\widetilde{mm'}} = \rho_{mm'} + (-1)^{m-m'} \rho_{-m'-m})$.

Typical experimental results for (34) are shown in Fig. 38 (which contains the same data shown in Fig. 37). This seems slightly more convenient than (31) for discussing SSD. For instance, Fig. 38 shows that the deviation from (34), as often as not, involves negative $\rho_{\widetilde{33}}$. This is, of course, impossible if the resonance was pure spin $3/2^+$: so this deviation cannot be attributed to a failure of the quark model. Rather it no doubt represents evil background.

The formulation of the spin structure in terms of either longitudinal t-channel or perversity frames is slightly embarrassing. Thus we have already agreed that the zero structure of the imaginary part of s-channel longitudinal amplitudes may be universal (Section 2.1). It is impossible that both (30) be true in the t-channel and that the s-channel amplitudes have canonical absorption zeros$^{80)}$. This may represent an interesting theoretical problem--how can these two pictures be reconciled? We look at it again in Section 4.6 when we consider explicit absorption model calculations.

4.4. Dynamics of the Black Box

(i) Regge Poles or Cuts?

So far we have not specified the dynamical nature of the production mechanism. If we assume that the quark black box on the right hand side of (30a) is dominated by Regge poles, then we deduce that the corresponding hadronic amplitude is also controlled by poles: in this example, ρ exchange with M1 coupling to the $N\Delta$ vertex. To this extent, the quark relations are implied by Regge pole models with specific choices for the coupling structure. This was pointed out by Maor[81) but our formalism (i.e. plugging in poles for the black box), is trivially extended to π, A_2, B, etc. exchange. This gives a very quick method of deriving not only his results but also more general pole couplings that imply all the quark relations. So we can distinguish three models:

(a) The hadronic amplitudes are given as in Fig. 36(b) in terms of a black box which is dominated by Regge poles. (35a)

(b) As in (a) but the black box contains poles, cuts, conspiracies, absorption zeros, etc. (35b)

(c) The *Born* hadronic amplitude is as in (a) given by Fig. 36(b) with Regge pole black boxes. The *observed* hadronic amplitudes are given by addition of cuts, e.g., (strong) absorption corrections. (35c)

(a) was suggested by Maor but we have already agreed in Section 2 that poles alone cannot describe scattering data. Correspondingly, (a) does not seem tenable and I will not consider it further. However, current data seems to be consistent with either (b) or (c). These are fundamentally different models and it is important to try to distinguish them. First we consider the most attractive (to me) model (b) and a particular realization in terms of dual models. This in turn sheds light on the region of validity of the basic quark relations--a hotbed of controversy in the classical derivation in terms of real live quarks[82).

(ii) *The Naive t-Channel Dual Model*:

Most dual models involving a realistic particle spectrum are based on combining a relativistic spin structure based on the duality diagrams of Fig. 36(a), with an orbital part given by the Veneziano form. In the original models[12) of Mandelstam and Delbourgo and Rotelli, the relativistic spin structure was achieved by interpreting the basic quark line $\twoheadrightarrow$ as a δ-function in Dirac spinor indices. For this purpose the quarks are given the mass and momentum of the relevant external particle, e.g., the line $\alpha_1 \twoheadrightarrow \alpha_3$ at the bottom of Fig. 36(b) becomes $\bar{u}(p_3)\, u(p_1)$ with $(\gamma \cdot p_1 + m_1)u(p_1) = 0$, etc. It is easy to see that this model gives the quark model predictions with the *t-channel as the additivity frame*.

(iii) External Mass Dependence:

Further, we note that the above interpretation for the mass and momentum of the inactive quarks (i.e., they are the same as those of the external particles) extends to those entering the black box of Fig. 36(b). This is a general rule in all the dual models and indeed is the only sensible interpretation. So:

> The black box is the scattering amplitudes for spin $1/2^+$ quarks with the mass and momentum of the corresponding external particles. (36)

This clarifies the application of discrete symmetries to the black box: parity is always true but, for instance, time reversal is only a constraint if the masses of the initial and final state particles are the same. (True $np \to pn$, False $\pi N \to \rho\Delta$). The rule (36) implies that one must be careful when interpreting quark relations in reactions between particles of different mass. Only if the relevant black box amplitudes depend weakly on the external masses can they be true. For instance, consider the relations (6.1) and (6.2) of Ref. 11; namely

$$\sigma\,(pp \to n\Delta^{++}) = \frac{8}{3}\;\sigma\,(K^+n \to K^{*o}p) \tag{37a}$$

$$\sigma\,(pp \to n\Delta^{++}) = \sigma\,(K^+p \to K^o\Delta^{++}) + \frac{25}{9}\,\sigma\,(K^+p \to K^{*o}\Delta^{++}) \tag{37b}$$

The first is reasonable--the dominant π pole amplitude being proportional to $\sqrt{-t}\,/\,(t-m^2_\pi)$ in both cases. The second is ridiculous, $\sqrt{-t}\,/\,(t-m^2_\pi)$ being equated to $1/(t-m^2_\pi)$. Clearly it would be worthwhile to re-do the preliminary data comparison of Bialas and Zalewski[11)], taking care to consider only those relations which are kinematically consistent.

(iv) Domain of Validity of Relations:

One interesting feature of the model described in Section 4.4(ii) is that the quark relations are valid over all energies and momentum transfers transfers that the diagram 36(a) dominates over the s-u type diagram indicated in Fig. 36(c). In particular, for $K^\pm N$ reactions there is no s-u diagram and one predicts the quark relations to be valid everywhere; this includes, for instance, the resonance region in $\bar{K}N$ scattering.

A K^+p exposure from 0.864 to 1.585 GeV/c reports reasonable agreement with the Stodolsky-Sakurai distribution in $K^+p \to K^o\Delta^{++}$ 83) for this low energy region 84): however, there have been few other tests of the quark relations in either the large momentum transfer or low energy regions where one might naively expect it to fail.

(v) Better Dual Models:

The model described in (ii) suffers from the disadvantage of being obviously wrong. For instance, it predicts parity doubling for all the observed particles; a feature which is ruled out by experiment. Attempts 13) to avoid this in a dual framework have been based on a trick due to Green, Heimann, and Montvay (GHM) 85). This is illustrated in Fig. 36(d) for 2 → 2 scattering which indicates that one inserts in, say, $\alpha_1 \twoheadrightarrow \alpha_3$ the factor:

$$\gamma\cdot p_s \mathbb{F}_s + \mathbb{M}_s \tag{38}$$

where $p_s = p_1 + p_2$ is the total s-channel momentum. $\mathbb{F}_s$ and $\mathbb{M}_s$ are cunning functions adjusted to both give correct asymptotic behavior and ensure that (38) reduces to $\gamma\cdot p_s + m$ at an s-channel pole $s = m^2$. This removes the undesirable parity doubling. We note that the model of Ref. 13(b) has the full horror of the Carlitz-Kislinger cuts 86) and may very well have sufficient complication to be a realistic model without further (absorption cut) modifications. However, it is clear that (38) is not diagonal in these sophisticated models (in any longitudinal frame) and so there is no quark additivity frame. Nevertheless, if a form such as (38) contains no γ_5's--as the current models predict--then one can show that it is diagonal and of the form

$$\begin{bmatrix} c_1 & 0 \\ 0 & c_2 \end{bmatrix} \tag{39}$$

in a perversity frame. This is sufficient to derive the SSD. Some of the relations to be discussed in Section 4.5 also require $|c_1| = |c_2|$ which follows from (38) if $\mathbb{F}_s/\mathbb{M}_s$ is real: a relation which depends on technical details of the model. So this model has the intriguing feature that SSD is true at all energies but the basic amplitude structure varies rapidly (as $\mathbb{F}_s$, $\mathbb{M}_s$ do) and is certainly not a simple t-channel ρ exchange with M1 $N\bar{\Delta}$ vertex. As we indicate later, in Section 4.7(iii), such interesting predictions can be easily checked by, say, $\pi N \to KY^*$ off a polarized target. For completeness we note that in the model, of Ref. 13(b), (38) tends to a δ-function at high energies and in this case we have SSD at all energies but a t-channel additivity frame only in asymptotia.

A beautiful prediction of the specific dual model of Ref. 13(b) is that the π amplitude should conspire ($M = 0, 1$, cf. Section 2.4, Section 4.6(ii)) but that the pole cut amalgams, in the ρ, A_2 segments, are completely $M = 0$. This predicts, for instance $d\sigma/dt\,[\gamma n \to p\pi^-] = d\sigma/dt\,[\gamma p \to n\pi^+]$ at $t=0$ which is in splendid agreement with experiment. Taking a more general view of the data, we find that $M = 0$. ρ, A_2 agrees with the current results but is not decisively tested because of (a) data at too low an energy for good $K^+n \to K^{0*}p$ $K^-p \to \bar{K}^{0*}n$ tests (b) the absorption model - which gives the ρ, A_2 $M = 1$ cut components-- predicts smaller corrections for the ρ, A_2 than the π. [cf. Figs. 23(a) (b), 24(a)].

There is an interesting distinction between models with and without a longitudinal additivity frame. In the former, for instance, the theorem in Section 4.2(ii) is true in the arbitrary $2 \to n$ process: in the latter, one can only define a perversity frame for two-body or quasi-two-body processes and the quark relations cannot be proven for genuine multiparticle reactions. This has yet to be tested experimentally.

4.5. Double Resonance Production

The most extensive tests of the quark spin structure are to be found in double resonance reactions. For instance, in $\pi N \to \rho\Delta$, and its SU_3 related friends $\pi N \to \omega\Delta$, $\overset{(-)}{K}N \to \overset{(-)}{K}{}^*\Delta$, the twelve hadronic amplitudes are given in terms of five black box quantities. This gives rise to six so-called class-A relations which are written in terms of perversity frame statistical tensors as

$$\begin{aligned} &A.1 : T^{20}_{00} = \sqrt{2}\ T^{02}_{00} \\ &A.2 : \mathrm{Re}\ T^{22}_{20} = 1/2\ \mathrm{Re}\ T^{20}_{20} \end{aligned} \qquad (40)$$

$$\begin{aligned} \text{A.3} &: \operatorname{Im} T^{22}_{20} = 1/2 \operatorname{Im} T^{20}_{20} \\ \text{A.4} &: \operatorname{Re} T^{22}_{02} = 1/\sqrt{2} \operatorname{Re} T^{02}_{02} \\ \text{A.5} &: \operatorname{Im} T^{22}_{02} = 1/\sqrt{2} \operatorname{Im} T^{02}_{02} \\ \text{A.6} &: T^{22}_{00} = 1/2\sqrt{6} - 1/\sqrt{2} \cdot T^{02}_{00} \end{aligned} \qquad (40)$$

These relations are, as prophesied in Section 4.3, rotation invariant. Figures 39 through 41 summarize the current status of their experimental validity. Here we mark the left hand side (●), right hand side (X) and difference (■ = 0 according to quark) of the above six equations. The t scales and theoretical curves should be temporarily ignored. We can comment that the errors are generally large (compared, say, with the separate values of the left and right hand sides) but the quark model is successful with parhaps one exception. This is $\pi N \to \omega\Delta$ for (A.6) at 2.3 and 2.67 GeV/c. However there are many more successes than failures: particularly striking are the low energy $K^+p \to K^{*0}\Delta^{++}$ results (B and E in Fig. 41) for (A.1), (A.3) and (A.5). These successes are at energies where explicit high energy models give poor quantitative fits: thus they support models like the dual theories of Section 4.4 which predict the quark relations to be true at all energies. [cf. Section 4.4(iv)].

We should note here that (40) separates into three equations corresponding to the theorem of Section 4.2(v)--the τP+ exchange obeys SSD--and three expressing conditions on τP- exchange. The former are always valid in the dual models of Section 4.4(i) but the latter three need $|c_1| = |c_2|$ in (39)--a result which depended on extra assumptions over and above the general form of the amplitude. It would again be nice to see if future data shows the τP+ conditions to be better satisfied than the τP-.

4.6. Absorption Model

It is interesting to consider the consistency of the quark relations with absorption--in particular to ask if the model (36(c)), where we absorb input Regge poles satisfying the quark amplitude predictions, is tenable. I was surprised to find that this latter model seems to be quite possible and in the following I will examine the relevant information.

(i) $\underline{\pi^+ p \to \pi^0 \Delta^{++}}$:

Fig. 37, in fact, shows the expected Δ^{++} density matrix elements in $\pi^+ p \to \pi^0 \Delta^{++}$ for SCRAM and WIZKID where we have absorbed an input Regge pole obeying the quark predictions with a t-channel additivity frame. The absorption models differ negligibly[87)] from the SSD compared with current and probably any future experimental error-bars. This is not too surprising: the reaction is dominated by the two s-channel helicity flip amplitudes whose ratio is unaltered by absorption. Further, the s-channel nonflip amplitude generated by crossing the pure helicity flip t-channel amplitude vanishes in the forward direction and is not altered much by absorption. The observables off a polarized target are more sensitive: Fig. 42 shows that the predicted asymmetry, integrated over the whole Δ^{++} decay, is quite large above -t of .5 $(\mathrm{GeV}/c)^2$. We note that in any quark model with an additivity frame there can never be any polarization in Δ^{++} production by natural parity exchange; this follows at once from the observation that all hadronic amplitudes are proportional to the one black box quantity--Equ. (30a). This contrasts with the similar $\pi^- p \to \pi^0 n$ which has its full two amplitudes; complicated quark models, including cuts and poles in the black box, can give polarization in this case. It would be nice to check this distinctive difference experimentally.

(ii) $\underline{\gamma p \to \pi^- \Delta^{++}, \quad \pi^+ p \to (\rho^0, \omega)\Delta^{++}, \quad \overset{(-)}{K}N \to \overset{(-)}{K}{}^* \Delta}$:

A more interesting case is $\gamma p \to \pi^- \Delta^{++}$ which is dominated by π exchange near t = 0. The nonzero cross-section in the forward direction is indicative of sizeable absorption corrections and, in fact, the total natural parity component is--dependent on t--some 25°/o to 50°/o of the cross-section. One can separate the two exchanged parities using incident polarized photons and so find $\rho_{ij}^{(\pm)}$: the Δ^{++} decay density matrix elements for $\tau P \pm$ exchange respectively. The quark model predicts

$$\rho_{33}^{(+)} = 3/8 , \quad \rho_{3-1}^{(+)} = \sqrt{3}/8 , \quad \rho_{31}^{(+)} = 0$$

$$\rho_{33}^{(-)} + \sqrt{3}\ \rho_{3-1}^{(-)} = 0 \tag{41}$$

the first line being an example of the theorem in Section 4.2(ii). We can compare these relations with the data[88] in Fig. 43: statistics are too limited to allow any significant conclusions. This figure also shows the predictions of a simple absorption model with just input π exchange. The theory reproduces the SSD quite amazingly in $\rho^{(+)}$: remember, in this simple calculation there is not a ρ or A_2 exchange in sight. This figure dramatically illustrates that the automatic association of the SSD in this and other processes with $\rho(A_2)$ exchange is rather dangerous. It is easy to see that absorbing π (or B) exchange will reproduce approximate SSD in its $\tau P+$ component for $\gamma p \Rightarrow \pi\Delta$, $\pi p \Rightarrow (\rho, \omega)\Delta$ and $\overset{(-)}{K}N \Rightarrow \overset{(-)*}{K}\Delta^{++}$. It is thus very hard to distinguish the quark model from simple absorption models in these processes. This is illustrated again in Figures 39 and 40 which show the deviations from the class-A relations predicted by simple π, B, ρ, and A_2 plus absorption models[89]. The theoretical predictions are almost always small and even rather less than the experimental deviations! Certainly this data does not favor the quark over the absorption model.

There are reactions where the quark and the absorption models give different predictions--examples are $\pi^+ p \Rightarrow f^0\Delta^{++}$ (selecting helicity flip 2 for the f^0) and $\gamma p \Rightarrow (\rho, \omega)\Delta$ with polarized photons. Both are very difficult and perhaps even impossible experiments. There is an easy way to see the distinction between the quark and absorption models in these cases. Thus absorption generates all M (the Toller quantum number, see Section 2.4) values--in particular M = 2 in the above reactions. The quark model can only have M = 0 and 1 as $M \geq 2$ cannot be generated from a $1/2^+ \, 1/2^+ \rightarrow 1/2^+ \, 1/2^+$ black box. Now people have long given up the π as a lost cause as analysis of the data (Section 2.4) indicated it was a complicated mixture of M = 0 and 1. It would certainly restore one's faith in the importance of quantum numbers if the π exhibited _just_ the complication suggested by the quark model and no more.[90] Tests for M = 2 are thus urgent.

Theoretically it seems to us very striking that the absorption model and quark model should so closely coincide for simple processes. Perhaps it has some cosmic significance. In particular, we note that the

ρ and A_2 have very similar helicity coupling structure to absorbed (π, B) exchange in all processes constructed out of $N\bar{N}$, $N\bar{\Delta}$, $\pi\rho$, $K\bar{K}^*$, $\pi\omega$ and $\gamma\pi$ vertices. This coherence of amplitudes leads to tremendous differences in the line reversed reactions, e.g., $K^-p \rightarrow \bar{K}^{*0}n$ v. $K^+n \rightarrow K^{*0}p$, $p\bar{p} \rightarrow n\bar{n}$ v. $np \rightarrow pn$, $\gamma p \rightarrow n\pi^+$ v. $\gamma n \rightarrow p\pi^-$, which differ by a sign change in the ρ (and B) components [cf. Section 2.4(e)]. This difference comes from the coherent interference between the ρ and the absorption corrections to π exchange. We note that the observed systematics determine a relative sign for the π and ρ couplings. This is given correctly in the SU_6 quark model of Ref. 13(b).

(iii) Class-B Relations:

There are also a series of relations--additional to the class-A relations of Section 4.5--which follow on making explicit assumptions about the black box in Fig. 36(b). The assumption 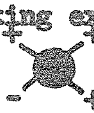

+ 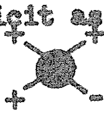

+ 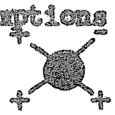

+ 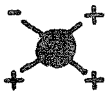

= 0, gives six class-B relations while putting in addition 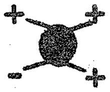

+ 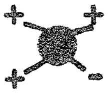

= 0, gives seven class-C relations. The status of these is unclear in general as neither assumption is justifiable from discrete symmetries in the physical situation with unequal external masses. The dual model of Ref. 13(b) makes the interesting prediction that the class-B relations should be true but that the class-C are wrong. This is intriguing for the class-C are indeed violated by experiment while the class-B are quite well satisfied. We show typical results for class-B$^{91)}$ **and** $\pi^+p \rightarrow \omega^0\Delta^{++}$ **in Figure 44. It is interesting that--as indicated on the figure--the absorption model predicts quite striking violations of these relations. In view of their hazy justification in the quark model, the significance of this is unclear to me at present**$^{93)}$.

4.7. Summary

In the preceding we have tried to give a flavour of the wide range of implications for scattering amplitudes inherent in the quark model. In particular, no model being an island, we have tried to describe its relation to other dynamic theories of exchange processes. It seems to us quite amazing that such symmetries should be present in complicated scatterings as $\pi^+p \rightarrow \omega^0\Delta^{++}$ which require the fingers of fully three physicists just to enumerate the independent observables. In the following we indicate some of the important areas for future theoretical and experimental endeavour.

(i) The success of the quark relations indicates that the dual models of Section 4.4 are building in the correct spin structure. It would be interesting to develop such models to the stage where they could be explicitly compared with experiment. An essential step is the splitting of the π and ρ, N, and Δ which are degenerate in the SU_6 limit.

(ii) As indicated in Section 4.4(iii) the analysis of Bialas and Zalewski11) should be reconsidered--using the new data now available and distinguishing quark relations that are kinematically ridiculous from those that are sensible.

(iii) An extremely exciting experiment is the R and A type experiments in $\pi N \rightarrow KY^*$ and $\bar{K}N \rightarrow \pi Y^*$ off a polarized target with observation of the final Λ polarization: These are clearly the best experiments to determine the quark additivity frame79,94)--if it exists--and how it varies with energy. As we discussed in Section 4.4(iv) the quark relations are not just valid at high energy, and such experiments should be done over a wide range of energies--say from 2 GeV upwards. Typical predictions are given in Figure 45. Another reason for interest in such experiments was discussed in Section 2.1B.

(iv) In Section 4.6 and Figure 42, we indicated that measurements of $\pi N \rightarrow \pi\Delta$ (and its SU_3 friends) off a polarized target would be useful. (See also Section 5.)

(v) It is interesting to examine the quark relations in as wide a range of circumstances as possible. In particular one should look at it in multiparticle as well as quasi-two-body situations (Section 4.4(v) and Refs. 95, 96). For instance, in $K^+n \rightarrow (K^+\pi^+)\Delta^-$ with low mass nonresonant s-wave $K^+\pi^+$ production one predicts for the Δ decay density matrix elements

$$\rho_{33} + \sqrt{3}\,\rho_{3,-1} = 0 \qquad (42)$$

--as always for τP- exchange.

(vi) It is vital to find evidence for or against M = 2 components in exchange processes at high energies. (Section 4.6(ii)). Good reactions are $\gamma p \rightarrow (\rho,\omega)\Delta$, $\pi N \rightarrow f^0\Delta$, and $p\bar{p} \rightarrow \Delta\bar{\Delta}$. In the latter reaction, the double correlation $\rho^{3-1}_{3-1} + \rho^{1-3}_{3-1}$ should vanish like t if only M = 0 and 1 are present. Again it is important to check for M = 1 components of ρ, A_2 exchange. (Section 4.4(v))--this can be done through studies of $\pi^- p \rightarrow \omega^0 n$, $\pi^+ p \rightarrow \omega^0 \Delta^{++}$, $K^- p \rightarrow \bar{K}^{*0} n$ v. $K^+ n \rightarrow K^{*0} p$ with attention to the energy dependence of the forward cross-section. (to distinguish M = 1 π, B from M = 1 ρ, A_2).

(vii) The classical quark tests in double resonance production (Section 4.5, Section 4.6(iii)) should be critically examined over a wide range of energy and momentum transfer. Consideration should be given to background problems (cf. Fig. 38). Further it is probably best to formulate tests in terms of s-channel longitudinal density matrix elements--as is always possible. These are more sensitive to differences between the quark and absorption pictures as they clearly exhibit the distinctive t-dependence of amplitudes predicted in the latter model.

(viii) The reaction $\vec{\gamma} p \rightarrow \pi^- \Delta^{++}$, with polarized photons and the Δ^{++} decay observed, is a very sensitive test of theories. (Section 4.6(ii)) Do the quark predictions--Eq. (41), Fig. 43--really hold over a wide range of t? Perhaps measurements in this reaction could give a clue to the amplitude structure underlying the e^{3t} dependence of $d\sigma/dt$ commented on in Section 3.

5. MULTIPARTICLE REACTIONS

Here we must be very brief because there is a deplorable lack of attention to amplitude structure in current multiparticle phenomenology. Spasmodic items include:

(i) What is the role of absorption in multiparticle processes? In particular, why isn't the S-wave deck enhancement (A_1) absorbed away as are two body π exchange low partial waves (Section 2.4)?

(ii) Continuing on the A_1, we can note that the two fashionable theories, Deck and resonance, predict respectively purely real and purely imaginary amplitudes. Polarization measurements in the analogous $(\pi)pp \rightarrow (\pi)pN^*_{1400}$ reaction may help to resolve this distressing ambiguity.

(iii) In 2 → 2 scattering, the single flip (ρ, A_2) exchange amplitude (e.g., $\pi^-p \rightarrow \pi^0 n$) agrees well with Regge pole theory (Section 2.1). The most successful B_5 calculation was for $K^+p \rightarrow K^0\pi^+p$ and $K^-p \rightarrow \bar{K}^0\pi^-p$[97] which are also single flip in most important subchannels ($K^{\pm}p \rightarrow K^{*\pm}p$, $K^+p \rightarrow K^0\Delta^{++}$, $K^-p \rightarrow \bar{K}^0 n$). Again no theoretically reasonable B_5 formula has been written except when all subchannels are spinflip. (The usual kinematic factor $\epsilon^{ijk\ell}\, p_i p_j p_k p_\ell$ producing this.) These three facts must be related. As corollaries we deduce that (a) $K^{\pm}p \rightarrow K^0\pi^{\pm}p$ and the similar $\pi^{\pm}p \rightarrow \pi^0\pi^{\pm}p$ are good reactions to test subtler parts of 2 → 3 Reggeism (WSNZ, double Regge limits), (b) more negatively 2 → 3 reactions, in which quasi two body subchannels have large nonflip amplitudes (e.g., $\pi^-p \rightarrow \pi^+\pi^-n$, $\pi^+p \rightarrow K^+\pi^+\Lambda$) and so poor agreement with Regge pole theory, will have large cut contributions. There are more type (b) reactions than type (a), i.e., corrections to Regge poles (cuts) dominant multiparticle reactions.

(iv) It is interesting to note that it is not necessary both to polarize the target and measure the final baryon polarization in quasi-two body reactions to find all the amplitudes. The final resonance density matrix elements off a polarized target are sufficient. This is summarized in the table below.

TABLE 4

Generic Reaction	Independent Observables	Unpolarized Target Observables	Polarized Target Observables
$\pi N \rightarrow \pi\Delta$	7	4	10
$\pi N \rightarrow \rho N$	11	4	10
$\pi N \rightarrow \rho\Delta$	23	20	56

In the Δ production reactions, we have many more observed quantities than we need: only in $\pi N \rightarrow \rho N$ do we need an extra one to find all the amplitudes. This and other useful observables can be found by measuring the final baryon polarization off an unpolarized target. This seems quite possible in the Argonne 12-foot bubble chamber. Here one can imagine a useful collaboration between a counter experiment on $\pi N \rightarrow \rho N$ with a polarized target, together with the bubble chamber experiment on the final baryon polarization. Some of the physics obtainable from such experiments has been discussed in Section 2.2 and Section 4.6, Fig. 42.

ACKNOWLEDGMENTS

Much of the work reported here has been done with Ed Berger and Charles Chiu. I am indebted to them for many stimulating discussions. Further I am grateful to J. Baton, D. Chu, E. Colton, S. Hagopian, T. Jenkins, P. Katz, J. MacNaughton, B. Musgrave, J. Prentice, W. Wittek and H. Yuta for their generous provision of unpublished data used in this article.

REFERENCES AND FOOTNOTES

1. $K(s)$ is $0.3893/(64\pi\ m\ p_{lab}^2)$ in meson-baryon scattering and half this in baryon-baryon and photon-baryon scattering.
2. G. C. Fox, in High Energy Collisions, ed. by C. N. Yang et al. (Gordon and Breach, Inc., New York, 1969).
3. E. L. Berger and G. C. Fox, Phys. Rev. Letters 25, 1783 (1970).
4. C. B. Chiu, Caltech preprint CALT-68-281 (1970), Nucl. Physics (to be published); C. B. Chiu, Caltech preprint CALT-68-300 (1971).
5. J. D. Jackson, Rev. Mod. Phys. 42, 12 (1970); L. Durand III, in Proceedings of the International Conference on Expectations for Particle Reactions at the New Accelerators, April 1970 (University of Wisconsin, Madison, 1970).
6. H. Harari, SLAC-PUB-914 preprint (1971). This references his earlier work.
7. M. Ross, F. S. Henyey, and G. L. Kane, Nucl. Phys. 23B, 269 (1970).
8. This model was discussed in Ref. 2 where it was staidly, if more relevantly, termed the HPW (High Partial Wave) model.
9. C. B. Chiu and G. C. Fox, unpublished data compilation. This will document the data plotted in Figs. 26 and 28 - 35.
10. R. Diebold, SLAC-PUB-673, published in Proceedings of the 1969 Boulder Conference on High Energy Physics, ed. by K. Mahanthappa, W. Walker, and W. Brittin (Colorado Associated University Press, 1970).
11. A. Bialas and K. Zalewski, Nucl. Phys. B6, 449, 465, 478, 483 (1968).
12. S. Mandelstam, Phys. Rev. 184, 1625 (1969); Phys. Rev. D1, 1734 (1970). R. Delbourgo and P. Rotelli, Physics Letters 30B, 192 (1969); Imperial College preprint "Veneziano Model for the Scattering of Meson and Baryon Supermultiplets" (1969).
13. (a) G. C. Fox, Cambridge University preprint "A Veneziano Model Without Parity Doubling for Production Processes" (1970); I. Montvay, ITP-Budapest Reports No. 273, 277, and 280 (1970). (b) R. Carlitz, S. Ellis, P.G.O. Freund, and S. Matsuda, Caltech preprint CALT-68-260 (1970). S. Ellis, Ph.D. thesis, Caltech (1971), unpublished.

14. R.J.N. Phillips and G. A. Ringland, "Polarization Test of Absorptive Cut Models", Nucl. Phys. (to be published).

15. A good fit to the $\pi^- p \to \pi^0 n$, $\pi^- p \to \eta n$, $\overset{(-)}{K} N$ CEX $d\sigma/dt$ data in SCRAM requires a low value of $C \approx 0.8$. Unfortunately this does not give the correct crossover position in Im N. We have plotted in Figs. 5 and 6 the curves for $C = 1.33$ -- using the same unabsorbed amplitude from our best $C \approx 0.8$ fit. This gives a reasonable zero position in Im N ($t \approx -0.25$ (GeV/c)^2). For contrast, we also plot Im N(ρ) for $C = 1$.

16. R. Dolen, D. Horn, and C. Schmid, Phys. Rev. 166, 1768 (1968).

17. V. Barger and R.J.N. Phillips, Phys. Rev. 187, 2210 (1969).

18. M. Davier and H. Harari, SLAC-PUB-893 preprint (1971).

19. R. D. Mathews, Nucl. Phys. B11, 339 (1969).

20. R. D. Field and J. D. Jackson, UCRL-20287 preprint (1971).

21. G. Belletini, at Moriond Conference (1970); E. L. Berger and G. C. Fox, NAL Summer Study on Polarization (1970).

22. S. Y. Chu and A. Hendry, Phys. Rev. Letters 25, 313 (1970), and preprint "Analysis of $\pi^+ p$ Scattering from 2.74 to 4 GeV/c at All Angles" (1971).

23. We used the accepted values $\epsilon_N/\epsilon_F = -1$ for $\pi^- p \to \pi^0 n$, $\pi^- p \to \eta^0 n$, $\pi^- p \to K^0 \Lambda$, and $K^- p \to \bar{K}^0 n$; $\epsilon_N/\epsilon_F = +1$ for $\pi^+ p \to K^+ \Sigma^+$ (cf. Section 2.5).

24. A. Yokosawa, this conference (page 612).

25. D. D. Drobnis et al., Phys. Rev. Letters 20, 274 (1968); P. Bonamy et al., Nucl. Phys. B16, 335 (1970).

26. S. M. Pruss et al., Phys. Rev. Letters 23, 189 (1969).

27. K. W. Lai, private communication.

28. Hypercharge exchange data are good for such tests as the flip and nonflip amplitudes are of similar size. Reference 20 has analyzed the FESRs for hypercharge exchange processes. Present data does not seem to favor any one channel as having the canonical zero structure.

29. The polarization in $K_L^0 p \to K_S^0 p$ is predicted to be similar to that in $\pi^- p \to \pi^0 n$. This follows because it has the same type of exchange as $\pi^- p \to \pi^0 n$ -- it differs only in the numerical ratio N/F. Correspondingly, simultaneous studies of $K_L^0 p \to K_S^0 p$ and $\pi^- p \to \pi^0 n$ will be very valuable.

30. Note from Figs. 1 - 4 that whereas Im N, F are independent of the exchange type, the real parts depend greatly on the exchange. Re N for reactions (R2) - (R4) is discussed in Section 2.1B (iii).

31. A Regge pole rather than a SCRAM explanation of Im F is much preferred. Even though they have a similar zero structure, the energy dependence ($\alpha_{eff} \approx \alpha_\rho(t)$) of $\pi^- p \to \pi^o n$ is very hard to understand in SCRAM (Ref. 2).

32. G. S. Abrams et al., Phys. Rev. Letters 25, 617 (1970).

33. In this Section, taking for example $\pi^+ p \to p\pi^+$, I use N and F to denote the amplitudes that are α 1 and $\sin \theta_s$ at $\cos \theta_s = -1$. Regarded as amplitudes for (forward) $\pi^+ p \to \pi^+ p$, they are, of course, respectively the flip and nonflip s-channel amplitudes.

34. E. L. Berger and G. C. Fox, Nucl. Phys. B26, 1 (1971) contains further details and references on backward πN scattering.

35. D. J. Crenell et al., Phys. Rev. Letters 23, 1347 (1969).

36. D. J. Sherden et al., Phys. Rev. Letters 25, 898 (1970); H. Aoi et al., Physics Letters 35B, 90 (1971). See also L. Dick and A. Yokosawa at this conference (pages 594 and 612).

37. The prediction only holds if you neglect the Δ_δ exchange component. $N_\alpha - \Delta_\delta$ interference is expected to give negative polarization for small -u; for $u \approx -0.6$ (GeV/c)^2, the Δ_δ is negligible.

38. V. Barger, C. Michael, and R.J.N. Phillips, Phys. Rev. 185, 1852 (1969).

39. E. L. Berger and G. C. Fox, Nucl. Phys. B30, 1 (1971).

40. The kinematic -t cutoff is of course larger at a given energy for class III compared with class II reactions. Exploitation of the immense vitality of a fully fledged π, requires rather high incident energies.

41. This comes from the fit to all $K^- p \to \bar{K}^{*o} n$ and $K^+ n \to K^{*o} p$ data presented in G. C. Fox et al., Argonne preprint "The Charge Exchange Production Mechanism for K^* 1890" (1971).

42. E. Leader, Phys. Rev. 166, 1599 (1968).

43. C. F. Cho and J. J. Sakurai, Phys. Rev. D2, 517 (1970).

44. J. D. Jackson and C. Quigg, Physics Letters 29B, 236 (1969) and Nucl. Phys. B22, 301 (1970).

45. N. Byers, Phys. Rev. 156, 1703 (1967) (crippled π); P. R. Stevens, Phys. Rev. D1, 2523 (1970) (fully-fledged and half-asleep π).

46. P. K. Williams, Phys. Rev. D1, 1312 (1970). The attribution of (equal) form factors in this reference to flip and nonflip amplitudes is both dubious and outside the spirit of PMA. To the extent such things matter, PMA cannot be trusted.

47. Equation (24) holds at $t = 0$. ρ_{00}^{H} has extra t-dependence $1/(t - m_{\pi}^{2})^{2}$, but $2\rho_{11}^{H}$ is $\alpha\left[1 + (t/m_{\pi}^{2})^{2}\right]/(t - m_{\pi}^{2})^{2}$. (The $(t/m_{\pi}^{2})^{2}$ term comes from the s-channel double flip amplitude.)

48. C. D. Froggatt and D. Morgan, Phys. Rev. 187, 2044 (1969).

49. $\bar{p}\Delta^{++}$ helicity nonflip is half asleep, the helicity flip one vertices make up the crippled π component.

50. C. Michael, in *Proceedings of the Ruhestein Meeting on Low Energy Hadron Interactions and Coupling Constants*, Springer Tract Vol. 55 (1970).

51. C. Michael and R. Odorico, Physics Letters 34B, 422 (1971). The comments in this paper on $\gamma N \to K(\Lambda, \Sigma)$ should be treated with caution. Explicit calculations reveal that K exchange, which they neglect, can be important.

52. A. C. Irving, A. D. Martin, and C. Michael, CERN preprint TH-1304 (1971).

53. W. B. Johnson *et al.*, Phys. Rev. Letters 26, 1053 (1971).

54. H. Harari, Phys. Rev. Letters 22, 562 (1969); J. L. Rosner, Phys. Rev. Letters 22, 689 (1969).

55. K. W. Lai and J. Louie, Nucl. Phys. B19, 205 (1970); B. Musgrave, talk at this conference (page 467); and C. B. Chiu, in *Proceedings of the Workshop on Particle Physics at Intermediate Energies*, UCRL-20655 (1971).

56. P. R. Robrish *et al.*, Physics Letters 31B, 617 (1970).

57. B. A. Barnett *et al.*, Physics Letters 34B, 655 (1971), and A. Yokosawa, this conference (page 612).

58. A. Firestone *et al.*, Phys. Rev. Letters 25, 958 (1970).

59. (a) R. Worden, Caltech preprint (1971). (b) A. Goldhaber, G. C. Fox, and C. Quigg, Physics Letters 30B, 249 (1969).

60. D.R.O. Morrison, Phys. Rev. 165, 1699 (1968) and Proceedings of XVth International Conference on High Energy Physics, Kiev (1970); T. T. Chou and C. N. Yang, Phys. Rev. 175, 1832 (1968); R. Carlitz, S. Frautschi, and G. Zweig, Phys. Rev. Letters 23, 1134 (1969).

61. F. Zachariasen, CERN preprint TH-1284 (1971).

62. P.G.O. Freund, Phys. Rev. Letters 21, 1375 (1968).

63. W. Frazer, this conference (page 48); C. Quigg, in Proceedings of the Workshop on Particle Physics at Intermediate Energies, UCRL-20655 (1971).

64. D. Z. Freedman, C. E. Jones, F. E. Low, and J. E. Young, Phys. Rev. Letters 26, 1197 (1971).

65. F. Gilman, J. Pumplin, A. Schwimmer, and L. Stodolsky, Physics Letters 31B, 387 (1970).

66. J. Ballam et al., Phys. Rev. Letters 24, 960 (1970).

67. ABBCCHLV Collaboration, Physics Letters 34B, 160 (1971); G. Ascoli et al., Phys. Rev. Letters 26, 929 (1971); U. Kruse, this conference (page 27).

68. We have already mentioned in Section 2.1B the somewhat circular argument that the elastic polarization data is well explained if you assume that both the ρ, A_2 (s-channel) is helicity flip and agrees with Regge pole theory and that the Pomeron is helicity nonflip and purely imaginary.

69. Large $-t$ elastic or diffraction dissociation data (e.g., $\gamma p \to \rho^0 p$, $pp \to pN^*_{1688}$) is also interesting. It awaits another day.

70. See Fig. 2 of the first cited paper in Ref. 4, for a similar comparison of forward cross sections.

71. The plotted points are determined by interpolation of data at energies around 5 GeV/c. Details and the explicit data references will be presented elsewhere.

72. This is expected in the quark model; cf. Eq. (37a) in Section 4.

73. D. F. Grether and G. Gidal, Phys. Rev. Letters 26, 792 (1971).

74. Large $-t$ ηN data is from Case-Western group and T. L. Jenkins, private communication. Small $-t$ ηN data in Fig. 31 is from O. Guisan et al., Physics Letters 18, 200 (1965).

75. $d\sigma/dt\ (\pi^- p \to \eta^0 n) = 2/3 \cos^2 (\pi\alpha/2)\ \ d\sigma/dt\ (K^- p \to \bar{K}^0 n)$, $\alpha = 0.4 + 0.9\ t$: This method has been exploited at smaller $-t$ in Refs. 4 and 19. Similar prediction $d\sigma/dt\ (\pi^- p \to \pi^0 n) = 2 \sin^2 (\pi\alpha/2)$ $d\sigma/dt\ (K^- p \to \bar{K}^0 n)$ is a rather poor representation of 3.67 GeV/c $\pi^- p \to \pi^0 n$ above $-t = 1\ (\mathrm{GeV}/c)^2$.

76. We note that the value of $pp \to d\pi^+$ in Fig. 26 is artificially high. The e^u dependence of this data at 5 GeV/c has turned into the "universal" e^{3u} at 21 GeV/c (Ref. 39). There is well over an order of magnitude decrease in $(p_{lab}/5)^3\ d\sigma/du$ at $u \approx -1\ (\mathrm{GeV}/c)^2$.

77. The only crossing even amplitude in $\gamma p \to \pi^0 p$ has $\tau P-$. The reaction is dominated by $\tau P+$ exchange as the asymmetry from polarized photons is near 1 up to t of $-1\ (\mathrm{GeV}/c)^2$. (R. L. Anderson et al., Phys. Rev. Letters 26, 30 (1971).)

78. We treat for definiteness meson baryon processes. There are, of course, analogous results for baryon baryon and meson meson scattering. See Ref. 11.

79. A. Bialas, A. Kotanski, and K. Zalewski, Nucl. Phys. B28, 1 (1971).

80. There would be no trouble if the imaginary part had the s-channel as its additivity frame. As we mentioned in the text, this is impossible for the real part at the ρ pole. Analyticity unfortunately forbids different additivity frames for the real and imaginary parts!

81. U. Maor, Nucl. Phys. B19, 20 (1970).

82. H. J. Lipkin, Nucl. Phys. B20, 652 (1970).

83. R. W. Bland, M. G. Bowler, J. L. Brown, G. Goldhaber, S. Goldhaber, J. A. Kadyk, V. H. Seeger, and G. H. Trilling, Nucl. Phys. B18, 537 (1970).

84. S. Loken (private communication) also finds good agreement with SSD in $K^+ p \to K^0 \Delta^{++}$ for p_{lab} in the range 1.37 to 2.17 GeV/c.

85. M. B. Green and R. L. Heimann, Physics Letters 30B, 642 (1969); I. Montvay, Physics Letters 30B, 653 (1969) and 33B, 540 (1970).

86. R. Carlitz and M. Kislinger, Phys. Rev. Letters 24, 186 (1970).

87. See also P. Gizbert-Studnicki, A. Golemo, and K. Zalewski, TPJU-2/71 preprint.

88. H. H. Bingham et al., Phys. Rev. Letters 25, 1223 (1970).

89. Here the ρ and A_2 were given the usual t-channel SSD -- Eqs. (30a,b). The π and B -- in accordance with the spirit of the model -- were allowed any couplings consistent with the t-channel quark constraints. This is more general than simple one pion exchange for $\pi N \rightarrow \rho\Delta$ where you are only allowed πρ and $N\bar{\Delta}$ nonflip couplings.

90. All M values would be generated by applying PMA (poor man's absorption, Section 2.4) to the full hadronic amplitude; M values of 0 and 1 only, come from PMA for the quark black box. Both schemes are consistent with current data.

91. Our class B relations are defined and labelled as in Ref. 92.

92. M. Aderholz et al., Nucl. Phys. B8, 485 (1968).

93. I have not investigated the sensitivity of these results to the input pole coupling structure. ρ was as usual t-channel SSD and B pure $N\bar{\Delta}$ and πω nonflip in the reported calculations. Maybe the violations in Fig. 44 are simply an indication that this is too naive. For the class A case, the violations were small for a wide class of couplings (Footnote 89).

94. A. Bialas and A. Kotanski, Nucl. Phys. B19, 667 (1970).

95. P. Gizbert-Studnicki and A. Golemo, TPJU-22/70 preprint.

96. A. Eskreys et al., TPJU-1/71 preprint.

97. H. M. Chan et al., Nucl. Phys. B19, 173 (1970); E. L. Berger, this conference (page 83).

98. Data $\pi^+ n \rightarrow \omega^0 p$:
1.44, 1.65, 1.86 GeV/c: J. S. Danburg, UCRL-19275 preprint (1969).
1.5 GeV/c: J. Katz (Minnesota), private communication (1970).
2.7 GeV/c: R. J. Miller et al., Phys. Rev. 178, 2061 (1969).
3.65 GeV/c: G. C. Benson et al., Phys. Rev. Letters 22, 1074 (1969).
4.19 GeV/c: G. S. Abrams et al., Phys. Rev. Letters 23, 673 (1969).
5.1 GeV/c: N. Armenise et al., Nuovo Cimento 65, 637 (1970).
5.4 GeV/c: University of Notre Dame preprint (1971).
6.95 GeV/c: J.A.J. Mathews et al., Phys. Rev. Letters 26, 400 (1971).

99. Data $K^+ n \rightarrow K^{*0} p$:
2.3 GeV/c: S. Goldhaber et al., Phys. Rev. Letters 15, 737 (1965).
3 GeV/c: G. Bassompierre et al., Nucl. Phys. B16, 125 (1970) and W. Wittek, private communication (1971).

100. Data $K^-p \to \overline{K}^{*0}n$:

2 GeV/c: D. Chu (Caltech), private communication (1971).

3.9 GeV/c: M. Aguilar-Benitez et al., Phys. Rev. Letters 26, 466 (1971).

5.5 GeV/c: B. Musgrave and H. Yuta (ANL), private communication (1971).

10.1 GeV/c: A. Angelopoulos (CERN), private communication to B. Musgrave (1970).

101. Data $\pi^-p \to \rho^0 n$, $\pi^+n \to \rho^0 p$, $\pi^-p \to \rho^- p$:

1.5 GeV/c: J. Katz, private communication (1970).

2.3 GeV/c: S. Hagopian (Florida), private communication (1971).

2.06, 2.46, 3.12 GeV/c: E. Colton (LRL), private communication (1971).

2.77 GeV/c: J. P. Baton (Saclay), private communication (1971).

4.16 GeV/c: P. B. Johnson et al., Phys. Rev. 176, 1651 (1968).

6.95 GeV/c: Toronto-Wisconsin Collaboration, private communication (1971).

8 GeV/c: W. Selove et al., Phys. Rev. Letters 21, 952 (1968), and J. A. Poirier et al., Phys. Rev. 163, 1462 (1967).

11.2 GeV/c: CERN-Munich Collaboration, Nucl. Phys. B7, 1 (1968).

102. Data $\pi^+p \to \rho^+p$:

3.7 GeV/c: J. MacNaughton (LRL), private communication (1971).

4 GeV/c: ABBBHLM Collaboration, Phys. Rev. 138, 897 (1965).

5 GeV/c: DNPT Collaboration, Nucl. Phys. B22, 45 (1970).

8 GeV/c: ABC Collaboration, Nucl. Phys. B8, 45 (1968).

103. np CEX 1.73 GeV/c, R. E. Mischke et al., Phys. Rev. Letters 23, 542 (1969); 8 GeV/c, E. L. Miller, et al., Phys. Rev. Letters 26, 984 (1971). The normalization of this data is a factor of two bigger than the old 8 GeV/c data. This has markedly improved the agreement of the PMA model with $np \to pn$. $\bar{p}p$ CEX 1.8 GeV/c, W. Atwood et al., Phys. Rev. D2, 2519 (1970); 7 GeV/c, P. Astbury et al., Physics Letters 22, 537 (1966); 23, 160 (1966); 8 GeV/c, W. Beusch et al., preprint (1970). $\gamma p \to n\pi^+$, $\gamma n \to p\pi^-$ 16 GeV/c, A. M. Boyarski et al., Phys. Rev. Letters 20, 300 (1968), ibid. 21, 1767 (1968) and preprint (1968).

104. The data in Fig. 39 is taken from: (A) $0 \leq -t' \leq 0.2$ (GeV/c)^2, p_{lab} = 8 GeV/c (Ref. 92); (B) $0 \leq -t' \leq 0.2$ (GeV/c)^2, p_{lab} = 5 GeV/c (BDNPST Collaboration, Physics Letters *28B*, 72 (1968).)

105. The data in Fig. 40 is taken from: (A) $0 \leq -t' \leq 0.55$ (GeV/c)^2, p_{lab} = 8 GeV/c; (B) $0 \leq -t' \leq 0.6$ (GeV/c^2), p_{lab} = 5 GeV/c; (C) all t, p_{lab} = 2.67 GeV/c; (D) all t, p_{lab} = 2.3 GeV/c. (A, B) are from papers cited in Ref. 104 while (C, D) is from W. Ko, G. Gidal, and D. F. Grether, UCRL-19779 preprint (1970) and Winston Ko, private communication (1971).

106. We did not plot the data of J. H. Freidman and R. R. Ross, Phys. Rev. Letters *22*, 152 (1969), as it uses a different notation. The plotted data in Fig. 41 is from: (A) $K^+p \to K^{*o}\Delta^{++}$, $0 \leq -t' \leq 0.25$ (GeV/c)^2, p_{lab} = 5 GeV/c, W. de Baere *et al.*, Nuovo Cimento *61A*, 397 (1969); (B) $K^+p \to K^{*o}\Delta^{++}$, $1 \leq \cos\theta_{c.m.} \leq 0.8$, p_{lab} = 2.53, 2.76, 3.2 GeV/c, G. S. Abrams, L. Eisenstein, J. Kim, D. Marshall, T. A. O'Halloran, W. Shufeldt, and J. Whitmore, Phys. Rev. *D1*, 2433 (1970); (C) $K^-n \to \bar{K}^{*o}\Delta^-$, $0 \leq -t' \leq 0.25$ (GeV/c)^2, p_{lab} = 3 GeV/c, SABRE Collaboration, Nucl. Phys. *B17*, 289 (1970); (D) $K^-n \to \bar{K}^{*o}\Delta^-$, $0 \leq -t' \leq 0.5$ (GeV/c)^2, p_{lab} = 5.5 GeV/c, B. Werner *et al.*, Nucl. Phys. *B23*, 37 (1970), and B. Musgrave, private communication (1971); (E) $K^+p \to K^{*o}\Delta^{++}$, all t, p_{lab} = 1.81 to 2.17 GeV/c, Ref. 84.

107. The curves in Fig. 45 correspond to A-type measurements: target polarized along beam, final nucleon polarization observed in respectively the ρ_{33} and ρ_{11} Δ^{++} decay elements. These are impossible experiments: however, the feasible $\pi^+p \to K^+Y^{*+}$ and $K^-p \to \pi^-Y^{*+}$ reactions give essentially identical results. The curves are plotted for both the s and t channel choices for the Δ decay reference frame. We plot predictions of the quark model with s (- . -) and t-channel (– – – –) additivity frames. The theoretical curves (strong cut (——), weak cut (········)) come from absorbing an input Regge pole obeying t-channel SSD (Eq. (30)). R-type measurements -- target polarized ⊥ beam -- give similar differences between models and channels.

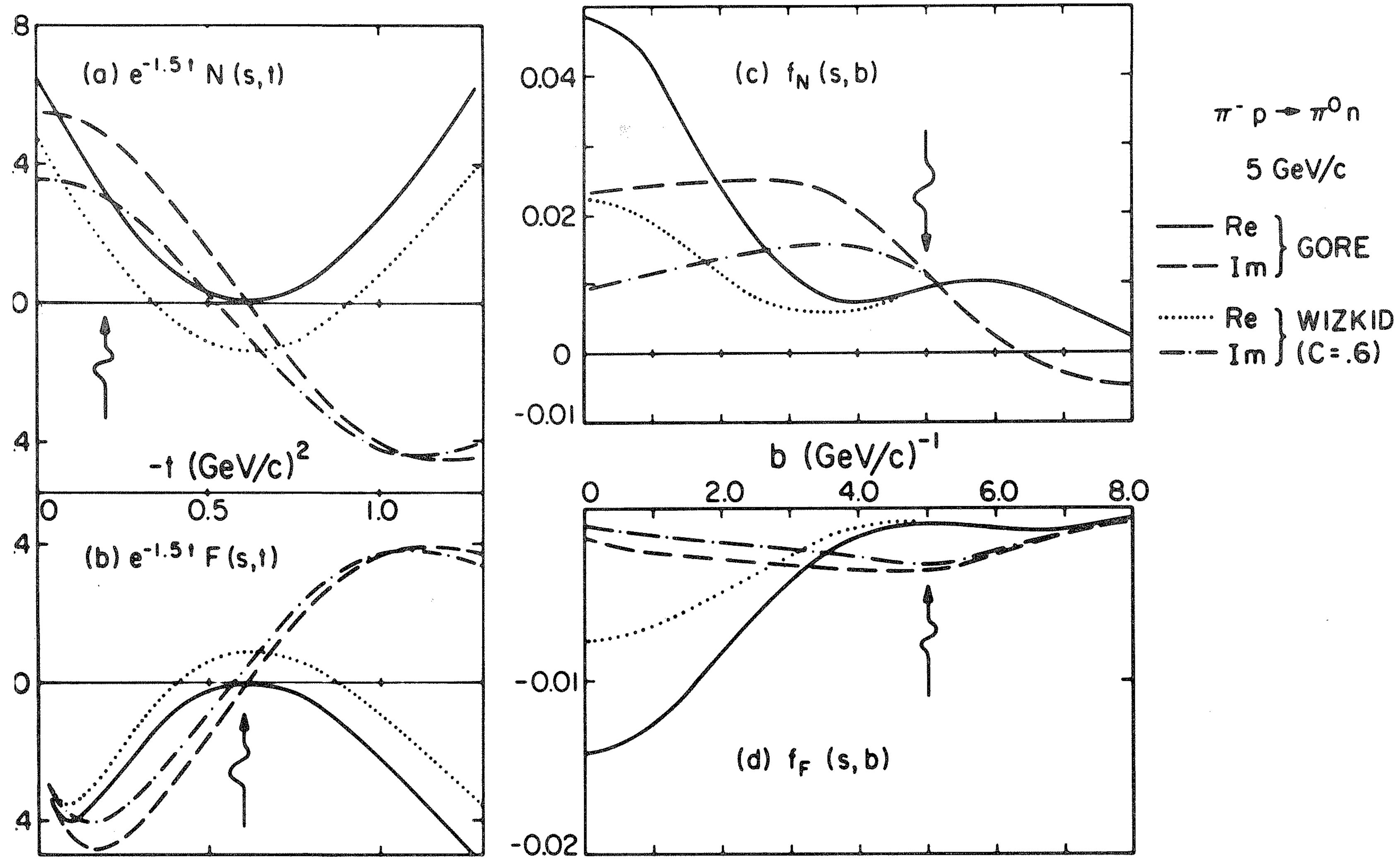

Figure 1: Nonflip (N) and spinflip (F) s-channel amplitudes for $\pi^- p \to \pi^0 n$ at 5 GeV/c. Amplitudes are normalized as in Eq. (1a). Also shown are their respective Fourier-Bessel transforms (f_N, f_F) defined by Eq. (5). Shown are the real and imaginary parts for two theories: EXD Regge pole theory (GORE) and the weak cut model (WIZKID) which results from absorbing GORE with S-wave absorption constant C = 0.6 (cf. Eq. (6)). The jagged arrow ($\rightsquigarrow$) marks magic points: $t = -0.2$ in N and -0.6 $(\mathrm{GeV}/c)^2$ in $F(s,t)$; $b = 5$ $(\mathrm{GeV}/c)^{-1} \simeq 1$ fermi in $f_{N,F}(s,b)$.

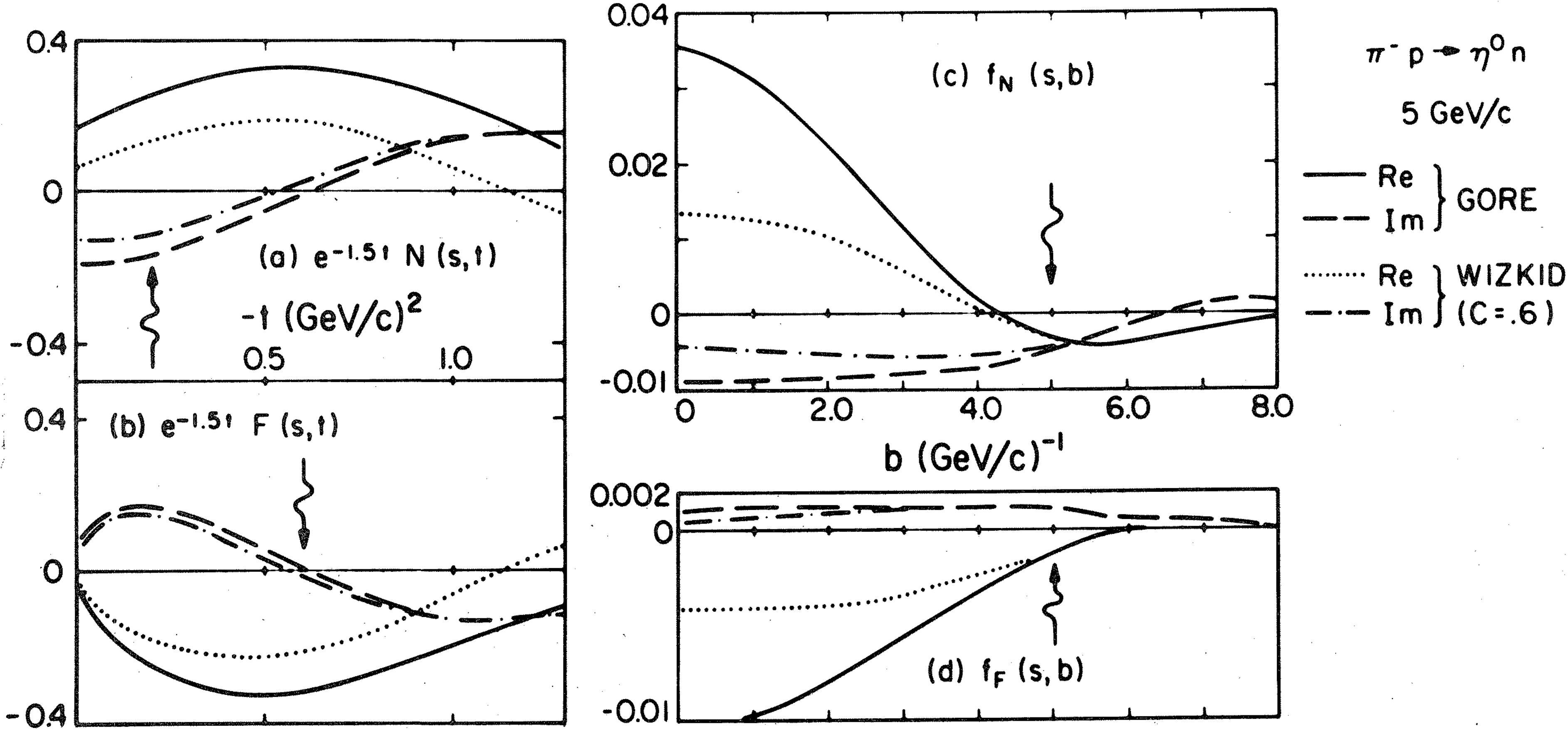

Figure 2: All quantities have the same meaning as Fig. 1 except that they are calculated for $\pi^- p \to \eta^0 n$ at 5 GeV/c.

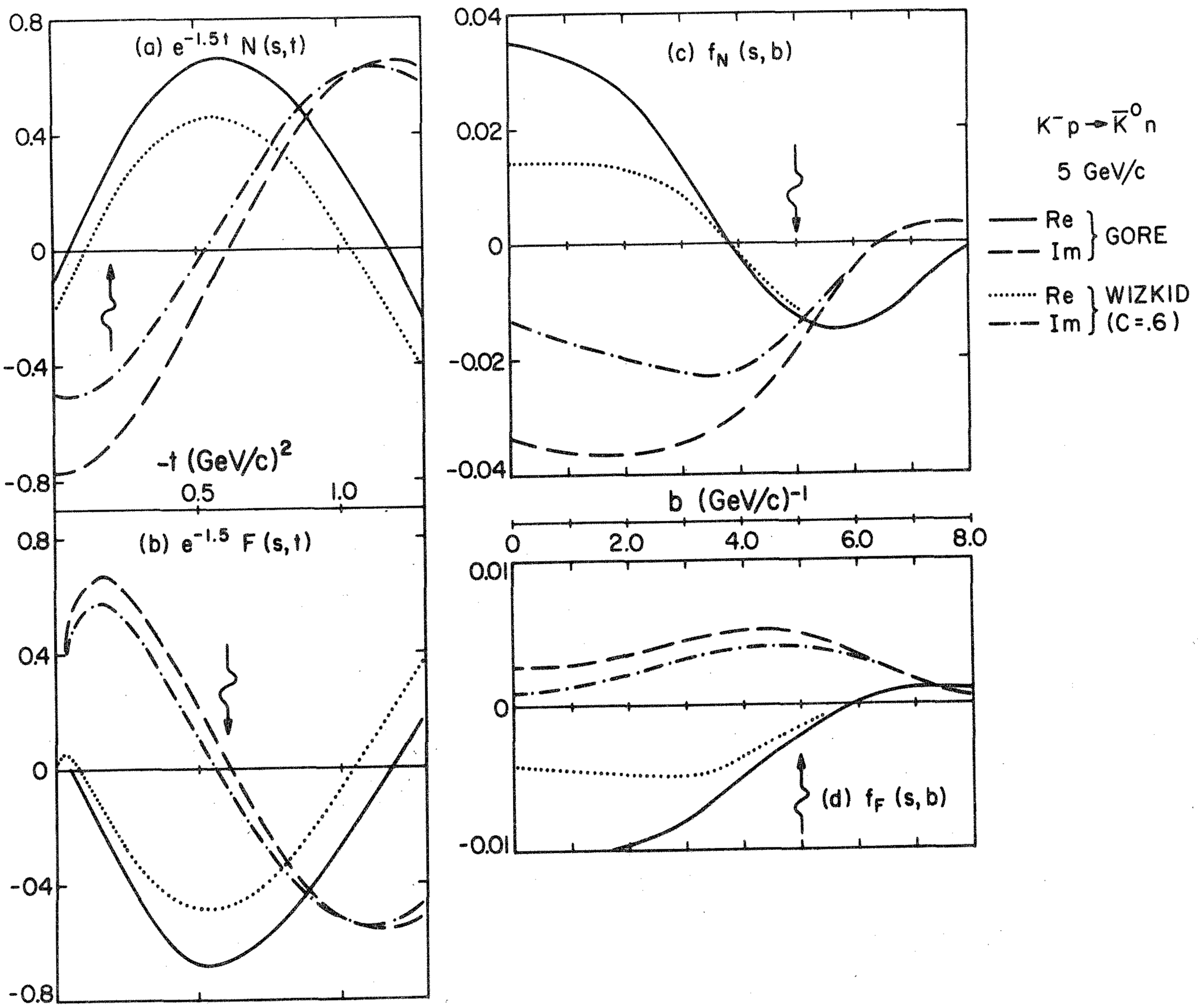

Figure 3: All quantities have the same meaning as Fig. 1 except that they are calculated for $K^-p \rightarrow \bar{K}^0 n$ at 5 GeV/c.

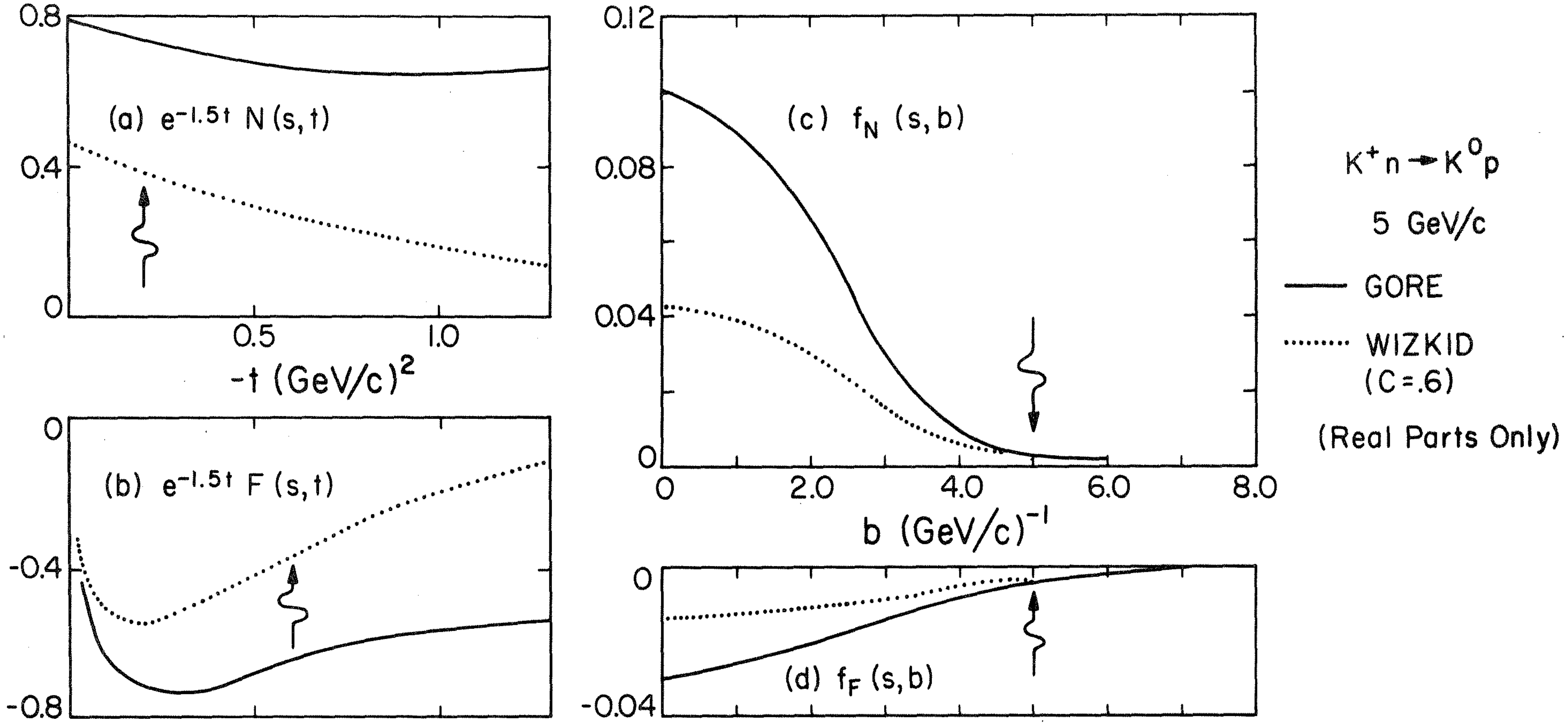

Figure 4: All quantities have the same meaning as Fig. 1 except that they are calculated for $K^+n \rightarrow K^0p$ at 5 GeV/c. Imaginary parts for amplitudes are not shown for they are zero in these simple theories.

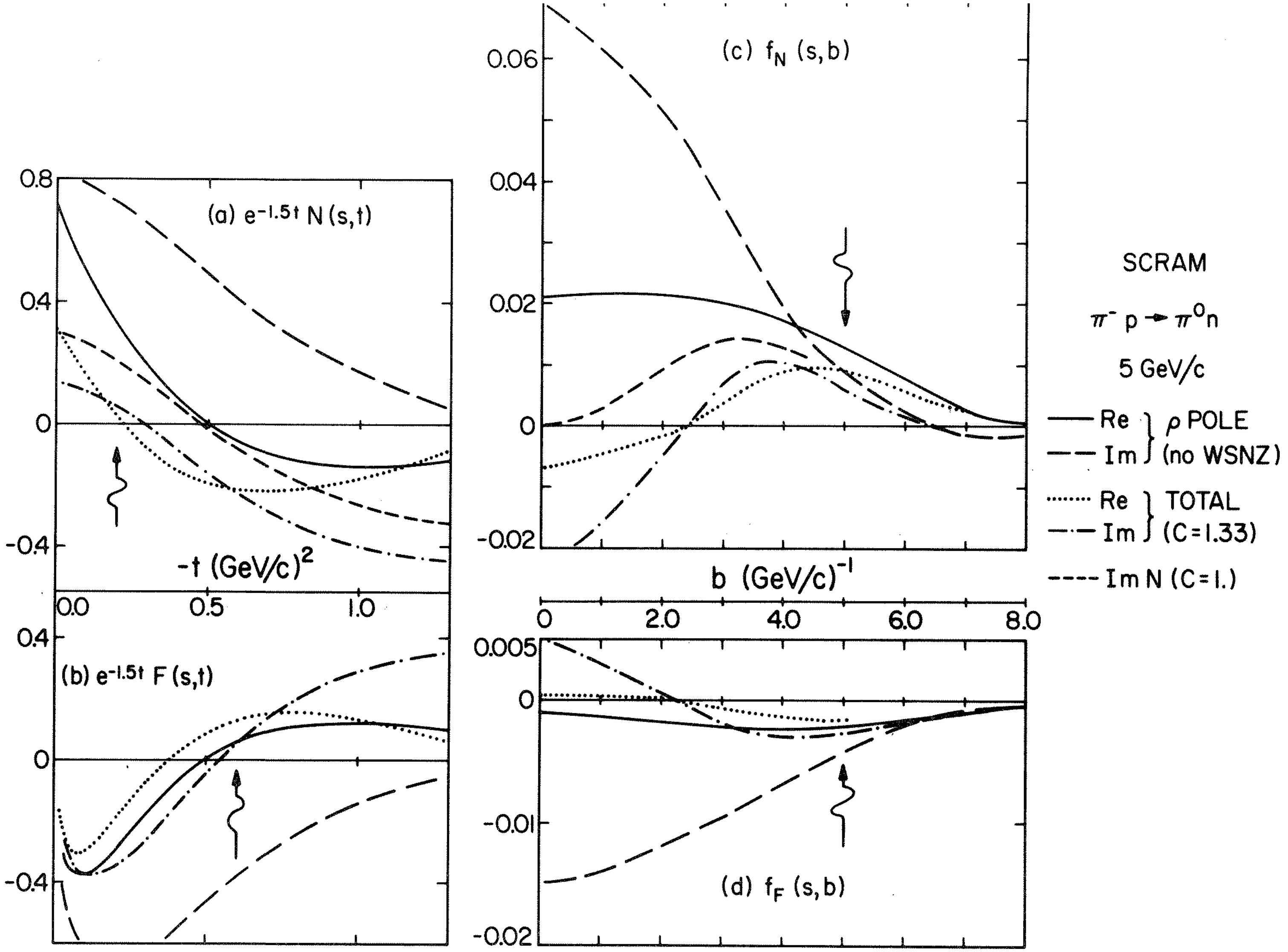

Figure 5: All quantities have the same meaning as Fig. 1 except they are calculated from a different theory. The pole terms have no WSNZ and the absorbed amplitudes correspond to the strong cut (SCRAM) model[7)] with S→wave absorption C = 1.33. We also show ImN for C = 1 which gives a better overall fit[15)] but the wrong position for the crossover zero in ImN.

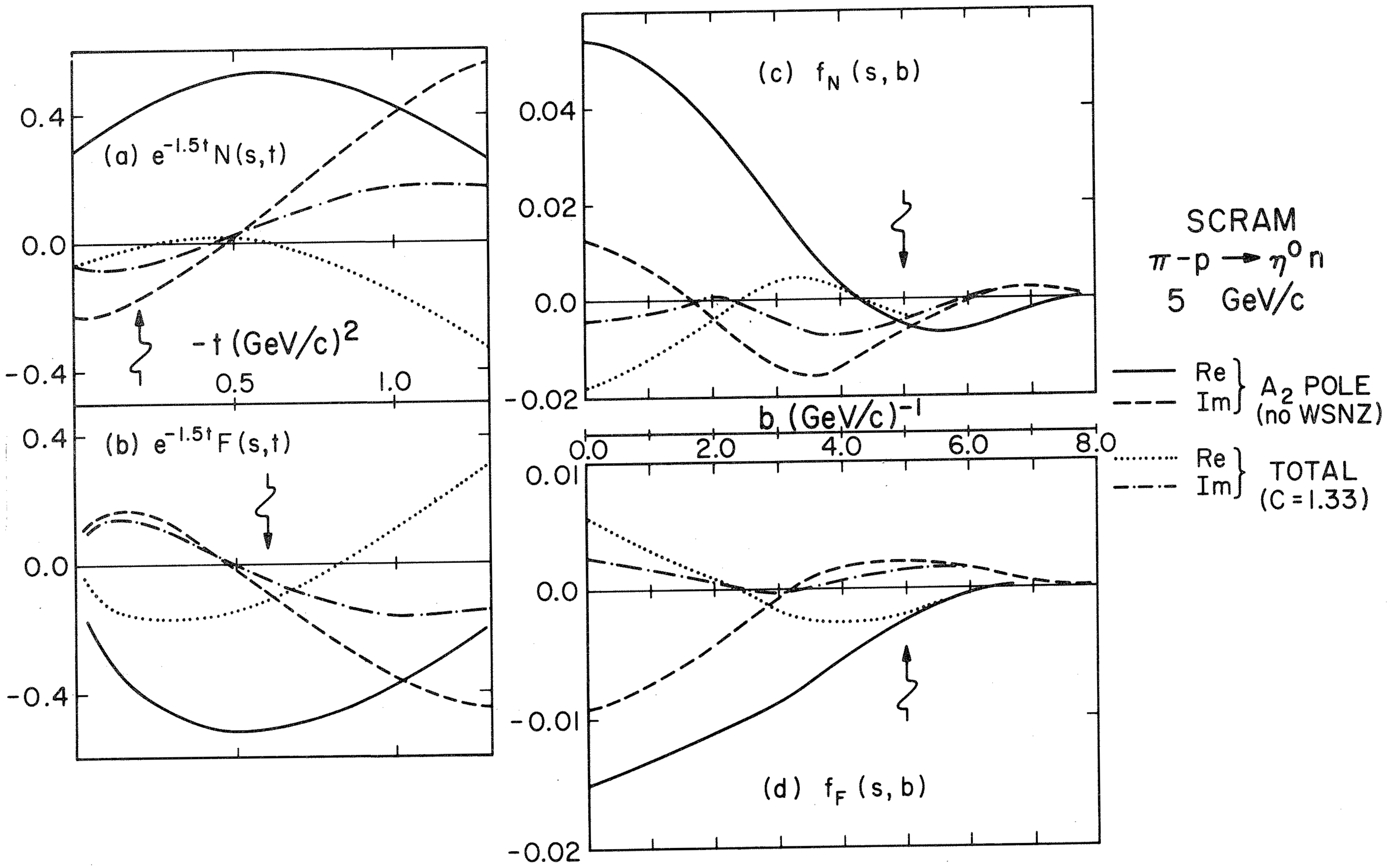

Figure 6: All quantities have the same meaning as Fig. 5 except they are calculated for $\pi^- p \rightarrow \eta^0 n$ at 5 GeV/c.

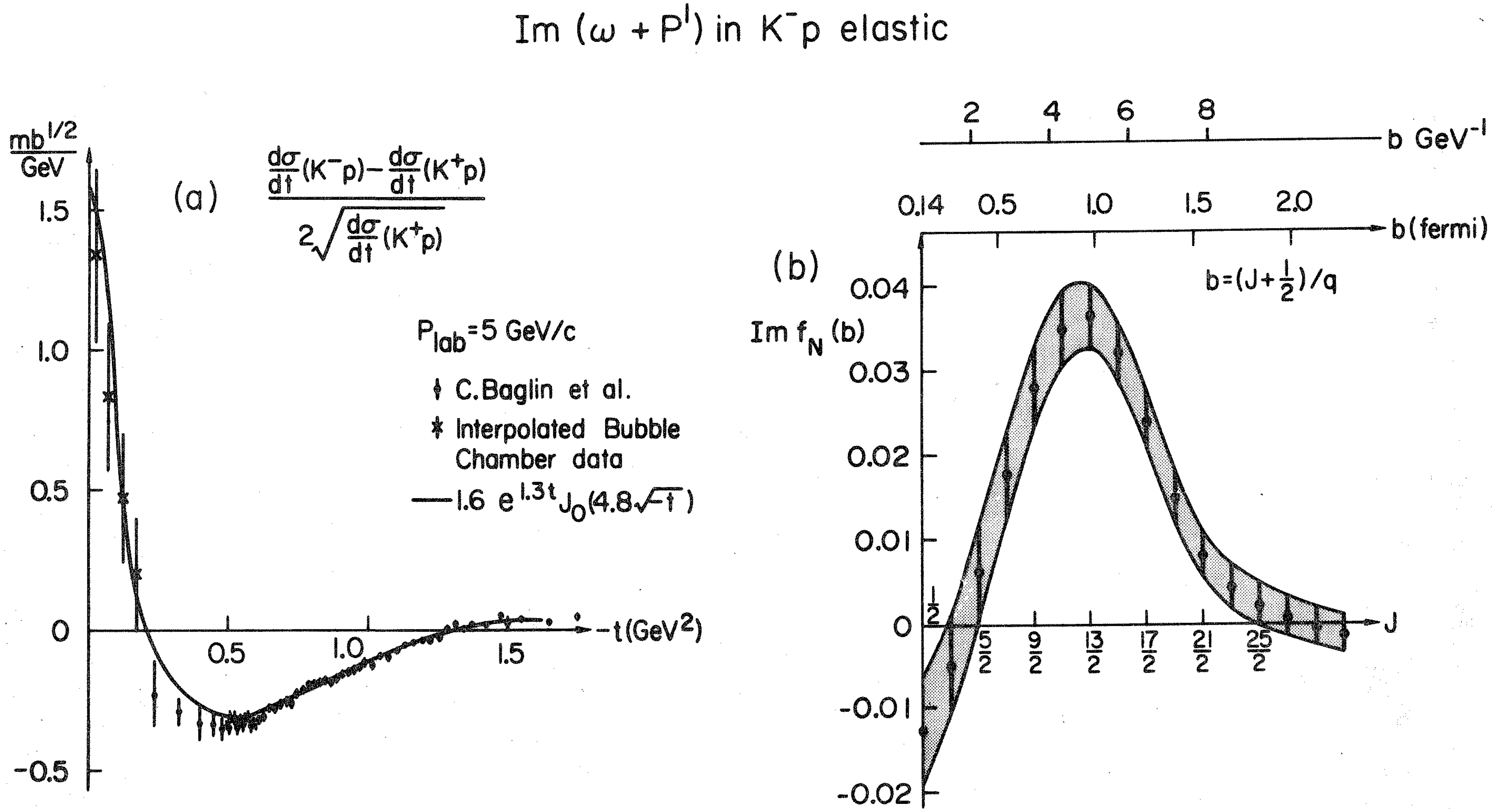

Figure 7: (a) 2 Imω = Im (ω + P') for K^-p elastic at 5 GeV/c. The curves are taken from ref. 18 and calculated as in Eq. (9). (b) Fourier-Bessel transform of (a) calculated from Eq. (5). (I have changed the scale: the original in ref. 18 was a factor of 2 bigger due to different convention for the normalization of partial wave amplitudes.)

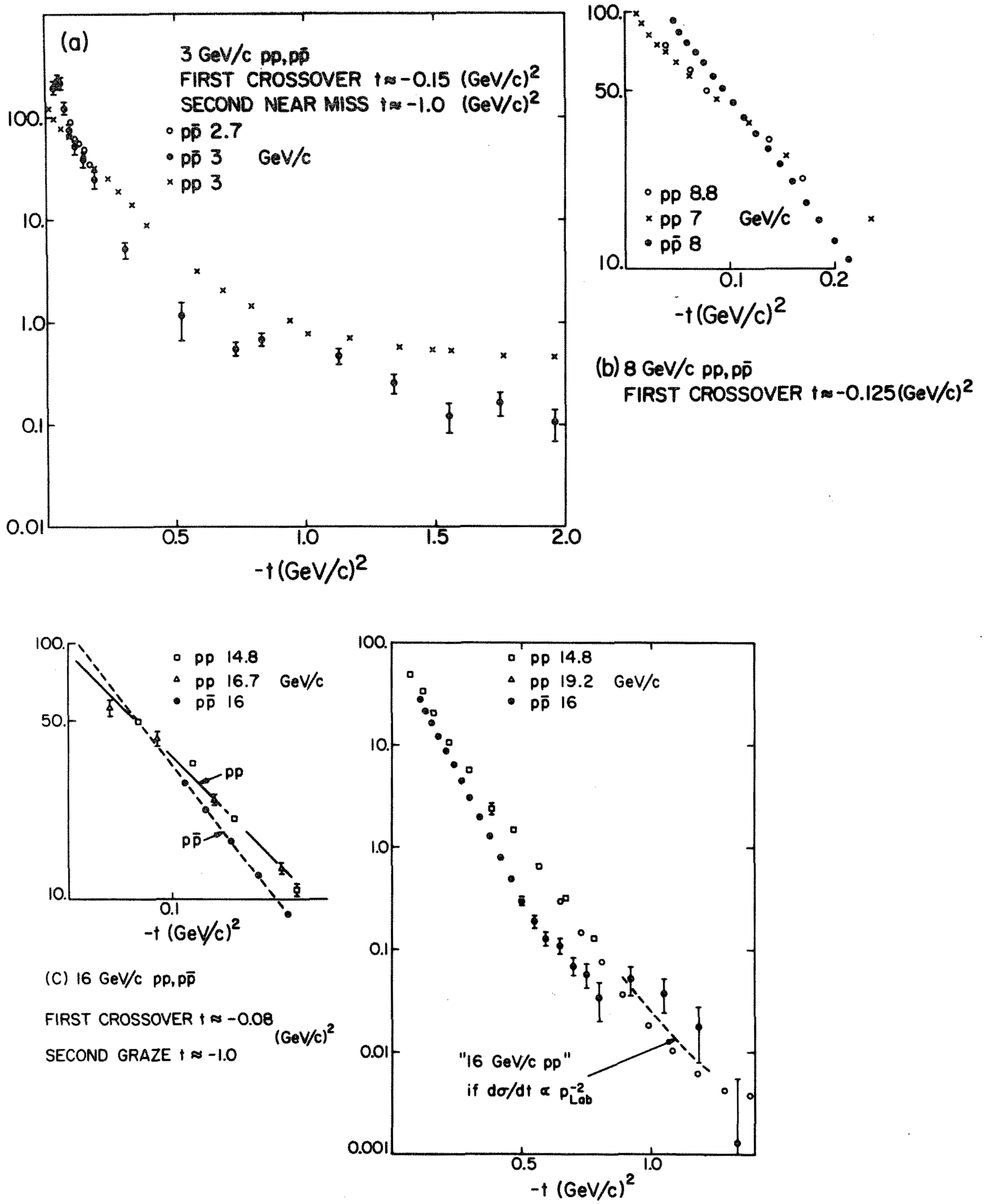

(b) 8 GeV/c pp,pp̄
FIRST CROSSOVER t≈-0.125(GeV/c)^2

(C) 16 GeV/c pp,pp̄

FIRST CROSSOVER t ≈ -0.08 (GeV/c)^2

SECOND GRAZE t ≈ -1.0

Figure 8: First and second crossovers in pp and pp̄ elastic scattering at (a) 3 (b) 8 and (c) 16 GeV/c. Plotted is dσ/dt in mb/(GeV/c)^2. Data is from: 3,7 GeV/c pp, A.R. Clyde UCRL-16275; 2.98 GeV/c pp, C.M. Ankenbrandt et al., Phys. Rev. 170, 1223 (1968); 8.8, 14.8 GeV/c pp, K.J. Foley et al., Phys. Rev. Letters 11, 425 (1963); 19.2 GeV/c pp, J.V. Allaby et al., Phys. Letters 28B, 67 (1968); 3 GeV/c pp̄ , B. Escourbes et al., Phys. Letters 5, 132 (1963); 8, 16 GeV/c pp, D. Birnbaum et al., Phys. Rev. Letters 23, 663 (1969).

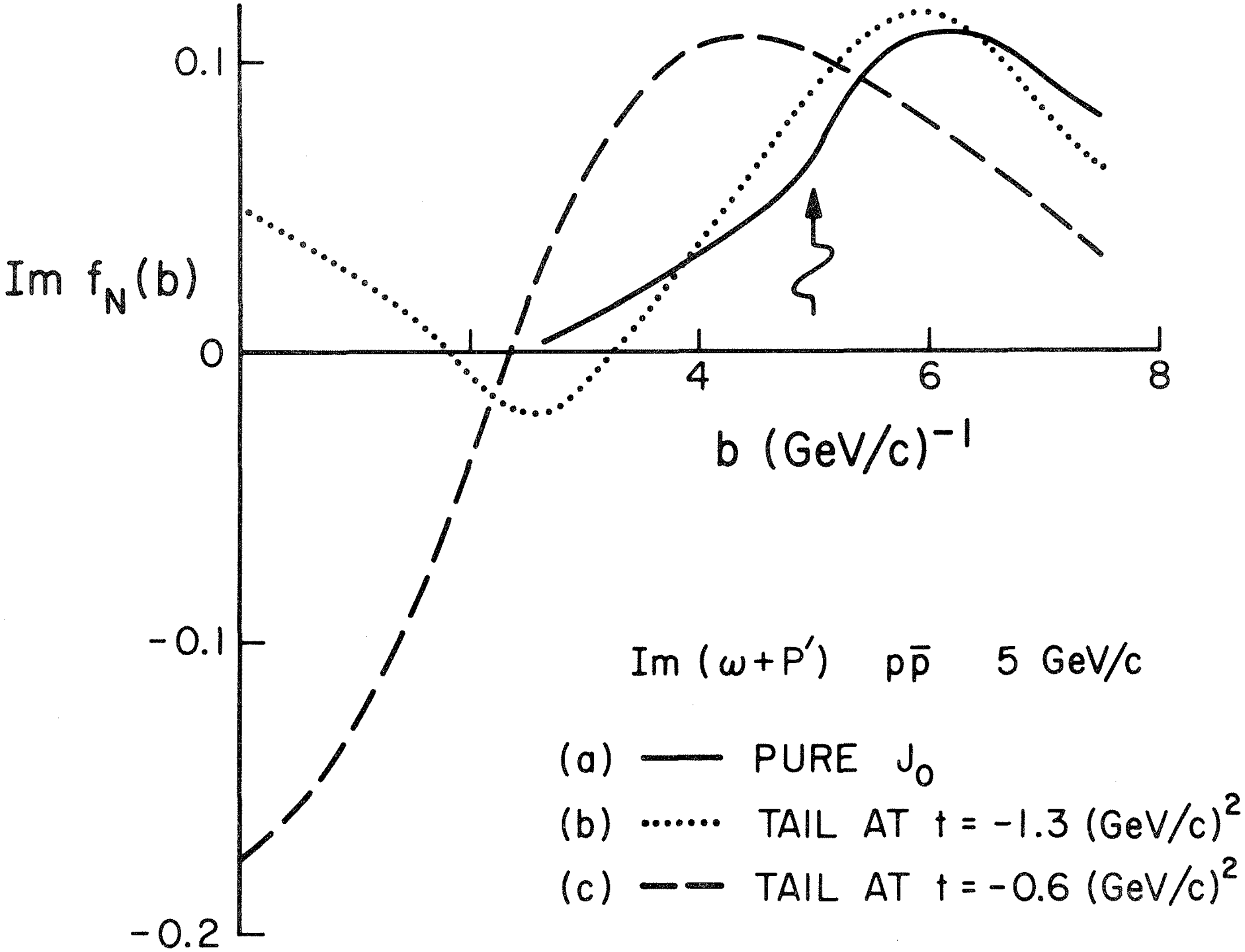

Figure 9: Im (ω + P') for $p\bar{p}$ elastic scattering at 5 GeV/c. The three curves come from partial wave analysing amplitudes (analogous to Eq. (9) and Fig. 7(a)) that agree with experiment for small $-t$ but have different forms in the larger $-t$ region (where assumptions underlying Eq.(9) may break down). The precise forms used to generate curves (a), (b), (c) are detailed in (respectively) Eq.'s (10 a,b,c) of the text. Jagged arrow marks magic value b = 1 fermi. This figure reports unpublished work with C. B. Chiu.

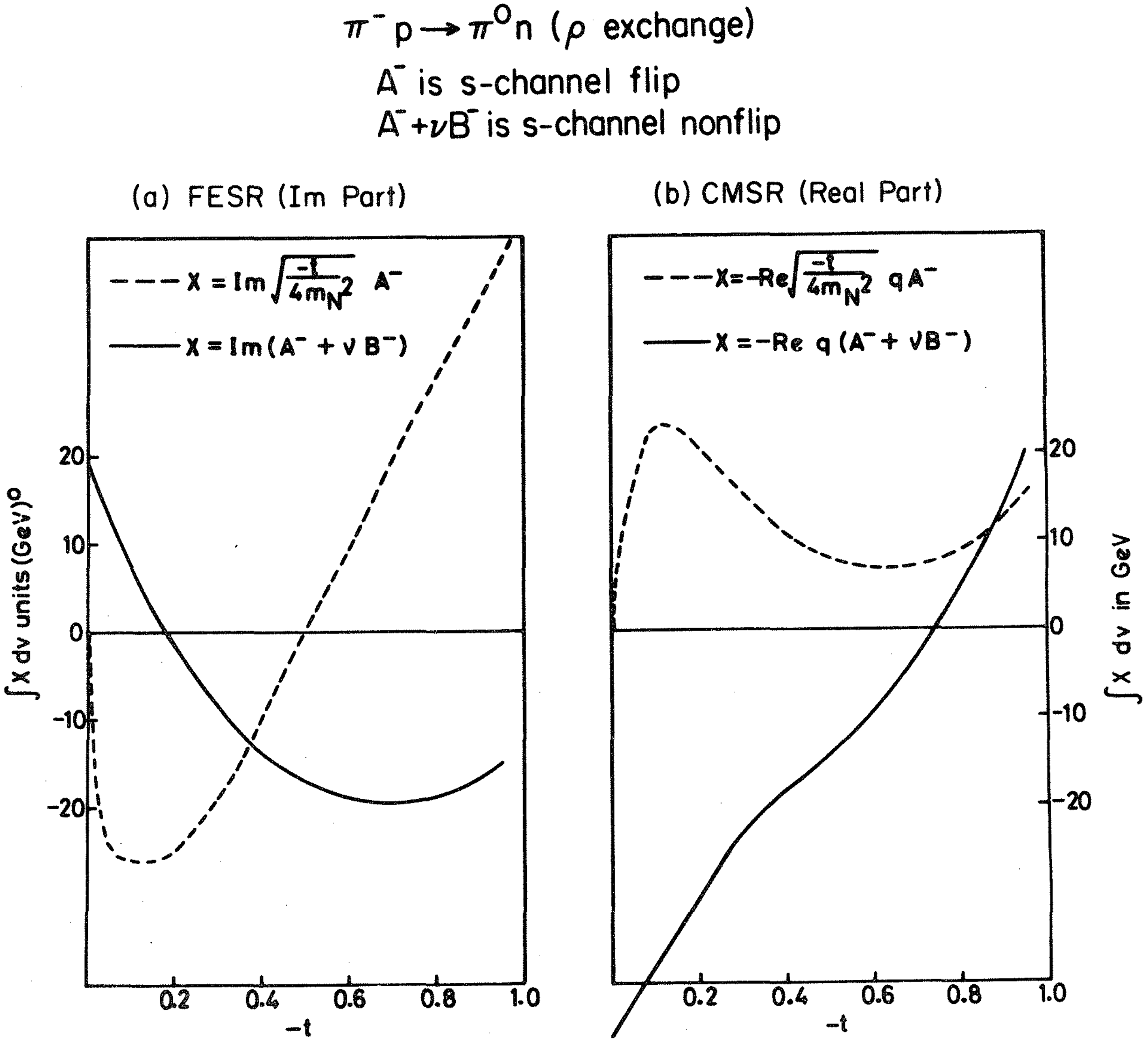

Figure 10: Real and imaginary parts of the ρ exchange s-channel helicity nonflip ($A^- + \nu B^-$) and helicity flip (A^-) amplitudes. These were determined by FESR (imaginary) and CMSRs (real parts) in ref. 14. The attribution to real and imaginary parts is only correct in the pole approximation.

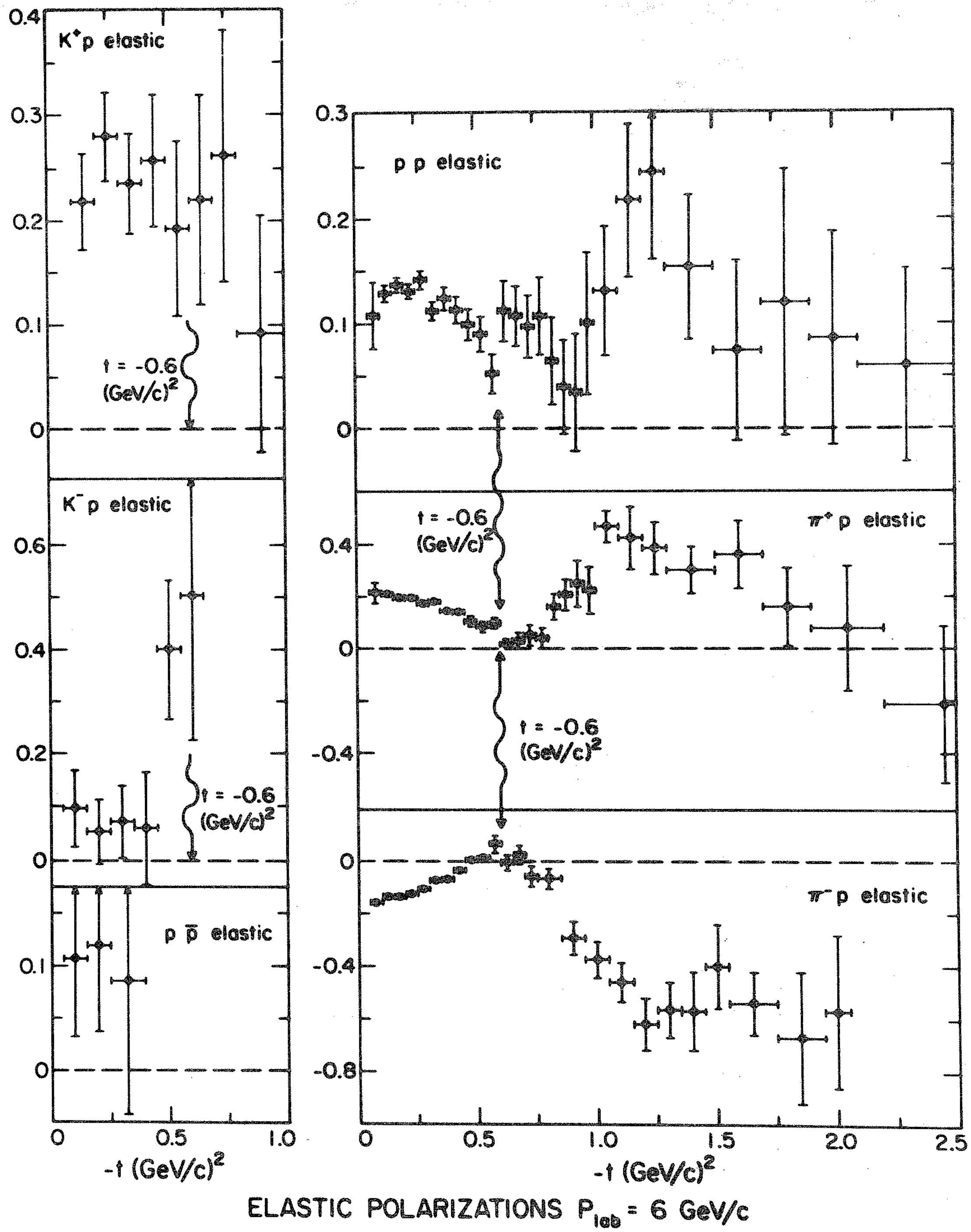

Figure 11: $K^{\pm}p$, $\pi^{\pm}p$, pp and $p\bar{p}$ elastic polarizations at 6 GeV/c from M. Borghini et al., Phys. Letters 31B, 405 (1970). The arrow marks t = −.6 (GeV/c)^2. The simple absorption model predicts a single zero there, for all elastic polarizations, in contradiction to experiment. The data instead agrees very well with EXD Regge theory. [Double zero in $\pi^{\pm}p$, no zero in $K^{\pm}p$, $p\overset{(-)}{p}$ at −.6]. See Section 2.1B of text and Figure 1 of Lovelace's talk. The new data presented by Dick at this conference strengthens these conclusions.

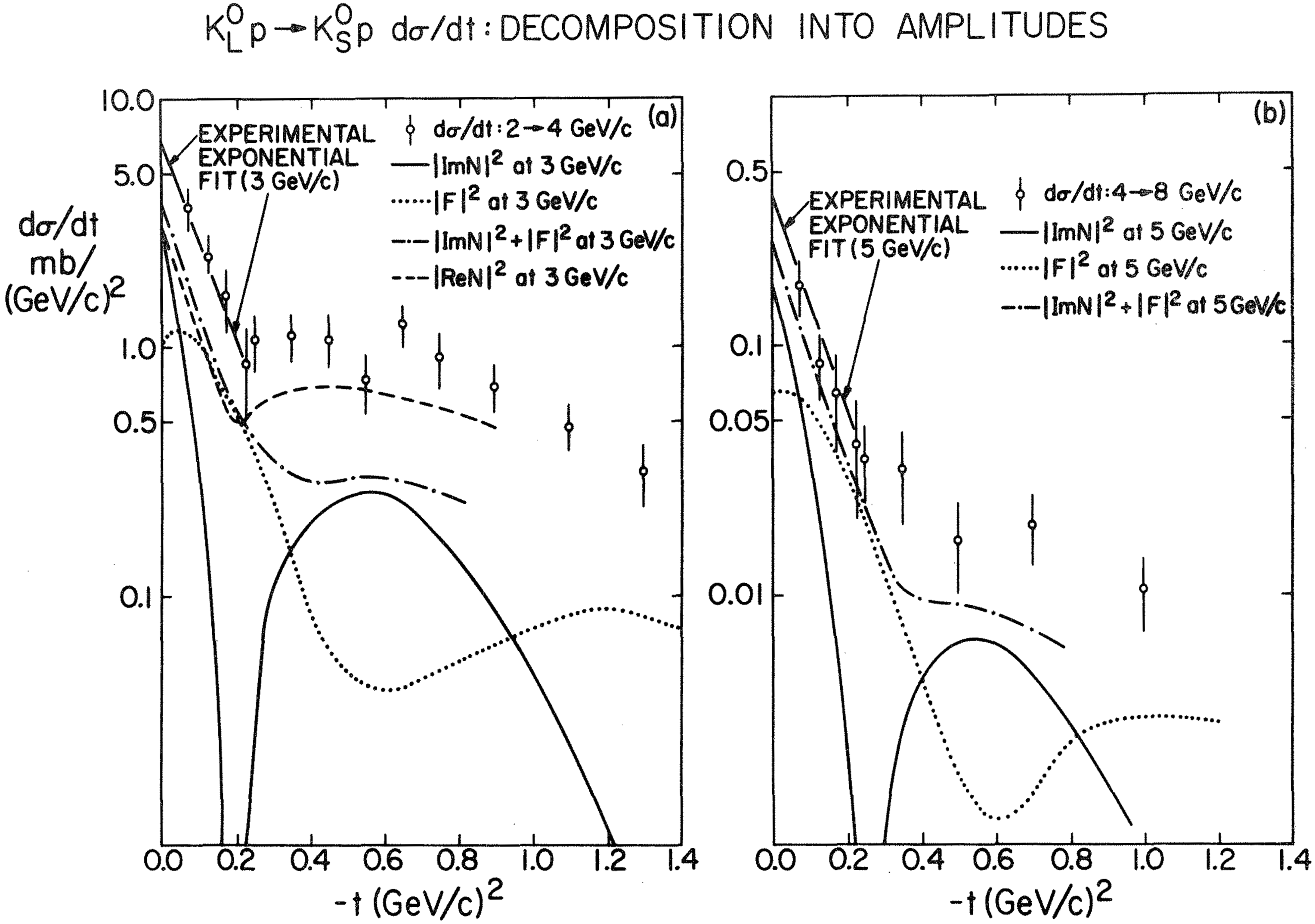

Figure 12: Decomposition of $K_L^o p \to K_s^o p$ (data from A. D. Brody et. al., Phys. Rev. Lett. 26, 1050 (1971)) into constituent amplitudes (Eq. (13)) at (a) 3 and (b) 5 GeV/c. The determination of the $|ImN|^2$ and $|F|^2$ curves is described in Section 2.1B of the text; —·— represents the sum of these two. At 3 GeV/c, (the higher energy has too low statistics) we mark (----) $|ReN|^2$ determined by subtraction of data (ɸ) and remainder —·— curves. This reports unpublished work with C. B. Chiu.

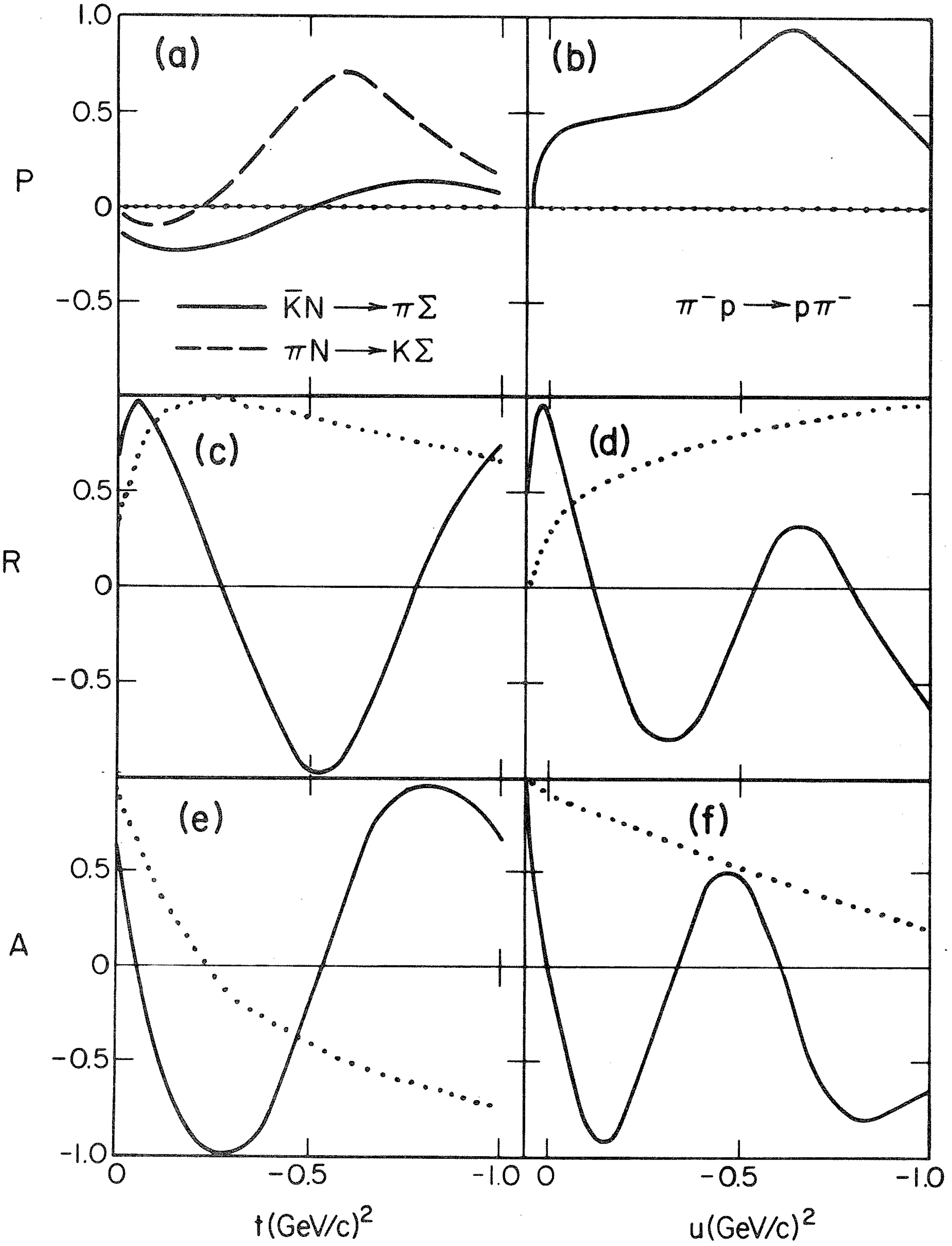

Figure 13: Observables (Equations (3), (14)) (a) P (c) R and (e) A for $\bar{K}N \to \Sigma\pi$ at 4.07 GeV/c; (b) P (d) R and (f) A for $\pi^- p$ backward elastic at 9.85 GeV/c. —— line denotes SCRAM and ······· GORE model. R and A predictions are similar for $\pi N \to K\Sigma$ w.r.t. $\bar{K}N \to \pi\Sigma$ and $K^- p \to \Sigma^+\pi^-$ w.r.t. $\pi^- p \to p\pi^-$. See Ref. 3 for details.

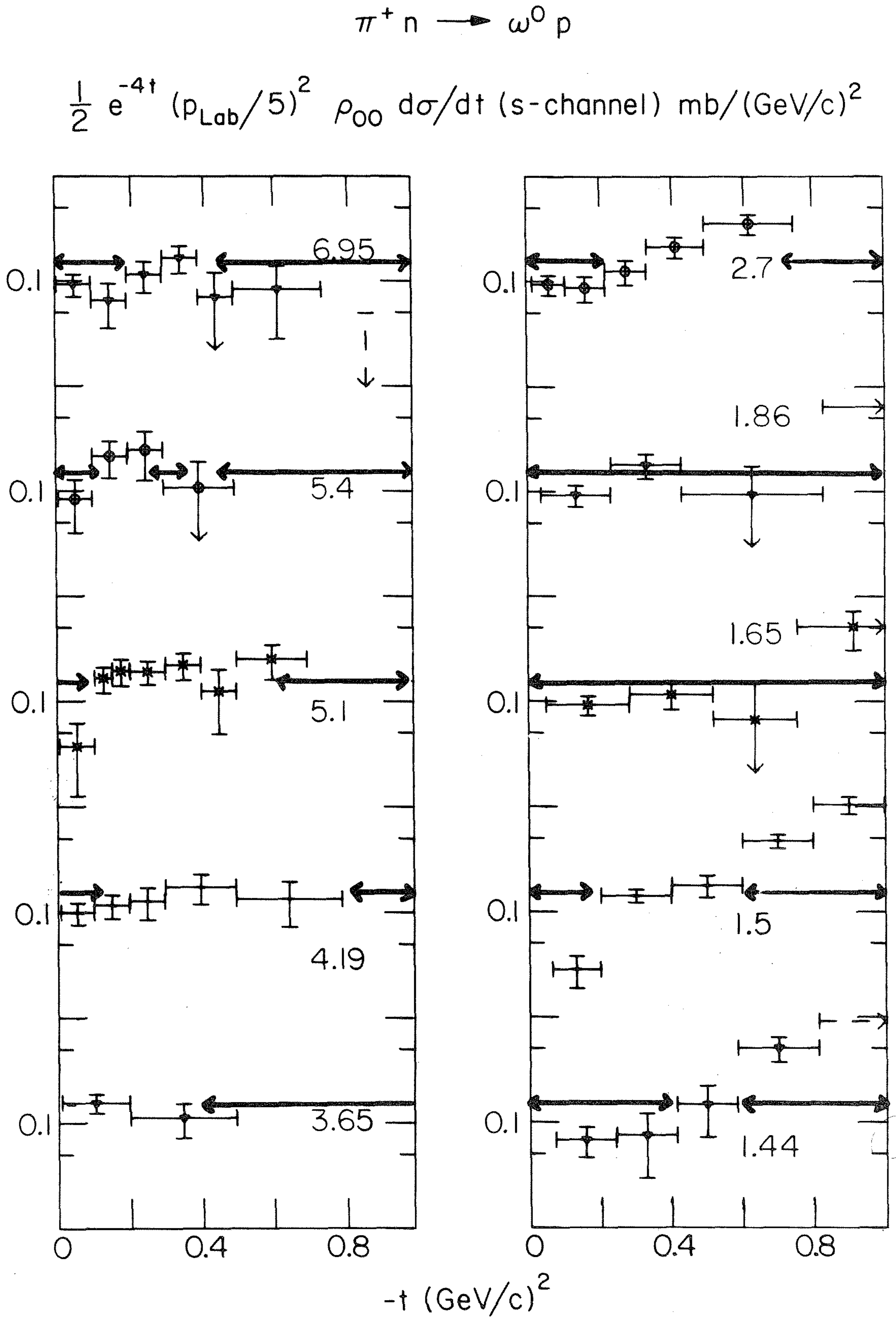

Figure 14: s-channel ρ_{00} $d\sigma/dt$ $\pi^+ n \to \omega^0 p$ data from Ref. 98. Solid line marks 0.15 approximate "fit" to $\pi N \to \omega N$.

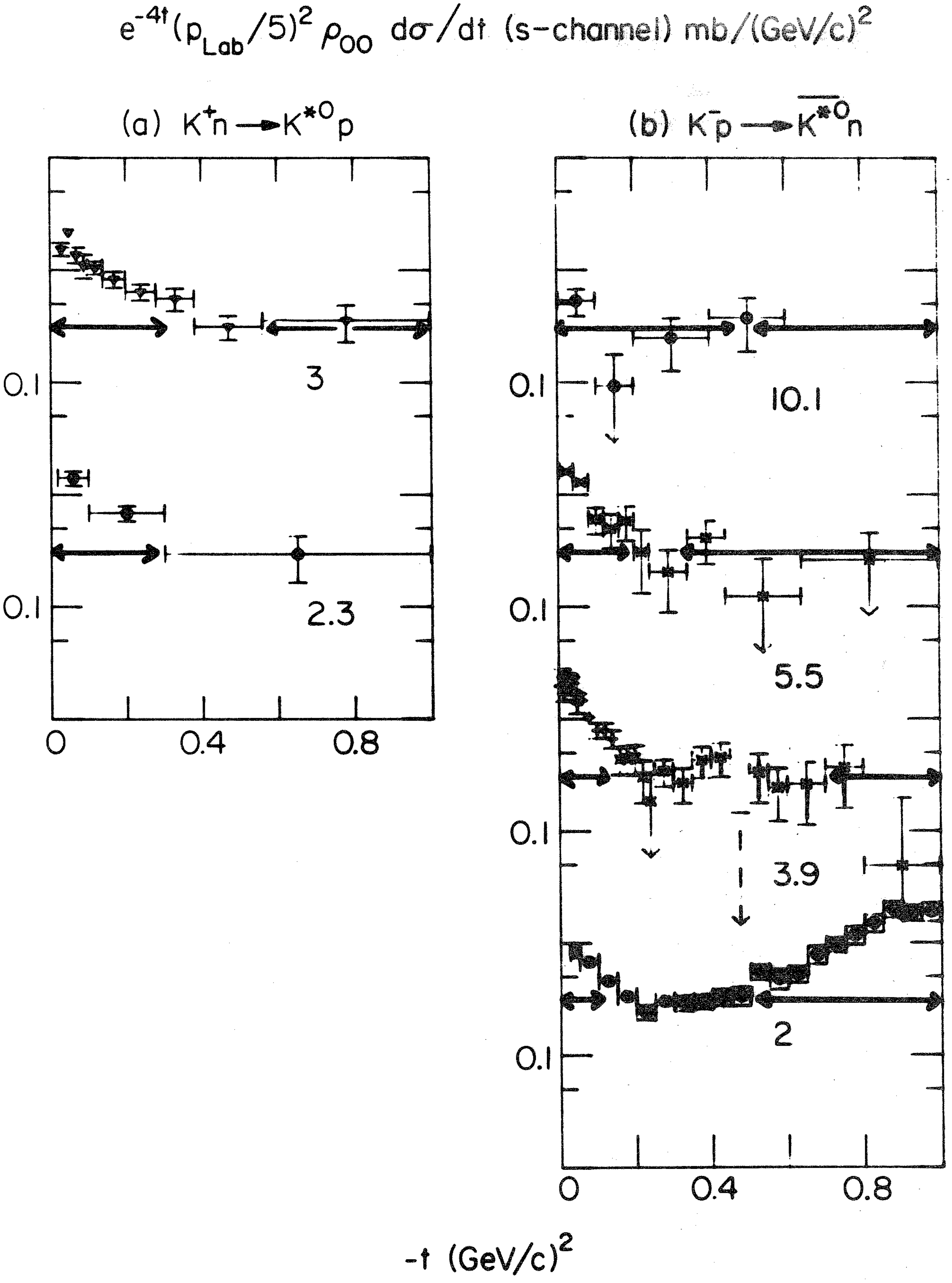

Figure 15: s-channel ρ_{00} dσ/dt (a) $K^+n \rightarrow K^{o*}p$ (b) $K^-p \rightarrow \bar{K}^{o*}n$ from refs. 99 and 100. Solid line marks 0.3; twice approximate "fit" to $\pi N \rightarrow \omega N$.

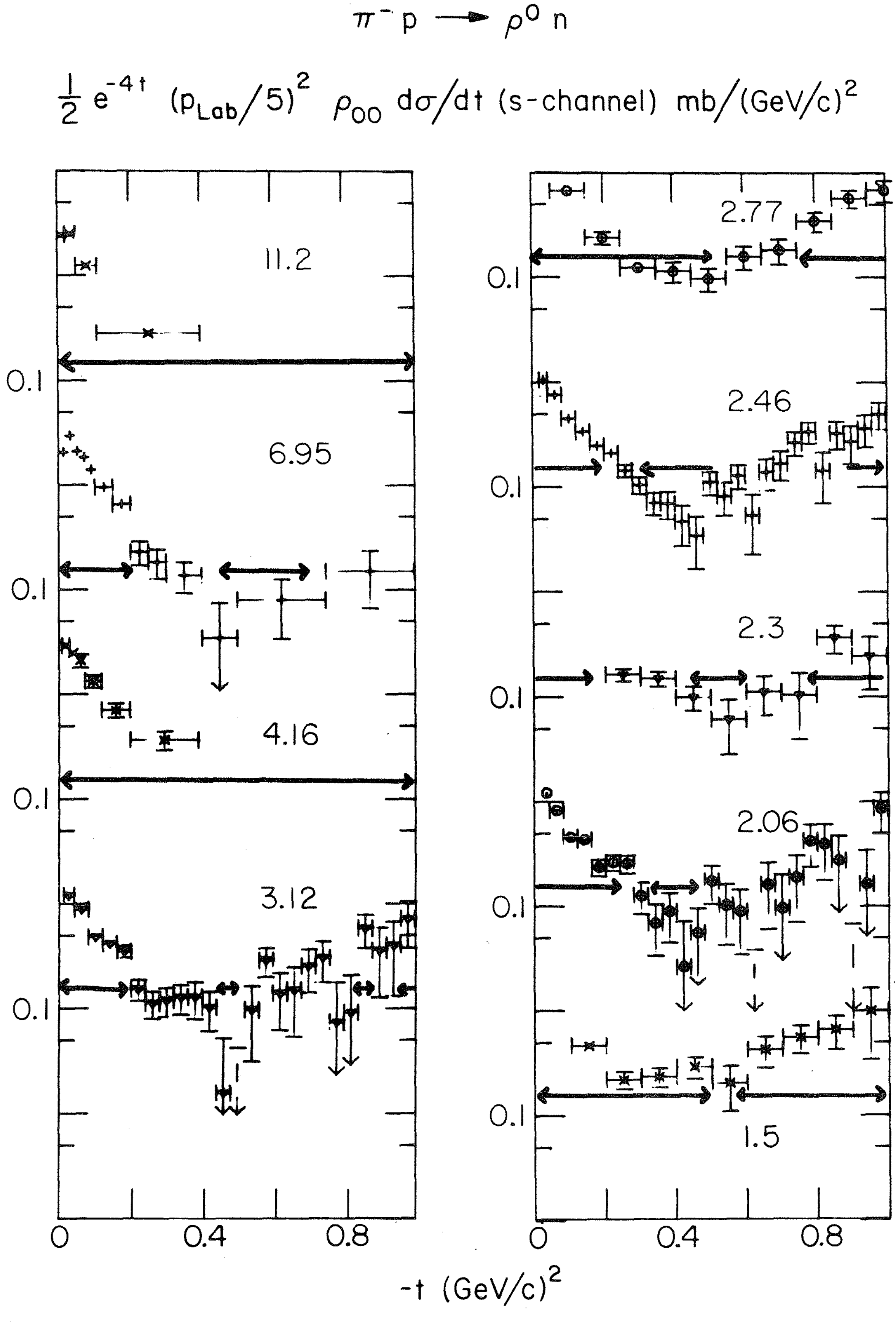

Figure 16: s-channel ρ_{00} $d\sigma/dt$ $\pi^- p \to \rho^0 n$, $\pi^+ n \to \rho^0 p$ data from Ref. 101. Solid line marks 0.15: approximate "fit" to $\pi N \to \omega N$.

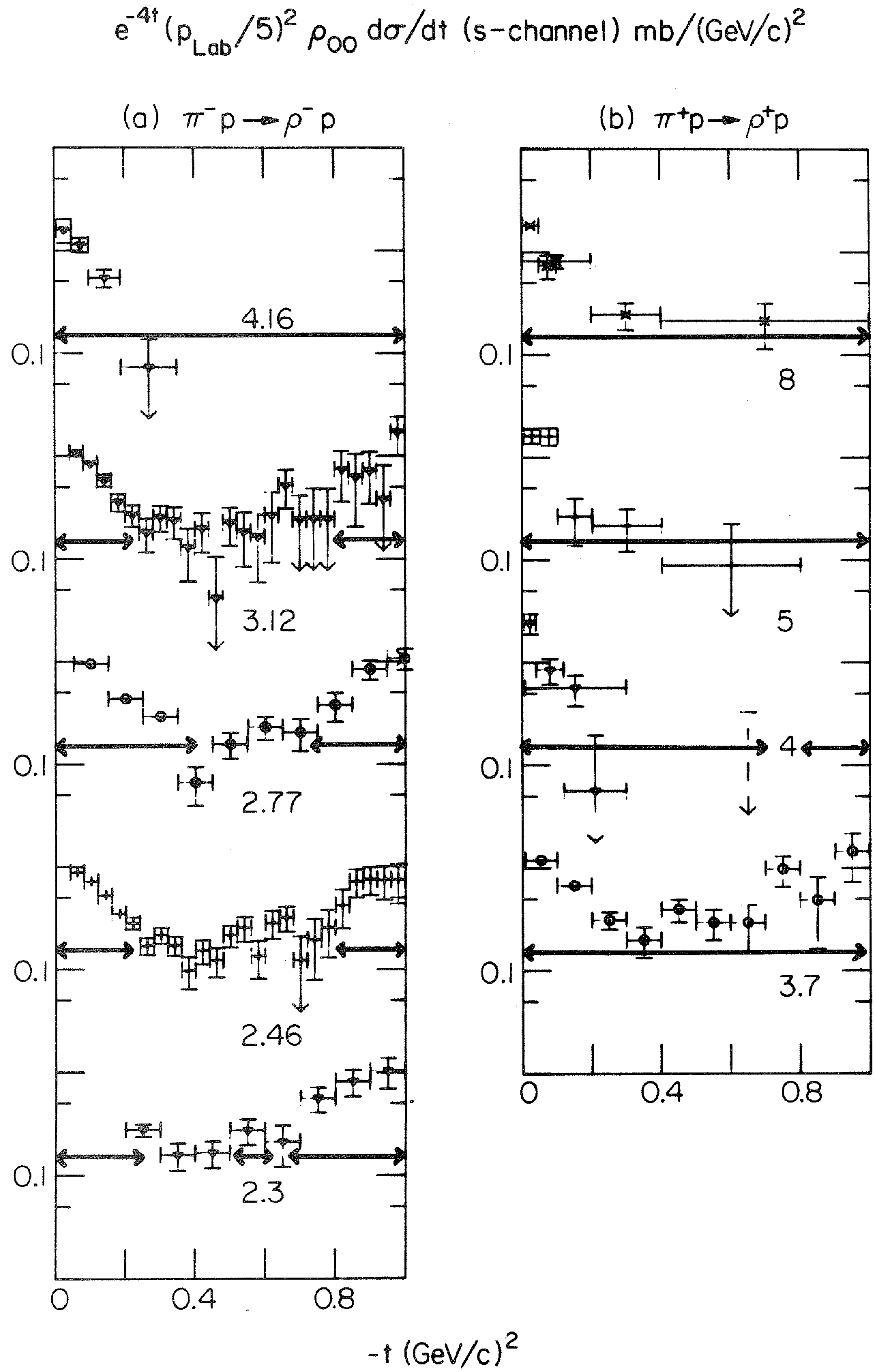

Figure 17: s-channel ρ_{00} $d\sigma/dt$ (a) $\pi^- p \rightarrow \rho^- p$ from Ref. 101; (b) $\pi^+ p \rightarrow \rho^+ p$ data from Ref. 102. Solid line marks 0.15: approximate "fit" to $\pi N \rightarrow \omega N$.

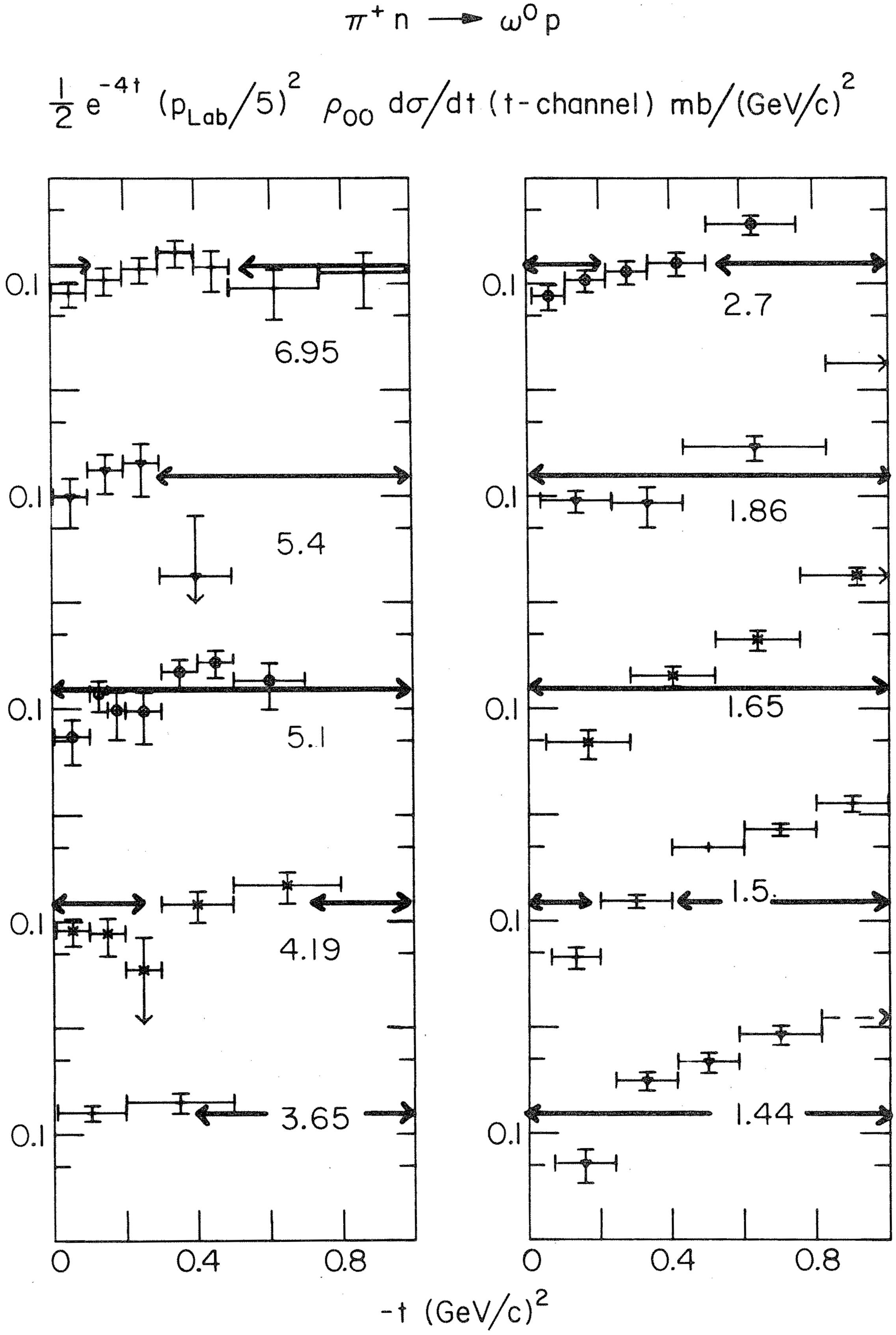

Figure 18: t-channel ρ_{00} $d\sigma/dt$ $\pi^+ n \rightarrow \omega^o p$ data from Ref. 98. Solid line marks 0.15 approximate "fit" to $\pi N \rightarrow \omega N$.

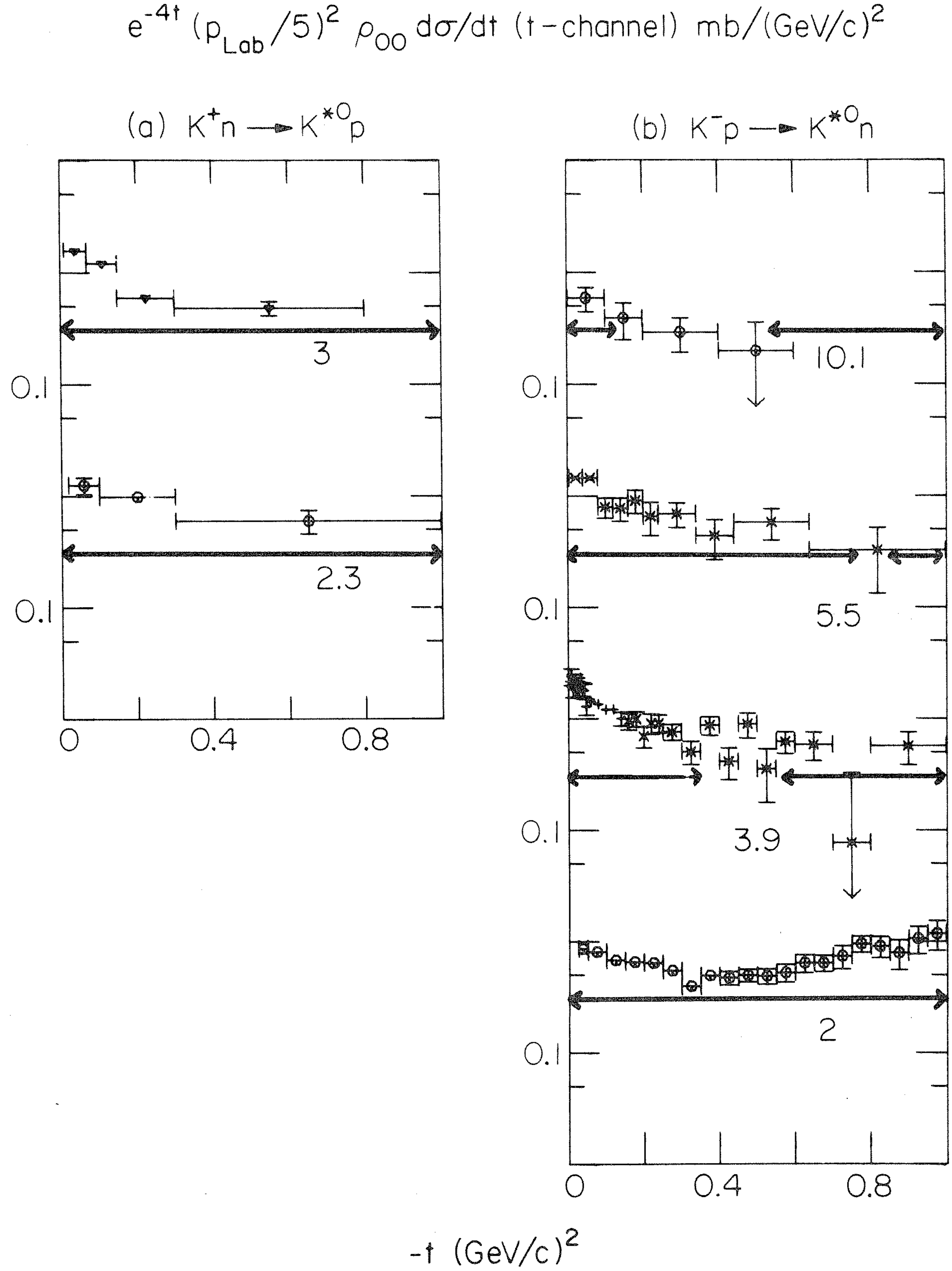

Figure 19: t-channel ρ_{00} $d\sigma/dt$ (a) $K^+n \to K^{o*}p$ (b) $K^-p \to \overline{K}^{o*}n$ from refs. 99 and 100. Solid line marks 0.3: twice approximate "fit" to $\pi N \to \omega N$.

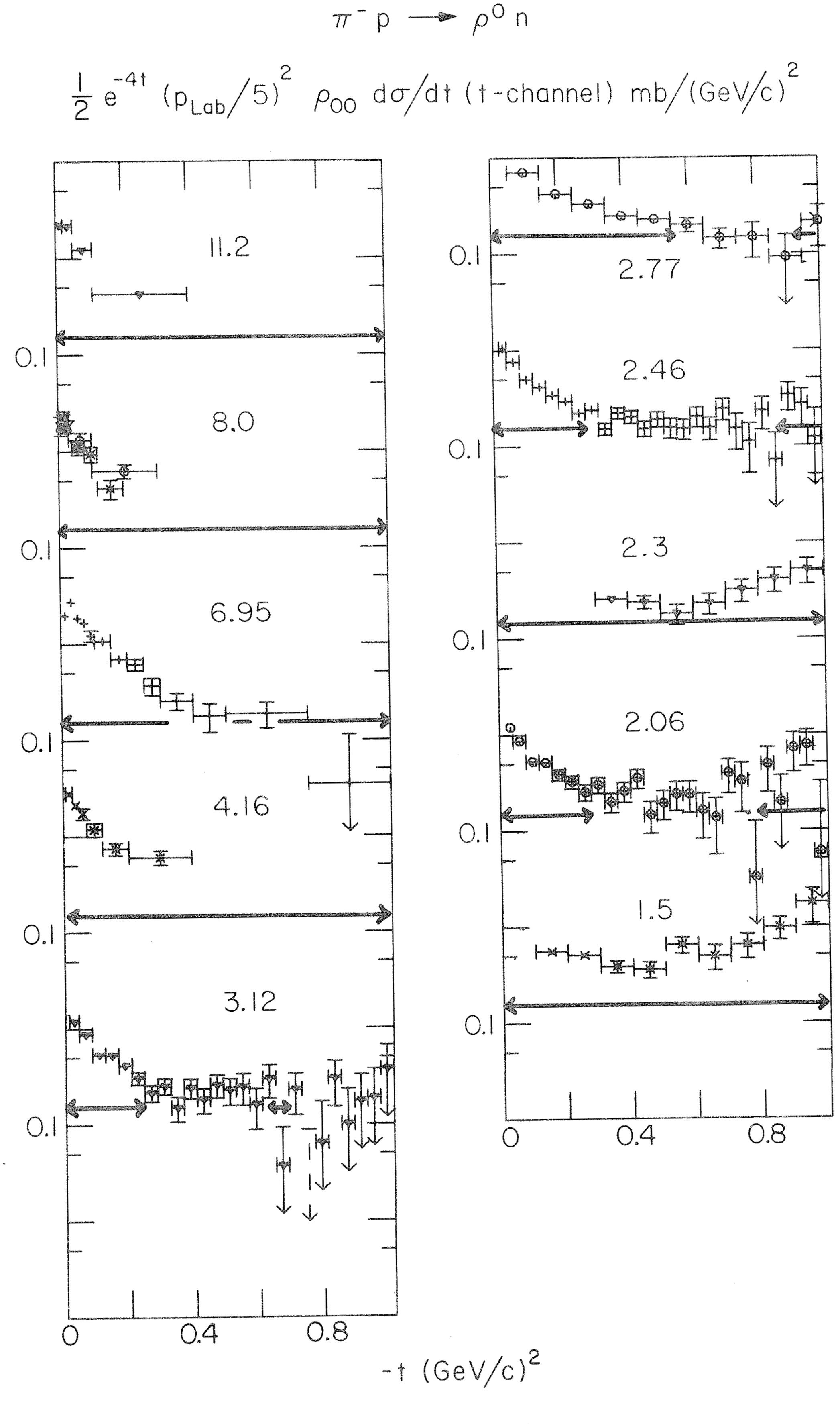

Figure 20: t-channel ρ_{00} $d\sigma/dt$ $\pi^- p \rightarrow \rho^0 n$, $\pi^+ n \rightarrow \pi^0 p$ data from ref. 101. Solid line marks 0.15: approximate "fit" to $\pi N \rightarrow \omega N$.

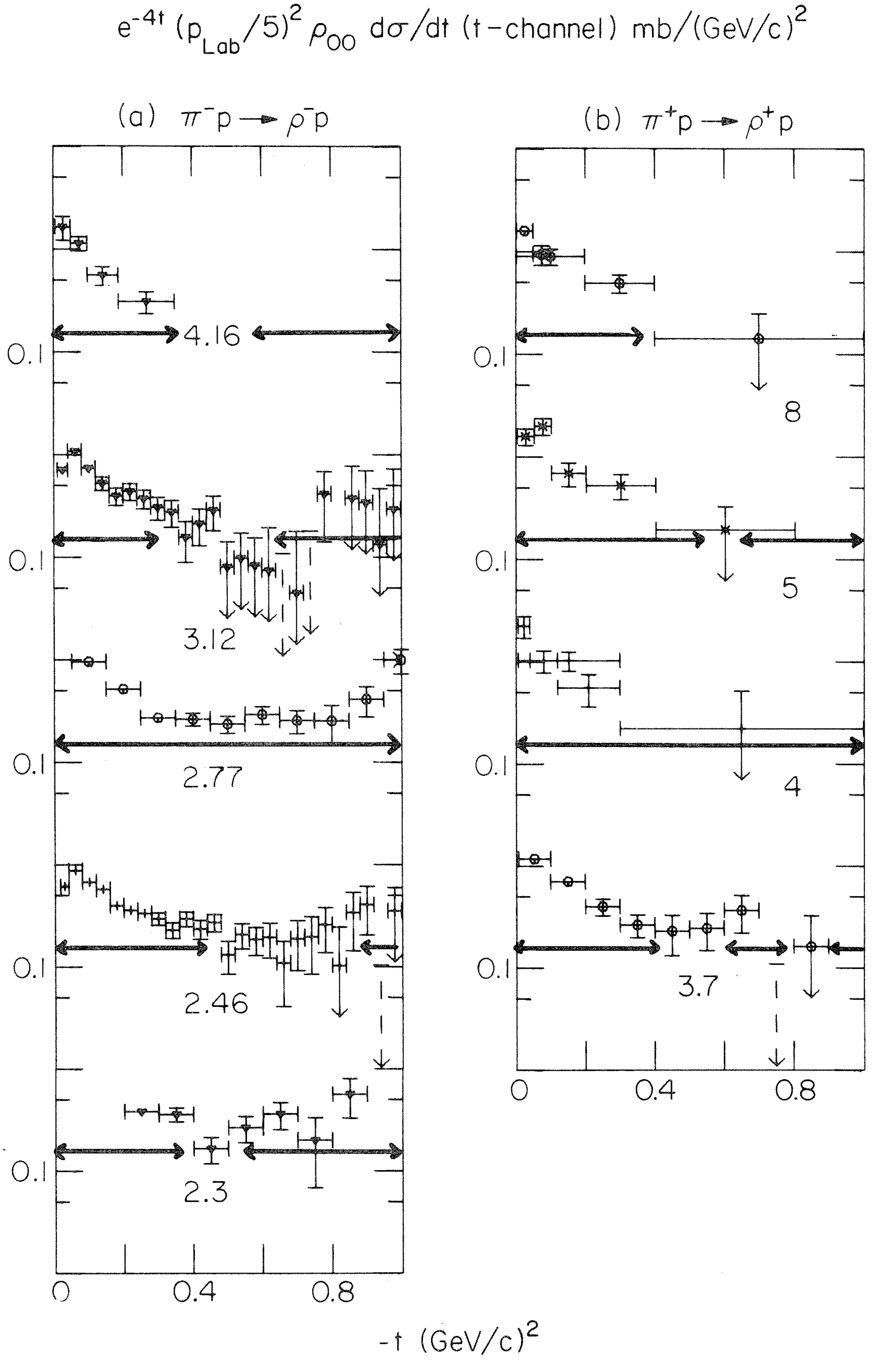

Figure 21: t-channel ρ_{00} dσ/dt (a) $\pi^- p \to \rho^- p$ from ref. 101 (b) $\pi^+ p \to \rho^+ p$ data from ref. 102. Solid line marks 0.15: approximate "fit" to $\pi N \to \omega N$.

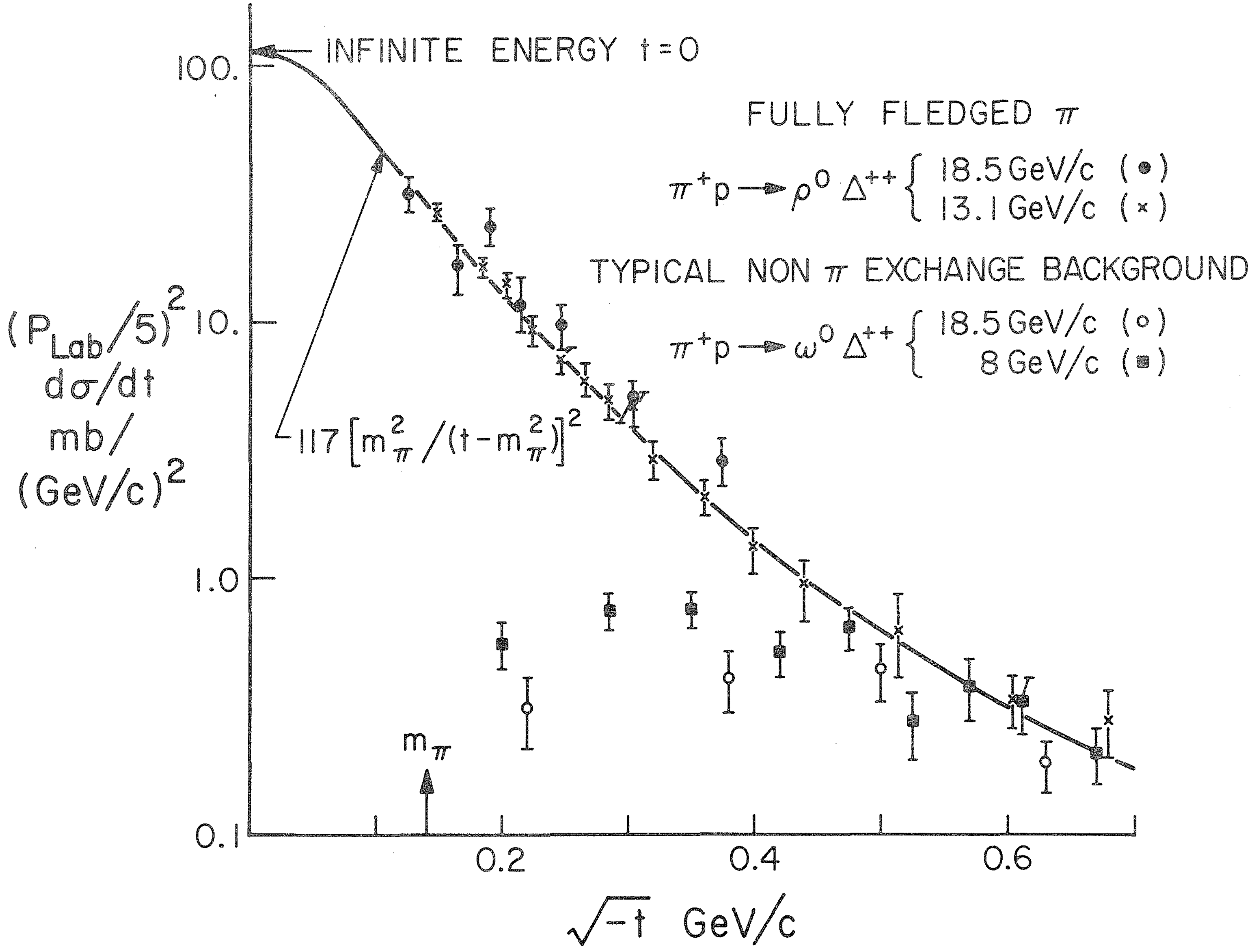

Figure 22: $\pi^+ p \rightarrow \rho^o \Delta^{++}$ at 13.1 GeV/c (J. A. Gaidos et. al., Phys. Rev. D1, 3190 (1970)) and 18.5 GeV/c. (N. N. Biswas et. al., preprint (1970)): The solid curve is a eyeball fit. $\pi^+ p \rightarrow \omega^o \Delta^{++}$ at 8 GeV/c (ABC collaboration, Nucl. Phys. B8, 45 (1968)), and 18.5 GeV/c (as above).

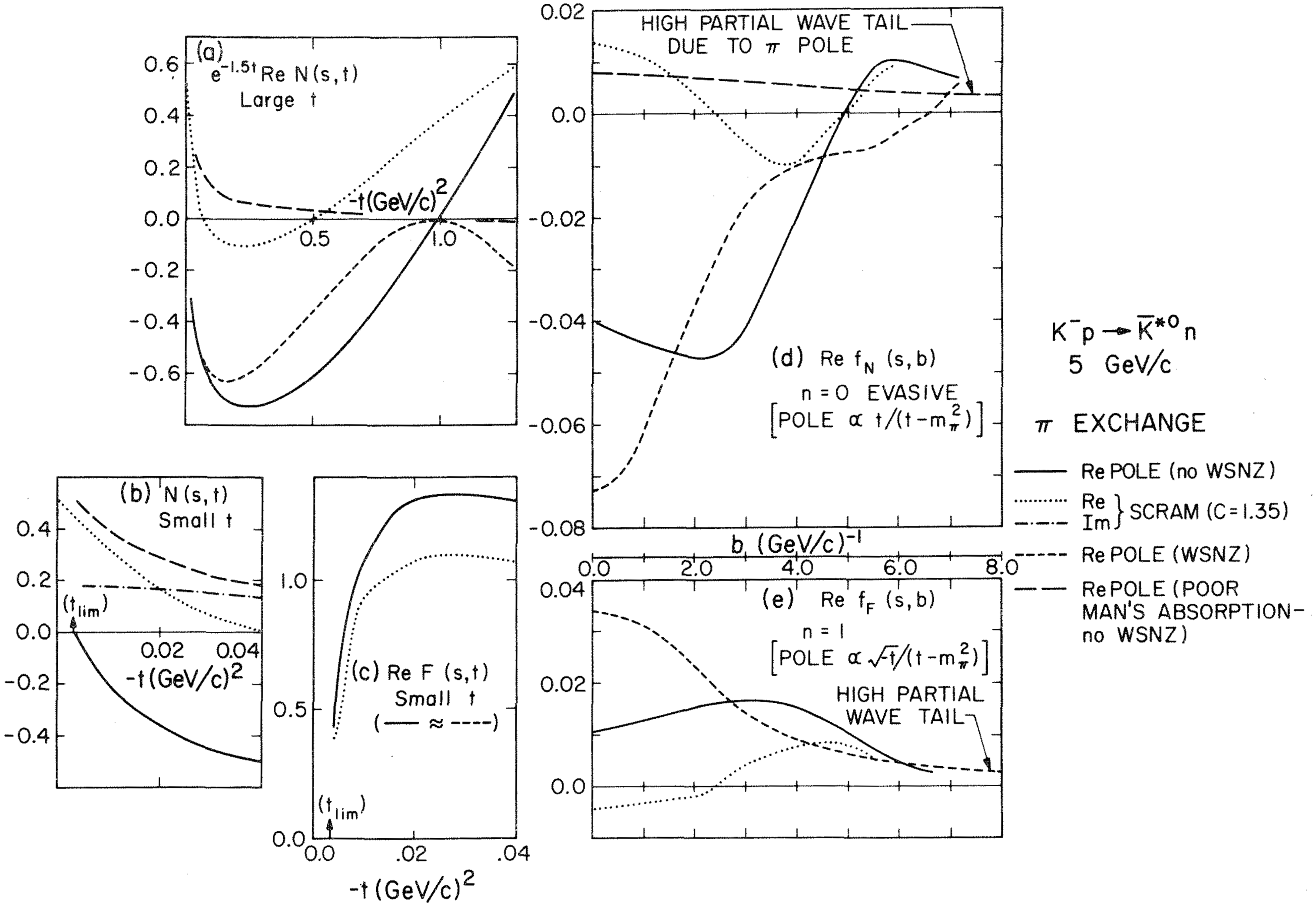

Figure 23: Nonflip ($N \propto H_{0\,-1/2 \to 1\,1/2}$) and flip ($F \propto H_{0\;-1/2 \to 0\;1/2}$) s-channel amplitudes for π exchange part of $K^-p \to \bar{K}^{o*}n$ at 5 GeV/c[41]. Amplitudes are normalized as in Eq. (1a). Also shown are their Fourier-Bessel transforms (f_N, f_F) defined by Eq. (5). Shown are pole terms with no WSNZ--the result of SCRAM absorption with C = 1.35--and the poor man's absorption amplitude. (The latter has been renormalized by 20% in 23(b) to agree with SCRAM at t=0.) We also give an unabsorbed π Regge pole with WSNZ predicted in GORE.

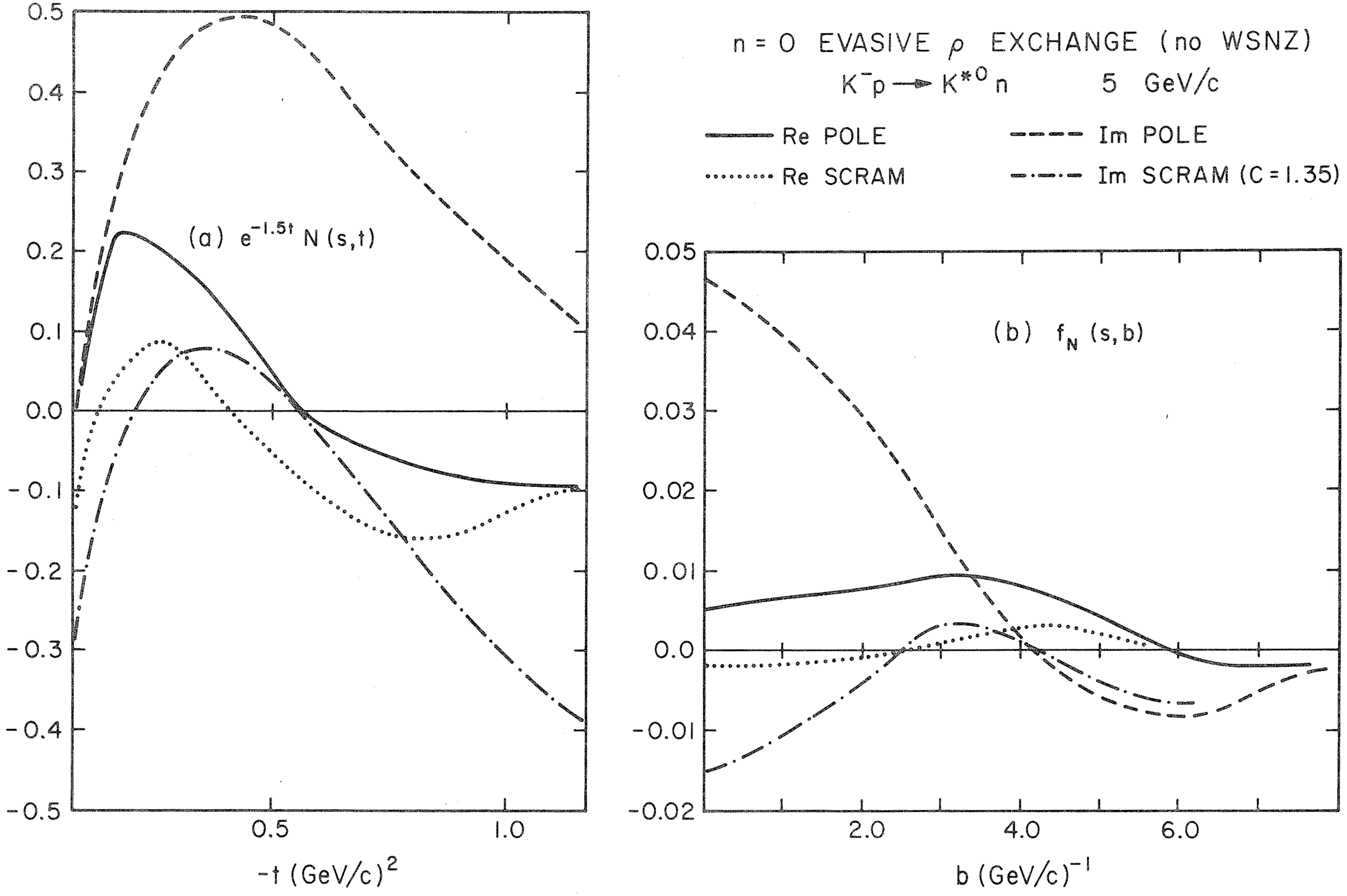

Figure 24: All quantities are as in Fig. 23 but refer to the ρ exchange contribution to the fit to $K^-p \to \bar{K}^{o*}n$ at 5 GeV/c. The spin flip amplitude is not shown--it is similar to F in Fig. 1 (GORE) or Fig. 5 (SCRAM). The PMA model is of course irrelevant for ρ exchange. Further we do not show curves for GORE when ρ has WSNZ--they are not very exciting. Note the zero at t=0 in the unabsorbed pole terms in Figs. 23 and 24. It follows from factorization

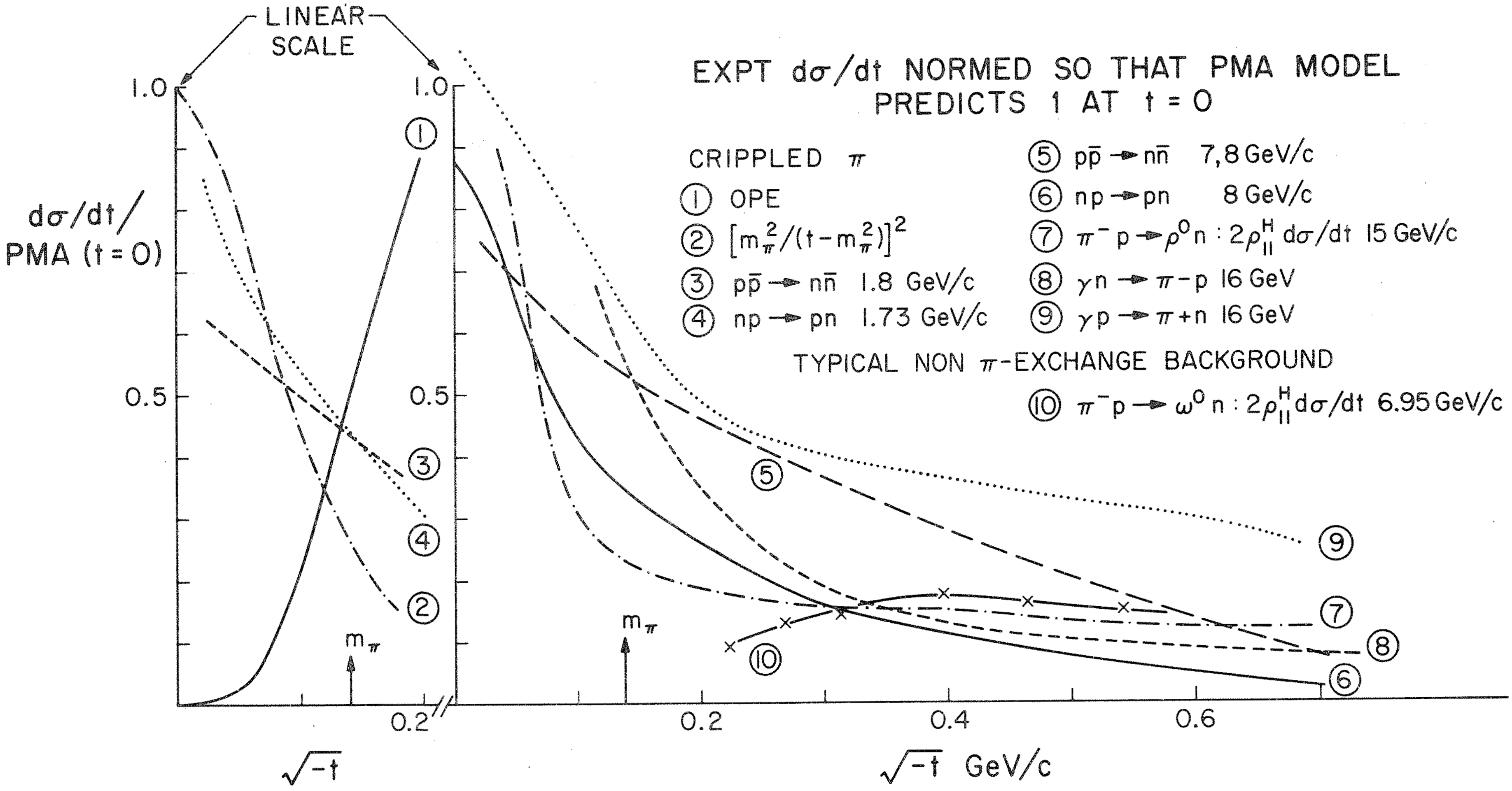

Figure 25: Crippled π dσ/dt normalized so that Poor Man's Absorption predicts 1 at t=0. OPE represents $2[t/m_\pi^2 - t)]^2$, $\pi^- p \rightarrow \rho^0 n$ comes from Leith (this conference) and $\pi^+ n \rightarrow \omega^0 p$ from ref. 98. The remainder of the data is from ref. 103.

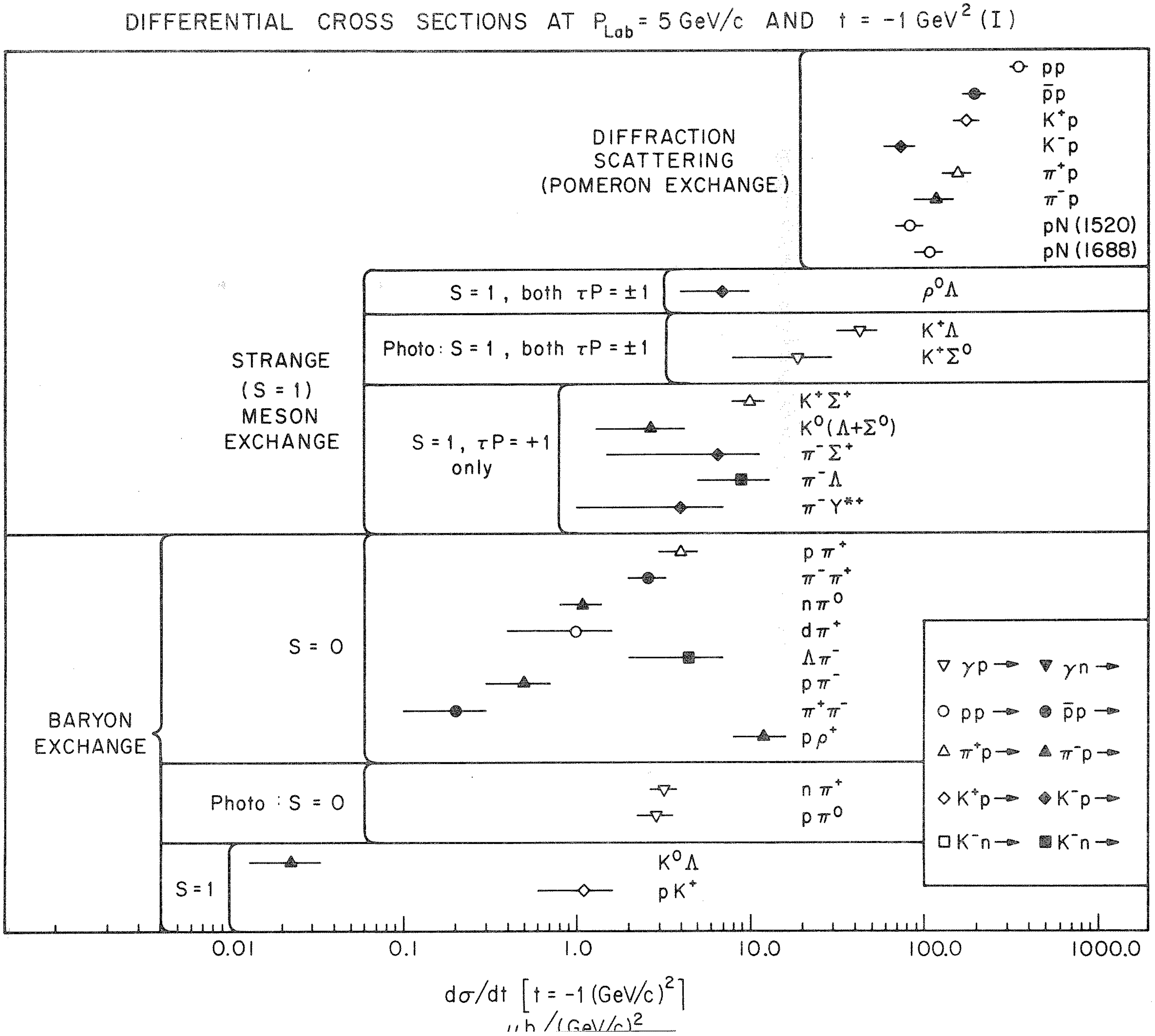

Figure 26:

Part I of a self explanatory figure in two parts. (Ref. 9 and Section 3). Photoproduction has been scaled by the 550 suggested by VDM and $\gamma_\rho{}^2/4\pi = 0.5$.

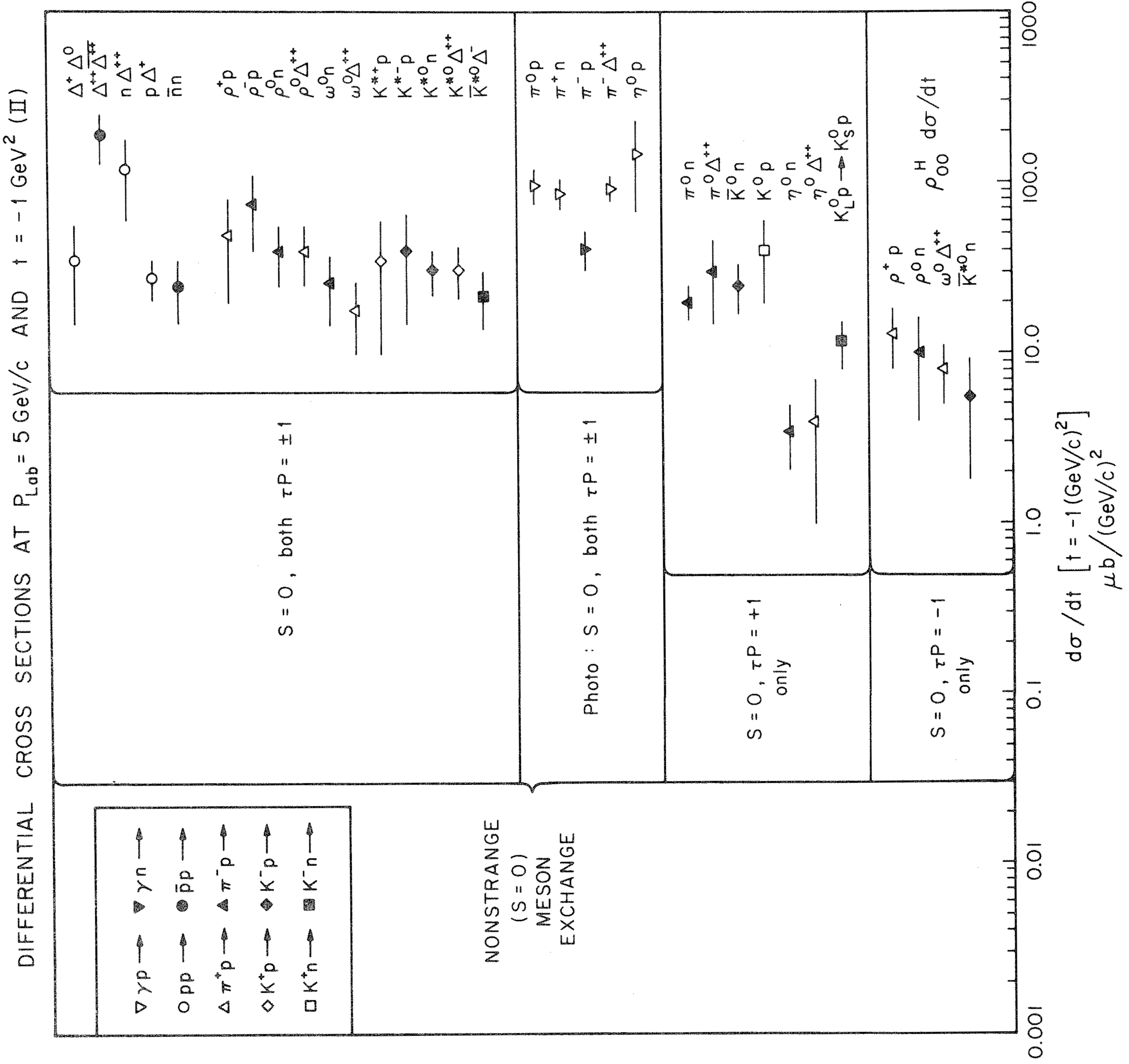

Figure 26: Part II of a self explanatory figure in two parts. (Ref. 9 and Section 3). Photoproduction has been scaled by the 550 suggested by VDM and $\gamma_\rho^2/4\pi = 0.5$.

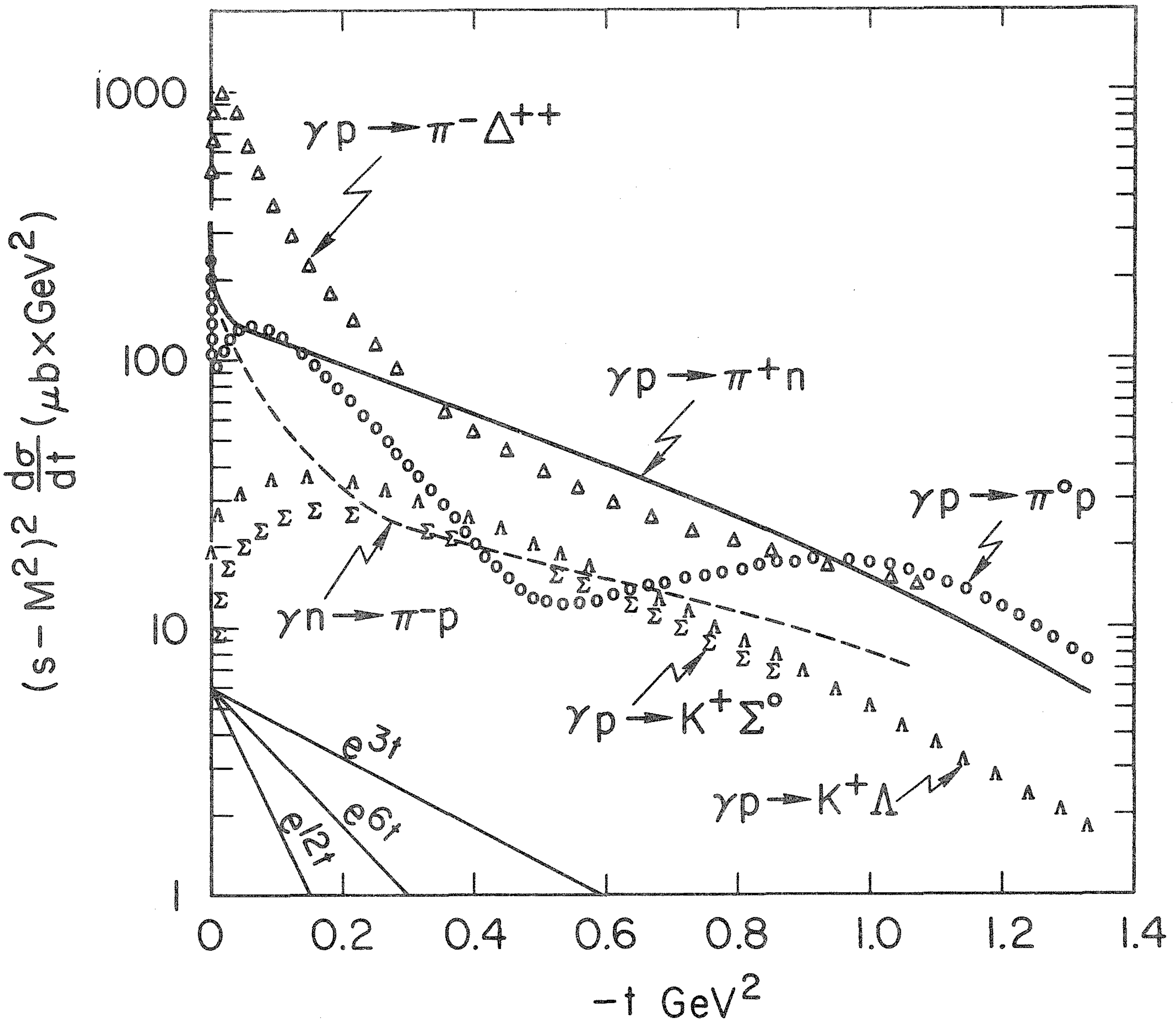

Figure 27: Schematic representation of universal $(s-m^2)^2$ dσ/dt curves for photoproduction (ref. 10).

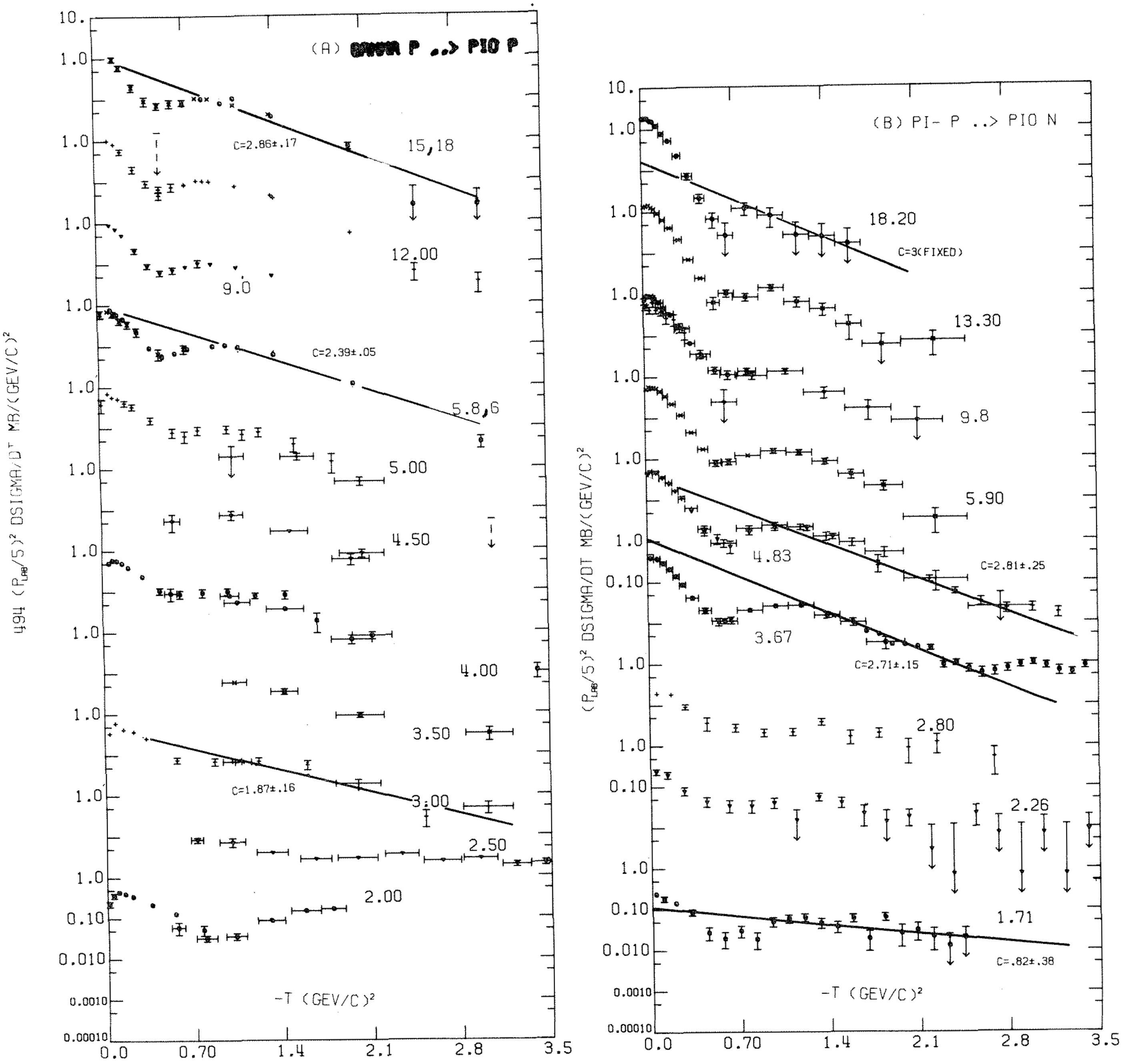

Figure 28: Forward Dip Reactions (a) 494 $(E_{1ab}/5)^2$ $d\sigma/dt$ mb/(GeV/c)^2 for $\gamma p \to \pi^0 p$. Coefficient is suggested by VDM for $\gamma_\rho{}^2/4\pi = 0.45$ (e.g., refs. 39, 41 and Section 3). (b) $(p_{1ab}/5)^2$ $d\sigma/dt$ mb/(GeV/c)^2 for $\pi^- p \to \pi^0 n$ (ref. 9). Exponential fits are those presented in Table 3 of Section 3. Note ratio of intercept of large $-t$ fit at $t=0$ v. value of $d\sigma/dt$ there. This indicates ratio A_{FP}/A_R in Eq. (28). It is energy independent above 5 GeV and big in photoproduction while it falls with energy in $\pi^- p \to \pi^0 n$. Further both reactions exhibit marked shrinkage up to p_{1ab} = 5 GeV/c. Backward dip reactions are shown in Fig. 32.

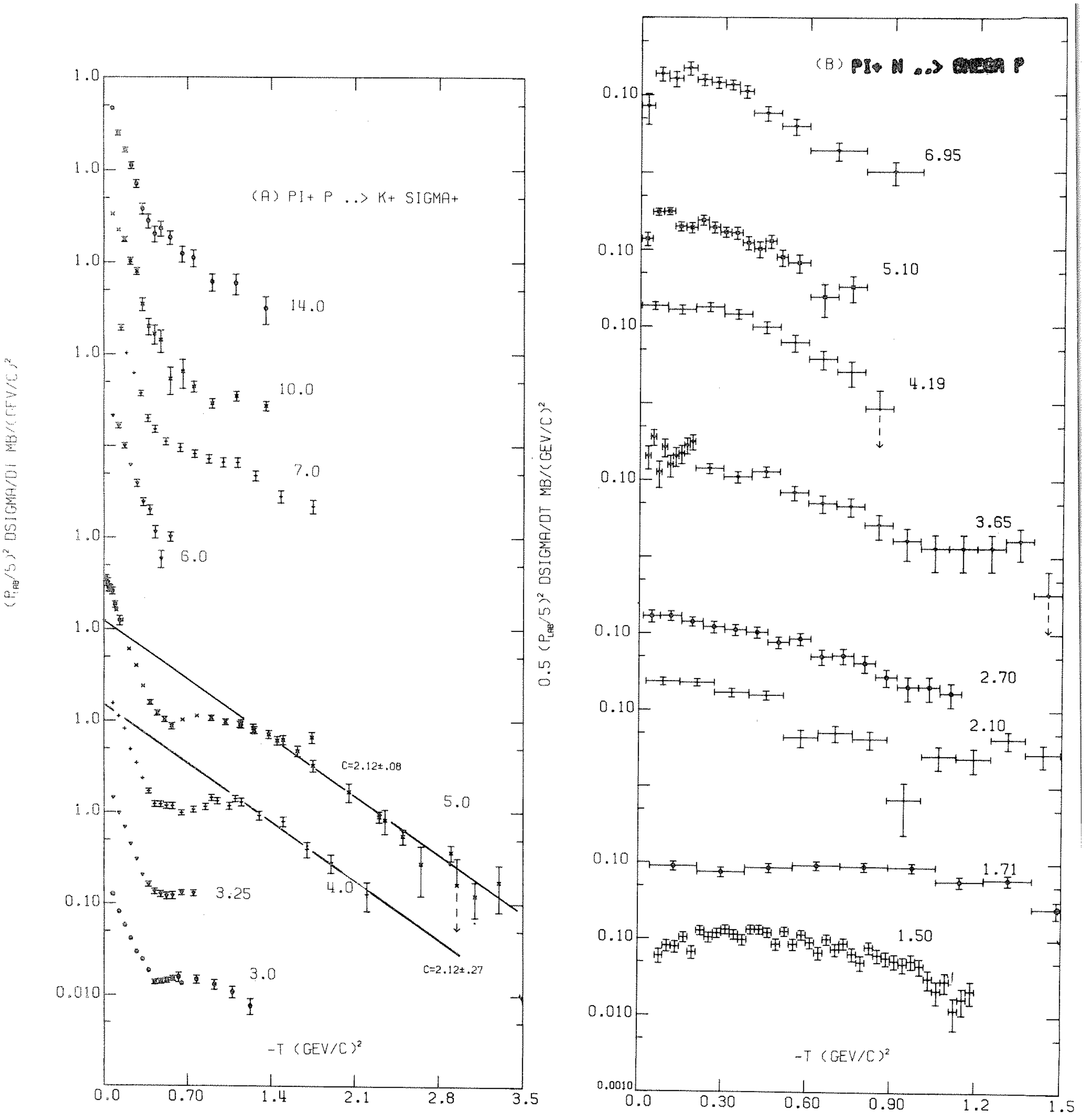

Figure 29: (a) $(p_{lab}/5)^2$ dσ/dt mb/(GeV/c)^2 for $\pi^+p \to K^+\Sigma^+$. (b) 1/2 $(p_{lab}/5)^2$ dσ/dt mb/(GeV/c)^2 for $\pi^+n \to \omega^o p$ (ref. 9). Exponential fits are those presented in Table 3 of Section 3. Note in (b) the strong shrinkage up to p_{lab} = 3.65 GeV/c; there is no significant change in slope after this value.

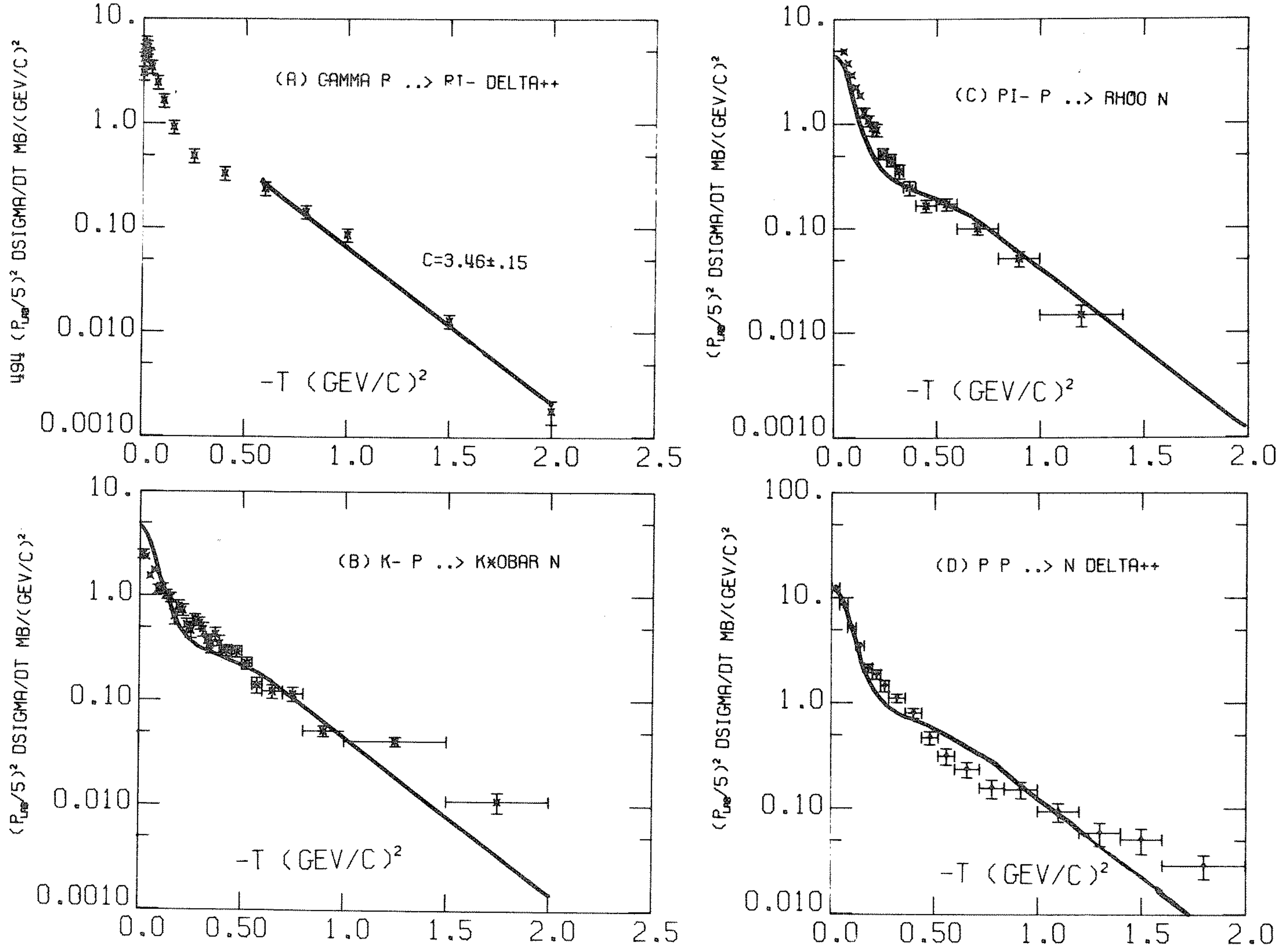

Figure 30: Half-asleep π-exchange reactions: $(p_{lab}/5)^2\ d\sigma/dt$ for: (a) 494$(\gamma p \to \pi^- \Delta^{++})$ at 16 GeV: (b) $K^- p \to \bar{K}^{o*} n$ at 3.9 GeV/c; (c) $\pi^- p \to \rho^o n$ at 6.95 GeV/c and (d) $pp \to n\Delta^{++}$ at 6.6 GeV/c. Exponential fit in (a) is that presented in table 3 of Section 3. Solid curves on (b) → (d) are the 16 GeV $\gamma p \to \pi^- \Delta^{++}$ in (a) scaled to reproduce the trend of the strong interaction data. These curves show that for reactions going by similar exchanges (in this case half asleep π) there is little qualitative difference between photoproduction and strong interactions.

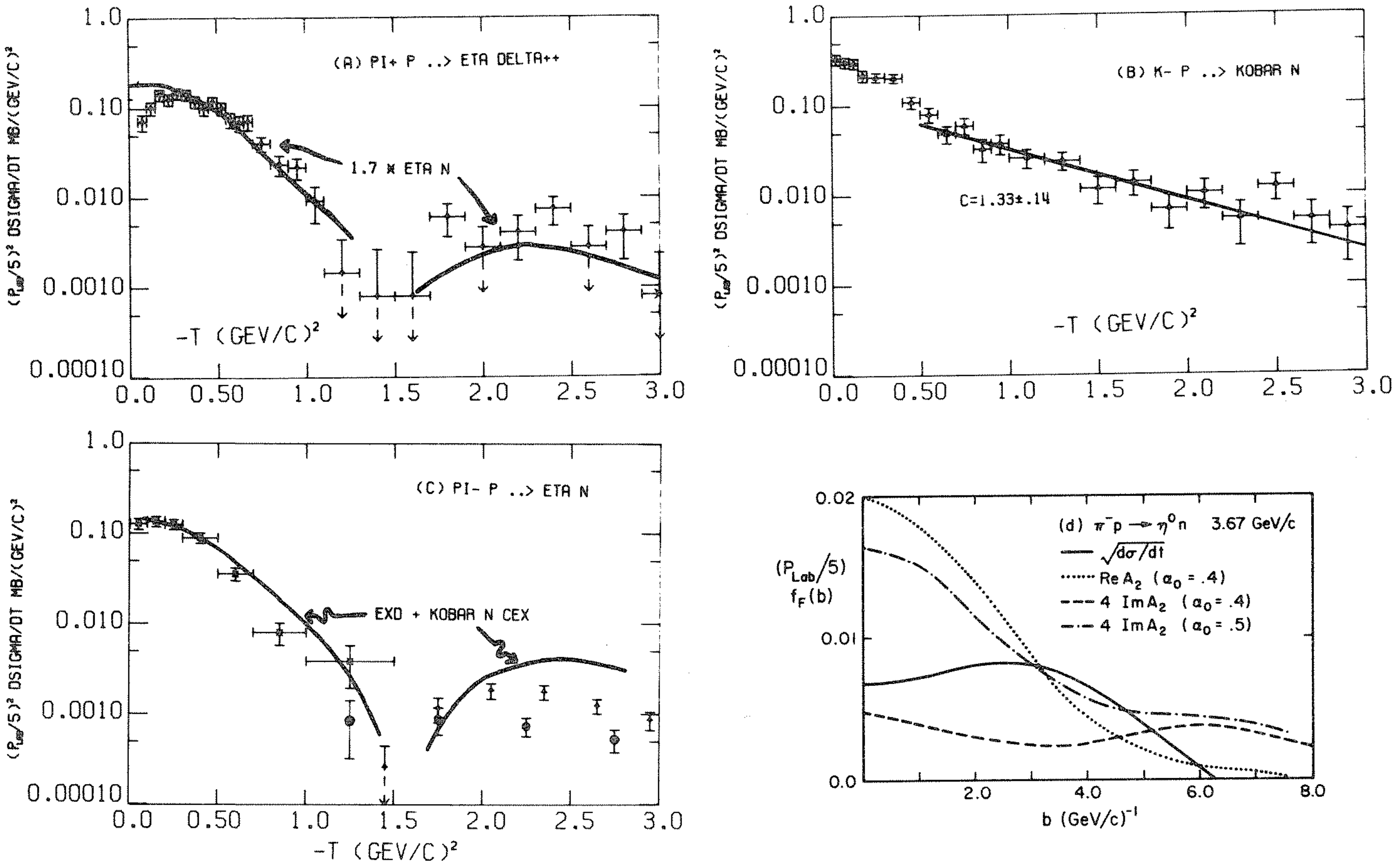

Figure 31: Patchwork quilt of Regge in Wonderland up to t = -3 (GeV/c)^2. $(p_{1ab}/5)^2$ $d\sigma/dt$ for (a) $\pi^+p \to \eta^o\Delta^{++}$ at 3.5 GeV/c (ref. 73), (b) $K^-p \to \bar{K}^o n$ at 3.95 GeV/c (ref. 9), (c) $\pi^-p \to \eta^o n$ at 3.72 (x), 3.67 (▲) and 4.83 (●) GeV/c. (ref.74) The exponential fit in (b) is that presented in Table 3 of Section 3. The attribution of the dip in (a) and (c) to the $\alpha_{A_2} = -1$ WSNZ is confirmed by the solid line in (a) which is 1.7 x the ηn data at 3.67, 3.72 in (c). The deviation near t=0 is due to nonflip component of ηn ($\eta\Delta^{++}$ is purely flip). Further solid curve in (c) is Regge pole prediction (ref. 75) based on EXD and data in (b). The empirical partial wave analysis shown in (d) assumed $\pi^-p \to \eta^o n$ was purely spinflip and used the methods described in Section 3.2. Shown are $\sqrt{d\sigma/dt}$ and $\sqrt{d\sigma/dt}$ x appropriate Regge phase to give real and imaginary parts of A_2 exchange. $[\alpha_{A_2} = (.4,.5) + .9t]$. These curves have been scaled to 5 GeV/c as if $d\sigma/dt \propto p_{1ab}^{-2}$.

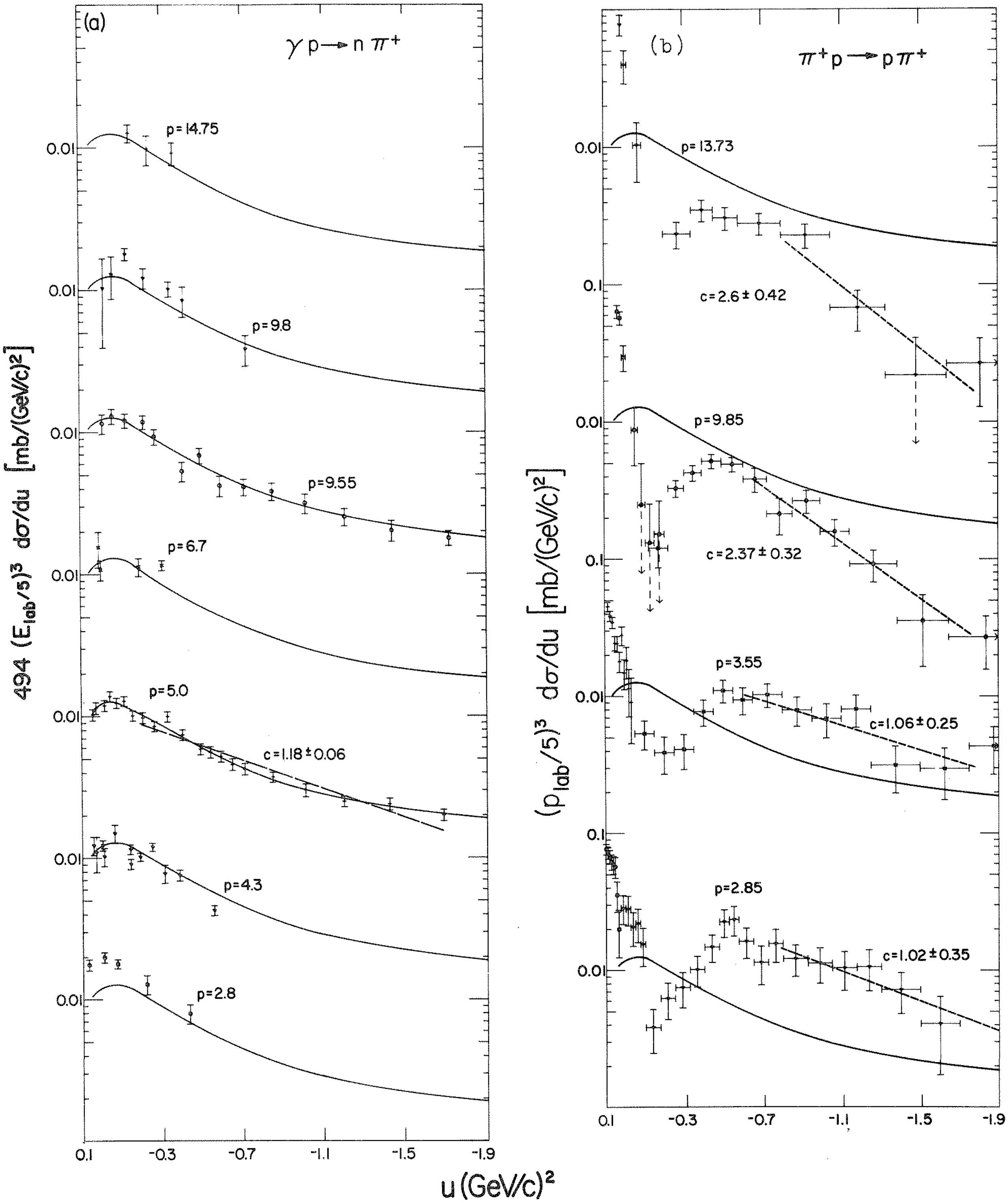

igure 32: Backward scattering: $(p_{1ab}/5)^3$ dσ/du mb/(GeV/c)^2 for (a) 494 (γp → nπ+) (b) π+p → pπ+ (Ref. 34). The solid curve in (a) and (b) is an eyeball representation of the universal form exhibited by (a) for $E_{1ab} \gtrsim 4$ GeV. This emphasizes the amazing differences in shape between the curves in (a) and (b). Exponential fits are those presented in Table 3 of Section 3. Note the marked shrinkage in (b) below 5 GeV/c; above this momentum, the large -t slopes show no significant change. Compare 32(b) with the other dip reactions in Fig. 28. The fourth of our dip reactions--backward π−p → nπ0--is similar at large -t to π+p → pπ+. It is shown in Ref. 39.

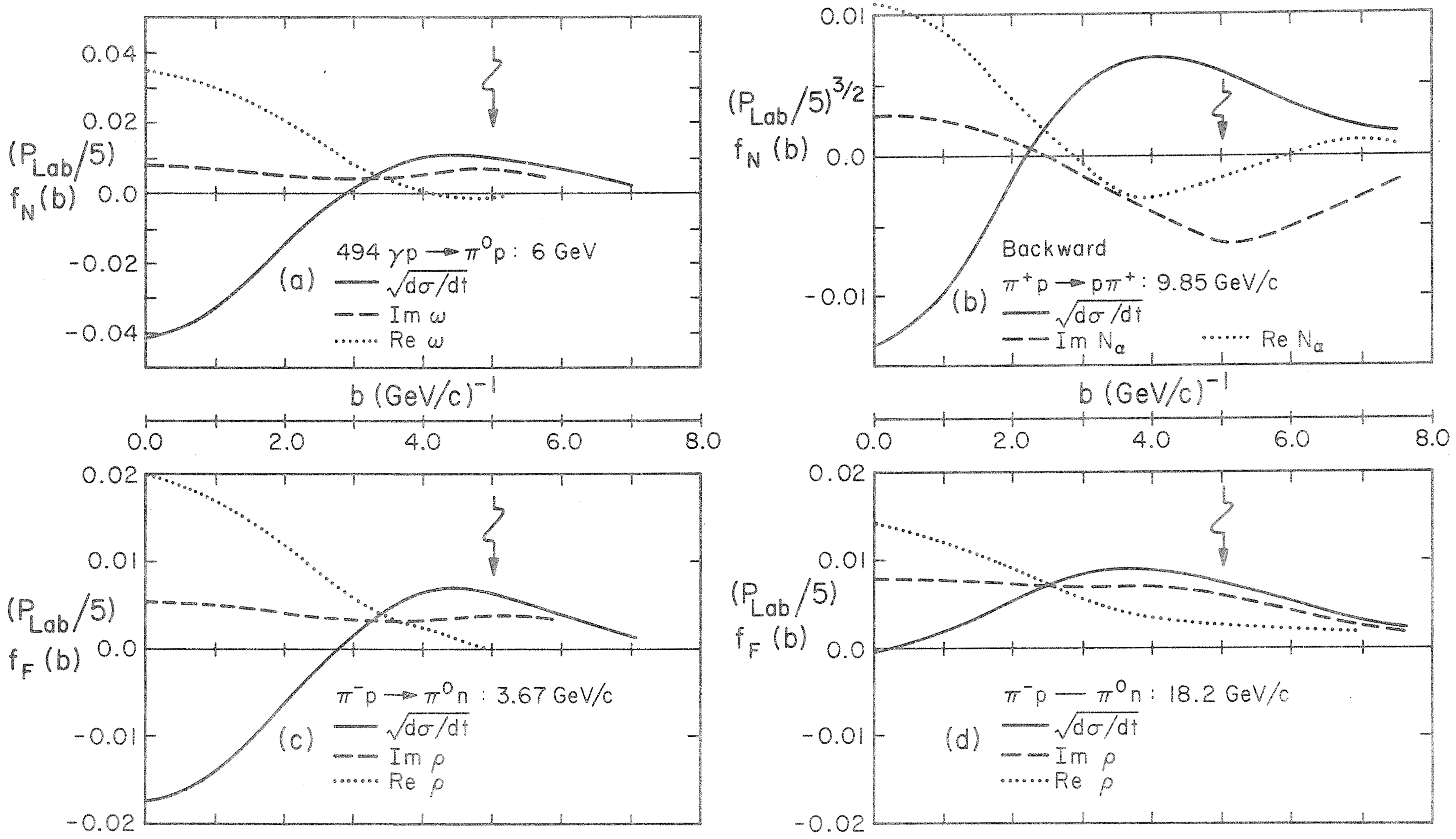

Figure 33: The Dip reactions. Empirical partial wave analyses described in Section 3.2 of (a) 6 GeV 494 ($\gamma p \rightarrow \pi^0 p$) single flip, (b) 9.85 GeV/c backward $\pi^+ p \rightarrow p\pi^+$ nonflip, (c) 3.67 GeV/c $\pi^- p \rightarrow \pi^0 n$, (d) 18.2 GeV/c $\pi^- p \rightarrow \pi^0 n$ assumed single flip. (Ref. 9) Shown are $\sqrt{d\sigma/dt}$ and $\sqrt{d\sigma/dt}$ x appropriate Regge phase to give real and imaginary part of dominant exchange. [(a) $\alpha_\omega = .4 + .9t$; (b) $\alpha_{N\alpha} = -.35 + .9u$; (d) $\alpha_\rho = .5 + .9t$]. Curves have been scaled to 5 GeV/c as if $d\sigma/dt \propto p_{lab}^{-2}$ ((a, (c), (d)) and p_{lab}^{-3}((b)).

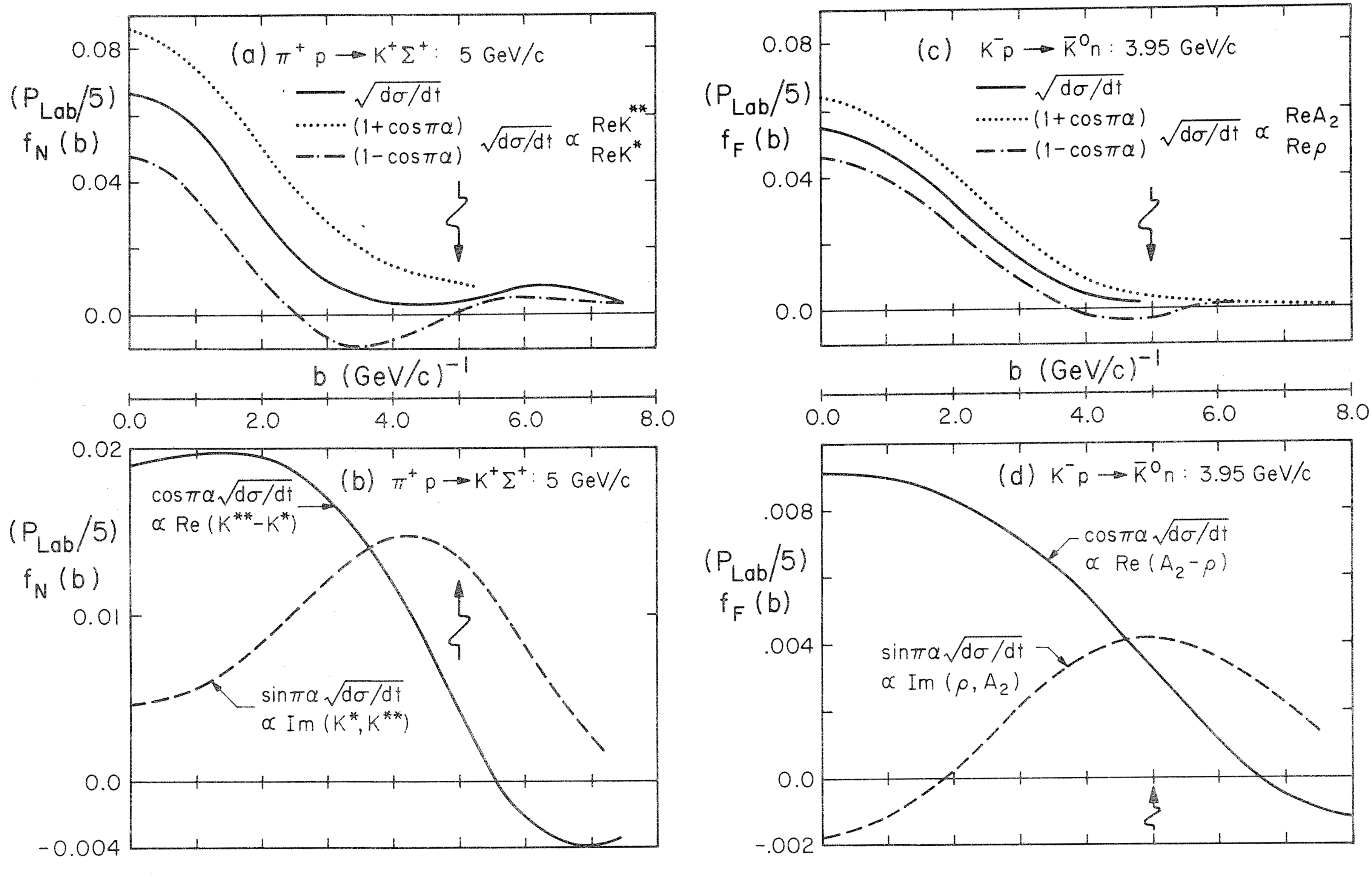

Figure 34: Empirical partial wave analyses described in Section 3.2 of (a), (b) 5 GeV/c $\pi^+p \to K^+\Sigma^+$ nonflip, (c), (d) 3.95 GeV/c $K^-p \to \bar{K}^0n$ assumed single flip. (Ref. 9). Shown are $\sqrt{d\sigma/dt}$ and $\sqrt{d\sigma/dt}$ x various Regge phases, scaled to 5 GeV/c as if the $d\sigma/dt \propto p_{lab}^{-2}$. In (a), (c) $\sqrt{d\sigma/dt}$ is appropriate for real reactions (Eq. (7/IV)); $(1 + \cos\pi\alpha)\sqrt{d\sigma/dt}$ is real part of (7/II), and $(1-\cos\pi\alpha)\sqrt{d\sigma/dt}$ real part of (7/I). In (b), (d) $\cos\pi\alpha\sqrt{d\sigma/dt}$ is real part of moving phase reactions (7/III) and $\sin\pi\alpha\sqrt{d\sigma/dt}$ imaginary part of (7/I → III). In (a), (b) $\alpha = .35 + .9t$; (c) (d) $\alpha = .5 + .9t$.

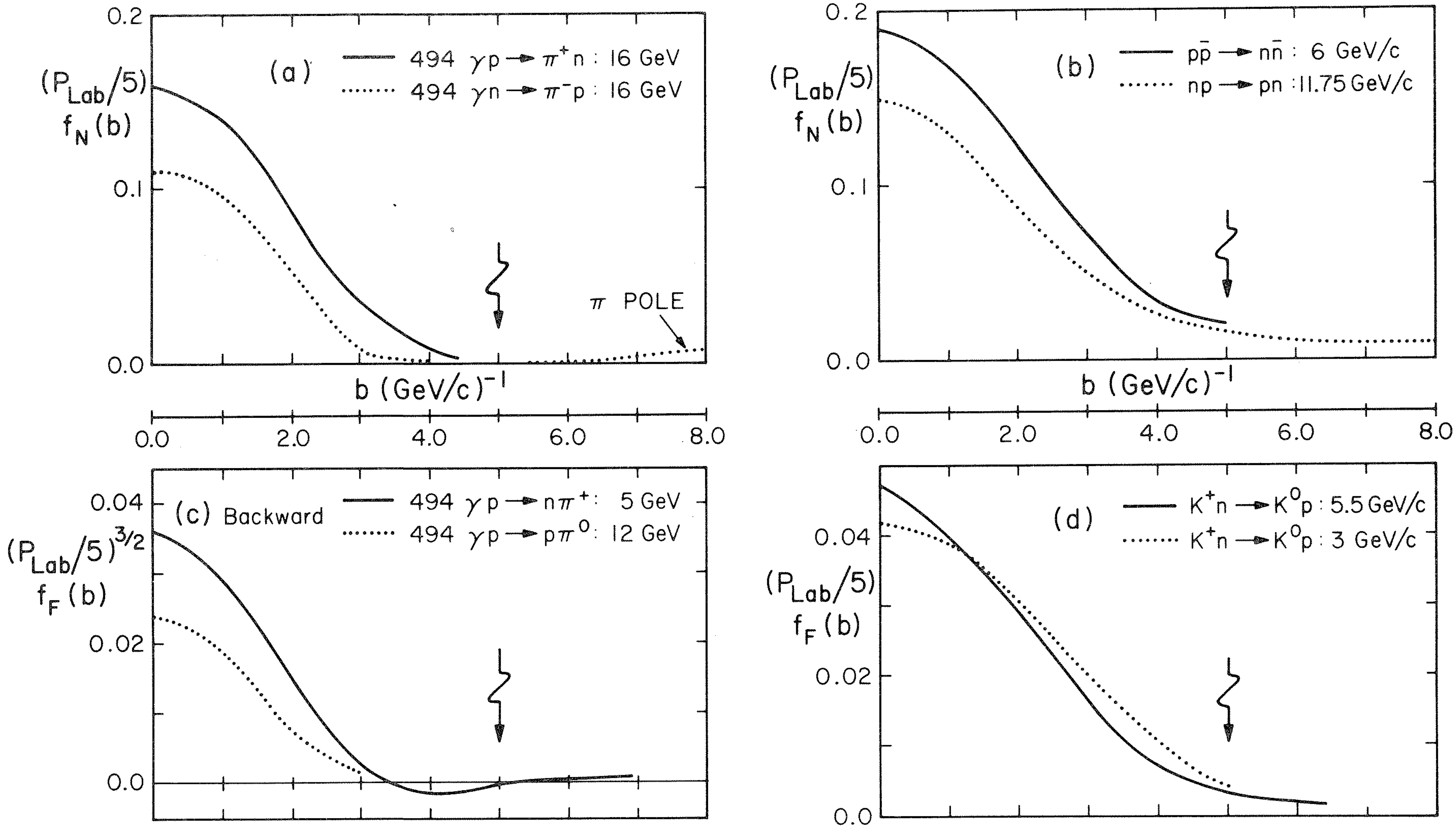

Figure 35: Empirical partial wave analyses described in Section 3.2 of (a) 16 GeV $\gamma p \to \pi^+ n$, $\gamma n \to \pi^- p$ nonflip, (b) 6 GeV/c $p\bar{p} \to n\bar{n}$, 11.75 GeV/c $np \to pn$ nonflip (c) backward $\gamma p \to n\pi^+$, $\gamma p \to p\pi^0$ single flip (d) 3, 5.5 GeV/c $K^+ n \to K^0 p$ assumed single flip. Only $\sqrt{d\sigma/dt}$ curves are shown. They have been scaled to 5 GeV/c as if $d\sigma/dt \propto p_{lab}^{-2}$ ((a), (b) (d)) and $\propto p_{lab}^{-3}$ ((c)). (d) and $np \to pn$ are expected to be purely real and so $\sqrt{d\sigma/dt}$ curve does give Regge phase; in others there are many exchanges--expected phase is unclear.

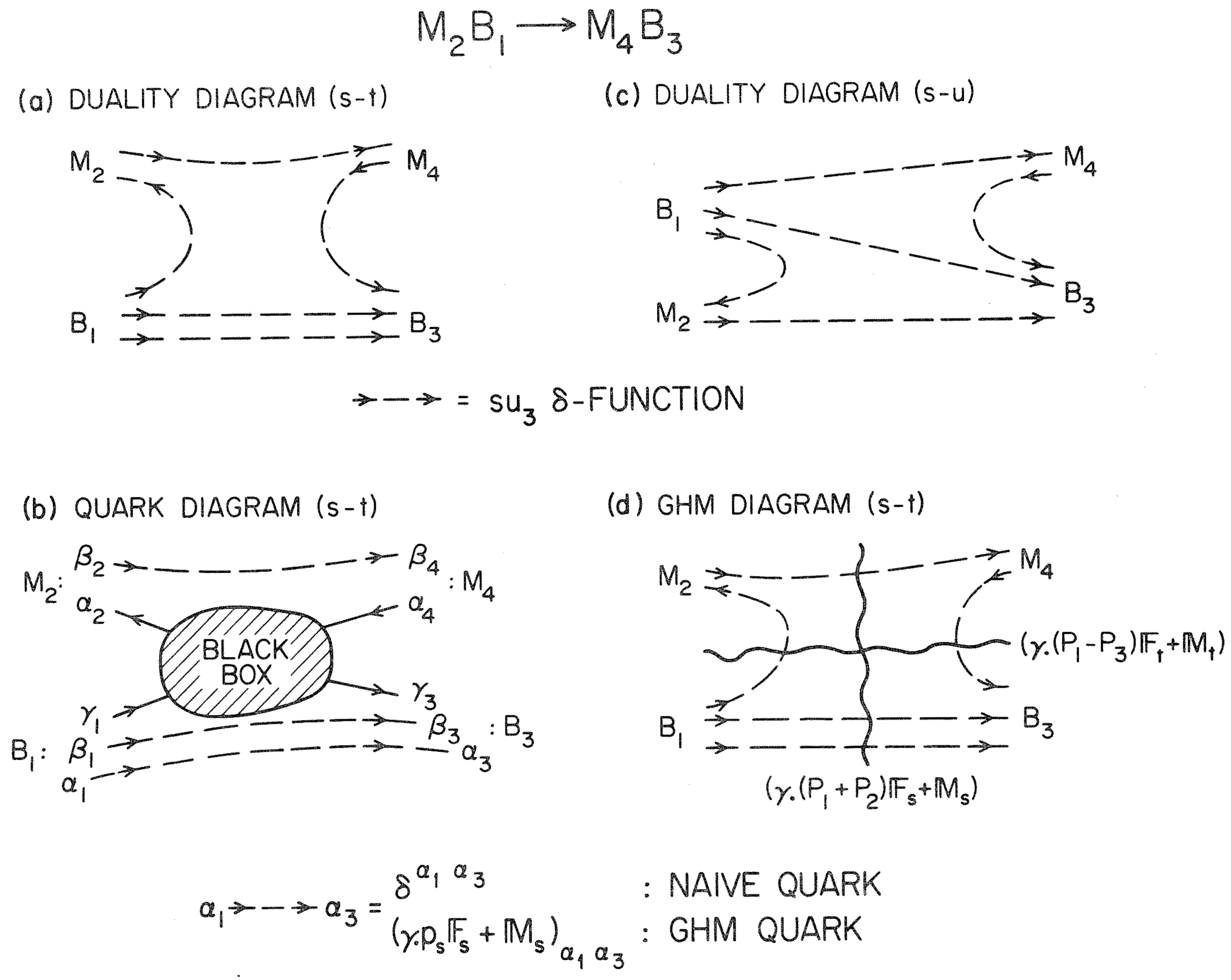
$M_2B_1 \longrightarrow M_4B_3$
(a) DUALITY DIAGRAM (s-t)
M_2
M_4
B_1
B_3
(c) DUALITY DIAGRAM (s-u)
B_1
M_2
M_4
B_3
= su_3 δ-FUNCTION
(b) QUARK DIAGRAM (s-t)
M_2: β_2 α_2
β_4 : M_4
α_4
BLACK BOX
γ_1
γ_3
B_1: β_1 α_1
β_3 α_3 : B_3
(d) GHM DIAGRAM (s-t)
M_2
M_4
B_1
B_3
$(\gamma.(P_1-P_3)\mathbb{F}_t+\mathbb{M}_t)$
$(\gamma.(P_1+P_2)\mathbb{F}_s+\mathbb{M}_s)$
$\alpha_1 \rightarrow - \rightarrow \alpha_3 = \delta^{\alpha_1\alpha_3}$: NAIVE QUARK
$(\gamma.p_s\mathbb{F}_s+\mathbb{M}_s)_{\alpha_1\alpha_3}$: GHM QUARK

Figure 36: Drunken duality and quark diagrams for meson baryon scattering. The SU_3 duality diagrams (a), (c) were introduced by ref. 54: the spin analogues (b), (d) of these correspond to the models discussed in Section 4.4(ii) for NAIVE QUARK and Section 4.4(v) for GHM QUARK.

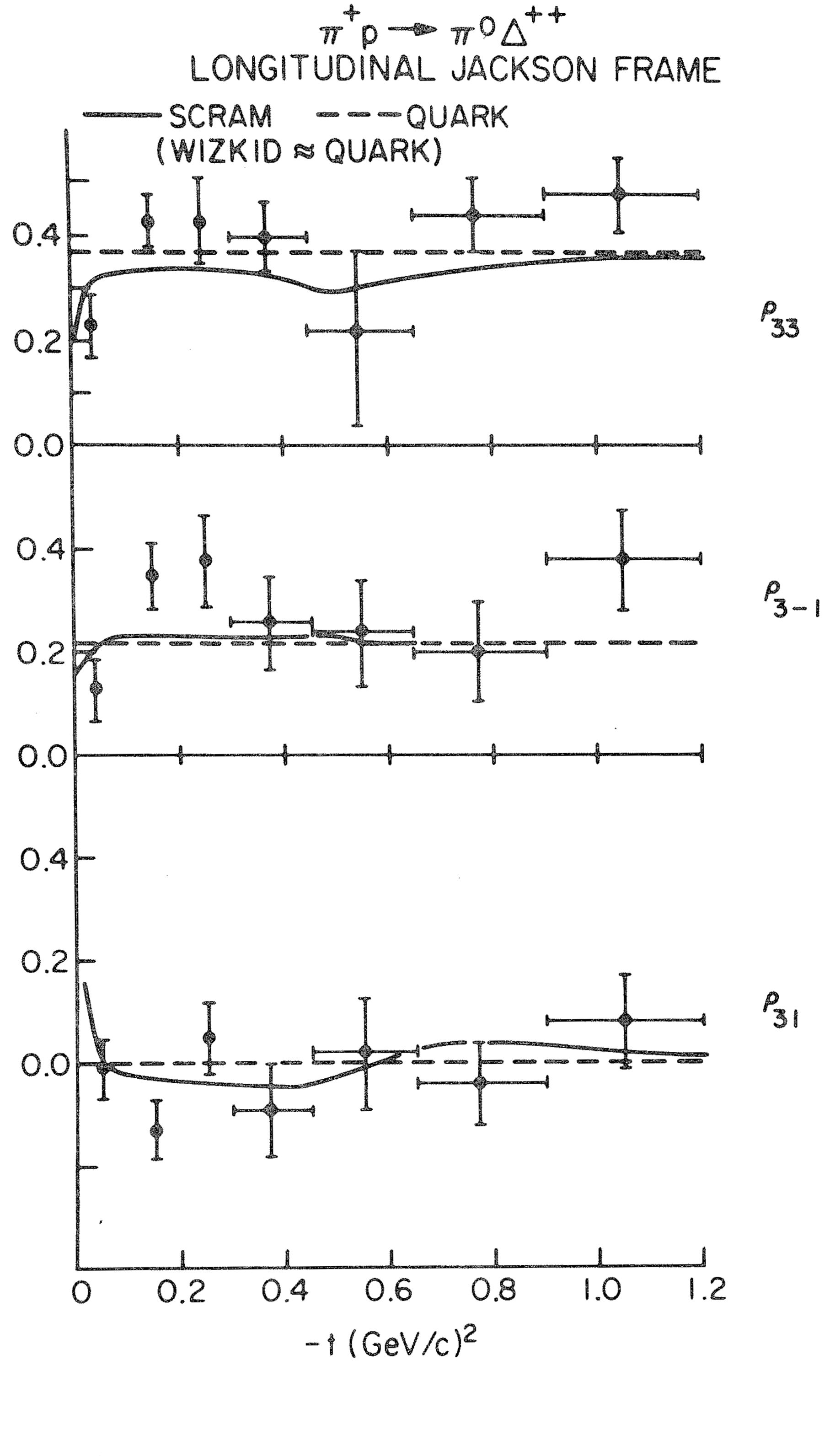

Figure 37: Decay density matrix elements, in the longitudinal Jackson Frame, for the Δ^{++} produced in $\pi^+ p \to \pi^0 \Delta^{++}$ for p_{lab} averaged between 3 and 4 GeV/c. (G. Gidal et. al., UCRL-18351, preprint 1968). The (——) theoretical curve corresponds to a strong cut (SCRAM) calculation absorbing a ρ Regge pole which obeyed the SSD (Eq. (30)) in the t-channel. The weak cut (WIZKID) calculation is indistinguishable from the SSD distribution predicted by the quark model, (– – – –).

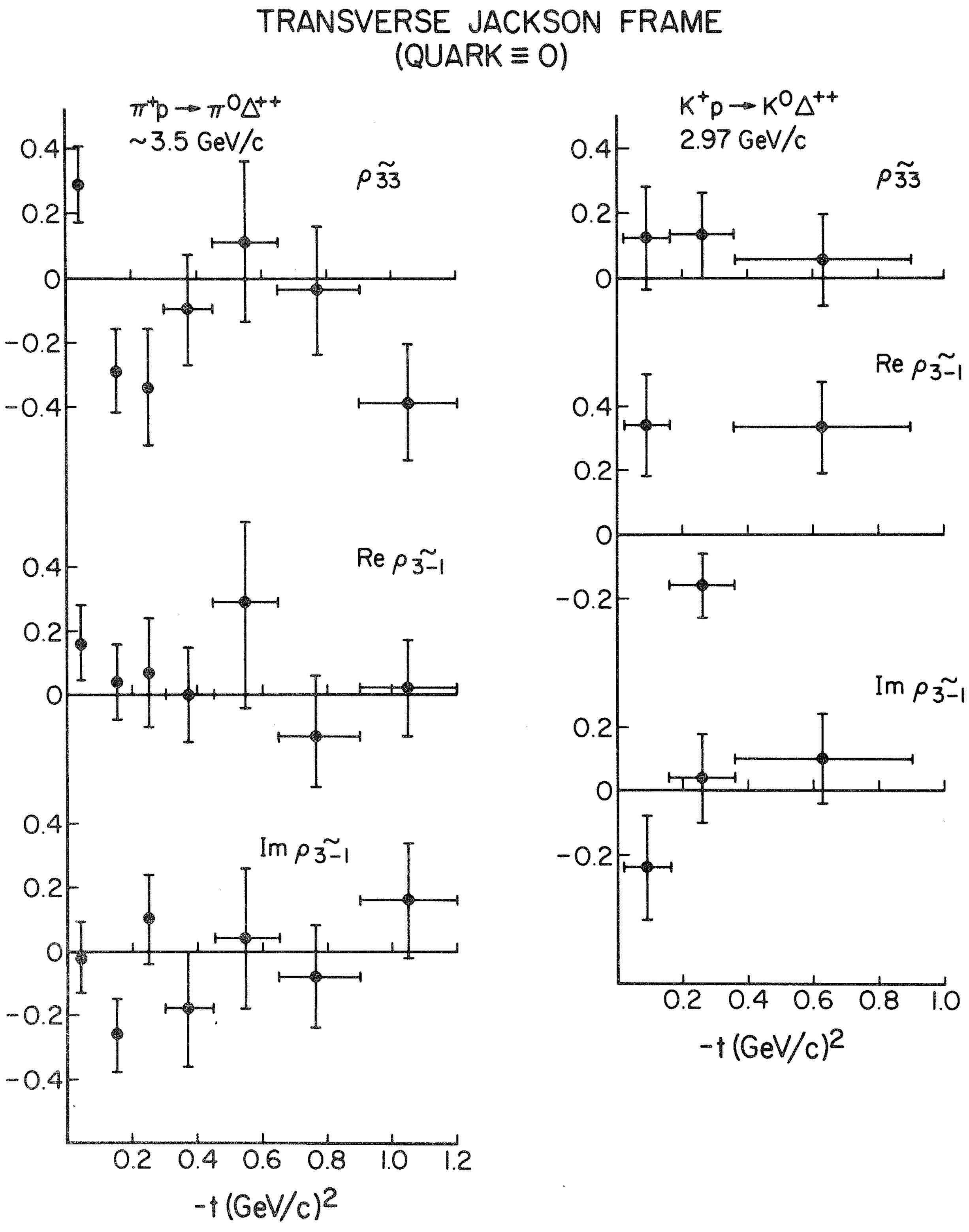

Figure 38: Decay density matrix elements in the transverse Jackson frame for the Δ^{++} produced in $\pi^+p \to \pi^0\Delta^{++}$ (Same data as Fig. 37) and $K^+p \to K^0\Delta^{++}$ (p_{1ab} = 2.97 GeV/c, M. Ferro-Luzzi et. al., Nuovo Cimento 36, 1101 (1965).) The quark model predicts that all 3 density matrix elements should be zero. (Eq. (34))

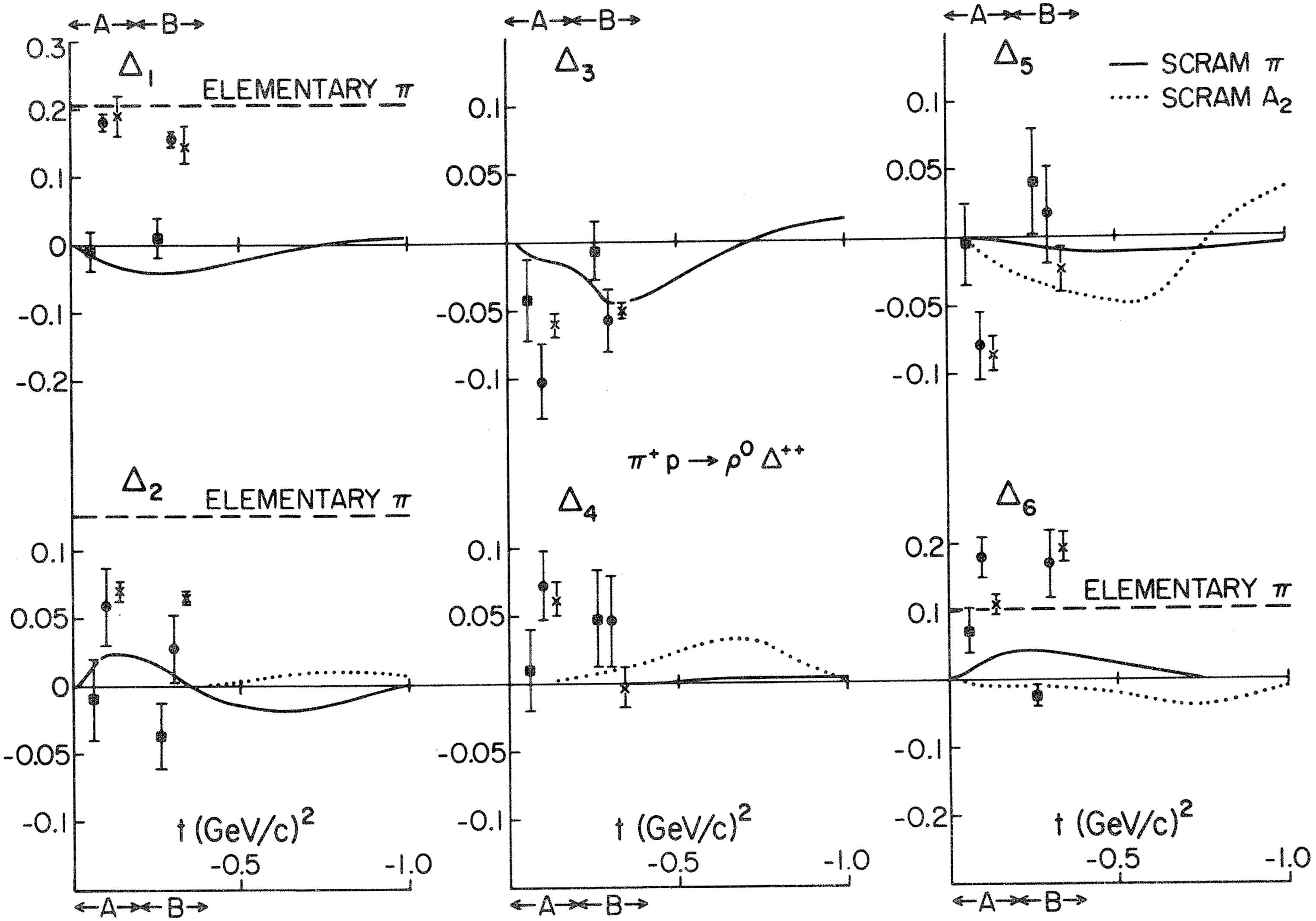

Figure 39: The experimental values for the left (●) and right (x) hand sides of the six class A relations defined in (40) and calculated in the s-channel perversity frame: we also show their difference Δ_i (▩) which should be zero in the quark model. The data is from $\pi^+p \rightarrow \rho^o\Delta^{++}$ and is taken from ref. 104. The t-scales at the bottom do not pertain at all to the experimental points but only to the theoretical curves. These are strong absorption (SCRAM) calculations for Δ_i and are described in Section 4.6(ii).

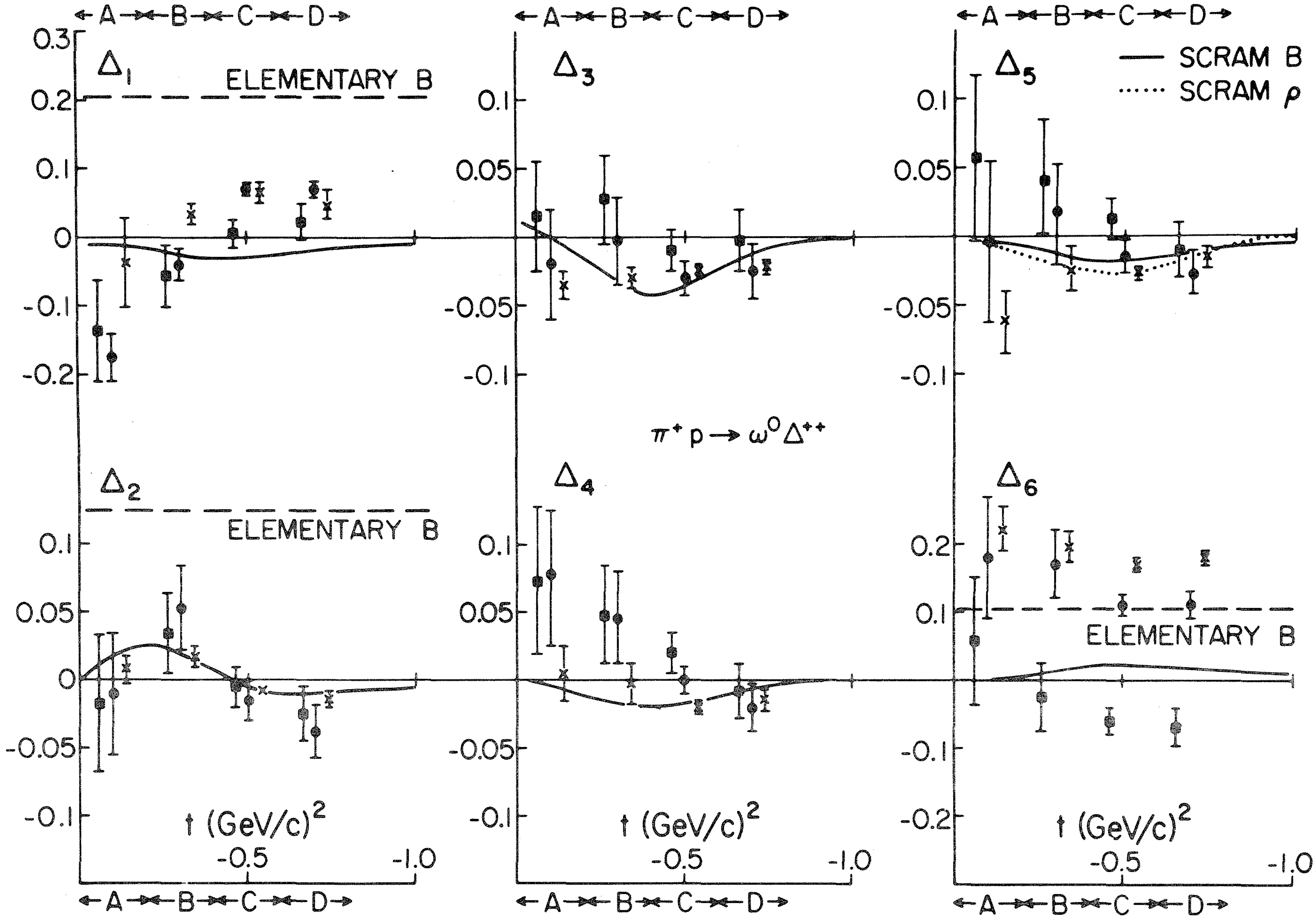

Figure 40: The experimental and theoretical values for Δ_i plotted as in Figure 39 while the data is for $\pi^+p \rightarrow \omega^o\Delta^{++}$ and taken from ref. 105.

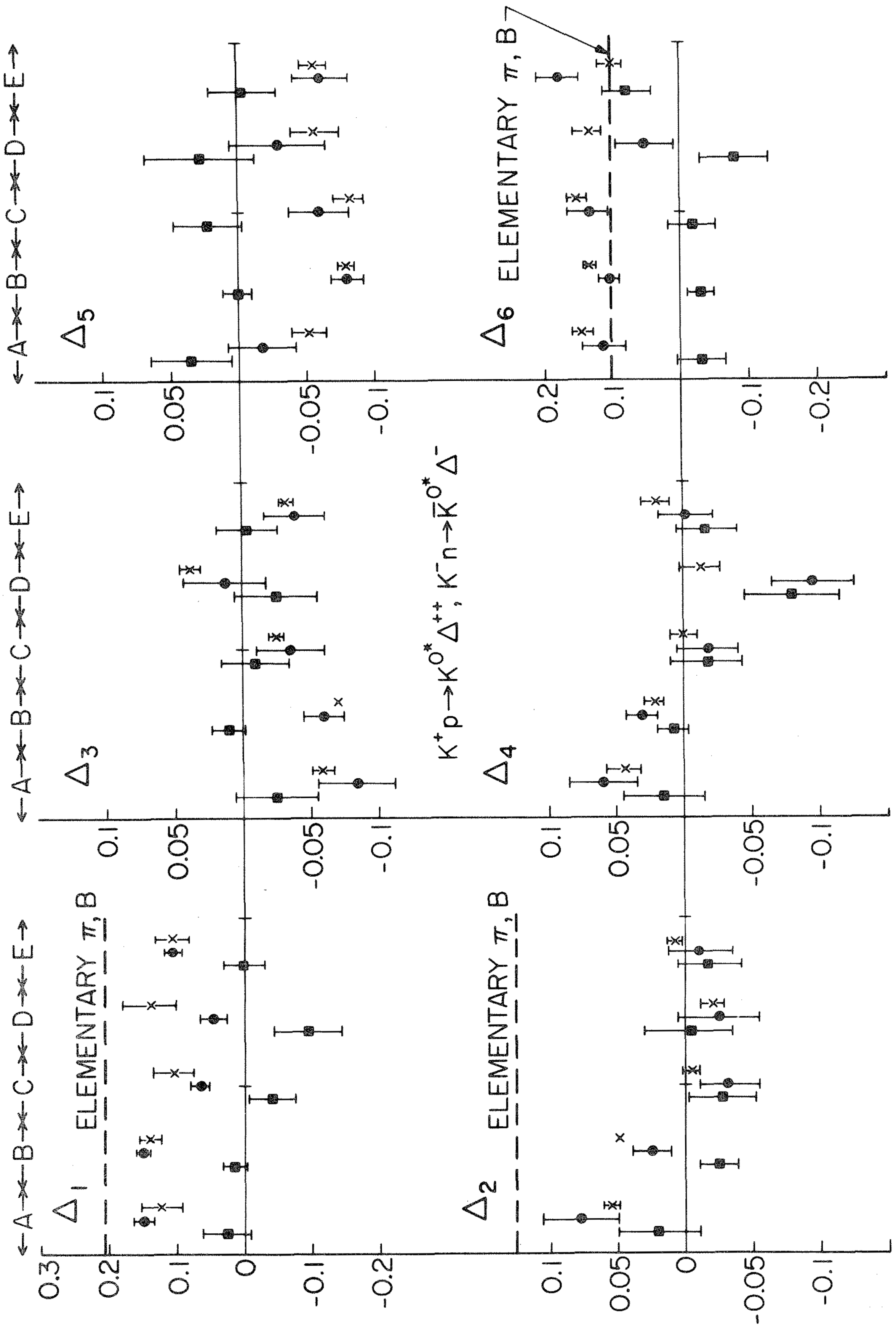

Figure 41: The experimental values for Δ_i in $\overset{(-)}{K}N \to \overset{(-)}{K}{}^*\Delta$, plotted as in Figure 39 and taken from ref. 106.

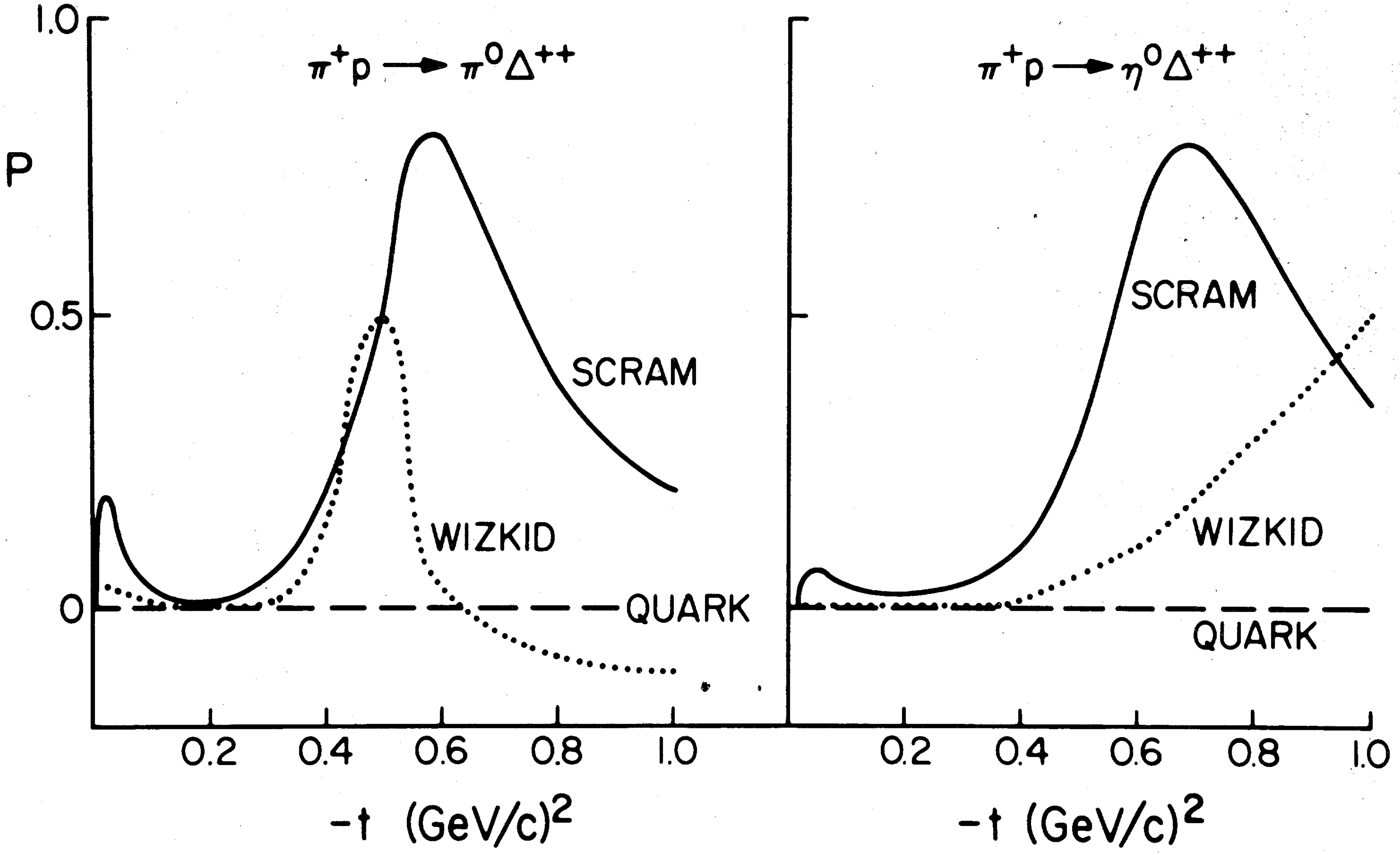

Figure 42: The total asymmetry – integrated over the Δ^{++} decay – in $\pi^+p \to \pi^o\Delta^{++}$ and $\pi^+p \to \eta^o\Delta^{++}$ interactions off a polarized proton target at 8 GeV/c. Shown are the predictions of the quark model (=0, – – –) strong cut (SCRAM, ——) and weak cut (WIZKID, ·······)

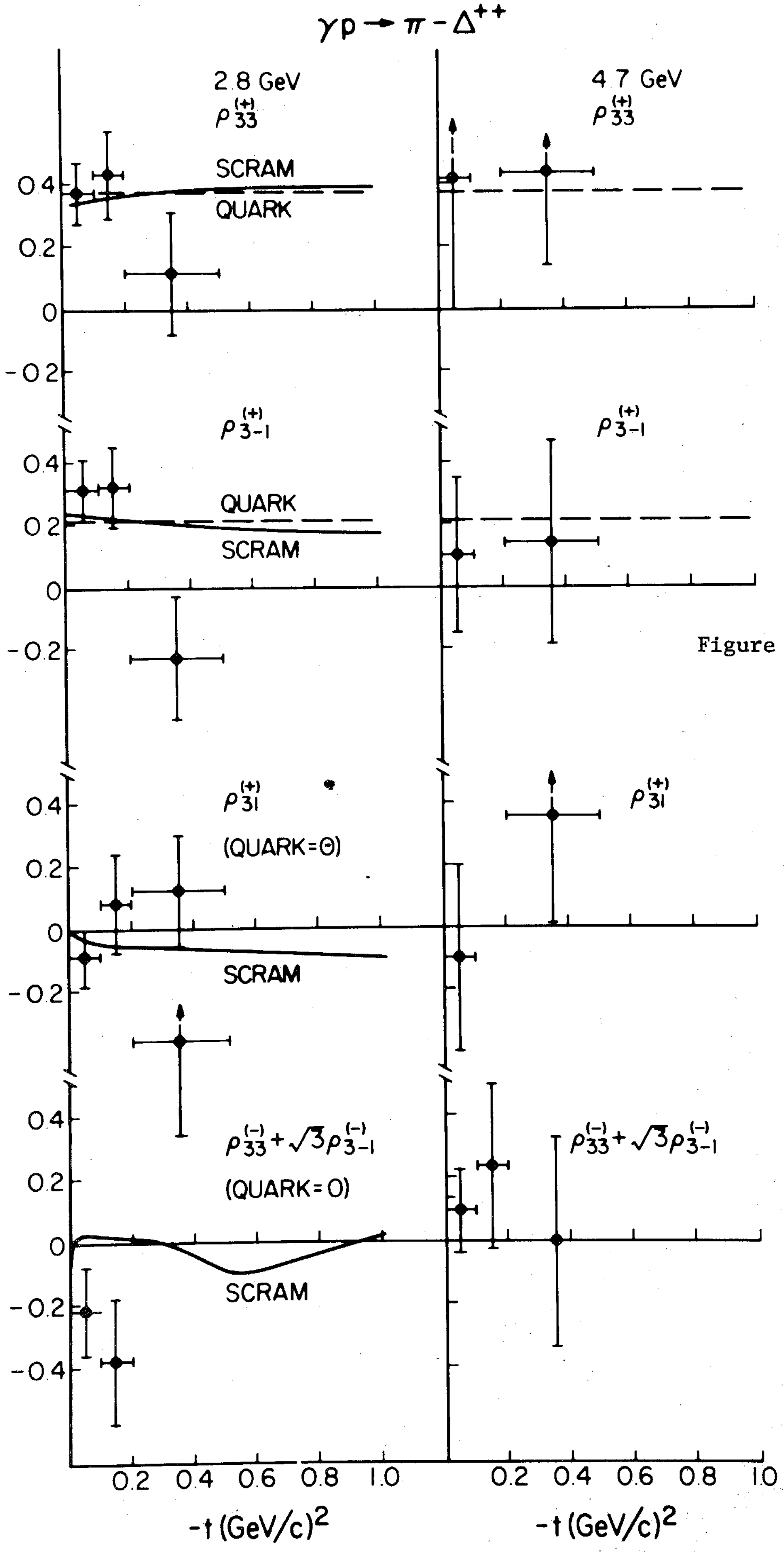

Figure 43: $\gamma p \rightarrow \pi^- \Delta^{++}$ with a polarized γ at 2.8 and 4.7 GeV (Ref. 88). Shown are the experimental Δ^{++} decay density matrix elements $\rho^{(\pm)}$ for $\tau P^{\pm}$ exchange. At the lower energy, we show the predictions of the quark model (– – – –) and the strong cut absorption model. (SCRAM, ———). The latter used as input π exchange only and no ρ, A_2 exchange at all--the $\tau P+$ is all generated from absorption. The theory predicts no significant energy dependence in the $\rho(\pm)$.

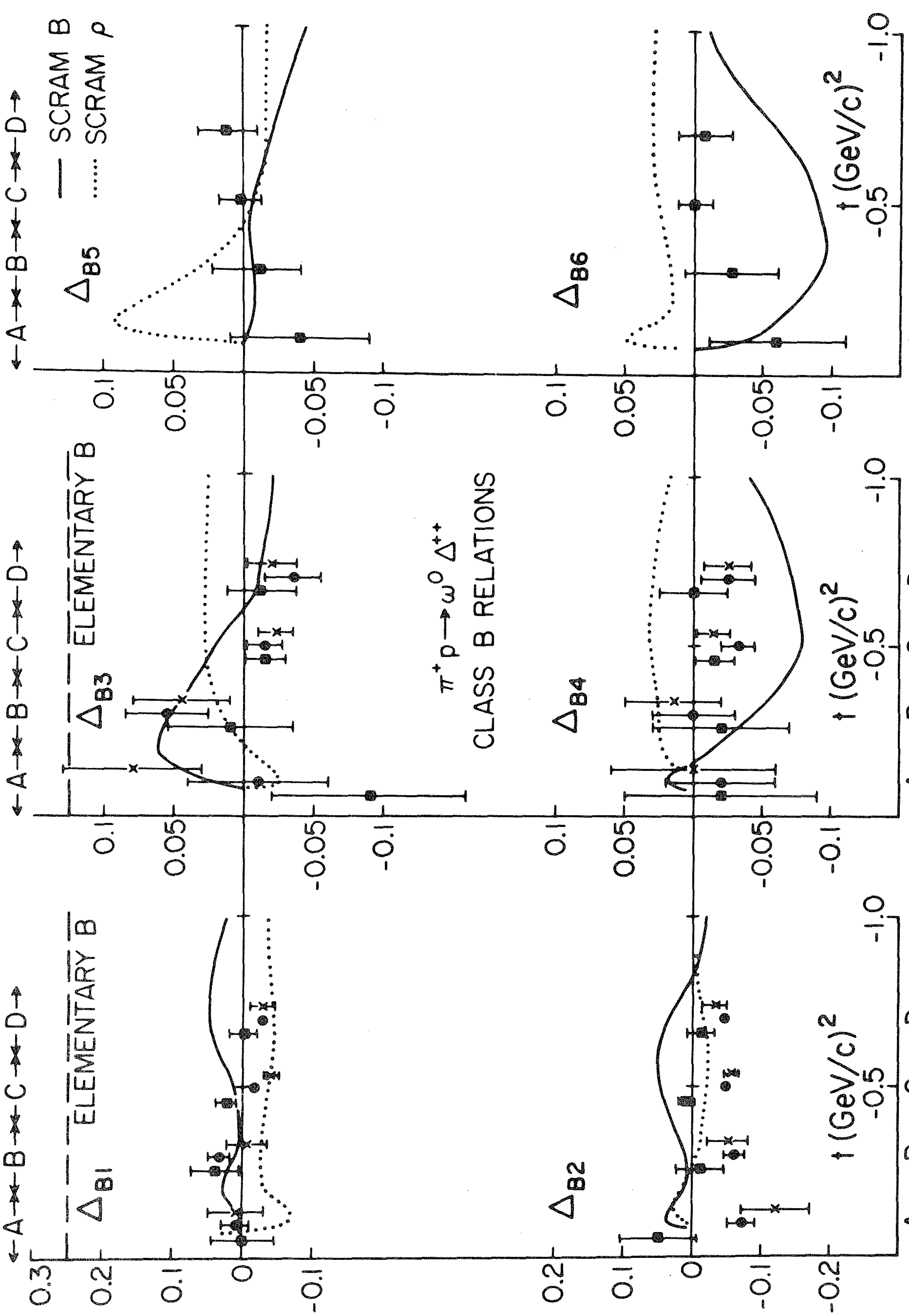

Figure 44: All theoretical and experiment values are as in Fig. 40 except we now plot the six class B[91] instead of the class A relations. The relations (B.5), (B.6) have zero right hand side. Only one entry (■) is made.

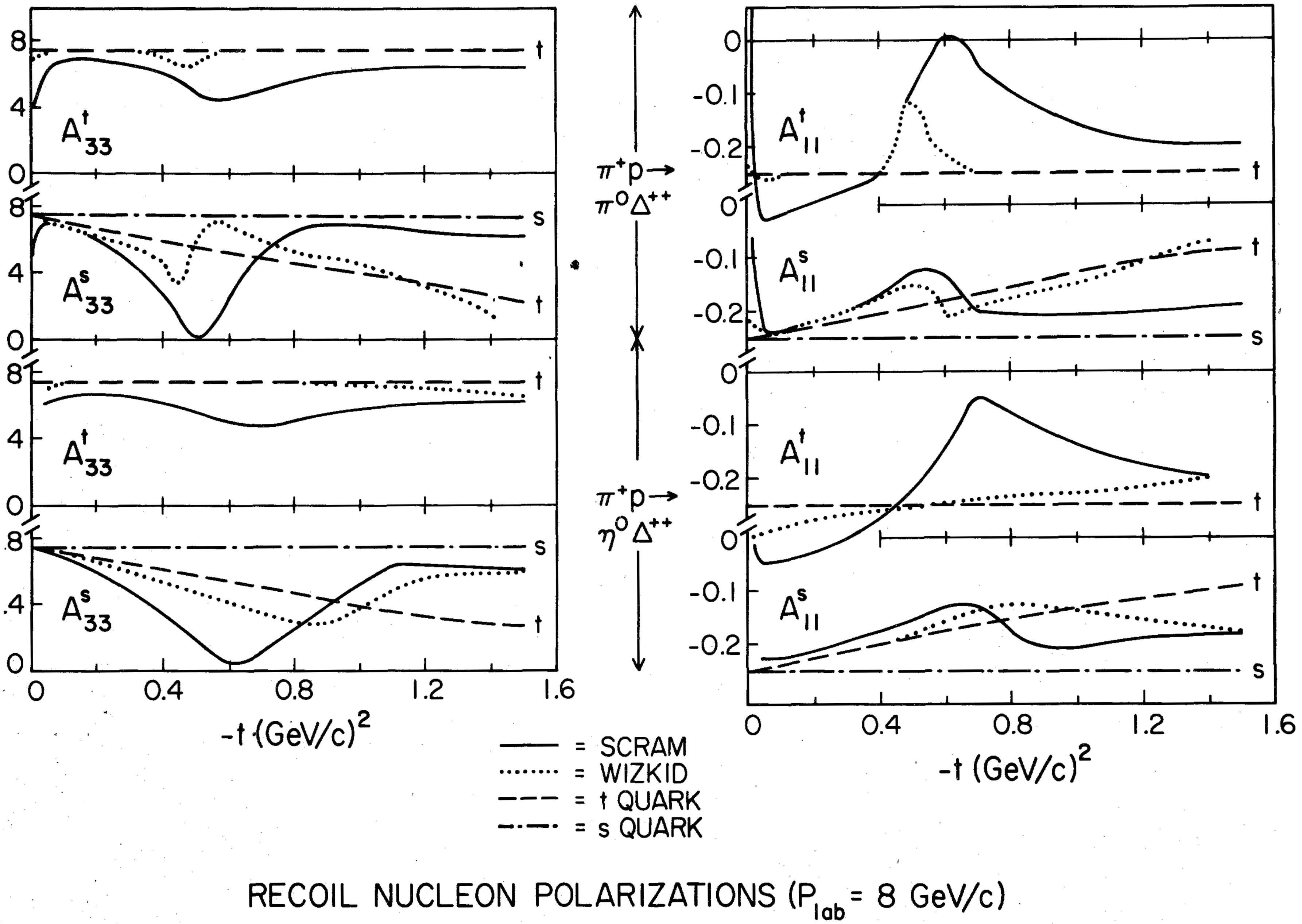

Figure 45: Theoretical predictions for the decay density matrix elements A_{33} and A_{11} describing the Δ^{++} in $\pi^+p \to \pi^o\Delta^{++}$ and $\pi^+p \to \eta^o\Delta^{++}$ at 8 GeV/c. This figure is discussed in Section 4.7 and explained in footnote 107.

DISCUSSION

On the behavior of partial wave amplitudes and large -t behavior (Section 3)

Schmid (CERN): It is interesting to contrast partial waves in K^-p and K^+n charge exchange scattering. Simple exchange degeneracy says the cross sections are the same, but the phases for both reactions are very different. For K^-p charge exchange we have a rotating phase; while for K^+n charge exchange, we have a real phase. If you analyze the latter, you get large low partial waves. In the K^-p case, due to the oscillations and consequent sign changes in the real and imaginary parts of the amplitude, one gets the peripheral partial waves. This is very nice, and consistent with the low energy data, where indeed the K^-p is much more peripheral than, for example K^+p. At 1 GeV/c, there is very strong Y^* formation in K^-p, i.e., in D waves and F waves, while in K^+p one finds large low partial waves. This is a dramatic example where the absolute magnitudes are identical, but the phases are very different. Consequently, the partial waves for these two cases behave very differently.

Fox: I agree. (See Figures 34 and 35 for K^-p and K^+n charge exchange partial waves.)

Schmid: On this work of Harari and Davier, let us emphasize what they did. Once you accept their model, it explains the difference of the cross section in terms of the interference effect between the Pomeron and the nondiffractive amplitude, with the added principle that the imaginary part of the nondiffractive amplitude is peripheral.

Fox: Yes, the imaginary part in their model is small at large $|t|$. (See Figure 7.) It is difficult to understand why you obtain the e^{3t} behavior in the large $|t|$ region. (Note the small contribution of ImN in Figure 12 outside the forward peak.) Maybe in the strong interaction case, such a behavior is associated with the real part --although in photoproduction, it is difficult to explain the large $-t$ behavior of $\gamma p \rightarrow \pi^o p$ with the real part alone. (See p.739).

Schmid: I have an independent point here. In strong interactions, say for t between -1 and -3 $(GeV/c)^2$, and lab momenta rather intermediate, say 3-5 GeV/c, there is exceedingly strong shrinkage.

Fox: I agree entirely. There is large shrinkage between 3-5 GeV/c. The data I show you is actually around 5 GeV/c. However, if we think of 3-5 GeV/c as being the transition region, you cannot interpret this shrinkage in terms of an asymptotic theory like Regge theory, unless there is high energy data which agrees with the trend. In particular, photoproduction shrinks between 3 and 5 GeV/c. (Figure 28.) However, above that energy, the cross-section shape is energy independent--there is no shrinkage. Unfortunately, there is essentially no experimental information as to shrinkage in strong interaction exchange reactions above 5 GeV/c, for $-t \gtrsim 1\ (GeV/c)^2$. It is an important experiment.